Satyajit Patel
C. H. Solanki
Krishna R. Reddy
Sanjay Kumar Shukla   *Editors*

Proceedings of the Indian Geotechnical Conference 2019

IGC-2019 Volume II

Springer

Lecture Notes in Civil Engineering

Volume 134

Lecture Notes in Civil Engineering (LNCE) publishes the latest developments in Civil Engineering - quickly, informally and in top quality. Though original research reported in proceedings and post-proceedings represents the core of LNCE, edited volumes of exceptionally high quality and interest may also be considered for publication. Volumes published in LNCE embrace all aspects and subfields of, as well as new challenges in, Civil Engineering. Topics in the series include:

- Construction and Structural Mechanics
- Building Materials
- Concrete, Steel and Timber Structures
- Geotechnical Engineering
- Earthquake Engineering
- Coastal Engineering
- Ocean and Offshore Engineering; Ships and Floating Structures
- Hydraulics, Hydrology and Water Resources Engineering
- Environmental Engineering and Sustainability
- Structural Health and Monitoring
- Surveying and Geographical Information Systems
- Indoor Environments
- Transportation and Traffic
- Risk Analysis
- Safety and Security

To submit a proposal or request further information, please contact the appropriate Springer Editor:

- Pierpaolo Riva at pierpaolo.riva@springer.com (Europe and Americas);
- Swati Meherishi at swati.meherishi@springer.com (Asia - except China, and Australia, New Zealand);
- Wayne Hu at wayne.hu@springer.com (China).

All books in the series now indexed by Scopus and EI Compendex database!

More information about this series at http://www.springer.com/series/15087

Satyajit Patel · C. H. Solanki · Krishna R. Reddy ·
Sanjay Kumar Shukla
Editors

Proceedings of the Indian Geotechnical Conference 2019

IGC-2019 Volume II

Editors
Satyajit Patel
Department of Applied Mechanics
Sardar Vallabhbhai National Institute
of Technology
Surat, India

C. H. Solanki
Department of Applied Mechanics
Sardar Vallabhbhai National Institute
of Technology
Surat, India

Krishna R. Reddy
Department of Civil, Materials,
and Environmental Engineering
University of Illinois
Chicago, Chicago, IL, USA

Sanjay Kumar Shukla
Department of Civil Engineering
Edith Cowan University
Joondalup, WA, Australia

Preface

The Indian Geotechnical Society, Surat Chapter, and Sardar Vallabhbhai National Institute of Technology (SVNIT), Surat, India, organized the Indian Geotechnical Conference (IGC) in Surat during 19–21 December 2019. The main theme of the conference was "GeoINDUS: Geotechnics for INfrastructure Development and UrbaniSation". The sub-themes of the conference included:

1. Characterization of Geomaterials and Physical Modelling
2. Foundations and Deep Excavations
3. Soil Stabilization and Ground Improvement
4. Geoenvironmental Engineering and Waste Material Utilization
5. Soil Dynamics and Earthquake Geotechnical Engineering
6. Earth Retaining Structures, Dams and Embankments
7. Slope Stability and Landslides
8. Transportation Geotechnics
9. Geosynthetics Applications
10. Computational, Analytical and Numerical Modelling
11. Rock Engineering, Tunnelling and Underground Constructions
12. Forensic Geotechnical Engineering and Case Studies
13. Others Topics: Behaviour of Unsaturated Soils, Offshore and Marine Geotechnics, Remote Sensing and GIS, Field Investigations, Instrumentation and Monitoring, Retrofitting of Geotechnical Structures, Reliability in Geotechnical Engineering, Geotechnical Education, Codes and Standards, and other relevant topics.

The proceedings of this conference consists of selected papers presented at the conference. The proceedings is divided into six volumes, including a special volume with all keynote/invited presentations.

We sincerely thank all the authors who have contributed their papers to the conference proceedings. We also thank all the reviewers who have been instrumental in giving their valuable inputs for improving the quality of the final papers. We greatly appreciate and thank the student volunteers, especially Vemula Anand Reddy, Mohit Mistry, Rahul Pai, Manali Patel, Rohan Deshmukh, Hrishikesh Shahane, Anand M. Hulagabali, Jiji Krishnan and Bhavita Dave for their unwavering support that was

instrumental in preparation of these proceedings. Finally, thanks to the Springer team for their support and full cooperation for publishing six volumes of this IGC-2019 proceedings.

Surat, India   Satyajit Patel
Surat, India   C. H. Solanki
Chicago, USA   Krishna R. Reddy
Joondalup, Australia   Sanjay Kumar Shukla

Contents

About the Editors

Dr. Satyajit Patel is Associate Professor at the Civil Engineering Department, Sardar Vallabhbhai National Institute of Technology, Surat, India. His research area includes utilization of industrial solid wastes in civil engineering constructions, geoenvironmental issues, soil stabilization, ground improvement, and geosynthetics for road pavements. He has published 13 journal papers and presented 7 research papers internationally. He has guided more than 29 M.Tech. students and 9 students are currently pursuing their Ph.D. under his guidance. He is a life member of Indian Geotechnical Society, Institution of Engineers (India), and Indian Road Congress (IRC). He has received a research grant from the Department of Science and Technology, Government of India.

Dr. C. H. Solanki is Professor (Geotechnical Engineering) at the Civil Engineering Department, Sardar Vallabhbhai National Institute of Technology, Surat, India. He has guided 50 postgraduate dissertations and 16 Ph.D. thesis and he is currently supervising 11 Ph.D. research scholars. He has published 165 research papers in the reputed national, international journals and conferences. Dr. Solanki received the "Shri. M. S. Jain Biannual Award" for the Best Paper in IGC 2013, Prof. Dinesh Mohan Award in IGC 2017 and "Distinguished Faculty Award" form The Venus International Faculty Awards-2016. He has organized 20 national level events including STTP, FDP, conferences and seminars and he was the chairman for the Indian Geotechnical Conference (IGC 2019) held at Surat, Gujarat. Dr. Solanki has been elected as a member of executive committee of IGS

for the terms (2015–2022). His research interests include subsoil characteristics, predictions in geotechnical engineering, soil dynamics, ground improvement and geoenvironmental engineering. He has given 50 expert talks throughout India and abroad. He is a life member of Indian Geotechnical Society, Indian Society for Technical Education (ISTE), and Institution of Engineers (India).

Dr. Krishna R. Reddy is Professor of Civil and Environmental Engineering, Director of Sustainable Engineering Research Laboratory, and also Director of the Geotechnical and Geoenvironmental Engineering Laboratory at the University of Illinois at Chicago, USA. He received his Ph.D. in Civil Engineering from the Illinois Institute of Technology, Chicago, USA. Dr. Reddy has over 28 years of teaching, consulting, and research experience in the fields of civil engineering, geotechnical and geoenvironmental engineering, environmental engineering, and sustainable and resilient engineering. He is the author of 4 books, 246 journal papers, 21 edited books/conference proceedings, 22 book chapters, and 225 full conference papers. He has received several awards for excellence in research and teaching, including the ASCE Wesley W. Horner Award, ASTM Hogentogler Award, UIC Distinguished Researcher Award, the University of Illinois Scholar Award, and the University of Illinois Award for Excellence in Teaching.

Dr. Sanjay Kumar Shukla is the Founding Research Group Leader (Geotechnical and Geoenvironmental Engineering) at the Edith Cowan University, Perth, Australia. He is the Founding Editor-in-Chief of the International Journal of Geosynthetics and Ground Engineering. He holds the Distinguished Professorship in Civil Engineering at Delhi Technological University, Delhi, VIT University, Vellore, Amity University, Noida, Chitkara University, Himachal Pradesh and V. R. Siddhartha Engineering College, Vijayawada, India. He graduated in Civil Engineering from BIT Sindri, India, and earned his M.Tech. in Civil (Engineering Geology) Engineering and Ph.D. in Civil (Geotechnical) Engineering from the Indian Institute of Technology (IIT) Kanpur, India. His primary areas of research interest

include geosynthetics and fibres for sustainable developments, ground improvement techniques, utilization of wastes in construction, earth pressure and slope stability, environmental, mining and pavement geotechnics, and soil–structure interaction. He is an author/editor of 15 books, including 7 textbooks, and more than 260 research papers, including 160 refereed journal papers. He has been honoured with several awards, including IGS Award 2018 by the International Geosynthetics Society, USA, in recognition of outstanding contribution to the development and use of geosynthetics. He is a fellow of Engineers Australia, Institution of Engineers (India), and Indian Geotechnical Society, and a member of American Society of Civil Engineers, International Geosynthetics Society, and several other professional bodies.

Analysis of the Effect of Plastic Waste Strips on Characteristics of Fine-Grained Soils

Mouneesh Meka and Anjan Patel

Abstract Most of the developing countries like India are facing a severe crisis in solid waste management. Among all, plastic waste is considered to be more harmful because of its non-biodegradable nature and abundant usage. The current work deals with an engineering technique in order to eliminate this problem of plastic waste management, by using plastic waste as a potential reinforcing element in soils. This saves a lot of effort, intellect and money which would be otherwise invested to manage plastic waste from various sources. In this study, the effects of mixing low-density polyethylene (LDPE) strips on some of the physical properties of fine-grained soils are presented. These LDPE strips act like reinforcement for the soils and could be well used in the construction of embankments and roads. In the present analysis, unconfined compressive strength (UCS) test, proctor compaction test and bender/extender tests were conducted. Four different types of fine-grained soils (i.e., CH, CL, MH and ML) were taken, and five different percentages by weight (i.e., 0%, 0.25%, 0.5%, 0.75% and 1%) of LDPE strips were added to each of these soils. The optimum percentage of LDPE strips that result in maximum improvement of soil characteristics was evaluated. It was observed that the UCS value increases up to a certain percentage of plastic waste and then it starts decreasing. Poisson's ratio was found to decrease with increase in plastic content, thus increasing the soil stiffness.

Keywords LDPE · Unconfined compressive strength · Proctor compaction · Bender-extender

1 Introduction

Since last few decades, environmental degradation is taking place at an alarming rate due to various reasons including human activities like extreme usage of

M. Meka (✉) · A. Patel
Department of Civil Engineering, Visvesvaraya National Institute of Technology, Nagpur, India
e-mail: mouneesh.meka@gmail.com

non-biodegradable materials and non-renewable resources. The disposal of non-biodegradable material is one of the most facing challenges in present day's situation. These plastic wastes create a lot of problems like blockages in pipelines, water pollution, threat to the marine species and release of toxic gases on burning. Some of the plastic materials are recyclable, whereas some are not. The non-recyclable plastic wastes and the waste which is not cost-effective in recycling can be used in construction industries quite effectively.

Some of the researchers have used different types of plastic waste materials for the improvement of various soil properties. Ilies et al. [1] used polyethylene waste material and binder for soil stabilization and then compared the results with that obtained from cement stabilization. Even though better results are obtained when cement is used, the usage of plastic waste is an eco-friendly technique and has a lower carbon footprint unlike cement. Choudhary et al. [2] have conducted studies on HDPE strips for the improvement of local sands. It was observed that the CBR and secant modulus values increase with addition of the HDPE strips. Consoli et al. [3] have highlighted the benefits of utilizing randomly distributed polyethylene terephthalate fiber, obtained from recycling waste plastic bottles, alone or mixed with rapid hardening Portland cement to improve the engineering behavior of uniform fine sand. Similarly, Sobhan and Mashnad [4] carried out an experimental investigation on soil–cement–fly ash mixture reinforced with recycled plastic strips that were collected from post-consumer milk and water containers. It is found that the use of fiber reinforcement significantly increases the post-peak load carrying capacity of the mix. In the present study, one time usable plastic which is generally manufactured for snack packaging is used for improving the strength characteristics of different soils.

2 Materials

2.1 Soil

In the present study, four different types of fine-grained soils were used due to the reason that fine-grained soils in general possess less strength as compared to the coarse-grained soils. An attempt has been made in this paper for improving the strength characteristics of fine-grained soils by using the plastic waste as soil reinforcing element. The soils were characterized in the laboratory for their basic geotechnical properties, and the results obtained are summarized in Table 1. These soils are classified as CL, CH, ML and MH according to the unified soil classification system (USCS).

Figure 1 shows the position of the selected soils in the plasticity chart.

Table 1 Properties of soil used

Property	CL	CH	ML	MH
Liquid limit (%)	34	59	49	65
Plastic limit (%)	23	30	40	44
Plasticity index (%)	11	29	9	21
75 μ passing (%)	54	85	73	61
Maximum dry density (g/cc)	1.68	1.58	1.64	1.67
Optimum moisture content (%)	21	23	17	20
Specific gravity	2.53	2.54	2.61	2.62
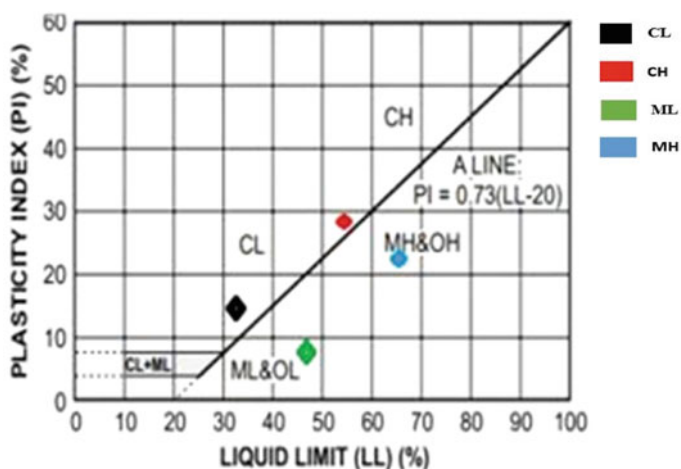
Fig. 1 Location of the used samples in soil plasticity chart

2.2 Plastic Waste

For the present study, plastic waste was collected from hostel areas of the Visvesvaraya National Institute of Technology, Nagpur. The selected plastic waste consists of packets used for snack packaging manufactured by the OMNIPLAST Pvt. Ltd. After collection, these wastes were cut into pieces (10 mm length × 10 mm width) as shown in Fig. 2, and then, the plastic strips were mixed with the soil. The percentage of plastic content in the mix was kept as 0, 0.25, 0.50, 0.75 and 1% by weight.

The mechanical properties of the plastic waste, viz. tensile strength, elongation at break and Young's modulus, are summarized in Table 2. In order to obtain these values, tensile strength test was conducted on the plastic strips as per the procedure presented in ASTM D638-14 (Standard Test Method for Tensile Properties of Plastics) by using the INSTRON Series IX automated material testing system. Using the computer interface, mechanical properties of the plastic strips were automatically

Fig. 2 Plastic waste strips
used in present study

Table 2 Properties of plastic
waste

Properties	Values
Tensile strength (MPa)	50.6
Elongation at break (%)	60.9
Young's modulus (MPa)	971.1

obtained from the tests. The load–displacement curve as obtained from the test is
shown in Fig. 3.
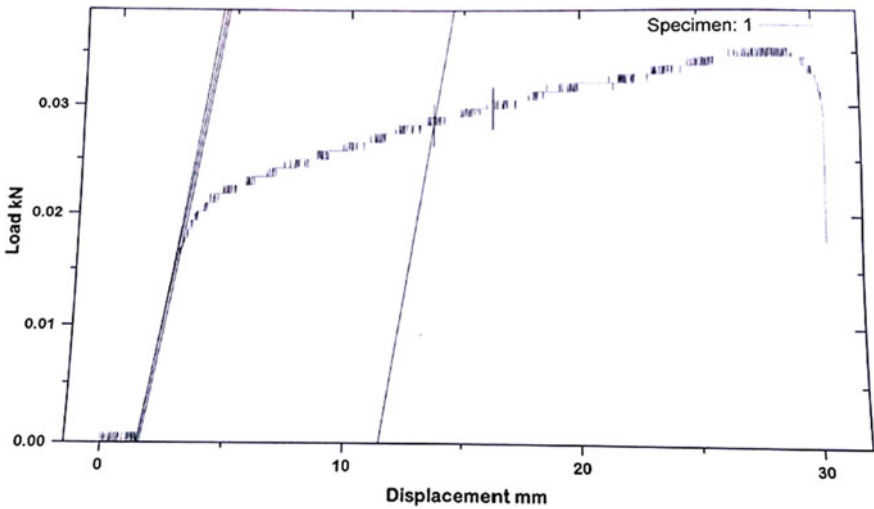
Fig. 3 Load settlement curve obtained from tensile strength test on the plastic strips

3   Experimental Investigations

As mentioned earlier, the plastic strips were mixed with the soils at five different percentages, i.e., 0, 0.25, 0.5, 0.75 and 1%, by dry weight of the soils. Then, proctor compaction tests were conducted to obtain the optimum moisture content (OMC) and maximum dry density (MDD) of the soils mixed with plastic strips.

In order to determine the unconfined compressive strength (UCS) of the reinforced soils (i.e., soil–plastic mix), soil specimens of size 5 cm diameter × 10 cm length were prepared in the laboratory. However, before conducting the UCS tests, bender/extender tests were conducted on these prepared specimens. For this purpose, small grooves were made on top and bottom of the soil specimens (as shown in Fig. 4a). The bender/extender system consists of a piezo-ceramic transmitter which is fixed to a triaxial pedestal and a receiver fixed to a top acrylic plate as shown in Fig. 4b. A schematic representation of the test setup is also shown in Fig. 5. The piezo-ceramic transmitter generates shear or compression wave which transmits through the soil specimen and is captured by the receiver. If the piezo-ceramic element generates and captures shear wave, then it is known as a bender element. On the other hand, if the piezo-ceramic element generates and captures compression wave, then it is known as an extender element. The generation of shear or compression wave was facilitated by a master control unit and the waveforms were analyzed with the help of GDS bender element system software. Then, the travel time was determined by using peak-to-peak method as shown in Fig. 6. Knowing the length of wave propagation (i.e., tip-to-tip distance between the transmitter and the receiver, L_{tt}) and the travel time (i.e., time lag between the I/P and O/P waves, t), the shear and compression wave velocities (V_s and V_p, respectively) were calculated using Eq. (1).

(a)   (b)
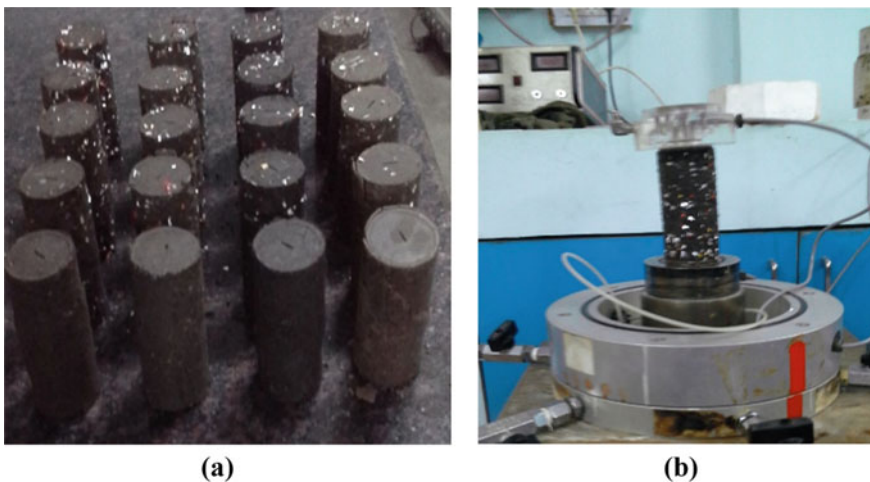
Fig. 4   a Soil samples used for the bender/extender testing **b** bender/extender test
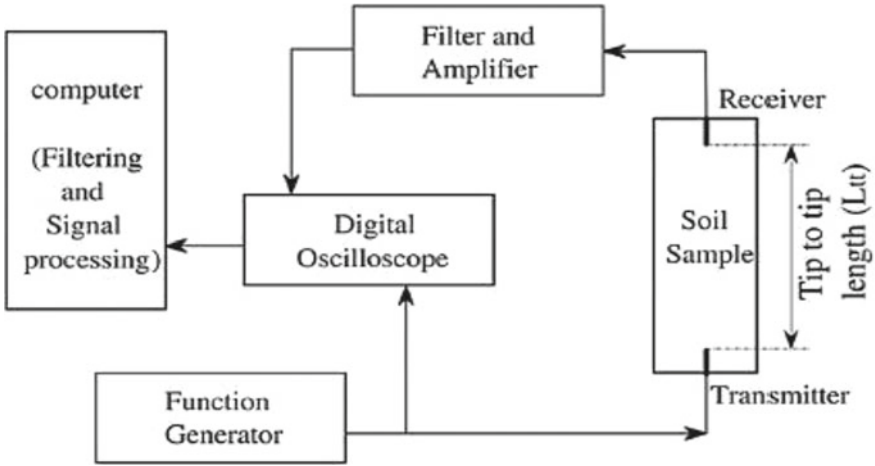
Fig. 5 Schematic representation of bender/extender test setup

$$V = L_{tt}/t \qquad (1)$$

where V is either V_s or V_p depending upon whether bender or extender elements have been used (Fig. 6).

Further, Poisson's ratio (v) was determined by using Eq. (2).

$$v = \frac{0.5r^2 - 1}{r^2 - 1} \qquad (2)$$

where r is the ratio between V_p and V_s.
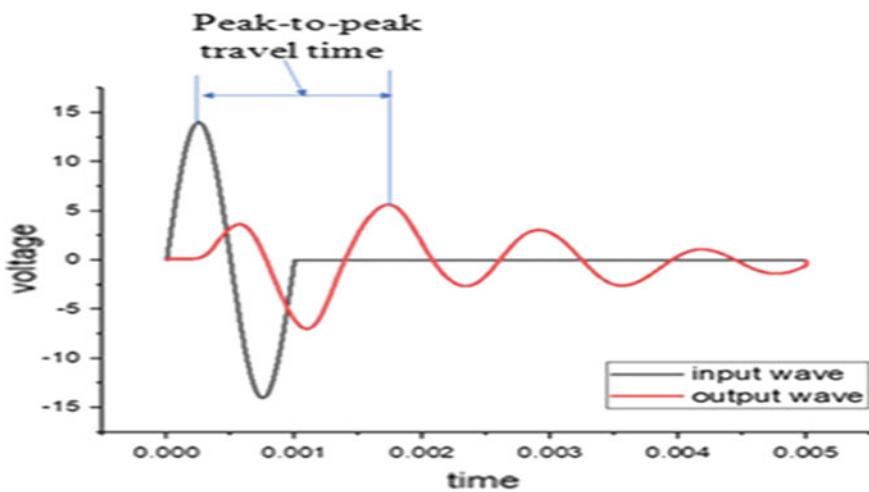
Fig. 6 Determination of peak-to-peak travel time

Fig. 7 Test setup used for
the UCS test

The unconfined compressive strength (UCS) test was conducted on all the samples used for the bender/extender test. It is worth mentioning that the bender/extender test is non-destructive in nature, and hence, the same samples after bender/extender test can be used for other tests like UCS. The test setup used to conduct the UCS test is shown in Fig. 7.

4 Results and Discussion

4.1 Compaction Characteristics

The variation in maximum dry density (MDD) and optimum moisture content (OMC) of different soils with addition of different percentages of the plastic strips is shown in Fig. 8 and Fig. 9, respectively.

From Fig. 8, it can be observed that the MDD decreases with increase in plastic content in all types of soils. This is due to fact that the density of plastic strips is less as compared to that of the soil. No clear trends were obtained between OMC and % of plastic strips as shown in Fig. 9. The plastic strips added to soil result in a more
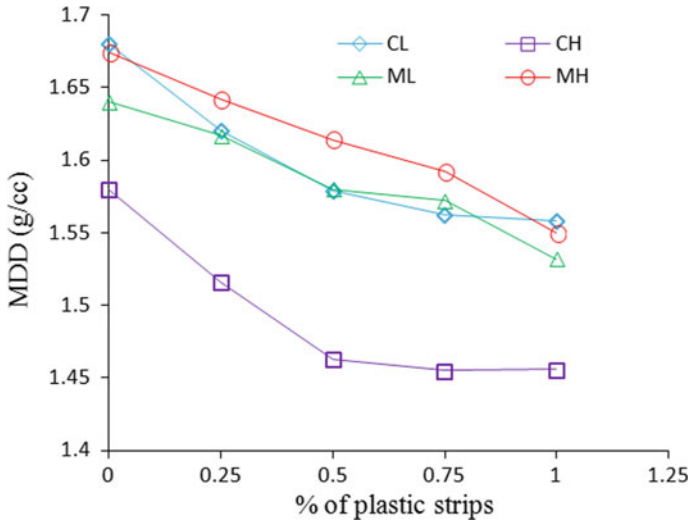
Fig. 8 Variation of MDD with % plastic strips
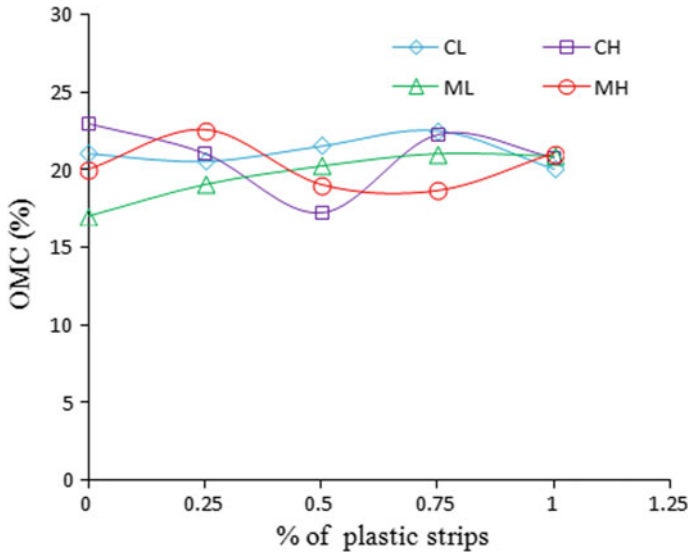
Fig. 9 Variation of OMC with % plastic strips

dispersed and disturbed structure of the mixture. Hence, based upon the inter-voids created in the soil–plastic mixture, it is expected that within the small range of plastic strip added, a clear trend could not be obtained for OMC.

4.2   Unconfined Compressive Strength

The variation of UCS with % of plastic strips added in different types of soils is shown in Fig. 10. For the sake of completeness, all the stress–strain curves obtained from the UCS tests are also shown in Fig. 11.

Based upon the results as shown in Fig. 10, the optimum UCS value was obtained at about 0.75% of plastic strips in all the soils. With addition of plastic strips more than 0.75%, the UCS value started decreasing. This might be again attributed to the more disturbed structure of the soil samples at higher plastic content. Further, the percentage increase in the UCS value at 0.75% plastic content was calculated, and it was found to be almost similar (varying between 33 and 41%) for all the soils. The strain value corresponding to failure stress was found to decrease with increase in plastic content as shown in Fig. 11. Hence, it is quite useful to reinforce the soils with addition of plastic waste where soil deformation is an issue. However, at higher plastic content, the soil becomes more brittle as shown in Fig. 11 at 1% plastic. This is due to the fact that at higher plastic content the bonding between soil solids decreases.
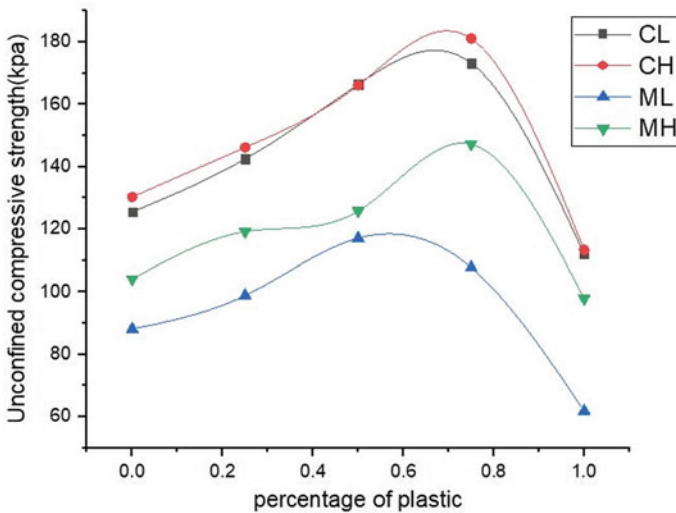
Fig. 10 Variation of UCS with % of plastic strips
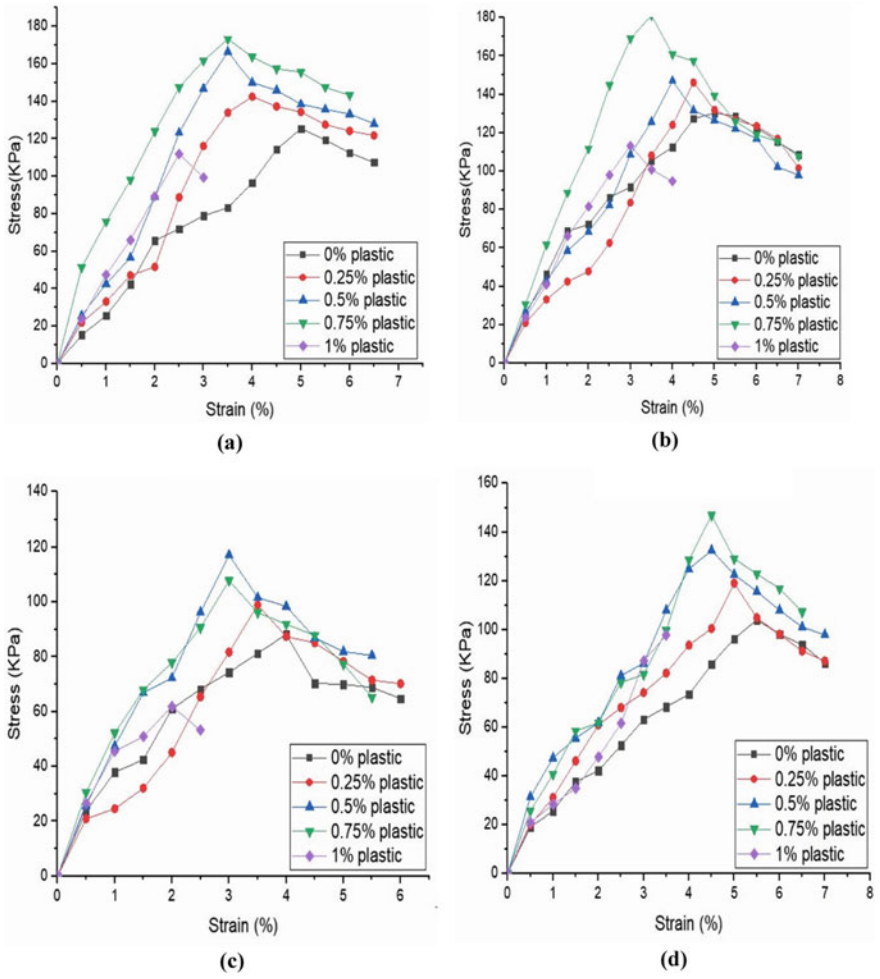
Fig. 11 Stress–strain curves obtained from UCS tests for **a** CL **b** CH **c** ML **d** MH soils

4.3 Wave Velocities and Poisson's Ratio

The results obtained from bender/extender test are presented in Table 3. The V_s, V_p and ν values were determined as per the procedure presented in Sect. 3 (Table 3)

Further, as shown in Fig. 12, Poisson's ratio value was found to decrease with increase in the plastic content. The decrease in ν value is about 4 to 6% and 11 to 14% in clayey and silty soils, respectively. With decrease in ν value, the soil stiffness

Table 3 Wave velocities and Poisson's ratio results

Soil type	Percentage of plastic	V_p (m/s)	V_s (m/s)	Poisson's ratio, ν
CL	0	325	86	0.4620
	0.25	352	94	0.4614
	0.5	282	88	0.4459
	0.75	281	94	0.4375
	1	264	84	0.4425
CH	0	249	92	0.4358
	0.25	223	77	0.4321
	0.5	184	71	0.4258
	0.75	192	68	0.4264
	1	169	63	0.4104
ML	0	235	70	0.4503
	0.25	163	63	0.4115
	0.5	163	64	0.4082
	0.75	169	64	0.4162
	1	124	53	0.3862
MH	0	235	79	0.4346
	0.25	223	77	0.4321
	0.5	202	69	0.4328
	0.75	176	71	0.4007
	1	146	63	0.3847

increases. This increase in soil stiffness is another reason that at higher plastic content, the soils become more brittle.

5 Conclusions

The following conclusions can be derived from the present study:

- The MDD value was found to decrease with increase in plastic content.
- The UCS value was found to increase with increase in plastic content up to a certain percentage and then it starts decreasing.
- Soil brittleness increases with increase in plastic content.
- The percentage increase in the UCS value was found to be almost similar for all types of soils.
- Poisson's ratio decreases with increase in plastic content, and thus, there is an increase in soil stiffness.
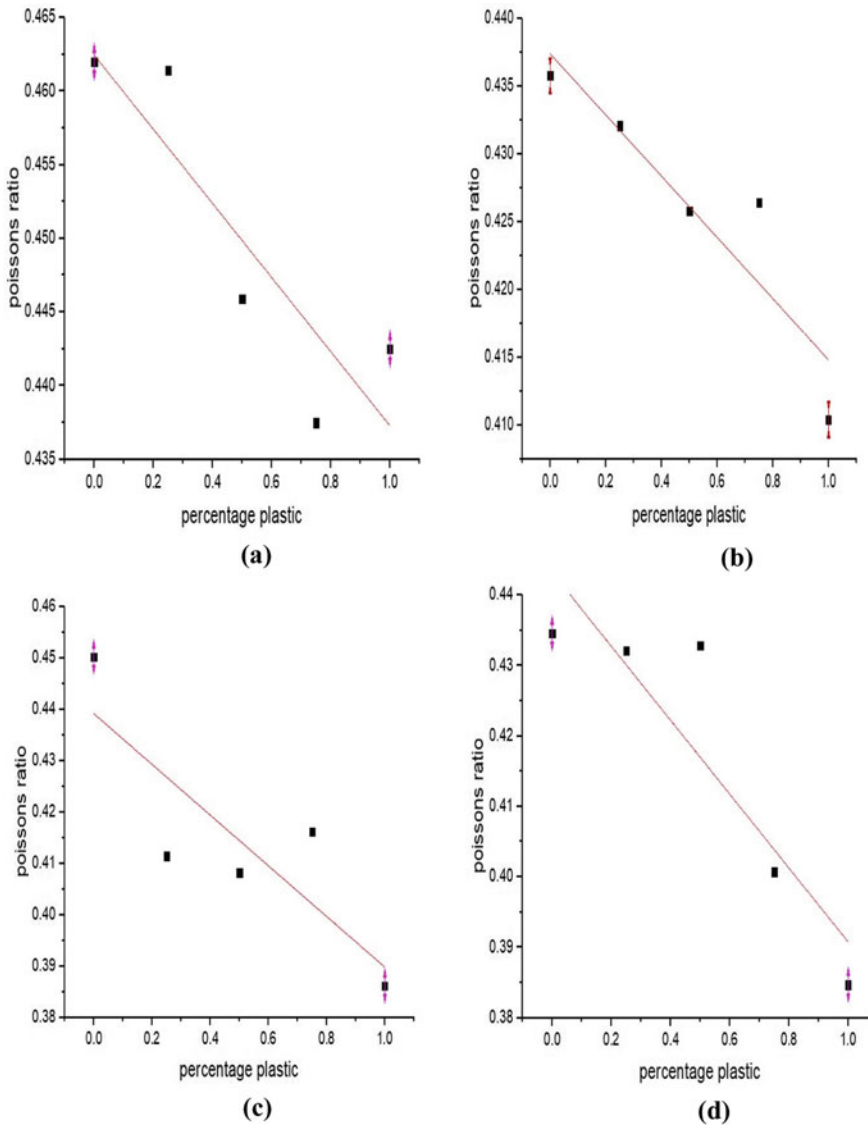
Fig. 12 Variation of Poisson's ratio with plastic content for **a** CL **b** CH **c** ML **d** MH soils

References

1. Ilies, N.M., Circu, A.P., Nagy, A.C., Ciubotaru, V.C., Kisfaludi-Bak, Z.: Comparative study on soil stabilization with polyethylene waste materials and binders. In: 10th International Conference Interdisciplinary in Engineering, INTER-ENG 2016. Procedia Eng. **181,** 444–451 (2017)

2. Choudary, A.K., Jha, J.N., Gill, K.S.: Utilization of plastic waste for improving the sub-grades in flexible pavements. In: Geoshanghai 2010 International Conference on Paving Materials And Pavement Analysis, Geotechnical Special Publication (2010). https://doi.org/10.1061/411 04(377)39
3. Consoli, N.C., Montardo, J.P., Prietto, P.M., Pasa, G.S.: Engineering behaviour of a sand reinforced with plastic waste. J. Geotech. Geoenv. Engg. **128**(6), 462–472 (2002)
4. Sobhan, K., Mashnad, M.: Mechanical stabilization of cemented soil fly ash mixtures with recycled plastic strips. J. Environ. Engg. **129**(10), 943–947 (2003)

Siting of New Landfill for Municipal Solid Waste Using GIS and MCDA-A Review

Swati A. Patil and Mahesh S. Endait

Abstract Due to rapid change in urban areas and the exponential growth in population, accelerated the huge generation of municipal solid waste (MSW). The management of the disposal of MSW is a substantial and complex process. Landfilling is the most common method used for the disposal of MSW, at the same time identifying the suitable site for disposal of MSW is a difficult task. Stakeholders are very much concerned about the disposal of solid waste and its landfilling. Sitting of the new landfill using spatial data and Geographical Information System (GIS) approach on conflicting points among social, economic and environmental effects. In this review paper literature related to new landfill sitting using GIS and Multi-Criteria Decision Analysis (MCDA) methods are cited. Review paper concentrates on MCDA techniques, method of disposal, type of solid waste and country.Most common methods have been used by researchers are Analytic Hierarchy process, Fuzzy, Dynamic-modeling, Analytical Network Process, Analytic Neural Network, site screening method and Artificial Neural Network. It can be concluded that GIS provides accurate mapping, quick collection of data, high accuracy, better predictions, and analysis by eliminating unsuitable areas.Moreover, MCDA methods Analytic Hierarchy process(AHP) is found best from a set of available alternatives and gives the error-free solution to the users because of simplicity in pairwise comparisons,consistency in evaluation and versatility. It helps inidentifying the optimum site for the construction of a landfill. Limitations of AHP are found in random assumptions for various criteria and due to that consistency ration increases more than10%. Hence, there is a need forthe application of artificial intelligence with AHP.

Keywords Municipal solid waste · GIS · Landfill sitting · MCDA techniques

S. A. Patil · M. S. Endait (✉)
Department of Civil Engineering, Sandip University, Nasik, Maharashtra 422213, India
e-mail: mahesh.endait@sandipuniversity.edu.in

S. A. Patil
e-mail: swati.patil@sandipuniversity.edu.in

1 Introduction

In developing countries due to urbanization, industrialization, and increasing population, the problem of solid waste generation is increases and it causes environmental pollution and degradation. In India, the rate of increase in urban population changes from 11% in 1901 to about 31% in 2011. The census of 2011 indicates the fact that presently 31.2% of the total population resides in the urban centers [1]. As per Central Pollution Control Board (CPCB), thequantity of solid waste generated in India during the year 2016–17 is 135,199 tonnes per day (TPD), which has been forecast to rise to 33% in the next 15 years. Out ofthetotal waste generated, 47,416 TPD is sent for landfilled [2, 3].

Engineering landfill is the best-suited method used for disposal of solid waste in India but finding a location of new landfill sitting remains a critical management issue.Wherein the selection is based on a number of considerations,the process is suffered from environmental, social, and political issues. In India, CPCB is a statutory organization under the Ministry of Environment, Forest, and Climate Change (MoEFC) provided the guidelines for selection of appropriate landfill site selection criteria for disposal of MSW [4].

Landfill sitting method involved the conventional method as well using spatial data, GIS and MCDA techniques. Methods aim at the low impact on environment, high social acceptance and low cost is preferable. New landfill sitting includes (i) setting up of a locational criteria; (ii) identification of search area; (iii) drawing up a list of potential sites; (iv) data collection; (v) selection of few best-ranked sites; (vi) environmental impact assessment; and (vii) final site selection and land acquisition [4]. The final selected site must satisfy the existing legislative guidelines. Application of GIS using spatial data and attribute data and multi-criteria decision analysis (MCDA) is being used by many authors for analysis of best possible sites of landfilling.MCDM methods able to make the comparisons against each criterion given in the legislation and assign the weights to the available existing sites. A few of the important methods of MCDM have been summarized. [5–11].

This paper aims to review of MCDA techniques in selection criteria on landfill sitting using GIS and its future scope for further research. Various thematic maps are required for new landfill sitting using GIS, RS for overlay analysis. These maps with different scales have been used by researchers for initial screening in order to eliminate unsuitable areas.

MCDA used in every field where we required to take a decision from the available alternatives, it gives the best solution in assigning the ranking. Various methods are developed to solve these multi-criteria problems [6, 12]. In the literature, many researchers considered the weights for different criteria and it was found that environmental, economic, and social criteria influence more in new landfill siting.

MCDA methods used in Literature are Analytic Hierarchy process, Fuzzy logic, Dynamic modeling, Analytical Network Process, Analytic Neural Network and Artificial Neural Network. This paper focused on MCDA techniques with GIS and RS for landfill site identification of MSW. The various factors and their weights with

their importance are discussed. In available methods found the AHP technique was frequently used by researchers with its advantages and limitations.

2 Literature Review

In this paper, the various methods used by researchers have been cited for new landfill sitting of MSW. Some of the most popular methods are summarized below like AHP, ANP, Fuzzy, Sitescreening, Site Sensitivity Index and Delphi technique, C Programme, Boolean logic and binary evidence, Weighting method and Artificial Neural Network.

2.1 AHP-Analytic Hierarchy Process

Analytical hierarchy process (AHP) has been introduced and developed by Saaty [13]. AHP method is used for pairwise comparisons. In AHP technique consistency ratio is always less than 10%, which shows the strong pairwise relations in criteria. As the pairwise comparisons were based on a random basis so there are chances of inconsistency. Hence 10% inconsistency is allowed. If the consistency ratio is not less than 10%, then the standard procedure is revised the pairwise comparisons needs to improve it. Spatial-AHP technique was used by Siddiqui et al. [14] for Oklahoma country to give the ranking for MSW landfill site. The factors considered are hydrogeology/geology, land use, and proximity for decision ranking. Considered factors were assigned the weights as per AHP technique and sensitivity was checked. Soil and land-use maps used were in raster format 200 m cell resolution published by soil survey maps (USDA SCS 1987). Same techniques were used by Kontos et al. [15] for MSW landfill site of the island of Lemons in the North Aegean Sea (Greece). The factors considered are hydrology/hydrogeology, environmental, social, and technical/economic.

In 2008 Sumathi et al. [3] used GIS-AHP for Pondicherry by considering the factors lake and ponds, rivers, water supply sources, groundwater table, groundwater quality, infiltration, air quality index, geology, fault line, elevation, land use, habitation, highways, and sensitive sites. An algorithm was formed and it performs GIS-based constraints mapping technique to eliminate the unsuitable sites. Afterward, the same technique was used by Sharifi et al. [16] for hazardous waste landfill sitting in Kurdistan Province, western Iran. The factors like geology, hydrogeology, hydrology, climatology, and eco-sociology were considered for identifying the best possible sites from 15 sites.

Natesan et al. [17] used AHP for Chennai city for MSW and used FIC, ANN and Delphi techniques in sanitary landfill siting. The reason of using these three techniques was that AHP is best in giving weights to the multiple alternatives. The Delphi

model sets the priority as per the opinion of the experts, but fail to establish interrelationship between the decision factors and elements in the decision factors. FIC is converted as a score of each decision factor. ANN model found to best to overcome the AHP, FIC and Delhi models.The results obtained were15.34%, 17.33%, 25.91% and 19.13% respe. The factors considered are land use, geology, geomorphology, drainage density, slope, soil, and runoff base map was used.

Moeinaddini et al. [9] also used AHP and weighted linear method in combination with GIS and foundeffective in handling of qualitative and quantitative data. The Landfill site was identified at Karaj, Iran, for MSW. Weighted-linear combination method and spatial cluster analysis (SCA) were used and suitable sites for allocation of landfill for a 20-year period were identified and found 6% suitable area for landfill. Same AHP technique was used by Sener et al. [18] in Konya, Turkey for MSW. Factors considered were such as geology/hydrogeology, land use, slope, height, aspect and distance from settlements, surface waters, roads, and protected areas. Four suitability classes like high, moderate, low and very low suitability areas were represented 3.24, 7.55, 12.70, and 2.81%, respectively, and remaining 73.7.% was found the unsuitable area for landfill. Geneletti [19] also used AHP and GIS for an inert landfill in the Sarca's Plain, located in southwestern Trentino. Found 8 potential sites in northern Italy and gave the ranking on the basis of visibility, accessibility, and dust pollution. The ranking was given on the basis of criterion scores and weights. Finally, out of the eight sites, finally, compare three suitable sites.

Tavares et al. [20] investigated new landfill sitting for incineration plant in Cape Verde of Africa using AHP& GIS. The major factors were considered were economic, environmental, health, and social costs 0.75% weighting was given to non-environmental factors and 25% weight was given to environmental factors. The identified sites found on the basis of factors were socioeconomic, technical, and environmental issues with weights 48%, 41%, and 11% respectively. Same AHP with ordered weighted average and GIS in combination with fuzzy was used by Gorsevski et al. [8] for landfill site selection in the Polog Region, Macedonia. Environmental factors were given more weight as compared tothe economic factor.

Gbanie et al. [13] did the case study for Bo, Southern Sierra Leone for Municipal landfill using weighted-linear combination and ordered weighted method in addition with GIS. The results showed 83.3% ofthe land area was unsuitable for landfill construction and only 2.1% ofthe land was suitable for construction. AHP and GIS technique also used by Kumar et al. [21]. Identified six potential sites in Delhi, India. While applying AHPtechnique, difficulty was found in ranking irregularities of the considered factors used and weights are given on 9-point scale. Feo et al. [5] considered total 22–23 constraints for new landfill sitting for different waste disposal sites like hazardous waste, non-hazardous waste landfills, inert waste landfill, waste to energy, mechanical biological treatment using multiple criteria decision analysis and GIS. Three phases such as "non-suitable areas," "preferential and penalizing criteria," and "most suitable sites" were considered. Finally, apply the AHP–Priority Scale Weighting and Simple Additive weight–Paired Comparison Technique approaches to the alternatives matrix gave the same ranking lists.

Khodaparast et al. [22] used AHP and GIS for MSW in Qom city, Iran and considered the factors like geomorphology–hydrography, environmental–social factors. Different criteria are selected according to the regional condition; therefore, important factors such as distance from sea and forest areas were not considered. Using AHP and WLC only 7% area was found as a suitable area for landfill construction. Md.Mohib et al. [23] considered 12 constraint factors in the first attempt and screened 45.7% area was screened. In the second attempt with the help of location-allocation analysis 10 locations were selected. The author found this AHP technique efficient for sitting of landfill. Luciana et al. [24] identified the landfill sitting for MSW using GIS and SAW method for ranking scale 0 to 10. Author addressed the method for a limited area and got the benefit of human health protection.

In summary parameters and their weights used in the analysis during the sitting problem affects the results. Table 1 summarizes the different criteria, sub-criteria, and corresponding weights used by various researchers. It can be seen that most of the researchers convinced that environmental, economic, and social criteria are more sensitive.

2.2 Site Screening Method

A site selection process usually proceeds through a phased approach. It begins with the use of regional screening techniques to reduce a large study area, such as an entire state or region, to a manageable number of discrete search areas.

Mehmet et al. [28] used the site screening method for HW landfill without using GIS in Turkey. He worked manually and used overlay technique as the methodology for preparing a final site selection map. He suggested this method is used for more general conditions and locations.

2.3 Fuzzy-Logic

Fuzzy logic is an extension of Boolean logic by Lotfi Zadeh in 1965 based on the mathematical theory of fuzzy sets, which is a generalization of the classical set theory Zadeh [29]. Nowadays fuzzy logic has been successfully used in various disciplines.

Omar et al. [30] investigated landfill sitting using the fuzzy intelligent system at capital city Amman, Jordan. The authorconsidered mainly four factors namely topography and geology, natural resources, socio-cultural, and economy, and safety. Fuzzy techniques can be used in vast areas especially in computer vision, weather prediction, image processing, nuclear reactor control, control of biomedical processes, automatic tuning, and many other fields of research [31–33]. IF–THEN rule was used for the fuzzy interface. Author finds different grades for different landfill sites 91.19%, 53.00%, 23.33%, and 52.09% grade I, II, III, and IV resp.The first landfill site was excellent and the third landfill site has proven to be worst and unacceptable.

Table 1 Criteria and their weights used in AHP from literature

Sr. No	Criteria	Sub-criteria	[3]	[9]	[16]	[15]	[8]	[25]	[26]	[19]	[27]	[20]
1	Environmental	Aspect	0.0510									0.11
2		Distance From Settlement	0.2350					0.134		0.21		
3		Distance From Surface Water	0.4080	0.1794	0.078	0.1266						
4		Distance From Protected Areas	0.1430		0.052			0.0168				
5		Distance From Power Lines		0.0186								
6		Temp		0.0428								
7		Rain		0.0983	0.039							
8		Flooding Over 100 Yrs		0.0813								
9		Lithology			0.09							
10		Sensitive Ecosystem		0.2830		0.0731						
11		Climatic Regimes			0.053							
12		Evapotranspiration			0.039							
13		Distance From Forest										
14		Dist.from Agri. Land										
15		Vegetation				0.0252						
16	Geology/Hydrogeology	Geology/Hydrogeology	0.0950				0.2936					
17		Distance from Faults		0.1393	0.087		0.1705	0.015				
18		Permeability of Soil		0.2140						0.07		
19		Distance from Aquifers			0.12							
20		Distance from Qantas,Springs& Wells		0.0735	0.11	0.2074	0.0571	0.171		0.15	0.07	
21		Distance from Lakes/Streams/Ponds					0.0571					

(continued)

Table 1 (continued)

Sr. No	Criteria	Sub-criteria	[3]	[9]	[16]	[15]	[8]	[25]	[26]	[19]	[27]	[20]
22		Distance from Rivers					0.0571					
23		Distance from Ground Water		0.01827								
24	Geomorphology	Depth of Water Table										
25		Water Permeability				0.2074						
26		Morphology				0.0459						
27		Slope (%)	0.1680				0.0312	0.025	0.1623	0.13		
28		Height	0.2872		0.01		0.1705			0.08		
29		Depth Of Bed Rock										
30		Soil Type										
31		Texture										
32	Economic	Land use&Landcover	0.6700	0.0570	0.064	0.0731	0.1058	0.073	0.3784		0.02	0.5
33		Depth Of The Soil		0.2153				0.111				
34		Distance From Road	0.5450		0.02	0.0163		0.037			0.23	
35	Socio-Cultural	Visibility/Distance From Residential Areas/Urban		0.2040 & 0.1622	0.053	0.1266	0.0571	0.052	0.1623		0.03	0.41
36		Wind Direction And Wind Gust		0.1755		0.0252						
37		Distance From Historical & Tourism Centers		0.0883				0.026				
38		Distance From Industries		0.0332	0.2			0.014				
39		Distance From Airport		0.0623				0.0731				
40		Cultural Areas				0.0731						
41		Distance From Villages						0.046				
42		Distance From School										
43	Design	Distance From Power Line										0.09
44		Design										

Chang et al. [34] used fuzzy multi-criteria decision-making methods for landfill siting in urban areas of south Texas. The author identified seven landfill sites and gave ranking to each. Landfill site one was found the ranking of 0.786689, which was the best site for landfill construction. The same technique was used by Alexandra et al. [26] for landfill siting of MSW. The author divides the factors into two parts, one part is the physical environment and the other part is the socioeconomic environment. No cost was considered in the first part and another factor was with consideration of cost. The fuzzy technique was associated with the first part as well AHP was associated with the second part. Combination of these two techniques results in composite suitability map for landfill siting. The author considered exclusionary and exclusionary criteria and wasexamined. The final decision of landfill site suitability was also depended on public response and political issues.

2.4 Site Sensitivity Index (SSI) & Delphi Technique

Paul et al. [35] used site sensitivity index, Delphi technique and RS,GIS for new landfill sitting at Kolkata, India. The author considered the factors for the ranking purpose was accessibility, receptor, environmental, socioeconomic, waste management practices, and climatologically and geological. Lowest SSI score indicates the less sensitive site.

2.5 Analytical Network Process

Analytical network process (ANP) is a mathematical theory that was involved as a systematic with varied dependences and has been successfully employed in different fields. This method is useful in flexibility consideration in solving more complex interrelationships among different elements.

Zeynab et al. [25] used ANP, weighted linear combination, ordered weighted average methods and got the results ranges in 1–7, 62.69%, 32.41%, 21.45%, 18.71%, 13.65%, 4.60%, and 0.05% of region area is in the very suitable class. Khan et al. [27] proposed ANP techniques by considering decision models, different criteria and alternatives. The author suggested for segregation at the source only so that burden and cost invested on landfilling can be minimized.

Aragones et al. [36] used the ANP method in Spain for landfill sitting with its strength and weakness and suggested the best method to the decision-makers. Two ANP models were analyzed and compared with each other. The author also suggested AHP and ANP models. The factors were grouped into plant exploitation costs, facilities and infrastructures, environmental issues, and legal requirements.

2.6 C Programme

Kao et al. [37] used a raster-based C program for landfill sitting, the author developed an algorithm. This technique was helpful in implementing multi-factor analysis for compactness and other siting factors with weights specified by the user. In this method sitting time is reduces using the C program algorithm.

2.7 Boolean Logic and Binary Evidence, Weighting Method and EVIAVE

Delgado et al. [38] made an analysis of land suitability for sitting of landfills in Mexico using spatial decision-support models and overlapping index of multiple class maps. The factors considered were grouped into land use, base map, soil and geomorphology, geology and roads. Results show the Boolean logic model was effective to apply as compared to the other two models. Emanuel et al. [39] used a weighting method for site selection and identified the factors like cost, environmental risk, and equity affects on landfill sitting decision. The dynamic model was designed by the author is a hypothetical and tested for the real world. Zamorano et al. [40] used EVIAVE method in Spain. This method is used for landfill and environmental diagnosis. The environmental factors considered are surface water, groundwater, atmosphere, soil, and human health. It was found that the environmental component was most affected in site selection.

2.8 Artificial Neural Network

Kuo et al. [41] used a combination of Artificial Neural Network and two multi-attribute decision analysis using data envelopment analysis and ANP. This technique used for the green supply chain management. The three steps involved were input layer, hidden layer, and output layer. Whereas the input layer represents the different criteria, the hidden layer is an experimental approximation to minimize the expected value of target variance for certain classes of problems. And the output layer used for the performance of each selection criteria. With the help of these three layers, the problem of data missing at various places can be minimized. It also overcomes traditional data development analysis drawbacks, limitations of data accuracy. In summary above Table 2 shows the review of papers MCDA and GIS techniques used for new landfill sitting by the researchers.

Table 2 Review of papers used MCDA and GIS for landfill sitting

Sr No	Year	Author	Methodology	Location
1	1986	Jensen and Christensen et al.	GIS	United States
2	1996	Siddiqui et al.	AHP	Oklahoma
3	2000	Natesan et al.	AHP, FIC, ANN and Delphi	Chennai,India
4	2005	Kontos et al.	AHP	Greece
5	2005	Mehmet et al.	Site screening method	Turkey
6	2006	Omar et al.	Intelligent system-Fuzzy	Jordan
7	2006	Alexandra et al.	AHP & OWA	–
8	2008	Chang et al.	Fuzzy	South Texas,USA
9	2008	Sumathi et al.	AHP	Pondicherry India
10	2008	Khan et al.	ANP	–
11	2008	Zamorano et al.	EVIAVE	Granada,Spain
12	2009	Sharifi et al.	weights	Western Iran
13	2009	Guiqin et al.	AHP	Beijing,China
14	2010	Geneletti et al.	Weight method	Italy
15	2010	Moeinaddini et al.	Weighted linear combination & AHP	Karaj,Iran
16	2010	Sener et al.	AHP	Konya,Turkey
17	2010	Kuo et al.	ANN-ANP	
18	2010	Aragones et al.	ANP	Spain
19	2011	Tavares et al.	AHP	Cape Verde
20	2012	Eskandari et al.	AHP & SAW	Iran
21	2012	Gorsevski et al.	AHP and OWA	Macedonia
22	2013	Gbanie et al.	WLC and OWA	Southern Sierra
23	2013	Kumar et al.	AHP	Delhi,India
24	2014	De Feo et al.	AHP (SAW–PCT)	Southern Italy
25	2014	Paul et al.	Delphi technique	Kolkata,India
26	2015	Zeynab et al.	OWA and ANP	Birjand plain, Iran
27	2018	Md.Mohib et al.	AHP	Alberta,Canada
28	2018	Khodaparast et al.	AHP	Qom city, Iran
29	2018	Luciana et al.	AHP & SAW	Italy
30	1996	Kao et al.	C PROGRAM	–
31	1996	Emanuel et al.	weighting method,	U.S

3 Conclusions

Multiple criteria decision analysis is a sub-discipline of operations research that explicitly evaluates multiple conflicting criteria in decision making, applicable every-where. MCDA techniques are useful in giving weights and ranking so that it is easy to find the best possible. Finding a new landfill sitting using MCDA and GIS is possible. These techniques have been used since 1986 and the MCDA methods like AHP, Fuzzy, ANN, OWA and Boolean logic, binary evidence, and overlapping index. A literature survey was conducted on new landfill sitting using GIS and MCDA tech-niques shows the increasing awareness at the social, environmental and economic level and moving toward the research scenario.

Out of the available methods used for new landfill siting, AHP techniques was found best as compared to the other methods. One of the advantages of AHP is that there is no need for any manipulations in the data. While giving weights environ-mental factors were found more weight as compared to social and economic factors. Environmental factors are more important, as it is related to human beings and health effects. The problem faced by using AHP is the weights are considered randomly so that there are chances of increasing the consistency ratio more than 10%. If consis-tency ratio increases more than 10%, then there is the need torevised the weights to different criteria. In the future, it is the need forthe application of artificial intelli-gence with AHP to minimize the errors. MCDA techniques found a scientific way as compared to the conventional method for landfill sitting, which saves time and got the accurate results, saves the money as invested in conventional methods, scientific and technical approach in the society. MCDA required accurate inputs so that we got the accuracy in the final results and easy to find the best landfill site from the available alternatives. It was found that in India the landfill sitting was not done at up to the mark. In the future, there is the scope of research in India regarding MCDA and GIS for new landfill sitting at the social, economic, political, and environmental level. GIS is also the best tool for mapping and overlay of maps. New landfill sitting using GIS and multi-criteria decision methods can save the effective use of available land resources [42].

References

1. Population-India RUD of (2011) CENSUS 2011 (PCA—Final Data) Population—Persons (PCA—2011 Final Data) Sex Ratio—2011 CENSUS 2011 (PCA—Final Data) Population—Males Population—Females % Decadal Growth Female
2. Central Pollution Control Board, Ministry of Environment and Forests.: Consolidated Annual Review Report 2015–16 on Implenetation of Solid Waste Management Rules 2016. Central Pollution Control Board, New Delhi (2017)
3. Sumathi, V.R.: GIS-based approach for optimized siting of municipal solid waste landfill. Wate Manag. **28**, 2146–2160 (2008). https://doi.org/10.1016/j.wasman.2007.09.032
4. Central Public Health and Environmental Engineering Organisation: Manual on SWM 2016 Ministry of Urban Development. Government of India, New Delhi (2000)

5. De, F.G., De, G.S.: Using MCDA and GIS for hazardous waste landfill siting considering land scarcity for waste disposal. WASTE Manag. (2014). https://doi.org/10.1016/j.wasman.2014.05.028

6. Figueira, J., Greco, S., Ehrogott, M.: Multiple Criteria Decision Analysis: State of the Art Surveys (2005)

7. Gal, T., Stewart, T .J., Hanne, T.: Multicriteria DecisionMaking: advances in MCDM Models, Algorithms, Theory, and Applications (1999)

8. Gorsevski, P.V., Donevska, K.R., Mitrovski, C.D., Frizado, J.P.: Integrating multi-criteria evaluation techniques with geographic information systems for landfill site selection: a case study using ordered weighted average. Waste Manag. **32**, 287–296 (2012). https://doi.org/10.1016/j.wasman.2011.09.023

9. Moeinaddini, M., Khorasani, N., Danehkar, A.: Siting MSW landfill using a weighted linear combination and analytical hierarchy process (AHP) methodology in a GIS environment Waste Manag. **30**, 912–920 (2010). https://doi.org/10.1016/j.wasman.2010.01.015

10. Yoon, K., Hwang, C.-L.: Multi-attribute Decision Making: An Introduction. Thousand Oaks Sage Publications, Inc (1995)

11. Zeleny, M.: Multiple Criteria Decision Making. Tata Mc Graw Hill, inc., New York (1982)

12. Ishizaka A, Nemery, P.: Multi-Criteria Decision Analysis Methods and Software(2013)

13. Peter, S., Bobby, P., Samuel, J., Medo, J., Tamba, V., Kabba, S.: Modelling landfil location using geographic information systems (GIS) and multi-criteria decision analysis (MCDA): case study Bo Southern Sierra Leone. Appl. Geogr. 1–10 (2001)https://doi.org/10.1016/j.apgeog.2012.06.013

14. Everett, J.W., Member, A., Vieux, B.E.: Landfill siting using geographic information systems. J. Environ. Eng. **122**, 515–523 (1996)

15. Kontos, T.D., Komilis, D.P., Halvadakis, C.P.: Siting MSW landfills with a spatial multiple criteria analysis methodology. Waste Manag. **25**, 818–832 (2005). https://doi.org/10.1016/j.wasman.2005.04.002

16. Sharifi, M., Hadidi, M., Vessali, E., Mosstafakhani, P., Taheri, K.: Integrating multi-criteria decision analysis for a GIS-based hazardous waste landfill sitting in Kurdistan Province, western Iran. Waste Manag. **29**, 2740–2758 (2009). https://doi.org/10.1016/j.wasman.2009.04.010

17. Natesan, U., Suresh, E.S.M.: Site suitability evaluation for locating sanitary landfills using GIS. J. Indian Soc. Remote Sens. **30**, 261–264 (2002)

18. Sener, S., Sener, E., Nas, B., Karaguzel, R.: Combining AHP with GIS for landfill site selection: a case study in the Lake Beysehir catchment area (Konya, Turkey). Waste Manag. **30**, 2037–2046 (2010). https://doi.org/10.1016/j.wasman.2010.05.024

19. Geneletti, D.: Combining stakeholder analysis and spatial multicriteria evaluation to select and rank inert landfill sites. Waste Manag. **30**, 328–337 (2010)

20. Tavares, G., Zsigraiová, Z., Semiao, V.: Multi-criteria GIS-based siting of an incineration plant for municipal solid waste. Waste Manag. **31**, 1960–1972 (2011). https://doi.org/10.1016/j.wasman.2011.04.013

21. Kumar, S., Hassan, M.I.: Selection of a landfill site for solid waste management: an application of AHP and spatial analyst tool. J. Indian Soc. Remote Sens. **41**, 45–56 (2013). https://doi.org/10.1007/s12524-011-0161-8

22. Khodaparast, M., Rajabi, A.M., Edalat, A.: Municipal solid waste landfill siting by using GIS and analytical hierarchy process (AHP): a case study in Qom city. Iran. Environ. Earth Sci. **77**, 1–12 (2018). https://doi.org/10.1007/s12665-017-7215-3

23. Khan, M., Vaezi, M., Kumar, A.: Science of the Total environment optimal siting of solid waste-to-value-added facilities through a GIS-based assessment. Sci Total Environ. **611**, 1065–1075 (2018). https://doi.org/10.1016/j.scitotenv.2017.08.169

24. Randazzo, L., Cusumano, A., Oliveri, G., Di, S.P., Renda, P., Perricone, M., Zarcone, G.: Landfill site selection for municipal solid waste by using AHP method In GIS environment: Waste management decision-support In Sicily (Italy). Multidiscip. J. Waste Resour. Residue. **02**, 78–88 (2018)

25. Motlagh, Z.K., Sayadi, M.H.: Siting MSW landfills using MCE methodology in GIS. Envir. Waste Manag. (2015). https://doi.org/10.1016/j.wasman.2015.08.013

26. Gemitzi, A., Tsihrintzis, V.A., Petalas, C.: Combining geographic information system, multi-criteria evaluation techniques and fuzzy logic in siting MSW landfills. Env. Geol. **51**, 797–811 (2007). https://doi.org/10.1007/s00254-006-0359-1

27. Khan, S., Faisal, M.N.: An analytic network process model for municipal solid waste disposal options. Waste Manag. **28**, 1500–1508 (2008). https://doi.org/10.1016/j.wasman.2007.06.015

28. Irfan, M., Cetin, H.: Site selection for hazardous wastes : a case study from the GAP area, Turkey. Eng Geol **81**, 371–388 (2005). https://doi.org/10.1016/j.enggeo.2005.07.012

29. Zadeh, L.A.: Fuzzy Sets. Inf Control **8**, 338–353 (1965)

30. Al-jarrah, O., Abu-qdais, H.: Municipal solid waste landfill siting using the intelligent system. Waste Manag. **26**, 299–306 (2006). https://doi.org/10.1016/j.wasman.2005.01.026

31. Gzogala, E., Rawlik, T.: Modelling with a fuzzy controller with application to the control of biomedical processes. Fuzzy Sets Syst. **31**, 13–32 (1989)

32. Al-Jarrah, O.M., Bani-Melhem, O.Q.: Building maps for mobile robot navigation using fuzzy classification of ultrasonic range data. J. Intell. Fuzzy Syst. **11**, 171–184 (2001)

33. Yager, R.R., Zadeh, L.A.: An Introduction to Fuzzy Logic Applications In Intelligent System (1993)

34. Chang, N., Parvathinathan, G., Breeden, J.B.: Combining GIS with fuzzy multicriteria decision-making for landfill siting in a fast-growing urban region. J. Environ. Manage. **87**, 139–153 (2008). https://doi.org/10.1016/j.jenvman.2007.01.011

35. Paul, K., Dutta, A., Krishna, A.P.: A comprehensive study on landfill site selection for Kolkata City, India. J. Air Waste Manage. Assoc. **64**, 846–861 (2014). https://doi.org/10.1080/109 62247.2014.896834

36. Aragone, P.: An analytic network process approach for siting a municipal solid waste plant in the metropolitan area of valencia (Spain). J. Environ. Manage. **91**, 1071–1086 (2010)

37. Kao, J., Lin, H., Chen, W.: Network geographic information system for landfill siting. Waste Manag. Res. **15**, 239–253 (1997)

38. Delgado, O.B., Mendoza, M., Lo, E., Geneletti, D.: Analysis of land suitability for the siting of inter-municipal landfills in the Cuitzeo Lake Basin, Mexico. Waste Manag. **28**, 1137–1146 (2008). https://doi.org/10.1016/j.wasman.2007.07.002

39. Emanuel, M., Min, H., Wu, X.: A Multiobjective Model for the Dynamic of Landfills. Dyn. Locat. Landfills **3**, 143–166 (1996)

40. Zamorano, M., Molero, E., Hurtado, A., Grindlay, A., Ramos, A.: Evaluation of municipal landfill site Southern Spain with GIS-aided methodolohy. J. Hazardous Mater. **160**(2008), 473–481 (2008)

41. Kuo, R.J.,Wang, Y.C.,Tien, F.C.: Integrationofartificial neural network and MADA methods for green supplier selection. J Cleaner Prod.**18**, 1161–1170 (2010)

42. Philadelphia, S., Pennsylvania, W.: A scaling method for priorities in hierarchical structures. J. Math. Psychol. **15**, 234–281 (1977)

Performance Analysis of GCLs as Barriers-A Review

Nazeema Basheer and Jaskiran Sobti

Abstract Geosynthetic clay liner has been used over a decade to stave off problems such as leaching of hazardous chemicals from landfill containments which otherwise could cause ecological issues and endanger the environment. Low permeability is a highly desirable property for use as a liner material in landfills to effectively control the seepage of highly contaminated leachate which can pollute the soil and groundwater in the vicinity. GCLs contain bentonite essentially, which has a high montmorillonite content imparting swelling characteristics. The usage of GCLs is booming day by day in engineered landfills and they are being extensively researched on their different characteristics such as hydraulic conductivity, diffusion characteristics, mechanical properties, reaction to various chemicals, and durability. This paper presents an overview of the major findings on the critical aspects affecting the various characteristic properties of GCLs. The performance of GCLs upon coming in contact with a higher concentration of salts considering the actual composition of leachate has also been dealt in this study.

Keywords Geosynthetic clay liners · Landfills · Bentonite · Hydraulic conductivity

1 Introduction

1.1 Background

Geosynthetic clay liners are made up of a layer of sodium or calcium bentonite which is sandwiched between two layers of geosynthetics or geomembrane. Clay liners have picked up a ton of consideration over years as treatment to leachate problems because of very low hydraulic conductivity to water, k ($\leq 10^{-10}$ m/s) [7, 8, 10–12, 27, 28] (Jo

---

N. Basheer · J. Sobti (✉)
Lovely Professional University, Jalandhar, Phagwara 144411, India
e-mail: jaskiran24362@lpu.co.in

N. Basheer
e-mail: nazeemawani93@gmail.com

et al. 2001). Lesser the hydraulic conductivity lesser will be the permeation of water and hence can be used for waste containment [2, 6, 14–17, 20] (Rosin-Paumier and Touza-Foltz 2012).

Apart from this, there are different points of interest of utilizing GCLs such as they have limited thickness, can be installed easily, cost effective, and can resist differential settlement in the soil. Besides having so many advantages GCLs can lose their properties with time. The characteristic property of GCLs is their low hydraulic conductivity which can deteriorate when subjected to higher concentration of salts. There are other aspects also which lead to the deterioration of GCLs and it has been a major concern to protect this property. Various researches have been carried out in which the hydraulic conductivity was analyzed and factors which led to its rise.

This study further discusses the factors analyzed by various researchers which lead to an increase in hydraulic conductivity.

2   Bentonite Quality and Hydraulic Conductivity

The characteristic property of bentonite that is hydraulic conductivity is principally influenced by montmorillonite content [27]. Bentonites are vulnerable to chemical composition of pore liquids that can cause the thinning of bentonite layer, can also cause increase in hydraulic conductivity [13, 22]. The distinction in hydraulic conductivity of two GCLs containing diverse characteristics of bentonite was evaluated based on permeation with water and chemical solution ($CaCl_2$) of different concentration [10, 11]. The test was continued till chemical equilibrium in terms of solute concentration was not attained (i.e., $C_{out}/C_{in} = 1$). Moreover, it was found that GCLs having higher-quality bentonite (GCL-HQB) which are characterized by having higher content of sodium montmorillonite (86%), higher plasticity index (548%), and higher cation exchange capacity (93 meq/100 g) had three times lower hydraulic conductivity than GCL having lower-quality bentonite (GCL-LQB) which have lesser montmorillonite content (77%), lesser plasticity index (393%), and lower cation exchange capacity (64 meq/100 g), when permeated with water[10, 11]. However, when treated with $CaCl_2$ solution the GCL-HQB resulted in higher hydraulic conductivity. Subsequently it was noted that GCL-HQB is possibly more vulnerable than GCL-LQB.

The results in the difference of hydraulic conductivity were demonstrated by plotting the conductivity of specimen as a function of $CaCl_2$ liquid permeant (Fig. 1).

3   Cation Exchange in GCLs

For bentonites utilized in GCLs, sodium (Na) is the essential interlayer cation, which binds water, boosts swelling, and lessens the pore spaces accessible for flow [26]. Consequently, Na bentonites have very low hydraulic conductivity [4, 5, 7, 8, 22].
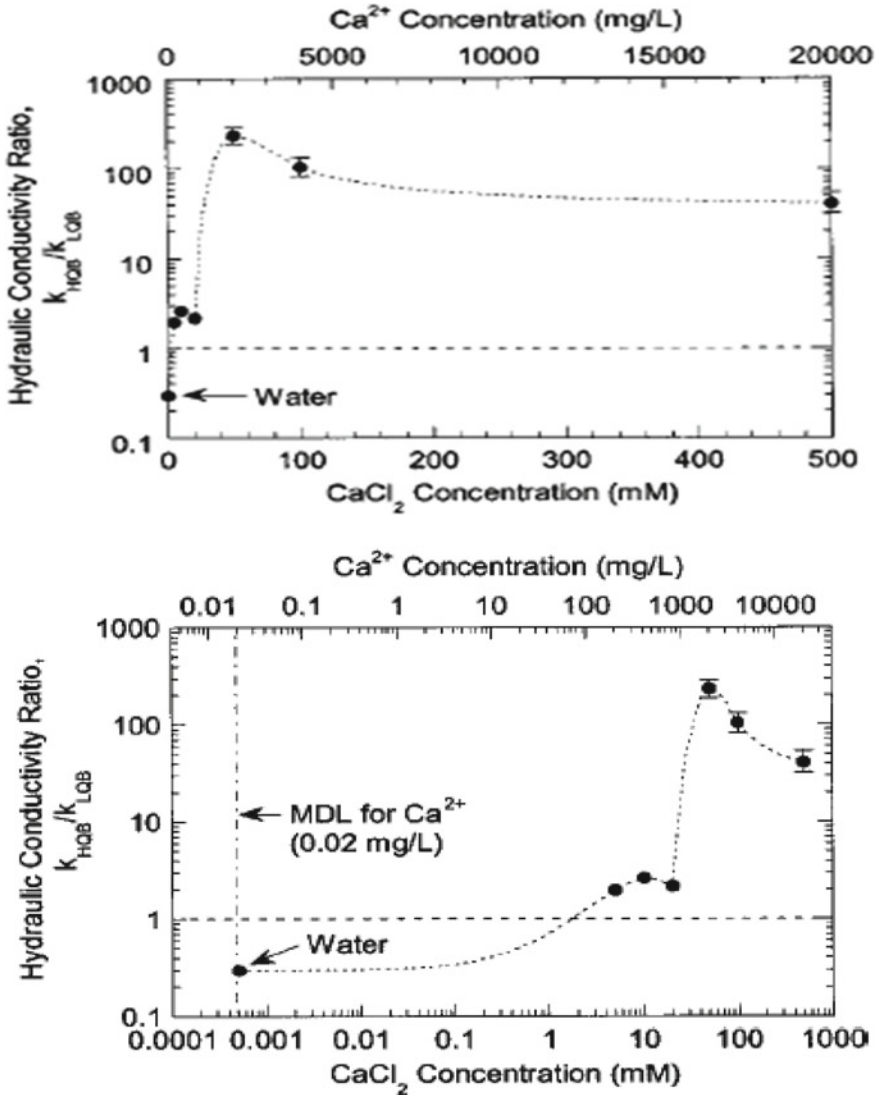
Fig. 1 Ratio of hydraulic conductivity of higher quality and lower quality bentonite [10, 11]

Past studies have demonstrated that substitution of Na by multivalent cations can diminish the swelling ability of bentonite and resulting in increment of conductivity in GCLs [4, 5, 8, 13, 23, 25, 27, 30, 31] (Jo et al. 2001, 2004; Egloffstein 2002). This can also occur even when bentonites are permeated with low concentration of multivalent cations [7, 21, 27] (Engloffstien 2002; Jo et.al 2004).

Most studies have researched how cation trade during permeation with simulated or actual MSW leachates can influence the conductivity of GCLs [1, 4, 5, 23, 25, 29].

For a given concentration, GCLs penetrated with arrangements containing monovalent cation displayed the best swelling and most minimal water-driven conductivity, whereas GCLs provided with arrangements having trivalent cations had the least swelling and most elevated conductivity (Jo et al. 2001). Examinations were done that how circumneutral pH containing cations (both monovalent and divalent) disturbed swelling property of GCLs which is dependent on RMD [8]. If the value of RMD lessens, the swelling decreases and hence increase in hydraulic conductivity. RMD is the measure of relative abundance of monovalent and multivalent cations that is defined as

$$\text{RMD} = \frac{M_m}{\sqrt{M_d}}$$

where M_m is the molar concentration of monovalent cation and M_d is the molar concentration multivalent cation.

An equation is used to predict the hydraulic conductivity of GCLs to a chemical solution or leachate (K_L) as a function of the hydraulic conductivity to deionized water (K_{DI}) and the ionic strength and RMD of the permeant solution [8]

$$\frac{\text{Log KL}}{\text{Log KD}} = 0.965 - 0.976 \, I + 0.0797 \, \text{RMD} + 0.251 \, I^2 \, \text{RMD}$$

3.1 Effects of Municipal Solid Waste (MSW) and Stabilized Inorganic Hazardous Waste.

A few examinations have shown as to how the performance of GCLs is influenced by saturation with the leachate from municipal solid waste [5, 25, 29] (Bradshaw et al. 2016). Liners which are passed through synthetic leachates can have conductivity multiple times (up to 50,000) higher than liners passed through deionized water (DIW), whereas hydraulic conductivities of GCLs permeated with actual MSW leachates generally are about the same as those obtained with actual MSW [24]. The long-term hydraulic conductivity of GCLs in equilibrium with MSW leachate is no greater than 5.6 times the hydraulic conductivity of DIW [26]. The ratio of hydraulic conductivity of actual leachate relative to hydraulic conductivity of deionized water (K_L/K_{DI}) is shown as a function of pore volume of flow (PVF) in Fig. 2.

The permeation of bentonite with solidified/stabilized inorganic hazardous waste (SIHW) can possibly deteriorate the water retention property of GCLs (Wang et al. 2019). Effective stresses additionally assume a vital job in conclusion of hydraulics conductivity at 30 kPa permeation with SIHW leachate had a detrimental effect on hydraulic performance (Wang et al. 2019). However, it was also concluded that
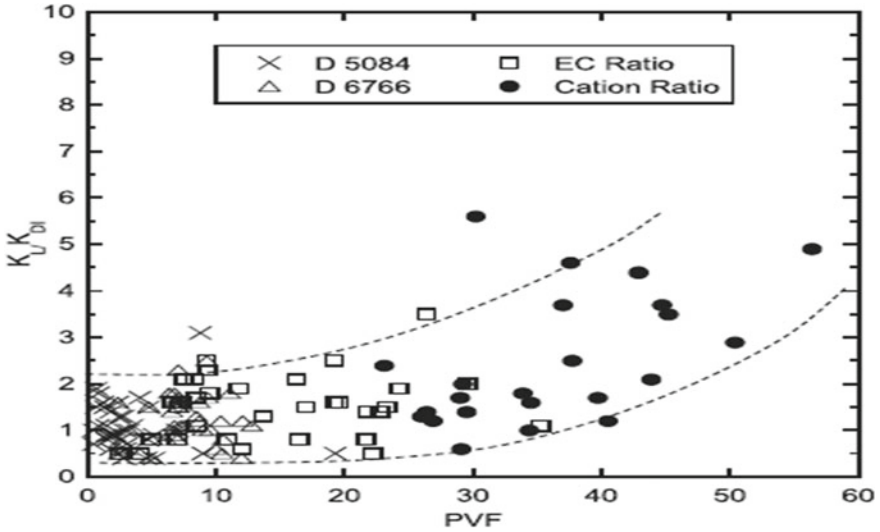
Fig. 2 Hydraulic conductivity of synthetic MSW leachate relative to hydraulic conductivity of deionized water as a function of PVF [26]

increasing stresses can check the negative impact initiated by SIHW leachate permeation. When the stresses were increased to 200 kPa, the GCLs had k values estimated below 1.0×10^{-9} m/s, with the exception of non-pre-hydrated GCL-S specimen.

4 Diffusion and Membrane Characteristics

Void ratio and confining stresses have a strong impact on diffusion coefficient, in addition to this, the solute concentration can have predominant effect on diffusion coefficient [9] (Rowe 1998). Since solute restriction is a function of clay size, the size of the pores of clay fluctuates, the degree of solute limitations in clays, that behave as membrane, also fluctuates with the result that few pores confine solute movement while other do not [18, 19] (Shackleford et al. 2003; Shackelford 2013a, b).

Membrane behavior of GCLs depends primarily on the solute concentration because as the concentration of solutes increases in the pores, the diffused double layer (DDLs) and electric field, maintaining membrane behavior, also decrease which causes pores to expand and subsequently lessen the solute restriction [3].

The concentration at which membrane behavior ceases to exist is known as threshold concentration (Shackelford et al. 2003). Chemico-osmotic pressure (ΔP) is directly related to membrane efficiency coefficient; the reduction in ΔP results in decrease of solute restriction (Shackelford and Lee 2003). Studies have indicated that the relation between the membrane efficiency coefficient (ω) and the logarithm of average salt concentration across the specimen ($\log C_{\text{ave}}$) becomes nonlinear

with increasing salt concentration (Shackelford et al. 2016). It was found that the membrane behavior of GCL was demolished when the KCl concentration across the specimen was increased. The diffusion coefficient, D^*, for both Cl^- and K^+ increased by a factor of 1.6 and 2.0, respectively.

5   Conclusion

The main grail of this study was to collectively find the causes which fostered reduction in the performance of GCLs as a barrier. There is no unsureness that GCLs have proved to be the best substitute to the leaching problem of hazardous waste containments yet they should not be contemplated as a nostrum to perfectly control all problems. There are certain sources which can devastate the long-term service of GCLs and some of them have been discussed in this paper. The desiccation or thinning of bentonite can be related to many aspects such as quality of bentonite used, cation exchange, soil water characteristic curves, and diffusion properties. The comprehensive contributions made by various researchers have led to the widespread knowledge of GCLs in using it as a barrier. However, there are certain aspects which need to be investigated more thoroughly such as effects of temperature on soil water characteristic curve because for wet paths the curves are difficult to measure. More importantly GCLs can be designed using different structural feature and inclusion of polymeric material fiber in such a way that they are recommendable for foreseen settlements.

References

1. Ashmawy, A.K., El-Hajji, D., Sotelo, N., Muhammad, N.: Hydraulic performance of untreated and polymer-treated bentonite in inorganic landfill leachates. Clays Clay Miner. **50**(5), 546–552 (2002)
2. Bouazza, A., Gates, W.: Overview of performance compatibility issues of GCLs with respect to leachates of extreme chemistry. Geosynth. Int. **21**(2), 151–167 (2014)
3. Fritz, S.: Ideality of clay membranes in osmotic processes: a review. Clays Clay Miner. **34**, 214–223 (1986)
4. Guyonnet, D., et al.:Geosynthetic clay liner interaction with leachate: correlation between permeability, microstructure, and surface chemistry. J. Geotech. Geoenviron. Eng. **131**, **6**(740), 740–749 (2005).
5. Guyonnet, D., et al.: Performance based indicators for controlling geosynthetic clay liners in landfill application. Geotext. Geomembr. **27**(5), 321–331 (2009)
6. Ishimori, H., Katsumi, T.: Temperature effects on the swelling capacity and barrier performance of geosynthetic clay liners permeated with sodium chloride solutions. Geotext. Geomembranes **33**, 25–33 (2012)
7. Jo, H., Benson, C., Shackelford, C., Lee, J., Edil, T.: Long-term hydraulic conductivity of non-prehydrated geosynthetic clay liner permeated with inorganic salt solution. J. Geotech. Geoenviron. Eng. **131**(4), 405–417 (2005)

8. Kolstad, D., Benson, C., Edil, T.: Hydraulic conductivity and swell of non-prehydrated GCLs permeated with multi-species Inorganic solutions. J. Geotech. Geoenviron. Eng. **130**(12), 1236–1249 (2004)
9. Lake, C., Rowe, R.: Diffusion of sodium and chloride through geosynthetic clay liners. Geotext. Geomembranes **18**, 103–131 (2000)
10. Lee, J., Shackelford, C.: Concentration dependency of the prehydration effect for geosynthetic clay liner. Soils Found. **45**(4), 27–41 (2005)
11. Lee, J., Shackelford, C.: Impact of bentonite quality on hydraulic conductivity of geosynthetic clay liners. J. Geotech. Geoenviron. Eng. **131**(1), 64–77 (2005)
12. Lee, J., Shackelford, C., Benson, C., Jo, H., Edil, T. : Correlating index properties and hydraulic conductivity of geosynthetic clay liners. J. Geotech. Geoenviron. Eng. **131**(11), 1319–1329 (2005)
13. Lin, L.-C., Benson, C.H.: Effect of wet and dry cycling on swelling and hydraulic conductivity of GCLs. J. Geotech. Geoenviron Eng. **126**(1), 40–49 (2000)
14. Liu, Y., Bouazza, A., Gates, W.P., Rowe, R.K.: Hydraulic performance of geosynthetic clay liners to sulfuric acid solution. Geotext. Geoembranes **43**(1), 14–23 (2015)
15. Liu, Y., Gates, W.P., Bouazza, A.: Acid induced degradation of bentonite component used in geosynthetic clay liners. Geotext. Geomembranes **36**, 71–80 (2013)
16. Liu, Y., Gates, W.P., Bouazza, A.: Fluid loss as a quick method to evaluate hydraulic conductivity of geosynthetic clay liners under acidic condition. Can. Geotechnical J. **51**(2), 158–163 (2014)
17. Makusa, G.P., Bradshaw, S.L., Berns, E., Benson, C.H., Knutsson, S.: Freez-thaw cycling concurrent with cation exchange and the hydraulic conductivity of geosynthetic clay liners. Can. Geotechnical J. **51**, 591–598 (2014).
18. Malusis, M., Daniyarov, M.: Membrane efficiency and diffusive tortuosity of a dense prehydrated geosynthetic clay liner Geotext. Geomembranes (2016)
19. Malusis, M., Shackelford, C., Olsen, H.: Flow and transport through clay membrane barriers. Eng. Geol. **70**(2–3), 235–248 (2003)
20. Mazzieri, F., Di Emidio, G., Fratalocchi, E., Di Sante, M., Pasqualini, E.: Permeation of two GCLs with an acidic metal-rich synthetic leachate. Geotext. Geomembrane **40**, 1e11 (2013).
21. Meer, S., Benson, C.: Hydraulic conductivity of geosynthetic clay liners exhumed from landfill final covers. J. Geotech. Geoenviron. Eng. (2007). https://doi.org/10.1061/(ASCE)1090-0241(2007)133:5(550),550-563
22. Mesri, G., Olson, R.E.: Mechanism controlling the permeability of clays. Clay Liner Miner. **19**, 151–158 (1971).
23. Petrov, R.J., Rowe, R.K.: GCL-chemical compatibility by hydraulic conductivity testing and factors impacting its performance. Can. Geotech. J. **34**(6), 863–885 (1997)
24. Rauen, T.L., Benson, C.H.: Hydraulic conductivity of a geosynthetic clay liner permeated with leachate from a landfill with leachate recirculation, pp. 76–83. Geoamericas, International Geosynthetics Society (IGS), Jupiter, FL (2008)
25. Ruhl, J.L., Daniel, D.E.: Geosynthetic clay liners permeated with chemical solutions and leachates. J. Geotech. Geoenviron. Eng. **123**(4), 369–381 (1997)
26. Bradshaw, S.L., Benson, C.H.: Effect of municipal solid waste leachate on hydraulic conductivity and exchange complex of geosynthetic clay liners. Geotech. Geoenviron. Eng. **140** (2014)
27. Shackelford, C., Benson, C., Katsumi, T., Edil, T., Lin, L.: Evaluating the hydraulic conductivity of GCLs permeated with nonstandard liquids. Geotext.Geomembranes **18**(2–4), 133–162 (2000)
28. Shackelford, C., Sevick, G.: Hydraulic conductivity of geosynthetic clay liners to tailing impoundments solution. Geotext. Geomembranes **28**(2), 149–162 (2010)
29. Shan, H.Y., Lai, Y.J.: Effect of hydrating liquid on the hydraulic properties of geosynthetic clay liners. Geotext. Geomembr. **20**(1), 19–38 (2002)
30. Shan, H.Y., Daniel, D.E.: Results of laboratory tests on a geotextile/bentonite liner material. Proc. Geosyn. **91**(2) 517–535 (1991)

31. Vasko, S.M., Jo, H.Y., Benson, C.H., Edil, T.B., Katsumi, T.: Hydraulic conductivity of partially prehydrated geosynthetic clay liners permeated with aqueous calcium chloride solutions. In: Proceedings of Geosynthetics'01. Industrial Fabrics Association International (IFAI), pp. 689-699. Saint Paul, Minnesota

Effect of Alkaline Environment on the Swell Pressures of Compacted Bentonite Under Thermal History

Rohini C. Kale, Kapil Bhanwariwal, and K. Ravi

Abstract Bentonite is used as a buffer material in the deep geological repository for the safe disposal of high-level nuclear waste (HLW). The repository consists of a natural barrier system and an engineered barried system. Natural barrier system consists of a host rock and its surroundings and engineered barrier system consists of a buffer material as well as a waste canister. Bentonite is compacted around the waste canister to isolate it from the atmosphere as well as to provide long-term stability to the barrier. The high temperature (150–250 °C) of the waste canister reduces over thousands of years till the radioactivy of the waste degrades as well as while the long-term operation of the repository, the concrete components will deteriorate and produce alkaline fluids having pH > 12. This long-term influence of high temperature may create a thermal history on the compacted bentonite, and the highly alkaline solution may alter the bentonite near the concrete affecting the physical and chemical properties of compacted bentonite. Hence, it is necessary to investigate the influence of alkaline environment along with the induced thermal history on the swelling pressure of compacted bentonite. The paper discusses an assessment of swell pressures of compacted bentonite [Barmer 1 (B_1)] from Barmer district of Rajasthan, India, with an initial dry density of 1.5 Mg/m^3 and subjected to 110 °C, hydrated with cement solution and distilled water. The swelling load is recorded with the help of digital load frame and compared with non-heated samples of the same density. The swelling time data of compacted bentonite is presented and compared. Experimental evidence indicated that the swelling pressure of compacted bentonite was less when hydrated with cement water as compared to distilled water. But the time taken for saturation was more when hydrated with cement water as compared to distilled water. However, further investigation is required to understand the swelling mechanism under highly alkaline solutions.

R. C. Kale · K. Bhanwariwal · K. Ravi (✉)
Civil Engineering Department, IIT Guwahati, Guwahati, Assam 781039, India
e-mail: ravi.civil@iitg.ac.in

R. C. Kale
e-mail: k.rohini@iitg.ac.in

K. Bhanwariwal
e-mail: b.kapil@iitg.ac.in

1 Introduction

Compacted bentonite is used as a buffer material for constructing a deep geological repository for the disposal of high-level nuclear waste [1–3]. The bentonite used as a buffer material in repositories is under unsaturated conditions, and these conditions influence the behavior of compacted bentonite, including its hydraulic conductivity, shrinkage, and swelling. The swelling behavior and stability of bentonite depend on its contents and the percentage of swelling clays, i.e., smectite. He et al. [4] reported that smectite remained dominant in Wyoming MX80 bentonite after alteration but significant changes in the morphology of smectite were observed in rich brine solutions of NaCl and $MgCl_2$ at high temperature (<150 °C). Such interactions of bentonite with different solutions like KOH at 80 °C may change the mineralogical composition of bentonite and its swelling characteristics. According to [5], the direction of compaction results in the higher value of swell pressure along with it. Karnland et al. [6] observed a higher value of swell pressure of compacted bentonite in the axial direction than in the radial direction. Rao and Ravi [7] defined a coefficient of anisotropy as the ratio of radial to axial swelling pressure to describe the bentonite anisotropy. Thus, the long-term performance of repository depends on these interactions.

According to [8], when clayey soils are subjected to elevated temperature, soil changes its index and engineering properties. The compacted buffer material is subjected to heat by (i) radiations coming from the waste canister released by waste material and (ii) other end of buffer material which is in contact with the host rock. According to [9], elevated temperature affects the index, physicochemical, and hydromechanical properties of bentonite and increases the permeability of the bentonite [10]. Pusch et al. [11] observed a decrease in soil suction when the temperature was increased from 22 to 80 °C. Cho et al. [12] observed the decrease in swell pressure of bentonite when the temperature was increased. However, the effect of high temperature on the properties of the bentonite buffer depends on the type of clay minerals present in the sample [13]. These observations have suggested researchers to study the effects of thermal history on the properties of bentonite. Recent studies were reported on the influence of thermal history on the performance of bentonite buffer by [14, 15]. It was observed that with the increase in temperature, the properties of powdered bentonite such as swell pressure, liquid limit, plastic limit, specific gravity, specific surface area, cation exchange capacity, etc., were reduced. Estabragh et al. [16] performed experiments on montmorillonite and concluded that an increase in time duration of heating and increased temperature results in decreased liquid limit and plastic limit. The swelling potential and swelling pressure tests were conducted on samples with a dry, optimum, and wet side of optimum water content. For dry samples, the swelling potential was higher than the other two cases. Both the

swelling potential and swelling pressure depend on the temperature the sample was exposed and the duration of exposure. The swelling pressure decreases with increase in temperature and duration of heating. Increasing the temperature and duration of heating reduces the concentration of Na^+ but no such effect was observed in dry unit weight.

During the operation of repository, pore fluids come from the host rock, may get percolated through the cement/concrete layer, and becomes alkaline that further hydrate the bentonite. Due to hydration, of pore fluids, the technological or natural gaps could be gradually sealed by swelling of bentonite [17]. The properties of compacted bentonite get altered by coming in contact with cement water having a high pH of 12–13.5 due to the release of sodium (Na^+) and potassium (K^+). The properties such as cation exchange capacity change due to the adsorption of these released sodium (Na^+) and potassium (K^+) cations. The presence of moisture seeps through the layer of cement from the host rock and creates the alkaline environment (pH > 12) inside the repository. The prolonged degradation produces the highly alkaline fluids that diffuse through the compacted bentonite buffer and changes the behavior of bentonite that is useful to act as a buffer in the repository [15, 18, 19]. The alkaline pore fluids may enhance the chances of solubility of radioactive elements [1]. The engineering properties of bentonite are different at room temperature and high temperature, and there is a requirement of suitable swell pressure for the long-term operation of the repository. The buffer must be designed to perform well for safety against both radioactive waste and reactive solutions flowing through the buffer material. Significant studies have been conducted to understand the effects of high temperature on the clayey and expansive soils in the past, and the studies on the effect of thermal history on the bentonite under hyperalkaline environment are still not clear. Hence, a proper quantified study is essential to develop a deep geological repository (DGR). Barmer bentonite is chosen as buffer material for its favorable physical and mineralogical properties [20]. Again, a lot of studies are presented concerning the effects of salinity on the swelling properties of bentonite. However, very few studies are focused on the effect of swelling pressure of bentonite in the presence of alkaline cement solution at elevated temperature. Therefore, in current experiments, swell pressure tests are performed on Barmer bentonite with infiltration of distilled and cement water solutions. The variation in swell pressure of bentonite due to these solutions and elevated temperature is discussed.

2 Materials and Methodology

2.1 Materials

Bentonite [Barmer 1 (B_1)] from Barmer district of Rajasthan, India, was used in this study. The basic characterization of the bentonite was determined by ASTM procedure (ASTM D4318, D7928-17, D720, D698) (Table 1).

Table 1 Properties of bentonite used in the study [14]

Properties	Barmer Bentonite
Specific gravity	2.79
Clay content (%)	89
Sand-sized fraction (4.75–0.075 mm)	1.63
Liquid limit (%)	447.28
Plastic limit (%)	49.23
Plasticity index (%)	398.05
Specific surface area (m^2/g)	507.74
Maximum dry density (g/cm^3)	1.42
Optimum moisture content (%)	35
Cation exchange capacity (meq/100 g)	94.58
Free swell index (%)	833.33
pH	8.29

2.2 Methodology

2.2.1 Determination of Swell Pressure

The swell pressures of compacted bentonite specimens were determined using constant volume consolidation cell [2] [21]. An air-dried sample of bentonite was compacted in a consolidation ring (diameter = 61 mm; height = 20 mm) and a thickness of 8 mm. The water content of the bentonite during compaction was 14%, and the specimens were prepared at a compaction density of 1.5 Mg/m^3. The compacted samples were mounted on the swell pressure assembly consisting of a 10 kN load cell (capacity = 10 kN; sensitivity = 0.01 kN) and LVDT (maximum displacement = 20 mm; sensitivity = 0.01 mm). The specimens were saturated using distilled water and cement water. A photograph of the test setup is presented in Fig. 1. The load during different stages of saturation was indicated by the load cell and was noted down at the regular intervals of time. The experiment was stopped when the load cell showed a constant reading of load [22]. The equilibrium load divided by the cross-sectional area of the specimen gave the swell pressure of the compacted specimen.

2.2.2 Preparation of Cement Solution

The cement pore water was prepared by mixing the ordinary portland cement with distilled water maintaining the w/c ratio equal to 1.0 and separating the supernatant water. The pH value of the cement solution used in this study is 12.5, i.e., hyperalkaline solution.

Fig. 1 Swell pressure apparatus

2.2.3 Influence of Thermal History

To study the influence of thermal history on the swell pressure of bentonite, the compacted bentonite specimens of density 1.5 Mg/m^3 were exposed to 110 °C for about three h, and results were compared with the non-heated specimen.

3 Results and Discussions

3.1 Time Swelling of Compacted Bentonites Without Heating

The plot of swell pressure with time for the specimens compacted at densities 1.5 Mg/m^3 and without heating (WH) for distilled water and cement water is presented in Fig. 2a. The specimens compacted to 1.5 Mg/m^3 and without heating
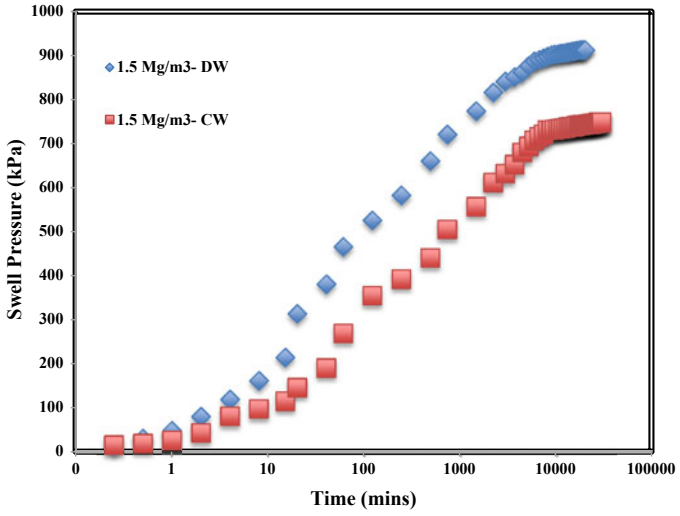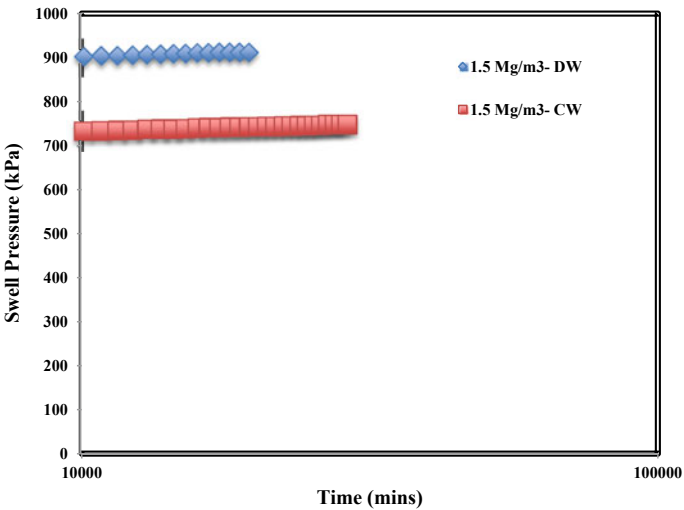
Fig. 2 **a** Swell pressure versus time of compacted bentonite (without heating) with distilled water (DW) and cement water (CW) **b** magnified image of swell pressure versus time while saturation

started attaining the equilibrium swell pressure after 18,720 min. of starting the test when infiltrated with distilled water. Comparatively, the specimens without heating started attaining the equilibrium swell pressure after 26,640 min of starting the test when infiltrated with cement water. The final swell pressure values of compacted

bentonite specimen are 913.78 kPa and 749.45 kPa for distilled water and cement water, respectively.

The important observation found was, though the swell pressure in case of distilled water was greater than the cement water the time of saturation for the sample saturated with cement water was more than in case of distilled water (Fig. 2b).

In case of cement water, the exact reason behind the long duration taken for the saturation may be due to clogging of pores by the precipitation of cementitious products, which was further investigated by microstructural behavior by FESEM (Fig. 3a and b). The observed swell pressure is less than that of sample hydrated with distilled water. The reason behind the reduced swell pressure may be due to the rapid exchange of Na^+ and Ca^+ ions with the hyperalkaline cement solution. From Fig. 3a and b, it can be observed that there is a deposition of cementitious material in between the pores of the bentonite particles. The presence of calcium in highly alkaline cement water may have exchanged with the active ions present with the bentonite, and therefore, the deposition is observed.

3.2 Time Swelling of Compacted Bentonites Subjected to High Temperature

The plot of swell pressure of compacted bentonite against time having compaction density 1.5 Mg/m^3 heated at 110 °C for about three hrs for both distilled water and cement water is presented in Fig. 4a. The specimens compacted to 1.5 Mg/m^3 and heated at 110 °C started attaining the equilibrium swell pressure after 16,640 min after starting the test when infiltrated with distilled water. Comparatively, the specimens without heating started attaining the equilibrium swell pressure after 18,720 min after starting the test when infiltrated with cement water. The final swell pressure values of compacted bentonite specimen having 1.5 Mg/m^3 densities are almost same, i.e., 661 kPa and 660 kPa for distilled water and cement water, respectively. However, the time of saturation for the samples in case of cement water was more than that of distilled water (Fig. 4b) (Table 2).

In Fig. 5a and b, the deposition of cementitious material in between the pores of the bentonite particles is observed when the sample was heated at 110 °C. The presence of calcium in highly alkaline cement water may have exchanged with the active ions present with bentonite, and therefore, the deposition is observed. The flaky structure of bentonite is shown in Fig. 5a.

When the compacted samples are heated at high temperature such as 110 °C, the available moisture will be lost, and the sample is completely dry as can be observed from Fig. 5a and b.

Table 3 shows the percentage of variations in swell pressure at different temperatures when saturated with distilled water and cement water. It is observed that the percentage change is more in case samples without heating than heated at 110 °C.
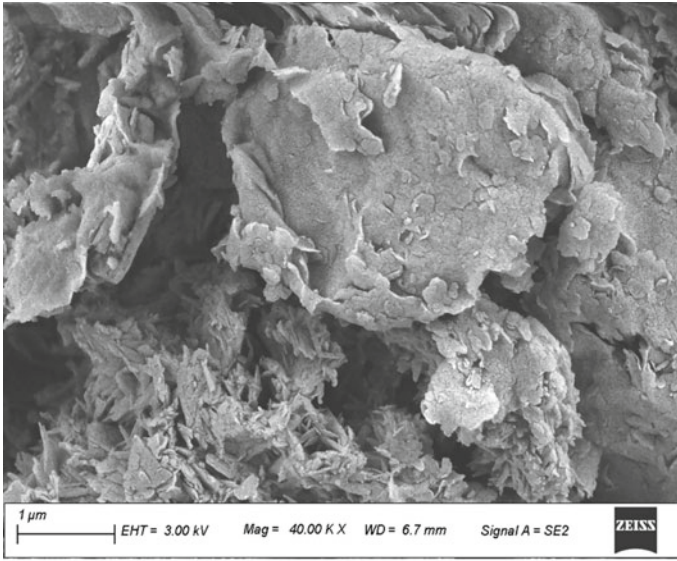
(a)
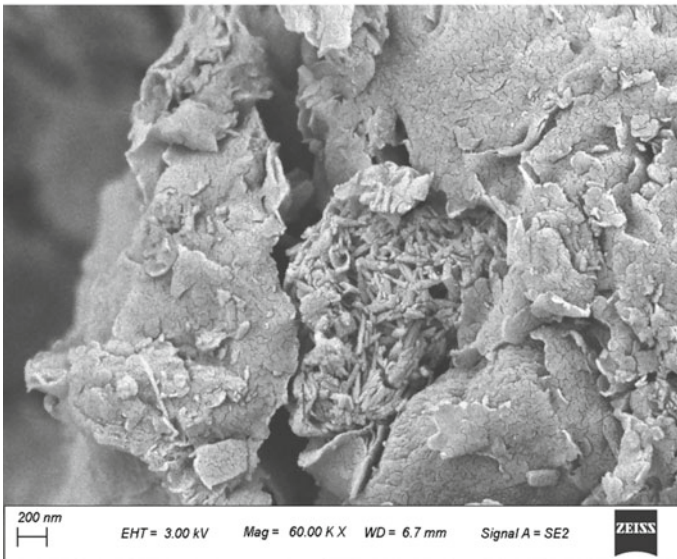
(b)

Fig. 3 a FESEM images of compacted bentonite specimen saturated with cement water (WH).
b Magnified image (cement water saturation)
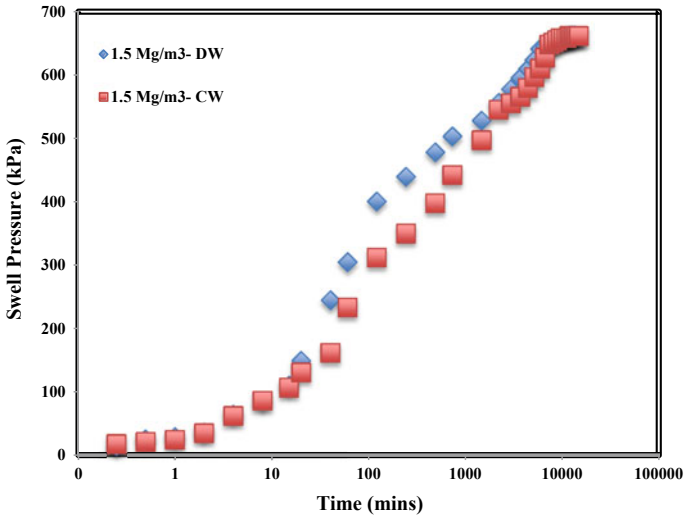
(a)
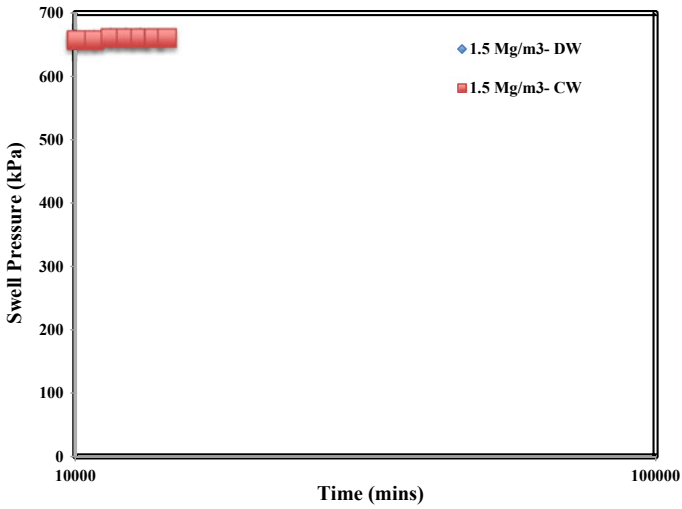
(b)

Fig. 4 **a** Swell pressure versus time of compacted bentonite (heated at 110 °C) with distilled water (DW) and cement water (CW) **b** magnified image of swell pressure versus time while saturation

Table 2 Variation in a final time of saturation of compacted bentonite samples

Temp (°C)	1.5 Mg/m³ (min)	
	DW	CW
WH	19,940	28,800
200	12,960	14,400
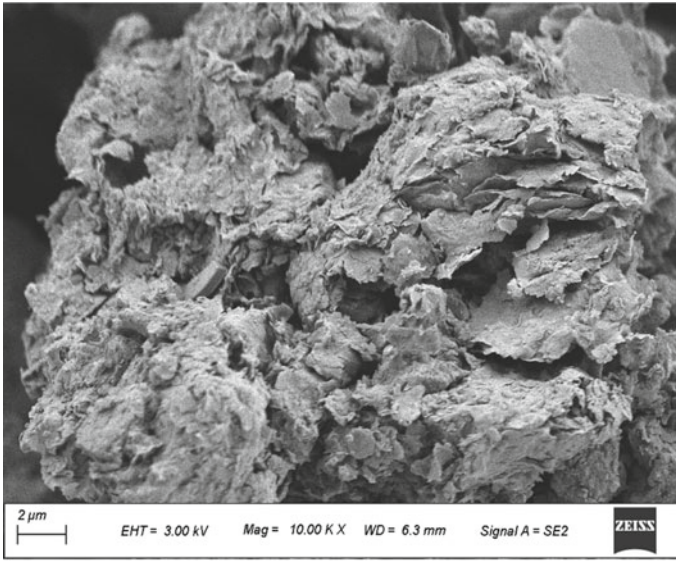
(a)
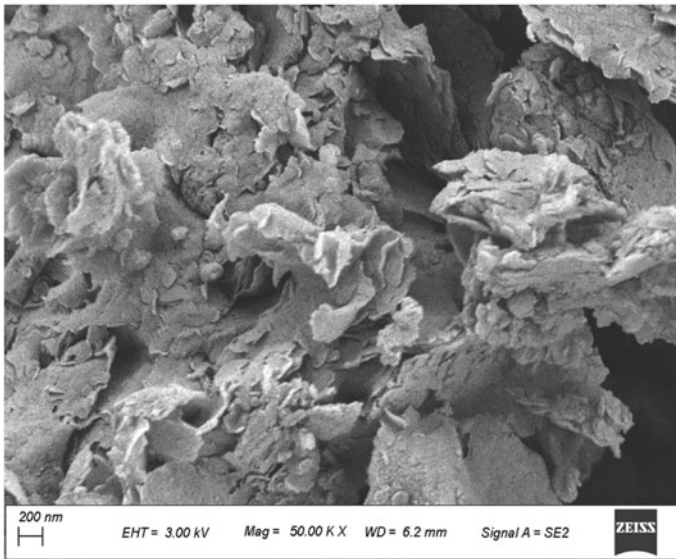
(b)

Fig. 5 a FESEM images of compacted bentonite specimen saturated with cement water (110 °C). **b** Magnified image with cement water saturation

Table 3 Percentage variations in swell pressure at different temperatures

Temp (°C)	1.5 Mg/m^3 (kPa)		
	DW	CW	% Change
WH	913.78	749.75	17.95
110	661.71	660.74	0.15

4   Conclusion

In this study, swelling pressure tests were conducted on densely compacted Barmer bentonite specimens, which had an initial dry density of 1.5 Mg/m^3. Influences of highly alkaline cement water on swelling behavior as well as the combined effect of thermal history and alkaline solution on the microstructural changes of the compacted Barmer bentonite were analyzed.

1. The highly alkaline (pH = 12.5) cement solution significantly influenced the swelling properties of the compacted Barmer bentonite.
2. The swell pressures of the compacted specimen of bentonite infiltrated with distilled water were more than the specimens infiltrated with cement water.
3. The swell pressure decreased with the increase in temperature in both the cases of distilled water and cement water.
4. The time taken for saturation in case of cement water was more than that of distilled water.

References

1. Gaucher, E., Blanc, P.: Cement/clay interactions–a review: experiments, natural analogues, and modeling. Waste Manage. **26**(7), 776–788 (2006)
2. Karnland, O., Birgersson, M.: Montmorillonite stability with special respect to KBS-3 conditions. In: Technical Report TR-06–11 Clay Technology AB (2006)
3. Lee, J.O., Cho, W.J., Chun, K.S.: Swelling pressures of a potential buffer material for a high-level waste repository. J. Korean Nucl. Soc. **31**(2), 139–150 (1999)
4. He, Y., Cui, Y.J., Ye, W.M., Conil, N.: Effects of wetting-drying cycles on the air permeability of compacted Téguline clay. Eng. Geol. **228**, 173–179 (2017)
5. Cui, Y.: On the hydro-mechanical behavior of MX80 bentonite-based materials. J. Rock Mech. Geotech. Eng **9**(3), 565–574 (2017)
6. Karnland, O., Olsson, S., Nilsson, U.: Mineralogy and sealing properties of various bentonites and smectite-rich clay materials. In: SKB TR-06–30. Swedish Nuclear Fuel and Waste Management Co, Stockholm, Sweden (2006)
7. Rao, S., Ravi, K.: Influence of initial degree of saturation on swell pressures of compacted Barmer bentonite specimens. Ann. Nuc. Energy **80**, 303–311 (2015)
8. Saba, S., Barnichon, J., Cui, Y., Tang, A., Delage, P.: Microstructure and anisotropic swelling behavior of compacted bentonite/sand mixture. J. Rock Mech. Geotech. Eng. **6**(2), 126–132 (2014)
9. Kale, R., Ravi, K.: Influence of thermal history on swell pressures of compacted bentonite. Process Saf. Environ. Prot. **123**, 199–205 (2019)

10. Abuel-Naga, H., Bergado, D., Ramana, G., Grino, L., Rujivipat, P., Thet, Y.: Experimental evaluation of the engineering behavior of soft Bangkok clay under elevated temperature. J. Geotech. Geoenviron. **132**(7), 902–910 (2006)
11. Pusch, R., Muurinen, A., Lehikoinen, J., Bors, J., Eriksen, T.: Microstructural and chemical parameters of bentonite as determinants of waste isolation efficiency. In: Project Report EUR 18950 EN. European Commission, Nuclear Science, and Technology (1999)
12. Cho, W., Lee, J., Kang, C.: Influence of temperature elevation on the sealing performance of the potential buffer material for a high-level radioactive waste repository. Ann. Nuc. Energy **27**, 1271–1284 (2000)
13. Romero, E., Villar, M., Lloret, A.: Thermo-hydromechanical behavior of heavily overconsolidated clays. Eng. Geol. **81**, 255–268 (2005)
14. Herbert, H., Kasbohm, J., Moog, H., Henning, K.: Long term behavior of the Wyoming bentonite MX-80 in high saline solutions. Appl. Clay Sci. **26**, 275–291 (2003)
15. Jenni, A., Gimmi, T., Alt-Epping, P., Mäder, U., Cloet, V.: Interaction of ordinary Portland cement and Opalinus Clay: dual porosity modelling compared to experimental data. Phys. Chem. Earth Parts A/B/C **99**, 22–37 (2017)
16. Estabragh, A., Khosravi, F., Javadi, A.: Effect of thermal history on the properties of bentonite. Environ. Earth Sci. **75–8**, 657 (2016)
17. Chen, Y., Cui, Y., Tang, A., Wang, Q., Ye, W.: A preliminary study on hydraulic resistance of bentonite/host-rock seal interface. Géotechnique **64**(12), 997–1002 (2014)
18. Torres, E., Turrero, M., Escribano, A., Martín, P.: Geochemical interactions at the concrete-bentonite interface of column experiments. PEBS, FP7–249681, **73** (2013)
19. Zhu, C., Ye, W., Chen, Y., Chen, B., Cui, Y.: Influence of salt solutions on the swelling pressure and hydraulic conductivity of compacted GMZ01 bentonite. Eng. Geol. **166**, 74–80 (2013)
20. Kale, R., Ravi, K.: Influence of thermal loading on the index and physicochemical properties of Barmer bentonite. Appl. Clay Sci. **165**, 22–39 (2018)
21. Pusch, R.: Swelling pressure of highly compacted bentonite. In: SKB Technical Reports TR-80–13 (1980a).
22. Komine, H.: Simplified evolution on hydraulic conductivities of sand-bentonite mixture backfill. Appl. Clay Sci. **26**, 13–19 (2004)

Utilization of Municipal Solid Waste as Backfill Material

Parul Rawat and Supriya Mohanty

Abstract One of the major problems in developing India is waste generation and its management. The total municipal solid waste generated by urban India is about 68.8 million ton per year and which is likely to be increased up to 160.5 million ton per year by 2041. Agricultural wastes like rice husk ash, and organic fibers and industrial wastes like fly ash, slag, and silica fumes which are also a part of solid waste are already being used in various civil engineering purposes. The paper is focused on the analysis of geotechnical use of municipal solid waste as backfill material in a cantilever retaining wall. Retaining walls are stabilizing structures that hold the soil at different levels without sliding of backfilled soil. In this study, conventional backfill soil of a cantilever retaining wall is replaced by MSW material, and stability analysis has been performed using Geo5 fine software. Then, stress and settlement analysis of the retaining wall under static and seismic condition has been done by using two-dimensional finite element software Plaxis2D.

Keywords Municipal solid waste · Retaining wall · Geo5 · Plaxis2D

1 Introduction

Waste generation and management have become one of the upcoming challenges not only for India but also for the whole world. As the world is moving toward urbanization, one of its most important by product is over looked by urban society which is growing even in faster rate than urbanization. Improper management of waste not only affects the environment on local and global basis but also the health and economy of the society. World Bank in 1999 published, What a waste: solid waste management in Asia [1] which predicted the MSW generation rate in Asia would be 1.8 million tonnes per day which is approximately equal to the present scenario as Pacific, East and West Asia combined produced about 1 million tonnes per day of MSW. India itself produced about 62 million tonnes of waste per annum according

P. Rawat (✉) · S. Mohanty
Department of Civil Engineering, Indian Institute of Technology (BHU), Uttar Pradesh, Varanasi 221005, India
e-mail: parulrawat.rs.civ18@itbhu.ac.in

to last censes (Censes 2011), the number is going to increased by 165 million tonnes per annum by 2031 as predicted by planning commission [2]. Another source revels similar generation by urban India of about 68.8 million ton per year and which is likely to be increased up to 160.5 million tonnes per year by 2041[3]. This problem of waste can be sorted, if it is handled properly in initial levels. The waste generated is dumped directly in open sites or landfills without treatment. Although this waste gives opportunity and source to energy programs, for that also a proper segregation system is required. The focus of this study is toward the waste which has already being produced and dumped in the landfill sites. Considering limited low lying areas which in near future are going to exhaust, so there is a need of alternative ideas to either use that filled land or to use the waste which has been filled. This paper deals with the reuse of soil-like material of the waste for geotechnical purpose. This technique of reusing finer fraction from waste is also known as waste mining. Research is going on to predict the geotechnical, physical, and chemical behavior of the MSW, so that either it can be reused or stabilized where it has been dumped. Research shows 60–70% of waste from landfill appeared to be soil-like [4, 5]. A hyperbolic relation was proposed by Zekkos et al. to see the variation of MSW unit weight with compaction effort, confining stress and soil content in the waste [6]. A phased approach was proposed as a best practice for the physical characterization of MSW for geotechnical purposes as most of the mechanical properties of waste depend on the physical composition of the same waste [7]. Experimental investigations were done to find out the impact of fibrous reinforcement angle on shear strength of the specimen. It was found that largest increase in shear strength was observed at reinforcement angle of 60° [8]. The dynamic properties of MSW like shear wave velocity and small strain shear modulus profile, material damping curve, and dynamic Poisson's ratio were compiled by Zekkos et al. [9].

In the present study, a particular case of Cantilever RCC retaining wall has been considered for the analysis and comparisons are made between a granular fill material and MSW fill, to check the suitability of MSW as a backfill material. The analysis for stability and retaining structure design for both fill materials were first conducted in Geo5 Fine software, and then stress and settlement analysis were conducted on Plaxis2D.

1.1 Objective of the Study

The objective of study is to reuse the soil-like fraction from MSW as a backfill material. This particular study deal with a comparative study of granular fill and MSW fill material in cantilever-type retaining wall. A typical section of wall is designed by using Geo5 software (limit state analysis) and checked for stability, the passed design is then checked for settlement and stress analysis by finite element-based software Plaxis2D. Analysis was conducted for both static and dynamic cases (Uttarkashi Earthquake M_w: 6.5). The data used in this study are based on the past research and presented in Tables 1 and 2.

Table 1 Concrete model parameters

Material model	Concrete (non-porous)
γ_{unsat} (kN/m^3)	25
E_{28} (kN/m^2)	27.79E6
ν	0.2
F_{c28} (kN/m^2)	6950
F_{con}, f_{cfn}, f_{cmm}	0.1
G_{c28} (kN/m)	35
Φ (°)	55.9
Ψ (°)	0
F_{t28} (kN/m^2)	2760
G_{t28} (kN/m)	0.09
$t_{hydration}$	28
E_1/E_{28}	0.7
Damping parameters α β	0.4189 −0.01061

Table 2 Properties of foundation soils and back fill materials

Parameter	Foundation Soil		Back fill material	
	Sand	Silty sand	Granular Soil	MSW
Material Model	Hardening soil	Hardening soil	Hardening soil	Hardening soil
Material Behavior	Drained	Drained	Drained	Drained
γ_{Dry} (kN/m^3)	17	15	18.85	16
γ_{Sat} (kN/m^3)	20	18	19.25	18.25
$E_{50}{}^{ref}$ (kN/m^2)	3.0E4	7.0E4	4.9E4	3.09E4
$E_{oed}{}^{ref}$ (kN/m^2)	4.038E4	8.025E4	6.5E4	3.09E4
$E_{ur}{}^{ref}$ (kN/m^2)	10.5E4	21E4	14.7E4	9.27E4
m (power)	1	1	0.5	0.5
c' (kN/m^2)	1	20	0	25
ϕ' (°)	34	28	38	28
Ψ (°)	4	0	0	0
ν'_{ur}	0.3	0.35	0.3	0.3
$e_\circ$	0.5	0.5	0.5	0.8
k (m/day)	1E-4	1.002E-3	34.56	1.0454E-3
Damping parameters α β	0.4189 0.02122	1.074 1.29E-3	1.698 0.82E-3	1.047 0.02122

2 Design Methodology

2.1 Stability Analysis Using Geo5

Geo5 program runs on the basis of limit state analysis. The program evaluates normal and shear force in the footing bottom and then verifies the wall against overturning and sliding. A typical geometry of reinforced cantilever wall was considered with height of wall of 6 m with horizontal backfill. The foundation of the wall was considered 0.7 m thick and of 4.29 m wide (Fig. 1). The retaining wall was provided with shear key of 0.3 m at the end of the heel. The water table was considered at 4 m from top of the wall. The front face of wall is supported by a sand fill of 1.5 m. The design has been done as per IS 456 standards, and materials used were Fe 456 (reinforcement) and M25 (concrete). The parameters used for backfill and foundation soil are discussed below. The angle of friction for structure–soil was considered as 20°, which is common value for non-cohesive soils.
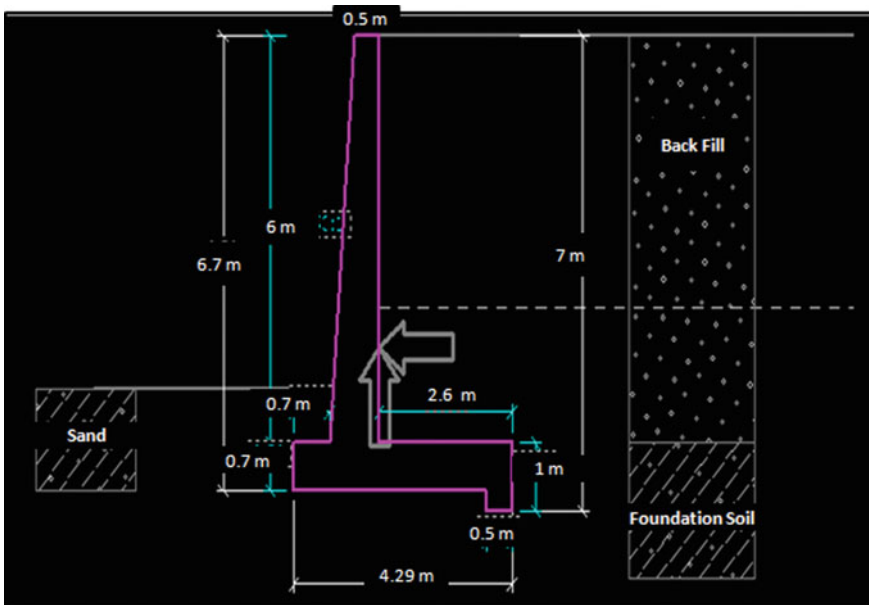
Fig.1 Dimension of cantilever retaining wall
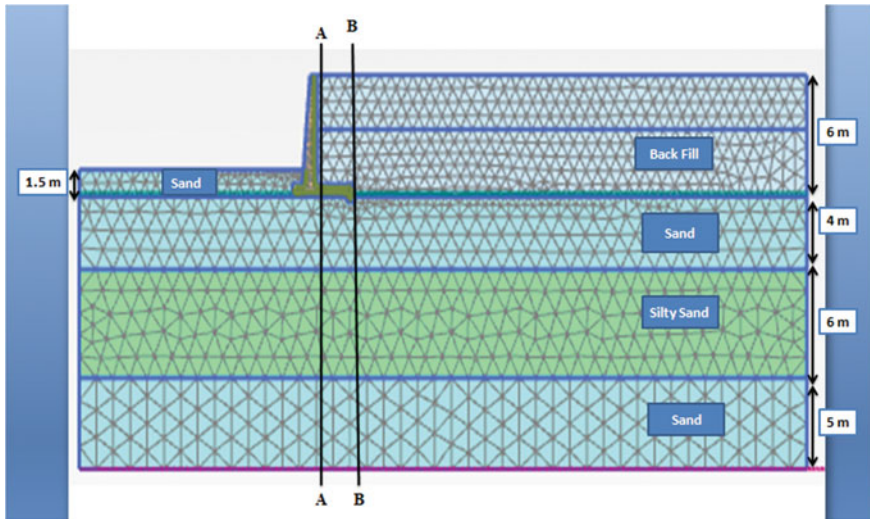
Fig. 2 Generated finite element mesh of cantilever retaining wall with backfill material

2.2 Numerical Analysis Using Plaxis2D

Finite element software Plaxis2D has been used for stress and deformation analysis of the retaining wall. 15-noded triangular elements were used for the meshing of the domain. The maximum, minimum boundary of the model was considered as Y boundaries from -15 to 15 m and X boundaries from -15 to 36.2 m. The structure which passed through Geo5 was used in Plaxis2D with concrete model. The general parameters were considered from Plaxis manual [10]. The parameters of the model used for cantilever wall are mentioned in Table 1.

Once the geometry and input parameters were defined, mesh was generated. The results converge for very fine meshing with 2275 elements and 18,728 nodes (Fig. 2). The backfill was then filled with two layers, and both static and seismic analyses were carried out. Two sections Section 1(A-A), i.e., just behind the wall and Section 2(B-B), i.e., near the heel of wall were considered for further analysis.

2.3 Input Motion Parameters

The input motion selected was Uttarkashi Earthquake of magnitude 6.5 and total duration of 39.9 s with peak ground acceleration (PGA) of 3.04 m/s^2 (Fig. 3). The pseudo-static coefficient of horizontal (K_H) and vertical (K_V) acceleration considered was 0.154645 and 0.103296, respectively. The K_H and K_V coefficients of earthquakes for this study were computed from the equation given by Hynse and Franklin [11];

$$K_{H,V} = (PGA)/2 \text{ g} \tag{1}$$

Fig. 3 Uttarkashi
Earthquake Input motion
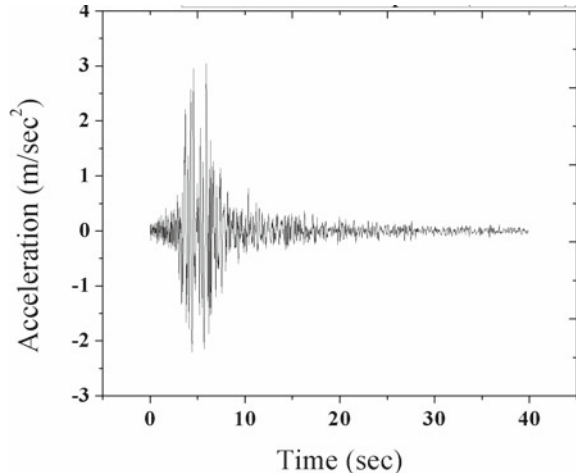
2.4   Material Parameters

Foundation Soil

A layered foundation soil of 15 m depth was considered in study. Sand and silty sand type soils were assumed in model in alternative layers of 4, 6, and 5 m. The parameters considered for foundation soils were taken from Plaxis manual and previous study [12, 13, 14]. The hardening soil (HS) model available in Plaxis was used in study for both foundation soil and backfill material to represent stress–strain behavior. HS model is considered superior to any linear elastic model as it produce more realistic results and capable of modeling modulus reduction with increase in strain. The HS model input parameters for foundation soils, and backfill materials are shown in Table 2.

Backfill Material

Granular fill and MSW backfill were considered in the model as fill materials. The parameters for conventional cohesionless granular soil were considered from the previous study [12]. The parameters of MSW fill were considered from the static and dynamic research done on Indian MSW [4, 15, 16]. The equivalent Young's modulus was considered from the correlation between SPT 'N' (number of blows) and 'E' (modulus of elasticity of soil) for non-cohesion soil [17]. MSW is considered as silty sand or gravel.

3   Results and Discussions

The study was conducted for a cantilever retaining wall with two backfill materials, each consists of two cases (static and seismic). Stability analysis of the cantilever

retaining wall was conducted by using Geo5 and deformation, and stress analysis was performed by using Plaxis2D software.

3.1 Results of Stability Analysis Using Geo5

Stability analysis of the cantilever retaining wall was conducted by limit state analysis in Geo5 for overturning, sliding, and bearing capacity. There are two classic theories proposed for retaining walls, i.e., Rankine's and Coulomb's earth pressure theory. The active earth pressure has been computed according to Coulomb's theory for both the fills (Table 3). The computed values of earth pressure show that MSW is lightweight material than conventional granular fill although there is slight variation of active earth pressure on wall.

Table 4 shows the FOS obtained from Geo5 analysis for all four cases. The FOS for static cases 1 and 3 shows that MSW fill has more safety factor than granular fill but for seismic conditions 2 and 4 granular fill has more values.

The slope stability analysis was carried out according to Bishop, Fellenius, and Spencer theories. A trial failure surface passing through the toe of the wall was assumed which was optimized and confirms that MSW fill has higher slope stability factor than granular fill.

Table 3 Earth pressure analysis according to Coulomb's theory

Material fill	K_a (Coefficient of active earth pressure)	P_a (Active earth pressure) kN/m^2	Wt. of fill kN/m
Granular backfill	0.279	45.94	296.14
MSW backfill	0.320	45.53	261.30

Table 4 Factor of safety from stability analysis using Geo5

	[*]Case 1	[*]Case 2	[*]Case3	[*]Case 4	Min. condition(static)
FOS for overturning	4.47	2.86	6.13	2.72	> 2
FOS for sliding	2.96	2.04	3.04	1.65	> 1.5
FOS for bearing capacity (vertical)	4.70	2.65	6.35	2.43	> 2
FOS for bearing capacity (horizontal)	2.97	2.05	3.05	1.66	> 2

[*]**Case1 =** Granular backfill (Static Condition)
Case2 = Granular backfill (Seismic Condition)
Case3 = MSW backfill (Static Condition)
Case4 = MSW backfill (Seismic Condition)

3.2   Results of Numerical Analysis Using Plaxis2D

3.2.1   Stress Analysis

Stress analysis of the cantilever retaining wall was done using Plaxis2D under static as well as seismic condition at two different sections considered behind the wall (Fig. 2). A typical contour plot of shear stress for seismic case for both the fill material is shown below (Fig. 4), which shows that most of the shear stress confined behind the wall near heel area which is also a probable failure zone. Also, as compared to granular fill stress value is less in MSW fill.

Stresses at Sect. 1(A-A): Effective stresses were considered in backfill material, i.e., upto 6 m depth. The effective horizontal stresses behind the wall section shows less stresses for MSW as compared to granular fill under static condition. But, in seismic case the top portion experience more stress (away from wall) in case of MSW fills (Fig. 5).

The variation of effective shear stress with depth for static and dynamic condition has also been studied. The average stress values were less for MSW fill as compared to granular fill. Maximum shear stress was noticed at depth of 2.5–3 m in static case, and in seismic case, it is just above the base of the retaining structure.

Maximum value = 221.0 kN/m² (Element 331 at Node 14037)

Minimum value = -1001 kN/m² (Element 354 at Node 13709)

Maximum value = 817.1 kN/m² (Element 358 at Node 13614)

Minimum value = -4466 kN/m² (Element 354 at Node 13709)
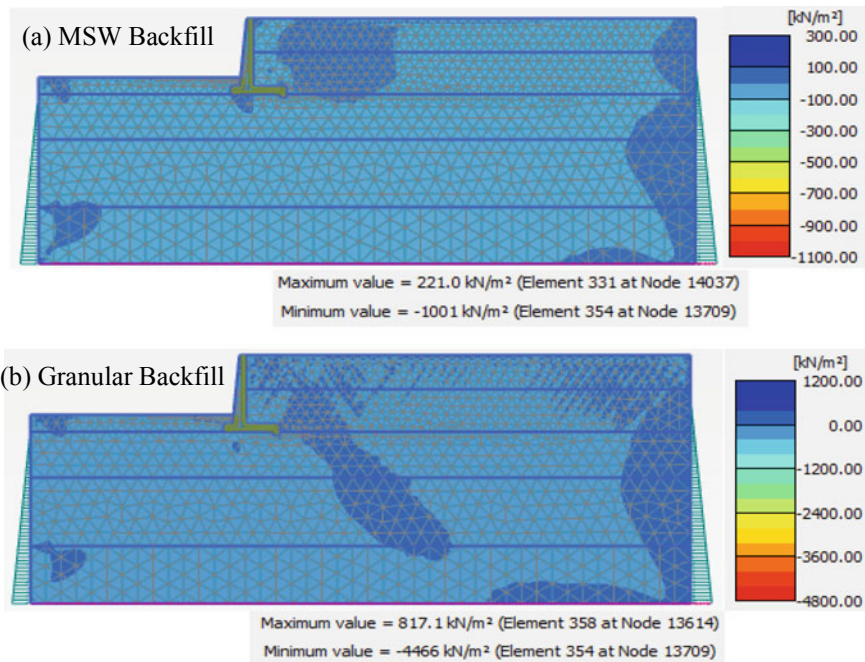
Fig. 4   Contour plot for shear stresses for (a) MSW backfill (b) Granular backfill model
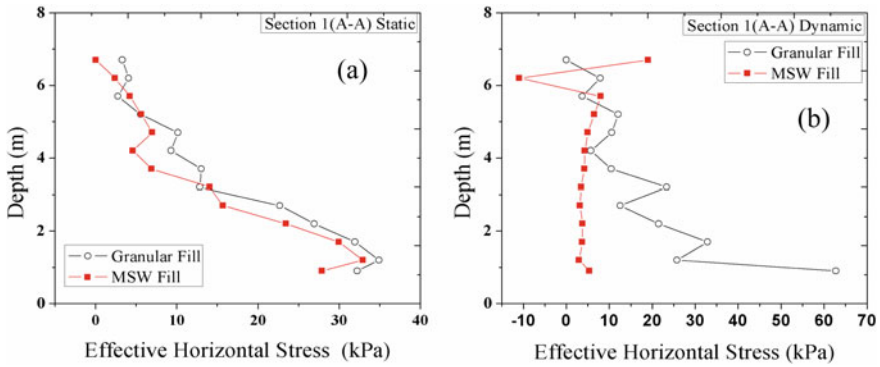
Fig. 5 Variation of effective horizontal stress with depth **a** Static and **b** Seismic case at section A-A

In static case within top 1.5 m, the vertical stresses in MSW fill can be seen more but below that it reduces (Fig. 6a). In seismic case, vertical stresses can be seen more in MSW fill for full backfill depth (Fig. 6b).

Stresses at Sect. 2 (B-B). Second section is considered near the heel of the wall which is considered as a critical section as most of the stresses concentrated near the heel area. As compared to granular fill material, MSW shows more effective horizontal stress within top 2 m depth of backfill but with increase in depth stresses shows reverse trends for both static and dynamic conditions (Fig. 7).

Shear stress result also concluded that stresses induced in MSW case are less as compared to granular fill in seismic case but in static case, shear stress is induced in opposite directions for two fill materials.

Vertical stresses can be seen more in granular fill upto the depth of top 4 m for both the cases (Fig. 8) but for last 2 m backfill vertical stresses for MSW can be seen more than granular fill. The reduction in the stresses from 0 to 2 m behind the wall could be because of the fill present in front side of the wall upto 1.5 m.
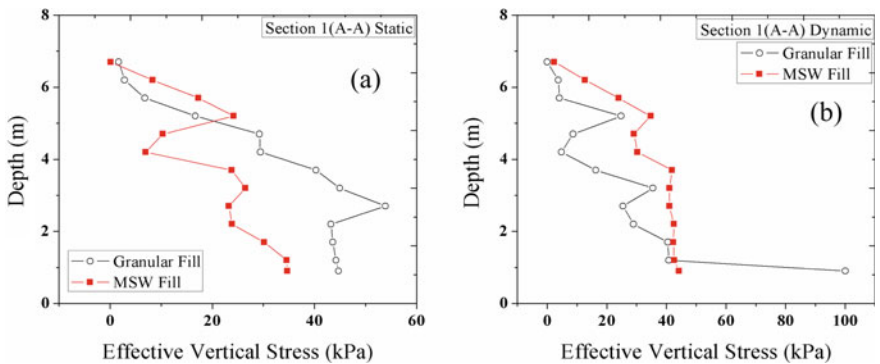
Fig. 6 Variation of effective vertical stress with depth **a** Static and **b** Seismic case at section A-A
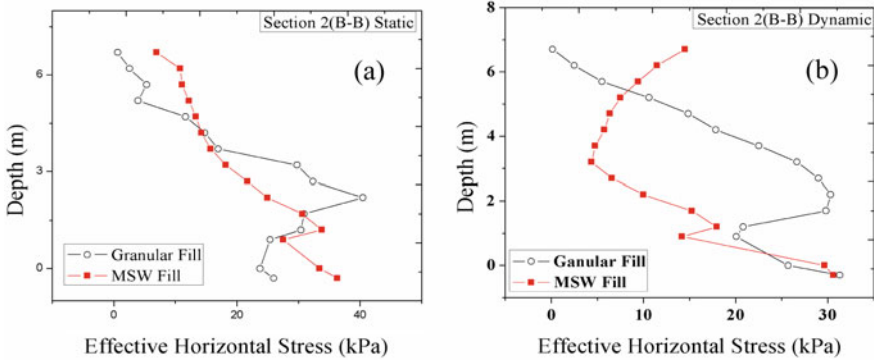
Fig. 7 Variation of effective horizontal stress with depth **a** Static and **b** Seismic case at section B-B
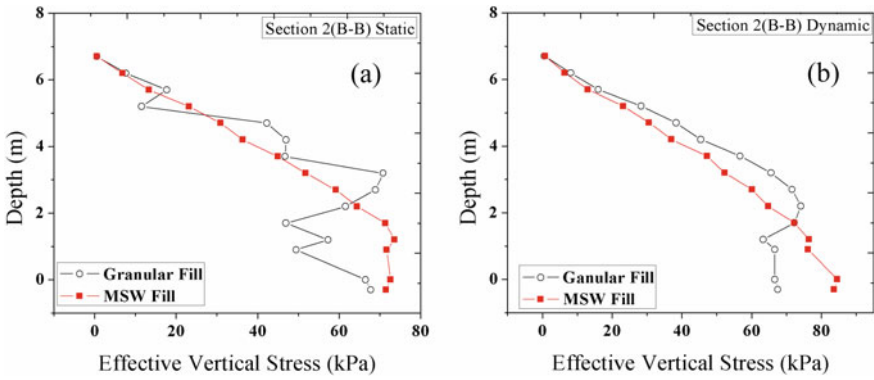
Fig. 8 Variation of effective vertical stress with depth **a** Static and **b** Seismic case at section B-B

3.2.2 Deformation Analysis

The deformation analysis was conducted on Plaxis2D model of the retaining wall. Typical contour plots for granular backfill are shown below (Fig. 9) for static as well as seismic case. Maximum deformations can be seen within 6 m depth of backfill in static case, whereas in seismic case deformations were more in free field location. Similar contours were seen for MSW fill also.

Deformations at Sect. 1(A-A). Resultant, horizontal, and vertical displacements were recorded at Sect. 1(A-A), i.e., behind the wall. In static case, MSW backfill shows less deformation than granular backfill and it goes on decreasing with depth but for seismic case deformations are more for granular backfill within top 2 m depth (Fig. 10).

It was noticed that horizontal displacements behind the wall for static case had more deformation within top 6 m depth and then it decreases with the depth but, for
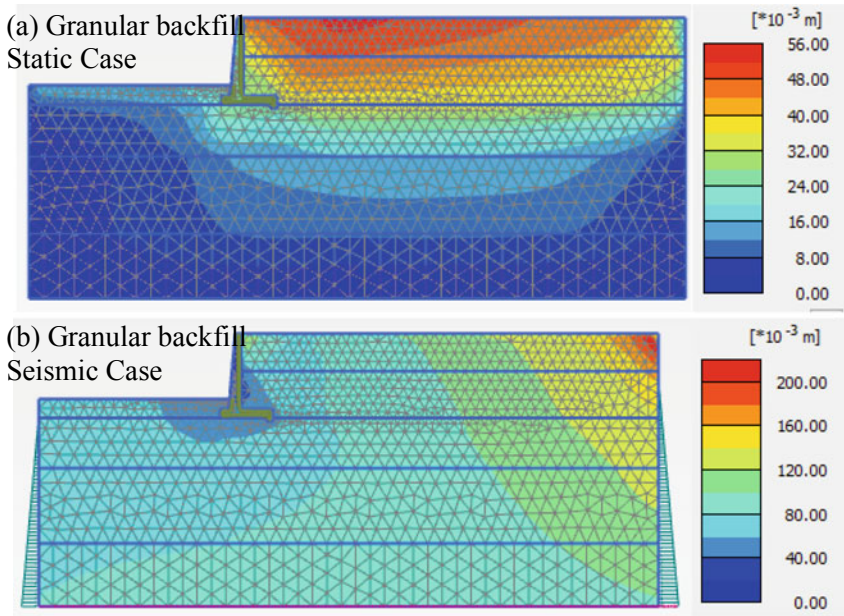
Fig. 9 Contour plots for resultant displacement of granular backfill for **a** Static **b** Seismic case
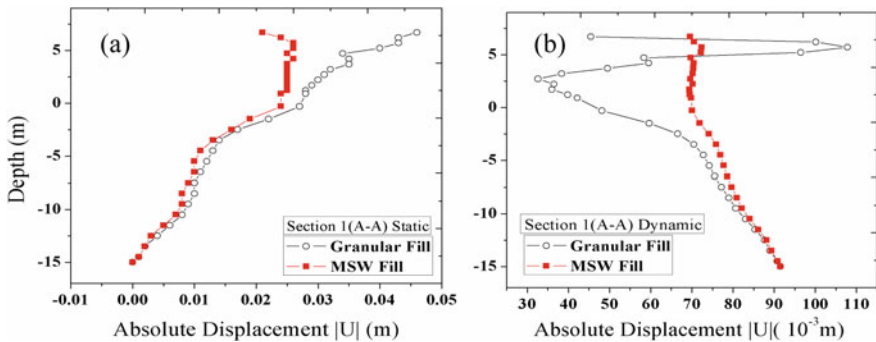
Fig. 10 Variation of resultant displacement with depth **a** Static and **b** Seismic case at section A-A

seismic case horizontal displacement continuously increasing with depth for both the fill materials. The horizontal displacements are found to be less as compared to vertical displacements.

The vertical displacement for both static and seismic case noticed more variations in backfills upto 6 m and then decrease with depth, but the deformations were low in MSW backfill. This may be due to less unit weight of MSW fills. From the literature, it can be seen that soil-like materials of MSW has low specific gravity then soil of same gradation [13].

Deformations at Section 2 (B-B). Heel of the wall is a critical place for failure, so deformation analysis has been carried out at the points selected in line near heel of the wall. The analysis shows that deformation patterns are similar to the deformation behind the wall, i.e., Section 1(A-A).

The deformation trend reduces near the heel of wall (at depth 0) and then increases again in seismic case and reduces in static case (Fig. 11). The resultant deformations can be seen more in case of MSW (seismic condition), and this could be because waste has property of more damping than natural soil [18] and even the initial parameters taken from previous study shows MSW initial voids more than any soil, and this could lead to more deformations during shaking.

Horizontal displacements variation noticed same trends like in resultant displacement trends but these deformations are almost negligible. Due to lightweight or low unit weight of MSW fills, the vertical displacements were noticed less in case of MSW fills than that of granular fills.

Table 5 shows the values of deformations at the end of static and dynamic phases. The maximum displacements in static case occurred behind the wall in backfill areas but for seismic case displacements are more in free field locations. At the end of phase, MSW fill shows less displacements and acceleration, one of the reason could be the low unit weight of MSW and low acceleration observed may be due to material
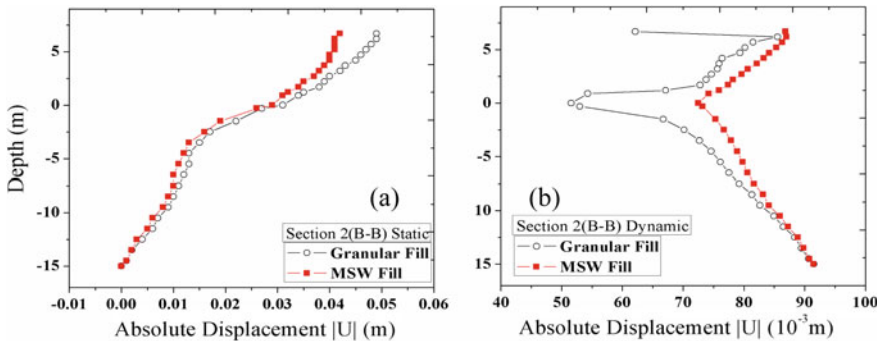
Fig. 11 Variation of resultant displacement with depth **a** Static and **b** Seismic case at section B-B

Table 5 Deformation results at the end of static and seismic phases for two backfills

		U (Resultant deformation) m	Ux (Horizontal deformation) m	Uy (Vertical deformation) m	a_x (Horizontal acceleration) m/s^2
Granular backfill	Static	0.053	0.0165	0.0526	
	Seismic	0.217	0.1952	0.1236	1.182
MSW backfill	Static	0.048	0.0154	0.0476	
	Seismic	0.127	0.1263	0.0318	0.358
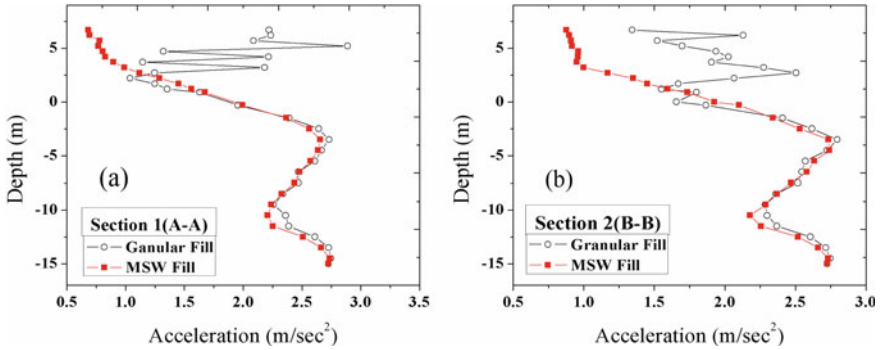
Fig. 12 Variation of acceleration with depth at two positions **a** Section 1(A-A) and (b) Section 2(B-B)

properties, i.e., damping ratio of MSW shows higher damping characteristics than soils.

3.2.3 Acceleration Responses

Backfill materials are filled upto 6 m depth, and the trends for the acceleration shows that for Sections 1 and 2 (Fig. 12) MSW fill has low acceleration values, which means most of the waves passing through it during earthquake get de-amplified.

4 Conclusions

The present study represents a comparative numerical model study to identify the suitability of MSW as a replacement of the conventional fill material. From the results of stability, deformation, and stress analysis, it can be concluded that MSW can replace granular backfill in field as MSW fill retaining structure surpass the minimum stability criteria. Also, due to its low unit weight MSW fill possess low stresses as compared to granular fill. Most of the acceleration got de-amplified when it travels through the MSW backfill. The horizontal displacements observed at critical sections were below the permissible limits generally considered, i.e., 0.5–0.7%H, where H is height of fill for static case. Although model verifies that MSW can be use as alternative fill material in field, this requires detailed study before practical implementation, like chemical study of MSW (leachates, heavy metal, and organic content study, etc.), long-term settlement analysis, and proper segregation methodology.

References

1. What a waste: Solid waste management in Asia. https://web.mit.edu/urbanupgrading/urbane nvironment/resources/references/pdfs/WhatAWasteAsia.pdf (1999)
2. Planning Commission Report.: Reports of the task force on waste to energy, vol. 1, (in the context of Integrated MSW management). https://planningcommission.nic.in/reports/genrep/rep_wte1205.pdf (2014)
3. WMW waste management world. https://waste-management-world.com/a/waste-to-energy-for-integrated-waste management-in-India
4. Havangi, V.G., Sinha, A.K., Parvathi, G.S., Chandra, S.: Municipal solid waste in road embankment construction-a case study. J. Indian Road Congress Paper **669**, 79–90 (2017)
5. Somani, M., Datta, M., Ramana, G.V., Sreekrishnan, T.R.: Investigations on fine fraction of aged municipal solid waste recovered through landfill mining: Case study of three dumpsites from India. Waste Manage. Res. **36**(8), 744–755 (2018)
6. Zekkos, D.P., Bray, J.D., Kavazanjian, E., Matasovic, N., Rathje, E., Riemer, M., Stokoe, K.H.: Framework for the estimation of MSW unit weight profile. 10th international waste management and landfill symposium, pp. 3–7, Santa Margherita di Pula, Cagliari, Italy (2005).
7. Zekkos, D., Kavazanjian, E., Jr., Bray, J.D., Matasovic, N., Riemer, M.F.: Physical characterization of municipal solid waste for geotechnical purposes. J. Geotech. Geoenviron. Eng. **136**(9), 1231–1241 (2010). https://doi.org/10.1061/ASCEGT.1943-5606.0000326
8. Zekkos, D., Grizi, A., Athanasopoulos, G.: Experimental investigation of the effect of fibrous reinforcement on shear resistance of soil-waste mixtures. Geotech. Test. J. **36**(6), 867–881 (2013). https://doi.org/10.1520/GTJ20120190
9. Zekkos, D., Matasovic, N., El-Sherbiny, R., Athanasopoulos-Zekkos, A., Towhata, I., Maugeri, M.: Dynamic properties of municipal solid waste geotechnical characterization, field measurement and laboratory testing of municipal solid waste. Geotech. Special Publ. **209**, 112–134 (2011)
10. PLAXIS Material Models Manual (2019)
11. Hynes-Griffin, M.E., Franklin, A.G.: Rationalizing the seismic coefficient method. U.S. Army Corps of Engineers Waterways Experiment Station, Vicksburg, Ms Geotechnical Lab (1984)
12. Shrestha, S., Ravichandran, N., Raveendra, M., Attenhofer, J.A.: Design and analysis of retaining wall backfilled with shredded tire and subjected to earthquake shaking. Soil Dyn. Earthquake Eng. **90**, 227–239 (2016)
13. Khan, S.A., Abbas, S.M.: Numerical modelling of highway embankment by different ground improvement techniques. Int. J. Inn. Res. Adv. Eng. **1**(10), 350–356 (2014)
14. Yadav, R., Shrivasthava, A., Jain, S.: Design and analysis of reinforced road embankment on soft soil by using finite element modeling software PLAXIS. IJSRD Int. J. Sci. Res. Develop. **5**(12), 634–643 (2018)
15. Naveen, B.P., Sitharam, T.G., Sivapullaiah, P.V.: Evaluating the dynamic characteristics of municipal solid waste for geotechnical purpose. Curr. Adv. Civ. Eng **2**(1), 28–34 (2014)
16. Ramaiah, B.J., Ramana, G.V.: CPTu at a municipal solid waste site in Delhi, India. 3rd international symposium on cone penetration testing, pp. 1083–1091, Las Vegas, Nevada, USA (2014).
17. Brahma, P., Mukherjee, S.P.: A realistic way to obtain equivalent Young's modulus of layered soil. In: Indian Geotechnical conference, pp. 305–308. Bombay, India (2010).
18. Towhata, I., Kawano, Y., Yonai, Y., Koelsh, F.: Laboratory tests on dynamic properties of municipal wastes. 11th Conference in Soil Dynamics and Earthquake Engineering and the 3rd International Conference on Earthquake Geotechnical Engineering, vol. 1, pp. 688–693 (2004).

A Study on Contaminant Transport Through Soil

Rajeshwari Puranik and Prasanna Patil

Abstract Soil in ecosystem is contaminated by various environmental activities taking place in day-to-day life. Major contaminants in soil are chlorides, fluorides, nitrates, iron, silicates, etc. The present study deals with the transportation of contaminants like sodium chloride (Nacl) and sodium fluoride (NaF) in soil by advection–diffusion method. The tests are carried on soil mixed with varying percentages of sand from 10 to 40%. In the present study, the dosage of contaminants, i.e., Nacl and NaF, is varied from 0.1 N to 0.4 N, respectively. The column of size 60 cm is utilized, and up to 40 cm height, soil is compacted from the base. The solutions of additives are pumped at the rate of 0.208 ml/s. The time of flow at the entry and exit of soil column is observed, and solution is collected from the exit point to evaluate percentage absorption by the soil. For different normalities of sodium chloride such as 0.1 N, 0.2 N, 0.3 N, 0.4 N, corresponding relative concentrations obtained are 0.078, 0.073, 0.062, 0.056, and similarly, relative concentrations for sodium fluoride are also determined. The soil absorption capacity increases with increasing the concentration of contaminants. For all normalities of contaminants, the nature of results obtained follows the footprint of breakthrough curves. Strength parameter of contaminated soil is evaluated by unconfined compressive strength test. The strength of sodium chloride contaminated soil is increased irrespective of concentrations and decreased with increase in percentage addition of sand. The strength of sodium fluoride contaminated soil is decreased with longer curing period.

Keywords Soil column · Sodium fluoride · Sodium chloride · Breakthrough curves

R. Puranik · P. Patil (✉)
Civil Engineering Department, Basaveshwar Engineering College, Bagalkot 587103, India
e-mail: pvpatil026@gmail.com

R. Puranik
e-mail: rajeshwarip0077@gmail.com

1 Introduction

Contaminants regardless of whether as a harmful liquid or as a solution of a harmful chemical type solvate in water are sometimes overflowed at ground surface by accidentally. A liquid contaminant will pass downward through the surface zone, finally reaching a bottom-line water table. Various organic, physical and chemical processes may take place along its surface zone. Once reaching the water level, the liquid contaminant will be transported through the water level to the latter's outlets. Along its way toward the water outlets, the concentration decreases by various processes. The executive of the water level must carry both management of water quantity as well as water quality. Definitely, the best action is to make every possible effort, relevant technological means, regulation and education, to prevent contamination. Contamination of groundwater has become a key environmental issue particularly with the ever increasing demand for energy and resource development. Geotechnical engineers as a result are more and more faced with the difficult task of designing waste management facilities that prevent the contamination of groundwater. To design such facilities requires an understanding of processes that govern tile transport of contaminants. The complexities of designing these structures are compounded by the lengthy required design life which may be hundreds of years or more [1, 2]. The main motto of the work is to analyze the mass transport phenomenon from a geotechnical point of view and to demonstrate the significance of the processes by analyzing the contaminant migration through soil media. The transport processes is based on the equations of flow laws. The flow laws combined the mass balance equation and casing where reduction of contaminant. It is called as the general governing differential equation for contaminant migration. Advection and dispersion are two basic processes. Advection means the contaminant will move along with the moving water. Dispersion means contaminant is mixed with the water or flow system. The advection and dispersion transport processes can be studied by a steady flow of water in a long the soil column [3].

2 Materials and Methodology

The soil sample is collected from Bagalkot at a depth of 1.5 m beneath the ground surface. Soil is classified as an inorganic soil with a group symbol CI as per IS classification system. To ease the flow of contaminant through the soil, different percentages of sand are mixed, and further solutions of sodium chloride (Nacl) and sodium fluoride (NaF) with different concentrations are added to determine absorption capacity. Sodium chloride is having a 1:1 ratio of sodium and chloride ions and molar mass of 58.443 g/mol. Sodium fluoride is an inorganic ionic compound, and its molar mass is 41.988 g/mol. Table 1 gives a summary of laboratory tests which are conducted as per relevant IS codes.

Table 1 Basic properties of the soil

Properties	Values
Specific gravity	2.58
Grain size distribution (%)	
Sand	37.2
Silt and clay	62.8
IS soil classification	CI
Consistency limits (%)	
Liquid limit	39
Plastic limit	18
Plasticity index	21
Compaction characteristics	
Optimum moisture content (%)	16.4
Maximum dry density (kN/m^3)	18.6
pH	7.86

2.1 Sample Preparation for Soil Column Experiment

For the present study, the transparent acrylic pipe of 60 cm height and diameter of 10 cm is used. For calculated maximum dry density and optimum moisture content, the soil sample is compacted up to the height of 40 cm from bottom of the column, and outlet is provided to collect the solution. The schematic of experimental setup is portrayed (Fig. 1). The soil is placed in four layers, and each layer is compacted using light compaction. To increase the permeability of base soil, sand is used randomly with varying percentages of 10, 20, 30 and 40% by weight.

2.2 Preparation of Solutions

Sodium chloride and sodium fluoride are weighted according to their molecular weights. For 0.1 normality, 5.844 g of NaCl is dissolved in 1000 ml distilled water to prepare solution of contaminant, and similarly, 4.2 g of NaF is dissolved in 1000 ml distilled water to prepare solution [2]. The solution is pumped with peristaltic pump with keeping constant flow rate of 0.208 ml/s into the column. The initial time is noted down at the start of pumping and also at different intervals of distance up to 30 cm without disturbing the column until solution oozes out from the outlet, and final time is recorded.
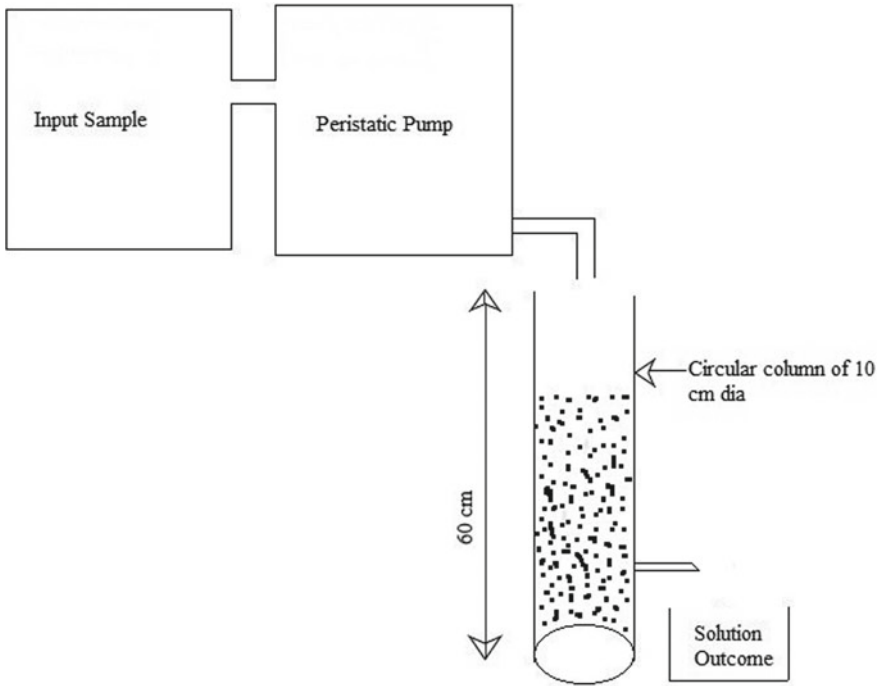
Fig. 1 Schematic of experimental setup

2.3 Sample Preparation for Unconfined Compressive Strength Experiment

The unconfined compressive strength test is conducted for both contaminated soil samples. The modules are tested after 7 days, 14 days and 28 days of curing period.

3 Results and Discussions

3.1 Breakthrough Curves

Breakthrough curve represents the plot between time and the measured solute concentration at the outlet of soil column. If the supplied solute source at the inlet has a constant concentration, it remains throughout the experiment, and it is known as continuous solute source. The plot between relative concentration and number of pore volumes is reproduced (Fig. 2) [4]. Based on the soil column experiment, the relative concentrations to time plots are obtained.
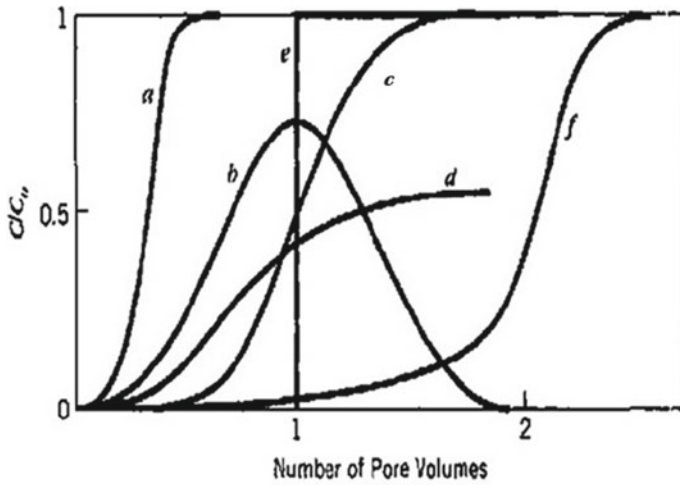
Fig. 2 Different types of breakthrough curves

The variation of relative concentration for sodium chloride solutions with different normalities to base soil with respect to time is plotted (Fig. 3). For 0.1 N, initially relative concentration was zero, as time period increases, the relative concentration incremented from 0 to 0.078 and reaches peak. Further increase in the time resulted in the reduction of relative concentration and remains constant throughout, and similar trend is observed for all other normalities.
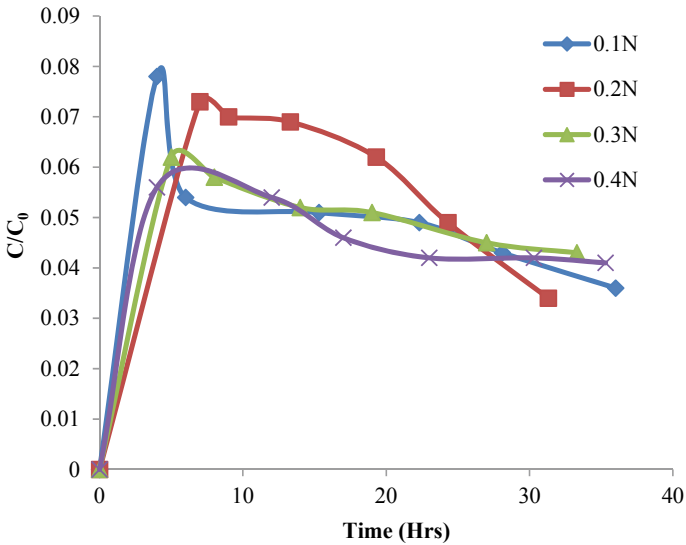
Fig. 3 Variation of relative concentration with time

The breakthrough curves for sodium chloride solutions with time to the different normalities to base soil mixed with 10% sand and base soil mixed with 20% sand with time, respectively (Figs. 4 and 5). Initially, relative concentration was zero as percolation period increases, the relative concentration increased for 0.1 N of about 0.0884 and reaches the peak. For different combinations of soil + sand, similar trend is attained. Further as time period increases, the relative concentration reduced and remained constant irrespective of normalities. The variation of relative concentration for sodium fluoride solutions with different normalities to base soil with respect to time is depicted (Fig. 6). Initially, relative concentration was zero, as time increases,
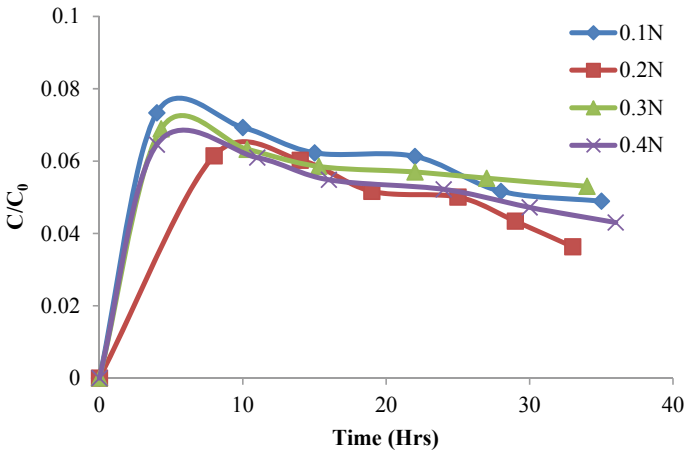
Fig. 4 Breakthrough curves of sodium chloride contaminated soil + 10% sand
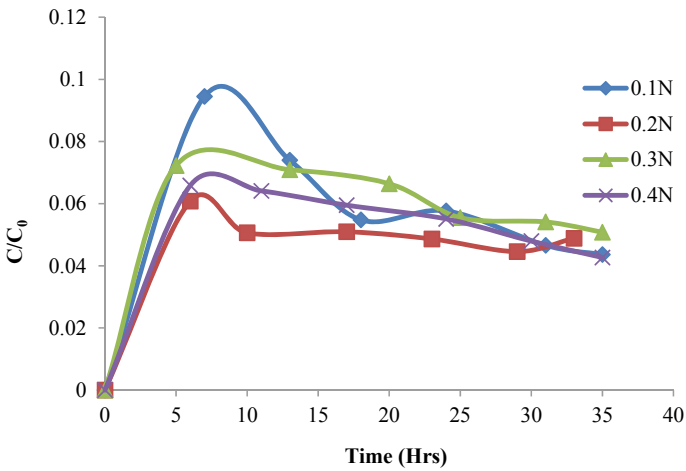
Fig. 5 Breakthrough curves of sodium chloride contaminated soil + 40% sand
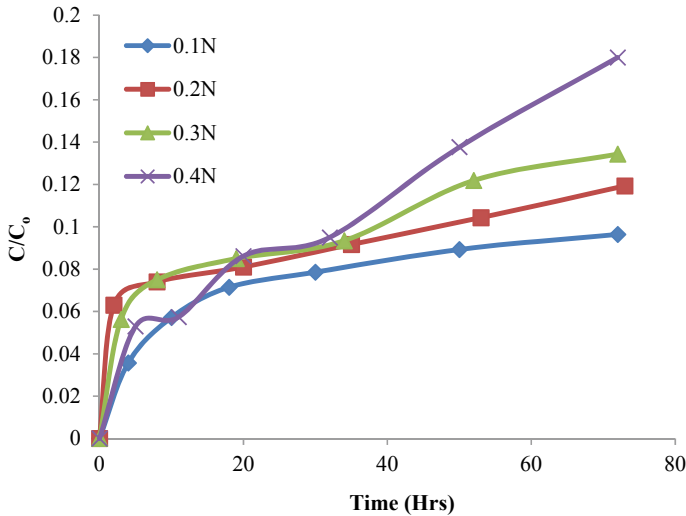
Fig. 6 Variation of relative concentration with time

the relative concentration increased for 0.1 N gets increased till 0.04 and reaches the peak. Further relative concentration increased with time increment and remained constant, and similar nature for all normalities is observed.

Plot showing the variation of relative concentration for sodium fluoride solutions with different normalities to base soil with respect to time is depicted (Fig. 6). Initially, relative concentration was zero as percolation period increases, the relative concentration increased for 0.1 N of about 0.03 and reaches the peak. For different combinations of soil + sand, similar trend is attained. Further as time increases, the relative concentration increased and remained constant throughout similar trend is observed for all normalities.

The breakthrough curves for sodium fluoride solutions with time to the different normalities to base soil mixed with 10% sand and base soil mixed with 20% sand with time, respectively, are obtained (Figs. 7 and 8). Initially, relative concentration was zero as percolation period increases, the relative concentration increased for 0.1 N of about 0.03 and reaches the peak. For different combinations of soil + sand, similar trend is attained. Further as time increases, the relative concentration increased and remained constant throughout similar trend is observed for all normalities.

3.2 Unconfined Compression Strength of Different Proportions

The unconfined compressive strength is carried out for four different contaminated soil samples, i.e., soil, soil + 10% sand, soil + 20% sand, soil + 30% sand and soil
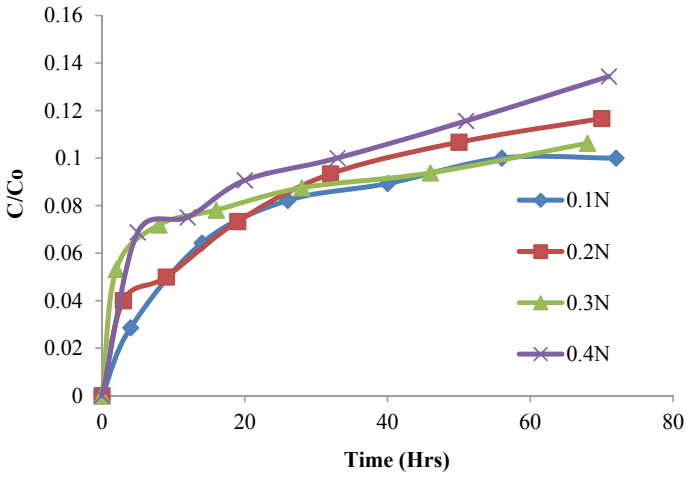
Fig. 7 Breakthrough curves of sodium fluoride contaminated soil + 10% sand
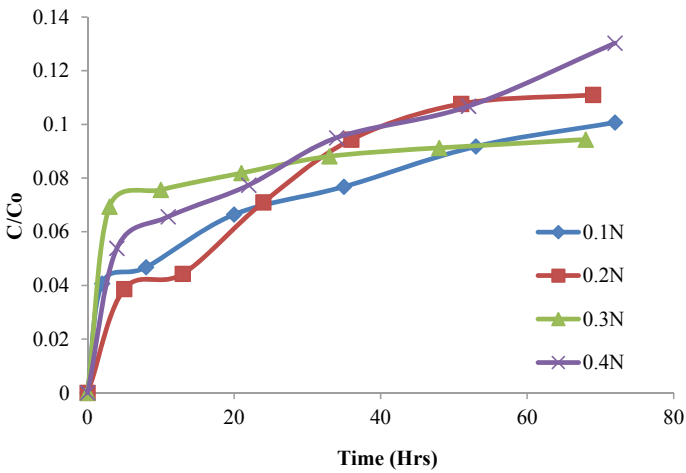
Fig. 8 Breakthrough curves of sodium fluoride contaminated soil + 40% sand

+ 40% sand. Unconfined compressive strength of sodium chloride contaminated soil and sodium fluoride contaminated strength is depicted (Figs. 9 and 10), respectively. The strength of sodium chloride contaminated soil is increased irrespective of concentrations and decreased with increase in percentage addition of sand. For sodium fluoride contaminated soil, reduction in strength is observed.
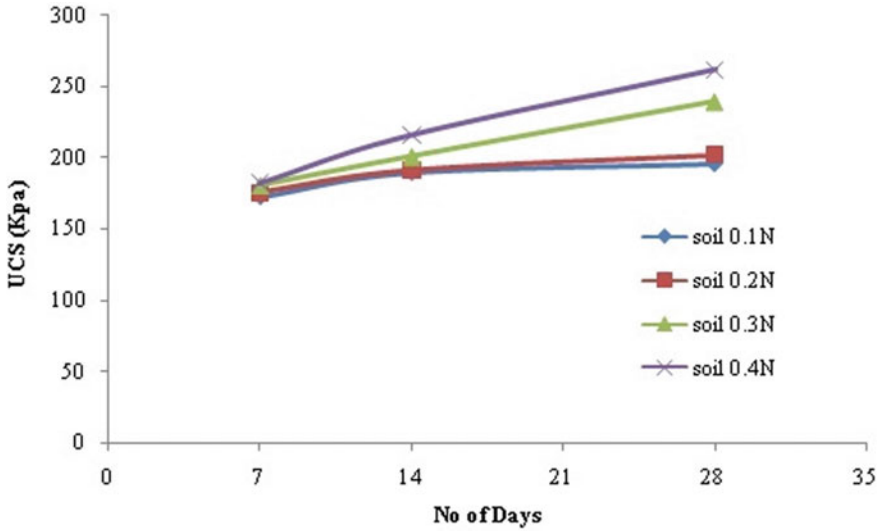
Fig. 9 UCS of contaminated soil with different concentrations sodium chloride
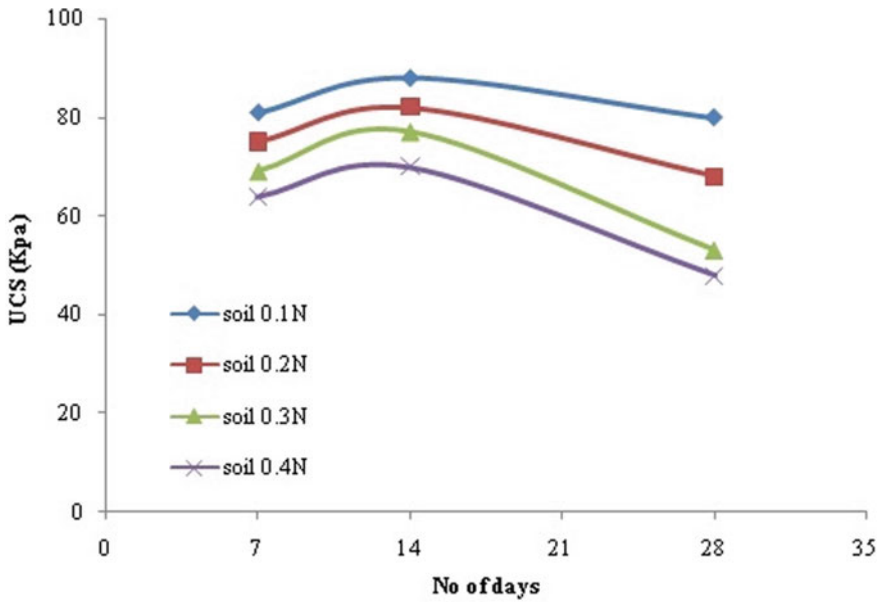
Fig. 10 UCS of contaminated soil with different concentrations sodium fluoride

4 Concluding Remarks

The following conclusions are drawn based on the results of laboratory studies.

1. The soil absorption capacity increases with increase in concentration of contaminants.
2. The result indicates a linear increase in relative concentration for sodium chloride contaminated soil. Different relative concentrations for different combinations are for soil 0.28, 0.32 for soil + 10% sand, 0.33 for soil + 20% sand, 0.33 for soil + 30% sand, 0.34 for soil + 40% sand.
3. For sodium fluoride contaminated soil, the relative concentrations obtained were 0.58 for soil, 0.52 for soil + 10% sand, 0.52 for soil + 20% sand, 0.52 for soil + 30% sand and 0.52 for soil + 40% sand. The trend of decrement in relative concentration is observed for all different normalities of sodium fluoride contaminated soil.
4. As porosity increases, the flow path for the contaminants increases and spreads through the soil longitudinally, and as it spreads laterally, the concentration of contaminant reduces.
5. For all normalities of contaminants, the nature of results obtained follows the footprints of breakthrough curves.
6. The strength of UCS increased for sodium chloride contaminated soil samples. For soil, the UCS value obtained for 0.4 N is 262 kPa, and for different combinations, the strength increased.
7. For different combinations of sodium fluoride contaminated soil, the UCS value corresponding to 0.4 N is 48 kPa, soil + 10% sand is 56 kPa, soil + 20% sand is 54 kPa, soil + 30% sand is 49 kPa, and soil + 40% sand is 44 kPa.
8. It provides a much closer approximation of the physical conditions and chemical processes occurring in the field. When soil is contaminated by sodium chloride, strength of the soil is increased. It can be concluded that sodium chloride is not a harmful contaminant and it can be used as a stabilizing agent. The strength of sodium fluoride contaminated soil is decreased with longer curing period.

References

1. Kumar, P.K., et al.: An experimental methodology for monitoring contaminant transport through geotechnical centrifuge models. J. Environ.l Monitor. Assess. **117**(1–3), 215–233 (2006)
2. Sharma, P.K., et al.: Experimental and numerical simulation of contaminant transport through layered soil. Int. J. Geotech. Eng. **8**(4), 345–351 (2014)
3. Bear, J., Cheng, A.: Modelling Groundwater Flow and Contaminant Transport (Theory and Application in Porous Media) (2010). Springer
4. Domenico, P.A., Schwartz, F.W. Physical and Chemical Hydrogeology, 2nd edn. (1997). Wiley
5. Javadi, S., et al.: Advection and retardation of non-polar contaminants in compacted clay barrier material with organoclay amendment. J. Appl. Clay Sci. **142**, 30–39 (2017)

6. Hou, L., et al.: Evaluation equilibrium and non-equilibrium transport of ammonium in a loam soil column. Water Environ. J. **32**(1), 80–92 (2017)
7. Yu, C., et al.: Study on transport and transformation of contaminant through layered soil with large deformation. J. Environ. Sci. Pollut. Res. **25**(13), 12764–12779 (2018)

Effect of Induced Osmotic Suction and Bentonite Content on Swell Behaviour and Hydraulic Conductivity of Compacted Red Soil

A. S. Devapriya and T. Thyagaraj

Abstract Clay liners are integral part of both hazardous and municipal waste landfills that prevent leachate from percolating into the soil beneath and polluting it. Hence, the compacted soils must have very low hydraulic conductivity ($<10^{-7}$ cm/s) to act as effective clay liners. Locally available red soil may be used as a liner material as it satisfies the design criteria. To meet the hydraulic conductivity requirement, the locally available red soil was modified by adding 10% and 20% bentonite by dry weight. Multiple identical compacted specimens were set-up in oedometric assemblies under a surcharge pressure of 12.5 kPa and were inundated with distilled water, 0.4 M $CaCl_2$ and 0.4 M NaCl solutions to study the swelling behaviour of red soil and red soil modified with different bentonite contents. The specimens were compacted at their respective optimum moisture content values to their maximum dry unit weights. Falling head permeability tests were conducted to measure hydraulic conductivity using the rigid wall permeameters at a hydraulic gradient of 20 and surcharge pressure of 12.5 kPa. The nature of the inundating fluid and the bentonite content is seen to greatly affect the swelling behaviour and the hydraulic conductivity of the compacted red soil.

Keywords Compacted soil · Modified clay · Clay liners · Swell–shrink paths · Hydraulic conductivity

1 Introduction

Clay liners are integral part of both hazardous and municipal waste landfills. They are compacted using clay soils of very low permeability so that the leachate does not percolate into the underlying ground and pollute it. Different environment Protection

---

A. S. Devapriya (✉) · T. Thyagaraj
Department of Civil Engineering, IIT Madras, Chennai, India
e-mail: devapriya.as09@gmail.com

T. Thyagaraj
e-mail: ttraj@iitm.ac.in

Agencies specify that the soils used for clay liners should have a hydraulic conductivity value as low as 10^{-7} cm/s [1, 2]. Bentonite is commonly mixed with locally available in-situ soils when they do not have the required hydraulic conductivity characteristics as the bentonite is known to possess high specific surface area and sealing characteristics [3–5]. In addition to the hydraulic conductivity characteristics, the swell–shrink behaviour of the compacted clay liners is also of importance. Daniel and Wu [6] recommended a maximum volumetric shrinkage of 4% for soils to be used as clay liners. The extent of volume change depends on the type and amount of the clay mineral, soil structure, compaction conditions, physico-chemical factors and environmental factors [7].

In the field, constant leachate interactions occur with the compacted soil, which causes the physico-chemical changes in the soil. Because of the difference in dissolved salt concentration between the soil and leachate, an osmotic gradient is developed, which in turn causes diffusion of salt into the soil, and thereby a reduction in the diffused double layer thickness [8, 9]. Previous studies show that the swell potential decreases with the reduction in the diffused double layer thickness [10]. The increase in osmotic gradient also causes an increase in the hydraulic conductivity. Further, the divalent cations impart higher osmotic suction and cause greater increase in hydraulic conductivity than with the monovalent cations [11].

This paper presents the effect of bentonite content and induced osmotic suction on the swell and hydraulic conductivity of compacted red soil. To study the swelling behaviour, series of one-dimensional oedometric swell tests were conducted on identical soil specimens prepared using distilled water and inundating them with distilled water, 0.4 M NaCl and 0.4 M $CaCl_2$ solutions. After complete swelling, the hydraulic conductivity was determined for each specimen by conducting falling head permeability tests.

2 Material Properties

Red soil used for the present study was collected from IIT Madras campus, Chennai, Tamil Nadu. It was air dried, passed through 2 mm sieve (No.10 sieve), and mixed thoroughly for homogenous base material and stored in containers. Commercially available sodium bentonite was procured and used for the study. Red soil–bentonite mixtures were prepared in two proportions: 10% and 20% bentonite by dry weight, and they were designated as B1 and B2, respectively (Table 1). Characteristics of the red soil, bentonite and red soil–bentonite mixtures are presented in Table 2. Figures 1 and 2 show the grain size distribution and the compaction curves of the soils used for the present study, respectively. Laboratory grade NaCl and $CaCl_2$ dehydrate were used for the preparation of solutions.

Table 1 Soils used for the present study

Soil	Soil designation	Proportions of soils	
		Red soil (%)	Bentonite (%)
Red soil	A	100	0
Red soil–bentonite mixture-1	B1	90	10
Red soil–bentonite mixture-2	B2	80	20

Table 2 Characteristics of red soil, bentonite and red soil–bentonite mixtures

Property	Soil designation			
	A	Bentonite	B1	B2
Liquid limit (%)	34	224	86	113
Plastic limit (%)	20	48	27	35
Shrinkage limit (%)	15	8.4	15	13
Plasticity index (%)	14	176	59	78
Specific gravity	2.68	2.92	2.70	2.73
Soil classification	SC	CH	SC	SC
Maximum dry unit weight (kN/m^3)	19.4	–	18.75	17.6
Optimum moisture content, OMC (%)	11	–	12.5	15
Unconfined compressive strength (kPa)	212	–	230	251

Fig. 1 Grain size distribution curves
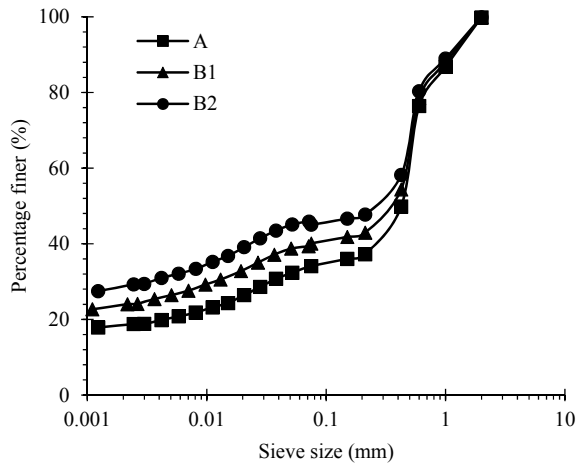
Fig. 2 Compaction curves
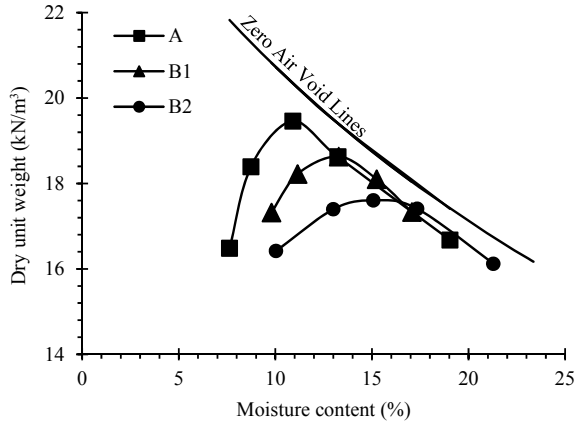
Table 3 Details of compacted specimens and inundating fluids

Soil specimen	Inundating fluid	Osmotic suction induced (kPa)
A	DW	0
	DW	0
B1	0.4 M NaCl solution	1,951
	0.4 M CaCl$_2$ solution	2,927
B2	DW	0
	0.4 M NaCl solution	1,951
	0.4 M CaCl$_2$ solution	2,927

3 Experimental Programme

3.1 Preparation of Soil Specimens

Red Soil, A and red soil–bentonite mixtures, B1 and B2, were pre-wetted with desired volume of water corresponding to their respective OMC values and stored in plastic covers for 48 h in the desiccator for moisture equilibration. The water content was then measured to ensure that the target water contents were achieved. Identical samples were prepared using these pre-wetted soils by statically compacting them in oedometer rings of height 30 mm and diameter 75 mm, to an initial height of 20 mm such that their respective standard Proctor maximum dry unit weight values were attained.

3.2   One-Dimensional Oedometer Swell Tests

The identical soil specimens were placed between two porous stones and filter papers and were assembled in the test set-ups under a surcharge pressure of 12.5 kPa. The identical soil specimens were then inundated with distilled water, 0.4 M NaCl solution and 0.4 M CaCl$_2$ solutions separately. The details of the compacted specimens and inundating fluids are given in Table 3. The vertical deformations were noted using dial gauge of 0.002 mm least count till the vertical deformations became constant, and the swell potential was calculated using Eq. 1.

$$\text{Swell}(\%) = \frac{\Delta H}{H} 100 \tag{1}$$

where ΔH is the increase in height of soil specimen during swelling and H is the initial as compacted height of soil specimen.

The induced osmotic suction is calculated using the van't Hoff equation (Eq. 2)

$$\pi = iMRT \tag{2}$$

where M is the maximum dissolved salt concentration of the inundating fluid (mol/L), R is the universal gas constant, T is the absolute temperature (K) and i is the van't Hoff factor ($i = 2$ for NaCl solution and $i = 3$ for CaCl$_2$ solution).

3.3   Rigid Wall Hydraulic Conductivity Tests

After the completion of swelling, the hydraulic conductivity of the saturated specimens was determined using falling head method in rigid wall permeameters in accordance with ASTM D 5856-15 [12]. The tests were conducted using the same inundating fluid used for swelling under a hydraulic gradient of 20 and a surcharge pressure of 12.5 kPa.

4   Results and Discussions

4.1   Effect of Bentonite Content on Swell and Hydraulic Conductivity

Figure 3 presents the time-swell plots of compacted red soil and red soil–bentonite mixtures. The swell curves are S-shaped curves with three distinctive phases: (i) initial swelling, (ii) primary swelling and (iii) secondary swelling. The initial swell
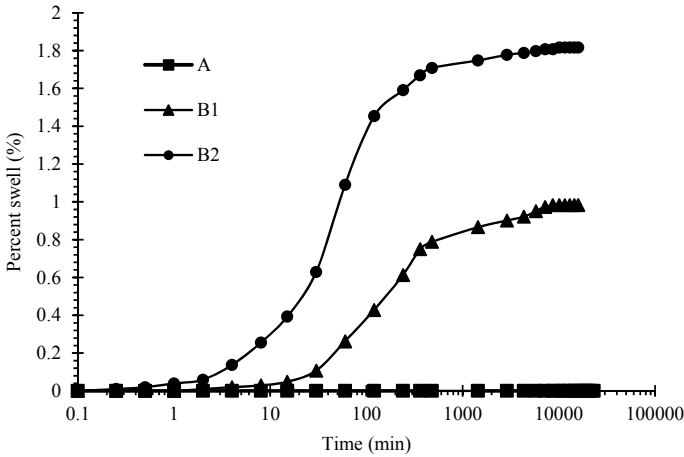
Fig. 3 Time-swell plots of compacted red soil and red soil–bentonite mixtures inundated with distilled water
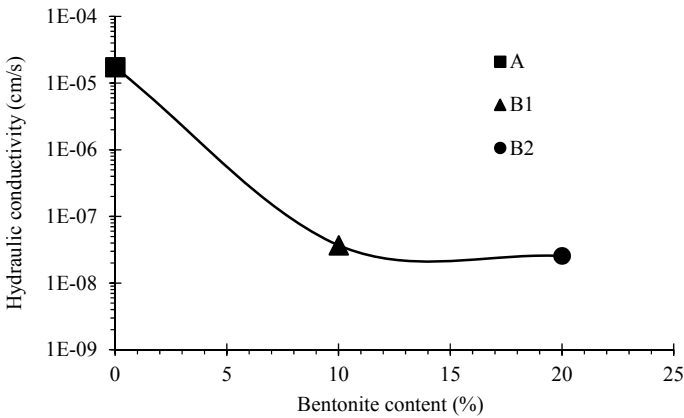
Fig. 4 Effect of bentonite content on hydraulic conductivity of red soil using distilled water as inundating fluid

takes more time to finish in B1 than in B2 owing to its lesser bentonite content, resulting in larger voids, and hence longer intervoid swelling [13]. Figure 3 shows that the compacted red soil showed no swell when inundated with distilled water, whereas red soil containing bentonite swelled. As the bentonite content increased, the magnitude of swell also increased. By adding bentonite to the red soil, a fraction of non-swelling red soil was replaced by a fine-grained soil with high swelling potential, which absorbs water into its crystal lattice. Thus, the diffused double layers around the soil particles expanded, and hence the swell potential is higher.

Figure 4 brings out the effect of bentonite content on hydraulic conductivity of compacted red soil. It can be seen that the addition of bentonite to the red soil reduces the hydraulic conductivity values. This is because of the high specific surface area and high swelling potential of bentonite which absorbs more water into its crystal lattice and expands its double layers, thereby reducing the macropores in the soil specimen and thus the hydraulic conductivity [3].

4.2 Effect of Osmotic Suction on Swell Potential and Hydraulic Conductivity

Figure 5(a and b) brings out the effect of osmotic suction on compacted red soil with 10% and 20% bentonite contents, respectively. The figures clearly show that the specimens inundated with salt solutions show a reduction in swell potential than the specimens inundated with distilled water. The reduction in swell is more for specimen inundated with divalent Ca^{2+} cations than monovalent Na^+ cations. When the soil specimen is inundated by salt solutions, it is being subjected to an osmotic gradient because of the difference in dissolved salt concentration in the soil pore water and the external reservoir solution. Soil being an imperfect semi-permeable membrane allows the transfer of salt through diffusion. This diffusion of salts results in the reduction of diffused double layer thickness, which in turn reduces the swell potential [9]. In Fig. 5b, all the three plots of B2 are S-shaped. However, there is a delay in the beginning of primary swelling of soil inundated with $CaCl_2$ solutions. Figure 5a shows that soil specimen B1 inundated by $CaCl_2$ solution shows no swell. $CaCl_2$ solution induces higher osmotic suction, resulting in a larger reduction of double layer, and hence the swelling occurs only in the intervoid space.

Figure 6(a and b) brings out the effect of salt concentration and induced osmotic suction on the hydraulic conductivity of the red soil–bentonite mixtures, respectively. The hydraulic conductivity increased with inundating fluid concentration and osmotic suction. When the soil is inundated with salt solution, because of the concentration gradient between the soil pore water and the external reservoir solution, the induced osmotic suction develops in the soil. This increase in suction is dissipated by absorbing salt solution into the partially saturated soil pores [9]. The diffusion of salt into the soil causes a reduction in the diffused double layer thickness which decreases the volume of micropores and increases the volume of macropores in the soil, which in turn results in a higher hydraulic conductivity in specimens inundated with salt solution. Higher the salt concentration and the valency of the ions, higher will be the induced osmotic suction.
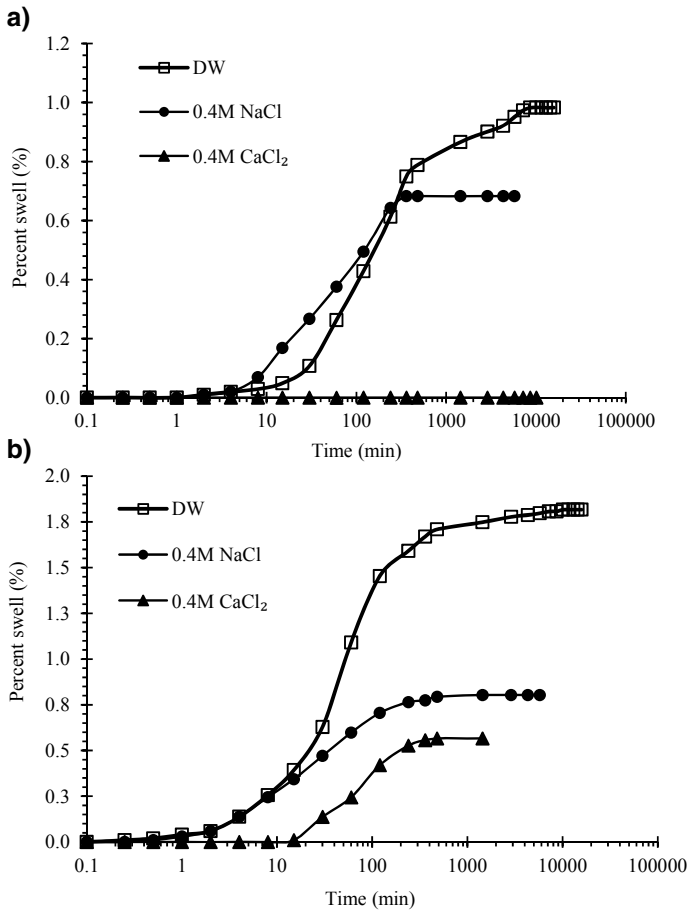
Fig. 5 **a** Effect of salt concentration on time-swell plots of compacted red soil–bentonite specimen B1. **b** Effect of salt concentration on time-swell plots of compacted red soil–bentonite specimen B2

5 Conclusions

Based on the above study, the following conclusions can be drawn.

- Addition of bentonite to the red soil increases the swell potential of the soil due to the expansion of diffused double layers. The hydraulic conductivity of soil which is largely dependent on macropores in the soil reduces due to the closing of macropores when the double layers expand.
- Exposure of compacted red soil–bentonite specimens to salt solutions has significant effect on the swell potential and hydraulic conductivity as well. The swell potential decreases, and hydraulic conductivity increases when the compacted soil
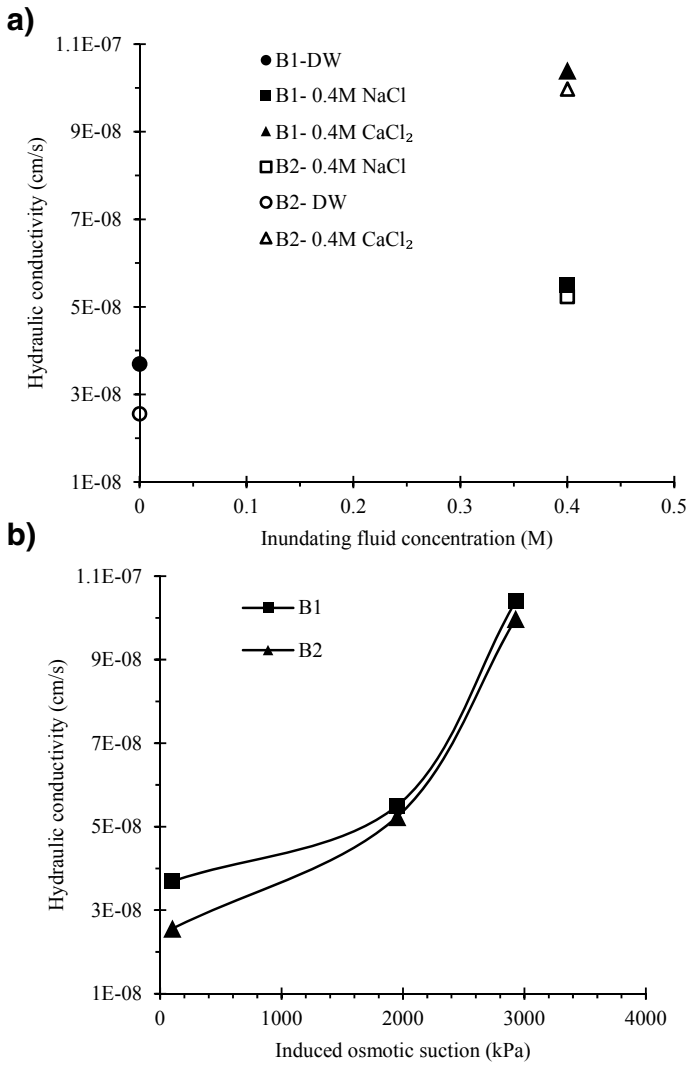
Fig. 6 **a** Variation of hydraulic conductivity with inundating fluid concentration. **b** Effect of induced osmotic suction on hydraulic conductivity of red soil–bentonite mixtures

is inundated with solutions, rather than with distilled water. This effect is more with divalent Ca^{2+} cations than with monovalent Na^+ cations.

References

1. UK Environmental Agency: LFE04—earthworks in landfill engineering. Eng. Guid. 1–66 (2011)
2. US EPA: Industrial Waste Management: Protecting Land, Ground Water, Surface Water, and Air, Chap. 7, 7B-1–7B-30 (2009)
3. Kumar, S., Yong, W.L.: Effect of bentonite on compacted clay landfill barriers. Soil Sediment Contamination Int. J. **11**, 71–89 (2002)
4. Sallfors, G., Oberg-Hogsta, A.L.: Determination of hydraulic conductivity of sand-bentonite mixtures for engineering purposes. Geotech. Geol. Eng. **20**, 65–80 (2002)
5. Sivapullaiah, P.V., Lakshmikantha, H.: Properties of fly ash as hydraulic barrier. Soil and Sediment Contamination **13**, 391–406 (2004)
6. Daniel, D.E., Wu, Y.K.: Compacted clay liners and covers for arid sites. J. Geotech. Eng. ASCE **119**(2), 223–237 (1993)
7. Yong, R.N., Warkentin, B.P.: Soil Properties and Behaviour, 1st edn. (1975). Elsevier Scientific Publishing Company
8. Di Maio, C.: Exposure of bentonite to salt solution: osmotic and mechanical effects. Geotechnique **46**(4), 695–707 (1996)
9. Rao, S.M., Thyagaraj, T.: Swell–compression behaviour of compacted clays under chemical gradients. Can. Geotech. J. **44**, 520–532 (2007)
10. Thyagaraj, T., Rao, S.M.: Influence of osmotic suction on soil-water characteristic curve of compacted expansive clay. J. Geotech. Geoenviron. Eng. **136**(12), 1695–1702 (2010)
11. Mishra, A.K., Ohtsubo, M., Li, L., Higashi, T.: Effect of salt concentrations on the permeability and compressibility of soil-bentonite mixtures. J. Faculty Agric. Kyushu Univ. **50**(2), 837–849 (2005)
12. ASTM D5856-15: Standard test method for measurement of hydraulic conductivity of porous material using a rigid-wall, compaction-mold permeameter, ASTM International, West Conshohocken, PA (2015)
13. Sivapullaiah, P.V., Sridharan, A., Stalin, V.K.: Swelling behaviour of soil-bentonite mixtures. Can. Geotech. J. **33**, 808–814 (1996)

Use of Fly Ash as Weak Cementing Agent to Strengthen Marine Clay

Sayali Belawadikar, D. S. Patil, and Ashish Juneja

Abstract Constructions on problematic soils are inevitable due to the increasing demand for land in the existing scenario. India has a coastline of 7500 km with large deposits of marine clay. Soft soils like marine clay are considered problematic due to its swelling behavior, low permeability, and highly compressibility. Landfill sites and reclamation areas formed due to dumping of dredged soft soils experiences high settlement and poor bearing capacity making it unsuitable as a foundation material. Atterberg limits represent the water holding capacity of soil. It can also contribute to estimation of shear strength, settlement, and permeability of soil. Researchers have explored various methods to reduce water holding capacity of marine clay and thereby enhance its engineering properties. Effective additives like fly ash, rice husk ash, marble dust, granite dust are widely mixed with marine soil to stabilize and improve its engineering behavior. Fly ash is a waste material produced in large amount at coal or lignite-based thermal power station. It requires large area of land for disposal as ash ponds as well as it causes air and water pollution. To address the adverse impact of dumping of fly ash on environment, wise utilization of fly ash is essential. In the present study, the effect of addition of Class F fly ash on liquid limit and plastic limit of marine clay and bentonite was studied. Marine clay obtained from Mumbai coast and bentonite from Kutch, Gujarat, was used in the tests. The liquid limit of the soil was determined using fall cone apparatus. Initially, the tests were performed on virgin clay only. Then the fly ash was added, and the percentage of fly ash in the soil was varied. The percentage of fly ash mixed in the soil ranges from 10 to 70%. The variation in liquid and plastic limit with the addition of fly ash was examined. It was observed that the plasticity index reduced by 60% in marine soil. Addition of fly ash reduced water absorption capacity of soil which in turn resulted in significant reduction in plasticity of soil. The usage of fly ash in improving clay with active minerals is novel and beneficial for reusing industrial waste products.

S. Belawadikar (✉) · D. S. Patil
Rajarambapu Institute of Technology, Islampur, Maharashtra, India
e-mail: sayalibelewadikar@gmail.com

A. Juneja
Indian Institute of Technology Bombay, Mumbai, Maharashtra, India

1 Introduction

The stability of structure largely depends upon the performance of soil underlying it. Understanding the behavior of soil under various loading conditions is necessary for appropriate design of foundations. Water present in the soil matrix has a significant effect on the engineering properties of soil. Water holding capacity of any soil generally depends on the mineralogical composition. Soil can be classified in to four types according to water content as solid state, semisolid, liquid, and plastic state. Atterberg limits, namely liquid limit, plastic limit, and shrinkage limit, gives an idea about soil state transformation from liquid to plastic, plastic to semi-solid, and then finally to solid. Atterberg limits indicate how much a soil is likely to settle or consolidate under load. Higher settlement is expected if the field moisture content is close to the liquid limit and vice versa. Behavior of soil will be different in every state of soil. Hence, these tests are conducted at primary stage of soil investigation. Liquid limit can be determined using Casagrande apparatus as well as fall cone. Casagrande method has some limitations such as human error associated with cutting of ideal groove, and type of base. This may lead to improper results. In this study, fall cone apparatus was preferred as it is comparatively accurate and easy to perform. It can be used to determine shear strength as well. This study follows the method given by Mahajan and Budhu [7] in which instrumented fall cone penetrometer was used to determine viscosity close to liquid limit.

Fly ash is a residue of coal combustion at power generation and incineration plants. As compared to imported coal, Indian coal is of low grade with 30–45% ash while imported coal contains only 10–15% ash. In India, large amount of fly ash is produced yearly which require large area for disposal and is a major cause for water as well as air pollution. Fly ash can be used to lower water content of soils. Fly ash reduces the potential of plastic soil to undergo volumetric expansion by a physical cementing mechanism. Fly ash acts as cementing material to bind soil particles together to control expansion similar to Portland cement bonds between aggregate to form concrete. Polidori [10] conducted test on six types of soils and their mixtures with silica sand to determine relation between Atterberg limits. Kumar and Wood [6] conducted test on mixture of kaolin and fine gravel to determine change in liquid limit with respect to clay content in mixture. Linear relation was observed in order to logarithm of cone penetration. Fall in liquid limit value was noted with reduction of clay content. Zainuddin et al. [15] noted reduction in liquid limit and plastic limit with addition of demolished tile dust in marine clay.

2   Materials and Experimental Setup

In the present study, Marine clay was used collected from Mumbai coast. This soil had liquid limit (LL) of 75.92% and plastic limit (PL) of 31.74%. The specific gravity of clay was 2.82, and it comes under CH group. This soil has 8.2 pH values. Maximum dry density of 1.42 Mg/m^3 at corresponding optimum moisture content of 22% was observed.

A fall cone apparatus (BS 1377, British standard Institution, 1990) with 30º smooth cone was used in this study. Its dial gauge was replaced by potentiometer (LVDT) and connected to high-speed data logger as previously done by Budhu [7]. Figure 1 shows the experimental set up. The total mass of cone assembly with cone, shaft, and LVDT was 0.89 N.

2.1   Sample Preparation

About 150 g of oven-dried soil passing through 425 micron sieve was used to determine the Atterberg limits. Fly ash was mixed with dry marine at varying percentage ranging from 10 to 70% by weight of soil. Distilled water was added to the above mixture and mixed homogenously. The sample was then kept in airtight container and left overnight to ensure proper absorption of moisture.
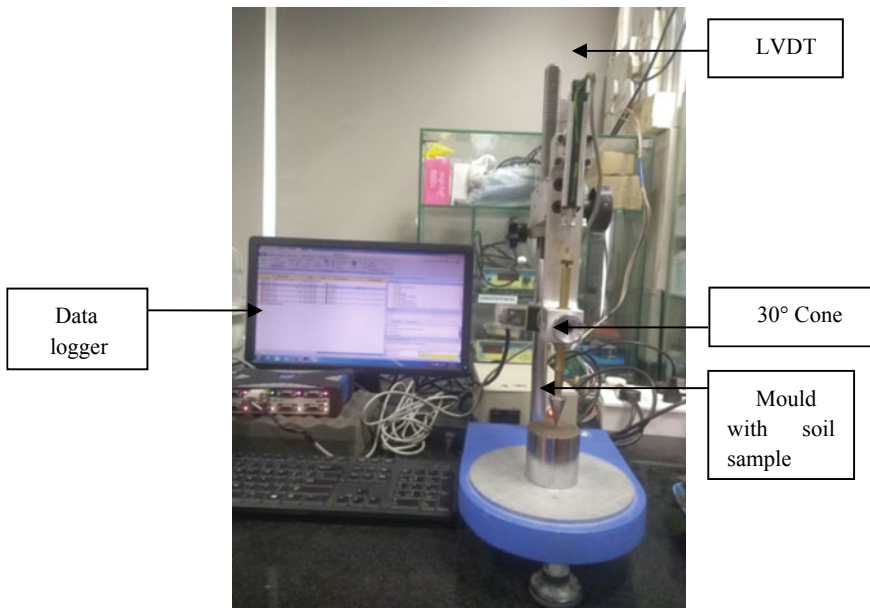
Fig. 1   Modified fall cone apparatus

2.2   Test Procedure

About 150 g of sample was taken with different percentage of clay–fly ash mixture as mentioned earlier. The mold was then filled with wet sample paste by tamping to remove the entrapped air. The cone was lowered just to touch the surface of the soil sample and then allowed to penetrate freely for 5 s. Depth of penetration of cone was recorded by the data logger at the sampling rate of 0.01 s. Same procedure was adopted for every trial by slowly adding water to the soil mixture. Water contents of the sample corresponding to 14–24 mm penetration were taken. Relation between the water content and penetration depth was plotted, and the liquid limit was obtained by interpolating the results at 20 mm depth of penetration.

3   Results and Discussion

The procedure followed for conducting the fall cone test is as per IS [3] (Part 5). Conventional cone was modified by attaching a potentiometer to the apparatus. Table 1 shows one of the trial result obtained by fall cone penetration which represents all the tests. Shear viscosity was determined using the equation proposed by Budhu [7]

$$\mu_p = 2.94 \text{KW} \sqrt{h_f} \left(\frac{0.67}{h_{\text{eq}}} - \frac{1}{h_{\text{f}}} \right)^2 \tag{1}$$

Table 1 Determination of shear strength and shear viscosity

S. No.	h_{f} (mm)	h_{eq} (mm)	Water content (%)	LI	Weight (N)	τ_{cs} (kPa)	τ (kPa)	$\Upsilon^{\cdot\cdot}$/s	μ (pa s)
1	13.94	4.28	70.65	0.88	0.89	6.09	28.89	2.88	2955
2	14.5	4.73	71.81	0.91	0.89	5.63	23.65	2.82	2214
3	15.6	6.3	73.07	0.94	0.89	4.86	13.33	2.72	776
4	16.88	6.75	74.52	0.97	0.89	4.15	11.61	2.62	724
5	18.73	7.52	77.3	1.03	0.89	3.37	9.36	2.48	607
6	19.34	8.17	78.32	1.05	0.89	3.16	7.93	2.44	444
7	21.47	9.58	81.92	1.14	0.89	2.57	5.77	2.32	278
8	22.2	9.75	82.36	1.15	0.89	2.40	5.57	2.28	291
9	23	10.3	84.01	1.18	0.89	2.24	4.99	2.24	246
10	24.47	11.25	86.79	1.25	0.89	1.98	4.18	2.17	190

where μ is the shear viscosity, h_f is the final depth of penetration, h_{eq} is equilibrium depth of penetration at which velocity reaches to its maximum as shown in Fig. 4, K is modified cone factor (Koumoto and Houlsby, [5] and W is weight of cone assembly.

As well the shear strength of the soil as shown in Eq. (2), Mahajan and Budhu [7] were determined using equilibrium depth.

$$\tau = \frac{W}{Fh_{eq}^2} \tag{2}$$

where

W	is the weight of the cone assembly (cone and shaft)
τ	is the maximum shear strength of the soil sample
h_{eq}	is the dynamic equilibrium height
F	is the non-dimensional cone resistance factor define by [5].

$$F = \pi N_{ch} \tan^2 \theta$$

where

| N_{ch} | is the modified bearing capacity factor for a 30° semi-rough cone |
| θ | is the half angle of cone. |

Sample time penetration data recorded by the data logger is shown in Fig. 2. Velocity of the cone was obtained by differentiating the polynomial conforming to the time penetration data and plotted with respect to penetration depth in Fig. 3.
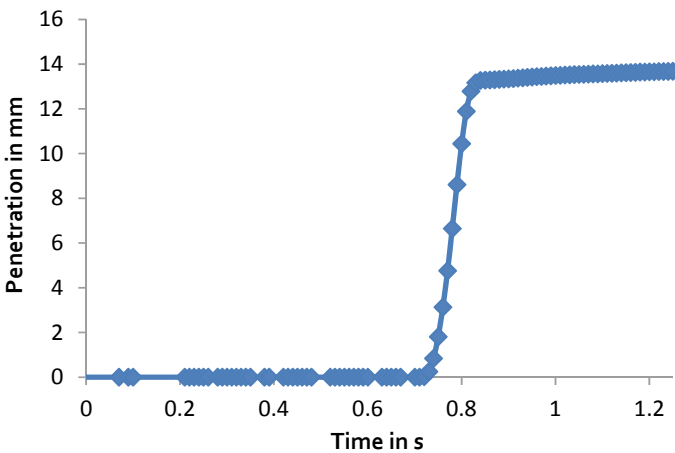
Fig. 2 Time penetration data obtained by data logger
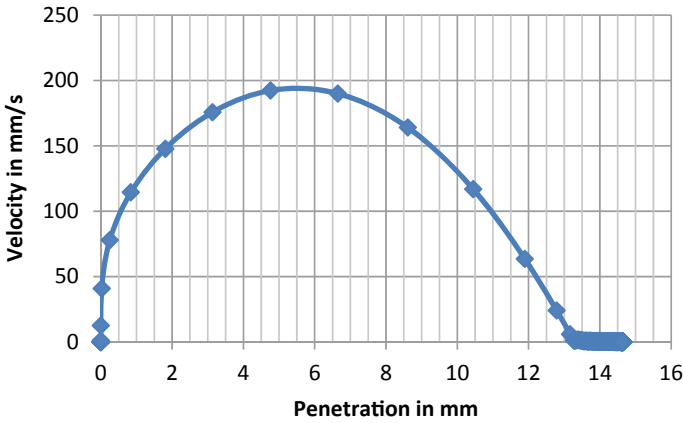
Fig. 3 Velocity versus penetration plot
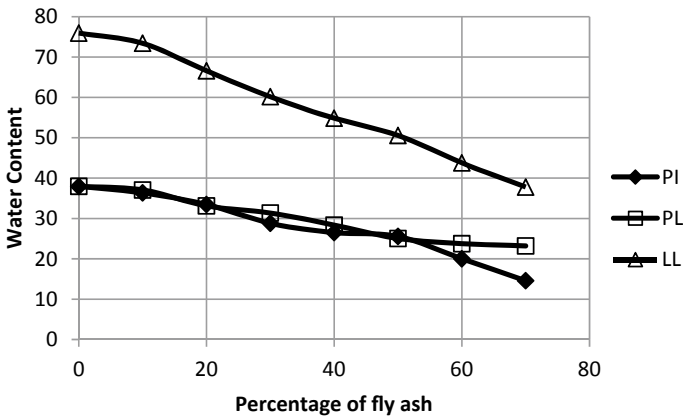
Fig. 4 Atterberg limits with different fly ash content

Figure 3 shows plot of velocity versus penetration depth. Velocity is obtained by differentiating polynomial when velocity of cone increases up to its maximum value at equilibrium depth and starts decreasing. In this case, equilibrium height of 4.76 mm was obtained at maximum cone velocity of 191 mm/s.

4   Results and Discussion

The water holding capacity of marine clay mixed with varying percentage of fly ash was determined using fall cone test. Shear viscosity and shear strength were

also interpreted from the fall cone test results using the equations given by previous researchers Hansbo [2], Koumoto and Houlsby [5], Mahajan and Budhu [7].

Figure 4 shows the variation in liquid limit and plastic limit with addition of fly ash in marine clay. Clear decrease in the plasticity index of about 60% was observed for soil mixtures. The workability of the soil–fly ash mixture improved with rise in fly ash percentage, besides drop in volume of soil sample at similar water content. The probable reason for this change can be attributed to the replacement of montmorillonite mineral with fly ash.

Liquid limit and plastic limit were plotted against the varying clay fractions for the soil mixtures as shown in Fig. 5. The Atterberg limits varied linearly with clay fraction.

The variation of water content with depth for different combination of Marine clay–fly ash is plotted in Fig. 6. Significant reduction in the water content was observed at identical penetration depth for higher fly ash content. This indicates reduction in water absorption and thereby improving the engineering properties.

Figures 7 and 8 represent relationship between shear strength, shear viscosity, and water content for marine clay, respectively. Figure shows approximately similar pattern with sand and clay mixture studied by Cabalar and Mustafa [1]. Mixing fly ash with marine clay regulates its water holding capacity and improves its shear strength and shear viscosity. Water content reduced linearly with increase in fly ash percentage. However shear strength reached peak value at 50% and then dropped on further addition of fly ash. Therefore, optimum fly ash content can be considered as 50%.
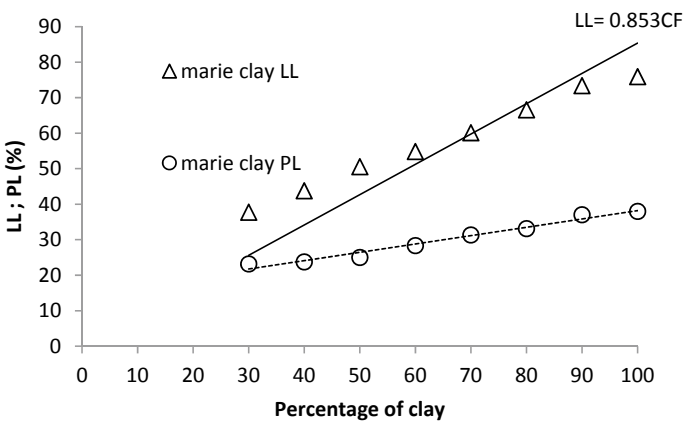
Fig. 5 Relationship between clay fraction and liquid limit; plastic limit of soil
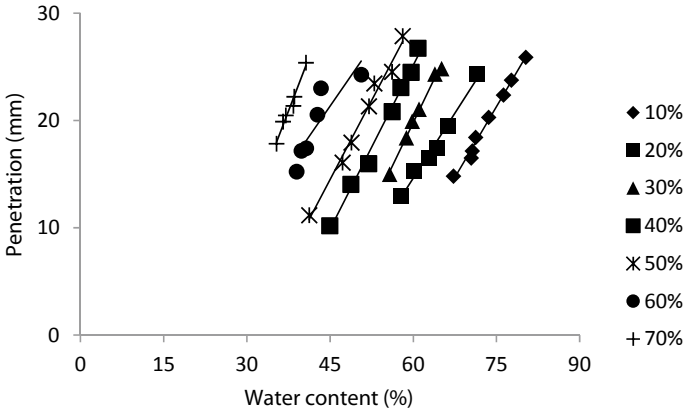
Fig. 6 Water content with respect to penetration for marine clay
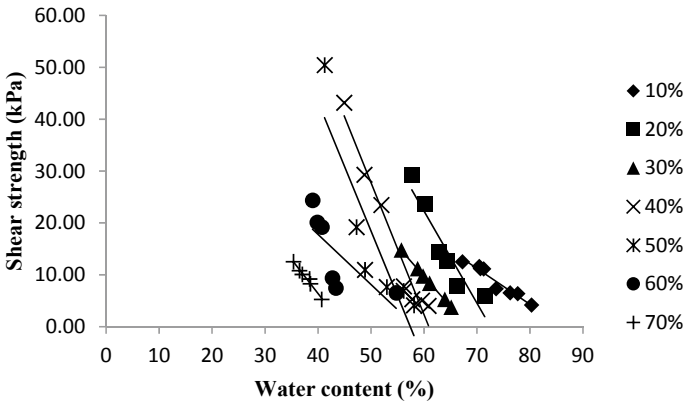
Fig. 7 Shear strength versus water content relationship of soil

5 Conclusions

Fall cone tests were performed using marine clay in the study. Dredged marine soil is problematic due to its high water absorption capacity. Fly ash was added to soil in varying percentage to reduce its water holding capacity and improve its engineering properties. Following conclusions were drawn from the present study:

- Mixing of fly ash to marine clay results in notable reduction in plasticity index. About 60% reduction in plasticity index was observed in the soil mixtures.
- Clay content in the soil mixture predominantly affects the liquid limit. Clay content varies linearly with liquid limit and plastic limit.
- Shear strength and shear viscosity decreased exponentially with increase in liquidity index. Addition of 50% fly ash with marine clay exhibited maximum
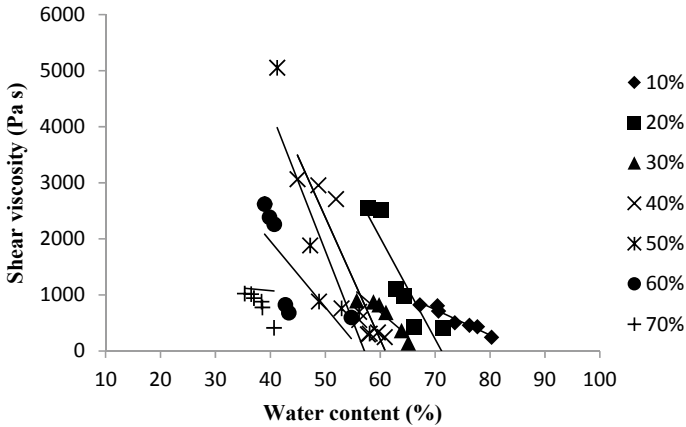
Fig. 8 Relationship between water content and shear viscosity

shear strength and viscosity. Replacement of cohesive clay with non plastic fly ash might be the reason for reduction in strength on further addition of fly ash in soil.

References

1. Cabalar, A.F., Mustafa, W.S.: Fall cone tests on clay–sand mixtures. Eng. Geol. **192**, 154–165 (2015)
2. Hansbo, S. (1957). A new approach to the determination of the shear strength of clay by the fall-cone test. In: Proceeding Royal Swedish Geotechnical Institute, vol. 14. Royal Swedish Geotechnical Institute, Stockholm, pp. 1–47
3. IS 2720: 1983 Method of test for soils, part 5, Determination of liquid and plastic limits (Second revision)
4. Juneja, Krishnan: The use relationship between shear strength, shear viscosity and liquidity index. Conference paper (2015)
5. Koumoto, T., Houlsby, G.T.: Theory and practice of the fall cone test. Géotechnique **51**(8), 701–712 (2001)
6. Kumar, G.V., Wood, D.M.: Fall cone and compression tests on clay-gravel mixtures. Geotechnique **49**(6), 727–739 (1999)
7. Mahajan, S.P., Budhu, M.: Shear viscosity of clays using the fall cone test. Géotechnique **59**(6), 539–543 (2009)
8. Mitchell, J.K.: Fundamental of soil behavior (1976). Wiley, Inc.
9. Nagaraj, H.B., Sridharan, A., Mallikarjuna, H.M.: Re-examination of undrained strength at Atterberg limits water contents. Geotech. Geol. Eng. **30**(4), 727–736 (2012)
10. Polidori, E.: Relationship between the Atterberg limits and clay content. Soils Found. **47**(5), 887–896 (2007)
11. Report on fly ash generation at coal/lignite based thermal power station and its utilization in country for year 2017–2018 by Central electricity authority
12. Sridharan, A., Prakash, K.: Percussion and cone methods of determining the liquid limit of soils: controlling mechanisms. Geotech. Test. J. **23**(2), 236–244 (2000)

13. Prakash, K., Sridharan, A.: Critical appraisal of the cone penetration method of determining soil plasticity. Can. Geotech. J. **43**(8), 884–888 (2006)
14. Wood, D.M., Wroth, C.P.: The use of the cone penetrometer to determine the plastic limit of soils. Ground Eng. **11**(3) (1978)
15. Zainuddin, N., Yunus, N.Z.M., Al-Bared, M.A.M., Marto, A., Harahap, I.S.H., Rashid, A.S.A.: Measuring the engineering properties of marine clay treated with disposed granite waste. Measurement **131**, 50–60 (2019)

Physical and Swell Behaviour of Sand–Bentonite and Marble Dust–Bentonite Mixes

Ankush Kumar Jain, Ayush Kumar, and Arvind Kumar Jha

Abstract Numerous researches have been carried out on bentonite amended with soils (commonly sand) to form barriers material for waste disposal projects such as landfill, cores of earth dams and radioactive waste repository systems. However, the development of sustainable geo-materials is still a greater concern for geotechnical engineer. Bulk utilization of marble dust, produced in the Rajasthan, is a serious concern for safe environment. In the present study, an attempt has been made to modify the behaviour of marble dust with bentonite to develop a novel liner material for landfill system. Further, the behaviour of marble dust amended with bentonite has been compared with sand–bentonite mixture which is known to be used as a liner material. Atterberg's limits, free swell index (FSI) and compaction characteristics (i.e. optimum water content and maximum dry density) of various proportion of both sand–bentonite and marble dust–bentonite mixtures (0:100–100:0) were determined. It is observed that MDD and OWC of sand reduce and, increase with an increase in its substitution with bentonite, respectively. The similar tendencies have been observed for marble dust–bentonite mixes. Further, the FSI of sand and marble dust is also observed to be increased drastically with its substitution with bentonite. The physicochemical examinations (pH and electrical conductivity (EC)) of entire mixes have been performed to elucidate the mechanism**.**

Keywords Bentonite · Liner · Marble dust · Sand · Swell

1 Introduction

The generation of hazardous wastes gradually due to rapid advancement in technology and population has led to create many problems such as waste management [1]. Until the middle of this century, all unwanted waste were being used to discard

A. K. Jain · A. Kumar
Manipal University Jaipur, Jaipur, Rajasthan 303007, India

A. K. Jha (✉)
Indian Institute of Technology Patna, Patna, Bihar 801106, India
e-mail: jhaarvind@iitp.ac.in

in open un-engineered dumps or, to bury it in land with very little attention given to their environmental impact [2]. The natural depressions like creeks, low lying areas and flood plains were used to dump the waste. No attempt was made, neither, to segregate waste nor, was consideration given to leachate control. Groundwater contamination due to improper past waste disposal practices, leaking underground storage tanks and accidental spills has been a growing concern on a global scale [3]. One of the main objectives in the design of a landfill site should be the proper management of polluted water and leachate migration, therefore mitigating the risk of health and environmental damage.

Conventionally, compacted liner materials were constructed by using soils having rich in clay mineral due to their low hydraulic conductivity (i.e. less than 10^{-7} cm/s) [4]. Bentonite is also the most suitable material which can be used as a liner material in an engineered landfill. Bentonite is mainly composed of SiO_2 (61.03%) and Al_2O_3 (14.59%) [5]. Bentonite has a high-water absorption capacity causing it to expand and swell due to the presence of montmorillonite minerals. To overcome the problem associated with low shear strength and swell–shrink in clay and bentonite, granular material such as sand was used to improve their properties [1, 6]. However, the major challenges with conventional liner (bentonite, bentonite–clay, bentonite–sand, etc.) include: (i) damage during the placement of the wastes, (ii) alteration in the properties of liner materials, (iii) reduction in capacity of primary leachate drainage layer over time because of biologically induced clogging and (iv) poor sustainability and economical. Further, sand seems like an infinite resource—especially when one imagines endless beaches and deserts—but the granular material is one of the most-consumed resources on the planet, and it could be running out. The problem of conventional liner and replacement of sand can be resolved by innovating a suitable liner material.

In developing countries, marble are still one of the most popular and decorative construction materials. India is the largest producer of waste marble dust. Around 95% of the total marble in the country are being produced only in Rajasthan state, India, and, hence, can be considered as the World's largest marble production [7]. Among them about 70% of marble waste generated from 4000 marble mines in Rajasthan, India, possesses a major environmental concern and local ecosystems due to its unscientific disposal [7, 8]. Therefore, usage of the marble dust in various construction industries would help to protect the environment. Marble dust can be used as filler materials to fill the voids present due to its fineness and to enhance the property of expansive clays [9]. Further, marble powder has been used as an additive for brick manufacturing, concrete production and highway construction [10, 11]. Some research has been done on the application of marble powder to improve the properties of clay soil [7, 9]. Marble dust has large percentage of CaO (66.60%) and MgO (22.13%), and sand has large percentage of SiO_2 (78.67%) and Al_2O_3 (12.20%) [3]. Further, the coarser particles and significant shear strength of marble dust improve the workability, plasticity and strength soils, particularly for cohesive soils [11]. However, attempt has not been made to study the potential of marble dust to be used as a liner material in combination with bentonite and is prime motive of present work.

The present work is focused to develop the novel liner material by capturing the advantageous properties of marble dust in improving the behaviour of bentonite. The detailed physical properties (Atterberg's limits and swell index), physicochemical (pH and EC) and compaction characteristics of marble dust–bentonite mixes has been studied to examine its suitability in developing linear material. Further, comparative study of marble dust–bentonite mixes has been done by determining the properties of sand–bentonite mixes to understand the potential of marble dust to be used as a liner material in replacement of sand.

2 Materials Used and Methodologies Followed

2.1 Materials Used

The geotechnical properties of bentonite, sand and marble dust are presented in Table 1. Micro-analyses (XRD, SEM and EDAX) of parent materials are shown in Fig. 1a–f and Table 2.

Bentonite (B)

The bentonite used for the study was collected from Bikaner District, Rajasthan, India. The geotechnical properties of bentonite are presented in Table 1. Particle size analysis of bentonite shows the presence of sand-sized particle (4.75–0.075 mm) of 8.00%, silt-sized particle (0.075–0.002 mm) of 15.00% and clay-sized particle

Table 1 Geotechnical properties of parent materials

Property	B	MD	S	Methodologies followed
Sand (4.75–0.075 mm), %	8.00	96.50	98.50	IS-2720 (Part-4) [12]
Silt (0.075–0.002 mm), %	15.00	3.50	1.50	
Clay (<0.002 mm), %	77.00	–	–	
Specific gravity	2.55	2.74	2.63	IS-2720 (Part 3) [13]
Liquid limit, %	185.00	17.60	30.76	IS-2720 (Part 5) [14]
Plastic limit, %	67.33	–	–	IS-2720 (Part 5) [14]
Plasticity index, %	117.67	–	–	
Shrinkage limit, %	8.05	–	–	IS-2720 Part 6 [15]
Differential FSI, %	490.00	–	–	IS 2720 Part 40 [16]
Modified FSI, (ml/gm)	13.04	–	–	Sivapullaiah et al. [17]
Optimum water content, %	45.76	15.03	14.44	Sridharan and Sivapullaiah [18]
Max. dry density, g/cc	1.12	1.87	1.58	
pH value	7.97	8.20	8.31	IS 2720 Part 26 [19]
EC, mS/cm	0.28	0.11	0.14	
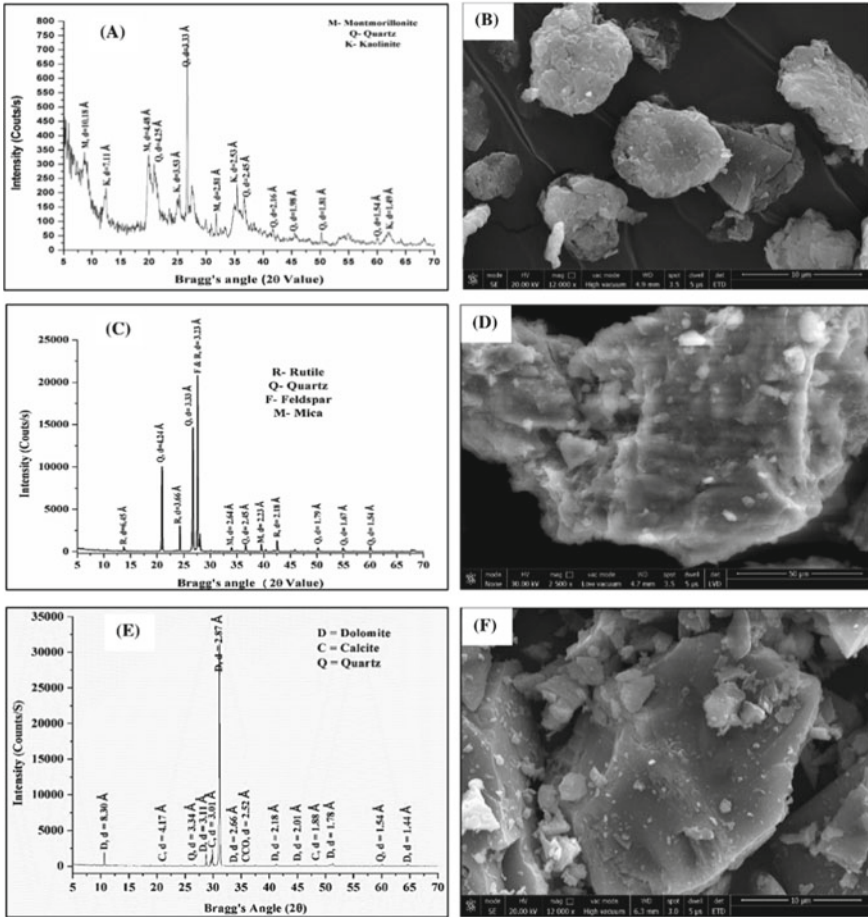
Fig. 1 XRD analyses and SEM images of **a** and **b** bentonite; **c** and **d** sand and **e** and **f** marble dust

(<0.002 mm) of 77.00%. Bentonite has liquid limit of 185% and specific gravity of 2.55. Further, free swell index (FSI) and modified free swell index MFSI of bentonite are observed to be 490% and 13.04 ml/gm, respectively.

The XRD analysis of bentonite (Fig. 1a) shows the presence of montmorillonite, kaolinite and quartz as predominant minerals. The microscopic image of bentonite (Fig. 1b) illustrates the rounded particle shape and more symmetrical particle size distribution, with smaller average grain sizes. The elemental analysis of bentonite by energy dispersive X-ray spectrometer (EDAX) confirms the presence of oxygen, carbon and silica with large percentage and potassium, titanium and chlorine in small percentage (Table 2).

Table 2 Chemical composition of bentonite, sand and marble dust

Element	Atomic %		
	Bentonite	Sand	Marble dust
O	56.85	71.28	60.52
Si	12.95	21.24	0.51
Al	8.42	3.99	–
Fe	2.94	1.01	–
K	0.25	0.72	–
Mg	1.42	0.81	8.40
Ca	–	0.31	8.77
Na	2.46	0.50	–
Ti	0.54	0.15	–
C	13.83	0.00	21.81
Total	100.00	100.00	100.00
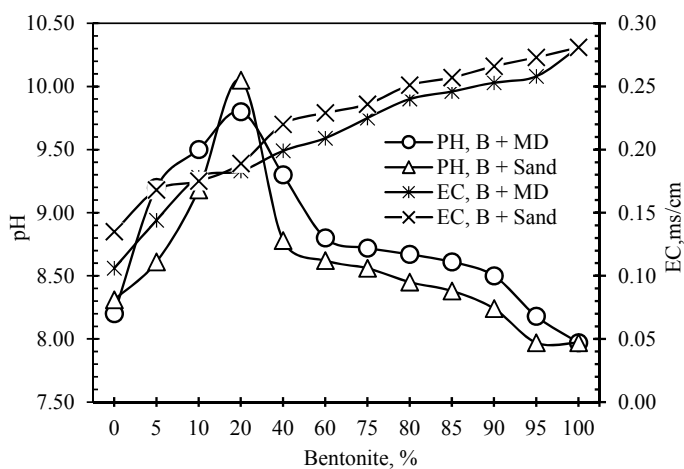
Fig. 2 pH and electrical conductivity of marble dust–bentonite and sand–bentonite mixes

Soil

The soil used for the study was collected from Manipal University Jaipur, Rajasthan, India. The soil used for the present study is from the depth of 1–1.5 m below the ground surface. The material passing from IS 425 micron sieve is used for all experimental purpose. The geotechnical properties of soil are presented in Table 1. The particle size analysis of soil confirms the presence of predominated amount of sand-sized particles (98.50%), and hence, it is represented as a sand (S) in the present study. The sand has a maximum dry density (ρ_{max}) and optimum water content (OWC) of 1.58 g/cc and 14.44%, respectively.

Soil predominated with sand-sized particles is predominated with rutile, quartz, feldspar and mica (Fig. 1c). The SEM image (Fig. 1d) and EDAX examination (Table 2) of sand confirm the irregular shape of particles and presence of silica as a key element, respectively.

Marble Dust (MD)

The marble dust used for the study was collected from Kishangarh, Ajmer District, Rajasthan, India. The particle size analysis shows the predominated amount of sand-sized particle of 96.50%. The specific gravity of marble dust is obtained to be 2.74. The maximum dry density and OWC of MD are observed to be 1.87 g/cc and 15.03%, respectively.

Mineralogical analysis of MD (Fig. 1e) confirms the presence of dolomite and calcite as predominated minerals having minor component of quartz. The SEM image of marble dust (Fig. 1f) enunciates the irregular and flaky shape of particles. The chemical composition (Table 2) analysis of marble dust shows the presence of calcium (8.77%) and magnesium (8.40%) as a predominant element.

2.2 Methodologies Followed

The methodologies followed to determine the geotechnical properties of parent materials are listed in Table 1. The pH tests are conducted according to IS 2720 Part 26 1987. The instrument was calibrated with standard buffer solution of pH 4.0, 7.0 and 9.0 prior determining pH values of all the samples. The same samples are used to measure the electrical conductivity.

The X-ray diffraction (XRD) of materials is performed by using graphite monochromator and Cu-Kα radiation. The scanning angle (also known as Bragg's angle) is kept in the range from 3° to 90°. The X'pert HighScore software is used to analysis and to identify the presence of various minerals as per sample data file of Joint Committee on Powder Diffraction Standards (JCPDS) [20]. Scanning electron microscope (SEM) coupled with energy dispersive X-ray spectroscopy (EDAX) is performed to examine microstructural and chemical composition of materials used. The sample was coated with 100 Å thin layer of gold palladium for 38 s using a sputter coater, polaron E5100 at 10^{-3} Torr vacuum. The same samples are used for elemental analysis by EDAX.

The sample prepared to determine the physical properties of B-S and B-MD mixes are based on their dry weight. Varying percentage of bentonite up to 100% is substituted by dry weight of S and MD to prepare the mixes. The dry mixes are done prior to wet mixing with water to determine the properties.

3 Results and Discussion

3.1 pH and Electrical Conductivity (EC) of Bentonite with Marble Dust and Sand

The physicochemical properties of marble dust and sand mixed with bentonite are measured in terms of pH and electrical conductivity and are shown in Fig. 2.

It is observed that the pH of soil amended up to 20% bentonite content increases and reduces thereafter up to 95%. The availability of calcite increases the concentration of salt cations in the soil solution which increases the ionic strength, resulting to the change in pH of soil amended up to 20% bentonite [21].Whereas, the reduction in the buffering capacity of soil due to decreasing percentage of calcite with addition of bentonite causes a reduction in pH after 20%. Similar result is shown for B-S mixes. Further, electrical conductivity of soil and marble dust also increases with increase of bentonite percentage. Electrical conduction in soil occurs due to the presence of moisture and surface charge. Soil–water interaction depends on the surface charge of clayey soil [22]. Na^+ and Ca^{++} become higher with increase in amount of bentonite [23]. Because of increase of charges in the solution with increase of bentonite electrical conductivity increases, further, bentonite has higher electrical conductivity value compared to sand and marble dust (Table 1). However, it is interesting to note that pH and EC of both sand and marble dust follow similar trends with increase in bentonite percentage.

3.2 Plasticity Characteristics of Bentonite with Marble Dust and Sand

Influence of bentonite on Atterberg's limit (liquid limit, plastic limit and plasticity index) of marble dust and sand is shown in Figs. 3 and 4, respectively. It is observed that liquid limit increases with increasing in bentonite content up to 95%, i.e. from 30.76% to 180% and 17.6% to 164% for B-S and B-MD mixes, respectively. Similar trend is obtained for plasticity indexes which increase from 30.76% to 115.77% and 17.60% to 97.55% for B-S and B-MD mixes up to the addition of 95% of bentonite, respectively. It is observed from Fig. 3 and Fig. 4 that plastic limit increases to 66.44% and 64.22% up to addition of 95% bentonite to MD and S mixes, respectively. Hence, the plasticity index of S and MD increases with addition of bentonite. These increment are attributed to (i) surface charge of bentonite, (ii) thinner particle size of bentonite, (iii) greater amount of water absorbed and (iv) increase in the diffuse double layer (DDL) thickness [6].

It was noticed from Fig. 5 that shrinkage limit increases to 17.454% and 10.611% with increasing amount of bentonite up to 40% for B-S and B-MD mixes, respectively. Further increment in bentonite content up to 95% results in the reduction of shrinkage
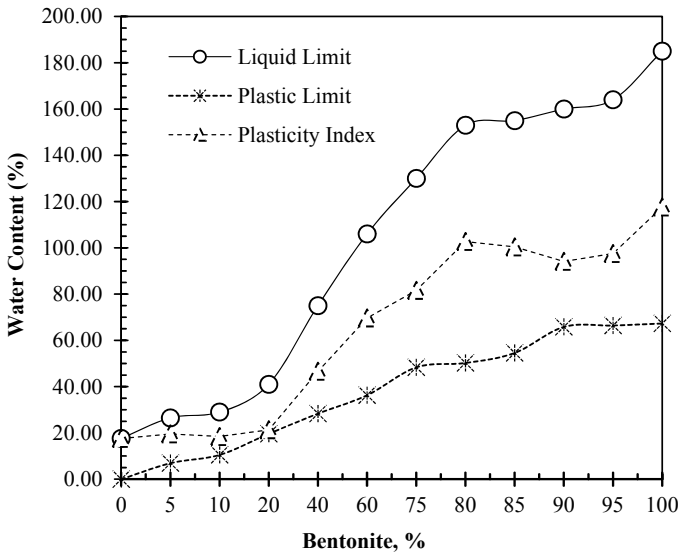
Fig. 3 Variation on liquid limit, plastic limit and plasticity index of marble dust with addition to bentonite
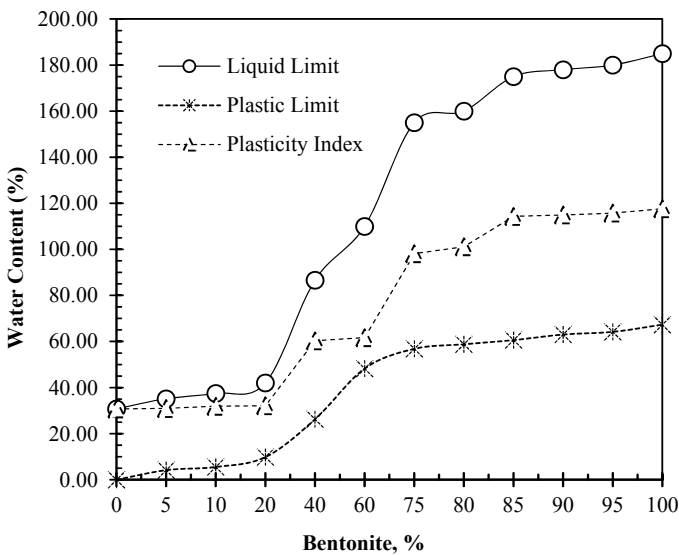
Fig. 4 Variation on liquid limit, plastic limit and plasticity index of sand with addition to bentonite
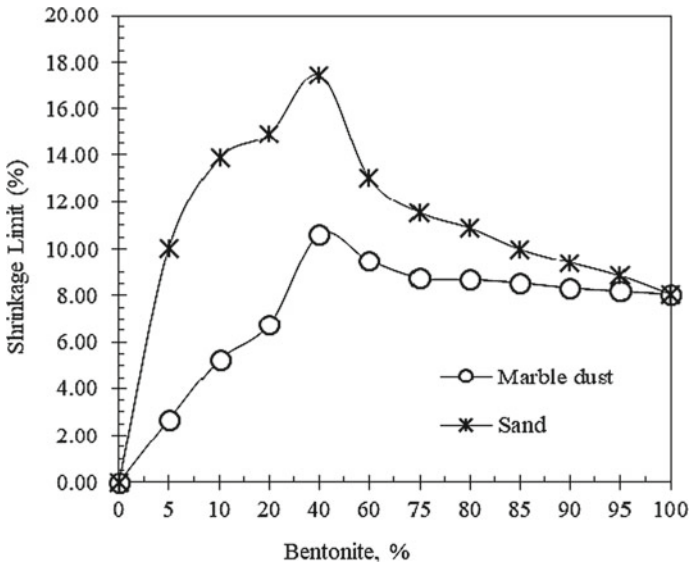
Fig. 5 Shrinkage limit of B-S and B-MD mixes

limit from 17.454% to 10.835% and 10.611% to 8.053% for B-S and B-MD mixes, respectively. The variation in shrinkage limit is attributed to change in the fabric of the sand and MD with addition of bentonite [24]. It can be summarized that bentonite in combination of marble dust possesses similar plasticity behaviour than that of bentonite–sand mixes.

3.3 Compaction Characteristics of Bentonite with Marble Dust and Sand

Figure 6 represents the compaction characteristics (ρ_{max} and OWC) of B-S and B-MD mixes.

It is observed that dry density of MD and S reduce from 1.87 gm/cc to 1.07 gm/cc and 1.58 gm/cc to 1.10 gm/cc with addition of bentonite up to 90%, respectively. However, OWC of MD and S enhances drastically with increase in bentonite percentage from 15.03% to 54.52% and 14.44% to 56.03%, respectively (Fig. 6). Comparing the results of B-S and B-MD confirm the potential of marble dust to achieve the similar dry density and OWC than that of sand in combination of bentonite. The reduction in dry density with increment in bentonite is due to (i) high surface charge of bentonite which resist the compactive effort, (ii) high repulsion capacity and (iii) formation of diffuse double layer [24]. The reduction in dry density is very small up to the addition of 20% bentonite because the particles of bentonite fill the voids present in sand and marble dust. Further addition of bentonite
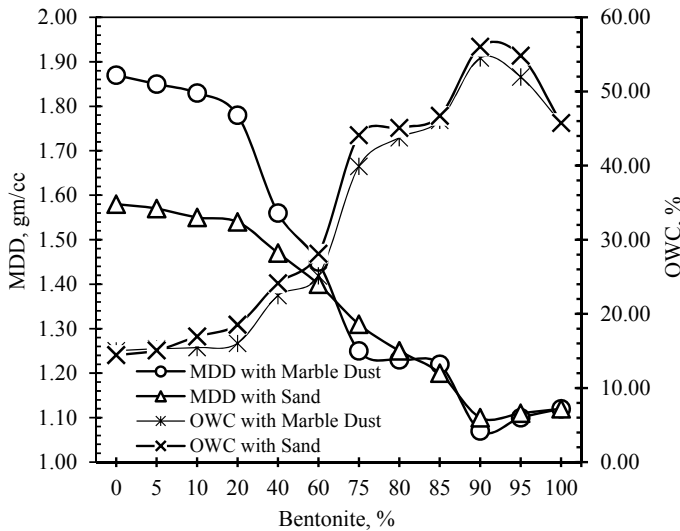
Fig. 6 Compaction characteristics of sand and marble dust with addition of bentonite

causes a drastic reduction in dry density as an excess addition of bentonite occupies the outside space of sand and marble dust particles, resulting decrease in dry density.

3.4 Swell Index of Bentonite with Marble Dust and Sand

Figure 7 shows the swell indexes in terms of free swell index (FSI) and modified free swell index (MFSI) of B-S and B-MD mixes. It is observed that swell indexes of MD and S increase drastically from 0 to 420% and 0% to 380% with addition of bentonite up to 95%, respectively. Hence, swell indexes of B-MD are observed to be same as B-S mixes. This increment is due to the addition of swelling particles of bentonite in non-swelling materials and increase in the thickness of diffuse double layer. Similar results are reported by previous researchers with sand–bentonite mixes.

4 Conclusion

Detailed study on the behaviour of varying percentage of bentonite with sand and marble dust has been done to understand the potential of marble dust to be used as a possible liner material. The major conclusions drawn from the present study are as follows:
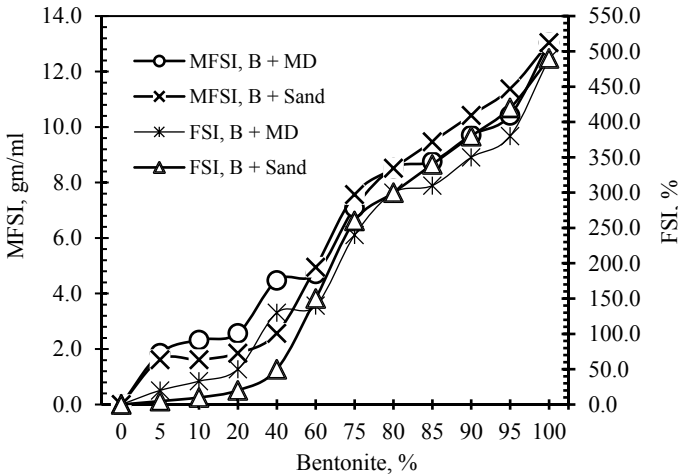
Fig. 7 Swell index (FSI and MFSI) of marble dust and sand with addition of bentonite

1. The pH of sand and marble dust increases initially up to 20% and decreases after further addition of bentonite. Electrical conductivity increases continuously for sand and marble dust with increase in bentonite percentage. Both pH and EC of bentonite–sand and bentonite–marble dust mixes represent similar trend.
2. The plasticity index of marble dust and sand increases continuously with increase in percentage of bentonite. However, shrinkage limit of sand and marble dust increases up to 40% bentonite and reduces thereafter. Further, plastic behaviour of bentonite–sand and bentonite–marble dust mixes is almost identical.
3. The compaction characteristics (maximum dry density and optimum water content) of bentonite possess an identical behaviour with sand and marble dust. In both combination, OWC increases with reduction in dry density.
4. Increasing trends of swell indexes (FSI and MFSI) are observed in sand and marble dust in combination of bentonite.

This study confirms that marble dust shows similar behaviour as compared to sand in combination with bentonite. Hence, marble dust can be used as a possible liner material for waste containment. However, further study on the engineering properties of bentonite–marble dust needs to be done and has to be compared with behaviour of bentonite–sand mixes.

References

1. Holtz, W.G., Gibbs, H.J.: Engineering properties of expansive soils. Trans. ASCE **121**, 641–679 (1956)
2. Day, S.R., Daniel, D.E.: Hydraulic conductivity of two prototype clay liners. J. Geotech. Eng. **111**(8), 957–970 (1985)
3. Shuaib-Babata, Y.L., Abegunde, A.J., Abdul, J.M.: Suitability of Ado-Ekiti (Nigeria) natural moulding sands for use as foundary sands in production of aluminium alloy cast. J. Prod. Eng. **20**, 91–100 (2017)
4. Benson, C.H., Trast, J.M.: Hydraulic conductivity of thirteen compacted clays. Clays Clay Miner. **43**, 669–681 (1995)
5. Kibria, G., Hossain, M.S.: Effects of bentonite content on electrical resistivity of soils. In: Geo-Congress 2014 Technical Papers: 2404–2413 (2014)
6. Chapuis, R.P.: Sand–bentonite liners: predicting permeability from laboratory tests. Can. Geotech. J. **27**(1), 47–57 (1990)
7. Sabat, A.K., Nanda, R.P.: Effect of marble dust on strength and durability of rice husk ash stabilised expansive soil. Int. J. Civil Struct. Eng. **1**(4), 939–948 (2011)
8. Arora, R.P., Ameta, N.K., Singhvi, B.S., Gupta, T.: Economical study on safety of earthen embankments by use of marble slurry. Eur. J. Adv. Eng. Technol. **3**(3), 49–54 (20160
9. Okagbue, C.O., Onyeobi, T.U.S.: Potential of marble dust to stabilise red tropical soils for road construction. Eng. Geol. **53**(3), 371–380 (1999)
10. Akbulut, H., Gürer, C.: Use of aggregates produced from marble quarry waste in asphalt pavements. Build. Environ. **42**, 1921–1930 (2007)
11. Jong, E.D., Warkentin, B.P.: Shrinkage of soil samples with varying clay concentration. Can. Geotech. J. **2**(1), 16–22 (1965)
12. Bureau of Indian standards IS 2720 (Part 4): Methods of test for soils: grain size analysis. New Delhi (1985)
13. Bureau of Indian Standards (second revision) IS 2720, (Part 3/Set 1): Methods of test for soils: determination of specific gravity, New Delhi, India (1980)
14. Bureau of Indian Standards (second revision) IS 2720, (Part 5): Methods of test for soils: determination of liquid limit and plastic limit, New Delhi, India (1985)
15. IS 2720: Methods of test for soils—part 6: determination of shrinkage factors. Bureau of Indian Standards, New Delhi, India (1972)
16. IS 2720-40: Methods of test for soils, Part 40: determination of free swell index of soils. Bureau of Indian Standards (1977)
17. Sivapullaiah, P.V., Sitharam, T.G., Rao, K.S.: Modified free swell index for clays. Geotech. Test. J. **10**(2), 80–85 (1987)
18. Sridharan, A., Sivapullaiah, P.V.: Mini compaction test apparatus for fine grained soils. Geotech. Test. J. **28**(3), 1–7 (2005)
19. Bureau of Indian Standards (second revision) IS 2720 (Part 26): Methods of test for soils: determination of pH value, New Delhi, India (1987)
20. JCPDS: Joint Committee for Powder Diffraction Studies International Centre for Diffraction Data (ICDD). The Powder Diffraction File Newtown Square Pa (1999)
21. Chesworth, W., ed.: Encyclopedia of Soil Science. Springer, Dordrecht, Netherlands, Xxiv. ISBN 1–4020–3994–8 (2008)
22. Komine, H., Ogata, N.: Experimental study on swelling characteristics of sand-bentonite mixture for nuclear waste disposal. Soils Found. **39**(2), 83–97 (1999)
23. Yassaad, H.R., Belkhodja, M.: The effects of bentonite on the physic chemical characteristics of sandy soils in Algeria. J. Appl. Sci. **7**(18), 2641–2645 (2007)
24. Sivapullaiah, P.V., Sridharan, A., Raju, K.V.B.: Role of amount and type of clay in the lime stabilization of soils. Proc. ICE-Ground Improv. **4**(1), 37–45 (2000)

Converting Agricultural Waste into Biochar for Improving Physical Properties of Soil

M. P. Choudhary ⓘ**, H. D. Charan, and Biswajit Acharya**

Abstract Biochar is a carbon-rich, fine-grained, porous material obtained from pyrolysis process, in which biomass is subjected to thermochemical conversion in the absence of either oxygen or very little oxygen. India is currently facing an acute problem of management of large quantities of agricultural waste which is either partially utilized or unutilized due to certain constraints. One of the indiscriminate uses of crop residues adopted by Indian farmers in the states of Punjab, Haryana and Uttar Pradesh is direct burning in open fields (in the form of *Parali*) which causes emission of greenhouse gases in the atmosphere. It is one of the sources of air pollution being faced every year during winter in the national capital region of Delhi. One of the recent advancements to combat this problem is the conversion of agricultural waste into biochar and applying it back into the soils to improve soil properties. Although biochar is not a new product, it has recently drawn attention of researchers because of its usefulness in improving the soil properties and as a means of carbon sequestration, thereby reducing greenhouse gas emission. Direct burning of agricultural wastes in fields cannot be called an environmental-friendly approach as it causes loss of biomass as well as introduces harmful gases into the environment. So converting agricultural wastes into biochar may be a better solution. In India, not much research has been carried out so far on biochar application in soils. The process of making biochar and the effects of utilizing biochar on the physical properties of soil have been presented in this paper, which will prove useful for Indian context where large quantities of agricultural waste are produced that creates environmental air pollution when directly burnt in fields.

Keywords Biochar · Agricultural waste · Greenhouse gases · Physical properties of soil · Carbon sequestration

M. P. Choudhary (✉) · B. Acharya
Rajasthan Technical University, Kota, Rajasthan, India
e-mail: choudhary_mp@yahoo.co.in

H. D. Charan
Bikaner Technical University, Bikaner, Rajasthan, India

1   Introduction

Agriculture is the main source of livelihood for about 60% of the Indian population, and at the same time, it is known to be the third largest source of greenhouse gas emissions, following the burning of fossil fuels and transportation [1], and in near future, the developing world as a whole is expected to witness an upsurge in the growth of agro-processing industry, and there will be a need to manage the waste generated from these industries. The agricultural and related agro-industries waste has the potential to supply feedstock for biochar production. Converting residual biomass into biochar can help in achieving long-term carbon sequestration and other beneficial effects on soils [2].

Biochar, a carbon-rich product, is obtained by heating biomass in the absence of or with a limited amount of oxygen at above 250 °C. This process is known as charring or pyrolysis which is also used for making charcoal. However, biochar is different from charcoal or other carbon products in that it is intended for use as a soil amendment [3]. Biochar has gained a great deal of attention in recent past due to its chemical and physical properties and has been portrayed as one of the potential drivers of climate change mitigation and sustainable agriculture [4]. Biochar is inspired by the fascinating properties of ancient Terra Preta, found in Amazon basin. It has been identified as a soil amendment and has very specific properties of adsorption and stability that make it unique among organic soil amendments [5].

The annual outburst of smog reportedly witnessed for last 3–4 years in the months of October–November in the national capital region of New Delhi is known to occur due to open burning of agricultural wastes by the farmers of nearby states like Haryana, Punjab, Uttar Pradesh and Rajasthan. During this period, the city witnesses the worst level of air quality, when the concentration of fine particulate matter ($PM_{2.5}$) is observed at the highest levels ever, e.g., at 640 μg/m^3 [6] against the annual permissible limits of 40 μg/m^3 as per the national ambient air quality standards of India [7].

After yielding the crops like wheat, rice or mustard from agricultural fields, generally the Indian farmers adopt the age-old practice of burning the wastes in their fields to clean up and prepare the fields for next crop as it is a fast, easy and cheap method of disposing off the wastes. Though the National Green Tribunal (NGT, New Delhi) has imposed a complete ban in 2015 on burning of crop residues and other materials which emit toxic pollutants into the atmosphere [8], farmers are still practicing it because they are unaware of the fact that it is harmful to their fields as it causes loss of biomass which may help positively in crop yield. So, there is a need for spreading awareness among the farmers regarding safe disposal of agricultural wastes in terms of biochar production. Figures 1, 2 and 3 show the burning of agricultural waste in fields near Kaithoon area of Kota district in Rajasthan.

The beneficial features of biochar are governed by the physical properties of the biochar which are altogether different from the physical properties of the soil and hence could change the physical properties of the soil also, if soil is amended with biochar [9].

Fig. 1 Crop residue of mustard plants after crop yield near Kaithoon, Kota, Rajasthan

Fig. 2 Crop residue put on fire by farmers near Kaithoon, Kota, Rajasthan

Fig. 3 Agricultural field after burning the waste near Kaithoon, Kota, Rajasthan

Furthermore, locally available weed biomass is an important source for preparing the biochar as it is not economically important as well as causes crop loss due to its presence. If biochar is prepared from the locally available weeds, then it can reduce the weed population in the agricultural fields on the one hand, and on the other, it can enhance plant growth by improving the physical, chemical and biological

characteristics of soil, all contributing to increased crop production and productivity [10].

2   Biochar Production

Biochar is produced by heating organic substances under conditions of incomplete oxygen [11]. Biochar can be produced either at individual farms or at large industrial setups [12], making it applicable for a large number of socioeconomic situations. Different types of pyrolysis technologies are commercially available that yield different proportions of biochar and bioenergy products, such as bio-oil and syngas [12]. The pyrolysis of biomass can be carried out in a reactor via gasification or carbonization at varying temperature and time depending on the final intended use of the end product [13].

Biochar can be made from a wide range of biomasses having different physical and chemical properties. Extensive feedstock biomasses have been used in the production of biochar such as bio-energy crops, forest residues, organic waste, agricultural waste, kitchen waste and even sewage sludge also [14].

For Indian conditions, biochar can be produced by individual farmers in their fields in conventional kilns made by locally available material or at community kilns by using the agricultural wastes and other by-products, so that the biochar produced can be utilized again for applying in the fields for the upcoming crops. To produce biochar from agricultural waste, a drum of 220 L capacity has been used as shown in Figs. 4, 5 and 6.

3   Materials and Methods

3.1   Biochar

The biochar produced as above at the field level from agricultural waste is crushed to small pieces, air-dried and passed through a 4.75 mm size sieve so as to get uniform size of biochar. The important characteristics of biochar like grain size distribution, pH, moisture content, specific gravity and electrical conductivity were determined in the laboratory as per the standard methods, and results are presented in Table 1.

3.2   Soil Sample

The soil samples used for study were collected from the agricultural fields of village Kosana, Jodhpur district, Rajasthan. The samples for various tests were prepared as

Fig. 4 Drum filled with agricultural waste

Fig. 5 Drum covered after initial burning and kept for 15 min for pyrolysis

Fig. 6 Biochar produced by
pyrolysis

Table 1 Physico-chemical characteristics of Biochar

Characteristic	Value	Test standards followed [15]
pH	10.2	IS: 2720 (Part 26)—1987 (Reaffirmed 2002)
Moisture (%)	7.9	IS: 2720 (Part II)—1973 (Reaffirmed 2010)
Specific gravity	1.56	IS: 2720 (Part III2)—1980 (Reaffirmed 2002)
Electrical conductivity (mS/cm)	4.28	IS: 14,767—2000
Grain size distribution		IS: 2720 (Part 4)—1985 (Reaffirmed 2006)
2–4.75 mm (coarse)	22.4	
0.425–2 mm (medium)	46.6	
0.075–0.425 mm (fine)	31.0	

the IS: 2720 (Part 1)-1983 in the geotechnical engineering laboratory of the Department of Civil Engineering, Rajasthan Technical University, Kota. The soil samples were first of all oven-dried, pulverized and then sieved through 4.75 mm size sieve to get an idea of the primary classification. The sieve size analysis gave us the constituents of soil as 68% of sand, 16.8% of silt and 15.2% of clay. Figure 7 shows the grain size distribution of soil samples and biochar.

The Atterberg limits of the soil sample were also found out in the laboratory. It was observed that liquid limit; plastic limit; and shrinkage limit of the soil were 41%, 22% and 15%, respectively. Further, the soil sample was classified as clayey
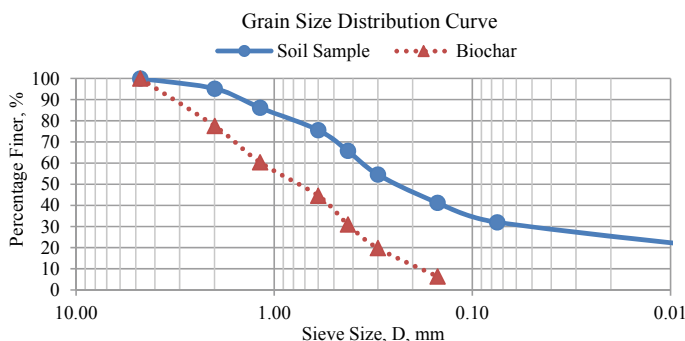
Fig. 7 Grain size distribution curve of soil sample and biochar

Table 2 Characteristics of soil sample

Characteristic	Value	Test standards followed [15]
pH	8.5	IS: 2720 (Part 26)—1987 (Reaffirmed 2002)
Specific gravity	2.62	IS: 2720 (Part III2)—1980 (Reaffirmed 2002)
Electrical conductivity (mS/cm)	0.90	IS: 14,767—2000
Grain size distribution		IS: 2720 (Part 4)—1985 (Reaffirmed 2006)
2–4.75 mm (coarse sand)	4.8	
0.425–2 mm (medium sand)	29.4	
0.075–0.425 mm (fine sand)	33.8	
0.002–0.075 mm (silt)	16.8	
<0.002 mm (clay)	15.2	
Consistency limits (%)		
Liquid limit	41	IS: 2720 (Part 5)—1985 (Reaffirmed 2006)
Plastic limit	22	IS: 2720 (Part 5)—1985 (Reaffirmed 2006)
Shrinkage limit	15	IS: 2720 (Part VI)—1972 (Reaffirmed 2001)

sand (SC) as per the Unified Soil Classification System (USCS). Table 2 represents summary of the important physical characteristics of the soil.

3.3 Biochar as Soil Amendment

To study the effect of biochar on physical properties of soil, tests were carried out in the geotechnical engineering laboratory to find out the liquid limit, plastic limit and shrinkage limit of the soil amended with different percent by weight (% w/w) of biochar like 5, 10, 15, 20 and 25%. For this purpose, the biochar was added in dry condition to the soil and the soil-biochar mix was thoroughly mixed with each

other. The tests of consistency limits were performed as per the standard methods described in Table 2.

4 Results and Discussion

The effect of biochar amendment on liquid limit of the soil is shown in Fig. 8. It was found that liquid limit of the soil amended with biochar increased from 41 to 47%, 49%, 54%, 55% and remained constant at 55% on addition of biochar at 5%, 10%, 15% 20% and 25% (w/w), respectively. It can be inferred from the results that liquid limit of the soil increases with addition of biochar into it up to a certain point due to the fact that biochar has high porosity and surface area which increases the liquid limit of the soil-biochar composite.

Figure 9 shows the effect of biochar amendment on plastic limit of the soil. It was observed that plastic limit of the soil-biochar composite increased from 22 to 28% when 5% biochar (w/w) was added to the soil, and thereafter, it decreased on 10 and 15% addition of biochar. Further, it was not possible to find plastic limit of the soil-biochar composite at 20 and 25% (w/w) biochar amendment because the composite
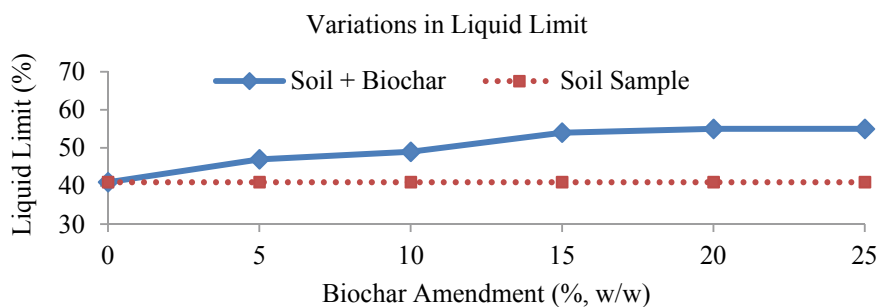
Fig. 8 Effect of biochar amendment on liquid limit of soil
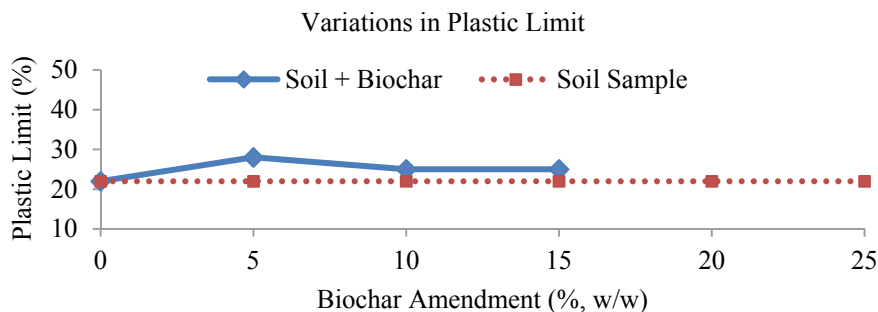
Fig. 9 Effect of biochar amendment on plastic limit of soil

did not show any plastic behavior. It crumbled at higher water contents. Hence, we can infer that the initial increase in plastic limit is because of the water-absorbing capacity of the soil-biochar composite up to a certain limit.

Figure 10 shows the variations in shrinkage limit of the soil amended with biochar at different ratios. The initial increase in shrinkage limit up to 10% addition of biochar is slightly slow, but thereafter it goes up sharply up to 25% (w/w). The increase can be seen from 15% in soil sample to 17%, 19%, 25%, 34% and 35%, respectively, in the soil-biochar composite. The increase in shrinkage limit indicates that there is higher void ratio in the biochar as compared to soil, and hence, soil amended with biochar requires more amount of water to change from solid state to semi-solid state.

Thus, we can see that values of all the consistency limits (liquid limit, plastic limit and shrinkage limit) have increased upon addition of biochar to the soil up to a certain percent by weight, and therefore, the physical properties of the soil are improved.

Similarly, Fig. 11 shows the variations in plasticity index (difference of liquid limit and plastic limit) for the soil sample and soil amended with biochar. The values after 15% addition of biochar are not shown as it was not possible to find plastic limits of the soil composite beyond 15% biochar (w/w).
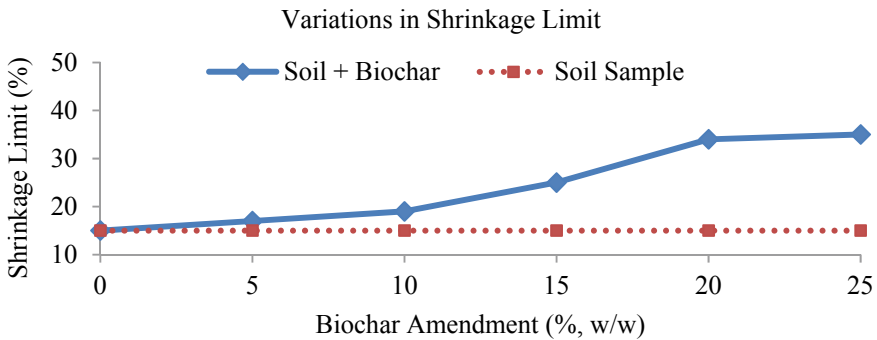
Fig. 10 Effect of biochar amendment on shrinkage limit of soil
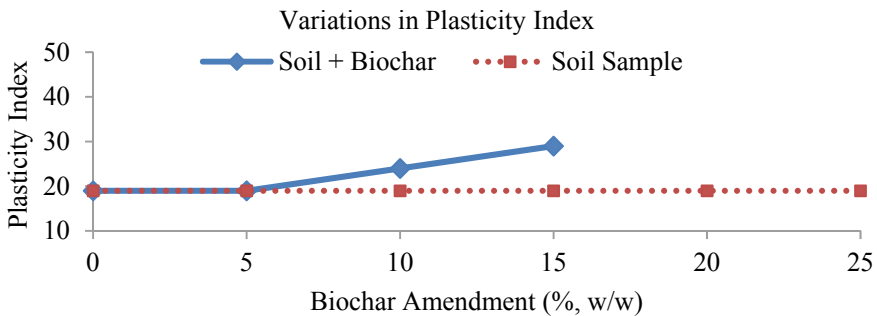
Fig. 11 Effect of biochar amendment on plasticity index of soil

5 Conclusion

The present study reveals that amendment of soil with biochar in different percent by weight has positive effect on the consistency limits of the soil. The liquid limit, plastic limit and shrinkage limit of the soil amended with biochar increase up to a certain level. Hence, the agricultural waste, which has otherwise no utility, shows a good potential of improving the soil properties. The important characteristics of high porosity and large surface area of biochar make it suitable for the soil amendment. This peculiarity of biochar can be very important in further investigation related to engineering properties like water retention capacity, hydraulic conductivity, shear strength and stability of the soil.

References

1. Worldwatch Homepage, https://www.worldwatch.org/agriculture-and-livestock-remain-major-sources-greenhouse-gas-emissions-0. Accessed on 26 May 2019
2. Parmar, A., et al.: Biochar production from agro-food industry residues: a sustainable approach for soil and environmental management. Curr. Sci. **107**(10), 1673–1682 (2014)
3. Lehmann, J., Joseph, S.: Biochar for environmental management: science, technology and implementation, 2nd edn. Routledge, London (2015)
4. Lehmann, J., et al.: Biochar effects on soil biota—a review. Soil Biol. Biochem. **43**(9), 1812–1836 (2011). https://doi.org/10.1016/j.soilbio.2011.04.022
5. Lehmann, J.: Bio-energy in the black. Front. Ecol. Environ. **5**, 381–387 (2007)
6. Economics Times Bureau Homepage, https://economictimes.indiatimes.com/news/politics-and-nation/odd-even-plan-for-five-days-in-delhi-from-monday/articleshow/61575418.cms. Accessed on 26 May 2019
7. CPCB Homepage, https://cpcb.nic.in/uploads/National_Ambient_Air_Quality_Standards.pdf. Accessed on 26 May 2019
8. DownToEarth Homepage, https://www.downtoearth.org.in/news/air/paddy-burning-ngt-orders-fine-imposition-on-erring-farmers-51698. Accessed on 26 May 2019
9. Ghosh, K.K., et al.: Effect of biochar on consistency behavior of soil. In: Indian Conference on Geotechnical and Geo-environmental Engineering (ICGGE) (2019). MNNIT Allahabad
10. Das, S.K., Avasthe, R.K.: Matber Singh: carbon-negative biochar from weed biomass for agricultural research in India. Curr. Sci. **110**(11), 2045–2046 (2016)
11. Lehmann, J.: A handful of carbon. Nature **447**, 143–144 (2007)
12. Woolf, D., et al.: Sustainable biochar to mitigate global climate change. Nat. Commun. **1**, 56 (2010). https://doi.org/10.1038/ncomms1053
13. Ogbonnaya, U., Semple, K.T.: Impact of biochar on organic contaminants in soil: a tool for mitigating risk? Agronomy **3**, 349–375 (2013). https://doi.org/10.3390/agronomy3020349
14. Nartey, O.D., Zhao, B.: Biochar preparation, characterization, and adsorptive capacity and its effect on bioavailability of contaminants: an overview. Adv. Mater. Sci. Eng. Hindawi Publishing Corporation (2014). https://doi.org/10.1155/2014/715398
15. Indian Standards (IS): 2720, Method of tests for soils, various parts published by Bureau of Indian Standards, New Delhi (2015)

Remediation of Cadmium-Contaminated Soil Using Biochar Derived from Wheat Straw, Rice Husk and Bagasse

Aarushi Joshi, Dharmaraj J. Patil, Jagabandhu Dixit, and Sailesh Narayan Behera

Abstract Improper waste disposal has resulted in rapid deterioration of the environment and the advent of fatal diseases. Carcinogenic substances that percolate into the ground deteriorate the quality of groundwater and soil. Moreover, pollution from large-scale burning of agricultural waste each time after the harvest season makes the goal of a healthy environment of utmost importance. Toxins, such as polycyclic aromatic hydrocarbons (PAH) and heavy metal contaminants, have several pathways to enter into the environment and bio-accumulate within living organisms. The objective of this study is to synthesise a substance that will break the source-receptor pathway resulting in cleaner water and soil. Biochar, through ion exchange or physical adsorption, has the capacity to adsorb heavy metal ions such as those of cadmium. The biochar was synthesised from biomass consisting of wheat straw, rice husk and bagasse. The biomass was then heated to temperatures ranging from 300 to 700 °C using the process of slow pyrolysis, in an environment in which the oxygen supply was limited. The samples were then subjected to Fourier transform infrared spectroscopy (FTIR) to ascertain the functional groups present followed by powder X-ray diffraction (XRD) to determine the elements or form of metal oxides present in the samples. The samples were mixed with a known amount of cadmium solution, and the final testing was performed using atomic absorption spectroscopy (AAS). The final testing directly showed the heavy metal ion adsorption efficiencies of biochar derived from different types of biomass, giving an insight into the future scope of using biochar has a remediating agent

Keywords Biochar · Heavy metal · Soil remediation

A. Joshi (✉) · D. J. Patil · J. Dixit · S. N. Behera
Shiv Nadar University, Greater Noida 201314, India
e-mail: aj579@snu.edu.in

D. J. Patil
e-mail: dp301@snu.edu.in

J. Dixit
e-mail: jagabandhu.dixit@snu.edu.in

S. N. Behera
e-mail: Sailesh.behera@snu.edu.in

1 Introduction

The use of burnt agricultural material as a means to enrich the soil has been used for the past several years. Farmers have the knowledge that using this burnt material from cook stoves, etc., and applying it to the soil makes it more suitable for cultivation. This process releases large amounts of pollutants into the atmosphere. However, burning in limited oxygen conditions produces liquid, gasses and solid matter. This solid matter, biochar, is the end product that effectively removes contaminants present in the soil that are generally bio-available for uptake by plants.

The property of biochar to bind carcinogens to its surface is governed by properties such as the feeder material and the temperature of synthesis. Variation in these properties result in changes in surface area available to adsorb toxins, pH changes in the soil, and the amount of different toxic substances taken up by the biochar through a series of differing surface chemical reactions. Biochar is the substance that breaks the source-receptor pathway through cation exchange, the physical processes of electrostatic attraction, pH increasing properties, etc.

These properties of biochar make it a highly researched into substance. Its applications could benefit several people and have a global impact in the reduction of soil and atmospheric pollutants. The objective of this study is to determine the effect of biochar derived from three different raw materials on the uptake and removal of cadmium heavy metal ion. The ideal temperature and the maximum amount of contaminant are to be determined for further research.

1.1 Mechanics of Remediation by Biochar

The properties of biochar such as the chemical process of chemisorption and the physical process of physisorption make it ideal for the removal of organic and inorganic contaminants. According to Gomez-Eyles et al. [7], the cation exchange capacity at low temperatures of pyrolysis takes place due to the presence of a high number of oxygen-containing functional groups. A higher temperature results in the increase in surface area of the biochar, making more sorption points available on the biochar surface. (Gomez-Eyles et al. 2011) It also results in the presence of a greater number of aromatic compounds available [10].

Physical adsorption is the main phenomenon responsible for the binding of metal contaminants to the surface of the biochar. High temperatures increase the aromaticity of the biochar resulting in the polarisation of the electron cloud and consequent attraction of positive metal ions to the pi-pi bonds of the aromatic group. (Gomez-Eyles et al. 2011). pH plays an important role in the removal of heavy metal ions since a high negative value results in competition for sorption points on the surface of biochar by hydrogen ions, while a positive pH prevents the dissociation of compounds into ions following the Le Chatelier's principle (Sizmur et al. 2015; Bolzan 2017).

This ensures that harmful compounds formed with the heavy metals on the surface of the char remain insoluble and are not bio-available for uptake.

1.2 Properties of Biochar

Various researches have provided insight into the composition of chars from different sources.

Bagasse. According to the study conducted by Figuerdo et al. (2017), the detectable elements in sugarcane biochar were potassium, phosphorous, magnesium, zinc, copper, silicon and aluminium. The presence of manganese in bagasse biochar increased in the temperature range of 450–550 °C, while the percentage of sulphur and phosphorous decreased in the same temperature range. [5]. The carbon content of the bagasse biochar decreases with an increase in temperature after a maximum temperature of 500 °C, and the highest phosphorous content is achieved at a temperature of 400 °C (Nwajiaku et al. 2017). Phosphorus, silicon and sulphur are responsible for the removal of zinc, mercury and lead.

Rice Husk. Biochar synthesised from rice husk has a high phosphorous content [18]. The highest percentage of silicon, about 31%, is present in chars synthesised at lower temperatures of 400 °C. (Sandhya et al. 2015). Rice husk biochar has a high carbon content, production potential and carbon storage potential (Zu et al. 2012). A direct correlation exists between carbon content and an increase in temperature, the highest yield of carbon, 74%, was found at a temperature of 525 °C (Ahmad et al. 2015).

Wheat Straw. An increase in temperature results in an increase in carbon content and a lower H/C ratio which showcases and increase in aromaticity of biochar [6]. There is an increase in phosphorous and manganese content of the char at a temperature range of 300–500 °C [14]. The highest potassium content and phosphorous content of 1 g/kg were found at a temperature of 550 °C [18].

2 Experimental Section

2.1 Material

Rice husk, bagasse and wheat straw are the raw materials obtained from the farms in the Dadri, Uttar Pradesh, and from Bulandshahr, Uttar Pradesh.

2.2   Instrumentation

A muffle furnace, B1410M-33 furnace, was used to synthesise the biochar. For ATR, samples were directly analysed after synthesis using the Thermo Nicolet iS5 with the software—Ominic Diamond. The results were plotted using origin. The Bruker D8 discover was used for XRD testing.

2.3   Raw Material Preparation

Each of the raw materials was prepared in a different way to remove impurities that may have been present. The rice husk and wheat straw were sieved to remove traces of soil, animal droppings and plastic. The bagasse was thoroughly washed by distilled water to remove soil dust and prevent the formation of molasses at high temperatures. Bagasse was then dried in an oven for 48 h at a temperature of 60°.

2.4   Synthesis of Biochar via Pyrolysis Process

For the synthesis of biochar: 2 g of rice husk and wheat straw were placed in silicon crucibles, and the temperature was slowly increased up to a starting temperature of 200 °C. The samples were carefully placed within the furnace for one hour. Fresh samples were then placed into the furnace for temperatures of 300, 400, 500, 600 and 700 °C for a residence time of 1 h each (Zhu et al. 2016). The bagasse biochar was prepared at temperature of 300° and 400° according to the FTIR data of the study by [11], and the resulting biochar at these temperatures has the highest heavy metal ion removal efficiency. The resultant products were analysed by ATR mode FTIR and XRD technique. After performing ATR and XRD, samples were shortlisted for further testing.

2.5   Removal of Cd (II)

Due to the presence of microscopic particles, AAS method was used for testing. The sample was prepared by introducing a set amount of 81 ppm cadmium solution to the biochar. Four samples were prepared using 25, 50, 75 and 100 mg of each type of biochar. 16 samples were selected based on maximum removal efficiency, after ATR and XRD, for further testing. These samples were placed in a shaker for 6 h, after which, they were centrifuged. The centrifuge was set at 10,000 rpm for the span of 20 min. After this process, the supernatant was extracted and placed in 10 ml

containers and allowed to rest, so that the suspended particles settle to the bottom of the container. The solution was then filtered for further testing.

3   Result and Discussion

3.1   FTIR

Findings. The characteristic peaks in all three kinds of biochar at various temperature comes at 1630, 1410, 1058 and 630 cm^{-1} showed the functional groups mainly including aromatic ring –C = C–, carboxyl, phosphate and aromatic –C–H–, and intensity of these peaks decreases by increasing the pyrolysis temperature (Li et al. 2018). Figures 1, 2 and 3 show the intensity of respective function group at various temperature.

Bagasse. Figure 1 shows FTIR spectra of the biochar synthesised from bagasse, the sample synthesised at 500 °C shows the presence of peaks in zone 5 indicating the presence of benzene ring, whereas the sample at 400 °C shows no such peak. The sample at 400 °C, however, shows the presence of oxygen-containing functional groups in zone 4 such as acid and amines. Thus, the most favourable condition for the synthesis of the product would be at 400 °C.

Wheat Straw. Based on the FTIR graph in Fig. 2, the wheat straw char shows the most favourable conditions at a temperature of 300 °C. This is due to the presence of aromatic hydrocarbon benzene indicated by the double peaks at approximately
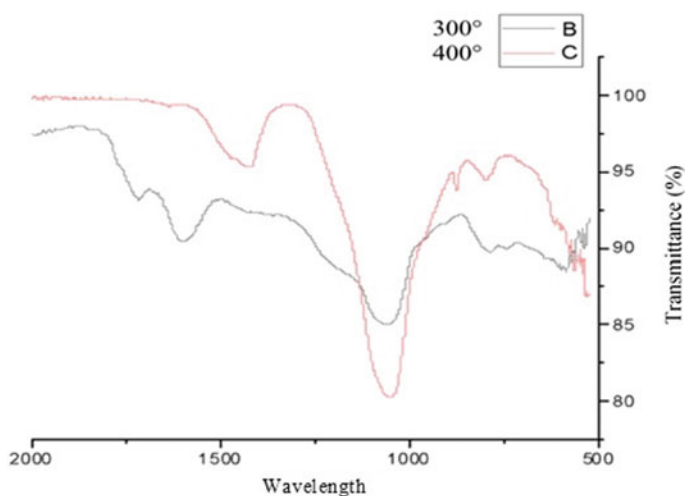
Fig. 1 Bagasse FTIR
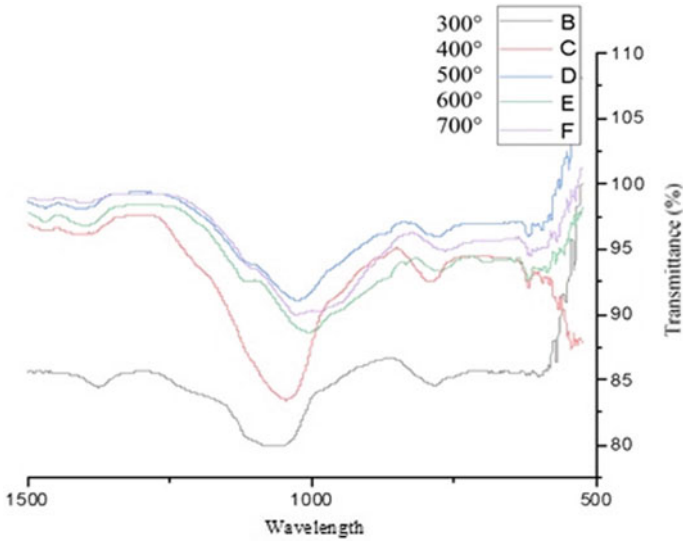
Fig. 2 Wheat straw FTIR
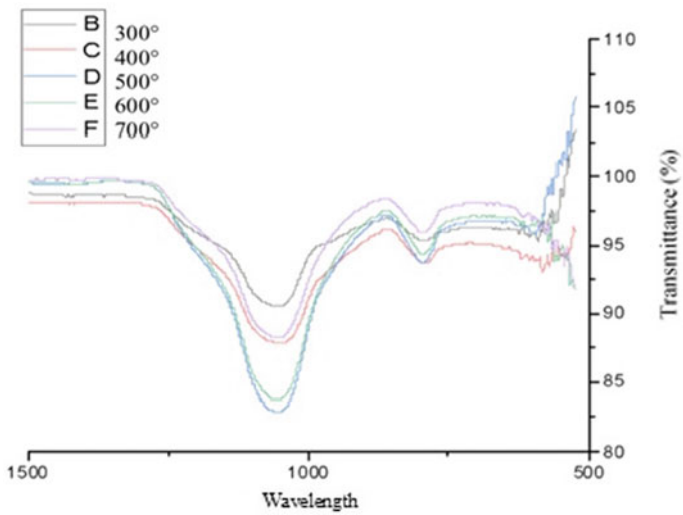
Fig. 3 Rice husk FTIR

1500 and 1600 cm^{-1}. The peaks at zone 4 (1850–1650 cm^{-1}) indicate the presence of oxygen-containing functional groups.

Rice Husk. On the basis of the FTIR analysis of rice husk in Fig. 3, the sample synthesised at 300 °C has the formation of slight double peak at zone 5, 1680–1450 cm^{-1}, indicating the presence of aromatic hydrocarbons such as benzene ring and alkenes. Thus, the product synthesised at 300 °C will be most efficient.

3.2 XRD

Findings. Distinct peaks were observed in two of the XRD graphs. The rice husk graph has not been included as the graph obtained contained no distinct peaks.

Bagasse. The XRD graph of bagasse Fig. 4 shows two distinct peaks which were found using the peak analyser software on Origin Lab. The graph look similar to the one studied during the literature review, and using the mineralogy database, the first peak at the two-theta value of 26.547 is indicative of silicon dioxide and the second peak indicated the presence of silicon dioxide, graphite and copper carbonate. Smaller peaks with lesser intensity could indicate the presence of copper oxide and calcium hydroxide.

Wheat Straw. The XRD graphs of wheat straw Fig. 5 shows 17 peaks using peak analysis on origin laboratory. The peaks of potassium chloride, calcium carbonate, magnesium chloride and silicon dioxide were found from the XRD graph.

Rice Husk. The XRD graph of rice husk complies with the literature review; however, no peaks were observed from the graph. The peaks of manganese dioxide, silicon dioxide, calcium oxide and aluminium oxide were to be observed for the samples.
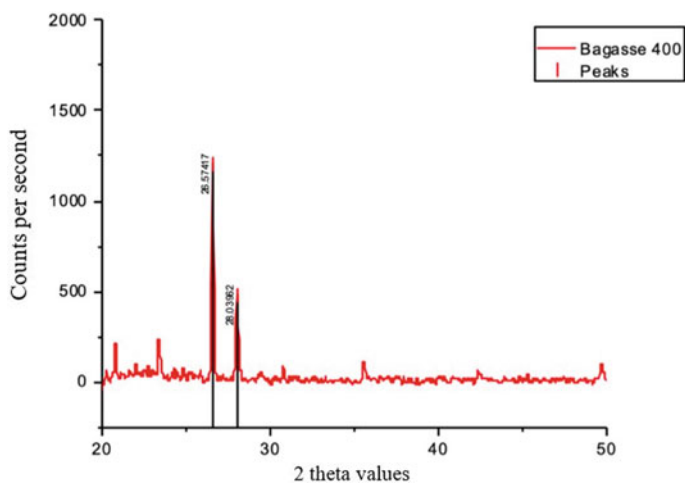
Fig. 4 Bagasse synthesised at 400 °C XRD
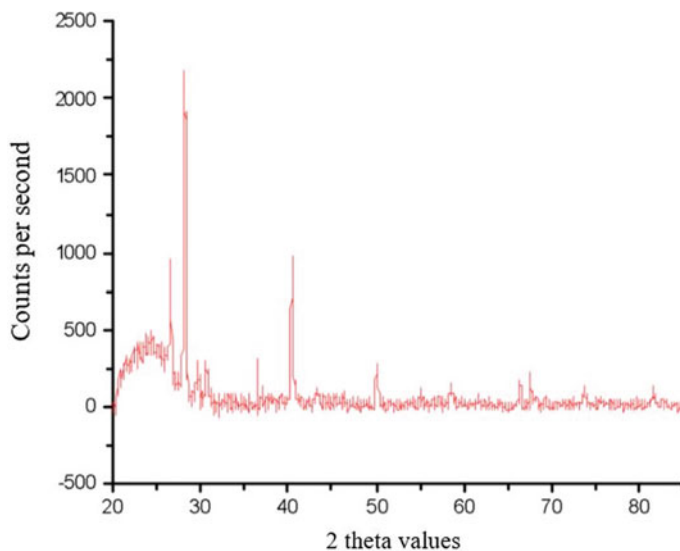
Fig. 5 Wheat straw synthesised at 300 °C XRD

3.3 Atomic Adsorption Spectroscopy

Findings. Each type of biochar removed a certain quantity of cadmium. From the graph Fig. 6, it is evident that wheat straw and bagasse had the highest removal efficacy at each quantity of biochar used.
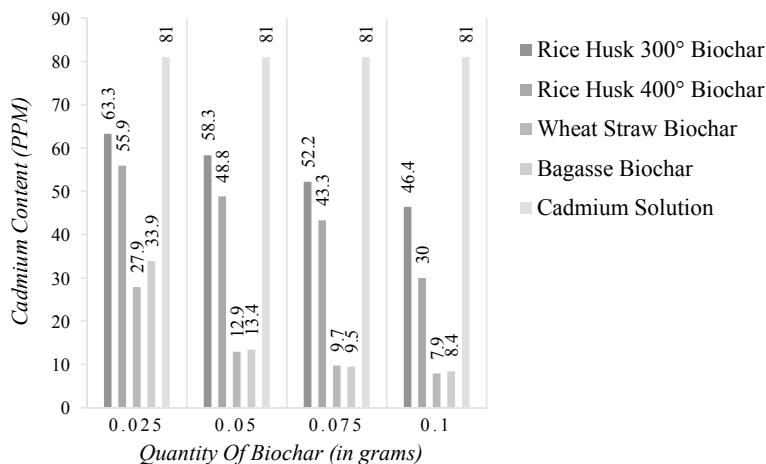
Fig. 6 Amount of cadmium removed across different char quantity and types

Effect of biochar dosage. As the quantity of biochar used increases, the amount of cadmium removed also increases. This could mean that more than 0.1 gm of biochar per 10 ml of contaminated water could potentially remove all cadmium heavy metal ions in an 81 ppm solution.

Effect of pyrolysis temperature. Two types of biochar were synthesised from the same feeder material but at different temperatures. It is evident from Fig. 6 that as the temperature of synthesis for rice husk increases from 300° to 400°, the amount of cadmium removed also increases.

Effect of feeder material. From the literature review, it was found that wheat straw has an increased aromaticity and carbon content as the temperature of pyrolysis increases from 300° to 400°. Bagasse has the presence of several minerals, and it is possible that cadmium was precipitated out of the solution or is bound on the surface of the char.

4 Conclusion

It is evident from the analysis that an increase in the amount of biochar applied to cadmium-contaminated water results in a higher removal capacity. While an increase in the temperature could also play a role in the removal efficiency, only rice husk was analysed at two different temperatures; hence, the data set is too small to support this. Bagasse and wheat straw biochar removed the highest amount of cadmium, and as the ration of biochar to contaminant was increased, the removal of heavy metal increased.

There is a further need to test the efficiency of a mixed ratio of biochar and the efficiency of removal of a mixed ratio of contaminants by a fixed ratio of char. A SEM analysis could further help in ascertaining the mechanism by which the heavy metal ion was removed by bagasse and wheat straw biochar.

References

1. Beesley, L., Moreno-Jiménez, E., Gomez-Eyles, J.L., Harris, E., Robinson, B., Sizmur, T.: A review of biochars' potential role in the remediation, revegetation and restoration of contaminated soils. Environ. Pollut. **159**(12), 3269–3282 (2011)
2. Camps-Arbestain, M., Amonette, J.E., Singh, B., Wang, T., Schmidt, H.P.: A biochar classification system and associated test methods. In: Biochar for Environmental Management: Science, Technology and Implementation, pp. 165–193 (2015)
3. Claoston, N., Samsuri, A.W., Ahmad Husni, M.H., Mohd Amran, M.S.: Effects of pyrolysis temperature on the physicochemical properties of empty fruit bunch and rice husk biochars. Waste Manage. Res. **32**(4), 331–339 (2014)
4. Das, P., Ganesh, A., Wangikar, P.: Influence of pretreatment for deashing of sugarcane bagasse on pyrolysis products. Biomass Bioenerg. **27**(5), 445–457 (2004)

5. El-Gamal, E.H., Saleh, M., Elsokkary, I., Rashad, M., El-Latif, M.A.: Comparison between properties of biochar produced by traditional and controlled pyrolysis. Alex. Sci. Exch. J. **38**, 412–425 (2017)

6. Gai, X., Wang, H., Liu, J., Zhai, L., Liu, S., Ren, T., Liu, H.: Effects of feedstock and pyrolysis temperature on biochar adsorption of ammonium and nitrate. PLoS ONE **9**(12), e113888 (2014)

7. Gomez-Eyles, J.L., Beesley, L., Moreno-Jimenez, E., Ghosh, U., Sizmur, T.: The potential of biochar amendments to remediate contaminated soils. Biochar. Soil Biota **4**, 100–133 (2013)

8. Gregorich, E.G., Carter, M.R.: Soil Sampling and Methods of Analysis. CRC press

9. Jeong, C.Y., Dodla, S.K., Wang, J.J.: Fundamental and molecular composition characteristics of biochars produced from sugarcane and rice crop residues and by-products. Chemosphere **142**, 4–13 (2016)

10. Jindo, K., Mizumoto, H., Sawada, Y., Sanchez-Monedero, M.A., Sonoki, T.: Physical and chemical characterizations of biochars derived from different agricultural residues. Biogeosci. Discuss. **11**(8) (2014)

11. Li, G., Zhu, W., Zhu, L., Chai, X.: Effect of pyrolytic temperature on the adsorptive removal of p-benzoquinone, tetracycline, and polyvinyl alcohol by the biochars from sugarcane bagasse. Korean J. Chem. Eng. **33**(7), 2215–2221 (2016)

12. Mahmoud, A.H., Saleh, M.E., Abdel-Salam, A.A.: Effect of rice husk biochar on cadmium immobilization in soil and uptake by wheat plant grown on lacustrine soil. Alex. J. Agric. Res. **56**(2), 117–125 (2011)

13. Muhammad, N., Aziz, R., Brookes, P.C., Xu, J.: Impact of wheat straw biochar on yield of rice and some properties of Psammaquent and Plinthudult. J. Soil Sci. Plant Nutrition **17**(3), 808–823 (2017)

14. Naeem, M.A., Khalid, M., Aon, M., Abbas, G., Tahir, M., Amjad, M., Murtaza, B., Yang, A., Akhtar, S.S.: Effect of wheat and rice straw biochar produced at different temperatures on maize growth and nutrient dynamics of a calcareous soil. Arch. Agron. Soil Sci. **63**(14), 2048–2061 (2017)

15. Nordic Council of Ministers Cadmium Review, Nordic Council of Ministers (2003)

16. Rodríguez-Vila, A., Forján, R., Guedes, R.S., Covelo, E.F.: Effect of waste mixed with biochar as soil amendment on trace element solubility in a mine soil. Span. J. Soil Sci. **7**(2) (2017)

17. Saleh, M.E., Mahmoud, A.H., El-Refaey, A.A.: Removal of cadmium from aqueous solution by biochars derived from peanut hull and wheat straw. Adv. Environ. Biol. 399–410 (2014)

18. Windeatt, J.H., Ross, A.B., Williams, P.T., Forster, P.M., Nahil, M.A., Singh, S.: Characteristics of biochars from crop residues: potential for carbon sequestration and soil amendment. J. Environ. Manage. **146**, 189–197 (2014)

19. Yahaya, Y.A., Don, M.M.: Pycnoporus sanguineus as potential biosorbent for heavy metal removal from aqueous solution: a review. J. Phys. Sci. **25**(1), 1 (2014)

20. Zhang, S., Luo, Z., Abdalla, M.A., Xia, S.: The wheat straw biochar research on the adsorption/desorption behaviour of mercury in wastewater. Desalin. Water Treatment **112**, 147–160 (2018)

Influence of Lime on the Unconfined Compressive Strength of Cnoal Gangue

Mohammed Ashfaq [ID]**, M. Heera Lal** [ID]**, and Arif Ali Baig Moghal** [ID]

Abstract Coal gangue is one of the largest industrial residues generated during the coal mining process. The surge in demand for coal has led to further increase in coal gangue production, and its safe disposal is an arduous effort in terms of costs involved and the associated environmental impacts. To address these issues, innovative methods are explored for coal gangue utilization in different fields. The bulk and effective utilization of coal gangue can be attained by using it for various geotechnical applications. Unconfined compressive strength (UCS) of any material plays a major role in its utilization for various geotechnical applications like reclamation fill, fill behind retaining wall, base and sub-base layer. In the present study, the UCS of coal gangue and its variation on addition of lime at different curing periods has been studied. The effect of lime content and curing period clearly manifested with a significant increase in UCS of stabilized coal gangue. The improvement in strength is attributed to the formation of pozzolanic compounds with the curing period.

Keywords Coal gangue · Unconfined compression strength · Pozzolanic compounds · Backfill; reclaimed fill

1 Introduction

Coal-based thermal power stations generate many residues during the combustion process, and collectively, they are referred to as coal combustion residues (CCRs). CCRs include fly ash, pond ash, bottom ash, etc., which create severe problems while handling and disposing them [1]. In India, the majority of coal produced is of inferior grade with a poor calorific value which has contributed to the increased level of CCRs' generation of about hundred million tons per year [2]. Disposal of these residues consumes large volumes of land contaminating the ground and surface water bodies, thereby leading to severe environmental and ecological impacts [3–6]. In a

M. Ashfaq (✉) · M. Heera Lal · A. A. B. Moghal
Department of Civil Engineering, NIT, Warangal, Warangal 506004, Telangana, India
e-mail: gmohdashfaq@gmail.com

vast and developing country like India, there is scarcity of quality construction materials with desired durability and strength properties. However, with the increase in costs of conveyance, there is a substantial increase in demand for alternate materials [7]. Hence, attempts are made to identify alternate avenues for the bulk utilization of these residues. Over the past few decades, the development of green construction materials has been promoted significantly by the higher sustainability standards of the construction industry [8–11]. The usage of such alternate materials can bring down energy consumption, greenhouse emissions and usage of raw materials [12, 13], and eventually, contributes to the reduction in overall project costs and to address environmental issues associated with its disposal. Hence, bulk utilization of the recycled materials can resolve all the above-mentioned issues to a large extent.

In this context, the present work intends to study the feasibility of utilizing coal mine waste, i.e. coal gangue as a fill material. The strength of the material is considered as one of the primary criteria for backfill applications. In the present study, an attempt has been made to study the unconfined compressive strength (UCS) of coal gangue. An attempt has been made to study the effect of lime addition on UCS of coal gangue. Moreover, the role of curing period on the UCS of lime-treated coal gangue has also been studied.

2 Materials and Methodology

Coal gangue was procured from Kakatiya Coal mines, Bhupalpally, Telangana. These samples were air-dried and crushed prior to passing through a 0.425 mm mesh sieve to homogenize them for the subsequent analysis. The powdered coal gangue samples were dried in a temperature-controlled oven at 100 °C for 24 h to remove moisture. Analytical grade hydrated lime has been used in the present study. Varying lime (2, 4 and 6%) percentages were added to the coal gangue on weight basis. To understand the influence of lime, moisture content was fixed at OMC of untreated coal gangue. The samples were cured for a period of 7, 14, 21 and 28 days in a desiccator. The UCS testing was done in accordance with ASTM D2166 [14]. The physical properties of coal gangue are presented in Table 1.

3 Results and Discussion

The unconfined compressive strength (UCS) of untreated coal gangue and its increment with lime addition at 28 days curing period is presented in Table 2.

Table 1 Physical properties of coal gangue

Properties	Values
Specific gravity	2.57
Grain size distribution	
Coarse fraction (%)	11
Fine fraction (%)	89
Atterberg limits	
Liquid limit (%)	28
Plastic limit (%)	NP
Plasticity index (%)	NP
Compaction characteristics	
Optimum moisture content (%)	17.6
Maximum dry density (kN/m^3)	21
pH	7.24
Carbon content (%)	3.5

Table 2 Increment in UCS of lime-stabilized coal gangue

Combinations	Unconfined compressive strength (kPa)
Coal gangue + 0% lime	118 (x)
Coal gangue + 2% lime	770 (6.54x)
Coal gangue + 4% lime	1041 (8.83x)
Coal gangue + 6% lime	1300.02x)

3.1 Effect of Lime Content

The UCS of the lime-stabilized coal gangue is shown in Fig. 1. From the figure, it can be noted that with the addition of lime, there is a substantial increase in UCS of coal gangue. The maximum increase in UCS was observed for 6% lime addition with an increment of 1100%. The initial increase in UCS at lower curing period can be attributed to the onset of pozzolanic reaction. Addition of lime triggers the breaking of Si–O bonds in the silica-rich coal gangue. Coal gangue with reactive silica can produce more cementitious compounds on reaction with lime addition as it increases the hydroxyl ion supply for the hydration of coal gangue [15–17]. Moreover, the rate of gain in UCS value with curing period for lime-stabilized coal gangue is low at the beginning but it increases with increase in curing period. Low UCS value at less curing period may be due to low pH values of the pore fluid.
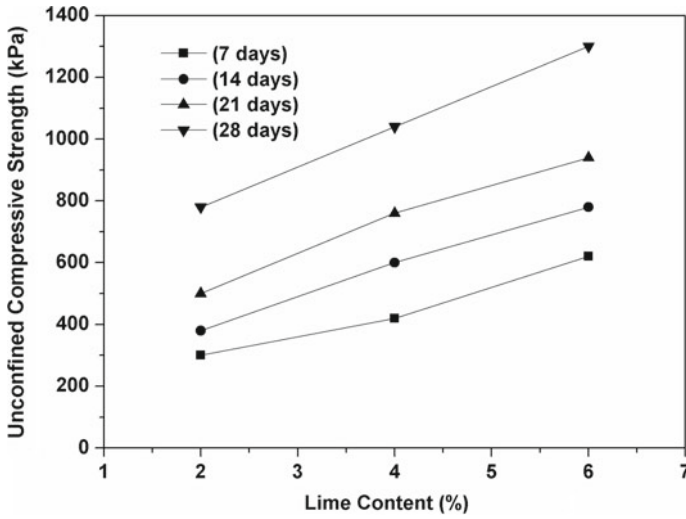
Fig. 1 Variation in UCS of coal gangue with lime content

3.2 Effect of Curing Period

Effect of curing over a period of 28 days for lime-stabilized coal gangue is shown in Fig. 2. It is evident from the figure that curing has a pronounced effect on unconfined compressive strength of coal gangue samples. There is a linear increase in UCS value
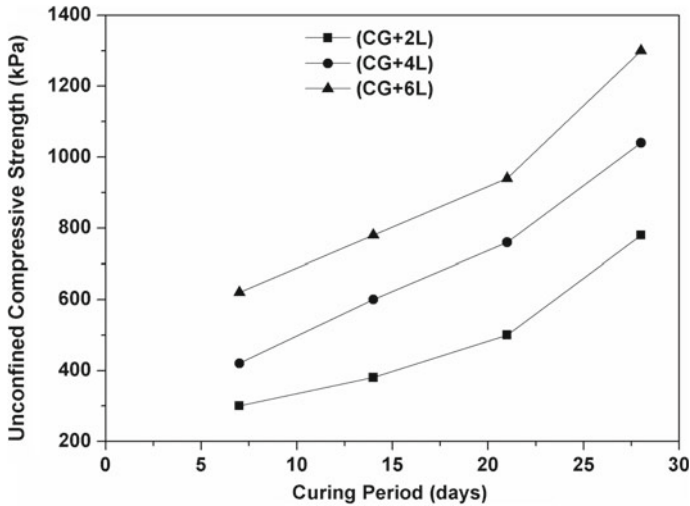
Fig. 2 Variation in UCS of coal gangue with curing period
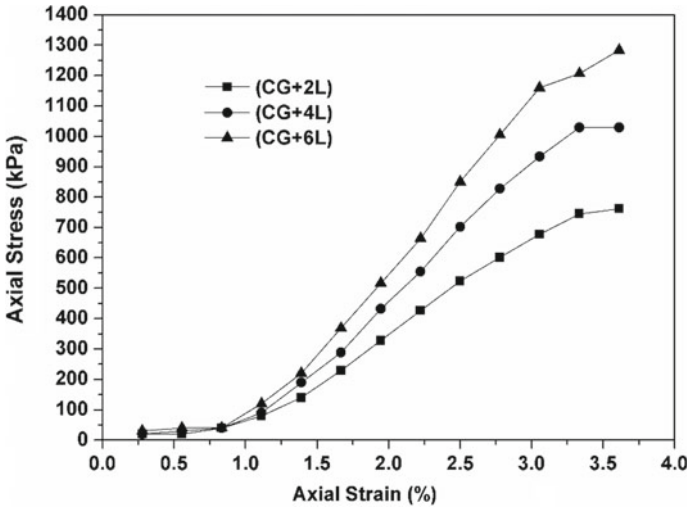
Fig. 3 Stress–strain behaviour of lime-stabilized coal gangue

with curing period. This behaviour is due to the fact that the addition of lime initiates the reaction between the silica and some alumina of the lattices of coal gangue. Further, highly alkaline environment produced due to lime addition helps in dissolution of alumina-silicates which are eventually precipitated as hydrated cementitious reaction products [18–20]. Furthermore, lime addition results in increased number of hydration products to fill the pore structures. The gain in strength due to lime is mainly believed due to substitution of other cations by calcium.

The stress–strain behaviour of coal gangue at varying lime contents is shown in Fig. 3. It was observed that the addition of lime has a profound effect on the stress–strain behaviour of coal gangue. A relatively linear behaviour of stress increase was noted for the corresponding strains. However, irrespective of stabilization, the failure point (at 4.3% strain) of coal gangue has remained constant for all the combinations considered. It was noticed that the application of load in excess of 3.5% strain has no significant impact on the stress-behaviour. Further, the effect of lime addition was noticeable from 2% strain, which may be due to the realignment of minerals of coal gangue [21] (Fig. 4).

4   Conclusions

In the present study, the strength behaviour of coal gangue was evaluated to assess its feasibility as a backfill material. The effect of lime (2, 4 and 6%) on UCS of coal gangue was also investigated. The following conclusions are drawn from the study:

Fig. 4 UCS samples of coal gangue and lime mixtures

- The addition of lime has led to a substantial increase in UCS of coal gangue. With an increment of 1100%, the maximum increase in UCS was observed for 6% lime addition.
- There is a linear increase in UCS value with the curing period. An enhancement in UCS of 400% was observed with the curing period.
- It was observed that the addition of lime has a profound effect on the stress–strain behaviour of coal gangue.
- It was noticed that the application of load in excess of 3.5% strain has no significant impact on the stress behaviour.

References

1. Sridharan, A., Pandian, N.S., Srinivasa Rao, P.: Shear strength characteristics of some Indian fly ashes. Ground Improve. **2**, 141–146 (1998)
2. Pandian, N.S., Krishna, K.C.: CBR behaviour of fly ash–murrum mixes. Ground Improve. **5**(4), 177–181 (2001)
3. Li, Y., Yao, Y., Liu, X., Sun, H., Ni, W.: Improvement on pozzolanic reactivity of coal gangue by integrated thermal and chemical activation. Fuel **109**, 527–533 (2013)
4. Chuncai, Z., Guijian, L., Dun, W., Ting, F., Ruwei, W., Xiang, F.: Mobility behaviour and environmental implications of trace elements associated with coal gangue: a case study at the Huainan Coalfield in China. Chemosphere **95**, 193–199 (2014)
5. Zhang, Y.Y., Nakano, J., Liu, L.L., Wang, X.D., Zhang, Z.T.: Trace element partitioning behaviour of coal gangue-fired CFB plant: experimental and equilibrium calculation. Environ. Sci. Pollut. Res. **22**, 15469–15478 (2015)
6. Yang, L., Song, J., Bai, X., Song, B., Wang, R., Zhou, T., Jia, J., Pu, H.: Leaching behavior and potential environmental effects of trace elements in coal gangue of an open-cast coal mine area, inner Mongolia. China. Miner. **6**(50), 1–18 (2016)
7. Sivapullaiah, P., Moghal, A.: CBR and strength behaviour of class F fly ashes stabilized with lime and gypsum. Int. J. Geotech. Eng. **5**, 121–130 (2011)

8. Xu, G., Shi, X.: Characteristics and applications of fly ash as a sustainable construction material: a state-of-the-art review. Resour. Conserv. Recycl. **136**, 95–109 (2018)
9. Wang, J., Qin, Q., Hu, S., Wu, K.: A concrete material with waste coal gangue and fly ash used for farmland drainage in high groundwater level areas. J. Clean. Prod. **30**, 1–8 (2016)
10. Wu, D., Hou, Y., Deng, T., Chen, Y., Zhao, X.: Thermal, hydraulic and mechanical performances of cemented coal gangue-fly ash backfill. Int. J. Miner. Process. **162**, 12–18 (2017)
11. Wu, H., Hu, L.: Feasibility study on the application of coal gangue as landfill liner material. Waste Manage. **63**, 162 (2017)
12. Praticò, F., Saride, S., Puppala, A.J.: Comprehensive life-cycle cost analysis for selection of stabilization alternatives for better performance of low-volume roads. Transp. Res. Rec. **2204**(1), 120–129 (2011)
13. Purnell, P.: The carbon footprint of reinforced concrete. Adv. Cement Res. **25**(6), 362–368 (2013)
14. ASTM D2166/D2166M–16: Standard test method for unconfined compressive strength of cohesive soil: West Conshohocken (2012)
15. Ghosh, A.: Compaction characteristics and bearing ratio of pond ash stabilized with lime and phosphogypsum. J. Mater. Civ. Eng. **22**(4), 342–351 (2010)
16. Ghosh, A., Subbarao, C.: Strength characteristics of class F fly ash modified with lime and gypsum. J. Geotech. Geoenviron. Eng. **133**(7), 757–766 (2010)
17. Sivapullaiah, P., Moghal, A.: Role of gypsum in the strength development of fly ashes with lime. J. Mater. Civ. Eng. **23**(2), 197–206 (2011)
18. Diamond, S., Kinter, E.B.: Adsorption of calcium hydroxide by montmorillonite and kaolinite. J. Colloid Interf. Sci. **22**(3), 240–249 (1966)
19. Bell, F.: Lime stabilization of clay minerals and soils. Dep. Geol. Appl. Geol. **42**, 223–227 (1996)
20. Rao, S.M., Shivananda, P.: Compressibility behaviour of lime-stabilized clay. Geotech. Geol. Eng. **23**, 309–319 (2005)
21. Mitchell, J.K.: Fundamentals of soil behavior. Wiley, New York (1993)

Potential Application of Treated Bauxite Residue

Sujeet Kumar, Abhay Kumar Verma, and Arun Prasad

Abstract Bauxite residue is a significant industrial solid waste residue produced by the Bayer process for the extraction of alumina from bauxite ores. It is usually disposed off in the form of slurry in the nearby areas of the alumina industry. About 400 million tons of bauxite residues are produced annually worldwide. However, it has some environmental and logistical problems in handling and disposal due to high alkalinity (pH 10–13.5), sodicity, fine particles, and some trace metal content. Thus, it cannot be used directly and requires pre-treatment before any civil engineering applications. In view of the given above, an attempt has been made to explore the potential of the bauxite residue for some civil engineering applications. The present study investigates the effect of various parameters on the strength and durability of bauxite residue. Further, a series of laboratory tests considering various parameters were carried out. The results indicate that treated bauxite residue with a certain combination of parameters (dry density, moisture content, and curing time) can be used as an unfired brick for low-cost housing.

Keywords Bauxite residue · Strength · Durability · Unfired brick · Subbase

1 Introduction

Most of the developing nations have one of the significant challenges to fulfill the demands of the rapidly increasing population. Industrialization and urbanization are the two common phenomena for these nations. Although it is quite essential for the betterment of the society regarding infrastructure and ongoing developmental activities at the same instance (time), we have to consider their negative impacts leading to disposal, environmental, and health problems. In the present scenario, the global researcher community is also dedicating its research to find out new ways to

S. Kumar (✉)
Civil Engineering Department, Shiwalik College of Engineering, Dehradun 248197, India
e-mail: Sujeet.rs.civ14@iitbhu.ac.in

A. K. Verma · A. Prasad
Civil Engineering Department, Indian Institute of Technology (BHU), Varanasi 221005, India

reduce the industrial wastes by using them as an alternative construction material. Bauxite residue is a major industrial solid waste produced during the extraction of alumina from bauxite ores. The worldwide deposits of bauxite ore are estimated approximately to be 55–75 billion tons, whereas India shares about 7% of global inventory [1]. Worldwide generation of this industrial waste was about 4 billion tons per annum till 2016 [2], whereas Indian alumina plants generate approximately 14 million tons of bauxite residue every year.

Various researchers have examined the chemical compositions of bauxite residue and found that it mainly contains minerals of ferrous (hematite, magnetite, and goethite), silica (quartz and sodalite), alumina (gibbsite, diaspore, and boehmite), calcite, anatase, rutile, perovskite, water, oxalate, occulants, some organic and inorganic carbon, and some trace and rare earth elements [1, 3]. From the literature, it appears that bauxite residue is predominately composed of oxides of iron, alumina, and silica. The availability of such elements (aluminate and/or silicate) is an essential constituent in any pozzolanic reactions in the presence of water and alkali. However, this waste has some environmental and logistical concerns with handling, storing, and disposal due to its characteristics such as high alkalinity (pH $10-13.5$), sodicity, fine particles, and heavy metals content [4]. Thus, bauxite residue cannot be used without treatment/stabilization and requires pre-treatment for any mass utilization. In view of the given above, researchers have carried out numerous studies covering various aspects such as metals recovery, water, wastewater treatment, and production of construction and building materials. However, civil engineering is one of the promising areas where mass utilization of these wastes can be utilized with some modification in different forms such as pavement materials, bricks, paving blocks, and embankment materials. Several investigators have been trying to develop construction and building materials using bauxite residue in conjunction with different types of industrial rejects (fly ash, silica fume, stone dust and lime, cement, gypsum, clay, etc.) and additives (traditional and non-traditional) [5–8]. However, in case of multivariate (multi-parameter) studies, conducting experiments and recording of results are bit expensive and time-consuming. In such situation, design of experiment can be used as an alternative for planning and designing the experiments which also overcome the deficiencies of conventional methods. Various researchers have applied design of experiment (DOE) in different areas such as sewage sludge ash optimization [9], optimized amount of lime, rice husk ash [10], fermentation, and bios option process [11, 12]. The present work is an attempt to treat bauxite residue. In this paper, experimental designed approach is used to assess the strength of treated bauxite residue. Finally, different possible applications of treated materials have also been tried for the possible utilization as construction and building materials.

Table 1 Geotechnical properties of the bauxite residue

Properties	Value
Maximum dry density (kN/m^3)	1.50
Optimum moisture content (%)	30
pH	10.2
Specific gravity	3.1
Sand content (%)	28
Silt size particle (%)	60
Clay size particle (%)	12
Effective diameter D10 (mm)	0.007
Coefficient of uniformity, C_u	8.57
Coefficient of curvature, C_c	0.69
Unified soil classification system (USCS)	ML
Unconfined compressive strength (kPa)	138.6

2 Materials and Methodology

2.1 Material

Bauxite residue used in the study was collected from Hindalco Industries Limited, Renukoot, and Uttar Pradesh, India. It appears reddish and contains mostly fine particles on visual examination. Commercial grade dry hydrated lime ($CaOH_2$) is used as the cementing agent, and it consists mainly of oxides of Ca and Mg. The physical and geotechnical properties of bauxite residue are summarized in Table 1.

2.2 Sample Preparation

Firstly, the required amount of bauxite residue and lime was mixed in a dry state to a uniform consistency. Water was then added while continuing the mixing process until a uniform, homogeneous mixture was obtained. After mixing, it was compacted in three layers in a split mold. After the molding process, the sample was extracted from the mold and placed in an airtight polythene bag. The sample was allowed to cure for desired curing periods in desiccators at room temperature (23 ± 3 °C) by maintaining the relative humidity of more than 95%. After the molding and curing processes, the sample was tested in an automatic load compression device of 50 kN capacity with a proving ring of 10 kN capacity.

Table 2 Factors and their ranges selected for the study	Factor	Variable type	Purpose
	Additive content (%)	Quantitative	Influence of cementing agent
	Curing time (days)	Quantitative	Effect of curing
	Molding moisture content (%)	Quantitative	Effect of molding moisture
	Dry unit weight (kN/m^3)	Quantitative	Effect of packing of particle

2.3 Selection of Factors

Five factors were selected for the investigation of the evaluation of strength and durability of bauxite residue on the basis of the literature review and were included in the experiment. Table 2 summarizes the factors and their range used in the present study.

2.4 Design Methodology

Different experimental design methods may be used for the design of the experiment, but it solely depends on the nature and operability region of the problem. In this study, Box-Behnken design (BBD) is used to design the experiment. It is a three-tier factorial method used in experimental design. The methodology of design of experiment is available in detail in [13], and thus, these are not described here. Input variables employed for this study are the lime content (L) and molding moisture (w) in percentage, dry density (γ_d) in kN/m^3, and curing time (t) in day. The operating ranges are taken as 3–11% for L, 26–30% for w, 13–15.5 kN/m^3 for γ_d, and 7–60 days for t. The experimental levels of independent variables are given in Table 3.

Table 3 Experimental level of independent variables used in the design of experiment	Input parameter	Range		
		−1	0	1
	W	26	28	30
	L	3	7	11
	γ_d	13	14.3	15.5
	T	7	34	60

3 Results and Discussions

Based on the experimental design, laboratory tests are performed and results are recorded for each combination. Results of the laboratory tests are presented as the response in Table 4.

Table 4 Design matrix of input and output based on the design of experiment

Run No	Input parameters				Response
	w	L	γ_d	t	UCS (kPa)
1	30	11	14.25	33.5	2381.09
2	28	3	14.25	60	1679.35
3	26	7	15.5	33.5	2295.68
4	28	7	14.25	33.5	1576.36
5	28	7	14.25	33.5	1464.13
6	28	7	14.25	33.5	1531.05
7	28	11	14.25	60	2568.24
8	28	11	15.5	33.5	3335.25
9	30	3	14.25	33.5	1108.35
10	26	7	13	33.5	947.02
11	28	7	15.5	7	1704.47
12	28	3	14.25	7	702.14
13	28	7	14.25	33.5	1347.08
14	30	7	13	33.5	1123.16
15	26	7	14.25	60	2214.05
16	28	7	14.25	33.5	1482.51
17	28	7	14.25	33.5	1525.4
18	28	7	15.5	60	3308.29
19	28	7	13	7	838.59
20	28	11	14.25	7	1387.41
21	30	7	14.25	7	1124.23
22	30	7	14.25	60	2189.8
23	26	3	14.25	33.5	997.38
24	26	7	14.25	7	1051.8
25	28	3	13	33.5	737.26
26	26	11	14.25	33.5	1856.25
27	30	7	15.5	33.5	2537.24
28	28	7	13	60	1549.35
29	28	3	15.5	33.5	1725.69
30	28	11	13	33.5	1324.05

Table 5 Summary of various predictive models based on Box-Behnken (BB) experimental design approach

Source	Std Dev	p-value	R^2	Adj R^2	Pre R^2	Remarks
Linear	247.18	<0.0001	0.96310	0.95460	0.92660	Significant
2FI	116.15	0.11130	0.97920	0.96680	0.90910	Insignificant
Quadratic	61.84	0.00340	0.99670	0.99250	0.95490	Opted
Cubic	21.02	0.04120	0.99950	0.99800	0.84960	Aliased

After successful experimental design and development, a predictive equation establishes the relationship between input parameters and response for the range of study. Thus, various linear and nonlinear empirical models were tried, and the details are presented in Table 5.

From Table 5, it is seen that quadratic models better satisfy the statistical criteria (as correlation coefficient ($R^2 = 0.92$)) and hence selected as predictive equations for the range of study. Further, the selection of the statistically significant input variables after choosing the best predictive model is the key step in the experimental design. It tells us if the independent variables and their interaction have significant influence on the dependent variables. In this case, variance analysis (ANOVA) could be beneficial in describing the interactions between variables. Thus, ANOVA was performed to establish the parameters found as statistically significant in the predictive model and their relative contributions to the dependent parameter (response), and the results are presented in Table 6.

From Table 6, it is also observed that the proposed models contain some statistically insignificant terms which have no active role in the prediction of the response. Thus, this term is discarded during the development of predictive equation. Hence, entire insignificant factors are discarded, and only significant parameters are considered for the development of predictive equations. Finally, a mathematical relationship linking all selected parameters is given as Eq. 1:

$$q_u = 31558.15 - 44.63w - 967.89L - 4214.54\gamma_d - 83.67t$$
$$+ 12.93w * L + 51.14L * \gamma_d + 6.74\gamma_d * t + 147.01\gamma_d^2 + 0.13t^2 \quad (1)$$

From the above results, it is seen that treated bauxite residue has good unconfined compressive strength ($460 \leq q_u \leq 4350$ kPa), for the range of studies ($3 \leq L \leq 11\%$, $13 \leq \gamma_d \leq 15.5$ kN/m^3, $26 \leq t \leq 60$ days, and $13 \leq w \leq 30\%$). Hence, treated bauxite residue may have potential to be used in some of the civil engineering applications.

Table 6 ANOVA results for BB design

Source	Sum of squares (SS)	df	Mean square (MS)	F-value	p-value Prob > F	Remarks
Model	1.36E+07	14	9.68E+05	83.09	<0.0001	Significant
W	1.01E+05	1	1.01E+05	8.68	0.01	Significant
L	2.90E+06	1	2.90E+06	249.23	<0.0001	Significant
γ_d	5.86E+06	1	5.86E+06	503.3	<0.0001	Significant
t	3.74E+06	1	3.74E+06	321.22	<0.0001	Significant
$W * L$	42,822.09	1	42,822.09	3.68	0.0744	Not significant
$W * \gamma_d$	1.07E+03	1	1.07E+03	0.0919	0.766	Not significant
$W * t$	2336.76	1	2336.76	0.2006	0.6606	Not significant
$L * \gamma_d$	2.62E+05	1	2.62E+05	22.45	0.0003	Significant
$L * t$	1.04E+04	1	1.04E+04	0.8899	0.3604	Not significant
$\gamma_d * t$	1.99E+05	1	1.99E+05	17.12	0.0009	Significant
w^2	1.05E+04	1	10,495.56	0.9011	0.3575	Not significant
L^2	8973.05	1	8973.05	0.7704	0.3939	Not significant
γ_d^2	3.92E+05	1	3.92E+05	33.66	<0.0001	Significant
t^2	69,371.46	1	69,371.46	5.96	0.0276	Significant
Residual	1.75E+05	15	11,647.39			
Lack of fit	1.43E+05	10	14,319.33	2.27	0.189	Not significant
Pure error	31,517.56	5	6303.51			
Cor total	1.37E+07	29				

3.1 Unfired Bricks

Since the unconfined compressive strength of some of the mix of stabilized red mud is more than 3500 kPa, these mixes have the potential to be used as unfired bricks. Thus, scaled bricks of size (100 × 50 × 50 mm) were prepared in accordance with IS 12894:2002 [14]. It was fabricated in our institute workshop. For preparing mix for brick, the required amount of red mud and lime was mixed in a dry state to a uniform consistency and water was then added while continuing the mixing process until a uniform, homogeneous mixture was obtained. After mixing, it was transferred into the mold and compacted using hydraulic press to achieve the correct dimension. After the molding process, the sample was extracted from the mold, wrapped in an airtight polythene bag, and kept in a desiccator to cure for desired curing period at room temperature (23 ± 3 °C) while maintaining the relative humidity of more than 95%. After the molding and curing processes, the sample was tested in an automatic load compression device of 50 kN capacity with a proving ring of 10 kN capacity. The results of various mix of red mud and lime used for the preparation of unfired bricks are shown in Table 7.

Table 7 Mix compositions used for the preparation of unfired brick

S. No.	Moisture content (w) %	Curing time (t) days	Dry density (γ_d) kN/m3	Lime content (L) %	Average compressive strength	Water absorption (%)
1	26	28	15.5	11	3408.25	19.05
2	26	60	15.5	7	3755.18	17.89
3	26	60	15.5	9	3924.15	15.68
4	26	60	15	11	3398.68	18.78
5	26	60	15.5	11	4075.58	13.81
6	28	28	15.5	11	3789.03	18.85
7	28	60	15.5	7	3645.48	17.94
8	28	60	15.5	9	3756.24	18.58
9	28	60	15	11	3623.08	17.90
10	28	60	15.5	11	4436.29	11.85
11	30	28	15.5	11	3845.72	17.87
12	30	60	15.5	7	4048.91	14.09
13	30	60	15.5	9	4124.19	12.68
14	30	60	15	11	4621.78	11.35
15	30	60	15.5	11	4989.27	12.82

Further, it is also seen that the stabilized red mud unfired bricks fulfill the requirement of compressive strength (>3.5 MP a) and water absorption (<20%) as per IS 12894:2002 [14]. Thus, the brick can be used in low-cost housing which will not only save the conventional constructional materials but also solve the storage problem. The discussed mix will also reduce the chance of contamination of surface and subsurface water bodies.

4 Conclusions

The primary objective of this work is to study the possible potential of treated bauxite residue for different civil engineering applications. An attempt has also been made to incorporate an alternative approach based on the design of the experiment to study the effects of multiple parameters on the compressive strength of bauxite. Further, the results reported in the previous section indicate that the treated bauxite can have scope in pavement layers and brick applications. However, the present study is limited to laboratory test only, and it will require detailed studies to validate these results with various model tests and ˝field studies. Further, the proposed predictive equations work well within the range of the present study. However, the proposed equation may or may not be efficient for the outside range of study like any other technique.

References

1. Sutar, H., Mishra, S.C., Sahoo, S.K., Chakravarty, A.P., Maharana, H.S.: Progress of red mud utilization: an overview. Am. Chem. Sci. J. **4**(3), 255–279 (2014)
2. Zhu, X., Li, W., Guan, X.: An active de-alkalization of red mud with roasting and water leaching. J. Hazard. Mater. **286**, 8591 (2015)
3. Mandal, A., Sinha, O.: New-generation aluminum composite with bottom ash industrial waste. JOM, 16 (2018)
4. Sutar, H., Mishra, S.C., Sahoo, S.K., Maharana, H.: Progress of red mud utilization: an overview. Master's thesis, National Institute of Technology, Rourkela (2014)
5. Feng, Y.L., Yu, L.J., Gao, J.P., Wang, P., Luo, Q.W., Huang, B., Wang, M.: Study on the preparation and properties of red mud unburned brick. Mater. Res. Innov. **19**(sup8), S8297 (2015)
6. Hongying, C.: Formula of environment-friendly red mud-brick or ceramsite, environment-friendly red mud-brick or ceramsite and preparation method thereof. Google Patents (2017), cN107056241 A
7. Jupei, X., Lixuan, G., Zhaoshu, Z.: Unburned brick prepared from main materials of red mud and magnesium slag. Google patents (2012), cN102381864 A
8. Shichao, C., Mianlian, B., Dongyang, M., Hui, S., Zhicheng, C., Xun, X., Daohong, W.: Method for manufacturing perforated brick by using red mud. Google patents (2017), cN106747317 A
9. Güllü, H., Fedakar, H.: Use of factorial experimental approach and effect size on the CBR testing results for the usable dosages of wastewater sludge ash with coarse-grained material. Eur. J. Environ. Civil Eng. **22**(1), 4263 (2018)
10. Olgun, M.: The effects and optimization of additives for expansive clays under freeze-thaw conditions. Cold Reg. Sci. Technol. **93**, 36–46 (2013)
11. Sen, R., Swaminathan, T.: Application of response surface methodology to evaluate the optimum environmental conditions for the enhanced production of surfactin. Appl. Microbiol. Biotechnol. **47**(4), 358–363 (1997)
12. Witek, A., Chojnacka, K., Podstawczyk, D., Dawiec, A., Pokomeda, K.: Application of response surface methodology and artificial neural network methods in modeling and optimization of biosorption process. Biores. Technol. **160**, 150–160 (2014)
13. Kumar, S., Prasad, A.: Strength retrieval of artiËcially cemented bauxite residue using machine learning: an alternative design approach based on response surface methodology. Neural Comput. Appl. (2018). https://doi.org/10.1007/s00521-018-3482-5
14. IS-12894: Pulverized fuel ash-lime bricks. Bureau of Indian Standards, New Delhi, India (2002)

Hydro-mechanical Behavior of Glass Fiber Reinforced Clay Barriers

Koteswaraarao Jadda, Sharon Kumar Injamala, and Ramakrishna Bag

Abstract The current study highlighted the inclusion of glass fiber reinforcement on various hydro-mechanical properties such as volumetric shrinkage, suction, compressibility and hydraulic conductivity of the clay. The effect of electrolyte on the compressibility and hydraulic conductivity of the clay and reinforced clay soil was studied using two NaCl salt concentrations of 0.5 and 1.0 molarity (M). The results showed that increase in glass fiber content leads to increase in the total suction and hydraulic conductivity of clay marginally, whereas compression index was found to be decreased. For 1.0 M NaCl concentration, the compression index of the clay and reinforced clay soils was found to be decreased by about 31% and 19%, respectively. However, the hydraulic conductivity of the clay and reinforced clay was noted to be increased by about 35 and 9 times, respectively. Therefore, the glass fiber can be used as an effective reinforcement material for contaminated barrier materials to improve its properties.

Keywords Clay · Glass fiber · Compression index · Hydraulic conductivity · Saline fluid

1 Introduction

The compacted clays are used as potential barrier materials for most of the municipal solid waste disposal. Due to the scarcity of high-quality bentonites, bentonite has been mixed with sand or clays and used as clay liners. The desiccation process in clays leads to form high shrinkage cracks, which caused to increase in the hydraulic conductivity significantly. In order to reduce desiccation cracking, various types of reinforcement materials such as natural fiber (coir, jute) and synthetic fibers (polypropylene fibers, polyethylene fibers, polyester, polyvinyl alcohol fibers and glass fibers) are extensively used as reinforcement materials in the clay barrier materials [10]. The effect of fiber reinforcement on hydraulic conductivity and desiccation cracking of expansive

K. Jadda (✉) · S. K. Injamala · R. Bag
Department of Civil and Environmental Engineering, IIT Patna, Patna 801106, India
e-mail: Jadda.pce17@iitp.ac.in

clays was investigated by several researchers [1, 3], 8. The above studies concluded that the inclusion of reinforcement leads to decrease in the volumetric cracks and increase in hydraulic conductivity marginally. Divya et al. [4] studied the significance of geo-fiber inclusions on hydraulic conductivity of soils. The study concluded that increase in both the length and concentration of fiber caused a marginal decrease in hydraulic conductivity of the soil.

Mukherjee and Mishra [10] found a decrease in hydraulic conductivity of soils with an increase in the aspect ratio of fibers. In contrast, Miller and Rifai [9] observed a significant increase in hydraulic conductivity with an increase in the aspect ratio of fibers. The fiber reinforcement changes the soil failure pattern from brittle to the ductile tensile [4, 7]. An increase in the fiber reinforcement leads to increase in the unconfined compressive strength (UCS) of soils up to the fiber content of 0.5%, followed by decrease in strength for higher fiber concentrations [2]. Similarly, Jiang et al. [5] observed that 0.3% fiber content was more optimal for stabilization of clays. A uniform increase in UCS with an increase in fiber concentration was noted by Soğancı [13]. Kar et al., [6] investigated the influence of fiber reinforcement on consolidation characteristics of cohesive soil. Thyagaraj and Soujanya [14] studied the effect of polypropylene fiber on waste containment bentonite barriers.

The effect of various leachate concentration on the hydraulic properties of barrier materials has been studied by many researchers [10, 12, 16]. The above studies suggested that the C_C, m_v and t_{90} of the bentonites decreased with increase in salt concentration. Further, the increase in electrolyte concentration caused a significant increase in the hydraulic conductivity of the barrier materials.

In the current study, a series of experiments were conducted to evaluate the significance of glass fiber reinforcement on various soil properties such as shrinkage limit, volumetric shrinkage, suction, compressibility and hydraulic conductivity of the clay.

2 Materials and Methodology

2.1 Materials

Locally available black cotton soil near Bihta village, Patna, Bihar and commercial bentonite procured from Bikaner, Rajasthan, India, were mixed in 50:50 weight ratios and used in the current study for conducting various experiments. The oven-dried black cotton soil passed through 425 micron sieve was used for mixing with bentonite. The basic engineering properties of the clay such as specific gravity, Atterberg limits and particle size distribution were determined following standard Indian soil classification system IS 2720 (Part 3, 1980), IS 2720 (Part 4, 1985) and IS 2720 (Part 5, 1985), respectively. The basic properties of clay mixture (50:50) along with bentonite and black cotton soil are presented in Table 1. The high tensile strength glass fiber of 10–15 mm length was used as reinforced material. The specific gravity and modulus of elasticity of glass fiber were approximately 2.64 and 71 GPa.

Table 1 Physical properties of mixture clay along with parent soils of bentonite and black cotton soil

Property	Specific gravity	Liquid limit (%)	Plasticity index (%)	% of clay fraction	IS classification
Bentonite	2.76	234	187	76	CH
Black cotton soil	2.69	41	21	34	CI
Mixture clay (50:50)	2.74	84.5	52.4	58	CH

2.2 Methodology

A series of experiments were conducted to evaluate the effect of glass reinforcement on various clay properties such as shrinkage limit, volumetric shrinkage, suction, compressibility and hydraulic conductivity. The standard compaction tests were performed as per the guidelines of IS: 2720 (Part-7-1980) by using different fiber contents, i.e., 0, 0.5, 1 and 2%. In order to find out the influence of glass fiber reinforcement on the volumetric shrinkage of the clay, the standard unconfined compressive strength (UCS) soil specimens of 36 mm diameter and 72 mm height were directly extruded from standard compaction mold to the corresponding MDD and OMC of different percentage of reinforcement condition. The initial void ratio of the extruded clay sample was noted as e_0. After that, soil specimens were allowed to dry at room temperature and followed by oven-dried at 110 °C for 24 h.

$$\text{The volumetric shrinkage noted as } V_\text{s} = \frac{e_0 - e_f}{1 + e_0} \times 100 \tag{1}$$

where e_0 and e_f are the void ratios in compacted and shrunken states, respectively [14]. The inclusion of glass fiber on the shrinkage limit of the clay was determined as per IS 2720 (Part 6, 1972). The effect of glass reinforcement on total suction of clay was determined by using WP4C device. The soil samples which were collected from compaction tests were used for suction measurement. The total suction at different gravimetric water contents was determined by drying soil specimens at the room temperature. Triplicate measurement was carried out for each percentage of reinforcement, and the average suction values were reported in the current study.

The effect of glass reinforcement on the compression index and hydraulic conductivity of the clay soil has been investigated using consolidation tests IS 2720-15 (1965). The oedometer clay specimens were prepared at a water content equal to the liquid limit by mixing clay with various percentages of glass fiber such as 0, 0.5, 1 and 2%. On the other hand, the effect of electrolyte concentration on the compression index and hydraulic conductivity of the clay soil and reinforced clay soil was studied using two NaCl concentrations of 0.5 and 1.0 M at a fixed reinforcement content

of 1%. The liquid limit of the clay was found to be 48.4% and 42% to the corresponding NaCl concentration of 0.5 and 1 M. The required quantity of the clay paste was carefully transferred into oedometer rings of size 60 mm diameter and 20 mm height. The consolidation tests were started with an initial pressure of 5 kPa to the maximum stress applied about 800 kPa. The compression index C_c was calculated as the slope of the straight-line portion of the virgin void ratio-effective stress (e-log P) curve.

$$C_c = \frac{e_i - e_j}{\log(\frac{p_i}{p_j})} \tag{2}$$

where e_i and e_j are the void ratios corresponding to the consolidation pressure of P_i and P_j at ith and jth steps of loading, respectively [10].

The hydraulic conductivity of the clay was indirectly calculated from the oedometer test results using Terzaghi's consolidation theory.

$$k = c_v m_v \gamma_w \tag{3}$$

where k is hydraulic conductivity, C_v is the coefficient of consolidation, m_v is the coefficient of volume compressibility and γ_w is the unit weight of pore water pressure. The settlement of the soil samples corresponding to various time intervals was recorded by using LVDT. The coefficient of consolidation (C_v) values of the clay was determined from Taylor's square root time ($\sqrt{T}$) method.

3 Results and Discussion

3.1 Effect of Glass Reinforcement on Shrinkage Limit and Volumetric Shrinkage

The effect of glass fiber reinforcement on the shrinkage limit and volumetric shrinkage of the clay is shown in Fig. 2. The results indicated that with an increase in the percentage of reinforcement, shrinkage limit increases, whereas volumetric shrinkage decreases.

The addition of reinforcement material caused to increase the ductility and tensile strength of clay resulting in the decrease in volumetric shrinkage. The reinforcement material attributes to increase the surface contacts in soils, which improves the resistance of soil against the volume change due to the desiccation process. Further, an increase in fiber content leads to a decrease in the fiber–fiber spacing in soil, resulting in an increase in the fiber soil effective contact area. This phenomenon is attributed to better crack-bridging [14]. The increase in shrinkage limit was found to be more pronounced up to 1% reinforcement, followed by the effect was decreased for
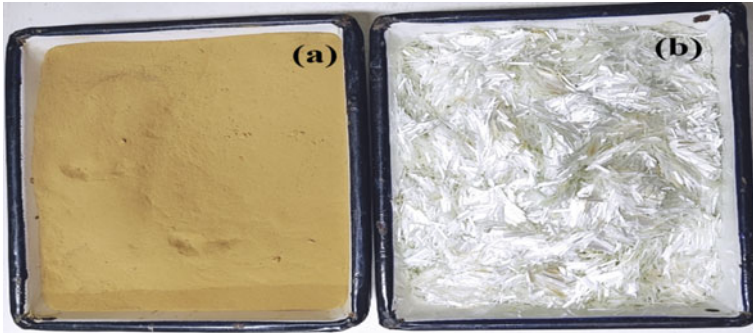
Fig. 1 Photograph of the materials used in the study, **a** mixture clay, **b** glass fiber
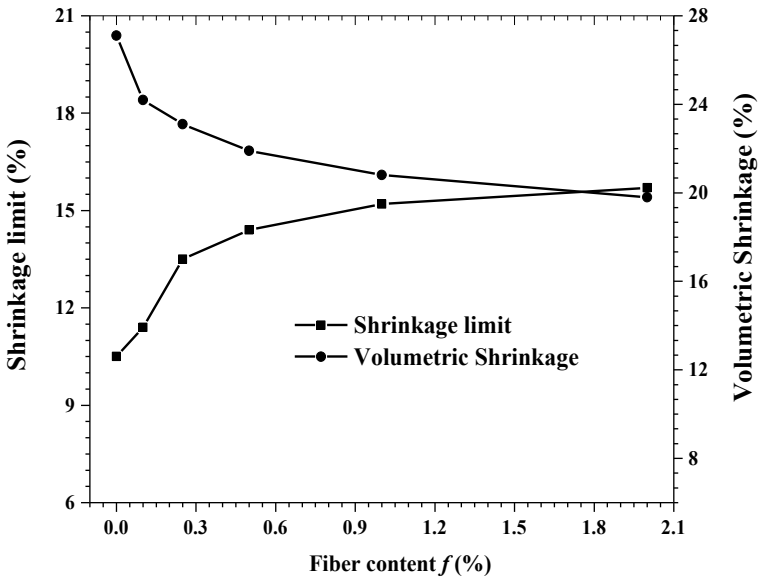
Fig. 2 Effect of glass reinforcement on shrinkage limit and volumetric shrinkage of clay

higher fiber content. Similarly, the volumetric shrinkage was noted to be decreased significantly up to 0.5% of reinforcement. Therefore, inclusion of glass fiber was an effective method to decrease the volumetric shrinkage in clays.
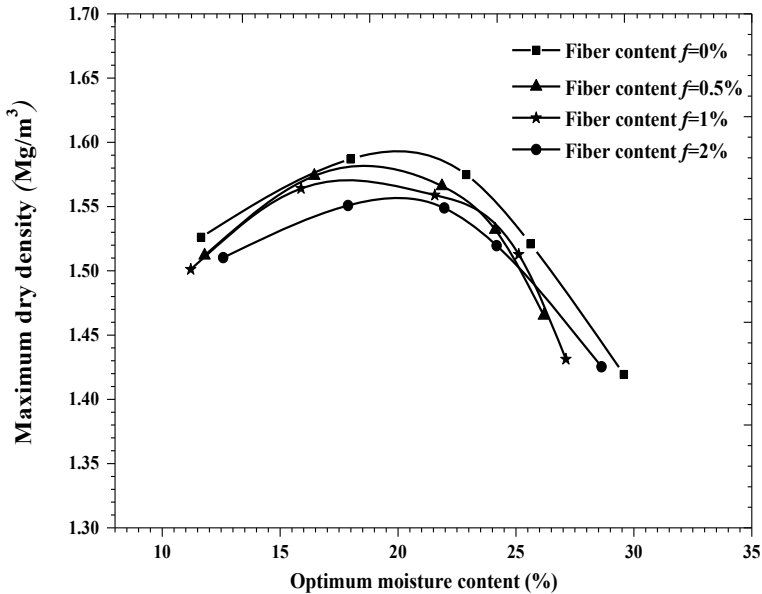
Fig. 3 Effect of glass reinforcement on compaction characteristics of clay soil

3.2 Effect of Glass Fiber Reinforcement on Compaction Tests

The effect of various percentages of glass fiber, i.e., 0, 0.5, 1 and 2% reinforcement on the compaction characteristics of clay, is shown in Fig. 3. The results indicate that the inclusion of glass fiber does not show any significant effect on the optimum moisture content (OMC) of clay.

However, the maximum dry density (MDD) was found to be marginally decreased with an increase in fiber concentration. During an increase in the fiber content, the lightweight material of the fiber can replace the soil clay particles [14]. This phenomenon reduces the total mass of the soil samples in mold, thereby decrease in MDD of clay.

3.3 Effect of Glass Fiber on Suction Properties of Clay

The inclusion of various percentage glass fibers on the total suction of the clay is shown in Fig. 4. The results showed that at a given water content, the increase in fiber content lead to marginally increase in the total suction of clay at lower range of suction below 8 MPa. Due to increase in fiber concentration, the macrospores of the clays could be decreased. Therefore, an increase in suction particularly at lower suction ranges has been noticed. However, at the higher suction range, the inclusion
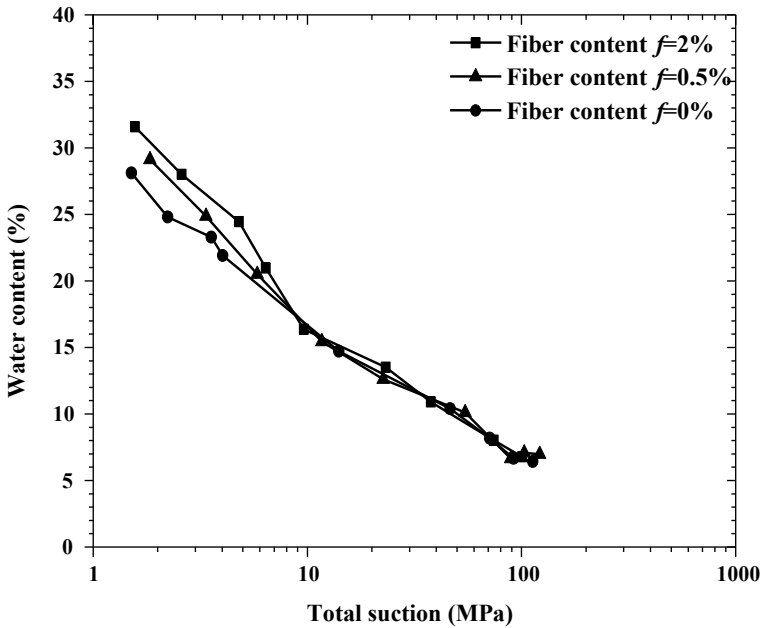
Fig. 4 Soil suction versus water content for the clay as a function of fiber content

of reinforcement does not show any effect on suction properties. Similar observations were reported by Malekzadeh and Bilsel [8]. The increase in fiber content attributed to increase in the air entry value (AEV) of clay. The reinforced fiber material may enhance the bonding between the fiber and soil, which can prevent air entry into the soil pores.

3.4 Effect of Glass Fiber Reinforcement on Compressibility and Hydraulic Conductivity of Clay Soil

The effect of glass fiber reinforcement on void ratio versus logarithm effective pressure, (e-logP) and hydraulic conductivity of the clay is shown in Fig. 5a, b, respectively. The results indicate that both the compression index and hydraulic conductivity of clay were marginally affected by fiber content. As fiber content increases from 0 to 2%, a marginal decrease in consolidation settlement occurred in the clay samples. Therefore, the compression index was noted to be decreased from 0.94 to 0.8. The percentage decrease in the compression index was found to be 14.5%. The fiber materials caused to increase the mechanical interactions between the fibers and soil particles, resulting in increased soil stiffness. Hence, consolidation settlement
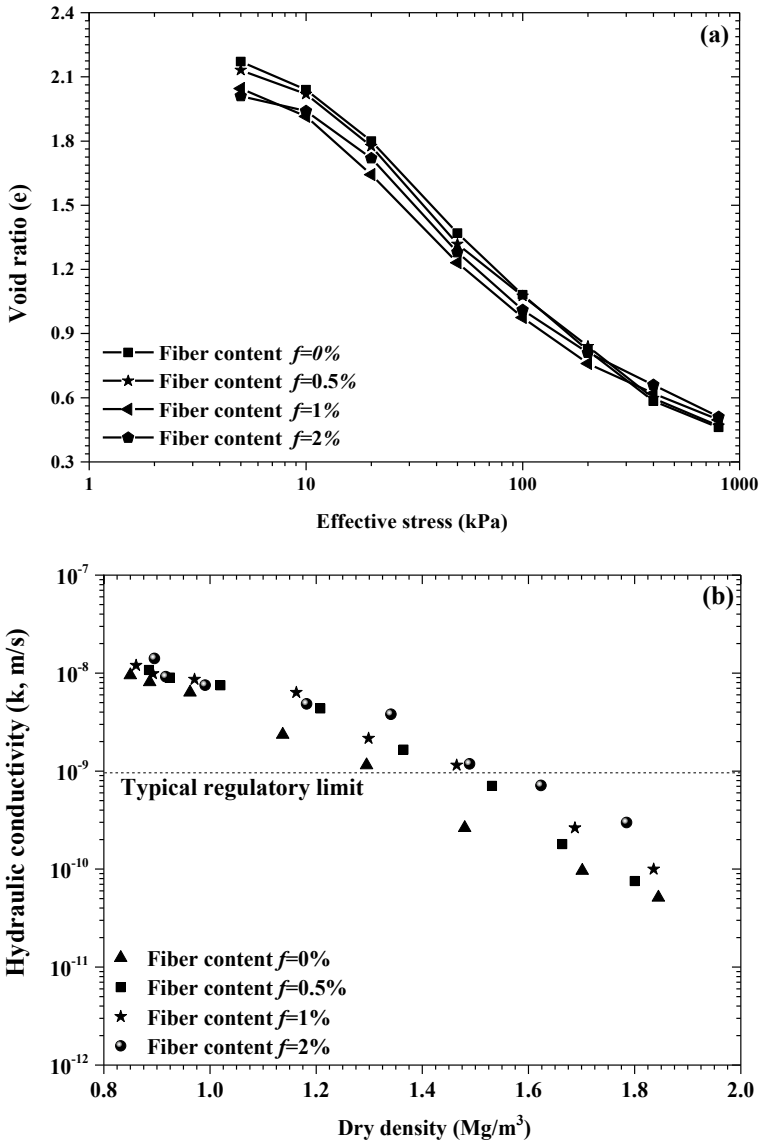
Fig. 5 Effect of inclusion of glass reinforcement on: **a** e-log(p) of the clay; **b** hydraulic conductivity of clay

decreased at higher fiber concentration. The hydraulic conductivity of the unreinforced clay was noted to be varied from 9×10^{-9} to 5×10^{-11} m/s to the corresponding dry density between 0.84 and 1.88 Mg/m^3. In addition to that at a given dry density, the hydraulic conductivity of clay increases marginally with an increase in glass fiber concentration.

As fiber concentration increases from 0 to 2%, the hydraulic conductivity of clay was found to be increased about 3.5 times. The similar observation was made by Abdi et al., [1]. However, the typical hydraulic conductivity value for landfill liner material is 10^{-9} m/s [10]. Therefore, even at higher fiber of 2%, the hydraulic conductivity of fiber reinforced clay was well below the critical hydraulic conductivity limit as shown in Fig. 5. Therefore, at a higher dry density of more than 1.5 Mg/m^3, the reinforced clays were fulfilling the basic criteria of hydraulic conductivity of barrier materials.

3.5 Effete of Saline Fluid on Compressibility and Hydraulic Conductivity of Clay and Reinforced Clay Soil

The effect of saline fluid concentration on both the compressibility and hydraulic conductivity of clay and reinforced clay soil is shown in Fig. 6a, b, respectively. The compression index for clay was noted to decrease from 0.944 to 0.65 to the corresponding increase in salt concentration from zero (Deionized water) to 1.0 M of NaCl. On the other hand, for reinforced clay at 1% glass fiber, the increase in NaCl concentration from 0 to 1.0 M caused to reduce the compression index from 0.786 to 0.63. The percentage of decrease in the compression index was found to be 31% and 19% for unreinforced clay and reinforced soil, respectively. The increase in salt concentration leads to a significant decrease in the diffused double layer thickness of clays. Therefore, the compression index values of unreinforced clay were decreased significantly with the increase in salt concentration. On the other hand, in case of reinforced clay, the effect of NaCl concentration on the compression index was found to be less as compared to unreinforced clay. In the presence of NaCl concentrations, the fiber amended clay experienced less consolidation settlement. The fiber concentration may affect the reduction in DDL thickness of clay. Further, the fiber materials could not allow any compression during the consolidation loading. This phenomenon controls the decrease in the compression index of the reinforced clays.

The results suggested that at a given dry density, due to an increase in NaCl concentration from 0 to 1 M, the hydraulic conductivity of the clay soil was found to be increased about 35 times. On the other hand, for reinforced clay, the hydraulic conductivity was noted to be increased about 10 times. It indicates that unreinforced clay was prone to be significantly affected by external pore fluid concentrations. Therefore, depending on the dry densities, both the unreinforced clay and reinforced clays were fulfilled the basic hydraulic conductivity criteria as engineered barriers
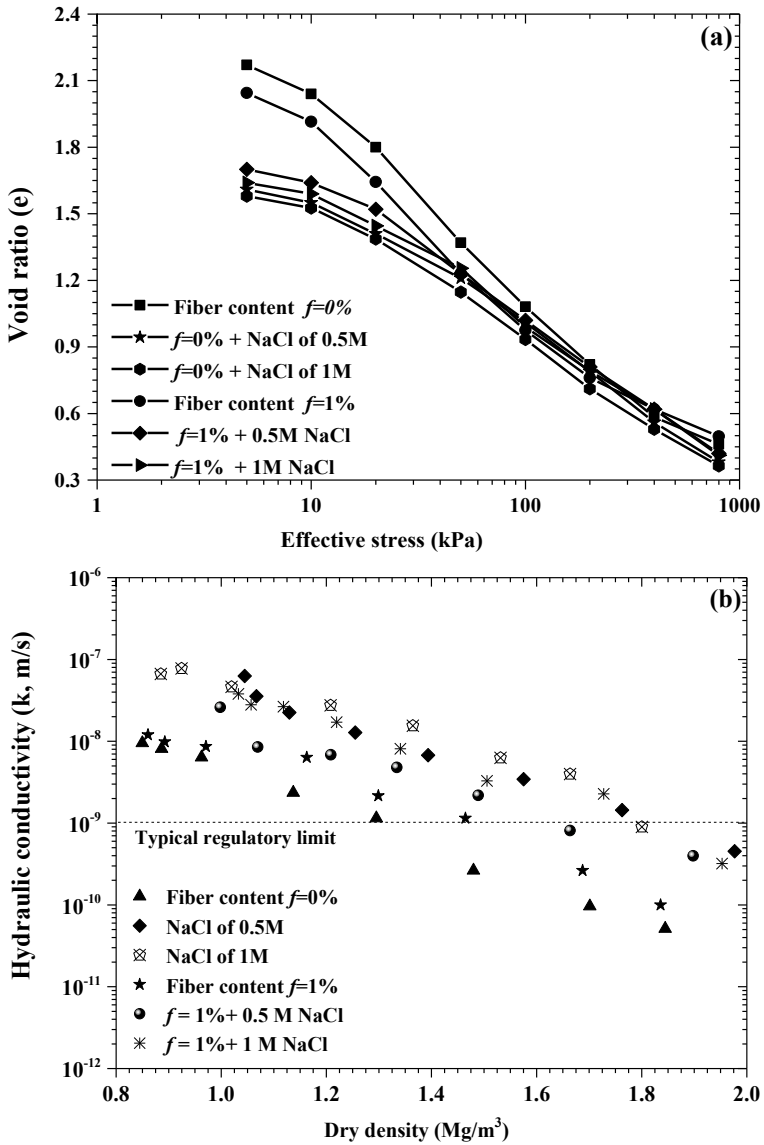
Fig. 6 Effect of saline fluid on: **a** e-log(p) of the clay and reinforced clay; **b** hydraulic conductivity of clay and reinforced clay

material. However, in the presence of the salt concentration, the hydraulic conductivity of unreinforced clay was significantly increased, whereas lesser effect was noticed for reinforced clay. In addition to that, the reinforced clay has experienced less volumetric shrinkage as compared to unreinforced clay.

4 Conclusions

The current study evaluated the effect of various percentages (i.e., 0, 0.1, 0.5, 1 and 2%) of glass reinforcement on various properties of clay such as shrinkage limit, volumetric shrinkage, suction, compressibility and hydraulic conductivity. The effect of saline fluids on the compressibility and hydraulic conductivity of the clay soil and reinforced clays was studied. The experimental results revealed that with an increase in percentage of reinforcement, the shrinkage limit and volumetric shrinkage were found to be increased and decreased, respectively. At lower suction range below 8 MPa, an increase in fiber content caused a marginally increase in the total suction of clay. Both the compression index and hydraulic conductivity of clay were marginally affected by fiber concentration. As fiber concentration increases from 0 to 2%, the compression index was found to be decreased by 15%. In the presence of 1.0 M NaCl, the compression index of the clay soil and reinforced clay soil was noted to be decreased by about 31% and 19%, respectively. Similarly, the hydraulic conductivity of the clay and reinforced clay soil was found to be increased by about 35 and 9 times, respectively. Therefore, the glass fiber can be used as effective reinforcement material for contaminated barrier materials.

References

1. Abdi, M., Parsapajouh, A., Arjomand, M.: Effects of random fiber inclusion on consolidation, hydraulic, conductivity, swelling, shrinkage limit and desiccation cracking of clays. Int. J. Civ. Eng. **6**, 284–292 (2008)
2. Ayeldeen, M., Kitazume, M.: Using fiber and liquid polymer to improve the behaviour of cement-stabilized soft clay. Geotext. Geomembranes **45**, 592–602 (2017)
3. Chaduvula, U., Viswanadham, B.V.S., Kodikara, J.: A study on desiccation cracking behavior of polyester fiber-reinforced expansive clay. Appl. Clay Sci. **142**, 163–172 (2017)
4. Divya, P.V., Viswanadham, B.V.S., Gourc, J.P.: Hydraulic conductivity behaviour of soil blended with geofiber inclusions. Geotext. Geomembranes **46**, 121–130 (2018)
5. Jiang, H., Cai, Y., Liu, J.: Engineering properties of soils reinforced by short discrete polypropylene fiber. J. Mater. Civ. Eng. **22**, 1315–1322 (2010)
6. Kar, R.K., Pradhan, P.K., Naik, A.: Consolidation characteristics of fiber reinforced cohesive soil. Electron. J. Geotech. Eng. **17**, 3861–3874 (2012)
7. Li, J., Tang, C., Wang, D., Pei, X., Shi, B.: Effect of discrete fibre reinforcement on soil tensile strength. J. Rock Mech. Geotech. Eng. **6**, 133–137 (2014)
8. Malekzadeh, M., Bilsel, H.: Hydro-mechanical behavior of polypropylene fiber reinforced expansive soils. KSCE J. Civ. Eng. **18**, 2028–2033 (2014)

9. Miller, C.J., Rifai, S.: Fiber reinforcement for waste containment soil liners. ASCE J. Environ. Eng. **8**, 891–895 (2004)
10. Mishra, A.K., Ohtsubo, M., Li, L.Y., Higashi, T., Park, J.: Effect of salt of various concentrations on liquid limit, and hydraulic conductivity of different soil-bentonite mixtures. Environ. Geol. **57**, 1145–1153 (2009)
11. Mukherjee, K., Mishra, A.K.: Influence of glass fiber on the behaviour of sand-bentonite mixture. IGC 2016, pp. 15–18 (2016). IIT Madras, Chennai, India
12. Singh, S., Prasad, A.: Influence of ferric chloride and humic acid on bentonite as clay liner. Int. J. Geotech. Eng. **4**, 45–53 (2010)
13. Soğancı, A.S.: The effect of polypropylene fiber in the stabilization of expansive soils. Int. J. Environ. Chem. Ecol. Geophys. Eng. **9**, 956–959 (2015)
14. Tang, C.S., Shi, B., Cui, Y.J., Liu, C., Gu, K.: Desiccation cracking behavior of polypropylene fiber–reinforced clayey soil. Can. Geotech. J. **49**, 1088–1101 (2012)
15. Thyagaraj, T., Soujanya, D.: Polypropylene fiber reinforced bentonite for waste containment barriers. Appl. Clay Sci. **142**, 153–162 (2017)
16. Tripathy, S., Bag, R., Thomas, H.R.: Effects of post-compaction residual lateral stress and electrolyte concentration on swelling pressures of a compacted bentonite. Geotech. Geol. Eng. **32**, 749–763 (2014)

Physical and Mechanical Behavior of Dredged Soil Acquired from Dal Lake—A Laboratory Study

Rakshanda Showkat , B. A. Mir, and K. M. N. Saquib Wani

Abstract This study deals with the characterization of dredged material obtained by dredging the world famous Dal Lake in Shrinagar, UT of J&K. Due to the non-availability of suitable dumping sites for the wastes generated around Dal Lake and owing to the concern of environmental and health issues of these waste materials, geotechnical engineers have been under tremendous pressure from geoenvironmentalists for the characterization of the same. Therefore, in this study, an attempt has been made to characterize the waste material generated from Dal Lake by studying its various physical and mechanical properties. Dredged material has been collected from three different sites viz Nishat, Shalimar, Telbal located on catchment of Dal Lake to conduct various field and laboratory tests for the determination of field density, soil classification, compaction characteristics, strength parameters like unconfined compressive strength, direct shear test and California bearing ratio. On the basis of results, it was found that the dredged material mostly comprised of silt, clay, and sand and the strength parameters revealed that dredged material cannot be used as construction and foundation material in its in situ state. Therefore, suitable and feasible treatments should be provided to dredged materials before being used for geotechnical applications.

Keywords Dredged material · Waste · Mechanical properties · Foundation material · Geotechnical applications

1 Introduction

Dal Lake (located at 34° 07′ N, 74° 52′ E, 1584 m above MSL), in Shrinagar, Union territory of Jammu and Kashmir, India, is the second largest Lake in state and has been integral to tourism and recreation in Kashmir, hence named as "jewel in the crown of Kashmir." The Lake having a total catchment area of 316 km^2, maximum depth of 6 m and shore length of 15.5 km is located in the Zabarwan mountain valley,

---

R. Showkat (✉) · B. A. Mir · K. M. N. S. Wani
National Institute of Technology, Srinagar, UT of Jammu and Kashmir 190006, India
e-mail: rakshandashowkat07@gmail.com
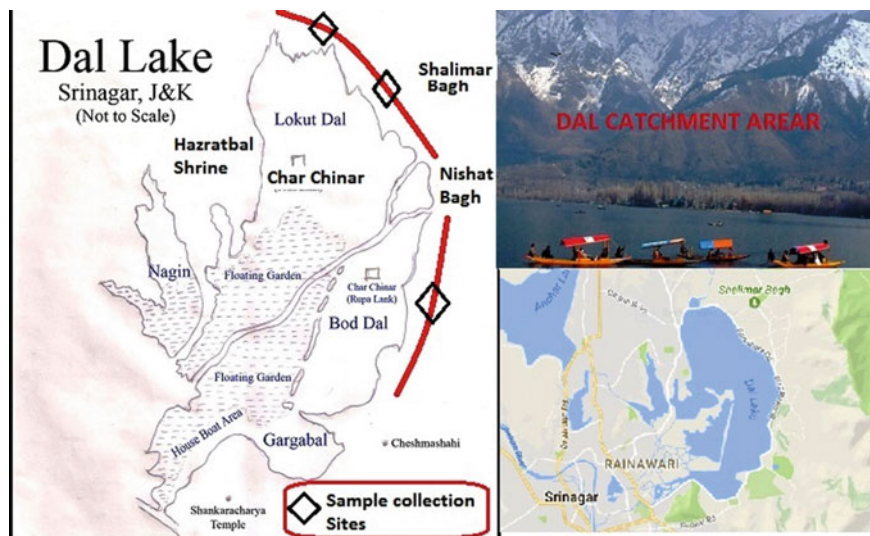
Fig. 1 Sample collection sites from the catchment area of Dal Lake

in the foothills of the Shankracharya hills, which surrounds it on three sides. The Dal Catchment consists of mountain ranges on its North and North-East and on the other sides it is enclosed by flat aerable land as shown in Fig. 1. The Lake receives large quantity of sediments and nutrients with the runoff from its catchment through Telbal Bota Khul during the downward movement of water from Marsar. The major silt and sediment loads enter the water body from the critical zone on northwestern portion of the catchment. A large amount of sewage from the settlements around the Lake and the habitation living on hamlets within the Lake, on floating islands and houseboats enters the Lake without treatment. Huge quantity of solid wastes and superfluous fertilizers from inlet channels produces algal blooms which ultimately results in eutrophication. Thick mats of red bloom and weeds give ugly look to the Lake besides affecting its flora and fauna. About 156 tons of phosphorus and 380 tons of nitrogen are estimated to flow into the Lake from various sources. The drains also carry sludge and solid wastes from the surrounding areas into the Lake. The interior channels connecting Dal with its other basins like Nagin, Pokhribal were found chocked due to the regular disposal of solid wastes. Also, vegetable growers regularly encroach into the Lake, planting trees. Because of urbanization, multi-storey buildings and small craft factories have been erected on the banks of Dal. In September 2014, the massive flood which occurred when the river Jhelum rose to the dangerous level due to intense rainfall from 1 to 7 September 2014, a huge amount of water entered the Dal Lake due to breach in embankment at Ram Munshi Bagh. This water brought large amount of silt and biological load in the Lake, thus causing siltation and pollution of Dal. As a result of this continuous disposal of wastes, silt deposition and encroachment, the load carrying capacity of the Lake has been reduced drastically. The problems of Dal Lake and its importance to the people,

tourists, sustainable development have been well recognized, and efforts are being made to clean the Lake which has been polluted as a result of rapid urbanization and disposal of solid wastes. The scheme for shoreline dredging of Dal Lake has been formulated with the primary objective to increase the clear water expanse of the Lake, improve water circulation and help in eco regeneration of Lake [1].

2 Dredging of Dal Lake

Dredging is the operation of removal of sediments and debris from the bottom of lake, river, harbor, and other water bodies. It is the form of excavation carried underwater or partially underwater in shallow water bodies. It is a routine necessity in water bodies because sedimentation gradually fills the channels. Dredging is focused on maintaining or increasing the depth of navigation channels, anchorages, or berthing areas to ensure the safe passage of boats and ships. The sediment removal process uses a machine known as a dredge to excavate the accumulated sediment and debris. A dredge is equipped with a powerful submersible pump that relies on suction to excavate the debris. A long tube carries the sediment from the bottom to the surface. Due to the rapid urbanization and population explosion particularly in developing countries, there is shortage of construction materials as well as scarcity of suitable construction sites. Thus, it forces the geotechnical engineers and specialists to adopt such soft soil sites for construction. Soft soil deposits which are very weak having low bearing capacity and undergo settlement for a considerable period of time. To assess the mechanical behavior of such soils, geotechnical engineers face a difficult task [1]. Using these soils as construction material, foundation medium, backfill, in dykes and embankments becomes a substantial problem for geotechnical engineers. The large quantities of dredged material obtained after carrying out dredging operation of Dal Lake also belong to the category of soft soils, enhancing load on engineers to use these deposits for constructional purpose. Since the capacity of Dal has tremendously decreased due to siltation, it becomes necessary to carry out dredging in order to maintain the Lake. Hence, there should be proper management of dredged material so that health and environmental hazards can be minimized [2]. Based on characterization, dredged material is now treated as a resource rather than waste. It can be used in the manufacture of large number of high value and beneficial products based on its mineralogical composition and geotechnical properties [2, 3]. It can be used in a number of ways such as fill material, sub-grade construction, reclamation, landscaping, agriculture, covers for landfills, and raw material for the production of riprap or blocks for the protection of dikes and slopes against erosion [2, 4], constructing wetlands for water quality improvement, bank stabilization, creation of islands, wildlife habitat wetlands, etc. [5]. Two broad categories of proposed uses are often distinguished: Engineering uses and Environmental uses [6]. Hence, this study becomes important for bulk utilization of dredged material obtained from Dal

Lake and also assesses the geotechnical properties of dredged soil. A number of techniques are available for dewatering and improving engineering properties of dredged material and other soft soils [7–12].

3 Materials and Methods

3.1 Materials

The soil samples for the present research study were taken from three different sites on the famous Dal Lake viz: site 1-Shalimar, site 2-Nishat, site 3-Telbal as shown in Fig. 1. At each site, soil samples were collected, sealed, and transported with utmost precaution for studying their various geotechnical properties and behavior as per relevant testing standards [13–23].

3.2 Testing Methodology

Physical Properties

(a) Field moisture content and dry unit weight: Field moisture content and bulk unit weight of samples of dredged material collected from three different sites were determined on undisturbed samples collected using core cutter method as per IS: 2720 part 2 and IS: 2720 part 29. The in situ samples possessed high moisture content. The dry unit weight of in situ samples was also low as compared to the maximum dry unit weight of the dredged samples.
Average values of moisture content and in situ dry unit weight were 33.12%, 35.2%, 34.7%, and 13 kN/m^3, 10.3 kN/m^3, 10.6 kN/m^3 for Shalimar, Nishat, and Telbal, respectively.
(b) Specific gravity: Specific gravity was determined as per IS: 2720 (part 3)—1980 using density bottle method with distilled water. The average value of specific gravity of Shalimar, Nishat, and Telbal was 2.4, 2.43, and 2.6, respectively.
(c) Particle size analysis: For measuring the distribution of particle sizes in a soil sample, it is necessary to conduct different particle size tests. It expresses quantitatively the proportions by mass of various sizes of different particles present in a soil, represented graphically on a particle size distribution curve. It is done in two stages: *Sieve analysis and Sedimentation* analysis.

Wet sieving is carried out for separating fine grains from coarse grains by washing the soil specimen on a 75 μm sieve mesh. Dry sieve analysis is carried out on particles coarser than 75 μm. Sedimentation analysis is used only for the soil fraction finer than 75 μm. Soil particles are allowed to settle from a suspension.
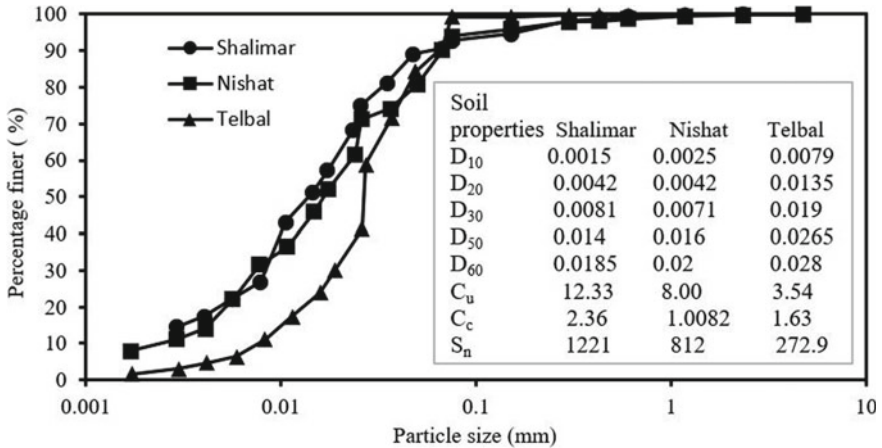
Fig. 2 Particle size distribution curves of different soil sample

In the present study, soil grading of dredged material from Shalimar, Nishat, and Telbal basin of Dal Lake was carried out on an oven-dried sample by dry and wet sieve analysis as per IS: 1498–1970 followed by sedimentation analysis as per IS: 2720 (part 4)—1985 using a hydrometer. The particle size distribution curves of the dredged material from three different sites (Site 1, Site 2, and Site 3) are given in Fig. 2.

The particle size distribution curve is used to know the classification of coarse grained soils and has a limited application for fine-grained soils like clay and silts, since the behavior of fine-grained soils (FGS) depends upon the plasticity characteristics and not on the particle size. The coefficient of uniformity (C_u) and coefficient of curvature (C_c) obtained from particle size distribution (PSD) curve represent the range and shape of PSD curve, thereby help in analyzing the gradation of soil. The particle size analysis is used to know the susceptibility to frost action, required for the design of drainage filters, an index to coefficient of permeability and the shear strength of the soils. The suitability of the backfill material also depends on gradation.

(d)   Index properties

Index properties are the properties of soil that help in identification and classification of soil and are indicative of the engineering properties of the soil. These properties are generally determined in the laboratory. The main index properties of fine-grained soils are Atterberg's limits which include liquid limit, plastic limit, and shrinkage limit.

Liquid limit tests

The Atterberg's limits were determined on oven-dried dredged soil samples passing through 0.425 mm IS sieve by wet to dry process using Casagrande's apparatus as per IS 2720-Part 5, (1985). The flow curves for the dredged material of the three sites are

shown in Fig. 3. As can be seen from Fig. 3, the dredged material under investigation possesses medium compressibility and depict that the soil obtained from Nishat is highly compressible with high rate of loss of shear strength. Furthermore, the in situ water content of the dredged material is more than its plastic limit resulting in a wet and sticky condition, impossible to compact and traffic.

Plastic limit tests

The plastic limit (PL) is determined by rolling out a thread of the fine portion of a soil on a flat, non-porous surface. If the soil is at moisture content where its behavior is plastic, this thread will retain its shape down to a very narrow diameter. The sample can then be remolded, and the test repeated the PL values were determined using
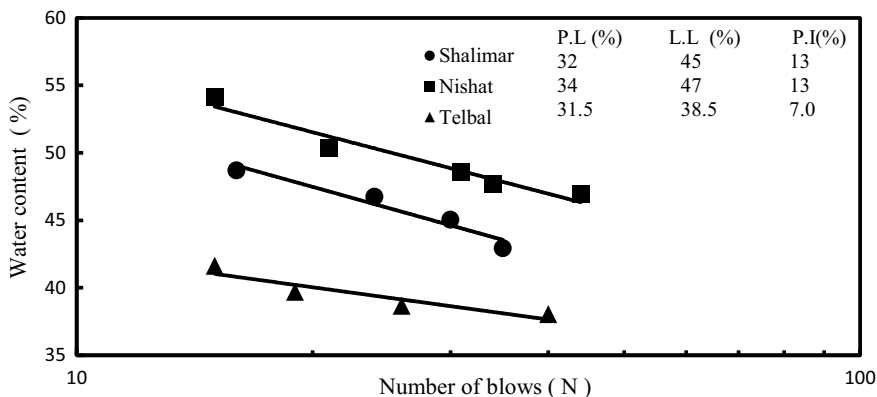
Fig. 3 Atterberg's Limits for three sites (Site 1, Site 2, Site 3)

Fig. 4 In situ stress–strain curves for site 1
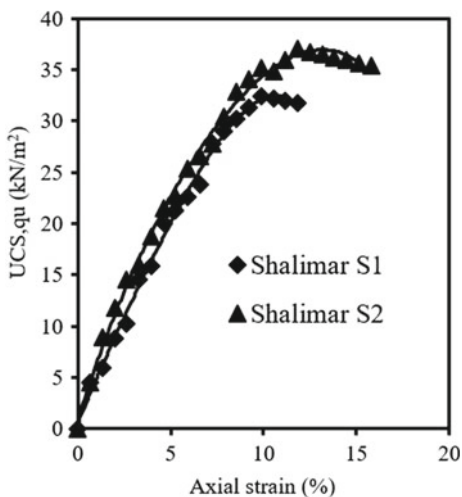
standard relevant testing procedures as per IS 2720-Part 5, (1985). The plastic limit values reported in Table 1 are an average of the three trial determinations. Based on the values of A-line and U-line in the plot of liquid limit versus plasticity index, mineral present in all three soil was found to be kaolinite.

Shrinkage limit tests

The shrinkage limit (SL) is the water content where further loss of moisture will not result in any more volume reduction. The shrinkage limit is much less commonly used than the liquid and plastic limits. It is used for understanding the shrinkage and

Table 1 Physical properties of dredged soil from three different sites on Dal Lake

Properties	Shalimar	Nishat	Telbal
Natural moisture content (%)	33	35.2	34.7
Bulk unit weight (kN/m^3)	15.5	14	14.3
In situ dry unit weight (kN/m^3)	13	10.3	10.6
Specific gravity (G)	2.4	2.43	2.6
% Finer than 75 μm	92.94	93.93	99.25
Clay (%)	12	10	3
Silt (%)	80	83	96
Sand (%)	7.06	6.06	0.745
Gravel (%)	0	0.07	0
Coefficient of uniformity, C_u	12.33	8	3.54
Coefficient of curvature, C_c	2.36	1.008	1.63
Suitability number, S_n	1221	812	272
Liquid limit (%)	45	47	38.5
Plastic limit (%)	32	34	31.54
Shrinkage limit (%)	18.0	17.0	17
Plasticity index (%)	13	13	6.96
P.I, A-line	18.25	19.71	13.505
P.I, U-line	33.3	35.1	27.45
Classification	MI	MI	MI
Clay mineral	Kaolinite	Kaolinite	Kaolinite
Flow index, I_f	11.11	25.4	8.96
Toughness index, I_t	0.85	1.95	1.28
Activity	1.08	1.3	2.32
Consistency index, I_c	0.92	0.90	0.54
Liquidity index, I_L	0.07	0.09	0.45

swell characteristics of the cohesive soils. Soil samples as prepared for the liquid limit are taken in a shrinkage dish without inclusion of air bubbles, weighed and kept for air drying until the color of the soil pat changes and then the dishes are oven dried at 110 °C for 24 h. Shrinkage limit was determined using the standard testing method as per IS 2720-Part 5, (1985).

Engineering Properties

Strength characteristics

In the present investigation, unconfined compression test and direct shear tests are performed on the in situ samples of the dredged materials of all three sites. Each site was tested for two samples and the weakest soil samples were compared for assessment of shear strength parameters. The test samples were tested in an unconfined compression testing (UCT) machine as per relevant standard testing procedures IS 2720-Part 10 (1991). These test values suggest that the soil under undrained condition is in soft state as shown in Figs. 4, 5 and 6 and needs treatment before being used for any engineering purpose. Direct shear tests were conducted on direct shear test machine under drained condition, as per standard testing procedures IS 2720-Part 13, (1986). The stress–strain behavior for all the three sites is shown in Fig. 7. The test results conducted under drained condition indicate angle of internal friction of Shalimar soil was found to be comparatively lower than other two sites which shows that it is possesses more cohesion than other two sites and that the dredged soil in natural condition is very soft and in a very loose state.

Compaction characteristics

In the present study, compaction was done by standard proctor test (light compaction test) in the laboratory by following proper codal provisions as per IS 2720-Part 7

Fig. 5 In situ stress–strain curve for site 2
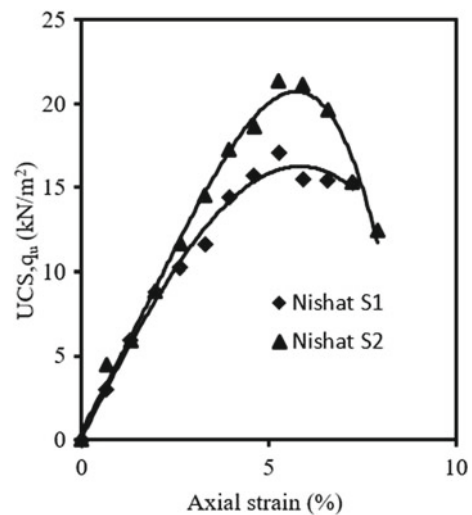
Fig. 6 In situ stress–strain
curves for site 3
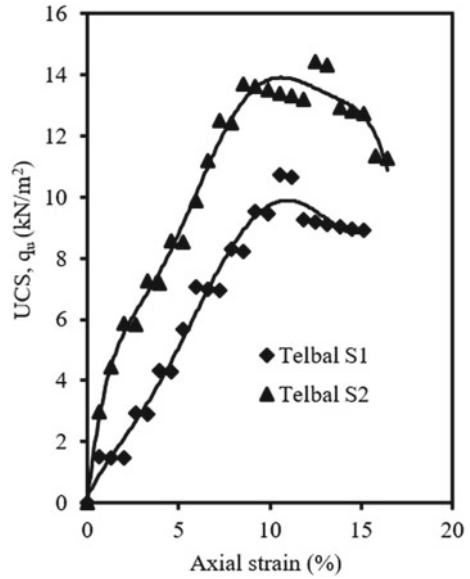
Fig. 7 Mohr failure
envelopes for 3
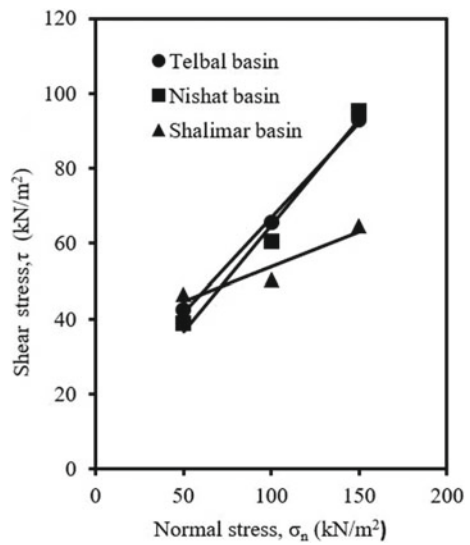
(1980). The results of the standard proctor tests are presented in a plot between moisture content (OMC) as abscissa and the corresponding dry unit weight as the ordinate Fig. 8. From the graph, OMC value of Shalimar soil was found to be comparatively lower than other two sites because OMC of highly cohesive soils is usually found to be very low. The zero air void line (ZAVL) based on specific gravity values of three sites is shown in Fig. 8.
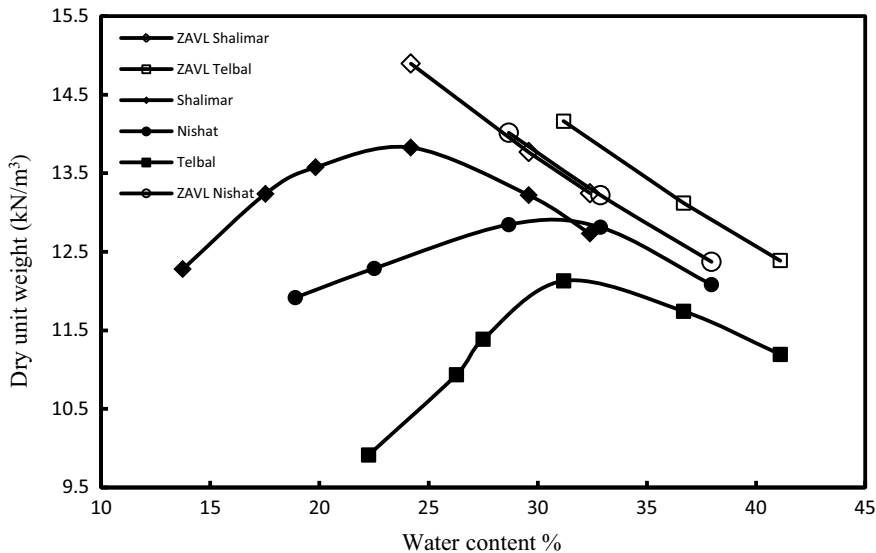
Fig. 8 Compaction curves for three different sites

CBR on dredged soil compacted on OMC

The California bearing ratio test is a penetration test meant for the evaluation of sub-grade strength of roads and pavements. In the present study, CBR tests were conducted on three soil samples compacted at OMC using relevant codal procedure IS 2720-Part 16 (2002). Figures 9 and 10 show the load-deformation curves of dredged
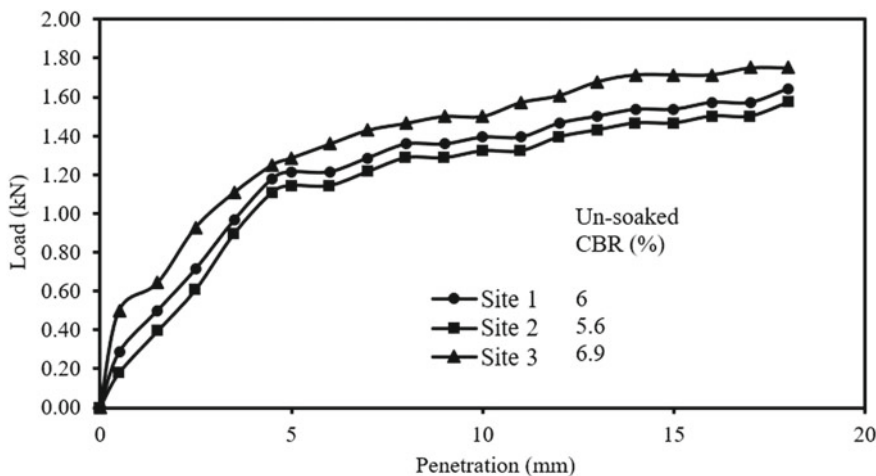
Fig. 9 Load versus deformation curves for CBR (un-soaked condition)
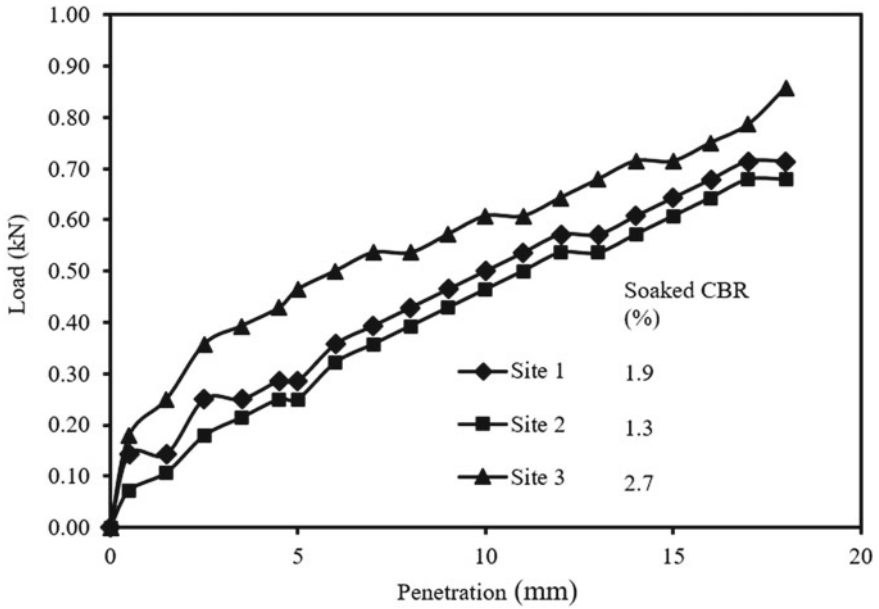
Fig. 10 Load versus deformation curves for CBR (soaked condition)

soil samples from three different sites of the Dal Lake. Table 2 gives the mechanical properties of the in situ soil samples from all the locations for comparison.

Table 2 Mechanical properties of dredged soil from three different sites on Dal Lake

Properties		Shalimar	Nishat	Telbal
DST @ In situ	Cohesion, c (kN/m^2)	35.69	8.57	16.35
	Angle of internal friction, Φ (Deg)	10.31	29.4	26.83
UC-test @ In situ	Unconfined compressive strength, q_u (kN/m^2)	34.17	19.17	12.57
Optimum moisture content (%)		25	32	31
Maximum dry unit weight (kN/m^3)		13.67	12.8	12.12
California bearing ratio un-soaked (%)		6.0	5.6	6.9
California bearing ratio soaked (%)		1.9	1.3	2.7

4   Conclusion

- Based on some of the physical properties of the dredged material investigated, the material from three different sites of Dal Lake has been classified as inorganic silt-MI of medium plasticity as per Indian Standard Soil Classification System.
- The specific gravity values are very low (2.4, 2.43, and 2.6 for Shalimar, Nishat, and Telbal, respectively) which is a cause of concern.
- The compaction curves show that soil has a low dry density ranging between 14 and 12 kN/m^3 at OMC varying between 27 and 32%.
- The dredged material is weak and has low values of shear strength parameters (UCS values being 34, 19.17, 12.57 kN/m^2 for Shalimar, Nishat, and Telbal respectively).
- The CBR values are also in a low range between 5 and 6% and hence the soil cannot be used as a construction material in sub-grade or for heavy construction work.

Hence it can be concluded that the dredged material collected from the Dal Lake is not suitable as an engineering material in its present in situ condition and hence needs stabilization before being able to be used as a construction material.

References

1. Mir, B.A.: Some studies on mechanical behavior of cement stabilised dredged soil from flood spill channel of Jhelum River Srinagar. In: Singh, D., Galaa, A. (eds.) Contemporary Issues in Geoenvironmental Engineering, Sustainable Civil Infrastructures, pp. 386–406. Springer, Cham (2017)
2. Mir, B.A., Mir, F.A.: Applications and geotechnical evaluation of dredged soil obtained from Dal Lake in Srinagar. In: Proceedings National Conference on Soils and Their Applications in Civil Engineering, pp. 26–37 (2004)
3. Bartos, M.J. Jr.: Classification and engineering properties of dredged soil. Technical Report D-77-18, U.S. Army Waterways Experiment Station, Vicksburg, MS (1997)
4. Aarninkhof, S., Luijendijk, A.: Safe disposal of dredged material in an environmentally sensitive environment. Port Technol. Int. **47**, 39–45 (2010)
5. DOER-C2: Dredged soil characterization tests for beneficial use suitability. Technical Note. U. S. Army Corps of Engineers (1999)
6. Mir, B.A., Wani, B.A., Ahmad, N., Ayoub, R., Dar, L.A., Rashid, S.U., Aziz, J.: Physical and compaction behavior of dredged material from Dal Lake, Srinagar. Int. J. Civil Eng. Appl. **3**(7), 4–8 (2013)
7. Haliburton, T.A.: Guidelines for dewatering/densifying confined dredged material, synthesis report. Technical Report DS-78–11, US Army Engineer Waterways Experiment Station, Vicksburg, MS (1978)
8. Jan, O., Mir, B.A.: Strength behavior of cement stabilised dredged soil. Int. J. Geosynthetics Ground Eng. (2018)
9. Mir, B.A., Amin, F., Majid, B.: Some studies on physical and mechanical behavior of dredged soil from flood spill channel of Jhelum river Srinagar. Acta Ing Civil **1**(1), 1–7 (2016)
10. Mir, B.A., Wani, K.M.N.S.: Mechanical behavior of Boulder Crusher Dust (BCD)-stabilized dredged soil. IGC (2018)

11. Wani, K.M.N.S., Mir, B.A.: Influence of microbial geo-technology in the stabilization of dredged soils. Int. J. Geotech. Eng. (2019). https://doi.org/10.1080/19386362.2019.1643099
12. Wani, K.M.N., Mir, B.A.: Effect of biological cementation on the mechanical behaviour of dredged soils with emphasis on micro-structural analysis. Int. J. Geosynth. Ground Eng. **5**, 32 (2019). https://doi.org/10.1007/s40891-019-0183-9
13. IS: 2720-part 3(1): Determination of specific gravity of fine grained soils (1980). BIS, New Delhi
14. IS: 2720-part 3(2): Determination of specific gravity of fine, medium and coarse grained soils (1980). BIS, New Delhi
15. IS: 2720-part 4: Determination of grain size distribution (1985). BIS, New Delhi
16. IS: 2720-part 5: Determination of Atterberg limits (1985). BIS, New Delhi
17. IS: 2720-part 6: Determination of shrinkage factors (1972). Bureau of Indian standards, New Delhi
18. IS: 2720-part 7: Determination of water content-dry density relation using light compaction (1980). BIS, New Delhi
19. IS: 2720-part 8: Determination of water content-dry density relation using heavy compaction (1980). BIS, New Delhi
20. IS: 2720-part 10: Method of Test for Soils: Determination of Shear Strength Parameter by Unconfined Compression Test (1973). Bureau of Indian Standards, New Delhi
21. IS: 2720-part 39: Method of Test for Soils: Determination of Shear Strength Parameter by Direct Shear Test (1977). Bureau of Indian Standards, New Delhi
22. IS: 2720-part 16: Method of Test for Soils: Laboratory Determination of CBR (1979). Bureau of Indian Standards, New Delhi
23. IS: 9669: Specification for CBR Moulds and Iits Accessories (1980). Bureau of Indian Standards, New Delhi

Investigation of Sub-surface Contamination Around the Landfill Site: A Case Study

Sagar Shinde, Arati Gaikwad, and Swapnil Joshi

Abstract Landfill leachate is a hazardous liquid that poses negative impacts if leaks out into environmental elements such as sub-surface soil and ground water systems. In the current study, detailed investigation was conducted on the municipal solid waste landfill site situated in northern part of Maharashtra, which is a non-engineered landfill. Ground water samples from nearby well and tube wells as well as soil samples around the landfill site were collected to assess the possible impact of leachate percolation on soil and ground water quality. Concentration of various physio-chemical parameters and heavy metals (Pb, Cd, Cr, Hg, As) in ground water was determined and compared with Indian Standard for drinking water. The soil samples were taken in the vicinity of landfill site at a shallow depth of 1 and 2 m using hand auger and were analyzed for presence of heavy metals and organic content. The contaminated soil near landfill was compared with normal soil samples taken at proximity of landfill site. The presence of high organic contents and heavy metals in soil samples indicates that there is appreciable contamination of soil due to leachate migration from landfill site. The result shows that there is a presence of contamination content in ground water table observed in surrounding wells. The study indicated that leachate can damage the soil and ground water properties and can cause greater threat to sub-surface environment if further action is not taken.

Keywords Environmental · Landfill · Leachate

1 Introduction

Currently, the solid waste disposal and management is one of the most important crises tackled by many of the urban and industrial areas in both developed and developing countries which direct the environmental issue in day today life [3]. Leachate is generated due to the percolation of water or precipitation into dumpsites and its permeation through waste as well as by the process of squeezing of the waste

S. Shinde (✉) · A. Gaikwad · S. Joshi
Civil Engineering Department, Matoshri COERC, 422003 Nashik, India
e-mail: shinde2609@gmail.com

due to its own self-weight [5]. Huge amount of solid waste is generated on daily basis and its management is a major issue. Solid waste generation has increased parallel to the development of industrialization, globalization, and urbanization [12]. However, today, due to increased land value, inadequate space, and limited nature capacity to handle unwanted emissions and residues pose long-term environmental and human health problems [20]. Unscientific and non-engineering open dumping of waste is commonly prevalent in most developing countries as it is the simplest and most cost-effective method of waste disposal [5]. This practice is also practiced in the developed countries up to a certain extent. Therefore, it desperately needs urgent action to be taken to minimize the associated harmful effects.

2 Study Area

The study area selected was a solid waste landfill site. The open dumping ground was actually situated in northern part of Maharashtra. It is a non-engineered landfill. There is no lining at the bottom of the dump yard. The total area occupied by dumping was near about 28 Acres [19]. Daily about 300 Tons of waste was generated was dumped at the site. The height of landfill heap varies from 8 to 10 m. The dumping was done at site since last 25–30 years. The annual average rainfall is noted to be 533 mm. The region experiences rainfall in the months of June to September. The study aims at addressing current and potential negative environmental impacts due leachate discharge by systematically examining the quality and condition of both soil and water which forms part of the study area and the surrounding environment. Therefore, this research study deals with the soil and water quality issue, thereby providing remedial actions for the study [18]. The proportion of solid waste in the landfill site are identified on the basis of dry weight of the representative daily solid waste generated and collected from various sectors of the city and finally the average is taken into consideration [19]. The details of solid waste and its categories are shown in Table 1.

Table 1 Details of solid waste collected from the city

S. No.	Types of waste	Percentages (%)
1	Organic waste	57.3
2	Paper waste	7.25
3	Plastic waste	13.25
4	Metal waste	1.95
5	Glass waste	2.00
6	Leather and rubber waste	2.75
7	Textile waste	6.25
8	Inert miscellaneous waste	9.25

Fig. 1 Layout of sampling at landfill site

3 Methodology

3.1 Leachate and Groundwater Sampling

Figure 1 shows the sampling pattern adopted at the landfill site to collect ground water, contaminated soil and leachate samples. The landfill leachate samples were collected which was flowing on the ground surface around waste dumped [10]. The sample collection was carried out both during monsoon (September 2018) and during summer (April 2019). The leachate samples were collected both from old waste dumped area as well as one from where the latest dumping is carried out [4, 10].

The physio-chemical parameters of leachate samples were determined. The 6 No's groundwater sampling locations in the study area are shown in Table 2. Water was collected from open wells by drawing buckets tied with ropes, while tube wells were pumped for 5–15 min before sampling [9, 11]. These samples were collected in pre-cleaned polypropylene containers which was cleaned before storage of samples and kept at room temperature [9]. Water was analyzed for Physio-Chemical Test and Heavy Metals as per Table 3.

3.2 Soil Sampling and Analysis

Soil samples were collected from the dumpsite, by removing the surface debris and sub-surface soil dug to a vertical depth of 1 and 2 m from ground surface using a

Table 2 Details of ground water sampling

Sample No	Water sample type	Distance from site boundary (m)	Depth from G.L
1	Open well water (OW)	184	4.87 m
2	Open well Water (OW)	322	5.48 m
3	Tube well (TW)	315	–
4	Tube well (TW)	402	–
5	Open well water (OW)	490	6.40 m
6	Open well water (OW)	762	5.80 m

Table 3 Methodology for physio-chemical test [13]

S. No.	Parameter	Method adopted	Apparatus/Instruments Used
1	Turbidity	Laboratory method	Nephelometer turbidity meter
2	pH	Electrometric method	Electronic pH meter
3	Electrical conductivity	Laboratory method	conductivity meter
4	Total hardness	EDTA titrimetric method	Laboratory method
5	Bio-chemical oxygen demand (BOD)	D.O. meter	BOD bottle, Incubators
6	Dissolve oxygen	Laboratory method	Digital D.O meter
7	Chemical oxygen demand (COD)	Titration method	COD reflux apparatus
8	Heavy metals (As, Cd, Cr, Hg, Pb)	Atomic absorption spectrometric method	Atomic absorption spectrometric

manual hand auger [8]. Samples were collected in horizontal direction around the landfill site. As shown in Fig. 1, total 9 contaminated soil sampling locations (one at boundary of site and other two at interval of 50 m from site in each direction) were identified in order to determine the horizontal extent of contamination level. Along with these one normal soil sample was collected at distance of near about 520 m away from the landfill site. In this way total 19 No's soil samples (at depth of 1 m and 2 m at each sampling location) were carried to laboratory and analyzed for chemical analysis such as organic content and heavy metals. These chemical parameters were then compared with normal soil sample at greater distance from the site. The soil sample can be also investigated for the presence of heavy metals in Atomic Absorption Spectrophotometer [8]. Hazardous heavy metals detected are Lead (Pb), Arsenic

(As), Cadmium (Cd), Chromium (Cr), and Mercury (Hg). The parameters for analysis were decided by considering the types of solid waste generated and the toxicity of the leachate at the landfill site.

4 Results and Discussion

4.1 Characteristics of Leachate

Leachate characteristics were identified by conducting physio-chemical parameters test on leachate samples collected from the dump site. From the result shown in Table 4, it seems that fresh leachate is more polluted than the older one. Leachate was also detected for the presences of heavy metals like lead, Cadmium, Chromium, Mercury Arsenic, etc. as these are considered to be hazardous elements in heavy metals. Heavy metals were detected under Atomic Absorption Spectrophotometer [8, 17].

From Table 4, it seems that the characteristics of leachate at new dump site are more hazardous as compared to old dump due to presence of active microorganism for decomposition [9]. pH Value for leachate ranges from 8.90 to 9.10 and in summer

Table 4 Characteristic of leachate samples

S. No.	Parameter	Concentration				Unit
		Monsoon		Summer		
		Sample 1	Sample 2	Sample 1	Sample 2	
		Old dump	New dump	Old dump	New dump	
1	Color	Black	Black	Black	Black	–
2	Odor	Foul smell	Foul smell	Foul smell	Foul smell	–
3	Turbidity	17.7	19.2	15.45	20.02	ppm
4	pH	8.9	9.1	9.22	10.12	–
5	Electrical conductivity	7291	13,212	10,873	15,442	u/cm
6	Total hardness	823	729	741	913.12	ppm
7	B.O.D	7560	10,500	10,255	17,522	ppm
8	D.O	0.7	0.6	0.04	0	ppm
9	C.O.D	9530	14,050.4	22,186	26,735.76	ppm
10	Pb	1.92	0.22	3.12	1.91	ppm
11	Cd	0.78	2.47	1.59	2.12	ppm
12	Cr	0.21	0.98	1.02	0.51	ppm
13	Hg	0.52	0.24	1.91	1.02	ppm
14	As	0.12	1.009	1.91	2.61	ppm

these values range from 9.22 to 10.12 which infers that it is alkaline in nature [9]. High COD value in the range of 9530 ppm to 26,735.76 ppm in leachate samples shows the presence of oxidizable organic materials that had leached from domestic refuse in the landfill site [9]. The leachate generated at the landfill site carries considerable amount of organic matter, percolated through the soil, and entered into ground water showing increase in BOD value. Higher value of electrical conductivity indicates the presence of inorganic material in the samples [8]. The concentration of contamination is observed more in summer as compared to monsoon since there is no dilution of precipitation.

4.2 Characteristics of Ground Water Quality

Water samples were collected from the existing groundwater sources around the landfill site at varying depth and distances from the boundary of the disposal site and was analyzed for physio-chemical characteristics as well as heavy metals [1].

Comparison was made between the observed contamination parameter values with Indian Standards for drinking water. It was found that the pH of the ground water samples ranged from 6.95 to 7.90. The values of pH were within the prescribed limit of Indian Standards for Drinking water [6, 9]. The Bio-Chemical Oxygen Demand (BOD) ranges from 0.19 to 0.61 ppm which state that the organic content concentration has decreased and not percolated into the ground water. Ground water was also analyzed for the presences of heavy metals like lead, Cadmium, Chromium, Mercury Arsenic, etc. The water table is located at 5 m from the ground surface as observed in wells. The rise in water table was observed due to monsoon. The flow of water table was in the direction opposite to highway (evidence from previous local bore observation and technician reports) (Fig. 2).

As per obtain results in Table 5, the tube well water samples have shown less contamination concentration as compared to samples collected from open well water at higher depth. The ground water contamination parameters seem to be reducing beyond 500 m landfill site as observed from samples 5 and 6, the contamination parameters are with the permissible limit stated by Indian standards for drinking water [6]. From the observed parameters of ground water, it can be concluded that the contamination flume is transported in the direction opposite to the highway. This may have followed the ground water flow path.

4.3 Chemical Analysis of Soil

4.3.1 Organic Content in Soil Samples

The organic content in the soil samples was determined in laboratory in order to obtain the decomposable content present in sub-surface soil. The temperature maintained
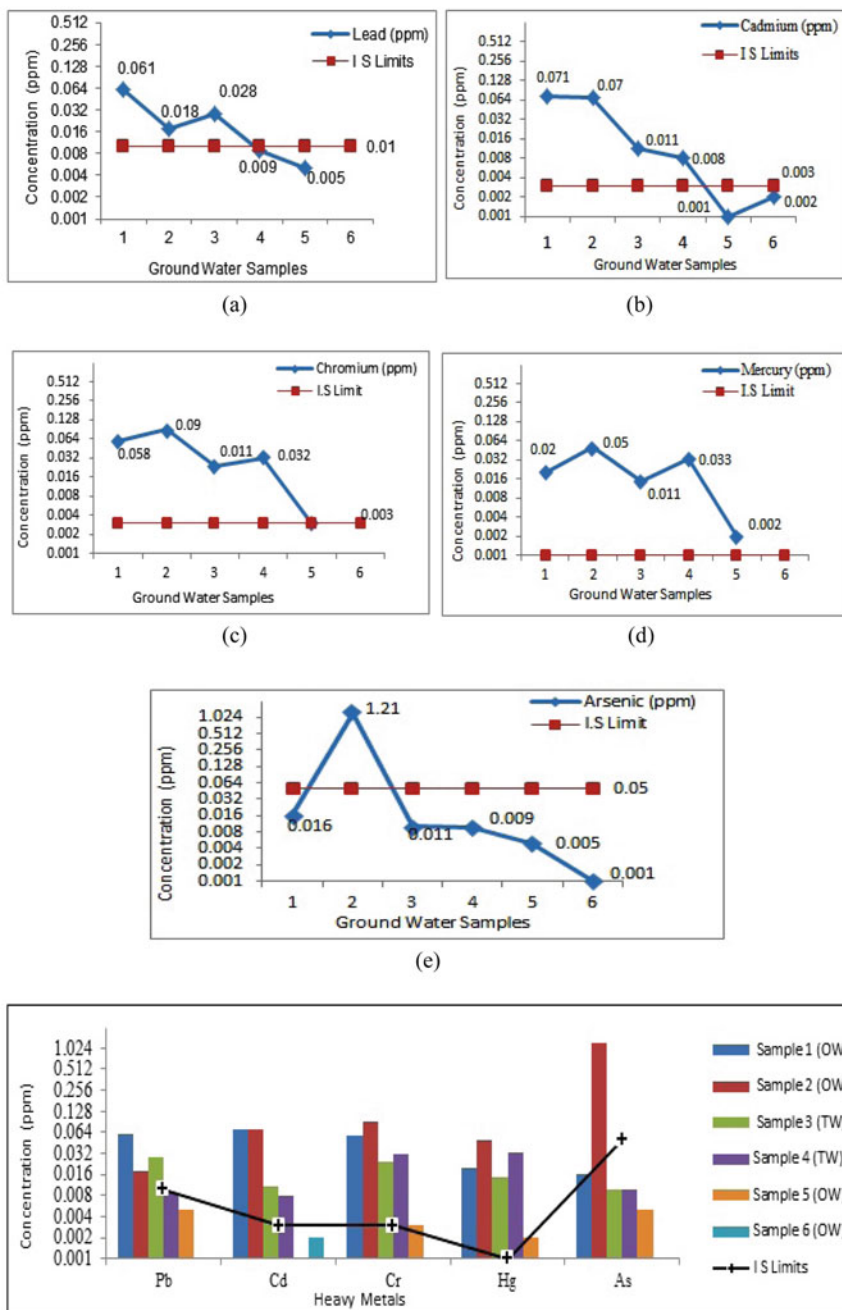
Fig. 2 Comparison of heavy metals in ground water samples with drinking water standards **a** Lead **b** Cadmium **c** Chromium **d** Mercury **e** Arsenic

Table 5 Characteristics of ground water samples

S.No.	Parameter	Concentration in samples						I.S limit	Unit
		1	2	3	4	5	6		
1	Color	Transparent	Transparent	Transparent	Transparent	Transparent	Transparent	–	–
2	Odor	Odor less	Odor less	Odor less	Odor less	Odor less	Odor less	Agreeable	– –
3	Turbidity	0.2	4.51	1.02	0.2	0.42	0.31	5–10	ppm
4	pH	7.8	7.1	7.3	7.75	6.95	7.9	6.5–8.5	– –
5	E.C	1271	1125	1012	987	1008	662	– –	μ/cm
6	Total hardness	229	153	163.7	120.01	130.1	112.5	200	ppm
7	B.O.D	0.61	0.38	0.31	0.26	0.41	0.19	– –	ppm
8	D.O	4.1	6.5	6.96	7.25	5.21	8.12	– –	ppm
9	C.O.D	2.52	2.15	1.96	1.71	2.32	1.32	– –	ppm
10	Pb	0.061	0.018	0.028	0.009	0.005	BDL	0.01	ppm
11	Cd	0.071	0.07	0.011	0.008	0.001	0.002	0.003	ppm
12	Cr	0.058	0.09	0.024	0.032	0.003	BDL	0.003	ppm
13	Hg	0.02	0.05	0.015	0.033	0.002	BDL	0.001	ppm
14	As	0.016	1.21	0.01	0.009	0.005	0.001	0.05	ppm

Table 6 Presences of organic content in (%) present in soil samples

S. No.	Depth below G.L (M)	Soil samples									
		1	2	3	4	5	6	7	8	9	10
1	1	0.78	3.24	7.31	2.12	4.37	5.89	6.89	2.34	2.69	2.13
2	2	–	1.87	4.55	1.67	3.47	2.62	4.01	1.57	2.15	1.16

Fig. 3 Organic content in soil samples at varying depth
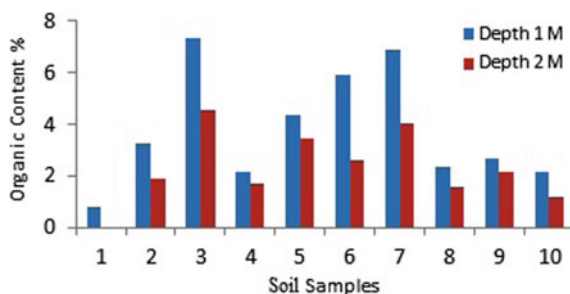
for the analysis was 105–110 °C in oven and muffle furnace at 400 °C for 24 h. From the values in Table 6, the maximum organic contamination in the range of 2.12–7.31% has been observed in samples 2, 3, 5, 6, and 7, i.e., in the direction opposite to highway. This infers that the soil at the boundary of the dump site has high organic content due to the seepage of leachate when compared to the control sample (Fig. 3).

4.3.2 Heavy Metal Contaminations.

Contamination of heavy metals in the environment is of major concern because of their toxicity and threat to human life and the environment [2]. Many investigators have conducted researches on heavy metal contamination in soils. Heavy metals were detected under Atomic Absorption Spectrophotometer [8, 16]. Heavy Metals are deposited in soil due to municipal waste containing refused batteries, paint products, metallic items phosphate fertilizers, presence in sewage sludge and waste water percolation, etc. [20]. The heavy metal concentration present in normal soil sample is due to the geological formation of the soil strata. There is no Indian standard available to indicate the presences of heavy metals in particular soil sample. Therefore, many researchers have tried to compare the contaminated soil at the landfill side with the normal soil samples available at particular distance away from the landfill site (Fig. 4) and (Table 7).

From the analysis of the heavy metals detected at study site, it seems that the elements are presents in the following sequences (Pb > Cr > Cd > As > Hg) with varying depth [8].
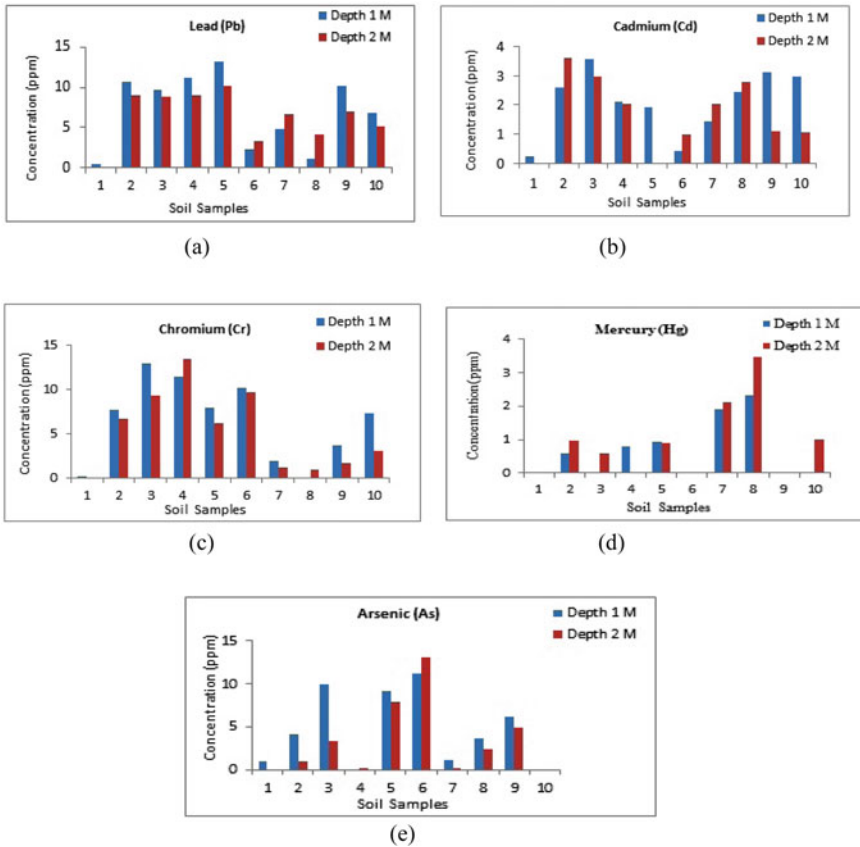
Fig. 4 Heavy metal concentration in soil samples at varying depth. **a** Lead **b** Cadmium **c** Chromium **d** Mercury **e** Arsenic

4.4 Geotechnical Aspect of Soil

The index properties of the soil samples are analyzed to identify the profile and characteristic of the contaminated soil and also that of normal soil sample [3, 14]. From the results shown in Table 8, it seems that the characteristics of the contaminated and uncontaminated soil are nearly comparable and not much difference was found. Also the contaminated soil in the vicinity of the landfill is more permeable than the normal or uncontaminated soil. This may be due to permeation of leachate through the soil mass [14].

Table 7 Heavy metal concentration in Soil samples

S. No.	Heavy metals	Depth below G.L (M)	Soil Samples									
			1	2	3	4	5	6	7	8	9	10
1	Pb	1	0.4	10.7	9.7	11.13	13.2	2.31	4.7	1.12	10.1	6.75
		2	–	8.9	8.8	8.92	10.1	3.22	6.6	4.12	7.02	5.21
2	Cd	1	0.2	2.5	3.5	2.12	1.92	0.41	1.4	2.45	3.12	2.96
		2	–	3.6	2.9	2.04	0.01	0.98	2.0	2.79	1.09	1.07
3	Cr	1	0.1	7.7	12	11.3	7.91	10.12	1.9	BDL	3.61	7.32
		2	– -	6.6	9.3	13.3	6.12	9.72	1.0	0.84	1.62	2.97
4	Hg	1	0.1	0.5	0.5	0.8	0.92	BDL	1.9	2.31	0.01	BDL
		2	– -	0.9	0.5	BDL	0.89	BDL	2.1	3.49	BDL	1.05
5	As	1	0.9	4.2	10	BDL	9.1	11.19	1.1	3.64	6.1	BDL
		2	– -	0.9	3.2	0.05	7.85	13.12	0.1	2.36	4.92	BDL

BDL Below Detection Level.
All values in ppm.

Table 8 Geotechnical aspect of soil samples

Sr No	Properties of soil	Normal soil	Contaminated soil			
		1	2	3	4	5
1	Specific gravity	2.64	2.56	2.52	2.54	2.59
2	Cu	1.69	0.92	1	0.781	1.14
3	Cc	18.80	13.33	17.50	12.83	17.75
4	Coarse sand (%)	14.8	19.04	21.86	18.48	15.02
	Med sand (%)	28.82	39.52	35.62	39.20	38.02
	Fine sand (%)	39.754	25.84	29.12	27.66	31.53
	Silt and clay (%)	16.40	15.60	13.40	14.80	15.42
5	W_L (%)	28	22	20	23	24.50
6	Soil classification	SW	SP	SW	SP	SW
7	K in cm/s	0.0038	0.00371	0.00475	0.00397	0.00410

5   Conclusion

The solid waste dumping site is observed to be non-engineered. The characteristics of leachate from new dumping area show more contamination than the old dumped leachate. Leachate in monsoon has comparatively less contamination potentials but more amount due to the effect of dilution, whereas the leachate observed in summer has more contamination potential but in less quantity. The physio-chemical and heavy metals contamination parameters of ground water exceed beyond the permissible Standards of Drinking Water. Hence, it is not useful for potable and domestic purpose and may cause public health problems [10, 15]. It will be recommended to treat water before use for domestic purpose. The groundwater quality improves with the increase in depth and distance of the well from the pollution source. Particularly beyond 500 m of the radius of the landfill site, the ground water quality meets the permissible limits for domestic uses. The soil at site was contaminated for organic content varies from 2.12 to 7.31%. Heavy metals present in soil (Pb > Cr > Cd > As > Hg) with varying depth and ground water contents heavy metals as (Cd > Cr > Pb > Hg > As). There is a need to determine the remediation measures for the contamination based on the present scenario. It is recommended to apply Electro Kinetic technique for remediating the contaminated land around landfill site [11].

References

1. Aderemi, A., Oriaku, A., Adewumi, A, Otitoloju, A.: Assessment of groundwater contamination by leachate near a municipal solid waste landfill. African J. Environ. Sci. Technol. **5**(11), 933–940 (2011)
2. Schiopu, A.M., Brindusa, M., Ion, A., Maria, G.: Impact of landfill leachate on soil quality in Lasi Country. Environ. Eng. Manage. J. **8**(5), 1155–1164 (2009)

3. Anchal, S., Ashok, G., Rajiv, G.: Impact of open dumping of municipal solid waste on soil properties in mountainous region. J. Rock Mech. Geotech. Eng. 1–15 (2018)
4. Archana, V.: Seasonal variation on phsio-chemical characteristics of leachate in active and closed Municipal solid waste landfill site in Lucknow, India. G-J. Environ. Sci. Technol. **1**(4) (2014)
5. Eshanthini, P., Padmini, T.: Impact of leachate on ground water quality near Kodungaiyur dumping site Chennai, Tamil Nadu, India. Int. J. Pharm. Tech. Res. **8**(10), 171–179 (2015)
6. Indian Standard Code (10500:2012) Standards Specification for Drinking Water Quality
7. Irma, D., Jelenadoki, A.: The impact of leachate on the quality of surface and groundwater and proposal of measures for pollution remediation of environmental protection **7**, 745–759 (2016)
8. Kanmani, S., Gandhimathi, R.: Assessment of heavy metal contamination in soil due to leachate migration from an open dumping site. Spinger Appl. Water Sci. **3**, 193–205 (2013)
9. Kanmani, S., Gandhimathi, R.: Investigation of physicochemical characteristics and heavy metal distribution profile in groundwater system around the open dump site. Spinger Appl. Water Sci. **3**, 387–399 (2013)
10. Kurakalva, R., Aradhi, K., Mallela, K., Venkatayogi, S: Assessment of groundwater quality in and around the Jawaharnagar municipal solid waste dumping site at greater Hyderabad, Southern India. Proc. Environ. Sci. **35**, 328–336 (2016)
11. Lianwen, L., Mingxin, G.: Remediation techniques for heavy metal-contaminated soils: principles and applicability. Sci. Total Environ. **633**, 206–219 (2018)
12. Magda, M. Abd, E.-S., Abu-Zuid.: Impact of landfill leachate on the groundwater quality: a case study in Egypt. J. Adv. Res. **6,** 579–586 (2015)
13. Maiti, S., De, Hazra, T., A. Debsarkar, A., Dutta, A.: Characterization of leachate and its impact on surface and groundwater quality of a closed dumpsite—a case study at Dhapa, Kolkata, India. Proc. Environ. Sci. 391–399 (2016)
14. Nanda, S., Shivaraju, R., Ramakrishnegowda, C.: Impact of municipal solid waste disposal on geotechnical properties of soil. In: Proceedings of Indian Geotechnical Conference December 15–17, Kochi, Paper NoL-183 (2011)
15. Nevenka, M., Bozena, C., Marijan, A., Svjetlana, A., Zdenka, T.: Assessment of groundwater contamination in the vicinity of a municipal solid waste landfill (Zagreb, Croatia), Wat. Sci. Tech. **37**(8), 37–44, IAWQ (1998)
16. Samadder, S., Prabhakar, R., Khan, D., Kishan, D.: Analysis of the contaminants released from municipal solid waste landfill site: a case study. Sci. Total Environ. https://doi.org/10.1016/j.scitotenv.12.003
17. . Senthamil, S., Palanivel, M., Amsaveni, M.: Assessment of ground water contamination in soil due to leachate migration from an open dumping site of Dharapuram Municipality, Tamilnadu, India. Adv. Appl. Sci. Res. **6**(12), 53-58 (2015)
18. Suman, M., Khaiwal, R., Dahiya, R., Chandra, A.: Leachate characterization and assessment of groundwater pollution near municipal solid waste landfill site. Spinger Environ. Monitoring Assessment **118**, 435–456 (2006)
19. Yakub, A., Chavan, F.: Assessment of solid waste management of malegaon city. Int. J. Innov. Res. Sci. Eng. Technol. **6**(1) (2017)
20. Yulia, M., Murzayeva, A.I.: Urban soil contamination. Proc. Eng. **153**, 162–166 (2016)

Geotechnical Characterization of Recycled Aggregates (RA) Comprising of Mixed Waste from Construction & Demolition (C&D) Plants

Apoorva Agarwal, Manoj Datta, G. V. Ramana, N. K. Soni, and Rajiv Satyakam

Abstract India produces approximately 100 million tonnes of C&D waste per annum. Attempts are being made to separately process the C&D waste by segregating it from MSW stream. For this, C&D waste processing plants have been established in Delhi. About 1.15 million tons of C&D waste is annually processed in these plants. The bulk output from these plants is Recycled Concrete Aggregate (RCA) (10%), Recycled Aggregate (RA) (55%), and silt like fraction (below 0.075 mm) (35%). RCA and silt like fraction have reasonable demand in industry. RA comprising of mixed waste which has brickbats in highest proportion have low demand. It is coined as MRA (Mixed Recycled Aggregate) thereafter. Some areas in which gravel or sand-sized fraction of the MRA can be used are filters, drains, and backfill for embankments.

The geotechnical characteristics of MRA from two C&D plants C&D P1 and C&D P2 were studied in laboratory for the sand-sized fraction. Grain size distribution, compaction, specific gravity, permeability, and shear strength test were done on MRA. The results have been compared with the locally available Badarpur Sand (BS). From the testing results it is observed that geotechnical properties like specific gravity, compaction, permeability, and shear strength of MRA are similar to BS. This study serves as a starting point for use of MRA to be used in various geotechnical application.

Keywords C&D waste · Recycled aggregate · Brickbats · Mixed recycled aggregate

A. Agarwal (✉) · M. Datta · G. V. Ramana
Indian Institute of Technology Delhi, New Delhi, India
e-mail: apoorvaagarwal6@gmail.com

N. K. Soni · R. Satyakam
NTPC-Netra, NTPC Limited, Greater Noida, India

1 Introduction

Reuse of waste materials is a topic of global concern and of great international interest. The urgent need for reuse of waste materials is driven primarily by environmental considerations attributable to the increased scarcity of natural resources and the increasing cost of landfill in most countries [1]. C&D waste generation globally exceeds 3 billion tonnes [2]. For United States, the generation of C&D waste has increased from 519 MT in 2012 to 548 MT in 2015 [3]. Globally, it is estimated that about 35% of the quantities of C&D waste produced are directed to landfills, without any further treatment, although efforts to recycle and reuse C&D waste are increasingly being made [4]. Recycling rate varies from 7% or less for various countries like Canada, Croatia, Africa, etc. to more than 90% in Estonia, South Korea, etc. In the countries, where there is no recycling, this waste mostly ends up in a landfill. For proper recycling or reutilization of C&D waste, the focus should be on the proper collection of data. Two largest producers of C&D waste countries China and India both have limited focus in the area of proper data collection.

In the Indian scenario, the total quantum of waste from the construction industry generated was estimated as 12–14.7 million tons per annum in the year 2000. According to CSE report [5], the amount of C&D waste generated in India just by buildings in one year is 530 MT. This figure is 44 times more than the official estimate of C&D waste generation in India.

Most of the data available for the assessment of C&D waste production in India is underestimated. There is an uncertainty of the quantum of C&D waste generation in India. It is estimated that the C&D waste comprises of 25–30% of total solid waste generation. India produces approximately 25–30 million tonnes of C&D waste annually, of which less than 5% is processed, the remaining being sent for dumping, adding to the already overburdened dumping sites and attendant problems [6]. There is no concrete data available on the quantity of generation and reutilization of C&D waste in India. Previous researchers have shown the potential reuse of recycled C&D waste in various geotechnical applications like backfill for retaining walls, sub-base material, reclaimed soil for pipes, soft soil improvement [7].

In India so far, no study is reported which gives the systematic geotechnical characterization of waste material from C&D waste processing plants. Thus, through this paper it is an attempt to understand the feasibility of using mixed waste coming out of processing plants in Delhi in the form of Recycled Aggregate Bricks in various geotechnical applications. The results were compared with locally available sand, i.e., Badarpur Sand.

2 Materials and Testing Methods

2.1 Material

C&D waste was collected from two C&D waste recycling plant C&D P1 and C&D P2 in Delhi. Both the plants do pre-sorting of waste into two streams (concrete waste and mixed waste) before processing. The concrete waste undergoes dry processing which mainly includes breaking the large chunks of concrete into a smaller size fraction and separating it out in different fractions. The mixed waste undergoes breaking off big chunks of waste material and washing it so that soil or any foreign particle sticking to the big particle can be removed. After washing it was also separated into different fractions. The processed sample coming out from concrete waste is termed as Recycled Concrete Aggregate (RCA) and from mixed stream is termed as Recycled Aggregate (RA)/Mixed Recycled Aggregate (MRA). MRA is comprising of concrete, brickbats, and other waste material in mixed form. For this research Mixed Recycled Aggregate (MRA) was considered for analysis.

2.2 Sampling

The output of both C&D waste processing plant C&D P1 and C&D P2 was subdivided into different fraction range, i.e., sample size ranging from 20 to 10 mm, 10 to 4.75 mm, 4.75 to 0.075 mm, and less than 0.075 mm. For the analysis, material size passing from 4.75 mm and retained on 0.075 mm was sampled from both the processing plants C&D P1 and C&D P2. This part contributes to about around 16 to 18% of the total waste received at the processing plant (as reported by recycling plants). In order to do various geotechnical testing, about 100 kg of sample was collected from both the recycling plant. The reference material for comparison comprising of Badarpur Sand (BS) was sampled locally.

2.3 Testing Methods

Extensive geotechnical testing was carried out on MRA procured from two processing plants. The following tests were conducted:

Grain Size Distribution: This test was carried out according to ASTM D 6913. The material in the test was separated into various fractions. According to ASTM D 6913, if particle size is less than or equal to 4.75 mm, then single-set sieving is applicable.

Specific Gravity: Specific gravity of material was found adopting procedure in IS 2720: Part III using Density Bottle.

Standard Proctor Test: The test was conducted according to ASTM D698-12e2 in order to obtain Maximum Dry Density (MDD) (γd) and Optimum Moisture Content (OMC) using Standard Proctor Test.

Permeability: As the material seems to be in the range of sand, thus constant head method was employed for measuring the permeability of material. The test was conducted as per the method laid in IS: 2720—Part 36.

Shear Strength Characteristics: For any geotechnical purpose, shear strength of material plays an important role to play. In order to find shear strength parameters of material, Direct Shear Test (DST) was carried out at dry condition on a shear box of size 60 × 60 mm cross section. The testing was done as per the method described in IS: 2720—Part 13. The samples were prepared at two different densities, i.e., one at dense condition (around 80% R.D.) and one at loose condition (around 30% R.D.). The test was performed at three different normal stresses, i.e., 100, 200, and 400 kPa for both the conditions. The strain rate employed during the test was 0.25 mm/min. The test was run till 15% strain so that residual characteristics can also be studied.

3 Results and Discussion

3.1 Grain Size Distribution

Particle size distribution and gradation characteristics are presented in Table 1 for MRA from C&D P1 and C&D P2 and reference material Badarpur Sand (BS). MRA was not washed and no wet sieving was carried out as materials received from both the plants were already washed at the processing plant.

From the grain size distribution, it can be inferred that the C&D waste from two processing plants P1 and P2 are very much similar to that of reference material

Table 1 Comparison of grain size distribution of MRA with reference material

Properties	C&D P1	C&D P2	BS
Coarse sand size, 4.75–2.0 mm, %	14.3	1.16	2.6
Medium sand size, 2.0–0.425 mm, %	36.5	26.4	58.0
Fine Sand Size, 0.425–0.075 mm, %	42.0	62.9	37.9
Silt and Clay Size, less than 0.075 mm, %	7.3	9.5	1.5
D10, μm	100	77	240
D30, μm	250	160	370
D60, μm	580	294	570
Coefficient of Uniformity, Cu	5.80	3.81	2.38
Coefficient of Curvature, Cc	1.08	1.13	1.00

Fig. 1 Comparison of grain size distribution of MRA from two processing plant P1 and P2 with reference material
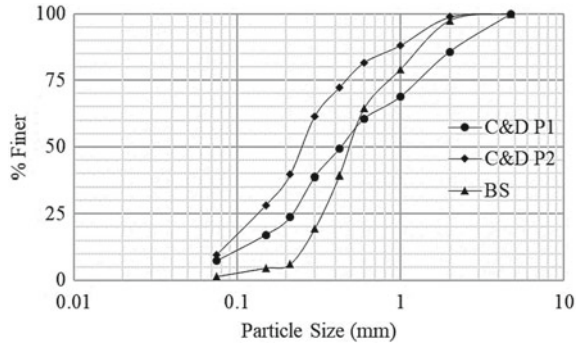
Fig. 2 Grains shape of MRA from two processing plants at 50X magnification

BS. Majority of material in P1 and P2 is medium to fine sand. The fraction below 0.075 mm is less than 10% in both the cases (Fig. 1).

The C&D waste from both the plants have brick bats in major quantity. It was not feasible to do compositional analysis for material below 4.75 mm by naked eyes. Thus, shape of the particles was studied with the help of digital microscope. The grains were angular with sharp edges (Fig. 2).

3.2 Specific Gravity

From Table 1 it is evident that most of the fraction of sample is in range of medium to fine sand. Thus, specific gravity of sample from C&D P1 and C&D P2 and reference material BS was found using specific gravity bottle. The specific gravity of sample from both the plants (P1 and P2) along with BS is summarized in Table 2:

The variation in specific gravity is more for C&D waste as compared to reference material due to heterogeneity of material.

Table 2 Specific gravity of C&D waste from two processing plant

Sample	Specific gravity
C&D P1	2.54–2.66
C&D P2	2.58–2.72
BS	2.63–2.69

Table 3 MDD and OMC of C&D waste from two processing plant P1 and P2 and reference material

Sample	MDD (kN/m^3)	OMC (%)
C&D P1	17.2	16.7
C&D P2	16.9	16.4
BS	17.6	16.0

Fig. 3 Comparison of compaction behavior of MRA from two processing plant P1 and P2 with reference material
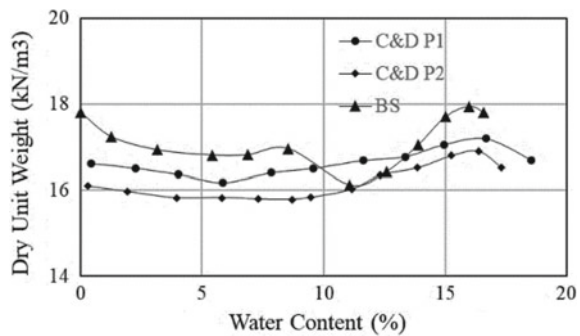
3.3 Standard Proctor Test

The test was conducted using Standard Proctor Test. Table 3 and Fig. 3 give the maximum dry density and optimum moisture content for C&D P1, C&D P2 and BS.

The compaction curve of the waste material from both the plants P1 and P2 does not show a significant peak.

3.4 Permeability

The permeability of C&D waste was evaluated using constant head method. Table 4 summarizes the permeability value for C&D waste from P1 and P2 along with reference material BS.

Table 4 Permeability values of C&D waste from two processing plant

Sample	Permeability (cm/sec)
C&D P1	10^{-3}–10^{-2}
C&D P2	10^{-3}–10^{-2}
BS	10^{-2}

Table 5 Shear Strength parameters of waste from processing plant P1 and P2 and reference material

Properties	C&D P1		C&D P2		BS	
	Dense	Loose	Dense	Loose	Dense	Loose
ϕ peak (°)	48.7	39.3	44.7	34.8	43.9	32.6
ϕ residual (°)	36.1	37.7	36.6	34.1	32.4	29.8
ψ (°)	12.6	1.6	8.1	0.7	11.5	2.8

3.5 Shear Strength Characteristics

Shear test was conducted using Direct Shear Test. Table 5 shows the resulting peak and residual angle of shearing resistance (φ) at dense and loose condition. It also gives dilation angle (ψ) for both the cases, i.e., at dense state and at loose state. Figure 4 gives the shear stress behavior of the materials with the increase in horizontal displacement and volume change behavior of material with increase in horizontal displacement. Finally, Fig. 5 gives the failure envelops of material from plant P1 & P2 and BS for dense and loose condition.

From the shear strength curves, it can be concluded that the angle of shearing resistance for C&D waste from both the plants P1 and P2 is high as compared to reference material. When the sample is compacted in dense compaction state, i.e., at R.D. 80%, the peak angle of shearing resistance converges to residual strength parameters with the increase in horizontal displacement. When the sample is loose compaction state, i.e., at 30% R.D., the convergence of peak shear strength value to residual shear strength value was negligible with the increase in horizontal displacement. At 80% R.D., all the materials exhibited positive dilation for all the normal stresses and the dilatancy decreases with increase in normal stresses. This is the typical characteristics behavior of granular material [8].

4 Conclusions

The material from both C&D waste processing plant P1 and P2 is comprising mainly of mixed waste and which is termed as Mixed Recycled Aggregate (MRA). From the extensive geotechnical testing carried out on sample from both the plants P1 and P2 and Badarpur Sand as reference material, following can be concluded:
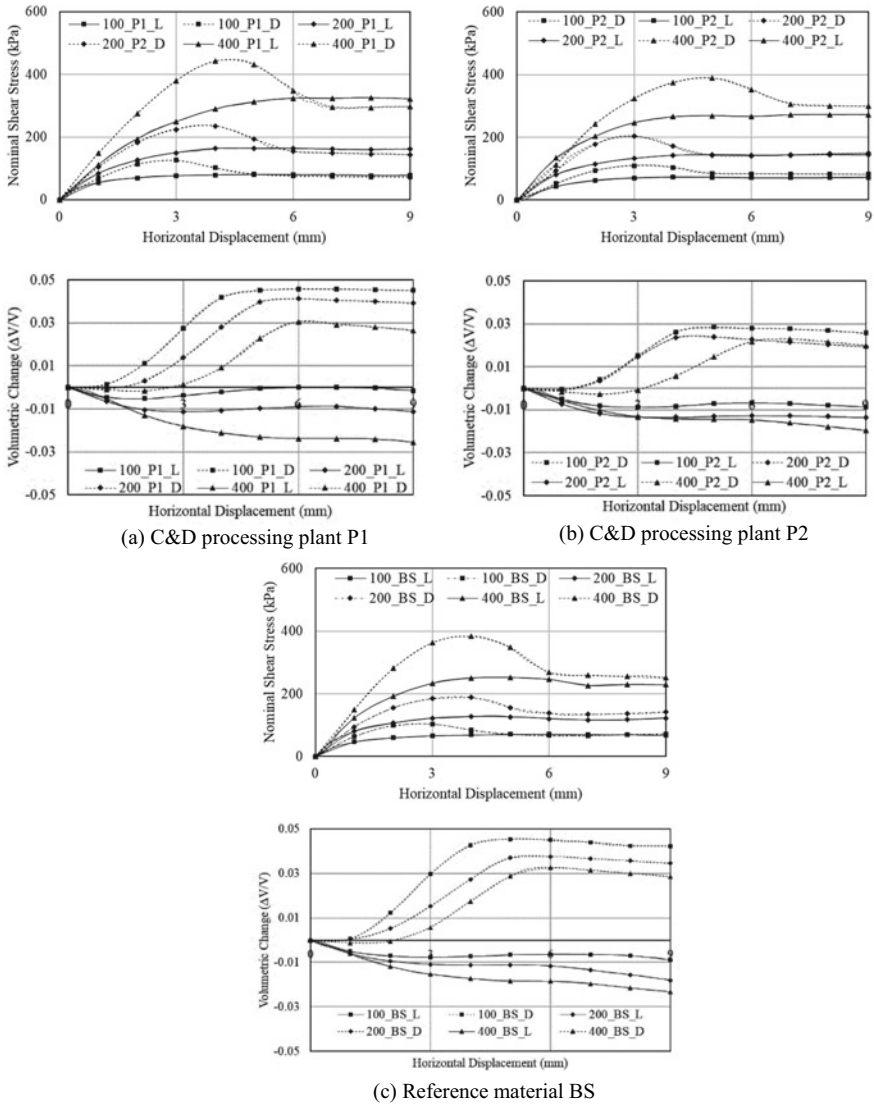
Fig. 4 Nominal shear stress—horizontal displacement and volume change—horizontal displacement behavior of material from plant P1 & P2 and BS

1. The particle size of the MRA waste is comprising predominantly of medium to fine sand.
2. The specific gravity and permeability are in the same range as that of reference material.
3. From the compaction characteristics, it can be concluded that the material shows similar behavior as that of granular material.

(a) C&D processing plant P1

(b) C&D processing plant P1

(c) Reference material BS
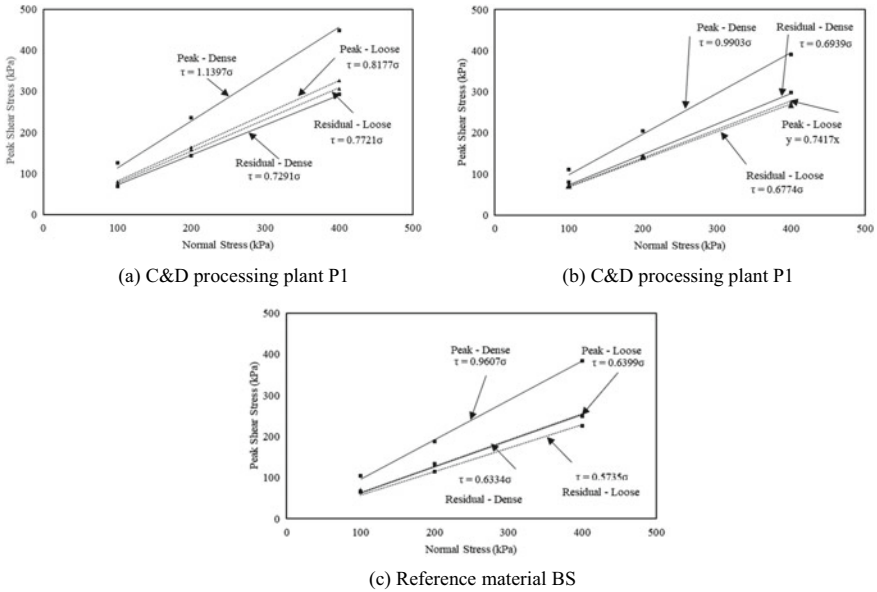
Fig. 5 Failure envelops of material from plant P1 & P2 and BS for dense and loose condition

4. The shear strength behavior of material is similar to that of reference material. The φ values obtained for the MRA are in the range of 49°–36° for plant P1 and 45°–34° for plant P2. The C&D waste exhibits convergence of peak shear strength to residual shear strength at dense condition, w*ith the increase in horizontal displacement.*

5. C&D waste shows positive dilation for all the normal stress in dense condition and compression in loose condition. This behavior is similar to that of granular material.

This paper gives the geotechnical characteristics of C&D waste derived from Mixed Recycled Aggregate which are similar to those of reference material i.e., Badarpur Sand. The chemical characteristics which include pH, TDS and heavy metals in the waste material have to be studied prior to use in the field.

References

1. Arulrajah, A., Ali, M.M.Y., Piratheepan, J., Bo, M.W.: Geotechnical properties of waste excavation rock in pavement subbase applications. J. Mater. Civ. Eng. **24**(7), 924–932 (2011)
2. Akhtar, A., Sarmah, A.K.: Construction and demolition waste generation and properties of recycled aggregate concrete: a global perspective. J. Cleaner Prod. **186**, 262–281 (2018)
3. USEPA: EPA Advancing Sustainable Materials Management: 2015 Fact Sheet 23 (2018). https://www.epa.gov/sites/production/files/2018-07/documents/2015_smm_msw_factsheet_07242018_fnl_508_002.pdf

4. Menegaki, M., Damigos, D.: A review on current situation and challenges of construction and demolition waste management. Current Opinion Green Sustain. Chem. (2018)
5. Centre of Science and Environment India (CSE): Construction and Demolition waste (WWW document) (2013). https://cdn.cseindia.org/userfiles/Construction-and%20-demolition-waste.pdf
6. Central Pollution Control Board (CPCB): Guidelines on Environmental Management of Construction & Demolition (C&D) Waste (2017)
7. Park, S.S., Kim, S.J., Chen, K., Lee, Y.J., Lee, S.B.: Crushing characteristics of a recycled aggregate from waste concrete. Constr. Build. Mater. **160**, 100–105 (2018)
8. Pant, A., Datta, M., Ramana, G.V.: Bottom ash as a backfill material in reinforced soil structures. Geotextiles and Geomembranes (2019)

Characterization of Heavy Metals from a Contaminated Industrial Site

Vemula A. Reddy, Deepak Haritwal, Chandresh H. Solanki, Shailendra Kumar, and Krishna R. Reddy

Abstract Soil contamination due to heavy metals has become a global problem. The knowledge of heavy metal speciation in soils must be understood for the rational investigation of risk and remediation of contaminated soils. This study presents a systematic investigation of an industrial site soil, known as Jarosite, which is obtained from a zinc smelter. The soil was found to be clayey soil with low to medium consistency, with organic content of 2.13% and pH of 5.59. The total heavy metals in the soil were determined using acid digestion procedure, and TCLP (toxicity characteristic leaching procedure) tests were also conducted for understanding the leachable metals from the soil. The total concentrations of heavy metals were found to be: zinc (Zn) = 13653 mg/kg, lead (Pb) = 6871 mg/kg, cadmium (Cd) = 1371 mg/kg, copper (Cu) = 128 mg/kg, nickel (Ni) = 37 mg/kg, arsenic (As) = 19 mg/kg, and cobalt (Co) = 13 mg/kg. TCLP concentrations were found to be: Zn = 1263 mg/kg, Pb = 503 mg/kg, and Cd = 251 mg/kg. The total heavy metals and TCLP metals are found to exceed the allowable limits, hence remediation action is required. Stabilization/solidification is considered to be promising technology to use for the site conditions.

Keywords Heavy metals · Soil · Leaching · Remediation · Stabilization

V. A. Reddy (✉) · D. Haritwal · C. H. Solanki · S. Kumar
Civil Engineering Department, Sardar Vallabhbhai National Institute of Technology (SVNIT), Surat, Gujarat, India
e-mail: vemulaanandreddy@gmail.com

D. Haritwal
e-mail: deepakharitwal009@gmail.com

C. H. Solanki
e-mail: chandresh1968@yahoo.co.in

S. Kumar
e-mail: skumar1863@gmail.com

K. R. Reddy
Department of Civil, Materials, and Environmental Engineering, University of Illinois at Chicago, Chicago, IL 60607, USA
e-mail: kreddy@uic.edu

1   Introduction

During the last few decades, rapid industrialization has led to manifold decline in the quality of environment [1, 14]. Particularly, the waste generated from the smelting activities all over the world [10]. Several studies indicated that people living near to the smelter have been affected significantly with the most toxic elements such as lead (Pb) and cadmium (Cd) [6]. Surveys showed that high (Pb) levels in blood were observed in the children who lived near the smelter [3, 9]. The increase in the production of various non-ferrous metals leads to solid waste generation in large quantities. Some of the non-ferrous metals include aluminum, lead, zinc, and copper [1]. Red mud which is generated during the production of 1 ton alumina has about 1.0–1.5 ton of waste generated [4, 11] likewise natrojarosite residue is the waste generated during the production of zinc and lead [5]. Currently, about 960 million tonnes of waste is generated during mining and industrial activities of these about 4.5 million tonnes are hazardous in nature Mehra et al. [12]. The disposal/dumping of such type of solid waste and resulting contamination of soils is a matter of concern to the geotechnical/geoenvironmental engineers. In this study, the characterization of Zn–Pb smelter waste was evaluated for potentially toxic heavy metals and leaching concentrations under weak acid environment. The goal of the study is to evaluate the most suitable remediation process for the successful application as an engineered and sustainable material.

2   Materials and Methods

2.1   Industrial Contaminated Site Soil

The soil contaminated with heavy metals was collected from Pb-Zn smelter (Latitude 24.60289°, Longitude 73.814657°), Hindustan zinc limited, Debari district, Rajasthan, India. The annual production of zinc is about 435,666 MT and lead 51, 759 MT [1, 2]. About 500 kg of sample was collected from the dumping site in sealed containers. The soil is air dried, homogenized, and sieved through a 10 mesh (2 mm) sieve. The basic properties and oxide composition of heavy metal contaminated soil are given in Tables 1 and 2.

Table 1 Basic properties of heavy metal contaminated soil

Property	Value
Specific gravity	2.78
pH	5.59
Color	Light Yellow
Organic content (%)	2.13
Natural water content (%)	14.20

Table 2 Oxide chemistry of field contaminated soil

Oxide	Value (%)
Aluminum oxide (Al_2O_3)	16.63
Calcium oxide (CaO)	11.18
Ferric oxide (Fe_2O_3)	36.21
Magnesium oxide (MgO)	2.89
Sulfate oxide (SO_4)	23.57
Phosphorus oxide (P_2O_5)	1.13
Potassium oxide (K_2O)	0.31
Loss of ignition	7.93

2.2 Determination of Total Heavy Metals

Several methods are available to evaluate the heavy metal concentrations in the contaminated soils. The most common method adopted is decomposition by Aqua Regia method ISO 11466:(1995) [13] where 3:1 concentrated hydrochloric acid (HCL) and nitric acid (HNO_3) is used for the determination of total heavy metals. The strong oxidizing power chemically decomposes the organic substances and dissolves the most insoluble metals available in the soil. About 3 grams of oven dried soil is taken and mixed with 21 ml of HCL and 7 ml of (HNO_3) in the digestion vessel and the sample is heated to 95 °C $\pm$ 5 °C and refluxed for 15 min. Later 5 ml of (HNO_3) is added and refluxed for 30 min, the procedure is repeated till the brown fumes are unseen in the sample. Further the sample is made up to 100 ml using distilled water and subjected to heavy metal concentrations analysis using atomic absorption spectrophotometer (AAS).

2.3 Toxicity Characteristic Leaching Procedure Test

During landfilling of any toxic materials, it is essential to fulfill TCLP limits given by Hazardous Waste Management Rules [8] in India. In this study leaching test was carried using toxicity characteristic leaching procedure test TCLP 1311 [16], which represents landfilling conditions in the field. The same TCLP procedure is used to characterize hazardous characteristics of contaminated soils and assess the need for remediation [14]. Approximately 10 grams of soil is mixed in TCLP extraction solution 200 ml with pH 4.93 $\pm$ 0.05 (glacial acetic acid CH3COOH and NaOH diluted in deionized double distilled water) is used. The mixture is tumbled in a 500 ml high density polyethylene bottle for 18 $\pm$ 2 h in a TCLP extractor. Later the soil-solution mixture is subjected to centrifugation of 5 min at 3000 rpm, then leachant is acidified with nitric acid at pH 2 and subjected to heavy metal concentration analysis by AAS. All the samples in the study were tested in triplicates for reproducibility of results.

Table 3 Total heavy metal concentrations of contaminated soil

Metal	Concentrations (mg/kg)
Lead (Pb)	6871
Zinc (Zn)	13653
Cadmium (Cd)	1371
Copper (Cu)	128
Nickel (Ni)	37
Arsenic (As)	19
Cobalt (Co)	13

3   Results

3.1   Total Heavy Metals Concentrations

Table 3 shows the distribution of heavy metal concentrations present in the contaminated soil sample. The lowest concentrations are for Cobalt (Co), Arsenic (As), Nickel (Ni), and Copper (Cu) and the highest for Zinc (Zn), Lead (Pb), and Cadmium (Cd). The order of heavy metal content is as follows: Zn > Pb > Cd > Cu > Ni > As > Co. The order of distribution of heavy metals is similar for many Zn–Pb smelters in the world [7, 17, 15]. The contaminated soil revealed high concentrations of Zn, Pb, and Cd which are attached to various metallic and complex phases.

3.2   Leaching of Heavy Metals

Based on the TCLP results, Table 4 shows the extremely high toxicity levels for Zn, Pb, and Cd, indicating 100 times for Pb, 5.05 times for Zn and 251 times for Cd as compared allowable limits. The acceptable limits for Zn are 250 mg/kg, Pb 5 mg/kg, and Cd 1 mg/kg according to Hazardous Waste Management rules [8]. The results are pertaining to weak acidic environment and are extracted from the acid-soluble phases of the contaminated soil particles which are easily available for leaching.

Table 4 TCLP concentrations of heavy metal contaminated soil

Heavy metal	Concentration (mg/kg)
Lead	503
Zinc	1263
Cadmium	251

4   Conclusions

An industrial Zn-Pb smelter soil was characterized for total heavy metal concentrations and leachable heavy metal concentrations. The following conclusions were drawn from this study:

1. High concentrations of Pb, Zn, and Cd are due to pyro-metallurgical process involved in the removal of Zn and Pb.
2. Leachability study indicated that the heavy metals are mobile in weak acidic environments.
3. Remediation of the soil is necessary to convert hazardous soil into non-hazardous form. Our ongoing studies show that solidification/stabilization can be one of the most appropriate methods in treating the contaminants in such soils.

References

1. Agrawal, A., Sahu, K.K., Pandey, B.D.: Solid waste management in non-ferrous industries in India. Resour. Conserv. Recycl. **42**(2), 99–120 (2004)
2. Asokan, P., Saxena, M., Asolekar, S.R.: Recycling hazardous jarosite waste using coal combustion residues. Mater. Charact. **61**(12), 1342–1355 (2010)
3. Beiyuan, J., Tsang, D.C., Valix, M., Zhang, W., Yang, X., Ok, Y.S., Li, X.D.: Selective dissolution followed by EDDS washing of an e-waste contaminated soil: extraction efficiency, fate of residual metals, and impact on soil environment. Chemosphere **166**, 489–496 (2017)
4. Borra, C.R., Pontikes, Y., Binnemans, K., Van Gerven, T.: Leaching of rare earths from bauxite residue (red mud). Minerals Eng. **76**, 20–27 (2015)
5. Catalan, L.J., Merlière, E., Chezick, C.: Study of the physical and chemical mechanisms influencing the long-term environmental stability of natrojarosite waste treated by stabilization/solidification. J. Hazard. Mater. **94**(1), 63–88 (2002)
6. Carvalho, F.M., Tavares, T.M., Silvany-Neto, A.M., Lima, M.E.C., Alt, F.: Cadmium concentrations in blood of children living near a lead smelter in Bahia, Brazil. Environ. Res. **40**(2), 437–449 (1986)
7. De Andrade Lima, L.R.P., Bernardez, L.A.: Characterization of the lead smelter slag in Santo Amaro, Bahia Brazil. J. Hazard. Mater. **189**(3), 692–699 (2011)
8. Government of India.: In: Waste Management Rules 1981. pp. 1–68. (2016)
9. Li, P., Lin, C., Cheng, H., Duan, X., Lei, K.: Contamination and health risks of soil heavy metals around a lead/zinc smelter in southwestern China. Ecotoxicol. Environ. Safety **113**, 391–399 (2015)
10. Li, Y., Perederiy, I., Papangelakis, V.G.: Cleaning of waste smelter slags and recovery of valuable metals by pressure oxidative leaching. J. Hazard. Mater. **152**(2), 607–615 (2008)
11. Liu, Z., Li, H.: Metallurgical process for valuable elements recovery from red mud—a review. Hydrometallurgy **155**, 29–43 (2015)
12. Mehra, P., Gupta, R.C., Thomas, B.S.: Assessment of durability characteristics of cement concrete containing jarosite. J. Clean. Prod. **119**, 59–65 (2016)
13. International Organization for Standardization.: Soil quality-Extraction of trace elements soluble in aqua regia. ISO (1995)
14. Sharma, H.D., Reddy, K.R.: Geoenvironmental Engineering: Site Remediation, Waste Containment and Emerging Waste Management Technologies. Wiley, Hoboken, NJ, USA (2004)

15. Voglar, G.E., Leštan, D.: Solidification/stabilisation of metals contaminated industrial soil from former Zn smelter in Celje, Slovenia, using cement as a hydraulic binder. J. Hazard. Mater. **178**(1–3), 926–933 (2010)
16. USEPA Method 1311.: Toxicity Characteristic Leaching Procedure (TCLP), United States Environmental Protection Agency, (USEPA), Washington, DC (1992)
17. Xia, W.Y., Feng, Y.S., Du, Y.J., Reddy, K.R., Wei, M.L.: Solidification and stabilization of heavy metal–contaminated industrial site soil using KMP binder. J. Mater. Civil Eng. **30**(6), 04018080 (2018)

Experimental Study of Engineering Properties of Kota Stone Slurry Powder and Fly Ash Mixed Expansive Soil

Dayanand Tak, J. K. Sharma, and K. S. Grover

Abstract Black cotton soils have the properties to shrink and develop cracks without any warning when water content is reduced in hot season and expand when it comes in contact with water content in rainy season. So, for a civil engineer it is very difficult task to design a foundation on black cotton soil. The properties of black cotton soils can also be improved by stabilizing the soils by mechanical means or by mixing of additives in different proportions by weight. The present study explores the behavior of black cotton soil when it is stabilized with Kota stone slurry powder (KSSP) and fly ash. Kota stone slurry powder and fly ash are locally available materials in abundance in Kota district in Rajasthan state. Kota stone slurry powder is generated during cutting, sawing, and polishing process in Kota stone industries. Fly ash is generated during thermal electricity production. Due to improper disposal, it considerably affects prime land, vegetations, surface, and underground water. There should be great priority to dispose these generating waste materials in scientific manner. The study reveals that mixing of KSSP with black cotton soil as a stabilizing agent improves the properties of the soil due to presence of silica and lime in it. The present study deals with determination of optimum percentage of utilization of KSSP and fly ash to improve the expansive soil. Index properties, Proctor test, and swelling index test were conducted to evaluate the magnitude of KSSP and fly ash mixed expansive soil.

Keywords Black cotton soil (BCS) · Kota stone slurry powder (KSSP) · Fly ash (FA) · Stabilization

D. Tak (✉)
Civil Engineering Department, Government Polytechnic Kota, Kota, India
e-mail: dayanandtak83@gmail.com

J. K. Sharma · K. S. Grover
Civil Engineering Department, University Department, Rajasthan Technical University, Kota, India
e-mail: jksharma@rtu.ac.in

K. S. Grover
e-mail: kdsgrover@gmail.com

1   Introduction

Black cotton soil is found in western part of Madhya Pradesh, some part of Andhra Pradesh, Karnataka, Southern part of Rajasthan, almost entire part of Deccan plateau and Utter Pradesh. Land area covered with black cotton/expansive soil is about 20–25% of total land area of India. Black cotton soil is highly problematic due to its detrimental volume changes corresponding to change in moisture content, swells, when contact with moisture in rainy season and shrinks in hot/dry season when it is dried [1, 2]. Black cotton soil is very dangerous for construction over it because of its swelling and shrinkage behavior but very fruitful for farmers because of its fertility. Lightly loaded civil engineering structures like residential buildings, pavements, and linings founded on expansive soil are severely damaged due to its swelling and shrinkage behavior.

Kota stone has been commonly used as a building material since the ancient times. Kota stone slurry powder contains siliceous and also having free lime to react chemically and forms cementitious compound [3]. It is very fine powder generated from Kota stone industries during the process of cutting, sawing, and polishing. Still a proper disposal system of Kota stone slurry powder is not developed. In present time, it is disposed to any convenient places like nearby Nallah, river, pasture land, forest land, and nearby roads. During the stormy days, these fine powder particles transfer from one place to another place and also available in suspension state in environment, which hazardous to health for living beings and affect the fertility of the nearby soil areas. Disposed quantities can be reduced by using the KSSP in various engineering applications and give solution to the problems of disposal. This will help in reduction to pollute the environment and also reduce the bad effects on fertility of nearby fertile soils [4, 5]. Kota stone is basically a calcareous sedimentary rock available in different colors and texture (blue, brown, green, gray, etc.) and fine-grained limestone [6].

Need one of the major environmental problems around the world. It can be used to improve strength and durability parameters [7].

Fly ash is a byproduct from burning pulverized coal in electric generating plant. Fly ash available in district Kota in Rajasthan till dated May 31, 2019 is 500 MT and stock in ash pond 0.67 Lac Metric Ton. Fly ash is defined as the material extracted from the flue gases of a furnace fired with coal. During stormy weather if fly ash is not disposed in proper manner, fine particles transfer from one place to another place and some particles are in suspension also, create the bad effects like damage lungs, damage nervous system, Kidney disease, swelling of the brain and hearing impairment. So, there is a need to dispose it in proper manner and used as an engineering material to improve the engineering properties of expansive soils. Several studies have shown that use of industrial waste materials like fly ash, pond ash, etc. to improve the engineering behavior and also suppress the swelling-shrinkage characteristics of expansive soil [8, 9, 10]. Fly ash is also used in stabilization of expansive soils [10]. Many researchers have shown that fly ash and stone dust are additives have great potential to stabilize the expansive soil [11, 12]. Experimentation to analyze

compaction and swelling behavior of black cotton soil mixed with different non-cementitious materials like fly ash and stone dust is presented [13]. Present paper deals a comprehensive experimental work to analyze the index properties, swell behavior, and compaction characteristics of black cotton soil mixed with KSSP and fly ash.

Many researchers did work on stabilization of black cotton soil with different cementitious and non-cementitious materials in the past to analyze the improvement in black cotton soil mixed with different materials like stone dust, fly ash, marble dust, Kota stone slurry powder, etc. The test results revealed that there is a significant improvement in engineering properties of expansive soils.

Tak et al. [14] presented the use of Kota stone powder to improve properties of black cotton soil and value of consistency liTakmits, swelling pressure, standard proctor, and UCS.

Shalendra et al. [15] analyzed black cotton soil mix with lime by different proportions and found that properties of soil such as plasticity index, shrinkage limit, and CBR value are improved.

Parte and Yadav [16] founded that marble dust has a potential to modify the characteristics of black cotton soil.

Anu et al. [17] perform experiments on soft soil mixed with fly ash and lime and found improvement in engineering properties like dry density and strength of soft soil.

Baba and Haripriya [18] presented the effect of granite dust and lime which mixed with different proportions with black cotton soil and found improvement in the engineering properties of the black cotton soil.

Materials

- **Soil**:-Soil was collected from Amrit Nagar, near Bohr Khera, district Kota in Rajasthan state. Soil engineering properties are listed in tables.
- **Kota stone slurry powder**:-The KSSP was collected from Indraprastha Industrial area dumped behind Mittal Factory, Road No. 5, district Kota in Rajasthan state.
- **Fly ash**:-Fly ash was collected from brick manufacturing yard near Nanta, generated during thermal power generation at district Kota in Rajasthan state.

2 Experimental Program

Objectives

- To stabilize and study the behavior of the Black cotton soil using KSSP and fly ash as a stabilizer.
- To mix KSSP and fly ash as a stabilizer at an interval of 5% from 0 to 20%.

Table 1 Laboratory experimental test result values of black cotton soil, Kota stone slurry powder and fly ash

Descriptions	Black cotton soil	Kota stone slurry powder	Fly ash
Specific gravity	2.57	2.63	2.1
Liquid limit (%)	55	32.0.8	35.5
Plastic limit (%)	26.62	NP	NP
Plasticity index (%)	28.38	–	–
Shrinkage limit (%)	9.20	22.49	35.5
Unified soil classification Symbol	CH	CI	CI
Maximum dry density(g/cm^3)	1.67	1.69	1.23
Optimum moisture content (%)	19.4	18.3	23.4

Experimental details

Properties of the black cotton soil studied by using varying percentage of Kota stone slurry powder and fly ash:

Atterberg,s limit, IS: 2720 (Part V)—1985.
Standard proctor compaction test, IS: 2720 (Part VII)—1980.
Shrinkage limit, I.S: 2720 (Part VI).
Free swell index, IS: 2720 (Part XL).
Specific gravity test, IS: 2720 (Part III).
Proctor compaction test. IS: 2720 (Part VII) (Tables 1 and 2).

Table 2 Chemicals composition of Kota thermal fly ash

Constituents of fly ash	Value–II (%)	As per IS: 3812 (Part 1); 2003
Silica (SiO$_2$)	60.9	35.0
Alumina (Al$_2$O$_3$)	26.5	
Ferric Oxide (Fe$_2$O$_3$)	5.50	
Calcium Oxide (CaO)	5.98	
Magnesium Oxide (MgO)	0.62	5.0
Titanium Oxide (TiO$_2$)	0.24	
Free lime content	2.75	
Moisture	0.76	
LOI (Loss On Ignition)	0.28	5.0
SiO$_2$ + Al$_2$O$_3$+ Fe$_2$O$_3$	92.9	70.0

2.1 Liquid Limit

The object of the test is to determine the liquid limit that shows the lowest water content at which the sample is in liquid state. Table 3.

Figure 1 shows continuous decreasing liquid limit of the black cotton soil mixed specimens. Liquid limit of the black cotton soil was 55%, it decreases up to 45.50%. Proportions of fly ash and Kota stone slurry powder in the Black cotton soil by dry weight of the soil. Specimens having fixed 15% Kota stone slurry powder but fly ash varying from 5 to 20% at the interval of 5%. Decreasing in liquid limit shows reduction in volume. This behavior indicates improvement in the engineering characteristics of the soil. Proportion of 15% Kota stone slurry powder is the optimum dose in the soil. Liquid limit test performed by the Uppal Cone Penetrometer (IS: 2720-V). Table 4 and Fig. 2.

Figure 1 shows continuous decreasing the liquid limit of mixed of the black cotton soil specimens. Liquid limit of the black cotton soil is 55%, it decreases up to 44.51%. Proportions of fly ash and Kota stone slurry powder in the black cotton soil by dry weight of the soil. Specimens having fixed 10% fly ash but Kota stone slurry powder varying from 5 to 20% at the interval of 5%. Decreasing in liquid limit shows reduction in volume. This behavior indicates improvement in the engineering characteristics of the soil. Proportion of 10% fly ash is the optimum dose in the soil.

Table 3 Liquid limits and percentage variations of mixes 15% KSSP and 5% to 20% fly ash at an interval of 5% with black cotton soil

Descriptions	Liquid limit (%)	Percentage decreasing (%)
BCS + 05% Fly ash + 15% KSSP	49.81	9.43
BCS + 10% Fly ash + 15% KSSP	47.95	12.82
BCS + 15% Fly ash + 15% KSS	46.80	14.91
BCS + 20% Fly ash + 15% KSSP	45.50	17.27

Fig. 1 Percentage variations in liquid limit of BCS mixed specimen

Table 4 Liquid limits and percentage variations of mixes 10% fly ash and 5% to 20% KSSP at an interval of 5% with black cotton soil

Particulars	Liquid limit (%)	Percentage decreasing (%)
BCS	55	–
Fly ash	35.5	–
BCS + 10% Fly ash + 05% KSSP	51.06	7.16
BCS + 10% Fly ash + 10% KSSP	50.11	8.90
BCS + 10% Fly ash + 15% KSSP	47.95	12.82
BCS + 10% Fly ash + 20% KSSP	45.92	16.51
BCS + 10% Fly ash + 25% KSSP	44.51	19.07
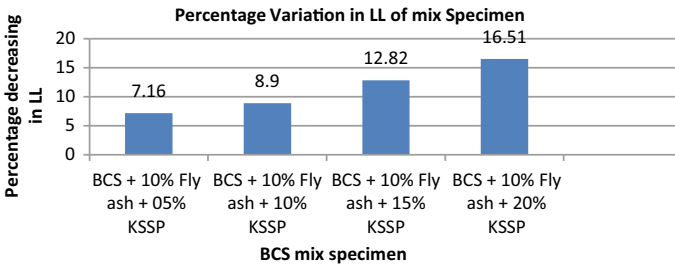
Fig. 2 Percentage variations in liquid limit BCS mixed specimen

2.2 Plastic Limit Test

See Table 5.

Table 5 Plastic limits and percentage variations of mixes 15% KSSP and 5% to 20% fly ash at an interval of 5% with black cotton soil

Descriptions	Plastic limit (%)	Percentage decreasing (%)
BCS + 05% Fly ash + 15% KSSP	25.05	5.90
BCS + 10% Fly ash + 15% KSSP	23.76	10.74
BCS + 15% Fly ash + 15% KSSP	23.05	13.41
BCS + 20% Fly ash + 15% KSSP	22.10	17.0

Figure 3 represents the relationship of mixed specimens with variation in the plastic limit. Plastic limit of the black cotton soil is 26.62% but mixing fly ash and Kota stone slurry powder are non-plastic (NP). Decreasing in plastic limit of the Black cotton and it mixed specimens from 26.62 to 22.10%. Mixed specimens having 15% Kota stone slurry powder but other admixture material was fly ash percentage varying from 5 to 20% at the interval of 5%. Decreasing in plastic limit showed reducing the volume change behavior that indicated improvement in the characteristics of the soil. Table 6.

Figure 4 represents the relationship of mixed specimens with varying in the plastic limit. Plastic limit of the black cotton soil is 26.62% but mixing fly ash and Kota stone slurry powder are non-plastic (NP). Decreasing in plastic limit of the black cotton and it mixed specimens from 26.62 to 22.28%. Mixed specimens having 10% fly ash but other mixing material was Kota stone slurry powder and percentage was varying from 5 to 20% at the interval of 5%. Decreasing plastic limit shows reducing the volume change behavior that indicated improvement in characteristics of the soil. Tables 7 and 8.

Fig. 3 Percentage variations in plastic limit (PL)

Descriptions	Plastic limit (%)	Percentage decreasing (%)
Black cotton soil	26.62	–
BCS + 10% Fly ash + 05% KSSP	25.05	5.90
BCS + 10% Fly ash + 10% KSSP	24.25	8.90
BCS + 10% Fly ash + 15% KSSP	23.76	10.74
BCS + 10% Fly ash + 20% KSSP	22.88	14.05

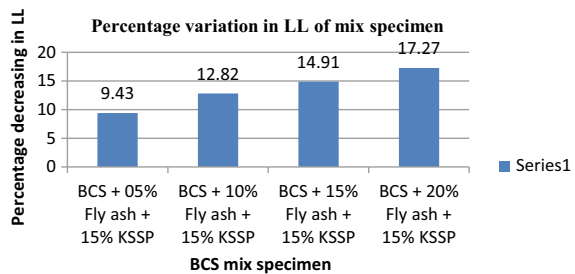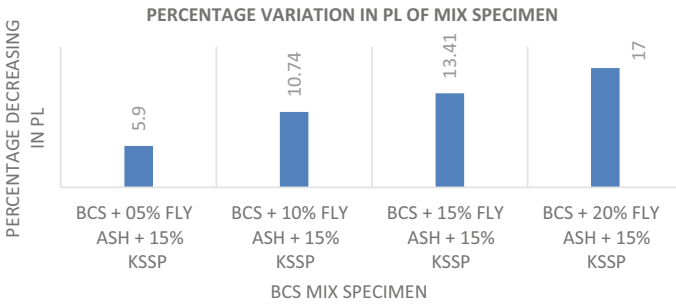**Table 6** Plastic limits and percentage variations of mixes 10% fly ash and 5% to 20% KSSP at an interval of 5% with black cotton soil
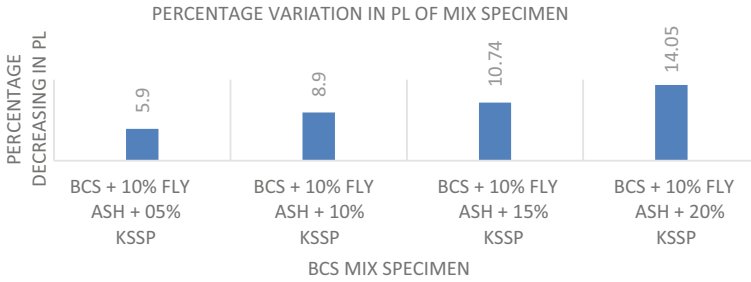
Fig. 4 Percentage variations in Plastic limit (PL)

Table 7 Plasticity index and percentage variations of mixes 15% KSSP and 5% to 20% fly ash at an interval of with black cotton soil

Descriptions	Plasticity index (%)	Percentage decreasing (%)
BCS + 05% Fly ash + 15% KSSP	24.76	12.76
BCS + 10% Fly ash + 15% KSSP	24.49	13.71
BCS + 15% Fly ash + 15% KSSP	23.75	16.31
BCS + 20% Fly ash + 15% KSSP	23.40	17.55

Table 8 Plasticity index and percentage variations of mixes 10% fly ash and 5% to 20% KSSP with black cotton soil

Particulars	Plasticity index (%)	Percentage decreasing (%)
BCS	28.38	–
BCS + 10% Fly ash + 05% KSSP	26.01	8.35
BCS + 10% Fly ash + 10% KSSP	25.86	8.88
BCS + 10% Fly ash + 15% KSSP	24.49	13.71
BCS + 10% Fly ash + 20% KSSP	23.04	18.82

2.3 Plasticity Index

Figure 5 represents the plasticity index variations in different mixed specimens and found decreasing in plasticity index of different mixed as compare to the black cotton soil. Mixed specimens of the black cotton soil having different percentage of fly ash but Kota stone slurry powder was fixed. Proportion of the admixtures in the mixed specimens was by weight of the dry soil. Figure 6 shows mixed specimens having

Fig. 5 Percentage variation in plasticity index (PI)

Percentage variation in PI of mix specimen
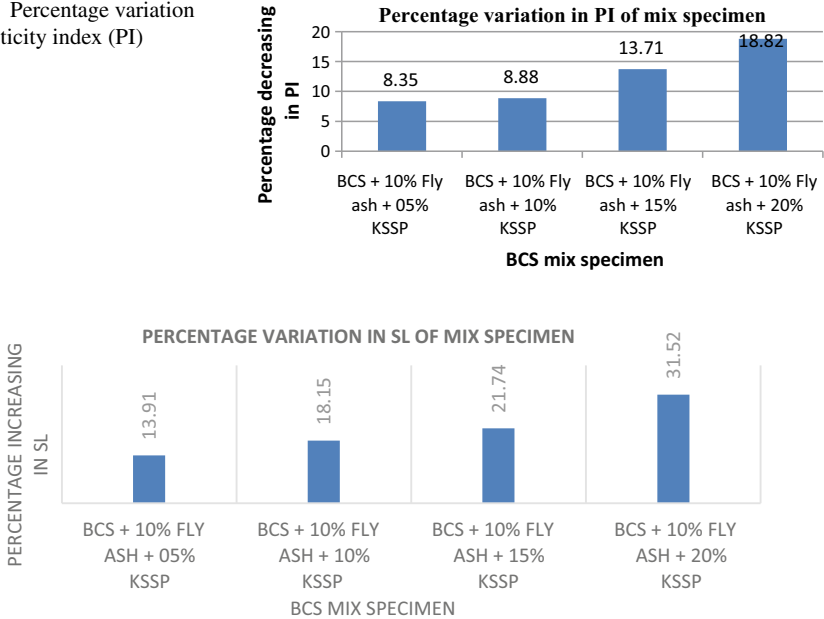
Fig. 6 Percentage variation in Shrinkage limit (SL)

15% KSSP but varying the percentage of fly ash from 5 to 20% at the interval of 5%. Mixing of 15% Kota stone slurry powder is the optimum dose. The plasticity index of the Black cotton soil is 28.38% and decreases up to 23.04%. Decreasing in plasticity index indicates improvement in strength of the soil.

2.4 Shrinkage Limit

Table 9 represents a comparison of mixed specimens shrinkage limits and shrinkage limit of the black cotton. Shrinkage limit of the black cotton soil was 9.20 and 22.49, 35.5% for Kota stone slurry powder and fly ash, respectively. Increasing in shrinkage limit was from 9.20 to 13.08%. Percentage of Kota stone slurry powder was remained 15% but percentage of fly ash varying from 5 to 20% at the interval of 5%. Percentage increasing in shrinkage limit was 42.17%. Presence of more percentage of fly ash founded more variations in mixed specimens Table 10.

Figure 6 draws a relationship between mixed specimens shrinkage limit. Shrinkage limit of the Black cotton was 9.20% and 22.49%, 35.5% for Kota stone slurry powder and fly ash, respectively. Increasing in shrinkage limit was from 9.20% to 12.10%. Percentage of fly ash was remained 10% but percentage of Kota stone

Table 9 Shrinkage limit of mixed specimen

Descriptions	Shrinkage limit (%)	Percentage increasing (%)
BCS + 05% Fly ash + 15% KSSP	10.78	17.18
BCS + 10% Fly ash + 15% KSSP	11.20	21.74
BCS + 15% Fly ash + 15% KSSP	12.16	32.17
BCS + 20% Fly ash + 15% KSSP	13.08	42.17

Table 10 Shrinkage limits and percentage variations of mixes 10% fly ash and 5% to 20% KSSP at an interval of 5% with black cotton soil

Descriptions	Shrinkage limit (%)	Percentage increasing (%)
BCS	9.20	–
BCS + 10% Fly ash + 05% KSSP	10.48	13.91
BCS + 10% Fly ash + 10% KSSP	10.87	18.15
BCS + 10% Fly ash + 15% KSSP	11.20	21.74
BCS + 10% Fly ash + 20% KSSP	12.10	31.52

slurry powder (KSSP) varying from 5 to 20% at the interval of 5%. Percentage increasing in shrinkage limit was 31.52%.

2.5 Specific Gravity

Tables 11 and 12 represent specific gravity of mixed specimens having varying percentage of Kota stone slurry powder and fly ash.

2.6 Swell Index

See Tables 13 and 14.

Tables 11 and 12 represent swelling index of the black cotton soil and its mixed with different proportions of fly ash and Kota stone slurry powder. Swell index of the black cotton soil is 50% and reduced up to 30% in mix of 20% ash with 15% Kota stone slurry powder and 10% ash with 20% Kota stone slurry powder.

Table 11 Specific gravity of mixed specimens

Descriptions	Specific gravity	Percentage variation (%)
BCS + 05% Fly ash + 15% KSSP	2.59	+ 0.8
BCS + 10% Fly ash + 15% KSSP	2.57	0.00
BCS + 15% Fly ash + 15% KSSP	2.55	−0.8
BCS + 20% Fly ash + 15% KSSP	2.52	−1.95

Table 12 Specific gravity of mixed specimens

Descriptions	Specific gravity	Percentage variation (%)
BCS	2.57	–
BCS + 10% Fly ash + 05% KSSP	2.56	−0.4
BCS + 10% Fly ash + 10% KSSP	2.56	−0.4
BCS + 10% Fly ash + 15% KSSP	2.57	−0.4
BCS + 10% Fly ash + 20% KSSP	2.59	+ 0.8

Table 13 Swell index and percentage variations of mixes 15% KSSP and 5% to 20% fly ash at an interval of 5% with black cotton soil

Particulars	Swell index (%)	Percentage decreasing (%)
BCS + 05% Fly ash + 15% KSSP	40	20
BCS + 10% Fly ash + 15% KSSP	40	20
BCS + 15% Fly ash + 15% KSSP	35	30
BCS + 20% Fly ash + 15% KSSP	35	30

2.7 Proctor Test

See Table 15 and Fig. 7.

Figure 8 represents a relationship between dry density versus moisture content. The maximum dry density of the black cotton soil was found 1.67 g/cm^3 corresponding to moisture content 19.4%. The maximum dry density obtained was

Table 14 Swell index and percentage variations of mixes 10% fly ash and 5% to 20% KSSP at an interval of 5% with black cotton soil

Particulars	Swell index (%)	Percentage decreasing (%)
BCS	50	–
BCS + 10% Fly ash + 05% KSSP	45	10
BCS + 10% Fly ash + 10% KSSP	45	10
BCS + 10% Fly ash + 15% KSSP	40	20
BCS + 10% Fly ash + 20% KSSP	35	30

Table 15 Variations in dry density of mixes 15% KSSP and 5% to 20% fly ash at an interval of 5% with black cotton soil at different moisture content

Descriptions	Optimum moisture content (%)	Maximum dry density (g/cm3)
BCS	19.4	1.67
BCS + 05% Fly ash + 15% KSSP	16.82	1.73
BCS + 10% Fly ash + 15% KSSP	17.23	1.73
BCS + 15% Fly ash + 15% KSSP	17.62	1.72
BCS + 20% Fly ash + 15% KSSP	17.90	1.71
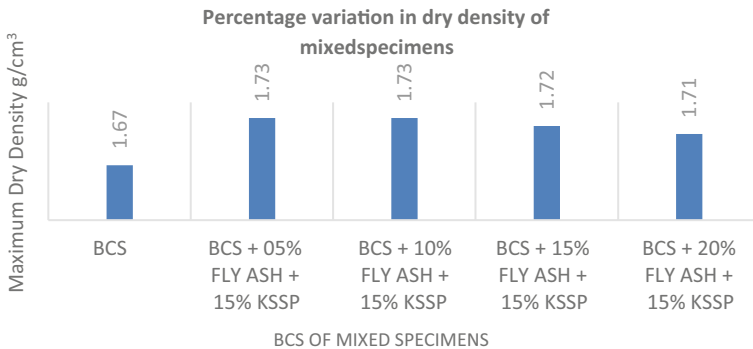
Fig. 7 Variations of maximum dry density of mixes 15% KSSP and 5% to 20% fly ash dosage at an interval of 5% with black cotton soil

1.73 g/cm^3 of the mix having 10% fly ash and 15% KSSP corresponding to moisture content 17.23%. Percentage increasing in maximum dry founded was 3.6%. Percentage increasing in maximum dry density indicates improvement in the characteristics of the black cotton soil. Test specimens having 15% Kota stone slurry
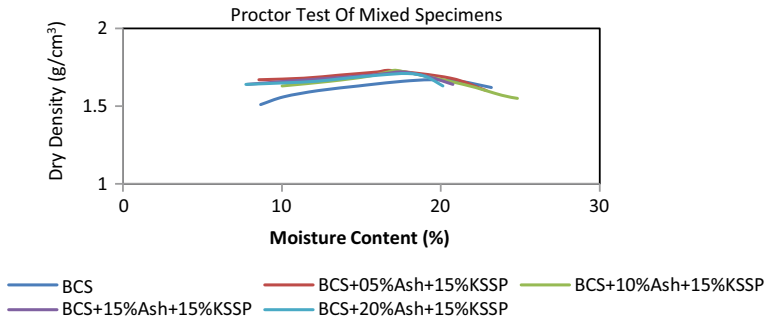
Fig. 8 Variations in dry density of mixes 15% KSSP and 5% to 20% fly ash at an interval of 5% with black cotton soil of different percentage dosage of moisture content

Table 16 Variations in dry density of mixes 10% fly ash and 5% to 20% KSSP at an interval of 5% with black cotton soil at different moisture content

Descriptions	Optimum moisture content (%)	Maximum dry density (g/cm3)
BCS	19.4	1.67
BCS + 10% Fly ash + 05% KSSP	18.96	1.71
BCS + 10% Fly ash + 10% KSSP	18.74	1.72
BCS + 10% Fly ash + 15% KSSP	18.43	1.73
BCS + 10% Fly ash + 20% KSSP	18.08	1.75

powder but varying percentage of fly ash varying from 5 to 20% at the interval of 5%. The test was conducted as per IS: 2720-VII. This test equivalent to the standard Proctor test AASHO—American Association of State Highway Officials. Table 16 and Fig. 9.

Figure 10 represents a relationship between dry density versus moisture content. The dry maximum density of the black cotton soil was found 1.67 g/cm3 and the corresponding to moisture content was 19.4%. The maximum dry density obtained was 1.75 g/cm^3 of the mix having 10% fly ash and 20% KSSP corresponding to moisture content 18.08%. Percentage increasing in maximum dry founded was 4.8%. Percentage increasing in maximum dry density indicates improvement in the characteristics of the black cotton soil. Test specimens having 10% fly ash but varying percentage of Kota stone slurry powder from 5 to 20% at the interval of 5%.
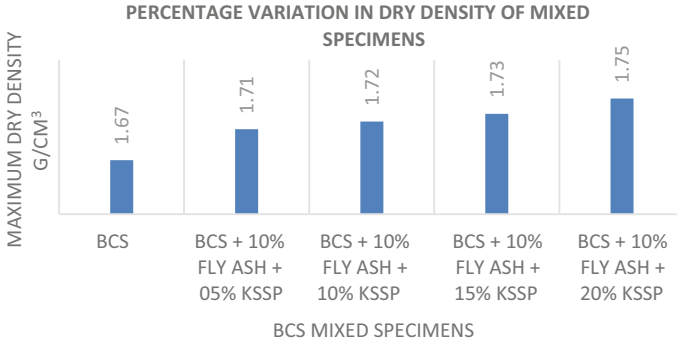
Fig. 9 Variations in maximum dry density of mixes 10% fly ash and 5% to 20% KSSP at an interval of 5% with black cotton soil
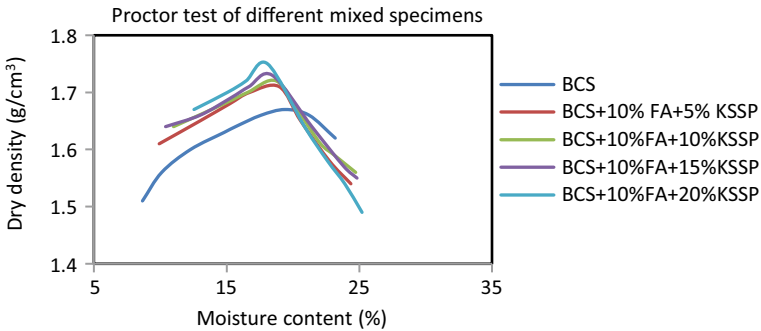
Fig. 10 Variation in dry density of mixed specimens

3 Conclusions

This experimental study investigates the incorporation of fly ash and Kota stone slurry powder to improve the characteristics of the Black cotton soil. Following conclusions are described as bellow,

1. Liquid limit of the black cotton soil found 55%, it decreased at different proportions of fly ash and Kota stone slurry powder in the black cotton soil. 19.07% decreased in LL of the black cotton soil mixed having 10% fly ash and 25% KSSP, 17.27% decreased in LL mixed having 15% KSSP and 20% fly ash. The black cotton soil classification changed from CH (high compressible) to CI (medium compressible).

2. The plastic limit of the black cotton soil found 26.62%. Reduction in PL of mix having different proportions of KSSP and fly ash. 14.05% reduction in mixed having 20% KSSP and 10%% fly ash and 17% reduction in PL of mix having 15% KSSP and 20% fly ash.

3. Determined the plasticity index of the black cotton soil was 28.38%. Plasticity index is reduced in mixed having different proportions of KSSP and fly ash. Maximum reduction in PI of the specimen having 20% KSSP and 10% fly ash was 18.82%. Reduction in PI indicates improvement in strength characteristics of the BC soil.

4. Free swell index of the black cotton soil was 50%, it reduced up to 35%. Reduction in the swell index was 30%. Reduction in free swell index meant reduced in swell behavior of the BC soil. This behavior indicates improvement in the properties of the BC soil.

5. The maximum dry density (MDD) and optimum moisture content (OMC) of the black cotton soil are determined 1.67 g/cm^3 and 19.4%, respectively. The MDD increased at different proportions of mixed used KSSP and fly ash as an admixture. The dry density was at most of the specimen having 10% fly ash and 20% KSSP and found 1.75 g/cm^3. Increased in the MDD also indicates improvement in the engineering properties of the BC soil.

References

1. Nevels, J.B.: Longitudinal cracking of a bicycle trial due to drying shrinkage. In: Proceeding of the Civil Engineering Conference, ASCE, Reston, pp. 132–157 (2001)
2. Walsh, K.D., Houston, W.N., Houston, S.L.: Evaluation of in-place wetting using soil suction measurements. J. Geotech. Eng. **119**(5), 862–873 (1993)
3. Bell, F.G.: Engineering Treatment of Soils. E & FN Spon Publishers, London (1993)
4. Martin, J.P., et al.: Properties and use of fly ashes for embankments. J. Energy Eng. **116**(2), 71–86 (1990)
5. Misra, A., Biswas, D., Upadhyaya, S.: Physico-mechanical behavior of self-cementing class C fly ash–clay mixtures. Fuel **84**, 1410–1422 (2005)
6. Mehta, Jitesh et al.: Experimental investigations for the Kota stone powder as replacement of marble powder in marble brick. Int. J. Current Trends Eng. Res. **2**(4), 105–111 (2016)
7. Jain, A., Rohan, M.: Strength permeability and carbonation properties of concrete containing Kota stone slurry. SRG Int. J. Civil Eng. **3**(6), (2016). ISSN: 2348-8352
8. Khattab, S.A.A., Al-Mukhtar, M., Fleureau J.M.: Long-term stability characteristics of a lime-treated plastic soil. J. Mater. Civil Eng. **19**(4), 358–366 (2007)
9. Babu, S.G.L., Vasudevan, A.K., Sayida, M.K.: Use of coir fibers for improving the engineering properties of expansive soil. J. Natural Fibers **5**(1), 61–75 (2008)
10. Reddy, et al.: Evaluating the influence of additives on swelling characteristics of expansive soils. Int. J Geotech. Ground Eng. **1**(7), 1–13 (2015)
11. Chen, F.H.: Foundations on expansive soils. Elsevier Science, Amsterdam (1975). https://doi.org/10.1080/19386362.2017.1288355
12. Schaefer, V.R. et al.: Ground improvement, ground reinforcement and ground treatment. Geotech. Special Publ. No. 69, ASCE, New York (1997)
13. Malik, V., Priyadarshee, A: Studied compaction and swelling behavior of Black cotton soil mixed with different non-cementitious materials like fly ash and stone dust. Int. J. Geotech. Eng. (2017). ISSN–1938–6362
14. Tak, D., Sharma, J.K., Grover, K.S.: Use of Kota stone slurry powder to improve properties of black cotton soil. Indian Geotechnical Conference, Indian Institute of Science, Bengaluru (2018)

15. Shalendra, S., Vasaikar, H.B.: Stabilization of black cotton soil using lime. Int. J. Sci. Res. 2319–7064 (2013) ISSN Online
16. Parte, S.S., Yadav, R.K.: Effect of marble dust on index properties of black cotton soil. Int. J. Eng. Res. Sci. Technol. **3**(3), 158–163 (2014). ISSN 2319–5991
17. Anu, K., Gurung, D., Yadav, R., Lollen, L.: Stabilization of soft clay using fly ash and lime stone dust. Int. J. Sci. Eng. Res. 7(5), (2016). ISSN 2229–5518
18. Baba, S.K.V., Haripriya, S.: Analysis of black cotton soil treated with granite dust and lime. Int. J. Civil Eng. Technol. **8**(8), 1341–1350 (2017). ISSN Print 0976–6308
19. IS: 2720 (Part 3). Determination of specific gravity of black cotton soil, fly ash, KSSP and mixes of different percentage of fly ash & KSSP with the black cotton soil. Bureau of Indian Standards, New Delhi, India (1980)
20. IS: 2720 (Part 40), Determination of swell index of black cotton soil, fly ash, KSSP and mixes of different amount in percentage of dry mass of the soil of fly ash & KSSP with the soil. Bureau of Indian Standards, New Delhi, India (1977)
21. IS: 2720 (Part 5), Determination of liquid limits and plastic limits of black cotton soil, fly ash, KSSP and mixes of fly ash and KSSP with the soil at different proportions of dry mass of the soil. Bureau of Indian Standards, New Delhi, India (1985)

Effect of Ground Granulated Blast Furnace Slag and Fly Ash on Geotechnical Properties of Expansive Soil

Parmanand Meena, J. K. Sharma, and Biswajit Acharya

Abstract Expansive soil is the most predominant geological hazard. As they get wet, the clay minerals assimilate water molecules and expand, on the other hand, as they shrink, leaving large voids in the soil which is a significant hazards for further construction stabilization is found to be the most ideal way of reducing shrinkage and swelling nature of expansive soils. In modern days of industrialization, it is essential to utilize waste material from various industries to use for expansive soil to decrease the contaminating impact of waste material and to achieve beneficial outcomes. Likewise, use of Ground Granulated Blast Furnace Slag (GGBS) is served to be a good stabilizing agent for expansive soils and also being a by-product it fills in as an eco-friendly way of using the product without dumping it on ground. In the present study, local fly ash and GGBS are used as a mix to investigate the properties of expansive soil in various proportions. Various laboratory tests such as standard proctor test, unconfined compressive strength, California bearing ratio test are done to figure out the strength characteristics of compacted soil using GGBS and fly ash as well as tests like specific gravity to obtain the physical properties of soil.

Keywords Expansive soil · Ground granulated blast furnace slag (GGBS) · Fly ash · Unconfined compressive strength · California bearing ratio test

1 Introduction

In evolving nation like India, due to the remarkable improvement in infrastructure, soil stabilization has turned the serious issue into development activity. The strength

P. Meena (✉) · J. K. Sharma · B. Acharya
Department of Civil Engineering, Rajasthan Technical University, Kota, Rajasthan, India
e-mail: parmanandmeena72020@gmail.com

J. K. Sharma
e-mail: jksharma@rtu.ac.in

B. Acharya
e-mail: bacharya@rtu.ac.in

of the local soil is satisfactory for supporting the superstructure over it. Soil stabilization is an unavoidable practice which improves the durability or bearing capacity of the soil by the utilization of controlled compaction, addition of reasonable stabilizer or admixture, improve toughness which at last improves the performance. The industrial waste materials which are commonly toxic, ignitable, corrosive, or reactive pose serious health and environmental consequences. Their use has just been demonstrated as the promising solution for disposal issues and cuts the production cost.

2 Literature Review

Zha et al. [1] presented the study of behavior of the soil stabilization with fly ash. It was found that the free swell, swelling pressure, swelling potential, and linear shrinkage were decreased with the increase in the content of fly ash and lime-fly ash. This increment decreased Optimum Moisture Content and Maximum Dry Density. Negligible changes in the UCS value were observed. With increase in the content of fly ash without curing, shear strength was increased with the addition of lime. It was concluded that the optimum content of fly ash for treating soils with curing time of 7 days is 9–12%.

Sharma and Sivapullaiah [2] represented the experimental study on the improvement of strength of expansive soil with waste granulated blast furnace slag. It was observed that the Optimum Moisture Content and Maximum Dry Density were decreased with the addition of GGBS to the black cotton soil. The strength was observed when GGBS added up to 20% for the curing period of 7 days and 14 days up to 40% for the curing period 28 days. Further addition decreased the strength. When GGBS content was added up to 20% the initial tangent modulus was improved, further addition made a small change.

Yadu and Tripathi [3] presented the study on the effect on the properties of soft soil with GGBS and fly ash. It was observed from the study that the Optimum Moisture Content goes on increasing with the addition of definite percentage of fly ash and GGBS to the black cotton soil. CBR value was increased with the increase in the GGBS percentage. It was found that 3% fly ash and 6% GGBS give the best result with black cotton soil.

Oormila and Preethi [4] presented a study on using fly ash and GGBS for improving soil characteristics. Series of test have been conducted on black cotton soil mixed with fly ash (5, 10, 15, 20%) and GGBS (15, 20, 25%). The UCS test results were found to give optimum strength when added with 10% fly ash. The addition of 20% GGBS to black cotton soil gives optimum strength. The CBR test was performed with combination of 10% fly ash and 20% GGBS and with combination of 10% fly ash and varying percentage of GGBS (15, 20, 25%). It was found that the combination of 10% fly ash and 25% GGBS gives an increment of 78.29% in the CBR value when combined with the CBR value of virgin soil.

Dayalan [5] conducted a comparative study on stabilization of soil with GGBS and fly ash. It was observed from the study that the OMC keeps on decreasing while MDD keeps on increasing with the addition of GGBS and fly ash. It was observed that CBR value increases with increase in percentage of fly ash up to 15% and again decreasing likewise for GGBS up to 15%. The OMC is 14.8% found at 10% of fly ash and of 13.7% is found at 10% of GGBS. The overall study concluded that the optimum value is 15% and 20% for fly ash and GGBS, respectively.

Neeladharan et al. [6] presented a study on stabilization of soil using fly ash with Ground Granulated Blast Furnace as binder. It is observed that with the increase in the addition of fly ash and GGBS, Optimum Moisture Content decreases and Maximum Dry Density increases. The soil group changed from CH to ML when 15% fly ash and 10% GGBS were added in combination. At this percentage, the shear stress increases and decreases with further addition. The CBR value was found to be increased at this percentage. It is concluded that 15% fly ash and 10% GGBS by weight of soil gives the better results.

3 Methodology Materials Used

3.1 Methodology

This study deals with the details of the experimental work carried out using black cotton soil, Ground Granulated Blast Furnace Slag (GGBS), and Fly ash. Soil sample used for this experimental work was collected from Borkheda (devaliarab road) area, Kota, Rajasthan, India. GGBS was collected from Bajaj TMT Prem Jain Ispat Pvt. (RIICO, Ranpur), Kota, and Rajasthan. Fly ash used in this study was collected from Thermal Power Plant, Kota, and Rajasthan. The soil sample was collected at the depth of 1.5–2 m to avoid upper soil which may contain other waste and can affect the experimental results. It is very necessary to improve the geotechnical properties of expansive soils before using it for any constructional work due to their swelling and shrinkage characteristics. Hence an attempt is made in this study to improve the strength of raw soil by stabilizing it with different percentages of GGBS (4, 8, 12, 16, 20%) and fly ash (4, 8, 12%).

3.2 Materials Used

3.2.1 Black Cotton Soil

Soil sample was collected at the depth of 1.5 to 2 m from Borkheda, Kota, Rajasthan. The soil sample was air dried to remove natural water present in it, which may affect test results.

Table 1 Geotechnical properties of black cotton soil

S. No.	Properties	Values
1.	Specific Gravity(G)	2.46
2.	Consistency Limits Liquid Limit (%) Plastic Limit (%) Plasticity Index (%)	54.52% 34.70% 19.81%
3.	IS soil classification	CH
4.	Proctor Test MDD (g/cc) OMC	1.773 21.2%
5.	CBR Value (%)	1.29%
6.	UCS (KN/m^2)	1.039

The following laboratory tests are conducted on soil

- Atterberg Limit Test (As per IS 2720—Part 5: 1985).
- Specific Gravity Test (As per IS 2720—Part 3 (Sect. 1): [7].
- Differential Free Swell Test (As per IS: 2720—Part 40: [8]).
- Compaction Test (As IS 2720—Part 7: [9] and Part 16: [10]).
- California Bearing Ratio Test (As per IS 2720—Part 16: [10]).
- Unconfined Compression Test (As per IS 2720—Part 10: 1991).

Some geotechnical properties of raw black cotton soil, as obtained from these laboratory test conducted in soil mechanics laboratory are mentioned in Table 1.

3.2.2 Ground Granulated Blast Furnace Slag (GGBS)

The Ground Granulated Blast Furnace Slag is as a by-product during the manufacturing of iron in a blast furnace. Molten Blast furnace slag has a temperature range of 1300–1600 °C and cooled very rapidly to prevent the crystallization. The cementing property of GGBS is very useful to improve the strength of the black cotton soil when it is blended with the soil.

The general characteristics of GGBS are as following:-

- Composition:- CaO (30–50%), SiO$_2$ (28–38%), Al$_2$O$_3$ (8–24%), MgO (1–18%) and few percentage of Fe$_2$O$_3$, K$_2$O.
- The specific gravity is between 2.7 and 2.9.
- The particle size is from 75 µm to 2.5 mm.

3.2.3 Fly Ash

Fly ash is fine, glass powder recovered from the gases of burning coal during the producing of electricity. The fly ash is also known as "pulverized fuel ash." Fly ash

includes substantial amount of silicon dioxide (SiO_2), aluminum oxide (Al_2O_3), and calcium oxide (CaO).

General characteristics of fly ash as following:-

- Specific gravity −1.9–2.96
- Particle size–10–100 micron.
- Type of fly ash based on IS 3812-1981.

    Grade-1 ($SiO_2 + Al_2O_2 + Fe_2O_3$) > 70%
    Grade-2 ($SiO_2 + Al_2O_2 + Fe_2O_3$ > 50%

4 Result and Discussion

4.1 Standard Proctor Test

This test was conducted based on IS: 2720, Part VIII (1983), Bureau of Indian Standards, New Delhi, 1–9. The standard proctor test is conducted in soil laboratory to find out the maximum dry density (MDD) and optimum moisture content (OMC) of black cotton soil and GGBS mix specimen.

(01) **Standard proctor Test for Black cotton soil mixed with GGBS**

From Table 2, it is observed that the MDD of black cotton soil is increased up to 1.892 gm/cc at 16% with the addition of GGBS and after further addition, the MDD of soil is decreased while OMC of soil is increased. The MDD is found to be increased by 6.28%.

From Fig. 1, it is observed that 16% GGBS gives the best results.

(02) **Standard Proctor Test For Black Cotton Soil Mixed with GGBS and Fly ash**

From Table 3, it is observed that the MDD of black cotton soil is increased up to 1.933 gm/cc at 16% GGBS + 8% fly ash, further addition decreases the MDD. Whereas

Table 2 Test results obtained for the black cotton soil mixed with GGBS

Mix Specimen	OMC (%)	MDD (g/cc)
BC Soil	21.23	1.773
BC + 4% GGBS	19.23	1.785
BC + 8% GGBS	18.29	1.826
BC + 12% GGBS	17.26	1.856
BC + 16% GGBS	15.86	1.892
BC + 20% GGBS	16.4	1.873
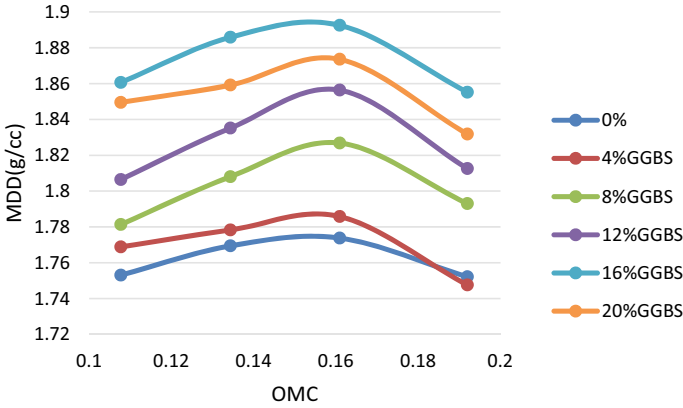
Fig. 1 Compaction characteristics of the black cotton soil and GGBS

Table 3 The results obtained for black cotton soil mixed with GGBS and fly ash

Mix specimen	OMC (%)	MDD (g/cc)
BC +16%GGBS +4%FA	17.05	1.90
BC + 16%GGBS + 8%FA	15.02	1.85
BC + 16% GGBS + 12%FA	16.09	1.89

the OMC of soil is observed to be increased, the MDD is found to be increased approximately by 9%.

From Fig. 2, we conclude that peak value observed at 16%GGBS +8% fly ash
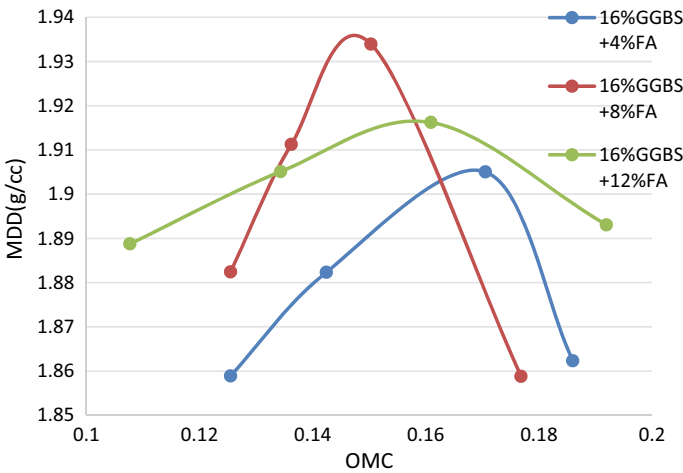
Fig. 2 Compaction characteristics of the black cotton mixed with GGBS and fly ash

4.2 California Bearing Ratio

This test was conducted based on IS: 2720, Part XVI (1987), Bureau of Indian Standards, New Delhi, 1–5. California Bearing Ratio Test is performed in soil laboratory to find out the CBR value of black cotton soil mixed with different percentage of GGBS and fly ash in soaked condition.

(01) **California Bearing Ratio Test for Black Cotton soil with GGBS**

From Table 4, it is observed that the CBR value of black cotton soil is 1.29% which is increased with the addition of GGBS up to 5.16% at 16% GGBS with black cotton soil, further addition of GGBS the CBR value of soil is decreased.

From Fig. 3, we see that on adding GGBS up 16% it gives optimum value, further increasing in percentage of GGBS CBR value found decreases.

(02) **California Bearing Ratio Test For black Cotton Soil with GGBS and Fly ash**

From Table 5, it is observed that when 16% GGBS + 8% fly ash is added with black cotton soil the CBR value of soil increased up to 376.74%,which is decreased on further adding 12% fly ash.

Table 4 CBR test results for black cotton soil mixed with GGBS and fly ash

Test specimen	CBR%	% Increase
BC Soil	1.29	–
BC + 4% GGBS	2.58	100
BC + 8% GBBS	3.42	165.11
BC + 12% GGBS	4.02	211.62
BC +16% GGBS	5.16	300
BC + 20%GGBS	4.93	282.17
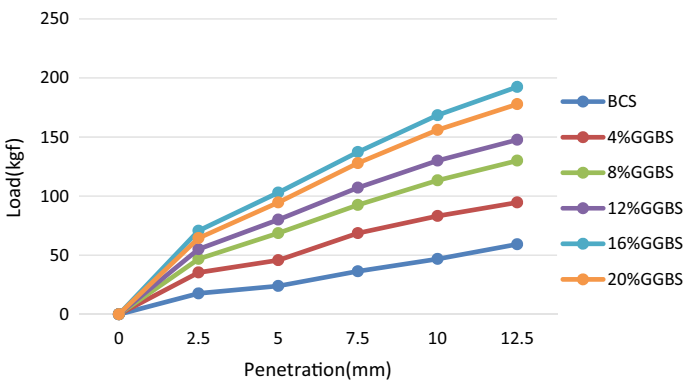
Fig. 3 CBR test results for black cotton soil mixed with various percentage of GGBS

Table 5 CBR test results for black cotton soil mixed with different percentage of GGBS and fly ash

Test specimen	CBR%	% Increase
BC + 16%GGBS + 4%FA	5.31	311.62
BC + 16%GGBS + 8%FA	6.15	376.74
BC + 16%GGBS + 12%FA	5.39	317.82
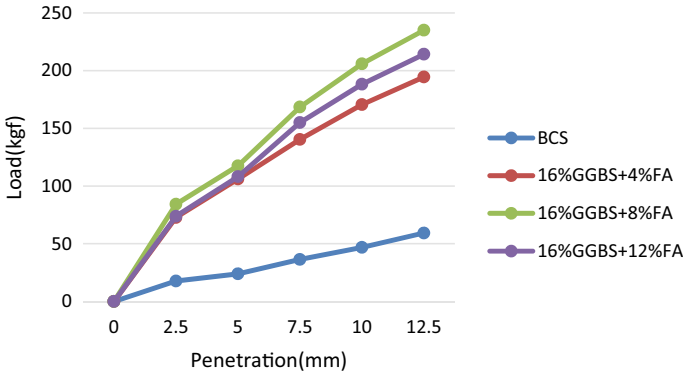
Fig. 4 CBR test results for black cotton soil mixed with GGBS and Fly ash

From Fig. 4, we observed that 16% GGBS with 8% fly ash gives the best results, peak value found on this combination.

4.3 Unconfined Compressive Strength Test

This test was conducted based on IS: 2720, Part X (1991), Bureau of Indian Standard, New Delhi, 1–4. To determine the unconfined compressive strength of black cotton soil by loading an axial cylindrical specimen in soil laboratory, Unconfined Compressive Strength test is conducted for 4 days in soaked condition. Variations of UCS results for black cotton soil with specimen are shown below:-

From Table 6, it is observed that the UCS value of black cotton soil is 1.045 kg/cm² which is increased up to 147.655% with addition of 16% GGBS. With further addition of GGBS, the UCS value of soil decreased.

From Fig. 5, it is observed that the UCS value with addition of 16% GGBS increases and with further addition of GGBS, the UCS value decreased.

From Table 7, it is observed that the UCS value of black cotton soil is 1.503 kg/cm² which is increased up to 187.751% with addition of 16% GGBS + 8% fly ash. With further addition of fly ash, the UCS value of soil decreased.

From Fig. 6, it is observed that combination of 16% GGBS with 8% fly ash gives the optimum value, peak value observed at this combination.

Table 6 UCS test results obtained for black cotton soil mixed with GGBS and Fly ash

Test specimen	Unconfined compressive strength (Kg/cm^2)	% Variation of compressive strength	Shear strength, C_u(Kg/cm^2)	% Variation of shear strength
BC Soil	1.045	0	0.5225	0
BC +4%GGBS	1.123	7.464	0.5615	7.464
BC + 8% GGBS	1.388	32.822	0.694	32.822
BC +12% GGBS	1.605	53.588	0.8025	53.588
BC +16% GGBS	2.588	147.655	1.294	147.655
BC +20% GGBS	2.433	132.822	1.2165	132.822
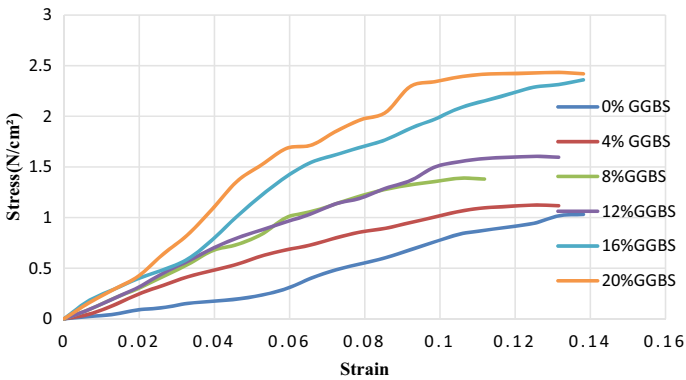
Fig. 5 UCS results obtained for black cotton soil with various percentage of GGBS

Table 7 UCS test result obtained for black cotton soil mixed with 16% GGBS and Fly ash

Test Specimen	Unconfined compressive strength, (Kg/cm^2)	% Variation of compressive strength	Shear strength, C_u(Kg/cm^2)	% Variation of shear strength
BC + 16% GGBS +4%FA	2.372	126.985	1.186	0.1513
BC + 16% GGBS +8%FA	3.007	187.751	1.5035	0.1184
23BC + 16% GGBS + 12%FA	2.855	173.205	1.427	0.1382
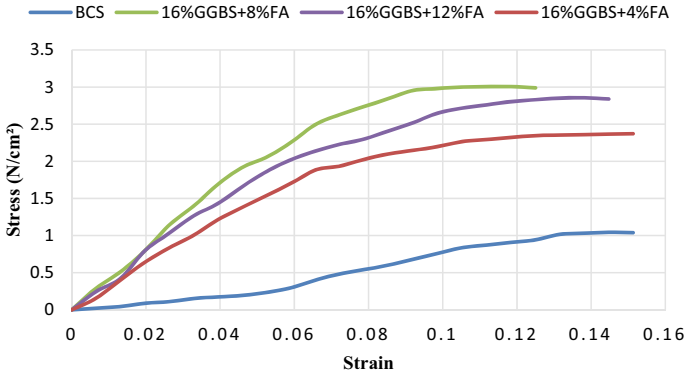
Fig. 6 UCS results for black cotton soil with GGBS and fly ash

5 Conclusion

(i)   It is concluded that on increase the percentage of GGBS and fly ash up to the definite percentage, optimum moisture content goes on decreasing while maximum dry density goes on increase.

(ii)   It is observed that the MDD of black cotton soil is increased up to 1.933 gm/cc at 16% GGBS and 8% fly ash.

(iii)   It is observed that the CBR value of black cotton soil is 6.15% on adding 16% GGBS and 8% fly ash, further addition of GGBS and fly ash decrease the CBR value.

(iv)   UCS value of black cotton soil is found 1.045 kg/cm^2, which is increased up to 187.75% with addition of 16% GGBS and 8% fly ash, so optimum value of UCS is found 2.855 kg/cm^2.

(v)   It is observed from the overall experimental work, that the 16% GGBS and 8% fly ash give the optimum results when mixed with black cotton soil.

References

1. Zha, F., Liu, S., Du, Y., Cui, K.: Behavior of expansive soil stabilized with fly ash. Nat. Hazards. **47**, 509–523 (2008) Published in© Springer Science + Business Media B.V. 2008. http://doi.org/10.1007/s11069-008-9236-4

2. Sharma, A.K., Sivapullaiah, P.V.: Improvement of Strength of Expansive soil with waste Granulated Blast Furnace Slag. Published in Geotechnical Special Publication-March, 2012. GeoCongress 2012 © ASCE (2012)

3. Yadu, L., Tripathi, R.K.: Stabilization of soft soil with granulated blast furnace slag and fly ash. Published Int. J. Res. Eng. Technol. **02**(02) (2013). ISSN: 2319–1163

4. Oormila,T.R., Preethi, T.V.: Effect of stabilization using fly ash and GGBS in soil characteristics. Presented in Int. J. Eng. Trends Technol. (IJETI). **11**(6), (2014)

5. Dayalan, J.: Comparative study on stabilization of soil with ground granulated blast furnace slag (GGBS) and fly ash. Published in Int. Res. J. Eng. Technol. (IRJET). **03**(05), (2016)
6. Neeladharan, C., Muralidharan, A., Mohan, K., Mohamed Sayeed, A., Arshad Azeez, V.I., Mohammed Faizan, V.S., Yasir Arafath, A.: Stabilization of soil using fly ash with ground granulated blast furnace slag (GGBS) as binder. Published in SurajPunj J. Multidisciplinary Res. **9**(4), (2019) ISSN NO: 2394–2886
7. Indian standard code: IS code 2720 (Part 3, 1980) Determination of specific gravity (1980)
8. Indian standard code: IS 2720 (Part 40, 1977) Determination of free swell index (1977)
9. Indian standard code: IS 2720 (Part 7, 1980) Determination content and dry density (1980)
10. Indian standard code: IS 2720 (Part 16, 1979) Determination of California bearing ratio (1979)

Effect of Crushing on Stress–Strain Behavior of Fly Ash Under Monotonic Compression and Repeated Loading–Unloading Conditions

Aparna Shrivastava, Ankit Ghanghas, and Ajanta Sachan

Abstract Use of fly ash in various geotechnical structures has increased instead of using conventional geomaterials. Million tons of fly ash is produced every year and its safe disposal is an issue as it creates health hazards if exposed to air directly. Fly ash is largely used as structural fill material in highway, railway embankments and as a backfill material in Geosynthetic reinforced structures. Fly ash is a by-product generated on coal combustion. It contains spherical, hollow particles (cenospheres), and particles filled with smaller particles (plerospheres). Due to presence of air voids in cenospheres, specific gravity of fly ash is obtained to be lower as compared to soil. Due to the hollow nature of fly ash particles, they undergo crushing and deformation when subjected to external loading. The present study evaluates the effect of crushing on stress–strain behavior under monotonic compression and repeated loading–unloading UU triaxial testing conditions. A successive cycles of standard proctor tests were performed on fly ash to induce different degrees of crushing. Specimens with different degrees of crushing (50 mm diameter and 100 mm height) were prepared at maximum dry density (MDD) of uncrushed fly ash. Stress-stain response under monotonic compression loading exhibited significant decrease in peak deviatoric stress with the increase in crushing of fly ash particles. There was significant reduction in accumulated axial strain with the increase in crushing under repeated loading–unloading conditions.

Keywords Fly ash · Cenospheres · Plerospheres · Crushing · UU triaxial

A. Shrivastava (✉) · A. Ghanghas · A. Sachan
Civil Engineering, Indian Institute of Technology, Gandhinagar, India
e-mail: aparna.shrivastava@iitgn.ac.in

A. Ghanghas
e-mail: ankit.ghanghas@iitgn.ac.in

A. Sachan
e-mail: ajanta@iitgn.ac.in

1 Introduction

Fly ash is a by-product generated by coal combustion from thermal power plant. Large amount of production of fly ash by coal combustion has raised the need for its safe disposal every year. Fly ash is health hazardous when exposed to air freely. It contains two types of particles: cenospheres and plerospheres. Cenospheres are the spherical particles which are hollow from inside and plerospheres are the particles filled with small spheres [1]. Fly ash particles are majorly spherical containing silicon, aluminum, and iron oxide [2]. Fly ash is largely used as a structural fill in highway and railway embankments. Also, fly ash is used as landfill covers and pavement subgrade material. Some of the researchers [2–4], and [5] studied the basic geotechnical properties of fly ash and its strength characteristics. Researchers [6] and [7] have studied the morphological characteristics of fly ash. Kim et al. [8] studied the suitability of fly ash and bottom ash mixtures in highway embankment as construction material. Fly ash particles being hollow in nature are highly susceptible to breakage and crushing on application of external loading. Researchers [9] and [10] studied the breakage of various soils due to external loading. Lade et al. [11] proposed particle breakage factor B_{10} based on effective particle size D_{10}. Hattamleh et al. [12] studied the effect of particle crushing on natural sand by performing direct shear test. Some of the researchers [13] and [1] reported that impact loading can crush the fly ash significantly. Gupta and Sachan [1] also reported that both microscopic and macroscopic (compactability, compressibility, and shear behavior) properties vary with the crushing of fly ash particles. Crushing of fly ash can significantly alter its shear strength parameters [1]. The current study mainly focuses on effect of particle crushing of fly ash on shear behavior under monotonic compression and repeated loading–unloading UU triaxial testing conditions.

2 Material Properties

Fly ash was collected from Gandhinagar thermal power plant and its basic geotechnical properties were determined by performing specific gravity, grain size analysis, and standard proctor test. Basic geotechnical properties of fly ash (uncrushed) are shown in Table 1. The specific gravity was found to be 2.11, which was obtained to

Table 1 Basic geotechnical properties of fly ash (uncrushed)

Properties	Values
Specific gravity	2.11
Sand	20.5%
Silt	79.5%
Optimum moisture content (OMC)	29%
Maximum dry density (MDD)	1.21 g/cc
Visual appearance	Grey
Nature	Non-plastic

be much lesser than soil due to presence of air voids in hollow cenospheres [2] of fly ash particles. The optimum moisture content (OMC) and maximum dry density (MDD) of Gandhinagar fly ash were obtained to be 29% and 1.21 g/cc, respectively. Grain size analysis showed 20.5% sand and 79.5% silt content. Fly ash particles were predominantly of silt size range and non-plastic in nature.

3 Experimental Program

In the present study, a series of UU (unconsolidated undrained) triaxial tests under monotonic compression and repeated loading–unloading conditions were performed at confining pressure of 100 kPa on fly ash specimens with different degrees of crushing. The tests were conducted at strain rate of 0.4%/min. In order to prepare samples with different degrees of crushing, fly ash was subjected to impact loading by conducting standard proctor tests as per the procedure mentioned in [14]. The uncrushed sample (S0) was obtained from Gandhinagar thermal power plant. Fly ash was compacted in three layers of equal mass by providing 25 blows using 2.6 kg hammer with a free fall height of 310 mm. In order to prepare S1, 13 such rounds were conducted on S0 thus imparting a total of 7702 kJ/m^3 energy in crushing. The sample was then oven dried for 24 h and was used to prepare S2. In order to prepare S2, S1 was subjected to above-mentioned energy. The same procedure was followed to prepare samples S3, S4, and S5. All the specimens were prepared at 1.21 g/cc of MDD (Maximum Dry Density) of uncrushed fly ash. Also, the saturation level was kept constant for testing of specimens with different degrees of crushing, i.e., 55%. The soils were compacted in equal layers and after compacting each layer of soil scratching with knife was done to ensure proper bonding between the layers. The specimens of 50 mm diameter and 100 mm height were prepared by moist tamping method using three-piece mold supported by collar at the top and base plate at the bottom. For repeated loading–unloading tests, the specimens were initially loaded at 0.4%/min till 40% of the peak deviatoric stress (obtained during monotonic compression tests) and then unloaded till 5% of the peak deviatoric stress. The test was continued upto 50 min to acquire 20% axial strain failure criteria. All the UU triaxial tests were performed as per IS 2720–11 [15], which gives c and ϕ parameters of material having inclined failure envelope UU tests were chosen to perform for analysis of the stress–strain response of fly ash under loading–unloading conditions to understand the degradation in stiffness response of fly ash. It was not dynamic loading rather it was monotonic compression strain-controlled loading–unloading condition at constant strain rate.

4 Results and Discussions

4.1 UU Triaxial Tests Under Monotonic Compression Conditions

The stress–strain of fly ash specimens with different degrees of crushing at confining pressure of 100 kPa under UU triaxial monotonic compression conditions is presented in Fig. 1. It was observed that the peak deviatoric stress decreased significantly with the crushing of fly ash from 968 kPa for S0 specimen to 425 kPa for S3 (Table 1). There was a significant decrease in peak deviatoric stress from S0 to S1 while it again increased for S2 and further decreased for S4. Specimen S5 exhibited similar response same as S1. Specimen S0 exhibited brittle behavior with well-defined post-peak softening response. However, the specimens S3, S4, and S5 indicated ductile behavior such that the deviatoric stress was more or less constant after achieving peak deviatoric stress. As per Gupta and Sachan [1], it was found that the particles in its uncrushed state were spherical in nature; either cenosphere or plerosphere. On application of impact loading, hollow cenospheres got crushed and crumbled. With the increase in crushing energy, the solid spheres (plerospheres) got ruptured and deformed. Such crushing of particles led the increased percentage of fines at higher crushing cycles. The fly ash specimens prepared at same dry density (1.21 g/cc) for specimens at higher crushing cycle will have more tendency to rearrange themselves during shearing, which resulted into ductile behavior of specimens at higher crushing
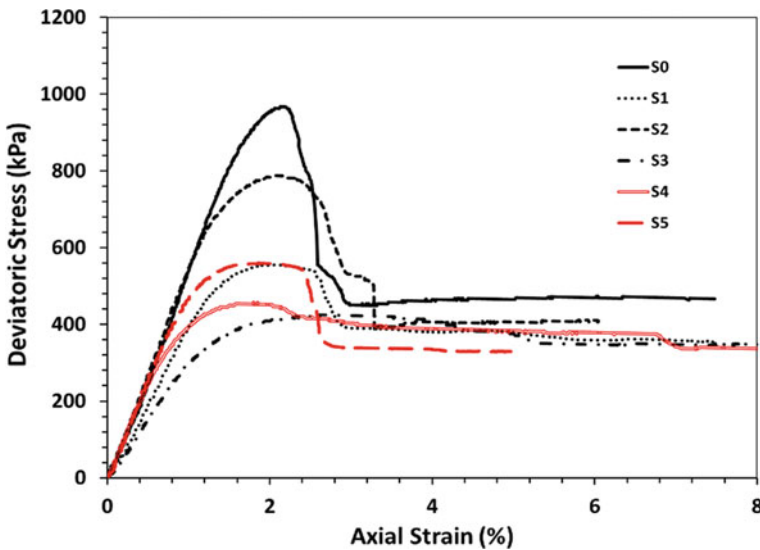
Fig. 1 Stress–strain response of fly ash specimens with different degrees of crushing under monotonic compression UU triaxial condition

cycles (S3-S5). At higher crushing cycles, the crushing of cenospheres and rupturing of plerosphere resulted into the increased percentage of fines leading to the greater void spaces. It caused reduction in peak deviatoric stress at higher crushing cycles.

4.2 UU Triaxial Tests Under Repeated Loading–Unloading Tests

The stress–strain behavior of fly ash specimens with different degrees of crushing at confining pressure of 100 kPa under repeated loading–unloading UU triaxial conditions is shown in Fig. 2. As per journal paper [16], three criteria were used to evaluate the effect of degrees of crushing of micaceous soil under repeated loading–unloading conditions: (1) total number of loading–unloading cycles completed in a particular time, (2) number of loading–unloading cycles completed in 2.5% axial strain, and (3) time required for completion of given loading–unloading cycle. Since none of the specimens could reach to even 2% axial strain, the specimens were compared based on the two criteria: total number of loading–unloading cycles completed in 50 min (N_t) and time required to complete 1st loading–unloading cycle (T_1).

It was observed that the total number of loading–unloading cycles completed reduced from S0 to S2 ($N_t = 135$ for S0 and 71 for S2) in the duration of 50 min. The number of loading–unloading cycles was then increased ($N_t = 97$ for S5) for S3 to S5 specimens (Table 2). Total accumulated strain for the uncrushed fly ash
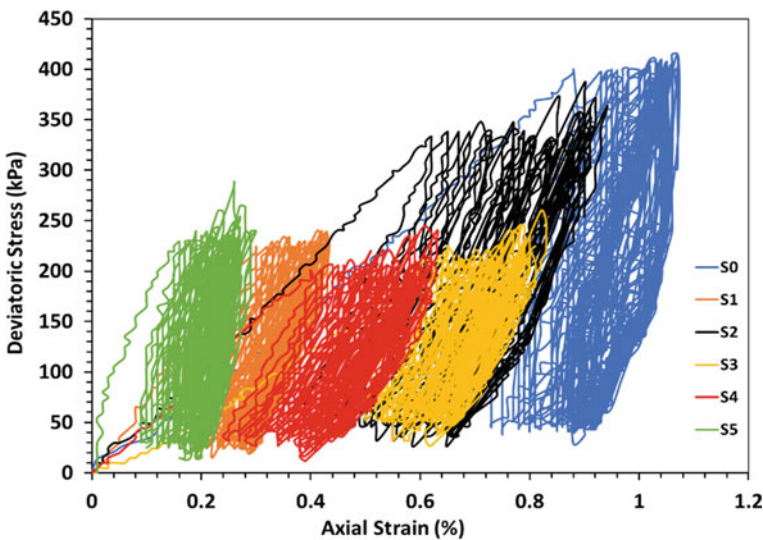

Fig. 2 Stress–strain response of fly ash specimens with different degrees of crushing under repeated loading–unloading UU triaxial condition

Table 2 Shear behavior of fly ash specimens with different degrees of crushing under UU triaxial condition

Specimens	Peak deviatoric stress (kPa)	Axial strain at failure (%)
S0	968	2.13
S1	556	2.01
S2	788	2.05
S3	425	2.56
S4	458	1.8
S5	560	1.85

specimen (S0) was obtained to be 1.1% and for specimen S5 to be 0.3% (Fig. 2). Looking into another criterion, it was found that time required to complete first loading–unloading cycle decreased with the crushing of fly ash.

As per previous literature [17], the behavior under repeated loading–unloading can be explained through dissipated energy concept (difference between the total strain energy stored during loading and the recovered elastic strain energy during unloading). According to [18], the dissipation of energy during any loading–unloading cycle was reported to be the cause of plastic strains that physically referred to the rearrangement of the particles and breakage of bonding and other part of energy stored as internal energy. For specimen S0, the accumulation of plastic strain would be more due to the rearrangement of cenospheres and plerospheres even at higher axial strain. The hollow air voids in the cenospheres would cause high probability of crushing during shear deformation itself leading to the rearrangement of the particles. This resulted into large shear deformation for the specimen S0 (1.1%) at given loading. Figure 2 also indicated that the recovery of strains decreased with the increase in crushing levels of fly ash. For specimen S0, the recovered elastic strain for the first loading–unloading cycle was obtained to be 0.15% and for highly crushed specimen S5 to be 0.07%. Lesser recovery of elastic strains would lead to the higher plastic strains for the crushed specimen S5 and resulted into higher dissipated energy. Greater plastic strains for the higher crushed specimens could occur with the greater rearrangement of the crushed cenospheres and ruptured plerospheres at higher crushing levels. (Table 3).

Table 3 Shear behavior of fly ash specimens with different degrees of crushing under UU triaxial repeated loading–unloading condition

Specimens	Number of loading–unloading cycles completed in 50 min (N_t)	Time to complete first loading–unloading cycle (seconds)
S0	135	157
S1	76	72
S2	71	129
S3	86	110
S4	91	89
S5	97	67

5 Conclusions

A series of UU triaxial tests under monotonic compression and repeated loading–unloading conditions were performed on fly ash specimens with varying degrees of crushing. The results are summarized as follows:

- The UU triaxial tests under monotonic compression conditions exhibited the significant reduction in peak deviatoric stress with the increase in crushing of fly ash particles. The uncrushed specimen S0 indicated brittle failure, whereas the higher crushed specimens indicated ductile failure.
- The UU triaxial tests under repeated loading–unloading conditions, total number of loading–unloading cycles completed in 50 min reduced with the particle crushing. Also, it was noted that time required to complete first loading–unloading cycle decreased with the crushing of fly ash.
- Total accumulated strain for the uncrushed fly ash specimen S0 was obtained to be 1.1% and for highly crushed specimen S5 to be 0.3%.
- For uncrushed specimen S0, the accumulation of plastic strain would be more due to the rearrangement of cenospheres and plerospheres. This resulted into the large shear deformation for the uncrushed specimen S0 (1.1%) at given loading.
- It was observed that the recovery of strains decreased with the increase in particle crushing of fly ash.

References

1. Gupta, K., Sachan, A.: Effect of crushing and strain rate on mechanical behavior of type-F fly ash. Transport. Infrastruct. Geotechnol. **5**(1), 4–23 (2018)
2. Martin, J.P., Collins, R.A., Browning, J.S., Biehl, F.J.: Properties and use of fly ashes for embankments. J. Energy Eng. **116**(2), 71–86 (1990)
3. Kim, B., Prezzi, M.: Evaluation of the mechanical properties of class-F fly ash. Waste Manage. **28**(3), 649–659 (2008)
4. Pandian, N.S.: Fly ash characterization with reference to geotechnical applications. J. Indian Inst. Sci. **84**(6), 189 (2013)
5. Jakka, R.S., Ramana, G.V., Datta, M.: Shear behaviour of loose and compacted pond ash. Geotech. Geol. Eng. **28**(6), 763–778 (2010)
6. Fisher, G.L., Prentice, B.A., Silberman, D., Ondov, J.M., Biermann, A.H., Ragaini, R.C., McFarland, A.R.: Physical and morphological studies of size-classified coal fly ash. Environ. Sci. Technol. **12**(4), 447–451 (1978)
7. Kutchko, B.G., Kim, A.G.: Fly ash characterization by SEM–EDS. Fuel **85**(17), 2537–2544 (2006)
8. Kim, B., Prezzi, M., Salgado, R.: Geotechnical properties of fly and bottom ash mixtures for use in highway embankments. J. Geotech. Geoenviron. Eng. **131**(7), 914–924 (2005)
9. Hardin, B.O.: Crushing of soil particles. J. Geotech. Eng. **111**(10), 1177–1192 (1985)
10. Hagerty, M.M., Hite, D.R., Ullrich, C.R., Hagerty, D.J.: One-dimensional high-pressure compression of granular media. J. Geotech. Eng. **119**(1), 1–18 (1993)
11. Lade, P.V., Yamamuro, J.A., Bopp, P.A.: Significance of particle crushing in granular materials. J. Geotech. Eng. **122**(4), 309–316 (1996)

12. Al Hattamleh, O.H., Al-Deeky, H.H., Akhtar, M.N.: The consequence of particle crushing in engineering properties of granular materials. Int. J. Geosci. **4**(07), 1055 (2013)
13. Choi, W., Son, Y., Park, J., Noh, S., Bong, T.: Changes in crushing and granularity characteristics of bottom ash as compaction energy. In: World of Coal Ash (WOCA) Conference, April, pp. 22–25. Lexington, (2013)
14. IS 2720-7: Methods of tests for soils, Determination of dry densty-water content relation using light compaction. Bureao of Indian Standards, New Delhi, India (1980)
15. IS 2720–11: Methods of tests for soils, Determination of the shear strength parameters of a specimen tested in unconsolidated undrained triaxial compression without the measurement of pore water pressure. Bureao of Indian Standards, New Delhi, India (1993)
16. Sachan, A., Seethalakshmi, P., Mishra, M.C.: Effect of crushing on stress–strain and pore pressure behavior of micaceous kutch soil under monotonic compression and repeated loading–unloading conditions. Geotech. Geolo. Eng. 1–15 (2020)
17. Polito, C., Green, R.A., Dillon, E., Sohn, C.: Effect of load shape on relationship between dissipated energy and residual excess pore pressure generation in cyclic triaxial tests. Can. Geotech. J. **50**(11), 1118–1128 (2013)
18. Voznesensky, E.A., Nordal, S.: Dynamic instability of clays: an energy approach. Soil Dyn. Earthquake Eng. **18**(2), 125–133 (1999)

Geotechnical Behaviour of Fly Ash-Bentonite Mixture as a Liner Material

Naman Kantesaria, Piyush Chandra, and Ajanta Sachan

Abstract The landfill liners are used to barrier the flow of leachate and hence prevent the migration of contaminants. Clay liners are increasingly used due to their low permeability and high attenuative capacity. The shrinkage of these liners during unsaturated state may cause cracking, and that lead to the leakage of leachate. Hence, it is needed to develop an alternative material having low shrinkage potential and low permeability. Treated fly ash is a good alternative and can be used as landfill liners. Fly ash is a by-product generated due to coal combustion and contains silt-sized hollow spherical particles. In the current study, an attempt has been made to reduce the permeability of fly ash by addition of bentonite and evaluate the suitability of this mixture as a liner material. Different percentages of bentonite (0, 2, 4, 6, 8, 10 and 12%) were mixed in the fly ash, and the geotechnical properties of this mixture were examined through various experiments such as liquid limit, unconfined compression and consolidation tests. The results of liquid limit tests indicated that water holding capacity of fly ash is increasing with the increase in bentonite content. The unconfined compressive strength and stiffness of the specimens were observed to be increased with the addition of bentonite till 8%, after that it started reducing. Swell pressure and permeability of these mixtures were determined through consolidation tests along with compressibility characteristics. Permeability was observed to reduce below $1*10^{-9}$ m/s with the increase in bentonite content in the fly ash indicating its suitability as a liner material.

Keywords Landfill liner · Fly ash · Bentonite · Permeability · Shear strength

N. Kantesaria (✉) · P. Chandra · A. Sachan
Civil Engineering, Indian Institute of Technology, Gandhinagar, India
e-mail: naman.kantesaria@iitgn.ac.in

P. Chandra
e-mail: piyush.chandra@iitgn.ac.in

A. Sachan
e-mail: ajanta@iitgn.ac.in

1 Introduction

The landfill liners are used to prevent the migration and leakage of leachate. They act as barrier and reduces the groundwater pollution through ingress of leachate. Mitigation of pollutant migration, low shrinkage and swelling, sufficient shear strength and resistance to erosion are the main requirements of any liner system [1]. Natural materials such as compacted clay, compacted shale, soil sealant and Bitumen materials are used as a liner material. Geomembranes are also used recently in a conjunction with natural materials in a liner system due to its less thickness and extremely low permeability. Out of above all mentioned materials, compacted clay liners (CCL) containing bentonite are widely used due to their low permeability, higher cost-effectiveness, higher resistance to damage and puncture, and higher sorption capacity. However, during unsaturated state, bentonite shrinks excessively and cracks are developed within soil mass, which increases the risk of leakage of leachate. Hence, it is required to develop an alternative material that has low shrinkage potential and low permeability. Bentonite mixed fly ash can be a good alternative material. Fly ash is a waste product of coal combustion generated from thermal power plant. The effective utilization and storage of fly ash itself is an issue. Both the above problem can be solved, if treated fly ash will be used as a liner material. Few previous researchers suggested to use fly ash in the construction of geotechnical and geoenvironmental applications [5, 16]. Edil et al. [6] examined the feasibility of fly ash-sand mixture as a liner material and found permeability values of mixture less than 10^{-9} m/s. Prashanth et al. [14] performed experiments on three different types of raw fly ash to access their suitability as a hydraulic barrier. They concluded that the pozzolanic fly ash developed low permeability with time and can be used as a hydraulic barrier. Cokca [4] and Phani Kumar and Sharma [13] investigated the effect of fly ash content on the basic geotechnical behaviour of expansive soil. They reported that the swelling pressure decreased and hydraulic conductivity increased with increase in fly ash content. Pal and Ghosh [12] performed falling head permeability tests on nine different fly ash with varying content of bentonite. They found reduction in permeability with decrease in degree of saturation and also proposed to use bentonite mixed fly ash as a liner material. Ravi Shankar and Niranjan [15] investigated the effect of compaction conditions on hydraulic and compressibility properties of fly ash-bentonite mixture. They found reduced hydraulic conductivity with decrease in compaction water content.

Very limited research has been done to investigate the applicability of fly ash in the construction of landfill as a liner material. Hence, the aim of the current study is to find the suitability of fly ash-bentonite mixture as an alternative material to conventional bentonite. Different percentages of bentonite (0, 2, 4, 6, 8, 10 and 12%) were added in the fly ash and a series of experiments such as liquid limit tests, unconfined compression tests, and consolidation tests were performed on these mixtures. The optimum bentonite content was evaluated based on the permeability, swell pressure and shear strength characteristics.

2 Material Properties

Fly ash used in the current research was obtained from Gandhinagar thermal power plant (Gujarat, India). Fly ash contains 80% silt-sized particles and 20% sand-sized particles having very low specific gravity (G_s) of 2.11. The other important geotechnical properties such as compaction parameters and Atterberg limits are presented in Table 1. Commercially available bentonite was used in the present study as an admixture and obtained from Pinal Corporation Ahmedabad (Gujarat, India). Bentonite is a high plasticity clay contains large amount of montmorillonite mineral. The specific gravity of bentonite was obtained to be 2.78 with all the particles had dimension less than 2 µm. The differential free swell index (DFSI) of bentonite was obtained as 662% and classified as highly expansive soil according to IS: 2911 Part III-1980 [11]. The Atterberg limits of bentonite are listed in Table 1. The scanning electron microscope (SEM) image of Gandhinagar fly ash and bentonite is shown in Fig. 1a

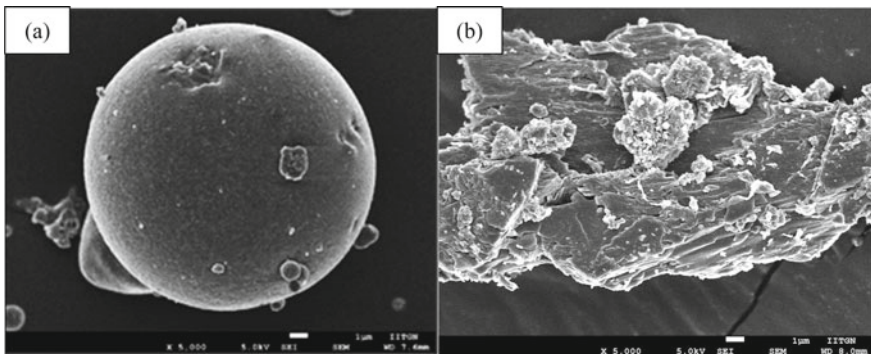| Table 1 Geotechnical properties of fly ash and bentonite	Soil	Fly ash	Bentonite
	Sand	20%	0%
	Silt	80%	0%
	Clay	0%	100%
	Specific gravity, G_s	2.11	2.78
	Liquid limit, w_L	50%	609%
	Shrinkage limit, w_S	–	6%
	Plasticity index, I_p	Non-plastic	558%
	Maximum dry density	1.21 g/cc	–
	Optimum moisture content	29%	–
	DFSI	–	662%

Fig. 1 Scanning electron microscope (SEM) image of **a** fly ash (Gupta and Sachan [7] **b** Bentonite

and b, respectively. Fly ash particles are spherical in shape whereas, the bentonite had layered structure of montmorillonite mineral, which contained sheets of silica tetrahedral and alumina octahedral.

3 Specimen Preparation and Experimental Program

Bentonite was mixed in the fly ash in a proportion of 0, 2, 4, 6, 8, 10 and 12% by weight to investigate the effect of bentonite content on geotechnical properties of fly ash. A small percentage of bentonite was selected, such that the adverse effect of excessive shrinkage and swelling do not overcome the benefits of its usage. The experimental program includes a series of liquid limit tests, unconfined compression (UC) tests and consolidation tests on all the specimens of raw fly ash and bentonite mixed fly ash. The oven-dried fly ash was mixed with specified percentage of oven-dried bentonite by weight to prepare the B-0 to B-12 specimens. The specimen name indicates the percentage of bentonite added. For example, B-12 indicates the 12% bentonite mixed fly ash specimen. The liquid limit tests were conducted using cone penetrometer method as per IS: 2720 (Part 5)-1985 [10]. All the specimens for UC test and consolidation test were prepared by moist tamping method at MDD (1.21 g/cc) and OMC (29%) of raw fly ash. The comparable compaction state was considered while preparing the specimens. The specimens of size 50 mm diameter and 100 mm height were prepared in four equal layers in three-piece metal mould for UC tests. The experiments were performed according to IS: 2720 (Part 10)-1991 [8] at a constant shearing strain rate of 1.25%/min. Three specimens of each bentonite content were tested to ensure repeatability of the results. The consolidation test was performed on the specimens of 20 mm height and 60 mm diameter prepared in three equal layers within the consolidation ring itself. The initial swelling of the specimens was allowed under the seating load of 5 kPa till the increase in the specimen height became constant. The specimen than loaded sequentially as 10, 20, 50, 100, 200, 400 and 800 kPa with an loading interval of 24 h. The unloading was done in the same sequence till 50 kPa normal stress. The procedure was followed according to guidelines of IS: 2720 (Part 15)-1986 [9]. The swell pressure and permeability were also determined through the results of consolidation test.

4 Result and Discussion

4.1 Variation in Liquid Limit Characteristics

Figure 2 shows the variation of liquid limit with bentonite content in fly ash. The liquid limit was found to increase from 50 to 74% with increase in bentonite content from 0 to 12%. The reason could be due to high water retention capacity of Bentonite
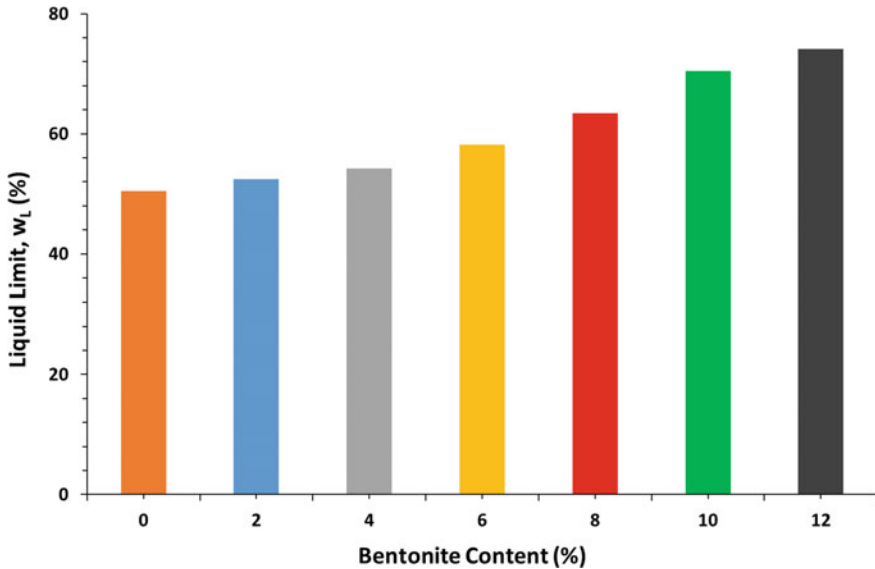
Fig. 2 Effect of bentonite content on liquid limit of fly ash-bentonite mixture

particles. Whenever, bentonite particles come in a contact with water, they formed diffused double-layer around them and that raised the their water holding capacity. Hence, addition of bentonite in the fly ash, induced plasticity in the non-plastic fly ash particles. The values of liquid limit for B-0 to B-12 specimens are presented in Table 2.

4.2 Variation in Shear Strength Characteristics

Figure 3 shows the results of UC tests in terms of axial stress-axial strain curves of B-0 to B-12 specimens. It is observed that unconfined compressive strength (q_u) increases with increase in Bentonite content till 8%. After that, it reduced with further addition of Bentonite up to 12%. The UCS increased from 325 kPa to 550 kPa with addition of Bentonite till 8%. In terms of percentage increase, the 84% strength increased with ingress of bentonite particles to fly ash. The initial stiffness of the specimens also improved till 8% Bentonite and then it reduced. The reason for that could be the pore filling phenomena, which happened with addition of very small-sized bentonite articles to larger fly ash particles. The small bentonite particles can go inside the void spaces created by the spherical fly ash particles and that will stiffen the whole soil matrix (Fig. 4a), which in turn enhances the strength and stiffness of mixture. After a particular percentage of Bentonite, with further addition can make the structure weakens as the Bentonite can now come in between the contact points of fly ash particles in addition to pore filling (Fig. 4b). These phenomena increased the

Table 2 Effect of bentonite content on liquid limit, unconfined compressive strength, consolidation behaviour, swell pressure and permeability

Property	Bentonite content (%)						
	0	2	4	6	8	10	12
Liquid limit, w_L (%)	50	52	54	58	63	70	74
Unconfined compressive strength, q_u (kPa)	325	358	413	446	591	578	550
Undrained cohesion, c_u (kPa)	162	179	206	223	296	289	275
Compression index, C_c	0.048	0.059	0.060	0.064	0.070	0.081	0.115
Swelling index, C_s	0.011	0.009	0.010	0.011	0.012	0.014	0.018
Swell pressure (kPa)	0	0	1	7	10	15	23
Permeability, k (m/s)	8.5×10^{-7}	8.9×10^{-9}	5.8×10^{-10}	3.5×10^{-10}	2.8×10^{-10}	2.7×10^{-10}	2.2×10^{-10}
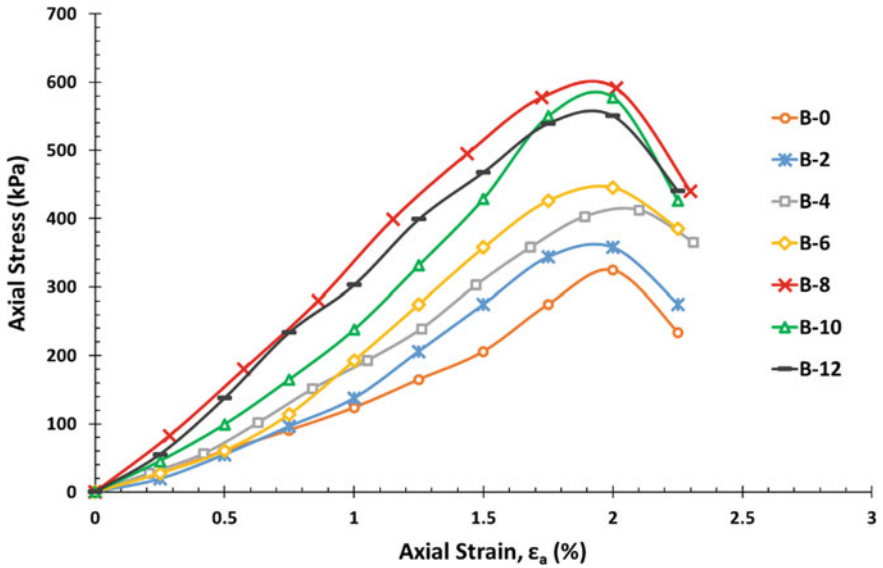
Fig. 3 Effect of bentonite content on unconfined compressive strength (q_u) of fly ash-bentonite mixture
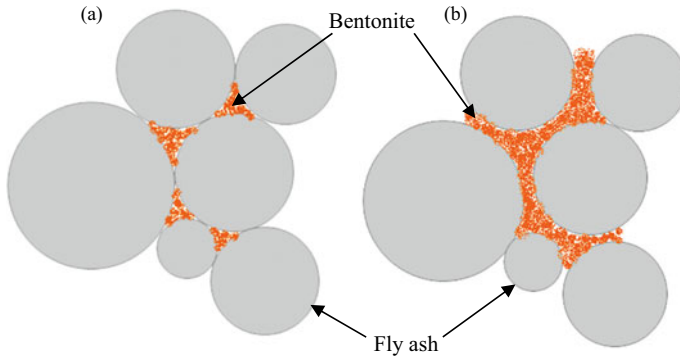
Fig. 4 Schematic diagram of possible mechanism: **a** Pore filling phenomena (bentonite content-2–8) **b** Lubrication phenomena (bentonite content >8%)

lubrication between fly ash particles and resulted in low value of shear strength. All the specimens showed sudden failure after achieving peak axial stress. The failure strain (ε_f) for most of the specimens was obtained around 2% axial strain. The variation in cohesion (c_u) value with bentonite content is shown in Fig. 5 and their values are presented in Table 2.
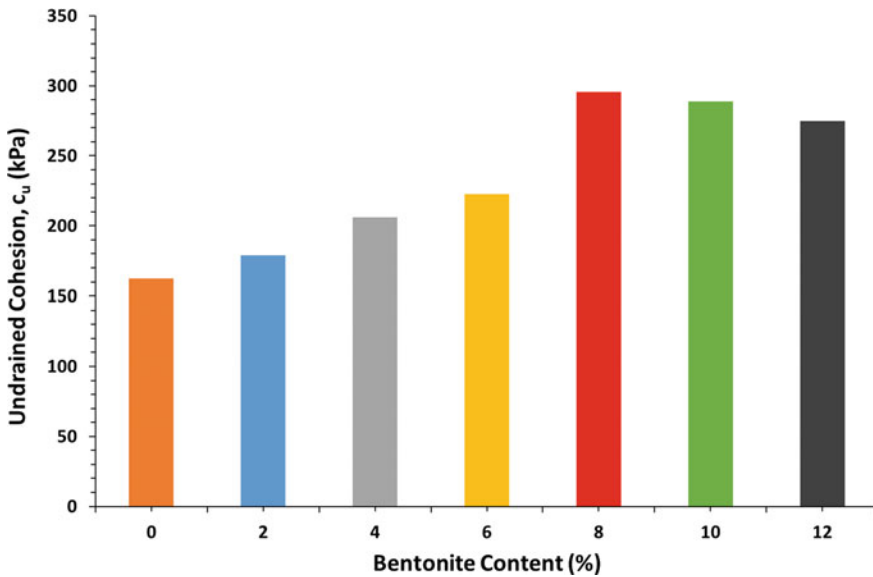
Fig. 5 Effect of bentonite content on cohesion (c_u) of fly ash-bentonite mixture
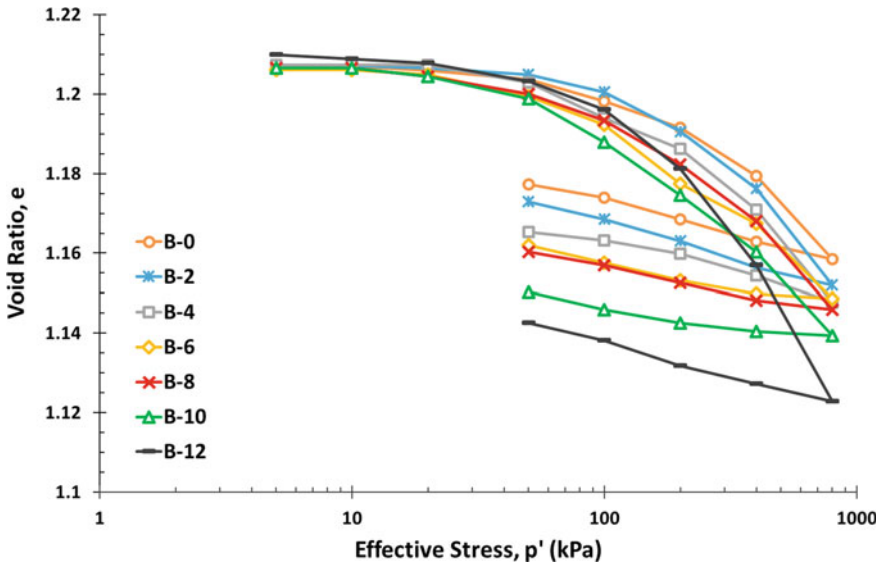
Fig. 6 Effect of bentonite content on consolidation behaviour of fly ash-bentonite mixture

4.3 Variation of Consolidation, Swell and Permeability Characteristics

Figure 6 shows the consolidation curves of B-0 to B-12 specimens plotted between void ratio (e) and effective stress (p') in semi-log scale. The results in terms of consolidation indices (C_c and C_s), swell pressure and permeability (k) are presented in Table 2. The compression index (C_c) and swelling index (C_s) of the specimens increased from 0.048 to 0.115 and 0.011 to 0.018 with increase in bentonite content from raw fly ash to 12% bentonite mixed fly ash, respectively. It indicates that addition of bentonite makes fly ash matrix more compressible due to possible lubrication effect of bentonite on rearrangement of fly ash particles with increased loading. The higher values of compression index made the clay liner more susceptible to differential settlement and damage. Hence, very high compression index (C_c) values are not recommended in the design of clay liners. Based on the determined values of C_c, the 4 to 8% bentonite content addition is recommended. The swell pressure was also determined through 1-D consolidation test for each bentonite mixed specimens and presented in Fig. 7. The maximum swell pressure of 23 kPa was obtained for highest bentonite content specimen (B-12). The 23 kPa swell pressure value was observed to be not very high and can be neglected as compared to huge swell pressure commonly observed for raw bentonite liners. The permeability of the B-0 to B-12 specimens was determined indirectly by taking average of permeability calculated for each loading increment from 200 to 800 kPa. The permeability (k) was found to decrease drastically from $8.5*10^{-7}$ m/s to $5.8*10^{-10}$ m/s from little variation in
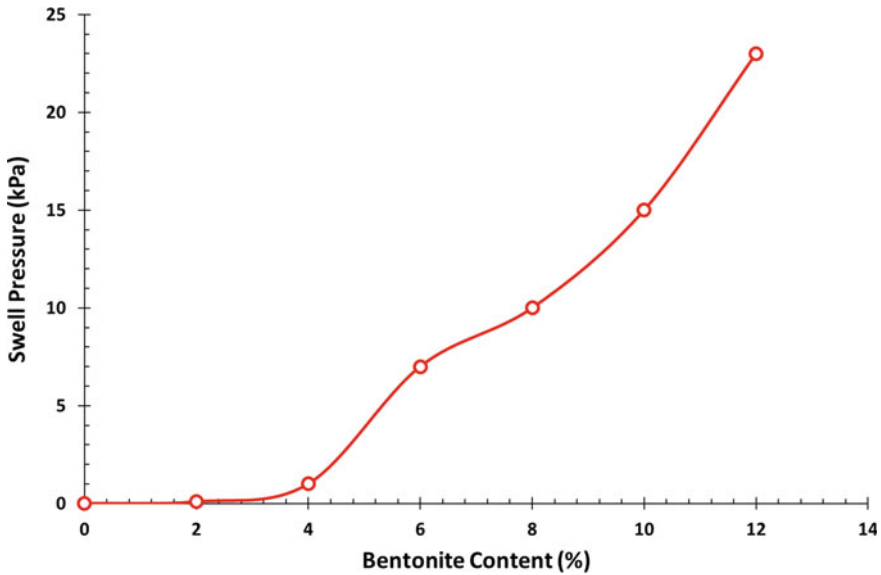
Fig. 7 Effect of bentonite content on swell pressure behaviour of fly ash-bentonite mixture

bentonite content from 0 to 4%. After that, very small reduction in the permeability (k) value was found till 12% bentonite content. Least permeability of $2.2*10^{-10}$ m/s was obtained for B-12 specimen. The permeability variation with bentonite content on semi-log scale is given in Fig. 8. Fly ash should have low permeability to act as a hydraulic barrier. Raw fly ash specimens had very high permeability in the order of 10^{-7} m/s and can not be used directly as a hydraulic barrier in its raw form. But, with addition of only 4% bentonite, fly ash permeability reduced less than 10^{-9} m/s, which is acceptable range for the permeability of hydraulic barrier or clay liner according to the minimum specifications given by Central Pollution Control Board (CPCB), Government of India (HAZWAMS/17/ 2000-01 [3]) and US Environmental Protection Agency (EPA/600/R-02/099) [2, 13].

5 Conclusions

The major conclusions derived from the current study can be summarized as follows:

- The water holding capacity and compressibility of fly ash increased with addition of bentonite content from 0 to 12%.
- The unconfined compressive strength (q_u) and stiffness of fly ash increased till addition of 8% bentonite content and thereafter it decreased with further Bentonite addition. The formation of strong matrix due to pore filling phenomena is responsible for the strength enhancement.
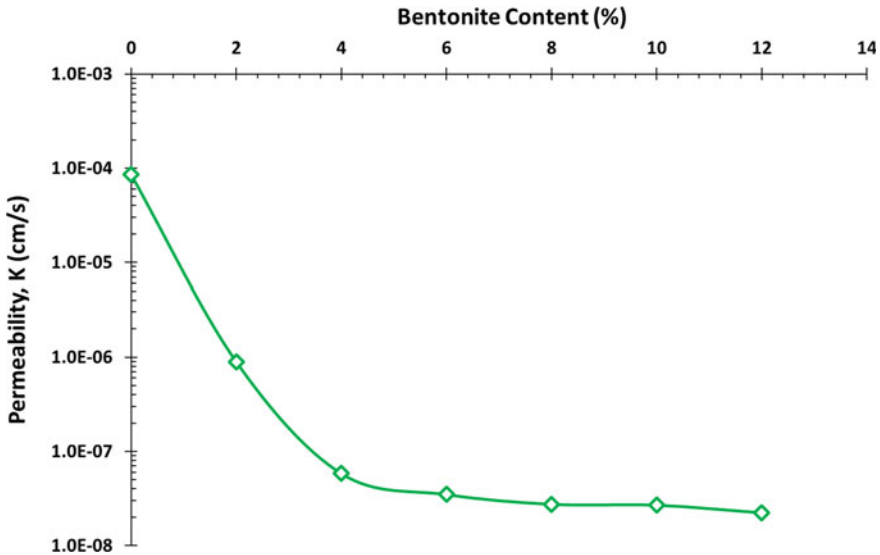
Fig. 8 Effect of bentonite content on permeability (k) of fly ash-bentonite mixture

- The order of permeability of the fly ash reduced from 10^{-7} to 10^{-10} m/s with addition of even small amount of bentonite (4%). The negligible swell pressure of 23 kPa was generated at highest Bentonite content of 12%.
- The optimum content of 8% bentonite was suggested as a admixture in the fly ash to make the mixture suitable for landfill liner with all the consideration of shear strength, compressibility, swell pressure and permeability.

References

1. Brandl, H.: Mineral liners for hazardous waste containment. Geotechnique **42**(1), 57–65 (1992)
2. Bonaparte, R., Daniel, D., Koerner, R.M.: Assessment and Recommendations For Improving the Performance of Waste Containment Systems. US Environmental Protection Agency, Washington, DC EPA Report EPA (2002)
3. Central pollution control board: Criteria For Hazardous Waste Landfills, Hazardous Waste Management Series, HAZWAMS/17/2000-01. Ministry of environments and forests, New Delhi, India (2001)
4. Cokca, E.: Use of class c fly ashes for the stabilizationof an expansive soil. J. Geotech. Geoenviron. Eng. **127**(7), 568–573 (2001)
5. Edil, T.B., Berthouex, P.M., Vesperman, K.D.: Fly ash as a potential waste liner. In: Geotechnical Practice for Waste Disposal'87, pp. 447–461. ASCE (1987)
6. Edil, T.B., Sandstrom, L.K., Berthouex, P.M.: Interaction of inorganic leachate with compacted pozzolanic fly ash. J. Geotech. Eng. **118**(9), 1410–1430 (1992)
7. Gupta, K., Sachan, A.: Effect of crushing and strain rate on mechanical behavior of type-F fly ash. Transport. Infrastruct. Geotechnol. **5**(1), 4–23 (2018)

8. IS: 2720-10: Methods of test for soils, Part 10: Determination of unconfined compressive strength, Bureau of Indian Standards, New Delhi (1991)
9. IS: 2720-15: Methods of test for soils, Part XV: Determination of Consolidation Properties, Bureau of Indian Standards, New Delhi (1986)
10. IS: 2720-5: Methods of test for soils, Part 5: Determination of liquid and plastic limit, Bureau of Indian Standards, New Delhi (1985)
11. IS: 2911 Part-III: Indian Standard Code of Practice for design and construction of pile foundations, Bureau of Indian Standards, New Delhi (1980)
12. Pal, S.K., Ghosh, A.: Hydraulic conductivity of fly ash–montmorillonite clay mixtures. Indian Geotech. J. **43**(1), 47–61 (2013)
13. Phani Kumar, B.R., Sharma, R.S.: Effect of fly ash on engineering properties of expansive soils. J. Geotech. Geoenviron. Eng. **130**(7), 764–767 (2004)
14. Prashanth, J.P., Sivapullaiah, P.V., Sridharan, A.: Pozzolanic fly ash as a hydraulic barrier in land fills. Eng. Geol. **60**(1–4), 245–252 (2001)
15. Ravi Shankar V.S., Niranjan D.V.: Effect of compaction conditions on the hydraulic and compressibility behaviour of fly ash—bentonite mixtures. J. Mech. Civil Eng. **12**(4) Ver. VII 01–28 (2015)
16. Sharma, R.S.: Geoenvironmental aspects of fly ash utilization and disposal. In; Ash Ponds and Ash Disposal Systems, pp. 347–357 (1996)

Impact of Municipal Solid Waste Landfill on Surrounding Environment: A Case Study

Antara Banerjee

Abstract Municipal solid waste in India is largely managed by disposal in landfill site due to its favorable economics. In this paper, the impact of municipal solid waste management and its disposal at Ghazipur landfill site which is approximately 72 acres is presented. The site on an average receives about 2000 tonne per day of MSW from North and South Shahdara, Delhi. The Ghazipur site is already matured and receives MSW over its full capability. The impact of Ghazipur landfill site on the surrounding environment was studied, and analysis of noise, air, soil, and groundwater pollution was conducted including a socio-economic impact survey. A comparative analysis of the above factors was done with the Boragaon waste dumping site in Guwahati. It was observed that the impact of this MSW on these sites to be negative on the surrounding environment which influences the nearby area greater than 10 km in diameter. Both the sites adversely affect the residents of the surrounding area and in near future with the increase of quantity of MSW, it would further result to a serious environmental hazard.

Keywords Municipal solid waste · Landfill · Pollution

1 Introduction

Solid waste includes all the discarded solid materials from commercial, municipal, industrial, and agricultural activities. According to UNEP data, the rate of waste generation generally increases in direct proportion to that of a nation's development [1]. In Delhi, the present MSW generation is nearly 8000 tonnes per day and is increasing by 3–4% per annum which is likely to increase to 18,000 tonne per day by the year 2021. Landfilling is the preferred method of municipal solid waste (MSW) disposal due to its favorable economics [2] According to various studies, researchers concluded that poorly designed landfills can create contamination of groundwater, soil, and air [3–5]. The most frequently reported hazard to the human health from

A. Banerjee (✉)
Department of Civil Engineering, The Assam Royal Global University, Ghy-35, Guwahati, Assam, India
e-mail: antarabanerjee22@gmail.com

these landfills is from the use of groundwater that has been polluted by leachate [6]. As water percolates through the landfill, contaminants are leached from the solid waste. Leachate is produced when moisture enters to refuse in a landfill, extracts contaminants into the liquid phase, and produces moisture content sufficiently high to initiate liquid flow. Leachate may contain dissolved or suspended material associated with wastes disposed of in the landfill, as well as many by-products of chemical and biological reactions [7]. Strength of leachate from MSW landfills varies with the progress of biological activity occurring in landfill. The study was carried on the Ghazipur landfill site that is nearly 72 acres. The site receives MSW from North and South Sahadara. The landfill site on an average receives about 2000 TPD of MSW. The Ghazipur site is accessible from National Highway-24 via Kondli road running parallel to Ghazipur drain. It is already matured and remains receiving MSW over its full capability. The effect of the existing landfill on the surrounding environment was studied which included the various environment attributes. The effects of landfill on the surrounding air, noise, soil, and groundwater environment were analyzed. Further the survey was conducted to study the impacts of landfill on the people residing in the nearby area. A comparative analysis of the above factors was done with the West Boragaon waste dumping site in Guwahati where dumping of garbage is nearly 500 metric tonne per day. The dumpsite is the only waste disposal ground of Guwahati city. The site is within the Brahmaputra flood plain having area of about 108 bigha which is located at a distance of about 15 km from the city and 2 km from NH-37.

2   Methodology Adopted

The impact of Ghazipur landfill site and Boragaon dumping site on the surrounding environment includes noise pollution, soil pollution, water pollution, air pollution, and socio-economic impact. The following methodologies were adopted for the study, viz (Figs. 1 and 2).

Fig. 1   Ghazipur landfill site

Fig. 2 Boragaon dumping site

2.1 Noise Pollution

An area of 5 acre was taken and analyzed for noise at three locations in and around Ghazipur. There were nine stations taken at each three locations, i.e., at Ghazipur, main road and apartments near Ghazipur landfill site. The noise monitoring was conducted during the peak hours as per National Monitoring system. The noise levels at Boragaon, Guwahati were checked mainly in the following stations: Basistha Chariali, N.H-37, Lokhra Chariali, N.H-37, Pachim Boragaon Chowk, N.H-37. The methodology adopted has been taken from IS Code 4954 (1968) and the manual provided by Central Pollution Control Board (Ministry of Environment and Forests, Govt. of India) which provides the guidelines for Noise Pollution Regulations in India [8].

2.2 Groundwater Pollution

Water sampling was done to determine the existing quality of water around both site areas of Ghazipur and Boragaon so as to assess the impact of municipal solid waste on the environment. After collecting samples from tube wells located near the sites sampling and testing were done following standard guidelines for physical and chemical parameters [9].

2.3 Air Pollution

For duration of 10 days, air monitoring was done on 4-hour basis for PM10, PM2.5, NO, NO2 and on 1-hour basis for CO. The methodology adopted has been taken from

the manual provided by Central Pollution Control Board (Ministry of Environment and Forests, Govt. of India) which provides the guidelines for the measurement of Ambient Air Pollutants [10].

2.4   Soil Pollution

An area around Ghazipur landfill and Boragaon dumping site was taken. The chemical properties of the soil sample collected at a depth of 0–50 cm were then analyzed as per standard procedure [11] and using IS 2720.

2.5   Socio-Economic Impact

A survey was conducted in the form of questionnaire to the residents in order to understand the impact on their day-to-day life. The sample size of 250 persons was taken for both the surveys conducted each at Ghazipur and Boragaon sites.

3   Test Results

3.1   Noise Monitoring

The comparison of results for the noise monitoring in and around Ghazipur is shown in Fig. 3.

As per Noise Pollution Regulations in India by Central Pollution Control Board (Ministry of Environment and Forests; Govt. of India), the permissible noise level in India for industrial areas is 75 dB for daytime and 70 dB at night, for commercial areas is 65 dB for daytime and 55 dB at night and for residential areas it is 55 dB for daytime and 45 dB at night. The noise monitoring results conducted in daytime for a month in both the respective site are listed in Fig. 3 (for Ghazipur landfill) and Table 1 (for Boragaon dumping site). So from the above-obtained values in Fig. 3 and Table 1, it can be observed that the noise levels have crossed the permissible limits as laid by CPCB in all the selected areas that was monitored both in Ghazipur landfill and Boragaon dumping site.
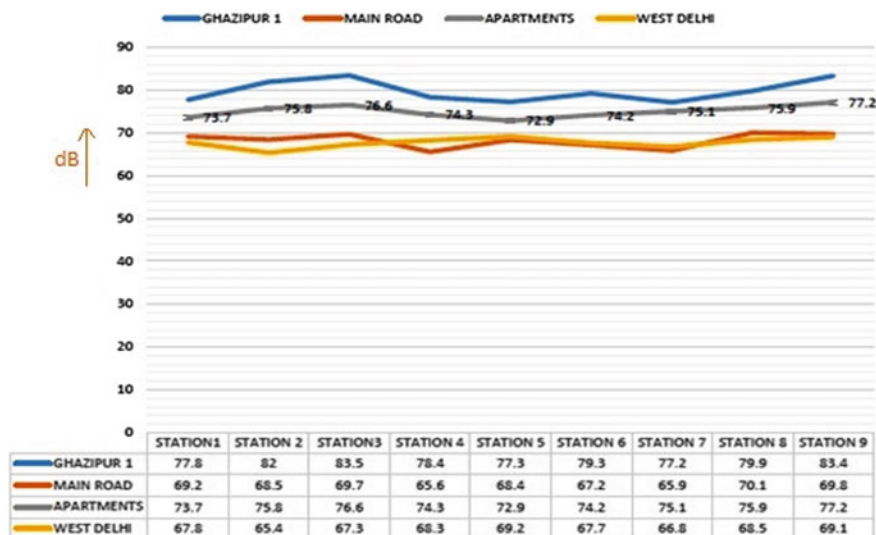
Fig. 3 Comparison of sound level in and around the Ghazipur landfill site

	STATION1	STATION 2	STATION3	STATION 4	STATION 5	STATION 6	STATION 7	STATION 8	STATION 9
GHAZIPUR 1	77.8	82	83.5	78.4	77.3	79.3	77.2	79.9	83.4
MAIN ROAD	69.2	68.5	69.7	65.6	68.4	67.2	65.9	70.1	69.8
APARTMENTS	73.7	75.8	76.6	74.3	72.9	74.2	75.1	75.9	77.2
WEST DELHI	67.8	65.4	67.3	68.3	69.2	67.7	66.8	68.5	69.1

Table 1 Report of noise-level monitoring carried out Near Boragaon Area in Leq dB(A)

Location	Date 6/04/19	Date 11/04/19	Date 18/04/19	Date 30/04/19
Basistha Chariali, N.H-37	78.6	75.6	77.4	78.3
Lokhra Chariali, N.H-.37	72.7	78.9	74.4	78.1
Pachim Boragaon Chowk, N.H-37	73.9	73.6	76.3	79.3

(All the data are collected during day time—hourly basis at each location between 9:00 AM and 5:00 PM)

Table 2 Comparison of result of different parameters range with Bureau of Indian Standards

Parameter	Unit	Results from Ghazipur landfill site	Results from Boragaon site	BIS Standards
pH	–	7.5–7.8	6.7–8.2	6.5–8.5
Conductivity	mS/cm	220–274	54.8–76.5	–
TDS	mg/l	771–1440	35–49	500
Total Hardness	mg/l	256–306	140–160	300
Alkalinity	mg/l	215–270	160–200	200
Chloride	mg/l	183–243	10–34	250
Residual Chlorine	mg/l	0.26	NIL	0.2

3.2 Result of Groundwater Quality

The results obtained above in Table 2, when compared with BIS standard permissible limits gives an idea about the water pollution in both the sites respectively. Except pH and chloride, all other parameters have shown values more than the BIS permissible limit at Ghazipur landfill site whereas parameters are still within BIS permissible range in case of Boragaon dumping site.

3.3 Result of Air Quality Parameters

The results obtained for air quality parameters have been listed above in Figs. 4, 5, 6, 7, 8 and Table 3. It can be observed from Figs. 4 and 5 that the PM_{10} and $PM_{2.5}$ values for Ghazipur landfill site have crossed the permissible limit as mentioned by NAAQ standards whereas NO, NO_2, and CO values as shown in Figs. 6, 7, and 8 are still within the limit, i.e., less than NAAQ standards. Again in Boragaon dumping site as shown in Table 3, it is observed that in some occasions the PM_{10} value exceeds the NAAQ standards but NO_2 is still within the permissible limit of NAAQ standards.
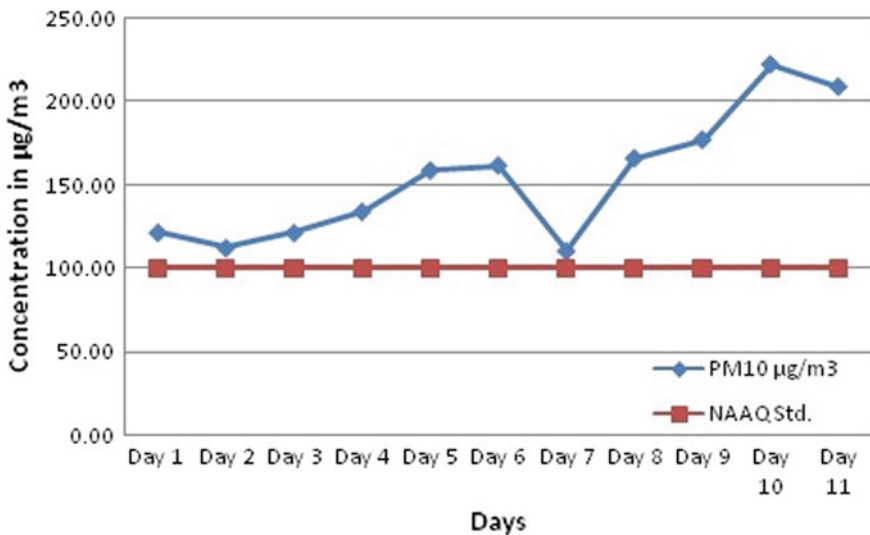
Fig. 4 Comparison of PM 10 with NAAQ Std. at Ghazipur landfill site
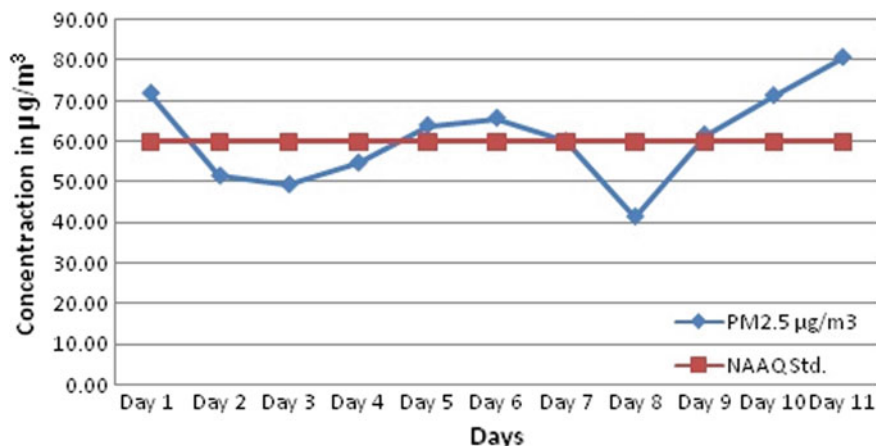
Fig. 5 Comparison of PM 2.5 with NAAQ Std. at Ghazipur landfill site
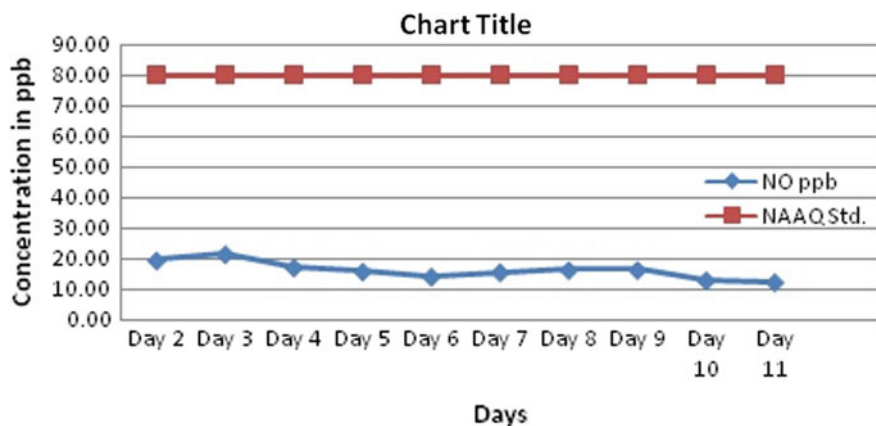
Fig. 6 Comparison of NO with NAAQ Std. at Ghazipur landfill site

3.4 Result for Soil Properties

From the result obtained for determination of the soil properties in Ghazipur landfill site, as listed in Table 4, it was found that the soil is acidic. Most plant nutrients, particularly calcium, potassium, magnesium were fluctuating from normal ranges whereas other parameters have also shown negative impacts. Thus, the soil is not only creating foul smell but also affecting water quality. The soil is unfit for any agricultural or irrigation works and due to the contamination it is posing health hazard to the residents nearby.
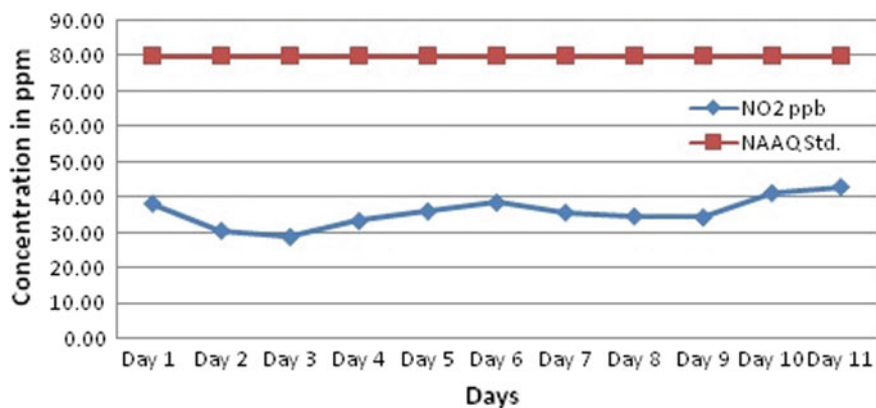
Fig. 7 Comparison of NO₂ with NAAQ Std. at Ghazipur landfill site
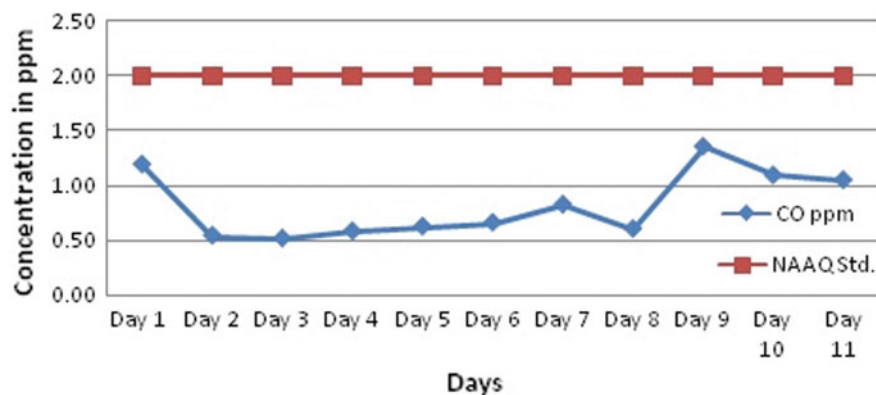
Fig. 8 Comparison of CO with NAAQ Std. at Ghazipur landfill site

Table 3 Ambient Air Quality Data of NO₂ and PM₁₀ of Boragaon dumping site for the month of April, 2019

Sampling date	General weather	N02 ($\mu g/m^3$)	PM10 ($\mu g/m^3$)
01-04-19	Cloudy/Rainy	17	99
03-04-19	Clear	20	88
05-04-19	Cloudy/Clear	17	71
08-04-19	Cloudy/Rainy	18	64
10-04-19	Clear	17	68
12-04-19	Clear	21	112
17-04-19	Clear	17	87
22-04-19	Clear	17	90
24-04-19	Clear	18	177
26-04-19	Clear	19	153
29-04-19	Cloudy	18	57

Table 4 Properties of soil

Point	1	2	2	3	3	4
Position Long	SE 147.4546	SW 147.4522	SW 147.4522	NW 147.453162	NW 147.453162	NE 147.456602
Lat	284.1598	274.1	274.1568	274.1537	274.1537	274.153
Depth (cm)	0–20	0–20	0–20	20–50	20–50	20–50
pH(1:5 Water)	4.9	3.9	4.5	4.7	4.3	4.8
%C	1	1.1	0.5	1.2	0.3	1
NO3(mg/kg)	6	4.3	1.2	9.8	3.1	13.6
SO4(mg/kg)	5	3	3	3	2	3
P(mg/kg)	27	20	6	19	9	30
K(mg/kg)	1.3	1.34	0.78	1.19	0.81	1.28
Ca(meq/100 g)	2.62	3.63	4.87	2.77	1.86	3.27
Mg(meq/100 g)	0.34	0.43	0.7	0.4	0.43	0.42
Al(meq/100 g)	0.1	0.07	0	0.16	0.78	0.07
Na(meq/100 g)	0	0	0.02	0	0.03	0
Cl mg/kg	10	10	5	5	10	10
EC ds/m	0.04	0.03	0.05	0.04	0.02	0.04
AmmN(mg/kg)	8	3	0	3	0	11
CEC (meq/100 g)	4.37	5.48	6.36	4.53	3.9	5.04
Ca/Mg ratio	7.68	8.35	6.96	6.95	6.95	4.37
Al Sat.%	2.3	1.2	0	3.4	3.4	19.9
ESP %	0	0.18	0.24	0.22	0.22	0.79

3.5 Result of Survey Conducted

See Figs. 9, 10, 11, 12, 13, 14.

Fig. 9 How often do you fall ill?
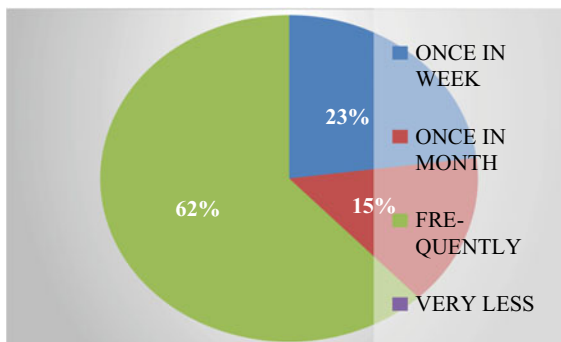
Fig. 10 What health problems do you face?
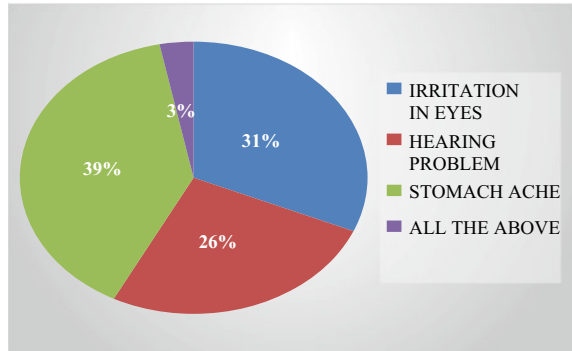
Fig. 11 How often do you find unbearable foul smell here?
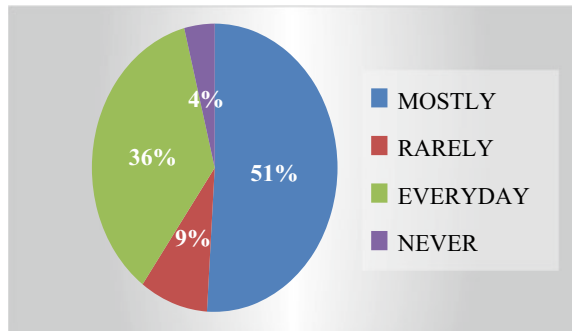
Fig. 12 How often your electric appliance stop working?
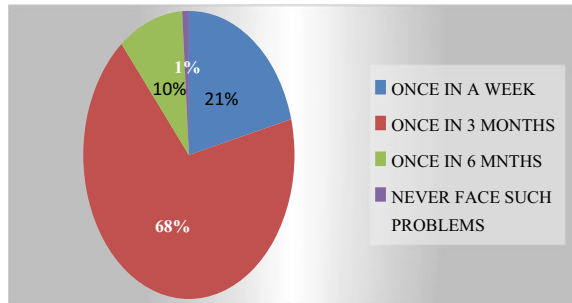
4 Conclusions

From the above observations of Ghazipur landfill site and Boragaon dumping site, the following conclusions can be made. The results of noise monitoring in and around both the sites show that the values are exceeding the Noise Pollution Regulations as framed by Government of India. Also the air monitoring for PM10 and PM2.5 shows that the results are again exceeding the NAAQ standards in both the sites, respectively. The value of total hardness, alkalinity and residual chlorine was found
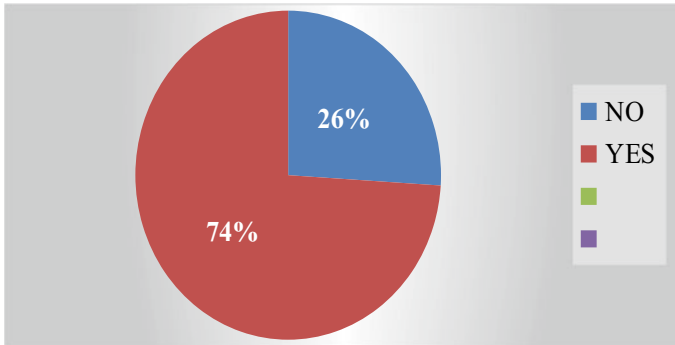
Fig. 13 Do you feel traffic problems here?
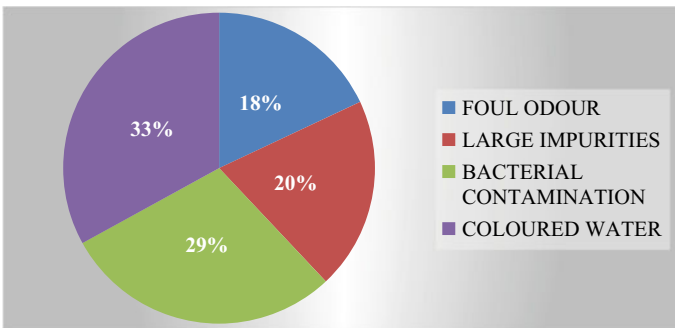
Fig. 14 What issues you face in the water?

to just exceed limits of BIS whereas TDS values were in much higher range than the acceptable limits given by BIS in case of Ghazipur landfill site. Further from the results of the soil properties in Ghazipur landfill site, it was found that the soil is acidic. Most plant nutrients, particularly calcium, potassium, magnesium were fluctuating from normal ranges thus depriving the concept of any agricultural or irrigation works. Hence results indicate that the effect of dumping of municipal solid waste in the study areas is slowly deteriorating the ground water quality. The soil is not only creating foul smell but also posing health hazard to the residents nearby. Based on the questionnaire survey conducted on the nearby residents, it was found that majority of the respondents were frequently falling ill. Also the foul smell from these sites was hampering their daily life and they were facing traffic-related issues too. Thus, it can be concluded that the impact of integrated solid waste on environment at landfill site is very negative. The impact is limited not just to landfill site but it is far-reaching. The area of influence of solid waste at landfill or dumping site is much greater than 10 km. People living adjacent to these areas are suffering the most in their day-to-day life.

References

1. UNEP report on Solid Waste Management (2005)
2. Taylor, A.A.R.: In: Waste Disposal and Landfill: Potential Hazards and Information Needs (2003). Available http://www.bvsde.paho. 2003org/bvsacd/cd59/protecting/sect2–12.pdf
3. Aljaradin, J.M., Persson, K.M.: Environmental impact of municipal solid waste landfills in semi-arid climates-case study Jordan. Open Waste Manage. J. **5**, 28–39 (2012)
4. Alam, P., Ahmade, K.: Impact of solid waste on health and the environment. Special Issue of Int. J. Sustain.Develop. Green Econom. (IJSDGE), **2**(I-1), 2 (2013) ISSN No: 2315–4721
5. Garg, S.: Findings from long-term monitoring studies as MSW landfill facilities with leachate recirculation. Waste Manage. **23**, 653–666 (2003)
6. Rajkumar, N., Subramani, T., Elango, L: Groundwater contamination due to municipal solid waste disposal—A GIS based study in Erode city. Int. J. Environ. Sci. **1**, 39–55 (2010)
7. Ilhan, F., Kurt, U., Apaydin, O., Gonullu, M.: Talha: Treatment of leachate by electocoagulation using aluminium and iron electrodes. J. Hazard. Mater. Elseiver **154**, 381–389 (2008)
8. Noise Pollution Regulations in India, Central Pollution Control Board (Ministry of Environment and Forests; Govt. of India). http://www.enfor.nic.in/cpcb
9. Garg, S.K., Garg,R.: In: Water Supply Engineering. 19th revised edn. Khanna Publishers, Delhi (2009)
10. Guidelines for the Measurement of Ambient Air Pollutants. Vol. 1, Central Pollution Control Board (Ministry of Environment and Forests; Govt. of India). http://www.cpcb.nic.in
11. Chaurasia, S., Gupta, A.D: In: Handbook of Water Air and Soil Analysis (A lab manual). 1st edn. International Science Congress Association E-publication, M.P. India (2014)

Settlement of Landfill Clay Cover Barriers with Geogrid Reinforcement

Akshit Mittal and **Amit Kumar Shrivastava**

Abstract Deformations in landfill clay cover barriers due to settlement in waste pills is a prevalent issue amassing to development of tensile cracks within the barrier, which reduces its usefulness and has a detrimental impact on its performance to reduce waste-water interaction. Geogrids have been widely used for reduction of differential settlement and preserve the utility and integrity of the barrier. However, these geogrids cannot mobilize maximum lateral resistance unless they are placed at optimum locations within the barrier. These locations need to be determined so as to obtain maximum possible benefit from the reinforcement. Hence, in this paper, laboratory-scale modeling of the landfill system has been carried out. Different landfill components such as the bottom liner, drainage layer, municipal solid waste pill, foundation layer/gas collection layer and the cover barrier have been scaled in accordance to the cover barrier height and a uniformly distributed load has been applied using a load frame. Filters, separators and protectors have been provided at suitable interfaces in the form of geotextiles throughout the landfill configuration. Kaolin clay and locally available sand blend in (4:1) proportion is used to simulate the bandwidth of clay cover material properties generally reported in the literature. Municipal waste was collected from different sources and mixed in proportion equivalent to the waste compositions of a typical Indian landfill. The waste was filled in five different horizontal phases, filled every two months and replaced with a new waste pill, which was prepared simultaneously in separate tanks, for different experimental program. Geogrids were applied in cover soil and different parameters such as initial layer spacing, vertical clearance between the reinforcement, effect of mechanical and physical properties of geogrids and the number of reinforcements have been analyzed in this study. The study showed the improvement in load-carrying capacity of the landfill cover with application of geogrids, subject to its optimum placement within the landfill cover. The mobilization of maximum tensile force in a geogrid occurred when the geogrid was placed at optimum positions.

Keywords Geogrids · Deformation · Covers · Settlement · Modeling

A. Mittal (✉) · A. K. Shrivastava
Delhi Technological University, Delhi 110042, India
e-mail: akshit97mittal@gmail.com

1 Introduction

Efficient designing and construction of waste containment systems is critical to ensure that the enclosed waste does not cause deleterious effects on the nearby environment. This requires providing effective barriers at the sides, bottom and the top of the landfill, so as to ensure efficient containment of municipal soil waste. Various types of barriers exist, such as the Compacted Clay Barrier (CCB), Geosynthetic Clay Liners (GCL), different admixtures, geomembranes and the respective combinations of each of the above. The selection of the barrier material depends upon the availability of the material near the site. CCBs are adopted at locations where clay is readily available and hence is economical to be used as the material to design a cover barrier [14, 17]. There are general geotechnical requirements required to be fulfilled to choose the best clay material to be used for the designing of the barrier, the most significant of which is the permeability of the clay. However, municipal solid waste landfills are subjected to differential settlements occurring as a result of waste biodegradation, collapse within the waste cavities or the falling over of the waste containers [8, 36]. Hence, it is inevitable to find solutions to enhance the strength of the soil and to prevent the deleterious outcomes occurrence of cracks might have on the performance of the Cover soil barriers of a landfill. Various researchers have presented methods of reinforcement for bolstering the strength of soil for different civil engineering structures such as embankments, foundations, slope and retaining earth walls [7, 15, 19, 21, 25, 38]. Similar study has been conducted on use of different reinforcement materials for increasing the strength of the clay cover barrier soils. Viswanadham et al. [37] conducted a centrifuge study on utilization of geofibers in the landfill clay covers and proffered that use of geofibers can have beneficial impacts in reducing cracks in the cover soil. They also proved that geofiber reinforced soil barrier sustained higher strains than unreinforced soil barriers at water breakthrough. Utilization of old dump waste for slope stability has also been studied by Koda [22]. In the past few years, geosynthetics have emerged as a low cost method for improving the strength of the soil and has gained wide acceptance as a good reinforcement material. Various studies have been conducted to analyze the performance of geosynthetics in Civil Engineering structures [4, 5, 9, 16, 18, 24, 26–29, 33]. This beneficial reinforcement effects of geosynthetics has also been utilized for reducing differential settlement and occurrence of cracks in landfill cover barrier soil. Material such as geogrid has found wide range of applications in landfill cover barriers. Various researchers have presented studies on use of geosynthetics as a reinforcement material in landfill cover. Palmeira and Viana [30] conducted a large-scale ramp study to assess the potential of geogrids in reducing the deformability of the cover soil and for reducing the tensile forces developed in the geomembranes. The study concluded that geogrids successfully reduced tensile forces developed in the geomembranes and simultaneously proffered that the inclusion of geotextiles over geomembranes further reduced deformability of the cover soil. Also, the study suggested that geogrid properties, especially stiffness plays a major role, with deformation lower for stiffer geogrids. Rajesh and Viswanadham [32] carried out centrifuge study to analyze the cracking

behavior of the landfill clay cover with and without the application of geogrid at different cover thicknesses. The study concluded that the inclusion of geogrids within the cover soil significantly restrained cracking in the cover soil. Divya et al. [11] investigated the potential benefit of utilizing geomembranes for curbing deformations in the clay cover, by conducting centrifuge model tests. They concluded that geomembranes acts as a hydraulic sealant even at high influx of cracks, thus preventing entry of water into the landfill even while differential settlement has taken place. Bacas et al. [3] conducted direct shear tests to analyze to investigate the effect of geotextile and geomembranes interface on the shear strength of cover systems and liners in the landfill. The study concluded that the characteristics of the geomembranes play a substantive role in choosing the best-suited type of geotextile for the cover systems. Feng et al. [12] presented a analytical study for computation of factor of safety of a geogrid reinforced landfill cover soil. The study analyzed different slope parameters such as slope angle, slope length, cover soil cohesion, frictional angle and interface friction and proffered that these parameter bear a significant effect on the stability of the slope of a landfill.

Review of existing literature showed that less study has been conducted to analyze the optimum locations of geogrids within the cover barrier. These locations can be significant to mobilize maximum possible tensile resistance within the reinforcements. Hence, in this study, an effort has been made to analyze the optimum locations of the reinforcements within the barrier by varying the top layer spacing of the reinforcements, number of layers of geogrids, types of geogrids and the vertical spacing between two consecutive reinforcements. For this purpose, a laboratory-scale model was designed, consisting of the different components of the landfill, significant to design a scientific landfill, which would be useful for the environment.

2 Materials Used

2.1 Cover Soil

The property of the soil plays a vital role in choosing the suitable material for the landfill clay cover barrier generally reported in the literature. Clay-based landfill barriers are usually designed for a hydraulic conductivity of less than or equal to 10^{-7} cm/sec for MSW type landfills. However, soil properties such as soil grain size and plasticity index of soil also play an important role in selection of suitable material for design of landfill clay barriers as they are directly related to the hydraulic conductivity of the soil. Koerner and Daniel [23] proffered a plasticity index ≥ 7–15% and percentage fines ≥ 30–50% for a suitable clay cover material, as these parameters directly influence the permeability of the soil. Daniel and Wu [10] suggested sand-clay mixture as an efficient material for reducing desiccation induced cracking in the landfill covers, which might be caused due to variable moisture content in the soil. Desiccation cracking can also cause expansion and softening of soil on water

Table 1 Properties of CCB soil and MSW

Properties	Soil blend	MSW
Specific gravity	2.63	2.26
Liquid limit (%)	41.2	
Plastic limit (%)	20.44	
Maximum dry unit weight (kN/m^3)	15.41	5.31
Optimum moisture content (%) Maximum dry unit weight (OMC + 5%) (kN/m^3) Coefficient of permeability(cm/sec)	24.52 14.02 8.19×10^{-7}	63% 2.34×10^{-4}
Coefficient of permeability(cm/sec) (OMC + 5%)	1.12×10^{-7}	

entry into the soil. Taking into consideration all the proposed characteristics of the landfill clay cover soil, a blend of kaolin and locally available sand (4:1) was chosen to simulate the characteristics of a typical landfill cover barrier. To ensure a permeability less than 10^{-7} cm/sec, the specimen was compacted at OMC + 5% as [6] proffered that soils compacted on the wet side of the OMC achieved permeability less than 10^{-7} cm/sec. The properties for the same are represented in Table 1.

2.2 Municipal Solid Waste (MSW)

Waste chosen for the testing was such that it reflects the typical characteristics of the MSW waste prevalent in Indian landfills. The waste reaching the landfill in India is typically mixed waste. The waste is found to be having 42.51% biodegradables, 9.63% paper waste, 10.11% plastic/rubber, 0.63% metal waste, 0.96% glass waste, and 17% inert waste [20]. The waste has typically high moisture content, pertaining to the presence of high amount of kitchen waste. For preparing waste simulating the characteristics of typical waste in Indian landfill, waste was procured from different places such as hostel mess (kitchen and food waste), recycle plant (paper, cardboard, glass, bottles, cans, metal and plastic waste), lawns and grounds (flowers and leaves), and construction site (debris, dirt and construction and demolition waste). The obtained waste was shredded and waste passing the 10 mm sieve was used for modeling of the landfill structure. The shredded waste was then mixed in the respective proportions using hands, and the prepared waste was stored for analysis. The geotechnical properties of the waste obtained after analysis are shown in Table 1. It should be noted that the age of the waste used for analysis was 2–3 weeks and thus some of the organic matter would have decomposed, leading to the small value of specific gravity. The moisture content obtained was typical of the Indian waste.

Table 2 Properties of Ggeogrids

Parameters	GG1		GG2	
	MD	TD	MD	TD
Tensile strength	7.8	8.2	5	5
Tensile modulus	550	350	115	115
Aperture size	30×30		12.5×12.5	

[**]Notes
[a] Tensile Modulus and Tensile Strength are in KN/m.
[b] MD and TD are Machine Direction and Transverse Direction, respectively.

2.3 Geogrids

Two geogrids with different mechanical and physical characteristics were chosen for the purpose of the study. The properties of the same were procured from the manufacturer (H.M.B.S. Textiles Pvt. limited). For the purpose of convenience, first and second type of geogrid has been termed using nomenclature as GG1 and GG2, respectively. The properties of the same are presented in Table 2.

3 Experimental Testing

3.1 Experimental Testing Model Preparation

The experimental model of the MSW landfill was prepared in a steel tank of dimensions 750 mm length, 450 mm width and 750 mm height, respectively. The steel tank modeled for the analysis consisted of uniform thickness steel sheets along the back and side portion of the tank and an acrylic sheet of 8 mm thickness along the front portion. The acrylic sheet used provided visual observation for each loading case and hence helped analyze the failure patterns. To prevent the buckling in the acrylic sheet, angles across the cross section of the sheet were used. The effect of friction was minimized using petroleum jelly along the edges of the steel tank. Each of the soil used for the study was first subjected to curing so that they achieve moisture equilibrium. For this purpose, they were stored in airtight bags for two week after adding sufficient moisture. The model preparation was started by first applying the bottom liner. A Geosynthetic Clay Liner (GCL) was chosen to simulate the characteristics of the bottom liner. Bentonite soil, encapsulated in two geotextiles, woven and non-woven, respectively, was needle punched and applied as a bottom liner. After placing the bottom liner, the drainage layer was designed using uniform gravels. A separator in the form of non-woven geotextile was then placed over the drainage layer to prevent the puncturing of the waste was a result of drainage layer. The MSW was placed in the model in five horizontal phases, with each phase completed in 2 months.

Each day, waste was placed in the tank and an intermediate cover was provided and this was repeated until the first phase was not complete. After the completion of one phase, similar procedure was applied on the other phases, until the entire waste was placed at the end of one year. After placing the MSW, a suitable separator was applied and then two layers of sand, one being a coarse sand followed by fine sand of equal thickness were applied. The angle of internal friction obtained for the sands was 45.1° and 36.9°, respectively. After placing the sand layers, the CCB was placed. The CCB was prepared in the form of slope with slope angle corresponding to 45°. The slope was prepared in four lifts, in form of cubical blocks and the excess soil was removed to form a smooth soil slope. After preparation of a lift, the surface was scarified using a spatula, to promote bonding between the lifts. A spirit level was used at the end of the model creation to ensure the alignment of the structure.

3.2 Testing Program

The tests were carried to find the optimum positions for placement of the geogrid within the cover barrier. For this purpose, the first series of tests was performed to determine the initial layer spacing (u). The u/H ratios were varied as 0.08, 0.16, 0.24, 0.32, and 0.40, respectively for both the geogrids at uniform thickness. After the completion of each test, the MSW was replaced with waste prepared in separate tanks with similar procedure as mentioned before. After determining the optimum top layer spacing, the next series of tests was performed to analyze the effect of increasing the number of layers of geogrids. The tests were carried out by fixing the top layer at the optimum position obtained from the previous test and varying the number of layers as $N = 1,2,3,4,5$, and 6, respectively, placed at 0.16 H, 0.32, 0.48, 0.64, 0.80, and 0.96 H, respectively. After determining the effect of number of layers of reinforcement, the final series of tests was performed to analyze the effect of vertical spacing between the geogrids. The first layer of reinforcement was placed at the optimum location obtained from the first test and the second layer was varied as 0.08, 0.16, 0.24, 0.32, and 0.40, respectively. Figure 1. shows the schematic of the testing model.

3.3 Testing Procedure

The tests to analyze the load-settlement characteristics of the landfill model were carried out in a Compression Testing Machine of overall capacity of 30 KN with geogrids placed at varying positions in the CCB. Two dial gauges were used for measurement of settlement with the increase in the load, each with an accuracy of 0.001%. The average of the dial gauge readings were used for computation of settlement. Two data logger, one for measurement of the load applied using the compression frame and other for the measurement of settlement using a LVDT. Each
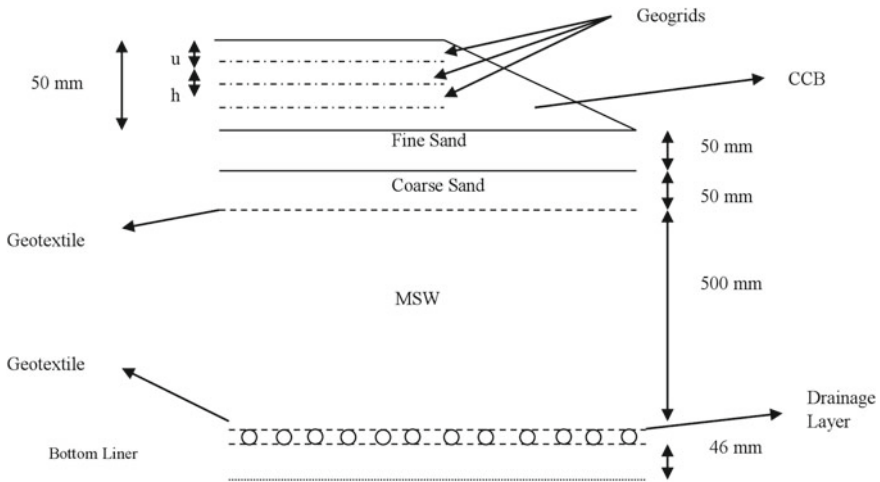
Fig. 1 Schematic of the testing model

of the test was performed in accordance to ASTM D 1196–93 [2], according to which the load was increased until the rate of settlement achieved was lower than 0.03 mm/min for three minutes consecutively. Two tests were repeated to analyze the variations in the results, if any. The average of the two values was reported.

4 Results and Discussion

4.1 Optimum Single-Layer Spacing

The first series of tests was performed to analyze the effect of top layer spacing (u) of the geogrid on the performance of geogrid reinforced CCB. To analyze the improvement in the load-carrying capacity of the CCB, a factor called Improvement Factor (IF) was used. This factor was analyzed at different s/H ratios, where s is the settlement in mm, induced due to the application of the overburden pressure. Improvement Factor can be defined as the ratio of the load carried by the Geogrid Reinforced CCB to the load carried by the unreinforced CCB at different s/H ratios. I.F. can be mathematically represented as

$$IF = \frac{q_r}{q}, \text{ for } s/H = 2\%, \ 4\%, \ 8\%, \ 12\% \text{ and } 16\% \tag{1}$$

where, q_r is the load carried by geogrid reinforced CCB and q is the load carried by unreinforced CCB.

The optimum top layer spacing was analyzed by varying the u/H ratio at five different points as discussed in the testing program. Figure 2a–b. shows the Pressure-Settlement graphs for GG1 and GG2, respectively. As can be observed from the graphs, application of a single layer reinforcement for each of the geogrid improves the stress carrying capacity of the landfill and also decreases the settlement under loading, for each of the u/H ratios. Figure 3a–b shows the improvement factor versus *u/H* curves for both the geogrids. As can be observed from the figure, the maximum possible benefit is obtained at *u/H* = 0.16, thus suggesting that the maximum mobilization in the reinforcement occurs at this ratio. It thus signifies the necessity of providing a suitable cover to the reinforcement, so as to obtain the maximum possible benefit from it. Similar results have been obtained for each of the geogrid. As can be observed, at *u/H* = 0.08, the improvement obtained is lower than that obtained at *u/H* = 0.16, thus signifying that at *u/H* < 0.16, the depth available for mobilizing sufficient tensile resistance in the reinforcement is not available, as a result of which maximum plausible benefits from the reinforcements cannot be obtained. In other words, the cushion of soil is not sufficient over the geogrids, as a result of which maximum lateral resistance cannot be obtained. It can thus be proffered that sufficient embedment of the geogrid should be ensured, so as to obtain maximum lateral resistance from the geogrids. Similar findings have also been reported by other researchers for geosynthetic reinforced structures. Shinand Das [35] reported a top layer spacing corresponding to 0.4 times the footing width (B) for geogrid reinforced foundation constructed over clay soil foundations. Similar observations were also reported by Chen et al. [9] reported a top layer depth of 0.33B for both geogrid and geotextile reinforced clay foundations.
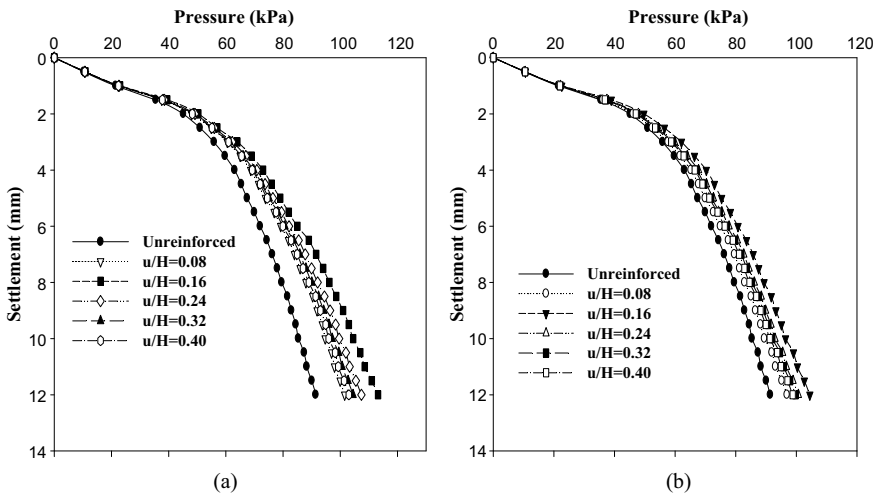
Fig. 2 Pressure-settlement curves for **a** GG1 and **b** GG2
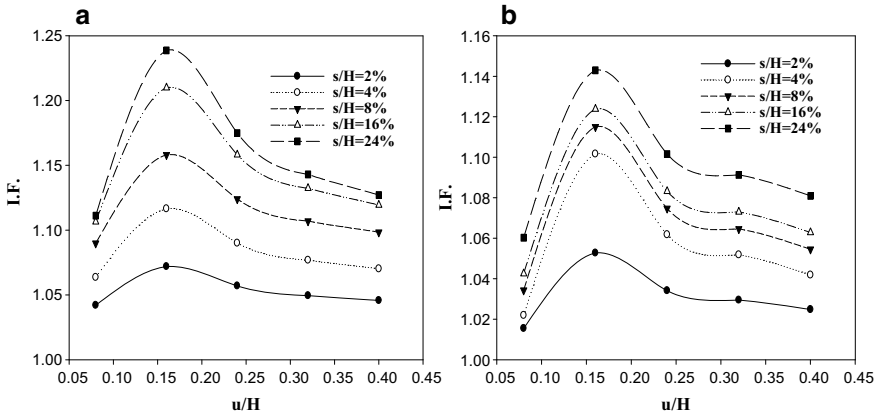
Fig. 3 Improvement factor versus u/H curves for **a** GG1 and **b** GG2

4.2 Effect of Number and Types of Geogrids

Number of layers of geogrids within the cover barriers would play a significant role during the construction of reinforced barriers. Hence, the next set of analysis was performed to determine the effects of increasing the number of layers of geogrids within the landfill CCB. Figure 4a–b. shows the pressure settlement curves for GG1
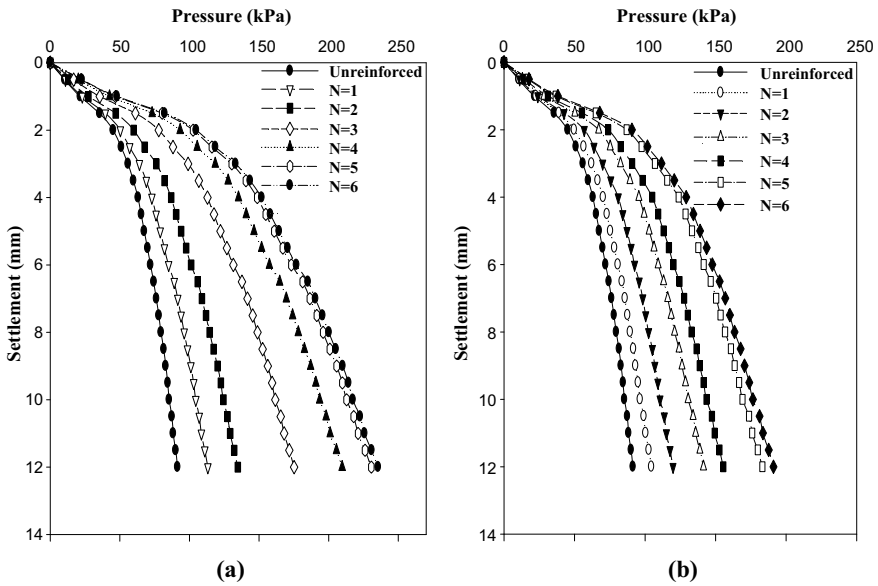
Fig. 4 Pressure settlement curves for **a** GG1 and **b** GG2 for different number of layers of reinforcements
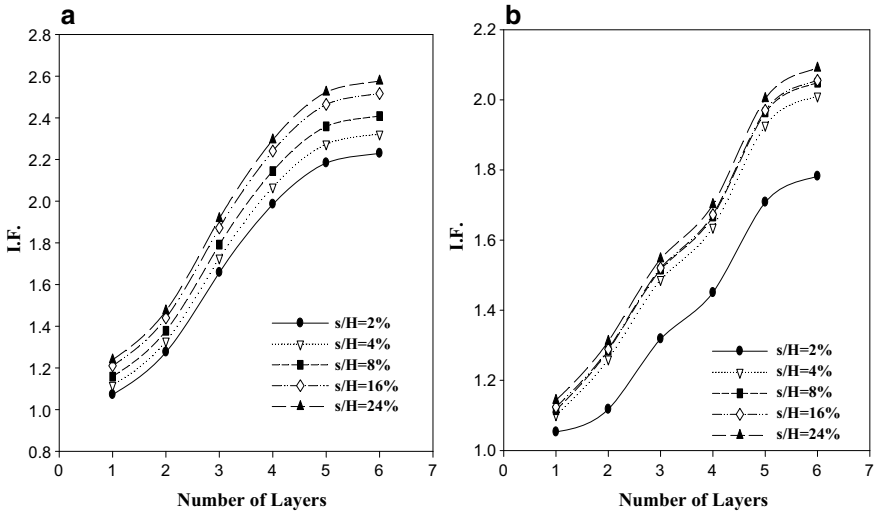
Fig. 5 Improvement factors versus number of layers curves for **a** GG1 and **b** GG2

and GG2, respectively. As can be observed, the inclusion of multiple layers of geosynthetics significantly improves the stress carrying capacity. This increase in the load-carrying capacity of the reinforced CCB with the increase in the number of layers of reinforcements can be attributed to the increase in the interface friction between the geogrids and the CCB, which increases with the increase in the number of layers of geogrids. Also, the increment in the number of layers of geogrids enhances the interlocking between the soil blend and the geogrid, as a result of which the lateral resistance provided by the geogrid increases and hence better improvement in load-carrying capacity is observed. The stiffness of the CCB increases with the addition of multiple layers of geogrids. Similar observations were reported by researchers such as [1] and [34] for geosynthetic reinforced foundations. Figure 5a–b shows the Improvement Factor versus Settlement curve for GG1 and GG2, respectively. As can be observed, the stress carried by the CCB increases upto $N = 5$, beyond which any further increase in the number of reinforcement layers does not increase the load-carrying capacity substantially. In other words, addition of further reinforcement layers beyond $N = 5$ in the CCB would be insignificant for the landfill design. Such an observation can be attributed to the stress envelope, which has its influence only upto a particular depth. Moving deeper than this point would not help in improving the load-carrying capacity of the reinforced CCB.

Comparing the performance of GG1 and GG2 shows that under similar conditions, both the geogrids perform differently, thus signifying that the properties of the geogrids play an important role in the reinforced CCB [31]. GG1 with higher stiffness provides better improvements at all the s/H ratios. Significantly, CCB is subjected to low overburden pressure (around 25 kPa) in typical field conditions. Performance of the geogrids at low over burden pressures thus becomes significant. GG1 would be the
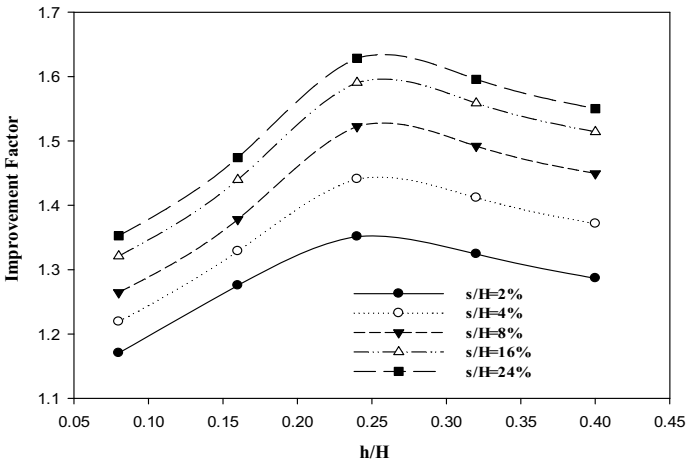
Fig. 6 Improvement Factors versus *h*/*H* curves for GG1

recommended geogrid for field operations, because it provides higher improvement at all the s/H ratios and significantly at lower overburden pressures.

4.3 *Effect of Spacing Between Geogrids*

The vertical spacing between the reinforcements plays an important role in designing reinforced structures, as it determines the cost of the project [13]. The effect of vertical spacing (*h*) was analyzed by fixing the top layer of the geogrid at *u*/*H* = 0.24 and varying the spacing of the second layer of reinforcement. As can be observed from Fig. 6, when the second layer of GG1 was placed at *h*/*H* = 0.24, maximum improvement in the load-carrying capacity of the CCB was obtained, thus signifying that the maximum mobilization of the second layer was obtained at this depth.

5 Conclusions

Inclusions of geogrids within the CCB significantly improve its load-carrying capacity; however, the maximum benefit is obtained when the geogrids are placed at optimum locations. Some of the key findings obtained from the study are:

1.   Inclusion of even a single layer of geogrid significantly improves the stress carrying capacity of the CCB.
2.   Maximum improvement in case of a single layer reinforcement was obtained when GG1 and GG2 were placed at u/H = 0.16, respectively, thus suggesting that

a suitable cover has to be provided to the reinforcement to mobilize significant lateral resistance within itself.

3. The effect of increasing the number of layers of reinforcement becomes redundant after placing the sixth layer of the geogrids, thus signifying that beyond N > 5, the inclusion of geogrids would not be beneficial for the design of the CCB.

4. Properties of the geogrid play an important role in choosing the right material to be applied in the CCB.

5. GG1 with higher tensile modulus performed much better than GG2 at every confining pressure and settlement ratio.

6. The maximum improvement, when varying the vertical spacing between the two layers of GG1 was obtained at $h/H = 0.24$.

References

1. Abu-farsakh, M., Chen, Q., Sharma, R.: An experimental evaluation of the behavior of footings on geosynthetic-reinforced sand. Soils Found. **53**(2), 335–348 (2013)
2. ASTM: Standard test methods for nonrepetitive static plate load tests of soils and flexible pavement components, for use in evaluation and design of airport and highway pavements. 112–113 (1997)
3. Bacas, B.M., Cañizal, J., Konietzky, H.: Shear strength behavior of geotextile / geomembrane interfaces. J. Rock Mech. Geotech. Eng. **7**(6), 638–645 (2015)
4. Badakhshan, E., Noorzad, A., Zameni, S.: Eccentrical behavior of square and circular footings resting on geogrid-reinforced sand. Int. J. Geotech. Eng. **6362**, 1–11 (2018)
5. Benmebarek, S., Djeridi, S., Benmebarek, N., Belounar, L.: Improvement of bearing capacity of strip footing on reinforced sand. Int. J. Geotech. Eng. **12**(6), 537–545 (2018)
6. Benson, C.H., Daniel, D.E., Boutwell, G.P.: Field performance of compacted clay liners. J. Geotech. Geoenviron. Eng. **125**(5), 390–403 (1999)
7. Binquet, J., Lee, K.L.: Bearing capacity tests on reinforced earth slabs. J. Geotech. Geoenviron. Eng. **101**(ASCE# 11792 Proceeding) (1975)
8. Camp, S., Rey, D., Kaelin, J. : Presentation of a new French site for storing very lowlevel radioactivewaste. Int. Landfills '"HPM1"'. LIRIGM, Grenoble 1 Univ. Fr. 21–22 March (2005)
9. Chen, Q., Abu-Farsakh, M., Sharma, R., Zhang, X.: Laboratory investigation of behavior of foundations on geosynthetic-reinforced clayey soil. Transp. Res. Rec. J. Transp. Res. Board. **2004**, 28–38 (2007)
10. Daniel, D.E., Wu, Y.-K.: Compacted clay liners and covers for arid sites. J. Geotech. Eng. **119**(2), 223–237 (1993)
11. Divya, P. V, Viswanadham, B.V.S., Gourc, J.P.: Influence of geomembrane on the deformation behaviour of clay-based landfill covers. Geotext. Geomembranes. **34**, 158–171 (2012)
12. Feng, S.-J., Ai, S.-G., Huang, R.-Q.: Stability analysis of landfill cover systems considering reinforcement. Environ. Earth Sci. **75**(4), 303 (2016)
13. Goodarzi, S., Shahnazari, H.: Strength enhancement of geotextile-reinforced carbonate sand. Geotext. Geomembranes. **47**(2), 128–139 (2019)
14. Gourc, J.P., Camp, S., Viswanadham, B.V.S., Rajesh, S.: Deformation behavior of clay cap barriers of hazardous waste containment systems: Full-scale and centrifuge tests. Geotext. Geomembranes. **28**(3), 281–291 (2010)
15. Gray, D.H., Al-Refeai, T.: Behavior of fabric- versus fiber-reinforced sand. J. Geotech. Eng. **112**(8), 804–820 (1986)

16. Haeri, S.M., Noorzad, R., Oskoorouchi, A.M.: Effect of geotextile reinforcement on the mechanical behavior of sand. Geotext. Geomembranes. **18**(6), 385–402 (2000)
17. Heerten, G., Koerner, R.: Cover systems for landfills and brownfields. L. Contam. Reclam. **16**(4), 343–356 (2008)
18. Huang, Z., Qutaibah, A.S., Nasrazadani, S., Felix, W.H.: Understanding and optimizing the geosynthetic-reinforced steep slopes. Electron. J. Geotech. Eng. **19**, 5793–5811 (2014)
19. Jellali, B., Bouassida, M., De Buhan, P.: A homogenization method for estimating the bearing capacity of soils reinforced by columns. Int. J. Numer. Anal. Methods Geomech. **29**(10), 989–1004 (2005)
20. Joshi, R., Ahmed, S.: Status and challenges of municipal solid waste management in India: a review. Cogent Environ. Sci. **2**(1), 1139434 (2016)
21. Juran, I., Guermazi, A.: Settlement response of soft soils reinforced by compacted sand columns. J. Geotech. Eng. **114**(8), 930–943 (1988)
22. Koda, E.: Anthropogenic waste products utilization for old landfills rehabilitation. Ann. Warsaw Univ. Life Sci. L. Reclam. **44**(1), 75–88 (2012)
23. Koerner, R.M., Daniel, D.E.: Materials. In: Final Covers for Solid Waste Landfills and Abandoned Dumps. pp. 78–79 (1997)
24. Koerner, R.M., Soong, T.Y.: Use of geosynthetics in infrastructure remediation. J. Infrastruct. Syst. **1**(1), 66–75 (1995)
25. Lal, B.R.R., Mandal, J.N.: Feasibility study on fly ash as backfill material in cellular reinforced walls. Electron. J. Geotech. Eng. **17**, 1437–1458 (2012)
26. Latha, G.M., Murthy, V.S.: Effects of reinforcement form on the behavior of geosynthetic reinforced sand. Geotext. Geomembranes. **25**(1), 23–32 (2007)
27. Luo, F., Zhang, G., Liu, Y., Ma, C.: Centrifuge modeling of the geotextile reinforced slope subject to drawdown. Geotext. Geomembranes. **46**(1), 11–21 (2018)
28. Mandal, J.N., Joshi, A.A.: Design of geosynthetic reinforced embankments on soft soil. Geotext. Geomembranes. **14**(2), 137–145 (1996)
29. Oberhagemann, K., Hossain, M.M.: Geotextile bag revetments for large rivers in Bangladesh. Geotext. Geomembranes. **29**(4), 402–414 (2011)
30. Palmeira, E.M., Viana, H.N.L.: Effectiveness of geogrids as inclusions in cover soils of slopes of waste disposal areas. Geotext. Geomembranes. **21**(5), 317–337 (2003)
31. Rajesh, S., Viswanadham, B.V.S.: Centrifuge modeling and instrumentation of geogrid-reinforced soil barriers of landfill covers. J. Geotech. Geoenviron. Eng. **138**(1), 26–37 (2012)
32. Rajesh, S., Viswanadham, B.V.S.: Hydro-mechanical behavior of geogrid reinforced soil barriers of landfill cover systems. Geotext. Geomembranes. **29**(1), 51–64 (2011)
33. S.Adhana, Mandal, J.N.: Proceedings of Indian Geotechnical Conference. In: Proceedings of Indian Geotechnical Conference. pp. 553–556 (2011)
34. Sawwaf, E. M.: Behavior of strip footing on geogrid-reinforced sand over a soft clay slope. Geotext. Geomembranes. **25**(1), 50–60 (2007)
35. Shin, E.C., Das, B.M.: Ultimate bearing capacity of strip foundation on geogrid-reinforced clay slope. KSCE J. Civ. Eng. **2**(4), 481–488 (1998)
36. Sivakumar Babu, G.L., Reddy, K.R., Chouksey, S.K.: Constitutive model for municipal solid waste incorporating mechanical creep and biodegradation-induced compression. Waste Manag. **30**(1), 11–22 (2010)
37. Viswanadham, B.V.S., Sathiyamoorthy, R., Divya, P. V, Gourc, J.: Influence of randomly distributed geofibers on the integrity of clay-based landfill covers : a centrifuge study. Geosynth. Int. **18**(5), 255–271 (2011)
38. Yetimoglu, T., Inanir, M., Inanir, O.E.: A study on bearing capacity of randomly distributed fiber-reinforced sand fills overlying soft clay. Geotext. Geomembranes. **23**(2), 174–183 (2005)

Desiccation Induced Cracking Characteristics of Locally Available Soils in Warangal

Nirbhay Narayan Singh , **Y. Sudheer Kumar, and P. Hari Krishna**

Abstract In this study, locally available soils in Warangal (Telangana) are chosen to assess the feasibility of using as clay liner. The focus of the work is to carry out a laboratory study on locally available prominent clayey soils for the effect of desiccation induced cracks and hydraulic conductivity on the compacted clay soils under the influence of varying pH as well as organic and inorganic chemicals. Three types of locally available soils were selected (red earth, black cotton soil and the soil that is available near Rampur dumping yard location in Warangal) and the tests were conducted by compacting these soils at optimum moisture content with varying pH, organic (Humic Acid, EDTA, Dichloromethane) and inorganic (NaOH, HCl) chemicals. These compacted soil samples were tested for the desiccation cracks and hydraulic conductivity with the same solutions which were used in the preparation of soil sample. Variation of pH and organic–inorganic chemicals has shown a significant effect on crack intensity factor (CIF) and hydraulic conductivity. From the test results, it is observed that in acidic condition, CIF values of soil are decreasing with a decrease in pH while in basic condition, CIF values are increasing with the increase in pH. With the decrease of pH, the hydraulic conductivity of soil is increasing for an uncracked sample and decreasing for cracked sample in acidic condition. While in basic condition both cracked and uncracked permeability is increasing with the increase in pH. In all the cases of tests done with different pH and organic–inorganic chemicals, red earth soil showed minimum values of CIF, hydraulic conductivities and also permeability ratios hence red earth soil should be chosen as a liner material among selected locally available soils.

Keywords Crack intensity factor · Humic acid · EDTA · pH · Desiccation cracks

N. N. Singh (✉)
Indian Institute of Technology, Delhi, New Delhi 110016, India
e-mail: nirbhay.mnnit@gmail.com

Y. S. Kumar · P. H. Krishna
National Institute of Technology Warangal, Warangal 506004, India

1 Introduction

Among the various waste disposal methods, landfilling is considered to be safe and cost-effective compared to others. Without appropriate treatment, landfill leachate could be a potential source of surface and groundwater contamination, as it could seep into soils and subsoil causing severe pollution to receiving water body [1]. The main concern about these landfills is that the bottom clay liner should prevent the migration of toxic leachate into the ground. Compacted clay liners and geo-synthetic clay liners are commonly used in modern sanitary landfill designs. If the clay liner undergoes desiccation cracking, there is a possibility of leachate to escape into ground/groundwater.

The presence of high amounts of clay particles in a soil, particularly highly active clay minerals such as smectites and vermiculites, promotes the formation of cracks [2]. A high plasticity index (PI) and low shrinkage limit indicate a high potential for shrinkage and swelling. In soils having PI more than 35%, excessive shrinkage can be expected [3] and the chemistry of the pore fluid also affects crack formation. It is known that surface tension affects the air–water-solid contacts inside the soil and generates negative pore-water pressures in the unsaturated soil [4]. The matrix suction may result in soil contraction, and ultimately soil shrinkage and cracking. There is a phenomenon called self-healing that occurs in some types of clays, which plays an important role in desiccation studies as it is beneficial in waste containment because of the decrease in hydraulic conductivity of the clay liners. The basic criterion for a soil to be used as a liner is that it should have hydraulic conductivity less than 10^{-7} cm/sec [5]. For the fabrication of a liner in arid sites [6] suggested the use of clayey sand with low hydraulic conductivity and low shrinkage values. The coefficient of permeability (K) represents the soil's ability to permit passage to water through the soil. This, in turn, indicates the ability of the soil to change matric suction as a result of environmental changes [7].

2 Material and Testing Procedure

2.1 Soils

Three types of soils, namely red earth soil, dump yard soil, and black cotton soil were selected. Red earth and black cotton soil were collected from locations nearby to NIT-Warangal campus premises and dump yard soil was collected from dumping yard location near Rampur in Warangal. Sieve analysis is performed to determine the distribution of coarser, larger-sized particles and the hydrometer method is used to determine the distribution of finer particles as per IS 2720 Part IV [8]. Atterberg's limits such as liquid limit, plastic limit, and shrinkage limit were estimated as per IS 2720 Part V [9] and Part VI [10], respectively. Optimum moisture content (OMC) and corresponding maximum dry density (MDD) were also being reckoned through

Table 1 Index properties of soils used

Parameters	Red Earth	Black cotton	Dump yard
Gravel (%)	6	0	2
Sand (%)	27	30	54
Silt (%)	41	39	10
Clay (%)	26	31	34
Soil classification	CI	CH	SC
Liquid limit (%)	38	61	84
Plastic limit (%)	21	21	24
Plasticity index	17	40	60
Shrinkage limit (%)	19.32	11.67	18.14
Maximum dry density (g/cc)	1.8	1.68	1.77
Optimum moisture content (%)	19.7	19.6	17.5
Free swell index	5	90	240

standard proctor compaction test as per IS 2720 Part-VII [11]. Free swell index test conformed to IS 2720 Part XL [12] was performed for quantitatively assessing the swelling potential of soil. All index properties of soil are listed in Table 1.

2.2 Chemicals

Organic chemicals such as ethylenediaminetetraacetic acid (EDTA), dichloromethane (DCM), and humic acid were accounted for in this study. Inorganic chemicals such as hydrochloric acid (HCl) and sodium hydroxide (NaOH) were also taken into account for evaluating the effect of varying pH on cracking characteristics and hydraulic conductivity of the soil. All chemicals were diluted to 9% concentration for testing purpose after preparing a 1 N stock solution of each chemical except humic acid.

2.3 Experimental Scheme and Sample Preparation

The desiccation test and hydraulic conductivity tests were conducted on soils compacted at seven different pH (2, 4, 5, 6, 7, 8, 10), three organic chemicals and two alkalides. The reason for not opting higher pH was that usually in a landfill, waste is lying in acidic condition. For these tests, using cylindrical oedometers ring, soil samples were prepared to diameter 6 cm and thickness 2 cm. Soil, sieved by 425μ was

mixed at optimum moisture content with different pH solutions and organic–inorganic chemical solutions and was compacted in the mold to the required maximum dry density (Day 0). CIF is defined as the time-variable ratio of the surface crack area (A_c), to the total surface area of the sample (A_t).

$$\text{CIF} = \frac{\text{CrackedArea}(A_c)}{\text{TotalSurfaceArea}(A_t)} \quad (1)$$

A computer-aided image analysis program was used to determine CIF from photographs of the desiccation process in four stages, as shown in Fig. 1. Firstly, the compacted soil sample was taken and kept in the oven for 24 h at 70 °C temperature (Day 1). Due to this process, the soil sample experienced cracks on the surface. The dried sample was then saturated with the same pH solution or organic–inorganic chemicals for 24 h (Day 2). After completion of saturation, it was observed the width of cracks in the soil reduced to a significant extent. This could be due to the self-healing property of soil through the swelling process. The saturated sample was again allowed for drying for 24 h at the same temperature for observing the effect of cycles of wetting and drying on the cracking behavior of soil (Day 3). At the end of each of the steps, a photograph of the sample was taken and these images were converted to binary images using open source software GIMP 2.0. A MATLAB program was developed for calculating CIF values through analysis of the binary images. A higher value of the CIF indicates more number of cracks formed in the soil specimen. The
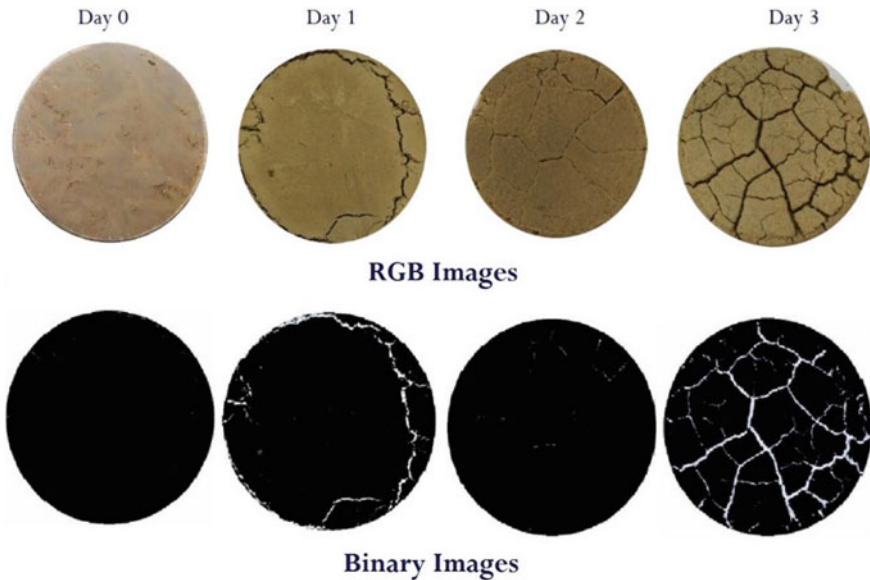
Fig. 1 Images of the desiccated sample at different stages

closing of cracks mainly depends on the mineralogical composition and self-healing properties of the soil.

To understand the influence of variation of pH alongside organic–inorganic chemicals on hydraulic conductivity of desiccated clay liner materials, variable head permeability tests were performed, and the coefficient of permeability was calculated in accordance with IS 2720 Part XVII [13].

3 Experimental Results and Analysis

3.1 Variation of CIF with Desiccation Cycles

The values of crack intensity factors (CIF) for the three soils (red earth, dump yard soil, and black cotton soil) compacted at optimum moisture contents with different pH solutions and saturated with same solutions are presented in Tables 2, 3, and 4.

From the results furnished in Tables 2, 3, and 4, it can be observed that the CIF value of the soil during desiccation is increasing and it can be observed from Figs. 1,

Table 2 CIF values for red earth soil at different pH

pH	Stage of testing (day)			
	Initial soil (0)	On drying (1)	On wetting (2)	On drying (3)
2	0	0.208	0.082	0.282
4	0	0.272	0.106	0.322
5	0	0.306	0.165	0.482
6	0	0.354	0.098	0.511
7	0	0.598	0.088	0.806
8	0	0.622	0.094	1.454
10	0	0.623	0.111	1.896

Table 3 CIF values for dump yard soil at different pH

pH	Stage of testing (day)			
	Initial soil (0)	On drying (1)	On wetting (2)	On drying (3)
2	0	0.548	0.094	2.668
4	0	0.478	0.222	3.785
5	0	1.696	0.287	3.847
6	0	1.852	0.036	4.949
7	0	2.382	0.165	5.236
8	0	2.411	0.201	5.988
10	0	3.598	0.231	7.016

Table 4 CIF values for black cotton soil at different pH

pH	Stage of testing (day)			
	Initial soil (0)	On drying (1)	On wetting (2)	On drying (3)
2	0	0.536	0.105	2.999
4	0	0.88	0.298	3.568
5	0	1.778	0.321	4.645
6	0	2.074	0.045	5.905
7	0	2.567	0.184	5.964
8	0	2.634	0.225	6.785
10	0	2.765	0.258	6.806

2, and 3. From Table 1, for red earth soil at pH 7, for the first cycle of desiccation, the CIF value increased from initial value of zero (i.e., on day 0) to 0.598 (i.e., on day 1) whereas during the second attempt of desiccation (i.e., on day 3), the value got increased to 0.806 from 0.088 (i.e., on day 2). Similarly, for dump yard soil, CIF is increased from 2.382 to 5.236 (220%) after the second cycle of desiccation at pH 7. For black cotton soil also, CIF is increased from 2.567 to 5.964 (232%) after the second cycle of desiccation. These values clearly indicate that the rate of increase in the CIF value is increasing with the number of desiccation attempts. This is mainly because the cracks formed in the first desiccation attempt remained as weaker zones even after saturation period and the cracks reopened and progressed easily with drying for the second time of desiccation.

It is evident from Figs. 1, 2, and 3 that CIF values are minimum for red earth soil and maximum for black cotton soil for all type of pH solution. This observation is mainly because when the soil sample which is compacted at a particular moisture content, during the drying process the matric suction produced on the surface of soil
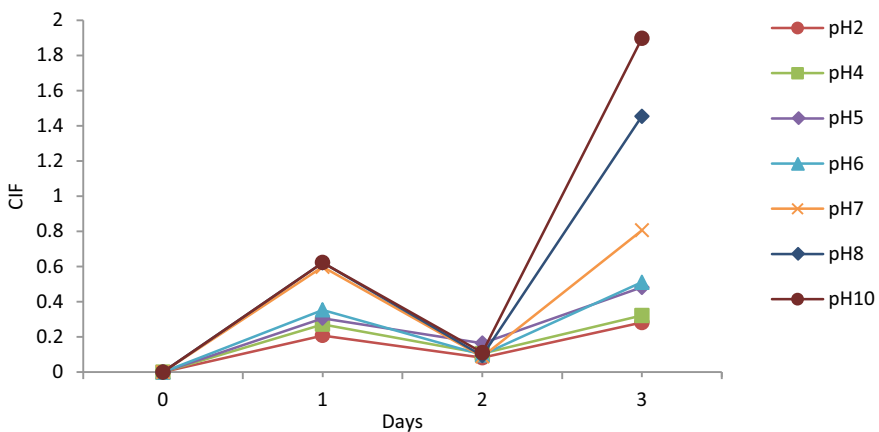

Fig. 2 Variation of CIF for red earth soil with the stage of drying and saturation
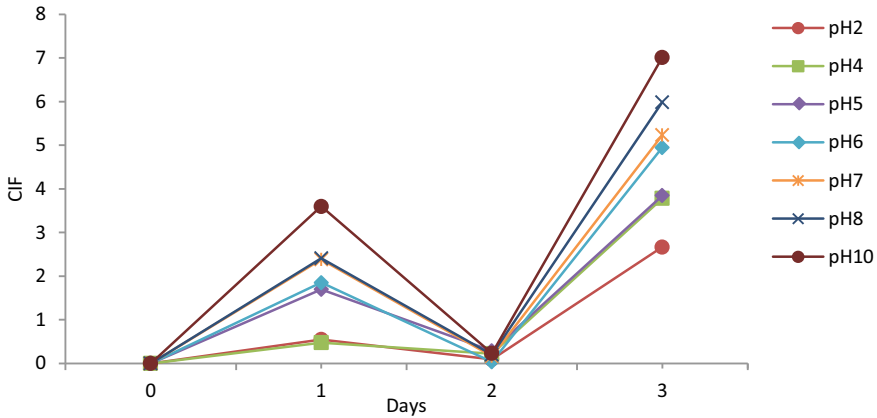
Fig. 3 Variation of CIF for dump yard soil with the stage of drying and saturation

sample may increase the tensile stresses and cause more negative pore pressures, thus leading to cracks in the soil sample. It was observed that the applied W-D cycles resulted in significant rearrangement of specimen structure: the initially homogeneous and non-aggregated structure was converted to a clear aggregated-structure with obvious interaggregate pores after the second W-D cycle.

Therefore, the cracking behavior of soils mainly depends on the moisture content and rate of evaporation within the soil mass. Miller et al. [4]. Cracks which are generated in the first cycle of desiccation, they are not closed completely after saturation. Hence after the first cycle when soil is saturated and dried again leads to an increase in the crack. CIF values at day 2 (i.e., after saturation) reduced remarkably indicating the self-healing of soil (Fig. 4).

3.2 Variation of CIF with pH

From Fig. 5, it can be observed that the CIF value increased when the pH of the solution varies from acidic to basic. This can be due to the fact liquid limit of the soil decreases as the soil gets acidic resulting in the reduction of plasticity index and hence the cracking of the soil is decreased [14]. In acidic condition, the leaching of alumina, silica, and iron occurs which erodes the lattice structure of clays and releases undissolved fragments for the migration with the leachate. These undissolved fragments form precipitation and fill the cracks as seen in SEM images [15]. Hence closing of the crack starts and overall crack width decreased resulting in decrease in CIF. While in the basic condition, the dissolution of alumina, silica, and iron starts while forming hydroxides which in turn get dissolved and corrode the cracks furthermore and results in an increase in crack width increasing CIF values [16]. It was observed that most of the cracking occurred in the initial 18-h time period. Upon
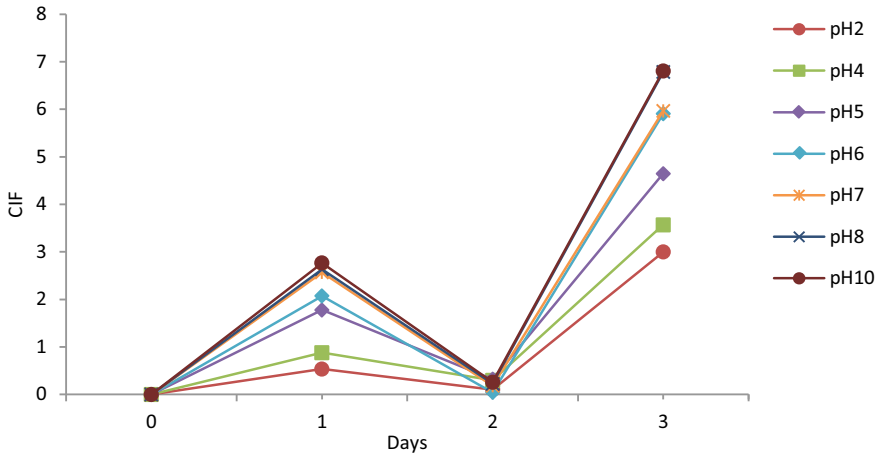
Fig. 4 Variation of CIF for black cotton soil with the stage of drying and saturation
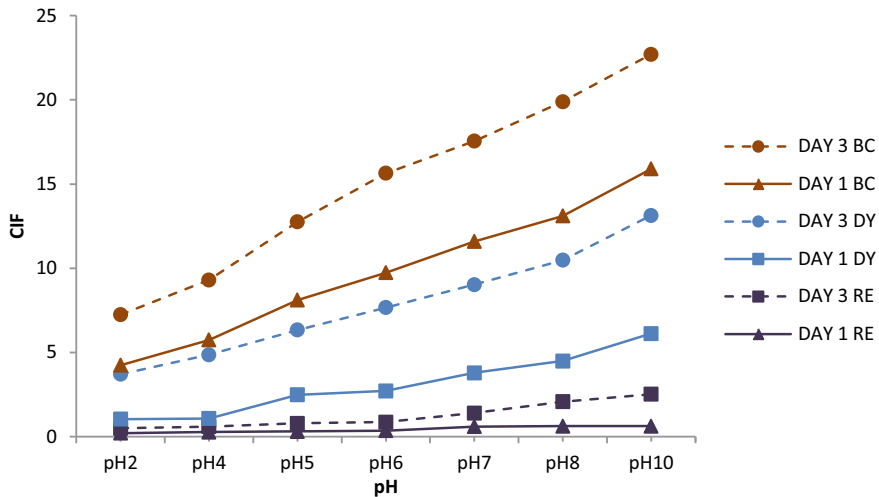
Fig. 5 Variation of CIF for red earth (RE), dump yard (DY), and black cotton (BC) soil with pH after desiccation

the second cycle of drying, the crack features (width, thickness, etc.) have progressed significantly compared to that of the first cycle. In the first cycle, the cracking pattern was observed to be linear with small branches whereas in the second cycle the pattern of polygon network.

To further understand the effect of organic–inorganic chemicals, NaOH and HCl as inorganic chemical solutions were used to see the variation in extreme acid–base condition. Cracking characteristics of soils (red earth, dump yard soil, and black

Table 5 CIF values for soils with different organic–inorganic chemicals

(a) Red earth soil

Stage of testing (day)	CIF				
	HCl	DCM	EDTA	Humic	NaOH
Initial soil (0)	0	0	0	0	0
On drying (1)	0.178	0.738	0.269	0.487	1.423
On wetting (2)	0.047	0.102	0.041	0.146	0.197
On drying (3)	0.356	1.128	0.476	0.953	2.112
(b) Dump yard soil					
Initial soil (0)	0	0	0	0	0
On drying (1)	0.207	3.505	0.673	2.748	3.118
On wetting (2)	0.088	0.378	0.213	0.211	0.289
On drying (3)	0.971	6.275	1.391	5.487	7.648
(c) Black cotton soil					
Initial soil (0)	0	0	0	0	0
On drying (1)	0.239	3.895	0.735	3.111	3.727
On wetting (2)	0.089	0.421	0.233	0.228	0.305
On drying (3)	1.186	6.982	1.968	6.101	7.945

cotton soil) is shown in Table 5. It can be observed from the following table that CIF values are minimum for HCl and maximum for NaOH for all three types of soils which is also evident from Fig. 5 which shows similar variation when all soils were subjected to varying pH. CIF values for organic chemicals are lying in between HCl and NaOH owing to their natural acidic-basic behavior. Since DCM is nearly neutral when mixed with water at room temperature; it is showing more CIF then EDTA (acidic in nature) and humic acid. Among organic chemicals, DCM is showing maximum CIF and EDTA is showing minimum CIF; while for humic acid, CIF is lying in-between, supporting the explanation that as the solution becomes acidic and CIF value decreases substantially.

3.3 Variation of Permeability with pH

The values of hydraulic conductivity for the three soils (red earth, dump yard soil, and black cotton soil) compacted at optimum moisture contents with different pH solutions and saturated with same solutions in terms of uncracked permeability constant (K_0) and cracked permeability constant (K_1) are presented in Table 6. From Table 6, it can be observed, for an uncracked sample as acidity increases permeability increases. This could be because of the increase in acidity attributing to the decrease in the thickness of Diffuse Double Layer (DDL), resulting in flocculation of the clay

Table 6 Variation of permeability with pH

(a) Red earth soil

pH	K_0 (10^{-7} cm/s)	K_1 (10^{-7} cm/s)	K_r
2	0.351	2.011	5.73
4	0.322	2.991	9.29
5	0.301	3.369	11.19
6	0.289	3.428	11.86
7	0.288	3.525	12.24
8	0.291	4.072	13.99
10	0.312	4.447	14.25

(b) Dump yard soil

2	0.663	4.896	7.38
4	0.609	7.312	12.01
5	0.569	8.210	14.43
6	0.546	8.355	15.30
7	0.544	8.601	15.80
8	0.551	9.945	18.05
10	0.614	11.851	19.30

(c) Black cotton soil

2	1.492	18.099	12.13
4	1.369	26.909	19.66
5	1.279	30.321	23.70
6	1.228	30.842	25.11
7	1.224	31.726	25.92
8	1.244	36.546	29.38
10	1.286	40.051	31.14

particles. Flocculated and dispersed structures have different hydraulic conductivities. The thickness of the DDL can influence the soil structure, resulting in permeability changes. Hence as solution acidity is increasing, there is enormous loss in DDL thickness, and increase in hydraulic conductivity. While in the basic condition also permeability is increasing with the increase in basicity confirming that the increase in chemical concentration results in higher permeability in soils [17]. While for cracked soil, permeability is mostly depending on how much the soil specimen is cracked. For higher CIF values of sample, higher permeability constant is observed. Permeability ratio is observed to be increasing as the pH of the soil is changing from acidic to basic. With an increase in acidity, the liquid limit of the soil decreases and hence plasticity index of the soil is also reduced. Hence permeability ratio is increasing with the increase in soil plasticity and as well as varying from acidic to basic condition.

Table 7 Variation of permeability of soil with organic–inorganic chemicals

(a) Red earth soil

Chemical	$K_0 (10^{-7}$ cm/s)	$K_1 (10^{-7}$ cm/s)	K_r
HCl	0.366	2.768	7.56
Dichloromethane	0.289	3.429	11.87
EDTA	0.299	2.433	8.14
Humic	0.342	2.877	8.41
NaOH	0.360	5.465	15.18

(b) Dump yard soil

HCl	0.692	6.753	9.76
Dichloromethane	0.546	8.337	15.26
EDTA	0.565	5.886	10.42
Humic	0.646	7.111	11.00
NaOH	0.591	13.325	22.55

(c) Black cotton soil

HCl	1.556	24.882	16.00
Dichloromethane	1.228	30.851	25.12
EDTA	1.271	21.907	17.24
Humic	1.454	25.883	17.81
NaOH	1.205	49.187	40.82

3.4 Variation of Permeability in the Presence of Organic–Inorganic Chemicals

Values of uncracked permeability constant (K_0) and cracked permeability constant (K_1) of soil with different organic–inorganic chemicals are presented in Table 7. From Table 7, it can be seen that irrespective of acid and base permeability is increasing with chemicals. Permeability of cracked sample is significantly higher than the uncracked sample and permeability ratio is higher for black cotton soil and lesser for red earth soil while for dump yard soil, it is lying in between earlier two.

4 Conclusions

The desiccation cracking and hydraulic conductivity of the selected locally available soils are controlled by soil properties like plasticity index and clay content. The crack intensity factor (CIF) values are observed to be more for soils having high plasticity index values. All soils have shown an increase in the CIF value with the increase in the number of desiccation attempts. In acidic condition, CIF values of soil are decreasing with a decrease in pH and in basic condition, CIF values are increasing with the increase in pH. Hydraulic conductivity of soil is increasing for an uncracked

sample and decreasing for cracked sample in acidic condition with a decrease in pH. While in basic condition, both cracked and uncracked permeability is increasing with the increase in pH. In the case of organic chemicals, CIF value is increasing with desiccation cycles and significantly affecting the cracks developing in the soil. Hydraulic conductivity is increasing with increasing chemical concentration and plasticity of the soil. The values of permeability ratios increased with an increase in plasticity index of the soils. In all the cases with different pH and organic chemicals, red earth soil showed minimum values of CIFs, hydraulic conductivities and also permeability ratios; hence red earth soil should be chosen as a liner material among selected locally available soils.

References

1. Azmi, N.B., et al.: Recent development in landfilll eachate treatment using low-cost adsorbent prepared from waste material. Advanced Wastewater Treatment System IJSRPUB, Wastewater Engineering (2014)
2. Holtz, D.R., Kovacs, D.W.: In: An Introduction to Geotechnical Engineering. Prentice-Hall, Inc. (1981)
3. Daniel, D.E., Estornell, P.: Hydraulic conductivity of three geosynthetic clay liners. J. Geotech. Eng. ASCE **118**(10), 1592–1606 (1992)
4. Miller, C.J., Mi, H., Yesiller, N.: Experimental analysis of desiccation crack propagation in clay liners. J. Amer. Water Res. Assoc. **34**, 677–686 (1998)
5. EU Landfill Directive-European Council: Council Directive 1999/31/EC. Council of European Union (1999)
6. Daniel, D.E., Yung-Kwang, Wu.: Compacted clay liners and covers for arid sites. J. Geotech. Eng. ASCE **119**(2), 223–237 (1993)
7. Fredlund, D.G., Rahardjo, H.: Soil Mechanics for Unsaturated Soils. Wiley, New York (1993)
8. IS 2720 (Part IV): Grain size analysis (1985)
9. IS 2720 (Part V): Determination of liquid and plastic limits (1985)
10. IS 2720 (Part VI): Determination of shrinkage factors (1972)
11. IS 2720 (Part VII): Determination of water content-dry density relation using light compaction (1980)
12. IS 2720 (Part XL): Determination of free swell index of soils (1977)
13. IS 2720 (Part XVII): Laboratory determination of permeability (1986)
14. Rayhani, M.H.T., Yanful, E.K., Fakher, A.: Desiccation induced cracking and its effect on the hydraulic conductivity of clayey soils from Iran. Can. Geotech. J. **44**, 276–283 (2007)
15. Amulya, M., Prasad, C.H.R.V., Reddy, P.H.P., Kalyan Kumar, G.: Effect of sulphuric acid on black cotton soil. Int. J. Earth Sci. Eng. (2015). ISSN 0974–5904
16. Singh, N.N. et al.: A study on cracking behaviour of black cotton soil. Geotech. Infrastruct. Projects (2017)
17. Seracettin, A.: Effect of chemicals on geotechnical properties of clay liners: a review. Res. J. Appl. Sci. Eng. Technol. **2**(8), 765–775 (2010)

Study the Potential of Plastic Waste Bottles as Geo-Cells for Maintenance of Pot-Holes in Flexible Pavement

Siddharth Shah, Yogesh Alwani, and Morvin Solanki

Abstract Flexible pavements are frequently damaged with excessive cracks, settlements, and potholes. Due to various reasons, these defects are occurring namely: less bitumen content, overload and poor subgrade compaction, poor drainage or poor subgrade itself. There are many options to maintain and repair such defects. Since last few decades, geo-synthetics material is introduced in market for various geotechnical application. These include use of geotextiles, geo-nets, geo-grids, geo-membrane, geo-cell etc. for ground improvement, providing drainage, separating two layers, as impervious layer and reinforcement. Out of all these applications geo-cell have great capacity to overcome poor bearing capacity of subgrade by its installation. On other hand use of plastic bottles for storing water, juice, oil, milk and other multiple things have increased exponentially. The polyethylene bottles have same material properties as that of geo-synthetic material. In this study, an attempt is made to study the effectiveness of waste plastic bottle fabricated in geo-cell for repair of potholes. For this, geo-cell derived as above is placed at the area of pothole near base course. This is simulated in the laboratory model of $1 \times 1 \times 1$ m pit and plate load test as well as CBR is carried out for pavement performance after repair in terms of settlement and bearing capacity.

Keywords Potholes · Repair techniques · Geo-synthetics · Geo-cells · Plastic waste

1 Introduction

Majority of the roads in India are flexible and are under heavyweight. Further, they are in incredible need of modernization with a specific end goal to deal with the expandable growth of the vehicles. Increase and development of potholes on Indian streets

S. Shah · Y. Alwani · M. Solanki (✉)
Marwadi University, Rajkot 360003, India
e-mail: morvinsolanki14@gmail.com

S. Shah
e-mail: siddharth.shah@marwadieducation.edu.in

still continued from the time of bitumen macadamized road arises. The problem behind these defects of road is climate, weather, wheel load, and workmanship [1, 2]. From few decades, many techniques are followed for the repair and maintenance of such defects such as cementitious and polymers [3–5]. Geo-synthetics, the synthetic polymer product which has become popular from last few decades and manufacturing is also increased. Geo-synthetics have wide range of application in civil engineering such as embankments, separation, retaining structures, reservoir, dams, canals, sediment and erosion control, reinforcement, filtration [6, 7]. Geo-cell are the honeycombed structure made up of high-density polyethylene materials have great capacity of confining the cohesionless soil particularly gravels and has proven versatile in stabilizing slope and increasing the bearing capacity of poor soils beneath footing and pavements [8–11] also it has good performance in dynamic conditions too [12].

On the other hand, plastic bottles are used tremendously for drinking water, cola, oil, and other soft drink, which are only single use and its waste management is a great challenge. Daily approximately 10 tons of plastic bottles are generated in a city like Ahmedabd [13]. In this study, the aim is to re-use the plastic waste bottle and make geo-cell out of it and check its feasibility to act as geo-cell. This has many fold advantages like reduction of plastic (environment friendly), employment (for collecting plastic bottles, cutting, and joining) and Cost-effective (Less price than original geo-cell).

2 Materials

2.1 Plastic Waste Bottle Geo-Cell

The polyethylene (PET) bottles were obtained from the local scrap shop after that it was cut in to three pieces at equal height. The cap portion was not utilized but the middle and bottom portions were joined by the fishnet strips and perforations were made by soldering rod to make it permeable Fig. 1. Thus, a three-dimensional structure with interconnected like honeycomb was prepared as shown in Fig. 2.

Before using the geo-cell derived from such plastic waste in place of traditional geo-cell, it was necessary to check its properties and its behaviour. Therefore, few basic tests like load-carrying capacity, permeability, and its physical properties were tested, Table 1 shows the comparison of the physical properties of both the geo-cells.

Fig. 1 Preparation of geo-cell from plastic bottles (cutting, joining, and perforations)
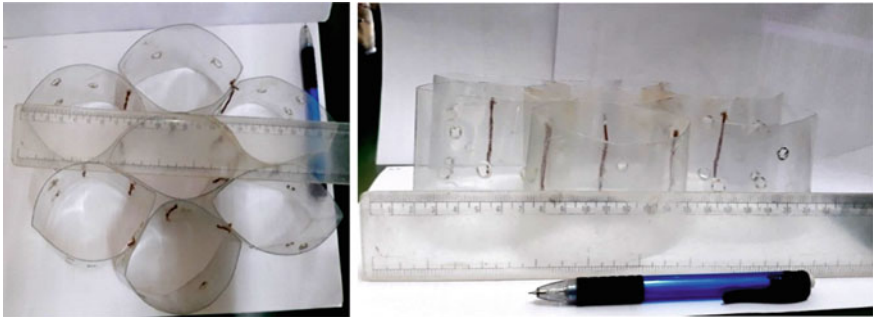
Fig. 2 Sample size of geo-cell

Table 1 Comparison of properties regular geo-cell with geo-cell derived from plastic waste bottles

Properties	Geo-cell	Plastic waste bottles geo-cell
Materials	HDPE	LDPE
Density	930–970 kg/m^3	917–930 kg/m^3
Temperature	90 °C	80 °C
Welded space	712 mm	110 mm
Depth	100 mm	60 mm
Width	3 mm	0.5 mm

2.2 Simple Tests on Geo-Cell Derived from Plastic Waste Bottles

To check the performance, two simple preliminary tests like its compressive strength, sand heap test and permeability were performed to ensure its final use in the experiment.

Test 01 Heap of sand with and without geo-cell. Here, the sand volume was done by freely falling on 24 × 24 cm square section without geo-cell and then it was loaded the height of heap was 20 cm and after and loading of 106.36 kg it was deformed by 7.5 cm as shown in Fig. 3.

The same experiment was repeated but now with geo-cell, and when same load was applied deformation was only 4 cm.

Test 02 Compressive strength of geo-cell. In this, compressive loading-carrying capacity of geo-cell was checked by increasing the loading step by step, approximately 300 kg of load was bearded by such geo-cell without substantial deformation (Fig. 4).

Drainage in geo-cell with sand. In this, only simple drainage test was carried out for the perforated geo-cell, placing geo-cell and filled with soil and water is passed from geo-cell for checking of perforated geo-cell as shown in Fig. 10 (Fig. 5).

Fig. 3 Demonstration of geo-cell with sand

(Side view)   (Top view)

Fig. 4 Static compressive strength test of plastic waste geocell(right-loaded, left specimen)

Fig. 5 Drainage test of geo-cell (left full saturation, right free drainage of water)

3 Experimental Work

After the confidence of the preliminary tests success, the authors have attempted the final testing of the geo-cell derived from the plastic waste bottles.

3.1 CBR Test with and Without Geo-Cell

CBR is the ratio expressed as a percentage of force per unit area required to pass through the soil mass of a standard circular plunger having a diameter of 50 mm at a rate of 1.25 mm/min, which is the ratio required for corresponding penetration in standard materials. This ratio is usually determined to be a penetration depth of 2.5 and 5 mm. When the ratio at 5 mm is always higher than 2.5 mm, the ratio at 5 mm is used. A different type of apparatus is required for this test like CBR Testing machine, cylindrical mould, Collar, Spacer Disc, Compaction Rammer. This test result is taken without geo-cell only for base coarse and reading of 2.5 and 5 penetration was carried out and for aggregate as shown in Fig. 6. Further, the same test was repeated with geo-cell same as above but with geo-cell in base course while filling aggregate as shown in figure.

3.2 Plate Load Test with and Without Geo-Cell

The plate load test was carried on a plate of 300 × 300 mm size having 25 mm thickness. The location and depth test pit (1 m) were selected as per the Layer Criteria: for the 2 MSA traffic with CBR 4%, (Source: IRC:37 (2001) Page No. 23, Pavement Design Catalogue) Granular Sub base = 265 mm, Base Course = 225 mm, Binder Course = 50 mm, wearing Course = 20 mm [14] and then loading platforms were created above which the sand bags were placed. Field CBR machine

Fig. 6 CBR test under performance

with necessary proving ring and dial gauges were taken at the site. The entire setup is shown in Fig. 7. After assembling the sitting load was given and test was started and settlements were observed for each increment of load for an interval of 1, 2.25, 4, 6.25, 9, 16, and 25 min and thereafter at hourly intervals, when the settlement is less than to the nearest 0.02 mm then the loading was increased. The rutting behaviour was observed the test was stopped because of failure in base course, and this test was carried out two times first without geo-cell and second with geo-cell (Fig. 8).

Fig. 7 Plate load test using geo-cell

Fig. 8 Closed views of geo-cell and plates for plate load test

4   Results and Discussions

As discussed earlier in this section, the results of CBR and plate load tests are discussed. Tables 2 and 3 show the CBR values of without and with geo-cell, it is clear that CBR value of the aggregates with geo-cell has increased from 8.5 to 9.6, thus increase of around 10% is found this may be due to the confinement of the geo-cell. Thus, we can say that geo-cell is showing its effect and plastic waste bottle geo-cell is showing its action perfectly as geo-cell.

Additionally, Fig. 9 is showing the results of the plate load test carried out in the field. From the figure, it is evident that, when geo-cell is used the load-carrying capacity has increased from the 700 to 1200 kg for sudden failure where as the

Table 2 When geo-cell is not added

CBR observation sheet (without geo-cell)				
Penetration (mm)	Proving Ring reading	Factor (kg)	Load (kg)	CBR value
2.5	102	1.199	112.29	8.1
5	146	1.199	175.0	8.5

Table 3 When geo-cell is added

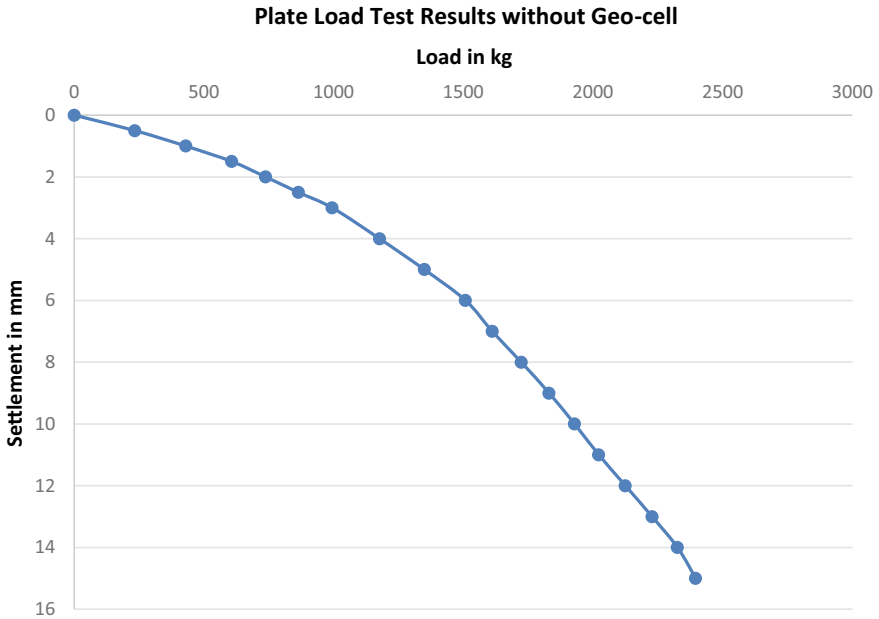| CBR observation sheet (with geo-cell)				
Penetration (mm)	Pro. ring reading	Factor (kg)	Load (kg)	CBR value
2.5	112	1.199	134.29	9.8
5	165	1.199	197.84	9.6

Plate Load Test Results without Geo-cell

Fig. 9 Plate load test results without geo-cell

final load is 2157–2559 kg. Therefore, one can predict that the geo-cell's confining effect is mobilized and load-carrying capacity of the aggregate has increased by approximately 40% (Fig. 10).

5 Conclusions

Based on the experiments and analysis, the following broad conclusions are drawn:

1. Geo-cell derived from the plastic waste bottle has potential to act as HDPE geo-cell available commercially in the market.
2. The performance of geo-cell derived from the plastic waste bottle is increasing the CBR value by 10% and bearing capacity by 40%, approximately
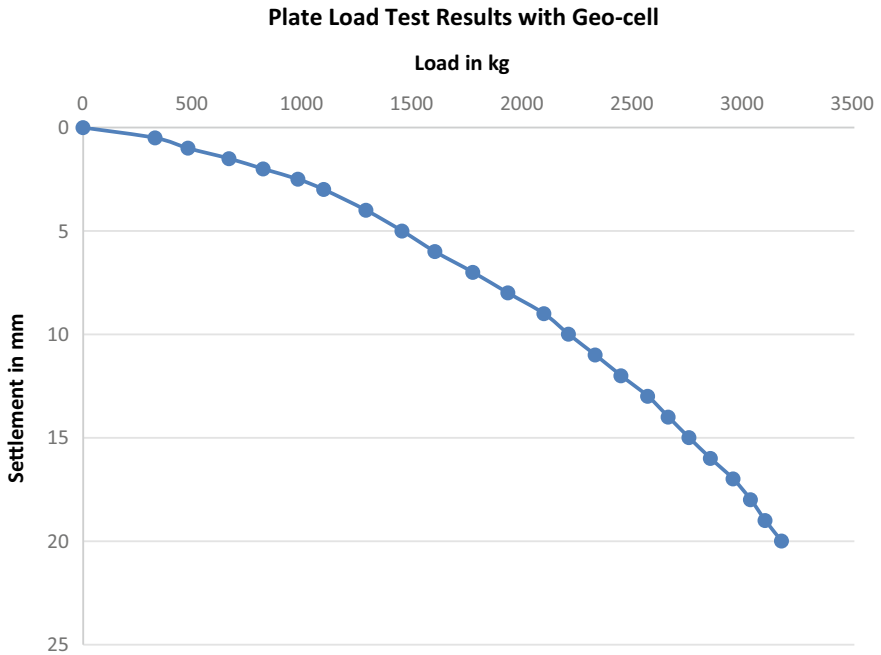
Plate Load Test Results with Geo-cell

Fig. 10   Plate load test results with geo-cell

References

1. Adlinge, S.S., Gupta, A.K.: present journal on "Pavement Deterioration and its Causes". IOSR J. Mech. Civil Eng. (IOSR-JMCE) pp. 09–15 ISSN: 2278-1684 (2015)
2. Kumar, P., Gupta, A.: Case Studies on Failure of Bituminous Pavements Compendium of Papers from the First International Conference on Pavement Preservation, Chap. 7(52), pp. 505–518 (2008)
3. Obaidi, H., Garcia, A.: A Fast Pothole Repair Method Using Asphalt Tiles and Induction Heating. Department of Civil Engineering, University of Nottingham, UK
4. Liu, M., Han, S., Han, X., Qi, X., Dong, S .: Microcapsule and polymer rein-forcement techniques developed asphalt for use of pothole repairs in winter and rainy sea-sons. Cold Reg. Sci. Technol. **167**, 102865 (2019)
5. Singh Kandhal, P.: A simple and effective method of repairing potholes in India. IRC, vol. 69-3, paper No. 544, October–December 2008
6. Kumar Shukla, S.: Introduction to geosynthetics and their applications. ITCIGA-2015
7. Yadav, M.: Application of geocells in reinforcement of soil: a review **1**(5) (2014) ISSN: 2349-8404; Online ISSN: 2349-879X

8. Moghaddas, S.N.: Performance of circular footings on sand by use of multiple-geocell or -planar geotextile reinforcing layers. Soils Found. **56**, 984–997 (2016)
9. Moghaddas, S.N.: Tafreshietal, "Repeated load response of soil reinforced by two layer of geocell." Proc. Earth Planetary Sci. **15**, 99–104 (2015)
10. Davarifardetal, S.: Plate load test of multi-layered geocell reinforced bed considering embedment depth of footing. Proc. Earth Planetary Sci. **15**, 105–110 (2015)
11. Kumar, V., SireeshSaride, V.: Rutting behavior of geocell reinforced base layer overlying weak sand subgrades. Proc. Eng. **143**, 1409–1416 (2016)
12. Pokhareletal, S.K. : Experimental evaluation of geocell-reinforced bases under repeated loading. Int. J. Pavement Res. Technol. **11**, 114–127 (2018)
13. CPCB Annual Report 2016–17, Regional Directorate, Page 18
14. IRC 37: 2001, Guidelines for the Design of Flexible Pavement, 2nd Revision

Effect of Low-Frequency AC Supply and Purging Solution on Remediation of Nickel-Contaminated Soil Using Electrokinetics

Lalit S. Thakur, Nirali B. Hasilkar, and Avani R. Umatt

Abstract The complete earth is prone to natural hazards, cannot be prevented, but through an understanding of the earth condition and the processes which could culminate in damage to life and property, it is possible to minimize the damage through proper disaster management measures. Man-made hazards have today taken over natural hazards in terms of the loss of life and the long term effect on mankind and the ecosystem on the whole. Reddy et al. reported on laboratory electrokinetic experiments that were conducted on different soils, namely, commercial kaolin and Na-montmorillonite as well as a field-derived glacial till. The presented work is an attempt to study effect of various variables, i.e. type of anodic and cathodic purging solution, periodic supply as well as improvement of soil with application of low-frequency AC supply instead of DC supply. The complete study has been carried out on models having different length with the Nickel (Ni(II)) & commercially available Kaolinite being artificially spiked using Nickel Chloride salt. This study on feasibility of using different extracting solution at various use of 0.1 M Ethylenediamine tetra-acetic acid (EDTA) better as compared to 1 M Sodium Nitrate. The Nickel removal efficiency of organic acid such as citric acid was found to be low as compared to other solution, the best removal being achieved with 1 M NaCl.

Keywords Reactor size · Low-frequency AC supply · Electrokinetics · Remediation of nickel contaminated soil

1   Introduction

There are many remediation technologies available for treating contaminated soils and groundwater that are classified as either ex-situ or in-situ techniques [5]. Ex-situ techniques treat the contaminated soil and/or groundwater after it has been removed

L. S. Thakur (✉) · N. B. Hasilkar
Civil Engineering Department, BITS Edu Campus, Vadodara 391240, India
e-mail: lalitthakur.cv@bitseducampus.ac.in

A. R. Umatt
Department of Health, Life & Applied Sciences, TLSU, Vadodara 390010, India

Fig. 1 Process of electrokinetic remediation
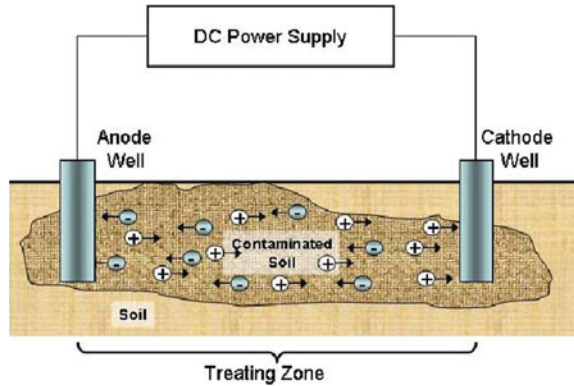
from the subsurface, whereas in-situ techniques treat the soil and/or groundwater within the subsurface itself.

Electrokinetics is a process that has shown a great potential for remediating heavy metal contaminated soils, including low permeable clays and/or heterogeneous soils (Fig. 1). Electrokinetic remediation technique uses the combined effect of electric, chemical and hydraulic potential for remediation of problematic/contaminated soil. In this method, a low DC voltage is applied to soil through carbon/sacrificial electrodes and the metals are extracted from contaminated soil in aqueous form. This method is one of the most promising remediation processes; it also has low operational cost and potential applicability to a wide range of contaminant types.

2 Literature Survey

The interaction between the soil system and contaminants is of course dependent on soil conditions other than organic matter content. For example, the solubility of metals can vary with pH—lead solubility increases as pH drops [1].

Generally, clay has a net negative charge on its surface. This negative surface electric charge of a clay particle is due to the presence of isomorphous substitution and broken structure. The negative charge on the clay surface is balanced by excess positive charge distributed in the fluid zone adjacent to the clay surface. This distribution adjacent to the clay surface is called the diffuse layer. A diagram of the effect of these charges around an idealized spherical particle is shown in Fig. 2 and a qualitative graph of the variation of electrical potential with distance from particle surface is presented in Fig. 2 along with the idealized distribution of charge [3].

Electroosmosis is the transport of pore fluid in soils under the influence of an electric field. Several theories have been formulated to describe the flow of water by electroosmosis. The most widely accepted model is the Helmholtz Smoluchowski (H–S) theory. According to this theory, the net water flow results when the excess positive charge is transported to the cathode [4]. Characteristics of the soil, which
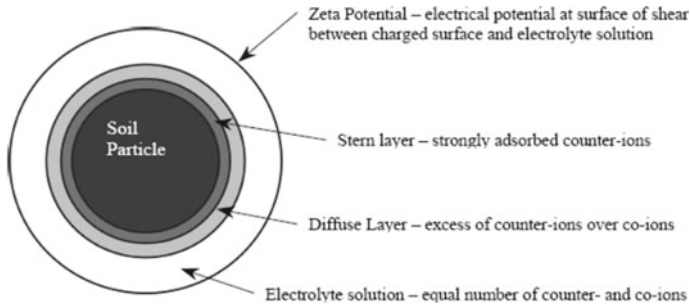
Fig. 2 Idealized representation of water around a clay particle [3]

influence kinetics of contaminant removal, include adsorption, ion exchange, and buffering capacity [2, 6]. Soil contaminant interaction is especially high in fine-grained soils.

3 Material Characteristics

The present work is carried out on Kaolinite sieved through 425 μ sieve and then tested for basic geotechnical properties and found to be CH type, as per IS classification system. Geotechnical properties of Kaolinite were found out using standard methods prescribed in relevant IS codes (IS 2720), and are summarized in Table 1. This soil is dried and then mixed with 1.012 gm of Nickel Chloride/kg soil with water content kept equivalent to liquid limit. The mixed soil was kept to mature for 1 month before filling them in the models. Model for the study is prepared using PVC pipes of pressure capacity 20 kg/cm^2, with flange end connections. For the entire set of tests, 0.1 M Ethylene Diamine Tetra-Acetic Acid solution is used at cathode and 1 M

Table 1 Geotechnical properties of virgin soil

Property	Value
Liquid limit (%)	73.8
Plastic limit (%)	33.2
Plasticity index (%)	40.6
Shrinkage limit (%)	24.0
Specific gravity	2.3
Maximum dry density (gm/cc)	1.38
Optimum moisture content (%)	32.3
Free swell (%)	96
Cohesion, c (kg/cm^2)	1.12
Angle of internal friction (φ)	3.65

Sodium Chloride solution is used at anode. Voltage applied for all the experiments is kept at 25 V in DC and AC mode.

4 Effect of Periodic Supply

Experiments in this phase were to determine contaminant mass removal by using a periodic voltage application in different combinations, i.e., one day on and one day off, one day on and two days off and two days on and one day off. The applied voltage and purging remains constant during all tests as mentioned above. Other details are as per Table 2.

4.1 One Day On-One Day off

This study is carried out to study the effect of supply period on remediation of contaminated soil keeping the purging solutions as 0.1 M ethylenediamine tetra-acetic acid (EDTA) at cathode and 1 M sodium chloride (NaCl) at anode. Figure 3 shows variation of voltage at anode, middle and cathode compartment along with applied voltage with respect to time. Sudden increase in the voltages is observed subsequent to addition of solutions in the anode and cathode compartments and/or when there was high sacrificial behaviour of electrode at anode. Figure 4 shows variation of current and current density. During electrokinetics, the fluctuation in currents can occur due to different reason. The current drop with the shutting down of the supply and shows a low value the next day when reading are noted down after the supply is restarted. The temperature profile also almost follows the current and voltage patterns drop in temperature on the off days. Figure 5 shows variation of pH of solution at anode and at cathode at the end of every week.

Table 2 Details of different phases of work

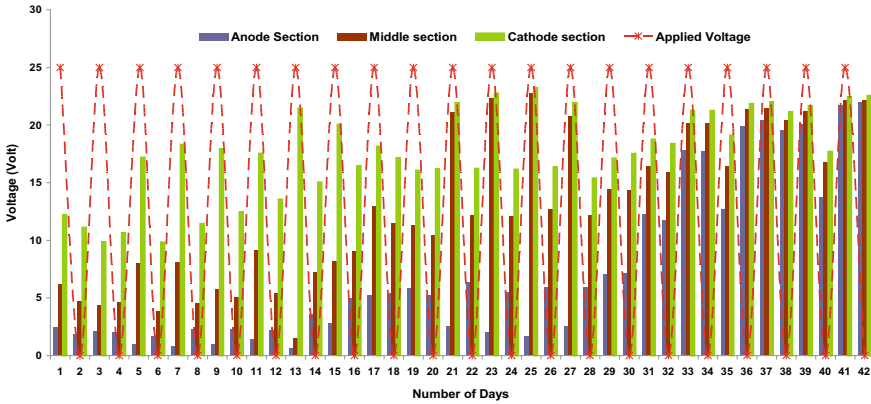| Type of supply	Frequency (Hz)	Duration of supply
Effect of periodic supply		
DC	0	1 day on—1 day off
DC	0	1 day on—2 day off
DC	0	2 day on—1 day off
Effect of low-frequency AC supply		
AC	0.25	Continuous
AC	0.50	Continuous
AC	0.75	Continuous
AC	1.00	Continuous

Fig. 3 Variation of voltage at different sections along length of sample and applied voltage with time for one day on and one day off model [7]
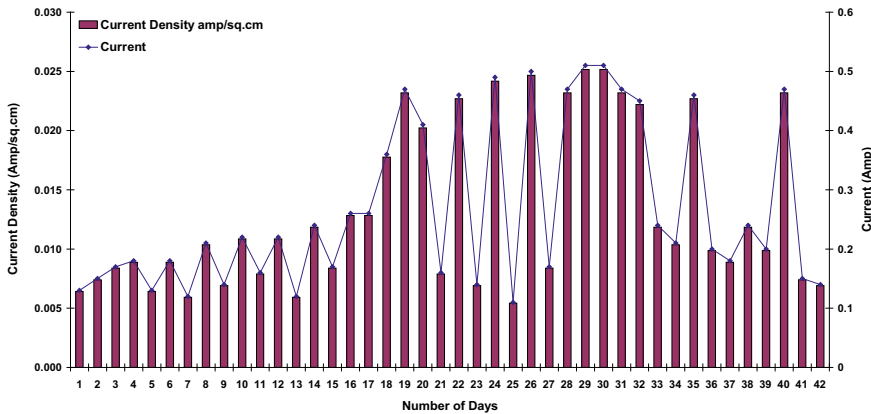
Fig. 4 Variation of current and current density with respect to time for one day on and one day off model

4.2 One Day On-Two Days off

This is the second variation used for study where in the shutoff time was double of the supply on time. Figure 6 shows variation of voltage near anode, cathode and at middle section along with applied voltage with respect to time. Sudden increase in the voltages is observed subsequent to addition of solutions in the anode and cathode compartments, the current also drops to zero in the off time, the second day shows a current reading since it was taken once the supply was switched on once again. Figure 7 shows variation of current and current density. Initially, when the voltage gradient was first applied, the current is low and starts build up slowly because it takes time for the solution migrates into the electrode reservoirs and for the salts and/or

Fig. 5 Variation of temperature and ambient temperature with time for one day on and one day off model

Fig. 6 Variation of voltage at different sections along length of sample and applied voltage with time for one day on and two days off model

contaminants to dissolve. The variation continues showing no stabilizing trend due to the supply off period. Figure 8 shows variation of pH of solution at anode and at cathode at the end of every week.

4.3 Two Days On-One Day off

This is the third variation wherein the supply on time was double as compared to the supply off time. Figure 9 shows variation of voltage at anode, middle and
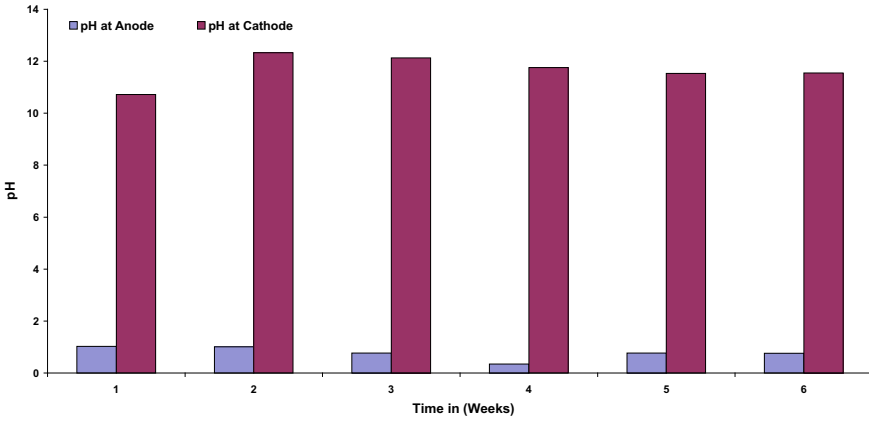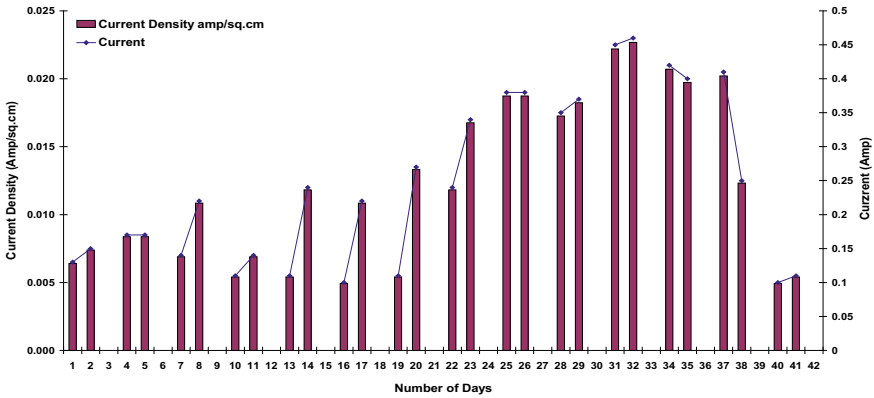
Fig. 7 Variation of temperature and ambient temperature with time for one day on and two days off model
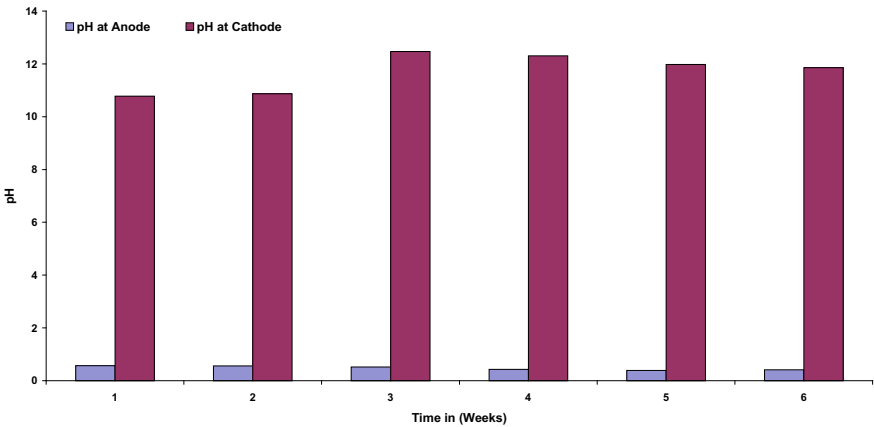
Fig. 8 Variation of pH at every week for one day on and two days off model

cathode compartment along with applied voltage with respect to time. Figure 10 shows variation of current and current density. During electrokinetics, the fluctuation in currents can occur due to different reason. The graphs follow the trend with the supply on time, there being a decreases in the current, current density, and voltage at various sections as well as temperature during this period. Figure 11 shows variation of pH of solution at anode and at cathode at the end of every week, which shows no appreciable change.

After completion of the experiment three soil samples were collected near anode, mid-section and near cathode from all the models and then tested on EDS. Figure 12 shows concentration of Nickel(II) after electrokinetic remediation and Fig. 13 shows the percentage removal with respect to the original concentration of 250 mg/kg.
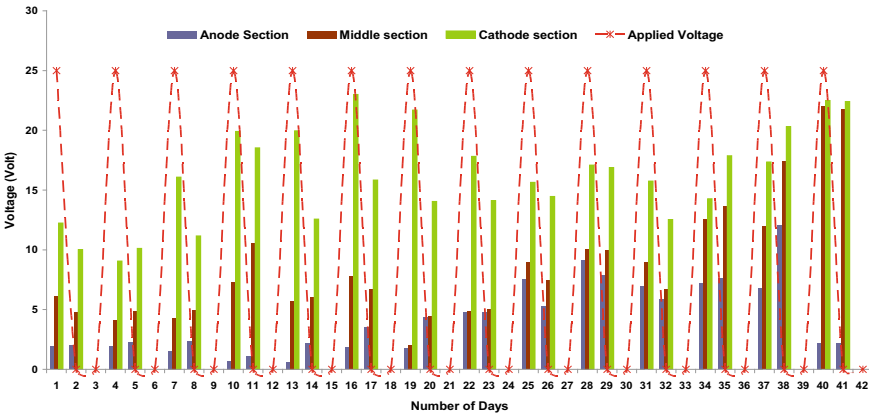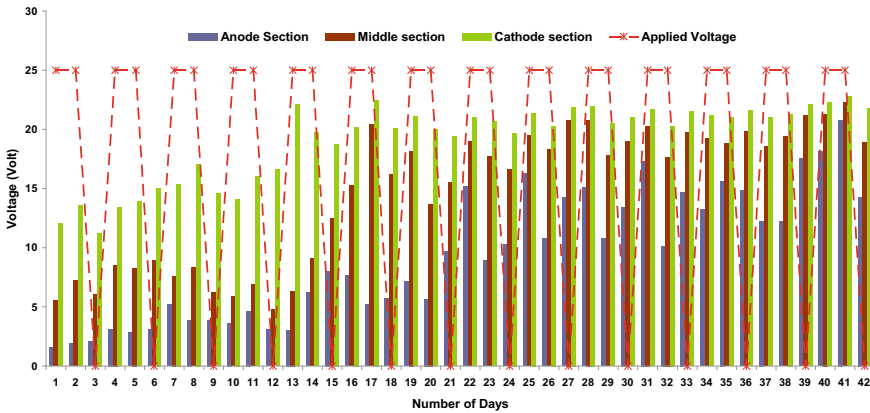
Fig. 9 Variation of voltage at different sections along length of sample and applied voltage with time for two days on and one day off model

Research has shown that the applied electric potential produces complex physical, chemical, and electrochemical changes within clay soils that affect mass transfer and overall efficiency. From the graphs, it can be concluded that greater removal of Nickel is achieved during two days on-one day off supply as compared to one day on-one day off and one day on-two days off periodic supply.

5 Effect of Low-Frequency AC Supply

For this phase, the required information is as per Table 2, four different frequency of sinusoidal waveform, i.e. 0.25, 0.5, 0.75 and 1 Hz has been used in the four models to study the effect of low-frequency AC supply. Purging solution used is same as 1st Phase.

5.1 Frequency = 0.25 Hz

Sinusoidal waveform of 0.25 Hz frequency was set in AC supply instead of DC supply. Figure 14 shows effect of temperature near anode and cathode and at middle section with ambient temperature with time. During experiment, at an interval of one week, samples from both anode and cathode compartments were collected, filtered and tested on pH value. Figure 15 shows variation of pH of solution at anode and at cathode at the end of every week. Reading for current could not be taken since the variation was too fast to be recorded. Since it is sinusoidal waveform, the voltage cannot be also recorded.
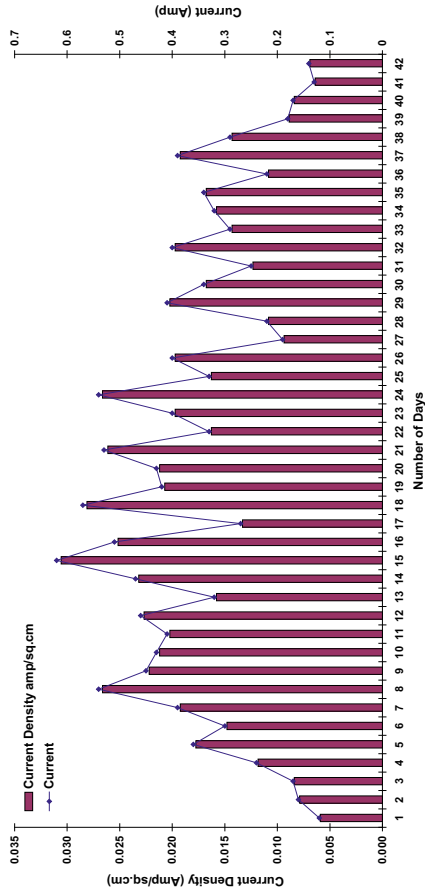
Fig. 10 Variation of current and current density with respect to time for two days on and one day off model
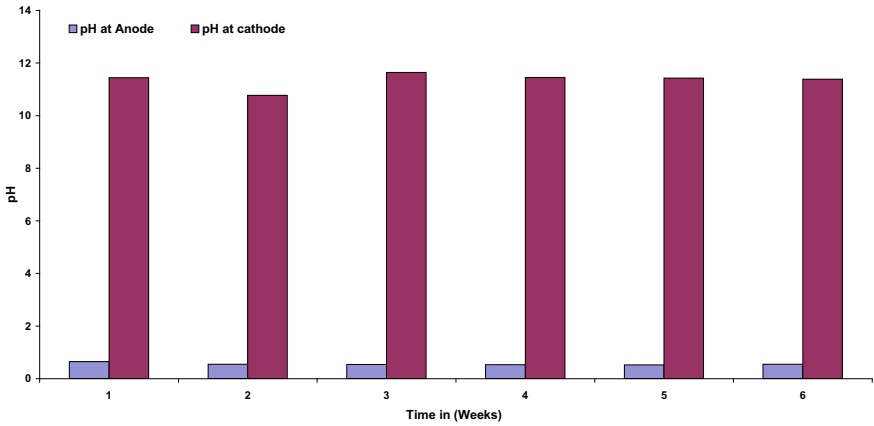
Fig. 11 Variation of pH at every week for two days on and one day off model
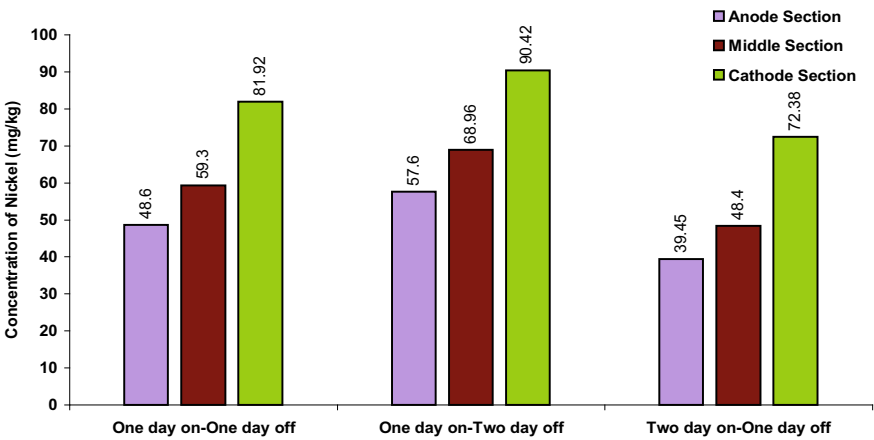
Fig. 12 Concentration of metal after electrokinetic remediation

Fig. 13 Total percentage removal of nickel after electrokinetic remediation

One day on-One day off, **74.69%**

One day on-Two day off, **71.07%**

Two day on-One day off, **78.64%**
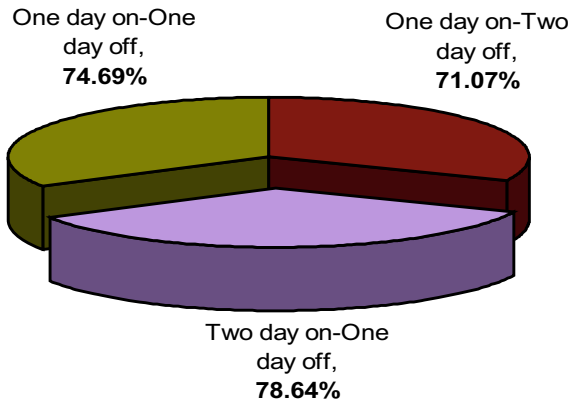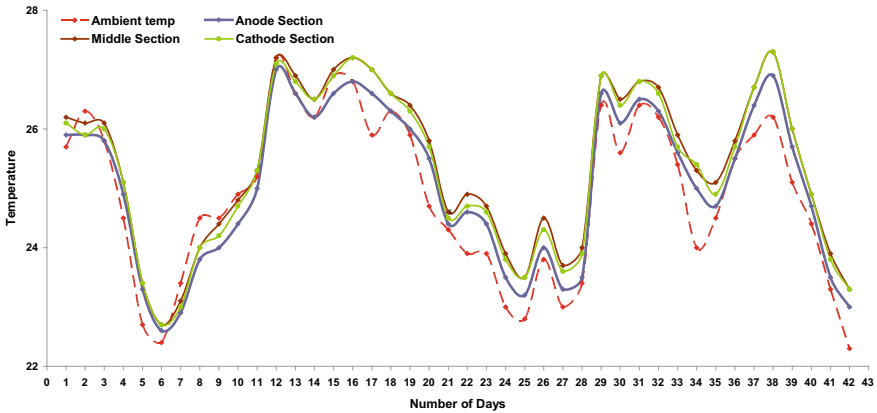
Fig. 14 Variation of temperature and ambient temperature with time for 0.25 Hz frequency
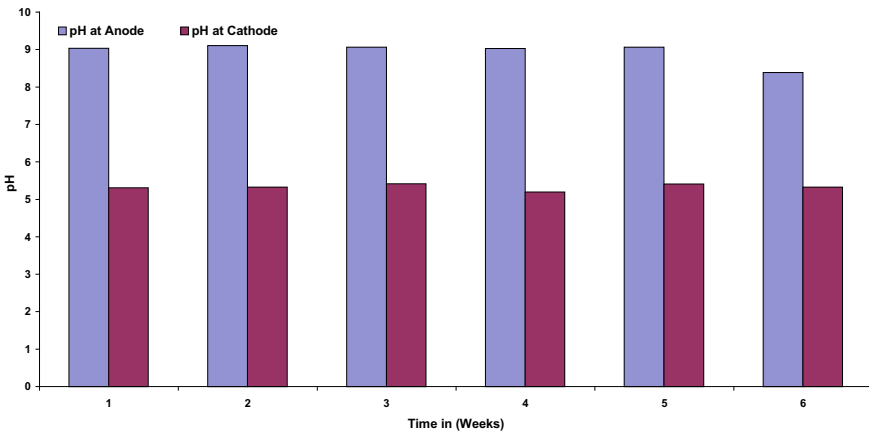
Fig. 15 Variation of pH at every week for 0.25 Hz frequency

5.2　Frequency = 0.5 Hz

Sinusoidal waveform of 0.5 Hz frequency was set in AC supply next for the study. Figure 16 shows effect of temperature near anode and cathode and at middle section with ambient temperature with time. Figure 17 shows variation of pH of solution at anode and at cathode at the end of every week. The low variation in pH shows that the movement of particle is effected due to change in anode and cathode, respectively, due to AC supply.
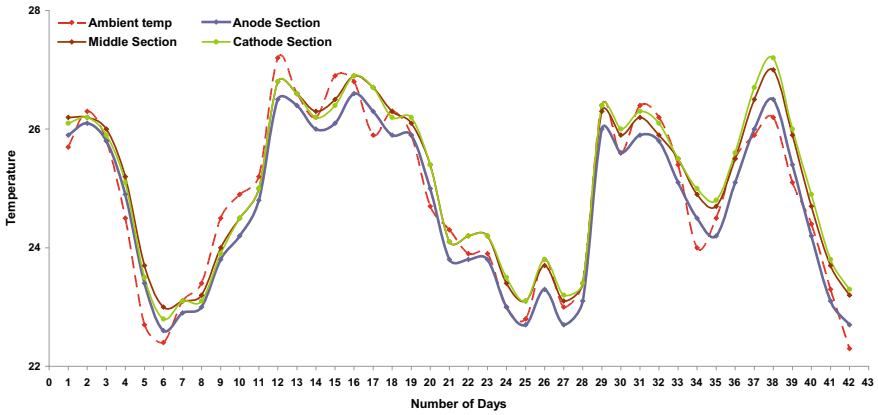
Fig. 16 Variation of temperature and ambient temperature with time for 0.5 Hz frequency
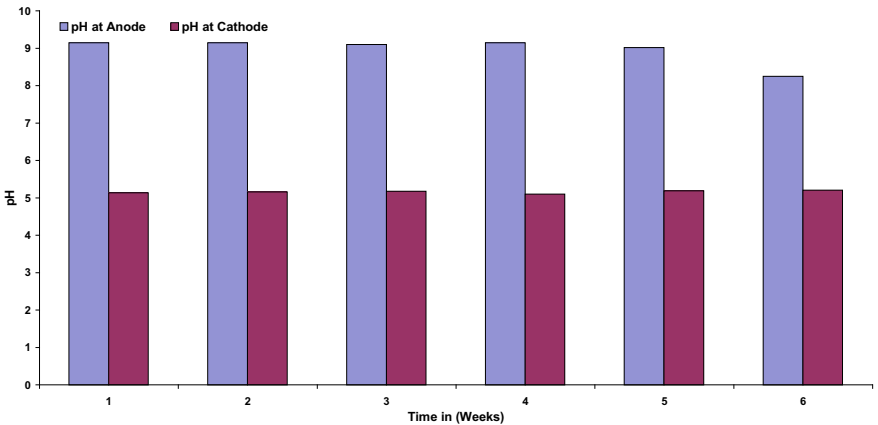
Fig. 17 Variation of pH at every week for 0.5 Hz frequency

5.3   *Frequency = 0.75 Hz*

Sinusoidal waveform of 0.75 Hz frequency was set in AC supply after 0.5 Hz further carrying on the study further. Figure 18 shows effect of temperature near anode and cathode and at middle section with ambient temperature with time. Figure 19 shows variation of pH of solution at anode and at cathode at the end of every week. The pH follows the same trend showing no appreciable change in the values, but temperature variation shows appreciable change of 4–5 °C giving an idea that some flow of ions does definitely occur.
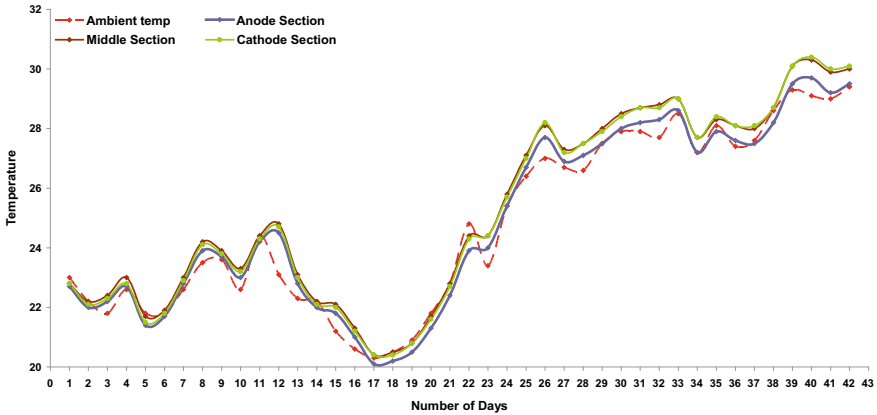
Fig. 18 Variation of temperature and ambient temperature with time for 0.75 Hz frequency
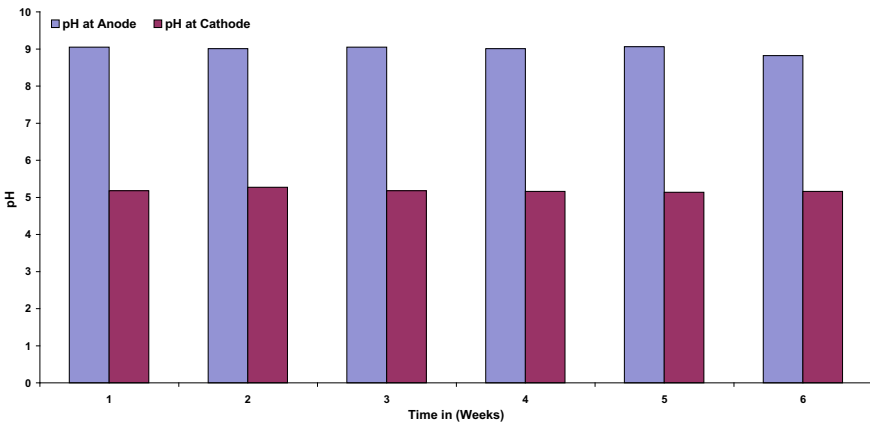
Fig. 19 Variation of pH at every week for 0.75 Hz frequency

5.4 Frequency = 1.0 Hz

Sinusoidal waveform of 1.0 Hz frequency was set in AC supply instead of DC supply. Figure 20 shows effect of temperature near anode and cathode and at middle section with ambient temperature with time. Figure 21 shows variation of pH of solution at anode and at cathode at the end of every week.

After completion of the experiment, three soil samples were collected near anode, mid-section and near cathode from each model and then tested on EDS. Figure 22 shows concentration of Nickel(II) after electrokinetic remediation. Nickel concentrations were low in the sections closer to the anode and higher near the cathode.
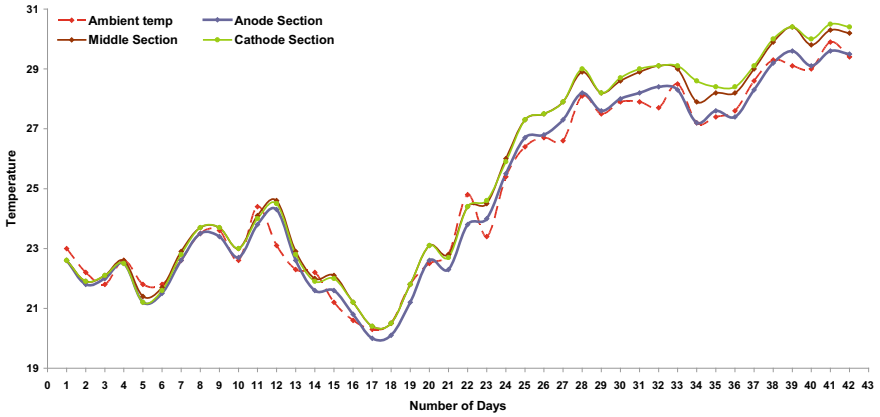
Fig. 20 Variation of temperature and ambient temperature with time for 1 Hz frequency
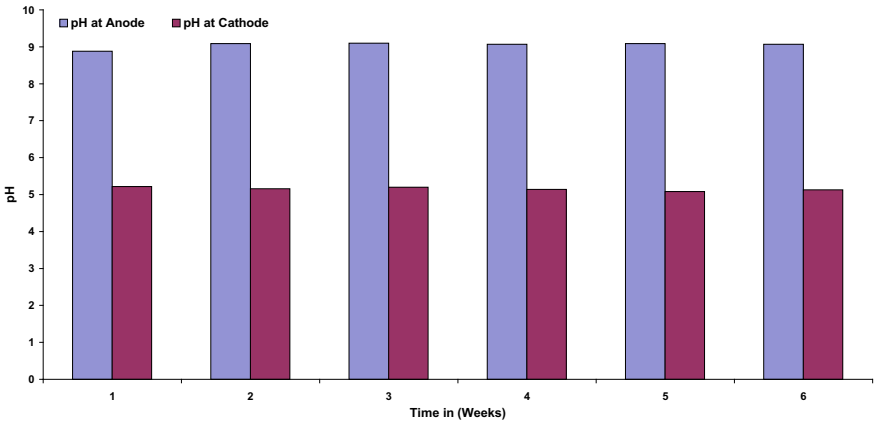
Fig. 21 Variation of pH at every week for 1 Hz frequency

Figure 23 shows the highest percentage removal of nickel when used 0.25 Hz frequency AC supply.

The remediation using low-frequency AC supply is relatively small as compared to the DC supply. When using an AC supply even at a low frequency as low as 0.25 Hz there is change in anode and cathode supply once every four seconds which affects and hinders the movement of ions, thereby the electrical gradient not helping in the movement of the metal ions. This same effect does not allow electromigration and/or migration potential to develop fully neither do other process work as efficiently as with DC supply. AC supply also does not allow the water to break up as speedily as in DC supply also hindering the electroosmosis process which helps in keeping a balance of the pH at the anode and cathode.
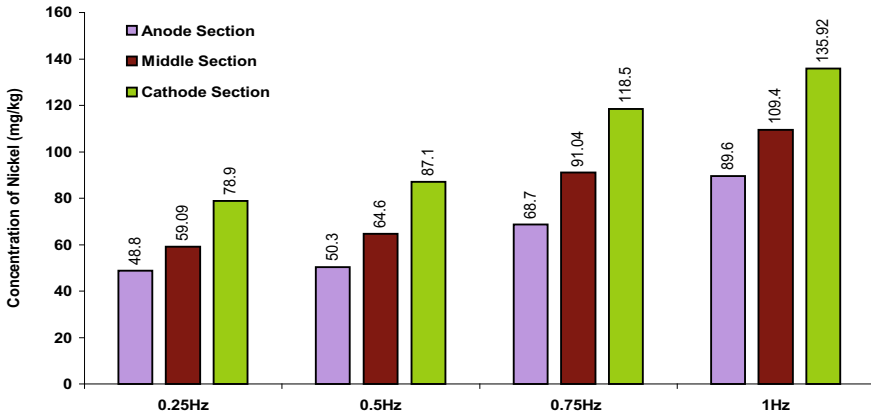
Fig. 22 Concentration Of metal after electrokinetic remediation

**Fig. 23** Total percentage removal of nickel after electrokinetics remediation using low frequency AC supply
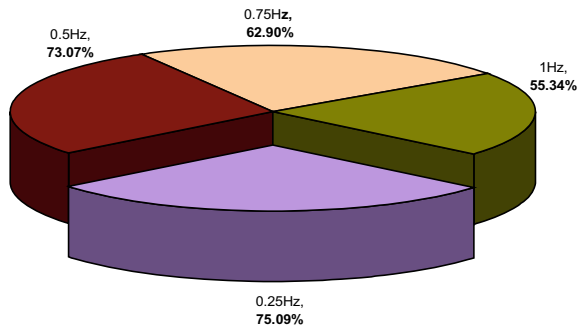
6   Conclusions

The following conclusions are deduced from the experimental results:

- It can be concluded that greater removal of Nickel is achieved during two days on-one day off supply as compared to one day on-one day off and one day on-two days off periodic supply. The applied electric potential produces complex physical, chemical, and electrochemical changes within clay soils that affect mass transfer and overall efficiency

- The low-frequency AC supply at 0.25 Hz gives a percentage removal of 75% only, since an AC supply even at a low frequency of 0.25 Hz has change in positive and negative amplitude once every four seconds which affects and hinders movement of ions. This effect also does not allow electromigration and/or migration potential to develop fully; neither do other processes work as efficiently. It also does not allow the water to break up as speedily as with DC supply, hindering the

electroosmosis process which helps in keeping a balance of the pH at the anode and cathode.

- The above results can be used for treating grounds contaminated by various heavy metals caused due to spilling of waste or untreated disposal of plating waste. As opposed to the traditional electrokinetics which uses DC current use of AC supply is easier to work with. The use of AC current reduces the operational hazards on the field. The use of AC current gives an added advantage of breaking of the pH and ion barriers formed in the soil when using DC supply.
- Application of intermittent supply, i.e. periodic supply has an added advantage of allowing the reversing of the created pH barrier which in DC supply becomes a major drawback in increasing the removal percentage. It gives an advantage of reducing the energy consumption without major decrement in removal percentage.

References

1. Alshawabkeh, A.N., Açar, Y.B.: Electrokinetic remediation II: theoretical model. ASCE J. Geotech. Eng. pp. 186–196 (1996)
2. Grim, R.E.: Clay mineralogy, McGraw-Hill, New York (1968)
3. Harbottle, M.J.: The use of electrokinetics to enhance the degradation of organic contaminants (2003)
4. Probstein, R.F., Hicks, R.E.: Removal of contaminants from soils by electric fields pp. 498–503 (1993)
5. Reddy, K.R., Chinthmreddy, S.: Electrokinetic remediation of heavy metal contaminated soils under reducing environments. Waste Manage. **19**(4), 269–282 (1999)
6. Sposito, G.: The Surface Chemistry of Soils. Oxford University Press, New York (1984)
7. Thakur, L.S., Umatt, A.R., et al.: Electrokinetic grouting for soft soil strengthening: effect of model size, supply frequency, reactant type and its concentration. In: International Congress of Environmental Research, SVNIT, Surat (2011)

The Effect of Water Table Depth on Bearing Capacity of Randomly Distributed Waste Tyre Rubber Fibre Reinforced Clayey Soil

P. Venkateswarlu ⓘ**, M. Upendra, Mohit Mistry** ⓘ**, C. H. Solanki** ⓘ**, and S. K. Shukla** ⓘ

Abstract The bearing capacity (BC) of footing is considerably governed by soil settlement. In practice, the BC of soil can be improved by reinforcing the soil. The laboratory model tests were performed to investigate the effect of water table depth (WTD) on BC of reinforced soil. Randomly distributed shredded waste tyre rubber fibre (length-19 mm, width-4.5 mm) of 0.75% by dry weight of soil as reinforcement. The circular moulds (height-250 mm, diameter-300 mm) were used to prepare the test samples. A shallow depth, surface loading, smooth base mild steel circular footing (diameter (B)-75 mm, height-60 mm) was used in the study. The WTD maintained at different positions, where the ratio of depth of water table below the base (b) to the base width of the footing (B) is 0, 1, and 2 for both unreinforced and reinforced clayey soil. The samples were kept 96 h for soaking. Tri-axial test loading frame was used to apply compressive load at a strain rate of 1.25 mm/min. The improvements in bearing capacity of reinforced soil over un-reinforced soil are 33% without water table effect and 28%, 23%, 20% with water table effect at b/B ratios are 0, 1, 2, respectively. The WTD greatly decreases the BC. The BC of reinforced soil is greater than that of unreinforced soil for all b/B ratios.

P. Venkateswarlu (✉)
Civil Engineering Department, IIT Delhi, New Delhi 110016, India
e-mail: pvenkateswarlu95@gmail.com

M. Upendra · M. Mistry · C. H. Solanki
Applied Mechanics Department, SVNIT-Surat, Surat 395007, India
e-mail: upendarjntuk@gmail.com

M. Mistry
e-mail: mohit.aryan1@gmail.com

C. H. Solanki
e-mail: chandresh1968@yahoo.co.in

S. K. Shukla
Discipline of Civil and Environmental Engineering, School of Engineering, Edith Cowan University, Joondalup, Perth, WA 6027, Australia
e-mail: s.shukla@ecu.edu.au

1   Introduction

The non-biodegradable tyre fibres can take long time to decompose completely and causes the environmental problems. The method of disposal by landfilling is not applicable due to the low density of the material causes the occupation of large volume. Every year millions of tyres were discarded, thrown away, or buried all over the world. Using waste tyres in the form of shreds in Civil Engineering projects is a promising method of recycling this waste material [1]. In 2011, 7.8% of scrap tyres were utilized in various Civil Engineering projects as reinforcement [2].

Reinforcement introduced to the soil or similar materials to improve engineering properties, e.g. strength, stiffness, permeability, compressibility, etc. [3]. Reinforcement is necessary in soils where chances of high erosion (soils with high sand and silt content) and the areas with soft soils (expansive soils) [4]. Soil erosion is due to physical movement of the soil particles caused by the wind, water, ice, animals, and human activities are required reinforcement [5]. Expansive soils, foundations damage to highways, bridges and buildings due to volume change are required improvement. Both cohesive and non-cohesive soils required reinforcement dealing with the different problems at a given site. The present study conducted on expansive soil with waste tyre rubber fibres as reinforcement elements. Kolay et al. (2013) investigated the improvement in the bearing capacity of silty clay soil with thin sand layer on top and placing geogrids at different depths, concluded that the bearing capacity increases significantly with the increased number of geogrid layers [6]. Soil reinforced with optimum percentage of treated fibres at various H/B ratios of 0.2, 0.4, 0.6, 0.8, up to 2 [7]. The reinforcement of highly compressible clayey soil with randomly distributed fibres caused an increase in the ultimate bearing capacity and decrease in settlement at the ultimate load [8]. In this paper, the effect of water table depth on bearing capacity of tyre fibre reinforced expansive soil was studied experimentally.

2   Materials

2.1   Clay

The present investigations have been made on the expansive (clayey) soil obtained from the deposits of "Vesu" area, Surat, Gujarat, India. The index properties of the soil were determined as per the IS test procedures [9–14]. The soil is classified as the high plasticity (CH) soil according to the IS Soil Classification [15]. The index properties of soil were presented in Table 1.

Table 1 Physical and mechanical properties of soil

Soil properties	Values
Specific gravity	2.56
Grain size analysis	
Gravel (%)	0
Sand (%)	10
Silt (%)	64
Clay (%)	26
Consistency limits	
Liquid limit (%)	64.45
Plastic limit (%)	30.66
Shrinkage limit (%)	10.41
Volumetric shrinkage limit (%)	57.98
Plasticity index	33.78
IS classification	CH
Differential free swell index (%)	70.35
Compaction study	
Optimum mixing moisture content (%)	23.39
Maximum dry unit weight (kN/m^3)	15
Unconfined compressive strength (kN/m^2)	114.25
Cohesion (kN/m^2)	57.12

2.2 Tyre Fibres

The waste tyre rubber fibres (WTRFs) were collected from "National Precured Retreaders" located at NH No. 8 nearby Navsari. As the WTRFs had various lengths and diameters, it was not possible to define a specific aspect ratio. For the simplification, it was divided into three groups using conventional sieve analysis procedure (retained on 4.75 mm IS sieve, passing through 4.75 mm IS sieve and retained on 2 mm IS sieve & passing through 2 mm IS sieve). The fibres retained on the 4.75 mm sieve size were used in the study. Type c fibres were shown in Fig. 1.

3 Methodology

3.1 Test Moulds

The GI sheet of 1.21 mm (18 gauge) thickness was used in the study to prepare the moulds. The sheet was cut into three rectangular pieces of each sheet width is 300 mm, which is a height of mould and length is 880 mm, which is a perimeter of

(a) Fiber width (diameter)　　(b) Fiber width (diameter)　　(c) Fiber width (diameter)

(<2mm)　　　　　　　　　(2mm-4.75mm)　　　　　　　(>4.75mm)
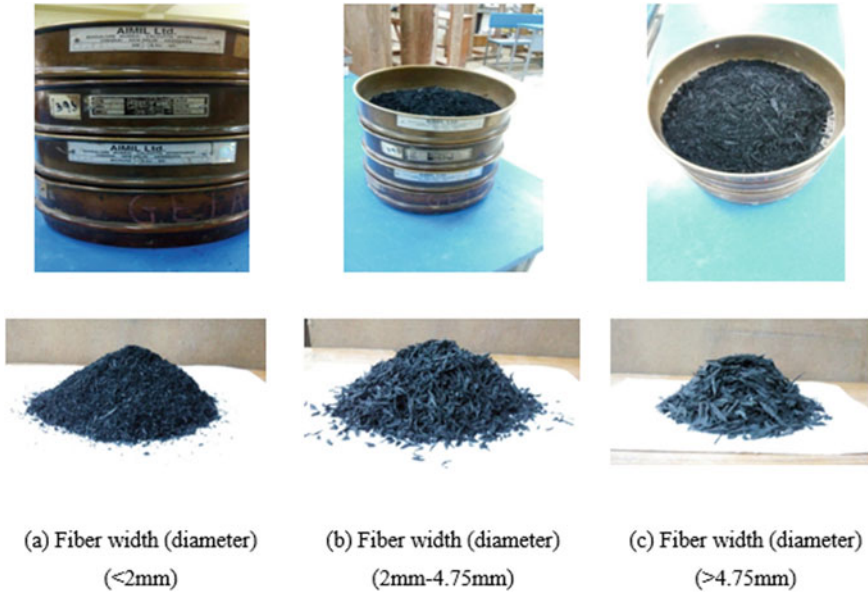
Fig. 1 Step-by-step procedure of seiving of fibres for the classification

the mould. The sheets were drilled with a hole of 10 mm at a horizontal and vertical spacing of 20 mm and 30 mm centre to centre to allow the passage of water through holes into the soil sample. For the first, second, third, and fourth moulds, the holes are up to the height of 250 mm 170 mm, 50 mm, and 0 mm from the bottom. The holes were made up to different heights to maintain water table depth at different heights. Now, the rectangular sheet of each case rolled along the length direction and the ends were welded to make cylindrical mould. Proper care has been taken while making markings and welding. The cylindrical moulds diameter is 280 mm and height is 300 mm. Figure 2. Shows the process of preparation of the moulds.

3.2 Test Footing

The circular footing was used in the study made up of steel with a diameter of 76.2 mm and height is 65 mm. Smooth surface footing condition is used in the study. Top surface of the footing is grooved about a diameter of 15 mm and depth is 5 mm to transfer load to the footing in a point load condition. Figure 3a–c shows the physical model of the footing.
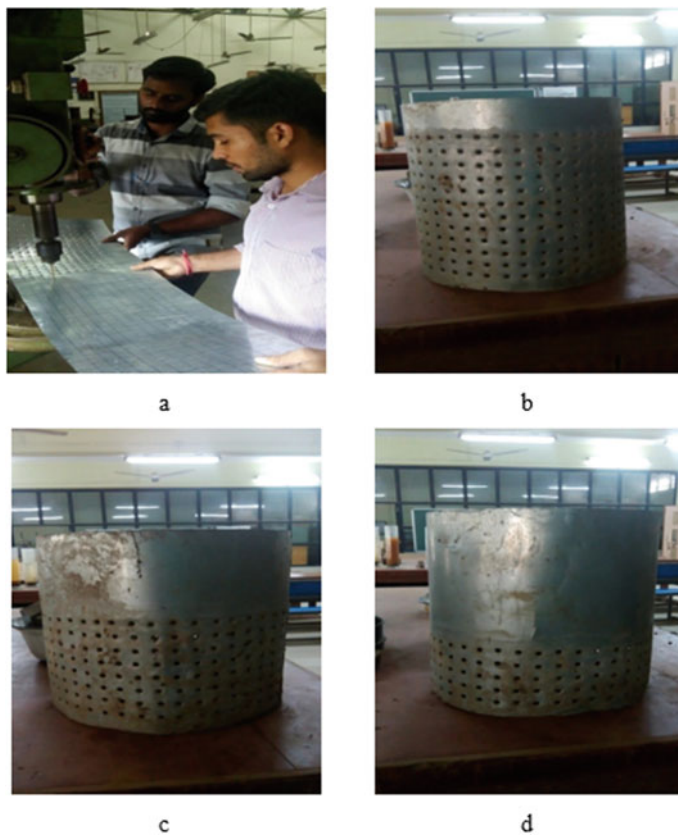
Fig. 2 **a** Placing of holes in both the directions, **b** b/D = 0 mould, **c** b/D = 1 mould, **d** b/D = 2 mould
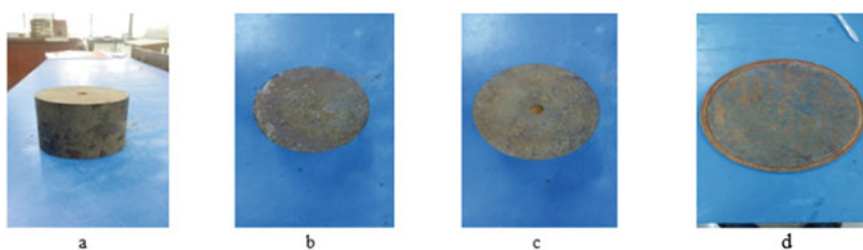
Fig. 3 Footing geometry **a** Circular steel footing **b** Smooth base footing, **c** grove at top to apply point load to the footing, **d** Base plate

3.3   Base Plate

The base plate of 300 mm diameter and 10 mm thickness was prepared to place at the bottom of the sample during the test. Base plate is made up of steel as shown in Fig. 3d.

4   Sample Preparation

The oven-dried soil sample around 23 kg, optimum fibre content 0.75% and optimum mixing moisture content (OMMC) were used to prepare test samples. Total sample is prepared in three different trays of 7.6 kg oven-dry soil in each tray. After the individual preparation, three trays soil sample poured in a single tray and mixed thoroughly to achieve uniform mixing. The prepared soil sample was left for 30 min to obtain uniform mix in terms of moisture equivalent. Soil was compacted in the mould with 2.65 kg hammer at a free fall height of 310 mm, placed by 3 layers and each layer having 103 blows. The process was depicted in Fig. 4.

Both the reinforced and unreinforced soil samples were prepared with the same procedure as described above. Un-soaked and soaked laboratory tests were performed at four conditions. Test-1 was performed on un-soaked in condition. Test-2, Test-3, and Test-4 are same as the test one except that the mould has holes at different depths
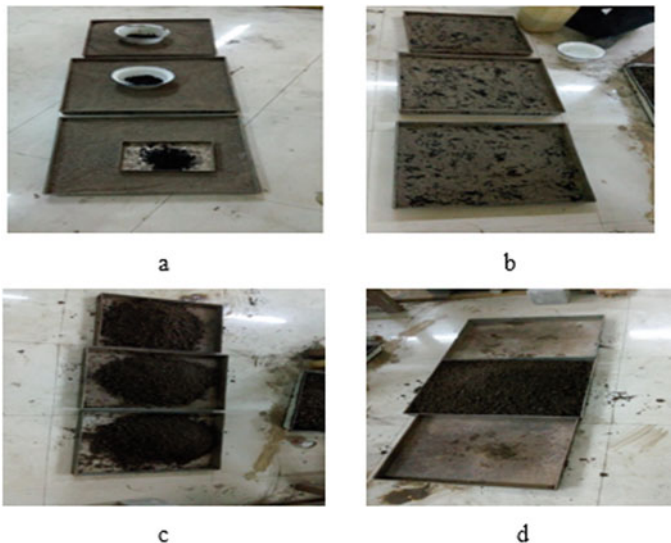
Fig. 4 Stages in the preparation of fibre-reinforced soil **a** Weight of samples were taken to prepare FRS, **b** Fibres mixed with oven-dry soil, **c** Adding water and thoroughly mixed, **d** Three parts combined to form uniform mix

of 250 mm, 170 mm and 50 mm from bottom of the moulds, respectively, for 48 h soaked condition.

5 Testing Procedure

The tri-axial loading apparatus was used for applying the compressive load to the footing. The loading frame attached a load cell of capacity 5000 kg as shown in the figure. The bottom of the load cell connected to a circular shank of size 50 mm to transfer load to the footing as point load. Small size of 10 mm diameter ball is used in between the load cell shank and footing to apply point load on to the footing. Figure 6. shows the instrumentation of the sample for bearing test of the circular footing.

Prepared sample is placed on the movable jack as shown in Fig. 5. Linear variable differential transducer (LVDT) connected to base plate by placing bottom of the test sample. LVDT and load cell connected to the data acquisition system to record the load and settlement. All the tests were performed on the strain rate of 1.25 mm/min (gyre = 2).

Fig. 5 Testing apparatus and instrumentation

Fig. 6 Testing procedure **a** Removing top cover after soaked for 96 h, **b** Placing mould under loading frame along with footing at centre, **c** Applying point load to the footing, **d** Footing after testing, **e** Settlement of the footing, **f** Removing sample from the mould

Figure 6a The sample is taken out from the water tank after the soaking period of 96 h and kept 30 min at outside for removing of surface water. Figure 6b Places the circular footing at the centre of the prepared test mould. Transfer the test mould along with footing to triaxial loading frame to the centre to load cell. Figure 6c Place the circular ball between the footing and load cell shank to apply point load. The loads were calculated up to the maximum displacement of 30 mm. Failure load is taken as 7.5 mm displacement, which is the 10% of the footing diameter. Figure 6d

after loading, the sample was released from the load. The LVDT removed from the sample and kept out of the sample. Figure 6e footing is removed from the test mould and observes the settlement behaviour of the footing. Settlement of the footing is uniform throughout the 30 mm depth as shown in the figure. Figure 6f the sample is taken out and removed from the mould. Sample is not reusable.

The water table effect was simulated by varying the height of holes of 10 mm diameter at horizontal and vertical centre to centre spacing of 20 mm × 30 mm on the mould to allow the passage of water through holes into the soil sample (Fig. 2). The water level in the soaking tank was up to the height of holes to maintain water table depth from b/B = 0 to b/B = 2 (Fig. 2). The effect of capillary rise above the water table depth was neglected. All tests were performed on Unconsolidated Undrained (UU) conditions at a strain rate of 1.25 mm/min.

6 Results and Discussions

6.1 Effects of Water Table Depth on Bearing Capacity of Fibre-Reinforced Soil

The presence of water in the soil causes the reduction in shear strength of the soil. Moisture content between the soil grains acts as the lubrication finally causes the reduction in strength. Problematic soils should be protected from the entrance or presence of moisture. The water table greatly changes the moisture content in the soil. Bearing capacity of soil greatly depends on the depth of water table from the ground level.

Four model tests were performed to find out the bearing capacity of randomly distributed waste tyre rubber fibre reinforced clayey soil with the presence of water table at different b/B ratios and without water table effect.

Figure 7 represents the bearing capacity of untreated and FRS without water table effect. The bearing capacity at 10% settlement ratio is 280 and 380 kPa for untreated and FRS soil. Improvement in bearing capacity is 100 kPa, which is 35.71% over untreated soil. Considerable improvement is achieved with the inclusion of tyre fibre at optimum fibre content of 0.75%.

The tyre fibres elements act as a tensile elements in the soil mass to enhance its natural stability and strength. The reinforcing elements bringing in contact with the surface of aggregate of soil mass. When load applied on soil mass cause's pressure and a strain on the tyre fibre, it creates a tensile load which resist soil movement and provide additional support for increased strength. This way, a tyre fibre-reinforced soil system is created which provides greater shear strength than the soil mass alone [4].

Figure 8 shows the bearing capacities at 10% settlement ratio are 70 and 90 kPa for untreated and FRS soils. The reduction in bearing capacity, when compared with the untreated and FRS soils without water table effects are 75% and 76.31%. The
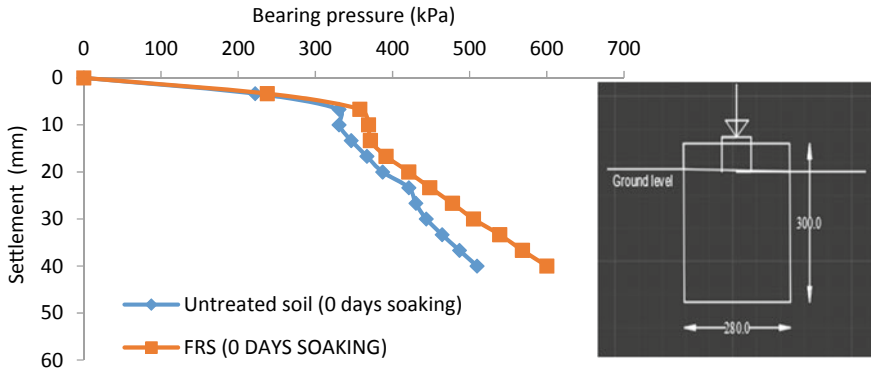
Fig. 7 Bearing pressure vs settlement curve for FRS and untreated soil without water table
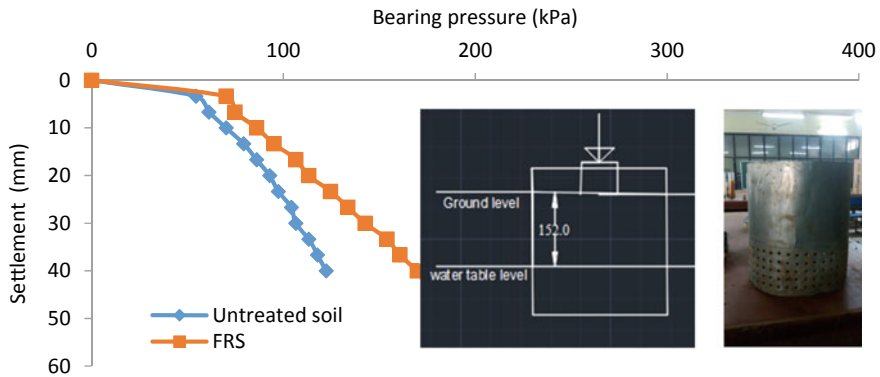
Fig. 8 Bearing pressure vs Settlement curve for FRS and Untreated soil with water table effect at b/B = 2

percentage reduction in bearing capacity is more in FRS compared with untreated soil. With the presence of water table, the bearing capacity greatly reduced.

Figure 9 represents the b/B = 1. The bearing capacities at b/B = 1 are 35 and 43 kPa as shown in the figure at 10% settlement ratio. The reduction in bearing capacities is 87.5% and 88.68% for untreated and FRS soils, respectively. Percentage reduction in bearing capacity is more in FRS, when compared with untreated soil.

Figure 10 represents the b/B = 0. The water table depth is at the base of the footing. Lesser the water table depth from the ground surface, greater the reduction in bearing capacity. The bearing capacities are 25 and 3 kPa for untreated and FRS soils at 10% settlement ratio. Percentage reduction in bearing capacities are 91.0% and 99.21% for untreated and FRS soils, respectively when compared with the absent of water table effect on both the cases.

From Fig. 7, 8, 9 and 10, the bearing capacity of fibre-reinforced soil is higher than the untreated soils except in the case of the when the water table depth at a
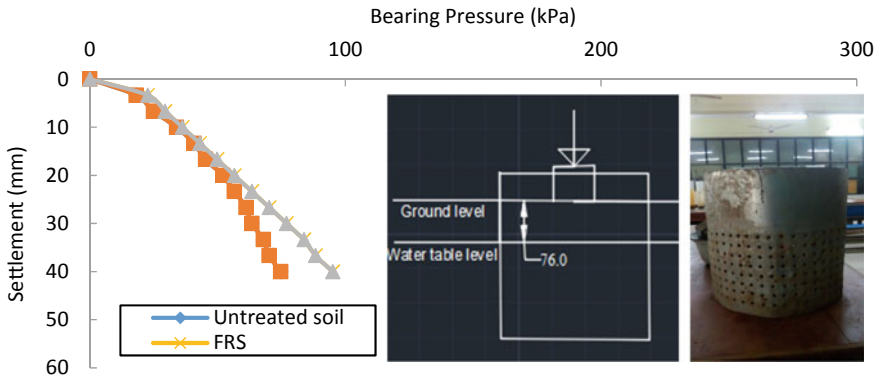
Fig. 9 Bearing pressure vs Settlement curve for FRS and Untreated soil with water table effect at b/B = 1
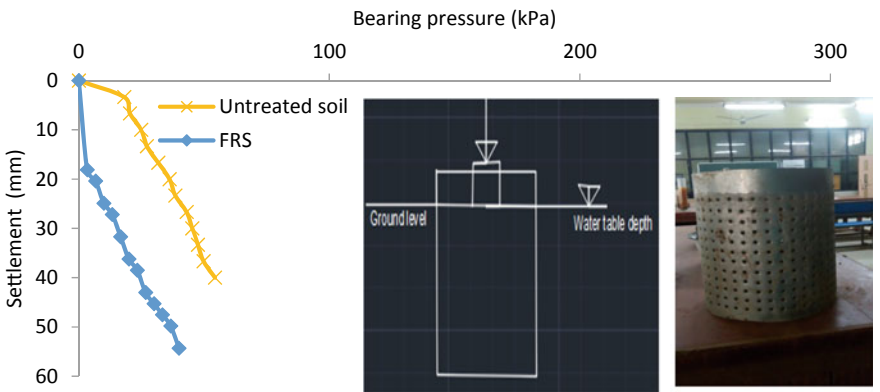
Fig. 10 Bearing pressure vs Settlement curve for FRS and Untreated soil with water table effect at b/B = 0

ground surface. The bearing capacity of FRS is less than the untreated soil, when the water table depth at the top of the ground surface. In the above case, the water acts as a lubricant between the fibres and soil particles, causes the shear sliding of tyre fibres over the soil sample.

7 Conclusions

The improvements in bearing capacity of reinforced soil are 33%, 23% and 20% over unreinforced soil at without water table effect and with water table effect at b/B are 1, and 2, respectively. The bearing capacity of untreated soil is more than the FRS, when the water table depth at the top of the ground surface. Percentage reduction in

bearing capacity is more in soaked FRS, when compared with soaked untreated soil. Fibres are not applicable for the modification of clayey soil, when the soil touches the moisture due to change in water table depth. Tyre fibres can be successfully used for the modification of clayey soils, where the effect of water table is absent.

References

1. Yang, S., Lohnes, R.A., Kjartanson, B.H.: Mechanical properties of shredded tires. Geotech. Test. J. **25**, 44–52 (2002)
2. ETRMA. In: Association ETRM, editor. European Tire & Rubber Manufacturers' Association. The annual report and statistic, Belgium (2013)
3. Shukla, S.K.: Fundamentals of Fibre Reinforced Soil Engineering. Springer Nature, Singapore, ISBN 978-981-10-3063-5 (eBook) (2017). https://doi.org/10.1007/978-981-10-3063-5
4. https://www.ccr-mag.com/what-is-soil-reinforcement-and-how-is-it-done/. Last accessed 15 Sept 2019
5. https://www.edu.pe.ca/agriculture/erosion.pdf. Last accessed 15 Sept 2019
6. Kolay, P.K., Kumar, S., Tiwari, D.: Improvement of Bearing Capacity of Shallow Foundation on Geogrid Reinforced Silty Clay and Sand. Hindawi Publishing Corporation J. Const. Eng. Volume (2013). Article ID 293809, 10 pages https://doi.org/10.1155/2013/293809
7. Jairaj, C., Prathap Kumar, M.T., Sridhar, R., Kumar, G., Prasad, G: 6th International Conference on Advances in Engineering Sciences and Applied Mathematics, (ICAESAM'2016) Dec. 21–22, Kuala Lumpur (Malaysia) (2016)
8. Maheshwari, K.V., Desai, A.K., Solanki, C.H.: Model footing tests on fiber reinforced soil. In: Indian Geotechnical Conference, GEOtrendz December 16–18, IGS Mumbai Chapter & IIT Bombay (2010)
9. BIS 2720 Part 3: Determination of specific gravity. Method of test for soils (1980)
10. BIS 2720 Part 5: Determination of liquid and plastic limit. Method of test for soils (1985)
11. BIS 2720 Part 6: Determination of shrinkage factors. Method of test for soils (1972)
12. BIS 2720 Part 7: Determination of water content – dry density relation using light compaction. Method of test for soils (1985)
13. BIS 2720 Part 10: Determination of unconfined compressive strength. Method of test for soils (1991)
14. BIS 2720 Part 40: Determination free swell index of soils. Method of test for soils (1977)
15. BIS 1498: Classification and identification of soils for general engineering purpose (1970)

On Improving the Performance of Silty Soil by Treating with Ferrochrome Slag: An Experimental Study

Suvojit Patla, Somenath Mondal, and Anil Kumar Choudhary

Abstract Establishing synergy between industrial slags and soils to apply as a ground improvement technique has been one of the prime focuses for geotechnical engineering researchers. This solves the issue of scarcity of "good soil" for construction of embankments and aids to maintaining the sustainable practices of the industries producing slags. In this context, this study analyses the performance of ferrochrome slag as additive in silty soil (ML). The ferrochrome slag passed through 4.75 mm and retained in 1.0 mm IS sieves is used and mixed with the silty soil in different ratios by weight (10:90) to (60:40), to find out the most suitable ratio of mixture. Therefore, the present study describes series of triaxial (Unconsolidated Undrained) and CBR tests on soil and slag individually, and mixture of both by different weight ratios as mentioned before. This exercise demonstrates the fact that, the mixture of soil and ferrochrome slag by ratio 50:50 shows maximum overall improvement of strength. Furthermore, it has been observed that the CBR value of the mixture illustrates an increment of about 500% and the result of the triaxial test of the mixture demonstrates an enhancement of shear strength by 16.5% of the mixture.

Keywords Ferrochrome slag · Silty soil · Experimental investigation

1 Introduction

Soil with low CBR and bearing capacity is the most troublesome and challenging to the geotechnical engineers to make it suitable for the construction of durable sub-grade courses of pavement. Most of the road failure occurs due to poor characteristics

S. Patla · S. Mondal (✉) · A. K. Choudhary
Department of Civil Engineering, National Institute of Technology Jamshedpur, Jamshedpur, Jharkhand 831014, India
e-mail: smondal.ce@nitjsr.ac.in

S. Patla
e-mail: suvojitp6@gmail.com

A. K. Choudhary
e-mail: akchoudhary.ce@nitjsr.ac.in

of sub-grade, causing loss of wealth and lives. Thus, there should be some remedy to overcome this crisis.

Traditionally, natural materials were used as additives to fill the lacuna of incapable soil, for civil engineering purposes, but exponential population growth and its demands in civil engineering field lead to scarcity of natural material and causing its depletion.

Additionally, alarming population and progressive industrialization results in cumulative accumulation of huge amount of by-products which if not utilized may cause several types of socio-environmental and economic problems.

By considering all these factors, a suitable and effective ground improvement technique is required, which will act as a symbiosis and may pave the way toward sustainable development.

So many soil stabilizing methods are there, but stabilizing with industrial by-products is found to be most promising in term of cost feasibility and simplicity. Ferrochrome slag is one such by-product, generated 12–16 million tons across the world and increasing 2.5–3% per year [10] India contributes 10% of total production. Being new in the field only limited work is done with it. So there is a vast scope of it being used as additive material for pavement construction on virtue of its high CBR and strength.

Chromium particles in it in small percentages (less than 6) [11]. There is a threat of using ferrochrome slag in practical field on lest of leaching of "Chromium". On this, showed low leachability of slag except potassium (k^+) under suitable lab. Condition [11], yet to confirm by leachate analysis. But the superior physical and chemical properties of ferrochrome slag overpower its drawback and becomes attractive construction material. Researchers showed ferrochrome slag is very stiff, and exhibit all over superior performance in construction field [1, 10, 12, 13, 15] compared to natural aggregate [14] and very suitable for construction of pavement Sub-grade [1, 2, 15] layers material.

The study infers that the mechanical and chemical properties of ferrochrome slag indicate suitability for using in road construction applications, such as base or sub-grade materials. Environmental impact assessment studies proved that ferrochrome is non-hazardous material and not harmful to be used as a green construction material in substitute of natural material to prevent its depletion. Additionally, utilization of ferrochrome slag will lead toward sustainability of industries generating it and reduce the cost of construction.

2 Experimental Methodology

2.1 Materials

Silty Soil: Local silty soil is collected from Balasore, Odisha and its basic geotechnical properties were determined by standard test procedure as per the provision of IS
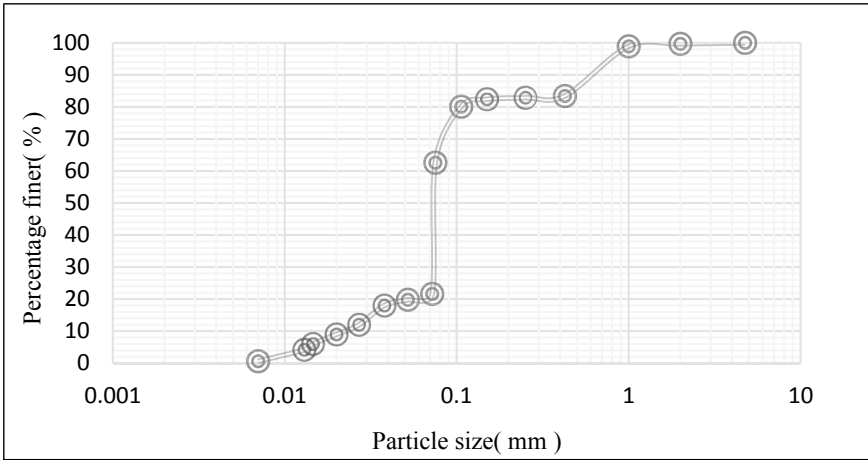
Fig. 1 Grain size distribution curve for local soil

Table 1 Basic geotechnical engineering properties of soil

Property	Value
Specific gravity	2.65
Natural moisture content (%)	25.00
LL (%)	48.00
PL (%)	28.00
I_P	20.00
Dry density (kN/m^3)	17.80
OMC (%)	16.20
C_{uu} (kPa)	28.42
CBR (unsoaked in %)	4.97
CBR (soaked in %)	2.97

2720 of practice. Figure 1 shows the grain size distribution curve Table 1 summarize the properties of soil used.

Ferrochrome Slag: The slag was collected from Balasore Ferro. Alloy Ltd, Odisha, passing through 4.25 mm and retained in 1 mm IS sieve is used. Figure 2 shows the grain size distribution curve and Table 2 shows the engineering properties.

2.2 Sample Preparation

Different percentages of ferrochrome slag content adopted in the present study were 10, 20, 30, 40, 50, and 60 by dry weight of the silty soil used. Mixing between soil
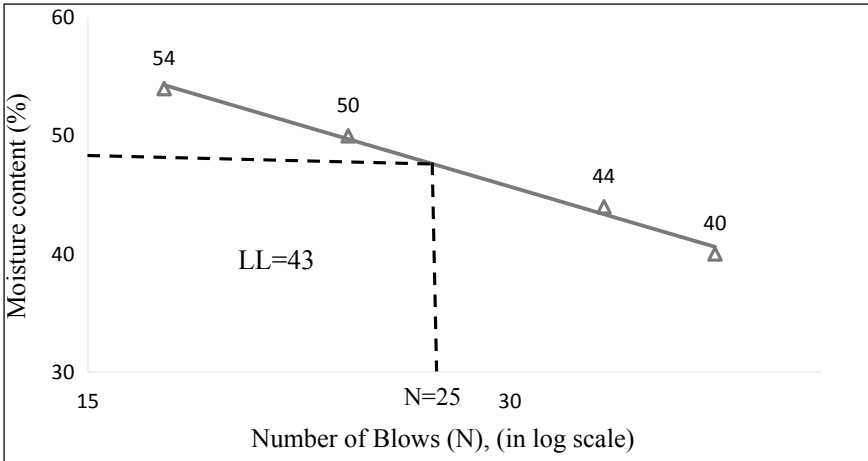
Fig. 2 Liquid limit curve

Table 2 Basic geotechnical engineering properties of ferrochrome Slag

Property	Value
Colour	Dark black
Specific gravity	2.92
Percentage finer than 75μ sieve	2.42
C_u	3.74
C_c	3.74
Soil classified as per ISSCS	SP
Maximum dry unit weight (kN/m^3)	14.60
Minimum dry unit weight (kN/m^3)	11.80
Field dry density (kN/m^3) at 100 cm fall	13.50
Peak frictional angle at 70% relative density	43.00
Cohesion C (kPa)	0.00

and slag was done manually and proper care was taken while preparing the sample in order to maintain a homogeneous mix.

2.3 Laboratory Test Program

The test program adopted for this study is described here. The Atterberg's limits (liquid limit & plastic limit) of original soil were found out to determine the consistency of soil. The proctor and modified proctor test were carried out on both soil and different proportion soil-ferrochrome slag composites to determine OMC and

MDD. Then, the value achieved in proctor test was used to prepare sample for triaxial test (UU) to determine undrained shear strength of soil for different designated soil and soil-ferrochrome slag composite mixes. And a cylindrical specimen with slender ratio (38 mm diameter and 76 mm height) was extracted from it. OMC value achieved in the modified proctor test were used to prepare the sample of unsoaked and soaked CBR test for different proposed mixes.

3   Results and Discussions

For the grain size distribution, wet sieve analysis was conducted as per the provision of IS: 2720 (Part IV)-1985. Since the percentage of fines (<0.075 mm) is 5–12% so we have to go for hydrometer analysis.

Since, the percentage of fines is greater than 50% so Atterberg's test as per provision of IS: 2720 (part 5) & IS: 9259–1979, was conducted to classify the soil.

With the help of plasticity chart and A-line of IS code, the above soil was classified as ML.

In order to designate the soil and check its suitability or its deficiency for being used as sub-grade soil, basic tests were conducted as per IS code which is tabulated in Table 1.

Now, in case of ferrochrome slag only dry sieve analysis was found sufficient in order to classify the soil, as Percentage of fines (<0.075 mm) is very less as mentioned above.
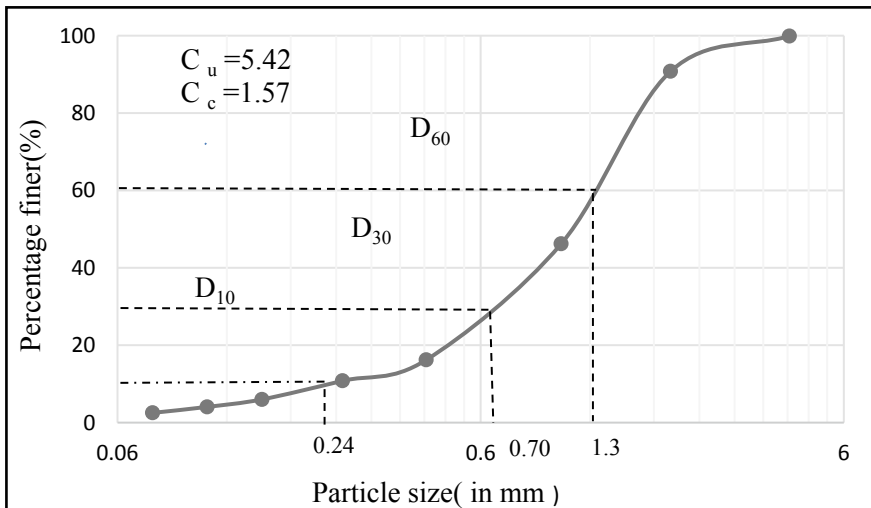
Fig. 3   Grain distribution curve for ferrochrome slag

The above slag is classified as SP from Fig. 3 by using C_u & C_c value. And to justify the suitability of ferrochrome slag for being used as additive material for improving the performance of soil, few basic tests were required is delineate in Table 2.

3.1 Effect on Compaction Characteristics

Compaction test were conducted to establish co-relation between moisture content and dry density for both unreinforced and different proportions ferrochrome slag reinforced soil. Two trials were conducted for each mix for more creditable comparative outcomes. We can observe, as the percentage of FS in the mixture increases, with increase in compacting energy MDD value increases and OMC decreases. These changes may be attributed high specific gravity of FS, low water absorption of FS and better interlocking of soil-FS composite, which results in decrease in void ratio. Graph 1 for zero % slag, 2 for 10% slag and so on up to 60% inclusion of ferrochrome slag (Fig. 4).
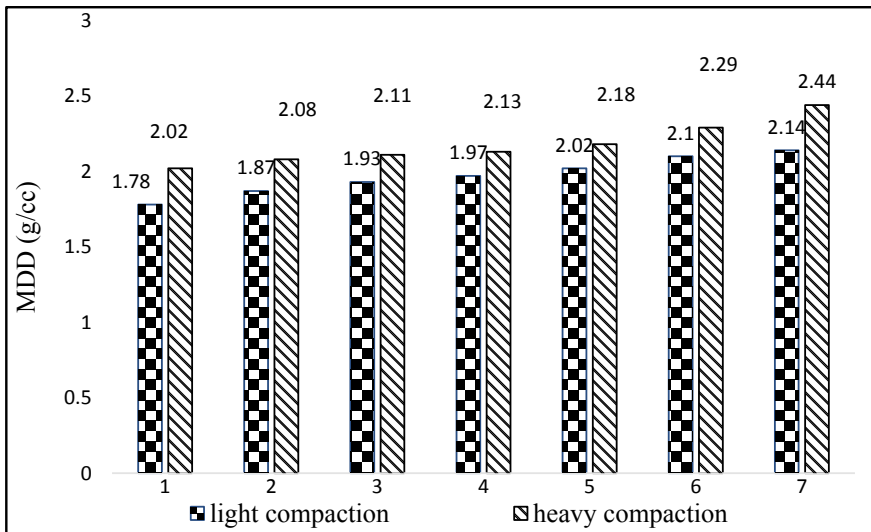
Fig. 4 Showing the improvement of MDD value with inclusion of ferrochrome slag and comparing

Table 3 Shear parameters obtained from UU test for soil slag mixture of different proportions

Mixture	C (kPa)	φ (degree)
100% SS	28.40	6
90:10	30.20	14
80:20	34.00	18
70:30	36.00	20
60:40	37.40	22
50:50	34.40	27
40:60	28.00	29

3.2 Effect on Undrained Shear Strength

The value of undrained shear strength obtained from stress–strain curve of UU test by plotting Mohr's circle. Increase in the undrained shear strength of soil mixed with ferrochrome slag composites may be attributed due to better interlocking resulting in decrease in void ratio, which provides more stress resistance for a particular strain. However, cohesion decreases after 40% inclusion, due to too many fibre or poor gradation, but frictional angle keeps on increasing and approaches the value that of ferrochrome slag.

The ratio of the mixture is ratio of silty soil to that of ferrochrome slag by weight. The shear parameters obtained from the UU test, from Table 3 are used to evaluate the shear strength for the specific mixture, tested at its respective OMC (%).

Undrained shear strength of the soil is calculated as per the formula given below

$$q = 2C + \tan(\varphi) \tag{1}$$

where $q =$ undrained shear strength of specimen.

The value undrained shear strength for different soil and soil-ferrochrome composite mixture are plotted in the bar graph, Fig. 5. Here also the sequence of curve is same as mentioned above from 1 to 7.

3.3 Effect on the CBR Value

The typical load versus settlement behaviour of soil and ferrochrome slag mixed soil in different proportions under unsoaked and soaked condition of CBR test is plotted in Figs. 3 and 4.

It can be observed that with the increase in percentage of ferrochrome slag in composite mixture, the load value increases and deformation value decreases significantly, subsequently shows nearly linearity in its behaviour at higher percentage (Fig. 6).
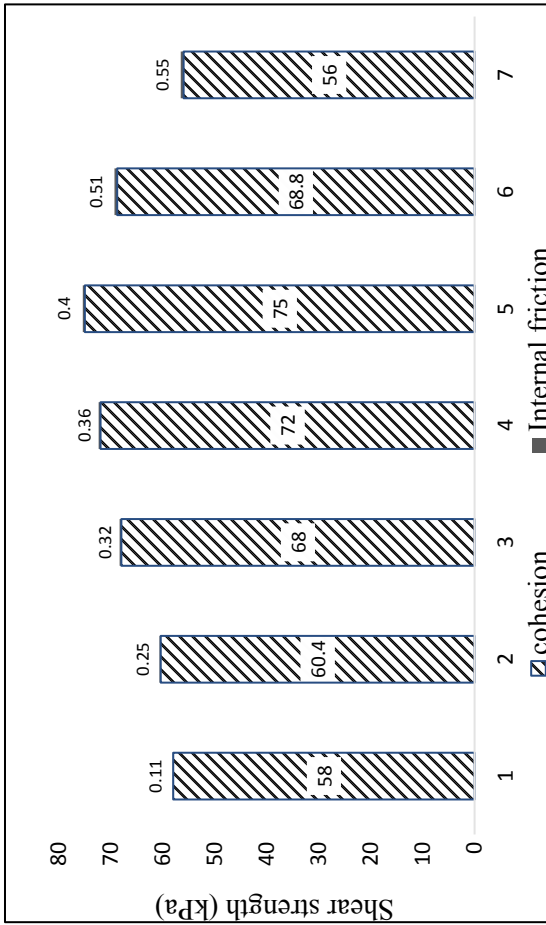
Fig. 5 Change in undrained shear strength with inclusion of ferrochrome slag
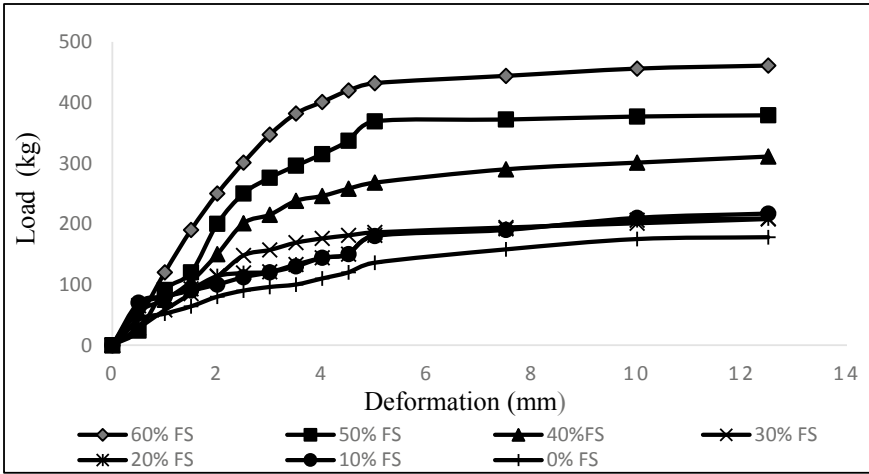
Fig. 6 CBR curve for soil and different soil-slag composite mixture in unsoaked condition

In case of unsoaked test, from the stress–strain for higher percentage of slag in the composite mixture, showing linearity. The unsoaked CBR value however finds very limited application in practical field, because in real practical field the sub-grade courses get subjected to moisture due to precipitation or other sources. But in semi-arid and arid condition the unsoaked CBR value may be used to construct pavement courses and will show superior behaviour due to its linearity in stress–strain relationship (Fig. 7).
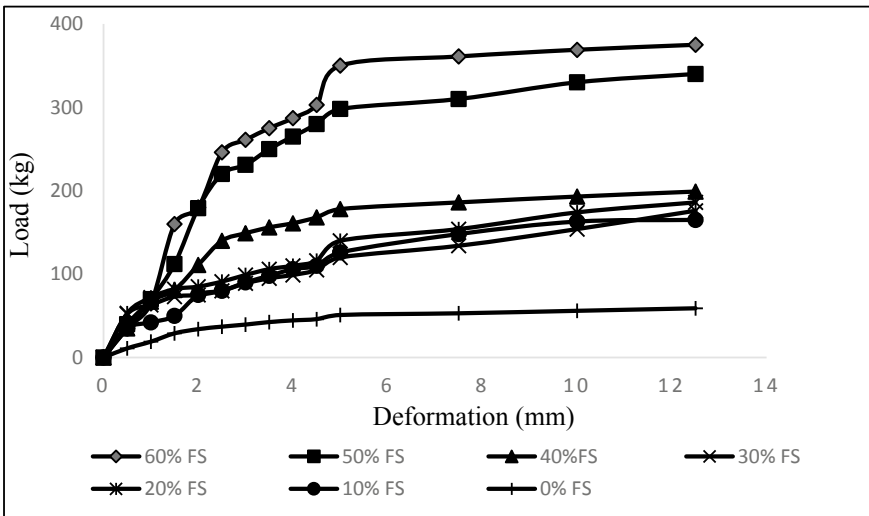
Fig. 7 CBR curve for soil and different soil-slag composite mixture in soaked condition

Table 4 Showing CBR value in unsoaked and soaked condition

Constituents	Un-soaked CBR (%)	Soaked CBR (%)
100% SS	5.60	2.97
90% SS + 10% FS	7.65	6.34
80% SS + 20% FS	8.42	6.50
70% SS + 30% FS	10.72	8.47
60% SS + 40% FS	15.69	11.94
50% SS + 50% FS	18.36	14.96
40% SS + 60% FS	21.95	17.94

Where in case of soaked condition the curve is non-linear even in higher percentage, this may be attributed due to forming of lumps in wet condition, causing uneven settlement. This can be attributed to elasto-plastic behaviour of the soil-slag mixture with soaked condition. The improvement in CBR value in wet condition is significant but on account of settlement behaviour dry condition may be called superior. However, soaked CBR finds large-scale applications in practical field. From the CBR curve or result of CBR test, CBR value is calculated and given in Table 4.

CBR value is calculated at 2.5 mm settlement with surcharge load of 2.5 kg at OMC. From the table, it can be observed that the CBR value increases as the percentage inclusion of ferrochrome slag increases.

4 Conclusions

With the increase in percentage of ferrochrome slag inclusion in the soil-ferrochrome composite, the following conclusions can be drawn on the basis synthesis of test results. From proctor and modified proctor compaction test, it is observed from Fig. 4 that, inclusion of ferrochrome slag, significantly changes the MDD value of the mixture. MDD goes on increasing and OMC decreases, since water absorption of slag is very low. Therefore, a huge amount of water can be saved and heavy-duty pavement sub-grade courses can be constructed, which will reduce post-construction settlement. Undrained shear strength of soil also goes on increasing up to 40% (Fig. 4) therefore shear failure can be minimized to. However, it starts decreasing after further increase in percentage of slag. CBR value of soil in soaked condition was 2.96% the value increased to 17.94% in case of 60% slag in the soil-slag composite mixture. However, according to our requirement of pavement sub-grade construction to be constructed we can adopt the suitable soil-ferrochrome mixture from Table 3.

References

1. Altan, Y., Mustafa, K.: Mechanical properties of ferrochromium slag in granular layers of flexible pavements. Mater. Struct. **43**, 309–317 (2010)
2. Das, B.B.: Characterization of ferrochrome slag as an embankment and pavement material. Master thesis, Department of Civil engineering, NIT Rourkela, India (2014)
3. IS: 2720 (Part-XIV)-1980. Methods of test for soils: Determination of density index (relative density) of cohesion less soils. Published by Bureau of Indian standard, New Delhi, India
4. IS: 2720 (Part-XVI)-1961. Methods of test for soils: CBR test. Published by Bureau of Indian standard, New Delhi, India
5. IS: 2720 (Part-II)-1983, reaffirmed in 2002. Methods of test for cohesive soil: Determination of shear strength parameter of soil, by triaxial test. Published by Bureau of Indian standard, New Delhi, India
6. IS: 2720 (Part III, sec.2)-1980. Methods of test for soils: Determination of Sp. gravity. Published by Bureau of Indian standard, New Delhi, India. Published by Bureau of Indian standard, New Delhi, India
7. IS: 2720 (Part-IV)-1985. Methods of test for soils: Grain size distribution of soil
8. IS: 2720 (Part-VIII)-1980. Methods of test for soils: Determination of water content dry density relation using heavy compaction. Published by Bureau of Indian standard, New Delhi, India
9. IS: 2720 (Part-XIII)-1986. Test for cohesion less soil: Direct shear test. Published by Bureau of Indian standard, New Delhi, India
10. Kauppi, M., Pekka, N.: Production, characteristics and use of ferrochrome slags. In: International Ferro–Alloys Congress XI, New Delhi, pp. 171–179 (2007)
11. Lind, B.B., Fallman, A.M., Larsson, L.B.: Environmental impacts of ferrochrome slag in road construction. Waste Manage. **21**, 255–264 (2001)
12. Nkhola, M.A.: Characterization of Ferrochrome Smelter Slag and its Implication in Metal Accounting. Dissertation submitted in Magister technology (M.tech) in Chemical Engineering, Cape Peninsula University of Technology (2006)
13. Sahu, N. et al.: A short review on utilization of ferrochrome slag. Min. Process. Extract. Metall. Rev.: Int. J (2016)
14. Sanghamitra, B., Satyanarayana Reddy, C.N.V.: Potential of ferrochrome slag as construction material. In: Conference: Young Geotechnical Engineers Conference of Andhra Pradesh, Hyderabad, India (2012)
15. Yilmaz, M., VuralKo, B.: Effect of ferrochromium slag with neat and polymer modified binders in hot bituminous mix. Indian J. Eng. Mater. Sci. **16**, 310–318 (2009)

Experimental Studies on Utilization of Blast Furnace Slag for Cohesionless Soil

Bhavin G. Buddhdev and **M. V. Chauhan**

Abstract In the present state, utilization of various waste materials in different geotechnical application is increase manifold. All the waste materials possess different characteristics depending upon its raw materials and processing techniques. Utilization of these waste materials needs greater concern of its properties and compatibility with parent material. Out of many waste materials available, blast furnace slag is one of them. Blast furnace slags are by-products of metallurgical processes. It is glassy material, vesicular textures, typically with sand-to-gravel-size particles can be converted into powder form as well as particular desire size particles. In this paper, experimental work has been carried out on cohesionless soil with utilization of BFS to improve its properties for various geotechnical applications. Based on the literature review, it was evident that no much experimental work had been done on cohesionless soil as compared to cohesive soils. Therefore, attempt has been made to check the effect of utilization of BFS in cohesionless soil with various proportions of BFS mixed with cohesionless soil. Experimental results indicate positive outcome in terms of soil improvement for cohesionless soil with utilization of BFS. This research is very much useful for utilization of this waste material for soil improvement especially for cohesionless soil with poor characteristics for many geotechnical applications. Utilization of this waste material will also solve many environmental issues related to its stockpiling and dumping which ultimately protect the environment.

Keywords Blast furnace slag · Cohesionless soil · Waste materials · Soil improvement

B. G. Buddhdev (✉) · M. V. Chauhan
Applied Mechanics Department, Vishwakarma Government Engineering College, Chandkheda, Ahmedabad, Gujarat, India
e-mail: bhavin_buddhdev@hotmail.com

M. V. Chauhan
e-mail: mukeshchauhan4809@gmail.com

1   Introduction

Research into new and innovative uses of waste materials in geotechnical engineering is need of days in the era of sustainability. Utilization of waste materials can be decided based on factors like availability, technical suitability, environment impact, and economic benefits. Presently, along with series of waste materials production, most of the countries including India are producing tons of blast furnace slag (BFS) which is the by-product of steel industries. This unutilized BFS is stock piled in the steel plants, and eventually land filled at slag disposal sites. Since the current methods of stockpiling and land filling are not sustainable, disposal of BFS has become a significant concern both to slag processor companies and to environmental agencies. There was very limited information on the engineering properties of BFS in the literature, so research that focuses on engineering properties of blast furnace slag was scarce. BFS is the by-product of metallurgical operations, typically containing gangue from the metal ore, flux material, and unburned fuel constituents. As a product of calcinated flux stone and the alumina and silica phases present in iron ore, the four major oxide phases present in BFS are CaO, SiO_2, Al_2O_3, and MgO. These oxides account for approximately 95% of the BFS composition [1]. The physical properties of BFS are largely controlled by how it cools and solidifies. The color of BFS coarse aggregate usually varies from light to dark gray, depending on chemical composition. The void structure of the BFS heavily influences the physical properties, including the bulk specific gravity and the absorption [2]. Based on the chemical and physical properties, BFS can be converted into any desire size fraction to make it suitable for various geotechnical applications. Utilization of BFS in geotechnical application till now is mainly for soil improvement of expansive soil like black cotton soil as well as in road construction as aggregate in flexible and rigid pavements. Some of the cases, in which BFS is utilized as improvement in subbase materials for road construction, have been noted. Still utilization of BFS with cohesionless soil based on site-specific condition as well as application in foundation of various structures is missing in literature. Based on the availability of BFS in national context, the proper guidelines at the production unit as well as collection and convergence in required form are not established as compared with global context. In this paper, extensive experimental program was carried to evaluate the properties of virgin soil as well as BFS. Based on the characterization results, effect of BFS in cohesionless soil was studied by replacing BFS with virgin soil in proportion of 15% and 25% by weight. The selection of percentage proportions of BFS with virgin soil was based on the literature as well as to know the proper effect of BFS with wide range of difference in percentage. This mixture of BFS and cohesionless soil has been evaluated for OMC-MDD, CBR, and shear strength parameters. The results of this selected parameters for both the proportions indicated the better improvement with BFS in the virgin soil. This experimental study opens the new area of utilization of BFS especially with cohesionless soil in many geotechnical applications. This study is an attempt to understand the effectiveness of utilization of BFS in certain area which provides greater economy with saving of precious nature resources.

2   Literature Review

Many researchers had put their sincere efforts to use the BFS coming out from steel processing units in various geotechnical applications. Many research papers were reviewed related to cohesionless soil with BFS and other waste materials. Many of them were about BFS which was utilized for geotechnical applications like earth-fill, embankment, subbase, base course for pavement, etc. The following paragraph illustrates the development in the utilization of BFS with cohesionless soil as well as scenario for different geotechnical applications.

"According to Hendrik [3]," slag has been used for construction purposes—especially road metal since Roman times. The dramatic expansion in Europe of iron and steel production associated with the industrial revolution led to a commensurate increase in slag production. By the early nineteenth century, slag output was rapidly outpacing consume\piton and there was an alarming growth of unattractive slag heaps on valuable industrial land. By the mid-nineteenth century, research had demonstrated a number of new uses for slag, particularly as an aggregate for concrete and as a cementations material in its own right. Consumption remained relatively modest until the twentieth century, when a major new use—in asphalt blend for road paving—was developed and became popular in step with demand for smooth roads by the growing automobile owning public. This use, together with the rapid growth of concrete usage worldwide, led to the consumption of most existing slag heaps and a current consumption roughly apace with new slag production. The utilization of slag, therefore, is one of the great, yet relatively unsung, stories of recycling. Research is ongoing to expand and refine the uses of slag. Slag is properly recognized as a valuable coproduce of iron and steelmaking, not a waste product [3].

BFS is obtained during the manufacture of iron and steel and possesses inherent hydrated properties. It was utilized for making different types of construction materials "(www.Academicjournals.org/ijps/pdf/…/ Safiuddin %20et%20al.pdf)" [4]. "According to Emery [5]," loose dry unit weight values for palletized BFS range from 8.2 to 10.4 kN/m^3. BFS is glassy material, typically with sand-to-gravel-size particles [5]. Most of the studies in the literature focus mainly on the chemical composition and mineralogy of BFS to assess its cementitious properties rather than its mechanical properties. "Noureldin et al. (1990)" reported on some of the engineering properties of blast furnace slag [6].

Maximum dry density of soil increases while plasticity characteristics gradually decreases with increase in slag content and thus the CBR value of soil increases and therefore increases soil strength [7–9]. Slag content in natural soil increases its workability by reducing its liquid limit and thus its plasticity [8]. It was recommended [9] for natural soil with 25% slag as an optimum stabilization ratio for soil and can be used for subgrade as well as in pavement [9]. Poh et al. [10] showed that there is potential in utilizing BOF slag fines in stabilization of fine-grained soils when activators are used [10].

Dayalan [11] studied on the stabilization of soil with BFS and fly ash. Soil stabilization has become the major issue in construction engineering, and the researches

regarding the effectiveness of using industrial wastes as a stabilizer are rapidly increasing. This study briefly describes the suitability of the local fly ash and BFS to be used in the local construction industry in a way to minimize the amount of waste to be disposed to the environment causing environmental pollution. In this study, different amount of fly ash and BFS are added separately, i.e., 5, 10, 15, and 20% by dry weight of soil are used to study the stabilization of soil. The performance of stabilized soil is evaluated using physical and strength performance tests like specific gravity, Atterberg's limits, standard proctor test and California bearing ratio (CBR) test at optimum moisture content. From the results, it was found that optimum value of fly ash is 15% and BFS is 20% for stabilization of given soil based on CBR value determined [11].

Pramanik [12] studied the behavior of soil for subgrade by using marble dust and BFS. In this paper, sandy clayey soil was stabilized using the combination of marble dust and BFS in different proportion (i.e., 0% + 0%, 5% + 5%, 10% + 10%, 15% + 15%, and 20% + 20%) and characteristic behavior (i.e., OMC, MDD, UCS, CBR, and permeability) of modified soil in the laboratory was studied. The series of test has been conducted in laboratory and it is found that marble dust and BFS (15% + 15%) are sufficient to increase the California bearing ratio in unsoaked and soaked condition value up to 195% and 100% approximately [12].

Kavaki [13] studied on the reuse of BFS in lime-stabilized embankment materials. In this paper, an effective way of utilizing the BFS with lime has been presented for stabilization of road materials. In the study, Ankara clay was used for stabilization. Although slag, lime, and clay mixtures do not affect optimum water contents of clay significantly, they decrease dry density and smoothes proctor curve. Then, the soil transforms into a rapid structure and the modulus of elasticity increases. When the results of the experiments were evaluated, unconfined compressive strength (UCS) and soaked California bearing ratio (CBR) values of the soils have shown significant increases. These increases reach to 46 times in CBR values for Ankara clay compared to natural case in 28 day cured samples. This stabilization technique is more effective than the lime alone and also the slag will prevent the ettringite formation that occurs in lime stabilization with sulfate rich soils that leads swelling behavior. Finally, the slag may turn from a waste material into a valuable product for road construction works with huge volumes even at faraway from the steel factories [13].

Ms. Radha Gonawala et al. evaluated soil and GGFS (10, 15, and 20%), soil and lime (3, 4, and 5%), soil and cement (0.5, 1, and 1.5%) for their engineering characteristics by laboratory investigations for embankment construction. Different laboratory tests carried out included: grain size analysis, Atterberg's limit test, proctor compaction test, CBR test, aggregate impact value test, abrasion test, and moisture absorption test [14].

Akin Musuru (1991) studied the cause of mixing of BFS on the consistency, compaction, characteristics, and strength of lateritic soil. It was observed decrease in both the liquid and plastic limit. The compaction, cohesion, and CBR improved with increasing BFS up to 10%, then if add 15% of BFS decrease the strength. The angle of internal friction decreased with increase in BFS [15].

Based on literature review, experimental program was decided to understand the effect of BFS when mixed with cohesionless soil in different proportions to evaluate certain parameters. Literature review suggested that very less experimental work was done in past considering only BFS as substitute material with cohesionless soil.

3 Experimental Work

3.1 Introduction

In the present study, an exhaustive experimental program was conducted to evaluate effect of the blast furnace slag available locally when it is used as construction material in various proportions to the soil in different geotechnical applications. The characterization of blast furnace slag is done which is locally available. Some soil samples (representative of both coarse and fine grained) were adopted for the study. Geotechnical parameters like OMC-MDD, CBR, and shear strength parameters values are studied for soil sample selected by adding various percentage of slag mix with it. Details of material used, processing test procedure adopted are described.

3.2 Material Used

Blast furnace slag: BFS obtained from industrial area of Rajkot city, Gujarat, India (Refer Photograph 1) of size-4.75 mm down up to 150 micron having gradation shown in Fig. 1 has been selected. Table 1 shows the chemical properties of BFS used in the study [16]. The characterization of BFS was done for properties necessary for the experimentation and shown in Table 2. BFS is a waste material mainly collected from steel processing units. It consists of some iron fractions that also may lead to some higher value of specific gravity. It cannot be directly compared with soil.

Photograph 1 Blast furnace slag sample

Table 1 Chemical properties of blast furnace slag

Chemical properties of BFS in %	CaO	SiO$_2$	Al$_2$O$_3$	MgO	Fe$_2$O$_3$	SO$_3$
	26.5	34.0	17.25	7.0	18.25	0.5

Table 2 Characterization of blast furnace slag and selected soil [17–19]

S. No.	Description	Virgin soil	Blast furnace slag
1	Classification as per IS	SM-SC	SM-SP
2	Water content	11.25	15.11
3	Specific gravity	2.66	2.72
4	Liquid limit	20.20	NP
5	Plastic limit	14.28	–
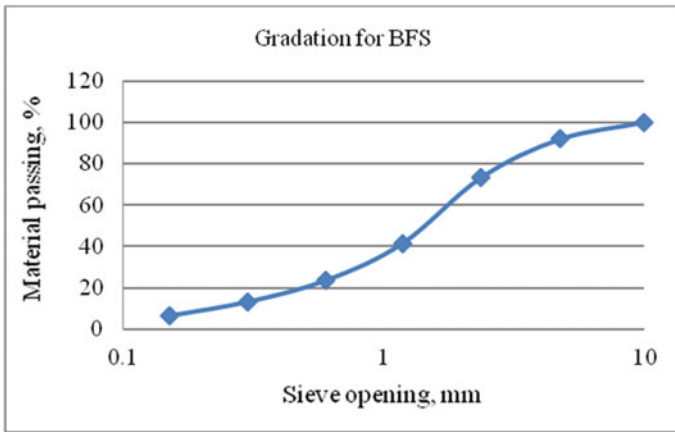
Fig. 1 Gradation of blast furnace slag [17]

Cohesionless soil: Soil samples are collected from riverfront area of Sabarmati River in Ahmedabad city for experiment purpose so that effect of slag for soil stabilization purposes can be worked out. Gradation of the soil sample considering size-4.75 mm down up to 150 micron is done and shown in Fig. 2. More than 90% is coarse-grained soil retained in 75 micron sieve, while fine-grained fraction is around 5 to 10%. The characterization of collected soil sample was done for properties necessary for the experimentation and shown in Table 2.

Fig. 2 Gradation of soil [17]
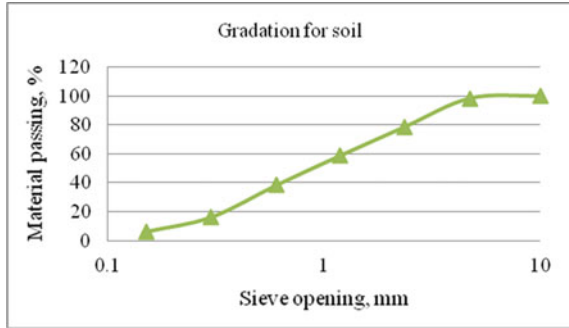
3.3 Experimental Test Procedure

All the experiments are performing as per the procedure and provision laid down in relevant IS codes.

4 Results and Discussions

The major aim to perform the experiment on BFS along with cohesionless soil is to evalute the feasability of this waste material with soil. The experimental outcome may lead to an extent for utilization of this BFS with soils.

BFS and representative soil samples were selected and taken for purposes of experimentation. The aim for soil improvement is to stengthen the virgin soil properties and enhance the soil properties to desired level. Both slag and selected soil are characterized for different geotechnical parameters (refer Table 2). OMC-MDD value of virgin soil and BFS is evaluated with standard proctor test. In this work, effect of BFS with soil under compaction behavior needs to be evaluated, that is why to start with first standard proctor test was selected. Yes, one can perform the same with modified proctor test also. Based on the OMC-MDD value obtained, it is decided to add 15% and 25% of BFS by weight to the soil. The appropriate change in the OMC-MDD is shown in Fig. 3. OMC-MDD value of mixture of soil and BFS shown increased in maximum dry density as compared with virgin soil. The percentage increase in maximum dry density was not much as increase in percentage of BFS from 15 to 25%. These behaviors in OMC-MDD witness that their was no significant effect of BFS with cohesionless soil. Still one can try for higher percentage of BFS replacement, but this trends indicative of not much improvement. California bearing ratio (CBR value) is considered as a most important geotechnical parameter for the pavement design. Design of pavement is unsafe and uneconomical on a poor subbase. To strengthen the poor subbase, certain amount of slag may be utilized to improve overall quality of strata. On a selected soil, BFS is added in amount of 15% and 25% by weight to the soil. The CBR test is done for both soaked and unsoaked condition.

Fig. 3 Summary of OMC-MDD for virgin soil and BFS [20]
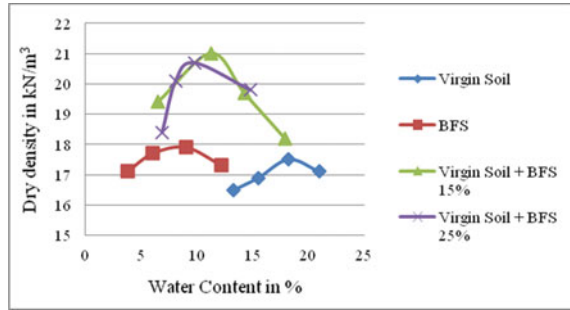
The details of results are shown in Table 3. CBR value (both soaked and unsoaked) was increased with mixture of BFS with virgin soil. The MDD value for 15% and 25% BFS + soil having very small marginal difference, while both unsoaked and soaked CBR values evaluated from experimentation, is higher may be due to higher resistance developed in presence of BFS. CBR value was also increased substantially with increased percentage of BFS from 15 to 25%. This increased value was indicative that there was very positive impact of BFS on CBR value with cohesionless soil. Shear strength parameters were evaluated by conducting direct shear test on virgin soil, BFS, as well as mixture of BFS and virgin soil in proportions of 15% and 25% by the weight to the soil. Based on the test carried out, cohesion (C) and angle of internal friction (ϕ) were evaluated as shown in Table 4. The angle of internal friction increases as the increased in the BFS percentage with virgin soil. This increased may be due to the granular form of BFS particle with virgin soil properties. As the BFS

Table 3 Summary of CBR for virgin soil and BFS [21]

S. No.	Description	Unsoaked CBR	Soaked CBR
1	Virgin soil	7.30	5.70
2	BFS	19.90	16.20
3	15% BFS proportion	10.12	8.60
4	25% BFS proportion	13.10	11.70

Table 4 Summary of shear strength parameter for virgin soil and BFS [22]

S. No.	Description	Cohesion (C) kN/m^2	Angle of internal friction (ϕ°)
1	Virgin soil	12	28°
2	BFS	– –	35°
3	15% BFS proportion	11	32°
4	25% BFS proportion	9	33°

is non-plastic granular material, no cohesion occurred during test. These effects lead to the decreased in the cohesion value when it is mixed with virgin soil.

5   Conclusions

An experimental work is carried out to study the use of BFS as soil improvement and used to enhance the overall quality of related geotechnical materials, by saving the natural resources which day by day become scared. The primary characterization indicates that the BFS has enough potential to use as a geomaterial for different geotechnical application. Further, the test results of OMC-MDD, CBR, and shear strength parameters are indication of improvement in soil property selected at very primary level but at the same time it will propagate for other secondary properties of soil as per the requirement of the projects. Analysis of experimental results showed a good improvement like CBR and angle of internal friction but at the same time OMC-MDD results indicate very little improvement. Pure cohesionless soil mix with properly graded BFS will give more improvement in terms of angle of internal friction as the negative effect due to cohesion not impact on shear strength parameters. Based on above discussion, BFS has a good potential to utilize in certain geotechnical application like embankments, roads, pavement construction, fill, etc. Furthermore as compared to the other waste materials like fly ash, bottom ash, etc., BFS is under-utilized till date. To facilitate and motivate the use of BFS, there is need to develop some crushing units which produced BFS of required size which will be available domestically at cheaper rates.

References

1. Hammerling, D.M.: Calcium Sulfide as Blast furnace Slag Used as Concrete Aggregate, M.S. Thesis. Michigan Technological University, Houghton, MI pp 1–8 (Page 3) (1999)
2. Lewis, D.W.: Properties and Uses of Iron and Steel Slags, National Slag Association, pp. 1–11 (1982)
3. Hendrik, G.: SLAG-IRON AND STEEL, U.S. Geological Survey Minerals Yearbook, pp. 1–24 (2002)
4. https://www.academicjournals.org/ijps/pdf/.../Safiuddin%20et%20al.pdf
5. Emery, J.J.: Palletized Lightweight Slag Aggregate, Proceedings of Concrete International, Concrete Society pp. 1–11 (1980)
6. Noureldin, A.S., McDaniel, R.S.: Evaluation of surface mixtures of steel slag and asphalt, Transportation Research Record 1269, Transportation Research Board, National Research Council, Washington, D.C., pp. 133–149 (1990)
7. Biradar, K.B., Kumar, A.U., Satyanarayana, P.V.V.: Influence of steel slag and fly ash on strength properties of clayey soil: a comparative study. Int. J. Eng. Trends Technol. (IJETT) **14**(2), 61–64 (2014)
8. Rao, et al.: A laboratory study on the effect of steel slag for improving the properties of marine clay for foundation beds. Int. J. Sci. Eng. Res. **5**(7), 253–259 (2014)

9. Chaubey, S., Ali Jawaid, S.M.: Soil stabilization using steel slag. Global J. Res. Anal. **5**(1), 2016 (2016)
10. Poh, H.Y., Ghataora, S.G., Ghazireh, N.: Soil stabilization using basic oxygen steel slag fines. J. Mater. Civ. Eng. ASCE **18**(2), 229–240 (2006)
11. Dayalan, J.: Comparative study on stabilization of soil with ground granulated blast furnace slag (GGBS) and fly ash. Int. Res. J. Eng. Technol. (IRJET) E-ISSN: 2395-0056 **03**(05), 2198–2204 (2016) www.irjet.net p-ISSN: 2395-0072
12. Pramanik, T .: Study the behaviour of soil for sub grade by using marble dust and ground granulated blast furnace slag. Int. J. Innov. Res. Sci. Eng. Technol. **5**(5), 37–41 (2016) (An ISO 3297: 2007 Certified Organization)
13. Kavakì, A.: Reuse of ground granulated blast furnace slag (GGBFS) in lime stabilized embankment materials. IACSIT Int. J. Eng. Technol. **8**(1), 11–14 (2016)
14. . Gonawala, R. et al.: Use of granular blast furnace slag in embankment construction. In: Recent Advances in Civil Engineering for Global Sustainability (RACEGS-2016), pp. 357–361, SVNIT, Surat, Gujarat, India
15. Musuru, A.: Potential beneficial steel slag wastes for civil engineering purposes. Resour. Conserv. Recycl. **5**, PT1, 73–80 (1991)
16. Buddhdev, B.G., Varia, H.R. : Feasibility study on application of blast furnace slag in pavement concrete. Int. J. Innov. Res. Sci. Eng. Technol. **3**(3), 10795–10802 (2014)
17. IS: 2720 (Part 3/See 2) 1980. Indian Standard Methods of Test for Soils Part 3 Determination of Specific Gravity Section 2 Fine, Medium and Coarse Grained Soils
18. IS: 2720 (Part 2) 1973. Indian Standard Methods of Test for Soils Part 2 Determination of Water Content
19. IS: 2720 (Part 5) 1985. Indian Standard Methods of Test for Soils Part 5 Determination of Liquid and Plastic Limit
20. IS: 2720 (Part 7) 1980 Determination of water content -dry density relation using light compaction
21. IS: 2720 (Part16) 1987 Laboratory CBR value
22. IS: 2720 (Part 39) 1977 Direct shear test for soil

Resilient Modulus of Compacted Fly Ash for Pavement Applications

Bhargav Kumar Karnamprabhakara, Prashant Vyankatesh Guda, and Umashankar Balunaini

Abstract Fly ash is one of the waste materials generated in large quantities across India. As per Central Electricity Authority (CEA) report, nearly 196 million tons of fly ash is generated in the year 2017–2018 in India from nearly 167 thermal power stations. Of the generated quantity, only about 60% is utilized for various applications, and a minor portion of it (about 3.4%) is being utilized in roads and flyovers. This study focuses on utilization of fly ash in large-volume embankment construction. When pavements are built over compacted fly ash, resilient modulus (M_R) of compacted ash is one of the key factors considered in the design of pavements. In the present study, fly ash collected from Neyveli Lignite Corporation (NLC), Neyveli, India is used to evaluate the resilient modulus of compacted fly ashes. Cyclic triaxial setup is used to test the resilient modulus of the fly ash. The resilient modulus tests are conducted at three different water contents, optimum water content, and ±2% of optimum water content. Samples are cured for two different curing periods, equal to 6 h and 24 h. The resilient modulus tests showed that the fly ash exhibited good pozzolanic property with the passage of time. The M_R value at OMC for fly ash at 6 h of curing is in the range of 70–80 MPa, whereas for 24 h of curing the M_R value is in the range of 80–115 MPa. The proposed M_R can be helpful to designers to design the thicknesses of pavement layers constructed over embankments made up of compacted fly ash.

Keywords Resilient modulus · Pavement · Fly ash · Waste materials

1 Introduction

Resilient modulus (M_R) is considered as one of the important design parameters for any pavement material. Resilient modulus of any soil is evaluated under the

B. K. Karnamprabhakara · U. Balunaini (✉)
IIT Hyderabad, Kandi, Sangareddy 502285, India
e-mail: buma@ce.iith.ac.in

P. V. Guda
Strata Geosystems, Mumbai 400093, India

application of isotropic confining pressure and repeated loading. Cyclic triaxial test is used to recreate the stress conditions that in general occur in the base and subgrade pavement layers. For the pavement design, US Federal Highway Administration considers resilient modulus as the primary performance parameter.

Resilient modulus defines the response of pavement material to the repeated loads. Resilient modulus is the measurement of the elastic property of soil recognizing certain nonlinear characteristics. M_R is defined as the elastic modulus based on the recoverable strain under repeated loading (see Fig. 1).

$$M_R = \frac{\sigma_d}{\varepsilon_r} \tag{1}$$

where σ_d is the deviator stress and ε_r is the recoverable strain under repeated loading.

Many studies are available on determining resilient modulus of the soils used for base, subbase, and subgrade layers in a pavement. Petry et al. [14] determined resilient moduli of 27 common Missouri subgrade soils and also of five unbound granular base materials. They noticed a loss in M_R for the soils with the increase in the percentage of fines in the soil. Sheng [19] developed correlation between the subgrade soil resilient modulus and the modulus of subgrade reaction, and also the correlation between the laboratory resilient modulus and the resilient modulus measured using test-pit in the field.

Figure 1 shows the developments of elastic and plastic strains for the repeated loading on the soil samples.

Research studies in the past have focused on determining resilient modulus of different waste materials like demolition wastes [13], reclaimed asphalt pavement (RAP) materials [15, 17], recycled plastic granules [5], tire derived aggregates [4] to utilize them as a pavement material either as a base or subgrade material. The
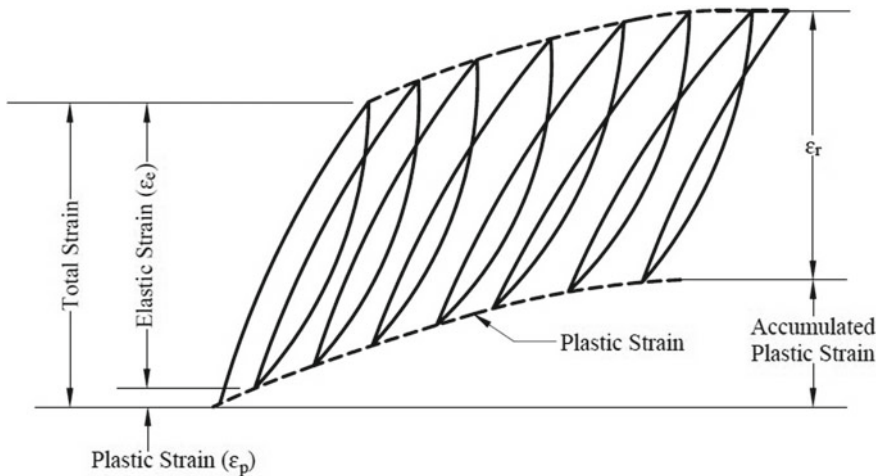
Fig. 1 Applied load versus accumulated strain (modified after [9])

studies in the literature encourage the usage of different waste materials in pavement applications. One such waste material that is generated in large quantities across the world is fly ash. Owing to increased urbanization, production of thermal power energy generates lot of fly ash. In developing countries like India, the handling of waste materials is a challenging task. Ash ponds cover for more than 66,000 acres of land in India itself. With increasing usage of thermal power, it is estimated that fly ash will be stored in more than 1.8 million acres of land by 2032 [6].

Central Electricity Authority (CEA) reports show that nearly 196 million metric tons of fly ash was generated for the year 2017 [7] in India. Only 67% of the generated fly ash is being used. The major modes of utilization cover cement sector (25.6%), mine filling (6.4%), bricks and tiles (9%), reclamation of low-lying area (10.5%), ash dyke raising (6.9%), roads and flyovers (3.4%), etc. Fly ash in its fine form is used as a stabilizing agent in cement sectors [16], and coarse fly ash is used as a fill material in retaining walls and embankments [10, 12].

Cementitious properties of fly ash with high amounts of CaO help in stabilizing soils and increase the strength [18, 20]. Edil et al. [8] studied the effect of addition of self-cementing fly ash to the soil on its California bearing ratio (CBR) and resilient modulus values. They found the addition of fly ash to the soil increased the M_R values from 3 to 15 MPa for 0% fly ash, to 51–106 MPa for 18% fly ash addition. However, there are limited studies on the resilient modulus of the fly ash material alone.

The objective of the present study is to determining resilient modulus of fly ash. The effect of water content and time of curing on resilient modulus of the samples are also studied.

2 Materials–Fly Ash

Fly ash used in the study was collected from Neyveli Lignite Corporation (NLC) Ltd., Neyveli, Tamilnadu. In general, fly ash captured in the electrostatic precipitators (ESP) is transferred to the silos and is collected in the dump trucks to the disposal pond. Fly ash used was collected directly in to air-tight containers from the silos. No loss of moisture content was ensured during transportation to the laboratory. Fly ash was finer in gradation and texture. Basic characterization tests like particle size distribution, specific gravity, morphology, chemical composition, compaction characteristics were performed on fly ash particles before commencing resilient modulus tests.

Fig. 2 Particle size
distribution of fly ash
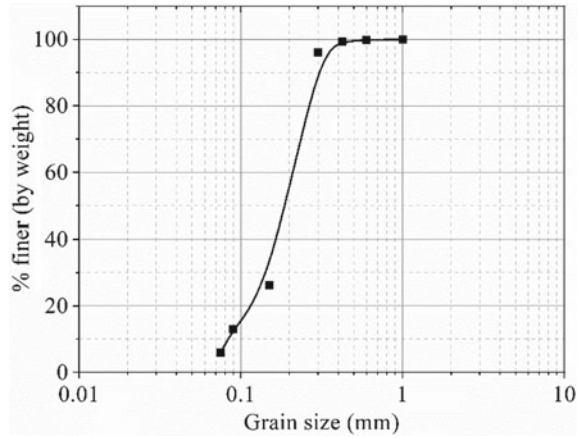
3 Experimental Work

3.1 Particle Size Distribution and Specific Gravity

Figure 2 presents the particle size distribution of the fly ash used in the present study. Sieve analysis on fly ash was conducted as per ASTM D 2487-98 (2000) [2]. Based on the gradation coefficients, fly ash was classified as poorly-graded sand type (C_c values ranged from 1 to 3, but C_u values was less than 6). The effective particle size (D_{10}) and average particle size (D_{50}) of fly ash were equal to 0.08 and 0.18, respectively. The specific gravity of fly ash was determined as per ASTM D854-10 [1] and it was equal to 2.62. The specific gravity and particle size distribution curve reported are an average of three trials.

3.2 Morphological Characteristics

Shape of the fly ash particles is studied under scanning electron microscope (SEM). Due to non-conductive nature of fly ash particles, gold coating was done on their surface. This procedure produced a clear scanning electron micrograph (SEM) image of the fly ash particles. Figure 3a, b presents the SEM images of fly ash at two different magnification factors equal to $500\times$ and $8000\times$. High magnification factors were used to observe the exact shape of the particles. It could be clearly observed from Fig. 3b that fly ash particles are highly rounded in shape. Similar shapes for fly ash particles are observed by Kim et al. [11].
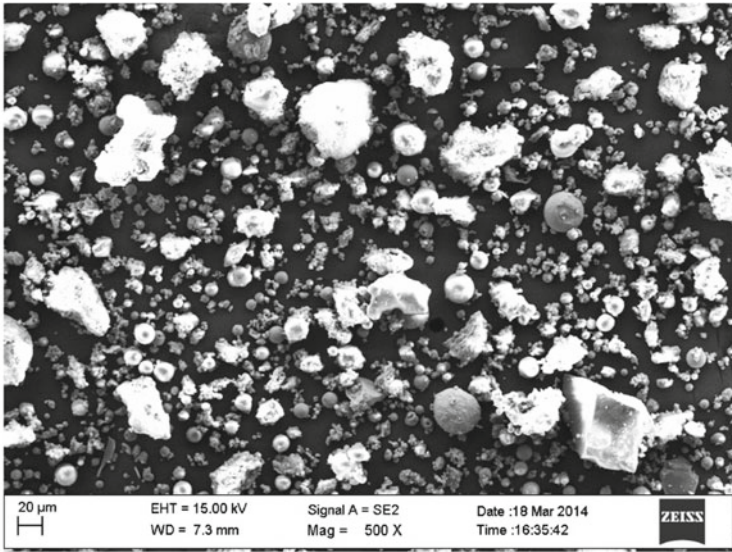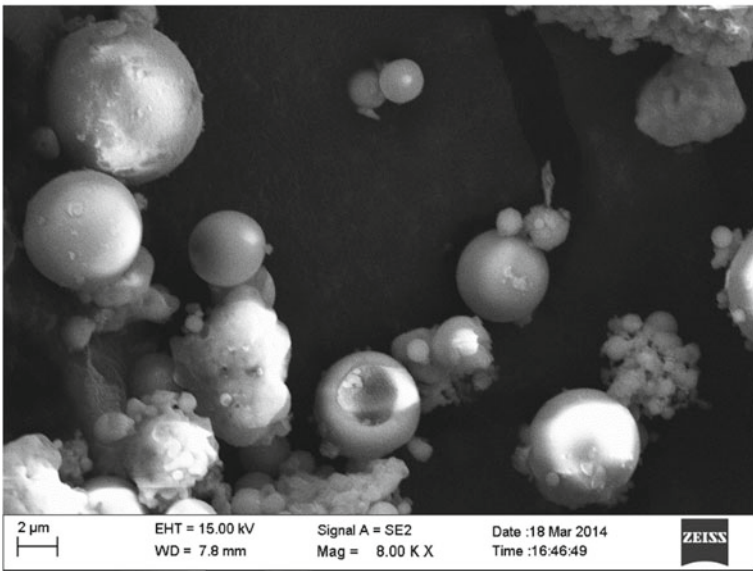
Fig. 3 SEM images of fine fly ash at a magnification factor equal to **a** 500× and **b** 8000×

Table 1 Chemical composition of fly ash used in the study

Chemical compound	% (by weight)
MgO	1.85
Al_2O_3	32.34
SiO_2	40.6
CaO	11.9
K_2O	0.11
Fe_2O_3	9.6

3.3 Chemical Composition

Using X-ray fluorescence (XRF) spectrometer, the chemical compounds present in the fly ash are studied and Table 1 gives the chemical composition of fly ash by percentage of weight. The main compounds are alumina Al_2O_3, silica SiO_2, and CaO. High percentage of CaO helps fly ash to utilize as a stabilizing agent as it gets harder with the time. Fly ash used in the study is classified as Class C (CaO > 10%) in accordance with IS 3812, however, ASTM specifications mention CaO should be higher than 20% to classify a fly ash as Class C.

3.4 Compaction Characteristics

Standard proctor compaction was carried on fly ash in accordance with ASTM D698-12 [3]. The variation of dry unit weight of fly ash with the addition of water is presented in Fig. 4. The maximum dry unit weight (MDD) and optimum water content (OMC) for fly ash were equal to 13.7 kN/m^3 and 26%, respectively.

Fig. 4 Variation of dry unit weight with the water content
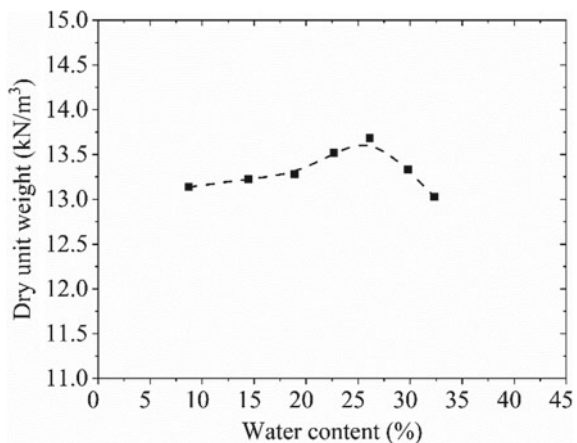
Fig. 5 Cyclic triaxial cell
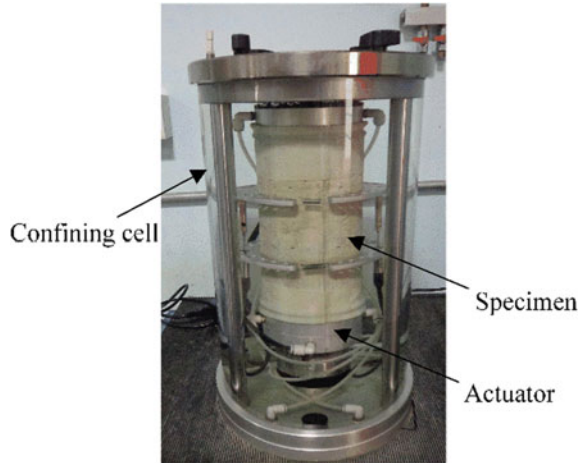
3.5 Resilient Modulus Tests

The resilient modulus testing was performed on fly ash samples prepared at three different water contents, optimum moisture content (OMC = 26%), wet side of optimum (OMC + 2% = 28%), and dry side of optimum (OMC-2% = 24%). The samples were cured under water for two different curing periods, 6 h and 24 h. The corresponding relative compaction of the samples prepared was equal to 97% of the maximum dry unit weight, satisfying the IRC specification for subgrade preparation.

Cyclic triaxial apparatus was used to determine the resilient modulus of all the fly ash samples. The main parts of the apparatus include cyclic triaxial cell actuator, air and water control valves, overhead water tank, and the monitoring system. Figure 5 shows the different parts in the cyclic triaxial cell, like confining pressure chamber, specimen, and the actuator.

The sequence of steps followed in the resilient modulus testing includes: specimen preparation, assembling of triaxial cell, application of confining pressure, stress conditioning, stress application through 15 additional stress states. The following sequence of steps was followed for all the samples tested in the study.

Sample preparation

All the samples tested in the study are prepared in split molds of dimensions, 100 mm in diameter and 200 mm in height. The fly ash samples were added with the water corresponding to pre-decided water contents and mixed homogenously. An aluminum foil was placed around split mold such that the sample did not stick to the surfaces of the split mold. After placing the aluminum foil, both the halves of the split mold were attached using the screws. The compaction was carried in three layers and energy equivalent to standard proctor was applied. The compacted samples were left to curing for 6 h and 24 h.

Conditioning and loading

The cured samples were placed in the cyclic triaxial cell with a rubber membrane around it, to avoid the direct contact of water on the sample. Cyclic triaxial cell was filled with the water to apply uniform confining pressure in all direction on the sample. Later, samples were subjected to 500 conditioning cycles and 15 different stress states (five deviatoric stresses and three confining stresses). Details of load and deformation were collected during all 15 cycles over the entire sequence of application of stress state, however, the last five applications of stress state were considered for the calculation of resilient modulus. Table 2 gives the different deviatoric stresses and confining stresses considered in the study. A constant confining stresses were maintained constant for every five cycles. The deviatoric stress applied was constant for cycles 1 to 5, 6 to 10, and 11 to 15. The application of stresses was carried in accordance with AASHTO-T307.

Results and discussion

Figure 6a–c shows the resilient modulus values for the fly ash samples prepared with different water contents equal 24%, 26%, and 28%. The resilient modulus of fly ash samples with curing period of 24 h was found to be higher than that of samples with six hours curing period. The pattern was found similar at all the water contents tested. This behavior could be attributed to the pozzolanic reaction of fly ash that takes place with the passage of time. Similar behavior was observed for red silty clay till mixed with 18% fly ash [8], reclaimed asphalt pavement (RAP) mixed with fly ash [17]. For curing period equal to six hours, the resilient modulus values of samples prepared with 24%, 26%, and 28% water contents ranged from 30 to 80 MPa, whereas for

Table 2 Resilient modulus testing sequence for a subgrade material

Cycles	Deviatoric stress (kPa)	Confining stress (kPa)
1	12.5	41.4
2	24.9	41.4
3	37.3	41.4
4	49.6	41.4
5	61.9	41.4
6	12.2	27.6
7	24.7	27.6
8	37.2	27.6
9	49.5	27.6
10	61.7	27.6
11	12.3	13.8
12	24.6	13.8
13	37.1	13.8
14	49.5	13.8
15	61.8	13.8

Fig. 6 Resilient modulus test results of fly ash alone at **a** 24% water content, **b** 26% water content, and **c** 28% water content
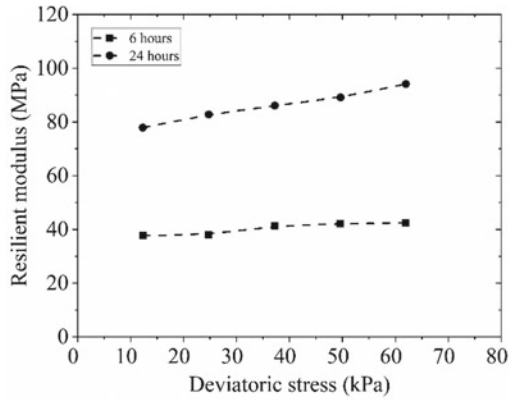
(a)
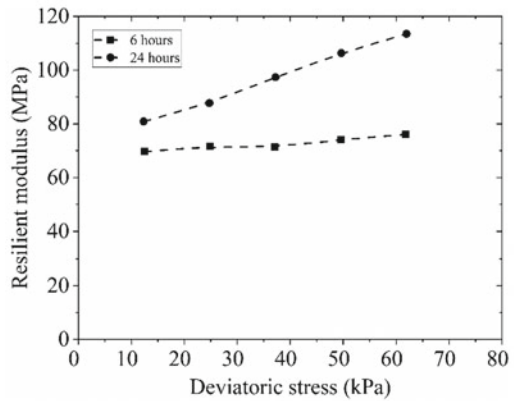
(b)
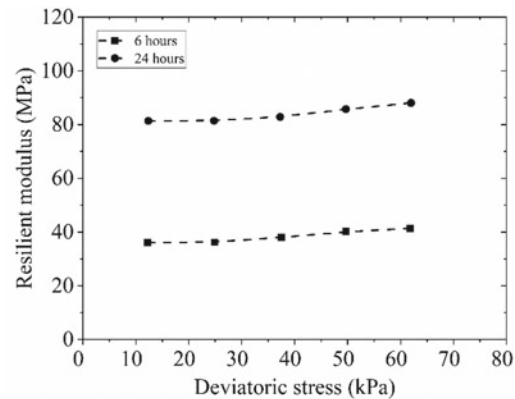
(c)

Fig. 7 Histograms of
resilient modulus values for
various curing times and
water contents of fine fly ash
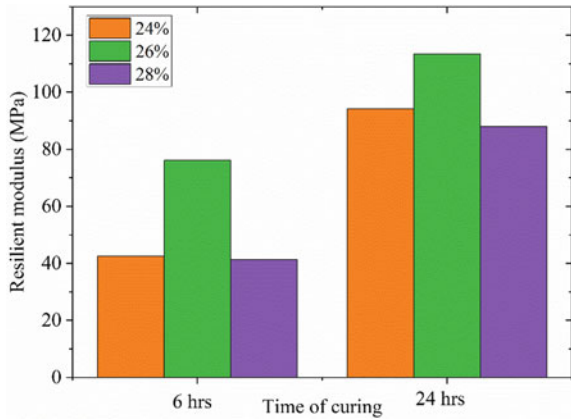
24 h of curing, the M_R value ranged from 75 to 120 MPa for samples prepared with
24%, 26%, and 28% water contents. High values of M_R ranging between 220 and
550 MPa for RAP and fly ash mixtures [17], and 87–205 MPa for crushed brick-
plastic granules and RAP-plastic granules mixtures [5] were reported in literature.
The difference in the resilient modulus mainly depends on the type of the material
used and the deviatoric stress applied on the sample.

In order to study the effect of water content on the resilient modulus, histograms
of M_R values corresponding to curing periods of 6 h and 24 h were plotted for
different water contents (see Fig. 7). For samples with 6 h and 24 h curing time, the
resilient modulus values at OMC were found to be considerably higher than that of
samples prepared at dry or wet side of OMC. The trend highlights that water content
significantly affects the strength and stiffness of the samples.

4   Conclusions

In this study, effect of the water content and the curing period was studied on fly
ash collected from Neyveli thermal power plant, Neyveli, Tamilnadu. The following
conclusions are derived from the study.

1. Resilient modulus (M_R) of fly ash samples with curing period of 24 h was found
   to be 30–50% higher than that of samples with 6 h curing period.
2. The resilient modulus (M_R) values of fly ash samples prepared at OMC were
   found to be higher than that of those of samples prepared at dry or wet sides of
   OMC by 44% and 45%, and 17% and 22% corresponding to curing periods of
   6 h and 24 h, respectively.

References

1. ASTM. D854. Standard test methods for specific gravity of soil solids by water pycnometer. West Conshohocken, PA: ASTM (2010)
2. ASTM D2487. Standard practice for classification of soils for engineering purposes (unified soil classification system). West Conshohocken, PA: ASTM (2011)
3. ASTM D698. Standard test methods for laboratory compaction characteristics of soil using standard effort. ASTM D698. West Conshohocken, PA: ASTM (2012)
4. Arulrajah, A., Mohammadinia, A., Maghool, F., Horpibulsuk, S.: Tire derived aggregates as a supplementary material with recycled demolition concrete for pavement applications. J. Clean. Prod. **230**, 129–136 (2019)
5. Arulrajah, A., Yaghoubi, E., Wong, Y.C., Horpibulsuk, S.: Recycled plastic granules and demolition wastes as construction materials: resilient moduli and strength characteristics. Constr. Build. Mater. **147**, 639–647 (2017)
6. Bordolai, B., Sarmah, E.: A re-think on fly ash ponds in India. Environmental Protection. eponline.com. Accessed 14 Feb 2021
7. CEA. (2018). "CAE, Anual Report 2017–18." Government of India, Ministry of Power, Central Electricity Authority. Last accessed 05 Feb 2016
8. Edil, T.B., Acosta, H.A., Benson, C.H.: Stabilizing soft fine-grained soils with fly ash. J. Mater. Civ. Eng. **18**(2), 283–294 (2006)
9. Huang, Y.H.: Pavement Analysis and Design, 2nd edn. Prentice Hall, Inc., New Jersey (2004)
10. Karnam Prabhakara, B.K., Guda, P.V., Balunaini, U.: Optimum mixing ratio and shear strength of granulated rubber-fly ash mixtures. J. Mater. Civ. Eng. **31**(4), 4019018 (2019)
11. Kim, B., Prezzi, M., Salgado, R.: Geotechnical properties of fly and bottom ash mixtures for use in highway embankments. J. Geotech. Geoenviron. Eng. **131**(7), 914–924 (2005)
12. Kim, H., Lee, M.S., Balunaini, U., Prezzi, M., Siddiki, N.Z.: Cmpaction quality control of fly and bottom ash mixture embankment using dynamic cone penetrometer and lightweight deflectometer. Transp. Res. Board, pp. 1–21 (2010)
13. Perera, S., Arulrajah, A., Wong, Y.C., Horpibulsuk, S., Maghool, F.: Utilizing recycled PET blends with demolition wastes as construction materials. Constr. Build. Mater. **221**, 200–209 (2019)
14. Petry, T.M., Richardson, D.N., Ge, L., Han, Y.P., Lusher, S.M.: Resilient Moduli of Typical Missouri Soils and Unbound Granular Base Materials. Missouri University of Science and Technology, Rolla Administration, Research and Special Programs, (January), 198p (2008)
15. Puppala, A.J., Hoyos, L.R., Potturi, A.K.: Resilient moduli response of moderately cement-treated reclaimed asphalt pavement aggregates. J. Mater. Civ. Eng. **23**(7), 990–998 (2011)
16. Sakai, E., Miyahara, S., Ohsawa, S., Lee, S.H., Daimon, M.: Hydration of fly ash cement. Cem. Concr. Res. **35**(6), 1135–1140 (2005)
17. Saride, S., Avirneni, D., Javvadi, S.C.P., Puppala, A.J., Hoyos, L.R.: Evaluation of fly ash treated reclaimed asphalt pavement for base/subbase applications. Ind. Geotech. J. **45**(4), 401–411 (2015)
18. Senol, A., Edil, T.B., Bin-shafique, S., Acosta, H.A., Benson, C.H.: Soft subgrades stabilization by using various fly ashes **46**, 365–376 (2006)
19. Sheng, B.: Evaluation of Granular Subgrade Modulus from Field and Laboratory Tests. Florida State University Libraries (2010)
20. Tastan, E.O., Edil, T.B., Benson, C.H., Aydilek, A.H.: Stabilization of organic soils with fly ash. J. Geotech. Geoenviron. Eng. **137**(9), 819–833 (2011)

Effect of Tiles Waste and Fly Ash Brick Waste on Permeability and Strength of Lower Granular Subbase Material

Mishra Pooja Mangalprasad and Hrishikesh Ashok Shahane

Abstract As there is growth in the construction industry, construction and demolition (C&D) waste generation is also growing with higher rates in India and hence dumping this waste is a major problem. The construction industry generates 12–15 million tonnes of C&D waste per annum. This C&D waste can be effectively utilized for construction of road pavement. Granular subbase course (GSB) acts as an important layer in the structure layer as well as a drainage layer in the pavement. Most of the pavements in India fail prematurely mainly due to the ineffective functioning of this drainage layer. In this study, engineering properties of fly ash brick (FAB) waste and tiles waste (TW) in a combination of murum to serve it as granular subbase materials were investigated. The objective is to compare the permeability as well as strength characteristics of GSB gradations prepared with different C&D mixes. Modified Proctor tests were conducted on different mixes of FAB waste and murum as well as TW and murum for determination of compaction characteristics. Proctor test result shows that as FAB waste content in murrum increases, the MDD value decreases, and the similar results were obtained for TW content. CBR test was conducted on the various mixes of waste material and murum from which CBR value of 70M + 30FAB was found to be highest. From permeability test, it was observed that the k value goes on increasing after the addition of FAB and TW in soil murrum mix. The permeability test indicated that FAB and TW materials are effective to drain off the water from the subbase layer. From the study, it was noticed that the strength parameter of FAB waste was found to be more effective than that of TW and both the materials show improvement in drainability property.

Keywords Granular subbase · Fly ash brick waste · Tiles waste · CBR · Permeability

M. P. Mangalprasad (✉)
Department of Civil Engineering, JESITMR, Nashik, Maharashtra 422222, India
e-mail: poojams01@gmail.com

H. A. Shahane
Department of Civil Engineering, S. V. National Institute of Technology, Surat, Gujarat 395007, India
e-mail: shahane.hrishi@gmail.com

1   Introduction

India is the fastest-growing economy in the world. The Indian construction industry is an essential part of the economy and people's expanding expectations for a better quality of living. As per the smart cities mission of the Government of India, strategic components of area-based development in the smart cities mission are city improvement, city renewal, and city extension [1]. The renovation will result in a replacement of the current built-up environment and enable co-creation of a new layout with enhanced infrastructure using mixed land use and increased density. In such missions, a large quantity of C&D is expected to be gendered as some existing infrastructure is going to replace with new infrastructure which will give the more intensive infrastructure service levels and a large number of smart applications. In this journey to maintain the equilibrium between demand and supply of materials, ensuring material prices stability, and conformance of materials to quality standards are the biggest challenges. Reuse of recycled C&D materials in civil engineering practices will decrease the demand for virgin natural resources and at the same time reduce the quantity of this waste material destined for landfills [2]. This will affect in a low carbon solution, considering that recycled materials have noteworthy carbon savings compared with virgin quarried materials [3]. C&D materials have been used in recent years in various civil engineering applications such as highways, embankments, concrete, and backfilling [2, 4–7].

In India, approximately 12–14.7 million tonnes of C&D waste is generated per annum as reported by CPCB [8]. According to Shen et al. [9], C&D waste is a combination of surplus constituents generated from the construction, renovation, and destruction activities such as site clearance, land excavation, and roadwork and demolition. Unfortunately, the C&D waste is usually dumped on the sides of canals, on minor roads, and at the entrances of cities and towns, even though there are allocated landfill areas for dumping this kind of waste; that causes environmental problems and affects people's daily lives [4].

The objective of this paper is to study the effect of tiles waste and fly ash brick waste on engineering and geotechnical properties of subbase material. As granular subbase course (GSB) is provided above the subgrade of pavement to serve both as a structural member of flexible pavement layer system and as a drainage layer in pavements, the Ministry of Road Transport and Highways [10] recommends 6 types of GSB mixes, to be laid in different combinations. It is recommended that gradings III and IV shall preferably be used in lower subbase. However, grading V and VI shall be used as a subbase cum drainage layer. The specification includes the strength requirements, liquid limit (LL), and plasticity index (PI) values but has no specific criteria or requirements for effective drainage based on an estimation of permeability/hydraulic conductivity (k) is given. These specifications often fulfill the requirements of the layer as a member however it is not clear whether these gradations fulfill the drainage requirements. Hence there is a need to check the permeability of the recommended GSB mixes. In most of the national highway development projects in India, modified specifications of GSB material using crushed aggregates with

quarry dust for the fines, to avoid the use of gravelly soils with fines having plasticity, are being adopted in order to ensure adequate drainage. Hence in the present study, GSB mixes with non-plastic C&D waste (tiles waste and fly ash brick waste) have been used to study the drainage characteristics. While the standard permeameter for measuring vertical permeability in the laboratory is used for materials of size less than 4.75 mm, there is no standard test by which the permeability of GSB mixes having greater aggregate sizes can be checked.

2 Background

Several researchers studied various types of C&D waste materials in an attempt to investigate the usage of it in several civil and geotechnical engineering applications. Arulrajah et al. [2] have done a comprehensive laboratory evaluation of the geotechnical and geoenvironmental properties of five predominant types of construction and demolition (C&D) waste materials. The C&D materials tested were recycled concrete aggregate (RCA), crushed brick (CB), waste rock (WR), reclaimed asphalt pavement (RAP), and fine recycled glass (FRG). In terms of usage in pavement subbases, RCA and WR were found to have geotechnical engineering properties equivalent or superior to that of typical quarry granular subbase materials. CB at the lower target moisture contents of 70% of the OMC was also found to meet the requirements of typical quarry granular subbase materials.

Mohammadinia et al. [6] investigated the reclaimed asphalt pavement (RAP), recycled concrete aggregate (RCA), and crushed brick (CB). The geotechnical properties of cement-treated C&D materials were evaluated to assess their performance in pavement base/subbase applications. The RAP exhibited the highest strength in all cases, with the same cement content and for the same curing duration, followed by RCA and CB. The resilient moduli of C&D materials increased with an increase in cement content, curing duration, and confining pressure. It is also indicated that cement-treated C&D materials are viable construction materials for pavement base/subbase applications. The behavior of C&D materials, when stabilized with geopolymers, was studied by Mohammadinia et al. [5]. Fly ash (FA) and ground-granulated blast furnace slag (S) were used as pozzolanic binders and a different alkaline activator solution to pozzolanic binder ratio was tested. Both the resilient modulus of the C&D materials and compressive strength were found to increase as a result of geopolymer stabilization. Geopolymer stabilization was found to be most effective for RCA. Higher compressive strength will be achieved by slag-based geopolymer stabilization when compared with fly ash-based geopolymer stabilization. Arisha et al. [4] investigated the suitability of recycled concrete aggregate (RCA) materials and recycled clay masonry (RCM) brick in pavement construction in Egypt. The preliminary recommendations after assessing the effect of RCA and RCM mixes on pavement performance were suggested. The recycled materials showed better pavement performance in terms of rutting and fatigue cracking in comparison with the typical virgin aggregate. Dungca and Jao [11] have determined the optimum

blending proportion of fly ash and bottom ash to the conventional road base materials used as highway embankments. Results show that the optimum strength can be produced at a blend of 100% bottom ash. However, permeability tests show a considerable decline in hydraulic conductivity with the addition of coal ashes to the typical aggregates. Thus, proper drainage must be carefully applied to these blended embankment materials so as to avoid substantial ingress of water. Richardson [12] has undertaken a study to determine the drainability characteristics of several types of unbound granular materials that are used in pavement bases. Hydraulic conductivity and effective porosity were determined for aggregates from two sources of crushed stone and two sources of gravel. For each material, two open gradations were tested in a rigid wall permeameter. Typical dense-graded gravel and crushed stone pavement base materials are relatively slow draining and effective porosities that average 27% of nominal porosities for a range of expected field compacted densities.

3   Material Characterization

Murrum is the coarse-grained soil mixed with fines which is used for road and embankment construction widely all over the world. The murum (M) used in this study was obtained locally from Nashik. On the basis of the particle size range, Cu (6.78), and Cc (2.14) the murrum was classified as clayey sand (SC) as per IS 1498 [13]. Tiles waste (TW) material and fly ash brick (FAB) waste material were collected from the waste generated at a locally available construction site in Nashik; the tile waste and fly ash brick waste were classified as poorly graded gravel (GP) category as per IS 1498 [13]. The TW and FAB materials were pulverized in the laboratory, as shown in Fig. 1b, c, with a maximum particle size of 20 mm to meet the requirements of specification for granular subbase grading III [10]. From direct shear test on murrum soil, shear parameters were evaluated, cohesion (c) = 0.09 kg/cm^2 angle of friction (φ) = 23.51°. The geotechnical properties of recycled C&D materials are presented in Table 1.

a   b   c
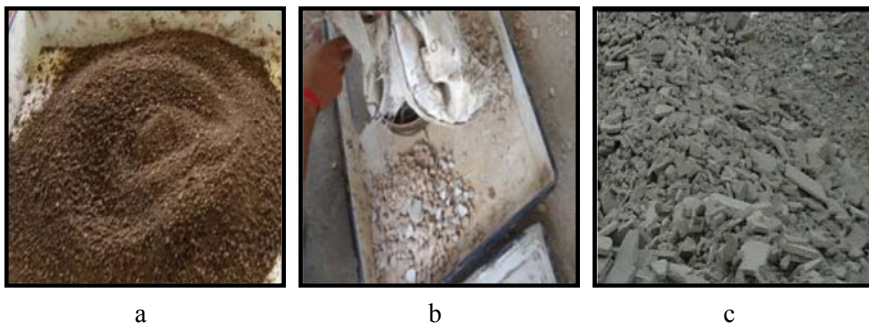
Fig. 1   Murrum and C&D materials

Table 1 Geotechnical properties of recycled C&D materials

Property	Murrum (M)	Tile waste (TW)	Fly ash brick waste (FAB)
Type of soil	SC	GP	GP
Specific gravity (G)	2.83	2.47	2.06
Plastic limit %	26.75	–	–
Liquid limit %	51.5	–	–
Plasticity index (Ip)	21.7	–	–
MDD (gm/cc)	1.95	1.78	1.90
OMC (%)	12	14.47	13.62
D_{10} mm	1.18	2.5	0.6
D_{30} mm	4.5	10	4.5
D_{60} mm	8	10.7	8
C_u	6.78	4.25	13.33
C_c	2.14	3.73	4.22

4 Methods and Sample Preparation

To study the engineering properties of the TW/FAB blends for use in pavement construction, a sequence of laboratory tests was conducted. The laboratory tests included basic characterization tests such as particle size distribution, specific gravity (coarse and fine fraction), as well as modified Proctor compaction, CBR tests, and falling head permeability test.

Fly ash brick waste and tile waste were added to the murrum samples to investigate the effects of these materials on permeability and strength on granular subbase material. Certain geotechnical properties of the murrum were determined by mixing tile waste and fly ash brick waste in the different percentage like 0, 10, 20, and 30% by weight of soil murrum samples [11]. Compaction, CBR test, and permeability test were performed on each of them. The effects of these wastes on soil murrum were thereafter determined.

5 Test Results and Discussion

Materials like metal brick, kankar, and crushed concrete are permitted to use in the lower subbase [10]. The particle size distribution curves of the C&D materials were determined from sieve analysis (Fig. 2). These plots were compared with upper and

Fig. 2 Grain size
distribution curve of C&D
materials
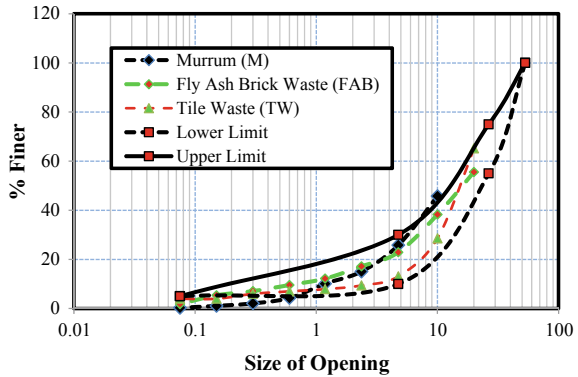
Fig. 3 Modified compaction
curves of murum and fly ash
brick waste
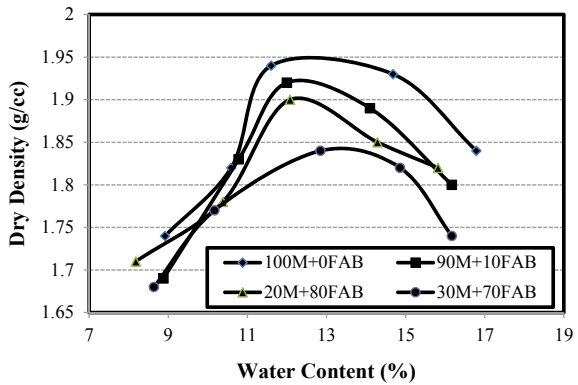
lower bound limits specified by the MORTH [10]. As shown in Fig. 2, the grading limits of the C&D materials were within the specified limits for pavement granular subbase materials, with some materials just below the marginal line.

Figure 3 shows the compaction curves of a mixture of murum and fly ash brick waste. The modified compaction test results indicated that murrum had the highest MDD. As the FAB waste content in murrum increases, the MDD value decreases. The fact is that FAB has lower density as compared to murrum. The compaction curve of murrum and FAB also shows its sensitivity to water content changes. It is also observed that the OMC value increases with the fly ash brick waste content which due to absorption of water by FAB grains during mixing and compaction (Fig. 3).

Similar compaction test results were obtained in case of TW and murum mixture. Results indicated that as the TW content in murrum increases, the MDD value decreases. However, the compaction curve of murrum and TW suggests its low sensitivity to water content changes in comparison with murrum which indicates that TW gives the stable compaction behavior and good workability over a wide range of

Fig. 4 Modified compaction curves of murum and tile waste
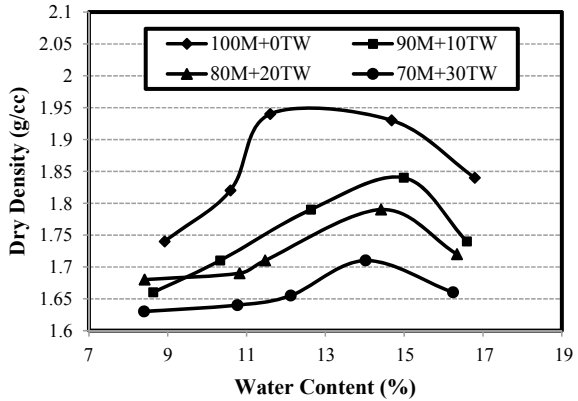
water. The various combination of M&TW shows the MDD value in the range of 1.7–1.8 g/cc and OMC value of 14–15%.

CBR test specimens were prepared by applying modified compaction efforts to murrum and FAB/TW mixed at their OMC as obtained in compaction tests and then the samples were soaked in water for a period of four days. The CBR values for M and FAB mixes were found in the range between 101 and 129% and satisfy the specifications of MORTH [10] requirements for a lower subbase material, which requires a least CBR value of 30%. The distinction in CBR results for the murum and 3 mixes is shown in Fig. 5. It was observed that with FAB content the CBR value increases. The CBR value with FAB contents was found to be higher than that of murum. Maximum CBR value was observed as 129% at 2.5 mm penetration value for the 70M + 30FAB mix.

Figure 6 shows the variation of CBR value with TW. It was observed that the CBR value decreases with TW content, however, it meets the specifications of MORTH [10]. Similar results were reported by Poon and Chan [14] in the investigation of crushed brick in CBR tests. By comparing CBR performance of both C&D material

Fig. 5 Variation of CBR value with FAB content
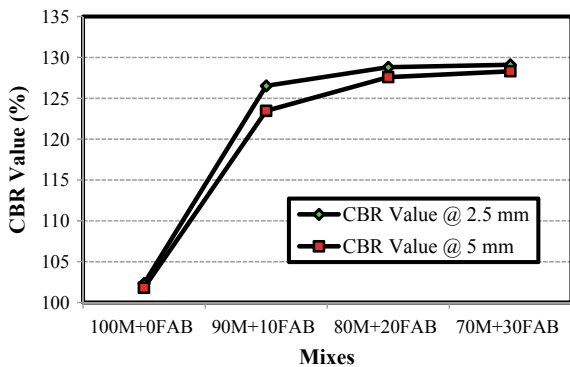
Fig. 6 Variation of CBR value with TW content
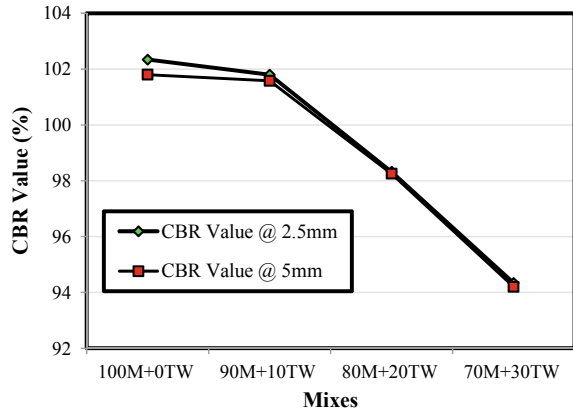
it was observed that the addition of fly ash brick waste gives the better replacement to the subbase material as its maximum CBR value is about 129% for 2.5 mm penetrations in soaked CBR condition of four days.

On comparing the results of various mixes, it was observed that the permeability value goes on increasing after the addition of FAB and TW (Fig. 7). This increase in the permeability is due to an increase in the void ratio of mixes as shown in Fig. 7. As the addition of FAB/TW creates the open-graded material, there was an effect of particle shape on the permeability of mixtures, thus making the mixture coarser. Test results show that both the mixes have good drainability property which is required for effective designing of a subsurface drainage system. The permeability of granular material is a function of particle size distribution, pore continuity, and pore shape. These are affected by particle size distribution, particle shape, and relative density [12].
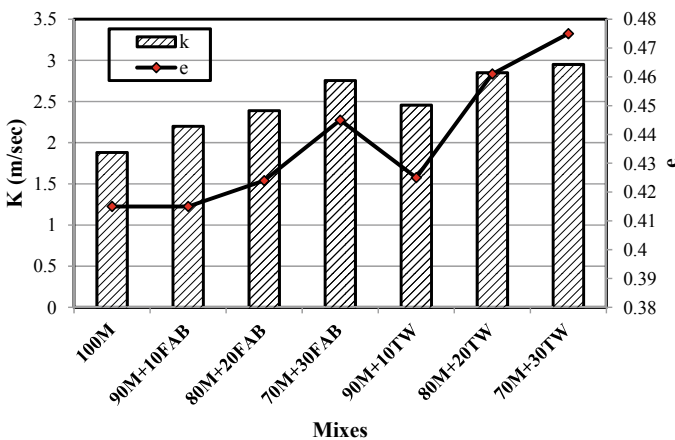
Fig. 7 Variation of 'k' value and 'e' for various mixes

6   Conclusions

The properties of the material and their particle size distribution were influenced greatly on OMC and MDD value. The CBR value with FAB contents was found to be higher than that of soil murum and TW mix. Maximum CBR value was observed as 129% at 2.5 mm penetration for the 70M + 30FAB mix, even though its void ratio was higher than that of other mixes. The FAB addition increases the frictional shear force between the matrix of murum and resists the load. Permeability result shows that both FAB and TW have good drainage property. The addition of FAB waste was found as more effective than that of TW waste as they satisfy the specifications Indian Road Congress for granular subbase layer.

References

1. Ministry of Urban Development Government of India (2015). Smart Cities Mission Statement & Guidelines
2. Arulrajah, A., Piratheepan, J., Disfani, M.M., Bo, M.W.: Geotechnical and Geoenvironmental properties of recycled construction and demolition materials in pavement subbase applications. J. Mater. Civ. Eng. **25**(8), 1077–1088 (2013)
3. Disfani, M.M., Arulrajah, A., Haghighi, H., Mohammadinia, A., Horpibulsuk, S.: Flexural beam fatigue strength evaluation of crushed brick as a supplementary material in cement stabilized recycled concrete aggregates. Constr. Build. Mater. **68**, 667–676 (2014)
4. Arisha, A.M., Gabr, A.R., El-Badawy, S.M., Shwally, S.A.: Performance evaluation of construction and demolition waste materials for pavement construction in Egypt. J. Mater. Civ. Eng. **30**(2), 1–14 (2018)
5. Mohammadinia, A., Arulrajah, A., Sanjayan, J., Disfani, M.M., Bo, M.W., Darmawan, S.: Stabilization of demolition materials for pavement base/subbase applications using fly ash and slag geopolymers: Laboratory investigation. J. Mater. Civ. Eng **28**(7), 1–9 (2016)
6. Mohammadinia, A., Arulrajah, A., Sanjayan, J., Disfani, M.M., Bo, M.W., Darmawan, S.: Laboratory evaluation of the use of cement-treated construction and demolition materials in pavement base and subbase applications. J. Mater. Civ. Eng. **27**(6), 1–12 (2015)
7. Arulrajah, J., Piratheepan, T.A., Bo, M.W.: Geotechnical properties of recycled crushed brick in pavement applications. J. Mater. Civ. Eng **23**(10), 1444–1452 (2011)
8. Gupta, S., Malik, R.K.: The impact of C&D waste on Indian environment: a critical review. Civ. Eng. Res. J. **5**(2), 1–07 (2018)
9. Shen, L.Y., Tam, V.W., Tam, C.M., Drew, D.: Mapping approach for examining waste management on construction sites. J. Constr. Eng. Manage. **130**(4), 472–481 (2004)
10. MORTH-2013 Specification for Road and Bridge Works. Indian Road Congress, New Delhi (2013)
11. Dungca, J.R., Jao, J.A.L.: Strength and permeability characteristics of roadbase materials blended with fly ash and bottom ash. Inter. J. GEOMATE **12**(31), 9–15 (2017)
12. Richardson, D.N.: Drainability characteristics of Granular pavement Base material. J. Transp. Eng. **123**(5), 385–392 (1997)
13. IS 1498 (2016). "Classification and identification of soils for general engineering purposes." Bureau of Indian Standards, New Delhi
14. Poon, C.S., Chan, D.: Feasible use of recycled concrete aggregates and crushed clay brick as unbound road sub-base. Constr. Build. Mater. **20**, 578–585 (2006)

Shear Strength Behavior of Soil-Sized Material Obtained from Landfill Mining, Waste-To-Energy Plants, and C&D Processing Plants

Lalit Kandpal and Manoj Datta

Abstract The quantity of waste produced in Delhi is around 10,000 tons/day, and all the existing landfills are running out of their capacity. Due to the scarcity of available land, the focus is on reuse of waste. The bulk utilization/high-volume reuse of waste material is possible in geotechnical applications such as earthfills and embankments. For assessing the potential of a waste material, shear strength behavior has to be studied. In this experimental study, strength behavior of soil-sized material (less than 4.75 mm) obtained from (a) landfill mining of aged waste (mined MSW), (b) waste-to-energy plant (MSW incineration bottom ash), and (c) C&D processing plant (C&D waste) has been evaluated. The shear strength behavior of these soil-like materials from MSW is compared with that of locally available soil, i.e., Badarpur sand and Delhi silt. Direct shear tests (DST) on dry samples of all the materials and DST (saturated) on mined MSW, Delhi silt and triaxial tests on saturated samples of MSWI bottom ash, C&D waste, and Badarpur sand were conducted. From the results, it was observed that all three materials exhibit effective angle of shearing resistance (ϕ') in the range of 36º–49º. The maximum value of shear strength was obtained for C&D waste (ϕ' in the range of 45º–49º) followed by MSWI bottom ash (ϕ' in the range of 42º–43º) and then by mined MSW (ϕ' in the range of 36º–42º).

1 Introduction

1.1 *Background*

In the past few decades, booming industrialization, rapid urbanization, and rampant growth of population have led to a significant increase in the generation of municipal solid waste (MSW) [11]. In developing countries like India, local authorities are struggling to find a sustainable and effective solution to manage the overwhelming

L. Kandpal (✉) · M. Datta
Indian Institute of Technology Delhi, New Delhi 110016, India
e-mail: lalitkandpal1996@gmail.com

growth of MSW. This has resulted in open dumping of waste in the form of mounds of garbage in the periphery of most of the metropolitan cities. As per the recent reports, around 55 million tons of waste is produced by India per annum [7]. Delhi in particular generates around 10,000 tons per day. At present in Delhi there are three dumpsites (Ghazipur, Bhalswa and Okhla) which have exhausted their capacities years back and running out of their capacities. Due to the scarcity of land available for dumping waste, several MSW incineration plants are being set up. This reduces the volume of the waste by 80–90% [5]. But the residues of these plants are sent back to the dumpsites. Recently construction and demolition (C&D) plants have been set up in Delhi with the aim of recycling of C&D waste. However, the use of C&D waste is a matter of concern in terms of its quality and demand.

1.2 Objectives

The primary objective of the study is to assess the shear strength behavior and other characteristics of soil-like material (SLM) obtained from the mining of landfills (mined MSW), residues of the incineration plants (MSWI bottom ash), and processed waste from C&D recycling plants (C&D waste) and assess their suitability for earth-fills and embankments. Also the shear strength behavior and other characteristics of the materials are compared among themselves and with locally available material, i.e., Badarpur sand and Delhi silt. SLM in the present study has been defined as the material having the particle size of less than 4.75 mm.

1.3 Literature Review

Landfill mining is still an evolving subject and is being improved in terms of utility of mined materials [4]. Numerous researchers have investigated the geotechnical characterization of mined MSW on different fraction [3, 6, 8]. However, due to the heterogeneity of the waste, there is wide variation in the values of the shear strength reported. Research on geotechnical behavior of MSWI ash of particle size less than 12 mm was carried out [13] and [1] but for SLM very few studies are conducted on shear strength behavior. Tay and Goh [12] carried out the triaxial CD test in Singapore on sand-sized particles of MSWI ash. Cristelo et al. [2] carried out research on C&D material from Portuguese recycling plant to assess the shear strength behavior.

Table 1 General information about the selected sites

Waste type	Location	Remarks
Mined MSW	Waste dump, Delhi	Aged MSW
MSWI bottom ash	Waste-to-energy plant, Delhi	–
C&D waste	C&D plant, Delhi	Processed C&D waste

2 Materials and Methodology

2.1 Materials

The material used in the current study was collected from various solid waste management facilities located at Delhi. The general information about all these facilities is presented in Table 1.

2.2 Methodology

Loss on ignition (LOI), grain size distribution (GSD), and shear strength parameters were determined for the SLM obtained from all the sites. The standards adopted are listed in Table 2. Shear strength parameters in dry condition in all the samples were determined from direct shear test (DST). Shear strength parameters in saturated condition for mined MSW were determined from DST (saturated). Consolidated drained (CD) triaxial tests were carried out on samples of saturated MSWI bottom ash and C&D waste.

Table 2 Standards adopted for tests

Property	Method	Standards
Organic content	Loss on ignition	ASTM D 2974-14 and [13]
Grain size distribution	Sieve analysis	IS2720(Part IV): 1985
Specific gravity	Density bottle	IS2720(Part III): 1980
Shear strength parameters	Direct shear and triaxial test	IS2720(Part XIII): 1986 and IS2720(Part XII): 1986

Table 3 Loss on ignition

Material	Loss on ignition (LOI) %
Mined MSW	8.5–9
MSWI bottom ash	3–4
C&D waste	2.5–2.8
Badarpur sand	0.3–0.4
Delhi silt	1–1.2

3   Results and Discussions

3.1   Loss on Ignition

The possible end use of the waste materials depends on the organic content [9]. LOI studies have been conducted by various researchers to estimate the percentage of organic material. LOI value of the samples is reported. LOI value ranges from 0 to 9% in all the materials studied. LOI above 5% indicates that organic content is higher than normally acceptable in earthworks (Table 3).

3.2   Grain Size Distribution

Figure 1 shows the grain size distribution (GSD) of all the tested materials. The coarsest material out of all the materials is C&D waste which is well graded. The fine content is less than 8%. After C&D waste, MSWI bottom ash is also coarse and
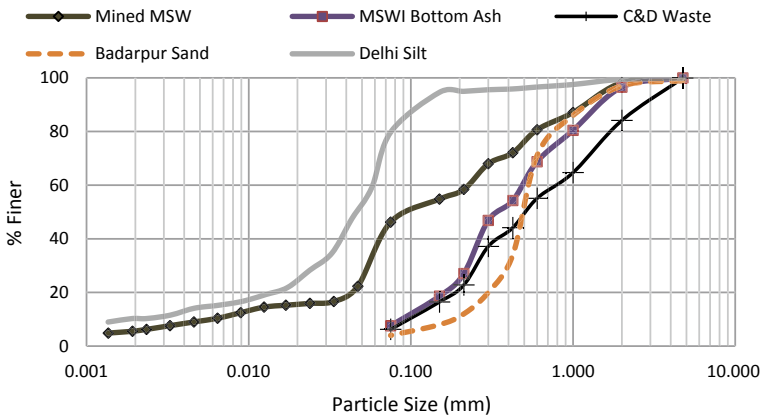
Fig. 1 GSD curve

Table 4 Specific gravity

Material	Specific gravity
Mined MSW	2.38–2.42
MSWI bottom ash	2.44–2.48
C&D waste	2.55–2.60
Badarpur sand	2.67–2.69
Delhi silt	2.65–2.66

well graded. Mined MSW has high content of fine fraction. Badarpur sand is medium coarse sand. Delhi silt is the finest of all the materials studied in this investigation.

3.3 Specific Gravity

The range of specific gravity of all the five samples is reported in Table 4. The sample with high organic content is found to have low specific gravity and vice versa. The effect of organic content on the specific gravity is well reported in the literature [10]. Mined MSW has the lowest specific gravity due to the high organic content.

3.4 Shear Strength

Mined MSW: DST (dry) and DST (saturated) were performed on mined MSW in order to investigate the shear strength parameters (c' and ϕ'). The sample was prepared by static compaction to get the dense sample. In contrast to the values reported in literature [8], the values are high in dry condition and due to the presence of high fine content, the saturated strength of the sample is significantly lower than the dry strength. The results are summarized in Table 5. The stress-displacement and volume change-displacement graph for both dry and saturated states are shown in Fig. 2.

MSWI Bottom Ash: DST (dry) and triaxial (CD) test (saturated) were performed on the material in order to investigate the shear strength parameters (c' and ϕ'). The dense sample was prepared by giving 30 blows in five layers using rubber tamping rod. The results obtained in the study are in accordance with the values reported in literature [13]. The material being coarser and freely draining has almost same angle

Table 5 Shear strength behavior of mined MSW

Test	c' (kPa)	Φ' (degree)	Failure strain (%) (Range)
DST (Dense, Dry)	0	42.9	3.3–6.6
DST (Dense, Sat.)	0	36.1	4.0–8.0
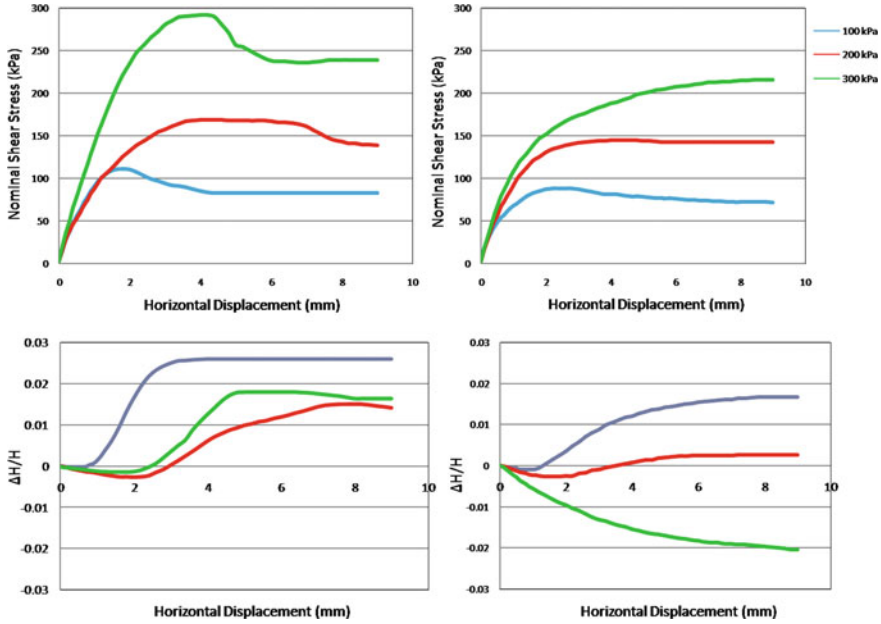
Fig. 2 Stress-displacement and volume change-displacement graph of mined MSW [DST dry (left) and DST saturated (right)]

of shearing resistance in dry and saturated condition. The results are summarized in Table 6. The stress-displacement and volume change-displacement graph for both dry and saturated states are shown in Fig. 3.

C&D Waste: DST (dry) and triaxial (CD) test (saturated) were performed on the material in order to investigate the shear strength parameters (c' and ϕ'). The dense sample was prepared by giving 30 blows in five layers using rubber tamping rod. In contrast to the values reported in literature [2], the values are high for both dry and saturated condition. The material being coarser and freely draining has high angle of shearing resistance in saturated condition also. The results are summarized in Table 7. The stress-displacement and volume change-displacement graph for both dry and saturated states are shown in Fig. 4.

Badarpur Sand: DST (dry) and triaxial (CD) test (saturated) were performed on the material in order to investigate the shear strength parameters (c' and ϕ'). The dense

Test	c' (kPa)	Φ' (degree)	Failure strain (%) (Range)
DST (Dense dry)	0	43.9	7.5–10.0
Triaxial CD test (Dense Sat.)	0	43.3	7.4–10.9

Table 6 Shear strength behavior of MSWI bottom ash

Fig. 3 Stress-displacement and volume change-displacement graph of MSWI bottom ash [DST dry (left) and Triaxial (CD) test saturated (right)]

Table 7 Shear strength behavior of C&D waste

Test	c' (kPa)	Φ' (degree)	Failure strain (%) (Range)
DST (Dense dry)	0	49.4	4.5–8.0
Triaxial CD test (Dense Sat.)	0	45.6	5.2–7.4

sample was prepared by giving 30 blows in five layers using rubber tamping rod The material being coarser and freely draining has almost same angle of shearing resistance in dry and saturated condition also. The results are summarized in Table 8. The stress-displacement and volume change-displacement graph for both dry and saturated states are shown in Fig. 5.

Delhi Silt: DST (dry) and DST (saturated) were performed on the material in order to investigate the shear strength parameters (c' and φ'). The sample was prepared by static compaction to get the dense sample. The results are summarized in Table 9. The stress-displacement and volume change-displacement graph for both dry and saturated state are shown in Fig. 6.
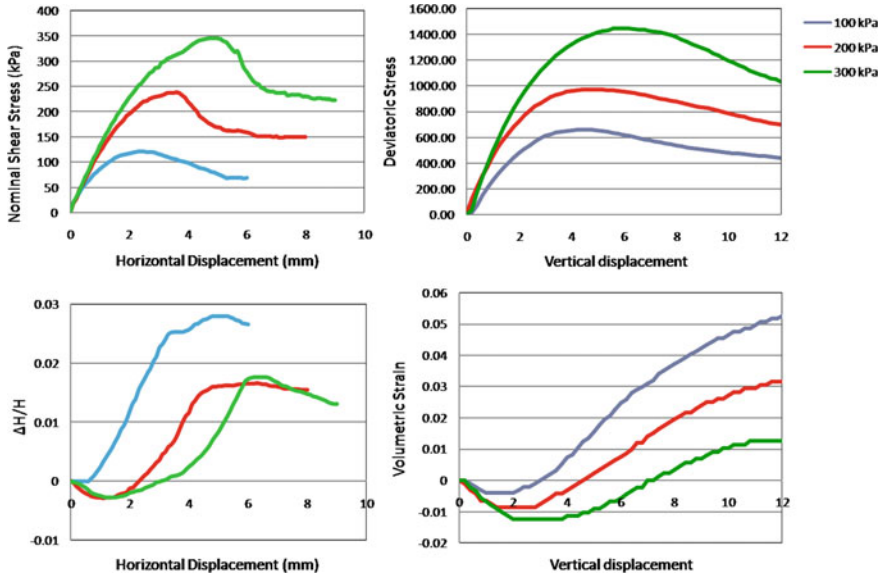
Fig. 4 Stress-displacement and volume change-displacement graph of C&D waste [DST dry (left) and triaxial (CD) test saturated (right)]

Table 8 Shear strength behavior of Badarpur sand

Test	c' (kPa)	Φ' (degree)	Failure strain (%) (Range)
DST (Dense dry)	0	43.1	3.3–6.0
Triaxial CD test (Dense Sat.)	0	42.2	2.5–5.0

4 Conclusions

In this experimental study, strength behavior of soil-sized material (less than 4.75 mm) obtained from (a) landfill mining of aged waste (mined MSW), (b) waste-to-energy plant (MSW incineration bottom ash), and (c) C&D processing plant (C&D waste) has been evaluated to assess if they can be used in earthfills, embankments. The shear strength behavior of these soil-like materials from MSW is compared with that of locally available soil, i.e., Badarpur sand and Delhi silt. The following conclusions can be drawn based on the results:

a. All the three materials exhibit effective angle of shearing resistance (ϕ') in the range of 36º–49º. The maximum value of shear strength is obtained for C&D waste (ϕ' in the range of 45º–49º) followed by MSWI bottom ash (ϕ' in the range of 42º–43º) and then by mined MSW (ϕ' in the range of 36º–42º).

b. C&D waste exhibits effective angle of shearing resistance (ϕ') high in comparison with the locally available material, i.e., Badarpur sand (ϕ' in the range of
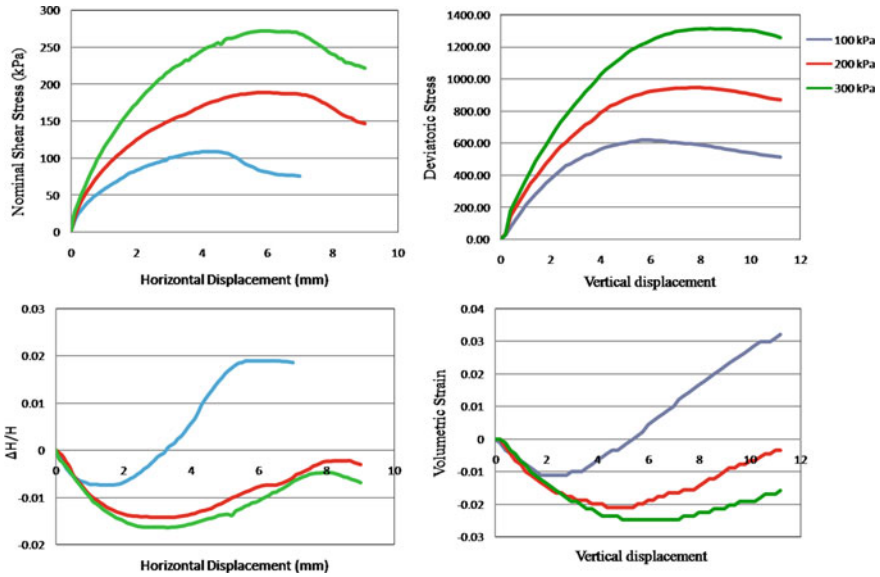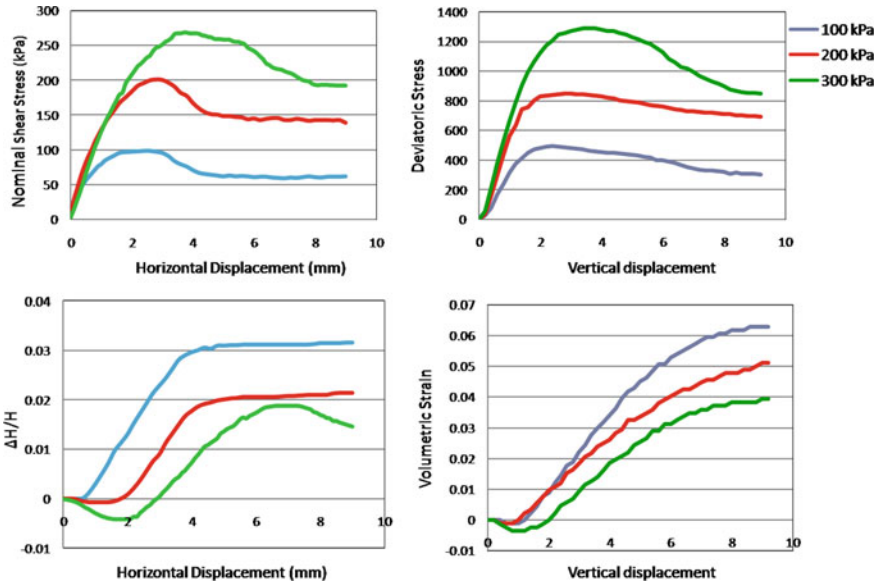
Fig. 5 Stress-displacement and volume change-displacement graph of Badarpur sand [DST dry (left) and triaxial (CD) test saturated (right)]

Table 9 Shear strength behavior of Delhi silt

Test	c' (kPa)	Φ' (degree)	Failure strain (%) (Range)
DST (Dense dry)	0	35.9	4.1–6.7
DST (Dense, Sat.)	0	32.0	10–12

41°–43°) and Delhi silt (ϕ' in the range of 32°–36°). MSWI bottom ash exhibits effective angle of shearing resistance (ϕ') almost same as that of Badarpur sand and higher than that of Delhi silt. Mined MSW exhibits effective angle of shearing resistance (ϕ') lower than that of Badarpur sand and higher than that of Delhi silt.

c. Mined MSW has high angle of shearing resistance in dry state but this reduces upon saturation. As the organic content is more than 5%, mined MSW cannot be used directly for embankments or earthfills since degradation of organic material will lead to excessive settlements. The use of this material can be undertaken in landfills as daily, intermediate, or final cover
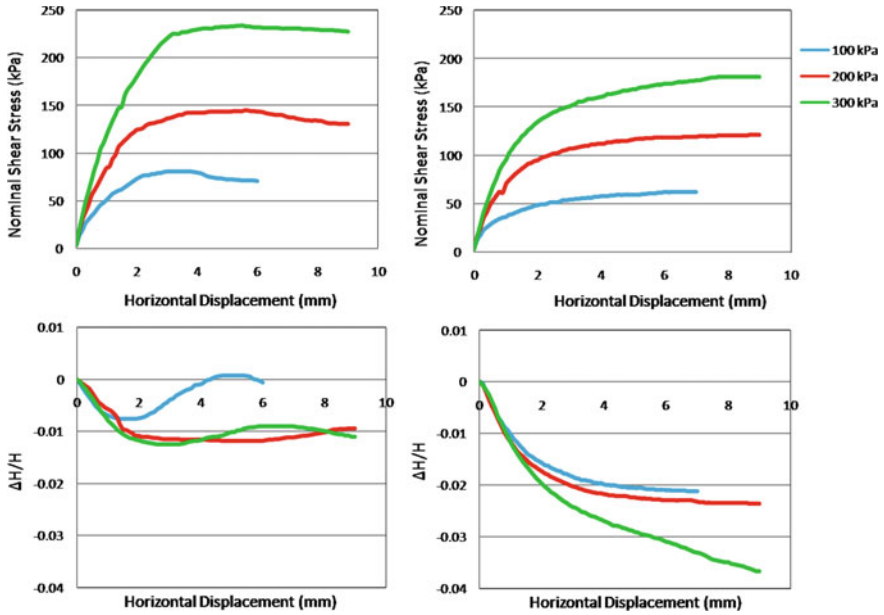
Fig. 6 Stress-displacement and volume change-displacement graph of Delhi silt [DST dry (left) and DST saturated (right)]

References

1. Becquart, F., Bernard, F., Abriak, N.E., Zentar, R.: Monotonic aspects of the mechanical behaviour of bottom ash from municipal solid waste incineration and its potential use for road construction. Waste Manage. **29**(4), 1320–1329 (2009)
2. Cristelo, N., Vieira, C.S., de Lurdes Lopes, M.: Geotechnical and geoenvironmental assessment of recycled construction and demolition waste for road embankments. Proc. Eng. **143**, 51–58
3. Gabr, M.A., Valero, S.N.: Geotechnical properties of municipal solid waste. Geotech. Test. J. **18**(2), 241–251 (1995)
4. Gaitanarou, Z., Tentes, G., Katselis, Y.: Landfill mining: an empirical review on past and state-of-the-art applications (2014)
5. Gupta, G., Datta, M., Ramana, G.V., Alappat, B.J.: Feasibility of using MSW incinerator ash in geotechnical applications. In: Indian Geotechnical Conference GeoNEst, p. 119 (2017)
6. Hyun Il, P., Borinara, P., Hong, K.D.: Geotechnical considerations for end-use of old municipal solid waste landfills. Int. J. Environ. Res. **5**(3), 573–584 (2011)
7. Kumar, S., Smith, S.R., Fowler, G.: Challenges and opportunities associated with waste management in India. R. Soc. Open Sci. **4**, 160764 (2017)
8. Naveen, B.P., Sivapullaiah, P.V., Sitharam, T.G.: Compressibility and shear strength of dumped municipal solid waste. J. Solid Waste Technol. Manage. **40**(4), 327–334 (2014)
9. Parrodi, J.C., Höllen, D., Pomberger, R.: Characterization of fine fractions from landfill mining: a review of previous landfill mining investigations. In: Proceeding of Sixteenth International Waste Management and Landfill Symposium, pp. 2–6 (2017, October)
10. Sen, P., Mukesh, M.D., Chitra, R., Ratnam, M.: Effect of organic content on the index properties and compaction parameters of soil. Int. J. Emerg. Technol. Adv. Eng. **4**(4), 354–359 (2014)

11. Somani, M., Datta, M., Ramana, G.V., Sreekrishnan, T.R.: Investigations on fine fraction of aged municipal solid waste recovered through landfill mining: Case study of three dumpsites from India. Waste Manage. Res. **36**(8), 744–755 (2018)
12. Tay, J.H., Goh, A.T.: Engineering properties of incinerator residue. J. Environ. Eng. **117**(2), 224–235 (1991)
13. Zekkos, D., Kabalan, M., Syal, S.M., Hambright, M., Sahadewa, A.: Geotechnical characterization of a municipal solid waste incineration ash from a Michigan monofill. Waste Manage. **33**(6), 1442–1450 (2013)

Strength and Permeability Characteristics of Fibre-Reinforced Liner Material

Debtanu Seth , **Suresh Prasad Singh** , **and Shubham Singh**

Abstract Sand–bentonite mixture is a widely used liner material. After optimisation, it is observed that sand–bentonite mix with bentonite content 15% satisfies the criteria of compacted clay liner (CCL) material stipulated by the United States Environmental Protection Agency (USEPA). Bentonite, one of the primary elements of the mixture, is an expensive material. So, the focus of this study is to reduce the bentonite content with reinforcing the mix by random inclusion of polypropylene fibres. In this study, sand–bentonite mixture with 10, 15 and 20% bentonite content is used and 0, 0.2, 0.5 and 1% polypropylene fibre by weight of the mixture is added. Unconfined compressive strength (UCS) test is done to observe the strength characteristics of the mix. The UCS specimens are statically compacted to their respective maximum dry densities (MDD) at optimum moisture content (OMC). UCS values are determined at this moulded water content as well as in fully saturated conditions. It is observed that the failure strength and ductility of a sample with a given bentonite content increases with increasing fibre content. It is also noticeable that normalised strain energy is improved and reduction of post-peak strength is minimised with increasing fibre content. However, at a particular fibre content, the strength initially increases up to 15% bentonite content and after that it reduces. This trend is observed for all the samples. The UCS value of sand–bentonite specimens, containing 15% bentonite and compacted at OMC with compaction effort of 595 kJ/m^3, increases from 60.92 to 483.46 kPa when the fibre content is increased from zero to 1% which is 694% increment of strength. Permeability test is done with distilled water under pressure head of 4 kg/cm^2 to find out the effect of fibre content on hydraulic conductivity of the mixtures. It is noticed that inclusion of fibres increases the hydraulic conductivity of the compacted sand–bentonite mixes. Scanning electronic microscopy (SEM) is performed to observe the distribution of fibres in the sand–bentonite mixture.

D. Seth · S. P. Singh (✉) · S. Singh
Civil Engineering Department, NIT Rourkela, Rourkela, Odisha 769 008, India
e-mail: spsingh@nitrkl.ac.in

D. Seth
e-mail: 217ce1033@nitrkl.ac.in

S. Singh
e-mail: 218ce1027@nitrkl.ac.in

1 Introduction

Liner is an essential part of a sanitary landfill system. Among the two types of liners, (i) compacted clay liner (CCL) and (ii) geosynthetic clay liner (GCL), CCL is extensively used due to its low installation cost and availability of material. The primary criterion of CCL is to have very low permeability (in the range of 10^{-7} cm/s) and adequate strength (more than 200 kPa). In most of the cases, the sand–bentonite mixture is used as a liner when the local soil is not fit for being compacted as liner. Due to high cost and less availability of bentonite, researchers showed interest in using less amount of bentonite in sand–bentonite mixture to achieve the previously mentioned criteria of liner material. Fibres are inserted randomly in the sand–bentonite mix to reduce the bentonite content in the sand–bentonite mix and to enhance the mechanical properties. There are two types of fibres (i) natural fibre and (ii) synthetic fibre. In this study, polypropylene fibre (Recron-3S) is used, which is a synthetic fibre.

Previously, researchers focused on the effect of fibre reinforcing on geotechnical properties of cohesionless soil and the strength characteristics of cohesive soil. There is limited literature on the feasibility of using randomly inserted fibre in sand–bentonite liner material for enhancing its mechanical and hydraulic properties. Gray et al. [1] investigated the effect of natural fibre, synthetic fibre and metal wires on the strength characteristics of sand and observed that fibre reinforcement increased the shear strength, decreased post-peak strength reduction and improved other strength behaviour. Maher and Gray [2] investigated the effect of random glass, reed and palmyra fibre inclusion in sand. It was found that the fibre reinforcing increases the failure strength significantly under static load and the stiffness of the sand although low modulus fibres have less contribution to the strength increment of the sand. Abdi et al. [3] studied the effect of short random fibre inclusion on the consolidation characteristics, compression behaviour, permeability and shrinkage property of a mixture of 75% kaolinite and 25% montmorillonite. Fibre of 1, 2, 4 and 8% was added as dry weight of soil with 5, 10 and 15 mm lengths. It was found that consolidation settlement and swelling of the soil decreased with increasing fibre content. Shrinkage limit increases with increasing fibre content. Although the length of fibre does not have any significant effect on the consolidation and compressibility characteristics of the soil, fibre content is constant. It was found that permeability increases slightly with increasing fibre content and length of fibre. However, this increase in permeability is not substantial enough to render the soil unsuitable to be liner or cover material. Miller and Rifai [4] investigated the effect of fibre reinforcing on workability, compaction and permeability characteristics of low plastic clay. The soil was compacted at 2% of wet of optimum and fibres added are 0.2, 0.4, 0.6 and 0.8% of dry weight of soil. Fibre inclusion has little effect on the compaction characteristics of the soil.

However, the crack reduction and tensile strength improved with increasing fibre content, although permeability rises slightly. The optimum fibre content is found to be 0.4–0.5%. Similarly, Moghal et al. [5] discussed the effect of fibre reinforcement in chemically treated soil specimens and compared the results with untreated soil specimens.

In this study, polypropylene fibres are randomly mixed with optimised sand–bentonite mixture. Strength criteria of the soil are observed, and the change is investigated by unconfined compressive strength test, and permeability test is performed to monitor the hydraulic conductivity of the samples with different fibre content. X-ray diffraction test is performed to obtain the compounds present in the mixture. Scanning electronic microscopy is performed to observe the surface texture of the sand and bentonite.

2 Experimental Programme

2.1 Materials

Sand and commercially procured sodium–bentonite are used in this study. The sand is obtained from a river situated in Rourkela. The sand is then dried in an oven to remove the moisture attached to the sand particles and sieved through no. 10 ASTM sieve. The passing portion of the sand is collected. The values of the coefficient of uniformity and coefficient of curvature of sand are obtained as 2.76 and 1.19, respectively. According to the IS classification system and from the C_u and C_c value, it can be concluded that the sand is poorly graded (SP). Bentonite is collected from Nilkanthar MineChemi, Jodhpur. X-ray diffraction confirms the presence of imontmorillonite, quartz, feldspar and aluminium silicate in sand–bentonite mixture. Physical properties of sand, bentonite and the mix are shown in Table 1. Figures 1 and 2 show the SEM images of bentonite and sand. Three sand–bentonite mixtures are prepared with bentonite content 10, 15 and 20% by weight of the mix. The sand and bentonite are dried individually in oven before mixing. Before every test, a desired proportion of water is added to the sand–bentonite mixture and the mix is kept at least for 24 h

Table 1 Geotechnical properties of bentonite and sand

Properties	Bentonite	Sand
Specific gravity	2.72	2.56
Fine contents (%)	97.07	3
Liquid limit (%)	341	–
Plastic limit (%)	32	–
Shrinkage limit (%)	7	–
Plasticity index (%)	291	–
Swelling index (%)	625	–

Fig. 1 Microscopic flaky structure of bentonite by SEM
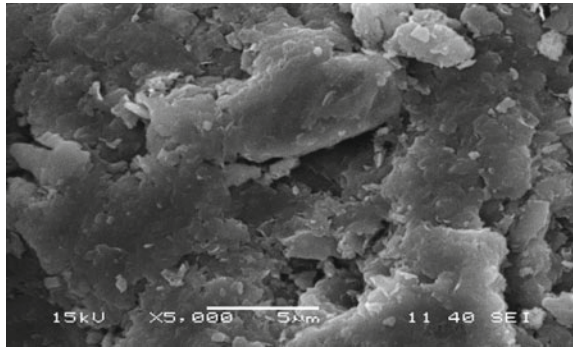
Fig. 2 Microscopic angular structure of sand by SEM
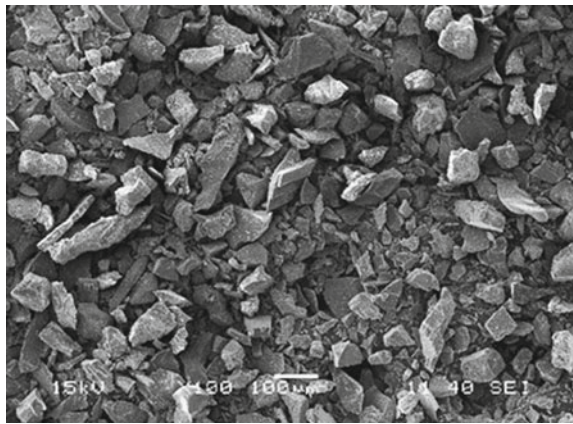
for homogeneous mixing of water. Different tests are performed following the IS codes.

Recron-3S fibre is used in this study to randomly mix with the soil. Recron-3S is a polypropylene (PP) fibre with triangular cross section, and it is developed by Reliance India Ltd, India to enhance strength criteria in different applications. Due to triangular cross section, more surface area of the fibre comes in contact with the soil particles causing better pull-out resistance in comparison with fibres with circular cross sections. Figure 3 shows the pull-out resistance mechanism of fibre, and in Fig. 4, the fibres can be seen embedded in a soil matrix in a SEM image and outlined with red dotted lines. The properties of the fibres are given in Table 2.

2.2 Methodology

Sample Preparation There is no stipulated method for mixing the fibre with the soil. While mixing the fibre and soil, the main difficulty is to attain homogeneity as

Fig. 3 Pull-out mechanism of PP fibre
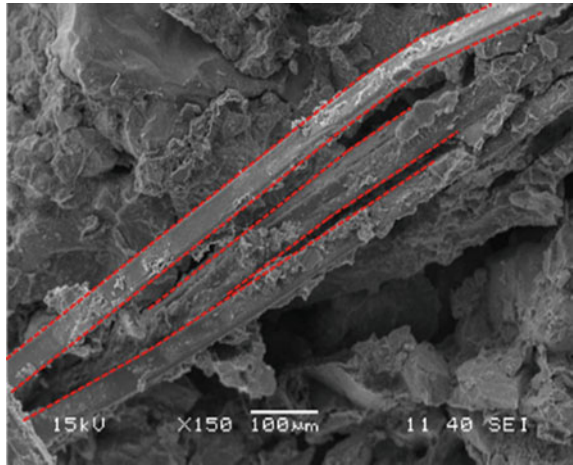
Fig. 4 PP fibre embedded in soil matrix
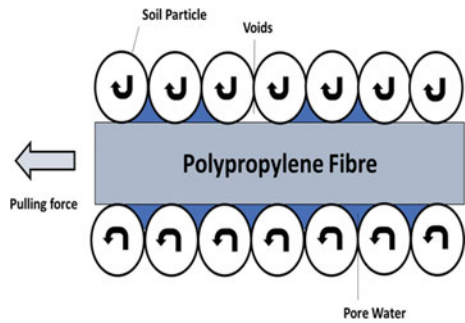
Table 2 Physical properties of polypropylene fibre

Polypropylene fibre	Specific gravity	Length (mm)	Equivalent diameter (mm)	Tensile strength (MPa)	Strain at failure (%)	Tensile modulus (GPa)
	0.91	6	0.023	120	80	3

the fibres are prone to be tangled, which causes an inhomogeneous mixture of fibre and soil. Three sand–bentonite mixtures are prepared with bentonite content 10, 15 and 20% by weight of the mix and by compacting them to their MDD at OMC and adding fibres as 0, 0.2, 0.3 and 0.6% of the dry weight of soil. The fibres are mixed thoroughly in random orientations with the soil to obtain a homogeneous mixture.

Unconfined Compression Test (UCS) The sample is prepared following the above process and for each percentage of mix two triplets are prepared, one triplet is tested in OMC, and another triplet is saturated before testing and later tested in saturated condition. Total 144 samples are tested for UCS among which, 72 are tested at their

OMC and the rest 72 in saturation condition. Again, among those 72 samples, 36 are compacted to their MDD obtained from standard proctor test, and the rest 36 are compacted to their MDD obtained from modified proctor test. During UCS test, load was applied at a strain rate of 1.25 mm/min until the sample fails.

Hydraulic Conductivity Samples are prepared as described above. The samples are compacted in permeability moulds to their MDD at OMC obtained from light compaction test and heavy compaction test. Due to very low permeability of the mixture, a hydraulic gradient of 2 kg/cm^2 is applied, and the head is kept constant throughout the experimental procedure. The samples are permitted with water until the soil is saturated and later the reading is taken.

Scanning Electronic Microscopy Scanning electronic microscopy (JSM-6480LV, magnification-100, 150 & 5000x, accelerating voltage-15 kV) of the bentonite, sand and the sand–bentonite–fibre mixture is performed to observe the shape of the particles and the embedment of the fibres in them. Samples are collected and dried carefully without disturbing the surface texture. Later the samples are coated with platinum and mounted to the instrument. Later pictures are taken through a computer screen attached to the microscope at different magnification.

3　Result and Analysis

3.1　Effect of Fibre Addition on the UCS Value of Compacted Soil

From Figs. 5 and 6, it is evident that with increasing fibre insertion, the unconfined compressive strength of the soil rises for both heavy and light compacted soil. The rate of increase in UCS is nonlinear unlike the linear trend observed by Das and

Fig. 5 Effect of addition of fibre for lightly compacted sample at their OMC
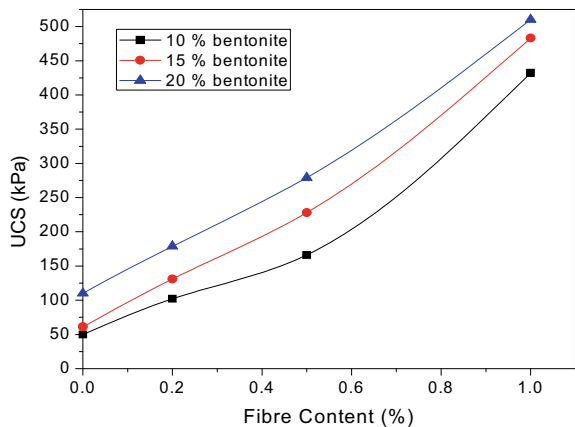
Fig. 6 Effect of addition of fibre for heavily compacted sample at their OMC
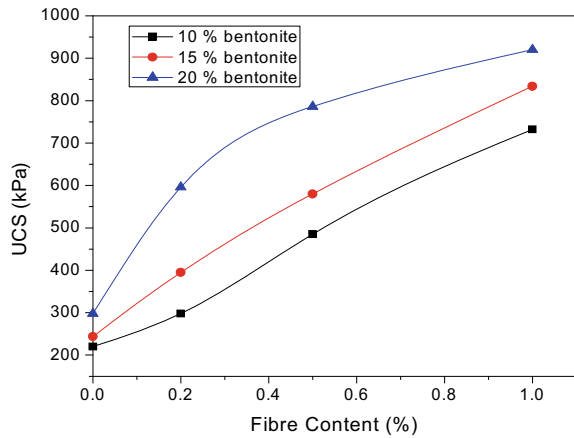
Singh [6]. The addition of fibre of 1% causes an increase in UCS value by 692% for standard compacted soil and 242% for heavy compacted samples in comparison with unreinforced samples for 15% bentonite content sample. It is evident that in case of standard compacted sand–bentonite mixture, percentage increase in UCS value is higher than percentage increase in case of heavy compacted sand–bentonite mixture, but the UCS value in case of heavily compacted soil is much higher than that of the lightly compacted soil. The variations of UCS value with fibre content are shown in Figs. 5 and 6, for sample compacted by standard compaction and heavy compaction methods, respectively, and tested in their OMC.

3.2 Effect of Fibre Addition on the UCS Value of Compacted Soil After Saturation

The compacted samples are saturated before testing for UCS. Similar to the previous case, the failure stress under static load increases with increasing fibre addition. The rate of increase in failure stress follows nonlinear and gradually decreasing trends. In this case, the light compacted sample has 103% increase in strength after 1% fibre inclusion and 186% increase in strength in case of heavy compacted soil after 1% fibre inclusion in comparison with unreinforced sample. The rate of increase in failure strength and value of failure strength both are higher in case of heavy compacted soil in contrast to lightly compacted soil. The variation of UCS with fibre content for mixes with different bentonite contents and compacted by standard proctor method is given in Fig. 7 and the same for the mixture compacted by heavy compaction method is given in Fig. 8. In both the cases, the samples were tested in saturated condition.

Fig. 7 Effect of addition of
fibre on UCS value for
lightly compacted sample at
saturated condition
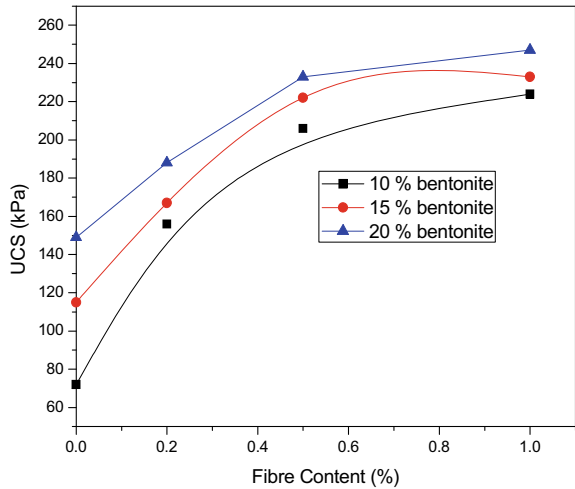
Fig. 8 Effect of addition of
fibre on UCS value for
heavily compacted sample at
saturated condition
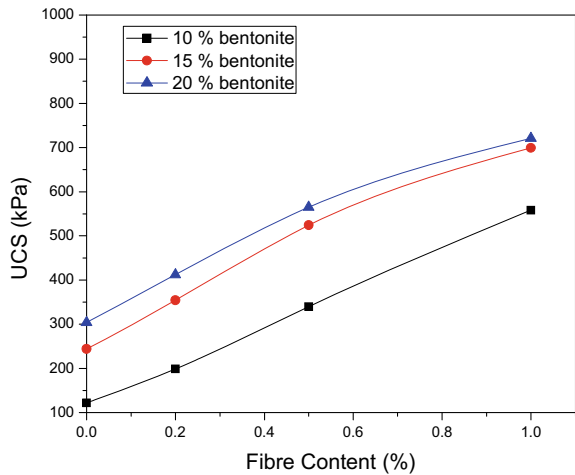
3.3 Effect of Moisture Content on the Stress–Strain Behaviour of Soil

It is noticeable that at OMC, the stress curve is steeper than that at saturation condition, given all other parameters are constant, which indicates that with increasing water content, the soil becomes more ductile. It is also observed that with increasing moisture content, the UCS value decreases. The decrease in failure stress due to increased water content can be attributed to the loss of contacts between particles and lubrication effect of water with increasing water content. The effect of water content should be considered while studying the impact of fibre insertion in soil.

Fig. 9 Effect of water content on stress–strain curve
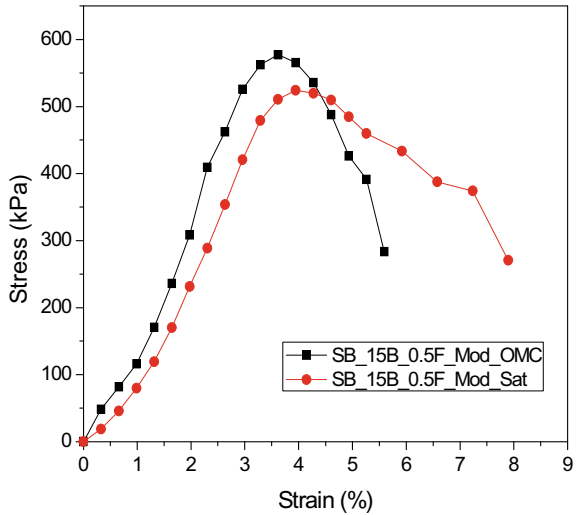
In Fig. 9, SB_15B_0.5F_Mod_OMC indicates a soil sample with 15% bentonite compacted at OMC by modified proctor and the other shows the same sample in saturated condition.

3.4 Effect of Fibre Inclusion on Strain Energy of Soil

It is evident from Fig. 10 that with addition of polypropylene fibre, the strain energy of the soil increases which indicates the capacity of soil to absorb energy increases with increasing fibre content. Thus, the ability of the liner to carry load without cracking increases, and also its resistance to sudden loads like earthquake loads enhances. This increase in strain energy of soil after the addition of fibre can be attributed to the anchorage action of the fibre in the soil matrix. Figures 9 and 10, which are given below, support the above statement.

3.5 Effect of Fibre Inclusion on Hydraulic Conductivity of Soil

The hydraulic conductivity of the heavily compacted soil is measured after the soil attains saturation state. It is observed that with increasing fibre content, the hydraulic conductivity of the soil increases. The permeability for unreinforced sand–bentonite mixture with 15% bentonite content and increases from 1.71×10^{-8} cm/s to $3.20 \times$

Fig. 10 Variation of strain energy with increasing fibre content for samples with different bentonite content
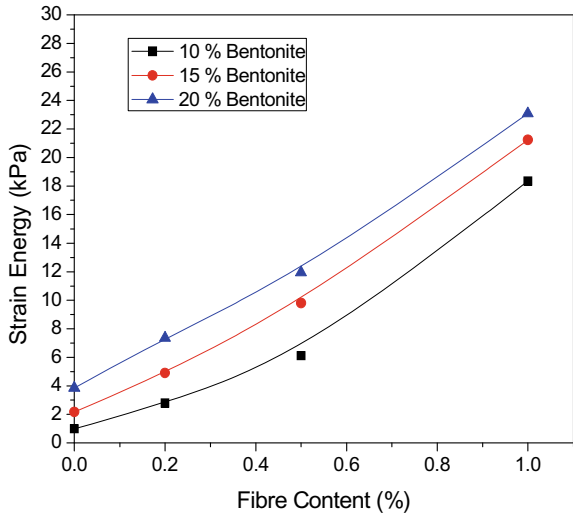
10^{-8} cm/sec when reinforced with 1% polypropylene fibre, i.e. increase in permeability by 87.1% in comparison with that of unreinforced soil. Although there is an increase in hydraulic conductivity of soil, the increase is not enough to render the soil unsuitable for being a liner material. The randomly inserted fibres are connected, and by drainage action, it increases the permeability of sand–bentonite mixture [7]. Thus, with increasing fibre content, the permeability of the mixture increases (Figs. 11 and 12).

Fig. 11 Variation of hydraulic conductivity with fibre content
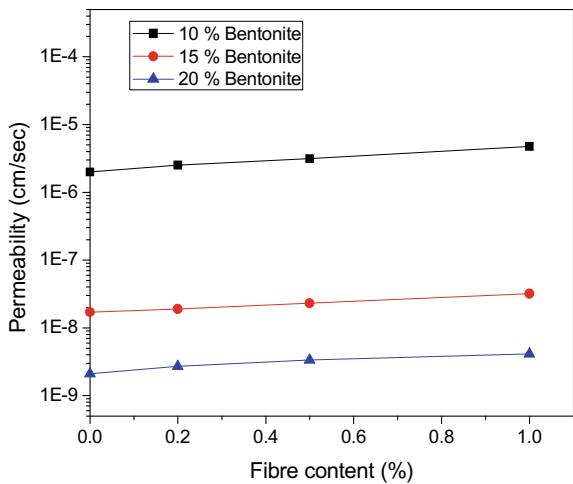
Fig. 12 Variation of hydraulic conductivity with fibre content as observed by Maher et al. [7]
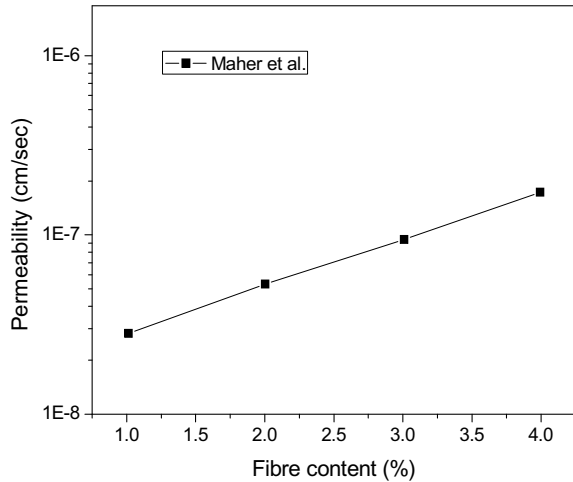
4   Conclusion

Polypropylene fibre is randomly mixed with sand–bentonite mixture and compacted. Various tests are performed to investigate the strength and hydraulic properties of the mix. The following conclusions can be drawn from the obtained test results.

The unconfined compressive strength of the mixture increases manifold with a slight increase in the percentage of fibre. The percentage increase in UCS value is more in lightly compacted soil in comparison with highly compacted soil, but the UCS value in case of heavily compacted sample is very much higher than samples compacted lightly. The saturated samples show an increasing trend in UCS value too. In this case, the percentage increase in both the lightly compacted samples and heavily compacted samples is almost same, although the UCS value for heavily compacted sample is much higher. It is also found that the strain energy increases and post-peak loss decreases with increasing fibre content. Addition of polypropylene fibre causes a slight increase in hydraulic conductivity.

From the above points and results, it can be concluded that sand–bentonite mixture with 10% bentonite content can proficiently satisfy the strength criteria of liner material after addition of fibre, but it will fail to fulfil the permeability criteria whereas 15% bentonite content can appropriately meet both strength criteria (minimum 200 kPa UCS value) and permeability criteria (not exceeding 10^{-7} cm/s). A bentonite content of 20% satisfies both strength and permeability criteria but for cost-effective design 15% bentonite content can be concluded as optimised bentonite content, and in the necessity of enhancing strength fibre can be added accordingly.

References

1. Gray, D.H., Ohashi, H.: Mechanics of fiber reinforcement in sand. J. Geotech. Eng. **109**(3), 335–353 (1983)
2. Maher, M.G.: Static response of sands reinforced with randomly distributed fibers. J. Geotech. Eng. https://doi.org/10.1061/(ASCE)0733-9410**116**(11):1661 (1990)
3. Abdi, M.R., Parsapajouh, A., Arjomand, M.A.: Effects of Random Fiber Inclusion on Consolidation, Hydraulic Conductivity, Swelling, Shrinkage Limit and Desiccation Cracking of Clays. Int. J. Civ. Eng. **6**4 December (2008)
4. Miller, C.J., Rifai, S.: Fiber Reinforcement for Waste Containment Soil Liners. J. Environ. Eng. https://doi.org/10.1061/(ASCE)0733-9372**130**8 891. (2004)
5. Moghal, A.A.B., Chittoori, B.C., Basha, B.M., Al-Mahbashi, A.M.: Effect of polypropylene fibre reinforcement on the consolidation, swell and shrinkage behaviour of lime-blended expansive soil. Int. J. Geotech. Eng. **12**(5), 462–471 (2018)
6. Das, N., Singh, S.K.: Geotechnical behaviour of lateritic soil reinforced with brown waste and synthetic fibre. Int. J. Geotech. Eng. **13**(3) (2019). https://doi.org/10.1080/19386362.2017.134 4002.
7. Maher, M.H., Ho, Y.C.: Mechanical properties of kaolinite/fiber soil composite. J. Geotech. Eng. **120**(8), 1381–1393 (1994)

Strength Properties of Alkali-Activated Fly Ash

Gaurav Anand, Murapaka Swamy Naidu, and Suresh Prasad Singh ⓘ

Abstract Fly ash is a by-product of coal-fired power plants and a rich source of aluminosilicate. This paper reports the compaction and strength properties of fly ash activated with different concentrations of lime, cement, and alkali solution. The lime and cement content has been varied as 0, 2.5, 5, 7.5, and 10% of dry weight of fly ash whereas the concentration of NaOH solution is varied as 0.5, 1, and 2 M. In general, an increase in stabilizer content increases the MDD value whereas the OMC decreases. The maximum UCS value of the stabilized specimens is found to be 3.5 MPa. However, stabilized specimens are found to be brittle in nature.

Keywords Fly ash · Activation · OMC · MDD · Unconfined compressive strength

1 Introduction

Industrialization and urbanization are the two major aspects of development both of which call for a scenario for high power generation. Fly ash produced from coal-fired power plants poses serious disposal as well as environmental issues. On the other hand, transformation of these deleterious waste products into suitable construction material might be a more suitable alternative owing to the fact that this technique would not only alleviate the environmental issue of waste disposal but also help decreasing the cost of construction business [1]. The self-hardening property of fly ash owing to its free lime content has made fly ash a suitable for construction material [2]. However, the cementitious property of fly ash can be further enhanced by activation [3]. The investigation of strength properties of fly ash has spurred the scientific curiosity in the past few decades. The variation of shear strength of pulverized fuel

---

G. Anand · M. S. Naidu · S. P. Singh (✉)
Civil Engineering Department, NIT Rourkela, Rourkela 769008, India
e-mail: spsingh@nitrkl.ac.in

G. Anand
e-mail: 217ce1023@nitrkl.ac.in

M. S. Naidu
e-mail: 218ce1490@nitrkl.ac.in

ash has been investigated by Raymond [4] and amelioration of the strength properties has been reported with progressing time. The enhancement of strength with lime stabilization at elevated temperature has also been studied by the investigators [5]. Enhancement of strength properties of class F fly ash via alkalization and gypsum addition has also been accomplished by Ghosh et al. [6]. Activation of fly ash has been attempted by various researchers [7–9]. Stimulation of the pozzolanic reactions upon the addition of lime to fly ash has been demonstrated by Mira et al. [10]. On the other hand, Ryu et al. [11] have concluded based on their study that the higher the molarity of alkaline addition the better the compaction, consequently improved strength. In this paper, an attempt has been made to investigate the effect of different stabilizers, i.e., lime, cement and NaOH on the compaction and strength properties of fly ash under various curing conditions.

2 Materials

Fly ash used in this study was collected from Rourkela Steel Plant (RSP), India. The collected sample has been passed through 425 μm sieve to remove foreign and vegetative matters. The samples were mixed thoroughly to obtain the homogeneity and were oven dried at temperature of 105–1100 °C. The physical and chemical properties of the fly ash have evaluated prior to the investigation and presented in Tables 1 and 2, respectively. Laboratory grade lime (CaO) of 95.6% purity is used in the test program. Similarly 43 grade slag cement is used. Sodium hydroxide solution of required concentration is prepared from NaOH pellets in the laboratory.

Table 1 Physical properties of fly ash

Physical parameters	Values	Physical parameters	Values
Color	Light gray	Shape	Rounded/Subrounded
Silt and clay (%)	88	Uniformity coefficient (Cu)	5.67
Fine sand (%)	12	Coefficient of curvature (Cc)	1.25
Medium sand (%)	0	Specific gravity	2.182
Coarse sand (%)	0	Plasticity index	Non-plastic

Table 2 Chemical analysis of fly ash

Elements	Composition	Elements	Composition	Elements	Composition
MgO	1.7	K_2O	1.97	MnO	0.3
Al_2O_3	28.1	P_2O_5	1.72	TiO_2	0.85
SiO_2	53.6	CaO	2.65	LOI	6.5
Fe_2O_3	1.8	Na_2O	0.5		

Fig. 1 Grain size distribution of fly ash
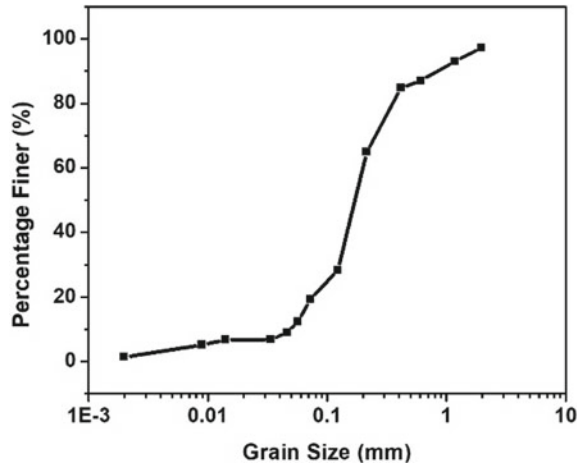
3 Methodology

The experimental procedure consisted of the treatment of fly ash with varying contents of lime, cement (0, 2.5, 5, 7.5, and 10%), and NaOH solution with varying molar concentration (0.5, 1, 2 M). The specific gravity of fly ash is found to be 2.182 [12]. Figure 1 presents the particle size distribution for the fly ash. Based on this analysis, it can be inferred that the fly ash consists of sand to silt-sized particles. As apparent from the figure almost 88 percentage of the fly ash is found to pass through 75 μm sieve [13]. The uniformity coefficient (Cu) and the coefficient of curvature (Cc) of the fly ash are evaluated to be 5.67 and 1.25, respectively, thus indicating uniform gradation of samples. All the tests are conducted as per Indian standards.

4 Results and Discussions

4.1 Compaction Characteristics

The light and heavy compaction tests are carried out in order to determine the relationship between the dry density and moisture content of the fly ash amended with different concentrations of the stabilizers. Figure 2a shows the relationship between dry density and water content at compactive effort of 595 kJ/m³ [14] whereas Fig. 2b gives for compaction effort of 2674 kJ/m³ [15]. The curves of dry density and moisture content for different lime content are present in Fig. 2c, d, respectively. It can be inferred that as the compactive energy increases the MDD increases and the moisture required to achieve this density decreases. Furthermore, it is seen that the nature

Fig. 2 Compaction curves for lime amended fly ash at compactive effort of **a** 595 kJ/m^3 **b** 2674 kJ/m^3, Variation of **c** MDD **d** OMC with lime content

of compaction curve is fairly flat. Such a slight variation of compaction properties with moisture content is desirable from the aspect of field application. Under such a circumstance, the variation of field moisture content may not alter the dry density of the compacted layer appreciably. Similar kinds of observations have also been reported for fly ash amended with lime in the literature [6, 16]. The variation of dry density with water content for cement amended fly ash subjected to light compaction energy and heavy compaction energy is represented in Fig. 3a–d, respectively. Cement amended fly ash also shows a similar behavior. However, under heavy energy compaction, a steady decrement in the moisture content values can be observed. The decrement in dry density values at higher cement content and an insignificant rise in the moisture content values are attributed to plasticity of the specimen imparted by cement. Figure 4a, b shows the variation of dry density with moisture content of the NaOH-treated fly ash specimen. Figure 4c, d shows the variation of OMC and MDD of the NaOH-treated fly ash specimen. It can be observed that with increase in NaOH content and increase in compaction energy the dry density of the specimen exhibits a steady enhancement. On the other hand, the OMC of the specimen decreases as the NaOH molar concentration increases. NaOH is viscous and much lubricating than normal water. During compaction when the load
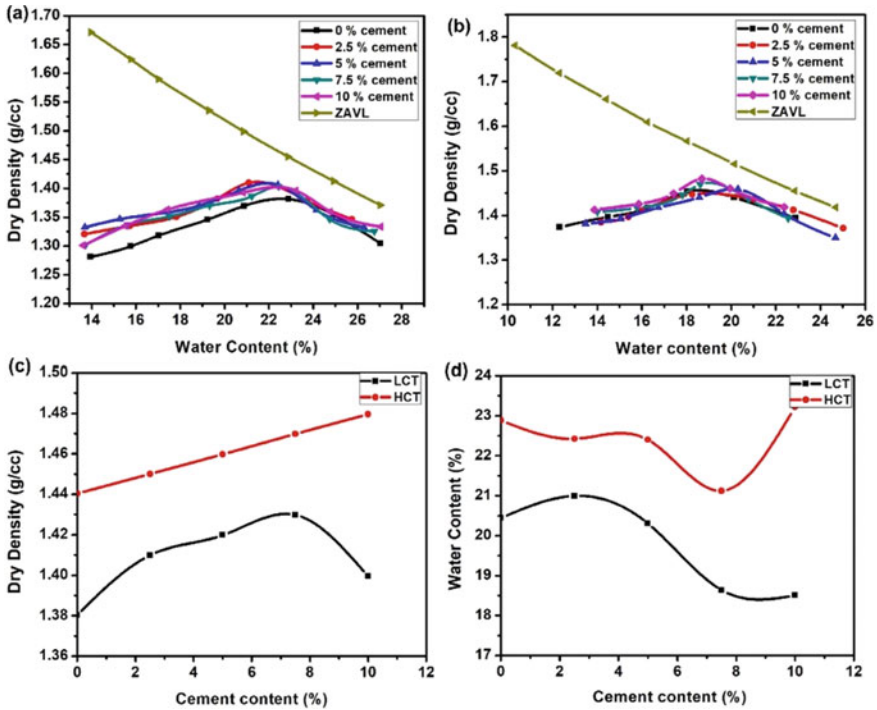
Fig. 3 Compaction curves for cement amended fly ash at compactive effort of **a** 595 kJ/m^3 **b** 2674 kJ/m^3, Variation of **c** MDD **d** OMC with cement content

is applied the coated fly ash particles shear along each other surface, resulting in a dense packing. Consequently, water, which is in between the particles, expels out. Hence, the maximum dry density increases and optimum water content decreases.

4.2 Unconfined Compressive Strength

Cylindrical specimens have been prepared with dimension 50 mm × 100 mm for each combination of stabilizers compacted to their respective MDD at OMC. These specimens are coated with wax and cured for 0, 7, 15, 30, and 60 days at 30 °C. The cylindrical specimen has been sheared at an axial strain rate of 1.25 mm/min till failure of the sample. For each lime, cement and NaOH content and curing period three identical specimens were tested and then the average compressive strength value has been reported. The stress–strain relationships of compacted lime-treated fly ash for varying curing periods are presented in Figs. 5 and 6 corresponding to light and heavy compaction energy levels, respectively. From these plots, it is envisaged
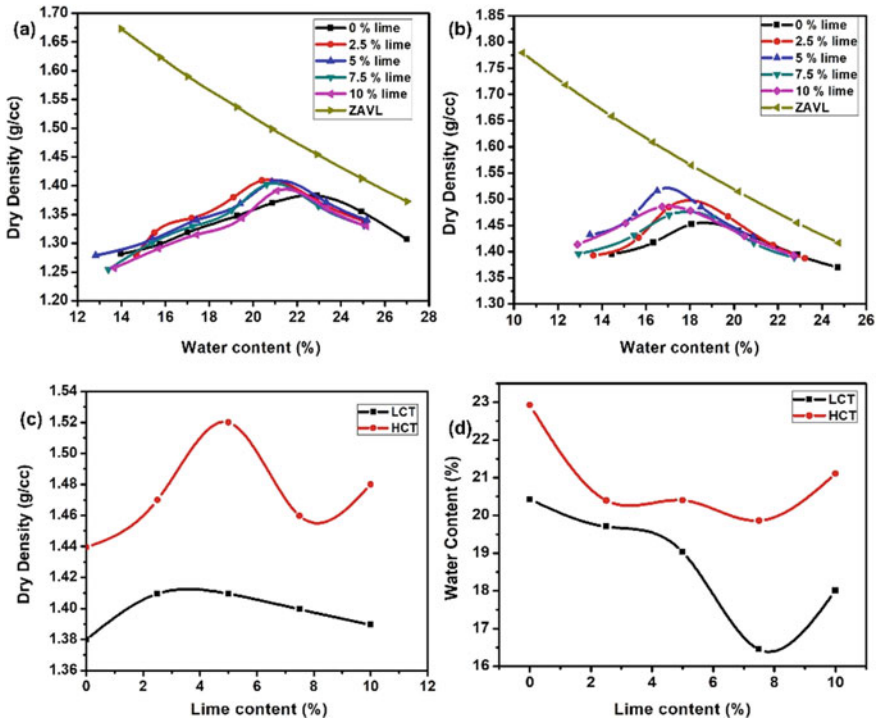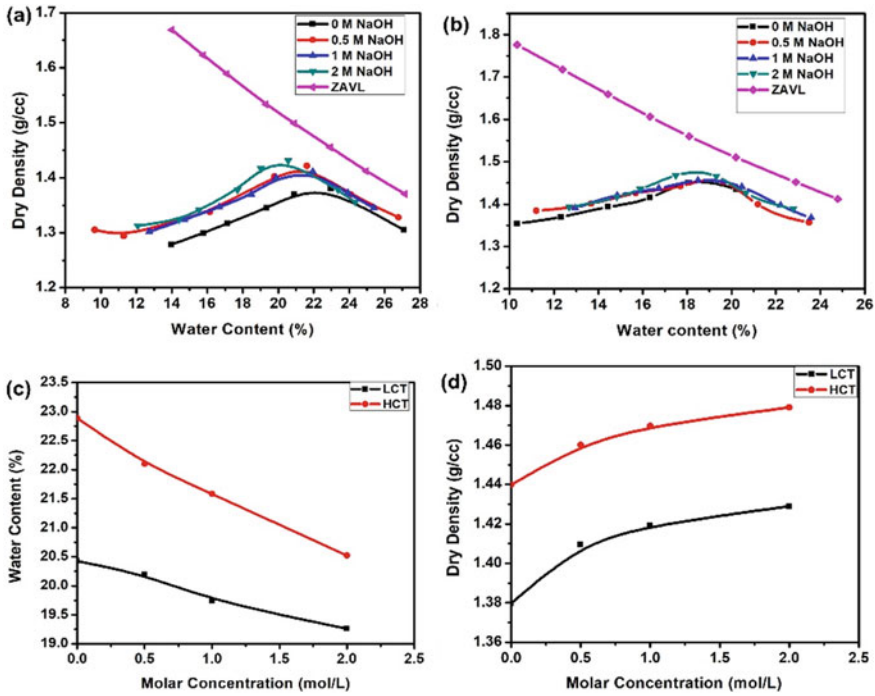
Fig. 4 Compaction curves for NaOH-treated fly ash at compactive effort of **a** 595 kJ/m^3 **b** 2674 kJ/m^3, Variation of **c** MDD **d** OMC with NaOH concentration

that the failure stress is higher when subjected to higher compaction energy than that of compacted with lower compaction energy.

However, with increasing curing time the unconfined compressive strength of the specimen increases appreciably. However, in general the failure strains are found to be lower for samples compacted with higher energies. The failure strains vary from a value of 1.5 to 2.75%, indicating brittle failure in the specimens with increasing lime content. The increase in unconfined strength of specimens with increased compactive effort is attributed to the closer packing of particles, resulting in the increased interlocking among particles. A closer packing is also responsible in increasing the cohesion component in the sample. With increasing curing period of lime-treated fly ash specimen shows improvement in UCS values.

Figures 7 and 8 show the stress–strain behavior of compacted cement-treated fly ash for varying curing periods corresponding to low compaction energy and high compaction energy, respectively. From these plots, it can be envisaged that the failure stress as well as failure strain of samples compacted with greater compaction energy are higher than the samples compacted with lower compaction energy However, in general the failure strains are found to be lower for samples compacted with higher energies. The failure strains vary from a value of 1.5 to 2.5%, indicating brittle failure in the specimens. Fly ash has alumina and silica both of which are
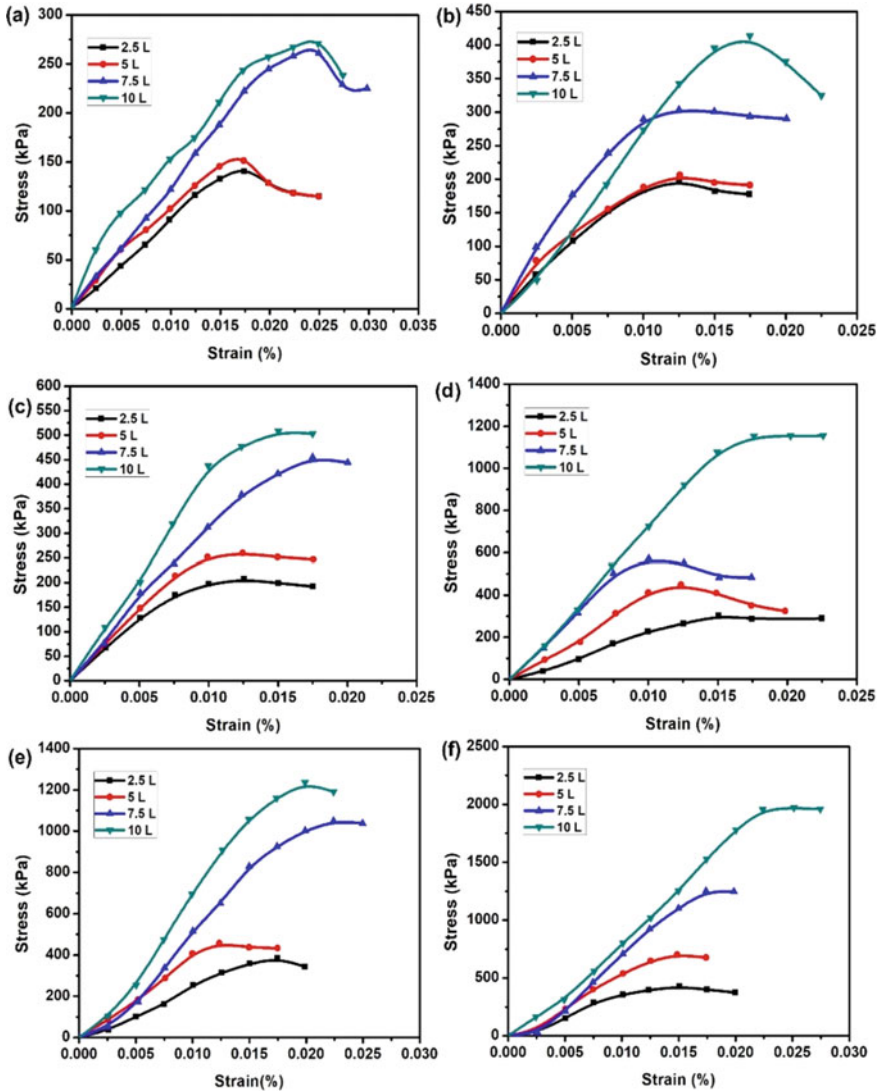
Fig. 5 Stress–strain curves for lime-treated fly ash compacted with low compaction energy and cured for **a** 0 day **b** 3 day **c** 7 day **d** 15 day **e** 30 day **f** 60 day

available for reactions leading to cementation process. Under such circumstance, the cement-stabilized fly ash imparts higher strength values. The variation in stress–strain behavior of the NaOH-treated fly ash specimen with increasing curing period has been illustrated in Figs. 9 and 10 for low compaction energy and high compaction energy, respectively. The variation is similar to previous two cases, i.e., lime-treated and cement-treated fly ash specimens.
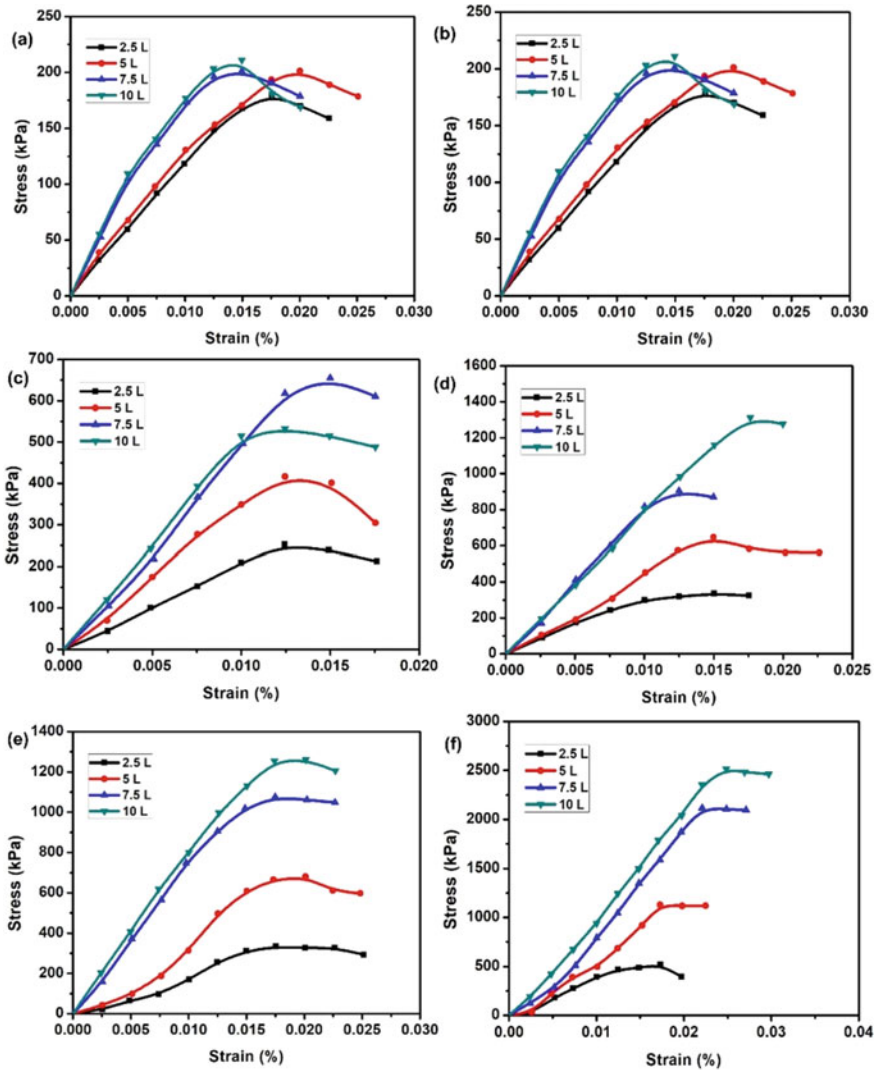
Fig. 6 Stress–strain curves for lime-treated fly ash compacted with heavy compaction energy and cured for **a** 0 day **b** 3 day **c** 7 day **d** 15 day **e** 30 day **f** 60 day

Additionally, it is observed that the failure strains vary from a value of 1.25–2.5%, indicating brittle failure in the specimens. As NaOH reacts with silica and alumina present in fly ash during the curing period and formed a gel like material called sodium aluminosilicate gel with a general formula $Na_n\{ -(SiO_2)_z -AlO_2-\}_n$. This gel filled the pore space in the specimens and developed strength. At lower NaOH content the amount of sodium available for the sodium alumina-silicate gel is not adequate thus the gel formation is unsubstantial thereby the strength properties do
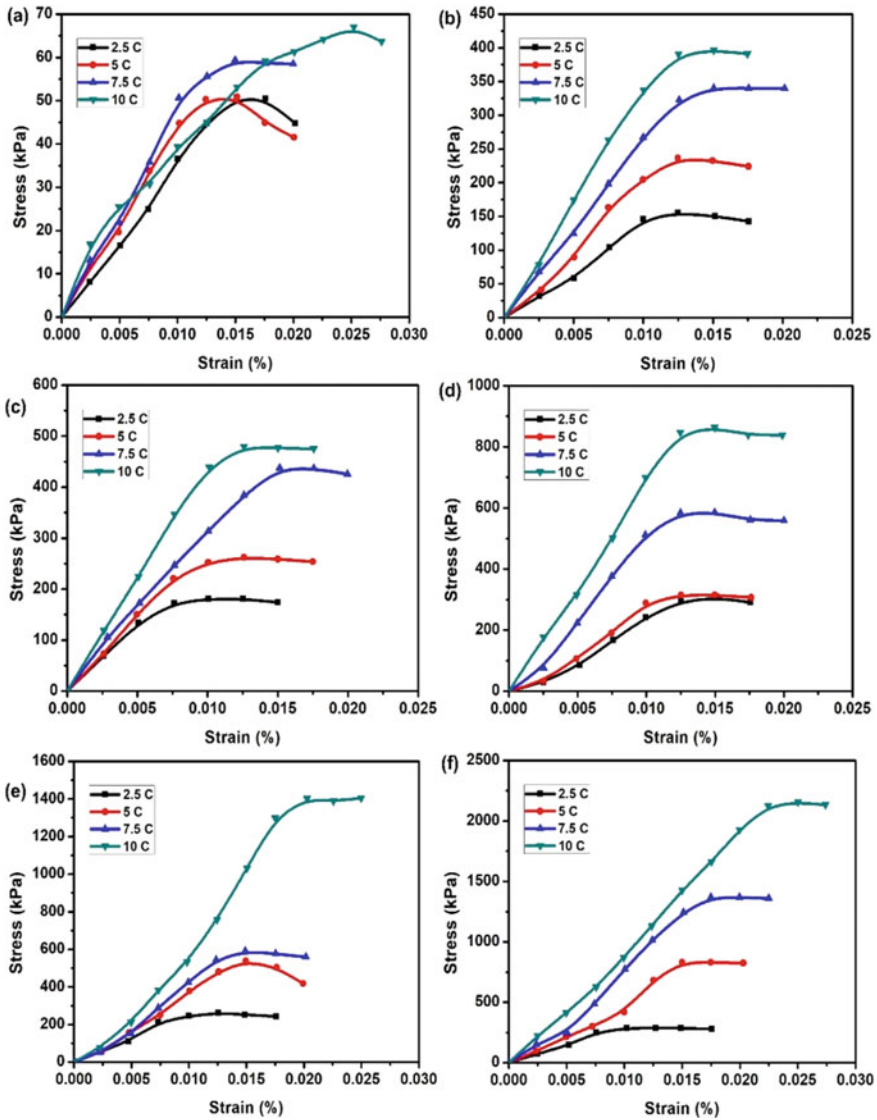
Fig. 7 Stress–strain curves for cement-treated fly ash compacted with low compaction energy and cured for **a** 0 day **b** 3 day **c** 7 day **d** 15 day **e** 30 day **f** 60 day

not show a significant enhancement. Although they exhibit appreciable plasticity, at higher alkali content the gel formation is adequate imparting high strength values. However, at higher alkali content and extended curing period excessive formation of gel eventuates.
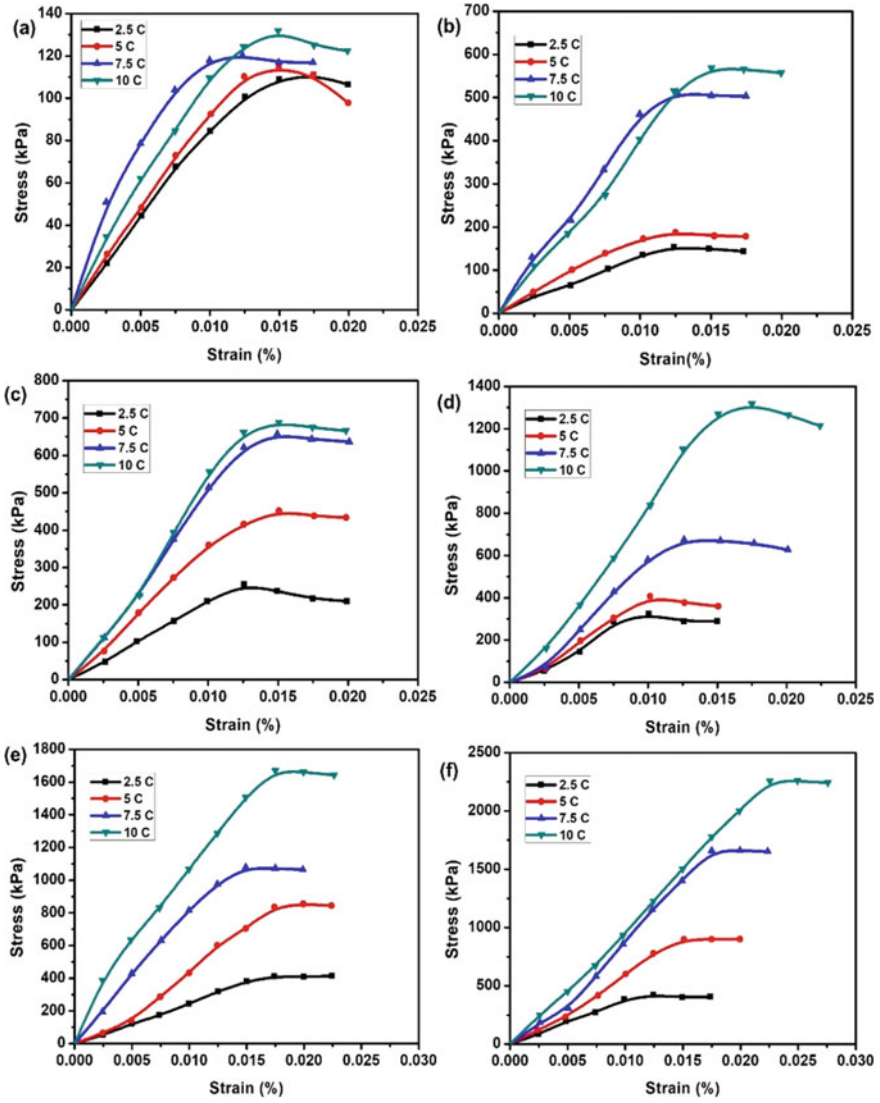
Fig. 8 Stress–strain curves for cement-treated fly ash compacted with heavy compaction energy and cured for **a** 0 day **b** 3 day **c** 7 day **d** 15 day **e** 30 day **f** 60 day

5 Conclusions

A comparative assessment on the stabilizing efficiency of lime, cement, and NaOH is made. In general, the MDD increases and OMC decreases with increase of stabilizer content or compaction energy. The enhancement in UCS for lime-stabilized and cement-stabilized fly ash specimen is attributed to the formation of pozzolanic
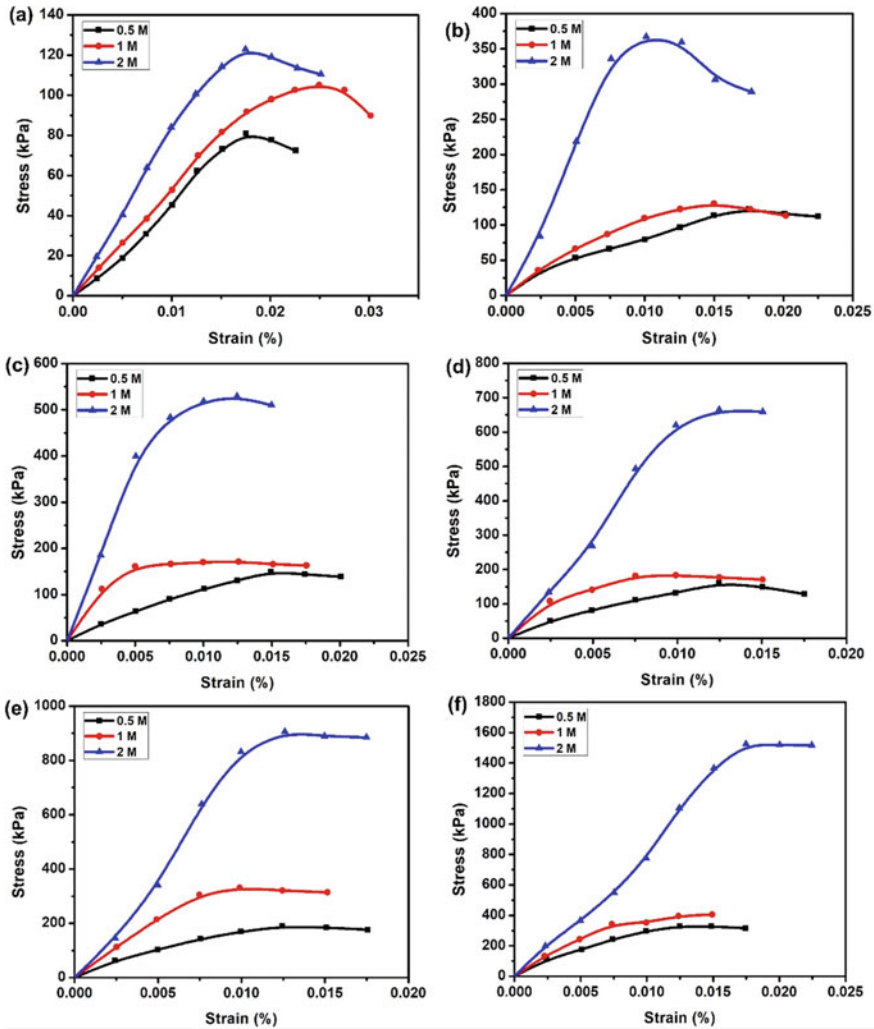
Fig. 9 Stress–strain curves for NaOH-treated fly ash compacted with low compaction energy and cured for **a** 0 day **b** 3 day **c** 7 day **d** 15 day **e** 30 day **f** 60 day

products whereas for NaOH-stabilized fly ash specimen it is due to the formation of sodium aluminosilicate gel with a general formula $Na_n\{-(SiO_2)_z-AlO_2-\}_n$. NaOH-activated fly ash gains strength much faster followed by cement and lime. An addition of 2 M NaOH solution to fly ash exhibits similar strength as obtained with 10% of cement addition. A maximum failure stress of 2.5 MPa is obtained. However, the failure strains reduce as the compaction energy or stabilizer content increases.
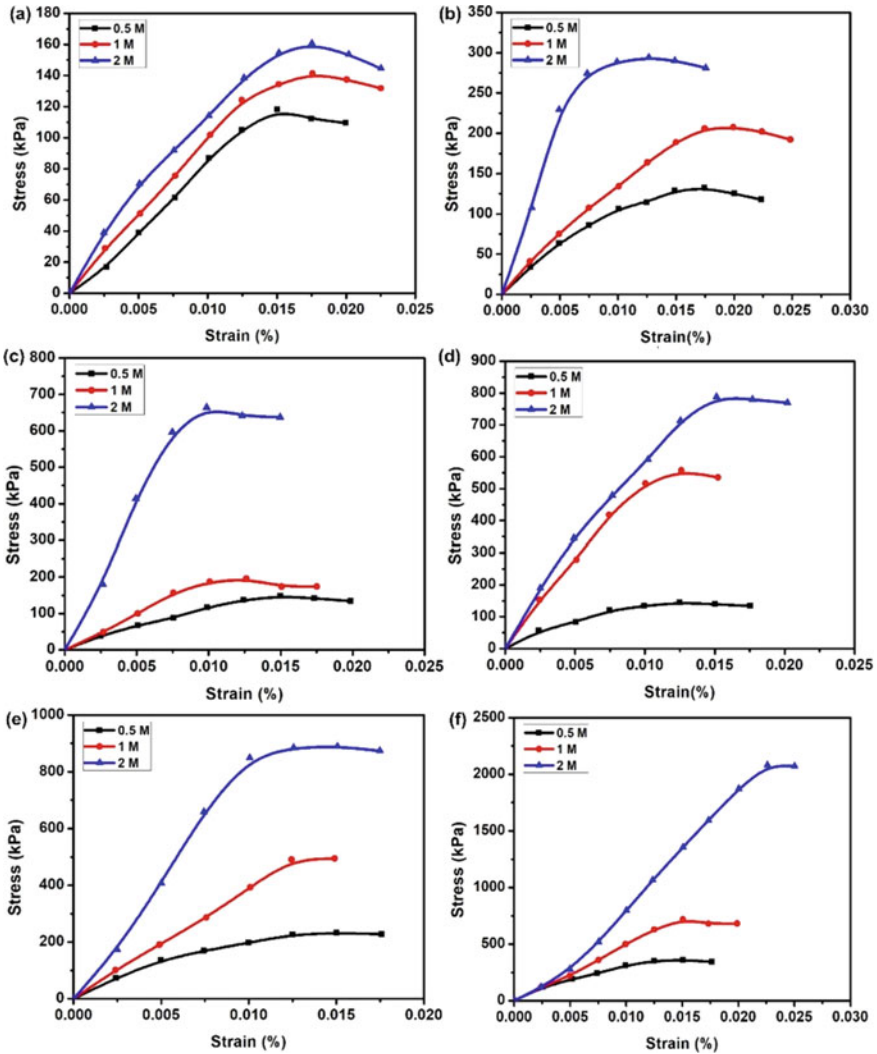
Fig. 10 Stress–strain curves for NaOH-treated fly ash compacted with heavy energy and cured for **a** 0 day **b** 3 day **c** 7 day **d** 15 day **e** 30 day **f** 60 day

References

1. Kisku, N., Joshi, H., Ansari, M., Panda, S.K., Nayak, S., Dutta, S.C.: A critical review and assessment for usage of recycled aggregate as sustainable construction material. Constr. Build. Mater. **131**, 721–740 (2017)
2. Yao, Z.T., Ji, X.S., Sarker, P.K., Tang, J.H., Ge, L.Q., Xia, M.S., Xi, Y.Q.: A comprehensive review on the applications of coal fly ash. Earth Sci. Rev. **141**, 105–121 (2015)

3. Palomo, A., Fernández-Jiménez, A.: Alkaline activation, procedure for transforming fly ash into new materials. Part I: applications. In: World of Coal Ash (WOCA) Conference, pp. 1–14 (2011)
4. Raymond, S., Hobbs, N., Evans, B., Knight, P., Akroyd, T., Cockroft, N., Sutherland, H.: Discussion. Pulverized fuel ash as embankment material. Proc. Inst. Civ. Eng. **24**(2), 235–246 (1963)
5. Gray, D.H., Lin, Y.K.: Engineering properties of compacted fly ash. J. Soil Mech. Found. Div. **98**(sm4) (1972)
6. Ghosh, A., Subbarao, C.: Strength characteristics of class F fly ash modified with lime and gypsum. J. Geotech. Geoenviron. Eng. **133**(7), 757–766 (2007)
7. Fan, Y., Yin, S., Wen, Z., Zhong, J.: Activation of fly ash and its effects on cement properties. Cem. Concr. Res. **29**(4), 467–472 (1999)
8. Palomo, A., Grutzeck, M.W., Blanco, M.T.: Alkali activated fly ashes A cement for the future. Cem. Concr. Res. **29**, 1323–1329 (1999)
9. Luo, X., Xu, J., Bai, E., Li, W.: Systematic study on the basic characteristics of alkali-activated slag-fly ash cementitious material system. Constr. Build. Mater. **29**, 482–486 (2012)
10. Mira, P., Papadakis, V.G., Tsimas, S.: Effect of lime putty addition on structural and durability properties of concrete. Cem. Concr. Res. **32**(5), 683–689 (2002)
11. Ryu, G.S., Lee, Y.B., Koh, K.T., Chung, Y.S.: The mechanical properties of fly ash-based geopolymer concrete with alkaline activators. Constr. Build. Mater. **47**, 409–418 (2013)
12. IS: 2720-Part-3 (Section 1) (1980) Determination of specific gravity-fine grained soils
13. IS: 2720-Part-4 (1985) Grain size analysis
14. IS: 2720-Part-7 (1983) Determination of water content-dry density relation using light compaction
15. IS: 2720-Part-8 (1983) Determination of water content-dry density relation using heavy compaction
16. Indraratna, B., Nutalaya, P., Koo, K.S., Kuganenthira, N.: Engineering behaviour of a low carbon, pozzolanic fly ash and its potential as a construction fill. Can. Geotech. J. **28**(4), 542–555 (1991)

Studies on the Effects of Addition of Shredded Plastic Waste as Reinforcement on Engineering Properties of Black-Cotton Soil

Siddharth Shah and **Amit Joshi**

Abstract Plastic waste is non-biodegradable and its disposal problem has become very critical issue nowadays. Black-cotton soil has been proved one of the problematic soil which requires improvement for its swelling and other characteristics. Therefore, this plastic waste has been attempted to be reused for improving the performance of this soil's engineering properties. For this, plastic waste was collected and shredded into strips of different aspect ratio of (5 mm × 10 mm, 5 mm × 20 mm, 3 mm × 10 mm, 3 mm × 20 mm). To decide the optimum aspect ratio, several tests were carried out by pilot study than for optimum aspect ratio, optimum amount of dosage was found out after adding 0.05–0.3% in the increment of 0.05% of the weight of soil sample. The results of the tests performed on black-cotton soil revealed that the optimum aspect ratio and economical dose for unconfined compression strength test were 5 mm × 20 mm and 0.1% of the weight of the soil sample. For California bearing ratio test, optimum dose of the fiber was found to be 5 mm × 20 mm and 0.1% of weight of soil sample collected, However, for free swelling test the results were varying and it was due to orientation of the flacks and was difficult to generalize the dose and percentage swelling control.

Keywords Plastic waste · Reinforcement · Black-cotton soil · Sustainable development

1 Introduction

In today's era, the dumping of the solid waste has been proved a great problem and further, the amount of plastic particularly the empty snacks and beverages pouches which has metalized coating is great problem. Plastic itself is non-biodegradable

S. Shah (✉)
Marwadi University, Rajkot, Gujarat, India
e-mail: siddharth.shah@marwadieducation.edu.in

A. Joshi
CED, Marwadi University, Rajkot, Gujarat, India
e-mail: amit.joshi@marwadieducation.edu.in

Fig. 1 Rajkot city's waste dumping yard at Nakrawadi

and all over the world the use of the plastic is now being restricted however in developing country like India still the awareness is less. Plastic bags, plastic pouches, PET bottles, etc., are few to list which are most common. This plastic's disposal is a great challenge and due to unsystematic disposal it is creating lot of trouble even to cattle. In Rajkot city of Gujarat only the amount of the waste plastic produced is about 15–20 tons/day. Therefore, the sustainable disposing of plastic is the need of the day. On the other hand, use of geosynthetics for soil improvement has been proved versatile in terms of the reinforcement. Similar efforts were made to utilize the metalized plastic waste in cohesionless soil to improve the strength properties [1]. Therefore, in this paper an attempt is made to use the shredded plastic (waste) and added to soil for its improvement in the engineering properties and check the feasibility of the amount of waste being utilized.

1.1 Plastic Waste Sample Collection

The plastic bags are collected from the Nakrawadi dumping yard station of Rajkot city as shown in Fig. 1. Then it was washed and dried, and after that it was shredded into various sizes of flakes to act as reinforcing element. More details are given in [2, 3]. The shredded plastic were produced in the varying sizes of flakes, viz. 5 mm × 10 mm, 5 mm × 20 mm, 3 mm × 10 mm, 3 mm × 20 mm few of them are as shown in Fig. 2.

1.2 Black-Cotton Soil

Since centuries this soil has remained problematic due to its montmorillonite mineral which has tendency to swell more than 100% of its original volume when subjected to moisture or saturation and equally shrinks and come back to original volume upon drying. This has many disadvantages which results in cracking of the super structure,
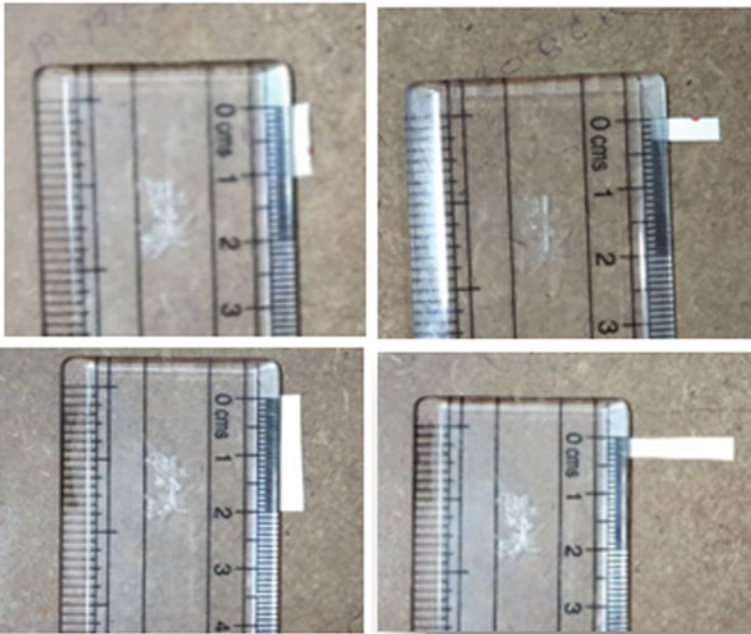
Fig. 2 Shredding the plastic waste sheet in different aspect ratios (typically shown for 3 × 20 mm and 3 × 10 mm)

be it road, or bridge or any other structure. Hence, many attempts are made like mechanical stabilization as well as chemical stabilization and use of geosynthetics to certain extent. However, very few attempts are made to utilize the plastic waste to control such behavior as well as study the changes in the other engineering properties

Table 1 Index properties of the black-cotton soil used in this study

S. No.	Index property	Value
1	Free swell index	53.9%
2	Liquid limit w_L	81.5%
3	Plastic limit w_p	33.2%
4	Plasticity index I_p	48.3%
5	IS soil classification	CH

of such soil. The black-cotton soil used in this study was collected from village Bedi near Rajkot city which has index properties as listed in Table 1.

2 Methodology

To utilize the waste plastic in expansive soil, the shredded waste plastic in different aspect ratios (5 mm × 10 mm, 5 mm × 20 mm, 3 mm × 10 mm, 3 mm × 20 mm) were tried one by one and added to the dry soil by the percentage weight of the soil ranging from adding 0.05–0.3% in the increment of 0.05%. The method adopted here was similar to [1]. The black-cotton soil was also tested in its virgin conditions and kept as the reference soil and the above-mentioned dosages were added and the engineering properties like California bearing ratio test (CBR) and unconfined compression test (UCS) were carried out to observe the effects of this shredded plastic on these properties. The total sets of the testing done are presented in Table 2 while Fig. 3 narrates the step-by-step procedure of preparation of the sample for these tests.

The unconfined compressive strength and CBR tests were carried out as per the relevant Indian standard codes.

3 Results and Discussion

As mentioned earlier, the different aspect ratio of shredded plastic was mixed with the black cotton soil and was tested for the different engineering properties as mentioned in Table 2.

The unconfined compressive strength UCS of raw soil was 200 kPa. Later the different aspect ratio was tried into the soil and it is mixed in the soil. Various aspect ratio and their different percentage were tried and optimum dose is found for each of the aspect ratio. The optimum dose is decided on the basis of maximum improvement in the UCS value. The best results obtained in UCS value corresponding to the different aspect ratio are tabulated below in Table 3. The aspect ratio 5 × 20 mm (dose of 0.1%) gives the improvement of 5% as the value of UCS increased to 210 kPa. The dosage and orientation of the fibers are crucial in the strength achievement, it

Table 2 Scope of the work

S. No.	.Fiber aspect ratio	Dose (%)	Tests carried out
1	No plastic/original	UCS, CBR, and free swell test	
2	5 mm × 20 mm	0.05	UCS CBR Free-swell
3		0.10	
4		0.15	
5		0.20	
6		0.25	
7		0.30	
8	5 mm × 10 mm	0.05	UCS CBR Free-swell
9		0.10	
10		0.15	
11		0.20	
12		0.25	
13		0.30	
14	3 mm × 20 mm	0.05	UCS CBR Free-swell
15		0.10	
16		0.15	
17		0.20	
18		0.25	
19		0.30	
20	3 mm × 10 mm	0.05	UCS CBR Free-swell
21		0.10	
22		0.15	
23		0.20	
24		0.25	
		0.30	

was observed that if the dosage of the plastic waste is increased, then the too much plastic by volume is accommodated in the sample and the strength reduces which may be due to slip among the fibers itself. Further, the orientation of the fiber across the failure plane may have imparted some higher strength due to the high tensile strength of fiber; however, the fibers were not failed, indicating the slip of the fiber and thus not much of the improvement in shear strength is observed; however, this dosage by weight has much volume and this is a positive sign for its usage in soil without adversely affecting strength.

Other geotechnical properties known as CBR value are also a important factor particularly in deciding the thickness of the pavement. The effect of this plastic waste is also seen on CBR value. The value recorded for raw soil was 8. The aspect ratio

Fig. 3 Step-by-step mixing and testing

Table 3 Maximum improvement in UCS corresponds to different aspect ratio

S. No.	Aspect ratio	Dose (%)	UCS (kPa)	Improvement (%)
1	5 mm × 20 mm	0.10	210	5
2	5 mm × 10 mm	0.15	208	4
3	3 mm × 20 mm	0.20	205	2.5
4	3 mm × 10 mm	0.30	207	3.5

Table 4 Maximum improvement in CBR corresponds to different aspect ratio

S. No.	Aspect ratio	Dose (%)	CBR	Improvement (%)
1	5 mm × 20 mm	0.10	12	50
2	5 mm × 10 mm	0.25	10	25
3	3 mm × 20 mm	0.20	10	25
4	3 mm × 10 mm	0.30	10	25

Table 5 Results of free swell tests for different aspect ratios

S. No.	Aspect ratio	Dose (%)	Swelling	Improvement (%)
1	5 mm × 20 mm	0.10	52	1.0
2	5 mm × 10 mm	0.25	53	0.5
3	3 mm × 20 mm	0.20	51	1.5
4	3 mm × 10 mm	0.30	53	0.5

used for UCS was kept the same in the CBR testing with same percentage of the dose. In the similar manner, the results obtained are tabulated in Table 4

It can be observed from Table 5 that for the aspect ratio 5 mm × 20 mm with 0.1% by the weight of the soil yields the maximum improvement in the CBR value of the soil. This might be possible due to 5 mm × 20 mm has large surface area to stick with soil and has given better grip; therefore, while deformation, the fibers placed across the plane would have shown resistance by mobilizing the tensile strength of fibers. However, in case of other aspect ratios the orientation and the grip length would have not been sufficient.

Further, the dosage and size of the fibers have negligible effects on swelling. The minor improvement is noticed. The reason for that may be because plastic waste is not contributing any chemical bonds to hold the molecules against swelling, neither the fibers are held by soil particles to mobilize its tensile strength, hence no improvement is found in swelling control.

4 Analysis for the Utilization of Plastic Shredded Waste

The analysis was done for the utilization of the plastic shredded waste in the construction of the pavement. In 1 km of road length, per lane width of 3.5 m and assuming the 30 cm of the average pavement thickness for the base and subbase layer then it will comprise of the 1050 m^3 of soil per lane per unit kilometer. Considering average unit weight of soil as 18 kN/m^3 then total 18,90,000 kg of soil would be utilized. Now from this study optimum dose of plastic waste is 0.1% by weight of soil, hence approximately 2000 kg of plastic waste would be utilized. 2000 kg of plastic waste has significant volume and therefore lot of space can be saved in dumping yard.

5 Conclusion

In this study, the metalized plastic waste was utilized in black-cotton soil and its engineering properties in terms of UCS and CBR were studied. After the careful analysis, the following broad conclusion can be drawn:

- After adding the fiber of an aspect ratio of 5 mm × 20 mm, 5 mm × 10 mm, 3 mm × 20 mm, 3 mm × 10 mm, we came to know that orientation of a fiber reinforcement is very important because fiber directly transfers the load and elongate up to the plastic capacity when their orientation is parallel to the load acting on the soil.
- After adding the fiber of different aspect ratio the optimum dose we got for unconfined compression strength test is 5 mm × 20 mm @ 0.1% of its weight.
- After adding the fiber of different aspect ratio the optimum dose we got from pilot test for California bearing ratio test is 5 mm × 20 mm @ 0.1% of its weight.
- Effect plastic fiber on controlling the swelling is not observed
- Although the improvement in the geotechnical properties is not huge, plastic can be used at construction site so that the dump ward land can be saved.

6 Limitation of the Study

These are the findings of the few laboratory test, however on the site the performance very much depends upon the cleaning and orientation of the fibers, accuracy of the adding fibers in proportion to soil as well as balling effects are the challenges for site conditions. But it is validated that if the plastic is added within this limit, it is not affecting the strength.

References

1. Benson, C.H., Khire, M.V.: Reinforcing sand with strips of reclaimed high-density polyethylene. J. Geotech. Eng. ASCE **120**(5), 838–855 (1994)
2. Chebet, C., Kalumba, D.: Laboratory investigation on re-using polyethylene (plastic) bag waste material for soil reinforcement in geotechnical engineering. F Civil Eng. Urban Plan. Int. J. (CIVEJ) **1**(1), 67–82 (2014)
3. Shah, S.G., Bhogayata, A.C., Shukla, S.K.: Feasibility of utilization of metalized plastic waste in cohesionless soil. In: International Congress and Exhibiion Sustainable Civil Infrastructures: Innovative Infrastructure Geotechnology, vol. 1, pp. 49–54, Springer, Cham. (2017). ISSN 2366–3405

Performance Evaluation of Rice Husk Ash and Phosphogypsum in Stabilizing the Problematic Expansive Soil

R. Dayakar Babu, K. Ramu, and M. S. Saandeepya

Abstract Various remedial measures adopted to overcome the problems posed by expansive soils like soil replacement, moisture control, prewetting, and lime stabilization have been practiced with varying degrees of success. However, these techniques suffer from certain limitations with respect to their adaptability. Stabilization using solid wastes is one of the emerging techniques to improve the engineering properties of expansive soils to make them suitable for use in construction. This paper presents an attempt made to study the influence of two wastes, rice husk ash (RHA), an agro-waste, and phosphogypsum (PG), an industrial waste from fertilizer industry, in different percentages, as stabilizing materials to improve the properties of problematic expansive soil. The percentage of phosphogypsum (PG) was varied from 0 to 8% with an increment of 2% in combination with 0, 5, and 10% percentages of rice husk ash (RHA). Different tests in the laboratory were conducted to evaluate the characteristics of treated expansive soil. The analyzed results clearly depict that the combination of 10% RHA + 6% PG had significantly improved the soaked CBR value and unconfined compressive strength (UCS) by about 3 times and 96%, respectively, when compared to that of virgin expansive soil. The parametric evaluation summarizes that the combined effect of waste materials phosphogypsum (PG) and rice husk ash (RHA) had shown promising influence on the strength characteristics of expansive soil, thereby giving a twofold advantage in improving problematic expansive soil and also solving a problem of waste disposal.

Keywords Expansive soil · Rice husk ash (RHA) · Phosphogypsum (PG) · Stabilization

R. Dayakar Babu (✉)
Kakinada Institute of Science and Technology, Divili 533433, India
e-mail: kitscivilian@gmail.com

K. Ramu · M. S. Saandeepya
University College of Engineering, JNTUK University Kakinada, Kakinada 533003, India
e-mail: kramujntu@gmail.com

M. S. Saandeepya
e-mail: saandeepya136@gmail.com

1 Introduction

Expansive soils were being a tough task for civil engineers in the design and construction of infrastructure projects. The major problems with clays, including low strength and high compressibility, can cause severe damage to civil engineering structures and can lead to very serious economic loss and environmental hazards. Therefore, these soils must be treated before commencing the construction operation to achieve desired properties. This has led to the development of soil stabilization techniques. Since the nature and properties of natural soil vary widely, a suitable stabilization technique has to be adopted for a particular situation after considering the soil properties. The chemical technique is a common soil stabilization approach, since it produces a better quality soil with higher strength and durability than mechanical and physical techniques. Soil stabilization can be explained as the alteration of the soil properties by chemical or physical means in order to enhance the engineering quality of the soil. The main objectives of the soil stabilization are to increase the bearing capacity of the soil, its resistance to weathering process, and soil permeability. The long-term performance of any construction project depends on the soundness of the underlying soils. Unstable soils can create significant problems for pavements or structures. Therefore, soil stabilization techniques are necessary to ensure better stability of soil so that it can successfully sustain the load of the superstructure especially in case of soil which are highly active, also it saves a lot of time and millions of money when compared to the method of cutting out and replacing the unstable soil. This paper deals with a parametric study on the influence of an agro-industrial waste, rice husk ash, and a fertilizer industrial waste, phosphogypsum, in stabilizing the problematic expansive soil.

2 Research Background

Expansive soils were being a tough task for civil engineers in the design and construction of infrastructure projects. Therefore, it is important to remove the existing problematic expansive soil and replace it with a non-expansive soil or improve the properties of the problematic soil by stabilization. The road network is planned and developed for fulfilling the requirements of transportation, keeping the total transportation cost in mind. In the process of network development, many a times, the alignment of the road may have to be finalized through the soil sub grades, which may not be suitable to bear the traffic loads with adequate strength [1]. The different techniques in use are chemical additives (cement, lime, salt treatments, and organic compounds), prewetting, soil replacement, moisture control, surcharge loading, and thermal methods [2]. Every method has got its own merits and demerits including cost factor. Among several techniques adopted to overcome the problems posed by expansive soils, lime stabilization gained prominence during the past few decades due to its abundance and adaptability [3]. Chemical additives, such as lime, cement,

fly ash, and other chemical compounds, have been used in expansive soil stabilization for many years with various degrees of success [4]. The recent research in the field of geotechnical engineering and construction materials focuses on agricultural and industrial wastes being locally available and has disposal problem.

Jasvir Singh et al. [5] presented the laboratory study of clayey soil stabilized with fly ash (FA) and rice husk ash (RHA). The soil was stabilized with different percentages of FA (i.e., 0, 8, 14, 18, and 24%) and RHA (i.e., 0, 4, 8 12, 16, and 20%). The Atterberg's limits, specific gravity, California bearing ratio, and unconfined compressive strength tests were performed on raw and stabilized soils. Results indicated that addition of FA and RHA reduces the plasticity index (PI) and specific gravity of the soil. It is observed that there is remarkable influence on CBR values of expansive soil at the 8% FA as the replacement and the addition of 12% RHA as an optimum percentage. Dahale et al. (2016) had reported the results of laboratory investigation carried out on problematic clayey soil stabilized with fly ash and hydrated lime. Experimental program shown that fly ash alters the strength properties of clayey soils significantly. Up to 50% of fly ash found effective in increasing strength properties and higher doses cause overall strength reduction.

Rathan Raj et al. [6] had used rice husk ash for stabilization of problematic soil, to study the effects of same on the index and engineering characteristics of problematic soil. The rice husk ash is mixed with soil in various proportions like 5, 10, 20, 30, 40, 50, and 80%. The various tests were conducted on these proportions and optimized proportion is arrived. The liquid limit and the FSI of the soil decreased steeply with the increase in the % of RHA. The undrained cohesion value of the soil mixed with RHA for clay soil decreased from 60 to 30 kN/m^2 and angle of internal friction value increased from 17°5′ to 38°. The unsoaked CBR value in the case of addition of RHA to clay soil increased from 3.2 to 9.3% and the soaked CBR value 2.4–4.4%.

Roshni et al. [7] evaluated the potential of phosphogypsum (PG) and wood ash (WA) to stabilize expansive soil. Results showed that the strength parameters of the soil are improved substantially by the addition of 4% phosphogypsum (PG) and 12% wood ash (WA). CBR and UCS values were increased due to the formation of cementitious compounds as a result of a chemical reaction between phosphogypsum (PG) and wood ash (WA).

The study carried out by Koteswara Rao et al. [8] on the expansive soil with rice husk ash, lime, and gypsum resulted in considerable improvement in the strength characteristics of the expansive soil. It was observed that the liquid limit of the expansive soil has been decreased by 22% with the addition of 20% RHA + 5% lime. It is observed that there is remarkable influence on the strength and CBR values of expansive soil at 20% RHA + 5% lime + 3% gypsum which is an optimum percentage.

3 Experimental Methodology

Tests were conducted in the laboratory on the expansive soil to study the behavior of expansive soil, when it is treated with an agro-industrial waste, rice husk ash, and a fertilizer industrial waste, phosphogypsum. Compaction, California bearing ratio, and unconfined compressive strength tests were conducted as per IS code of practice.

3.1 Materials Used

The details of the various materials used in the laboratory experimentation are reported in the following sections.

3.1.1 Soil

The soil used was a typical expansive soil collected from Appaniramuni Lanka, Near Dindi village, Sakhinetipalli Mandal, East Godavari district, Andhra Pradesh State, India.

3.1.2 Rice Husk Ash (RHA)

For the present study, the rice husk ash (RHA) has been brought from the captive power plant of Ms. Lalitha Rice Mill, Peddapuram, East Godavari district, Andhra Pradesh State, India.

3.1.3 Phosphogypsum (PG)

For the present study, the phosphogypsum (PG) has been brought from the fertilizer industry Ms. KPR Fertilizers, Balabadhrapuram, East Godavari district, Andhra Pradesh State, India.

3.2 Sample Preparation

The soil was initially air dried, pulverized, and then was sieved through a 4.75 mm sieve, prior to the testing. The samples were prepared by mixing the pulverized and sieved soil with the needed stabilizing agents in dry condition and then required amount of water is added to make a consistent mix by thorough mixing. The following

Table 1 Different variables studied

Stabilizing agent	Percentages varied
Rice husk ash	0, 5, 10
Phosphogypsum	0, 2, 4, 6, 8

table lists the different variables and their respective contents used in the present study (Table 1).

4 Discussion of Results

4.1 General

In the laboratory, various experiments were conducted by blending different percentages of rice husk ash (RHA) and phosphogypsum (PG) with the expansive soil. Compaction, CBR, and UCS tests were conducted as per IS codes of practice, with a view to determine the optimum combination of rice husk ash (RHA) and phosphogypsum (PG) as an addition to problematic expansive soil to improving its properties.

4.2 Combined Effect of Rice Husk Ash (RHA) and Phosphogypsum (PG) as Additives on the Compaction Properties of Problematic Expansive Soil

The influence of combination of rice husk ash (RHA) and phosphogypsum (PG) on the compaction parameters of expansive soil is clearly presented in Figs. 1 and 2. The percentage of rice husk ash was varied from 0%, to 10% with an increment of 5%. From Figs. 1 and 2, it was observed that the treatment as combination with 10% RHA + 6% PG has considerably improved the expansive soil. It can be inferred from the graphs, that there is a gradual improvement in the maximum dry density by about 9.6% when compared to that of virgin expansive soil. Also, the corresponding optimum moisture content had shown a reduction by about 14%.
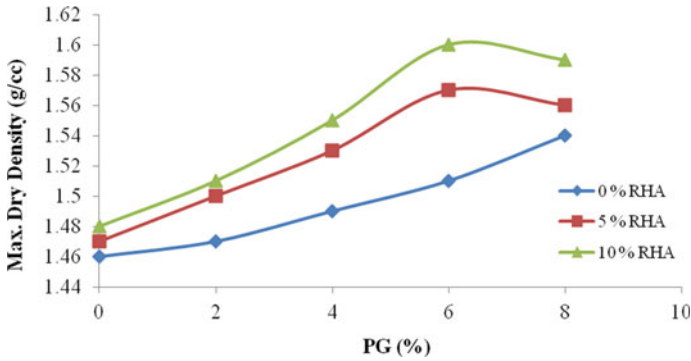
Fig. 1 Plot showing the variation of MDD values with percentage of PG for different percentages of RHA
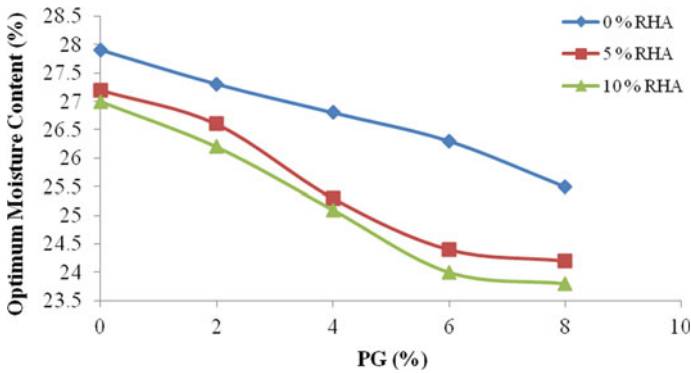
Fig. 2 Plot showing the variation of OMC values with percentage of PG for different percentages of RHA

4.3 Combined Effect of Rice Husk Ash (RHA) and Phosphogypsum (PG) as Additives on the Penetration Properties of Problematic Expansive Soil

The influence of combination of rice husk ash (RHA) and phosphogypsum (PG) on the CBR values of expansive soil is clearly presented in Figs. 3 and 4. The percentage of rice husk ash was varied from 0, to 10% with an increment of 5%. From Figs. 3 and 4, it was observed that the treatment as combination with 10% RHA + 6% PG has substantially improved the penetration properties of expansive soil. The graphs depict the improvement in the CBR values both unsoaked and soaked by about 155% and 310%, respectively, when compared to that of virgin expansive soil.
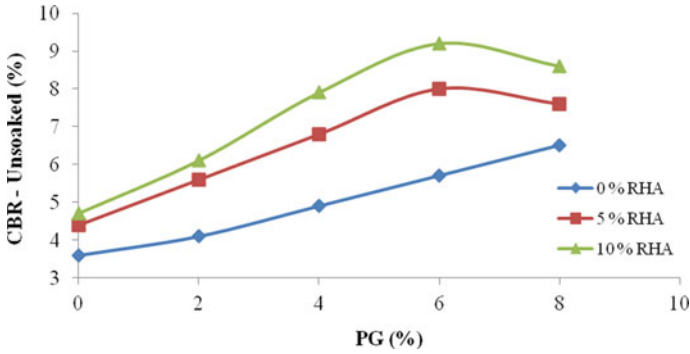
Fig. 3 Plot showing the variation of CBR-unsoaked values with percentage of PG for different percentages of RHA
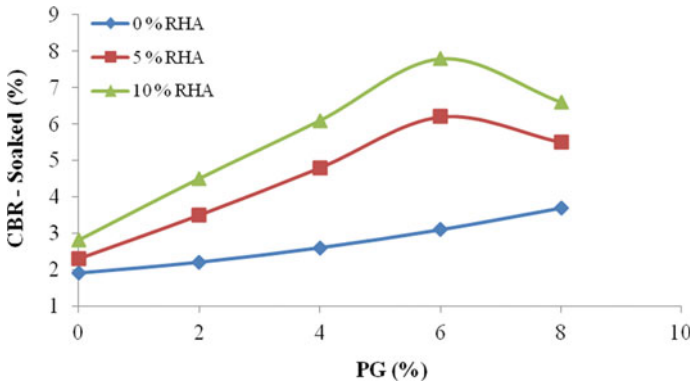
Fig. 4 Plot showing the variation of CBR-soaked values with percentage of PG for different percentages of RHA

4.4 Combined Effect of Rice Husk Ash (RHA) and Phosphogypsum (PG) as Additives on the Unconfined Compressive Strength (UCS) of Problematic Expansive Soil

The influence of combination of rice husk ash (RHA) and phosphogypsum (PG) on the unconfined compressive strength (UCS) of expansive soil is clearly presented in Fig. 5. The percentage of rice husk ash was varied from 0, to 10% with an increment of 5%. Figure 5 clearly shows that the combination of 10% RHA + 6% PG had significantly improved the unconfined compressive strength (UCS) by about 96%, when compared to that of virgin expansive soil.
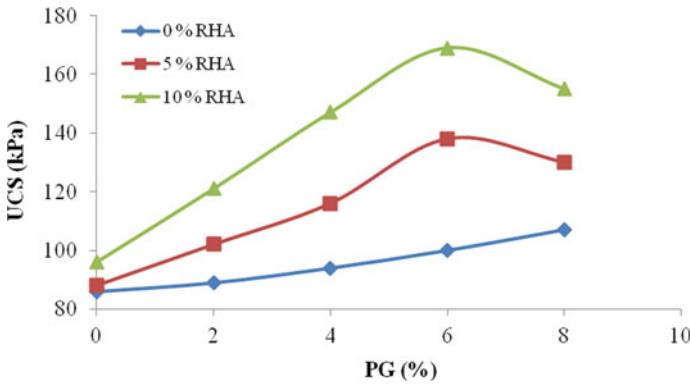
Fig. 5 Plot showing the variation of unconfined compressive strength values with percentage of PG for different percentages of RHA

4.5 Effect of Curing on the Penetration and Strength Properties of Problematic Expansive Soil Treated with Optimum Percentages of RHA and PG

Figures 6 and 7 show the performance impact of curing on the penetration and strength characteristics of expansive soil treated with optimum combination of rice husk ash (RHA) and phosphogypsum (PG). Figures 6 and 7 clearly depict the variation of CBR and UCS values, respectively, of expansive soil treated with optimum combination of RHA and PG (i.e., 10% RHA + 6% PG) cured for different time periods. The results ascertain that there is a significant increase in the CBR values both unsoaked and soaked by about 36% and 32%, when the treated expansive soil is cured for
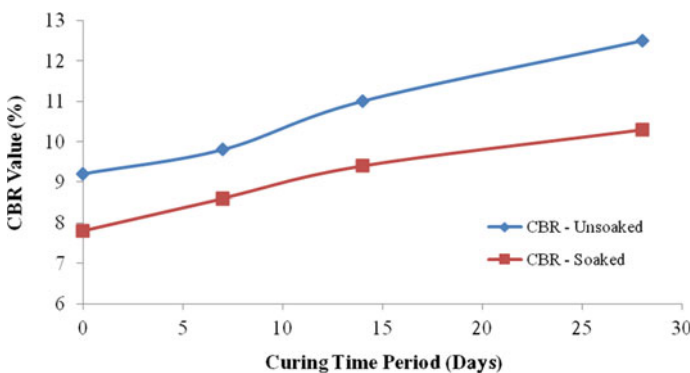
Fig. 6 Plot showing the variation of CBR values of expansive soil treated with optimum combination of RHA and PG cured for different time periods
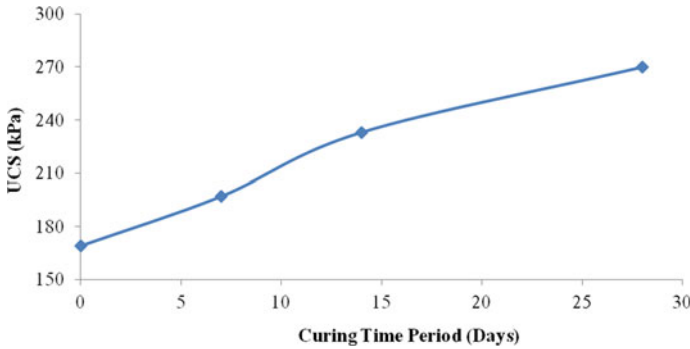
Fig. 7 Plot showing the variation of UCS values of expansive soil treated with optimum combination of RHA and PG cured for different time periods

28 days. The same trend of improvement in strength is seen with an increase of by about 60% for 28 days of curing.

Finally from the above discussions, it is evident that the addition of rice husk ash (RHA) and phosphogypsum (PG) to the virgin expansive soil showed an improvement in compaction, penetration, and strength properties to a significant extent. When the rice husk ash (RHA) was only added, there is a mild increase and on further blending it with phosphogypsum (PG), the improvement was more pronounced. The above said stabilizing agents in combination made the problematic expansive soil with a better particle orientation under compaction, thereby improving strength and penetration characteristics for 10% RHA + 6% PG. This is due to the pozzolanic reactions between soil, RHA, and PG resulting in the formation of better compact soil matrix with a better interparticle cohesive bond strength. This made the problematic expansive soil, which if not stabilized is a discarded material, a useful fill material with better properties. It can be summarized that the materials rice husk ash (RHA) and phosphogypsum (PG) had shown promising influence on the properties of expansive soil, thereby giving a twofold advantage in improving problematic expansive soil and also solving a problem of waste disposal.

5 Conclusions

The following conclusions are made based on the results discussed in this investigation.

(i) The addition of non-plastic, silica-rich waste material, rice husk ash (RHA), and other waste material, phosphogypsum (PG), as a binder bonded the soil particles closer with a better particle orientation, thereby making the problematic virgin expansive soil, a soil with better and enhanced properties.

(ii)   There is a gradual improvement in the maximum dry density and the corresponding optimum moisture content had shown a reduction on the addition of RHA + PG when compared to that of virgin expansive soil.

(iii) It was observed that the treatment as combination with 10% RHA + 6% PG has significantly improved the penetration and strength properties of properties expansive soil.

(iv)   There is a significant increase in the CBR and UCS values, when the expansive soil was treated with optimum combination of RHA and PG (i.e., 10% RHA + 6% PG) and cured for 28 days.

(v)   The materials rice husk ash (RHA) and phosphogypsum (PG) had shown promising influence on the properties of expansive soil, thereby giving a twofold advantage in improving problematic expansive soil and also solving a problem of waste disposal.

References

1. Chandrasekhar, B.P., Prasad Raju, G.V.R., Ramana Murthy, V., Hari Krishna, P.: Relative performance of lime and calcium chloride on properties of expansive soil for pavement subgrades. In: Proceedings of IGC-99, pp. 279–282, Calcutta (1999)

2. Nelson, J.D., Miller, D.J.: Expansive Soils, Problems and Practice in Foundation and Pavement Engineering. Wiley, New York (1992)

3. Snethen, D.R.: An evaluation methodology for prediction and minimization of detrimental volume change of expansive soils in highway sub grades. Research report, Vol. 1, prepared for federal highway administration, Washington (1979)

4. Al-Rawas, A.A., Taha R., Nelson, J.D., Al-Shab, T.B., Al-Siyabi, H.: A comparative evaluation of various additives used in the stabilization of expansive soils. Geotech. Test. J. **25**(2), 199–209 (2002)

5. Singh, J., Singh, M.H.: Soil stabilization using Fly Ash and Rice Husk Ash. Int. J. Innov. Res. Sci. Eng. Technol. **6**(7), 14412–14419 (2017)

6. Rathan Raj, R., Banupriya, S., Dharani, R.: Stabilization of soil using Rice Husk Ash. Int. J. Comput. Eng. Res. **6**(02), 43–50 (2016)

7. Roshni, R., Divya Krishnan, K., Ravichandran, P.T.: Experimental study on the strength behaviour of expansive soil treated with phospho gypsum and wood ash. Int. J. Sci. Res. **4**(10), 161–164 (2015)

8. Koteswara Rao, D., Pranav, P.R.T., Anusha, M.: Stabilization of expansive soil with Rice Husk Ash, Lime and Gypsum—an experimental study. Int. J. Eng. Sci. Technol. **3** (11), 8076–8085 (2011)

9. Evans, R.P., Mc Manus, K.J.: Construction of vertical moisture barriers to reduce expansive soil sub grade movement. TRR-1652, TRB, pp.108–112 (1999)

10. Fredlund, D.G., Rahardjo, H.: Soil mechanics for unsaturated soils. Wiley, New York (1993)

11. Sivapullaiah, P.V., et al.: Optimization of lime content for fly ash. ASTM J. Test. Eval. **23**(3), 222–227 (1995)

Estimation of Total Soluble Solids in MSW Incineration Bottom Ash by Higher Dilution Method: Assessment for Geotechnical Reuse

Garima Gupta, Manoj Datta, G. V. Ramana, and B. J. Alappat

Abstract The unavailability of new space and brimming of the existing ones to dump municipal solid waste (MSW) in cities like Delhi has caused the government to switch to MSW incineration (MSWI) in waste-to-energy (WtE) plants. Attempts are being made worldwide to utilize the residues from WtE plants as a substitute for natural soil in civil engineering applications. Though adequate from the strength perspective, MSWI bottom ash (BA) has significantly high total soluble solids (SS) which need to be addressed before being put to reuse. The present study assesses whether the existing Indian Standards IS-2720 Part-XXI for estimating SS in soil can be used for soil-like fraction of MSWI BA or if certain modifications are required. The study identifies that the dilution ratio (DR) or liquid-to-solid ratio of 10 l/kg used in the standard method to dissolve all the soluble solids is inadequate for estimation of SS in the soil-like fraction from MSWI BA. SS was measured in MSWI BA collected from three WtE plants in Delhi, and the results were compared with coal BA from a thermal power plant and two locally available soils. The procedure as mentioned in IS-2720 Part-XXI was adopted but with minor modifications and with varying DR ranging from 10 to 200 l/kg. DR of 10 l/kg, though adequate for SS determination in coal BA and local soils, underestimated SS levels in MSWI BA substantially. It is recommended that IS-code method be used with caution for estimating SS in materials which are soil-like but not exactly soil.

Keywords Total soluble solids · MSW incineration · Bottom ash

1 Introduction

Rapid urbanization, population explosion, and increase in the standard of living have laden the natural resources disproportionately and exacerbated the problems of waste disposal. Cities like Delhi, which have outgrown their boundaries, are striving hard for additional space to dump these alarming quantities of waste. The fallout has

G. Gupta (✉) · M. Datta · G. V. Ramana · B. J. Alappat
Indian Institute of Technology Delhi, New Delhi 110016, India
e-mail: gamma840@gmail.com

caused India to witness the rise of waste-to-energy plants wherein municipal solid waste (MSW) is burnt to ashes and energy is recovered as a by-product. This process of incineration reduces the waste quantities substantially. Literature reports 70–80% of mass reduction and up to 90% volume reduction of MSW in such plants worldwide [1–9].

Temperatures as huge as 850–1000 °C in incinerator furnace eliminates most of the organic material present in incoming MSW, leaving behind inorganic ash residues, namely bottom ash and fly ash. MSW incineration (MSWI) bottom ash constitutes 80–90% of these residues and relatively small quantities of fly ash are generated [1–9].

Coal combustion residues (CCRs) from thermal power plants have widely been recognized as a substitute for natural materials in numerous geotechnical applications and in building construction materials [10, 11]. Akin to CCRs, the residues from MSW incineration have similar potential and attempts are being made worldwide to reuse it in earthworks, road pavements, as landfill cover material, building construction material, etc. [1–9].

MSWI BA is a mixture of sand and gravel and though it has been found to perform satisfactorily from strength and mechanical perspective [1, 2, 8, 9], its environmental performance remains contentious. The non-volatile and incombustible salts which get concentrated in the bottom ash after incineration tend to leach out in various disposal or reuse scenarios. In literature, contamination potential of MSWI BA has been widely assessed in the context of heavy metal or metalloid leaching but not much attention is focused on the leaching of other soluble solids such as salts [2, 3, 6, 12, 13]. This is generally because their presence in excess does not classify them as a hazardous material. The most widely used toxicity characteristic leaching procedure (TCLP) omit the presence of such salts as a regulatory criterion for material's classification as hazardous or non-hazardous and hence misinterpreted sometimes as it does not necessarily suggest that the material's reusability but suggests only material's disposal condition.

Correct estimation of total soluble solids (SS) can provide a fair idea of the proportion of the total leachable components present in MSWI BA over its life cycle and would be beneficial to address its long-term impact on the environment. The present study contemplates the existing Indian standard practice IS-2720 Part-XXI [14] of estimating SS in soil and comprehends if the same can be used as such or with some modifications to assess SS in soil-like fraction of MSWI BA. The study emphasizes the role of dilution ratio (DR) or liquid-to-solid ratio on the accurate estimation of SS. It also draws a comparison between SS values of two locally available soils, coal bottom ash and MSWI bottom ash.

2 Material and Methods

MSWI BA was collected from three waste-to-energy plants in Delhi, P1, P2, and P3. The three plants combinedly contribute approximately 45 MW of power generation and accommodate nearly 5000 tons per day of MSW which is almost half of the city's daily MSW generation. All the three plants pre-segregated the incoming MSW through a various combination of techniques such as size-based segregation through trommels, density-based segregation through ballistic separators, and metal segregation through magnetic separators. The objective of pre-segregation operations aimed to increase the calorific value of the waste being fed to the furnace.

These plants reported a similar mass reduction of around 70% of the incoming MSW as reported worldwide. Bottom ash was recovered through hoppers after the water-quenching operation. Bottom ash averaged to be approximately 80–90% of the total residues and its laboratory grain-size analysis indicated the proportions of the soil-like fraction (passing 4.75 mm) and gravel-like fraction (above 4.75 mm) as given in Fig. 1. Bottom ash is being referred to as a combination of soil-like and gravel-like fraction because it is neither natural soil nor natural gravel but only appears to be so by the naked eyes. A stockpile of MSWI BA from one of the WtE plant and its soil-like fraction obtained after initial processing is shown in Fig. 2. If this soil-like fraction from MSWI BA can substitute natural soil in various applications, completely or partially, nearly 40–60% utilization of WtE rejects can be achieved. Only the soil-like fraction has been targeted for this study.

Coal bottom ash from a local thermal power plant and two locally available soils, Yamuna sand and Badarpur sand, were subjected to the same testing sequence for the comparison of results. Yamuna sand is natural river sand, whereas Badarpur sand is quarried sand.

2.1 Sample Collection

The incoming waste fed to the incinerators may vary from day-to-day, season-to-season, and regions-to-region. In order to capture the heterogeneity of the ash being

Fig. 1 Rejects from WtE plant

(a)   (b)
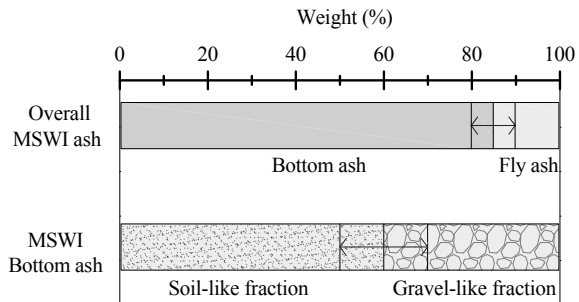
Fig. 2 **a** Stockpile of MSWI bottom ash and **b** soil-like fraction from MSWI bottom ash

generated in these WtE plants, the sampling was carried out in various seasons between 2017 and 2019. At each point of sampling, approximately a ton of bottom ash was collected in a period of 5–10 days. The material was then exposed to natural atmosphere under a shed at a landfill site for partial air-drying for a period of 4–5 days. MSWI BA was later sieved through various large-sized screens onsite, and the material passing 4.75 mm was collected and stored in plastic containers in the laboratory. Details of sample collection and the abbreviations used for different samples are given in Table 1.

Table 1 Sample collection details and the abbreviations used for different samples

Sample	Sampling period	Abbreviations used
MSWI bottom ash P1	Monsoon 2017	BA P1$_M$
	Winter 2018	BA P1$_W$
	Summer 2018	BA P1$_S$
MSWI bottom ash P2	Monsoon 2017	BA P2$_M$
	Winter 2018	BA P2$_W$
	Summer 2018	BA P2$_S$
MSWI bottom ash P3	Winter 2019	BA P3$_W$
Coal bottom ash	–	CBA
Badarpur sand	–	BS
Yamuna sand	–	YS

2.2 Experimental Methodology

Existing Practice for Estimation of SS. SS in soil is determined as per Indian Standard IS 2720-Part-XXI. The existing practice requires at least 10 g of sample (passing 2 mm) to be mixed with 100 ml of distilled water and shaken overnight for at least 15 h. The soil is then decanted and the filtered through Whatman no. 42 filter paper. The filtrate is then oven-dried to estimate SS. This method identifies the dilution ratio (DR) or liquid-to-solid ratio of 10 l/kg for SS determination. However, the DR of 10 l/kg may not allow the complete dissolution of soluble solids in MSWI BA as the solution may get saturated due to elevated concentration of salts in ash in comparison with natural soil. Hence, higher DR may be required to for SS estimation in MSWI BA.

Modified Procedure for Estimation of SS. The study aimed to determine DR that would be just necessary and enough to allow the complete dissolution of soluble solids in MSWI BA. SS was estimated at DR of 10, 20, 50, 100, 150, and 200 l/kg for all the samples mentioned in Table 1. If two successive DR would give negligible change in SS, the lower DR would be the required dilution for estimation of SS in the soil-like fraction from MSWI BA.

Since the capacity of flasks that could be placed on a rotary shaker was fixed to 500 ml, the amount of sample taken for each dilution was changed. To ensure that a representative quantity of sample is taken for the test, a number of repetitions were fixed such that at least 20 g of sample was used at each dilution. At least three repetitions were performed at each dilution. Table 2 shows the details of sample preparation. The samples were crushed in mortar and pestle to pass 425 µm sieve to ensure homogeneity. The samples were agitated at 200–250 rpm to ensure good mixing. The samples were later vacuum filtered. After measuring the pH, the entire extract was oven-dried at 105 ± 5 °C to estimate SS. All the weight calculations were done using a weighing balance of 0.1 mg readability.

Estimation of Constituents of SS. After fixing on a DR from the above-modified method, the SS extract was prepared again at that DR and tested for its constituents.

Table 2 Details of sample preparation for SS estimation

Dilution ratio (l/kg)	Diluted volume (ml)	Sample quantity for each iteration (g)	Number of repetitions	Total quantity of sample (g)
10	500	50.0	3	150
20	500	25.0	3	75
50	500	10.0	3	30
100	500	5.0	4	20
150	500	3.3	6	20
200	500	2.5	8	20

The SS extract of each sample was tested for volatile solids (VS), anions (chlorides and sulfates), and metal/metalloids using APHA standards [15].

VS gives a rough estimate of the organic component of total soluble solids that volatilize at temperatures up to 550 °C. The loss in weight when the SS residues were ignited from 105 ± 5 °C to 550 ± 5 °C is reported as VS. Chlorides were determined by Mohr's method using silver nitrate titration. Sulfates were determined using the turbidimetric method. Metals/metalloids in SS extract were determined using inductively coupled plasma mass spectrometry (ICP-MS).

3   Results and Discussion

Table 3 shows the change in SS of samples on increasing the DR. Figure 3 shows a comparison of SS in MSWI BA of three plants with YS, BS, and CBA. Table 4 shows the pH value, estimated SS, VS and ratio of VS to SS for all the samples.

3.1   Effect of DR on Estimation of Total Soluble Solids for Local Soils and Coal Bottom Ash

From Table 3, it is evident that the change in SS for Yamuna sand, Badarpur sand, and coal bottom ash at higher dilutions is insignificant. The slight increase in SS at higher dilution for the above three materials can also be attributed to the experimental error or heterogeneity of the samples. DR 10 is adequate to dissolve most of the soluble solids for soil or coal bottom ash.

Table 3 Total soluble solids at various dilutions (average $\pm$ standard deviation) in wt.%

Sample	Dilution ratio (l/kg)					
	10	20	50	100	150	200
YS	0.06 ± 0.01	0.07 ± 0.01	0.11 ± 0.01	–	–	–
BS	0.04 ± 0.01	0.05 ± 0.01	0.07 ± 0.01	–	–	–
CBA	0.07 ± 0.00	0.12 ± 0.00	0.21 ± 0.03	–	–	–
BA P1$_M$	–	–	–	–	3.13 ± 0.07	3.21 ± 0.11
BA P1$_W$	1.78 ± 0.01	–	2.31 ± 0.03	2.80 ± 0.11	3.46 ± 0.05	3.57 ± 0.06
BA P1$_S$	1.77 ± 0.02	–	2.41 ± 0.01	2.86 ± 0.02	3.46 ± 0.07	3.57 ± 0.10
BA P2$_M$	–	–	–	2.36 ± 0.07	2.43 ± 0.04	2.54 ± 0.06
BA P2$_W$	1.86 ± 0.06	–	2.27 ± 0.04	2.52 ± 0.07	–	2.65 ± 0.05
BA P2$_S$	1.31 ± 0.03	–	1.96 ± 0.03	2.47 ± 0.08	–	2.65 ± 0.03
BA P3$_W$	1.95 ± 0.09	–	2.29 ± 0.03	2.46 ± 0.06	–	2.79 ± 0.12

Fig. 3 Comparison of total soluble solids in MSWI BA, local soils, and coal bottom ash
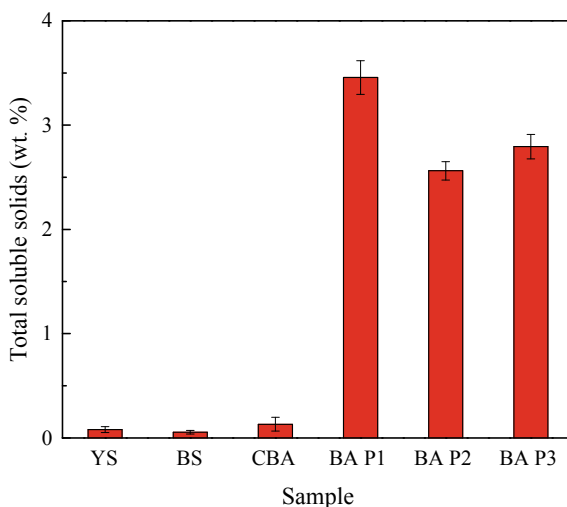
Table 4 pH, SS, VS, and ratio of VS/SS

Sample	pH	SS*	VS*	VS/SS
YS	7.7	0.08 ± 0.03	0.01 ± 0.01	0.12
BS	8.3	0.05 ± 0.02	0.01 ± 0.01	0.07
CBA	7.9	0.13 ± 0.07	0.02 ± 0.01	0.17
BA P1$_M$	10.3	3.18 ± 0.07	0.80 ± 0.06	0.25
BA P1$_W$	10.5	3.54 ± 0.07	0.83 ± 0.05	0.23
BA P1$_S$	10.6	3.5 ± 0.09	0.80 ± 0.10	0.23
BA P2$_M$	9.3	2.54 ± 0.06	0.57 ± 0.11	0.22
BA P2$_W$	9.5	2.58 ± 0.07	1.10 ± 1.10	0.43
BA P2$_S$	10.1	2.58 ± 0.10	0.75 ± 0.13	0.29
BA P3$_W$	8.9	2.79 ± 0.13	1.17 ± 0.12	0.42

*weight % (average ± standard deviation)

3.2 Effect of DR on Estimation of Total Soluble Solids for MSWI Bottom Ash

In contrary to YS, BS, and CBA, SS in MSWI bottom ash increases significantly at higher dilutions for all the three plants, for all the seasons. It almost gets stabilized at DR 100 for MSWI BA from WtE P2 whereas SS for MSWI BA from P1 and P3 gets evened out around DR 150. MSWI BA from P1 shows higher values of SS in comparison with P2 and P3. SS in soil-like fraction of MSWI BA is in the range of 2.5–3.6%. This value is considerably higher than the two local soils and the coal bottom ash having SS of the order of 0.1%.

Results suggest that higher concentration of soluble salts in MSWI BA saturates the water solution at lower DR preventing the further dissolution of salts. This results in underestimating the value of SS in soil-like fraction of MSWI BA. MSWI BA needs to be diluted at least 150 times to allow the complete dissolution of soluble solids.

3.3   pH and Volatile Solids

In Table 4, high pH values of MSWI BA are suggestive of their alkaline nature that may be due to the presence of soluble alkalis and alkaline earth metals such as Na, K, and Ca. The lower values of pH for BA $P3_W$ may be attributed to carbonation during the onsite processing of samples.

VS is ranging between 0.6 and 1.2% in MSWI BA, whereas it is found to be insignificant in local soils and coal bottom ash indicating the absence of any soluble organic solids in the same. Low VS/SS ratio signifies a little proportion of soluble organics in total soluble solids for YS and BS. This proportion is around 20–25% in MSWI BA and CBA and up to 40% in some MSWI BA samples.

3.4   Chemical Constituents of SS in MSWI BA

Preliminary studies show that soluble solids in MSWI ash comprised of high levels of chlorides and sulfates. Chlorides were in the range of 10–20%, whereas sulfates were of the order of 30% of the weight of total soluble solids in MSWI BA.

Major and minor metal ions present (in decreasing order of their weight percentage) were sodium, potassium, calcium, aluminum, and iron. They combinedly constituted 10–15% of the total soluble solids in MSWI BA. Other metals/metalloids present in trace amounts were zinc, copper, chromium, lead, antimony, nickel, vanadium, molybdenum, and manganese. These were approximately 0.1–0.2% of the total soluble solids in MSWI BA.

4   Conclusions

Previous studies [5, 6] indicate that the bulk utilization of soil-like fraction of MSWI bottom ash in geotechnical applications is feasible but the presence of soluble solids may thwart the same. Substituting it as backfill material in reinforced soil structures, for an instance, 20 m wide, 5 m high, and a kilometer long, would involve 0.1 million cubic meters of earthwork. With a compacted density of 1.5 g/cc [5], 0.15 million tonnes of MSWI BA would be used. An average of 3% of total soluble solids in MSWI BA would mean approximately 4500 tonnes of soluble solids that are likely to release into environment from backfill during its lifetime. Hence, precautionary

design measures to isolate such material from external environmental factors such as groundwater table and rainfall using impermeable barriers are crucial for bulk reuse in geotechnical applications.

Soil-like fraction of MSWI bottom ash, though a look-alike of natural soil or coal bottom ash, is not as benign as it may appear. The concentration of soluble solids in MSWI BA is highly elevated and may pose a serious risk to the environment. If used in an unbound form such as in earthworks, filling of low-lying areas or deep mining pits, it can potentially contaminate groundwater table. If used in a bound form such as in concrete, bricks, soluble solids may interfere with the associated chemical reactions resulting in poor quality products.

It is therefore essential to estimate the SS values accurately and gauge its deleterious effect on the environment before putting it to reuse. It is recommended that IS-code method be used with due caution for estimating SS in materials when more soluble solids are anticipated. The requirement of higher dilution ratio should be verified for such materials. An understanding of the mass balance of SS which will quantify all the soluble metals, metalloids, total organic carbon and anions such as chlorides, sulfates, fluorides, nitrates, carbonates in the SS extract would be beneficial to address its long-term impact on the environment and studies are underway to investigate the same.

References

1. An, J., Kim, J., Golestani, B., Tasneem, K.M., Al Muhit, B.A., Nam, B.H., Behzadan, A.H.: Evaluating the use of waste-to-energy bottom ash as road construction materials. Office of Materials, State of Florida Department of Transportation, Contract No.: BDK78-977-20 (2014)
2. Arm, M.: Variation in deformation properties of processed MSWI bottom ash: results from triaxial tests. Waste Manage. **24**(10), 1035–1042 (2004)
3. Chang, F.Y., Wey, M.Y.: Comparison of the characteristics of bottom and fly ashes generated from various incineration processes. J. Hazard. Mater. **138**(3), 594–603 (2006)
4. Forteza, R., Far, M., Seguı, C., Cerda, V.: Characterization of bottom ash in municipal solid waste incinerators for its use in road base. Waste Manage. **24**(9), 899–909 (2004)
5. Gupta, G., Datta, M., Ramana, G.V., Alappat, B.J., Bishnoi, S.: Laboratory investigations on geotechnical properties of bottom ash from two MSW incineration plants in Delhi. In: Indian Geotechnical Conference, Indian Institute of Science, Bengaluru, India (2018)
6. Gupta, G., Datta, M., Ramana, G.V., Alappat, B.J.: Feasibility of Reuse of Bottom Ash from MSW Waste-to-Energy Plants in India. In: The 8th International Congress on Environmental Geotechnics, Springer, Singapore, pp. 344–350 (2018)
7. Gupta, G., Datta, M., Ramana, G.V., Alappat, B.J.: Feasibility of using MSW incinerator ash in geotechnical applications. In: Indian Geotechnical Conference, IIT Guwahati, India (2017)
8. Lynn, C.J., Ghataora, G.S., OBE, R.K.D.: Municipal incinerated bottom ash (MIBA) characteristics and potential for use in road pavements. Int. J. Pavement Res. Technol. **10**(2), 185–201 (2017)
9. Margallo, M., Taddei, M.B.M., Hernández-Pellón, A., Aldaco, R., Irabien, A.: Environmental sustainability assessment of the management of municipal solid waste incineration residues: a review of the current situation. Clean Technol. Environ. Policy **17**(5), 1333–1353 (2015)
10. Blissett, R.S., Rowson, N.A.: A review of the multi-component utilization of coal fly ash. Fuel **97**, 1–23 (2012)

11. Kim, H.K., Lee, H.K.: Coal bottom ash in field of civil engineering: a review of advanced applications and environmental considerations. KSCE J. Civil Eng. **19**(6), 1802–1818 (2015)
12. Huang, C.M., Yang, W.F., Ma, H.W., Song, Y.R.: The potential of recycling and reusing municipal solid waste incinerator ash in Taiwan. Waste Manage. **26**(9), 979–987 (2006)
13. Lin, C.F., Wu, C.H., Ho, H.M.: Recovery of municipal waste incineration bottom ash and water treatment sludge to water permeable pavement materials. Waste Manage. **26**(9), 970–978 (2006)
14. Code, Indian Standard IS 2720-Part XXI: Determination of Total Soluble Solids (First revision) (1977)
15. APHA, AWWA, WEF: Standard methods for examination of water and wastewater, American Public Health Association, Washington DC (2012)

Characterization of Soft Soil Deposit of Indo-Bangla Railway Project

Rajat Debnath and Rajib Saha

Abstract Tripura, one of the northeastern state of India, Agartala being the capital city with fast growing infrastructural facilities and population due to its global importance by acting as business corridor for South East Asian countries through Bangladesh. Present study attempts to highlight the characterization of subsoil deposits encountered in Indian part of the Indo-Bangla railway project which may be an important study for safe and sustainable design of foundation. Total 47 number of exploratory bore holes up to 25–30 m depth were conducted physical and engineering parameters are accordingly investigated. This study presents properties of subsoil of that area from three undisturbed soil samplers. Laboratory investigation was carried out for evaluating grain size analysis, shear strength parameters, and consolidation parameters. From the tests conducted on the samples it was found that the samples had very low shear strength and high compressibility values. Rate of change of pore water pressure along with shearing was also developed which gave an idea of the effect of pore water on the clay and organic soil. Thus, the outcome of present study will be helpful for carrying out safe and economic foundation design of the proposed railway embankment as well as assess vulnerability of the proposed construction from future disasters.

Keywords Soft peat clay · Engineering parameters · Indo-bangla railway

1 Introduction

Very soft peaty-type clay mixed with decomposed matter is very problematic type of soil from constructional point of view for a geotechnical engineer due to high compressibility, amorphous nature of soil, settlements of high order, creep, and subsequently low bearing capacity which may ultimately lead to low bearing capacity, not suited for the superstructure [1]. Soil mixed with decomposed matter which may be characterized as organic soil (OS) consists of organic matter (OM) mixed in varying

R. Debnath · R. Saha (✉)
National Institute of Technology Agartala, Agartala, India
e-mail: rajib.iitbbsr@gmail.com; rd2100@gmail.com

percentages of decomposed plants and animals which are synthesized by chemical reactions.

The Indo-Bangla railway project which is to be constructed at Agartala, Tripura, whose 5 km stretch passes through India, mostly encountered soft clay(SC) and OS which were obtained during the 47 borings conducted in that stretch having boring length upto a depth of 25–30 m. The present study deals with the experimental investigation of the soil collected from three undisturbed soil samplers of bore holes which were collected from the site during subsoil investigation, which would give a detailed idea about the subsoil deposit. The collected samples were undergone tests to determine the physical parameters, percentage of OM, Atterberg limits, shear strength parameters, and consolidation properties.

2 Experimental Investigation

2.1 Sample Collection

SC and OS were obtained by samplers having inside clearance (C_i) ranging from 1 to 3% and having area ratio (A_r) of less than 10%. OS obtained was amorphous in nature with varying decomposition of plant and animal remains whereas two samples of SC were devoid of OM. Thin tube samplers were used for collecting undisturbed soil (UDS) samples from the site at a depth varying from 1.5 to 3.00 m from earth ground level (EGL). Collected samples were waxed on both the open ends in order to fully secure the collected samples and to minimize the moisture loss. Samplers were kept vertically in upright position in a room having 85% humidity and at a constant temperature of 20 °C.

2.2 Physical Parameters

Water content of the soil was determined by oven drying the SC at 105 °C and OS at 75 °C, as per Indian Standards (IS): 2720 (Part 2) [2]. Organic content (OC) of soil was obtained by igniting 50gm of ovendried soil sample in a muffle furnace at a temperature of 450 °C following ASTMD2974 (ASTM 2007). OC was obtained by igniting OS which had 26% OM and having 74% ash content as shown in Fig. 1. Grain size analysis and hydrometer test were further conducted in order to determine the percentages of sand, silt, and clay as per IS: 2720 (part4) [3]. In case of OS pretreatment of the soil was necessary in order to oxidize the OM of the soil, which was done by treating the OS with 20 volume hydrogen peroxide (H202). From the results obtained from grain size and hydrometer test it was found that almost the entire soil was finer than 75 μ and 36% finer than 2 mμ, in case of OS whereas in case of first and second sample of SC almost 10% was retained on 75 μ sieve,
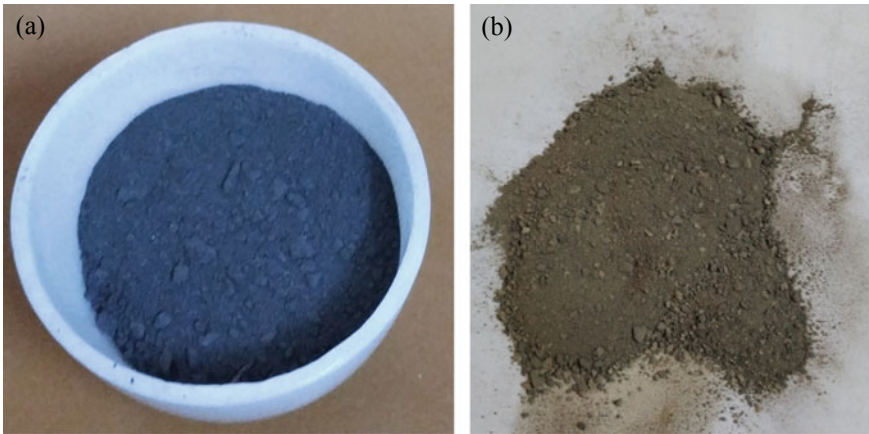
Fig. 1 **a** Ovendried OS. **b** Ash content of OS

nearly 55% passed through 2 mμ and 8% was retained on 75 μ sieve and nearly 48% passed through 2 mμ, respectively, as shown in Fig. 2, which indicated that there is an increase in the fines content with the increase in the OM in the soil which might be due to the chemical changes occurring in the soil during decomposition [4].

Laboratory investigation yielded different results in case of SC and OS which are presented in Table 1. Specific gravity yielded much lower value in case of OS compared to SC [5].

Liquid limits (LL) as per IS:2720 (Part 5) [6] were also on the higher side in case of OS which is mainly due to the fact that they are colloidal in nature and higher water absorption capacity compared to SC, whereas plastic limit (PL) had lower values mainly due to the fibrous nature of the soil due to decomposed matter, which resulted in higher plasticity index (PI), similar trends were observed by [7].

Fig. 2 Grain size distribution of soil
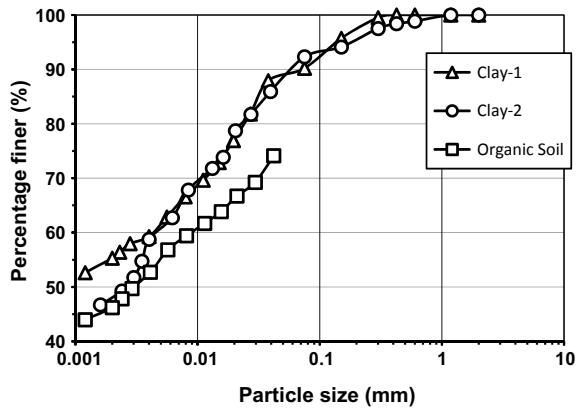
Table 1 Index parameters of soil

Nature of soil	Organic content (%)	Water content (%)	Liquid limit (%)	Plastic limit (%)	Plasticity index (%)	Specific gravity (G)
Clayey soil	Nil	42.12	49	23	26	2.69
Clayey soil	Nil	48.23	51	28	23	2.71
OS	26	116.64	179	87	92	1.98

2.3 Sample Preparation

Thin walled sampling tubes, as per IS:1892–1972 [8], were used to obtain UDS samples from the site, which were then mounted on the sample extractor to obtains UDS samples to carry out consolidated-undrained (CU) triaxial test and consolidation test, as shown in Fig. 3. In case of consolidation test, consolidation ring was used to obtain sample for the test from tube sampler having 20 mm height (H) and diameter (D) of 60 mm, having D to H ratio of 3:1, as per IS:2720 (Part 15). In case of CU triaxial test, small sampling tubes of 38 mm dia. were used to extract soil from the sampler, from which soil samples of 38 mm D and 76 mm H were obtained for undergoing the test maintaining a D to H ratio of 1:2, as per IS:2720 (Part 12).

2.4 Consolidation Test

Consolidation test was conducted on the UDS soil samples collected by the consolidation ring of three soil samples, out of which two were SC and one consisted of OS having 26% OM. Isotropic consolidation stresses were applied on each sample through consolidometer placed in position such that stresses are applied vertically on the specimen. Initially a seating pressure of 0.05kgf/cm^2 was applied for 24 h. and a stress sequence of 0.1, 0.2, 0.4, 0.8, 1.6, and 3.2 kgf/cm^2 and each loading deformations of the specimen were recorded at time intervals of 0, 0.25, 0.50, 1, 2, 4, 8, 15, 30, and 60 min. interval and 2, 4, 8, and 24 h. which would facilitate plotting of changing of thickness of specimen against sq.rt. of time ($\sqrt{t}$) [9].

2.5 CU Triaxial Test

Samples of 38 mm D and 76 mm H were used for this test in order to determine the shear strength parameters of the soil as per [10] along with change in pore water pressure (PWP) during shearing and also measuring changes in volume of sample during consolidation. Consolidation of the soil sample was carried out and the change

Fig. 3 **a** Extraction of sample from site. **b** Thin tube soil samplers. **c** Three types of soil samples. **d** Consolidation ring in sampler. **e** Soil sample for consolidation. **f** Extraction of soil sample from sampler for triaxial test. **g** Soil collected in small D samplers. **h** Samples for CU triaxial test

Fig. 3 (continued)

in soil volume can be recorded in the burette and the graph of change in volume change (ΔV) versus sq.rt. of time($\sqrt{t}$) is shown in Fig. 4, from this graph, time is recorded for 100% (t_{100}) consolidation of the sample and post consolidation length and diameter of the sample can be evaluated, coefficient of consolidation (C_v) of the specimen can also be determined at different cell pressure. After full consolidation, back pressure was applied to the samples in order to fully saturate the soil sample in such a manner that the ratio of change in cell pressure ($\Delta \sigma_c$) to change in PWP is 0.95–1.00, which is also known as B-factor, as per IS;2720(Part 12). After attaining a B-factor of 0.95, triaxial test were conducted at a strain rate of 1.25 mm/min. and at an effective confining stress of 1, 2 and 3 kg/cm^2, respectively. During shearing, PWP measuring apparatus was again taken into consideration in order to measure change in PWP during shearing of soil sample.

Fig. 4 Plot of ΔV versus $\sqrt{t}$
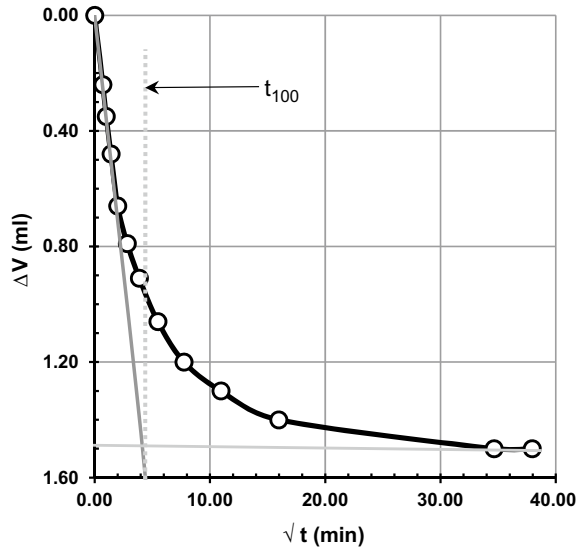
3 Results and Discussion

3.1 Consolidation Characteristics

Change in void ratio (Δe) under each stress increment (σ'_c) is deduced. From e vs logarithmic change in shear stress (log σ'_c) graph, compression index (C_c) can be determined, as shown in Fig. 5. Three samples were experimentally investigated to determine the consolidation parameters such as coefficient of compression (C_c), coefficient of volume compressibility (m_v), and coefficient of compressibility (a_v) which yielded nearly similar values in case of SC, whereas higher values in case of OS, as shown in Table 2.

3.2 Shear Strength Characteristics and PWP

Triaxial CU tests were conducted at different confining pressure of 1, 2, and 3 kgf/cm^2 and the corresponding change in PWP was recorded and plotted in graph, as shown in Fig. 5. Along with the increase in confining pressure, deviator shear stress also increased, which was on the higher side in case of SC compared to OS and the shear strength parameters cohesion (C) and angle of internal friction (φ) were obtained, as shown in Table 3. PWP initially increased slightly during shearing of the sample and showed a decreasing trend as shearing continued, as shown in Fig. 6 [11]. PWP parameter at failure showed a lesser value for OS [5].
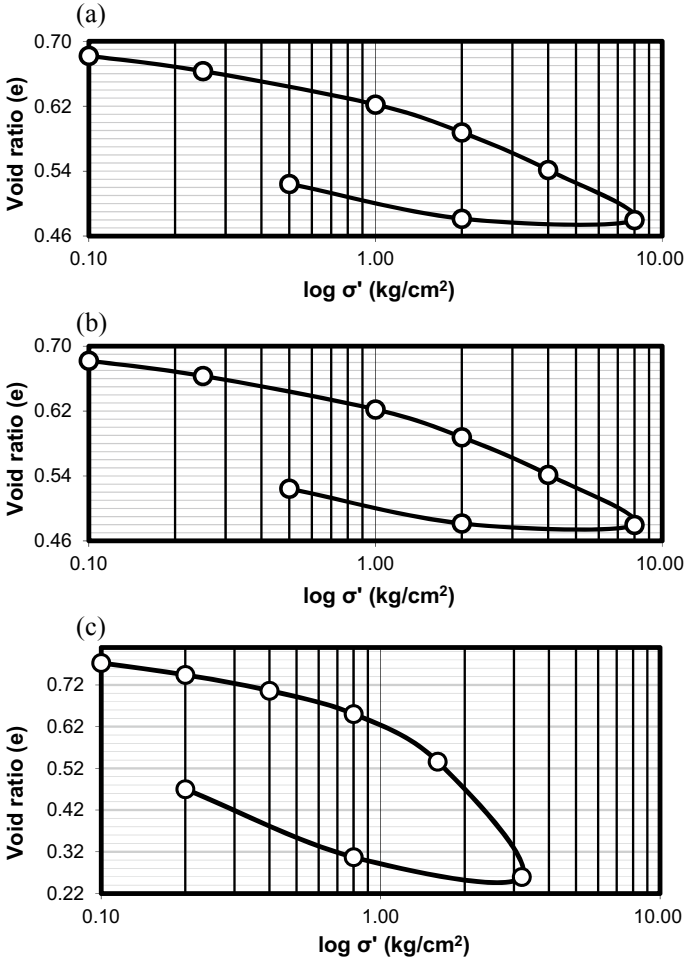
Fig. 5 Void ratio **e** versus $\log \sigma'$ graph **a** and **b** SC **c** OS

Table 2 Consolidation parameters of soil

Nature of soil	C_c	m_v (cm^2/kgf)	a_v (cm^2/kgf)
Clayey soil-1	0.292	0.014	0.022
Clayey soil-2	0.205	0.010	0.015
OS	0.998	0.118	0.188

Table 3 Shear strength parameters of soil

Nature of soil	C (T/m^2)	$\phi(\circ)$
Clay soil-1	1.40	2
Clay soil-2	1.20	1
OS	0.70	-
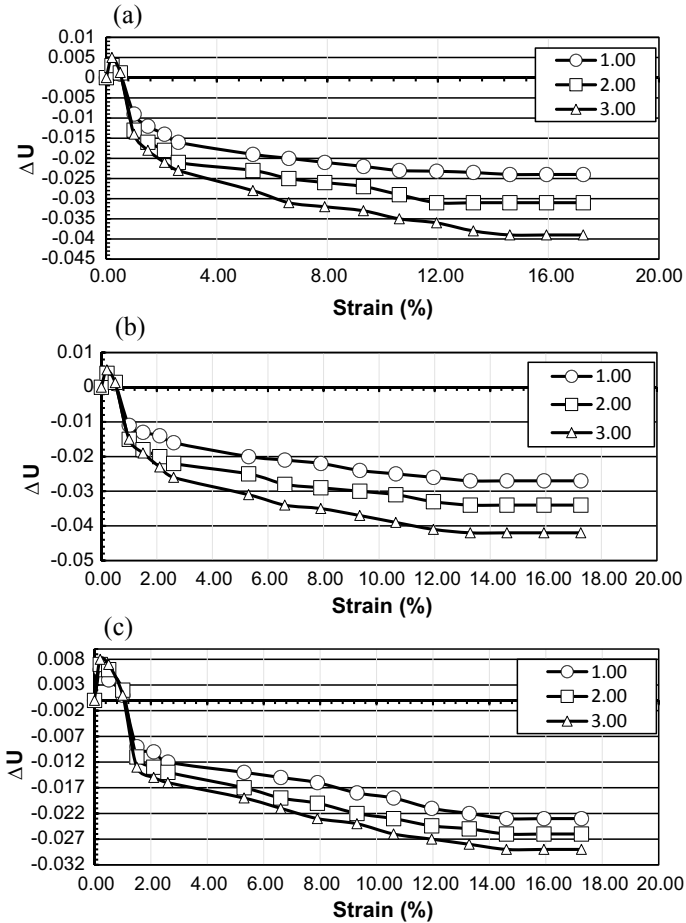
Fig. 6 Rate of change in PWP versus strain at varying cell pressure of 1, 2, and 3 kg/cm^2 in case of **a** and **b** SC **c** OS

4   Conclusion

Conducting consolidation test, CU triaxial test, and other experimental investigation on SC and OC, the following conclusions can be stated:

- Atterberg limits were on much higher side for OS having LL value of 116.64 which is a much higher value as compared to SC having LL of 49 and 51, respectively.
- Consolidation parameter such as C_c is also on the higher side for OS compared to SC which is mainly due to the amorphous nature of the soil having value of 0.998 compared to 0.292 and 0.205 in case of two clayey samples mainly due to high water absorbing capacity of the soil which might result in creep and inadmissible settlements.

- Shear strength parameter such as C value obtained for OS is on the lower side having value of 0.70 T/m^2 compared to 1.40 and 1.20 T/m^2 in case of both clayey soils.
- From the results obtained from the tests it can be stated that ground improvement in such type of soil is necessary and may be adopted as a future scope.

References

1. Terzaghi, K., Peck, R.B., Mesri, G.: Soil mechanics in engineering practice, 3rd edn. Wiley, New York (1996)
2. IS: 2720(Part 2)—1973: Determination of water content
3. IS: 2720(Part 4)—1985: Grain Size Analysis
4. Mesri, G., Ajlouni, M.: Engineering properties of fibrous peats. J Geotech. Geoenviron. Eng. **133**(7), 850–866 (2007)
5. Devi, R.D., Sahu, R.B., Mukherjee, S.: Shear strength of organic clay in Kolkata Region. Indian Geotech J. **45**(1), 25–34 (2015)
6. IS: 2720(Part 5)—1985: Determination of liquid limit and plastic limit
7. Andersland, O.B., Khattak, A.S., Al-Khafaji, A.W.N.: Effect of organic material on soil shear strength. Laboratory Shear Strength of Soil. ASTM International Published (1981)
8. IS: 1892–1979: Code for practice of subsoil investigation of soil
9. Leonards, G.A., Altschaeffl, A.G.: Compressibility of clay. J. Soil Mech. Found. Div. Am. Soc. Civ. Eng. **90**(5), 133–156 (1964)
10. IS: 2720(Part 12)—1981: Determination of shear strength parameters of soil from consolidated undrained triaxial compression test along with the measurement of pore water pressure
11. Roscoe, K.H., Burland, JB.: On the generalized stress-strain behavior of wet clay. In: Engineering plasticity, pp. 535–609, Cambridge (1968)

Site Characterization and Economization Through Pressuremeter Test: A Case Study in Katni, M.P

Kuppala Venkata Sivannarayana ⓘ**, Arnab Banerjee** ⓘ**, and Subhasish Pasupalak** ⓘ

Abstract Katni in Madhya Pradesh is proposed to have a railway elevated corridor spanning across 33 km, longer than any other in India. The geotechnical investigation spanning over two stages showed variations in SPT N value at deeper depths. The pile lengths derived from correlation with SPT N showed lot of variation. Hence, an effort has been made to characterize the site through in situ shear strength properties by conducting pressuremeter test. The variation of undrained shear strength (S_u) derived from SPT 'N' correlations and pressuremeter test is presented along with the site Np value. S_u derived from the pressuremeter test is much higher and appropriate than those derived from UU-triaxial tests and SPT 'N' correlations. The variation of S_u derived from pressuremeter tests, UU-triaxial test, and SPT 'N' correlation is illustrated in this paper. Through in situ testing, economization and standardization of foundation design were possible in this project.

Keywords SPT N · In situ · Pressuremeter test · Undrained shear strength · Economization

1 Introduction

Katni is a major junction of West Central railways, with heavy railway traffic meeting at the junction. The freight and passenger traffic are thereby planned to be decongested through the implementation of Katni Grade Separator project.

As a part of geotechnical investigation, boreholes were carried out at different intervals throughout the project stretch. The borehole investigation showed wide variation of SPT N value leading to a disparity in the pile lengths across the stretch.

K. V. Sivannarayana (✉) · A. Banerjee · S. Pasupalak
L&T Infrastructure Engineering Limited, Chennai 600089, India
e-mail: kvs@lntiel.com

A. Banerjee
e-mail: avik.arnab@gmail.com

S. Pasupalak
e-mail: subhasishpasupalak@gmail.com

Pressuremeter test (PMT) which is a specialized in situ test was carried out at various locations across the project stretch to characterize the site with respect to shear strength. The aim of this paper is to illustrate the variation of undrained shear strength (S_u) observed after analysis of PMT. The observed shear strength values are then compared with the undrained shear strength of soil correlated through SPT N and found to be higher and more consistent across the stretch. The reason for this can be stated that, the correlations are developed for geological conditions not inherent to local geology in present case study. In this paper, we will observe that cohesion values ranged from 400 to 600 kPa at deeper depths (i.e., greater than 15 m) in hard residual clay through analysis of PMT data across the stretch. Through the analysis of PMT, an effort was also made in this paper to characterize the site Np value which can be used to directly assess the undrained shear strength from limit pressure and initial stress of soil.

This paper also deals with on how the pile lengths can be reduced based on in situ test rather than relying on correlations helping in economizing the project.

2 Project Description

Katni is located in the central part of India, in state of Madhya Pradesh (M.P.). It is the largest railway junction of M.P. and second busiest railway junction of India connect more than 34 major cities of India. Approximately 342 passenger trains and 300 goods trains passes the junction every day. So, to address the easy moving of traffic, a grade separator in UP and DOWN line having a total length of 33 KM (in total) of which 12 KM is on viaduct, 4 KM on retaining wall, and remaining on the earthen embankment has been proposed. Based on the rail formation level and ground level difference, the grade separator is divided into three parts; Viaduct, retaining wall, and embankment. There are in total 645 supports for the viaduct portion along the alignment in both the lines. A U-trough type retaining wall is proposed for a smooth grade change from embankment to viaduct.

3 Background Study

3.1 Geotechnical Investigation

The project corridor being 33 KM in total, the geotechnical investigation was planned in different stages. Stage 1 comprised of boreholes being carried out at 450 m spacing for getting basic BOQ in order to float the tender. Later as a part of detailed design work, boreholes were carried out at a closer spacing of 75 m, i.e., at every third pier location to get a detailed understanding of the soil profile in terms of classification

and its origin. In total 200 boreholes were carried out including both stages. The whole borehole investigation was divided into two agencies.

The geological profile can be classified as a residual soil formation with limestone and lateritic bauxite as the parent material overlain by a shallow deposit of alluvial soil. The residual soil is in clay formation with intermediate to high plastic characteristics. In the project stretch around the Katni river, limestone rock was encountered from shallow depth. The core recovery and rock quality designation recorded during investigation was observed to vary from 10 to 40% and 0 to 10%, respectively.

3.2 Geology

The site is a mining area having major physiographic units of Vindhyan Plateau and valleys of Bhitrigarh ranges. The limestone and lateritic bauxite formations are the predominant geological formations in current site. The geological profile consists of residual soil of limestone and bauxitic origin overlain by a top layer of alluvium soil. The residual soil is mostly high to medium plastic clay in nature. Limestone rock was encountered in highly weathered state in and around the Katni river area.

3.3 Soil Profile

Field exploration and laboratory tests from stage 1 and stage 2 investigations of 200 boreholes up to 40 m depth shows the presence of brownish to gray color silty clay in medium stiff state at surface to hard at deeper depths. In Fig. 1, generalized soil profile, Atterberg limits, and SPT 'N' are shown at borehole locations where PMT was executed. The soil at deeper depth mostly after 10 m depth is found to be intermediate plastic clay in hard state, occasionally with gravel content varying from 12 to 20%. The clay with lime content (in residual soil form) is also located at depths greater than 15 m. Coarse sand with gravel content is also found as pockets at some depths.

3.4 Foundation Recommendations

Pile was recommended as foundation for the pier structures owing to the high loads transferred from superstructure and also due to space constraints given the project runs parallel to existing railway line and urban area. The undrained shear strength (S_u) where undisturbed sampling was not possible was calculated through correlations from SPT 'N'. The pile lengths were found to vary from 25 to 35 m across the project stretch owing to variation in SPT 'N' values. Around Katni river location, the pile length varies from 18 to 20 m length where rock was encountered. The variation
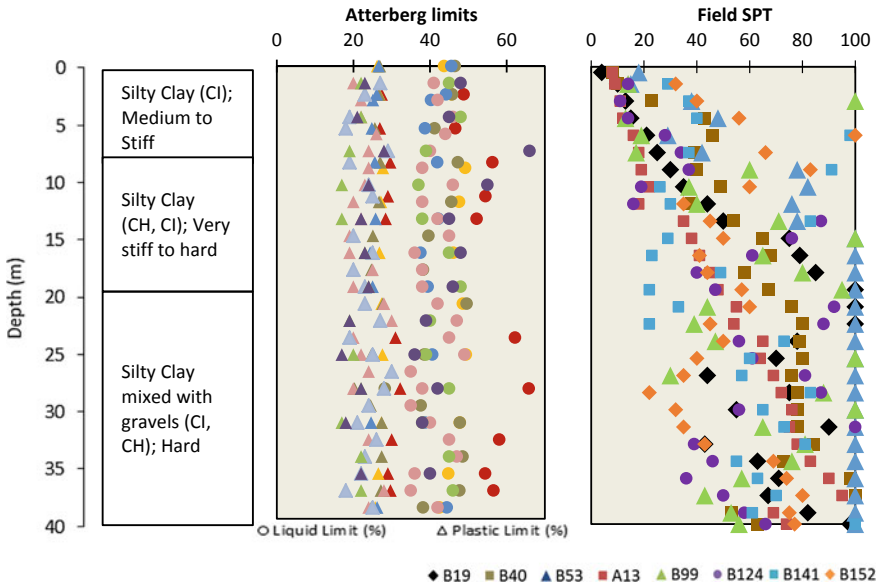
Fig. 1 Soil profile and parameters at pressuremeter locations

in SPT '*N*' values can be attributed to different agencies using different tools for carrying out drilling as well for execution of SPT. As a result, a lot of variation was observed in pile lengths for the similar soil characteristics. This led to the necessity of an in situ pressuremeter test to directly assess the undrained shear strength of soil strata instead of correlations developed in different geological conditions not inherent to local geology. The variation of pile length in the project stretch across the project is shown in Fig. 2.

4 Pressuremeter Test

4.1 Planning

Pressuremeter test is planned in 8 boreholes, at 4 test depths in each, total 32 tests. The pressuremeter is having an outer dia. of 74 mm and length of 500 mm. The maximum volume and pressure capacities are 800 cm^3 and 80 bar, respectively. The test locations and depths were decided by considering the soil\lithological profile from stage 1 and 2 investigations. As collecting undisturbed sample at depth more than 10 m is found critical, the pressuremeter test is adopted for strength characterization of the deeper strata.
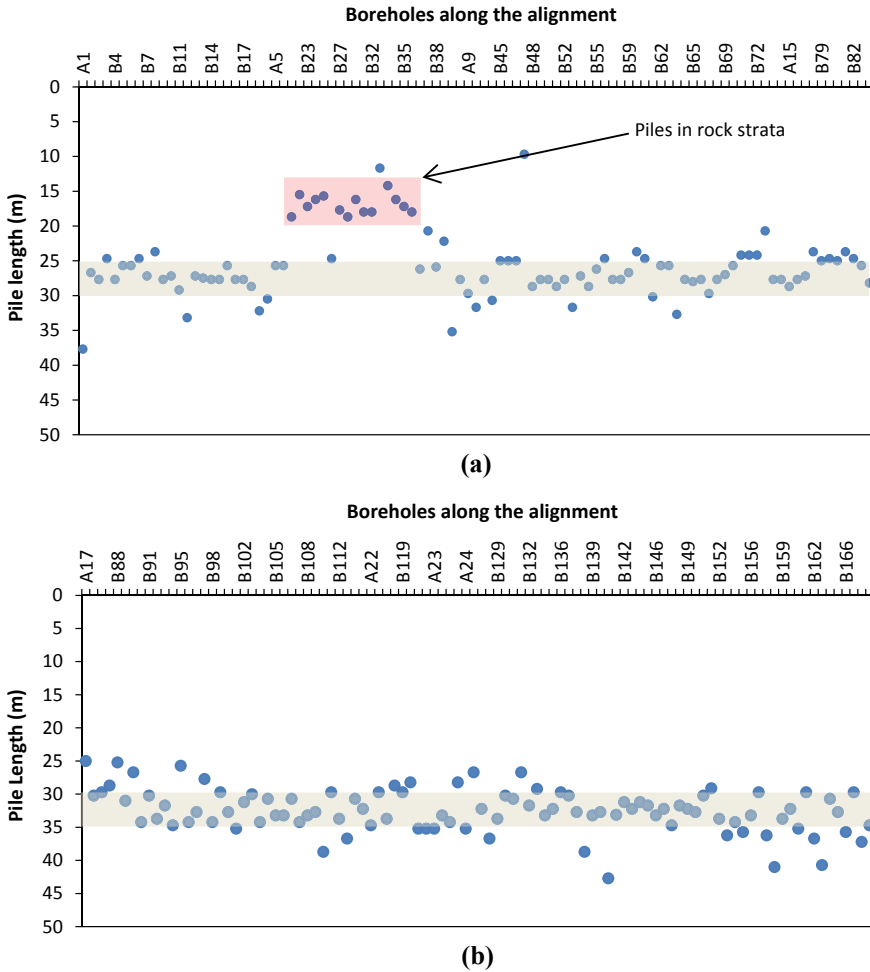
Fig. 2 Variation of pile length along the alignment **a** starting from Ch. 0 to 7.5 KM **b** from 7.5 to 14 KM (approx…)

4.2 Analysis

Figure 3 shows expansion of an ideal cavity in cohesive soil. The test is assumed as undrained because the duration of test is very small as compared to the drainage time which is going to occur in the drainage path of very large in order of the borehole dia [1]. When the borehole is drilled, the radial stress reduced to zero on the borehole wall. The soil will behave elastically if the disturbance caused due to drill is nominal. During the test, when the probe membrane touches the borehole wall the soil behaves an elastic trend in pressure–volume curve till strain softening stage. The volume (V_0) at which the curve became linear is equal to the difference between the volume of
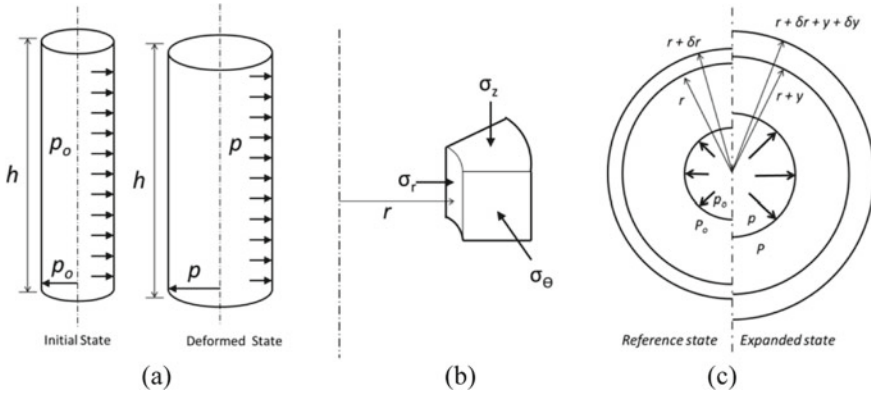
Fig. 3 Ideal expansion of cavity **a** expansion of cylindrical cavity, **b** element of soil in cylindrical symmetry, and **c** reference and expanded stage of cavity at a radius r

the hole and the initial volume of the probe. The reference pressure (P_0) and volume (V_0) is taken from the starting point of the linear portion. The expression for shear modulus for the expansion of a cylindrical cavity is given by Gibson and Anderson [2]:

$$G = (V_i + V_m)\frac{\Delta p}{\Delta v} \tag{1}$$

where G is the shear modulus of the soil, V_i is the initial volume of the probe, V_m is the mean volume of the probe in the elastic region, Δp is the corrected pressure increase in elastic region, and Δv is the corrected volume increase in the elastic region for the increment of Δp pressure.

In the analysis of expansion of cylindrical cavity in elastic-perfectly plastic soil, the reference state is taken as original in situ state before drilling the borehole at test depth location, which can be acquired by pushing the deformed borehole wall to the original state. This could be observed in the pressure–volume curve of the pressuremeter test. When the pressuremeter probe wall touches the borehole wall the soil responds elastically. The initial point from the linear portion of the pressuremeter curve is considered as the horizontal in situ stress. All volume is normalized with this reference volume (V_0) and volumetric strains were calculated from this volume.

According to Palmer [1], the shear strength of the soil from pressuremeter can be derived from the slope of P: ln ($\Delta V/V$) curve. The slope of elastic and plastic phase gives peak and ultimate strength of the surrounding soil, respectively. For a proper development of plastic phase, the applied strain should be large enough to yield the surrounding soil annulus. So, the undrained strength of the soil is given by:

$$S_u = \frac{\mathrm{d}p}{d\left(\ln\left(\frac{\Delta V}{V}\right)\right)} \tag{2}$$

As cavity pressure increases, in plastic stage the cavity strain increases continuously with a small increment of pressure. The pressure at which the change in volume equals the cavity volume is termed as limit pressure (P_L). The expression for limit pressure is:

$$P_L = P_0 + S_u\left(1 + \ln\left(\frac{G}{S_u}\right)\right) \tag{3}$$

$$N_P = 1 + \ln\left(\frac{G}{S_u}\right) \tag{4}$$

$$S_u = \frac{P_L - P_0}{N_P} \tag{5}$$

The limit pressure depends strongly on undrained shear strength (S_u) and shear modulus (G) [3]. Marsland and Randolph [4] proposed this method for estimation of S_u from P_L. S_u can be derived from Eq. (5) by successive estimation of S_u by equating both sides of equation. Marsland and Randolph [4] conducted a series of plate load test and pressuremeter test and compared the results. By comparing both the in situ test results suggested N_p value of 6.18 for London clay. Mair and Wood [5] suggested the variation of N_P with G/S_u presented in Fig. 4. The variation of N_P corresponding to G/S_u is presented in Fig. 4. In this study, the N_P value observed is in range of 4.25–5.26. From the figure it could be observed that N_p values are less than the values observed by Marsland and Randolph [4] but good agreement with Mair and Wood [5].
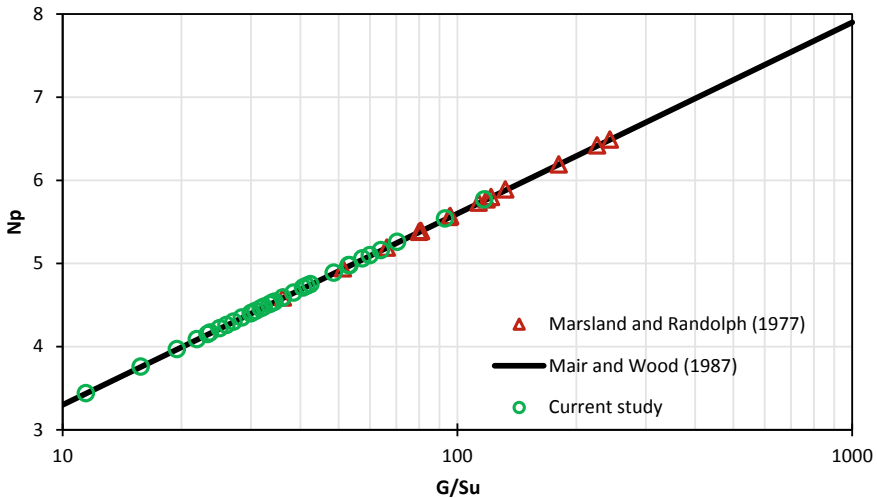
Fig. 4 Variation of pressuremeter constant with shear modulus/undrained shear strength
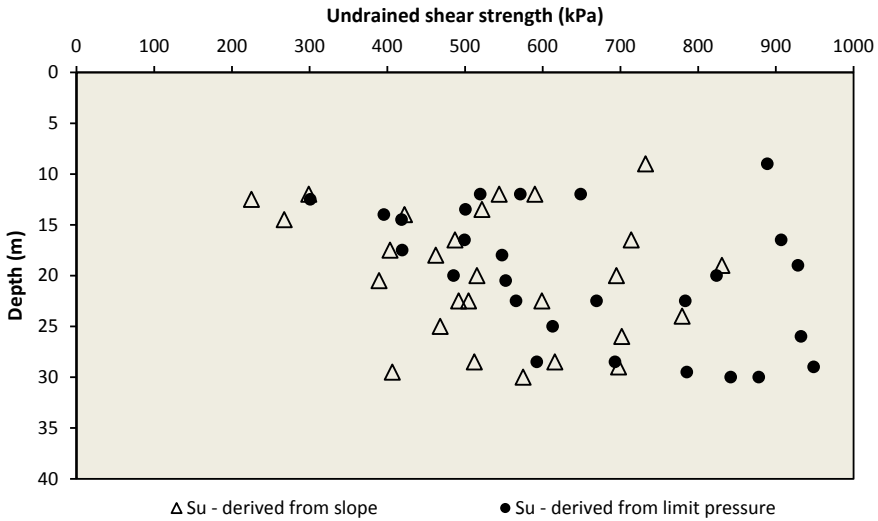
Fig. 5 Undrained shear strength derived from pressuremeter test

5 Site Characterization

5.1 Undrained Shear Strength (S_u)

The undrained cohesion values obtained from the analysis presented in the preceding section is shown in Fig. 5. From figure it can be observed that undrained shear strength (S_u) of soil at 10–15 m below ground level (GL) is reported to vary between 200 and 300 kPa with few values showing higher S_u of 500–600 kPa because of fewer readings in the plastic phase of the test. From 15 to 20 m below GL is reported to vary between 400 and 500 kPa and that between 20 and 30 m below GL the cohesion values is varying between 450 and 600 kPa.

Cole and Stroud [6] reported S_u ranging from 400 to 600 kPa for hard clay or very weak rock. IS 2911 Part 1 Sec 2 represents the same table given by Cole and Stroud [6], but recommends the table to be used only for judgment of shear strength properties of weathered rocks.

5.2 Comparison of Undrained Cohesion Values

The initial estimation of undrained shear strength of soil for foundation recommendation was carried out in this project through correlations from SPT 'N'. At later stage due to variation of SPT 'N' values leading to variation in pile length, the in situ shear strength of soil was analyzed through pressuremeter test.
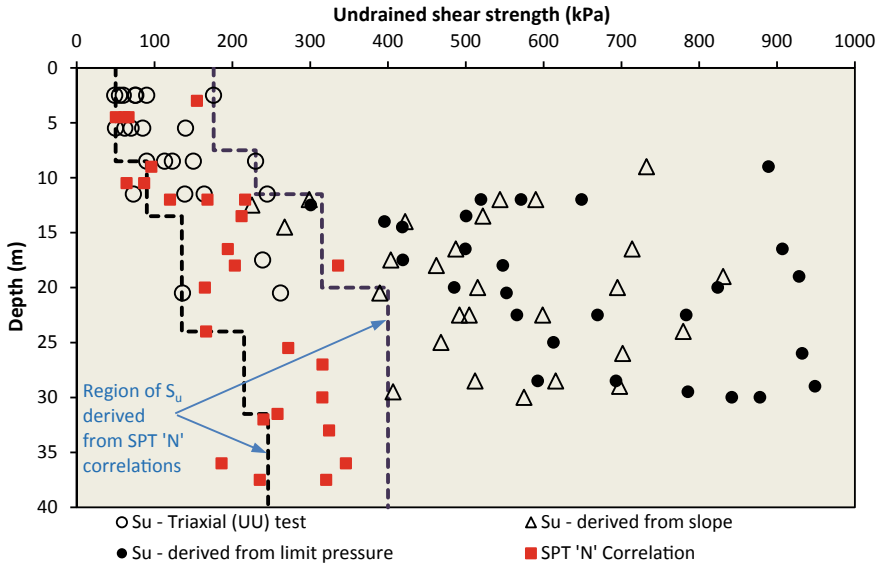
Fig. 6 Comparison of undrained shear strengths from UU-triaxial test, SPT '*N*' correlations and derived from pressuremeter tests (from slope and limit pressure)

In this section, a comparison of cohesion values obtained from SPT '*N*' with the cohesion values obtained from pressuremeter test is illustrated. From Fig. 6 it can be observed that the range of undrained shear strength (S_u) values obtained from correlations varies from 240 to 340 kPa. The in situ undrained shear strength values obtained from pressuremeter test at similar depth is observed to be higher. The reason for this may be explained in the shortcomings of the correlations developed in soil conditions not same as local geology. Moreover, the correlations being based on SPT '*N*', there is uncertainty about the efficiency of the hammer used at project site and that used for developing the correlation.

A comparison can also be drawn with the undrained shear strength (S_u) obtained from UU-triaxial tests (on UDS), with some amount of limitation as the numbers of UU-triaxial tests for comparison are less. It can be observed that at depth of 10–15 m from GL the UU-triaxial test gives S_u of 140–240 kPa whereas the same from pressuremeter test is reported as 210–300 kPa. In deeper strata, at same location the difference between S_u, derived from UU-triaxial test and pressuremeter tests increases. This can be observed from Fig. 6, where UU-triaxial test report S_u in the range of 250 kPa whereas in pressuremeter test it is of 400 kPa. The reason is explained by many previous researchers Hansen and Gibson [7], Wood and Worth [8]. According to Hansen and Gibson [7] the shear strength mobilized on a vertical plane as in pressuremeter test is much greater than; the shear strength mobilized a plane inclined 45 deg. to the horizontal in triaxial compression test; because the lateral earth pressure applied in pressuremeter test in in situ condition is very high than the confined pressure applied in triaxial compression test. Wood and Worth [8] stated
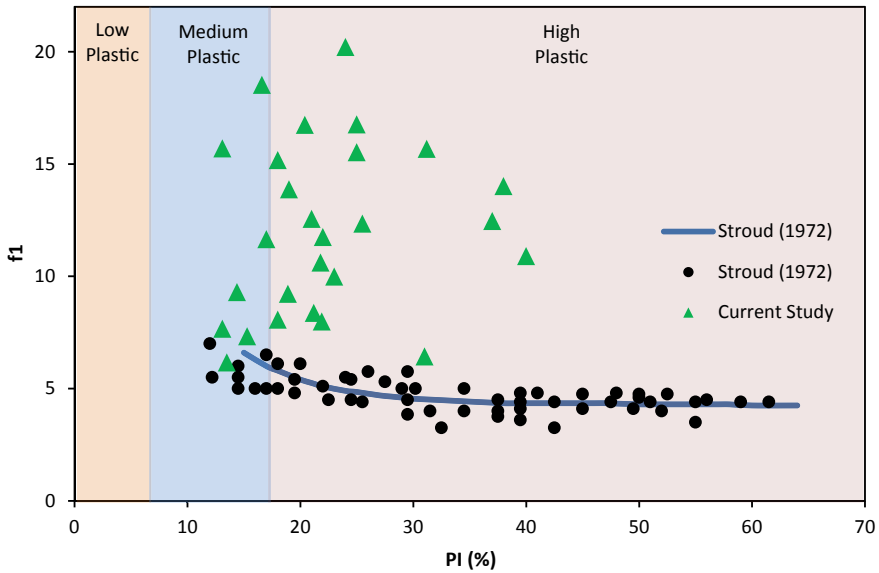
Fig. 7 Variation of f_1 values with respect to plasticity index

that on the expansion of cavity the radial stress σ_r becomes the major principal stress (more than existing vertical stress σ_z) and σ_θ becomes minor principal stress. Hence, these two principal stresses cause the failure on a vertical plane. So the vertical stress σ_z becomes an intermediate principal stress causing no effect on the soil element.

The correlation graph in current study and given by Stroud [9] is shown in Fig. 7. The factor f_1 (S_u/N_{60}) in current study is developed by dividing S_u derived from pressuremeter test by SPT 'N' observed at same depth corrected for 60% hammer efficiency. It can be observed that the f_1 factor ranges from 7.5 to 15. However, the range can be narrowed down to 7.5–13 by only considering those S_u which was derived from pressuremeter tests with fully developed plastic phase. This gives some evidence that the correlations developed on soil not inherent to local geology may not give correct assessment of undrained shear strength values.

6 Discussion

6.1 Economic Design

In the preceding sections, the variation in pile lengths was illustrated. Through soil classification the subsoil profile was observed to be same across the project stretch. As a result to understand the generalized undrained shear strength of soil, pressuremeter test was carried out across the project stretch at different locations. Through analysis

of pressuremeter test data, the undrained shear strength of soil at different depths was assessed as illustrated in preceding section.

The pile length calculation was done based on the range of S_u data achieved through pressuremeter and was observed to vary from 23 to 24 m. Pile length for the 645 pier supports was reduced through undrained shear parameters analyzed from pressuremeter data resulting in economization of project. Further to this, with the variation in pile length reduced from previous recommendations, the ease of construction for contractor in executing pile foundations for all pier supports at 26 m intervals (mostly) increased manifold.

Although the advantages of PMT are many, there are few site issues that were encountered during the execution. The issues can be taken care through proper checking of all equipment and discussion with experienced people having good knowledge on equipment of PMT. However, site-specific issues with PMT have to be resolved through wise engineering judgment and expertise.

7 Conclusion

Katni, located in central India, has stiff formations of limestone and bauxite in residual form. The soil stratum is of very stiff clay formation having high to intermediate plastic clay. The site characterization through conventional geotechnical investigation found to be difficult in current study. So, the adoption of PMT test had been done for strength characterization of the strata. The foundation had been designed based on the PMT test data obtained. Through this paper we have been able to illustrate the site-based undrained shear strength values and the effects of using the same for foundation analysis in correctly judging the strength characteristics of soil. The important points that can be inferred from this paper are:

1. The in situ shear strength parameters achieved through PMT are higher and more reliable than that analyzed through correlations.
2. The in situ shear strength of soil through PMT is higher than shear strength observed from unconsolidated undrained triaxial test because of different confining pressure and stress paths.
3. The f_1 factor is majorly used to correlate the undrained shear strength (S_u) of soil where undisturbed samples are not possible to be collected and grossly underestimates the shear strength of soil in the current case study. Hence, the applicability of correlations for different subsoil conditions needs to be checked.
4. The N_p value which is used to correlate cohesion value from PMT was found to vary from 4.25 to 5.26 for the current case which is slightly lower than suggested by different authors, albeit for different soil conditions.
5. Through correct assessment of undrained shear strength of soil (S_u), considerable quantity of pile length savings was made and being able to achieve generalized shear parameters helped in reduction of pile length variation.

References

1. Palmer, A.C.: Undrained plane-strain expansion of a cylindrical cavity in clay: a simple interpretation of the pressuremeter test. Geotechnique **22**(3), 451–457 (1972)
2. Gibson, R.E., Anderson, W.F.: In-situ measurements of soil properties with the pressuremeter. Civ. Eng. Public. Wks. Rev. **56**(658), 615–618 (1961)
3. Menard, L.: The menard pressuremeter: interpretation and application of pressuremeter test results to foundation design, 45 (1975)
4. Marsland, A., Randolph, M.F.: Comparisons of the results from pressuremeter tests and large in-situ plate tests in London Clay. Geotechnique **27**(2), 217–243 (1977)
5. Mair, R.J., Wood, D.M.: Pressuremeter testing: methods and interpretation, CIRIA Report, Butterworths, UK, 160 (1978)
6. Cole, K.W., Stroud, M.A.: Rock socket piles at Coventry point, market way, Coventry. Géotechnique **26**(1) (1976)
7. Brinch Hansen, J., Gibson, R.E.: Undrained shear strengths of anisotropically consolidated clays. Géotechnique **1**(3):189–200 (1949)
8. Wood, D.M., Wroth, C.P.: Some laboratory experiments related to the results of pressuremeter tests. Geotechnique **27**(2), 181–201 (1977)
9. Stroud, M.A.: The standard penetration test in insensitive clays and soft rocks. ESOPT, Stockholm 1974. Stockholm, National Swedish Building Research, pp. 367–375 (1974)

Agartala–Bangladesh Railway Embankment Construction Over Soft Soils Incorporated with Prefabricated Vertical Drains: A Case Study

Rai Bahadur Reang, Sujit Kumar Pal, and Sanjay Paul

Abstract Three embankments of different dimensions for the railway tract at contiguous locations are being constructed over soft soils using prefabricated vertical drains for connecting two cities, Agartala and Dhaka. Prefabricated vertical drains were supplied from Maccaferri and the installation rig machineries were provided by IRCON. PVDs were installed in triangular pattern with three different spacing (0.7, 0.8, and 1.0 m) with according depths (15, 6, and 7.5 m). For conducting physical and engineering properties, soils were collected from different locations as well as from different depths using auguring and wash boring method at suitable intervals along with SPT tests. It has been observed that the natural soil profile was composed of three different layers of different thickness; sandy silty-clay at top, silty-clay in the middle, and sandy silty-clay at bottom, respectively, overlying the hard stratum. A sand layer of thickness 0.2 m is being provided underlain by a strip drains made up of polypropylene, which accelerates and helps sand layer draining off the water from PVDs, over which paralinks were also laid that function as reinforcement to embankment soil deposits. Settlements predictions of the existing soils were made and determined. Different results were obtained at various locations. Without PVD, the settlement of the soil strata at chainage Ch-03 + 900 to Ch-04 + 400 km is observed to be 2305 mm and the corresponding settlement time is 189306 days. While the design was made considering PVD the consolidation settlement and time gave as 1660 mm and 122 days, respectively.

Keywords Prefabricated vertical drain · Stratified soft soil · Settlement

R. B. Reang (✉) · S. K. Pal · S. Paul
Department of Civil Engineering, NIT Agartala, Tripura, Tripura, India
e-mail: raireang@springer.com

S. K. Pal
e-mail: skpal1963@gmail.com

S. Paul
e-mail: sanjaypaul76@gmail.com

1   Introduction

Preloading combined with prefabricated vertical drains (PVDs) has been used extensively used in the construction of large-scale infrastructure for highways, railways, ports, and airports [1–7]. Barron [8] proposed the original analytical solutions to theoretically analyze the consolidation process of vertical drained ground. However, the performance of the PVD system is still difficult to accurately predict because the consolidation rate of PVD-improved foundation is controlled by several factors [9–12]. Prefabricated vertical drains are commonly used to decrease the drainage path within soft soils to accelerate the time of primary consolidation. PDVs are displacement drains of small volume that exhibits considerably with fewer disturbances to the soil mass than the displacement sand drains. In this railway project, there are three construction sites (under same project) for which settlements of soil mass due to installation of PVDs were predicted based on which the embankment shall be constructed. But, only one site is discussed in this paper. An analytical solution was proposed to predict the settlement and determined using IRC:75, IS:8009 (Part-1) and Bowles formula. Different settlements were observed for different sites. Since the three construction sites are consist of different types of soil layers, it has been observed that the proper knowledge of keep maintaining spacing and depth to which PVDs are thrust into the existing soil are important factors for settlement evaluation for stratified field soils. The size of the installation mandrel and installation rig shall be kept same all through the project. Installation of PVDs and construction of embankments are under progress. Laboratory and numerical study are also being carried out to validate the field settlement and other mechanism of reaction to soil disturbance and finding its solution. With this new approach, a modified effective drain spacing and depth of the PVD shall be evaluated for layered soil consisting of different type of soils.

2   Importance of Prefabricated Vertical Drain

It is very important to stabilize soft soil before commencing any major construction work to prevent out the settlement. Many soft clay strata contain thin bands of silt or sands which result in the instability of embankments due to the horizontal spread of excess pore pressure vertical drains relives these excess pore pressures and thus avoids the occurrences of instability. The time required to reach a higher degree of consolidation under preloading improved drainage should be used in the form of prefabricated vertical drains. In order to expedite the settlement process and reduce building of pore water pressure, it is necessary to restrain the flow path through the soil. This can be achieved by placing prefabricated vertical drains at a regular spacing in the soil. PVDs are selected over vertical sand drains for its feasibility in installation and its low cost. When a heavy load, such as a road embankment or other structure is placed on the top of clay or silty-clay soil, considerable sudden

settlement may occur due to squeezing out of excess pore water pressure, thus the soft soil consolidated. This kind of settlement often causes serious construction problems. But, when PVDs are installed before commencing any civil engineering construction and structure over the soil, the settlement takes place in gradual manner and thus no serious abruption of the soil and no consequent casualties are observed.

3 Field Study

In this project, prefabricated vertical drains are to be used in the construction of embankments for broad gauge railway lines between Agartala (India) and Dhaka (Bangladesh) at chainages Ch-03 + 900 to Ch-04 + 400 km, Ch-04 + 400 to Ch-04 + 700 km, and Ch-04 + 700 to Ch-05 + 100 km, i.e., there are three different construction sites (under same project) in between 3.9 and 5.1 km from Agartala railway station (Tripura) and only 0.7 km away from international fencing line (border between India and Bangladesh). The existing sites consist of stratified soft soils covering vast area all around extending to great depths. Embankments of different heights, such as 6, 6, and 9 m high, are to be established at stages on these sites. Installation of prefabricated vertical drains at chainage Ch-03 + 900 to Ch-04 + 400 km is under progress, and therefore only this chainage is discussed in this paper. The study of the soil profile indicated that the top of the stratification contains the light gray soft sandy silty-clay. The next layer observed in the stratification contains the silty-clay which is then followed by sandy silty-clay. The next layer of stratification is moderately weathered rock. Table 1 gives details of type of soil strata at the chainage Ch-03 + 900 to Ch-04 + 400 km.

3.1 Properties of the Soil Strata, Embankment Fill, PVD, Drainage Composite, Paralink

The settlements of the existing soil stratums can be accelerated by using prefabricated vertical drains (PVDs) with surcharge. With the use of PVDs, water flows out horizontally as well as vertically, i.e., three-dimensional consolidations occur while

Table 1 Type of soil strata at chainage Ch-03 + 900 to Ch-04 + 400 km

Stratum	Description	Depth below ground level (m)	Thickness (m)
I	Light gray soft sandy silty-clay	0.8	0.8
II	Silty-clay	11.50	10.70
III	Sandy silty-clay	13.20	1.70
IV	Moderately weathered rock (in situ rock)	–	–
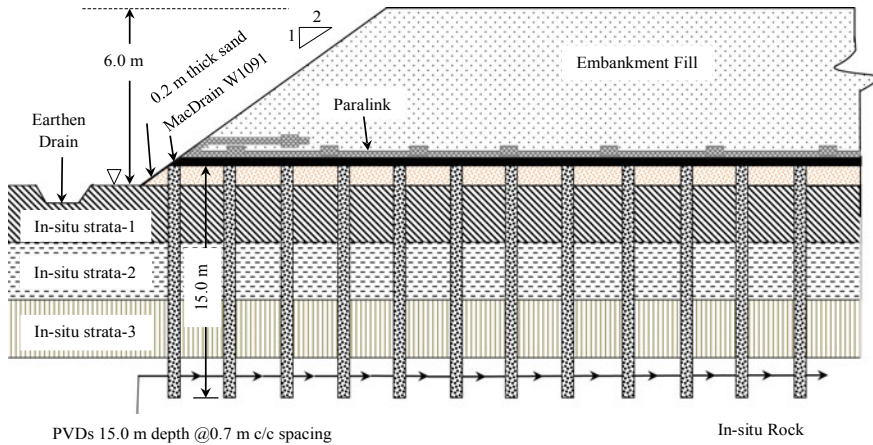
Fig. 1 Typical cross section (a portion of the total embankment width of 106 m) of railway track (Ch-03 + 900 to Ch-04 + 400 km)

prefabricated vertical drains are used. Therefore, on application of PVDs along with preload the time required for settlements can be drastically reduced. Based on the study of properties of existing soil, the ground improvement technique using prefabricated vertical drains (PVDs) was designed. The spacing of PVD was designed as 0.7, 0.8, and 1.0 m for these three sites. At chainage Ch-03 + 900 to Ch-04 + 400 km the spacing and depth were kept as 0.7 and 15 m, respectively, with triangular patterns to achieve the expected settlement within the desired consolidation period. At this chainage, the height of the embankments is 6 m. The consolidation settlement is expected to be 1660 mm. A typical cross section of the embankment is shown (Fig. 1).

The details and properties of the soil strata, embankment fill, prefabricated vertical drain, drainage composite, paralink, and sand blanket are given in the following.

The details of the soil strata are given in Table 3. Properties of the prefabricated vertical drains and paralinks are tested as per ASTM and EN ISO methods. The installing rig had been provided by IRCON (a central PSU of the Indian Government). The drainage composite is used in the field with the basis of pressure and discharge requirement and the type used in this project is Geocomposite MacDrain W1091 (having a "W" configuration as longitudinal parallel channels) and paralinks are also to be used as reinforcement to embankment. Paralinks is a high strength geogrid manufactured from high tenacity polyester yarns. Locally available well graded sand shall be applied over the field soil bed as sand blanket to facilitate the drainage of water. Properties of geocomposite and prefabricated vertical drains are given in Tables 2 and 4, respectively.

Table 2 Details of the geocomposite (MacDrain W1091) used in this project

Properties	Test method	Average value
Thickness (mm)	EN ISO 98,631	9.00
Tensile strength (kN/m)	EN ISO 10,319	18.00
In plane flow capacity (l/s)	EN ISO 12,958	0.38
Apparent opening size, O_{90} (μ)	EN ISO 12,956	110.00

Note All the data are collected from IRCON, a central PSU of the Indian Government, Agartala region

3.2 Construction of the Embankment

After the completion of installation of prefabricated vertical drains, preload (embankment material) along with surcharge loading shall be placed over the existing soil bed in stages up to the required height as shown in Table 5. The embankment material of which properties are different from the existing field soil shall be collected from other locations. In this project, 10 days interval for each 0.5 m rise in the embankment shall be adopted up to 60 days. After that, the next 3 m height shall be completed within 30 days and the other 3 m to be within 32 days. When the expected consolidation period is over and the soil has consolidated up to the required extent same as evaluated from the design, the surcharge loading has to be removed to arrive at the working level and the surface is to be properly rolled. Once this is completed commencement of construction of the railway lines may be carried out on the improved ground.

3.3 Estimation of Settlement

For cohesive soft soils, the consolidation settlements are of major concern as this is a long-term phenomenon. Since the very first objective of PVD installation is to consolidate the soil bed, the total settlement was determined by using conventional method of settlement analysis before the installation of PVDs started. Total settlement of a soil bed is summation of elastic (immediate) settlement (S_i), primary consolidation settlement (S_P), and secondary consolidation settlement (S_s) as shown in Eq. (2). In this project, primary consolidation settlement was mainly focused barring initial and secondary consolidation settlement for the calculation of total settlement [a conventional Eq. (1)] and was determined using IRC:75, IS:8009 (Part-1) and Bowles formula. Primary consolidation settlement (S_p) and total settlement (S_t) are calculated as,

$$S_p = \frac{C_c H}{1 + e_0} \log\left(\frac{p_0 + \Delta p}{p_0}\right) \tag{1}$$

where

Table 3 Parameters of the soil strata at chainage Ch-04 + 100 km

Sl. no	Stratum	Thickness (m)	Specific gravity (G)	Liquid limit (LL), %	Plastic limit (PL), %	Plasticity index (PI), %	Saturated unit weight (γ_{sat}), t/m³	Effective unit weight (γ_{sat}), t/m³	Influence factor after Osterberg ($I_{\sigma z}$)	Net incremental pressure at the layer top (Δp), t/m²	Initial void ratio (e_0)	Compression index (c_c)	Poisson's ratio (μ)	Influence factor (I_s)	Modulus of elasticity (E_s), t/m²
1	I	0.80	2.73	49	26	23	1.60	0.60	0.500	20.206	1.820	0.351	0.30	0.002	180
2	II	10.50	1.57	46	24	22	1.07	0.07	0.499	20.147	0.836	0.235	0.30	0.026	180
3	III	1.70	2.72	36	23	07	1.83	0.83	0.498	20.119	1.040	0.234	0.30	0.004	661

Note All the data are collected from IRCON, a central PSU of the Indian Government, Agartala region

Table 4 Details of the PVD used in this project

Properties	Test method	Typical value
Core configuration	⊓⌐⊓⌐⊓⌐⊓	
Core material	ASTM D 276	PP
Width (mm)	ASTM D 3774	100.00
Thickness (mm)	ASTM D 5199	4.00
Width-width tensile strength (kN/m)	ASTM D 4595	≥ 7.00
Tensile strength (kN/m)	ASTM D 4595 EN ISO 10,319	≥ 2.50
Elongation at 0.5 kN (%)	ASTM D 4595 EN ISO 10,319	≤ 10
Discharge capacity, 300 kPa ($i = 1$) (cm^3/s)	ASTM D 4716	≥ 100
Permeability (cm/s)	ASTM D 4491	$\geq 1.4 \times 10^{-4}$
Permittivity (s^{-1})	ASTM D 4491	0.44
Apparent opening size, O_{90} (μ)	EN ISO 12,956	<85

Note All the data are collected from IRCON, a central PSU of the Indian Government, Agartala region

Table 5 Embankment stage construction details for Ch-03 + 900 to Ch-04 + 400 km

S. No	Height of embankment (m)	Total number of days for construction and waiting period for consolidation
1	0.5	10
2	1.0	20
3	1.5	30
4	2.0	40
5	2.5	50
6	3.0	60
7	6.0	90
8	9.0	122

$$\Delta p = 2q\, I_{\sigma z}$$

q = Total pressure at the base of embankment.
$I_{\sigma z}$ = Influence factor after Osterberg.
C_c = Compression index.
e_0 = Initial void ratio.
And,

$$S_t = S_i + S_P + S_s \tag{2}$$

Table 6 Embankment geometry and its geotechnical parameters

S. No.	Parameter	Design value
1	Embankment height (m)	6.00
2	Embankment side slope (V:H)	1:2
3	Embankment width at top (m)	106.00
4	Embankment length at top (m)	106.00
5	Embankment width at base (B) (m)	130.00
6	Embankment length at base (L) (m)	130.00
7	Horizontal projection of embankment side slope along width (a) (m)	14.50
8	One half of the embankment width at top (b) (m)	53.00
9	Unit weight of embankment material (γ) (t/m^3)	1.90
10	Total pressure at the base of embankment (q) (t/m^2)	20.2061
11	Location of settlement estimation in embankment	Center

The results of various parameters and primary consolidation settlement of each layer are given in Table 7. Embankment geometry and its geotechnical properties are shown in Table 6. Total primary settlements are observed as 2305 mm. After applying depth factor (I_F), rigidity factor, and pore water correction factor, the estimated total consolidation settlement was observed as 1660 mm. By adopting this settlement value, the time required to reach the desired degree of consolidation was determined considering with and without PVD. The best fitted design was opted for this project thereafter.

3.4 Estimation of Time Required—without Using Prefabricated Vertical Drain

When huge surcharges are imposed on a natural soil bed, the soil consolidates, i.e., three-dimensional consolidations occur but in a slow manner while no PVDs are used. The time required for three-dimensional consolidation settlement onto this soil is calculated as,

$$t = \frac{T_V \times d^2}{c_v} \tag{3}$$

Laboratory test results revealed that the coefficient of vertical consolidation (c_v) of the soil of layer II was 2.45×10^{-4} cm^2/s (0.772632 m^2/yr) and this value was adopted in the calculation of settlement time required. The expected degree of consolidation (U) was 99% and therefore the corresponding time factor (T_V) was obtained as 1.781 from the design curve. The length of the PVD to be embedded was 15 m long. And, the length of the drainage path was also taken as 15 m. Hence, using

Table 7 Results of various parameters and primary consolidation settlement

Layer No	Thickness of layer (m)	Center of layer from base of the embankment (z), (m)	$\alpha = \tan^{-1}[(a+b)/z] - \tan^{-1}(b/z)$	$\beta = \tan^{-1}(b/z)$	$I_{\sigma z} = (1/\pi) \times [\alpha(1 + b/a) + \beta]$	Overburden pressure, (t/m²)	Total pressure at the base of embankment (q), (t/m²)	Primary consolidation settlement (S_P), (m)
I	0.80	0.40	0.002	1.563	0.500	0.240	20.206	0.192
II	10.70	6.15	0.025	1.455	0.500	0.855	20.206	1.907
III	1.70	12.35	0.048	1.342	0.498	1.935	20.206	0.206
Total primary consolidation settlement								2.305

Eq. (3) the consolidation time period to reach the required degree of consolidation was observed to be 518.649 years (189,306.97 days). This duration are minimized by multiple times by using PVDs that will reduce construction cost as well.

3.5 Estimation of Time Required—Using Prefabricated Vertical Drain

In order to accelerate the time of consolidation settlement, prefabricated vertical drains are used. Triangular pattern was selected over square pattern for PVD installation. From design calculation, spacing (s) and coefficient of horizontal consolidation (c_h) were opted as 0.7 m and $2c_v$, respectively. And, the time required was calculated using Hansbo's equation, as follows:

$$t = \frac{D^2}{8 \times c_h} \times \left[\frac{1}{1 - \left(\frac{d}{D}\right)^2} \times \ln\left(\frac{D}{d}\right) - \frac{3}{4} + \frac{1}{4}\left(\frac{d}{D}\right)^2 \right] \times \ln\left(\frac{1}{1 - U}\right) \quad (4)$$

where

$$D = 2\sqrt{\left(\frac{A}{\pi}\right)}$$ Effective diameter of area covered by each drain = 0.73511 m;

where A = Area treated by single PVD

$$= 0.866 \times s^2$$

where

$$= 0.866 \times (0.7)^2$$

$$= 0.42434 \, m^2$$

$$d = 2\left(\frac{b + t}{\pi}\right) = $$ Effective diameter of each drain = 0.0662;

where $b = 100$ mm, $t = 4$ mm

$$U = \text{Degree of consolidation settlement} = 99\%.$$

It has been observed that the time required for consolidation with prefabricated vertical drains is expected to be shorter as compared to the time required for the preloading alone without PVD. After putting values of all the parameters, the time required for settlement was obtained from Eq. (4) as 122 days that is only about

4 months of total consolidation period obtained without using PVDs and thus ultimately the construction cost will also be lessened that any civil engineer aims at.

4 Conclusion

All the results of the parameters required for PVD design are evaluated in the laboratory prior to commencement of the construction in the field. Installation of prefabricated vertical drains at site Ch-03 + 900 to Ch-04 + 400 km is under progress that will be followed by the installation at Ch-04 + 400 to Ch-04 + 700 km and Ch-04 + 700 to Ch-05 + 100 km. Without using PVD, the settlement of the soil strata at Ch-03 + 900 to Ch-04 + 400 km is observed to be 2305 mm and the corresponding settlement time is 189306 days. The PVD design revealed that the consolidation settlement of the existing soil strata is about 1660 mm when PVDs are used. The corresponding time required to obtain this settlement is 122 days. Thus, prefabricated vertical drains may be used to expedite consolidation settlement of the layered soft soils discussed in this paper.

References

1. Arulrajah, A., Bo, M.W., Leong, M., Disfani, M.M.: Piezometer measurements of prefabricated vertical drain improvement of soft soils under land reclamation fill. Eng. Geol. **162**, 33–42 (2013)
2. Cascone, E., Biondi, G.: A case study on soil settlements induced by preloading and vertical drains. Geotext. Geomembr. **38**, 51–67 (2013)
3. Indraratna, B., Rujikiatkamjorn, C., Ewers, B., Adams, M.: Class A prediction of the behavior of soft estuarine soil foundation stabilized by short vertical drains beneath a rail track. J. Geotech. Geoenviron. Eng. (2010). https://doi.org/10.1061/(ASCE)GT.1943-5606.0000270,686-696
4. Karim, M.R., Lo, S.C.: Estimation of the hydraulic conductivity of soils improved with vertical drains. Comput. Geotech. **63**, 299–305 (2015)
5. Karunaratne, G.P.: Prefabricated and electrical vertical drains for consolidation of soft clay. Geotext. Geomembr. **29**(4), 391–401 (2011)
6. Vu, V.: Optimal layout of prefabricated vertical drains. Int. J. Geomech. https://doi.org/10.1061/(ASCE)GM.1943-5622.0000434, 06014020 (2014)
7. Watabe, Y., Shinsha, H., Yoneya, H., Ko, C.: Description of partial sandy layers of dredged clay deposit using penetration resistance in installation of prefabricated vertical drains. Soils Found. **54**(5), 1006–1017 (2014)

8. Barron, R.A.: Consolidation of fine-grained soils by drain wells. Trans. ASCE **113**(2346), 718–754 (1948)
9. Abuel-Naga, H.M., Pender, M.J., Bergado, D.T.: Design curves of prefabricated vertical drains including smear and transition zones effects. Geotext. Geomembr. **32**, 1–9 (2012)
10. Bo, M.W.: Discharge capacity of prefabricated vertical drain and their field measurements. Geotext. Geomembr. **22**(1), 37–48 (2004)
11. Chai, J., Miura, N.: Investigation of factors affecting vertical drain behavior. J. Geotech. Eng. (1999). https://doi.org/10.1061/(ASCE)1090-0241(1999)125:3(216),216-226
12. Sathananthan, I., Indraratna, B., Rujikiatkamjorn, C.: Evaluation of smear zone extent surrounding mandrel driven vertical drains using the cavity expansion theory. Int. J. Geomech. **6**(355), 355–365 (2008). https://doi.org/10.1061/(ASCE)1532-3641(2008)8

A Geotechnical Study on Breached Summer Storage Tank

Nandyala Darga Kumar and C. Lavanya

Abstract This paper presents some of the observations made as well as geotechnical testing carried out in search of reasons of breached out summer storage tank, which was about to be commissioned for supply of water especially during summer season to the villagers of Nuzendla mandal in Andhra Pradesh. The tank has about 10 acres of storage area and the levels of water in the tank are not the same throughout the area but varying from 3 to 5.5 m. The breaching of tank was occurred, at a location where the water level is 5.5 m high, and where two mutually perpendicular bunds are joining. The disturbed and undisturbed soil samples collected from the location where breaching of tank took place were tested in the laboratory to understand the basic characteristics of the soil used for bund construction. The grain size analysis, compaction control, free swell index, liquid and plastic limits, permeability and shear characteristics are determined. It is noticed that the locally available soil is used for bund construction and it is of medium to high plastic in nature. The compaction levels at certain places are found to be inappropriate and the slopes of bund throughout are not as per the specifications. The filling up of water into the tank was done at a time, but not in stage by stage filling process. The reasons of breaching of earth bund are noticed as erosion of soil due to windblown water wave action, not providing the revetment on upstream slope and required slope as per the specifications.

Keywords Summer storage tank · Compaction control · Grain size · Liquid limit · Bund slope · Wave erosion

N. D. Kumar (✉)
JNTUH College of Engineering Manthani, Manthani, Telangana, India
e-mail: ndkjntu@gmail.com

C. Lavanya
GokarajuRangaraju Institute of Engineering and Technology, Hyderabad, Telangana, India
e-mail: lavanya.cc@gmail.com

1 Introduction

Water storage tanks are increasingly built commonly for irrigation and drinking water purposes especially in the dry areas. Several types of tanks such as clay bund, coffer dam, PVC lining, sand-bentonite lining, bitumen lining, lining of concrete or bricks, sand-cement sausages lining is in practice. The choice of a type of earth bund depends largely on the availability of the materials and the costs involved. Water storage tanks made of earth bunds are economical and require a people of minimum skills to construct it. Earth materials are usually three types: 1. granular: silts, sand, gravels, and boulders which are not cemented together; 2. cohesive: clays, or materials which have sufficient clay minerals in them for them to act as clays; and 3. lithified: rock. Generally, cohesive soils are preferred for earth bund construction. Several types of designs for tank bund sections are available. Since free-board varies from one tank to the other depending upon wave height, each tank proposal is required to be designed separately. As the variation in wave height for minor irrigation tanks is within a very small range, it is proposed to have the same free-board for all minor irrigation tanks considering the most severe condition. Increase in cost, if any by adopting such a method, would be marginal and thus it is negligible. Any marginal increase in free-board (by 0.1 or 0.2 m.) will have additional factor of safety during cyclones and in the event of any breach of tank on the upstream side. Thickness of revetment as 0.30 m may be considered. However, actual thickness of revetment can vary from 0.25 to 0.30 m depending upon the size of stone available. For bunds more than 16 m height, the sections are to be finalized based on soil test results. The stability of bund sections must be checked up with slip circle method [1].

In general the earth dams/levees fail by means of hydraulic failure, excessive seepage, and structural failure. About 40% of earth dam failures have been attributed to hydraulic failure and these may be due to overtopping, wave erosion, toe erosion, and gullying. The earth dam may also fail due to excessive seepage. Uncontrolled seepage can erode fine soil material from the downstream slope or foundation and continue moving toward the upstream slope to form a pipe or cavity often leading to a complete failure of the embankment. About 25% of the dam failures have been attributed to structural failures. Structural failure of an earthen embankment may take in the form of a slide or displacement of material in either the downstream or upstream face. Majority of times the earth dams fail due to hydraulic failures such as wave erosion, toe erosion, and gullying. Notching of upstream face by wave action reduces the embankment cross-sectional thickness and weakens embankment material. Hydraulic toe erosion occurs when flow is in the direction of a bank at the bend of the river and the highest velocity is at the outer edge and in the center depth of the water. Gullies are formed due to rainfall erosion of embankment slopes and also caused by traffic from people and vehicles [7–9].

In the recent past, there were many preventive and remedial measures came up into the real practice, which includes modifying the geometry of the slope, controlling the groundwater, constructing tie backs, spreading rock nets, providing proper drainage system and provision of retaining walls, etc. The destructive effects of

soil liquefaction, sudden drawdown, and groundwater flow would cause sometimes sudden or excessive settlements, causing breaching of earth bund. Proper design of foundation system requires the following: (i) purpose of engineering structures, probable service life loadings, types of framing, soil profile, construction methods, construction costs, and client/owner's needs, (ii) design without affecting environment and enough margin of safety with respect to unforeseen events and uncertainty in determination of engineering properties of soil and acceptable tolerable risk level to all the parties, i.e., public at large, the owner, and the engineer [2].

The geotechnical or structural failure is an unacceptable difference between expected and observed performance. The failure of a structure may be due to poor design, faulty construction, excessive loads, and soil-related failure. There are several factors contributing to the failure of foundation, if overlooked or addressed improperly, such as construction error, improper soil investigation, fluctuation of ground water table, and seismic loads [3]. Commonly we find two types of construction errors such as temporary protection measures and actual foundation work [4]. The response of clay to the construction of structures on it is not truly undrained. A significant consolidation develops initially in the over-consolidated natural clay, which becomes normally consolidated during construction. An undrained behavior develops only in the normally consolidated clay during the initial stages of the construction. The soil type is important in offering resistance against failure of earth mass and earth slope geometry to avoid slope failure [5, 6].

2 Description of Summer Storage Tank

The summer storage tank was built in an area of 10.8 acres in Nuzendla Mandal, Narasaraopet division, Guntur district, Andhra Pradesh state, India. Its storage capacity is 37580 m^3. The highest storage level is 5.65 m and this maximum storage level is spotted in the northeast corner of the tank. The plan area of tank is almost rectangular and its line diagram with salient points is shown in Fig. 1. Also, the photographs of breached portion are presented in Fig. 2. The bed is sloping toward northeast corner. The storage level in the southwest corner is 3 m. As the nature of soil in the original bed is pervious and to control the percolation losses, the bed is covered with 0.5 m thick clay layer which is of highly compressible in nature and its liquid limit and free swell index are 68% and 110%, respectively. The tank is made up of earth bunds in all the four sides with a slope of 2.5(H):1(V) in both the upstream and downstream sides. The soil used for earth bund construction is almost homogeneous and is intermediate to highly compressible clay. The breaching of earth bund took place in the northeast corner of the tank, where the highest water storage level is 5.65 m. The breaching of bund is occurred during filling up of water in the tank.

The summer storage tank consists of homogeneous earth bund made up of CI and CH soils. A 0.6 m deep concrete wall is built all around the tank from the bed level to downward in the upstream side, to avoid seepage beneath the bund section. Rock

Fig. 1 Line diagram of
summer storage tank
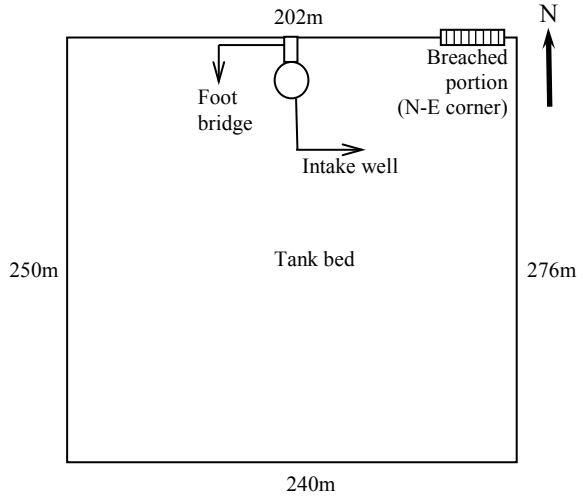
Fig. 2 Photographs showing breached sections of summer storage (SS) tank

toe is provided in the downstream side; from northeast corner of the tank, up to about
¼ of the distance either side in the north and east directions of the tank. The width
of the breached portion is about 6–7 m and it took place in the northeast corner. No
revetment and gravel cover is provided in the upstream side of the bund in all the
four sides.

3   Tests Conducted and Discussion of Results

The soil samples were collected from different locations in the vicinity of breached
portion of the tank. The location of soil samples collected is presented in Table 1.

Table 1 Location of soil samples collected for investigation

No	Sample location
1	71.00 m from intake well foot bridge at RL.101.625 toward breached location
2	71.00 m from intake well foot bridge at RL.101.255 toward breached location
3	71.00 m from intake well foot bridge at RL.101.165 toward breached location
4	60.00 m from intake well foot bridge at RL. 99.760 toward breached location
5	60.00 m from intake well foot bridge at RL.100.695 toward breached location
6	60.00 m from intake well foot bridge at RL.101.770 toward breached location
7	51.00 m from intake well foot bridge at RL.102.225 toward breached location
8	74.00 m from intake well foot bridge at RL.102.300 toward breached location
9	74.00 m from intake well foot bridge at RL.102.585 toward breached location
10	Bed portion of SS tank

The location of soil samples is measured with reference to the foot bridge of intake well in the tank area. The undisturbed soil samples are collected in the form of cores from sample locations 6, 7, 8, and 9 to ascertain their field dry density and field moisture contents. Also, the direct shear test is conducted on the undisturbed soil samples. The disturbed soil samples collected from the locations 1, 2, 3, 4, 5, 6, 7, 8, 9, and 10 are utilized for determining the index properties of soils such as liquid limit, plastic limit, free swell index, grain size distribution, and compaction characteristics. The respective test results are presented and discussed in the following subsections. The tests were conducted as per the Bureau of Indian Standard (BIS) test procedures [10–15].

3.1 Atterberg Limits and Free Swell Index

The liquid limit, plastic limit, and free swell index tests are conducted on all the ten samples which were collected from the site. The standard test procedure is followed while testing the soil samples in the laboratory [10, 11]. From the results presented in Table 2, it is observed that the liquid limit of soil samples 1–9 is varying from minimum 46% to maximum 66%. The bed clay, i.e., soil sample 10 has a liquid limit of 68%. The free swell index is varying from 65 to 85% and for bed clay, it is 110%. The compressibility of soils is varying from intermediate to highly compressible nature.

Table 2 LL, PL, PI, and FSI for soil samples 1–10

Sample No	Liquid limit (LL) in %	Plastic limit (PL) in %	Plasticity index (PI)	Free swell index (FSI) in %	
S1	62	28	34	76	
S2	66	29	37	80	
S3	48.5	19	29.5	70	
S4	64	27	37	75	
S5	48	18	30	70	
S6	47	19	28	65	
S7	46	18	28	65	
S8	61	26	35	70	
S9	56	22	34	75	
S10	68	28	40	110	

3.2 Sieve Analysis

The soil samples were tested for grain size distribution by conducting the wet sieve analysis as per the standard test procedure of testing of soils in the laboratory [12]. The results obtained are presented in Table. 3. Also, grain size distribution curves for the samples 1–5 and 6–10 are presented in Figs. 3 and 4, respectively.

From the results (Table 3), it is noticed that all the soil samples have percentage silt and clay fraction more than 50%. Fine sand fraction is varying from 8 to 22.5%, and remaining soil fractions such as gravel, coarse sand, and medium sand are negligible. With the help of test results presented in Tables 2 and 3, the soil samples are classified. The percentage of soil fraction available in each soil sample is further presented in Fig. 5 in the form of bar chart. From the classification of soil samples presented in

Table 3 Soil fractions in percent present in samples 1–10

Sample No	% Soil fraction				
	Gravel	Coarse sand	Medium sand	Fine sand	Silt and clay
S1	1	1	3	8	87
S2	0	1	3	8	88
S3	3.5	1.5	7.5	22.5	65
S4	1	1	3	8.5	86.5
S5	7	3	7	18.5	64.5
S6	2.5	1.5	8	15	73
S7	2	2	6	14	76
S8	3	2	5	11	79
S9	1.5	2	4.5	15	77
S10	1	1	2.5	5.5	90

Fig. 3 Grain size distribution curves for soil samples 1–5
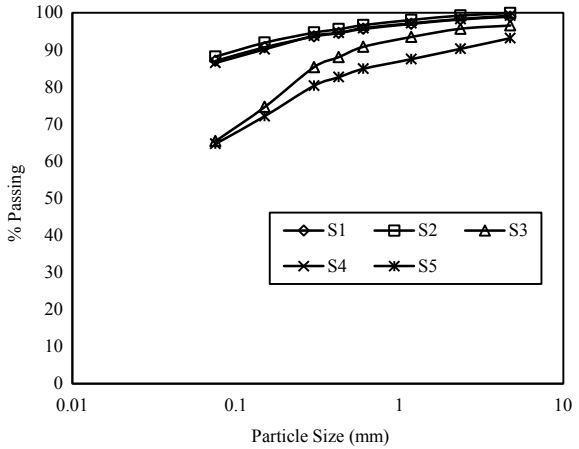
Fig. 4 Grain size distribution curves for soil samples 6–10
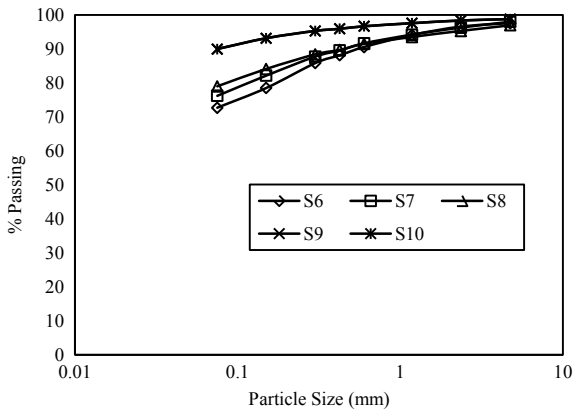
Table 4, it is noticed that some of the soil samples are in the intermediate compressible clay (CI) category and some of them are in the category of highly compressible clay (CH) soil.

Samples 1, 2, 4, and 10 have fine fraction (which is passing through 75 micron sieve) more than 85%. Soil samples 6, 7, 8, and 9 have the % fine fraction above 70 and below 80. Soil samples 3 and 5 have the fine fraction about 65%. Overall all the samples 1 to 10 have the fine fraction above 50%. The sample 10 is the bed sample and it has fine fraction 90%.
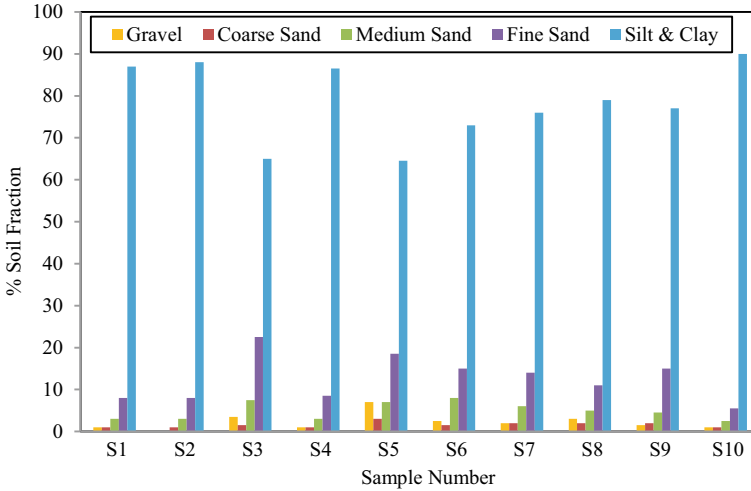
Fig. 5 Soil fraction in percent present in soil samples 1–10

Table 4 Classification of soil samples 1–10

Sample No	Soil classification	
1	CH	Highly compressible clay
2	CH	Highly compressible clay
3	CI	Intermediate compressible clay
4	CH	Highly compressible clay
5	CI	Intermediate compressible clay
6	CI	Intermediate compressible clay
7	CI	Intermediate compressible clay
8	CH	Highly compressible clay
9	CH	Highly compressible clay
10	CH	Highly compressible clay

3.3 Compaction Test

The standard Proctor's compaction test was conducted on all the samples in the laboratory as per the standard test procedure of testing of soils [13]. The compaction curves showing water content-dry density relationship are presented in Figs. 6 and 7. The optimum moisture content (OMC) and the maximum dry density (MDD) results obtained from the compaction curves are presented in Table 5. From the OMC, MDD results, it is noticed that the soil samples possess typical clayey soil behavior. The MDD of earth bund soil samples (1–9) is varying from 16.3 to 17.25 kN/m^3 and OMC is varying from 17 to 22.5%. The tank bed sample has OMC 25% and MDD 15.10 kN/m^3. The bed clay is highly compressible and impervious in nature.

Fig. 6 Compaction curves for soil samples 1–5
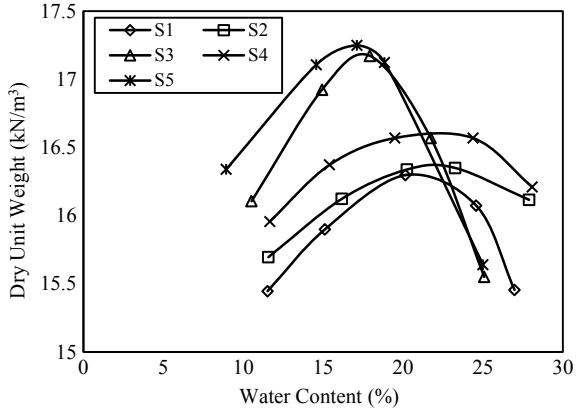
Fig. 7 Compaction curves for soil samples 6–10
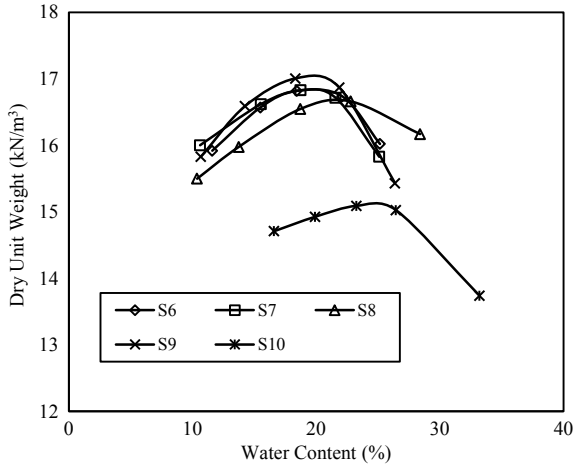
Table 5 OMC and MDD of soil samples 1–10

Sample no	Compaction characteristics	
	Optimum moisture content, OMC in %	Maximum dry density, MDD in kN/m^3
S1	21.00	16.30
S2	22	16.37
S3	17.5	17.2
S4	22.50	16.60
S5	17.00	17.25
S6	20.5	16.85
S7	20.00	16.86
S8	21.50	16.70
S9	20.00	17.05
S10	25.00	15.10

Table 6 Field dry density and field moisture content of core samples

Sample No	S6	S7	S8	S9
Field moisture content (FMC) in %	18.37	16.81	14.34	20.66
Field dry density (FDD) in kN/m^3	16.21	16.80	16.01	16.87
Maximum dry density (MDD) in kN/m^3	16.85	16.86	16.70	17.05
Relative compaction (%)	96.20	99.64	95.86	98.94

For soil samples 6, 7, 8, and 9, the degree of compaction is estimated and the result is presented in Table 6. For the above four samples, the degree of compaction is above 95%.

3.4 Direct Shear Test

A simple direct shear test (quick test) was conducted on the undisturbed soils collected from the locations 6, 7, 8, and 9 of an earth bund near the breached portion. The test was conducted as per the standard test procedure [14]. The strength envelopes obtained from the tests are presented in Fig. 8. The shear parameters such as cohesion and angle of shearing resistance obtained from the tests are presented in Table 6. The cohesive strength is varying from 30 to 50 kPa and the angle of shearing resistance is varying from 7.75° to 19.87° (Table 7).

Fig. 8 Shear stress versus normal stress curves for samples 6–9

Table 7 Direct shear test results of core samples

Sample No	S6	S7	S8	S9
Undrained cohesion, c in kPa	35	36	30	50
Angle of shearing resistance, ϕ (°)	15.22	17	19.83	7.75

3.5 Permeability Test

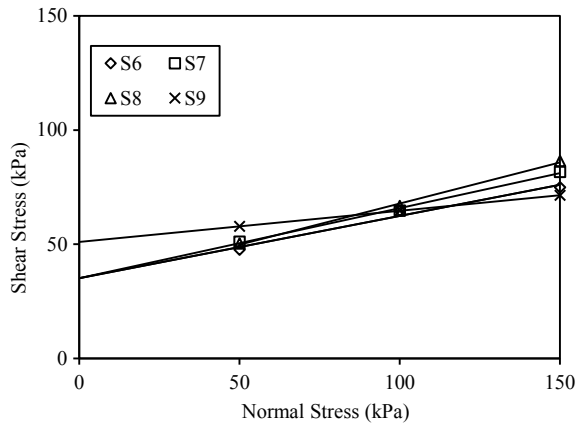The sample collected from the locations 6, 7, 8, and 9 is prepared at their respective OMC and kept for saturation in the permeameter mold as per the standard test procedure of testing of soils for permeability [15]. As the percent fine fraction present in soil samples is more, a falling head permeability test was conducted. The coefficient of permeability of four soil samples 6, 7, 8, and 9 is in the order of 10^{-6} to 10^{-8} cm/s and on an average 10^{-7} cm/s. From the permeability results, it is observed that the soil samples used for earth bund are impervious to highly impervious in nature.

4 Reasons of Breaching of Bund and Recommendations

From the field observations and laboratory test results of soil samples of breached portion, the following points are identified as reasons for earth bund breaching.

- The sloping of bed toward breached portion caused more concentration of water pressure as compared to the other portions of bund.
- Instead filling the tank with water in stages, the tank was filled up at a time to the full storage level.
- As per the specifications the revetment of thickness 0.25–0.3 m is required to be provided on the upstream slope, but it was not provided.
- The windblown water wave action was prevailed predominantly in the tank area.
- The compaction of soil was inappropriate.

5 Conclusions

From the field observations and test results, the following measures for closing the breached portion are suggested.

- No gullies and slope failures in the bund are noticed around the tank. The failure is due to hydraulic action on the upstream slope of bund where water concentration is high.
- The breached portion of the earth bund can be closed by selecting a suitable soil such as GC, GW, SC, SM and required to compact in layers as per the specifications and ensured the required degree of compaction.

- If it is expensive to get the suitable soil to close the breached portion of the earth bund, the same clay soil (CI or CH) which was used previously for earth bund formation can be used toward closing of the breached portion provided; the upstream and downstream slopes, respectively, are required to be changed from 2.5:1 and 2.5:1 to 3.5:1 and 2.5:1.
- A gravel cover and revetment layer each of minimum 300 mm thick as per the specifications is required to be provided so as to avoid the direct attack of wind generated water waves and to keep the upstream slope safe.
- It is required to ensure such that no gaps and uncompacted soil is left while closing the breached portion of the bund and it is also required to ensure the appropriateness of connectivity of bund formations.
- It is important to ensure that the filling up of water in the tank should be done in stages not at a time to the full capacity.

References

1. Government of Andhra Pradesh: Andhra Pradesh Community Based Tank Management Project Operational Manual: Vol. V(b) of VI, Technical Manual, Irrigation & CAD Department (2007)
2. Bowles, J.E.: Foundation Analysis and Design. McGraw-Hill Publications (1996)
3. Leonards, G.A.: Investigation of failures. J. Geotech. Eng. ASCE **108**(GT-2), 187–246 (1982)
4. Campbell, P.: Learning From Construction Failures. Wiley, Applied Forensic Engineering (2001)
5. Popescu, M.E.: A suggested method for reporting landslide remedial measures. IAEG Bull **60**(1), 69–74 (2001)
6. Glade, T., Anderson, M.G., Crozier, M.J.: Landslide Hazard and Risk. Wiley (2006)
7. BIS: 14954, Distress and Remedial Measures in Earth and Rock fill Dams-Guidelines, Bureau of Indian Standards, New Delhi (2001)
8. Garg, S.K.: Irrigation Engineering and Hydraulic Structures. Khanna Publishers, New Delhi (2012)
9. Stephens, T.: Manual of Small Earth Dams. Food and Agriculture Organization of the United Nations, Rome (2010)
10. BIS: 2720-Part 5, Bureau of Indian Standard methods of test for soils, Part5: Laboratory determination of Atterberg limits of soil (1985)
11. BIS: 2720-Part 40, Bureau of Indian Standard methods of test for soils, Part 40: Laboratory determination of free swell index of soil (1977)
12. BIS: 2720-Part4, Bureau of Indian Standard methods of test for soils, Part 4: Laboratorydetermination of grain size through sieve analysis (1985)
13. BIS: 2720-Part 7, Bureau of Indian Standard methods of test for soil, Part 7: Laboratory determination of compaction characteristics of soil (1980)
14. BIS: 2720-Part 13, Bureau of Indian Standard methods of test for soil, Part 13: Laboratory determination of shear characteristics of soil through direct shear test (1986)
15. BIS: 2720-Part 17, Bureau of Indian Standard methods of test for soil, Part 17: Laboratory determination of permeability of soil (1986)

Shear Strength Behavior of an Unsaturated Clayey Soil

P. B. Pande (ⓘD)**, S. R. Khandeshwar** (ⓘD)**, and S. P. Bajad** (ⓘD)

Abstract Recently, the study of shear strength of unsaturated soil is gaining more interest in research and practice. In this study, the triaxial shear test and filter paper method were undertaken to study the shear strength behavior of unsaturated soil. The clayey soil from central India was tested to understand the unsaturated shear strength behavior. The shear strength behavior was analyzed by plotting relationship between shear strength (τ) versus matric suction ($u_a - u_w$). The failure envelope resulting from relationship between the shear strength and matric suction shows nonlinear behavior and provides the shear strength parameter with respect to suction ($\emptyset^b$). In this experimental program, the shear strength behavior of unsaturated soil is studied using the soil–water characteristic curve (SWCC), and the nonlinearity between shear strength and the matric suction is observed. The nonlinearity is mainly due to desaturation of soil which starts from air entry value and continued till residual suction value and is affirmed and supported by the experimental results obtained in this study.

Keywords Unsaturated soil · Shear strength · Suction · SWCC

1 Introduction

The shear strength of unsaturated soil appeals more research in the geotechnical engineering and practice from last few decades. The shear strength of unsaturated soil governs the main parameters of geotechnical engineering such as bearing capacity, earth pressure, and slope stability. In India, engineers are mostly come across with the unsaturated clayey soils. The shear strength of unsaturated clayey soil is strongly influenced by the physico-chemical interaction between water and clay minerals.

P. B. Pande (✉) · S. R. Khandeshwar
Department of Civil Engineering, Yeshwantrao Chavan College of Engineering, Nagpur, India
e-mail: prashantbpande21@gmail.com

S. P. Bajad
Regional Board of Technical Education, Pune, India

Therefore, it is necessary to study the shear strength behavior of unsaturated clayey soil [1].

The thought process to study shear strength behavior of unsaturated clayey soils started from last five decades. Numerous experimental programs were conducted by various researchers to understand the shear strength behavior of unsaturated soils from different countries. A series of consolidated drained tests were performed with modified triaxial cell using axis translation technique to study the shear strength behavior of unsaturated Dhanauri clay and Madrid gray clay [2]. The series of six undrained and unconfined compression tests were conducted on unsaturated compacted clayey soil comprising 52% sand, 18% silt, and 30% clay [3]. Guadalix Red silty clay was investigated by performing the test under a net normal stress of 120–600 kPa for suction lower than the air entry value and obtained elliptical failure envelope [4]. The effect of suction on shear strength was studied by testing the clayey soil from Ningxia Hui, China with advanced triaxial test apparatus [5]. The suction-controlled direct shear test was performed on unsaturated expansive clay and studied the stiffness of clay with suction [5]. The consolidated drained test with modified direct shear apparatus was performed for investigating the Regina clay and Glacial till (clayey till), respectively [6, 7]. Most of the investigators were studied the shear strength behavior on various types of unsaturated soils and observed the nonlinear behavior of strength envelope. But very few researchers have studied the shear strength behavior of unsaturated clayey soil in Indian context.

Therefore, the clayey soil from central India was investigated to study the shear strength behavior in this research work. The conventional triaxial shear test and filter paper method were performed for shear strength and suction measurement, respectively. The soil–water characteristic curve was also developed from the data obtained from experimental work. The shear strength was interpreted for range of 60 and 275 kPa matric suction.

Unsaturated soil property functions can be used positively with reasonable accuracy by performing an indirect laboratory test such as a pressure plate test or filter paper method to develop the soil–water characteristic curve in research work. The filter paper is the only suction measuring method which measures the whole range of interest [8]. The failure envelope for an unsaturated soil was appeared to be nonlinear with respect to the matric suction axis.

2 Unsaturated Shear Strength

The concept of unsaturated shear strength was begin with the general theory of consolidation for an unsaturated soil [9]. Initially, the influence of suction on compacted cohesive soils was studied [10]. The Mohr–Coulomb strength relationship was proposed in the form of Eq. (1) to describe the shear strengths of unsaturated soils:

$$\tau_{\mathrm{f}} = C + \sigma \, \tan \emptyset \tag{1}$$

where

τ_f = shear strength,
C = cohesion,
σ = normal stress,
$\emptyset^b$ = angle of shearing resistance.

The two independent stress state variables such as the net normal stress $(\sigma - u_a)$ and the matric suction $(u_a - u_w)$ were recommended [11], instead of a single effective stress variable for interpreting stress–strain behavior of unsaturated soils. Later, the unsaturated shear strength equation comprising two independent stress state variables were proposed [12]. The net normal stress $(\sigma - u_a)$ and the matric suction $(u_a - u_w)$ are the two most commonly used stress state variables for expressing the unsaturated shear strength equation in the following form:

$$\tau_f = c' + (\sigma - u_a) \tan \emptyset' + (u_a - u_w) \tan \emptyset'^b \tag{2}$$

where

τ_f shear strength,
c' effective cohesion,
$\emptyset'$ effective angle of shearing resistance,
$\emptyset^b$ shearing resistance with respect to matric suction,
$(\sigma - u_a)$ net normal stresses,
$(u_a - u_w)$ matric suction.

$\emptyset^b$ indicates the rate of increase in shear strength with respect to matric suction. From experimental and theoretical studies, it is stated that $\emptyset^b$ is the nonlinearly decreasing function of matric suction. The modified Mohr–Columb's failure envelope is observed between the shear stress (τ) and matric suction $(u_a - u_w)$, and the $\emptyset^b$ can also be defined as an angle of internal friction with respect to $(u_a - u_w)$ variation under a constant $(\sigma - u_a)$.

Vanapalli [7] elaborated the detailed procedure for interpreting confined compression test results and derived the Eq. (3) for angle of friction with respect to suction. This equation was exclusively suggested for the confined undrained triaxial test.

$$\tan \emptyset^b = \frac{\{q_u (\cos \emptyset' + \sin \emptyset' \tan \emptyset')\}}{(u_a - u_w)} - \frac{\{(c_u + \sigma_3) \tan \emptyset' - c'\}}{(u_a - u_w)} \tag{3}$$

where

q_u failure deviator stress from the undrained triaxial test,
c_u undrained cohesion.

3   Material and Methodology

Triaxial shear test was selected to evaluate the shear strength clayey soil samples owing to its pervasiveness. The filter paper was used for measuring suction values in the range of 0–350 kPa. The suction values were obtained from the calibration curves developed in this study.

The highly plastic clayey soil available in central India was investigated in this research work. Primarily index properties were assessed to classify the soil. Results obtained from practical size distribution, liquid limit, plastic limit, and specific gravity are summarized in Table 1.

The soil was categorized as clay of high plasticity on the basis of results obtained from the various laboratory test conducted (Table 1). Furthermore, the standard proctor test was performed to obtain the maximum dry density (14.4 KN/m^3) and optimum moisture content (25%), respectively.

The soil specimens were compacted with different water contents and maintained the various optimum conditions, i.e., dry of optimum, optimum, and wet of optimum. The series of tests were performed on identical clayey soil samples. The same process was followed for the preparation of soil samples for performing triaxial shear test and filter paper method. The soil sieved through 2 mm sieve mixed with the required quantity of distilled water and it was placed for 24 h to establish the hydraulic equilibrium. After achieving, the equilibrium soil was compacted.

The compacted soil was then left for another one day (48 h) to achieve the equilibrium. The soil samples were extracted from the compacted soil for triaxial as well as filter paper test. The soil sample of size 38 mm diameter and 76 mm height was extracted for the triaxial test [13]. Similarly, the soil sample of size 50 mm diameter and 70 mm height was extracted for the filter paper method [14]. Figure 1 shows the molds used for extracting the samples for triaxial and filters paper method. After sampling, the samples were kept in a plastic bag which was labeled by the sample number and stored in the desiccator (see Fig. 2) for 24–48 h equilibration period until being tested. Density of each set was confirmed before commencing the triaxial and filter paper method.

Table 1 Index properties

Properties	Values
Gravel	0
Sand	9.47%
Silt	47.23%
Clay	43.30%
Liquid limit	68.60%
Plastic limit	29.10%
Plasticity index	35.50%
Specific gravity	2.61

Fig. 1 Moulds and samplers

Fig. 2 Soil samples in desiccator

3.1 Triaxial Test

The compacted soil samples obtained with different initial water contents and different dry densities were tested under undrained condition. Three soil samples from one set were tested with three different confining pressures, i.e., 50, 100, and 150 kPa. Confined compression triaxial shear tests were conducted on specimens with the same initial conditions. The specimens were sheared immediately after the application of the confining pressure at a constant strain rate. The confining pressures applied were in the range of 50–100 kPa. The tests were performed on soil samples at various optimum conditions, i.e., dry of optimum, optimum, and wet of optimum.

The effective shear strength parameters: Cohesion (c′) and angle of shearing resistance (∅′) were obtained from the consolidated drained test. The series of consolidated drained test was performed on the soil samples compacted at optimum moisture content and maximum dry density. Three samples were consolidated under pressure of 50, 100, and 150 kPa for twenty-four hours. Samples were tested under confining pressure of 50, 100, and 150 kPa. Consolidated samples were sheared at the rate of 0.0125 mm/min, which enabled drainage during the testing, as the sample was made of clayey soil [15].

3.2 Filter Paper Method

The combination of procedure suggested in [13, 16] was implemented to accomplish filter paper method. Suction was obtained from the calibration curve after attaining equilibrium between the soil and filter paper. The ash free and quantitative type II, i.e., Whatman No. 42 filter paper having a diameter 5.5 cm was used as per ASTM D5298 guidelines. The objective of the calibration of the filter paper for total suction was to place the filter paper above the salt solution in such a way that transfer of water to the filter paper takes place only by vapor absorption. The water content of filter paper at equilibrium stage and calibration equation gives the suction of soil. Both the non-contact and contact filter paper methods were used to quantify the total and matric suctions, respectively.

4 Results and Discussion

4.1 Soil–Water Characteristic Curve

The relationship between shear strength of unsaturated soil and soil–water characteristic curve is presented in Fig. 3. The soil–water characteristic curve is usually developed with the help of pressure plate method. However, it was developed using data obtained from filter paper method in this study. The use of the filter paper method is adequate to construct soil–water characteristic curve (see Fig. 3) for clayey soil of central India. The matric suction ($u_a - u_w$) is ranging from 60 to 300 kPa.

The results were studied by categorizing the compacted soil into three different initial conditions, wet of optimum, optimum, and dry of optimum. Suction was measured as soil de-saturate from the saturated to dry state as compacted soil. Suction increases slowly as water content decreases in wet of optimum condition. And in case of optimum condition, the suction values suddenly rise with decrease in water content. In dry of optimum condition, suction gradually decreases again due to inadequate capillary forces in pores. Also, when a soil sample is dry, with a suction value higher than 300 kPa, it was difficult to obtain good sample. Thus, it was not possible to
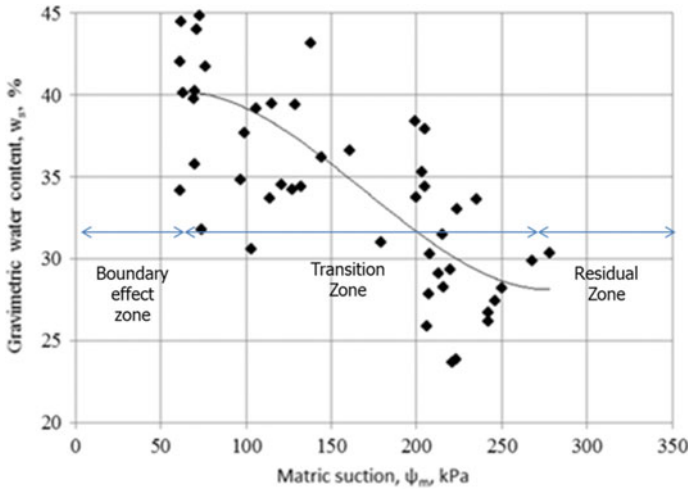
Fig. 3 SWCC (w_s versus ψ_m) for Central India clayey soil

establish proper contact between the soil and the filter paper. It causes inaccuracies in suction results and the same has been observed by other researchers [16, 17]. Thus, the use of filter paper method is restricted for developing the soil–water characteristic curve within the range of 0–300 kPa. The attempt of measuring the suction beyond 300 kPa was futile since it results scattered curves due to insufficient contact between soil and filter paper. However, all the data points were included within the range of 0–300 kPa.

4.2 Shear Strength

The shear strength test and suction results obtained from the triaxial test and filter paper method, respectively, were analyzed by plotting relationship between shear strength (τ) versus matric suction ($u_a - u_w$). The failure envelope obtained can be used to obtain the shear strength parameter with respect to suction $\emptyset^b$ that shows the nonlinear behavior.

The triaxial shear test results on unsaturated clayey soil and exhibits significant nonlinearity for the failure envelope with respect to the matric suction is illustrated in Fig. 4. The $\emptyset^b$ angle originates at a value equal to $\emptyset'$ (i.e., 15°) where the matric suction is equal to zero and decrease significantly at matric suctions in the range of 60–300 kPa. The scatter in the failure envelopes (Fig. 4) appeared due to deviations in the initial void ratios of the soil samples. However, it is difficult to quantify the change in void ratio of the soil at failure of specimen.

The strength behavior of soil was studied with soil–water characteristic curve of soil developed from the suction results. The linear increase in shear strength with
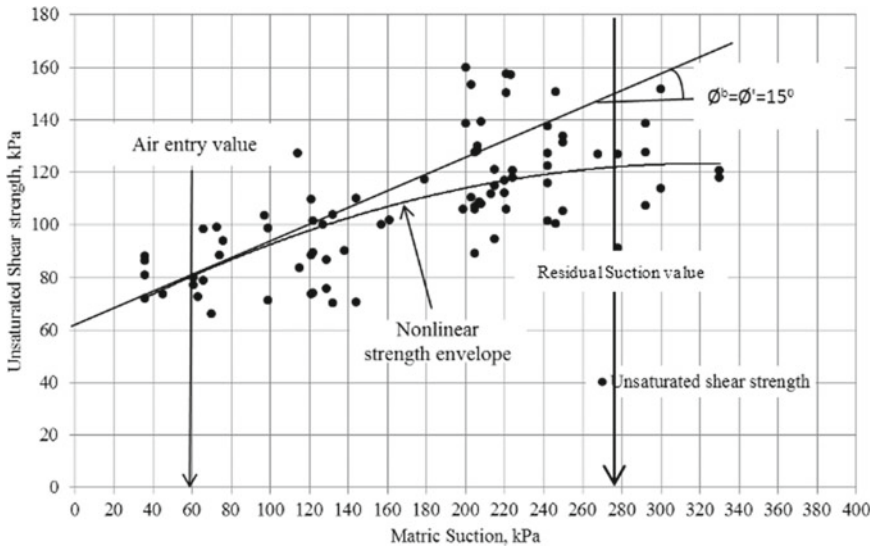
Fig. 4 Failure envelope from shear strength vs matric suction relation

respect to suction was observed up to the air entry value, i.e., 60 kPa. This value of suction corresponding to the air entry value gives the point at which air entered the largest pores of the soil. At this stage, the desaturation starts from and continues till the soil reaches the residual suction value, i.e., 275 kPa. In between air entry value and residual suction value, the rate of distortion was higher; and nonlinear increase in shear strength is observed. Beyond the residual suction value, the trend of curve is observed as horizontal which indicates the shear strength remains constant with increase in matric suction. During experimentation, it was observed that soil started losing its strength. The two parts of strength envelope, i.e., the linear and a curvilinear segment is usually detected. The linear segment was transformed to the curvilinear segment at about the air entry value of soil.

The boundary effect zone, almost voids are filled with water, i.e., soil is mostly saturated where suction is not observed. The nonlinear (curvilinear) variation in shear strength envelop was observed only in the transition zone (Fig. 4) due to desaturation process in this zone and the desaturation starts from air entry value (60 kPa). In desaturation stage, suction increases speedily and it is observed that small change in water content results in large change in suction. The nonlinear shear strength behavior is observed till residual suction value (275 kPa) up to which desaturation progresses. After this, the residual zone started in which soil tends to dry and the effect of suction is reduced. The unsaturated shear strength parameter $\emptyset^b$ is equal to the effective friction angle $\emptyset'$ up to air entry value; and $\emptyset^b$ decreases as the soil entered into the transition zone. The unsaturated shear strength at the stage of air entry value was observed as 80 and 120 kPa at the residual suction value.

5 Conclusion

The shear strength of unsaturated soil derived from the combination of filter paper and conventional triaxial test was demonstrated for the clayey soil from Central India. The identical unsaturated soil specimens were tested under different initial conditions, i.e., wet of optimum, optimum, and wet of optimum to validate the feasibility of this combined method.

The shear strength behavior of unsaturated soil is studied using the soil–water characteristic curve, and the nonlinearity between shear strength and the matric suction is observed in the failure envelope of the clayey soil within transition zone only. The nonlinearity is mainly due to desaturation of soil which starts from air entry value and continued till residual suction value and is affirmed and supported by the experimental results obtained in this study on compacted clayey soil. The air entry value and residual suction value are identified on the desorption curve; the residual zone is hardly noticeable. It can be stated that the failure envelope appearances the nonlinearity when wide range of matric suctions (e.g., 0–500 kPa) were quantified in the investigation, and more research is required to understand the properties of unsaturated soil.

References

1. Zhan, L., Ng, C.W.W.: Experimental study on mechanical behavior of recompacted unsaturated expansive clay. Chin. J. Geotech. Eng. **28**(2), 196–201 (2006)
2. Satija, B.S.: Shear behaviour of partly saturated soils. Ph.D. Thesis. Indian Institute of Technology, New Delhi (1978)
3. Chantawarangul, K.: Comparative study of different procedures to evaluate ef-fective stress strength parameters for partially saturated soils. M.Sc. Thesis. Asia Institute of Technology, Bangkok, Thailand (1983)
4. Escario, V., Juca, F.: Strength and deformation of partly saturated soils. In: Proceedings of the 12th International Conference on Soil Mechanics and Foundation Engineering, vol. 1, pp. 43–46, Rio, Balkema, Rotterdam (1989)
5. Yongfu, X., Yongzhan, C., Songyu, L.: Triaxial test on unsaturated expansive soils. Chin. J. Geotech. Eng. **20**(3), 14–18 (1998)
6. Gan, J.K.M., Fredlund, D.G.: Multistage direct shear testing of unsaturated soils. Geotech. Test. J. ASTM **11**(2), 132–138 (1988)
7. Vanapalli, S.K.: Simple test procedures and their interpretation in evaluating the shear strength of unsaturated soils. Ph.D. Thesis. Department of Civil Engineering, University of Saskatchewan, Saskatoon, SK (1996)
8. Houston, S.L., Houston, W.N., Wagner, A.M.: Laboratory filter paper suction measurements. Geotech. Test. J. **17**(2), 185–194 (1994)
9. Biot, M.A.: General theory of three-dimensional consolidation. J. Appl. Phys. **12**, 155–164 (1941)
10. Hilf, J.W.: An investigation of pore-water pressure in compacted cohesive soils, Ph.D. Thesis, Technical Memorandum. No. 654, U.S. Department of the Interior, Bureau of Reclamation, Design and Construction Division, Denver, CO (1956)
11. Coleman, J.D.: Stress strain relations for partly saturated soils. Geotechnique **12**(4), 348–350 (1962)

12. Fredlund, D.G., Morgenstern, N.R., Widger, R.A.: The shear strength of unsaturated soils. Can. Geotech. J. **15**(3), 313–321 (1978)
13. ASTM D2850: Standard test method for unconsolidated, undrained compressive strength of cohesive soils in triaxial compression. In: Annual book of ASTM Standards, ASTM, West Conshohocken, PA, USA (1995)
14. ASTM D5298: Test method for measurement of soil potential (suction) using filter paper. ASTM International, West Conshohocken, PA, USA (2007)
15. ASTM D7181: Standard test method for consolidated drained triaxial compression test for soils. ASTM International, West Conshohocken, PA USA (2007)
16. Bulut, R.: A re-evaluation of the filter paper method of measuring soil suction. Civil Engineering, Ph.D. Thesis (1996)
17. Leong, E.C., He, L., Rahardjo, H.: Factors affecting the filter paper method for total and matric suction measurements. Geotech. Test. J. ASTM **2**(3), 322–333

Effect of Drying and Wetting SWCCs on Unsaturated Soil Slopes

Ammavajjala Sesha Sai Raghuram and **B. Munwar Basha**

Abstract The soil water characteristic curve (SWCC) exhibits hysteresis. It is the relation between soil water and soil suction. Desorption (drying) and sorption (wetting) can be used to obtain SWCC. The suction is different in drying and wetting SWCC paths. The slope failures generally take place in wetting SWCC. Therefore, a few efforts have been made in this direction to investigate the effect of drying and wetting SWCCs on slope stability. In this study, the change in factor of safety (FoS) considering drying and wetting SWCCs of unsaturated infinite slope is presented. It is noted that there is a substantial change in the FoS during drying and wetting cycles. A significant difference in the fitting parameters of SWCC for drying and wetting cycles can be observed. In addition, a notable change can be observed in the suction stress of the unsaturated soil slope obtained using both drying and wetting SWCCs. Additionally, the FoS values obtained from experimental data are compared with the correlations available for wetting SWCC in the literature. The correlations available in the literature are in good agreement with the experimental data. The present study highlights the importance of wetting SWCC on the stability analysis of unsaturated soil slopes.

Keywords Infinite slope · Unsaturated soils · Hysteresis · SWCC

1 Introduction

Seasonal variations change the depth of slip surface in soil slopes. Many of the slope failures take place in the unsaturated zone, where the slip surface lies above the water table. The suction that exists in unsaturated soil increases the stability of slopes in dry conditions and decreases the stability in wet conditions. Until recently,

A. S. S. Raghuram (✉) · B. M. Basha
Department of Civil Engineering, Indian Institute of Technology Hyderabad, Kandi, Sangareddy 502285, India
e-mail: raghuram.ammavajjala@gmail.com

B. M. Basha
e-mail: basha@ce.iith.ac.in

conventional soil mechanics have been used for most of the slope stability analysis in which soil suction is neglected. In conventional soil mechanics, pore water pressure is assumed to be either zero or positive along the failure surface. However, in real field conditions, pore water pressures within the slope could be highly variable and it could be negative due to which slope failures occur in the unsaturated zone [1]. Therefore, it is of great importance to consider the soil suction in the slope stability analysis. The infinite slope analysis is conducted that accounts for the unsaturated soil shear strength.

Soil water characteristic curve (SWCC) relates soil water to the soil suction, which is a key element to model the unsaturated soil properties like shear strength. There are two possible ways to obtain SWCC, namely desorption (drying) and sorption (wetting). It is well recognized that for a given constant suction, soil water contents are not unique. Therefore, soil exhibits different SWCCs during drying and wetting cycles and is termed as hysteresis. The soil water content in the drying SWCC is greater than the soil water content in wetting SWCC for a constant value of suction. Drying SWCC can be obtained by considering a completely saturated soil sample and thereby drying the soil sample by applying suction in increments while measuring the corresponding soil water content and suction. Wetting SWCC can be obtained by considering the completely dried soil sample and thereby wetting the soil sample by decreasing the suction. Though both of these methods yield continuous SWCC's which are not the same. The direction of the process (drying or wetting) and dependency of soil water content lead to hysteresis [2]. The following are the reasons for the hysteretic behavior of SWCC:

1.   Inkbottle effect.
2.   Contact angle effect.
3.   Entrapped air.
4.   Aging of soil.

Figure 1 shows the typical hysteresis of SWCC. Drying SWCC (initial drying curve) is the SWCC from complete saturation to residual state. Upon wetting, SWCC starts from residual state to saturated state on the drying path, which is referred to as wetting SWCC (main wetting curve).

2   Studies Related to Hysteresis of SWCC

Several studies are reported to evaluate the SWCC by using various techniques like filter paper method [3, 4], Tensiometers [5], pressure plate apparatus [6, 7], axis translational technique [8], and dew point potentiometer [9, 10]. The hysteretic SWCCs of sands and loams are found by using the pressure plate apparatus [11]. The author proposed a simple method to estimate the scanning curves of SWCC. Tempe pressure cell and hanging column techniques are used to find the hysteresis of sands [12]. Similar work was done using dew point potentiometer to find the hysteresis of clayey silts and clays [13]. Pressure plate apparatus and dew point potentiometers are used to
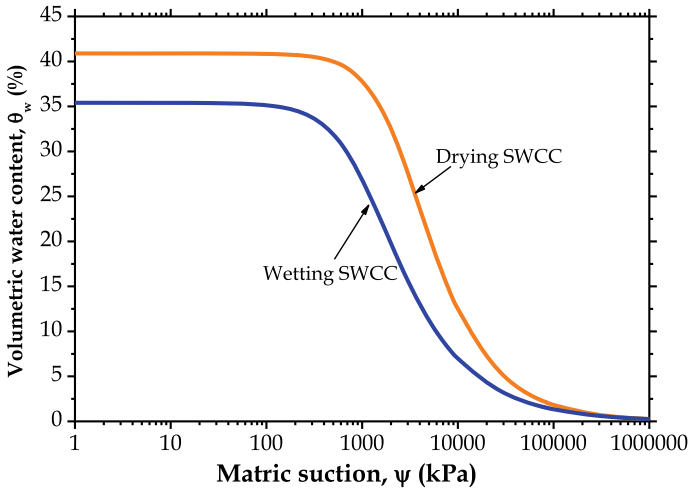
Fig. 1 Hysteresis of soil water characteristic curve

find the hysteresis of highly expansive clays [14]. The influence of relative density on the hysteretic SWCC of sand was presented using automated SWCC apparatus [15]. A simple method was proposed to predict the collapse behavior of soil in wetting [16]. The hysteretic SWCC behavior of bentonites was investigated and proposed a model to predict the boundary wetting SWCC [17]. Natural deposited soils and fine soils, when compacted at the dry of optimum, are subject to collapse upon wetting [18]. It was reported that most of the slope failures take place in wetting SWCC [19].

The previously published studies highlight the significance of hysteretic SWCC behavior of soils. However, no attempt has been made to evaluate the influence of hysteresis of SWCC on the infinite slopes. Therefore, a few efforts have been made to investigate the effect of hysteretic SWCC on slope stability.

3 Unsaturated Soil Slope Stability

Consider an infinite slope, which makes an angle 'ω' with the ground surface as shown in Fig. 2. Assume the depth of the slip surface is at $H = 1$ m in the present study below the ground surface. Let 'H_w' represents the depth of the water table (H_w is varied from 1.5 to 10 m in this study). The study proposed by [20] reported the factor of safety (FoS) for unsaturated soil slope by extending the Mohr–Coulomb failure criteria and is given as follows [21]:

$$\text{FoS} = \frac{c'}{\gamma H \sin \omega \, \cos \omega} + \frac{\tan \phi'}{\tan \omega} + \frac{\chi(\psi)}{\gamma H \, \sin \omega \, \cos \omega} \qquad (1)$$
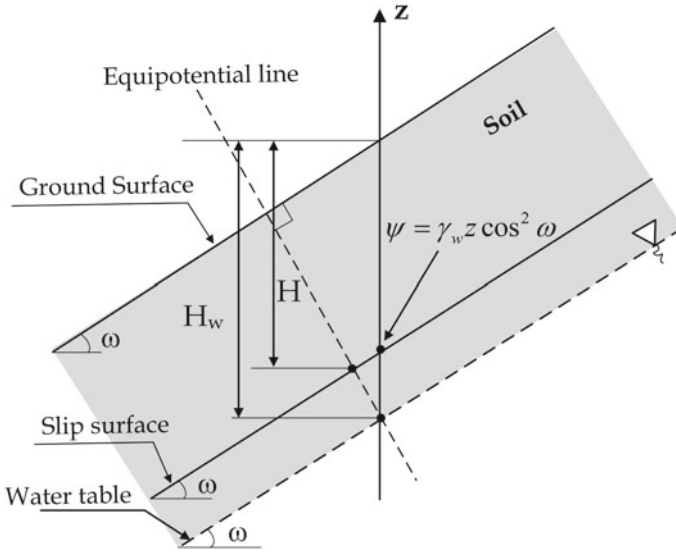
Fig. 2 Infinite slope considered in the study

where c' and ϕ' are the effective cohesion and effective internal friction angle, γ is the unit weight of soil, χ depends upon the degree of saturation, $\psi = (u_a - u_w)$ is the matric suction, u_w and u_a are the pore water and pore air pressures.

The parameter χ as shown in Eq. (1) varies with shear strength models for unsaturated soils. In the present study, nonlinear shear strength model proposed by Fredlund et al. [22] is assumed. Therefore, Eq. (1) becomes

$$F = \frac{c'}{\gamma H \sin \omega \cos \omega} + \frac{\tan \phi'}{\tan \omega} + \frac{\left(\frac{\theta_w}{\theta_s}\right)^{\kappa} \tan \phi' (u_a - u_w)}{\gamma H \sin \omega \cos \omega} \tag{2}$$

where κ is the fitting parameter which depends upon the type of soil, θ_w is the volumetric water content, and θ_s is the saturated water content. In atmospheric conditions, $u_a = 0$. Therefore, Eq. (2) becomes,

$$F = \frac{c'}{\gamma H \sin \omega \cos \omega} + \frac{\tan \phi'}{\tan \omega} + \frac{\left(\frac{\theta_w}{\theta_s}\right)^{\kappa} \tan \phi' (-u_w)}{\gamma H \sin \omega \cos \omega} \tag{3}$$

The matric suction along the slip surface is given by

$$\psi = -u_w = -\left[\gamma_w(-H_w)\cos^2 \omega\right] = \gamma_w H_w \cos^2 \omega \tag{4}$$

The study presented by Garven and Vanapalli [23] suggested an equation to find the fitting parameter κ which is based on plasticity index (I_p) of the soil and is given as

$$\kappa = -0.0016I_p^2 + 0.0975I_p + 1 \tag{5}$$

Equation (5) is used in this study to find the fitting parameter κ. In the literature, several equations are available to find the SWCC. In this study, van Genuchten (VG) model is considered [24]. The VG model represents the SWCC precisely. The dimensional-less water content (Θ) is given by

$$\Theta = \frac{\theta_w}{\theta_s} = \frac{1}{\left[1 + (\alpha\psi)^n\right]^m} \tag{6}$$

where α is the fitting parameter of SWCC and is related to the inverse of air entry value (AEV), n is the fitting parameter of SWCC and is related to the slope of SWCC, m is fitting parameter related to the symmetry of SWCC. The fitting parameter m as shown in Eq. (6) is directly related to the fitting parameter n as shown below.

$$m = \left(1 - \frac{1}{n}\right) \tag{7}$$

By imposing this relation in Eq. (6), it becomes

$$\theta_w = \frac{\theta_s}{\left[1 + (\alpha\psi)^n\right]^{\left(1 - \frac{1}{n}\right)}} \tag{8}$$

The FoS of the unsaturated infinite slope can be found by using Eqs. (3), (4), (5), and (8).

Three different soils are considered in the present study from the literature. Goh et al. [25] reported the shear strength of three different types of unsaturated soils considering the hysteresis of SWCC. The three soils have sand: kaolin ratios of 15: 85 (Inorganic silt), 35: 65 (Inorganic clay), and 55: 45 (clayey sand). The same soils are considered in the present study to evaluate the effect of hysteretic SWCC on slope stability. Table 1 summarizes the soil properties for three soils. The SWCC fitting parameters for the VG model are presented in Table 2.

4 Results and Discussions

Figure 1 shows the hysteretic SWCC of soil. The saturated water content in drying SWCC is greater than the wetting SWCC. This is due to the entrapped air in the soil.

Table 1 Basic and engineering properties of the soils considered

Property	Inorganic silt	Inorganic clay	Clayey sand
Specific gravity	2.66	2.67	2.66
Maximum dry density	15	16.7	18.6
Plasticity index	19.9	18.6	13.1
Grain size distribution			
Sand (%)	15.0	35.0	55.0
Silt (%)	73.6	44.5	39.0
Clay (%)	11.4	20.5	6.0
Unified soil classification system, USCS	MH	CL	SC
Effective cohesion, c' (kPa)	29.5	8.5	8.2
Effective friction angle, ϕ' (deg.)	26.8	26.9	33.2

Table 2 SWCC fitting parameters for three soils

Property	Inorganic silt	Inorganic clay	Clayey sand
Drying saturated water content, θ_{sd}	0.503	0.466	0.359
Wetting saturated water content, θ_{sw}	0.441	0.452	0.325
VG fitting parameters			
α_d (kPa^{-1})	0.016811	0.010746	0.016118
α_d (kPa^{-1})	0.054752	0.057118	0.085011
n_d	1.40	1.23	1.38
n_w	1.24	1.12	1.21

In general, the drying process initiates from the micro-pores of the soil at a higher suction range. On the other hand, the wetting process initiates from macro-pores in the soil at lower suction [17]. Figures 3, 4 and 5 represent the drying and wetting SWCC of inorganic silt, inorganic clay, and clayey sand for VG model. It can be noticed from Figs. 3, 4 and 5 that, there is a significant difference in between the drying and wetting SWCCs. Furthermore, the hysteresis is more in case of clayey sand followed by inorganic silt and inorganic clay.

In addition to the experimental data for wetting SWCC, correlations available in the literature are used to compare the suction stress and FoS values for different water table positions. Likos et al. [26] proposed correlations based on the type of soil (cohesive or cohesionless). Figures 6, 7 and 8 show the influence of water table position and hysteretic SWCC on the suction stress and FoS for both experimental data and correlations proposed by Likos et al. [26]. Figure 6 represents the change in suction stress and FoS with the depth of the water table for inorganic silt in drying and wetting cases. It can be observed from Fig. 6 that there is a noticeable change in the suction stress and FoS for drying and wetting SWCCs. As an illustration (compare drying and wetting experimental data fits), the suction stress and FoS values are
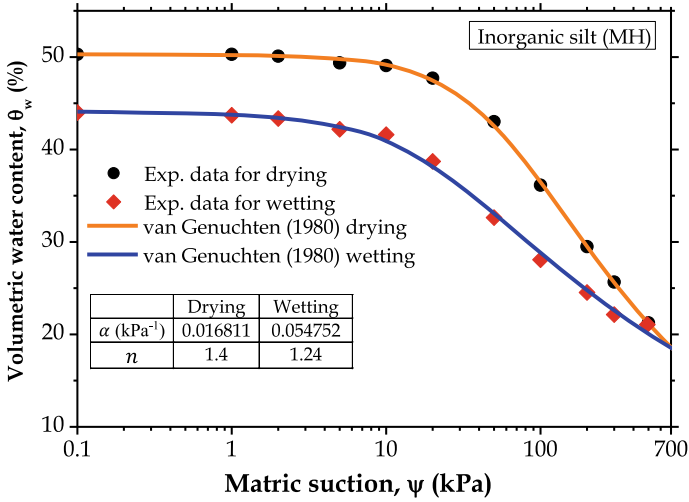
Fig. 3 Hysteresis of inorganic silt for the VG model
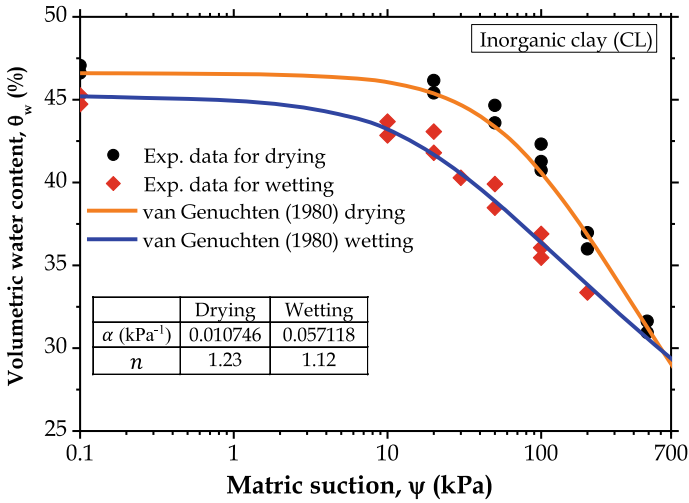
Fig. 4 Hysteresis of inorganic clay for the VG model

reduced from 0.9 to 0.79 kPa and 6.24 to 6.02 when the water table is at 10 m below the ground surface.

In addition, it can be observed that the hysteresis of SWCC does not show any impact when the water table is below 4 m from the ground level. This might be due to insufficient suction head. The suction stress and FoS values obtained from the experimental data lie within the ranges proposed by Likos et al. [26]. The difference
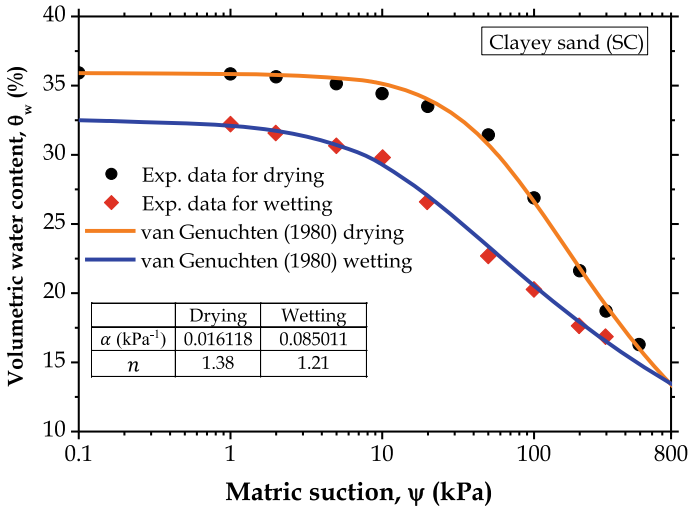
Fig. 5 Hysteresis of silty sand for the VG model

Fig. 6 Effect of water table position on suction stress and FoS for inorganic silt

Fig. 7 Effect of water table position on suction stress and FoS for inorganic clay

Fig. 8 Effect of water table position on suction stress and FoS for clayey sand

in suction stress and FoS values is very high for $\alpha_w = 2.67\alpha_d$ and $n_w = 1.05n_d$ correlations.

The effect of water table position on the suction stress and FoS of inorganic clay is presented in Fig. 7. Figure 7 shows that the suction stress and FoS values are reduced from 1.1 t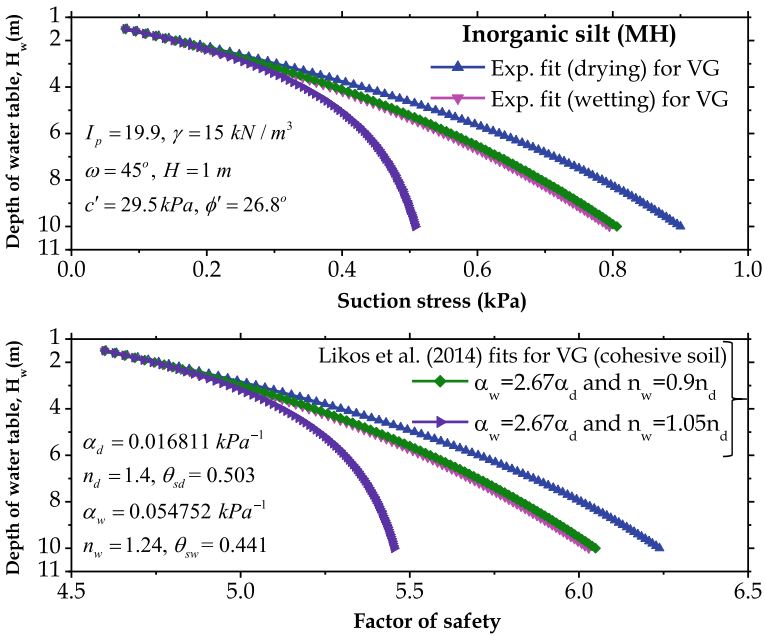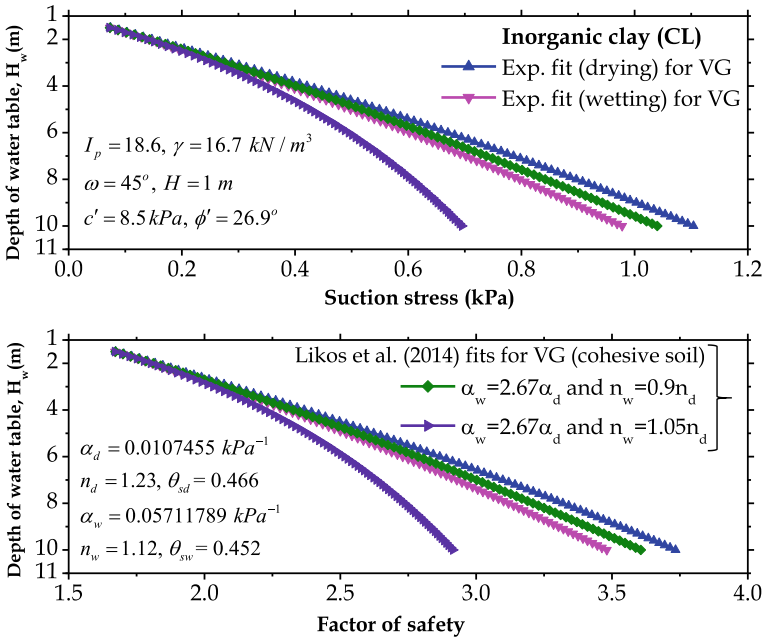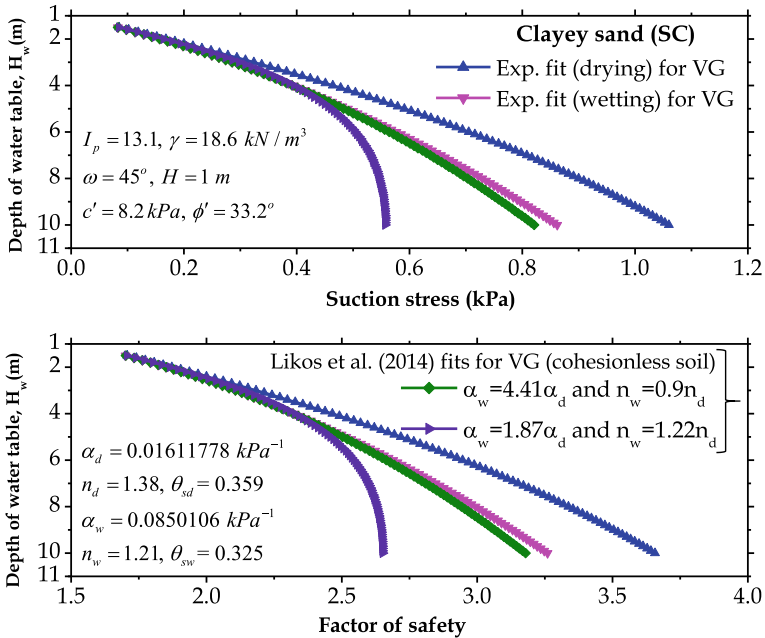o 0.97 kPa and 3.73 to 3.48 for a given water table position if 10 m below the ground level (compare drying and wetting experimental data fits). Though the suction stress reduction is negligible (0.13 kPa), the reduction in the FoS is significant. Figure 8 shows the variation of suction stress and FoS along with the depth of the water table for clayey sand. It can be observed from Fig. 8 that the effect of hysteretic SWCC and water table position on suction stress and FoS is very high. As an example, suction stress and FoS values are reduced from 1.06 to 0.86 and 3.66 to 3.26, respectively.

Figures 6, 7 and 8 depict the fact that, as the depth of the water table increases, the suction stress and FoS increases. This could be attributed to the increase in the suction head which increases the suction stress and FoS. A similar trend was noticed by Raghuram and Basha [27]. In addition, the FoS and suction stress are greater in drying SWCC when compared to wetting SWCC. This is due to the fitting parameters of SWCC. As mentioned in the earlier sections, the fitting parameter α is related to the inverse of AEV. As, the AEV increases, the slope stability increases [28]. Furthermore, the maximum decrease in the FoS due to hysteretic SWCC follows the order clayey sand > inorganic silt > inorganic clay. This is due to the fact that the increase in wet to dry ratio of AEV increases the hysteresis [29]. Therefore, as the hysteresis increases, the difference in suction stress and FoS between drying and wetting increases. In the present study, the hysteresis is more in clayey sand followed by inorganic silt and inorganic clay. The suction stress and FoS values for all the three soils overestimate FoS when the drying SWCCs are considered. However, wetting SWCCs results underestimate the FoS.

5 Conclusions

The effect of hysteretic SWCC on the slope stability is carried out by considering three different soils from the literature. The following are the major findings from the study:

1. The current study highlights the importance of hysteresis of SWCC on slope stability.
2. It can be observed that there is a significant difference in the suction stress and factor of safety due to drying and wetting SWCCs.
3. The difference in the suction stress and FoS between drying and wetting SWCC depends upon the wet to dry ratio of the AEV value, which intern depends upon the type of soil. In this study, it was observed that the maximum decrease in the FoS due to hysteretic SWCC follows the order clayey sand > inorganic silt > inorganic clay.

4. The correlations proposed by Likos et al. (2014) give good estimates of the wetting SWCC's.

It is shown that neglecting the hysteresis of SWCC overestimates the suction stress and FoS. Therefore, due to the consideration must be paid to wetting SWCCs for slope stability analysis for safe and reliable designs.

References

1. Godt, J.W., Baum, R.L., Lu, N.: Landsliding in partially saturated materials. Geophys. Res. Let. **36**, L02403 (2009)
2. Haines, W.B.: Studies in the physical properties of soil. V. The hysteresis effect in capillary properties, and the modes of moisture distribution associated therewith. J. Agric. Sci. **20**(1), 97–116 (1930)
3. ASTM, Designation: D5298–16: Standard test method for measurement of soil potential (suction) using filter paper. American Society for Testing and Materials, West Conshohocken, PA, (2016)
4. Puppala, A.J., Manosuthikij, T., Chittoori, B.C.S.: Swell and shrinkage characterizations of unsaturated expansive clays. Eng. Geol. **164**, 187–194 (2013)
5. Sreedeep, S., Singh, D.N.: A study to investigate the influence of soil properties on suction. J. Test. Eval. **33**(1), 1–6 (2005)
6. Hoyos, L.R., Suescún-Florez, E.A., Puppala, A.J.: Stiffness of intermediate unsaturated soil from simultaneous suction-controlled resonant column and bender element testing. Eng. Geol. **188**(7), 10–28 (2015)
7. Rahardjo, H., Satyanaga, A., Leong, E.C.: Effects of flux boundary conditions on pore-water pressure distribution in slope. Eng. Geol. **165**, 133–142 (2013)
8. Vanapalli, S.K., Nicotera, M.V., Sharma, R.S.: Axis translation and negative water column techniques for suction control. Geotech. Geol. Eng. **26**(6), 645–660 (2008)
9. Leong, E.C., Tripathy, S., Rahardjo, H.: Total suction measurement of unsaturated soils with a device using chilled mirror dew-point technique. Geotechnique **53**(2), 173–182 (2003)
10. Thakur, V.K.S., Sreedeep, S., Singh, D.N.: Parameters affecting soil-water characteristic curves of fine-grained soils. J. Geotech. Geoenviron. Eng. **131**(4), 521–524 (2005)
11. Pham, H.Q.: An engineering model of hysteresis for soil-water characteristic curves. M.Sc. thesis, University of Saskatchewan, Saskatoon, SK, Canada (2001)
12. Yang, H., Rahardjo, H., Leong, E.C., Fredlund, D.G.: Factors affecting drying and wetting soil-water characteristic curves of sandy soils. Can. Geotech. J. **41**(5), 908–920 (2004)
13. Ebrahimi-Birang, E., Fredlund, D.G., Samarasekera, L.: Hysteresis of the soil water characteristic curve in the high suction range. Ottawa Geo. Conf., pp. 1061–1068. Ottawa (2007)
14. Lin, B., Cerato, A.B.: Hysteretic water retention behavior of two highly clayey expansive soils. In: Hryciw, R.D., Athanasopoulos-Zekkos, A., Yesiller, N. (eds.) GeoCongress 2012. State of the Art and Practice in Geotechnical Engineering, pp. 1205–1212. ASCE, Reston, VA (2012)
15. Song, Y.K.: Suction stress in unsaturated sand at different relative densities. Eng. Geol. **176**, 1–10 (2014)
16. Li, P., Vanapalli, S.K.: Simple method for prediction of the soil collapse behavior due to wetting. Int. J. Geomech. **18**(11), 06018026 (2018)
17. Gapak, Y., Tadikonda, V.B.: Hysteretic water-retention behavior of bentonites. J. Hazard Toxic Radioactive Waste **22**(3), 04018008 (2018)
18. Sun, D.A., Sheng, D.C., Xu, Y.F.: Collapse behaviour of unsaturated compacted soil with different initial densities. Can. Geotech. J. **44**, 673–686 (2007)

19. Xie, Y., Chi, Y.: Geochemical investigation of dry- and wet-deposited dust during the same dust-storm event in Harbin, China: constraint on provenance and implications for formation of aeolian loess. J. Asian Earth Sci. **120**, 43–61 (2016)
20. Fredlund, D.G., Morgenstern, N.R., Widger, R.A.: The shear strength of unsaturated soils. Can Geotech J **15**(3), 313–321 (1978)
21. Raghuram, A.S.S., Basha, B.M.: Stability analysis of unsaturated infinite slopes—a reliability perspective. In: Hoyos, L.R., McCartney, J.S., Houston, S.L., Likos, W.J. (eds.) Second Pan-American Conference on Unsaturated Soils 2017. pp. 185–195. GSP 302, ASCE, Reston, VA (2017). doi.org/https://doi.org/10.1061/9780784481691.019
22. Fredlund, D.G., Xing, A., Fredlund, M.D., Barbour, S.L.: The relationship of the unsaturated soil shear strength to the soil water characteristic curve. Can. Geotech. J. **32**(3), 440–448 (1996)
23. Garven, E.A., Vanapalli, S.K.: Evaluation of empirical procedures for predicting the shear strength of unsaturated soils. In: Miller, G.A., Zapata, C.E., Houston, S.L., Fredlund, D.G. (eds.) Fourth International Conference on Unsaturated Soils 2006. vol. 2, pp. 2570–2581. GSP 147, ASCE, Reston, VA (2006)
24. van Genuchten, M.T.: A closed-form equation for predicting the hydraulic conductivity of unsaturated soil. Soil Sci. Soc. Am. J. **44**(5), 892–898 (1980)
25. Goh, S.G., Rahardjo, H., Leong, E.C.: Shear strength of unsaturated soils under multiple drying-wetting cycles. J. Geotech. Geoenviron. Eng. **140**(2), 06013001 (2014)
26. Likos, W.J., Lu, N., Godt, J.W.: Hysteresis and uncertainty in soil water-retention curve parameters. J. Geotech. Geoenviron. Eng. **140**(4), 04013050 (2014)
27. Raghuram, A.S.S., Basha, B.M.: Reliability analysis of rainfall induced slope failure at Seattle area near Washington. In: Indian Geotechnical Conference 2017, GeoNEst, December, IIT Guwahati, India (2017)
28. Zhang, L.L., Fredlund, D.G., Fredlund, M.D., Wilson, G.W.: Modeling the unsaturated soil zone in slope stability analysis. Can. Geotech. J. **51**(12), 1384–1398 (2014)
29. Al-Mahbashi, A.M., Elkady, T.Y., Al-Shamrani, M.A.: Hysteresis soil-water characteristic curves of highly expansive clay. Eur. J. Environ. Civ. Eng. **22**(9), 1041–1059 (2016)

Analysis of Suction Caissons in Soft Clay

Preethi Sekar, N. Preetham Rajan, and Satya Kiran Raju Alluri

Abstract The cost of establishing any offshore structure is quite expensive. One of the largest expenses in offshore infrastructure is the foundation as environment like wind, wave, and soil or a combination and poses a challenge in most cases. For observation platforms, suction piles offer an unique advantage that it can be reused any number of times by just shifting the location which helps reduce the cost of preliminary infrastructure for potential identification quite feasible. Suction piles or suction buckets are hollow cylindrical steel or concrete caisson, closed at the top and open at the bottom [1]. They are installed by applying suction inside the airtight caisson therefore not difficult for setting up. Once the required data is collected, the pressure inside the caisson is reversed, to be moved to another location. These suction piles resist loads due to the mobilized frictional resistance occurring inside shaft as well as the outside while the bearing resistance comes from the annulus and top plate as it rests on the ground surface (Houlsby and Byrne in Proc. Inst. Civil Eng. Geotech. Eng. 158, 75–82, 2005, [2]). An analysis on the aspect ratio of the caisson for soft clay encountered in the gulf regions is studied in detail [3]. An optimum aspect ratio of the bucket considering various failure conditions is obtained for the gulf regions using numerical computation which can be easily adopted to other location by changing the input parameters. The ratios which are ideal for the gulf regions are also stated in the paper. The suction pile installation has also been studied using a finite element analysis tool, and the failure pattern due to reversal is observed. It is observed that once the suction exceeds the required value, reverse bearing failure occurs causing the bucket to fail.

Keywords Suction caissons · Soft clay · Offshore foundation · Numerical computation

P. Sekar (✉) · S. K. R. Alluri
National Institute of Ocean Technology, Chennai, India
e-mail: preethi.seera.sekar@gmail.com

N. P. Rajan
Bhanes Engineering Pvt. Ltd, Chennai, India

1 Introduction

The foundations often encountered in offshore are monopiles, suction buckets and gravity foundations. These foundations are subjected to heavy lateral loads caused by wind, wave, and seismic forces. Therefore, the foundations account for a significant cost of the total construction or erection cost for offshore structures. For a wind turbine to be set up, extensive field studies and measurements are carried out with the help of coastal and offshore observation platforms. Suction buckets act as better alternative in economical and reuse point of view for observation platforms [4].

Suction buckets or suction caissons are large cylindrical structure, usually made of steel, open at the base and closed at the top. It might be used as a shallow foundation or as short stubby pile. The suction buckets as shallow foundations are generally used in sandy soils while the suction piles or anchors are used in clayey soil [2]. The suction bucket consists majorly of two installation stages: (i) Penetration due to self-weight and (ii) Penetration due to application of suction. By reversal of suction, the bucket can be removed from the area of installation. This application of suction is what makes suction buckets a viable alternative. The suction buckets can be shifted from one location to another after required observations are made.

The Gulf regions of India offer huge potential in terms of offshore wind energy. Based on three borelogs obtained during a geotechnical investigation carried out in this region, it is observed that it has very soft clays with the shear strength values ranging between 20 and 25 kN/m^2 to a depth ranging between 8 and 15 m. As per the literature, the bucket is to be designed as a short pile for clayey soils. However, this paper deals with the determination of preliminary dimensions and suitable aspect ratio for the particular soil. This methodology can also be used for all soil types with the same algorithm. The same aspect ratio is then modeled using a finite element package to validate the result.

2 Installation

The resistance offered to loads onto the suction bucket is offered by the mobilized skin friction both on the inner and outer sides of the wall, and the end bearing is met by the plate closing the cylinder on the top and the area of the annulus [1]. The areas of resistance offered are represented in Fig. 1. It is to be noted that the end bearing due to top plate occurs only after full installation of the suction bucket after a contact is established. The properties used in the analytical calculation are as given in Table 1. It is also to be noted that for the simplification of the study, a constant shear strength value is adopted. There are two main stages of installation: (1) self-penetration and (2) suction assisted penetration. Apart from this, the installation has to be checked for failure that maybe caused due to reverse bearing capacity failure, buckling of the suction walls and the maximum suction that can be applied. The terminologies used in the equations are given in Table 2.
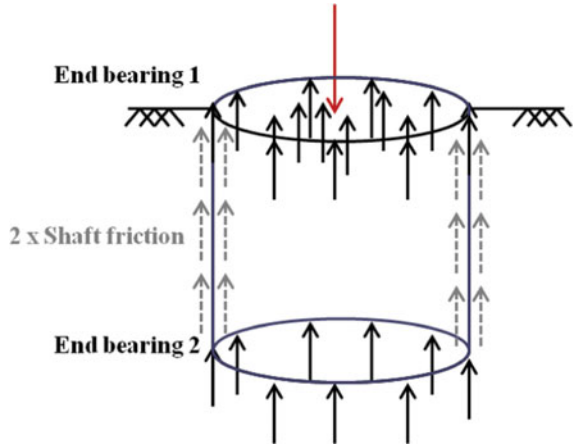
Fig. 1 Resistance offered by suction pile

Table 1 Material properties used in the study

Parameter	Symbol	Value	Units
Self-weight of the structure	P	220	kN
Factored self-weight of the structure	P_f	550	kN
Submerged unit weight of soil	γ'	6.5	kN/m^3
Adhesion factor	α	0.9	–
Undrained shear strength	c	20	kPa

The bearing capacity after installation is the sum of end bearing at the annulus given by $\pi DtcN_c$, end bearing of top plate given by $\pi D_i^2 cN_c/4$, skin friction on the inner and outer surfaces of the vertical walls given by $\pi \alpha hc(D_0 - D_i)$ to compensate the self-weight of the entire structure.

3 Capacity Calculation

As the aim is to determine the least aspect ratio of a suction bucket to successfully work for the gulf regions, the h/D ratios are varied from 0.1 to 5 [5] and checked to see if the bucket sustains all the failure mechanisms. The aspect ratios that need to be determined are the height of the bucket (h), average diameter of the bucket (s), and the thickness (t) of the bucket. Three simultaneous equations, namely Eqs. (1), (2) and (3), are utilized to determine these three unknowns.

Based on the final bearing capacity of the suction bucket explained above:

$$\frac{\pi D_i^2 cN_c}{4} + \pi DtcN_c + \pi \alpha hc(D_o + D_i) - P_f = 0 \tag{1}$$

Table 2 Symbolic notations with units

Parameter	Symbol	Units
Depth of penetration/Height of bucket	h	m
Depth of penetration due to self-weight	h_s	m
Depth of suction assisted penetration	h_{req}	
	$h\text{-}h_s$	m
Depth of water above seabed	h_w	m
Inner diameter of bucket	D_i	m
Outer diameter of bucket	D_0	m
Average diameter of bucket	D	M
Thickness of bucket	t	m
Selected aspect ratio(h/D)	β	–
Self-weight of the structure during installation	P	kN
Factored self-weight of the installed structure	P_f	kN
Atmospheric pressure	p_a	kPa
Unit weight of water	γ_w	kN/m^3
Submerged unit weight of soil	γ'	kN/m^3
Adhesion factor	α	–
Undrained shear strength	c	kPa
Suction	s	kPa

Based on the selected *h/D* ratio:

$$h - \beta D = 0; \tag{2}$$

Based on the minimum thickness required to prevent buckling of the caisson, as per API standards:

$$\frac{D}{100} + \frac{6.35}{1000} - t = 0; \tag{3}$$

By simultaneously solving all the three equations, the required aspect ratios are derived for a particular *h/D* ratio. With the obtained aspect ratio, the next step is to find the plug height or the height of self-penetration, h_s.

3.1 Self- Penetration

The self-penetration is achieved due to the weight of the superstructure and the self-weight of the bucket due to the action of gravity against the bearing capacity of the footing on the soil. This self-penetration creates a soil plug inside the annulus

which prevents the soil from flowing into the bucket during the application of suction, effectively preventing 'reverse bearing capacity' failure. The height achieved due to self-penetration is computed by equating the frictional and end resistance offered by the soil to the bucket and the weight acting against it. Substituting the P_f with P and h by h_s and rearranging Eq. (1) gives the height of self-penetration achieved as in Eq. (4).

$$h_s = \frac{P - (\pi D t c N_c)}{\pi \alpha c (D_o + D_i)} \tag{4}$$

The remaining height yet to be penetrated, h_{req}, is the difference between the total height of the bucket and the depth of self-penetration achieved, h_s.

3.2 Suction Assisted Penetration

The suction acts on the top plate of the caisson, upwards. The suction load is therefore computed by the multiplication of the suction pressure and the area of the top plate. This suction works on creating a differential pressure on the inside and the outside of the caisson. However, a huge difference in the stress inside and outside of the caisson creates a flow of soil instead of the installation of suction bucket. To maintain equilibrium of forces in the caisson, the equilibrium equation can be rearranged to find suction, as described in Eq. (5).

$$s = \frac{(2\pi h_{req} \alpha c D) + (\gamma' h_{req} + c N_c) \pi D t - P}{\pi D_0^2 / 4} \tag{5}$$

The suction acts on the top plate of the caisson, and the end and skin friction to be overcome by the suction is equated to obtain Eq. (5). The suction obtained for the equation is the required pressure to be applied to install the caisson flush on to the seabed level. This pressure is however theoretical and is limited to the cavitation pressure of water, pump capacity, and the pressure differential that can be created between the inside and the outside of the caisson, which depends on the water depth at the area of installation.

3.3 Reverse Bearing Capacity Failure

In case of failure of plugs, a plastic zone is created in the plug region. This plastic zone stops further penetration of the caisson during application of suction. The soil flows inwards during application of suction, effectively preventing the installation. The minimum height required for the reverse bearing failure not to occur as given by Houlsby [2] is computed from Eq. (6).

$$P + \frac{cN_c\pi D_i^2}{4} - h_f \alpha c\pi D_0\left(1 + \frac{D_i^2}{(0.01h^2 + 0.2D_0h_f)}\right) - \left(\gamma'h_f + cN_c\right)\pi Dt = 0$$

(6)

This value should always be less than the h_s for the effective plug formation. This phenomenon is further studied with the use of a numerical package, to understand the plastic zone formation, and the movement of soil inside the bucket foundation.

4 Optimization

Optimization is to be done to determine the maximum economical section and suction for a given weight and soil conditions in the Gulf regions. A computational tool, MATLAB R2019a [6] was utilized solve the equations and carry out the iterations. The input is as shown in Table 1. For h/D ratios ranging from 0.1 to 5 and the corresponding h_s, h_f and suction pressure required is computed and is as given in Figs. 2 and 3. The entire output of the program is seen in Table 3.

It is observed that as the *h/D* ratio is increased, the*h* of the bucket increases, which in turn increases the self-weight of the bucket, thus increasing the height due to self-penetration. It is also seen that as *h/D* increases, the suction to be applied also increases. For some cases of *h/D* as seen up to the case of 0.9, the suction obtained is negative. With regard to this study, it simply means that no suction is necessary for installation. It is seen to that the height of penetration is always kept high as compared to the height of failure for successful installation [7].

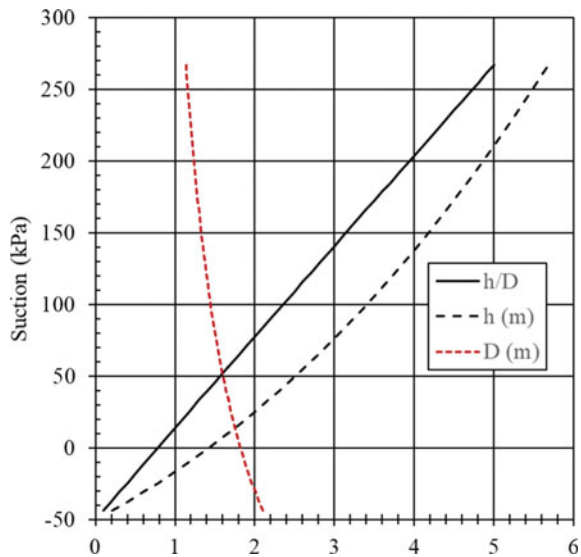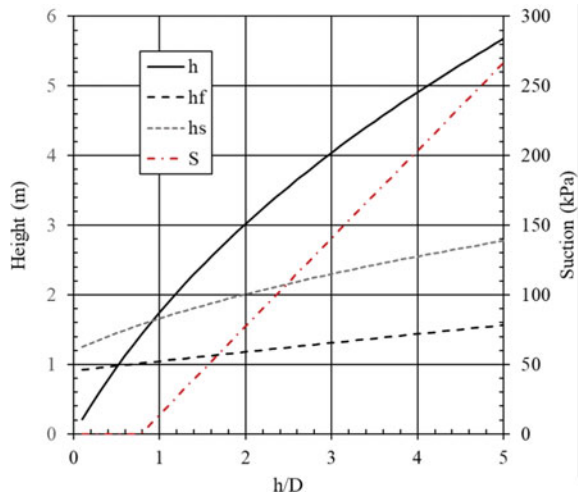**Fig. 2** Variation of suction on lateral dimensions of the caisson

Fig. 3 Design chart for optimization

5 Numerical Analysis

A numerical model using a finite element package called PLAXIS 3D [8] was utilized to study 'reverse bearing capacity failure' inside the caisson. The reverse bearing capacity of the suction plays a crucial role in the determination of the aspect ratio of the bucket. A study is to be carried out by increasing the suction value applied to the caisson and the reaction in studied. A suction bucket of 2 m nominal diameter, 3 m height is chosen for the study. Based on the formulation, it is observed that the bucket self-penetrates only to a depth of 7 cm on its own and the remaining height requires a suction of about 210 kPa.

The model consists of 39,993 elements with element size varying from 0.0656 to 2.012 m, and mesh refinement study was carried out. The boundary limits are considered so the results are not influenced by the boundary conditions. A suction bucket of dimensions as shown in Table 4 is considered in this study. The material properties of the model are provided in Table 5. The suction values are varied from 100, 150, 200, 250, and 300 kPa.

The vertical displacements, mobilized shear stress, and the deviatoric strains are studied to understand the effect of reverse bearing capacity as shown in Fig. 4a, b and c. From the graphs in Fig. 4, we can see the effect of suction on the reverse bearing capacity failure. We can see from the figures that until the suction pressure was 250 kPa, there was only nominal change in the displacements. However, as the pressure reaches 300 kPa, we can see an increase in displacement by 750%. For the mobilized shear stress, we can see that the maximum value flatlines after the suction increases more than 250 kPa. Any increase in suction pressure will not contribute to any further resistance of the caisson with the soil, leading to reverse bearing capacity of the soil. The strain value also increases rapidly once the pressure increases over 250 kPa, signifying a failure of the soil.

Table 3 Variation of study parameters with respect to *h/D*

h/D	*h* (m)	*t* (mm)	h_{f} (m)	h_{s} (m)	*S* (kPa)
0.1	0.21	28	0.92	1.25	−43.5101
0.2	0.41	27	0.93	1.3	−37.287
0.3	0.6	27	0.95	1.35	−30.4433
0.4	0.78	26	0.96	1.4	−24.7143
0.5	0.96	26	0.98	1.45	−17.9194
0.6	1.13	26	0.99	1.49	−11.4055
0.7	1.29	25	1	1.54	−5.12265
0.8	1.45	25	1.02	1.58	1.267024
0.9	1.6	25	1.03	1.62	7.769173
1	1.75	24	1.04	1.66	14.05291
1.1	1.89	24	1.06	1.7	20.34815
1.2	2.03	24	1.07	1.74	26.8036
1.3	2.17	24	1.08	1.77	33.82176
1.4	2.3	23	1.1	1.81	39.64401
1.5	2.42	23	1.11	1.84	45.80001
1.6	2.55	23	1.12	1.88	52.30547
1.7	2.67	23	1.14	1.91	58.7246
1.8	2.79	22	1.15	1.95	64.88228
1.9	2.91	22	1.16	1.98	71.55599
2	3.02	22	1.18	2.01	77.73983
2.1	3.13	22	1.19	2.04	84.04242
2.2	3.24	22	1.2	2.07	90.46671
2.3	3.35	21	1.22	2.1	96.64339
2.4	3.45	21	1.23	2.13	102.8924
2.5	3.55	21	1.24	2.16	109.0168
2.6	3.66	21	1.26	2.19	116.1052
2.7	3.75	21	1.27	2.22	121.7855
2.8	3.85	21	1.28	2.25	128.3912
2.9	3.95	20	1.3	2.27	134.6206
3	4.04	20	1.31	2.3	140.7282
3.1	4.14	20	1.32	2.33	147.5371
3.2	4.23	20	1.33	2.35	153.8268
3.3	4.32	20	1.35	2.38	160.1877
3.4	4.41	20	1.36	2.41	166.6249
3.5	4.49	20	1.37	2.43	172.4388
3.6	4.58	20	1.39	2.46	179.0571

Table 3 (continued)

h/D	h (m)	t (mm)	h_f (m)	h_s (m)	S (kPa)
3.7	4.66	19	1.4	2.48	184.709
3.8	4.75	19	1.41	2.51	191.4915
3.9	4.83	19	1.43	2.53	197.6067
4	4.91	19	1.44	2.55	203.7951
4.1	4.99	19	1.45	2.58	210.0539
4.2	5.07	19	1.46	2.6	216.3922
4.3	5.15	19	1.48	2.62	222.8074
4.4	5.23	19	1.49	2.65	229.2965
4.5	5.31	19	1.5	2.67	235.8689
4.6	5.38	19	1.52	2.69	241.7233
4.7	5.46	18	1.53	2.71	248.2117
4.8	5.53	18	1.54	2.74	254.214
4.9	5.61	18	1.55	2.76	261.1111
5	5.68	18	1.57	2.78	266.8439

Table 4 Physical parameters of the model

Parameter	Value	Units
Depth of penetration/ Height of bucket	3	m
Inner diameter of bucket	1.97	m
Outer diameter of bucket	2.03	m
Average diameter of bucket	2	M
Thickness of bucket	26	mm
Selected aspect ratio(h/D)	1.5	–
Suction pressure	Varies	kPa

Table 5 Parameters used in PLAXIS model

| Description	Value	Units
Type of analysis	Mohr-Coulomb	
Type of drainage	Drained	
Saturated unit weight of soil	17	kPa
Unsaturated unit weight of soil	16 kPa	
Young's modulus, E	15,000	kPa
Poisson ratio	0.2	–
Cohesion, c	20	kPa
Angle of internal friction	0	deg

Fig. 4 Variation in study parameters for different suction with **a** displacement **b** mobilized shear stress and **c** deviatoric strain. The red solid indicates maximum value in all graphs
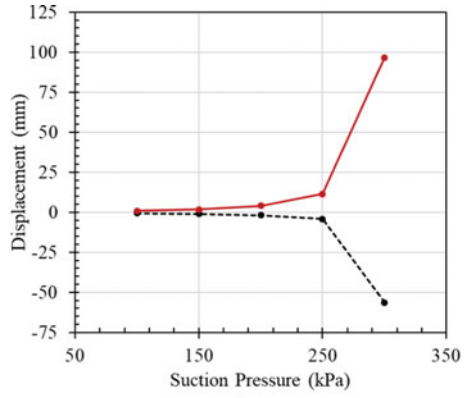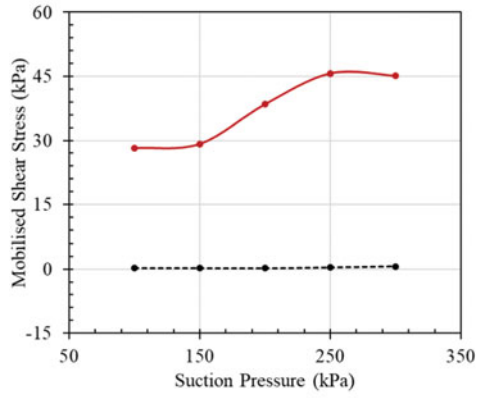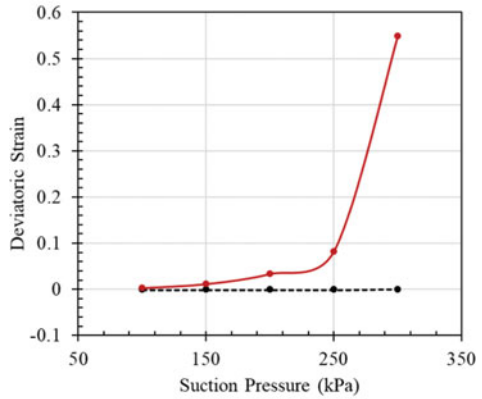
From Fig. 5, it is seen that the plastic zone is created inside and just below the area of installation of the caisson. This is due to the plug not being able to withstand the suction pressure applied. This causes the soil to move upwards into the caisson rather than the caisson move toward the bed level. It can also be seen from Fig. 6a that the pressure dissipation is attributed highly due to shear dissipation rather than bearing as seen from Fig. 5b [9]. Further models have to be studied to understand the complex behavior of suction buckets through numerical modeling. Study also needs to be carried out in understanding the undrained behavior.
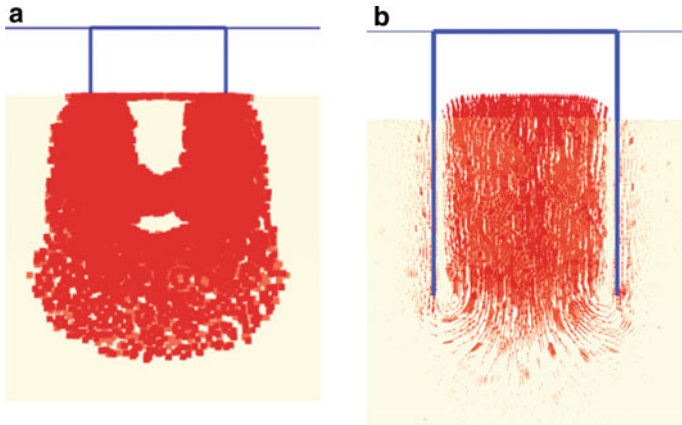

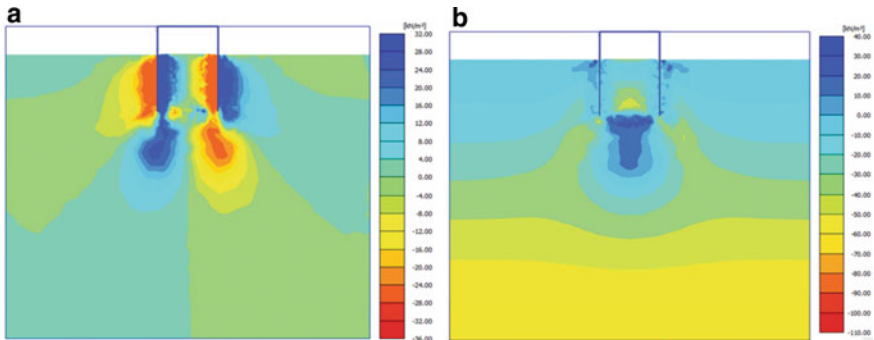**Fig. 5** **a** Plastic zone **b** upward movement of soil

Fig. 6 **a** shear dissipation **b** end bearing pressure

6 Conclusion

The optimal suction pile configuration has been studied for the Gulf coast of India. It has been found that for an observation platform for a soft clayey soil, increase in diameter increases the suction required to a large extent; however, increasing the height of the bucket, proves more effective. Heave inside the caisson due to the application of suction has to also be studied. It is also observed that in case of reverse bearing capacity failure, as simulated in PLAXIS 3D, a plastic zone is formed which effectively stops the penetration of the bucket into the soil. A check has been applied to assure that this failure is avoided for the h/D ratios studied. The stability of these foundations to static lateral and dynamic loading has to be further studied. The increase in strength of the soil due to the formation of plug has to also be studied in detail. A numerical model has been carried out to understand the bearing capacity failure based on the displacement, shear stress, and the deviatoric strain values. Further study on the complex load transfer mechanism and the behavior in undrained condition has to be studied. The lateral capacity of the bucket also plays a major role on the dimension, which has not been carried out in the study.

References

1. Hogervorst, J.R.: Field trials with large diameter suction piles. In: Offshore Technology Conference. Offshore Technology Conference (1980)
2. Houlsby, G.T., Byrne, B.W.: Design procedures for installation of suction caissons in clay and other soils. Proc. Inst. Civil Eng. Geotech. Eng. **158**(2), 75–82 (2005)
3. Randolph, M. F., House, A.R.: Analysis of suction caisson capacity in clay. In Offshore Technology Conference. Offshore Technology Conference (2002)
4. Senpere, D., Auvergne, G.A.: Suction anchor piles-a proven alternative to driving or drilling. In: Offshore Technology Conference. Offshore Technology Conference (1982)
5. Magued, I., El-Gharbawy, S., Olson, R.: Performance of suction caissons in sand and clay. Can. Geotech. J. **39**(3), 576–584 (2002)
6. Matlab 2019 Reference Manual
7. Guo, Z., Wang, L., Yuan, F., Li, L.: Model tests on installation techniques of suction caissons in a soft clay seabed. Appl. Ocean Res. **34**, 116–125 (2012)
8. Plaxis 3D 2018 Reference manual, Plaxis bv
9. Andersen, K.H., Jostad H.P.: Shear strength along outside wall of suction anchors in clay after installation. In: The 12th International Offshore and Polar Engineering Conference. International Society of Offshore and Polar Engineers (2002)

Thixotropic Properties of Deepwater Indian Marine Clays from Eastern Offshore—Evaluation and Correlations

Rohit Sinha and R. K. Ghanekar

Abstract Thixotropy of clays is an important parameter in offshore geotechnical engineering. Thixotropy is responsible for the short-term gain in undrained shear strength of clays after remolding, and hence, it is imperative to incorporate it in the analysis while estimating the short-term load carrying capacity of foundation systems at varying time after their installation. Different clays display different thixotropic properties, and so far, there has been negligible information available about Indian offshore clays. Hence, this paper presents and discusses the thixotropic properties of eastern offshore deepwater clays measured during a recent geotechnical investigation.The paper discusses different factors which affect the thixotropic behavior of clays along with the investigations done and reported in the literature to correlate thixotropy with other soil parameters such as plasticity index, liquidity index, and water content. Further, a comparison is presented between the eastern Indian offshore thixotropy data with the published data from other parts of the world. Evaluation of possibility of development of some correlation(s) for Indian offshore thixotropy data has also been presented.

Keywords Thixotropy · Offshore · Geotechnical · Deepwater · Clays

1 Introduction

The determination of undrained shear strength of clays is important for design of foundations for any structural system interacting with clays. There are numerous parameters which influence the shear strength at a given time, e.g., at undisturbed state, remolded state immediately after installation of foundations and at a state after some time—post-foundation installation. One such property is thixotropy which is of

R. Sinha (✉) · R. K. Ghanekar
Geotechnical Engineering Section, Institute of Engineering and Ocean Technology, ONGC, Panvel, Maharashtra 410221, India
e-mail: sinha_rohit1@ongc.co.in

R. K. Ghanekar
e-mail: ghanekar_rk@ongc.co.in

considerable importance in offshore geotechnical engineering defining the strength gain after installation of foundations in clays in short term.

Thixotropy is defined as "a process of softening caused by remolding which is an isothermal, reversible, time-dependent process occurring under conditions of constant composition and volume, whereby a material stiffens while at rest and softens or liquefies upon remolding" [1]. The measure of thixotropy is the ratio (called the thixotropy strength ratio) between the shear strength at a given time after thixotropic strength gain and the shear strength just after remolding.

Thixotropic properties are different for different clays, and there has been no information available about Indian offshore clays. Hence, the study presented in this paper was performed to get an insight into the thixotropic property of clays, particularly in the deepwater Indian Marine Clays from Eastern offshore. The data used for this study is from a recent deepwater project of ONGC. In the present paper, comparison and subsequent evaluation of the eastern Indian offshore thixotropy data with the published data from other parts of the world is made and possibility of the development of some correlation(s) for Indian offshore thixotropy data has also been examined.

2 Literature Survey

From literature search, it appears that the published material on thixotropy is very limited. It also appears that thixotropic property of clays was noticed quite early in the history of geotechnical engineering practice. As early as 1948, Moretto (1948) reported study on the thixotropic behavior of natural clays.

2.1 Effect of Mineralogy

Skempton and Northey [2] presented data for pure mineral clays—Kaolinite, Illite, and Bentonite and some natural clays, using the laboratory vane. Kaolin clay showed almost no thixotropy, Illite showed comparatively more thixotropic gain, and Bentonite showed comparatively large strength gain (and continued to gain strength even after a year). It was hence surmised that mineralogy plays an important part in the thixotropic behavior of clays.

2.2 Effect of Plasticity Characteristics

Santos-Soage [3] studied the factors affecting thixotropic behavior of clays and found that the factors which affect the consistency limits (Atterberg limits) of clays also affect the thixotropic behavior. Hence, clay microstructure, mineralogy, electrolyte

concentration, organic content, etc., which are reflected in the Atterberg limits, also affect the thixotropy of clays.

2.3 Effect of Water Content

Skempton and Northey [2] indicated that water content of the clay has influence on the thixotropic strength gain. They concluded that thixotropic strength gain decreases with decrease in water content below liquid limit, and thixotropic strength gain may be negligible at or close to the plastic limit. In their study, they used water content in terms of liquidity index.

2.4 Thixotropy Relationship with Sensitivity

Yang and Andersen [4] also investigated relation between sensitivity and thixotropy strength ratio. It was observed that a trend of increasing thixotropy strength ratio with sensitivity can be seen but it appears to level-off at higher time intervals (beyond 1 day) and sensitivity of 5.

3 The Data Used in the Present Study

The published data used for the present study has been taken primarily from Yang and Andersen [4]. To a limited extent, data presented by Colliat [5] has also been considered. The reason for choosing data primarily from Yang and Andersen [4] was that it is for marine clays (including also data from some Indian marine clays), is comparatively substantial, and is in easily usable form. These data were then compared with the data from recently concluded geotechnical investigation of ONGC Eastern offshore deepwater project.

3.1 Published Data

3.1.1 Data from Yang and Andersen [4]

The database used by Yang and Andersen [4] contained thixotropy data for marine clays from 15 offshore sites in Norway, Ghana, Angola, Egypt, India, and Malaysia. The database has a very good range of various geotechnical parameters as shown in Table 1.

Table 1 Range of basic parameters in the database [4]

Basic parameters	Marine clays
Water content, %	21–145
Plasticity Index, $I_{P,\%}$	19–97
Clay fraction, %	28–80
Sensitivity	1.5–10
OCR	1–4.5

3.1.2 Data from Colliat [5]

Colliat [5] presents thixotropy data from 22 sites from offshore Guinea (Gulf of Guinea), and Colliat et al. [6] present the geotechnical data for the Gulf of Guinea clays in details. The water depth ranged between 350 m and more than 1400 m. The water content at most of the sites ranges between 80 and 150%. The soils display very high plasticity index—ranging typically between 70 and 130%. The range of sensitivity is from 3 to 6. Mineralogical examination showed Kaolinite as the dominant mineral and Smectite also as a significant portion.

3.2 Eastern Indian Deepwater Offshore Data

3.2.1 Data from Eastern Indian Offshore Soil

The data pertains to a recent deepwater Eastern Indian offshore project of ONGC. Soft to firm clays were encountered at most places to considerable depth below seafloor. Thixotropy is measured in terms of thixotropy strength ratio: ratio between the shear strength after a time after thixotropic strength gain and the shear strength just after remolding. The strength test used is laboratory vane. The strength test of a number of samples of remolded clay is done immediately after remolding. The samples are then stored in a way that the water content remains the same as original sample. The tests were again performed at time intervals of 0, 1, 2, 4, 7, 14, 30, and 60 days. The thixotropy test results were available from 11 borings in the area. The water depth ranged from ~30 m to 1240 m. The sample depth (below seafloor) range (where the thixotropy data were available) was from 3.6 to 47.4 m. The clays are highly plastic clays and generally have very high clay fraction reaching up to 100%. The water content ranged from 53 to 101% and plasticity index ranged from 43 to 88. OCR best estimates varied from 0.65 to 1.8. The sensitivity ranged from 2 to 3. No mineralogical composition study is available; however, inferred from activity data, the soils are generally believed to be composed of Illite or a combination of Illite and Montmorillonite.

4 Data Analysis and Results

Primarily, the data from Yang and Andersen [4] and to much lesser extent data from Colliat [5] have been used to compare the eastern Indian offshore data.

The literature search resulted in getting comparatively limited data. However, the data from Yang and Andersen [4] was found to be suitable for the study purpose. Colliat [5] and Colliat et al. [6] did not present the data values and hence could not be directly incorporated in the study.

Yang and Andersen [4] had also checked thixotropy strength ratio against activity and plasticity index but the plots showed very high scatter without any clearly discernible trend. Inclusion of Indian data also did not improve the situation, and hence, these plots are not included in this paper.

4.1 Comparison of Data from Yang and Andersen [4] and Eastern Indian Offshore Marine Clays for Use in the Study

Before evaluating the Indian data against published data, the data from Yang and Andersen [4] and from Eastern Indian offshore were comapred to examine the compatibility and usability. Three basic differences were noticed:

- It can be seen that the time intervals at which the strength is measured are different for eastern Indian offshore and Yang and Andersen [4] paper. The common time intervals for thixotropy strength testing are 1, 30, and 60 days, and direct comparison of data is only possible for data for these time intervals.
- It was noted that the thixotropy tests and sensitivity tests in Yang and Andersen [4] data are all from fall cone tests while in eastern Indian offshore project laboratory vane tests were used.
- Yang and Andersen [4] state that their database contains only those test results where the change (decrease) in water content over the duration of the test-set was less than 1.5% of the original water content. Examination of the eastern Indian offshore data showed maximum variation of water content in most of the tests from 3 to 5%. Only a few tests show variation less than 1.5 or 2%.

It is to be noted that an increase of water content will tend to reduce the shear strength and vice versa. It was realized that the quantification of variation of shear strength due to these differences is not possible to do realistically. Also due to limited amount of data available from Eastern Indian Offshore project, it would not have been practical to use data only from tests where the water content variation is less than 1.5% as is the case in Yang and Andersen [4] database. It was hence decided to go ahead with further study and evaluate the results subsequently.

Also, Yang and Andersen [4] use liquidity index (LI) as one of the correlating parameter. During an earlier study done at ONGC [7], it was observed that the

intrinsic state parameter, w/w_L; i.e., ratio of natural water content and liquid limit [8] correlates extremely well with LI:

$$LI = 1.81.w_f/w_L - 0.81$$

$$(n = 841, \quad R^2 = 0.95, \quad \text{and standard deviation} = 0.09) \tag{1}$$

It is also noticed that the former parameter is much simpler and eliminates the arbitrariness of plastic limit definition and determination [8, 9]. Since data from Yang and Andersen [4] were also available for deriving the intrinsic state parameter, this parameter was used instead of liquidity index.

Since intrinsic state parameter also normalizes the water content, it was not considered worthwhile to separately investigate relationship between water content and thixotropy strength ratio.

4.2 Thixotropy Strength Ratio Versus Intrinsic State Parameter

Figures 1, 2 and 3 present the relationship between intrinsic state parameter and thixotropy strength ratio using Indian offshore data plotted along with data from Yang and Andersen [4] for 1 day, 30 days, and 60 days intervals, respectively.

4.3 Thixotropy Strength Ratio Versus Sensitivity

Figures 4, 5 and 6 present relationship between sensitivity and thixotropy strength ratio using Indian offshore data plotted along with data from Yang and Andersen [4] for 1 day, 30 days, and 60 days intervals, respectively.

4.4 Thixotropy Strength Ratio Versus Time

Figure 7 presents thixotropy strength ratio versus time in logarithmic scale. The figure plots the data from eastern Indian deepwater offshore along with ranges of data presented by Yang and Andersen [4] and Colliat [5].
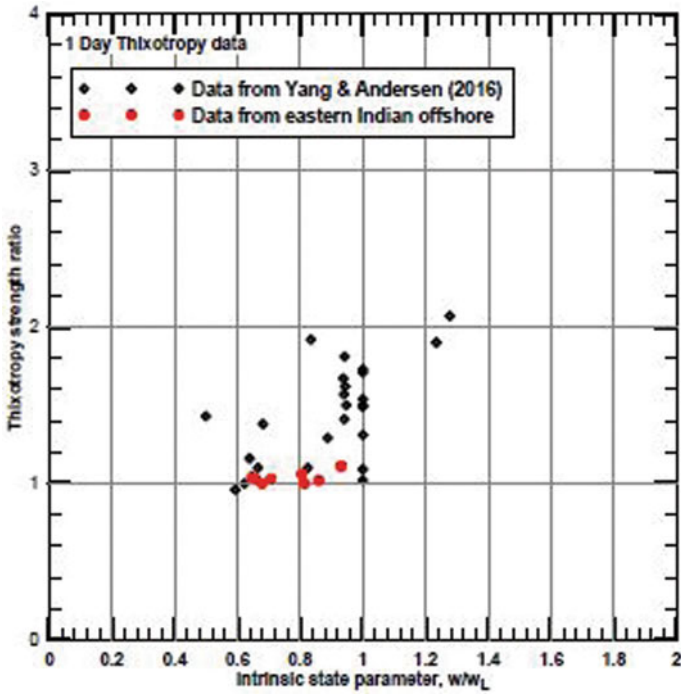
Fig. 1 Thixotropy strength ratio versus intrinsic state parameter—1 day interval

4.5 *Sensitivity Versus Intrinsic State parameter*

Bjerrum [10] has proposed a correlation between liquidity index (LI) and sensitivity (St) as follows:

$$St \ = \ 10(0.15 + 0.73.LI) \tag{2}$$

As stated earlier, a very good correlation was found between liquidity index and intrinsic state parameter [7]. Hence, it was decided to investigate the relation between intrinsic state parameter and sensitivity.

Figure 7 presents relationship between intrinsic state parameter and sensitivity using Indian offshore data plotted along with data from Yang and Andersen [4]. An attempt was made to develop a correlation between sensitivity and intrinsic state parameter. The best correlation is exponential and is shown on the figure. The correlation is not very strong with coefficient of determination, R^2 equal to 0.66. For comparison, correlation proposed by Bjerrum [10] for Norwegian clays is also presented on Fig. 8 by converting LI to W/W_L.
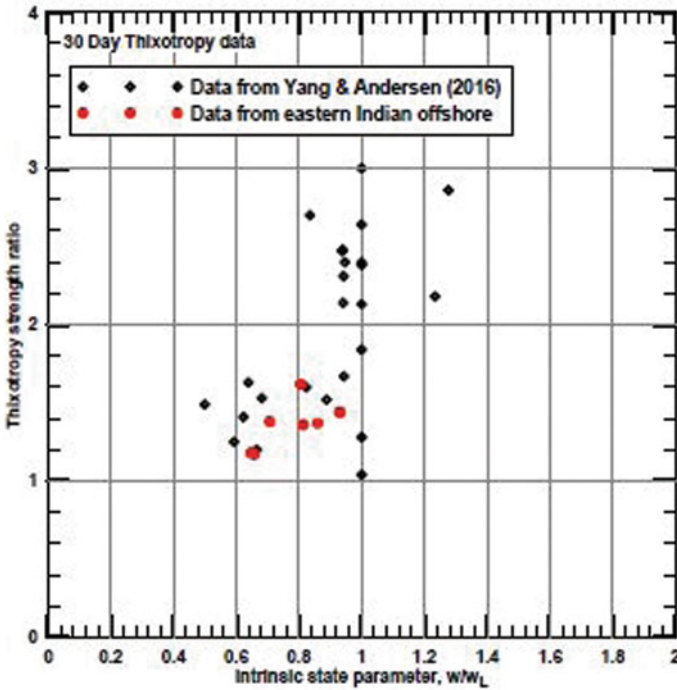
Fig. 2 Thixotropy strength ratio versus intrinsic state parameter—30 day interval

5 Discussion of Results and Recommendations

The thixotropy data from eastern Indian offshore were compared with data from Yang and Andersen [4] for the relationships with intrinsic state parameter and sensitivity. Time versus thixotropy strength ratio was also compared with data from Yang and Andersen [4], and Colliat [5].

5.1 Thixotropy Strength Ratio Versus Intrinsic State Parameter and Sensitivity

The data, for the two comparisons, could only be examined for 1 day, 30 days, and 60 days intervals.

Despite differences in the testing method and variation of water content during the tests, the eastern Indian data neatly plots within or close to the range of data presented by Yang and Andersen [4]—for thixotropy strength ratio versus intrinsic state parameter or sensitivity (refer Figs. 1, 2, 3, 4, 5 and 6). A difference can also be
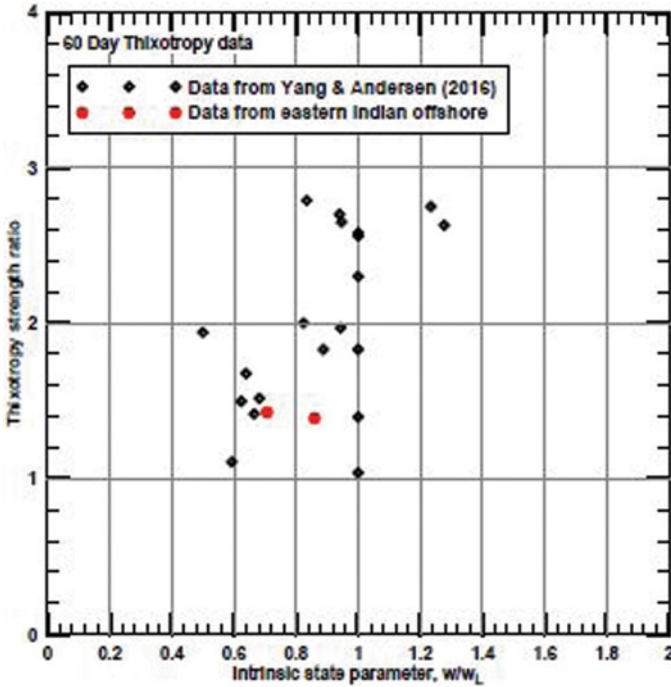
Fig. 3 Thixotropy strength ratio versus intrinsic state parameter—60 day interval

gleaned from the plots that the ranges for intrinsic state parameter and sensitivity is much lower for eastern Indian offshore as compared to Yang and Andersen [4] data.

It is also seen that due to the scatter in data, only trends can be discerned (especially for 30 days interval), and it is not worthwhile to try to develop correlations. In general, it can be stated at present that the thixotropy strength ratio increases with increasing intrinsic state parameter and sensitivity, confirming the trends reported in the literature.

5.2 Thixotropy Strength Ratio Versus Time

From Fig. 8, it can be seen that eastern Indian offshore data plots toward the lower side of the range reported by Yang and Andersen [4] and Colliat [5]. This generally matches with range of sensitivity of the two datasets and variation of thixotropy strength ratio with sensitivity. Although the lower bound of the range of sensitivity of Yang and Andersen data is lower than the Indian data, some of the curves from Indian data plot below the lower bound range of Yang and Andersen [4] data. The reason is not very clear. In the absence of definitive data about mineralogy and activity, it is not possible to evaluate or analyze the data further.
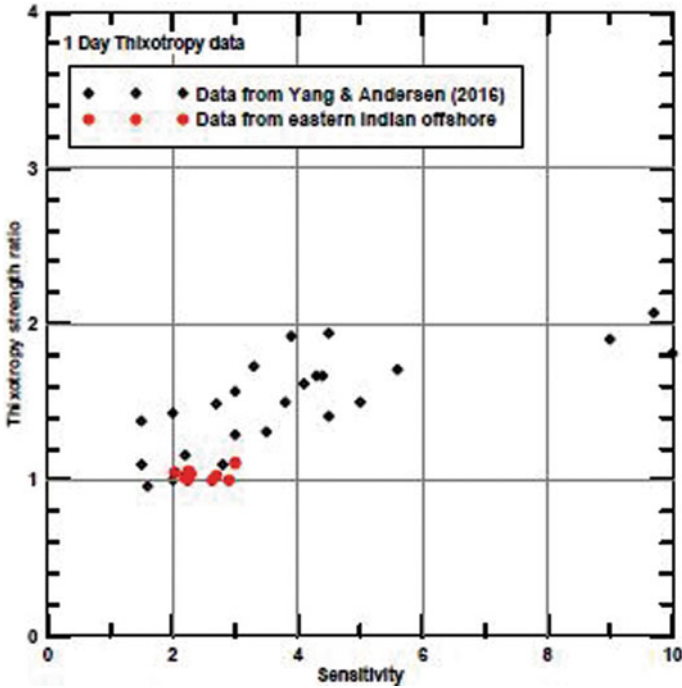
Fig. 4 Thixotropy strength ratio versus sensitivity—1 day interval

5.3 Sensitivity Versus Intrinsic State Parameter

The relation between liquidity index and sensitivity is well known in the literature. Yang and Andersen [4] had also presented the relation using their database. Figure 8 shows their data superimposed with data from eastern Indian offshore but using the intrinsic state parameter instead of liquidity index. The eastern Indian data neatly plots in the range shown by Yang and Andersen [4]. A clear trend of increasing sensitivity with intrinsic state parameter is observed which is also supported by Bjerrum [10] data as presented in the Figure.

6 Conclusion

The study presented in the paper gives an insight into the thixotropic behavior of eastern Indian offshore deepwater clays.
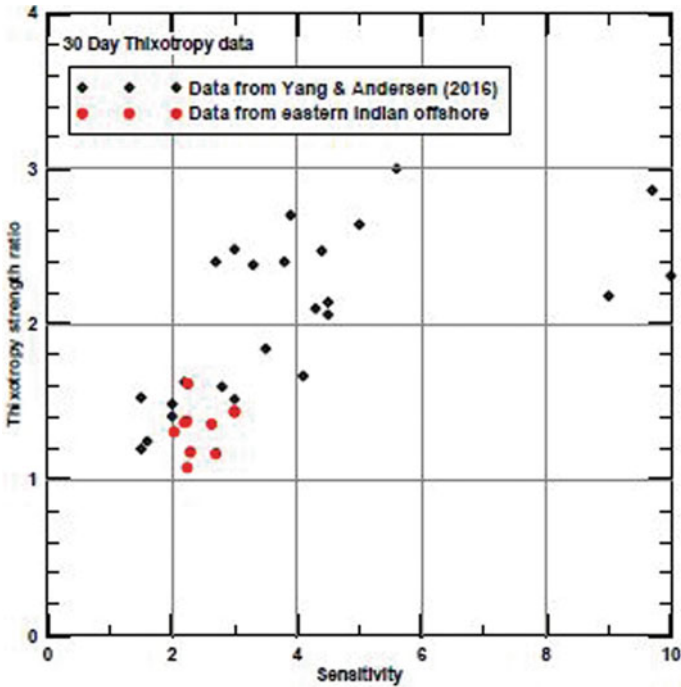
Fig. 5 Thixotropy strength ratio versus sensitivity—30 day interval

It was observed after a thorough literature review that the published material on thixotropy is very limited. However, it is noted that mineralogy, plasticity characteristics, and water content have an influence on the thixotropic behavior of clays.

Further, there exists some relationship between sensitivity and thixotropy. The investigations done by researchers reveal that for sensitivity values less than about 5, an increasing trend is seen between thixotropy and sensitivity which Indian data conforms to, as found in this study.

To evaluate and examine whether some correlations can be developed for Indian offshore deepwater data, the data from recently concluded deepwater geotechnical investigation for ONGC's Eastern Indian Offshore field were compared with data taken primarily from Yang and Andersen [4] and to some extent the data presented by Colliat [5]. It was found that the data trends from eastern Indian deepwater offshore conform to the data trends presented in the literature for clays encountered world over. However due to considerable scatter in data and data limitations, only trends could be discerned and correlations could not be developed.

Comparison of thixotropy strength ratio with intrinsic state parameter (an equivalent parameter to liquidity index but simpler and more rational) and sensitivity also confirmed the fact that the thixotropy strength ratio increases with increasing intrinsic state parameter and sensitivity.
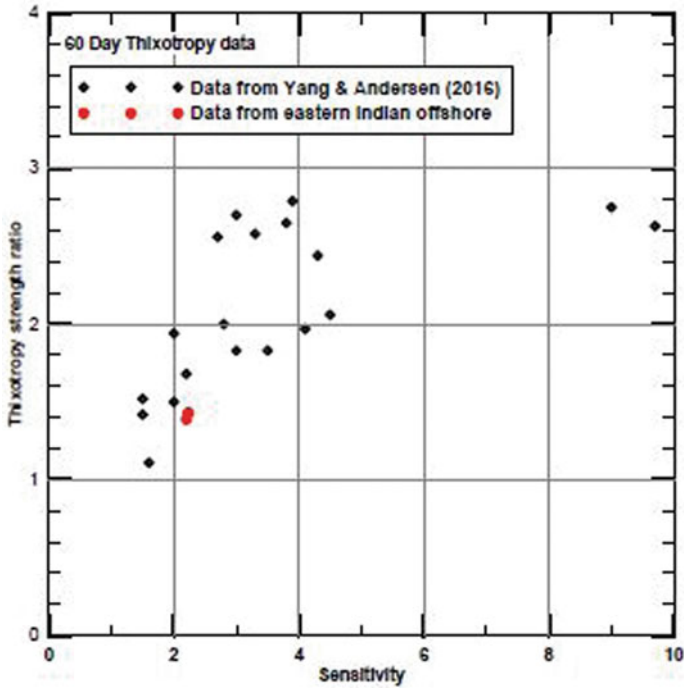
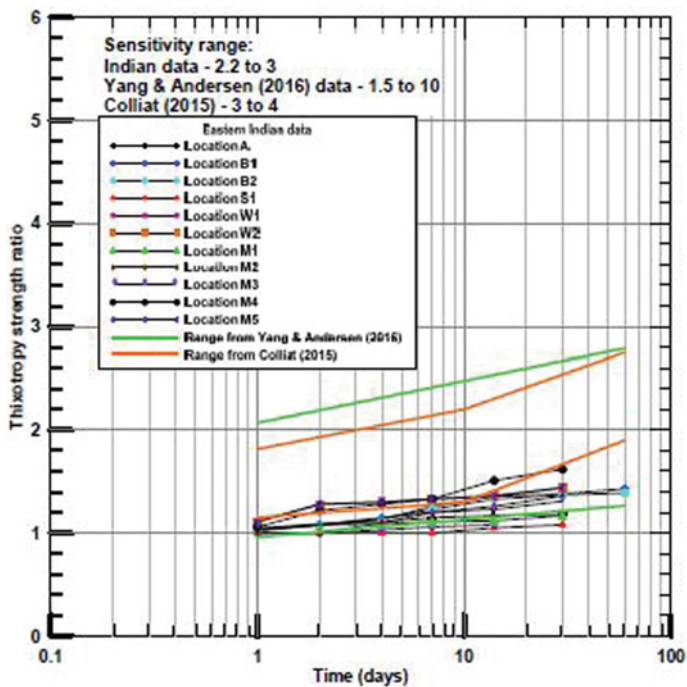**Fig. 6** Thixotropy strength ratio versus sensitivity—60 day interval
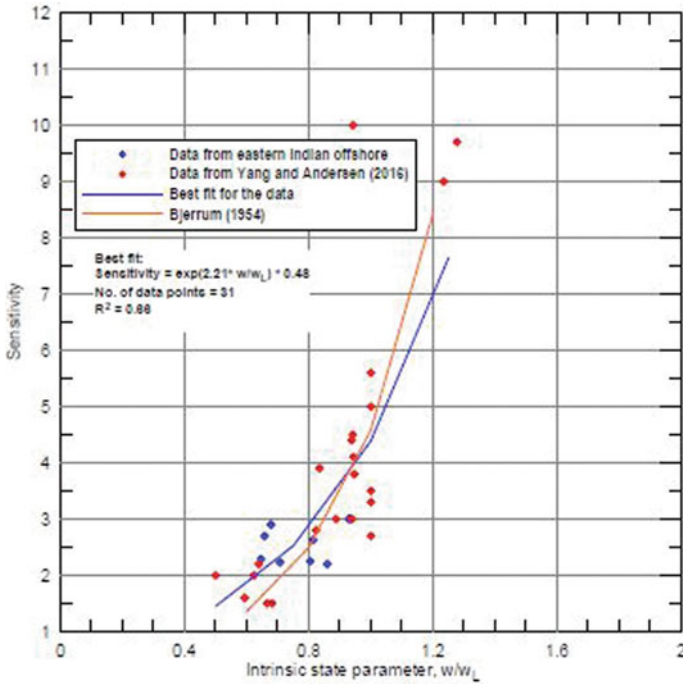
Fig. 7 TThixotropy strength ratio versus time

Fig. 8 Sensitivity versus intrinsic state parameter

References

1. Mitchell, J. K.: Fundamental aspects of thixotropy in soils. J. Soil Mech. Found. Div. Am. Soc. Civil Eng. **83**(3), 19–52 (1960)
2. Skempton, A.W., Northey, R.D.: The sensitivity of clays. Geotechnique **3**, 30–53 (1952)
3. Soage-Santos, R.: Study on thixotropy of marine soft clays. A report submitted in partial fulfillment of the requirements for the degree of MSc Soil Mechanics and for the Diploma of Imperial College London, Imperial College, London (2011)
4. Yang, S.L., Andersen, K.H.: Thixotropy of marine clays. Geotech. Testing J. (2016). https://doi.org/10.1520/GTJ20150020
5. Colliat, J.L.: Friction degradation and strength regain along suction piles in soft deepwater Gulf of Guinea clays. In: Meyer (Ed.) Proceedings of 3rd International Symposium on Frontiers in Offshore Geotechnics, Oslo, Norway. Ed. Meyer (2015)
6. Colliat, J.-L., Dendani, H., Puech, A., Nauroy, J.-F.: Gulf of Guinea deepwater sediments: geotechnical properties, design issues and installation experience. In: Proceedings of 2nd International Symposium on Frontiers in Offshore Geotechnics, Ed. Gourvenec and White (2010)

7. IEOT.: Establishment of soil design parameters from soil index parameters. Report—III—Statistical analysis of data and preliminary recommendations. A research project with Norwegian Geotechnical Institute (NGI) under Oil Industry Development Board (OIDB) funding (2002)
8. Nagaraj, T.S., Miura, N.: Soft Clay Behaviour. A.A. Balkema Publishers, Rotterdam, Netherlands (2001)
9. Ghanekar, R.K., DeGroot, D., Lunne, T.: Intrinsic properties' frameworks—comparative evaluation and use in engineering practice. In: Proceedings of 4th International Workshop on Soil Parameters from In Situ and Laboratory Tests, Scientific Conference—Natural and Technical Problems of Environmental Engineering, Poznan, Poland (2010)
10. Bjerrum, J.: Geotechnical properties of Norwegian marine clay. Geotechnique **4**, 49–69 (1954). https://doi.org/10.1680/geot.1954.4.2.49

Evaluation of SWCC Curves and Undrained Shear Parameters at Different Densities and Saturations of Unsaturated Clay

Kishan Bhadiyadra, Nehal Desai, and K. N. Sheth

Abstract The behaviour of unsaturated soils in terms of physical and mechanical properties is somewhat different than typical saturated soils. Undrained shear parameters of soil having an unsaturated state are analysed. Moreover, the influences of moisture content and dry density are also observed. The saturation of the specimens ranges from 20%, 40%, 60% and 80%, and the dry density ranges as per standard Proctor density and modified Proctor density of particular soil type. Fredlund's modified Mohr–Coulomb failure envelope is used to evaluate undrained shear parameters of unsaturated soils. The soil matric suction is evaluated using a contact filter paper technique. It is an effort towards how soil compacted fills and slopes have behaved after its construction while they are exposed to the natural environment.

Keywords Unsaturated soils · Shear strength · Matric suction · Moisture content · Density

1 Introduction

There are numerous soil materials encountered in engineering practice whose behaviour is not consistent with the principles and concepts of classical, saturated soil mechanics [1]. The presence of more than one fluid phase, for example, results in material behaviour that is challenging to engineering practice [2]. Unsaturated soils (i.e., water and air in the voids) form the largest category of soils which do not adhere in behaviour to classical saturated soil mechanics [3]. Almost 60% land area on earth is arid or semi-arid region, so that these soils strata are not in fully saturated state [3],

K. Bhadiyadra (✉) · N. Desai
Unique Engineering Testing & Advisory Services, Udhna, Surat 394210, India
e-mail: kjb.fetr@gmail.com

N. Desai
e-mail: nehal@uniquesurat.com

K. N. Sheth
Depaartment of Civil Engineering, Dharmsinh Desai University, Nadiad 387001, India
e-mail: hod.cl@ddu.ac.in

and moreover, conventional soil mechanics considers fully saturated soil condition for shear strength analysis as worst-case condition, but there were some landslides happened while soils are in unsaturated state also (Bharat et al. 2017) [4]. Artificial fills or earthen dam after construction does not remain in the same condition in terms of saturation during its life period. So that we need to analyse the soil condition in an unsaturated state as well to figure out the real-time behaviour of the soil strata out there. Here, CI and CH soils of south Gujarat region are used for the tests regarding evaluation in undrained shear parameters of unsaturated soils. Saturation ranges from 20%, 40%, 60% and 80% to simulate unsaturated state in soil specimen. The test was performed by remoulded soil specimens up to the desired saturation percentage. The densities derived from standard Proctor and modified Proctor test is considered. The physical tests of particular soil type also carried out for the check of the sensitivity of soils.

2 Method

2.1 Material

Two types of soils are collected from two different cities of south Gujarat region in this experiment which is (1) medium plastic clay and (2) high plastic clay from Dahej and Surat cities, respectively. Table 1 presents the physical properties and both Proctor test results, which mentions grain size analysis, Atterberg limits, IS classification, free swell index, specific gravity, standard Proctor test and modified Proctor test results. All of the tests are performed twice.

2.2 Instruments

The instruments used are a mould with a diameter of 100 mm and height 125 mm. There are three sample tubes with a diameter of 28 mm and height 130 mm. Sampler is with a diameter of 28 mm and height 74 mm, and a plunger is with 20 mm thickness and 98 mm the diameter. Hydraulic sample extractor is needed to compress and also extract the sample from the mould [5]. Three-layer measurement tools were also used. The instruments used are different than the universal remoulding tool. This old is used to extract three samples from the same old to get more uniformity in the specimens. Among three samples, two samples are for triaxial UU tests, and one sample is to check for the uniformity of desire density and saturation.

Table 1 Physical properties

Soil property	Dahej	Surat
Gravel %	1.5	5.5
Coarse sand %	1.5	4
Medium sand %	5	2
Fine sand %	22	8.5
Silt + clay (%)	70	79.5
Liquid limit%	40	60
Plastic limit %	18	21
Plasticity index %	22	39
IS classification	CI	CH
Specific gravity gm/cm^3	2.794	2.789
Free swell index %	15	64
S.OMC[a] (standard) %	17.50	20.30
S.MDD[b] (standard) gm/cm^3	1.70	1.60
M.OMC[c] (modified) %	16.82	16.32
M.MDD[d] (modified) gm/cm^3	1.84	1.84

[a]*S.OMC* Standard Proctor test optimum moisture content
[b]*S.MDD* Standard Proctor test maximum dry density
[c]*M.OMC* Modified Proctor test optimum moisture content
[d]*M.MDD* Modified Proctor test maximum dry density

2.3　Experimental Calculations

All the tests are done regarding the Indian Standards. Now, for calculation of saturation moisture content, specific gravity is an important factor, and thus, we determined specific gravity until we get the accuracy to 0.03gm/cm^3. The equations used in determining the saturation and bulk density are mentioned below as Eqs. (1) and (2),

$$\text{M/C} = \frac{S\gamma \text{x} \left(\left(\frac{G}{\rho d} \right) - 1 \right)}{G} \tag{1}$$

$$\rho = \rho d \text{x} \left(1 + \frac{S\gamma}{100} \right) \tag{2}$$

where

M/C　moisture content,
S_γ　saturation percentage,
G　specific gravity,
ρ_d　dry density and
ρ　ulk density.

2.4 Sample Preparation

Now to determine compaction test, we add 10% of moisture in the soil and put it into a desiccator and put the desiccator partly submerged in 27 °C water to let the soil distribute moisture evenly. By doing this, we encountered more accurate results of compaction test, and repetitions also gave the same accurate results. From this experiment, we followed these steps for remoulding the sample also. The remoulding is done in three equal layers and compressed it in the mould hydraulically. After the remoulding, the sample is extracted in three tubes with the help of sample extractor. From the tubes, extracted sample is used to prepare unconfined compressive strength test specimens. The size of the specimen is 38 mm in the diameter and 76 mm in height.

3 Results and Discussion

3.1 Evaluation of SWCC Curves for CI & CH Soils

Soil matric suction is measured having variation in dry density and degree of saturation using contact filter paper technique confirming ASTM 5298–10 [6]. For the achievement of the appropriate density, a sample is cast with three plungers made up of aluminium metal again that does not affect while in contact with soil and water mixture. The plungers are shaped in the manner that can compact soil sample in two layers in PVC moulds. The PVC moulds having 50 mm dia. And 60 cm of height with 10 mm of the freeboard is used. The dimensions of the moulds are so designed that it can accommodate enough soil samples that confirm ASTM 5298–10 [6]. Soil SWCC curves for both the soils then derived to understand unsaturated soil behaviour. All SWCC curves are validated by RETC software for soil water retention developed by Van Genuchten (1994). The relation between dry density, moisture content and soil matric suction can be understood by the following Fig. 1.

3.2 Triaxial UU Test Results of CI and CH Soils

The results of such shear parameters are evaluated as per unsaturated soil mechanics which is somewhat different from conventional saturated soil mechanics. This particular way of shear parameter evaluation from shear testing involves soil matric suction parameter that can impact remarkably in shear strength of soil, especially when the soil sample is unsaturated. In this method, two identical specimens are tested at each dry density having the same moisture content at different confining pressure. Furthermore, for the true shear parameter evaluation, the soil cohesion and angle of internal friction of two consecutive moisture variation of same dry density are taken
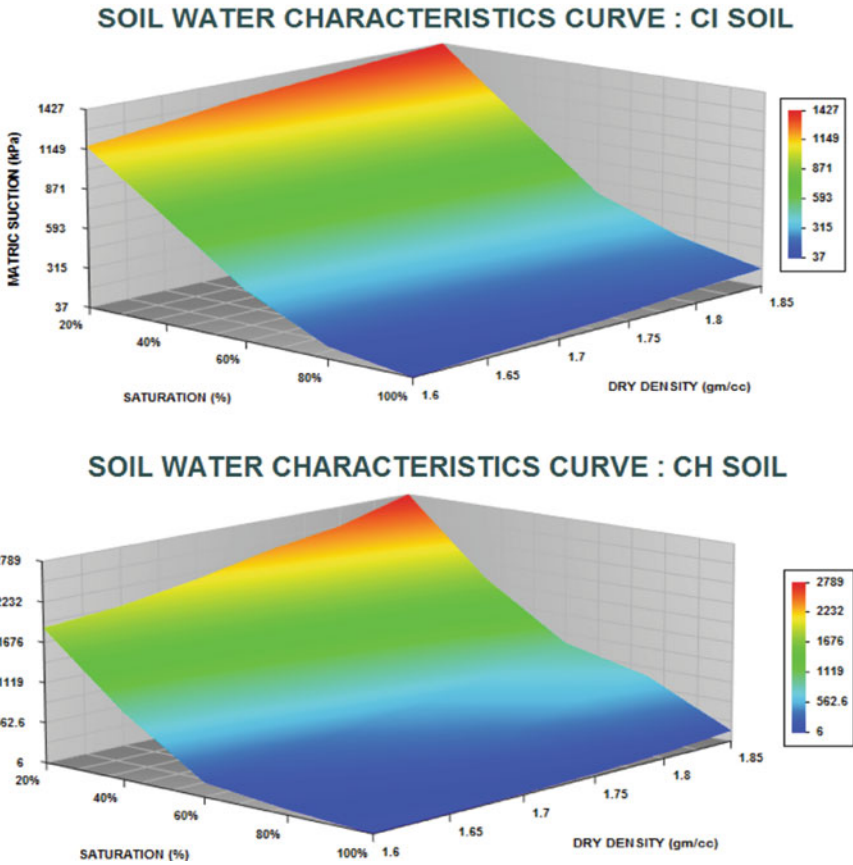
Fig. 1 SWCC curves for CI and CH soils

into account for the determination of true cohesion and the angle which reflects the shear strength due to soil matric suction or negative pore water pressure [7]. So that the results of the shear parameters can be considered as saturation group in particular like 20–40%, 40–60% and 60–80%. It can be evaluated by following the formula of Fredlund's extended Mohr–Coulomb failure envelope,

$$(\sigma_1 - u_a) = (\sigma_3 - u_a).\tan^2(45 + \phi'/2) + 2C_1.\tan(45 + \phi'/2) \qquad (3)$$

$$C'_1 = C' + (u_a - u_w).\tan\phi^b \qquad (4)$$

where.

$\sigma_1 - u_a$ net normal stress state on the failure plane at failure,
$(\sigma_3 - u_a)$ Confining Pressure at failure,

C'_1 Cohesion obtained from the test,
ϕ' Angle of internal friction obtained from the test,
$(u_a - u_w)$ Soil matric suction and.
ϕ^b angle indicating the rate of increase in shear strength concerning a change
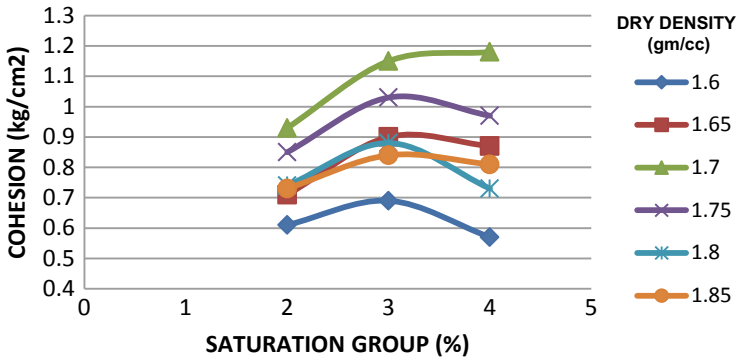   in matric suction.

The considered densities in CI and CH soils are 1.60, 1.65, 1.70, 1.75, 1.80 and 1.85 gm/cm^3 out of which 1.70 gm/cm^3 is standard Proctor test density and 1.85 gm/cm^3 is modified Proctor test density for CI soil and 1.60 gm/cm^3 is standard Proctor test density and 1.85 gm/cm^3 is modified Proctor test density for CH soil. Now, for each density, the saturation moisture content is introduced from 20 to 80% with an interval of 20%. The test results are mentioned in Table 2.

The confining pressure range for two identical specimens for triaxial UU test is 1.0 and 2.0 kg/cm^2, respectively. Two identical specimens having the same density and moisture content are tested, and the results in terms of cohesion, friction angle and the angle contributing soil matric suction are evaluated as per unsaturated soil mechanics using extended Mohr–Coulomb criterion proposed by D. G. Fredlund (Fig. 2).

Now, at standard proctor density, CI soil showed the highest cohesion and that is also got rise as we go the lowest saturation group to the highest saturation group which

Table 2 Evaluated shear parameters of CI and CH soils

γ_d (g/cc)	Sat. group (%)	C (kg/cm^2)		ϕ (°)		ϕ^b(°)	
		CI	CH	CI	CH	CI	CH
1.6	20–40	0.61	0.75	36.04	39.09	6.14	0.12
	40–60	0.69	0.84	35.13	38.82	11.6	0.3
	60–80	0.57	0.87	37.02	38.45	15.6	2.7
1.65	20–40	0.71	0.84	33.58	38.44	2.48	0.18
	40–60	0.9	0.93	32.51	38.07	4.65	0.78
	60–80	0.87	0.98	32.94	37.29	6.26	1.18
1.70	20–40	0.93	0.93	30.04	37.41	0.87	0.47
	40–60	1.15	1.05	29.56	36.43	1.07	0.47
	60–80	1.18	1.08	31.12	35.99	3.95	1.21
1.75	20–40	0.85	1.05	35.09	36.27	0.97	0.11
	40–60	1.03	1.10	33.66	35.85	3.16	0.67
	60–80	0.97	1.03	33.98	35.02	11.13	3.56
1.80	20–40	0.74	1.32	33.64	30.52	4.81	0.39
	40–60	0.88	1.44	35.51	28.13	8.56	0.93
	60–80	0.73	1.27	38.1	27.38	13.02	3.84
1.85	20–40	0.73	1.45	38.1	29.32	2.91	0.21
	40–60	0.84	1.46	36.23	27.78	5.29	1.05
	60–80	0.81	1.33	37.02	23.23	9.63	3.92
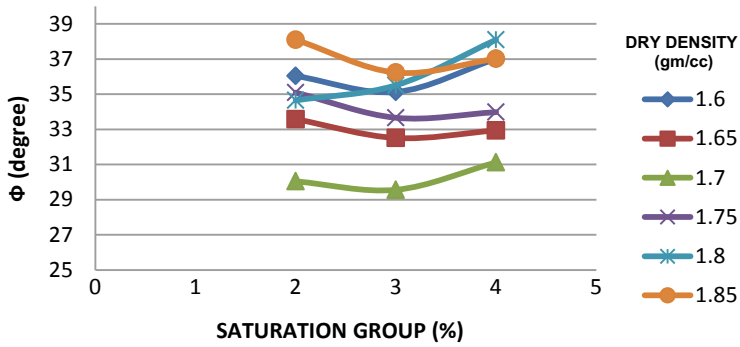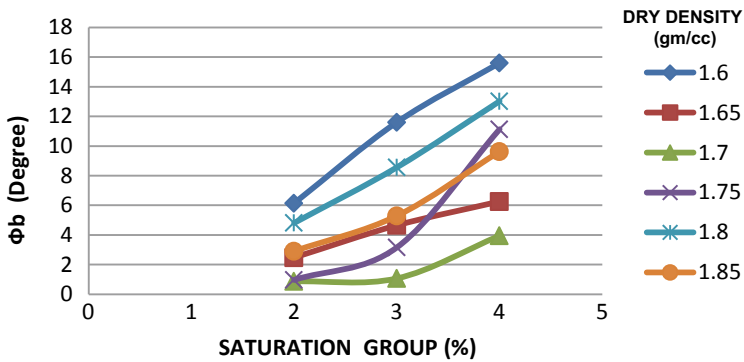
Fig. 2 a Saturation group versus cohesion, b saturation group versus friction angle, c saturation group versus friction angle w.r.t soil matric suction of CI soil

is taken for the evaluation. After standard proctor density cohesion goes down in all saturation groups having some variation within the saturation group in particular. It looks like modified proctor density that the cohesion goes down regarding lesser moisture content due to rise in dry density. When the angle of internal friction is a concern, it shows appropriate results as per the variation of cohesion at each density and saturation group variations. As per figure we can say conventionally that if the soil cohesion is more the angle of friction is less.

Lastly, a very important observation is noted that at the lower saturation group, the Φ^b angle is very less that means at that particular saturation group, the matric suction is the highest; in other words, the negative pore water pressure is more at that particular saturation. On the other hand at higher saturation group, the angle Φ^b got sudden rise because at higher saturation ranges the soil matric suction goes down so is a contribution in ultimate cohesion too. We can say that at fully saturation state, the angle Φ^b can be reported the same as the angle of internal friction and that onwards it may be analysed by conventional saturated soil mechanics (Fig. 3).

Now, at modified proctor density, CH soil showed the highest cohesion, and at 40–60% saturation group and after that, at highest saturation group lower value of cohesion at modified proctor density is reported. After standard proctor density, cohesion got a rise in all saturation groups having some variation within the saturation group in particular. It looks like modified proctor density that the cohesion goes highest regarding lesser moisture content due to rise in dry density. When the angle of internal friction is a concern, it shows appropriate results as per the variation of cohesion at each density and saturation group variations. As per figure we can say conventionally that if the soil cohesion is more, the angle of friction is less.

Observation is noted again in CH or high plastic soil that at the lower saturation group, the Φ^b angle is very less which means that at that particular saturation group, the matric suction is the highest; in other words, the negative pore water pressure is more at that particular saturation. On the other hand at higher saturation group the angle Φ^b got sudden rise because at higher saturation ranges the soil matric suction goes down so is a contribution in ultimate cohesion too. We can say that at fully saturation state, the angle Φ^b can be reported the same as the angle of internal friction and that onwards it may be analysed by conventional soil mechanics.

4 Conclusions

- Starting from the initial stage of evaluation of soil-specific SWCC curves, it is noticed that soil matric suction is depended mainly on chemical property of soil like water retention capacity, cohesion, temperature conditions, etc. It depends on density and saturation conditions as well. It is observed that more the plastic the soil is, more pressure we need to extract water from the soil mass.
- Below standard Proctor density, each soil shows almost the same strength behaviour at different saturations for both types of soils. From the triaxial UU test, it is noticed that CI soil gives maximum cohesion at standard Proctor density,
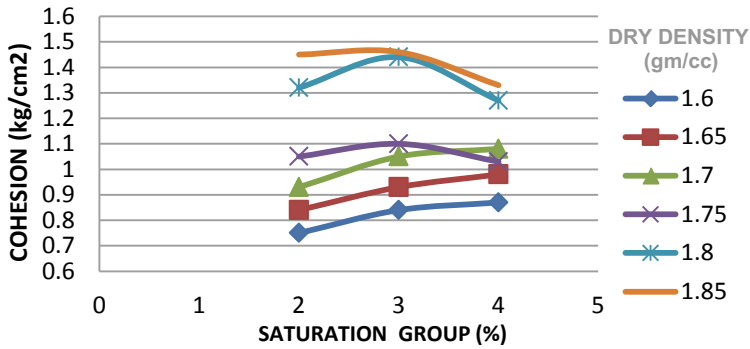
a)

b)
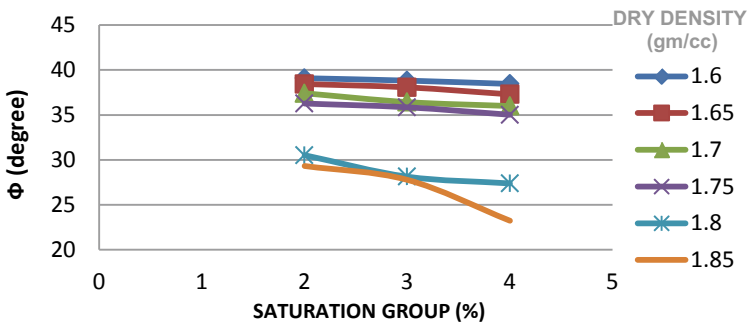
c)

Fig. 3 **a** Saturation group versus cohesion, **b** saturation group versus friction angle, **c** saturation group versus friction angle w.r.t soil matric suction of CH soil

whereas CH soil gives maximum cohesion at modified Proctor density at 40–60% saturation group. On the other hand, bentonite clay shows maximum cohesion after standard proctor density but before of modified Proctor density.
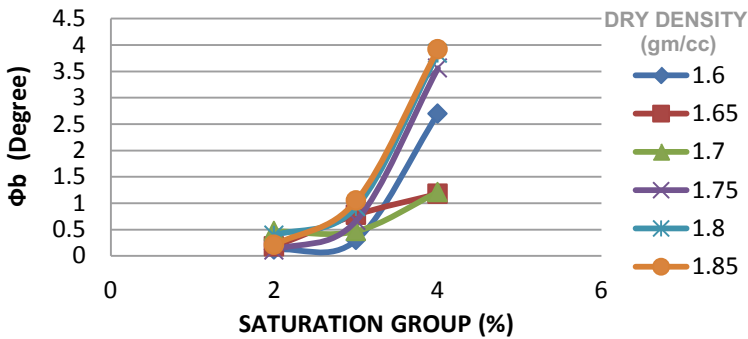
- The most important conclusion is the relation of soil matric suction with soil shear properties. At lower saturation or in negative pore pressure condition, the angle of friction due to matric suction is less which means the contribution of matric suction in true cohesion in that condition is maximum.
- On the other hand with an increase in saturation condition or increase in pore pressure conditions, the Φb angle range have sudden rise up to 15° from almost 1.0° results lesser contribution in actual shear strength conditions. And ultimately at fully saturation conditions, the angle that represents strength contribution due to matric suction (Φ^b) is equal to ϕ

References

1. Vanapalli, S.K.: Shear strength of unsaturated soils and its applications in geotechnical engineering practice. In: 4th Asia Pacific Conference on Unsaturated Soils, pp. 579–598 (2009)
2. Vanapalli, S.K., Pufahl, D.E., Fredlund, D.G.: Interpretation of the shear strength of unsaturated soils in undrained Loading condition. In: 52nd Canadian Geotechnical Conference, Regina, Saskatchewan, pp. 643–650 (1999)
3. Fredlund, D.G.: Use of soil-water characteristic curve in the implementation of unsaturated soil mechanics. Third In. Conf. Unsaturated Soils, Recife, Brazil **3**, 10–13 (2002)
4. Choudhury, C., Bharat, T.V.: Soil-water characteristic curve models for clays. In: Proceedings of Indian Geotechnical Conference IGC-2014 (Vol. c) (2014)
5. Shah, D., et al.: Experimental UCS of black cotton soil for Navsari and surat cities. In: Conference on Engineering and Technology: Smart Engineering (2018)
6. Astm-5298–10.: Standard test method for measurement of soil potential (suction using filter paper). ASTM Int. 1–6 (2010)
7. Fredlund, D.G., Rahardjo.: Unsaturated Soil Mechanics in Engineering Practice. Wiley (2012)

Reliability Analysis of Retaining Wall Using Artificial Neural Network (ANN) and Adaptive Neuro-Fuzzy Inference System (ANFIS)

Pratishtha Mishra and Pijush Samui

Abstract Reliability of geotechnical structures is the main concern of geotechnical engineers as is clear from previous studies and evaluations. It also helps us to determine the probability of failure. First-order second-moment method (FOSM) helps us to determine the reliability index of geo-structure. This study employs an artificial neural network (ANN) and adaptive neuro-fuzzy inference system (ANFIS) for determination of reliability index of retaining wall based on sliding criterion. ANN has played a vital role in the field of geotechnical engineering as it has reduced cumbersome calculations and has increased the precision of result. The strong nonlinear relationship between the known random variables and unknown output or result is mapped easily by using ANN. ANN also ascertains the result by removing the uncertainties involved in the problem. ANFIS is an ANN system which uses fuzzy logic in contemplating the data. It works on removing the fuzziness of the values entered (random variables) and gives more realistic values of the output as compared to other approaches. This study adopts ANN and ANFIS as regression techniques. The performance of ANN and ANFIS has been assessed based on different parameters such as coefficient of correlation, root mean square error, and mean absolute error. A comparative study has been presented between the FOSM, ANN-based FOSM, and ANFIS FOSM models. Therefore, this study concludes that ANN and ANFIS is a better alternative to solve for the reliability of the retaining wall.

Keywords Retaining wall · Reliability index · ANN · ANFIS

1 Introduction

Retaining wall, a geotechnical structure is of sheer importance for the stability of slopes. From geotechnical learning and rapid advancements, it is known that slopes

P. Mishra (✉) · P. Samui
Department of Civil Engineering, National Institute of Technology Patna, Patna 800005, India
e-mail: pratishthamishra22@gmail.com

P. Samui
e-mail: pijushsamui@gmail.com

fail due to different mechanisms. For instance, slopes suffer rotational failure, translational failure, compound failure, wedge failure, and other failures in the form of flows and spreads. Many remedial measures are followed to avoid the failure of the slope and construction of retaining wall is among one of the remedies. For the construction of a retaining wall, the soil parameters that influence the bearing capacity of the soil along with the earth pressure are evaluated. Primitive parameters that define the failure are cohesion intercept, angle of shearing resistance, unit weight, and angle of wall friction. Considering these parameters, the factor of safety is calculated. Also, to measure the ability to meet requirements under a specified period of time, reliability analysis is performed. For reliability analysis, first-order second-moment method (FOSM) is widely used, but this technique is quite a time consuming [1, 2]. This problem has been remedied by the researchers by using certain other methods such as response surface method [3, 4], multiple tangent plane surface [5], and multi-plane surfaces method which are used to solve the ambiguities of nonlinear limit state surface. But these approaches are limited to nonlinear convex or concave surfaces only. This article performed reliability analysis of retaining wall by using artificial neural network (ANN) [6, 7] and adaptive neuro-fuzzy inference system (ANFIS). ANN has made progress in many fields like in medical, geotechnical, defense, etc. Applications of ANN in geotechnical engineering are prediction of pile capacity, settlement of foundation, soil properties and behavior, characterization of site, determination of liquefaction potential, evaluation of stability of slopes, and prediction of settlement of underground structures such as tunnels and estimation of maximum deflection of earth retaining structures [8]. ANFIS has also covered many areas of geotechnical engineering, for example, applications employed in triaxial testing, resonant column testing, and liquefaction triggering. ANN and ANFIS amalgamates the different probabilities of occurring of events and pops up with accurate results considering all the possibilities as these are trained with set of data which when tested bring in modified correct output. The predicted values of the output are further used for reliability analysis. In this paper, the backpropagation technique is employed in ANN and clustering technique in ANFIS. Also, the reliability index of the results generated from both ANN and ANFIS is calculated and compared thereafter.

2 Artificial Neural Network (ANN) Model

Artificial intelligence has left a major mark in the computing field and other fields as well. ANN is a branch of artificial intelligence or precisely machine learning. Neural network is a representation of the human neural system. Networks here are defined using three components—transfer function, architecture of network, and learning law. These components depend upon the type of problem to be solved. Using this algorithm, the machine can be trained to give appropriate result by changing the weights given to the inputs and using certain formulations. One of the renowned neural networks is the backpropagation network. Although there are several other algorithms as well, but backpropagation (in ANN) [9, 10] is most versatile and robust

among all. Backpropagation is a concept of machine learning that works on reducing the cost function. After giving the first result and comparing it using the cost function, mechanism propagates backward changing the weight factors, and thereby bringing the change in the result until and unless it reduces the cost function resulting in accurate result. Neural networks train and test data like a human mind does. Mainly, backpropagation's objective is to change or reduce the error in a quick response of time. Also, it uses partial derivative of cost function for all the weights individually. Cost function (Eq. 1) is nothing but root mean squared error (RMSE).

$$C = \frac{\sum |y(x) - a|^2}{2n}$$ (1)

Here C is the cost function, x is the input from the training set, $y(x)$ is the observed output, n is the total number of input training set, and a is the output from the model. Cost function is minimized in order to get results up to the mark.

Backpropagation works in two phases. First phase is propagation in which setting and initialization of weights take place. Input is worked upon to generate proper output. Errors are calculated and then output is propagated back in the neural system to generate errors in the output and hidden MLPs. Second phase is concerned with updating weights of connections. In this phase, the calculation of the gradient of the weight is performed and certain percentage of this gradient (based on the learning) is subtracted from the weight. Each work of this technique is done in the hidden neuron layers where different compositions of inputs with different weights are taken. A network can have many hidden neurons in accordance with the need of the problem. The backpropagation technique is shown in Fig. 1. It can be seen that a primary level neural network has one input layer, at least one hidden layer (there can be many depending upon the complexity of the input), and one output layer, and all the connections are given particular weight. The hidden layers are also called perceptron which behave like human neurons. These can be contained in large number in a network to bifurcate large inputs into different possibilities. These multi-layer perceptrons (MLPs) are trained to give unbiased and learned results and these are highly capable
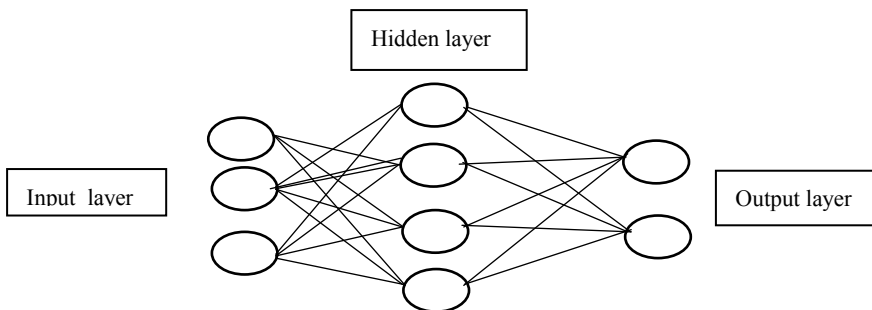

Fig. 1 ANN three-layer network

of data mapping. The weights of the connections are altered accordingly depending upon the error and weight gradient.

This model is fed with four inputs required for calculating the factor of safety of the retaining wall based on sliding criteria, i.e., are cohesion intercept (c), angle of shearing resistance (φ), angle of wall friction, (δ) unit weight (γ), and corresponding output to train the data. We have total 80 data out of which 70% is taken for training model and 30% is used for testing.

3 Adaptive Neuro-Fuzzy Interference System (ANFIS) Model

Role and perfection of ANN model are already explained in the previous section, but a shortcoming of the ANN model is the complexity of the connection weights of MLPs which cannot be deciphered. Therefore, the rules defining the relation between input and output variable are difficult to quantify. To overcome this drawback, neuro-fuzzy models are used. These models are trained to provide data mappings. Also, it extracts knowledge about the relationship between model input and corresponding output data. ANFIS has removed the drawbacks of the other models in use and has provided us with accurate results comparatively. Advancement in modeling techniques has led to soft computing, artificial intelligence, and fuzzy modeling system. ANFIS is a hybrid technique based on understanding of the researchers. Fuzzy logic works on 'if-then' rules to establish a qualitative relation between input and output variables, and it is a heuristic approach. Concept of clustering is used to resolve the problem. This approach is based on forming the unsupervised group of input and output data based on their similarities and dissimilarities. Neuro-fuzzy networks employ fuzzy conditional statement, i.e., if-then rule. For instance, **If U then V** where U and V are labels of unsupervised fuzzy set. This rule makes us aware of contribution of set of inputs to the output. All the fuzzy logic systems have two components: sets and rules. To determine fuzzy sets, linguistic terms are interpreted mathematically as membership functions and variables in the model are fuzzified to be fractional or partial members of the membership functions in the interval of (0,1). For each and every variable, fuzzy sets overlap and necessary range of variation are covered, and this process is called fuzzification. Now, as the output of the fuzzified input is fuzzified too, therefore, defuzzification algorithm such as the mean of maxima and center of gravity is applied to get real-valued outputs.

Fuzzy interference system is also known as fuzzy rule-based system, fuzzy associative memories, fuzzy models, or fuzzy controllers. This system is made of five blocks:

- *Rule base* (consists of neuro-fuzzy if-then rules)
- *Dataset* (defines membership functions of fuzzy sets used in the neuro-fuzzy rules)
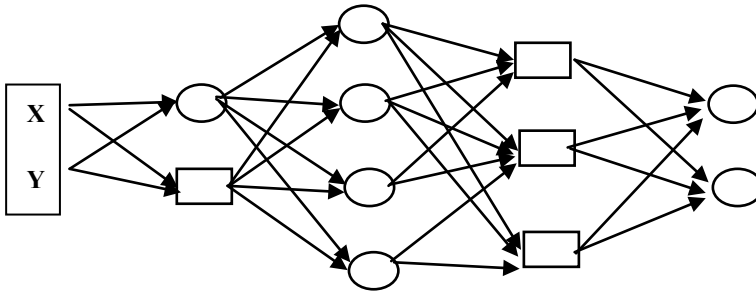- *Decision-making unit* (performs interference operation on rules)

Fig. 2 Adaptive network

- *Fuzzification interface* (converts real-valued inputs into degree of match with linguistic values)
- *Defuzzification interface* (converts fuzzified output into real value output)

Rule base and database are collectively referred to as *knowledge base*. Neuro-fuzzy system enhances the generalization capacity of the network, i.e., when data inputted is beyond the training dataset, networks inbuilt learning program helps it to extrapolate the result and revert back an appropriate result based on the learning. Learning process is knowledge-based but data driven. Being adaptive of the system explains the dependency of nodes to the linked parameters. It supports the learning rule which minimizes the errors by making changes in the linked parameters. Figure 2 shows an adaptive network.

This model was fed with the same variables as in ANN with 70-30% bifurcation of data for training and testing, respectively. Also, certain values are calculated which ascertain the model behavior and its accuracy in producing result. These values compare the results from both the models.

4   Model Performance Assessment and Reliability Index

Reliability index was calculated using first-order second-moment method which gave us the probability of failure of the retaining wall which is showed using reliability index 'β'. Deducing this value gives an overview of the structural reliability. And as it is a statistical value based on number of variations, when used for different models, function of model and accuracy of its prediction become understandable. This particular value along with other values predicts the failure probability of a model and the perfection of the model. As in this paper, the problem is modeled using ANN and ANFIS, and values measuring their extent of perfection are given as follows:

1.   Nash–Sutcliffe efficiency (NS) [11] indicates the predictive power of the models. More the NS value closer to 1 more is predictive power.

$$NS = 1 - \frac{\sum_{i=1}^{n}(d_i - y_i)^2}{\sum_{i=1}^{n}(d_i - d_{\text{mean}})^2} \tag{2}$$

2. Root mean square error (RMSE) [12] value closer or equal to 0 indicates that the error in prediction is less.

$$RMSE = \sqrt{\frac{1}{N}\sum_{i=1}^{n}(d_i - y_i)^2} \tag{3}$$

3. Variance account factor (VAF) [13, 14] value equal to 100% shows model performance gives good result.

$$VAF = \left(1 - \frac{\text{var}(d_i - y_i)}{\text{var}(d_i)}\right) \times 100 \tag{4}$$

4. R^2 (coefficient of determination) and Adj. R^2 (adjusted determination coefficient) [15] values should be closer to 1 and also closer to each other shows that the model used most of the variability in soil parameters.

$$R^2 = \frac{\sum_{i=1}^{n}(d_i - d_{\text{mean}})^2 - \sum_{i=1}^{n}(d_i - y_i)^2}{\sum_{i=1}^{n}(d_i - d_{\text{mean}})^2} \tag{5}$$

$$Adj\ R^2 = 1 - \frac{(n-1)}{(n-p-1)}\left(1 - R^2\right) \tag{6}$$

5. Performance index (PI) [16] indicates the performance of the models.

$$PI = adj.R^2 + 0.01\ VAF - RMSE \tag{7}$$

6. Bias factor is a factor whose value more than unity represents the overestimated model, value of less than unity represents an underestimation model, and a value of unity indicates a prediction, which is unbiased [17].

$$\text{Bias Factor} = \frac{1}{N}\sum_{i=1}^{n}\frac{y_i}{d_i} \tag{8}$$

7. Root mean square error to observation's standard deviation ratio (RSR) [18] has the benefit of error index statistics. More the value closer to 0 more the prediction power.

$$RSR = \frac{RMSE}{\sqrt{\frac{1}{N}\sum_{i=1}^{n}(d_i - d_{\text{mean}})^2}} \tag{9}$$

8. Normalized mean bias error (NMBE) calculates the model's ability to predict a value which is away from the mean value. NMBE equal to 0 indicates perfect model [19].

$$\text{NMBE}(\%) = \frac{\frac{1}{N}\sum_{i=1}^{n}(y_i - d_i)}{\frac{1}{N}\sum_{i=1}^{n}d_i} \times 100 \tag{10}$$

9. Mean absolute percentage error (MAPE) [20] value closer to 0 shows high prediction accuracy.

$$\text{MAPE} = \frac{1}{N}\sum_{i=1}^{n}\left|\frac{d_i - y_i}{d_i}\right| \tag{11}$$

10. Relative percentage difference (RPD) [21] is given in Eq. (13)

$$\text{RPD} = \frac{\text{SD}}{\text{RMSE}} \tag{12}$$

11. Willmott's index of agreement (WI) shows the degree of model prediction error. WI range is from 0 to 1 and WI = 1 shows perfect model [22, 23].

$$\text{WI} = 1 - \left[\frac{\sum_{i=1}^{N}(d_i - y_i)^2}{\sum_{i=1}^{N}(|y_i - d_{\text{mean}}| + |d_i - d_{\text{mean}}|)^2}\right] \tag{13}$$

12. Mean bias error (MBE) and mean absolute error (MAE) values closer to 0 show lesser error in prediction [24].

$$\text{MBE} = \frac{1}{N}\sum_{i=1}^{n}(y_i - d_i) \tag{14}$$

$$\text{MAE} = \frac{1}{N}\sum_{i=1}^{n}|(y_i - d_i)| \tag{15}$$

13. The range of Legate and McCabe's index (LMI) is ($-\infty$, 1) [25, 26]. Values closer to 1 represent a perfect model. The lesser the value, the more is divergence between observed and predicted values.

$$\text{LMI} = 1 - \left[\frac{\sum_{i=1}^{N}|d_i - y_i|}{\sum_{i=1}^{N}|d_i - d_{\text{mean}}|}\right] \tag{16}$$

14. Expanded uncertainty (U_{95}) indicates the short-term performance of the model. Smaller the value high the performance of model [27].

$$U_{95} = 1.96(\text{SD}^2 + \text{RMSE}^2)^{1/2} \qquad (17)$$

15. t-statistic smaller value indicates the superior performance of model [28].

$$t \text{ - stat} = \sqrt{\frac{(N-1)\text{MBE}^2}{\text{RMSE}^2 - \text{MBE}^2}} \qquad (18)$$

16. Global performance indicator (GPI) uses all the parameters to analyze model in a single parameter. Higher the value of GPI, higher is the accuracy of model.

$$\text{GPI} = \text{MBE} \times \text{RMSE} \times U_{95} \times t_{\text{stat}} \times \left(1 - R^2\right) \qquad (19)$$

17. Reliability index (β) is a parameter to check the reliability of the model. It is calculated using FOSM. Value of reliability index between 3 and 4 indicates good performance of model [29].

$$\beta = \frac{\mu - 1}{\sigma} \qquad (20)$$

Here, d_i and y_i are the observed and predicted ith value, respectively, d_{mean} is the average of observed value, SD is the standard deviation, σ is the standard deviation, and μ is the mean of the dataset generated. n is the number of training or testing samples and p is the model input quantity.

5 Result and discussion

All the models are analyzed on the basis of various parameters (Table 1) VAF, RMSE, R^2, Adj. R^2, MAE, PI, RSR, NS, the bias factor, LMI, NMBE, RPD, MAPE, U95, t-statistic, GPI, and β.

From the observation, Table 2, it is visible that ANFIS is a better model than ANN but with less deviation of assessment values from the desired values for instance bias

Table 1 RPD values for evaluating models

RPD	Model type
<1	Very poor models
1.0–1.4	Poor models
1.4–1.8	Fair models
1.8–2.0	Good models
2.0–2.5	Very good models
>2.5	Excellent models

Table 2 Performance assessment using various parameters of both the models ANN and ANFIS

S. No.	Assessment values	ANN (training)	ANN (testing)	ANFIS (training)	ANFIS (testing)
1.	WMAPE	0.0077	0.0201	8.83E-05	0.0224
2.	NS	0.9992	0.989	1	0.9832
3.	RMSE	0.0301	0.0722	0.0004	0.0894
4.	VAF	99.942	99.285	100	98.615
5.	R^2	0.9992	0.989	1	0.9832
6.	AdjR^2	0.9992	0.9867	1	0.9797
7.	PI	1.9685	1.9074	1.9996	1.8764
8.	RMSD	0.0301	0.0722	0.0004	0.0894
9.	Bias factor	0.9947	0.9831	1	0.9819
10.	RSR	0.028	0.1047	0.0004	0.1296
11.	NMBE	-0.5659	-1.739	0.0009	-1.53
12.	MAPE	0.021	0.0492	0.0002	0.0551
13.	RPD	0.8573	0.8073	0.9978	0.9078
14.	WI	0.9998	0.9972	1	0.9959
15.	MAE	0.021	0.0492	0.0002	0.0551
16.	MBE	-0.0155	-0.043	2.53E-05	-0.037
17.	LMI	0.9764	0.9096	0.9997	0.8988
18.	U_{95}	0.0776	0.1819	0.001	0.2366
19.	t-stat	4.4526	3.5057	0.4982	2.216
20.	GPI	-1.26E-07	-2.15E-05	6.16E-19	-2.95E-05
21.	β	1.6134	2.0884	1.6174	1.9751

factor is almost 1 in the ANFIS model and this predicts that model is neither overestimated nor underestimated. Also, RSR is almost zero in ANFIS which is as desired out of the model. RPD value is less than 1 in ANN which makes ANFIS comparatively better than ANN in performance. Also, MAE and MBE when calculated give result in the favor of ANFIS, but ANN shares the same range, i.e., its value is near to zero. There are other variables for which values are not distinct for both the models, but ANFIS has an upper hand, therefore, it is suggested to use ANFIS above ANN. But it is observed that the training data model is more appropriate as compared to that of testing in case of ANFIS, as there is ample amount of input in training model (70%), therefore, we can conclude that adaptive networks work good with fuzzy logic in wide range of data. Also, if value of reliability index is compared with the reliability index value of observed dataset (1.6174 for 70% observed data and 2.103 for 30% observed data), it is observed that both models data almost coincide the observed dataset. Overall assessment concludes that ANFIS is better to work with if wide range of data is to be worked upon, but ANN cannot be discarded as a model because it works equally well for both training and testing models.
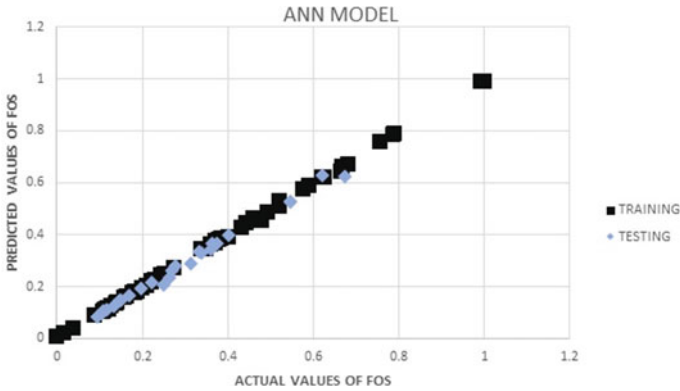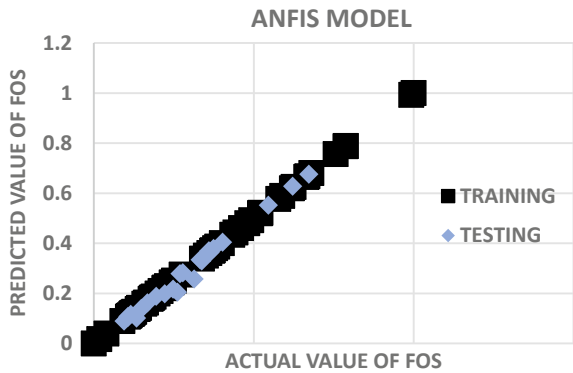
Fig. 3 Actual values versus. predicted values of FOS using ANN model

Fig. 4 Actual values versus predicted values of FOS using ANFIS model

   Figures 3 and 4 show the plot of predicted values against actual or observed values of both training and testing data using ANN and ANFIS model. It is observed that data points coincide each other and there is not much difference in the result. Therefore, it can be concluded that these models prediction power is high. But when they are examined with other parameters, the overall assessment shows that ANFIS model is better than the ANN model.

5.1 AOC-REC Curve

Regression error characteristics curve (REC) [30] is a probability curve and a metric system to check the performance of regression model. Area over curve (AOC) is the measure of distinction of predicted data of the model from the actual data.

   From the AOC value, it is clear that due to less value of AOC of ANFIS training model, and it proves to be a better model as compared to the other models. Also, it

Table 3 Area over REC plot value for ANN and ANFIS models.

Models	AOC
ANN (training)	0.0200
ANFIS (training)	2.2721e-04
ANN (testing)	0.0449
ANFIS (testing)	0.0498

is observed that AOC value of ANN testing model is less than ANFIS testing model, and it is already mentioned in sections above that fuzziness works good with wide range of data.

5.2 Taylor Diagram

Taylor diagram [31] is the graphical representation of how closely the pattern (or patterns) matches observation which is quantified in terms of **correlation**, **root mean square error,** and **amplitude of their variations (standard deviations)**. This diagram evaluates the aspects of different complex models and performs a comparative analysis of these models with the reference data (self-observed data) (Table 3).
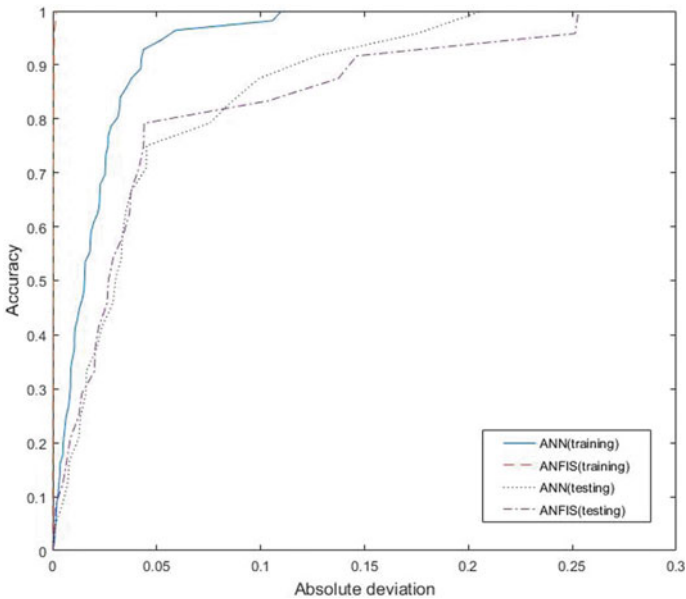

Fig. 5 REC curve plot for ANN and ANFIS (training dataset)

Figure 6 shows that both models lie near to the observed value and deviation is quite less. Therefore, both these models have a good performance and overall experimentation shows that there is a good agreement between the predicted values generated from the models and actual values calculated.

Figure 7 is the plot of Fp/Fm against cumulative probability for both ANN and ANFIS model, respectively. From Fig. 7, the result can be extracted that for ANFIS(training) at P_{50}, value of Fp/Fm is near to 1, i.e., for training set, value of Fp/Fm is 1.0000, and for testing set, value is 0.9916, whereas, for ANN model at P_{50}
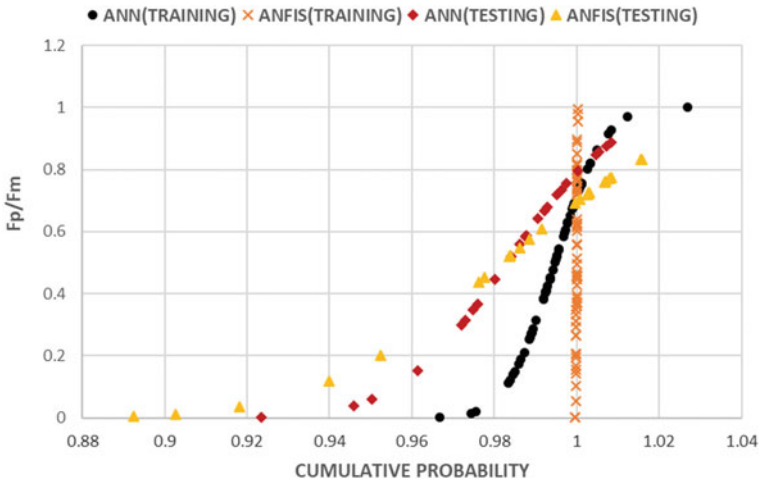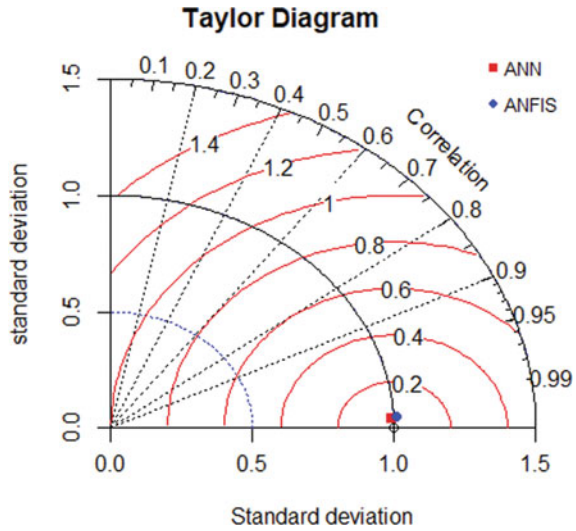
Fig 6 Taylor diagram for ANN and ANFIS

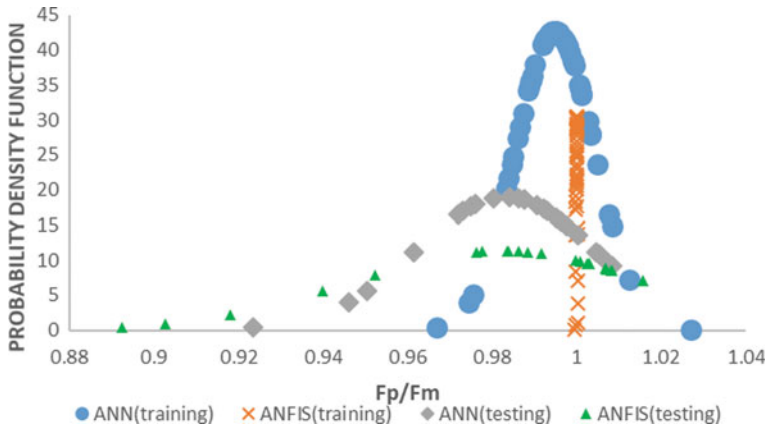**Fig. 7** Cumulative probability plot for Fp/Fm for ANN and ANFIS models

Fig. 8 Lognormal distribution for Fp/Fm for ANN and ANFIS for training and testing data

Fp/Fm is 0.9950, and 0.9876 for training and testing datasets, respectively. There-fore, ANFIS observation is comparable to ANN, but due to slight change and less deviation from the value 1, ANFIS acts as a better model. But when P_{90} is checked for, it is seen that all the values of all the models are almost one. Therefore, both these models stand a good chance, but ANFIS has already proven to be a better model. Figure 8 is the plot of probability density function against Fp/Fm for both ANN and ANFIS training and testing dataset. This plot is lognormal distribution for Fp/Fm, and from this plot, it is observed that ANFIS functions better in training period than ANN as probability of FOS within 20% accuracy level is concerned under lognormal distribution, and it is clear from Fig. 8 that most of the points lie in the region that is under 20% accuracy level, and also it is visible that for ANN there is deviation of graph from 1. Therefore, ANFIS is better than ANN. But for testing dataset, both ANN and ANFIS show the same accuracy levels.

6 Conclusion

In this paper, the reliability index of the retaining wall with c, φ, γ, and δ as input parameters along with other performance assessment values were calculated for ANN and ANFIS models. Both these models were compared with different parameters and both of them showed equal efficiency. Also, their results almost converged to the same value. But ANFIS with wide range of data outperformed as fuzziness works good with ample data. 70 % of total data was used for training and 30% for testing, therefore, in training dataset, modeling ANFIS performed better, but for testing dataset, both ANN and ANFIS performed equally well converging to same result or just say FOS value 1. Therefore, both these models can be used as soft computing technique for computing the factor of safety as testing model does and then calculating the reliability of the

retaining wall. With collective observations, ANFIS can be concluded as the better model among both.

References

1. Wu, T.H., Leland, M.K.: Safety analysis of slopes. J. Soil Mech. Foundat. Div. 609–632 (1970)
2. Cornell, C.A.: First-order uncertainty analysis of soils deformation and stability. In: Proceedings of the 1st International Conference on Application of Probability and Statistics in Soil and Structural Engineering (ICAPI), pp. 129–144, Hong Kong (1971)
3. Wong, F.S.: Slope reliability and response surface method. J. Geotech. Eng. Div. ASCE **111**(1), 32–53 (1985)
4. Faravelli, L.: Response-surface approach for reliability analysis. J. Eng. Mech. **115**(12), 2763–2781 (1989)
5. Guan, X.L., Melchers, R.E.: Multitangent-plane surface method for reliability calculation. J. Eng. Mech. **123**(10), 996–1002 (1997)
6. Gomes, H.M., Armando M.A.: Comparison of response surface and neural network with other methods for structural reliability analysis. Struct. Safety **26**(1), 49–67 (2004)
7. Deng, J., et al.: Structural reliability analysis for implicit performance functions using artificial neural network. Struct. Safety **27**(1), 25–48 (2005)
8. Shahin, M.A., Mark B.J., Holger R.M.: Artificial neural network applications in geotechnical engineering. Australian Geomech. **36**(1), 49–62 (2001)
9. Saravanan, K., Sasithra, S.: Review on classification based on artificial neural networks. Int. J. Ambient Syst. Appl. (IJASA) **2**(4) (2014)
10. Kandel, E.R., Schwartz, J.H., Jessell, T.M. (eds.).: Principles of Neural Science, vol. 4, pp. 1227–1246. McGraw-hill, New York (2000)
11. Jain, S.K., Sudheer, K.P.: Fitting of hydrologic models: a close look at the Nash–Sutcliffe index. J. Hydrol. Eng. **13**(10), 981–986 (2008)
12. Kisi, O., Shiri, J., & Tombul, M.: Modeling rainfall-runoff process using soft computing techniques. Comput. Geosci. **51**, 108-117 (2008)
13. Grima, M.A., Babuška, R.: Fuzzy model for the prediction of unconfined compressive strength of rock samples. Int. J. Rock Mech. Mining Sci. **36**(3), 339–349 (1999)
14. Gokceoglu, C.: A fuzzy triangular chart to predict the uniaxial compressive strength of the Ankara agglomerates from their petrographic composition. Eng. Geol. **66**(1–2), 39–51 (2002)
15. Babu, G., Sivakumar, L., Amit, S.: Reliability analysis of allowable pressure on shallow foundation using response surface method. Comput. Geotech. **34**(3), 187–194 (2007)
16. Kung, G.T., et al.: Simplified model for wall deflection and ground-surface settlement caused by braced excavation in clays. J. Geotech. Geoenviron. Eng. **133**(6), 731–747 (2007)
17. Prasomphan, S., Shigeru, M.: Generating prediction map for geostatistical data based on an adaptive neural network using only nearest neighbors. Int. J. Mach. Learn. Comput. **3**(1), 98 (2013)
18. Moriasi, D.N., et al.: Model evaluation guidelines for systematic quantification of accuracy in watershed simulations. Trans. ASABE **50**(3), 885–900 (2007)
19. Srinivasulu, S., Ashu, J.: A comparative analysis of training methods for artificial neural network rainfall–runoff models. Appl. Soft Comput. **6**(3), 295–306 (2006)
20. Armstrong, J.S., Fred C.: Error measures for generalizing about forecasting methods: empirical comparisons. Int. J. Forecast. **8**(1), 69–80 (1992)
21. Rossel, R.A., Viscarra, R.N., McGlynn, A., McBratney, B.: Determining the composition of mineral-organic mixes using UV–vis–NIR diffuse reflectance spectroscopy. Geoderma **137**(1–2), 70–82 (2006)
22. Willmott, Cort J.: On the validation of models. Phys. Geogra. **2**(2), 184–194 (1981)

23. Willmott, Cort J.: Some comments on the evaluation of model performance. Bull. American Meteorol. Soc. **63**(11), 1309–1313 (1982)
24. Raventos-Duran, T., et al.: Structure-activity relationships to estimate the effective Henry's law constants of organics of atmospheric interest. Atmosph. Chem. Phys. **10**(16), 7643–7654 (2010)
25. Legates, D.R., Robert E.D.: The continuing search for an anthropogenic climate change signal: Limitations of correlation-based approaches. Geophys. Res. Lett. **24**(18), 2319–2322 (1997)
26. Legates, D.R., McCabe, G.J.: Evaluating the use of "goodness-of-fit" measures in hydrologic and hydroclimatic model validation. Water Res. Res. **35**(1), 233–241 (1999)
27. Gueymard, Christian A.: A review of validation methodologies and statistical performance indicators for modeled solar radiation data: towards a better bankability of solar projects. Renew. Sustainable Energy Rev. **39**, 1024–1034 (2014)
28. Stone, R.J.: Improved statistical procedure for the evaluation of solar radiation estimation models. Solar energy **51**(4), 289–291 (1993)
29. USACE Risk-Based Analysis in Geotechnical Engineering for Support of Planning Studies, Engineering And Design. Dept Army, USACE Washington, DC ll, (1999)
30. Fawcett, T.: An introduction to ROC analysis. Patt. Recogn. Lett. **27**(8), 861–874 (2006)
31. Taylor, Karl E.: Summarizing multiple aspects of model performance in a single diagram. J. Geophys. Res. Atmosp. **106**(D7), 7183–7192 (2001)

Hyperspectral Image Classification Using Semi-supervised Deep Learning Strategies

Sourish Gunesh Dhekane, Shivam Tiwari, and Manan Sharma

Abstract Recent development in deep learning (DL) methodologies has shown promising results on various computer vision tasks including the classification of hyperspectral data. However, these methodologies are expected to suffer in the presence of lack of training data, due to complex network architecture and a large number of parameters. In this paper, various K-means-based clustering techniques are explored to generate pseudo-labels to facilitate the training of deep networks. To tackle the curse of dimensionality, an auto-encoder (AE)-based dimensionality reduction method is employed. Finally, the classification is done using convolutional long short-term memory cells (ConvLSTM) which outperforms the rest of the deep neural networks used. In addition, an analysis of the effect of the proposed dimensionality reduction method on classification accuracy is presented. The efficacy of the proposed approach is demonstrated on two real-world hyperspectral image datasets namely the "University of Pavia" (UP) and "Salinas".

Keywords Hyperspectral image classification · Semi-supervised learning · Auto-encoder · Convolutional long short-term memory cells

1 Introduction

A hyperspectral image can be denoted by a three-dimensional tensor (a, b, λ), where a and b denote the spatial coordinates and λ denotes the wavelength associated with the spectral bands. One of the key aspects of hyperspectral images is the presence of these large number of narrow, contiguous spectral bands [1] containing vast amount of information. This information can be used in various remote sensing applications like

S. G. Dhekane · S. Tiwari (✉) · M. Sharma
Indian Institute of Information Technology Guwahati, Guwahati, India
e-mail: shivam21ballia@gmail.com

S. G. Dhekane
e-mail: sourishdhekane@gmail.com

M. Sharma
e-mail: manansharma858@gmail.com

land cover classification [2], crop protection and analysis [3], and mineral detection [4]. In most of the applications, the task of classifying pixels of a hyperspectral image plays a key role. However, there are a number of challenges associated with this task. One of the biggest challenges is the lack of correctly labeled pixels (ground truth knowledge), which directly affects the quality of classification maps [5]. Also, the shortage of labeled pixels results in relatively less amount of training data compared to the spectral dimensions of the hyperspectral image. This introduces the curse of dimensionality in this application. Also, it has been observed that for a constant set of training data, and the classification performance increases with increase in distinctive features (dimensions) until an optimal number is reached [6]. As this optimal number is crossed, the performance of the classifier starts to degrade which is exactly what happens in case of this problem statement. The spectral dimensions of the hyperspectral image are large in number as well as redundant in nature. Hence, the extracting idiosyncratic features from the raw input data in order to reduce the dimensionality plays an important role in the classification task.

In recent years, due to the availability of massive amounts of data and the improvement in computational resources, deep learning [7]-based methodologies are gaining success in various computer vision applications like image classification [8], semantic segmentation [9], and estimation in generative models [10]. In the case of classification of hyperspectral images in a supervised scenario, Roy et al. [11] have achieved the state-of-the-art results using a hybrid spectral convolutional neural network (HybridSN). However, the same task in a semi-supervised scenario demands some modifications in the deep learning methodologies due to the aforementioned challenges. To incorporate these modifications, Liu et al. [12] proposed a semi-supervised convolutional neural network (CNN) containing skip connection parameters between encoder and decoder layer. On similar grounds, a semi-supervised ladder network [13] was proposed that jointly optimized a supervised as well as an unsupervised cost. In another work, Pan et al. proposed a multi-grained network (MugNet) [14] based on a multi-grained scanning approach where kernels are generated in a semi-supervised way. These approaches try to modify either the network architecture with its associated operations or the optimization problem. However, a relatively simple approach to deal with the scarcity of labeled samples is to generate pseudo-labels using a clustering approach on the abundant unlabeled data and a few available ground truth samples [15]. The generated pseudo-labels can then be used to train the deep neural network. Following this approach, a convolutional recurrent neural network (CRNN) was used for classification by treating each pixel as a sequence of spectral dimensions [16]. It used pseudo-labels generated by clustering based on constrained Dirichlet process mixture model (C-DPMM) to pre-train the proposed model. The fine-tuning was done using the limited labeled data. In this work, we further explore this approach by testing the performance of K-means-based clustering algorithms for pseudo-label generation. In the case of dimensionality reduction, AE have demonstrated good performance in encoding the high dimensional redundant input into a low-dimensional manifold [17]. Although traditional approaches for dimensionality reduction like PCA are good in the removal of correlated features, it is biased toward

features having large variance which leads to incorrect results. Hence, it is intuitive to check the efficacy of deep AE for this task.

In this paper, we explore the approach of pseudo-label generation via different conventional techniques based on semi-supervised version of K-means clustering algorithm to facilitate the pre-training of the model. Although CRNN has shown better results in this approach [16], recurrent neural networks (RNNs) are known to suffer from the vanishing and exploding gradient problem [18]. Long short-term memory (LSTM) cells overcome this drawback by introducing "update, forget, and output gates" in the architecture. Hence, we explore convolutional long short-term memory cells (ConvLSTM) in the aforesaid semi-supervised setting. Also, we explore AE to extract better representations from the raw feature set. Finally, we fine-tune the pre-trained architecture using the limited labeled samples and compare the performance of our approach with other classifiers in the same setting.

The remaining paper is organized into 4 sections. Section 2 contains the detailed description of the clustering methods, the dimensionality reduction algorithm, and the classifier that are chosen to be analyzed in this work. Section 3 contains the description of the proposed methodology. Section 4 covers the description of datasets used, experimental setups, and the results. Finally, Sect. 5 provides an analysis of the obtained results with conclusions and the scope of future work.

2 Related Work

2.1 Clustering Approaches

Clustering is a task of partitioning the given unlabeled data into different groups (clusters) such that the data samples in the same cluster have relatively high similarity with each other as compared to data samples from different clusters. Clustering algorithms are unsupervised, i.e., information about the class labels cannot be extracted from the clusters. However, when the label information about a few data samples is available, it is possible to make an approximation to relate the clusters with class labels [19]. This approach is known as semi-supervised clustering and the class labels predicted by this approximation are called pseudo-labels [15]. K-means clustering is one of the most widely used clustering algorithms in machine learning literature. In the following sub-sections, we describe the semi-supervised versions of K-means clustering and its variants: K-median and K-medoid-based K-means clustering.

K-means Clustering
It is an iterative hard clustering approach which groups the data into K clusters [20]. As K is a hyper-parameter in this algorithm, the very first step is to specify the value of K. Then, K number of cluster centers are initialized which are selected randomly from the set of data points. Next, the distance of every data point from each cluster center is calculated in terms of a chosen distance metric. The data points are assigned

to that cluster center to which they are the closest. After this process is completed, the position of cluster centers is updated by calculating the mean of the data points assigned to their respective cluster. These steps are carried until convergence where the updates in cluster centers are sufficiently small. In other words, the K-means clustering algorithm aims to minimize the objective function J denoted in Eq. (1), where x_j^i represents the assignment of data point x_j to the ith cluster with its center located at c_i.

$$J = \sum_{i=1}^{k} \sum_{j=1}^{n} x_j^i - c_i^2 \tag{1}$$

One way to make a semi-supervised version of this algorithm is to initialize the cluster centers at data samples for which the label information is provided. Suppose there are c number of classes present and the label information about l number of randomly selected data samples per class are provided. Then, K should be set equal to $l * c$. After the initialization of $l * c$ cluster centers, the assignment of data samples to cluster centers and the updation of the cluster centers is carried out as described before. Finally, each data sample is assigned a pseudo-label which is the class label of the cluster center to which the data sample is assigned. Hence, for each iteration, a unique pseudo-label is assigned to the data samples. The only assumption made in this semi-supervised version of K-means clustering algorithm is the availability of label information of at least one data sample per class. This assumption is reasonable for the task at hand.

Although K-means clustering is a relatively simple and scalable algorithm that guarantees convergence, it is affected adversely by the presence of outliers. To avoid this issue, different variants of K-means clustering, like K-medoid [21] and K-median [22] clustering, are considered.

K-medoid-based K-means Clustering (K-med)

The main difference between the K-medoid and K-means clustering algorithm lies in the assignment of cluster centers. In K-means clustering, the cluster center is not necessarily a data sample. However, K-medoid clustering imposes an additional condition that the cluster centers can only be located at data samples. Hence, it is more robust to the presence of outliers. However, the traditional K-medoid clustering algorithm becomes computationally expensive as the number of data samples increase. This is due to a step in K-medoid clustering algorithm where each medoid is swapped with every non-medoid data sample and the corresponding cost is calculated. If the cost in the new set of medoids is lesser than the previous set of medoids, then the new set is used for further iterations. In case of a large number of data samples, this implementation is infeasible due to a large number of swapping operations. This issue can be resolved by applying the approach of K-medoid clustering in K-means clustering. In K-med clustering algorithm, the cluster center is not updated to the mean of the data samples assigned to a particular cluster. Instead, it is updated to the

data sample which is nearest to this calculated mean. This solution ensures that the cluster center is always a data sample.

K-median Clustering

The K-median clustering algorithm is designed to reduce the cost associated with clustering which is calculated using the L1 norm. Hence, the objective function to be minimized for K-median can be written as in Eq. (2) where x_j^i represents the assignment of data point x_j to the ith cluster with its center located at c_i. The reduction in the cost of clustering is done by assigning the cluster center to the median instead of the mean of the data samples belonging to a particular cluster.

$$J = \sum_{i=1}^{k} \sum_{j=1}^{n} \left| x_j^i - c_i \right| \tag{2}$$

The K-median clustering algorithm does not impose the condition that a cluster center must be a data sample from the dataset. However, the median is calculated per feature using L1 distance. Thus, the values of individual dimensions of the cluster center come from the dataset.

2.2 Auto-Encoder

Traditional auto-encoder consists of two main components: the encoder and the decoder [23]. The task of the encoder is to map the input feature vector into an intermediate hidden representation. When the objective of the AE is to minimize the dimensionality of the data, the number of neurons in the hidden layer is set to be less than that of the input layer. Hence, the encoder embeds input into a low-dimensional manifold. The task of the decoder is to reconstruct the original input from its low-dimensional encoding. The working of AE can be mathematically represented for input X as shown in the set of Eqs. (3) where e is the encoded representation obtained by the set of weights w and bias vector b and X' is the reconstructed output features. Here, J denotes the squared loss which is minimized by the AE.

$$
\begin{aligned}
e &= f(wX + b) \\
X' &= g(w'e + b') \\
J(X, X') &= X - X'^2
\end{aligned}
\tag{3}
$$

In order to obtain a low-dimensional embedding, the number of hidden layer units should be considerably less than the number of features in the input. Another way to improve the AE is to introduce sparsity by restricting the number of active neurons in the hidden layer for any input [24]. This is done by including a penalty term in the objective function which maintains the value of sparsity parameter. Hence, AE

is a good choice to reduce dimensionality and learn useful representations in the presence of a large number of redundant features.

2.3 Convolutional Long Short-Term Memory Cells (ConvLSTM)

In the literature, the task of hyperspectral image classification has been achieved using deep neural networks like convolutional neural networks (CNN) [27], recurrent neural networks (RNNs) [28], convolutional recurrent neural networks (CRNN) [16], etc. CNNs are better at extracting the features based on information based on spatial relations, whereas RNNs are good at predictions on sequential data. Although it is not directly apparent that hyperspectral data is sequential, due to the high number of dimensions, a pixel of a hyperspectral image can be viewed as a sequence of spectral dimensions. Hence, RNN can be expected to perform well. However, for better understanding of the long-range dependencies in sequential data, LSTMs have been demonstrated to perform better than the RNNs [18]. The LSTM architecture consists of a memory cell and a number of gates having their own parameters. The input gets collected to the memory cell in case of activation of the input gate. Preservation of long-term context is the key aspect of LSTM. This is achieved by the forget gate. In case of activation of the forget gate, the state of the past cell is removed (forgotten). In this way, only important contexts are preserved. Also, the decision on whether the cell output will be propagated to the final state is done by the output gate. Due to this architecture, the vanishing/exploding gradient problem is addressed [25].

However, due to the use of fully connected layers, spatial information cannot be encoded in the LSTM framework [26]. Hence, the introduction of convolution layers instead of fully connected layers in input-to-state and state-to-state transitions in LSTM can help in the incorporation of information about the spatial relations. The mathematical representation of ConvLSTM is shown in the set of Eq. (4). The memory cell mem_t of the LSTM is the space where the information of the current state is stored. The input gate is represented by inp_t in which the information about the new input is accumulated. The forget gate frg_t decides whether the information about the past state should be forwarded into the upcoming states. The output gate out_t decides whether the recent output of the mem_t is passed to the final state h_t. It should be noted that the symbol $*$ represents the convolution operation and the symbol o represents the hadamard product.

$$\text{inp}_t = \sigma(w_{xi} * x_t + w_{hi} * h_{t-1} + w_{ci} o \text{ mem}_{t-1} + b_i)$$
$$\text{frg}_t = \sigma\left(w_{xf} * x_t + w_{hf} * h_{t-1} + w_{cf} o \text{ mem}_{t-1} + b_f\right)$$
$$\text{out}_t = \sigma(w_{xo} * x_t + w_{ho} * h_{t-1} + w_{co} o \text{mem}_t + b_o)$$
$$\text{mem}_t = \text{frg}_t o \text{mem}_{t-1} + \text{inp}_t o \tanh(w_{xc} * x_t + w_{hc} * h_{t-1} + b_c)$$
$$h_t = \text{out}_t o \tanh(\text{mem}_t) \tag{4}$$

Due to the aforementioned architecture, the ConvLSTM is better at predictions on sequential data in addition to the consideration of information based on spatial relations.

3   Proposed Methodology

The proposed semi-supervised deep learning framework consists of four steps. The first step consists of the use of semi-supervised clustering in order to generate pseudo-labels. The second step extracts meaningful features and reduces the dimensionality of the hyperspectral image using AE. In the third step, the pseudo-labels and extracted features are used to pre-train the ConvLSTM. Lastly, the ConvLSTM is fine-tuned using the same set of labeled samples used for semi-supervised clustering. The structure of the proposed methodology is shown in Fig. 1.

3.1   Pseudo-Label Generation

Pseudo-labels are the class labels predicted based on the cluster assignment obtained by a clustering algorithm along with a small set of labeled data samples. The semi-supervised versions of K-means, K-med, and K-median clustering algorithms are explored in this work to generate the pseudo-labels. The data samples for which the label information is available are assigned as the initial cluster centers. This is followed by the execution of aforesaid clustering algorithms. Finally, pseudo-labels are assigned as described in Sect. 2.1.
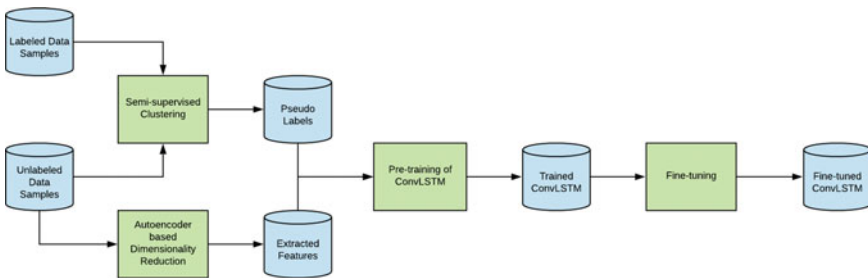

Fig. 1 Proposed semi-supervised deep learning strategy

3.2 Dimensionality Reduction

The set of unlabeled data is used to train the AE in an unsupervised manner. As the motive behind the use of AE is to reduce the dimensionality, the number of neurons in the hidden layer is set to be less than that of the number of neurons in the input layer. Sparsity regularizer is also introduced in the cost function in order to learn a better encoding. It should be noted that no label information is used in this step, i.e., fine-tuning of AE by stacking a softmax layer is avoided. The quality of extracted features is measured by using them to train the ConvLSTM along with the generated pseudo-labels. The analysis of information loss due to the reduction of dimensionality is carried out by decreasing the dimensions of the data by approximately 10% of the total dimensions in a step-wise manner and checking the classification accuracy obtained against it.

3.3 Pre-training the ConvLSTM

The pseudo-labels generated are used to pre-train the ConvLSTM which takes into input the features extracted by the AE. In this step, it should be noted that the proposed model is trained on the pseudo-labels, which might not be fully accurate when compared with the ground truth. As the training and test data is partitioned randomly, the training data is more likely to contain some falsely predicted pseudo-labels along with the majority of correctly predicted pseudo-labels. To improve the performance of the classifier in this step, one way is to increase the number of correctly predicted pseudo-labels by improving the accuracy of pseudo-label generation. The other way is to ensure that a less number of incorrectly predicted pseudo-labels are used for training. This can be done by introducing a metric of confidence in the pseudo-label generation step. For example, if a data sample P1 is more close to the cluster center to which it is assigned than another data sample P2 which is assigned to the same cluster center, then P1 is more likely to be having the class label of that cluster center than that of P2. Hence, P1 should more likely to be included in the training set than P2. Thus, P1 has more confidence in the generated pseudo-label as compared to P2. If this metric of confidence is used in the implementation, then the training data is selectively chosen to consist of data samples with the pseudo-labels having relatively high confidence. Otherwise, train and test data is divided in a random fashion.

3.4 Fine-Tuning the ConvLSTM

The full utilization of the given labeled data can be achieved by fine-tuning the pre-trained ConvLSTM with the labeled data. It is expected that the performance of the

classifier should improve with the training on this labeled set. The fine-tuning step can be done in a number of ways. A set of dense layers can be added to the pre-trained model followed by a softmax layer as proposed in [16] where the parameters of the pre-trained model are set to be frozen during the fine-tuning. Hence, only the parameters corresponding to the newly added dense and softmax layer are changed. However, we observe that the addition of a large number of dense layers to the pre-trained model decreases the performance. Hence, we propose to include only a single dense layer and a softmax layer to the pre-trained model.

4 Experiments and Results

4.1 Datasets

Two real-world hyperspectral image datasets are used to check the performance of the proposed methodology.

The first dataset used is called the "University of Pavia" (UP) dataset [29]. The dataset was captured using reflective optics system imaging spectrometer (ROSIS) sensors during a flight campaign over the targeted geographical region. The original dataset is a 610*340 pixel hyperspectral image. However, many pixels contain no information. Hence, they are discarded before the analysis. The spatial resolution of the image is 1.3 m. It contains 103 spectral dimensions within a narrow wavelength range of 430–860 nm. This dataset consists of nine different land cover classes such that the classes are not represented equally, i.e., the dataset does not have equal number of data samples in each class. Hence, the issue of class imbalance is present.

The second dataset used is called "Salinas" dataset [30]. This dataset is captured using airborne visible/infrared imaging spectrometer (AVIRIS) sensors. It is collected over the Salinas Valley in California. The spatial resolution of this image is 3.7 m, which is higher as compared to UP dataset. It is a 512*217 pixel image containing at sensor radiance data, and it consists of 224 spectral dimensions. However, 20 dimensions out of the total 224 dimensions are discarded as they correspond to the water absorption bands. The ground truth of this dataset contains 16 different classes and similar to the UP dataset, the classes are not represented equally. Thus, the issue of class imbalance is present in this dataset also.

4.2 Experimental Setup

In the experiment, the labeled set is constructed by randomly selecting 10, 20, 30, and 40 pixels per class. In the semi-supervised clustering step, K-means, K-medoid, and K-median clustering algorithms are tested. We define a configuration by the clustering algorithm and the number of labeled samples used in the semi-supervised clustering.

Hence, for 3 different clustering algorithms and 4 settings of the number of labeled samples used, there are 12 configurations in total. For each of the configuration, the same set of 10/20/30/40 labeled samples is used to remove the effect of initialization of cluster centers on the performance of pseudo-label generation. The number of iterations for which the clustering should be conducted is set as a hyper-parameter. As the proposed methodology requires only an approximation of the class labels in the form of pseudo-labels, the number of iterations is set to be a very small number. This implies that the clustering is forcefully terminated after a few iterations. This also helps in achieving less execution time.

To analyze the information loss in the process of feature extraction, the spectral dimension is reduced in steps of 10% of the total, till it reaches half of the total number of dimensions. For example, in case of UP dataset, the classification accuracy is obtained for the feature sets with 93, 83, 73, 63, and 53 dimensions (reduction of 10 dimensions in each step). The total number of dimensions of the UP dataset is 103. Finally, the effect of dimensionality reduction is analyzed by plotting a graph between the cardinality of the reduced feature set and the classification accuracy associated with it. The classification accuracies in this experiment are obtained by using ConvLSTM as the classifier over the reduced feature set.

Finally, the performance of the proposed model is compared with three different classifiers: CNN, LSTM, and CNN-LSTM. For CNN, the feature vector is passed to one-dimensional convolution layer with 64 filters, each having kernel size of 8. Padding is applied to keep the feature shape unchanged. ReLU activation and a dropout of 0.2 are used in all neural architectures. Then, a batch normalization layer is applied followed by a one-dimensional max pooling layer of stride 2. The training of the architecture is carried out with Adam optimizer. The LSTM model is implemented using an LSTM layer having the number of units equal to the size of input feature vector. Both the dropout and recurrent dropout are set to 0.2. The training of the architecture is carried out with Adam optimizer. In the case of CNN-LSTM, a one-dimensional convolution layer having 64 filters of size 8 is used with the "SAME" padding and ReLU activation. A max pooling layer is attached to it with stride 4. It is followed by an LSTM layer having number of units equal to the size of the original feature vector. Finally, a dense layer is applied with a softmax layer attached to it. The model is trained with "Adam" optimizer. In the implementation of ConvLSTM, instead of passing the one-dimensional feature vector for a pixel, a two-dimensional feature vector is constructed. To incorporate the spatial information, the spectral dimensions of the neighbor pixels are concatenated and passed to the two-dimensional ConvLSTM layer. The output of this layer is passed to a dense layer attached to a softmax layer. It should be noted that the number of units in the ConvLSTM layer is set to be equal to the number of spectral features of the input. Each of the classifiers is tested 10 times for each of the aforesaid 12 configurations. The average of all these results is reported.

4.3 Results

The classification accuracies for the UP and the Salinas dataset are shown in Tables 1 and 2. The accuracy of the best performing classifier in each configuration is high-lighted. The index numbers 1, 2, 3, and 4 represent the classifiers CNN, LSTM, CNN-LSTM, and ConvLSTM, respectively. It can be seen that for a classifier, the classification accuracy increases with the increase in the number of labeled samples used per class. Also, the use of K-med and K-median clustering algorithm has shown better performance on the UP dataset. However, the use of K-means has outperformed the other two clustering algorithms in case of the Salinas dataset. From the point of view of the classifiers, ConvLSTM has produced the best results for a majority of the configurations with a few exceptions, where CNN-LSTM can be seen to outperform the ConvLSTM. An important observation in this experiment is the improved results due to the combined use of spatial and sequential information (CNN-LSTM and ConvLSTM) as compared to its use separately (CNN and LSTM).

The classification accuracies obtained on the extracted features are shown in Fig. 2. The results clearly highlight the fact that the amount of information loss in the feature extraction is comparatively lesser than that of the reduction in dimensions. This shows the efficacy of the AE to extract distinguishing features from the large set of raw input features. Thus, from the mentioned results and the observations stated above, it can be clearly seen that the proposed methodology and the choice of classifier outperforms other classifiers in the same environment in the majority of configurations.

5   Conclusion and Future Work

This paper explores the semi-supervised deep learning-based strategies to classify hyperspectral images. The key aspect of this methodology is the generation of more accurate pseudo-labels via semi-supervised clustering. The highest overall accuracies of 95.61% and 96.97% are obtained for the UP dataset and Salinas dataset, respectively. Also, the relatively low information loss is observed which is marked by only 10% reduction in overall accuracy due to the dimensionality reduction. These two aspects highlight the effectiveness of the proposed methodology. Apart from these two measures, the proposed methodology is also computationally efficient due to early termination of the semi-supervised clustering algorithm. However, this methodology can be further explored as the pseudo-label generation step can be performed by several other more efficient clustering algorithms.

Table 1 Classification accuracies for UP dataset

No	K-means				K-med				K-median			
	10	20	30	40	10	20	30	40	10	20	30	40
1	88.76	89.31	90.03	92.57	90.08	92.31	93.28	94.86	89.93	90.91	92.33	94.30
2	88.12	90.63	91.32	92.08	89.80	90.22	90.87	91.21	88.12	90.97	91.41	92.55
3	90.44	92.12	93.47	94.07	91.32	93.62	93.86	94.01	90.94	93.26	93.84	94.71
4	**91.32**	**93.43**	**94.01**	**95.30**	**92.03**	92.77	93.54	**95.61**	**91.83**	92.96	**94.14**	**95.42**

Table 2 Classification accuracies for Salinas dataset

No	K-means				K-med				K-median			
	10	20	30	40	10	20	30	40	10	20	30	40
1	93.47	94.81	95.84	96.03	93.58	94.27	94.32	94.56	92.34	93.06	93.41	94.66
2	91.82	91.99	92.08	92.25	91.03	91.39	91.68	91.9	90.72	90.95	91.63	92.00
3	**93.78**	**95.91**	96.26	96.88	93.08	**94.44**	95.09	96.13	**93.21**	93.98	94.91	**96.26**
4	93.69	95.53	**96.44**	**96.97**	**93.25**	94.29	**95.38**	**96.52**	93.14	**94.33**	**95.12**	96.05

Effect of Dimensionality Reduction

	90%	80%	70%	60%	50%
UP	95.1	92.81	89.77	88.37	84.42
Salinas	93.81	90.02	87.59	86.64	83.82

Number of extracted features as compared to the total number of dimensions present in the dataset
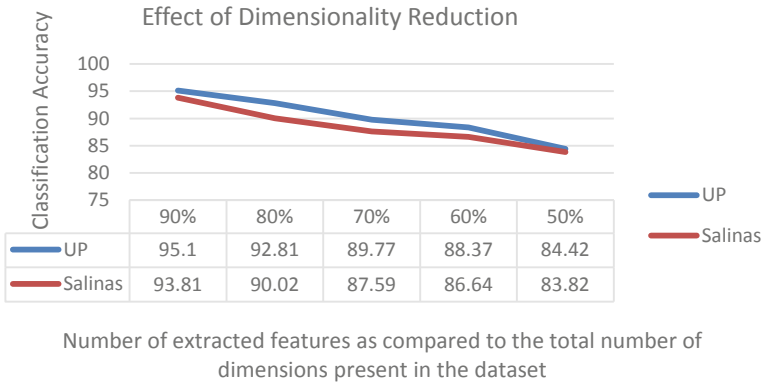
Fig. 2 Classification accuracies using the extracted features

References

1. Chang, C.I.: Hyperspectral Imaging: Techniques for Spectral Detection and Classification, vol. 1, Springer Science & Business Media (2003)
2. Xu, B., Gong, P.: Land-use/land-cover classification with multispectral and hyperspectral EO-1 data. Photogramm. Eng. Remote Sensing **73**(8), 955–965 (2007)
3. Mahlein, A.K., Oerke, E.C., Steiner, U., Dehne, H.W.: Recent advances in sensing plant diseases for precision crop protection. Eur. J. Plant Pathol. **133**(1), 197–209 (2012)
4. Schmidt, F., Legendre, M., Le Mouëlic, S.: Minerals detection for hyperspectral images using adapted linear unmixing: LinMin. Icarus **237**, 61–74 (2014)
5. Baraldi, A., Bruzzone, L., Blonda, P.: Quality assessment of classification and cluster maps without ground truth knowledge. IEEE Trans. Geosci. Remote Sens. **43**(4), 857–873 (2005)
6. Houghes, G.F.: On the mean accuracy of statistical pattern recognition. IEEE Trans. Inform. Theory **14**(1), 55–63 (1968)
7. LeCun, Y., Bengio, Y., Hinton, G.: Deep Learning Nature **521**(7553), 436 (2015)
8. Krizhevsky, A., Sutskever, I., Hinton, G. E.: Imagenet classification with deep convolutional neural networks. In: Advances in Neural Information Processing Systems, pp. 1097–1105 (2012)
9. Girshick, R., Donahue, J., Darrell, T., Malik, J.: Rich feature hierarchies for accurate object detection and semantic segmentation. In Proceedings of the IEEE Conference on Computer Vision and Pattern Recognition, pp. 580–587 (2014)
10. Goodfellow, I., Pouget-Abadie, J., Mirza, M., Xu, B., Warde-Farley, D., Ozair, S., Bengio, Y.: Generative adversarial nets. In Advances in neural information processing systems, pp. 2672–2680 (2014)
11. Roy, S.K., Krishna, G., Dubey, S.R., Chaudhuri, B.B.: HybridSN: Exploring 3-D-2-D CNN feature hierarchy for hyperspectral image classification. IEEE Geosci. Remote Sensing Lett (2019)
12. Liu, B., Yu, X., Zhang, P., Tan, X., Yu, A., Xue, Z.: A semi-supervised convolutional neural network for hyperspectral image classification. Remote Sensing Lett. **8**(9), 839–848 (2017)

13. Büchel, J., Ersoy, O.: Ladder Networks for Semi-Supervised Hyperspectral Image Classification. arXiv preprint arXiv:1812.01222 (2018)
14. Pan, B., Shi, Z., Xu, X.: MugNet: Deep learning for hyperspectral image classification using limited samples. ISPRS J. Photogramm. Remote Sensing **145**, 108–119 (2018)
15. Wu, H., Prasad, S.: Semi-supervised dimensionality reduction of hyperspectral imagery using pseudo-labels. Pattern Recogn. **74**, 212–224 (2018)
16. Wu, H., Prasad, S.: Semi-supervised deep learning using pseudo labels for hyperspectral image classification. IEEE Trans. Image Process. **27**(3), 1259–1270 (2017)
17. Wang, Y., Yao, H., Zhao, S.: Auto-encoder based dimensionality reduction. Neurocomputing **184**, 232–242 (2016)
18. Pascanu, R., Mikolov, T., Bengio, Y.: On the difficulty of training recurrent neural networks. In International ConFerence on Machine Learning, pp. 1310–1318 (2013)
19. Bair, E.: Semi-supervised clustering methods. Wiley Interdiscipl. Rev. Comput. Statist. **5**(5), 349–361 (2013)
20. MacQueen, J.: Some methods for classification and analysis of multivariate observations. Proc. Fifth Berkeley Symp. Mathe. Statist. Probabil. **1**(14), 281–297 (1967)
21. Kaufman, L., P.J. Rousseeuw, Y. Dodge.: Clustering by Means of Medoids in Statistical Data Analysis Based on the pp. 405–416 (1987)
22. Jain, A.K., Dubes, R.C.: Algorithms for Clustering Data, vol. 6. Prentice hall, Englewood Cliffs, NJ (1988)
23. Goodfellow, I., Bengio, Y., Courville, A.: Deep Learning. MIT Press (2016)
24. Makhzani, A., Frey, B.: K-sparse Autoencoders. arXiv preprint arXiv:1312.5663. (2013).
25. Hochreiter, S., Schmidhuber, J.: Long short-term memory. Neural Comput. **9**(8), 1735–1780 (1997)
26. Xingjian, S.H.I., Chen, Z., Wang, H., Yeung, D.Y., Wong, W.K., Woo, W.C.: Convolutional LSTM network: A machine learning approach for precipitation nowcasting. In Advances in Neural Information Processing Systems, pp. 802–810 (2015)
27. Hu, W., Huang, Y., Wei, L., Zhang, F., Li, H.: Deep convolutional neural networks for hyperspectral image classification. J. Sensors (2015)
28. Lyu, H., Lu, H., Mou, L.: Learning a transferable change rule from a recurrent neural network for land cover change detection. Remote Sensing **8**(6), 506 (2016)
29. Gamba, P.: A collection of data for urban area characterization. In: IGARSS 2004. 2004 IEEE International Geoscience and Remote Sensing Symposium, vol. 1. (2004)
30. https://www.ehu.eus/ccwintco/index.php/Hyperspectral_Remote_Sensing_Scenes

Integrated Geophysical and Geotechnical Study of a Southern Oil and Gas Field in Western Offshore, India

Sri Harsha Gamidi and R. K. Ghanekar

Abstract The field under study is located toward the south of petroleum producing area of western Indian offshore. The field was initially partly developed and redevelopment has been started in recent years. During the initial and redevelopment phases, many geotechnical investigations and geophysical surveys have been performed. A collated data study of old and new geophysical and geotechnical data was done with the objective to establish the field wide identification of different soil strata and their engineering parameters. The engineering parameters established from this study will help to verify the reasonability of newly measured in situ and laboratory parameters. They can also be used to optimize the costly field and laboratory testing programmes. Moreover, this study will help in assessing soil conditions and assigning design parameters for upcoming geotechnical investigations where either data are inadequate or missing. In this paper, the results and conclusions inferred from the integrated study, shallow geologic and geotechnical conditions of the field are presented.

Keywords Geophysical · Geotechnical · Integrated · Optimizing · Characterization

1 Introduction

To augment its hydrocarbon production, ONGC started the redevelopment of one of its field, located toward the south of petroleum producing area of western Indian offshore. The redevelopment involves the installation of a few offshore platforms, pipelines and cables. The pre-engineering surveys of the said field redevelopment had detailed geophysical surveys and geotechnical investigations. Geophysical surveys

S. H. Gamidi (✉) · R. K. Ghanekar
Geotechnical Engineering Section, Institute of Engineering and Ocean Technology, ONGC, Panvel, Maharashtra 410221, India
e-mail: gamidi_sriharsha@ongc.co.in

R. K. Ghanekar
e-mail: ghanekar_rk@ongc.co.in

were performed with the aim to identify hazards, which could affect the safety of the infrastructure. The other objectives achieved from geophysical survey were: collecting the bathymetry data; understanding the seafloor features, shallow geology and map the existing infrastructure. The geotechnical investigations were performed with the aim to estimate the design parameters and soil conditions for design and installation of structures.

Reasonably, a large amount of data from old and new investigations exists, and hence, a collated study of old and recent data was done, with the aim to understand the field wide stratigraphy and soil conditions. This paper presents various results and conclusions inferred from this study.

1.1 Origin of Soils in Indian Offshore

The continental shelf on western Indian offshore is wide, around 200 km. In the eastern offshore, it is narrow, with 40 km approximate width. The soils in Indian offshore are either terrigenic or pelagic origin. The terrigenic soils originate on land and transported to the sea. The ocean environment by its mechanisms such as cementation at times alters the terrigenic soils. The pelagic soils originate from biological remains of sea organisms either by mineral or chemical precipitation. Sometimes, these soils can also get modified from the actions of the ocean environment [1].

2 Data Considered for the Study

Data of two geophysical surveys and 64 geotechnical investigations for the platform, pipelines (development) and jack-up rig (exploratory) locations are available from the past and present pre-engineering surveys. Of the two geophysical surveys, the recently performed geophysical survey has more comprehensive information than the survey performed in the initial phase of field development.

The geotechnical data available has final soil investigation reports done for platforms, pipelines and jack-up rigs in hard copy from the initial phase. The data from redevelopment has data in digital form also, e.g., measured CPTU (cone penetration test with pore pressure measurement) data. A few exploratory locations are very far from others; hence, the data of these locations are excluded from the study.

3 Review of Geophysical Survey Data

Various tools were used to perform geophysical survey during the initial and recent field development. The tools used are multibeam echosounder, side-scan sonar, sub-bottom profiler and magnetometer. The multibeam echosounder survey helps to

assess the topography/bathymetry; the side-scan sonar survey is used to get a photograph like image of the seafloor; the sub-bottom profiler aids to know the stratigraphy; and the magnetometer identifies metal objects at or just below the seafloor. The study of these survey results shows that major hazards which may hamper infrastructure development are not present in this field. Important observations from the geophysical survey in comparison with geotechnical data are presented in the following sections.

3.1 Topography of Field

Water depths measured by echo sounders, bathymetry data from the geophysical survey and bathymetry data from National Oceanic and Atmospheric Administration (NOAA), USA database were studied together to understand the overall topography of the field. All the new and old (exploratory, development) locations, where geotechnical investigations were carried are plotted against contours of the field (see Fig. 1). The 3D surface of the field generated from NOAA data is shown in Fig. 2. By observing the contours and the 3D surface of the field, it can be inferred that the field (where most of the exploratory and development locations are) has a gentle slope toward west and southwest direction.

3.2 Seabed Sediments, Features and Sonar Contacts

The interpretation of acoustic reflectivity of the side-scan sonar data helps to identify the soil present at the seafloor. The side-scan sonar data of the present field were studied; low to medium reflective surficial sediments are interpreted as clay and medium reflective sediments can be interpreted as sand (see Fig. 3). Furthermore, few seabed scars/anchor drag marks, depressions and sonar contacts like debris, wellheads, etc., were also spotted (see Fig. 3).

3.3 Sub-bottom Profiling

Sub-bottom profiling is performed to understand the shallow soil layers below the seafloor. The sub-bottom profiling for pipeline routes and platform locations were done by Pinger system. The soil layers identified from the sub-bottom records can be classified into two types. The topmost soil layer (Unit A) is interpreted as 'sandy silty clay' and the second soil layer (Unit B) identified as a firm to stiff clay. The first soil layer thickness varied from 20 to 40 m and the thickness of the second soil layer could not be estimated due to the limitations of the acoustic signal penetration. It can also be observed that the thickness of first soil layer interpreted from sub-bottom
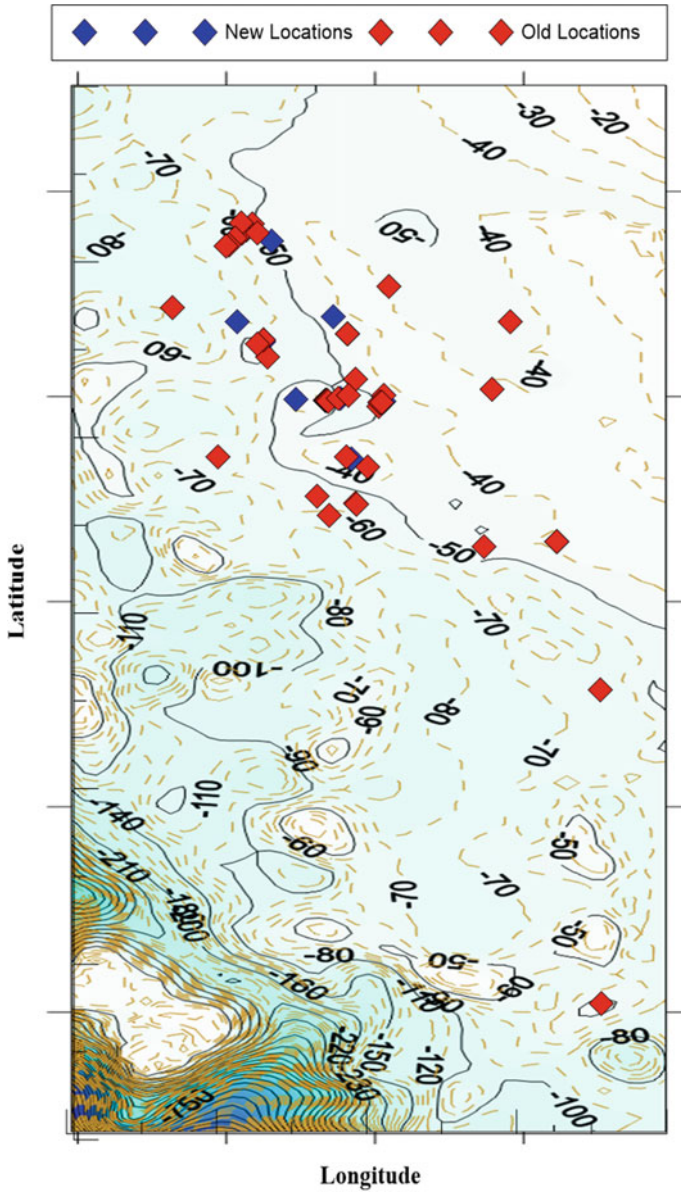
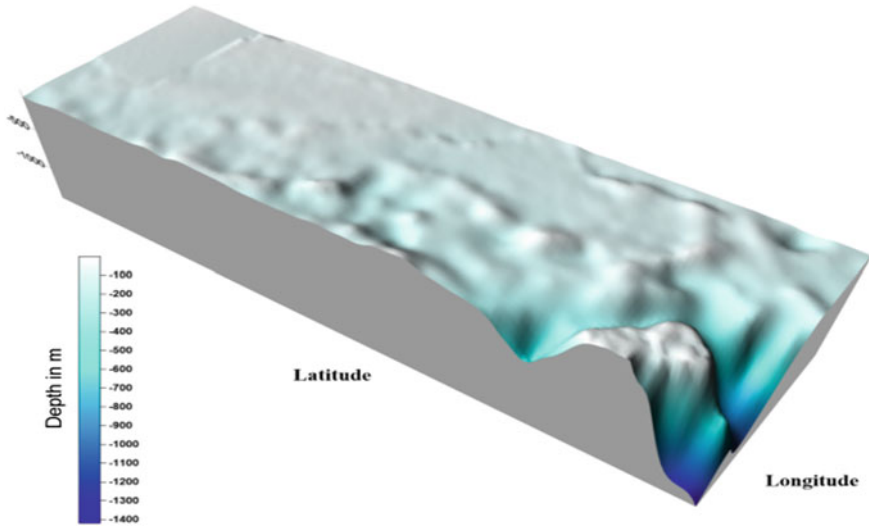**Fig. 1** New and old geotechnical investigation locations with respect to contours

Fig. 2 3D surface of field generated from NOAA (USA) data
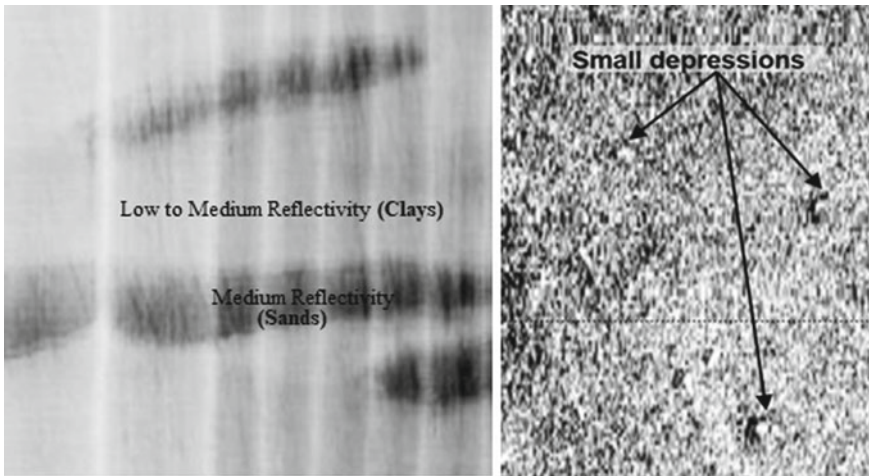

Fig. 3 Side-scan sonar image showing seafloor sediments and depressions

profiling data shows good agreement with CPTU interpretation (soil behavior type index and cone resistance) plots as shown in Figs. 4 and 5.

Finally, acoustic masking (possibly due to shallow gas) as shown in Fig. 6 was identified within the first soil layer (Unit A) occasionally along the proposed pipeline/cable routes.
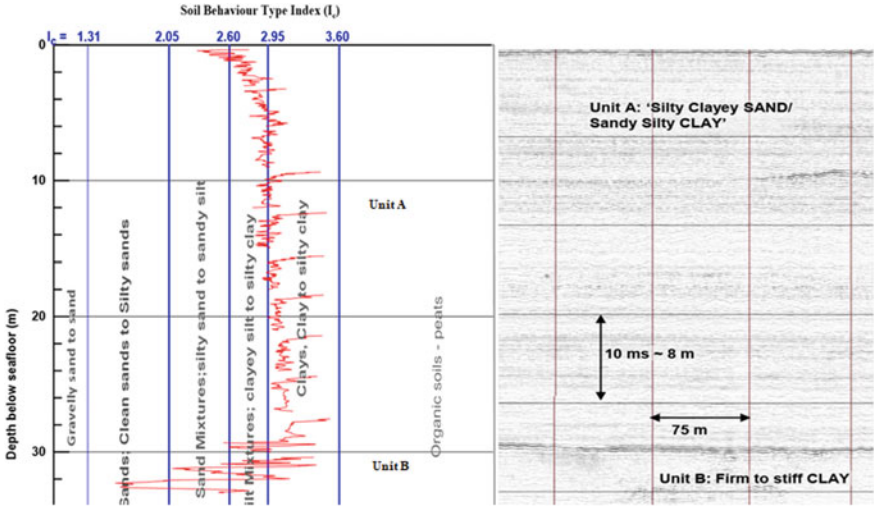
Fig. 4 Comparison of SBT and sub-bottom profiling records
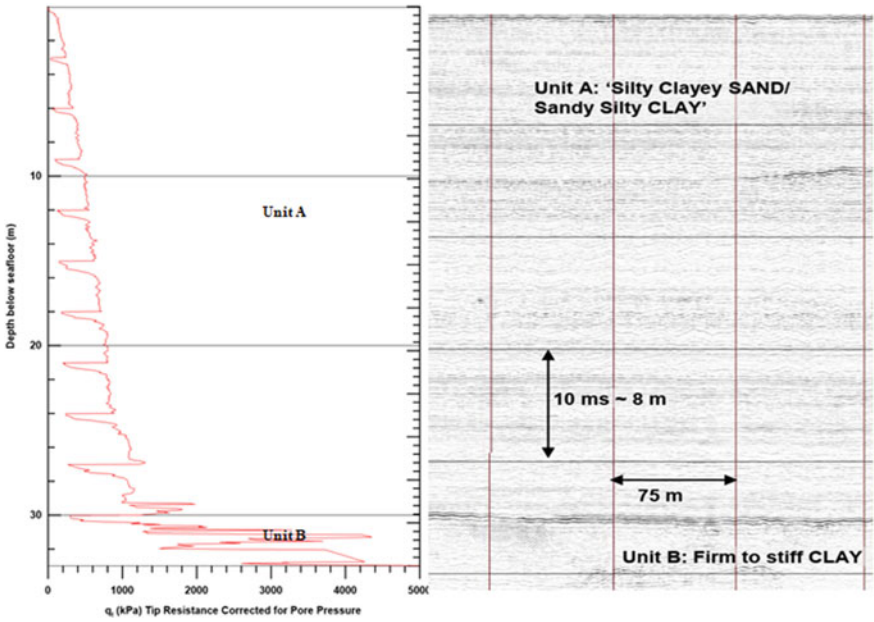
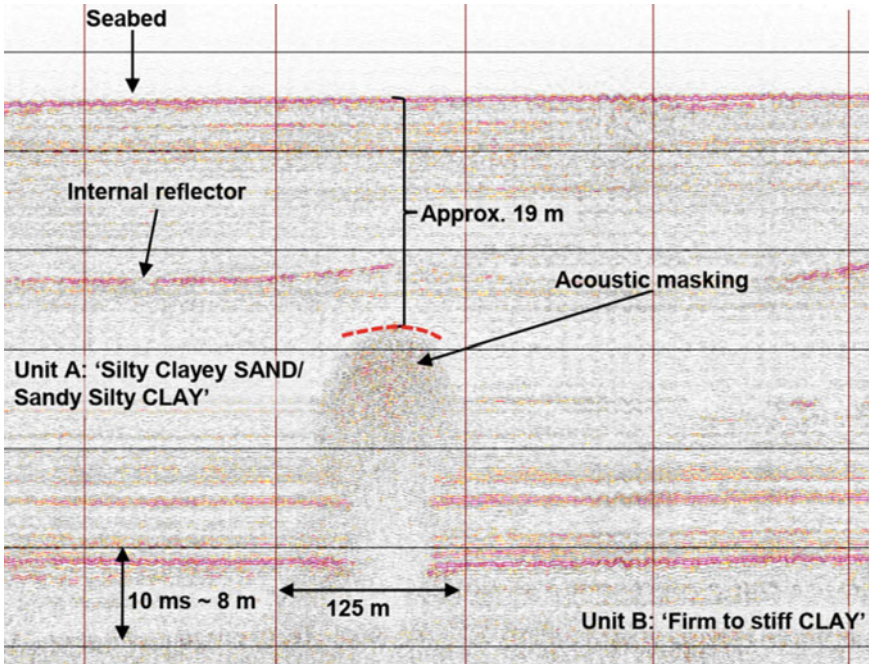Fig. 5 Comparison of q_t and sub-bottom profiling records

Fig. 6 Shallow gas in unit A

3.4 Magnetic Anomalies

Magnetic anomalies found during the magnetic survey were due to the existing pipelines and other sonar contacts.

4 Reviews of Geotechnical Investigations Data

The geotechnical investigation data considered for the study have been classified into two categories. The recent data, with digital CPTU records and final soil investigation reports and the hard copies of final soil investigation reports of locations investigated during the initial phase of the field development.

The raw CPTU data of the recently investigated locations were processed and parameters: q_t (measured cone resistance corrected for pore pressure effect and seabed reference), f_s (sleeve friction), B_q (pore pressure parameter—$\Delta u/(q_t-\sigma_v)$, $\Delta u = u_2-u_0$, $u_2 = $ pore pressure measured at the shoulder of piezocone, $u_0 = $ in situ equilibrium pore pressure, $\sigma_v = $ total vertical stress) [2], and soil behavior type index (I_c) [3] were plotted against the depth from seafloor.

The soil behavior type index (I_c) was developed by Robertson et al. [3] to identify the type of soil from the CPTU data. The stratigraphy at a location can be easily visualized from the plot of I_c against depth from the seafloor. The recent geotechnical investigations are located sufficiently far from each other within the field. Hence, a combined plot of all I_c against depth from seafloor identified a few major site-wide (see Fig. 7) and some locally present clay and sand layers. The parameter wise (q_t, f_s and B_q) combined plots of all locations (not presented here due to paucity of space) also support the above observation.

Furthermore, the bore logs from the old and new soil investigation reports were studied to understand the field wide soil stratigraphy. From the review of all the geotechnical information, it can be concluded that the soil stratigraphy in the present field is clay dominated. At any location, more numbers of clay layers and few sand layers are present. Likewise, some soil layers are having field wide and others having only local presence can be confirmed. Other important observations from the study of geotechnical data are presented in the following sections.

4.1   Carbonate Content

One of the important characteristics of soils in western Indian offshore is the presence of a high quantity of carbonate. The soils in the present field also have high carbonate content. For clays, the carbonate content affects the plasticity characteristics but has no significant influence on shear strength. For sands, higher carbonate content indicates higher particle crushing and compressibility resulting in lower pile-soil friction. The modified Clark and Walker [4] classification system was used to classify clays and sands in the present field.

4.2   Relative Density, Friction Angle of Sands in the Field

The sands in the present field have high quantities of carbonate content and varying degree of cementation. Hence, most of the sands were classified into siliceous carbonate sands, calcareous sands and calcarenites [4]. The relative densities of the coarse-grained soils present in the field were estimated by the correlation proposed by Jamiolkowski et al. [5]. The correlation used was developed for silica sands; hence, the API recommended frictions angles were adjusted to accommodate the nature of carbonate bearing sands.

A very thin loose silty sand layer (siliceous carbonate) was observed at the seafloor in some locations. Its thickness varies from 0.5 to 2 m. The presence of this layer can also be confirmed from side-scan sonar records. Another thin medium dense silty sand layer (siliceous carbonate) of 3–4 m approximate thickness is present around 25–35 m depth from the seafloor. At some locations, this layer is interbedded with clay.
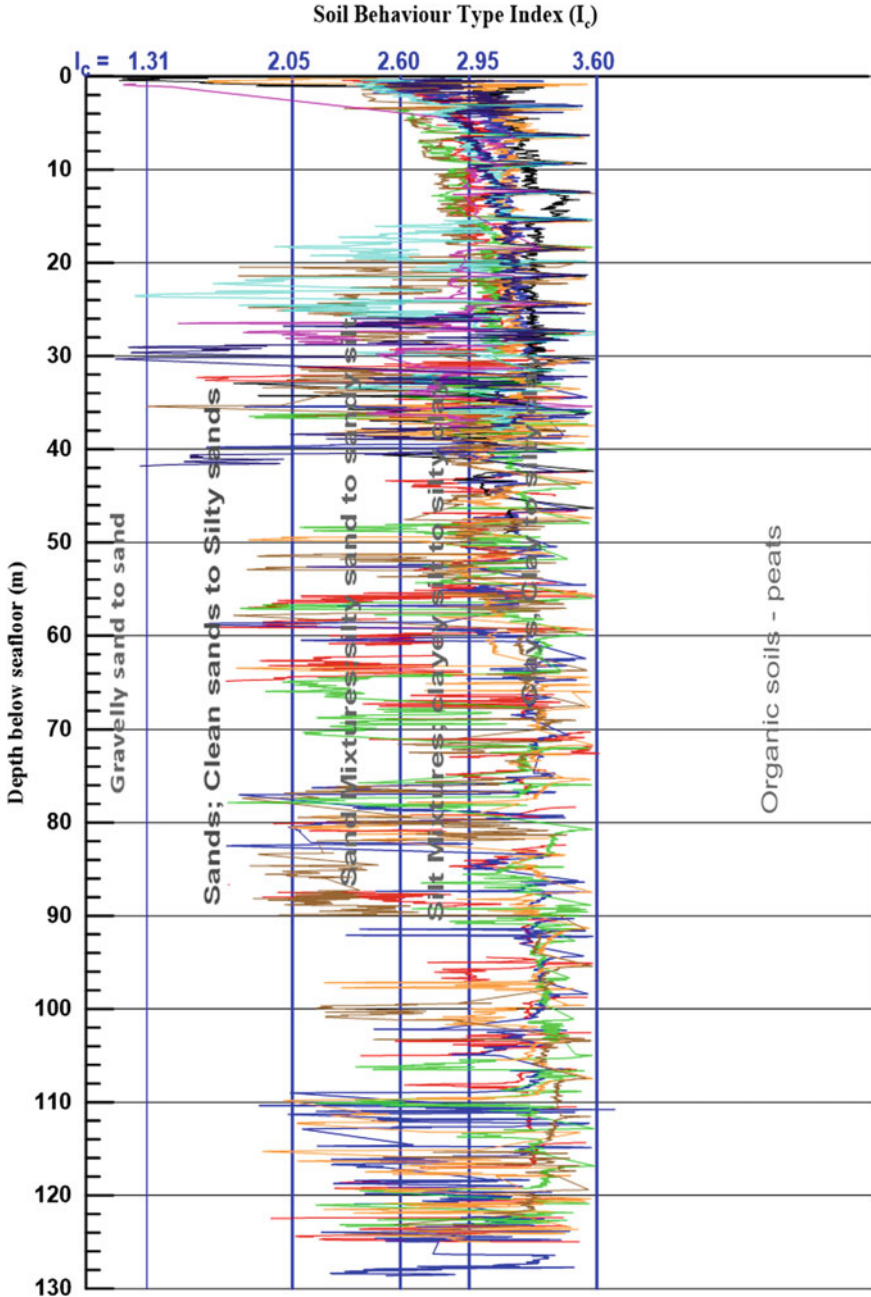
Fig. 7 Combined plot of all SBT (I_c) with respect to depth from seafloor

The other sand layers present in the field did not show any specific pattern in their position from the seafloor. Hence, their site-wide presence could not be established.

4.3   Shear Strength and Stress History of Clays in the Field

A number of in situ and laboratory tests were performed to measure the undrained shear strength of clays. In situ tests like field vane shear and CPTU were performed. Laboratory tests to measure shear strength like pocket penetrometer (PP), torvane (TV), motor vane (MV), unconsolidated-undrained triaxial test (UU) and consolidated-undrained triaxial test (CU) were performed. The final design strength profile was estimated considering in situ and laboratory strength results.

The soil stratigraphy of the field shows several calcareous and carbonates clay layers [4]. A large clay layer with consistency varying from very soft to firm is present all over the field located at a depth of 0 to 2 m from the seafloor. The presence of this layer can also be seen in sub-bottom profiling records (see Fig. 5). The thickness of this layer varies from 18 to 40 m. Effective unit weight of soil in this layer is between 4 and 6 kN/m^3. Also, the moisture content and liquidity index of this layer are more than 70% and 0.75, respectively. The S_{uUU}/σ'_v (S_{uUU} = unconsolidated-undrained shear strength of clays, σ'_v = effective vertical stress) on average are 0.2 indicating normally consolidated clays.

Several stiff and very stiff clay layers are present after the first clay layer. In these layers, the consistency of clays increases and liquidity index decreases with depth. The effective unit weights also support the trend in consistency. The moisture content of these stiff and very stiff clay soil layers is around 40% and liquidity indices are in between 0.1 to 0.3. The S_{uUU}/σ'_v values are around 0.5; and the OCR as per CPTU-based correlation by Mayne [6] is around 2 indicating the presence of slightly overconsolidated clays.

Some overconsolidated hard clay layers are present mostly after 125 m depth from the seafloor. But their field wide presence could not be established due to the deficiency of data.

5   Three Dimensional (3D) Soil Model of the Field

As a part of the integrated study, a 3D model was developed to get a better understanding of the soil stratigraphy. The creation of 3D soil model helps to visualize the spatial variation in stratigraphy. The isosurface obtained from the 3D model can help to locate a specific type of soil from the seafloor.
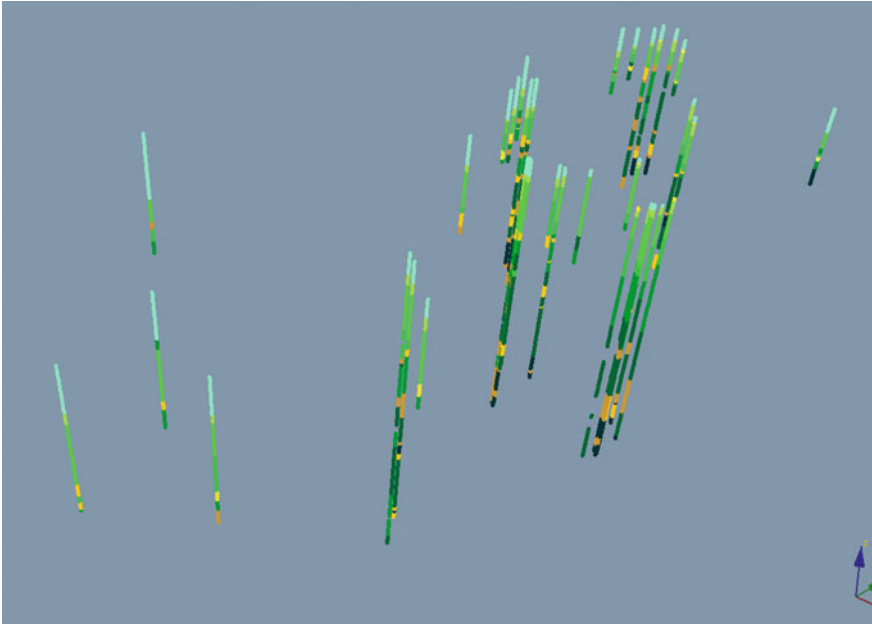
Fig. 8 Scatter plot of bore logs

5.1 Procedure to Create 3D Model

The *XYZ* data to create the model were obtained from the bore logs of each geotechnical investigation. The easting, northing and depth from the seafloor are chosen as Cartesian coordinates (*XYZ*) to create 3D scatter plots (see Fig. 8). The consistency of clays and relative density of sands were color-coded (clays in green and sands in brown) and displayed at each coordinate of the scatter plot. The increase in the intensity of green color from light to dark shows the increase in consistency. Similarly, the increase in the intensity of brown color, i.e., from light to dark shows the increase in relative density. Finally, the coordinates of the scatter plot along with their respective color are interpolated to create the 3D model (see Fig. 9) showing stratigraphy.

5.2 Inferences from the 3D Soil Model

A cross-section at the location of interest either orthogonal or oblique to the 3D model helps to view soil stratigraphy (see Fig. 10).

An isosurface from the 3D model shows the location of a particular type of soil present at different depths from the seafloor. (see Fig. 11).
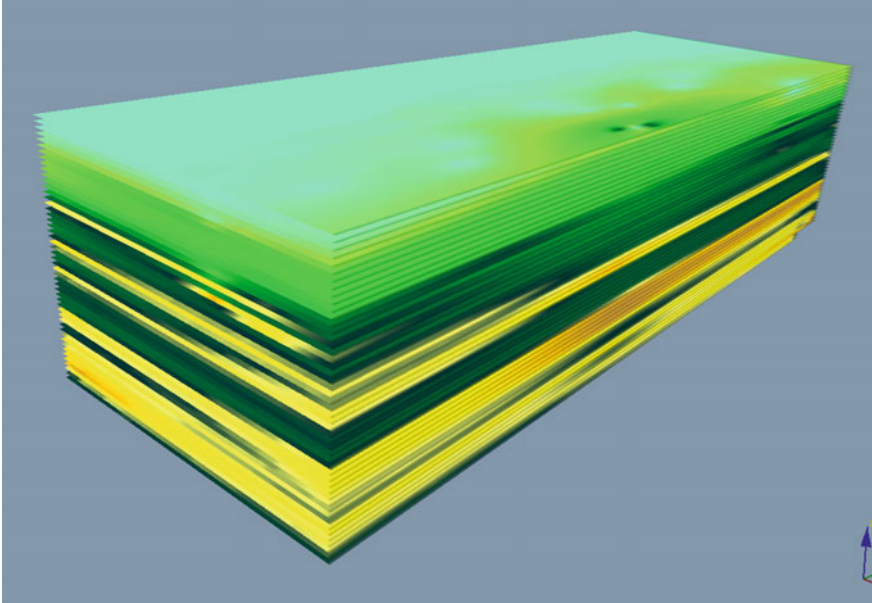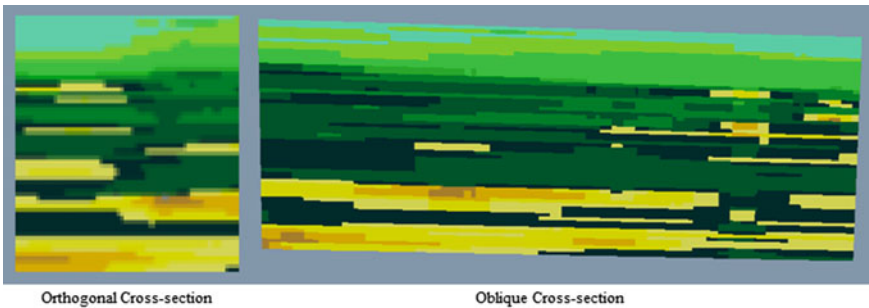
Fig. 9 3D model of the field

Orthogonal Cross-section   Oblique Cross-section

Fig. 10 Cross-sections showing soil stratigraphy

6 Conclusions

- The present study reaffirmed how large quantity of independent data from a given area can be integrated to derive useful inferences in site investigations.
- From the study of geophysical survey data, it can be concluded that serious hazards which may hamper field development are not present in the study area. Also, most of the field has a gentle sloping terrain.
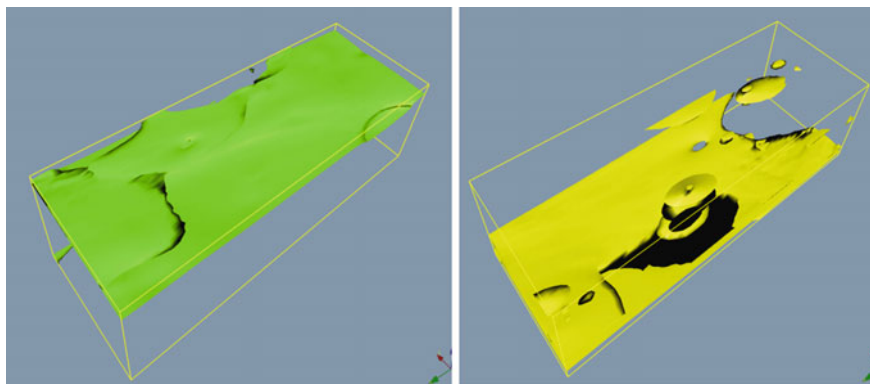
Fig. 11 Isosurface showing very soft clay and loose sand layers

- The soil stratigraphy is dominated by clayey strata with few sand layers. Few clay and sand layers having field wide presence are identified. A high percentage of carbonate is found in the soils of this field.
- The integrated study allowed the creation of a 3D soil stratigraphic model of the field. The 3D model helps is assessing the stratigraphy at locations where geotechnical information is not available.
- Even though the 3D model has many advantages, the quality of the 3D model depends on the number of data point available and numerical interpolation method used to interpolate that data. The users should be aware of the limitations of the 3D soil model while using it to optimize the project work of soil investigations.
- Since the redevelopment of the field is in progress, the presented model shall be used to forecast the stratigraphy at new locations to compare the results using actual field investigation data and to refine the model further. It is proposed that the results of such an endeavor shall be presented in a future paper.

References

1. Gulhati, S.K.: Geotechnical aspects of the Indian offshore environment. In: 31st Annual General Session, Indian Geotechnical Conference. Visakhapatnam, India (1989)
2. Lunne, T., Robertson, P.K., Powell, J.J.M.: Cone Penetration Testing in Geotechnical Practice. Blackie Academic & Professional/Chapman-Hall Publishers, London (1997)
3. Robertson, P.K., Wride, C.E.: Evaluating cyclic liquefaction potential using the cone penetrometer test. Can. Geotech. J. **35**(3), 442–459 (1998)

4. Clark, A.R., Walker, B.F.: A proposed scheme for the classification and nomenclature for use in the engineering description of Middle Western Sedimentary Rocks. Geotechnique **27**, 94–99 (1977)
5. Jamiolkowski, M., Lo Presti, D.C.F., Manassero. M.: Evaluation of relative density and shear strength of sands from CPT and DMT. J.T. In: Germaine, T.C., Sheahan, R.V., Whitman (eds.), Soil Behaviour and Soft Ground Construction, ASCE Geotechnical Special Publication, 119, pp. 201–238. American Society of Civil Engineers (ASCE), Reston, Virginia (2001)
6. Mayne, P.W.: Cone Penetration Testing State-of-Practice, Final Report, NCHRP Project 20–05, Topic 37–14, Transportation Research Board Synthesis Study (2007)

Large-Box Direct Shear Test of Municipal Solid Waste: A Case Study

Lalit Mohan Pathak and Sharique Khan

Abstract Improper disposal of municipal solid waste in landfill sites in the form of huge dump slopes led to various slope instability problems in metro cities. The stability of such slopes is largely governed by the shear strength parameters of the slope. In the present study, the shear strength parameters of a municipal solid waste disposal site were determined by conducting consolidated undrained direct shear test with a shear box size of 300×300 mm. Effective shear strength parameters were evaluated considering peak shear stresses corresponding to 25 mm shear displacement. Apparent cohesion, c′, of 7.4–14.5 kPa with effective friction angle, φ', of 27.5–30.10° were evaluated from the direct shear results. The results of these tests will lead to a better understanding of shear strength properties of municipal solid waste material and ensuring safe disposal of the material in the form of sustainable dump slopes.

1   Introduction

Improper management and uncontrollable disposal of municipal solid waste (MSW) at large landfill sites in India pose a huge risk in environment degradation and have led to various slope stability problems. As per Energy Alternatives India, the MSW generation is estimated to increase at the rate of 5% per annum and per capita waste generation is estimated to increase at 1.33% per annum. The increased waste generation and improper dumping of waste at landfill sites will lead to landfill slope failures causing loss of life and degradation of surrounding environment. The proper knowledge of shear strength properties of waste material is vital for safe and sustainable landfill design. The shear strength of waste governs the stable profile of landfill slope and hence dictates the overall landfill capacity [22].

L. M. Pathak (✉) · S. Khan
ATES, Aimil Limited, New Delhi, Delhi 110044, India
e-mail: lalitpathak@aimil.com

2　Background

Numerous studies have been carried out to ascertain shear properties of MSW [10, 13, 14, 16, 19, 22]. The available literature shows a clear distinction in behaviour of MSW with soil [8]. Models derived from soils, usually, the Mohr–Coulomb failure criterion, defined by cohesion (c) and friction angle (φ) can be used to study the behaviour of MSW in landfill stability analysis [19].

The overall strength characteristics of MSW can be summarized as follows [6, 23]:

- There is an increase in shear strength of MSW with increase in confining pressure in a nonlinear way;
- The fibrous material present in the waste gives rise to an equivalent cohesion at very low confining pressure;
- Presence of plastic bags, paper and cardboard reduces friction angle (φ) of MSW [4],
- An increasing fraction of soil-like, gravel and inert waste increases the friction angle (φ) of MSW [4],
- There is no change in strength of MSW due to variation of density of MSW;
- Age and degradation of MSW play an important role in the shear strength, there is an increase in friction angle and decrease in cohesion with the increment of age of waste material;
- There is a noticeable hardening observed in the shear stress–strain curve and a horizontal asymptotic level is generally not obtained even with large deformations [5, 15, 18]. Hence, it is important to describe a certain level of deformation at which it is assumed that the failure situation has been reached.

As per available literature, about 48% researchers have used laboratory direct shear test to estimate the shear strength properties of MSW [23]. Direct shear test is one of the standard tests employed for the estimation of shear strength properties of MSW. Advantages of direct shear test over alternative test methods are well documented [21, 24, 25]. Some documented aspects of direct shear test are listed as under:

- Samples with large particle sizes can be tested with relative ease;
- The sample can be made to shear in a predefined plane;
- Consolidation is relatively one-dimensional (K_o-consolidation);
- Preparation of sample and test conditions influence test results;
- For appropriate sample dimension, the shear deformation is generally plane strain and occurs by simple shear;
- The test operation is relatively simple and easy;

However, changes in shear surface area during shearing stage and uncertainty in interpretation of results due to non-uniform stress–strain behavior across the shear surface are the major disadvantage of direct shear test.

3 Methodology

Consolidated-undrained direct shear tests were conducted in accordance with IS: [17] (Part-13). Tests were conducted on MSW obtained from four different locations of a landfill site. The first two specimens were tested under imposed normal stresses ranging from 50 to 200 kPa, while the last two specimens were tested under imposed normal stresses ranging from 100 to 400 kPa. The main objective of these tests was to study the behavior of shear strength under different imposed normal stresses.

4 Apparatus and Sample Preparation

The direct shear test was carried out using a large-box direct shear apparatus having box size of 300 × 300 mm and depth 200 mm. The DST machine developed in-house by Aimil is capable of strain-controlled semi-automatic load application and real-time logging of load and displacements in both directions. All instrumentation data was displayed digitally and output was interfaced graphically with a personal computer during testing. A constant shearing rate of 0.6 mm/min was adopted for

Fig. 1 Large-box direct shear test apparatus, Aimil make

shearing. Figure 1 shows the Aimil direct shear test apparatus used to carry out these tests.

Landfill MSW samples were collected from four different pit locations. Samples were packed and transported to the testing facility in gunny bags of 80 kg capacity each. Figure 2 shows the sample preparation and segregation process. The composition of collected sample is shown in Table 1. The samples were air dried and properly segregated. Particle size greater than 50 mm diameter including inert wastes such as glass pieces, plastic bottles, metal parts and other organic biodegradable wastes such as garden wastes were removed before testing the specimen.

Moisture-density relation obtained from standard proctor test on samples Pit-02, Pit-09 and Pit-14 yielded a maximum dry density of 0.735 gm/cc at 57.82% optimum

Fig. 2 Removal of inert waste and organic biodegradable waste from air dried samples

Table 1 Composition of collected sample

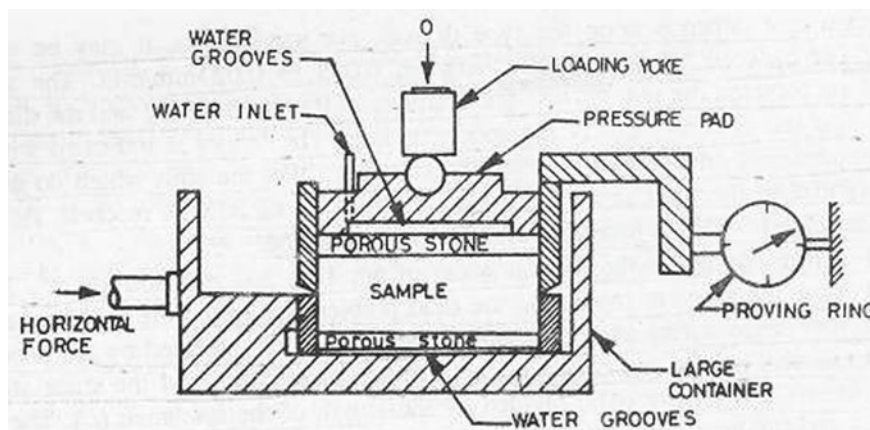| Category	Composition (% by dry mass)			
	Pit-02	Pit-09	Pit-14	Pit-04
Biodegradables	42.8	43.1	40.6	45.2
Paper	9.5	9.9	9.6	7.9
Inert waste	28.2	21.3	27.3	28.6
Others (residual fines)	19.5	25.7	22.5	18.3

Fig. 3 Schematic arrangement of sample in a typical DST setup

moisture content. A maximum dry density of 0.820 gm/cc at 52.43% optimum moisture content was obtained for sample Pit-04. The organic content of the samples ranged between 6.2% and 9.1%. The samples were compacted using a tamping rod in three different layers in the shear box before consolidation process.

The typical arrangement of sample and application normal and shear load on the sample is shown in a schematic diagram in Fig. 3.

5 Result and Discussion

The shear stresses reported were calculated by considering the shear load corresponding to 25 mm shear displacement and initial maximum shear area without applying area correction. The summary of tested samples subjected to different normal stresses is tabulated in Table 2.

Table 2 Summary of tested samples

Sample ID	Normal stress, kPa		Shearing rate, mm/min
	During consolidation	During shearing	
Pit 02 and Pit 09	50	50	0.6
	100	100	
	200	200	
Pit 14 and Pit 04	100	100	
	200	200	
	400	400	

Table 3 Unit weight of MSW samples pre and post-consolidation stage

Sample ID	Compacted total unit weight before consolidation (kN/m^3)	Applied vertical stress (kPa)	Total unit weight after consolidation (kN/m^3)
Pit 02	11.6	50	13.3
	11.6	100	14.3
	11.6	200	15.4
Pit 09	11.6	50	13.3
	11.6	100	14.8
	11.6	200	16.0
Pit 14	11.6	100	14.5
	11.6	200	15.7
	11.6	400	16.2
Pit 04	12.5	100	13.3
	12.5	200	13.5
	12.5	400	14.4

The unit weight of the samples before and after consolidation stage was calculated, with increase in the normal stress applied during consolidation stage there is an increase in the unit weight of the samples tabulated in Table 3.

Figure 4 shows the individual trends of shear stress vs. horizontal shear strain at different normal stresses for all the tests reported in this study.

As evident from Fig. 4, the MSW samples undergo strain hardening, as there is an increase in shear stress with the increase in horizontal displacement. Accordingly, the peak shear strength is interpreted specifically at 25 mm shear displacement from the graphs of shear stress vs. shear displacements. The peak shear strength of MSW is plotted as a function of normal stress and the shear strength parameters obtained are presented in Table 4. A linear Mohr–Coulomb trend has been fitted in each data set to obtain the values of apparent cohesion, c', and effective friction angle, φ', as shown in Fig. 5.

The results obtained from the tested samples indicate that the values of apparent cohesion, c', ranges from 7.4 to 14.5 kPa with effective friction angle, φ', of 27.5°–30.10°. The average value of apparent cohesion, c', is 9.75 kPa with average effective friction angle, φ' as 28°. The results obtained show close conformity with direct shear test results reported by Gabr and Valero [15] on MSW with resulting shear strength properties ranging from 0–28 kPa and 20–39°. Specimen No. Pit-04 shows relatively high value of apparent cohesion, this may be due to the presence of high organic matter which adds to the cohesion value.
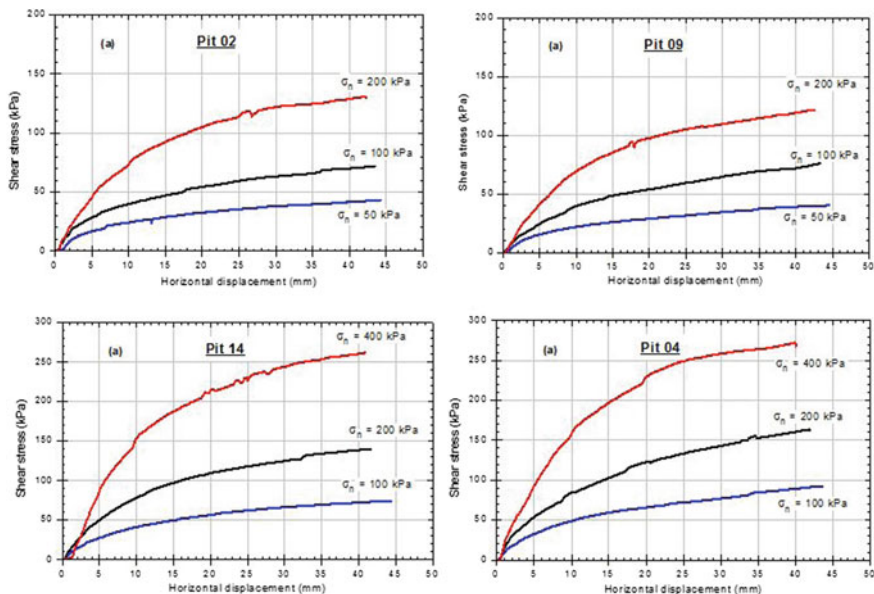
Fig. 4   Shear stress-horizontal displacement results for the tested MSW specimens

Table 4   Summary of results of direct shear test

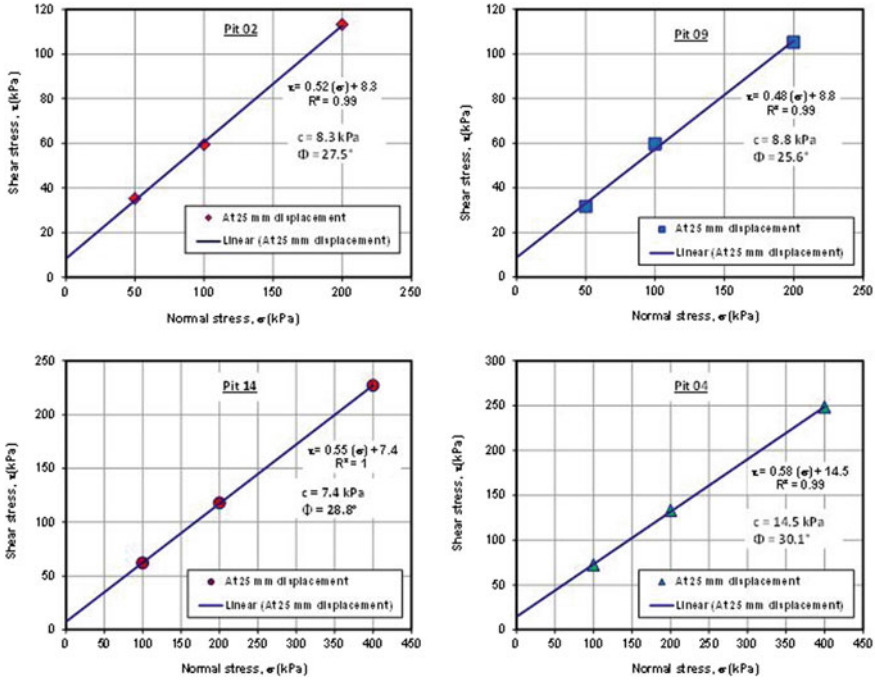| Sample ID	Applied vertical stress (kPa)	Peak shear stress at 25 mm shear displacement (kPa)	Apparent cohesion, c′ (kPa)	Effective friction angle, Φ′ (°)
Pit 02	50	36.00	8.3	27.5
	100	60.30		
	200	116.60		
Pit 09	50	34.10	8.8	25.6
	100	60.20		
	200	106.00		
Pit 14	100	62.70	7.4	28.8
	200	118.40		
	400	225.00		
Pit 04	100	69.50	14.5	30.1
	200	127.50		
	400	247.00		

Fig. 5 Shear strength parameters of tested samples

6 Conclusion

Apparent cohesion, c', of 7.4–14.5 kPa with effective friction angle, φ', of 27.5–30.10° were evaluated from the direct shear results. Based on the presented study, it can be suggested that carrying out the large direct shear tests on MSW samples provides critical engineering parameters for safe design and construction of landfill slopes.

The results of these tests will lead to a better understanding of shear strength properties of municipal solid waste material and ensuring safe disposal of the material in the form of sustainable dump slopes.

References

1. Anderson, D.G., Kavazanjian, E.: Performance of landfills under seismic loading. In: Proceedings of Third International Conference on Recent Advances in Geotechnical Earthquake Engineering and Soil Dynamics, vol. 3, pp. 1557–1587. St. Louis, Missouri (1995)
2. Augello, A.J., Bray, J.D., Seed, R.B., Matasovic, N., Kavazanjian, E.: Performance of solid-waste landfill during the Northridge earthquake. In: Proceedings of NEHRP Conf. on Research on the Northridge, California Earthquake of January 17, 1994 pp. II-71 to II-80. CUREe, Los Angeles, CA (1998a)

3. Augello, A.J., Bray, J.D., Abrahamson, N.A., Seed, R.B.: Dynamic properties of solid waste based on back-analysis of OII landfill. ASCE J. Geotech. Geoenviron. Eng. **124**(3), 211–222 (1998)
4. Bareither, C., Benson, C., Edil, T.: Effects of waste composition and decomposition on the shear strength of municipal solid waste. J. Geotech. Geoenviron. Eng. **138**(10), 1161 (2012)
5. Bouzza, A., Wojnarowicz, M.: Stability assessment of an old domestic waste slope in Warsaw Poland. In: Proceedings of Slope Stability 2000, Sessions of Geo-Denver 2000, no. 101, pp. 48–57. ASCE Geotech, Special Publication (2000)
6. Bray, J.D., Zekkos, D., Kavazanjia, E., Athanasopoulos, G.A., Riemer, M.F.: Shear strength of municipal solid waste. J. Geotech. Geoenviron. Eng. **135**(6), 709–722 (2009)
7. Caicedo, B., Giraldo, E., Yamin, L., Soler, N.: The landslide of Dona Juana landfill in Bogota. A case study. In: Proceedings of the Fourth International Congress on Environmental Geotechnics (4th ICEG), pp. 171–175. Rio de Janeiro, Brazil (2002)
8. Cañizal, J., Lapeña, P., Castro, J., Costa, A., Sagaseta, C.: Determination of shear strength of MSW. Field tests vs. laboratory tests. In: Fourth International Workshop Hydro-Physico-Mechanics of Landfills. Santander, Spain (2011)
9. Duncan, J.M.: Factor of safety and reliability in geotechnical engineering. J. Geotech. Geoenviron. Eng. ASCE **126**(4), 307–316 (2000)
10. Duncan, J.M., Wright, S.G.: Soil Strength and Slope Stability. Wiley (2005)
11. Eid, H., Stark, T.D., Evans, W.D., Sherry, P.: Municipal solid waste slope failure i: waste and foundation soil properties. J. Geotech. Geoenviron. Eng. ASCE **126**(5), 397–407 (2000)
12. Fassett, J.B., Leonards, G.A. & Repetto, P.C.: Geotechnical properties of municipal solid waste and their use in landfill design. In: Solid Waste Association of North America, Proceedings, Waste Tech'94, Silver, pp. 1–31. Springs, MD, USA (1994)
13. Gabr, M.A., Valero, S.N.: Geotechnical properties of municipal solid waste. Geotech. Test J. ASTM **18**(2), 241–251 (1995)
14. Gabr, M.A., Hossain, M.S., Barlaz, M.A.: Shear strength parameters of municipal solid waste with leachate recirculation. J. Geotech. Geoenviron. Eng. **133**, 478–484 (2007)
15. Grisolia M., Napoleoni Q., Tancredi G.: The use of triaxial tests for the mechanical characterization of MSW. In: Proceedings of the 5th International Landfill Symposium, Sardinia'95, Cagliari, vol. 2, pp. 761–768 (1995)
16. Hossain, M.S.: Mechanics of compressibility and strength of solid waste in bioreactor landfills. Ph.D. Dissertation, Department of Civil Engineering, North Carolina State University at Raleigh, NC (2002)
17. IS: 2720 (Part 13)-1986 Code of Practice for Direct Shear Test
18. Jessberger, H.L., Kockel, R.: Determination and assessment of the mechanical properties of waste. In Sarsby R.W. (ed.) Waste Disposal by Landfill—Green '93, pp. 313–322. Rotterdam-Balkema (1993)
19. Landva A.O., Clark J.I.: Geotechnics of waste fill. In: Geotechnics of Waste fills—Theory and Practice, ASTM STP 1070, pp. 86–113. ASTM, Philadelphia, PA, (1990)
20. Reddy, K.R., Hettiarachchi, H., Gangathulasi, J., Parakalla, N., Bogner, J., Lagier, T.: Compressibility and shear strength of municipal solid waste under short-term leachate recirculation operations. Waste Manage. Res. **27**(6), 578–587 (2009)
21. Saada, A.S., Townsend, F.C.: State of the art: laboratory strength testing of soils. Yong, D., Townsend, F.C. (eds.) Laboratory Shear Strength of Soil, pp. 7–77. ASTM STP 740, ASTM International, West Conshohocken, PA (1981)
22. Sharma, H.D., Reddy, K.R.: Geoenvironmental Engineering: Site Remediation, Waste Containment, and Emerging Waste Management Technologies. Wiley, NJ (2004)
23. Stark, T.D., Huvaj-Sarihan, N., Li, G.: Shear strength of municipal solidwaste for stability analyses. Environ. Geol. **57**(8), 1911–1923 (2009)
24. Takada, N.: Mikasa's direct shear apparatus, test procedures and results. Geotech. Test. J. **16**, 314–322 (1993)
25. Terzaghi, K., Peck, R., Mesri, G.: Soil Mechanics in Engineering Practice. Wiley, New York (1996)

Codal Provisions for Foundation Design on Soils and Rocks: A Review

Gaurav Sharma, Pradeep Kumar, Koushik Pandit , **and Sayantani Lala**

Abstract   Usual design of building foundations is performed based on prescribed serviceability and strength criteria as laid down by various standard codes adopted by different countries. Generally, the total settlement of a foundation is described under the serviceability criterion; whereas a strength criterion is described by bearing capacity of the soil or rock underlying the foundation. Both of these safeguard a foundation from its stability and structural integrity point of view against the acting design loads that may appear during its lifetime. The important most function of a foundation is to transfer super-structure load to the underlying strata which are composed of either soil or rock or both in layers. Engineering properties of both soils and rocks vary geo-spatially in small to large scale. In view of the wide spectrum of soil/rock characteristics, the analysis and design of foundations are provided by understanding of basic soil and rock mechanics principles. Although a detailed analysis of site-specific solutions is a must for a vital and large-scale project as well as for a problematic site condition. Building codes present the most relevant guidance in design and construction of foundations. An attempt has, therefore, been made in the present study to revisit and compare foundation design methodology, by studying and investigating three popular design codes, namely Indian Standard Code (IS code), American Concrete Institute Code (ACI) and International Building Code (IBC) by the International Code Council (ICC). In this study, the basic technical information on (i) 'general behavior of soil and rock,' i.e., nature of soil, rock types, stability and properties along with its behavior under foundation, (ii) 'effect of groundwater,' i.e., the effect of underground water on foundation, (iii) 'foundation settlement,' i.e., foundation failure modes, (iv) 'preventive and strengthening measures,' i.e., improvement of bearing capacity of strata through stabilizing methods, etc., have been covered in brief.

Keywords   Settlement · Bearing capacity · Foundation design · Standards and codes; comparative study

G. Sharma · P. Kumar · K. Pandit (✉) · S. Lala
CSIR—Central Building Research Institute, Roorkee 247667, India
e-mail: Koushik@cbri.res.in
URL: https://www.cbri.res.in

1   Introduction

Any building structure transmits its super-structure load through foundations which are constructed over soil or rock, together termed as sub-strata. Foundations are hence called the sub-structure buried beneath the natural ground level (NGL). Elementary design of a foundation is based on satisfactory bearing capacity and tolerable settlement of the sub-strata on which it rests [1]. Design load pressure in excess of the bearing capacity of the sub-strata causes ruptures and develops failure surfaces between the footing edges and ground surface. Diverse failure modes in the sub-strata have been observed and listed as (a) general shear failure: the load beyond ultimate bearing capacity develops, shear force within the soil underlying the footing causes its sudden settlement and bulging over the ground surface; (b) local shear failure: the settlement is accompanied by sudden jerks and little bulging over ground surface and further increase in load causes large settlement and heaving; and (c) punching shear failure: only vertical settlement of soil and footing occurs without any heaving on the ground surface [2, 3]. The design methodologies of sub-structure are thus formulated to suit the indigenous soil conditions for an efficient building design without foundation failure.

Some mechanical properties of soils and rocks are complex and difficult to determine precisely, probably because they are not a manufactured standard product like rolled steel or mix-designed concrete and the origin and process of rock and soil cycles are mainly governed by physical and chemical changes within their micro-structures. Further, the selection of site for construction of a building and its foundation is not entirely within the engineer's control and many times, and a structure is to be built on an apparently weak soil site or highly weathered and fissured rocky topography. Hence, the stability and function of a building largely depend upon the behavior of the soil or rock upon which it is built.

Characteristically, the serviceability is typically a long-term trait for a building foundation related to time-dependent consolidation phenomenon of the bearing sub-strata, whereas the bearing capacity may be a short-term feature (e.g., an embankment construction on an undrained clay foundation) or a long-term feature where the maximum foundation load may appear at an unknown time. Usually, the bearing capacity of shallow and deep or pile foundations is estimated using codal provisions developed after classical soil mechanics principles utilized by Terzaghi and Meyerhoff[4], Meyerhof [5] and static formula by Tomlinson [6], respectively.

For the purpose of design of foundation, a number of codes are available in various countries around the world. As the soil and climatic conditions differ geospatially, the design parameters also alter accordingly, even if the principles of the design methodologies are essentially the same. However, a comparative study of the foundation codes has revealed some inconsistency in the principles considered for design methodologies which should be studied and modified, if and when necessary.

An attempt has, therefore, been made in the present study to revisit and compare foundation design methodology, by studying and investigating three popularly referred and used design codes, namely Indian Standard Codes (IS codes) [7–18],

American Concrete Institute Codes (ACI) [19, 20] and International Building Codes (IBC) [21] by the International Code Council (ICC). In this study, basic information on nature of soil, rock types, stability and properties along with its behavior under foundation, effect of groundwater on foundation, foundation failures, improvement of bearing capacity of strata through soil stabilizing methods, etc., have been covered in brief.

2 Comparison of Codal Design Methodology

For the comparative study three international building codes, namely IS, ACI and UBC/IBC are considered. After studying and analyzing the different clauses of these codes, comparative discussions have been made along with highlighting some research gaps. These comparisons will facilitate the scope of improvement in building codes after further studies and validations.

There are several Indian Standards for foundation on soil and rocks like IS 1080 on "Code of Practice for Design and Construction of Shallow Foundations in Soils (Other Than Raft, Ring And Shell)" [7], IS 1904 on "Code of Practice for Design and Construction of Foundations in Soils: General Requirements" [8], IS 2911 (Part 1 to Part 4) "Design and Construction of Pile Foundations—Code of Practice" [9–12], IS 6403 [13], IS 12070 on "Code of Practice for Design and Construction of Shallow Foundations on Rocks" [14], IS 13063 on "Code of Practice for Structural Safety of Buildings on Shallow Foundations on Rocks" [15], IS 14243 (Part 2) on "Guidelines for selection and development of site for building in hill areas" [16], IS 14593 on "Design and Construction of Bored Cast-in-situ Piles Founded on Rocks - Guidelines" [17] and IS 14804 on "Siting, design and selection of materials for residential buildings in hilly areas—Guidelines" [18]. Prevailing building codes on concrete constructions in the USA are provided in ACI: 318-14 [19], and ACI: 332R-84 [20]. The main regulations for foundations in the International Building Code [21] are located in Section 1808 (Foundations), Section 1809 (Shallow Foundations), and Section 1810 (Deep Foundations).

2.1 Depth of Footing

According to all the considered codes in this paper, footing depth is the depth below the natural ground surface at which the required bearing capacity of soil/rock for load transmission is obtained. The clauses defining the depth of footing according to various codes have been listed below.

Indian Standard. All foundations shall extend to a depth of at least 0.5 m below NGL where the bearing strata are soil. This minimum depth is required to ensure the availability of safe bearing capacity and optimum frost depth [8] (sec. 7.1, 7.2). For

the foundation depth in rocks, Cl. 5.4 of [15] is referred to. It says that (i) in partially weathered, jointed and sheared rocks, foundation base is to be kept at least 0.5 m inside rock; whereas, (ii) for very low strength, rock, foundation material shall be treated to be as soil and depth is defined using IS 1904 [8] provisions; and (iii) for sound and massive rock, foundation line shall be above frost penetration limit.

ACI. Depth of footing above reinforcement should not to be less than 0.15 m even though firm bearing soil is found at a shallower depth. A practical minimum depth is taken as 0.25 m. However, the overall depth of pile foundation shall be selected such that the effective depth of bottom reinforcement is at least 0.3 m as per Cl. 13.3.1.2 and 13.4.2.1 of [19], and Cl. 8.3.2 [20].

IBC. According to IBC (sec. 1805.2 and sec. 1805.2.1) [21], concrete footings and solid masonry foundations shall extend below the frost line. Foundation walls supporting wood shall extend at least 0.15 m above the finish grade adjacent to the wall at all points. However, for masonry buildings, IBC suggests that the depth of footings shall extend to 0.3 m and should confirm to sufficient frost depth.

Discussion. After a preliminary overview, it is noted that the minimum foundation depth prescribed in IS codes is almost double than the other two referred standards. This may be due to heavy weight of solid masonry and concrete (the most common materials of construction used in India), as compared to various lightweight IBS prevalent in other countries [22]. The IBC [21] prescribes regulations about commercial construction, whereas IRC: The International Residential Code [23] prescribes the regulation on residential construction along with home remodeling issues. Hence, the UBC/IBC [21] is a more generic code and prescribes the range of values for the determination of the minimum depth of the foundation. IBC/UBC has also included considerations of frost depth in defining the minimum depth of foundation.

2.2 Cover to Footing Reinforcements

The main reason of providing the cover is to protect the reinforcement from the chemical agents present in the atmosphere. Because inappropriate cover depth results into the corrosion of constituent elements which ultimately reduce the life of the structure.

Indian Standard. Cl. 5.3.6 of [8] recommends a minimum cover of 50 mm for footings. But the actual cover may be even more depending on the presence of harmful chemicals, water table, etc. For locations with considerable salt and sulfate content in water, Cl. 26.4.2.2 of IS 456: 2000 [24] suggests that dense M-20 concrete along with pozzolana could be used. A thick layer of bitumen can be laid before laying foundation concrete to prevent infiltration of water from sulfate bearing soil.

ACI. American building code [19] specifies the cover depth for different regions (Table 1).

Table 1 Summary of concrete cover specification by ACI code [19]

Concrete exposure	Member	Specified cover (mm)
Permanent ground contact	All	75
Exposed to weather or in contact with ground	All	40–50
Not exposed to weather or in contact with ground	Slab joists	40
	Walls	20
	Beams, columns, pedestals and tension ties	40

IBC. There should be a minimum of 3 inches (7.62 cm) concrete between reinforcement and the other main structural member in which the concrete is deposited against the ground and 2 inches (5.08 cm) for concrete surfaces which are just in contact with natural ground level. IBC also suggests a concrete cover of 3.2 cm for prestressed square piles of 12 inches (30.5 cm) or smaller size and 3.8 cm for larger piles. For foundations exposed to seawater, the minimum 6.4 cm of protective concrete cover is prescribed in Sec. 1809.2.3.5 of [21].

The following Table 1 gives a summary of concrete cover specification by ACI code [19].

Discussion. ACI specifies the cover thickness depending upon the type of reinforcement. However, the IS and IBC codes specify concrete cover to foundation as per the climatic conditions irrespective of the provided diameter of the foundation slab reinforcements.

2.3 Longitudinal Reinforcement and Dowel length

The forces and moments developed at column face must be conveyed to footing through the pedestal. The compressive force is delivered to the concrete while the tensile force is taken by the reinforcement steel. However, for balancing large permissible bearing stresses, dowel bars or column extensions should be provided.

Indian Standard. As prescribed in IS, these extending bars should be at least 0.5 percent of the cross-sectional area of the supported column or pedestal. Minimum of four bars shall be provided whose diameter should not exceed the diameter of column bars by 3 mm as per Cl. 34.4 of [24].

ACI. For columns, minimum dowel reinforcement is given as, As (min.) = 0.005 Ag, where Ag is column gross cross-sectional area. Required dowel reinforcement is given by:

As (req) = (Pu – Φ * Pn)/(Φ * fy), where the value of strength reduction factor (Φ) is 0.65, as per Cl. 15.8.2.1 of [19].

IBC. According to IBC [21], the total sectional area of dowels shall not be less than the sectional area of the longitudinal reinforcement of the member and in no case less than four dowels should be used. Also, the diameter of the dowels shall not exceed the diameter of the column bars by more than 1/8 inch (nearly 3 mm) as per Sec. 2623 (h) of UBC [25].

Discussion. As per IS and ACI codes, the minimum sectional area of dowels should be 0.5% of the sectional area of the column or pedestal, whereas, in UBC/IBC, the corresponding minimum area is simply taken as equal to column reinforcement. This lead to contradiction and diverse values, because different codes have different methods for defining the minimum nominal reinforcement.

2.4 Allowable Lateral Soil or Rock Pressure and Bearing Capacity

The bearing capacity or allowable lateral soil pressure of soil is the gross pressure that the footing can withstand such that the soil does not fails in shear and settlement occur within the safe limits [3, 15].

Indian Standard. As per Sec 5.2.2.1 of [13], the equation for calculating of ultimate bearing capacity is:

$$Q_{nu} = c * (N_c i_c S_c d_c) + q * (N_q - 1) * (i_q S_q d_q) \\ + 0.5 B \gamma * N_\gamma * (i_\gamma S_\gamma d_\gamma) * W'$$

Where, $N_\gamma = 2(Nq+1) \tan\Phi$
$\underline{N_c} = (Nq-1) \cot\Phi$
and, $N_q = e\hat{\ }\pi*\tan\Phi*\tan^2(45°+\Phi/2)$
Here, S, d and i are empirical correlation factors for shape, depth and inclination of loading, respectively.
If depth of water below ground $> (D_f)$, then, reduction factor $W' = 1$
If water table at depth $= (D_f)$, then, $W' = 0$.
As per, IS 12070 [14], Cl. 4 gives the calculation of safe bearing pressure (SBP) on rock based on rock mass material types (massive crystalline bedrock having SBP 1000 t/m² to soft or broken bedrock having SBP 40 t/m²). Although, universally applicable SBP values based on rock mass classification cannot be given, but according to Cl. 5 of [14], rock mass rating (RMR) values (100–0) could be used to determine SBP values (600-448 t/m² for RMR = 100 to 81, to 55-45-40 t/m² for RMR = 20–0). For good quality rock with wide joint spacing, i.e., 1 to $\geq$ 3 m, Cl. 6.1 gives an empirical equation to determine SBP based on average UCS of rock cores. Alternatively, Cl. 7 of [14] suggests an empirical equation based on pressure-meter tests to determine SBP for low strength fragmented or weathered rock masses with closely spaced (5–30 cm) discontinuities. In common practice, such cases are considered as granular

Table 2 Allowable foundation pressure and lateral bearing pressure of soil/rock as per IBC [21]

Class of materials	Allowable foundation pressure (kN/m^2)	Lateral bearing pressure of soil (kN/m^2)
Bed rock	575	575
Sedimentary rock	190	19
Sandy gravel	145	9.5
Sand	95	8
Clay	70	5

mass and foundation design is based on conventional soil mechanics. Again, Cl. 9 of [14] outlines a different method to calculate the SBP based on plate load tests performed at field on poor rocks suspected to have bearing capacity less than 100 t/m^2.

Although SBP values can be calculated based on above methods, but the settlement criterion often plays the pivotal role in limiting the SBP value which is finally taken for foundation design. Total settlement shall not be more than permissible settlement as prescribed in Cl. 5.2.2 of [15], whereas differential settlement and tilt of the building shall be not more than the recommended values specified in Cl. 5.2.3 of [15].

ACI. The theoretical bearing capacity of soil (X_1) can be calculated as, $X_1 = (q_{ult} * m_1 - \gamma * D_f)$, where, $m_1 =$ model error for the bearing capacity. According to Meyerhof [5], the model error m_1 can be represented by a random variable with a bias factor of 1.0 and a coefficient of variation of 0.25.

IBC. Allowable foundation pressure and lateral bearing pressure of soil or rock as per IBC [21] is given in Table 2.

Discussion. Allowable bearing capacity in different building codes is different which can be used for proportioning footings. On the basis of the building's performance, a presumptive bearing capacity value is assumed. But these values are used only for preliminary design or for less important structures [26]. It is recommended by IS 1904 [8] that the safe bearing capacity should be estimated only after analyzing soil test data. If water table is present near the footing on non-cohesive soil, then these values should be further reduced to 50%.

2.5 Foundations Adjacent to Slopes

Cl. 10.2 of IS 1904 [8] stipulates the different requirements for construction of building foundations on a sloping terrain. It says that any construction on a suspected unstable landslip area should be avoided. Spread footing on sloping sites should be prepared resting on horizontal bearing strata by making a stepped ground profile by

cut and fill method. At all level changes, the footings should be lapped at the steps for a minimum distance of foundation thickness or twice the height of step, whichever is the maximum (Cl. 10.2.4 of [8]). On valley side, clearance on valley side, i.e., the minimum edge distance of the footing from slope's crest should be more than 1.5 m and should rest on a firm soil or rock as per Cl. 6.1 of IS 14243 Part 2 [16].

3 Strengthening Measures for Foundations

There are some guidelines provided by the IS codes to strengthen the foundation of buildings to make it stable under the prevailing design loads. These guidelines may be summarized as below:

- For water covered bearing strata, suitable drainage arrangement shall be provided (Cl. 6.2.5 of [15]). For prevention of water entry into foundation, a minimum of 0.75 m wide apron should be provided all around the building (Cl. 6.3 of [16]).
- For wide joints, cracks, areas of disintegrated rock, the foundation should grouted with 1:1 cement sand mortar up to maximum frost depth [15].
- If at the time of actual excavation, major solution cavities have been found which have rendered the ground surface uneven, the depth of foundation should be taken to a level such that 80% rock area is available. It must be ensured that the raft does not over hang at any corner (Cl. 10.1 of [15]).
- Due attention should be paid to problems of foundation on heterogeneous rocks, particularly, foundations on rock slopes and necessary remedial measures should be taken (10.5 of [15]).
- Foundations should be checked for total and differential settlements to trace any distress in the foundation after construction of the super-structure [27].
- The foundation should be well beyond the influence shear zone created due to cuttings or excavations or due to proximity of the foundation to a sloping ground (Cl. 10.2.5 of [8]).
- If the probable slip surface passes through a support structure like a retaining wall, then it should be made strong enough to resist any unbalanced thrust coming due to slope movement.
- The minimum horizontal spacing between an existing footing and a new one shall be equal to the width of the wider one (Cl. 14 of [8]).

4 Conclusion

The present comparative study of foundation design methodology was taken up by studying and investigating several design codes that prescribes the standards for the efficient foundation design. Later in this paper, contrasting discussions of clauses along with some propositions are thus been delivered for further detailed analysis for codal improvement. However, the study here has been limited to only three codes

of practice of foundation design. It has been found that in some sections, a common basic assessment criteria has not been followed and hence should be considered for future ongoing studies.

Though the codes listed above provide every necessary details of foundation design, but there is a need to update the depth consideration in the Indian Standards in accordance with the various climatic classifications. Footing located at insufficient depth is subjected to frost damage due to formation of ice lenses and consequent frost heave. During summer, thawing occurs and melted water is entrapped. As the soil water freezes and melts, the footing is lifted during cold weather and it settles during warm weather due to an increase in water content. To prevent frost damage, the footing should be placed below the frost depth, which may be 1 m or more in cold climate [1, 26]. India being considered a tropical country, the frost depth has not been taken into consideration while calculating minimum footing depth. However, several regions in India record snowfall in winter and hence these criteria should be considered in the codal methodology. Also, in Annexure-V of CPWD handbook of plinth area rates, the depth dependency is based upon the soil bearing capacity alone [28]. Between the different building codes of the USA, it is difficult to determine which frost penetration charts should be followed. However, in warm states for concrete or block wall foundations, frost depth could extend to 45 cm, whereas in regions like Canada and Alaska, the required depth can even extend to 150 cm. Similar to these charts, a frost depth map is also needed suiting to the geophysical conditions of the Indian terrain.

On the other side, the IBC and ACI codes give more descriptive details of concrete cover to reinforcements for foundations which should be followed in Indian Standards. According to ACI, even if the bearing strength of concrete is not exceeded, reinforcement must be provided at column interface. This type of specification is not provided in other two codes. Also, ACI provides the upper limiting value of dowel reinforcement, i.e., no. 36 (35.81 mm in dia.), while IS and UBC agree on the minimum diameter of dowel should not extend the diameter of reinforcement by 3 mm. Dowels should extend in supported member at least the greater of the development length of the longitudinal bar in compression which is entirely different due to different methods of design. Apart from this, there is requirement of a standard formula in IS code for calculation of dowel reinforcement.

The comparison drawn between different codes for the presumptive safe bearing pressures of foundations on different soils and rocks shows much variance in the values of SBP, even for the same type of soil. Though the soil characteristic of different regions is different but this much deviation should be taken into consideration and needed to be checked again.

References

1. Das, B.M.: Principles of Foundation Engineering, 7th edn. Cengage (2016)
2. Ranjan, G., Rao A.S.: Basic and Applied Soil Mechanics, 3rd edn., New Age International Publication (2016)
3. Murthy, V.N.S.: Textbook of Soil Mechanics and Foundation Engineering. Marcel Dekker Inc. (2005)
4. Terzaghi K.: Theoretical Soil Mechanics, 1st edn. Wiley (1943). https://doi.org/10.1002/9780470172766
5. Meyerhof, G.G.: The ultimate bearing capacity of foundations. Géotechnique **2**(4), 301–332 (1951). https://doi.org/10.1680/geot.1951.2.4.301
6. Tomlinson, M., Woodward, J.: Pile Design and Construction Practice, 5th edn. Taylor and Francis, New York (2008)
7. IS 1080: 1985 (RA 2002): Indian Standard Code of Practice for Design and Construction of Shallow Foundations in Soils (Other Than Raft, Ring and Shell). Bureau of Indian Standards, Manak Bhavan, 9 Bahadur Shah Zafar Marg, New Delhi 110002
8. IS 1904: 1986 (RA 2006): Indian Standard Code of Practice for Design and Construction of Foundation in Soil. Bureau of Indian Standards, Manak Bhavan, 9 Bahadur Shah Zafar Marg, New Delhi 110002
9. IS 2911 (Part 1/Sec 1): 2010, Design and Construction of Pile Foundations—Code of Practice Part 1 Concrete piles Section 1 Driven Cast In-situ Concrete Piles, 2nd revision. Bureau of Indian Standards, Manak Bhavan, 9 Bahadur Shah Zafar Marg, New Delhi 110002
10. IS 2911 (Part 1/Sec 2): 2010, Design and Construction of Pile Foundations—Code of Practice Part 1 Concrete Piles Section 2 Bored Cast In-situ Concrete Piles, 2nd revision. Bureau of Indian Standards, Manak Bhavan, 9 Bahadur Shah Zafar Marg, New Delhi 110002
11. IS 2911 (Part 1/Sec 3): 2010, Design and Construction of Pile Foundations—Code of Practice Part 1 Concrete Piles Section 3 Driven Precast Concrete Piles, 2nd revision. Bureau of Indian Standards, Manak Bhavan, 9 Bahadur Shah Zafar Marg, New Delhi 110002
12. IS 2911 (Part 1/Sec 4): 2010, Design and Construction of Pile Foundations—Code of Practice Part 1 Concrete piles Section 4 Precast Concrete Piles in Pre-bored Holes, 1st revision. Bureau of Indian Standards, Manak Bhavan, 9 Bahadur Shah Zafar Marg, New Delhi 110002
13. IS 6403: 1981 (RA 2002): Code of Practice for Determination of Bearing Capacity of Shallow Foundations. Bureau of Indian Standards, Manak Bhavan, 9 Bahadur Shah Zafar Marg, New Delhi 110002
14. IS 12070: 1987 (RA 2010): Code of Practice for Design and Construction of Shallow Foundations on Rocks. Bureau of Indian Standards, Manak Bhavan, 9 Bahadur Shah Zafar Marg, New Delhi 110002
15. IS 13063: 1991 (RA 2001): Structural Safety of Buildings on Shallow Foundations on Rocks Code of Practice. Bureau of Indian Standards, Manak Bhavan, 9 Bahadur Shah Zafar Marg, New Delhi 110002
16. IS 14243 (Part 2): 1995 (RA 2005): Selection and development of site for building in hill areas guidelines; part 2 selection and development, Bureau of Indian Standards. Manak Bhavan, 9 Bahadur Shah Zafar Marg, New Delhi 110002
17. IS 14593: 1998 (RA 2003): Design and Construction of Bored Cast-In-Situ Piles Founded on Rocks—Guidelines. Bureau of Indian Standards, Manak Bhavan, 9 Bahadur Shah Zafar Marg, New Delhi 110002
18. IS 14804: 2000 Siting, Design and Selection of Materials for Residential Buildings in Hilly Areas—Guidelines. Bureau of Indian Standards, Manak Bhavan, 9 Bahadur Shah Zafar Marg, New Delhi 110002
19. ACI: 318-14: Building Code Requirements for Structural Concrete (ACI 318M-14) and commentary (ACI 318 RM-14). American Concrete Institute (2014)
20. ACI: 332R-84: Guide to Residential Cast-in-Place Concrete Construction. American Concrete Institute (1999)

21. IBC: International Building Code. International Code Council (2012)
22. Brand, A.H., Trivedi, K.H.: Foundation design and construction in urban environments. In: Proceedings of the International Foundations Congress and Equipment Expo, pp. 1550–1559. ASCE, San Antonio (2015)
23. IRC: The International Residential Code. International Code Council (2012)
24. IS 456: 2000, Indian Standard Code of Practice for Plain and Reinforced Concrete. Bureau of Indian Standards, Manak Bhavan, 9 Bahadur Shah Zafar Marg, New Delhi 110002
25. UBC: International Conference of Building Officials. 10 South LOS Robles, Pasadena, California 91101 (1967)
26. Pillai, S.U., Menon, D.: Reinforced Concrete Design, 3rd edn. Mc Graw Hill (2003)
27. IS 8009 Part 1: 1976 (RA 1998), Code of Practice for Calculation of Settlement of Foundations: shallow Foundations Subjected to Symmetrical Static Vertical Loads. Bureau of Indian Standards, Manak Bhavan, 9 Bahadur Shah Zafar Marg, New Delhi 110002.
28. Plinth Area Rates Handbook. Central Public Works Department, M/s Jain Book Agencies, C-9, Connaught place, New Delhi 110001 (2012)

Influence of API *p–y* Procedures on Design of Offshore Piles in Clay

Rupam Mahanta and R. K. Ghanekar

Abstract In case of long piles used to support fixed offshore platforms, load in lateral direction is often a major component of design loads significantly influencing their design. Generally, American Petroleum Institute (API) recommendations are followed for design of piles for platforms in Indian offshore. In case of soft clay, API RP 2GEO [1] recommendation for generating lateral soil resistance-displacement (*p–y*) data is based on the procedure given by Matlock [2]. However, for clays, where undrained shear strength (s_u) is more than 100 kPa and *p–y* procedure for stiff clay is recommended to be followed, and relevant API codes have generally referred to the *p–y* procedure given by Reese et al. [3]. Problems are sometimes encountered in analysis when stiff clay occurs near the seafloor and the procedure for *p–y* data given by Reese et al. [3] is applied. Therefore, a comparative study was carried out by applying both these *p–y* procedures in stiff clays to examine the influence of the procedures on design of piles. Cyclic *p–y* data were generated in line with offshore loading environment. Comparative results show that the influence of the *p–y* procedures is significant, especially when the pile's lateral displacement normalized with pile diameter crosses certain limits.

Keywords Offshore · Pile · Lateral

1 Introduction

Open-ended steel tubular piles are the permanent foundation for offshore jacket platforms. In general, the diameter of piles for these fixed jacket platforms in Indian offshore is within the range of 1.2–2.4 m. Vertical penetration below the seafloor may be typically 60–150 m. As such, these piles are long or flexible piles. For design purpose, the piles should be safe in capacity against design loads, their displacement

R. Mahanta (✉) · R. K. Ghanekar
Institute of Engineering and Ocean Technology, ONGC, Panvel, Maharashtra 410221, India
e-mail: rupam.mahanta@gmail.com

R. K. Ghanekar
e-mail: rkghanekar@gmail.com

should be within allowable limit governed by the purpose for which the platforms are built and the structural stress should be within allowable limit. Design of offshore jackets and piles are carried out using interactive analysis of soil, pile and structure applying numerical technique. For the soil-pile interactive analysis, the lateral resistance versus displacement of soil at various depths below the seafloor is represented by 'p–y data'. These data represent the nonlinear lateral stress–strain behaviour of soil. For generating the p–y data, API [1] recommends, in the absence of other procedures, to follow the method based on Matlock [2] in case of soft clay. As per the referred code, undrained shear strength (s_u) limit for using the soft clay procedure is 100 kPa, beyond which the p–y procedure for stiff clay is recommended to be considered. Relevant API codes do not recommend any particular procedure for stiff clay, but, have generally referred to the procedure given by Reese et al. [3] for many years, although in recent version [1], the procedure is referred for 'structured' stiff clay only. The procedures already mentioned are hereafter referred as 'soft clay' and 'stiff clay' p–y procedures, respectively, in the paper.

2 Background of the Study

There are locations in western Indian offshore where the design value of s_u in some layers near the seafloor is 100 kPa or more. It was observed in certain cases that due to change of procedure for generating p–y data when s_u exceeded 100 kPa, there was an significant impact on analysis. For clays with value of s_u 100 kPa or slightly more, nearly the same result is ideally expected from analysis, irrespective of applying any of the two procedures for p–y data. It was of interest to verify this aspect. Further, practical difficulties sometime arise in carrying out analysis of existing piled structures when soil near seafloor at the site is predominantly stiff clay and the 'stiff clay' p–y procedure is applied for pile-soil-structure interactive analysis. In some of such cases, the analysis suddenly collapses while applying increasing lateral load on the structure. Therefore, a comparative study was carried out on the effect of the two p–y procedures on analysis of offshore piles where soil near seafloor was mainly stiff clay. Pile-soil interactive analysis was carried out on single, fixed-headed, vertical pile with purely lateral loads using cyclic p–y data as per the referred procedures.

3 Lateral Loading on Long Offshore Piles

In case of long offshore piles, the soil near the seafloor influences the result of lateral loading. Beyond a certain depth below seafloor, the soil reaction in response to applied lateral load at pile head is negligible. The bending moment, lateral displacement, shear and rotation in pile with respect to a specific lateral load depend on the soil characteristics (represented by characteristics of p–y springs), properties of pile material, pile geometry and pile head restraint. The focus of the present study is
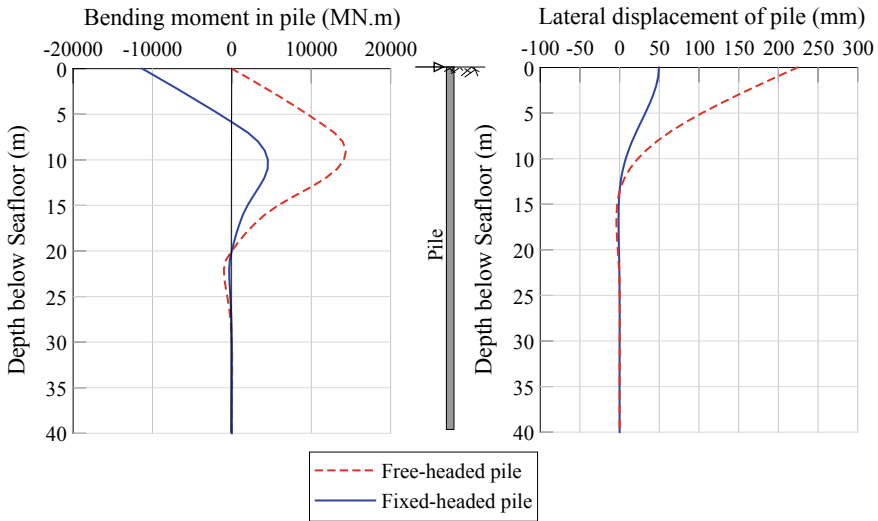
Fig. 1 Typical pattern of bending moment and displacement for a long pile in response to applied lateral load at pile head

primarily on the impact of application of the two API-referred 'soft clay' and 'stiff clay' procedures for generating cyclic *p–y* data for stiff clay layers. As mentioned already, the application of the two procedures on stiff clays is to find how the *p–y* procedures make difference in the analysis with the same soil, pile and lateral loads.

Figure 1 shows typical patterns of bending moment and displacement in response to lateral load for a long pile with free and fixed-headed conditions. However, the comparative analysis presented in the paper was carried out considering piles as 'fixed-headed' in view of very high restraint on pile head against rotation generally applicable for offshore jacket structures.

4 Pile and Soil Data

For the comparative study presented in this paper, first an ideal soil profile with 100 kPa as constant s_u has been considered since this is the transition s_u value where the procedure of *p–y* is to be changed as recommended by API [1]. This profile is subsequently referred to as 'soil-1' in the paper. Open-ended steel tubular pile with outer diameters ranging from 1.219 to 2.134 m with pile wall thickness of 50 mm and vertical penetration of 90 m were considered for the study with this profile. The purpose of selecting the range of pile diameters was to examine the variation of results of analysis with respect to the practical range of diameter for long piles generally used for fixed platforms in Indian offshore.

Table 1 'Soil-2' design parameters

Soil layer	Depth (m)	s_u(kPa)	ϕ' (deg.)	γ' (kN/m³)	k (MN/m³)	ε_{50}(%)
1	00.0–05.8	19	–	6	–	1.5
2	05.8–16.0	100	–	9	–	1
3	16.0–18.3	55	–	9	–	1
4	18.3–21.3	55	–	7	–	1
5	21.3–26.5	280	–	10	–	0.5
6	26.5–31.0	140	–	10	–	0.5
7	31.0–40.2	140–160	–	7.5	–	0.5
8	40.2–43.5	-	30	10	16.5	-
9	43.5–54.0	160–250	–	8.5	–	0.5

Note ϕ' = effective angle of internal friction; γ' = effective unit weight; ε_{50} =strain at 50% failure stress; k = rate of increase with depth of initial modulus of subgrade reaction for lateral soil resistance and limit unit end bearing pressure for layer-8 is 3 MPa

Subsequently, an actual soil profile from a platform location in western Indian offshore, where both soft clay and stiff clay exist near seafloor was also analysed. The pile outer diameter for the platform was 1.829 m with wall thickness of 44 mm for 80 m below seafloor and 50 mm for 2 m of the pile length above its bottom. Relevant part of soil (subsequently referred as 'soil-2') data for the platform location has been presented in Table 1.

Cyclic *p–y* data were generated with both 'soft clay' and 'stiff clay' procedures for clays with s_u of 100 kPa or more for the comparative analyses. Details of the procedures for generating the *p–y* data for clay layers are referred to the API code [1] and corresponding papers [2 and 3] for the procedures. Data of *p–y* for the sand (layer no. 8 in 'soil-2') were generated following API [1] procedure, although the influence of the layer on the analysis result is not significant.

For the analysis with data of 'soil-1', cyclic *p–y* curves generated by using both the referred procedures are shown in Fig. 2 for depths at seafloor and at 10 and 20 m below seafloor. However, for the interactive analysis, *p–y* curves have been used at every metre depth along the pile depth below seafloor.

It may be observed that the initial parts in the graphs with both the procedures are similar in pattern. But, as the soil displacement increases, the soil stiffness with respect to individual procedure may vary significantly. It may also be observed that except for the *p–y* curve at seafloor, post-peak degradation of stiffness of the *p–y* springs is more as per the 'stiff clay' procedure when compared with the 'soft clay' procedure. It may be due to the presence of secondary structures such as fissures and joints in the stiff clay where the tests were conducted for deriving the 'stiff clay' procedure. Further, the peak lateral resistance of soils is also different with the two procedures.

It may be mentioned that degradation of soil resistance is more with increasing displacement of soil in case of cyclic *p–y* data compared to static. However, analysis considering static *p–y* data is out of scope of this paper. Only cyclic *p–y* data have
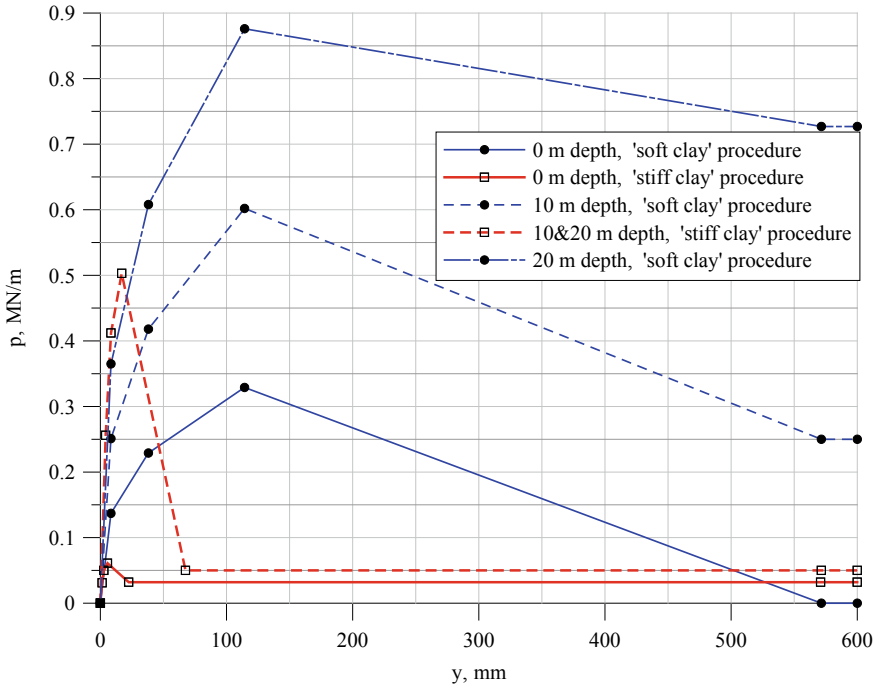
Fig. 2 *p–y* data as per the 'soft clay' and 'stiff clay' procedures at 0 m, 10 m and 20.0 m depths for pile diameter 1.524 m in soil with constant s_u of 100 kPa

been used in the present study in view of the standard practice of the offshore industry for analysis of piles for fixed platforms.

5　Analysis, Results and Discussion

5.1　Soil with Constant s_u (for Profile 'soil-1')

Analysis was performed by increasing the lateral load on pile and corresponding results of displacement, bending moment, etc., were noted. Lateral displacement and bending moment for pile diameter 1.524 m corresponding to an applied lateral load of 2000 kN have been shown in Fig. 3.

Lateral displacement and bending moment at pile head with respect to increasing lateral loads are shown in Fig. 4 for the pile (diameter 1.524 m) using both the *p–y* procedures.

It may be observed that the displacement at pile head is lesser by about 30–40% on applying the 'stiff clay' procedure when compared with the 'soft clay' procedure up
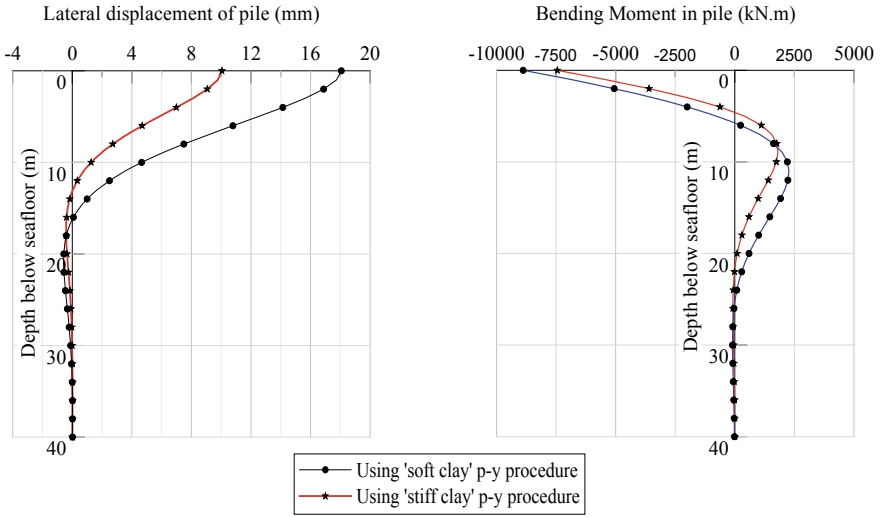
Fig. 3 Pile displacement and bending moment for pile diameter 1.524 m corresponding to lateral load of 2000 kN applied at pile head
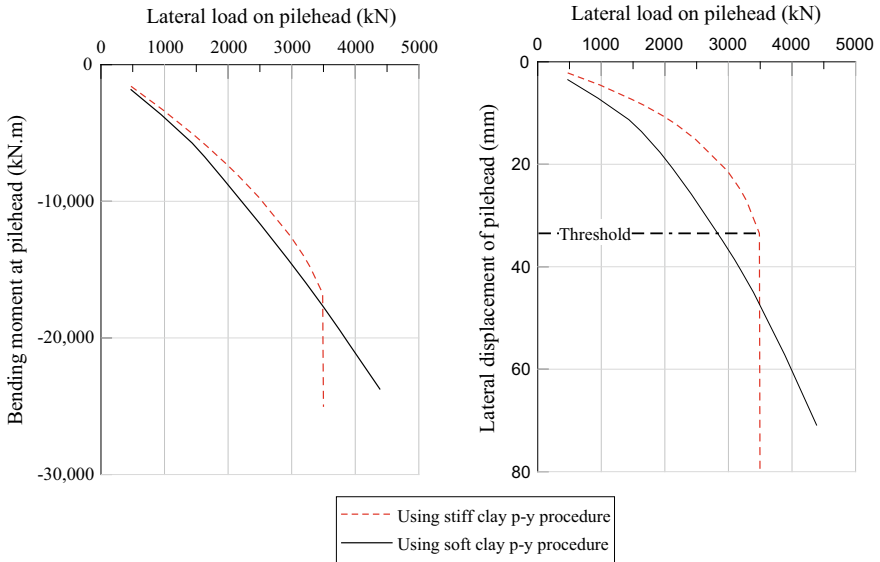
Fig. 4 Pile head displacement and bending moment with variation of lateral load with 'soil 1' for pile diameter 1.524 m

to a limit of lateral load on the pile. Similarly, the bending moment is also less with the 'stiff clay' procedure up to a limit of lateral load; however, the difference in case of bending moment is lesser compared to displacement.Thus, at relatively lower lateral loads, the pile response is found to be stiffer when using the 'stiff clay' procedure compared to results from using the 'soft clay' procedure. For the pile diameter of 1.524 m, limiting lateral load is found to be about 3500 kN up to which the 'stiff clay' procedure gives lesser bending moment and lateral displacement. When the load exceeds this limit, the displacement and bending moment increase rapidly and the foundation collapses.

Analysis using the 'stiff clay' *p–y* procedure indicates that at relatively higher load, the lateral stiffness of the soil-foundation system drastically reduces after reaching a certain limit of displacement resulting in sudden failure of the foundation. The foundation collapses at relatively smaller lateral displacement when the 'stiff clay' *p–y* procedure is applied. It is thought that this is the reason why problems are sometimes encountered in case of analysis related to modification/requalification of some existing offshore platforms. Generally, for those platforms, lateral load for analysis is higher than that considered in initial design due to change of design wave load over the period since original design and/or increased facilities built in many of them subsequent to their original installation. Generally, problems are faced in analysis of such cases where *p–y* data are generated using the 'stiff clay' procedure and predominantly stiff clay exist near seafloor. Numerical problem sometimes occurs as the foundation suddenly collapses in analysis after reaching the threshold lateral displacement of pile, although offshore piles or structures are permitted to undergo much higher displacement from serviceability point of view. As evident from Fig. 4, on using the 'soft clay' *p–y* model, this problem is not encountered as the lateral displacement and bending moment of pile increases gradually with increasing lateral load till a significantly higher level of displacement.

In order to verify the results for the practically used range of pile diameters, analysis was carried out with different pile diameters to derive the limiting lateral displacement with respect to pile diameter. Results of analysis on the displacement limit (normalized with pile diameter) where the use of the 'stiff clay' procedure may predict sudden collapse of foundation are presented as Table 2. It is observed that the average normalized lateral displacement is 2% at which the foundation is predicted

Table 2 Threshold displacement of pile for 'soil-1' profile with 'stiff clay' procedure

Pile diameter (m)	Displacement/diameter (%)	Displacement (mm)	Lateral load (kN)
1.219	1.9	23.3	2289
1.372	2.0	27.9	2857
1.524	2.2	33.5	3487
1.829	2.0	37.3	4683
1.981	2.1	41.4	5412
2.134	2.0	42.7	6050

to collapse. This was verified for the 'soil-1' profile, i.e., with s_u value of 100 kPa (constant with depth) for the range of pile diameters 1.219–2.134 m.

5.2   Analysis for Existing Platform with Soil Profile 'soil-2'

Analysis was performed for the 'soil-2' profile of a location from western Indian offshore where a fixed platform exists. The result of displacement and bending moment in pile in response to lateral pile head load shows a similar trend as in case of 'soil-1'. The result of displacement is shown in Fig. 5. In this case, the soil near seafloor was not completely stiff clay, but stiff clay occurs for a significant depth within the influence zone applicable for lateral resistance of pile. Therefore, the load–displacement response of the pile was expected to be significantly influenced by the stiff clay p–y characteristics in this case also. It is found from the analysis that the foundation is predicted to collapse at a threshold displacement of 3.7% of pile diameter if the 'stiff clay' procedure is used for the stiff clay layers. Therefore, the lateral load on the pile cannot be increased beyond a limit in this case also. However, on using the 'soft clay' procedure for the stiff clay layers, the pile continues to displace laterally for a large displacement with increasing lateral load without showing sudden failure of the soil-foundation system.
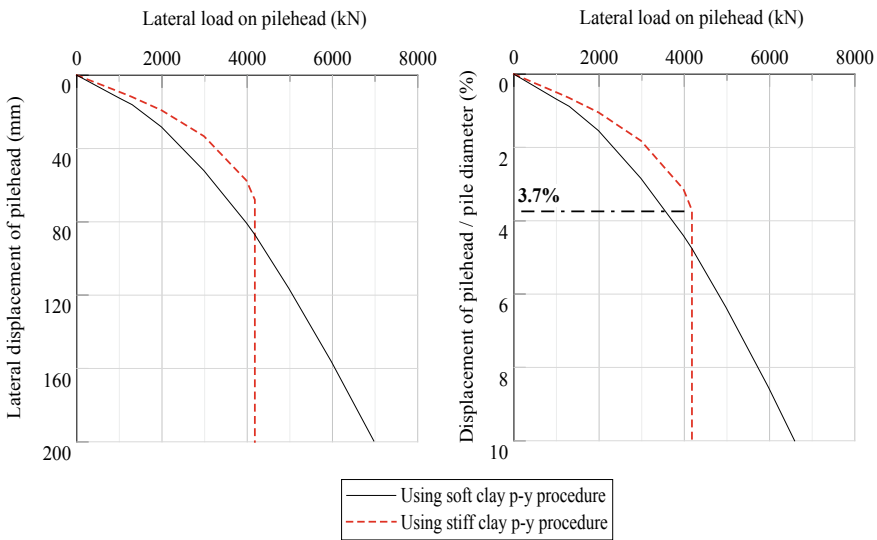
Fig. 5 Pile head displacement and bending moment with variation of lateral load for 'soil-2' and pile diameter 1.829 m

6 Conclusion

From the study influence of two *p–y* procedures on flexible and fixed-headed offshore piles, the following conclusions are made:

- Application of cyclic *p–y* data generated by using the procedure given by Reese et al. [3] on stiff clay results in a stiffer lateral response of the pile till a certain limit of lateral displacement of pile when compared to results from using the procedure of Matlock [2]. In a soil profile with constant undrained shear strength of 100 kPa ('soil-1'), sudden collapse of the soil-foundation system is predicted at displacement of about 2% of pile diameter if the 'stiff clay' *p–y* procedure is applied. For the case of an actual offshore platform mentioned as 'soil-2' profile, corresponding limit displacement of pile was found to be 3.7% of the pile diameter.
- Numerical problem that is encountered sometimes in the interactive analysis of soil, pile and structure in sites having predominantly stiff clay near seafloor may be due to the brittle nature of failure characterized by the *p–y* springs as per the 'stiff clay' procedure as indicated by the study. Numerical problem and the lesser limit of displacement before collapse may also be for the reason that except for the *p–y* curve at seafloor, post-peak degradation of stiffness of the *p–y* springs is more as per the 'stiff clay' procedure when compared with the 'soft clay' procedure.
- Both the 'soft clay' and 'stiff clay' *p–y* procedures are ideally expected to produce nearly the same results when the undrained shear strength of the clay is at or very close to the transition s_u value, i.e., 100 kPa. However, differences in results of analysis are found to be significant. Initial part of the lateral load–displacement response is stiffer when 'stiff clay' *p–y* procedure is used, but after some limit, the stiffness rapidly degrades leading to the prediction of sudden failure.

It is also indicated by researchers [4] that the *p–y* procedures referred by API recommended practice may be quite conservative for practical application in case of piles for offshore platforms. It is understood that many consultants use the 'soft clay' procedure much beyond the limit prescribed by API without any known consequent mishaps. In view of the analysis and general opinion of researchers/designers working on offshore geotechnical engineering, there is scope for further research on formulating more realistic *p–y* procedures for analysis of offshore piles, especially in stiff clays and layered soil profiles which can improve the results with respect to offshore loading environment and soil behaviour.

References

1. American Petroleum Institute: Geotechnical and Foundation design Considerations, ANSI/API RP 2GEO. 1st edn. API, Washington, DC (2011, Addendum 1, 2014)
2. Matlock, H.: Correlations for design of laterally loaded piles in soft clay. In: Proceedings of the Offshore Technology Conference, pp 577–594. OTC Paper No. 1204 (1970)
3. Reese, L.C., Cox, W.R., Koop, F.D.: Field testing and analysis of laterally loaded piles in stiff clay. In: Proceedings of the 7th Annual Offshore Technology Conference, pp. 671–690. OTC Paper No. 2312 (1975)
4. Nichols, N.W. et al.: Effect of lateral strength and stiffness on jacket foundation integrity and design for South China Sea Sites. In: Proceedings of the Offshore Technology Conference. OTC Asia Paper No. 24842-MS (2014)

Effect of Different Densities and Saturation on Unconfined Compressive Strength of Expansive and Yellow Plastic Clay

Dhruval Shah, Nazimali Chinwala, and Hitesh Desai

Abstract It is well-known that the effects of saturation and maximum dry density can be enormous on the unconfined compressive strength of the soil. This paper asserts the existence of a huge change in the behaviour of the unconfined compressive strength of soil at the combined effect of different densities and saturation conditions. This experiment was done on expansive soil and yellow plastic clay taken from different cities of South Gujarat region in India. The findings show a unique behaviour of the strength of soil at the standard Proctor test's maximum dry density with the combination of various saturation conditions. A unique upward trend was noticed at the standard Proctor test density at different saturation conditions. Also, different saturation conditions were derived from the experiment.

1 Introduction

During the construction of a fill or embankment, the degree of saturation of the compacted soils is usually, in an unsaturated condition, controlled at around 60–70% for maximum dry density [1]. Due to natural factors, the strength of soil decreases quickly, which will often cause the shear failure of soil during the rainy season [2]. Soil stabilization through mechanical and chemical processes is commonly used to enhance soil properties such as increasing the shear strength of the soil [3]. This

D. Shah (✉) · H. Desai
Unique Engineering Testing & Advisory Services, Surat 394210, India
e-mail: dhruvalshah9630@gmail.com

H. Desai
e-mail: hitesh@uniquesurat.com

N. Chinwala
Applied Mechanics Department, SVNIT Surat, Surat 395007, India
e-mail: nazimali.chinwala@gmail.com

work is mainly focused on the study of the unconfined compressive strength of saturated soil which mainly depends on saturation percentage and dry density [4]. In past decades, lots of research have been done by introducing various materials whether it maybe lime, fly ash or certain add mixtures. But this present study provides the relation between densities and various saturation conditions, to identify the particular saturation percentage at which soil gives better strength. The tests were made by remoulding the sample at each considered densities by the help of standard and modified Proctor test at 80, 85, 90, 95 and 100% of saturation [5]. The physical properties, standard and modified Proctor tests have been done twice to get accurate results, and the average value has taken into consideration. The unconfined compressive strength test has been done by remoulding the sample and from every mould, three samples were extracted an average value which has been considered. From specific gravity and dry density, saturation is derived and we consider 80–100% of saturation with the interval of 5%. Repetitions have been done if necessary. The purpose of this study is to discover the effect of saturation on unconfined compressive strength at every possible condition.

2   Method

2.1   Material

In this experiment, four types of soils are collected from two different cities of South Gujarat region which are (1) expansive soil (ES) and (2) yellow plastic clay (YS) from Silvasa and Bharuch cities. Table 1 presents the physical properties and both Proctor test results, which mentions grain size analysis, Atterberg limits, IS classification, free swell index, specific gravity, standard Proctor test and modified Proctor test results. All of the tests are performed twice.

2.2   Instruments

The instruments used are a mould with a diameter of 100 mm and height 125 mm. Three sample tubes with a diameter of 28 mm and height 130 mm. Sampler with a diameter of 28 mm and height 74 mm. A plunger with 20 mm thickness and 98 mm the diameter. Hydraulic sample extractor is needed to compress and also extract the sample from the mould [5]. Three-layer measurement tools were also used. The instruments used are different than the universal remoulding tool. This mould is used to extract three samples from the same mould to get more uniformity in the specimens.

Table 1 Physical properties

Soil Property	Silvasa ES	Bharuch ES	Silvasa YS	Bharuch YS
Gravel %	1	0	10	22
Coarse sand %	1	1	10	9
Medium sand %	0	0	8	6
Fine sand %	5	2	5	26
Silt + Clay (%)	91	97	66	37
Liquid limit%	52	60	53	41
Plastic limit %	22	25	24	20
Plasticity index %	30	35	29	21
IS classification	CH	CH	CH	SC
Specific gravity gm/cm^3	2.669	2.464	2.672	2.835
Free swell index %	54	55	24	36
S.OMC[a] (Standard) %	22.5	20.8	21.87	20.01
S.MDD[b] (Standard) gm/cm^3	1.602	1.651	1.633	1.652
M.OMC[c] (Modified) %	18.7	18.3	19.24	16.25
M.MDD[d] (Modified) gm/cm^3	1.851	1.752	1.771	1.805

[a]*S.OMC* Standard Proctor test optimum moisture content
[b]*S.MDD* Standard Proctor test maximum dry density
[c]*M.OMC* Modified Proctor test optimum moisture content
[d]*M.MDD* Modified Proctor test maximum dry density

2.3 Experimental Calculations

All the tests are done regarding the Indian Standards. Now for calculation of saturation moisture content, specific gravity is an important factor; thus, we determined specific gravity until we get the accuracy to 0.03gm/cm^3. The equations used in determining the saturation and bulk density are mentioned below as Eqs. (1) and (2),

$$M/C = \frac{S\gamma x\left(\left(\frac{G}{\rho d}\right) - 1\right)}{G} \qquad (1)$$

$$\rho = \rho d \times \left(1 + \frac{S\gamma}{100}\right) \qquad (2)$$

where M/C = moisture content, S_γ saturation percentage, G = specific gravity, ρ_d = dry density, ρ bulk density.

2.4   Sample Preparation

Now to determine compaction test, we add 10% of moisture in the soil and put it into a desiccator and put the desiccator partly submerged in 27 °C water to let the soil distribute moisture evenly. By doing this, we encountered more accurate results of compaction test and repetitions also gave the same accurate results. From this experiment, we followed these steps for remoulding the sample also. The remoulding is done in three equal layers and compressed it in the mould hydraulically. After the remoulding, the sample is extracted in three tubes with the help of sample extractor. From the tubes, extracted sample used to prepare unconfined compressive strength test specimens. The size of the specimen is 38 mm in the diameter and 76 mm in height.

3   Results and Discussion

3.1   UCS of Expansive Soils

The considered densities in Silvasa expansive soil are 1.60, 1.65, 1.70, 1.75, 1.80 and 1.85 gm/cm^3 out of which 1.60 gm/cm^3 is standard Proctor test density and 1.85 gm/cm^3 is modified Proctor test density. Now, for each density, the saturation moisture content is introduced from 80 to 100% with an interval of 5%. The test results are mentioned in Table 2 below, and all the units of unconfined compressive strength test results are in kg/cm^2. UCS describes unconfined compressive strength and is denoted as q_u.

The considered densities for Bharuch expansive soil are 1.55, 1.60, 1.65, 1.70 and 1.75 gm/cm^3 out of which 1.65 gm/cm^3 is standard Proctor test and 1.75 gm/cm^3 is modified Proctor test. The test results are mentioned in Table 3.

Now before the standard Proctor test density, both the soils show almost the same behaviour and gives better strength at 90% of saturation. At standard Proctor test density, the upward trend is noticed from 90 to 100% saturation which is remarkable.

Table 2 Silvasa expansive soil UCS results

Saturation (%)	q_u Avg. kg/cm^2					
	q_u @ 1.6	q_u @ 1.6	q_u @ 1.6	q_u @ 1.6	q_u @ 1.6	q_u @ 1.6
80	2.76	2.6	4.18	3.69	4.82	6.89
85	3.08	2.84	3.86	3.9	4.73	5.44
90	2.63	3.1	4.53	5.81	5.28	10.02
95	3.53	1.95	3.03	2.44	4.5	5.02
100	3.71	1.81	2.16	2.3	3.99	4.36

Table 3 Bharuch expansive soil UCS results

	q_u Avg. kg/cm^2				
Saturation (%)	q_u @ 1.55	q_u @ 1.60	q_u @ 1.65	q_u @ 1.70	q_u @ 1.75
80	7.34	8.32	9.81	9.14	12.25
85	7.55	8.21	7.61	11.18	16.89
90	8.48	10.64	5.88	13.03	21.51
95	4.64	9.49	6.87	12.39	19.08
100	3.68	6.9	7.93	11.36	12.58

And after standard Proctor to modified Proctor test density, soil gives better strength at 90% of saturation condition for both the soils.

3.2 UCS of Yellow Plastic Clays

For Silvasa yellow plastic clay, densities are 1.58, 1.63, 1.68, 1.73 and 1.78 gm/cm^3 from which 1.63 gm/cm^3 is standard Proctor test density and 1.78 gm/cm^3 is modified Proctor test density. All the densities are remoulded at 80, 85, 90, 95 and 100% saturation. Results mentioned in Table 4.

And for Bharuch yellow plastic clay, 1.6, 1.65, 1.70, 1.75 and 1.80 gm/cm^3 are the desired densities and 1.65 gm/cm^3 is standard Proctor test density and 1.80 is gm/cm^3 modified Proctor test density. All these densities are remoulded at 5% interval of saturation from 80 to 100%. Table 5 elaborates the test results.

Figure 1 clearly shows all the results of the standard Proctor test density at different saturation conditions.

In the beginning, before standard Proctor test density, soil shows almost the same strength behaviour and gives better strength at 90% of saturation. At standard Proctor test density, it goes rising from 90 to 100% saturation which is worthy of attention. And after standard Proctor test density till modified Proctor test density, soil shows the best strength at 95% of saturation.

Table 4 Silvasa yellow plastic clay UCS results

	q_u Avg. kg/cm^2				
Saturation (%)	q_u @ 1.58	q_u @ 1.63	q_u @ 1.68	q_u @ 1.73	q_u @ 1.78
80	4.41	5.18	4.73	5.63	5.99
85	4.38	7.68	4.81	7.52	5.2
90	5.13	5.63	5.19	7.88	6.55
95	4.26	6.58	7.1	9.72	8.76
100	3.53	8.22	3.25	5	5.76

Table 5 Bharuch yellow plastic clay UCS results

	q_u Avg. kg/cm^2				
Saturation (%)	q_u @ 1.6	q_u @ 1.65	q_u @ 1.7	q_u @ 1.75	q_u @ 1.80
80	2.82	3.22	5.04	6.16	8.52
85	2.7	2.87	3.92	5.25	5.34
90	2.08	3.06	4.47	5.29	4.91
95	1.59	3.56	4.87	5.61	5.51
100	1.31	3.78	3.09	3.49	4.75
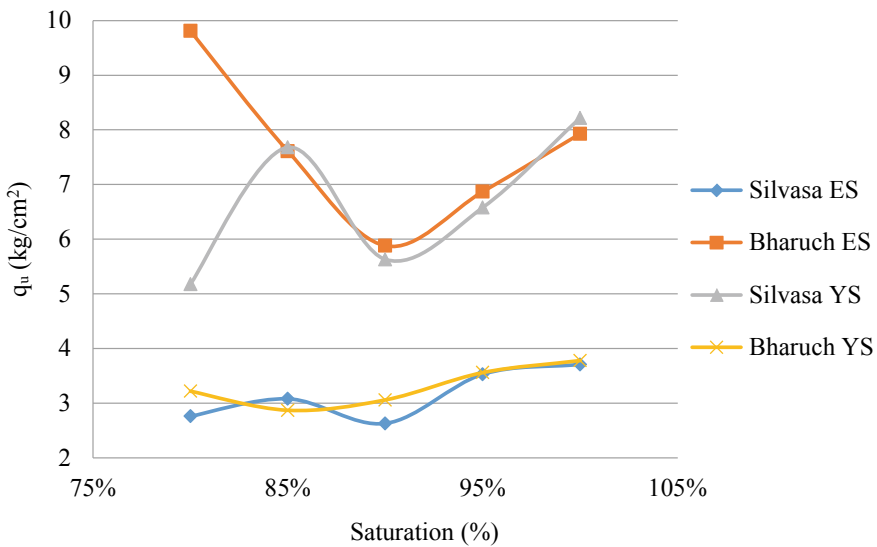
Fig. 1 UCS versus saturation

4 Conclusions

- In the early stage, before standard Proctor test density, soil behaves almost the same in both types.
- For expansive soil, it gives more strength at 90% of saturation before standard Proctor test density. At standard Proctor test density, it goes upward from 90 to 100% saturation. And after standard till modified Proctor test density, it also gives better strength at 90% of saturation.
- For yellow plastic clay, the peak saturation is 90% before standard Proctor test density. At standard Proctor test density, it goes upward from 90 to 100% saturation. And till modified Proctor test density it gives maximum strength at 95% of saturation.

- Hence, from this experiment, we can evaluate that, the expansive soil is saturated at 90% of saturation after and below standard Proctor test density and for yellow plastic clay, 90% is saturation condition below standard Proctor and 5% above standard Proctor test density. And for both the soils, 100% at standard Proctor test density is the saturated condition.

References

1. Jonggil, C., Byeongsu, K., Seong-wan, P., Shoji, K.: Effect of suction on unconfined compressive strength in partly saturated soils. KSCE J. Civil Eng. **14**(2), 281–290 (2010)
2. Wen, Y., Zi-Xin, X., & Yong-He, W.: Experimental study on unconfined compressive strength of completely weathered granite improved soil. In: Advances in Transportation Geotechnics and Materials for Sustainable Infrastructure, pp. 131–136 (2014)
3. Yuksel, Y., Jongwan, E., Aysegul, G.: Evaluation of Unconfined Compressive Strength for High Plasticity Clayey Soil Mixed with Cement and Dispersive Agents, pp. 270–279. Grouting (2017)
4. Hongsheng, L., Haitian, Y., Cheng, C., Xioutang, S.: Experimental investigation on compressive strength of frozen soil versus strain rate. J. Cold Regions Eng. 125–133 (2001)
5. Shah, D., Chinwala, N., Desai, H.: Experimental Study on Unconfined Compressive Strength of Black Cotton Soil for Navsari and Surat Cities. McGraw Hill Education, Vadodara (2018)

Influence of Grain Sorting and Grain Shape/Elongation on the Intergranular Porosity of Cubic Packing for Sedimentary Rocks

Shreya Katre, Arnab Kumar Pal, Siddharth Garia, K. Ravi, and Archana M. Nair

Abstract Porosity, being the main storage parameter in porous reservoir rocks, relates to the microscopic void spaces in rocks where oil and gas are accumulated. Diagenetic processes may damage porosity since they affect the systematic arrangements of grain particles and cause grain rearrangements. The extent to which the grain rearrangements may occur depends on the original packing of the grains and how extensively the packing has now been modified. The present study deals with the geometry of cubic packing of grains for a sandstone and carbonate rock core samples obtained from different parts of India which are known for undertaking hydrocarbon activities. Cubic packing is studied including the theoretical model along with the obtained model from the digitally analyzed image through Field Emission Scanning Electron Microscopy (FESEM) with the help of MATLAB coding. A set of particles (idealized as spheres of varying radii) was added to the ideal cubic assemblage of eight spherical particles, and thus, the effect of grain sorting on intergranular porosity was observed. The same model was taken into account to estimate the effect of degree of elongation. But the only difference was a set of particles (idealized as spheres of varying radii) that was added to the ideal cubic assemblage of eight elongated particles. Thus, it is concluded that the nature of pore systems at micrometer to millimeter scale gets affected by the grain sorting. Digital images acquired from FESEM-backscattered electron imaging gives promising inputs for grain size distribution which in turn discloses the frequency of available grain sizes corresponding to different size ranges. Porosity obtained from cubic assemblage influences the shape

S. Katre · A. K. Pal · S. Garia · K. Ravi · A. M. Nair (✉)
Department of Civil Engineering, IIT Guwahati, Guwahati 781039, India
e-mail: nair.archana@iitg.ac.in

S. Katre
e-mail: shreya.katre@gmail.com

A. K. Pal
e-mail: arnab.pal@iitg.ac.in

S. Garia
e-mail: sidd_41@iitg.ac.in

K. Ravi
e-mail: ravi.civil@iitg.ac.in

and degree of elongation of the grains responsible for the formation of interstitial pore spaces which may affect the storage capacity of porous reservoir rocks.

Keywords Porosity · Cubic packing · Grain size distribution · Degree of elongation

1   Introduction

The quantification and characterization of reservoir rock properties are most valuable in numerous fields, e.g., geology, geophysics, geochemistry, hydrology, hydraulic fracturing, reservoir engineering, petroleum exploration, mining, and civil engineering [19]. In each of these research areas, certain rock parameters are more important, depending on the particular area. Apart from other physical properties, porosity and permeability are the fundamental properties of sedimentary rocks to have a significant effect on the hydrocarbon storage and production [10]. For modeling flow through porous reservoir rocks, realistic numerical data of porosity is needful to characterize the nature of pore systems at various scales, prominently at minute scales. Primary syn-depositional porosity of sedimentary parameters may get varied due to differences in grain size, shape, roundness, sorting and packing, or due to the filling of finer reflux between larger grains. Also, porosity differences may result from post-depositional diagenetic processes such as grain rearrangement, pore filling with crystalline material or modification of the original grains by physical and chemical processes [15, 20]. Thus, depositional processes are most damaging to porosity during early burial because of packing changes and ductile grain deformation [2].

Grain rearrangements during these processes can be quantified indirectly by modeling different packing arrangements theoretically to calculate porosity. This effective utilization of space by mutual arrangement of the constituent grains of an aggregate is called packing [19]. Depending on the mode of deposition, all natural sediment particles existing in their natural form may or may not be packed in their tightest possible manner, and their packing can range from loose random packing to dense random packing. The extent to which the grain rearrangements may occur depends on the original packing of the grains and how extensively the packing has now been modified [20]. This modification in grain rearrangements will have an effect on the physical properties of the material. The present study focusses on the influence of packing of grain particles on the physical property called porosity.

Ideal assemblages of systematic packings composed of uniform size of grains have no influence of grain sizes on their porosity. It has also been shown that along with a grain size of uni-modal well-rounded spheres, the grain size of the uni-modal prolate grains also have no effect on the intergranular porosity of different types of ideal packings [15]. But it is very difficult to represent actual conditions with uniform size of grains available in it as this type of condition rarely occurs in nature. The presence of non-uniform sizes affects the porosity of rocks because they have a direct impact on the arrangement of grains and pore throat size which is the main

influential parameter in the porosity estimation [17]. The more non-uniformly graded the material is, smaller the pores between the grains, hence smaller the porosity values. At the same time, sorting also plays an influential role in porosity value as the comparatively smaller size of grains fills the space available between the larger grains resulting in lower porosity compared to the previous one. Spherical sized grains have less porosity compared to non-spherical grains as spherical grain settle in denser arrangement than that of non-spherical grains creating wider space which contributes to higher porosity. Packing of two or more shapes tends to block and cancel the effects of radical shape while in only single-shape packs, it causes a wide grain volume range and much wider space for porosity [22].

It is advantageous to consider the simple type of packing like cubic and then to examine the deviations that become more and more complex and chaotic [9]. Graton and Fraser [11] have established that in assemblages of uniformly sized spheres, the porosity ranges from a maximum of 47.6% if the spheres are cubically packed. Various experiments have been conducted to find out random packing density of spheres. The maximum packing density (volume fraction of spheres) is approximately 0.64 in the random close-packed (RCP) limit for hard spheres [4, 8, 21–23]. But the influential factors for packing density are particle shape and method of packing: regular or irregular (random), where the latter furthermore gets affected by the densification [3]. Packing density higher than 0.64 can be achieved by using a collection of particles with a variety of sizes that is grain size distribution. Desmod and Weeks [6] have numerically generated number of sphere packings with different particle radii distributions like binary, linear, Gaussian, and lognormal, varying polydispersity and skewness independently of one another. But, they truncate certain distributions with the particle size to generate packings within a reasonable time frame. Dexter and Tanner [7] have specified that granular materials have a grain size distribution which is well defined by a lognormal distribution function, that is, the weights of the particle sizes present are distributed normally with respect to the logarithms of the respective particle diameters. They have proved that as the standard deviation increases, packing density increases.

The present study deals with the cubic assemblage of discrete grain particles of different shapes that include equi-sized spherical as well as equi-sized elongated grains. Cubic assemblage is formed when a square layer, in which two sets of rows intersect at 90°, overlie upon the second square layer. Two hemispheres and one cylinder having a diameter equal to those hemispheres, together form each elongated grain. In the present study, an attempt is made to compose a model which has a framework of eight spherical grains, to which further a set of grains was added to observe the effect of sorting. The same model was repeated with eight elongated grains as a framework, and then, intergranular porosity was calculated.

2 Methodology

2.1 Sample Description

For the analysis, one carbonate and one sandstone core plug sample of approximately 2.5 cm diameter from different parts of India (Sandstones from upper Assam-Arakan basin and carbonate from Bombay offshore) were collected for porosity analysis. Bombay offshore basin is located on the western continental shelf of India between Saurashtra basin and Kerala Konkan in the south covering an area of 120,000 km^2 from the coast. The basin is in the late Cretaceous to Holocene age [14]. While upper Assam basin being a part of Assam-Arakan basin, it is mostly of Tertiary and Quaternary age [16].

2.2 Field Emission Scanning Electron Microscopy (FESEM)

A scanning electron microscope uses secondary electrons and backscattered electrons for imaging samples which gives enough data at sufficient resolution by which the pore space distribution can be realistically described. FESEM uses the field emission gun firing electrons to scan the area concerned. The ideal resolution of this microscope is 0.5 nm which can typically reach up to 5 nm with 30 kV with conducting material, whereas it can be reached up to 50 nm with non-conducting material such as rock [12]. Secondary electrons show morphology and topography on samples, while backscattered electrons illustrate contrasts in composition in multiphase samples [1].

The significance of FESEM study is its fixed magnification ratio for observing the pore structure on a given location of a sample and also the appropriate number of FESEM images need to be taken for the description of the sample as it is difficult to identify the features like smallest pore structure including matrix pores and organic matter nanopores of sample if the magnification is not appropriate enough [5].

Sample preparation for this instrument is very important as the smooth flat surface is required for clear imaging. Before analyzing it in the microscope, the sample surface should be dried to avoid absorption of X-ray and coated with gold to avoid charging [13]. This method is faster and less expensive than other conventional methods. Image collected by FESEM is a rich source of information for variability in porosity and mineral distribution [17]. Backscattered electron image is collected, and image processing is applied to make the image more informative by filtering it and extract the pore information quantitatively. Figure 1 shows a digital image of carbonate sample acquired from FESEM (Make-Ziess and Model-Sigma) backscattered electron imaging.

Fig. 1 FESEM-BSE image of a carbonate rock sample collected from Bombay offshore basin
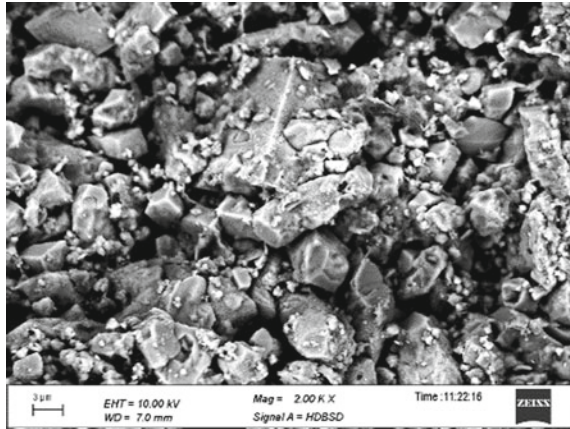
2.3 Analysis of FESEM Images

The analysis of the images obtained through FESEM can be done using various platforms such as ImageJ and MATLAB [18]. ImageJ enables to estimate porosity based on thresholding which includes connected and isolated pore spaces. In such case, grain size distribution plotting becomes tedious as one has to measure all grain sizes manually which may incorporate manual errors. Here, the whole study has been done using MATLAB software, to provide for an alternative for the much used ImageJ. The development of MATLAB code focus on plotting the grain size distribution instead of pore size distribution, because a set of grain sizes is needed to observe the effect of grain sorting on the intergranular porosity. Figure 2 shows the flowchart of the workflow to obtain porosity of available samples.

Filtering. Before performing calculations of porosity of the rock, it is important to apply noise removal filters which remove the arbitrariness in the images to a great extent. Processing of the image was started by applying Gaussian filter to enhance the image properties to remove noise as well as to remove small details from image prior to large object extraction and bridging of all small gaps in lines and curves. The new value of the pixel is assigned as the weighted average of the neighborhood pixels. Figure 3(a) and (b) shows the original and filtered images for carbonate sample respectively.

Thresholding. The FESEM images obtained are 2D raster images of the sample. A threshold value was used to differentiate pores from the rock grains which was obtained from Otsu's threshold method. After thresholding, the processed images were obtained and compared with the original FESEM obtained image manually to ascertain whether the threshold value actually represents the sample. Otsu thresholding was used to convert a grayscale image into a binary image. Iteration of all the possible threshold values to calculate a measure of spread for the pixel levels each side of the threshold is done by Otsu's thresholding method. The aim is to find
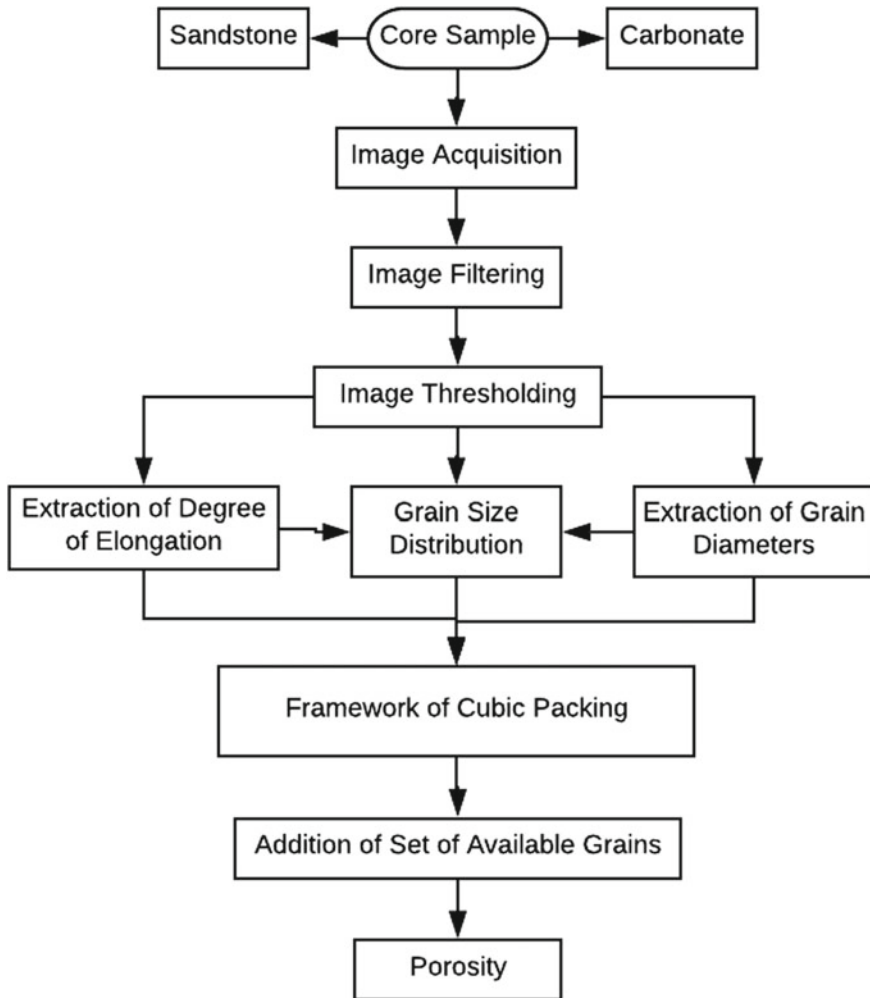
Fig. 2 Flowchart of the workflow to obtain porosity of available samples

the threshold value where the sum of foreground and background spreads is at its minimum. The original image (a) and image after thresholding (b) for a representative carbonate sample is presented in the Fig. 4.

Grain size distribution. The grain diameters, as well as the maximum length between the farthest pixels of the grains, were measured. The shape anisotropy expressed by grain elongation E was calculated using the equation given by Nabawy [15]:

Degree of Elongation (E) = the length of the grain/the diameter of the grain.
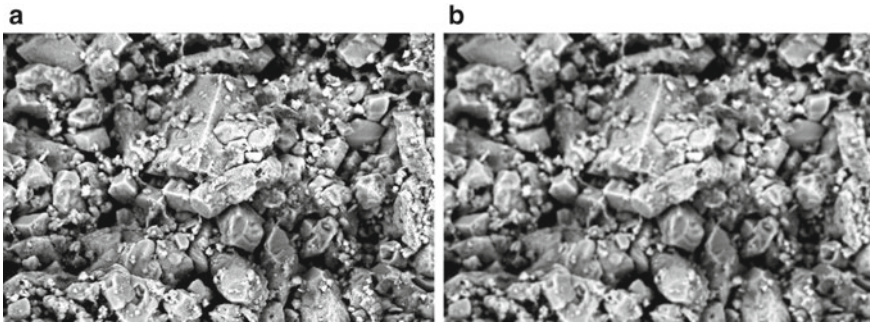
Fig. 3 Carbonate sample **a** original image and **b** filtered image
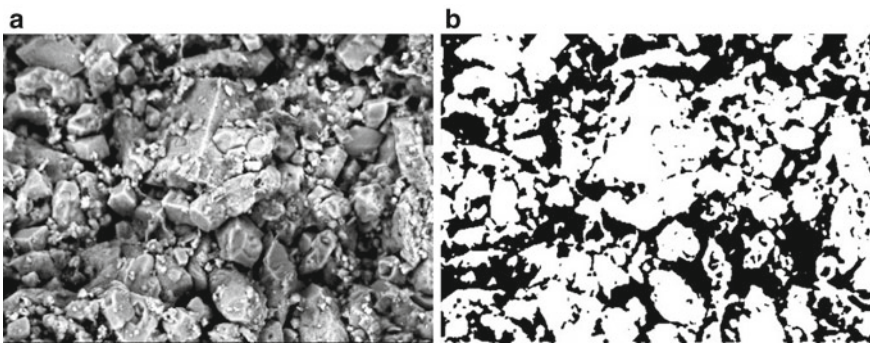
Fig. 4 Carbonate sample **a** original image and **b** image after thresholding

Different classes consisting of different range of particles were segregated so as to identify the diversity of the grain sizes present in the sample that was obtained through FESEM analyzed an image in turn to get a histogram of frequency versus grain sizes. Maximum likelihood technique was used to find out the distribution that fits best to the available data. The goal of maximum likelihood is to find the parameter values that give the distribution that maximize the probability of observing the data. In some cases, as the range of data is less, probability plots are plotted to find the goodness of fit of the distribution. If the probability plot is close to a straight line, then the specified distribution fits the data.

This grain size distribution was used to add another set of spheres within the available pore spaces of cubic packing. The limiting packing density to add another set of spheres was taken according to the equation given by Dexter and Tanner which takes into account the standard deviation of the available set of particles.

The equation to represent packing density as a function of standard deviation is given as

$$D = D_f - (D_f - D_0) \exp(-M\sigma) \tag{1}$$

where D is the packing density, $D_0 = 0.6366$ $D_f = 1$, is the final limiting packing density as $\sigma \to 0$, $M = 0.19$, and σ is the standard deviation of a given set of grain sizes. The given equation is valid for $0 < \sigma < 0.7$.

3 Results and Discussions

The estimated grain sizes from FESEM analyzed image were plotted against the frequency of their occurrence to get a grain size distribution as shown in Fig. 5. Similar histogram analysis was done for carbonate sample. Figure 5 shows that fine sized grains have more frequency of occurence in the focused part of the sample as compared to the coarse sized grains. Thus, the sample has a higher chance of getting filled by finer reflux within pore space. Figure 6 represents the statistical fitting on grain size distribution histogram of sandstone rock sample. The statistical analysis of grain size distribution for both samples shows that samples follow a lognormal three-parameter distribution with a P-value of 0.46 for a carbonate sample and that of 0.86 for sandstone sample. The standard deviation of the grain size distribution is presented in Fig. 7. The standard deviation of the carbonate and sandstone samples corresponds to 0.002 and 0.003, respectively. Such a less value indicates that addition

Descriptive Statistics
Mean=4.94483006603651E-03
Standard Error=0.000343
Median=3.74209187988445E-03
Standard Deviation=3.5265171192928E-03
Variance=1.2436322992665E-05
Sum=0.524151986999871
Count=106
Maximum=2.37057242436757E-02
Minimum=1.98526221859148E-03
Range=2.17204620250843E-02
Kurtosis=8.7674
Skewness=2.6555
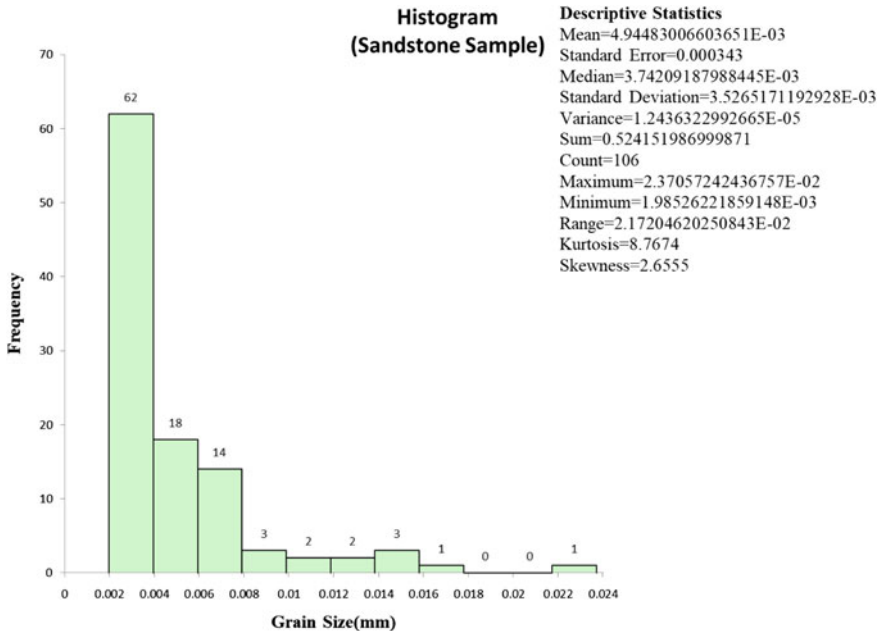
Fig. 5 Grain size distribution of sandstone sample
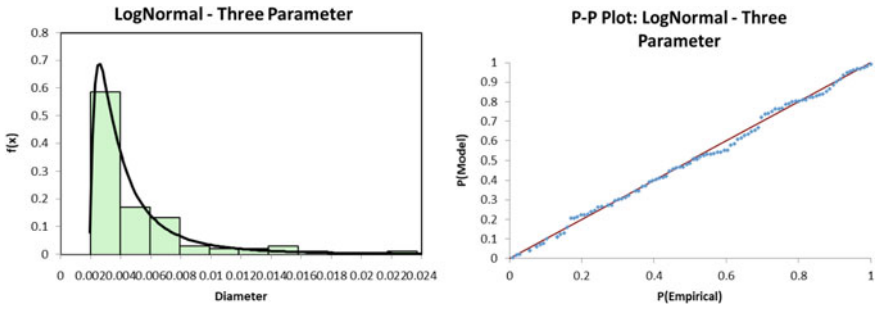
Fig. 6 Statistical analysis of grain size distribution of sandstone sample

Fig. 7 Intergranular porosities of cubic packing

of a set of grains to the remaining pore spaces can follow Eq. (1) given by Dexter and Tanner [7] to estimate packing density which in turn gives porosity of the packing.

Porosity values based on cubic packing assemblage in Fig. 7 show a different range of values of porosity. From the studied samples, the uniform size of grains irrespective of their shape does not influence on the porosity of packing. But the addition of a set of grains within the available void spaces affects the packing porosity. Addition of another set of grains occupies the remaining pores and causes porosity reduction from 47.60% to 20.26% and 17.44% for carbonate sample and sandstone sample, respectively.

The anisotropy of grains was observed by measuring the degree of elongation of both the samples. The maximum measured value of the degree of elongation (E) within all grain sizes was 2.07 for carbonate while 2.25 for sandstone sample. When sorting of grains is considered to add a group of grains within the available pores of cubic packing of elongated grains, the value of porosity gets considerably reduced as compared to spherical grains. Thus, observed results show a direct effect on the intergranular porosity of cubic assemblage. It was observed that the uniform grain size irrespective of shape does not influence on the intergranular porosity. But on the addition of a set of grains from available grain size distribution, mixing of different sizes of particles utilize the pore space available and thus reduce the porosity of resulting assemblage.

4   Conclusion

In this study, different grain sizes of carbonates and sandstones were measured from the obtained FESEM analyzed images. As an alternative for conventional ImageJ software, a MATLAB code was developed to serve as a substitute for measuring quantitative data from digital images. The code was successful in extracting grain sizes, which includes grain diameters and the degree of elongation of grains. The developed code is applicable to FESEM-BSE image of polished rock surface. These measured grain size values were then used to plot the grain size distribution. The statistical analysis of grain size distribution implied that both the distributions are lognormal three parameters. These parameters were then used to form cubic assemblage. A new methodology was developed in terms of packing density and grain sorting to introduce a set of grains to the existing assemblage, which made possible to mix different sizes of grains in a single model. Mixing of different sizes of discrete spherical particles to ideal cubic assemblage causes significant reduction in porosity. Anisotropy factor of grains was included in the model in terms of their elongation. It was observed that the extent of porosity reduction upon adding of different sizes of spherical grains to a cubic assemblage of elongated grains was more than the extent to which porosity reduction occurred in case of the cubic assemblage of spherical grains. Thus, it is concluded that the nature of pore systems at micrometer to millimeter scale gets affected by the grain sorting. Grain anisotropy has a significant influence on porosity as the value gets reduced considerably as compared to

isotropic grains. Digital image analysis technique focusses small area of the sample to derive grain size distribution. Hence, to estimate reservoir porosity, analysis on repetitive small samples is required to get an overall description. The study shows the effect of grain shape in terms of degree of elongation and grain size distribution in terms of degree of sorting on porosity.

References

1. Anantheshwara, K., Bobji, M.S.: Surface probe techniques. In: Tribology for Scientists and Engineers, pp. 555–580. Springer, New York, NY (2013)
2. Avseth, P.: Combining Rock Physics and Sedimentology for Seismic Reservoir Characterization of North Sea Turbidite Systems. Stanford University (2000)
3. Brouwers, H.J.H.: Particle-size distribution and packing fraction of geometric random packings. Phys. Rev. E **74**(3), 031309 (2006)
4. Cargill, G.S., III.: Dense random packing of hard spheres as a structural model for noncrystalline metallic solids. J. Appl. Phys. **41**(5), 2248–2250 (1970)
5. Deng, H., Hu, X., Li, H.A., Luo, B., Wang, W.: Improved pore-structure characterization in shale formations with FESEM technique. J. Nat. Gas Sci. Eng. **35**, 309–319 (2016)
6. Desmond, K.W., Weeks, E.R.: Influence of particle size distribution on random close packing of spheres. Phys. Rev. E **90**(2), 022204 (2014)
7. Dexter, A.R., Tanner, D.W.: Packing densities of mixtures of spheres with log-normal size distributions. Nat. Phys. Sci. **238**(80), 31 (1972)
8. Finney, J.L.: Random packings and the structure of simple liquids. I. The geometry of random close packing. Proc. Royal Soc. London. A. Mathe. Phys. Sci. **319**(1539), 479–493 (1970)
9. Fraser, H.J.: Experimental study of the porosity and permeability of clastic sediments. J. Geol. **43**(8, Part 1), 910–1010 (1935)
10. Garia, S., Pal, A.K., Ravi, K., Nair, A. M.: A comprehensive analysis on the relationships between elastic wave velocities and petrophysical properties of sedimentary rocks based on laboratory measurements. J. Petrol. Explorat. Prod. Technol. 1–13 (2019)
11. Graton, L.C., Fraser, H.J.: Systematic packing of spheres: with particular relation to porosity and permeability. J. Geol. **43**(8, Part 1), 785–909 (1935)
12. Huggett, J.M., Shaw, H.F.: Field emission scanning electron microscopy—a high-resolution technique for the study of clay minerals in sediments. Clay Miner. **32**(2), 197–203 (1997)
13. Korte, D., Kaukler, D., Fanetti, M., Cabrera, H., Daubront, E., Franko, M.: Determination of petrophysical properties of sedimentary rocks by optical methods. Sed. Geol. **350**, 72–79 (2017)
14. Mohan, M.: Geohistory analysis of Bombay high region. Mar. Pet. Geol. **2**(4), 350–360 (1985)
15. Nabawy, B.S.: Estimating porosity and permeability using digital image analysis (DIA) technique for highly porous sandstones. Arab. J. Geosci. **7**(3), 889–898 (2014)
16. Pahari, S., Prasad, I.V.S.V., Banerjee, A, Varshney, M.: Evaluation of petroleum source rocks of bengal basin, India. Petroleum Geochemistry and Exploration in the Afro-Asian Region (2008). (December): 21–26
17. Pal, A., Garia, S., Ravi, K., Nair, A.M.: 2018. Influence of Packing of Grain Particles on Porosity, Indian geotechnical conference (2018)
18. Pal, A., Garia, S., Ravi, K., Nair, A.M.: Porosity Estimation by digital image analysis. ONGC Bulletin **53**, 59–72 (2018)

19. Pandalai, H.S., Basumallick, S.: Packing in a clastic sediment: concept and measures. Sed. Geol. **39**(1–2), 87–93 (1984)
20. Rittenhouse, G.: Pore-space reduction in sandstone-controlling factors and some engineering implication. In: Offshore Technology Conference. Offshore Technology Conference (1973)
21. Rutgers, R.: Packing of spheres. Nature **193**(4814), 465 (1962)
22. Scott, G.D., Charlesworth, A.M., Mak, M.K.: On the random packing of spheres. J. Chem. Phys. **40**(2), 611–612 (1964)
23. Yerazunis, S., Bartlett, J.W., Nissan, A.H.: Packing of binary mixtures of spheres and irregular particles. Nature **195**(4836), 33 (1962)

Effect of Deployment of Jack-Up on Piles and Structure of Existing Offshore platform—A Case Study

Rupam Mahanta and Praveen Bhat

Abstract Jack-up rigs are mobile offshore platforms deployed mostly to carry out drilling and work-over activities related to exploration and production of oil and gas. For activities related to production of hydrocarbon, jack-ups are deployed near existing fixed jacket platforms frequently. Most of the jack-up rigs are, three-legged units supported by foundations known as 'spudcans' fixed at the bottom of their legs. Fixed offshore platforms are supported by open-ended steel tubular piles. Spudcans of a jack-up penetrate below the seafloor during its deployment in offshore. Diameter of spudcan is much larger compared to diameter of piles supporting a fixed platform. Due to penetration of spudcans into seafloor, capacity, loads and load–displacement behaviour of nearby piles of the fixed platform may be affected since displacement and remoulding of a large volume of soil occurs near the piles. Analysis was carried out for a case in western Indian offshore to examine the effect of spudcan penetration on the safety of piles and structure of a fixed platform. Also, the minimum distance to be maintained between pile and spudcan to avoid over-stressing of piles, and structure was worked out. The analysis and results are discussed in the paper.

Keywords Offshore · Pile · Jack-up

1 Introduction

Jacket-type fixed offshore platforms are supported by open-ended, steel tubular piles. In general, the diameter of piles for these platforms in Indian offshore is within the range of 1.2–2.4 m. The vertical penetration below the seafloor may be typically, 60–150 m. The load-deformation behaviour and the capacity of a pile depend on the soil condition surrounding the pile. Also, the stress and displacement of structural components are influenced by the stiffness of the soil-foundation system. Therefore,

R. Mahanta (✉) · P. Bhat
Institute of Engineering and Ocean Technology (IEOT), ONGC, Panvel, Maharashtra, India
e-mail: rupam.mahanta@gmail.com

P. Bhat
e-mail: bhat_praveen@ongc.co.in

an interactive analysis of soil, pile and the structure is carried out to analyse structural integrity and to predict performance of the piles. In-place analysis of structure must account for any changes in soil properties near the piles especially, due to deployment of jack-up rig as it may significantly influence the performance of the foundation and the jacket structure.

Jack-ups are deployed in offshore near well-head platforms to carry out drilling and work-over jobs in the wells installed on these platforms. They are, generally, three-legged units and supported by individual foundations, termed as spudcans, under the legs. To carry out drilling or work-over jobs in wells, drilling derrick is cantilevered-out from the jack-up over well positions (slots) located on the deck of the jacket platform. Deployment of a jack-up near the fixed platform causes disturbance to the soil around the spudcans. As the large foundations (spudcans) of a jack-up penetrate below seafloor, large volume of soil gets displaced and especially the clays get remoulded around the depth of penetration of the spudcans. Similarly soil disturbance takes place upon withdrawal of a jack-up from an offshore site after completion of their work. The effect of remoulding and movement of soil may have adverse effect on the piles falling in the zone of disturbance. Soil properties, distance between spudcan and pile, and spudcan's depth of penetration below seafloor are important factors which influence the magnitude of such effects. Cases where the spudcan of a jack-up is in close proximity of piles of the fixed platform, the effect needs to be incorporated in the analysis, so that the structure and the foundation remain safe due to jack-up deployment. This paper presents a case study on effect of spudcan penetration on nearby piles and structure due to deployment of a jack-up at specified position near an existing fixed-jacket platform.

2 Background of Study

There is limitation on the movement and length of extension of the drilling derrick mounted on the jack-up rig. Therefore, jack-ups are often required to be deployed close to the platforms so that all the wells in the platform are accessible. Position of the jack-up vis-a-vis the well-head platform is planned accordingly. Most of the piles for fixed offshore platforms in western Indian offshore are designed to be inclined with respect to the vertical. Figure 1 shows a sketch of typical foundation plan with four piles where two of the piles are inclined in both X- and Y-directions with respect to vertical, and the other two (piles near which the jack-up is installed) are inclined with respect to vertical in Y-direction only.

This is done to provide safe distance between spudcan and piles when jack-ups are deployed on that side of the platform. However, in the platform (supported by eight piles—two at each corner) considered in this case study, all piles were designed with inclination on both X- and Y-directions since originally deployment of jack-ups near this platform was not planned. Later on, due to some operational exigency, an option was to be examined if a particular jack-up could be deployed near the platform without compromising safety of the structure and foundation. Researchers

Fig. 1 Conventional plan of piles for a four-piled well-head jacket platform
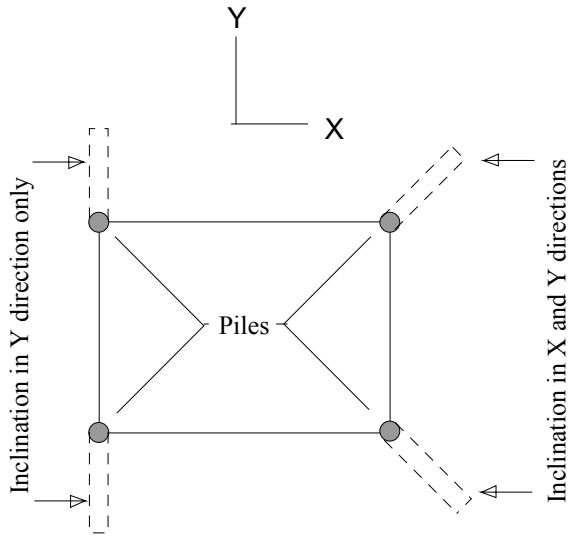
[1–3] have demonstrated that deployment of jack-up rig near an existing platform may have significant effect on the stress and displacement of nearby piles and jacket's structural components depending on the proximity of the spudcan, type of soil, depth of penetration of spudcan, etc.

In order to access all the wells of the fixed platform by the jack-up rig, due to the limitation on extension of the cantilevered part of the jack-up and piles being inclined on both X- and Y-directions, in this case, only available option was to deploy the rig at a position where two spudcans would be quite near to four of the eight piles of the platform. The relative positions of spudcans and the platform piles for carrying out the analysis are shown in Fig. 2.

Generally, for normal deployment of jack-ups near well-head platforms, a minimum clear gap of not less than 0.5 times diameter of spudcan is maintained between edge of spudcan and nearest surface of pile.

A study was carried out to examine whether the piles and structure of the platform would be safe with the design loads for the plan of deployment as shown in Fig. 2.

3 Soil, Pile and Spudcan Data

The soil profile at the location comprises of both sand and clay layers. However, the zone of soil near the seafloor where the spudcan penetration can take place is predominantly clayey. Relevant soil data have been presented in Table 1. The soil properties were derived on the basis of an in-situ test, i.e., CPTU (cone penetration test with pore pressure measurement) and laboratory test on samples recovered by an offshore geotechnical vessel.
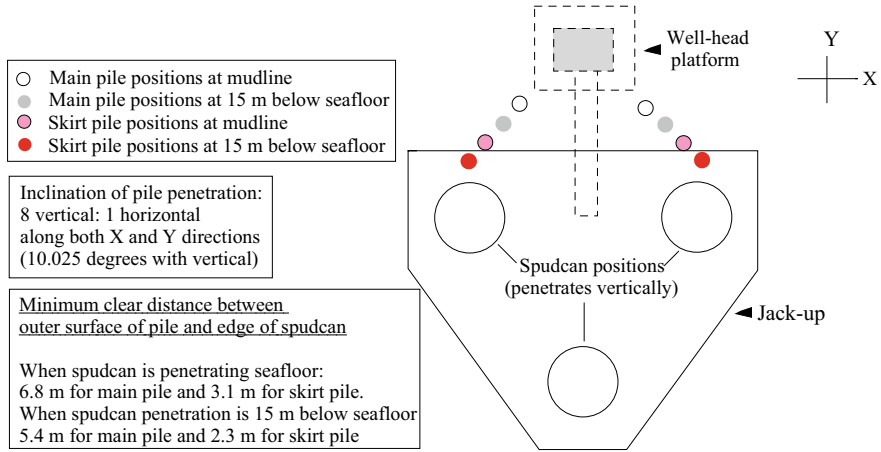
Fig. 2 Schematic showing the proposed deployment of jack-up near the fixed platform and relative positions of piles with respect to spudcans (figure is not to scale)

Table 1 Soil parameters in top layers for the location

Layer	Soil type	Depth (m)	s_u (kPa)	Φ' (deg.)	γ' (kN/m³)	ε_{50}	$q_{lim\ (MPa)}$	$k\ (MN/m^3)$
1	Sand	0–1.0	–	35	8	–	7	34.6
2	Sand	1.0–2.3	–	15	8	–	2	5.5
3	Clay	2.3–6.4	60–30	–	8	1.5	–	–
4	Clay	6.4–10.0	20–35	–	8	1.5	–	–
5	Clay	10.0–13.6	30	–	8	1.5	–	–
6	Sand	13.6–15.0	–	25	8.5	–	3	5.5
7	Sand	15.0–17.2	–	35	10	–	8	34.6
8	Clay	17.2–22.0	35–55	–	8	1.5	–	–
9	Sand	22.0–23.0	–	25	9	–	2	5.5
10	Clay	23.0–24.0	70	–	9	1.0	–	–
11	Sand	24.0–25.8	–	25	9	–	2	5.5
12	Clay	25.8–27.0	65	–	8.5	1.0	–	–
13	Sand	27.0–32.5	–	30	9	–	4	16.6
14	Clay	32.5–40	100	–	8.5	1.0	–	–

Note s_u = undrained shear strength; ϕ' = effective angle of internal friction; γ' = effective unit weight; ε_{50} = % strain at 50% failure stress; k = rate of increase with depth of initial modulus of subgrade reaction for lateral soil resistance; q_{lim} = Limit unit end bearing pressure

Table 2 Salient details of the platform and foundation

Feature	Description
Platform type	Well-head, fixed platform
Water depth	76 m
No. of wells in the platform	16
Diameter of piles	1.829 m (outer diameter)
Type of pile	Open-ended tubular; steel
Pile wall thickness	63.5 mm near seafloor; 50 and 44 mm downwards
Jacket leg and pile inclination	1(horizontal): 5.657 (vertical), double battered
Vertical penetration of main piles	116.2 m for main piles
Vertical penetration of skirt piles	m for skirt piles

The platform was supported by eight piles where four of the piles were main piles (driven through the main legs of the structure) and the remaining four piles were driven as skirt piles. Outer diameter was 1.829 m for all the piles. Wall thickness for pile sections near seafloor was 63.5 mm. For pile segments at greater depth below seafloor, wall thickness was 50 and 44 mm. Further details are described subsequently in Table 2. Equivalent diameter of spudcan was 15.2 m.

4 Structure of the Jacket Platform

The structural model, generated by using the software SACS, is shown in Fig. 3. The positions of the conductors, jacket structural members and piles are shown. The well conductors are in the middle of one side of the structure. The feasibility for using a three-legged, cantilever type, spudcan supported jack-up rig to be deployed near the fixed platform was to be examined under the present study. Some of the salient features of the platform are mentioned below at Table 2.

5 Methodology for Analysis

Offshore piles and structures are designed by carrying out interactive analysis of pile, soil and structure where the load–displacement properties of soil along with stress–strain behaviour of the structural material (steel) are taken into account. The analysis of the present case was carried out using software SACS where user-defined load–displacement data of soil was input with required modifications as explained subsequently.
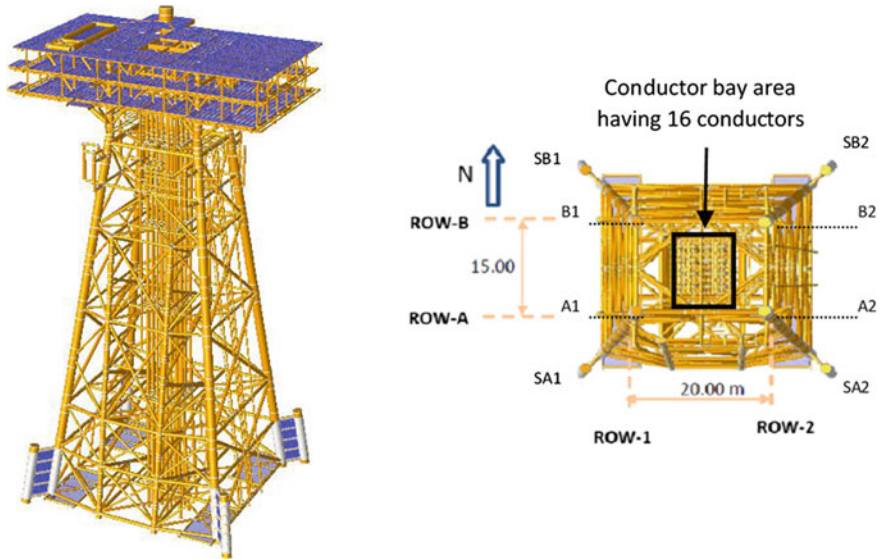
Fig. 3 Structural model of the platform and pile positions

The relative positions of spudcan of the jack-up and piles of the jacket structure was shown in Fig. 2.

During spudcan penetration, remoulding of soil occurs, and due to movement of soil, significant soil forces could be transmitted to nearby piles. Figure 4 indicates, through a simplified sketch, pile of a fixed platform getting affected by the lateral movement and remoulding of soil due to spudcan penetration below seafloor.

Therefore, interactive analysis of soil-pile-structure was carried out where the effect of penetration of the jack-up spudcan into the seafloor was also considered. Conventional interactive analysis was carried out using the pile load-transfer curves viz. *t-z*, *q-z* and *p-y*; where *t-z* is axial shaft resistance versus displacement, *q-z* is end bearing resistance versus displacement and *p-y* is lateral resistance versus displacement of soil. All the three types of curves represent nonlinear stress–strain response of soil. Cyclic *p-y* data were used in view of offshore environmental loading. Load-transfer data (*t-z*, *q-z* and *p-y*) were generated as per the code of practice [4].

In the present case, axial capacity of pile was found to be adequate even if soil disturbance due to jack-up deployment was considered since contribution of soil zone for the length of piles affected by jack-up deployment to the axial pile resistance is not significant. As such, effect of jack-up deployment on axial load-movement of pile in the present case was not further investigated.

Due to the proximity of spudcan to some of the piles, the possibility of spudcans fouling any piles while penetrating the seafloor was first examined. Spudcan penetration below seafloor was estimated considering the designated maximum axial load (preload) to be applied per leg of the unit. The leg-penetration analysis was carried out as per [5, 6], and penetration of the spudcan was estimated to be 15 m for the
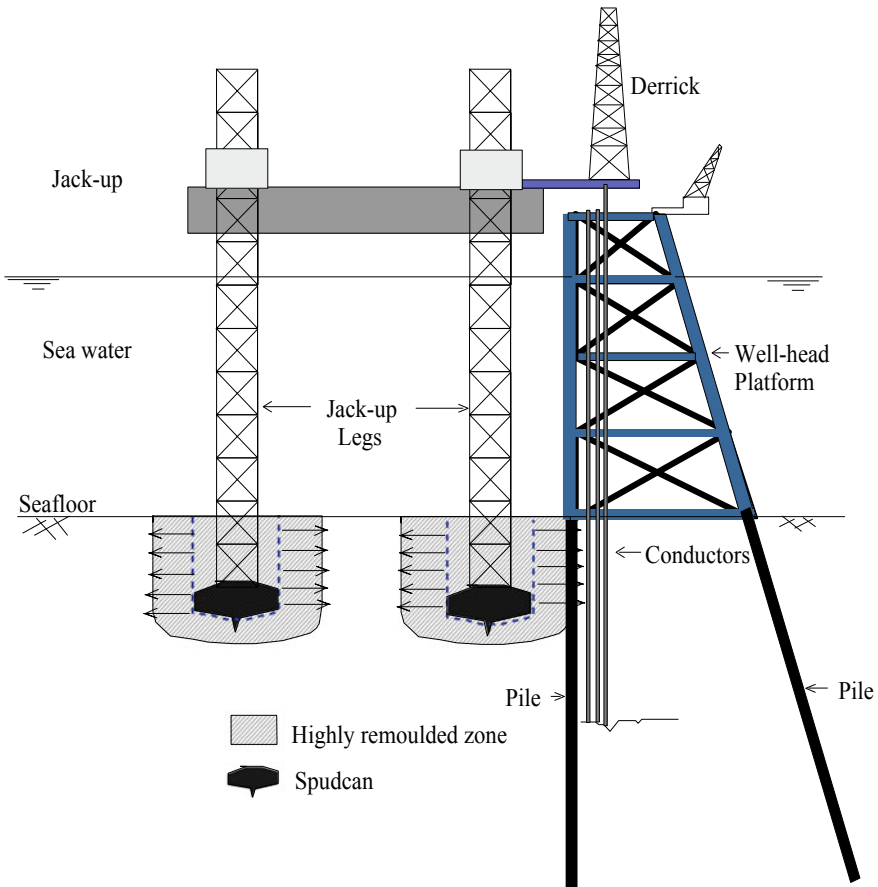
Fig. 4 Soil remoulding and lateral displacement of soil due to penetration of spudcan

subsequent analyses. Based on the estimated penetration, the soil lateral movement applicable for the piles near spudcan positions was calculated based on references [1, 2] using the concept of 'shifted *p-y*'. Remoulding of clayey soil within the estimated disturbed soil zone was also considered through modification of *p-y* data for the piles close to spudcans. Pile group effect with respect to lateral loading for the 2-pile groups was also considered by modifying *p-y* data with applicable *P* and *Y* multiplying factors as 0.8 and 4.5, respectively, which were derived as per method recommended by API [4].

Global static in-place analysis was carried out based on working stress method using SACS software for 100 year extreme storm and 1 year operating storm condition. Additional analysis was carried out for 100 year fair weather condition to explore the feasibility for deployment of jack-up rig for periods with less harsh weather conditions. In this paper, the structural analysis results for 100 year extreme storm condition have been presented. The one-third (33%) increase in allowable

stresses has been considered as per the provisions in design codes [7, 8]. Structural members were checked for yield, stability and nominal joint strength considering gravity and all lateral loads, i.e., wave, current and wind for eight (eight) directions. Marine growth of 100 mm thickness from elevation level (+) 6.0 m to (−) 30 m and 50 mm thickness from (−) 30 m to seafloor was considered. These elevations are with respect to chart datum for the offshore location. The piles have been checked for load carrying capacity and stress 'unity-check' (UC) ratio. The connection between main and skirt piles in the platform have been modelled using the advanced feature of meshing of plates for ensuring proper load-transfer mechanism.

6   Lateral Soil Movement and 'shifted *p-y*'

As mentioned already, when the spudcan position is close to an existing offshore structure, its penetration may cause significant deformation to the soil surrounding the nearby piles. Forces are transferred to nearby piles due to the soil displacement, and also forces are induced in the jacket structural components.

Soil displacement due to jack-up deployment has been considered in the analysis by modifying lateral load–displacement data (*p-y* characteristics) of soil for the piles located on the side facing the jack-up. Remoulded strength of clayey soils (with sensitivity of clay as 2.0) was considered for piles facing the jack-up for the estimated depth of penetration of the spudcan. In the *p-y* data, '*y*' values were shifted based on estimation of soil displacements following guidelines in references [1]. Two critical depths of spudcan penetration have been considered in the analysis and they are when spudcan of jack-up rig penetrates the seafloor, i.e., at the beginning of penetration, and when it penetrates 15 m below seafloor. Shifted values of '*y*' in relevant '*p-y*' data for the conditions are shown in Fig. 5.

Undisturbed soil condition without any '*y*-shift' in *p-y* data was considered for the piles on the opposite side of the fixed platform.

7   Results of Analysis and Discussion

The result for bending moment for the most critical pile is presented at Fig. 6. It is corresponding to condition of spudcan penetrations of 15 m below seafloor. The maximum increase of bending moment was observed to be about 215%. The maximum lateral displacement in pile was observed to be 13.6 cm which was not significantly high. It has been observed that significant re-distribution of loads occurs among the piles when spudcan penetration effect is considered due to different soil conditions considered on two opposite sides (near jack-up and far from jack-up) of the platform while analysing for jack-up deployment.

Analysis shows that due to jack-up deployment, significant increase in stress occurs in pile material. Maximum increase in pile stress was found to be 360%.
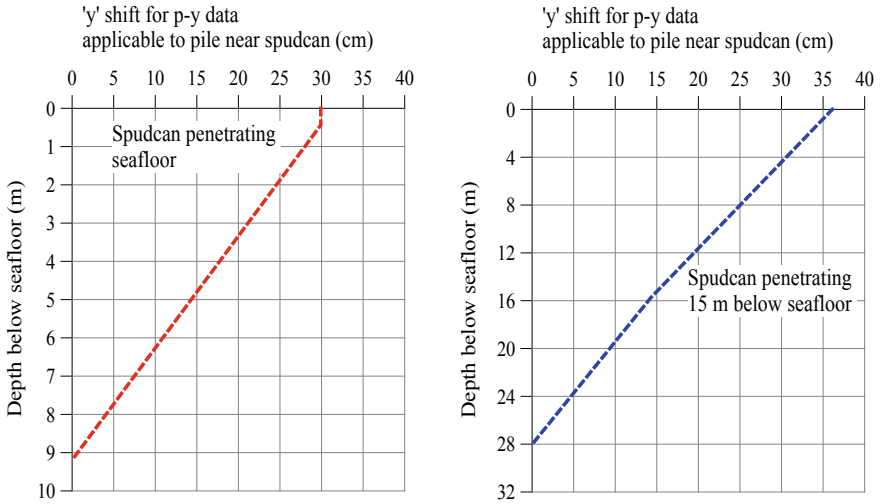
Fig. 5 Shifted 'y' values for spudcan penetration at seafloor and 15 m below seafloor

Fig. 6 Bending moment in the most critical pile (SA1) with the critical design load conditions
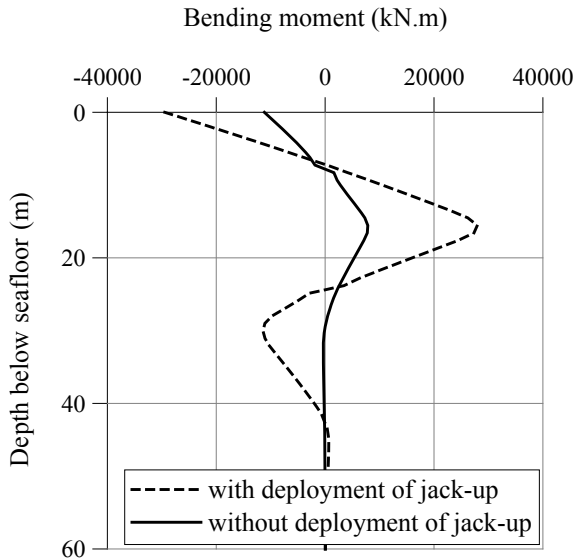
However, stress utility ratios for all piles are within allowable limit, i.e., less than 1.0.

The results have been summarised at Table 3 showing maximum increase of stress for individual piles. Pile numbers are indicated in Fig. 3.

Results in Table 3 are selected for different directions of environmental loading where such increase has been maximum due to the effect of jack-up deployment.

Table 3 Maximum increase in pile stress utility ratio for individual piles

Pile number	No jack-up deployment	With jack-up deployment	% increase
A1	0.42	0.74	076.2
SA1	0.25	0.85	240.0
A2	0.28	0.53	089.3
SA2	0.15	0.69	360.0
B1	0.31	0.57	083.9
SB1	0.20	0.43	115.0
B2	0.32	0.53	065.6
SB2	0.16	0.26	062.5

It may be noted that the comparison shown in Table 3 accounts for the re-distribution of loads in the piles and reduction of certain gravity loads (which were considered in original design) due to removal of some equipments from the structure when analysed for deployment of jack-up, which had influence on the stress utility ratios; further, stress in pile is also related to pile wall thickness (which varies along the length of piles). Thus, inspite of the jack-up deployment, pile stress was found to be within allowable limit for all the piles.

Regarding increase in stress for structural members, the condition with 15 m penetration of spudcan was found to cause maximum stresses in structural components. Calculated stresses were found to be beyond permissible limits in some of the members. Figure 7 shows the results with maximum effect due to jack-up deployment. Primarily, structural components near the seafloor were found to be over-stressed with stress utility ratio significantly exceeding the allowable limit. Maximum increase in
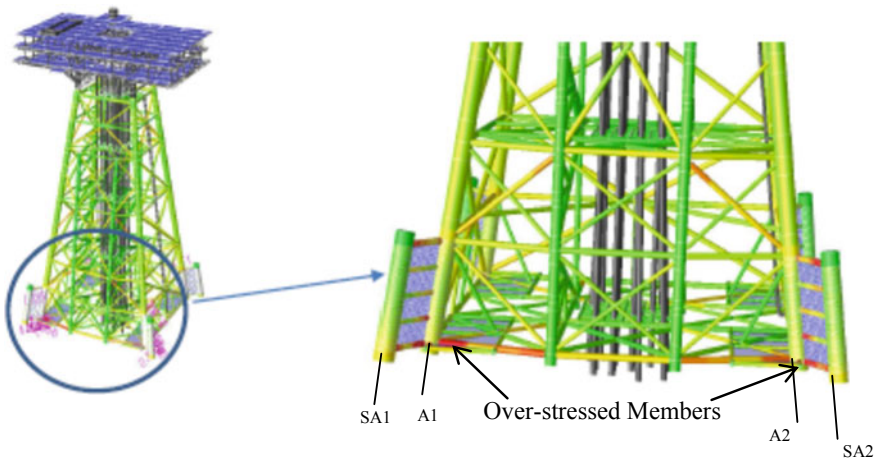
Fig. 7 Over-stressed structural components near the jack-up deployment position

stress for structural member was by more than 570% (stress utility ratio increased from 0.67 to 4.5) compared to original design.

Finally, the result of analysis indicated that stresses in many primary structural components would exceed the allowable limit if the jack-up rig was deployed at a position with the specified distance (Fig. 3) with respect to the nearby piles. However, all piles were found to be safe though stress and displacement increases in them due to the deployment of the jack-up. For the structure to be safe with the deployment of the jack-up, minimum spacing of about 8 m needs to be maintained between the edge of spudcan and outer surface of pile.

8 Conclusion

A case study on the effect of deployment of jack-up rig on piles and structure of existing offshore platform has been presented.

Given the large size of spudcan, offshore loading environment and spudcans' distance with pile being comparatively very small, the proposed deployment appeared to be practically very risky with possibility of physical contact of pile with spudcan.

The result of analysis shows that all piles meet the required limits of safety even with increase of stress in them arising from close proximity of spudcans. It is thought to be, due to having in-built margin on factors of safety in original design of the piles, reduction of some gravity load applicable for the analysis of jack-up deployment and re-distribution of loads among piles due to modified soil properties. Regarding the structural integrity, the result of analysis shows that some of the structural components of the jacket structure do not meet the structural integrity assessment criteria for deployment of the jack-up rig near the platform. In view of results of analysis, the proposed deployment was not recommended.

It is also found from analysis that a minimum spacing of about 8 m needs to be maintained between the edge of spudcan and outer surface of pile for the structure to be safe with deployment of the jack-up.

Analysis of such cases involving structure, soil, pile and disturbance of soil due to jack-up leg penetration are complex in nature. The analysis presented in the paper is only an approximate solution based on the methodology that is compatible for interactive analysis of soil, pile and structure although the soil condition is not exactly the same as per procedure [1, 2] used to estimate 'y shifts' in the case. More rigorous analysis specific to such cases preferably with 3D large deformation finite element analysis and model test may produce more refined outcome to arrive at a generalised formulation to use in practice in such cases. Given the significant cost and the importance of safety aspects in offshore operations, more research on the subject will benefit the offshore industry in terms of comprehensive guidelines and more reliable results of analysis.

References

1. Tirant, P.L., Perol, C.: Stability and Operation of Jackups. Editions Technip, Paris (1993)
2. Siciliano, R.J., Hamilton, J.M., Murff, J.D.: Effect of Jackup Spud Cans on Piles. 22nd Annual OTC, Houston Texas (1990)
3. Mirza, U.A., Sweeney, M., Dean, A.R.: potential effects of jackup spudcan penetration on jacket piles. In:Offshore Technology Conference, Houston-Texas, USA (1988)
4. American Petroleum Institute: Geotechnical and foundation design considerations. In: API RP 2GEO, 1st edn. API, Washington, DC (2011)
5. The Society of Naval Architects and Marine Engineers: Guidelines for Site Specific Assessment of Mobile Jack-Up Units, Technical & Research Bulletin 5-5A, 1st edn. Jersey City, New Jersey (2002)
6. International Organization for standardization ISO: International Standard ISO 19905–1:2012(E), Petroleum and natural gas industries - Site-specific assessment of mobile offshore units, (with errata and supplements), Part 1: Jack-ups, 1st edn0 ISO, Geneva, Switzerland
7. American Petroleum Institute: Structural integrity management of fixed offshore structures. In: API RP 2SIM, 1st edn. API, Washington, DC (2014)
8. American Petroleum Institute: Planning, designing, and constructing fixed offshore platforms—working stress design. In: API RP 2A (WSD). 22nd edn. API, Washington, DC (2011)

An Autonomous Program for Crack Length Calculation in an Unsaturated Soil in 1-D Column

Anangsha Alammyan , **Sai Krishna Kothapalli** , **and S. Sreedeep**

Abstract Cracks are widely present in natural and engineered soils. Their presence has the potential to significantly alter both hydraulic and mechanical properties of soil, thereby causing the performance to weaken with respect to different engineering disciplines, particularly geotechnical, environmental and geological engineering. This makes the quantification and characterization of cracks important, which would lead to a better understanding about their extent and complexity in soil under various conditions of seasonal rainfall changes. The length of individual cracks has been studied in the literature to determine the smallest volume with respect to which an averaging of a certain property of the cracked soil can be performed. In this regard, the analysis of images has been instrumental in crack length quantification. However, the currently used software-based methods involving manual adjustment through visual inspection of the cracks in two-dimensional surface images are a time-consuming task that lacks accuracy, sensitivity and reproducibility. There is, hence, the need to develop automated imaging techniques for analyzing crack length in drying soils rather than relying on software-based methods. The main objective of this study is to introduce a novel image analysis tool that employs an open source computer vision library coded in Python to effectively characterize crack length in soils. A simple experimental setup was developed using a one-dimensional column containing compacted red soil in an environment-controlled chamber. A series of images of soil sample was captured using commercially available camera model (Canon EOS 700D) to have a photographic time-lapse representation of the cracking process. A step-by-step strategy using a Python script is presented here to outline an approach to divide the circular two-dimensional image into equal radial slices and calculate the crack length in each slice. The approach can be further extended to calculate other crack parameters sector-wise in a circular image.

A. Alammyan (✉) · S. K. Kothapalli · S. Sreedeep
Indian Institute of Technology Guwahati, Guwahati, Assam 781039, India
e-mail: anangsha.nits@gmail.com

S. K. Kothapalli
e-mail: kothapalli@iitg.ac.in

S. Sreedeep
e-mail: srees@iitg.ac.in

1 Introduction

Upon drying, shrinkage might occur in soils due to loss of water by evaporation. A desiccation crack generally appears in soil when the volumetric shrinkage is constrained or when the induced surface tensile stress becomes equal to the soil tensile strength [1]. The presence of desiccation cracks in soil can fundamentally modify both its hydraulic and mechanical properties, thereby causing a weakened performance of soil. The stability of geotechnical structures that have been constructed on clayey soils is significantly affected directly or indirectly by the presence of desiccation cracks in the soil matrix. Study of desiccation crack is important while considering urban green infrastructure like terrace gardens, bare soil infrastructure like embankments, bio-engineered slopes and agricultural field.

Several field and laboratory studies have been carried out for the characterization of desiccation cracks in soils using variety of approaches like manual measurement [2], X-ray computerized tomography [3], electrical resistivity tomography [4] and numerical simulation [5] among many others. The analysis of digital images of the soil surface has been extensively used to get an idea of the two-dimensional crack characteristics of soil [6, 7]. As distribution and extent of crack network affect water storage and movement, it is important to measure the crack size and pattern. The determination of crack geometry is also important in characterizing the diverse phenomena associated with cracked soils. Studies have stressed on the need for an accurate description of spatial characteristics of joint systems and desiccation cracks [8]. Knowledge of the spatial characteristics of cracks is helpful in environmental applications to accurately model dispersion of contaminants and porous flow. In previously conducted laboratory studies, a commonly used parameter called the crack length density (CLD) has been defined as the total length of the crack skeleton in a soil mass. The calculation of crack length density involves computation by accumulating pixel lengths between two adjacent skeletal pixels. It has been studied to determine the crack geometry [9, 10] and to characterize the smallest volume for which a specific property of the cracked soil can be averaged over [11].

In previous studies, the computation of crack length was done by mapping the entire soil area using AutoCAD and calculating the lengths of individual cracks by approximating them as straight lines [9, 11]. There appears to be a lack of automation in the reported studies. In addition, a significant amount of computational time and human effort need to be spent in analyzing each image separately. This has significant impact in case of studies covering large areas which generate several photographs for which the CLD has to be determined. Moreover, the chances of reproducibility in the results from manual processing are less because of the effect of observer-dependent subjectivity. The main objective of the present study is to develop a program to automate the calculation of CLD of surface cracks in unsaturated soil in a one-dimensional (1-D) column. It aims to overcome the shortcomings of the existing

methods of determination of the CLD by using a program coded in Python language. The Python code analyzes two-dimensional photographs of cracked soil samples and gives the output in the form of a binary image showing the crack skeleton, from which the CLD can be determined. It is an effective image analysis technique valid for all types of soils tested in the laboratory using test pots of any size.

2 Methodology

2.1 Test Plan, Setup and Instrumentation

Soil properties. The tested soil was collected from a hill site in Guwahati, India. The index properties of the soil were determined following the standard procedures given by ASTM [12–14]. The sand, silt and clay contents were determined to be 26%, 50% and 24%, respectively. Liquid and plastic limit were found to be 42% and 24%, respectively. According to the unified soil classification system (USCS), the soil was classified as inorganic silt of low plasticity (ML). The maximum dry density (MDD) was determined to be 1690 kg/m^3 with corresponding optimum moisture content (OMC) of 17%. The other index properties of the tested soil are listed in Table 1.

Table 1 Index properties of the tested soil

Index properties	Value
Specific gravity	2.58
Particle-size distribution (%)	
Coarse sand (4.75–2 mm)	0
Medium sand (2–0.425 mm)	7
Fine sand (0.425–0.075 mm)	19
Silt (0.075–0.002 mm)	50
Clay (<0.002 mm)	24
Specific gravity	2.58
Atterberg limit (%)	
Plastic limit	24
Liquid limit	42
Plasticity index	18
Shrinkage index	21.3
Standard compaction tests	
Maximum dry density (kg/m^3)	1690
Optimum moisture content (%)	17

Sample preparation and testing procedures. The soil was first oven-dried. The soil samples were placed in a poly vinyl chloride (PVC) column with a height of 250 mm and an inner diameter of 300 mm. The soil column was placed on a perforated base plate, over which a filter paper was placed. This was done to prevent loss of soil particles with seeping water. All the soil samples were compacted statically to 0.9 maximum dry density (MDD), which is commonly used in embankment soil [15]. A thin layer of lubricant was applied on the inner surfaces of the column before compaction to reduce the soil-PVC interface friction. The compaction procedure was divided into three layers, each having an equal thickness to achieve uniform soil density. Three replicates (in three separate molds) were prepared to carry out the time-lapse study. The surface of the sample was leveled using a straight edge to get a uniform surface. This procedure was repeated for all the specimens. After compaction, the entire column was placed inside a temperature and relative humidity (RH) controlled chamber where the temperature (25 $\pm$ 2 °C) and RH (40 $\pm$ 5%) were controlled to minimize extreme environment variations. Ultraviolet lighting was turned on to simulate natural lighting conditions. This is shown in Fig. 1. During the process, the soil samples were monitored continuously for a period of 28 days.

Monitoring of cracks. During the experiment, continuous monitoring was done using a high-resolution digital still camera placed straight above the sample. The images were taken with a digital camera Canon EOS 700D with an exposure time of 1/50 s, ISO speed 160 and 39 mm focal length of lens. To get undistorted images directly above the testing specimen, the camera was placed on an adjustable steel mount above the sample. During the duration of the experiment, the camera settings remained fixed. The surface size of the three specimens used for the purpose of image
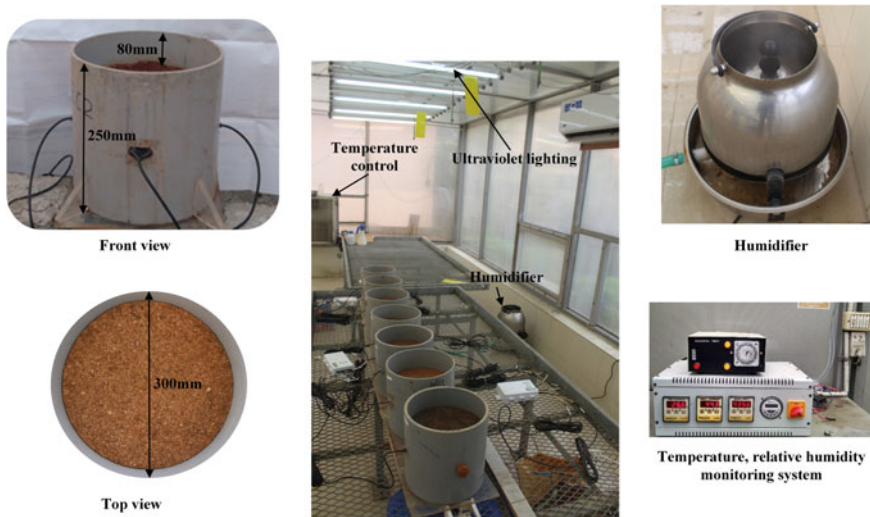
Fig. 1 Test setup for monitoring crack initiation and propagation by image analysis

analysis was taken as to be of diameter 300 mm in accordance with a scale-effect study carried out to find the representative elementary volume [11].

2.2 Image Analysis

Image analysis is a simple non-invasive technique of analyzing digital images of cracked soil surface for the characterization and quantification of desiccation cracks. The developed cracks have a distinct color which is significantly darker than the soil matrix. This assists in the identification of crack pixels and their distinction from the intact soil area. The present study puts forward a novel approach for measuring the lengths of all surface cracks in a cylindrical soil sample by analyzing the digital cracks using a script coded in Python. The thresholding is done with the aid of a novel image analysis algorithm using a step-by-step strategy with a script coded in Python [16]. The first step is the conversion of the original RGB image to gray scale which effectively removes all color information while retaining information on light intensity. The applied method employs the BGR2GRAY command in Python that converts the RGB image to gray scale. The second step uses a smoothing operation to blur out the surface irregularities. This is done by applying a bilateral filter, which removes irregularities without blurring out the crack edges. The next step is thresholding the original image to form a binary image where the crack skeleton appears in black and the soil matrix appears white. This is done using the Gaussian adaptive thresholding method. In this step, each pixel in the gray scale image is replaced with a black pixel if the image intensity is less than a threshold value, and it is replaced with a white pixel if the image intensity is greater than that particular threshold. The value of the threshold for a particular pixel is automatically selected depending upon the light intensity of the surrounding pixels.

The thresholded images then are divided into eight equal sectors to find the CLD in each sector. Summing up, the total crack length in the image can also be found. There were some challenges faced while developing this algorithm. Each image was clicked manually, and hence, the resulting circular soil sample had varying diameter and different dimension of shadow from the container enclosing it. Because of this, it was difficult to locate the center of each different circle with a single code for all images. Keeping the above difficulties in mind, the authors came up with an algorithm where a sector was created of specified angle of 45°. This individual sector was masked over the circular thresholded image of the soil sample and then rotated around it. With this method, the values of crack lengths could be found out sector-wise for the entire image. A Python script was written to incorporate the same. The procedure is explained in brief in the following steps.

At first, the image is thresholded as per a novel algorithm [16]. Following which, a sector having an angle of 45° is drawn and masked on the thresholded image of the

cracked soil. The rest of the image is made transparent, so, when the program runs, the analysis is carried out only on the selected area, which is one sector of 45°. The total length of the cracks in that particular sector is then measured by counting the number of black pixels in it. The novel script does this automatically, and no human input is required once the program starts running. After the measurement of crack length is done in the first sector, the original masked sector is rotated by 45° till the next portion of the image is covered. This leads to the formation of a second sector in which measurements can be carried out. The rest of the image including the first sector is made transparent to ensure that measurements are taken only in the selected area. After the crack length in the second sector has been calculated, the masked sector is further rotated by another 45° so that a third sector in the image is selected and the rest of the image is rendered transparent. After the measurements have been made, these steps are repeated until the whole image is covered by the masked sector leading to the original image of the circular soil sample being effectively divided into eight equal sectors of 45° each. Thus, the crack length density for each sector can be found separately, while the rest of the image has been taken out of consideration for calculation. As a summation of all the above, the total crack length in the image can be found. An additional parameter called the crack intensity factor (CIF) defined as the ratio of area of cracks to the total area of soil sample can be determined as the ratio of black pixels to white pixels in the thresholded image. CIF gives an idea of what percentage of the soil surface is cracked. The entire process with the corresponding segment of code is summarized in Fig. 2.

3 Results and Discussion

The scope of this novel approach is limited to the measurement of crack length by counting the number of dark pixels as the cracks in the thresholded image appear as dark, while the surrounding soil sample appears as white. Further studies can be carried out to use this masking algorithm to divide the circular images of soil samples into equal sectors and find out other crack parameters in each sector. Previous studies have been carried out where the entire circle was divided into an orthogonal network of square grids, along which, the crack parameters are counted [17]. This method of dividing the image into smaller areas leads to possible errors in estimation of crack parameters as the periphery of the image is curved and hence is not covered in full square grids. The Python script presented here for masking the image can be considered as a suggestion for improvement of this existing method. Dividing the image into radial slices with an equal angle rather than squares could be a more uniform way of dividing the image to estimate crack parameters. This could also save computational time otherwise in accounting for the discrepancies along the
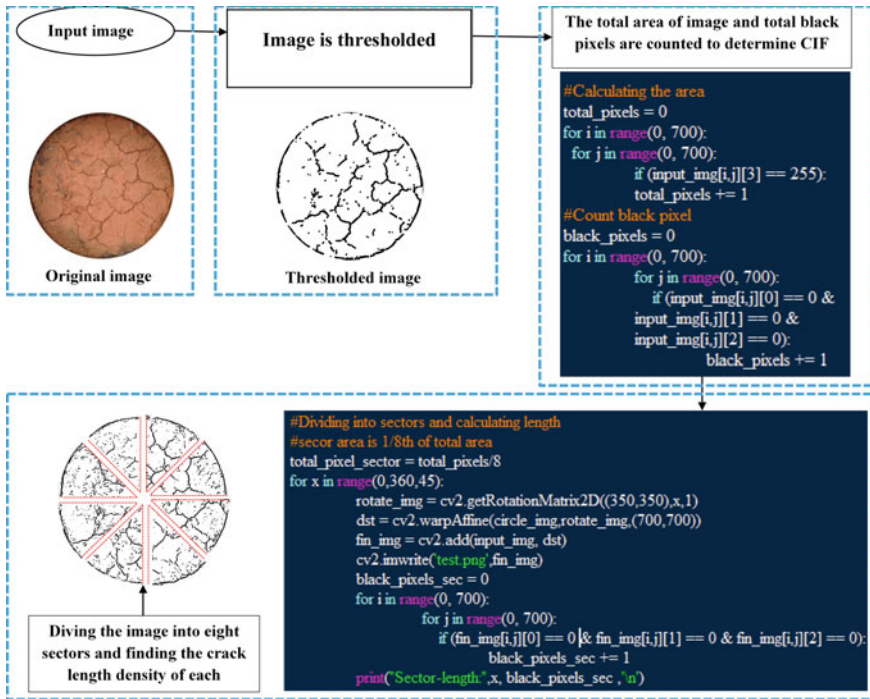
Fig. 2 Flowchart outlining the steps involved in splitting the image to sectors and calculating the crack length density

Table 2 Specimen geometry and main results from image analysis

Total area (cm^2)	Area of uncracked soil (cm^2)	Total crack area (cm^2)	CIF	Crack length density (cm)	Crack length/unit area (cm^{-1})
706.86	537.21	169.65	0.24	122.48	0.173

circumference of the circle in case of orthogonal grids. The results from the study calculated using the algorithm are shown in Table 2.

4 Conclusion

The study presented a simple autonomous program customized for quantifying the total length of surface cracks in unsaturated soil in a 1-D column. The program efficiency to compute CLD was validated using 1-D column experiments. Though a

simple program was introduced for quantifying cracks in 1-D column, however, the same can be easily modified for use in different setups. The authors would like to provide copy of the program as open source for allowing users to further modify it.

4.1 Scope for Future Work

Image analysis has proved to be a powerful tool for the qualitative and quantitative description of 2D patterns. The experimental setup and image analysis described in this paper are part of a long-term project investigating the cracking patterns of drying soils. Applications of the method described here to study the fundamentals of soil cracking and changes in suction can be found in related publications [16]. Research suggests that cracking is a three-dimensional phenomenon [18] and the three-dimensional quantification of crack patterns is a much more difficult task than the 2D process described in the current work. In addition to advanced techniques, the study requires more sophisticated equipment. In essence, the novel method described here can be considered as a first step toward this ultimate goal of quantification of crack networks in the field and in geotechnical projects.

Appendix: Python Script for Quantifying the CIF

```python
import numpy as np
import cv2
from matplotlib import pyplot as plt
import sys
from math import pi

if int(len(sys.argv)) < 2:
    print ("Usage :python script.py input.png output.png")
    sys.exit()
```

```
    # Read the Input Image
    input_img = cv2.imread(sys.argv[1],cv2.IMREAD_UNCHANGED)
    height, width, channels = input_img.shape
    #Resizing the Input Image
    input_img = cv.resize(input_img, (700, 700))
    #Splitting the channels
    (inp_r, inp_g, inp_b, inp_a) = cv2.split(input_img)
    #Convert to Grayscale
    input_img = cv2.cvtColor(input_img, cv2.COLOR_BGR2GRAY)
    #Blur it a bit to remove noise
    input_img = cv2.bilateralFilter(input_img,5,75,75)
    #Threshold the image using adaptive gaussian
    in-
put_img=cv2.adaptiveThreshold(input_img,255,cv2.ADAPTIVE_THRESH_GAUSS
IAN_C,cv2.THRESH_BINARY,11,7)
    #Find Contours
    input_img, contours, hierarchy = cv2.findContours(input_img, cv2.RETR_TREE,
cv2.CHAIN_APPROX_SIMPLE)
    #Draw Contours
    input_img = cv2.drawContours(input_img, contours, -1, (0,255,0), 1)
    #Adding the Alpha channel back
    input_img = cv2.merge((input_img,input_img,input_img,inp_a))
    #Save the image
    cv2.imwrite(sys.argv[2],input_img)



  #Calculating the area PI*radius*radius
  total_pixels = 0
  for i in range(0, 700):
     for j in range(0, 700):
        if (input_img[i,j][3] == 255):
           total_pixels += 1

  #Count black pixel
  black_pixels = 0
  for i in range(0, 700):
     for j in range(0, 700):
        if (input_img[i,j][0] == 0 & input_img[i,j][1] == 0 & input_img[i,j][2] == 0):
           black_pixels += 1

print ("Total Number Of Pixels: ", total_pixels)
print("Total Black Pixels: ", black_pixels)
print ("CIF:", black_pixels/total_pixels)

  #Dividing circle into sectors and calculating CLD
```

```
total_pixel_sector=totalpixels/8
for x in range(0,360,45):
        rotate_img=cv2.getRotationMatrix2D((350,350),x,1)
        dst=cv2.warpAffine((circle_img,rotate_img,(700,700)))
        fin_img=cv2.add(input_img,dst)
        cv2.imwrite('test.png',fin_img)
black_pixels_sec=0
for i in range(0,700):
    for j in range (0,700):
        if (fin_img[i,j][0]==0 &  fin_img[i,j][1]==0 & fin_img[I,j][2]==0):
        black_pixels_sec += 1
print("Sector Length",x, black_pixels_sec,'\n')
```

References

1. Corte, A, Higashi, A.: Experimental research on desiccation cracks. Soil Res. Rep. **66** (1960)
2. Ackerson, J.P., McInnes, K.J., Morgan, C.L., Everett, M.E.: Measuring crack porosity using three-dimensional electrical resistivity tomography. Soil Sci. Soc. Am. J. **81**, 1025–1035 (2017)
3. Zhou, H., Mooney, S.J., Peng, X.: Bimodal soil pore structure investigated by a combined soil water retention curve and X-ray Computed tomography approach. Soil Sci. Soc. Am. J. **81**(6), 1270–1278 (2017)
4. Samouëlian, A., Cousin, I., Richard, G. Tabbagh, A.: Soil cracks detection by 3D electrical resistivity. In: 9th EAGE/EEGS MEETING. Springer, Kyiv (2003)
5. Amarasiri, A., Kodikara, J., Costa, S.: Numerical Modelling of desiccation cracking. Int. J. Numer. Anal. Meth. Geomech. **48**, 336–340 (2010)
6. Yoshida, S., Adachi, K.: Effects of cropping and puddling practices on the cracking patterns in paddy fields. Soil Sci. Plant Nutrition **47**, 519–532 (2001)
7. Peng, X., Zhang, Z.B., Gan, L., Yoshida, S.: Linking soil shrinkage behavior and cracking in two paddy soils as affected by wetting and drying cycles. Soil Sci. Soc. Am. J. **80**, 1145–1156 (2016)
8. Bosscher, P.J., Douglas, E.C.: Measurement and analysis of jointing properties in fine-grained soils. J. Geotech. Eng. ASCE **114**(7), 826–843 (1988)
9. Zhang, Z.B., Peng, X., Wang, L.L., Zhao, Q.G., Lin, H.: Temporal changes in shrinkage behavior of two paddy soils under alternative flooding and drying cycles and its consequence on percolation. Geoderma **192**, 12–20 (2013)
10. Wang, C., Zhang, Z.Y., Liu, Y., Fan, S.M.: Geometric and fractal analysis of dynamic cracking patterns subjected to wetting-drying cycles. Soil Tillage Res. **170**, 1–13 (2017)
11. Li, J.H., Zhang, L.M.: Geometric parameters and REV of a crack network in soil. Comput. Geotech. **37**, 466–475 (2010)
12. ASTM: Standard Test Method for Particle-Size Analysis of Soils. ASTM International, West Conshohocken (2007)
13. ASTM: Standard Test Methods for Liquid Limit, Plastic Limit, and Plasticity Index of Soils. ASTM International, West Conshohocken, PA (2010)
14. ASTM: Standard Test Methods for Laboratory Compaction Characteristics of Soil Using Modified Effort. Annual Book of Standards 4 (2017)
15. Li, J.H., Li, L., Chen, R., Li, D.Q.: Cracking and vertical preferential flow through landfill clay liners. Eng. Geol. **206**, 33–41 (2016)

16. Anangsha, A., Gadi, V.K., Bordoloi, S., Kothapalli, S.K., Sreedeep, S., Guoxiong, M., Garg, A.: A New autonomous program customized for computing surface cracks in an unsaturated soil in a 1-D column. J. Test. Eval. **47**(5), 3822–3835 (2019)
17. Chaduvula, U., Viswanadham, B.V.S., Kodikara, J.: A study on desiccation cracking behavior of polyester fiber-reinforced expansive clay. Appl. Sci. (2017)
18. Zhang, Z.B., Zhou, H., Zhao, Q.G., Lin, H., Peng, X.: Characteristics of cracks in two paddy soils and their impacts on preferential flow. Geoderma **228**, 114–121 (2014)

A Case Study on Soil Quality Analysis Around Dumping Yard

Suraj D. Bhosale, Sanju R. Phulpagar, and Abhijeet Keskar

Abstract The groundwater is one of the most important water resources. The danger of pollution in groundwater has become one of the environmental factors of greatest concern in latest years, particularly in developing countries. The society is continually enhancing the amount of municipal and industrial waste generated. Growth in solid waste has increased due to the drastic population growth in India in recent years. Due to fast urbanization, solid waste generation has deepened and influences the quality of groundwater. In addition, human operations and lifestyle modifications have risen in solid waste resulting in contamination of the soil and polluting soil and groundwater. Aurangabad City is Maharashtra State's increasing industrial center. There are several manufacturing centers around the town that dispose their solid waste to neighboring areas. 300 MT of solid waste per day is produced in Aurangabad city, resulting in increased public health danger and environmental damage. Therefore, in the current study, Naregaon dumping yard located in Aurangabad city of Maharashtra is selected. Results of the study showed that, owing to leachate formation around the dumping yards, the quality of groundwater decreases. The study also showed that the contamination of the soil is nearer to the storage yard and reduces as distance increases.

Keywords Soil quality · Dumping ground · Naregaon · Irrigation

1 Introduction

Water is very important for every living organism [2]. The groundwater is one of the most crucial water resources. In recent years, the risk of pollution in groundwater has

S. D. Bhosale (✉) · S. R. Phulpagar · A. Keskar
Research Scholar, Sardar Vallabhbhai National Institute of Technology, Surat, Gujarat, India
e-mail: bhosalesurajd@gmail.com

S. R. Phulpagar
e-mail: sanjup1213@gmail.com

A. Keskar
e-mail: keskarabhijeet@gmail.com

become one of the most concerns environmental factor, especially in the developing countries [7]. The amount of municipal and industrial waste generated by the society is continuously enhancing. Due to drastically increasing population in recent years in India, growth of solid waste has increased [5]. As a result of rapid urbanization, the generation of solid waste has intensified, and it has influence on the ground-water quality [3]. People in the nearby vicinity mostly depend upon groundwater for domestic and drinking purposes. The pollution of soil arises because of the leaching of wastes from landfills that produce induce heavy metal such as lead, mercury, and copper [6]. The contamination of soil and groundwater is the most serious environmental risk linked to unsanitary land filling of solid waste [6]. Soil is an interface for infiltration, surface runoff, and precipitation event. Likewise, soil is a very crucial media to interflow of leachate/water into the ground reservoirs [1].

Porosity is directly proportional to the contamination of groundwater as well as leachate will spread in underground soil strata that will affect surrounding agricultural soil and land. The physico-chemical parameters of soil are crucial for site suitability, plant growth, and soil management [1]. Aurangabad city is a growing industrial hub in Maharashtra state [8]. Various industrial centers are located in regions of Paithan MIDC area, Chikalthana, Shendra, Waluj, and Pandharpur that disposes their solid waste to nearby sites. This solid waste disposal generates a concern as it causes land pollution when deposited openly, water pollution when stored in low lands, and air pollution when burned [8]. Due to rapid urbanization and enhancement in population, growth of solid waste and environmental pollution has increased [8]. In Aurangabad city, 300 MT per day solid waste is generated which lead to increase in public health risk and damages environment [8]. Therefore, in the current study, Naregaon dumping yard located in Aurangabad city of Maharashtra is selected [4]. Have analyzed the soil quality and chemical characteristics and concentration of heavy metals in Konabari area of Bangladesh for the period of six months (i.e., July to December 2011) by considering five different points at a distance of 10 m apart from each other at depth of 15 m and 30 m, respectively. The outcome of the study showed that waste material produce a drastic impact on soil quality, and heavy metal varies in order as, iron (Fe) > zinc (Zn) > lead (Pb) > copper (Cu) > cadmium (Cd). The metal contained were found more in the industrial effluent site and lesser in solid waste dumping site. Raman et al. (2008) have collected samples from solid waste dumping site in Chennai to find out the impact of a solid waste landfill site on groundwater. The physical and chemical parameters of soil and water such as hardness, temperature, pH, electrical conductivity, total suspended solids, alkalinity, total dissolved solids, calcium, magnesium, chloride, sulfate, phosphate, nitrate, and the metals like potassium, sodium, copper, manganese, lead, cadmium, chromium, palladium, nickel, organic carbon, organic matter, moisture contain, leaches, and pH antimony were studied using various analytical techniques. Its direct impact on groundwater and soil quality parameter was observed, which was exceeding the limits as stated by Indian Standards and concluded that contamination of water and sand in nearby vicinity is due to dumping of solid waste [1]. Studied physico-chemical parameters and textural analysis of soil around periphery of Davanagere Urban city. The study indicates that the soil has neutral pH and moderate permeability. The main

objective of the current study is to understand how the soil contamination variation occurs with respect to distance from the boundary of the Naregaon dumping yard located in Aurangabad city of Maharashtra.

2 Study Area

Aurangabad, the largest city of Maharashtra state, is located on a hilly upland terrain in the Deccan traps as shown in Fig. 1. It is located at latitudes 19° 53′ 35″ N and longitude 75° 23′ 55″ E. Aurangabad is the sixth most populous city in Maharashtra with a population of 1,175,116 (https://en.wikipedia.org/wiki/Aurangabad). On an average, 1000 metric ton/day of waste is dumped at the Naregaon dumping yard. The average rainfall of Aurangabad city is 714.6 mm (2011).

Fig. 1 Study area Naregaon in Aurangabad District of Maharashtra (Not to the scale)

3 Methodology

The present study is carried out, by collecting soil samples from the nine locations around the municipal dumping ground of Naregaon located in Aurangabad city of Maharashtra. The locations of sample collection sites are positioned on the basis of latitude and longitude. The latitude and longitude of nine sample sites and their distance from the boundary of dumping yard are given in Table 1. The preliminary survey on the quality soil samples was conducted in 2018, for the reason that the ground water and soil got polluted due to solid waste dumping, nearer to the location.

3.1 Soil Samples

The collection of soil sample was done by standard method (core-cutter method) that is used to collect the soil samples. The core cutter containing the soil is dug out from the ground. The dolly is removed, and the excess soil is trimmed off. The soil samples were then taken to the laboratory for testing. The method adopted

Table 1 Details of sampling site location

Well	Latitude	Longitude	Distance from boundary of MSW dumping ground (m)
Site 1 (S1)	19° 53′ 50.78″	75° 23′ 17.99″	1400
Site 2 (S2)	19° 53′ 32.1″	75° 23′ 26.09″	800
Site 3 (S3)	19° 53′ 25.98″	75° 23′ 27.31″	750
Site 4 (S4)	19° 53′ 12.19″	75° 23′ 57.95″	700
Site 5 (S5)	19° 53′ 26.66″	75° 23′ 51.29″	330
Site 6 (S6)	19° 53′ 36.13″	75° 23′ 50.82″	380
Site 7 (S7)	19° 53′ 49.09"	75° 23′ 50.6″	420
Site 8 (S8)	19° 53′ 49.49″	75° 23′ 51.86″	450
Site 9 (S9)	19° 53′ 45.85″	75° 23′ 45.67″	310

Table 2 Method adopted for physico-chemical analysis of soil

S. No.	Soil characteristics	Symbol	Unit	Test method
1	pH	pH	–	pH analyzer
2	Electrical conductivity	EC	dS/m	EC analyzer
3	Moisture content	MC	%	Oven dry method
4	Organic matter	OM	%	Titration method

Table 3 Textural characteristics of soil

Well	Clay (%)	Silt (%)	Sand (%)
Site 1 (S1)	29	35	36
Site 2 (S2)	28	38	34
Site 3 (S3)	28	42	30
Site 4 (S4)	29	38	33
Site 5 (S5)	28	35	37
Site 6 (S6)	30	36	34
Site 7 (S7)	29	41	30
Site 8 (S8)	28	43	29
Site 9 (S9)	30	33	37

Table 4 Physico-chemical properties of soil samples around Naregaon dumping ground

Well	pH	EC (dS/m)	Organic matter (OM) (%)	Moisture content (MC) (%)
Site 1 (S1)	7.5	0.19	0.54	10
Site 2 (S2)	7.6	0.44	0.58	12
Site 3 (S3)	7.4	0.49	0.56	11
Site 4 (S4)	7.3	0.51	0.34	15
Site 5 (S5)	6.9	0.65	0.43	12
Site 6 (S6)	7.1	0.70	0.18	16
Site 7 (S7)	6.8	0.81	0.13	17
Site 8 (S8)	6.9	1.16	0.23	14
Site 9 (S9)	7.6	1.23	0.17	19

for physico-chemical analysis of the soil sample is given in Table 2. The station-wise distributions of analytical parameters such as soil textural characteristics and physico-chemical parameters are given in Tables 3 and 4, respectively.

4 Results and Discussion

4.1 Soil Characteristics

Soil acts as a media to interflow of leachate into ground water (GW). If the soil have high porosity, the interflow is more, and GW contamination is more, and furthermore, the leachate will spread that affects the soil quality. Each of these soil conditions has distinct characteristics that can be observed in the field (Naregaon dumping ground). Experimental results obtained on the characteristics of soil samples are given in Table 3.

4.2 Soil Textural Characteristics

The textural characteristics of soil samples collected around the Naregaon dumping ground are given in Table 3. From the study, it was observed that the soil quality varied in different locations.

The results of textural analysis indicate that leachate can percolate deeper and has a high risk of ground water contamination for soils having the larger portion of sand content. The uncontaminated soil is relatively uniform, and contaminated soil is more fines than the uncontaminated soil. The high percentage of fine content for contaminated soil quality is from emanating the decomposed municipal solid waste above the soil. During bacterial degradation or decomposition of municipal solid waste, large amount of fines are produced.

4.3 Physico-chemical Parameters

The physico-chemical parameters of soil such as pH, electric conductivity (EC), organic matter (OM), and moisture content (MC) are analyzed in the MSW dumping yard of Naregaon located in Aurangabad city of Maharashtra and are given in Table 4.

pH. It decides the amount of hydrogen present in the soil and ranges from zero to fourteen (0–14). The low pH value of the samples indicates sour soil, and high pH value shows salty soil. The pH value of collected soil samples from nine locations were ranged from 6.8 to 7.6 as given in Table 4. The soil pH should be within the limits of 6–8.5. The leachate is acidic in nature and will reduce the soil pH [Pooja et al.]. Results of the study showed that the soil pH of all samples is less than 8.5 and is within the limits.

Electrical Conductivity (EC). The amount of soluble salts in the soil sample is expressed in terms of EC, and it is measured by a conductivity meter. The high salt content in the soil samples leads to plasmolysis and exosmosises and leads to inhibition of water and that condition of soil is unfavorable for crop growth [Pooja et al.]. The limitation of EC is 2 dS/m. Result of the study showed that the EC of all the collected soil samples ranges from 0.19 to 1.23 dS/m as given in Table 4.

Organic Matter (OM). Organic matter (OM) of the soil includes animal and plant waste with the rate of decomposition [Pooja et al.]. Its limitation is less than 0.5%. Result of the study showed that OM that ranges from 0.13 to 0.58% for all the soil samples as well as microbial activity is also less due to less holding capacity of water.

Moisture Content (MC). The MC of soil is the percentage (%) of water content available in the soil. The MC is the ratio of mass of free water in the collected soil samples to the mass of dry soil sample [Pooja et al.]. The MC of soil should be less than 20%. Results of the study showed that MC varies from 10 to 19% of the samples collected from all the nine locations around the dumping yard (Table 4) and is within

the limits. If the MC is greater than 20%, increase in the leachate formation and the gas production take place which further contaminates the ground water.

5 Conclusion

As India is developing country and Indian economy depends on agricultural yield, if suitable quality of ground water is not available in the ground, it will directly impact on agricultural growth. The quality of ground water is decreasing due to leachate formation around the dumping yards. The study has shown that the soil contamination is more near the dumping yard and decreases with increase in distance. This conclude that agricultural production around the study area is unfavorable due to the presence of dumping yard. Hence, selection of dumping yard is of major importance for agricultural productivity.

References

1. Bhagwat, T.N.: Soil suitability for solid waste dumping: implication for groundwater protection. Earth Sci. Int. J. (ESIJ) **1** (2018)
2. Chavan, B.L., Zambare, N.S.: Ground water quality assessment near municipal solid waste dumping site, Solapur, Maharashtra, India. **2**, 73–78 (2014)
3. Eshanthini, P,, Padmini, T.K.: Impact of leachate on ground water quality near Kodungaiyur Dumping Site, Chennai, Tamil Nadu, India (2016)
4. Islam, M.S., Tusher, T.R., Mustafa, M., Mahmud, S.: Effects of solid waste and industrial effluents on water quality of Turag River at Konabari Industrial Area, Gazipur, Bangladesh. J. Environ. Sci. Nat. Res. **5**(2), 213–218 (2012)
5. Prasanna, K., Annadurai, R.: Study on ground water quality in and around Perungudi Solid waste dumping site in Chennai. **9**(2) (2016)
6. Raman, N., Narayanan, D.S.: Impact of solid waste effect on ground water and soil quality nearer to Pallavaram solid waste landfill site in Chennai. RIC Rasayan J. Chem. **1** (2008).
7. Shenbagarani, S.: Analysis of groundwater quality near the solid waste dumping site. IOSR J. Environ. Sci. **4** (2012)
8. Tejankar, A., Pathrikar, R.K.: Analysis & recycling of municipal solid waste: a case study of Aurangabad City, Maharashtra, India. Int. J. Sci. Res. Eng. **2** (2017)

Uplift Capacities of Triple-Plate Horizontal Circular Anchors in Sand

B. Vidya Tilak (ID) **and Narendra Kumar Samadhiya** (ID)

Abstract Anchors have found varied applicability in the field of civil engineering; be it in foundations, in supporting diaphragm walls, to support waterfront structures, in bridge abutments, in supporting transmission towers. A variety of anchors have been experimented in small-scale model tests in the laboratory and tested in the field. Plate anchors, screw anchors, drag anchors, cement-grouted anchors, and shank anchors are a few to name. Researchers have studied, in both experimental studies, and analytical and numerical ones. The use of multi-plate anchors attached to the same tie rod has, however, been not yet considered. The authors present their idea of the use of multi-plate anchors here. The study describes the load–displacement behavior of both single-plate and triple-plate horizontal anchors of circular shape. The triple-plate anchors consist of three single-plate anchors attached to the same tie rod at a spacing (s) equal to the size of the anchor (d). The efficacy of additions of plates is checked by the detailed laboratory study, in the sand.

Keywords Plate anchors · Single-plate anchors · Multi-plate anchors · Pullout load · Sand

1 Introduction

Plate anchors have a multitude of applications in both civil engineering structures, and offshore structures. An anchorage system is used to resist tensile forces, wind forces, and wave action. The plate anchors are of different shapes, like square, circular, rectangular, and irregular anchors; different angle of inclinations, like horizontal, inclined, and vertical; and used with different angle of load application. Foundation systems of transmission towers, offshore floating structures, construction of oil and

B. V. Tilak (✉) · N. K. Samadhiya
Indian Institute of Technology Roorkee, Roorkee, Uttarakhand 247667, India
e-mail: vtilak@ce.iitr.ac.in

N. K. Samadhiya
e-mail: narendra.samadhiya@ce.iitr.ac.in

gas extraction wells, submerged pipelines, tunnels, and rock engineering structures are some of the applications of plate anchors.

The perpetual application of plate anchors has pioneered extensive research in the area. The early 1960s laid the groundwork for intensive laboratory studies in this domain. Kozlov [8] studied the application of horizontal loads to horizontal anchors. Das and Seeley [1] have worked with horizontal anchors in the laboratory. They used aluminum plates of 3.2 mm thickness, the plates were of rectangular size. The chosen tank was 0.6 m × 0.6 m × 0.6 m in size, the angle of friction of silica sand was 31°. The uplift load was applied to the model by a 6.5 mm diameter tie rod, attached to the center of the plate. Meyerhof's theory was used to predict the breakout factor of shallow anchors. Das and Seeley [2] have performed laboratory tests on eccentric loads. Saran et al. [15] developed constitutive laws for soil anchors. They performed model tests for strip, circular, and square anchors. Dickin [4] used a centrifuge to test the uplift resistance of horizontal plate anchors in sand. He also assessed the design method of previous researchers, like the finite element of Rowe and Davis, Vermeer and Sutjaiadi's predictions, Meyerhof and Adams' formulas, and Mayer's vertical slip surface model.

Subbarao and Kumar [16] used the method of characteristics coupled with a log-spiral failure surface to develop a theory for the vertical uplift capacity of shallow horizontal strip anchors in a general c–φ soil. Geddes and Murray [6] studied the collective behavior pattern of horizontal plate anchors placed in a row, with multiple configurations. Ilamparuthi et al. [7] conducted an experimental investigation on half-cut circular anchor plates in sand. They observed that the uplift capacity of circular anchors depends on their diameter, embedment ratio, and sand density. Merifield and Sloan [12] based their design practice on empiricism. They have performed numerical analysis to determine ultimate pullout loads of anchors in frictional anchors. Sakai and Tanaka [14] performed an experimental and numerical study of uplift behavior of shallow circular anchors in two-layered sand. The density of the layers was dense, medium, and loose. A set of the different combinational height of the layers was chosen. Dickin and Laman [5] performed centrifuge and numerical studies using PLAXIS, to study the response of strip anchors in cohesionless soil. Kumar and Kouzer [9] conducted numerical analysis to study the effect of group action of horizontal anchors in sand. Liu et al. [11] presented an experimental study of a series of scaled model tests to study the anchor behavior in air-dried sand. Rokonuzzaman and Sakai [13] performed model tests on rectangular anchor plates in a circular tank.

The literature study reveals a series of studies on horizontal anchors and group anchors. Kumar and Naskar [10] performed numerical studies on co-axial anchors in a general c–φ soil. However, the study on co-axial anchors, i.e., multi-plate anchors, is never resorted to, in the case of sand. The authors in the present study put forward their experimental investigation on multi-plate horizontal anchors in sand.

2   Methodology

A tank of dimension 1.1 m × 1.1 m × 0.75 m was utilized to perform the pullout tests on a single-plate and triple-plate anchors. Figure 1 shows the experimental setup. The sand was of uniform gradation. The dry sand was compacted to a relative density of 65% (medium-dense) using rainfall technique. The sand used had an angle of internal friction of 34° and unit weight of 14.8 kN/m³. The setup of the test includes a test tank, a loading system consisting of a loading frame and cable system, tie rod, and dial gauges with a magnetic base, strainer, load plates, load hanger, pedestal, and frame for sand raining.

The anchor plates were 50 and 75 mm in size, circular in shape, and of thickness 5 mm. The anchors were connected to a tie rod and pulled using a cable of 5 mm in diameter attached to the center of the pulley. At the free end of the cable, the authors made a provision for the application of load. Pullout load on the anchor plate was gradually applied. A set of two dial gauges were used to record the displacements after each application of the load. Displacement was recorded until the ultimate pullout failure occurred, and the anchor system failed.

The triple-plate anchors consist of three single-plate anchors attached to the same tie rod at a spacing equal to the size of the anchor Fig. 2. The weight of the triple-plate anchor system increases by two additional anchor plates and two connectors of length equal to the diameter of the plate, as compared to the single-anchor plate system. The spacing chosen between the plates for all the triple-plate anchor system was equal to the size of the anchor plate. For the present study, embedment ratios (h/d) of 2, 4, 6, and 8 were selected, where the embedment length (h) is the height of
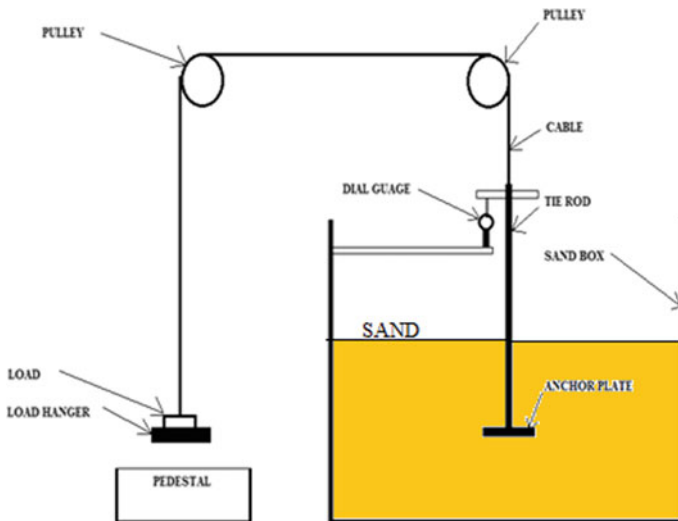
Fig. 1 Experimental setup

Fig. 2 a Single-plate
anchor, **b** triple-plate anchor
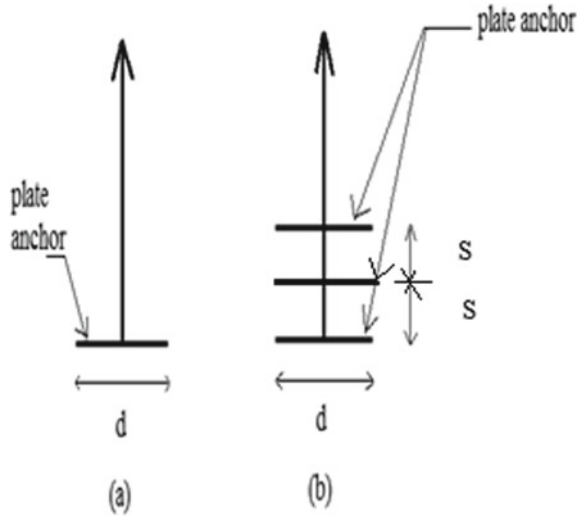
the anchor plate from the top surface of the filled-up tank and diameter of the anchor
plate (*d*).

3   Results and Discussions

3.1   *Load–displacement of Single-Plate Anchors*

The variation of load with displacement for the pullout tests on 50 mm single-plate
circular anchors with embedment ratios (*h/d*) of 4, 6, and 8 is shown in Fig. 3.

The pullout test result for 50 mm single-plate anchor is not shown in Fig. 3, as the
anchor was pulled out at the loading increment itself and registered a pullout load of
13 N for a displacement of 200 mm in case of embedment ratio of 2. The pullout load
of 13 N in this case, is the resistance offered due to the self-weight of the anchor plate
and the tie-rod. Hence, for the case of embedment ratio 2, the value of the pullout load
will not be considered. The actual pullout load needs to be experimentally found out
by a more sensitive arrangement of the test facility. The pullout load is mobilized by
the development of the passive resistance of sand between the horizontal anchor plate
and the top surface of the test tank filled with sand. Das and Shukla [3] recommend
the consideration of frictional resistance for anchors with limited width. An increase
in the pullout load was observed for an increase of embedment ratio from 2 to 8.
The increased embedment depth (*d*) encompasses a higher volume of soil mass
responsible in providing higher passive resistance.

The load–displacement behavior of 75 mm circular single-plate anchors with
embedment ratios of 2, 4, 6, and 8 is shown in Fig. 4. The increased size of the

Fig. 3 Load–displacement
curves of 50 mm single-plate
circular anchor
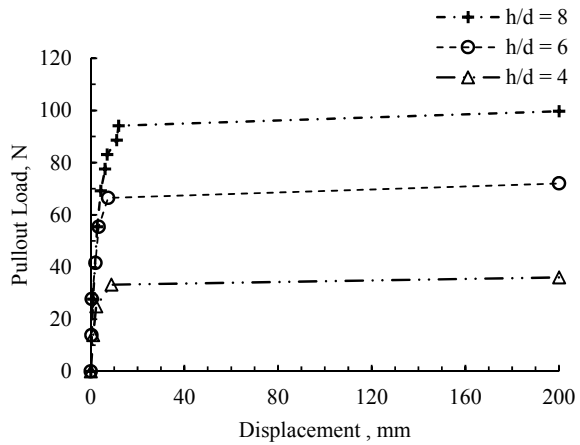
Fig. 4 Load–displacement
curves of 75 mm single-plate
circular anchor
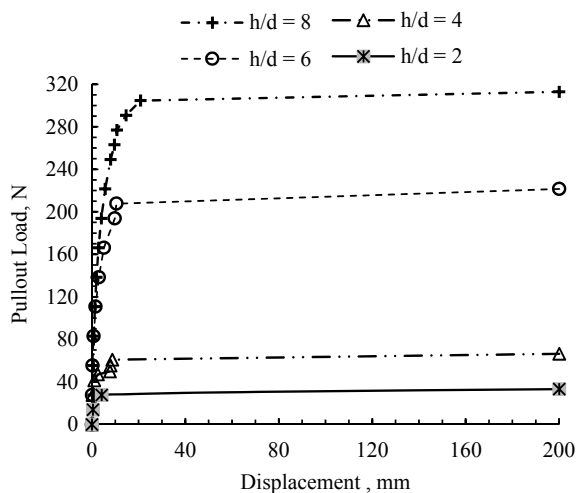
anchors provides higher area encompassing higher soil volume to generate better resistance and hence higher pullout capacity.

3.2 *Load–displacement of Triple-Plate Anchors*

The variation of load with displacement for the pullout tests on 50 mm triple-plate circular anchors with embedment ratios (*h/d*) of 4, 6, and 8 is shown in Fig. 5. The pullout load of 31 N was obtained at a displacement of 200 mm embedment ratio of 4 for the 50 mm triple-plate circular anchor. The pullout load is mobilized by the development of the passive resistance of sand between the horizontal anchor plates

Fig. 5 Load–displacement
curves of 50 mm triple-plate
circular anchor
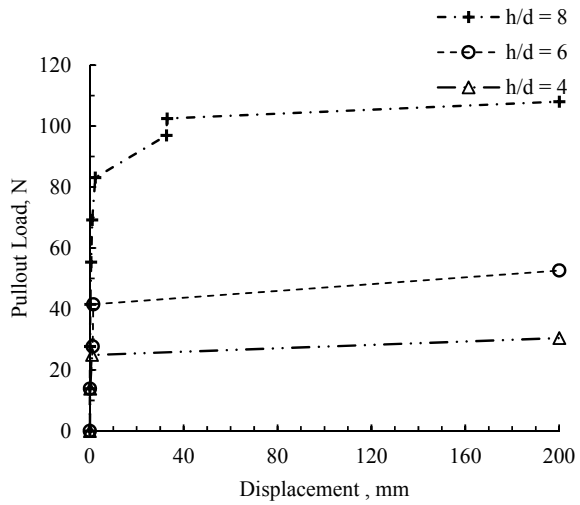
and the top surface of the test tank filled with sand. An increase in the pullout load was
observed for an increase of embedment ratio from 4 to 8. The increased embedment
depth (*d*) encompasses a higher volume of soil mass responsible in providing higher
passive resistance.

The variation of load with displacement for the pullout tests on 75 mm triple-plate
circular anchors with embedment ratios (*h/d*) of 4, 6, and 8 is shown in Fig. 6. The
increased size of the anchors provides higher area encompassing higher soil volume
to generate better resistance and hence higher pullout capacity.

Fig. 6 Load–displacement
curves of 75 mm triple-plate
circular anchor
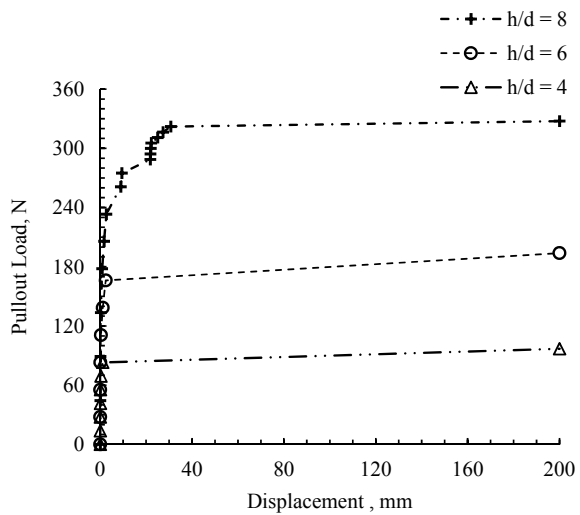
3.3   Comparisons of Single-Plate and Triple-Plate Anchors

Table 1 shows the comparative study of the 50 mm and 75 mm single-plate anchors and triple-plate anchors, respectively.

The results of the triple-plate anchors, for the varying embedment ratio of 4 and 6, do not show an increasing trend when compared with the single-plate anchors. The influence of the additional plates has led to a decrease in the pullout load. The influence of an additional plate becomes instrumental in reducing the embedment depth of the top-most plate, at the same embedment ratio for the ratios 2–6.

For the 50 mm triple-plate anchor at an embedment ratio of 4, the embedment ratio of the top-most plate was 2. The pullout load at failure recorded was 30 N. However, the pullout load of 50 mm single-plate anchor, at an embedment ratio of 4, was 36 N. The reason for this decrease is perhaps due to the placement of the three plates before the sand filling. This kind of placement of top plates does not necessarily provide uniform distribution of sand below the top plates. The result of the unavoidable manual error in the chosen method may be attributed to this decrease, especially in embedment ratios 4 and 6.

The sequence of construction for the horizontal anchors is: excavation, placement of anchors, and backfilling. An interesting comparative observation of 50 mm triple-anchor at embedment ratio of 6, with 50 mm single-plate anchor at embedment ratio of 4, brings to the next stage of the study. The pullout load of 50 mm triple-plate anchor at embedment ratio 6 had the top-most anchor plate at embedment ratio of 4, which was 52.63 N; which is greater than the 50 mm single-plate anchor at embedment ratio 4 with pullout load of 36.02 N. This brings us to the positive replacement of single-plate anchors with triple-plate anchors. This idea is not economical with the horizontal anchors but probably will be effective in inclined and vertical anchors.

Referring to Table 1, the pullout load of 50 mm single-plate anchor at embedment ratio of 8, was 99.72 N. The pullout load of 50 mm triple-plate anchor at embedment ratio of 8 was 108.05 N. The influence of additional plates affected an increase in the pullout load. The increase is credited to the effect of the top-most plate being at an embedment ratio of 6. The effect of top-plate of triple-plate anchor (of $h/d = 8$) being in embedment ratio of 6 is better than the single-plate anchor being placed at

Table 1 Summary of pullout load of single-plate and multi-plate anchors

Embedment ratio (h/d)	Peak pullout load, N			
	50 mm plate anchor		75 mm plate anchor	
	Single-plate	Triple-plate	Single-plate	Triple-plate
2	–	–	33.24	–
4	36.02	30.47	66.50	96.96
6	72.03	52.63	221.56	193.86
8	99.72	108.05	312.96	327.59

embedment ratio if 6. The pullout load of 50 mm triple-plate anchor at $h/d = 8$ is 108.05 N is better than pullout load of 50 mm single-plate anchor at $h/d = 6$.

The authors are of the view that the triple-plate anchors beyond the embedment ratio of 8 would also prove to be better than the single-plate anchors at similar depth ratios. The non-uniformity in sand filling between the plates takes less importance for the case of deep anchors than shallow anchors.

3.4 Remarks

Table 1 shows an increase in the pullout load of 75 mm triple-plate anchor as compared to the 75 mm single-plate anchor. It can be credited to uncontrolled errors in the sand filling process, the choice of application of a set of load plates during the succession of the experiment, or a disturbance in the surrounding area leading to the densification of sand layers before the application load. The case in consideration causes an 8% error in the tests mentioned. The authors refer this as an avertible error, common to the laboratory investigations owing to multiple facts stated above.

4   Conclusions

The laboratory study chooses the traditional single-plate anchors, tests them for the same, and compares it with the novel idea of triple-plate anchors. The pullout load of triple-plate anchors increased with the increase in the size of the anchors and embedment ratios. The use of triple-plate anchors, at shallow depths, proved ineffective. The use of triple-plate anchors, at larger embedment ratios, proved useful. The authors suggest direct replacement of existing methods with the triple-plate anchors.

References

1. Das, B.M., Seeley, G.R.: Breakout resistance of shallow horizontal anchors. J. Geotech. Eng. **101**(9), 999–1003 (1975)
2. Das, B.M., Seeley, G.R.: Shallow anchor resistance to eccentric uplift load. J. Geotech. Eng. **102**(4), 389–393 (1976)
3. Das, B.M., Shukla, S.K.: Earth Anchors, 2nd edn. J. Ross Publishing Inc., New York (2013)
4. Dickin, E.A.: Uplift behavior of horizontal anchor plates in sand. J. Geotech. Eng. **114**(11), 1300–1317 (1988)
5. Dickin, E.A., Laman, M.: Uplift response of strip anchors in cohesionless soil. Adv. Eng. Softw. **38** (8–9), 618–625 (2007)
6. Geddes, J.D., Murray, E.J.: Plate anchors groups pulled vertically in sand. J. Geotech. Eng. **122**(7), 509–516 (1996)

7. Ilamparuthi, K., Dickin, E.A., Muthukrisnaiah, K.: Experimental investigation of the uplift behaviour of circular plate anchors embedded in sand. Can. Geotech. J. **39**, 648–664 (2002)
8. Kozlov, S.M.: Investigation of the behaviour of anchorages acted on by horizontal loads. Leningrad. (Trans. from Osnovaniya) Fundamenty i Mekhanika Gruntov **6**, 19–21 (1967)
9. Kumar, J., Kouzer, K.M.: Vertical uplift capacity of horizontal anchors using upper bound limit analysis and finite elements. Can. Geotech. J. **45**, 698–704 (2008)
10. Kumar, J., Naskar, T.: Vertical uplift capacity of a group of two coaxial anchors in a general c−φ soil. Can. Geotech. J. **49**, 367–373 (2012)
11. Liu, J., Liu, M., Zhu, Z.: Sand deformation around an uplift plate anchor. J. Geotech. Geoenviron. Eng. **138**(6), 728–737 (2012)
12. Merifield, R.S., Sloan, S.W.: The ultimate pullout capacity of anchors in frictional soils. Can. Geotech. J. **43**, 852–868 (2006)
13. Rokonuzzaman, Md., Sakai, T.: Model tests and 3D finite element simulations of uplift resistance of shallow rectangular anchor foundations. Int. J. Geomech. **12**(2), 105–112 (2012)
14. Sakai, T., Tanaka, T.: Experimental and numerical study of uplift behaviour of shallow circular anchor in two-layered sand. J. Geotech. Geoenviron. Eng. **133**(4), 469–477 (2007)
15. Saran, S., Ranjan, G., Nene, A.S.: Soil anchors and constitutive laws. J. Geotech. Eng. **112**(12), 1084–1100 (1986)
16. Subbarao, K.S., Kumar, J.: Vertical uplift capacity of horizontal anchors. J. Geotech. Eng. **120**(7), 1134–1147 (1994)

An Observation of Methods of Pile Analysis Subjected to Different Load and Soil Condition

Alpesh Pandya and Atul K. Desai

Abstract Design of structures, subjected to lateral loads, is very much dependent upon lateral response of pile foundations. The lateral load acting on foundations may be sustained as earth pressure in a retaining wall, or alternated, as reciprocating machinery, as pulsated, from the traffic loading on a bridge pier. The response of pile which is laterally loaded is considered complex soil-structure interaction problem; because deflection of pile is dependent on soil reaction and soil reaction influences the pile deflection. A good number of methods have been developed for the analysis of laterally loaded piles like chin method, *p-y* relationships, *p-y* multiplier, modified *p-y* curves, strain wedge method, etc. An observation of a few methods is presented here with their limitations and capabilities of analysis of piles in different conditions of load application and soil type.

Keywords Analysis of piles · Chin method · *P-Y* curves · Strain wedge method

1 Introduction

Prediction of performance of pile under load can be calculated from many methods including very simple to complex with some where finite element methods are also used. In his Rankine Lecture, Poulos (1989) mentioned list of methods [8]. He not only tried to focus on variety of methods but also stressed on importance of input information on results, as they are dependent on quality of input. It is very difficult to obtain easily interpretable input data from routine procedure of site investigation. So a simpler approach is required which can correlate general properties of soil with site experience and which are easy to understand by users.

A. Pandya (✉) · A. K. Desai
Applied Mechanics Department, SVNIT, Surat 395007, India
e-mail: pandyaalpesh@yahoo.co.in

A. K. Desai
e-mail: atuldesai61@gmail.com

Fig. 1 Relationship of
settlement and
settlement/load
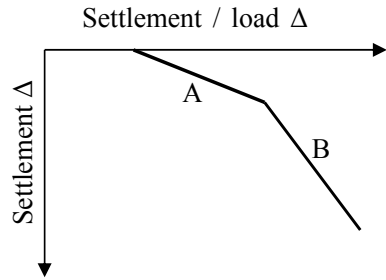
The hyperbolic method used by Chin was to plot the behavior of footing and piles. This method is used to determine ultimate loads and is very popular though it does not link with the soil parameters.

Fellenius (1980) and others have found that the Chin method appears to over predict when they compare the results of analysis of Chin method and other methods for defining ultimate loads. However, there is little doubt that in most cases, according to the plotting method, linear functions represent pile performance very well.

Chin (1970, 1972) expressed his method by $A/P = mA + C$, where A is settlement of pile head, P is numerical value of applied load and C is a constant. Thus, if A/P is plotted against an abscissa of A, a linear plot is obtained, and the inverse slope l/m gives an asymptotic limiting value of P. This is true for piles, where most of the load is carried out by shaft friction and also for footings and piles where end bearing carries the most of the load as explained by Chin. A typical relationship between pile head settlement A and settlement divided by load A/P is shown in the Figure. It has been suggested by Chin & Vail and has often been accepted where (A) of the relationship represents shaft friction while the second part (B) represents total load. This cannot be true for every case because of the nature of hyperbolic functions, but it can easily be accepted that individually shaft and base performance are of hyperbolic form (Fig. 1).

Chin [6] suggests that mobilization of stress in soil with increase of strain is a function of increasing number of effective soil contacts rather than of a general increase of intergranular stress on a constant number of grain contacts. He suggests that intergranular stress in flocculated clay, for example, is virtually constant and independent of the applied or effective stress. On this basis of hyperbolic function of stress–strain relationship developed by him, it may be understood that when soil is under compressive stress, the load is transmitted by internal column-shaped grain structures. As these reach limiting loads, number of columns begin to support this each having nearly similar yield load.

While laterally loaded piles are designed, lateral bearing capacity is calculated at failure, with deflection and moment of a pile under working load. Sometimes, while considering deformation controlling and serviceability requirement, the deflection and bending moment along the shaft are of greater importance in that. The over deformation and overstress make the moment overshoot the allowable moment of the pile materials and induce additional deformation for superstructures.

Active research has been carried out to find working load behavior of laterally loaded pile for many years, and many approaches were proposed for load deformation analysis of piles subjected to lateral loads, such as classical Winkler model (subgrade reaction method), *p-y* curve method and continuum analysis proposed by Xu et al. In continuum analysis, the soil is considered as a three-dimensional continuum, and numerical techniques such as boundary element methods, integral equations or finite element methods are used to give numerical solutions for laterally loaded pile. The others keep treating the pile as a flexible material and surrounding soil as number of horizontal linear springs for Winkler and discrete nonlinear springs for *p-y* curve method. Because of its simplicity in comparison with continuum analysis, beam on foundation model was more acceptable to practicing engineers due to accuracy and precise prediction of responses of laterally loaded piles. Vesic's expression for Winkler model is more in use in comparison with lot of various expressions developed by research because it is simple and it includes properties of both soil and beam.

2 Chin Method

A number of methods for prediction of settlement of single plies and pile groups and its analysis are available including load transfer method, empirical methods, elastic continuum method, the 'hybrid' type of approach, etc. Guo et al. presented an infinite layer approach for single pile, and Cheung et al. presented the same for pile groups.

2.1 *Validity of Chin's Method*

To check Chin's method, 50 loading tests were carried out by Borel et al. [15] under MLT procedure which was limited to head settlement greater than 10% of dia. of pile, and each load step was maintained for 60 min of time. Every test carried out with utmost care, and all readings were digital. Load cells were used to check load and linear potentiometers to measure settlements. Measurement of shaft and toe resistances was taken by removable extensometers. In all 50 tests, various pile techniques and variety of soils were used. With pile diameters ranging from 200 to 1000 mm, load applied was from 675 to 10,000 kN with pile length varies from 5 to 45 m. During tests, four piles were loaded in tension. Out of 50 piles tested, bored (6), impact-driven steel and concrete (17), CFA (12), vibratory-driven (5) and screwed displacement auger (10) were tested. There were 20 piles in clay, 15 in sand, 8 in calcareous and 7 in mixed soil.

Two different approaches were used to check the performance of Chin method: (1) complete load settlement curve and (2) partial load settlement curve taken into account, which was obtained by gradually removing the last points as if the test was stopped at lower loading step. To determine the result of ultimate resistance from the complete curve, each test result was plotted in hyperbolic coordinates to find part

B of load settlement curve which is useful to calculate Chin parameters. Except in five cases, the Chin method estimated very satisfactory ultimate resistance. The five cases where plunging failure was observed were not anticipated by Chin method, and ultimate resistance was 25% more than estimated. As per the second approach, the load settlement curves were altered by removing last point one after another to check sensitivity of Chin method for head settlement to the number of loading steps. A graphical representation is shown for the test carried out at Mittersheim site. To obtain a shortened load settlement curve, last two points out of 13 were removed. The maximum settlement observed is 3.3% of pile diameter against 92% of measured ultimate resistance. The same is repeated for other readings, and 1.4% of settlement is observed against 81% of ultimate resistance (Figs. 2 and 3).

The main conclusions for the Chin method are as following: It is observed that Chin method generally over predicts the shaft resistance. It was also observed that when shaft resistance is more than 55%, predicted shaft friction varies from 120 to 60% of the measured value.

Fig. 2 Performance of Chin method
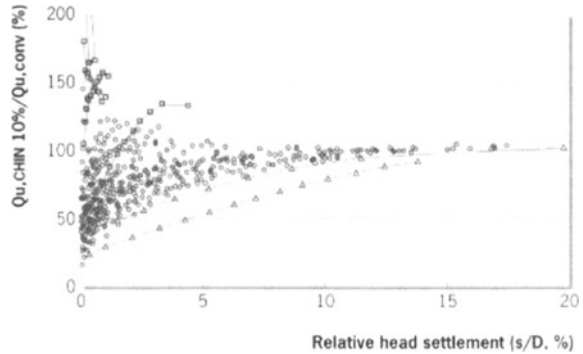
Fig. 3 Prediction of the ultimate resistance
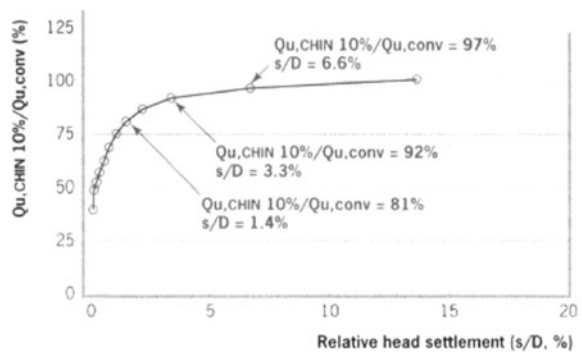
3 *P-Y* **Method**

3.1 *Introduction*

When a structure is subjected to earthquakes, high winds, ship impacts and wave action, it is essential to design lateral load capacity of pile foundations. For single pile design under static load, many researchers have proposed different methods, but for closely spaced pile groups, where spacing is less than six pile diameters, a very few methods are available for reference. It is seen many times that piles in front row show similar kind of load–displacement curve as shown by single pile, but piles in trailing rows show less resistance in comparison with front rows. This phenomenon is known as shadowing. The effect of shadowing becomes less as the spacing between piles increases and becomes unimportant once the spacing exceeds about six times pile diameters center to center. Due to this uncertainty, design of pile groups is very conservative. Some numerical methods [2] and models are available for this, but a large number of full-scale tests are essential for verification and to provide real information about the ground.

Two popular ways to analyze laterally loaded piles both numerically or analytically are as follows: continuum-based methods and load transfer methods. The most popular method is '*p-y*' curve, which is simple and reliable hence widely used. These curves can be produced by measuring soil resistance [1] directly or by measuring strain along the length of pile indirectly. There are some shortcomings due to differentiation procedure when '*p-y*' curve is generated indirectly as P values are sensitive to pile curvature [3]. Research shows that when a larger diameter shaft is used, stiffer response is measured than that of general curves.

3.2 **P-Y** *Curves for Laterally Loaded Piles in Sand*

Reese
The best available criterion for the analysis of behavior of single vertical pile in sand is subjected to static or cyclic loading suggested by Reese et al. To check the accuracy of prediction of behavior of piles which are laterally loaded, they are compared to measure analytical results of load tests [11]. For the purpose of analysis, different assumptions were made in selecting soil properties to correlate with the results of standard penetration test. Hence, all soil properties are not exact but were the best available from the information collected.

Arkansas River
Furgo and Associates have carried out a large number of lateral load tests for Corps of Engineers at a site on Arkansas river in Arkansas. Soil properties reported for all test piles were similar, but because of differences in loading condition, pile stiffness, etc., a number of different analyses were performed. Some of the results are presented

here. One boring was selected as representative of soil conditions at the test site which was done in a 20 ft deep test pit prior to testing the piles (Figs. 4 and 5).

Among number of piles, test pile 6, which was 14BP73, driven vertically, short-term and cyclic loading applied is presented here. The graph representing measured and computed deflection shows good similarities for static loading. For cyclic loading, only one deflection was reported. The computed deflection underestimates the measured deflection by 10%.

Fig. 4 Test setup for test pile 6 at Arkansas River
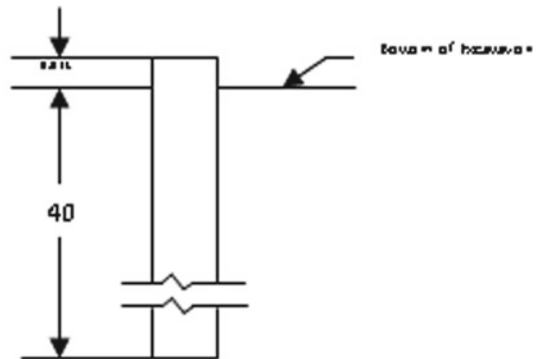
Pile properties, Section type = 14 BP73,
EI = 21.5X10¹⁰ lb-in², b= 14 in

Fig. 5 Comparison of measured and computed deflection for test pile 6 at Arkansas River
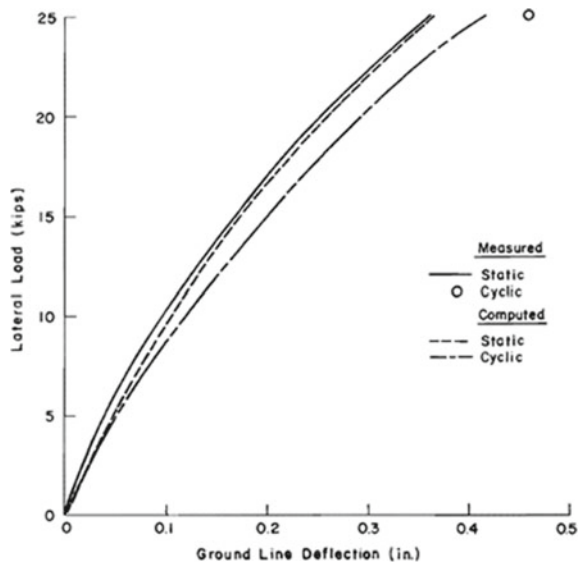
Fig. 6 Information for the analysis of tests at Appa
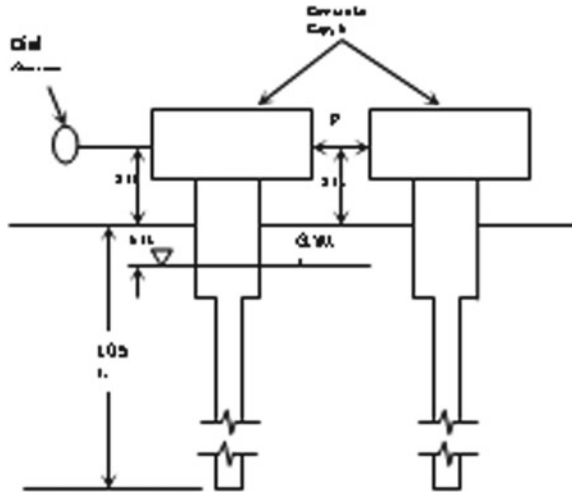
Apapa

Number of load tests were carried out on Raymond step tapered piles near Apapa, Nigeria. The load applied was short-term static lateral load. Only one analysis was performed for test piles 1 and 2 because of similarities in test conditions. These piles were driven vertically, and reinforced concrete was filled in steel shells. The soil profile at site was a layer of soft organic clay below 5 ft thick hydraulically placed sand. The sand layer governs the pile behavior, but clay layer is having some influence on it. Laboratory triaxial test and in situ vane test were used to find angle of internal friction and c. A graphical representation is shown to compare measured and computed deflections by load–deflection curves which are dissimilar in shape. This also represents that initial slopes were nearly similar for shorter loads, but at larger loads beyond 11 kips, the curves diverge much (Figs. 6 and 7).

Bailly

Bergstrom (1974) reported tests of two 14BP89 piles at a site for proposed nuclear power plant which were driven vertically, and loads were applied to free head piles at 1.5 feet above the ground surface. Maximum load applied incrementally was 39 kips, unloaded and then cycled 25 times at 22 kips.

For the test piles TP7 and TP8, a graphical representation is shown. At site, soil was fine sand, loose to moderately dense. As the soil properties were similar for both test piles, only one analysis was carried out. It can be seen that computed and measured deflections are very similar other than at 39 kips load point, where computed deflection is 12% more than measured one. The load–deflection curve for 25 cycles of loading also shows great similarities for measured and computed deflections though curve was developed from results of submerged sand it works equally for soil above water table (Fig. 8).

Fig. 7 Comparison of
measured and computed
deflection for tests at Appa
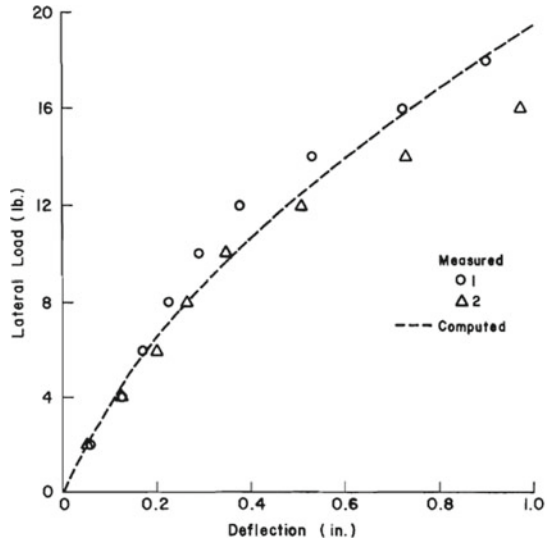
Fig. 8 Comparison between
measured and computed
deflection of tests at Bailly
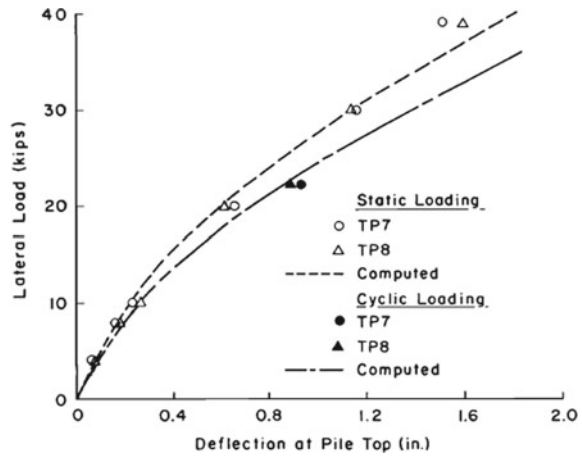
Conclusion for Sand (Reese)

Researchers have shown many measured versus computed deflections analysis from
the tests carried out in sand, which were very much in agreement with the criteria
adopted for *p-y* curve method though some results were conservative, but overall,
the comparison between measured and computed results for piles embedded in sand
shows excellent to very good for most of the cases at working loads.

Development of p-y curves for sand by other Authors

Khari et al.

In 2014, Khari et al. [12] developed other set of p-y curves for sand with very limited parameters with their experimental model which was for piles in offshore construction. The test setup includes soil tank with dimensions 900 mm × 700 mm × 65 mm, soil thickness below pile tip was at least 6D, two LVDTs to measure deflection and seven levels of strain gauges to measure bending moments. The soil samples were collected from Johor Bahru, Malaysia, and tested at laboratory temperature. Among many methods of reconstructing sand samples, they have used pluviation and tamping to prepare the samples.

Results of Khari et al.

Single fixed-head smooth and rough piles in loose and dense sand were chosen for series of tests. T44 and T45 were tests on smooth piles, while T48 and T48 were tests on rough piles in loose and dense sand samples. Sand was considered loose when relative density was 30% and dense when relative density was 75%. Incremental loads were applied to test piles in all cases. As seen from the figure due to active length of pile, it did not show any deflection at a depth of 26 to 28 cm. Differences in deflection at ground surface are also visible against applied load in all cases of pile type and relative densities. Computed results with integration process and measured by LVDT show similar nature. It is also observed that smooth pile in loose sand demonstrates 200% larger deflection than in dense piles. For rough piles, observed values of deflection were 175 and 23% larger for relative densities 75 and 30% compared to smooth pile (Figs. 9, 10 and 11).

Conclusion—Khari et al.

Khari et al. conducted number of experiments on their model to determine and compare their results with popular methods. They have adopted some modification factors to consider density of soil and wall friction. The *p-y* curves generated using

Fig. 9 Schematic diagram for the test carried out by Khari et al. [12]
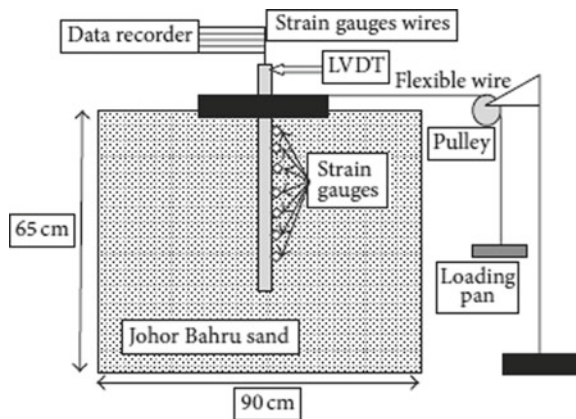
Fig. 10 Deflection versus
Depth, Khari et al. [12]
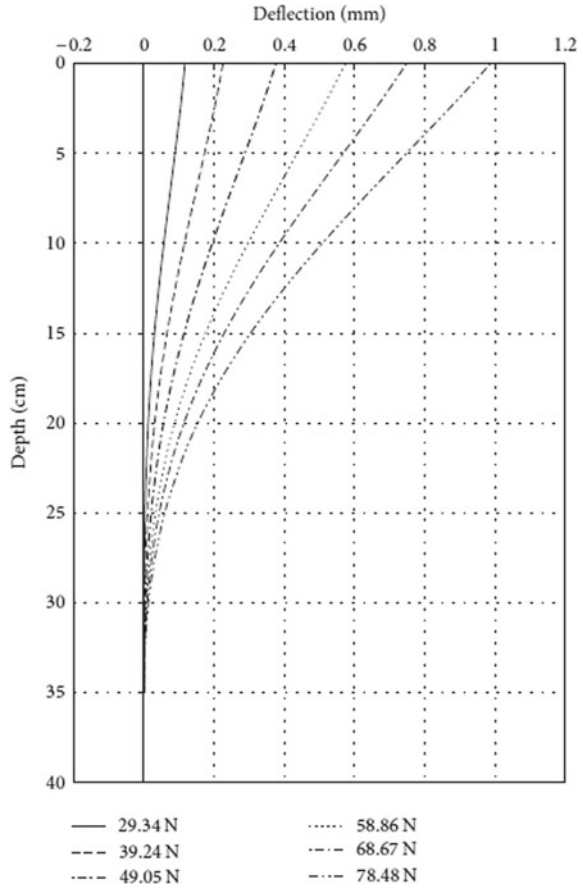
strains recorded along the length of pile as hyperbolic function showed good values
in comparison with older graphs available.

3.3 P-Y *Curves for Laterally Loaded Piles in Clay*

Reese

Numbers of lateral load tests [13] were also carried out on clay. To check the efficiency
of p-y curve method for the prediction of behavior of test piles in clay, thorough
analysis was done with reference to location of site wherever possible.

Test results: Bagnolet

A graphical representation for test piles B1 and B4 in uniform deposit of stiff clay,
carried out at Bagnolet, east of Paris, France, is shown. As the water table was below
the pile tips, Stiff A criteria were used for analysis. Comparison of both test piles

Fig. 11 Deflection at ground surface versus lateral load **a** Dr = 30%, **b** Dr = 75%

(a)

- • T45
- ○ T47

(b)
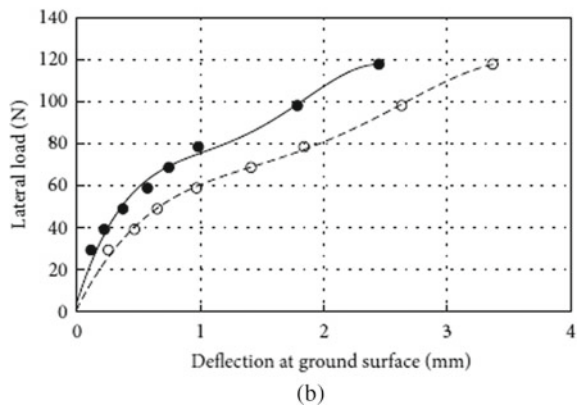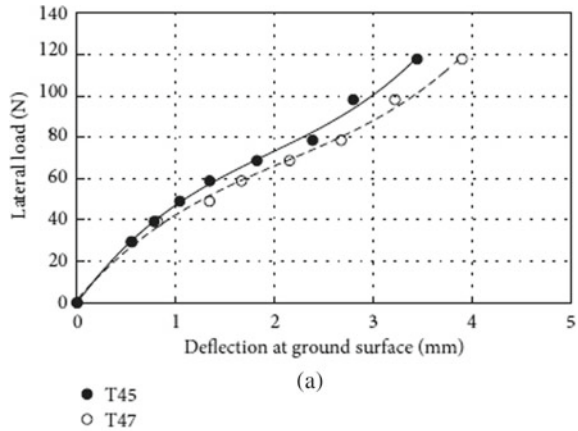
shows good results for B1 pile for measured and computed maximum moments, while some scattered results can be seen for B4. For deflections, both piles show fair comparison for measured and computed deflections (Fig. 12).

Bay Mud

To have different type of soil, site at bay mud was chosen for Gill for the purpose of testing. The soil which is classified as CH was composed of insensitive, slightly organic silty clay. Two test conditions were defined, and eight tests were carried out. For piles D1, D2, D3 and D4, water table was below ground level at 7.5 feet provided dry soil condition, and for these piles, Stiff A criteria were used for analysis. For test piles F1, F2, F3 and F4, soil was wet for number of days. Soft B and unified criteria were used for analysis of these piles. Type of piles used for all tests was same, but diameter was from 4.5 to 16 in. As seen in the figure, measured deflection for D1 and D2 both are large than computed results on non-conservative side by 33%. For D3 and D4, measured deflections are also larger (Fig. 13).
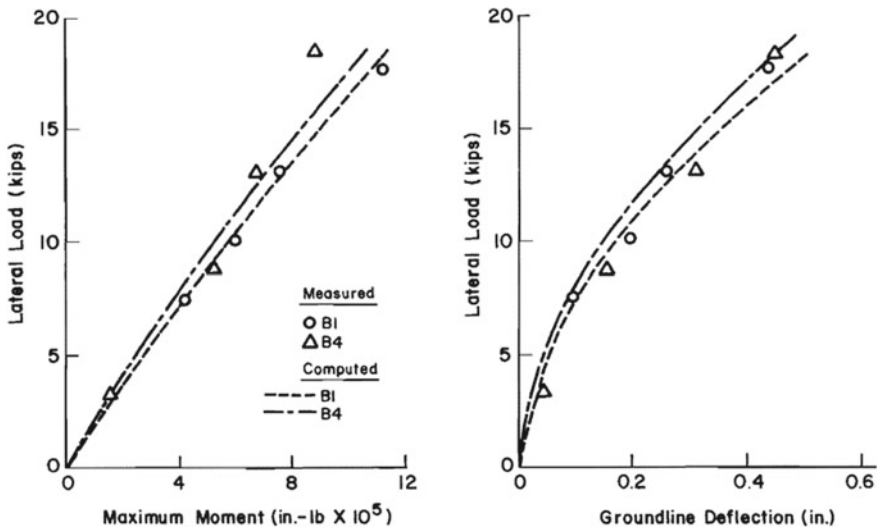
Fig. 12 Comparison of measured and computed results for test pile B 5 at Bagnolet
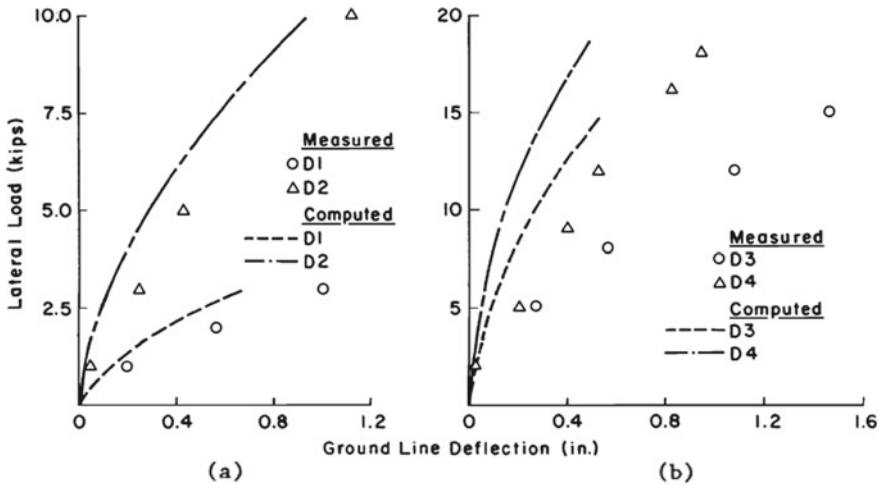
Fig. 13 Comparison of measured and computed deflection for tests at dry bay mud site **a** for test piles D1 and D2 **b** for test piles D3 and D4

For the piles in flooded site, comparison of computed deflection with measured deflection by Soft B and unified criteria shows that F1 and F2 show very good results for unified criteria while F1 shows non-conservative results for Soft B criteria. While for test piles F3 and F4, both criteria are used, and measured deflections are more than computed deflections. For F3 test pile, difference of 53% in Soft B criteria and

a difference of 36% in unified approach were reported. Similar kind of results can be seen for F4 as well (Figs. 14 and 15).

Conclusion (Reese)

As per the results provided by different researchers showed, while measured and computed results were compared, relatively good results for piles in clay for most
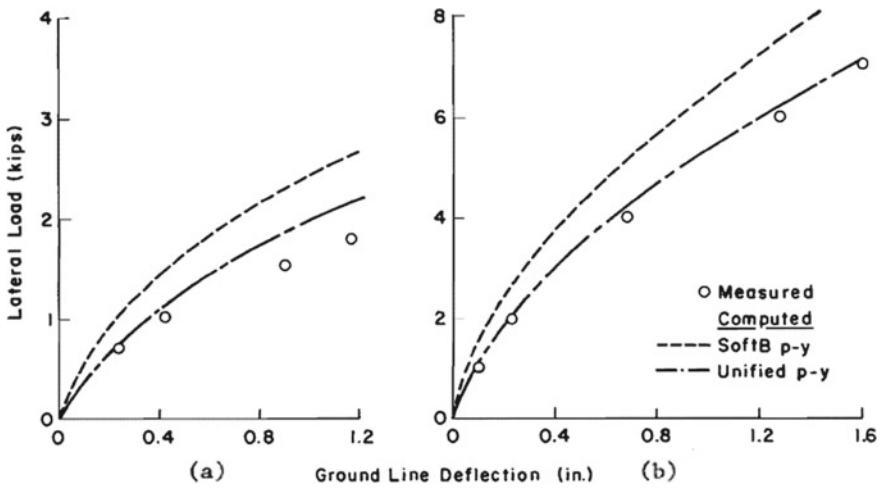
Fig. 14 Comparison of measured and computed deflection for tests at flooded bay mud site **a** for test pile F1
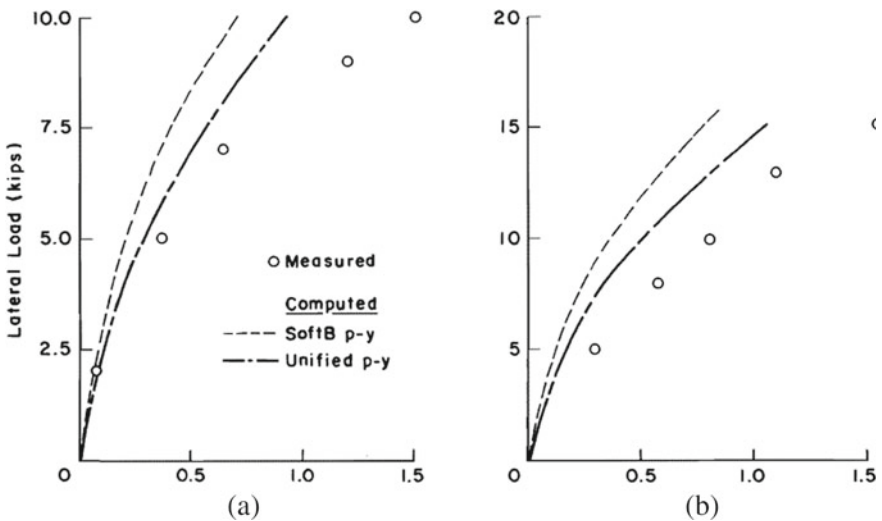
Fig. 15 Comparison of measured andcomputed deflection for tests at flooded bay mud site **a** and **b** for test pile F2 for test pile F3 and **b** for test pile F4

of the tests were seen at working loads. In those cases where there is noticeable difference in results, it was believed that it was due to lack of availability of better soil property results for analysis. It was observed through different cases that p-y method for the analysis of laterally loaded pile offers the best result among the various methods available. Results of full-scale pile tests can make this method better, and accurate results of soil properties will make this method more faithful in prediction of pile behavior.

Kyle et al.

A pile group in 3 × 3 patterns with center to center spacing of three times pile diameter was tested by Kyle et al. [14] under static and dynamic lateral loads. It was a full-scale test setup at Salt Lake International Airport. This assembly was accompanied by a single pile driven to 1.8 m depth. It was taken care that for both the cases soil properties should be the same. The piles used were closed ended steel pipes. To measure the resistance provided by each pile, strain gauges were attached to tie-rods. A computer program was designed for the analysis of results (Figs. 16 and 17).

A graphical representation of load–deflection curve for both single pile and group of piles is presented. For better comparison with single pile, average load carried by each pile of group was calculated by dividing total load carried by group with number of piles. It can be observed that for smaller displacements results are similar, but for
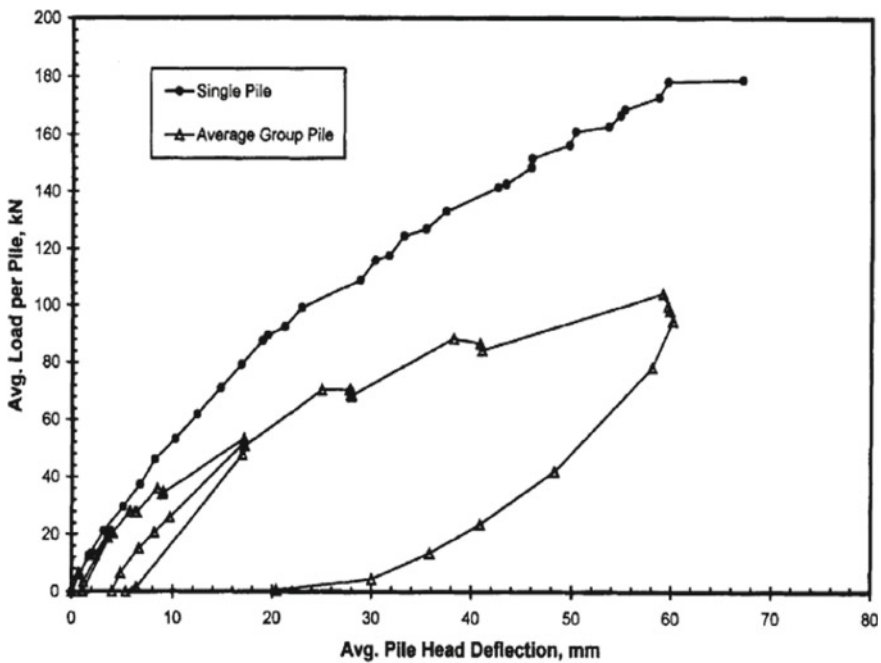
Fig. 16 Average load versus deflection curve for single pile test and pile group test
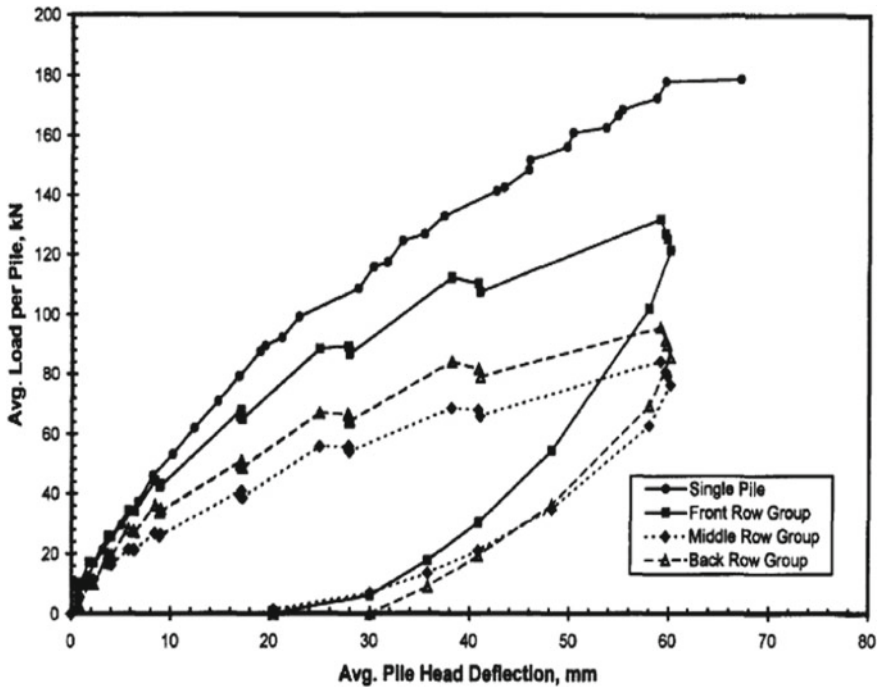
Fig. 17 Average load versus and single deflection curve for every row of pile group pile

increased deflection, average load carried by each group pile is considerably smaller than carried by single pile. It was also observed that for same pile, load displacement of single pile is noticeably smaller. It was very interesting to observe load–deflection curve of each row of pile group. When compared with single pile load–deflection curve, it was concluded that load distribution in pile group is not uniform but depends upon the position of pile row.

Conclusion (Kyle et al.)
It was concluded that single pile under given average load deflected very less in comparison with closely spaced pile group. It was also noticed that trailing row of pile group carried less load than load carried by front row, proving that load distribution is not similar and depends upon the row position. It was also concluded that single pile carried more load than load carried by piles in all rows.

3.4 Limitation of **p-y** Method

The basic limitation of *p-y* method is resistance due to shear deformation of soil because soil resistance against pile movement is not considered [8]. Apart from

this, subgrade modulus is considered to be dependent on relative density of soil. Clarification is also required for the use of friction angles to be used in p-y equation required to plot p-y curve.

4 Strain Wedge Method

4.1 Introduction

With a view to utilize traditional one-dimensional Beam on Elastic Foundation concept, the strain wedge approach was developed to predict the response of flexible pile under lateral loading. Initially, it was developed to analyze free head pile in uniform soil. Researchers have modified this to analyze pile in multiple soil layers and effect of pile head condition on behavior of soil and pile both. The cutting edge of this method over other approaches is simplicity of required soil properties. Very common properties of soil are required for the analysis. Soil layers are divided into layers [9] of smaller thickness, and each layer is considered as individual soil layer.

Properties employed for sand	Properties employed for clay
Effective unit weight (total above water table, buoyant below)	Effective unit weight
Void ratio, e, or relative density, Dr	Plasticity index, PI
Angle of internal friction, ø	Effective angle of friction, ø
Soil strain at 50% stress level, ε_{50}	Undrained shear strength, Su
	Soil strain at 50% stress level, ε_{50}

Las Vegas Field Test (Short Shaft)
An 8 feet diameter and 32 feet long reinforced concrete drilled shaft with 1% longitudinal steel reinforcement was tested at Las Vegas as short shaft. A team of University of Florida incorporated FLPIER/COM624 programs for soil input data and same data were provided to strain wedge model. The strength of concrete at 28 days was assumed to be 5.0 ksi. It is observed from the graph that SW model has predicted very good results which nearly similar to measured results while results obtained from FLPIER/COM624 are very different than actual (Fig. 18).

Full-scale Load Test on Pile in Liquefied Soil
With the help of soil properties reported by Weaver, Ashford and Rollins, a number of full-scale field tests were carried out at the Treasured Island [4]. The special characteristic of these tests was that they were carried out in liquefied soils. Controlled blasts were used to liquefy the soil without increasing its density. The sand at site contained 5% fines. The piles tested were of 0.61 m dia., long isolated pipe pile filled with concrete and laterally loaded at 1 m above the ground (Figs. 19 and 20).

Fig. 18 Measured and computed shaft response of Las Vegas Test
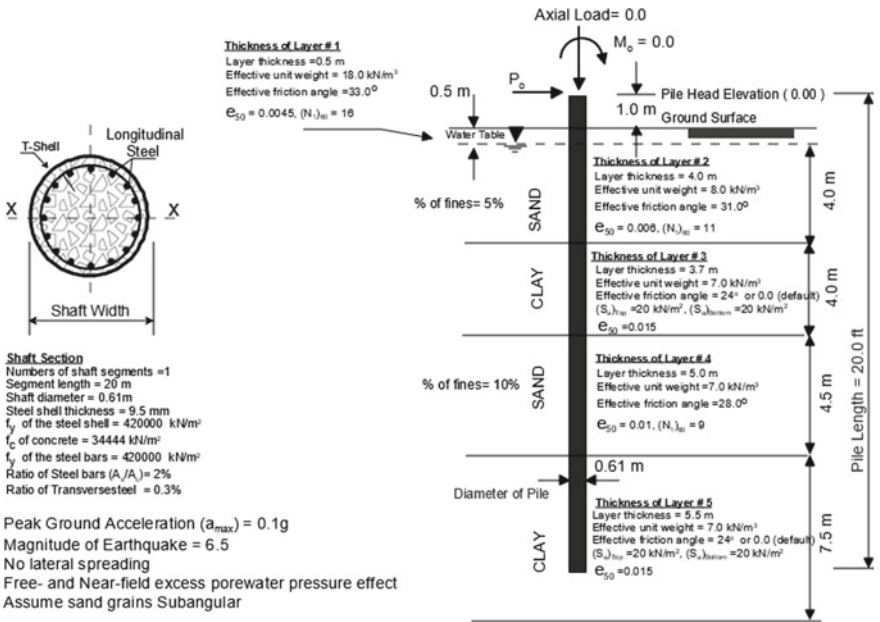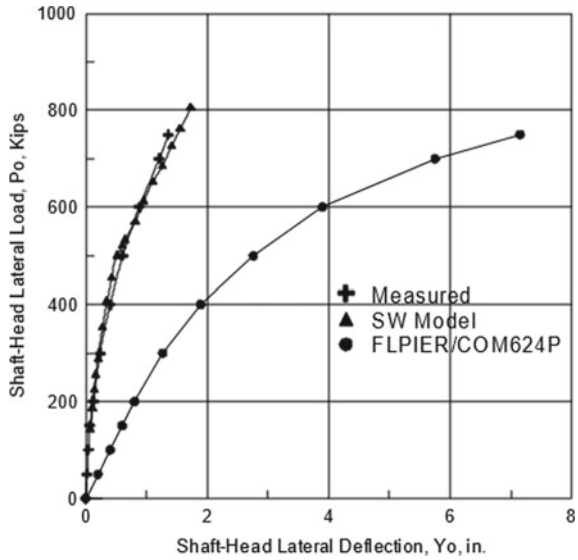
Fig. 19 Soil and pile properties at Treasure Island test
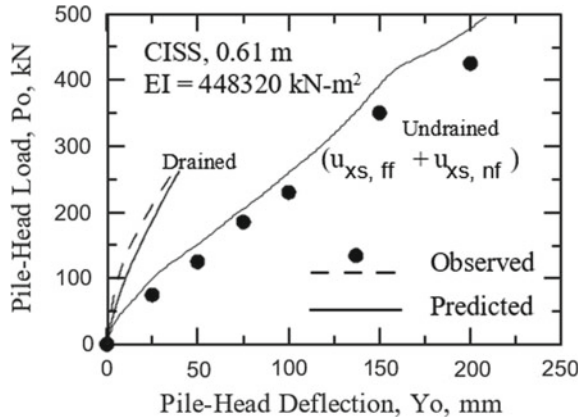
The piles tested at Treasure Island were loaded after the soil around it was lique-
fied for static drained test, and same was observed for SW model. Observation of
figure shows that SW model predicts the drained response in line with the observed
response. The behavior of pile in undrained post liquefaction status was with the
effect of excess pore pressure, both free field and near field. After providing the
first blast at site and maximum ground acceleration assumed as 0.11 g, piles were
loaded for cyclic load. Figure shows very similar measured and computed undrained
response. Analysis carried out with assumed maximum ground acceleration caused
an excess pore water pressure in most of the sand which was in line with measured
free field excess pore water pressure (Table 1).

The strength of SW model for prediction of p-y curves for piles or shaft in partially
or fully liquefied soil can be seen from the comparison shown in graph. The tradi-
tional p-y curve method used with reduction multiplier fails to show concave upward
movement for p-y curves which are back calculated (Fig. 21).

Table 1 .

Soil layer thick (m)	Soil type	Unit weight, (kN/m^3)	$(N_1)_{60}$	$Ö$ (deg.)	$å_{50}$ (%)	S_u (kN/m^2)
0.5	Brown, loose sand (SP)	18.0	16	33	0.45	
4.0	Brown, loose sand (SP)	8.0	11	31	0.6	
3.7	Gray clay (CL)	7.0	4		1.5	20
4.5	Gray, loose sand (SP)	7.0	5	28	1.0	
5.5	Gray clay (CL)	7.0	4		1.5	20
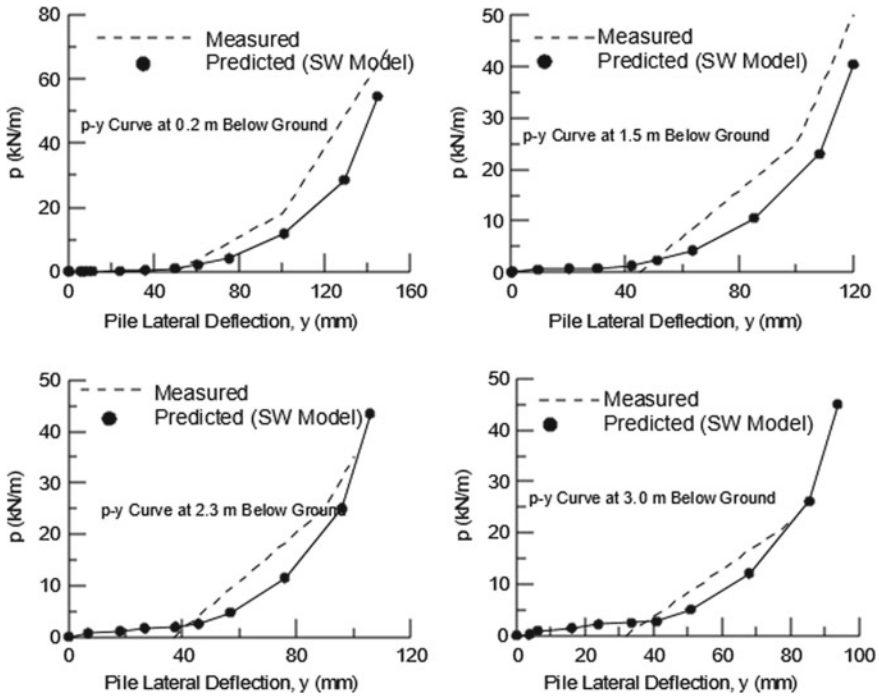
Fig. 21 Predicted *p-y* curves using strain wedge method versus observed ones from Treasure Island test

After the first blast at site, upper 4.6 m length of pile was almost liquefied, and pore water pressure was almost 1.0. This was measured after application of few cycles of load. When maximum ground acceleration was increased to 0.15 g for analysis in SW model, soil was completely liquefied, and load–deflection curve shows upward concave movement.

Full-scale Load Test on a Bored Pile in Layered Soil

Brown et al. carried out full-scale load test on bored pile [4], 1.5 m diameter and 34 m deep below ground surface in Chaiyi, Taiwan. The soil at the site was layered in which both sand and clay were present. FLPIER program was used for analysis which showed very poor prediction of p-y curves for both sand and clay layers [10]. Brown carried out another analysis with FLPIER program with modified soil properties which gave very good correlation with measured test results (Figs. 22 and 23).

To compare the results with SW model, original soil and pile properties were used for analysis without any site-specific modification. The response predicted single free head pile was comparative with results obtained through test. It should be noted that SW model uses nonlinear model for pile material behavior which plays an important role in prediction of results.

Fig. 22 Soil profile and pile
tested at Chaiyi test, Taiwan
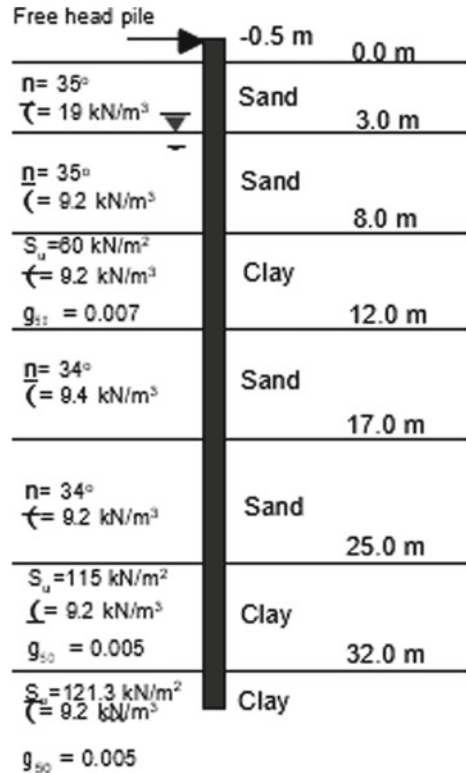
Conclusion (Strain Wedge Method)

It was observed through various comparisons with field test data that SW model
can carry out prediction of pile behavior without changing the original soil and pile
properties and it is the biggest advantage of this approach. Other approaches like
FLPIER/COM 624, etc., require fairly moderate soil properties for prediction of pile
behavior under laterally loaded condition [17].

5 Conclusion

It was observed that Chin method generally over predicts the shaft resistance.

The *p-y* curve method which was initially developed by Reese and then Matlock is
most widely used method for the analysis of laterally loaded piles. After incorporating
the results of some full-scale tests, this method is more trustworthy as p-y curves
can be back calculated. A lot of research is still going on to improve this method
using different test instruments/techniques. For soil under test, *p-y* curves are not
unique as it is affected by soil and pile properties. This is the biggest drawback of
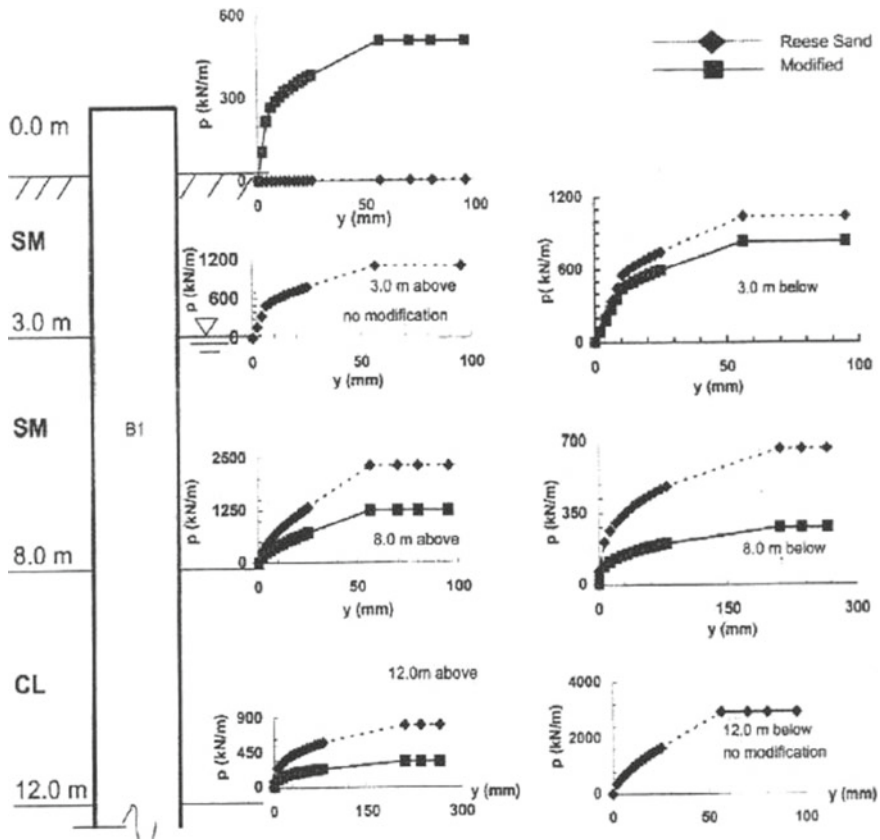
Fig. 23 Traditional *p-y* curves modified to obtain good match with field data, Chaiyi Test

this method. For partially and/or fully liquefied soil, it does not show the upward concave movement which can be seen in SW model analysis.

The SW model uses original soil and pile properties and predicts the behavior of pile under lateral load nearly similar to the results obtained on field. The biggest advantage of this method is that it does not require modified soil properties for prediction. The nonlinear model for pile material is one of the reasons for its successful observations.

The current SW model can be made better by incorporating effect of vertical side shear resistance which has greater impact on lateral response of piles/shafts with large diameter. Apart from this, in many cases, piles with large diameter are designed as long shafts. The behavior of these shafts is similar to intermediate shafts which give softer response in comparison with large shafts. The *p-y* curve method is having this advantage over SW method that it can be used for all types of shafts/piles.

References

1. Abdrabbo, F.M., Gaaver, K.E.: Simplified analysis of laterally loaded pile groups. Alexandria Eng. J. **51**(2), 121–127 (2012)
2. Ahmadi, M.M., Ahmari, S.: A Simple approach to investigate laterally loaded pile-soil interaction in clay. In: 4th International Conference on Earthquake Geotechnical Engineering, p. 1761 (2007)
3. Ashour, M., Norris, G., Pilling, P.: Lateral loading of a pile in layered soil using the strain wedge model. J. Geotech. Geoenviron. Eng. **124**(4), 303–315 (1998)
4. Ashour, M., Norris, G., Sherif, E.: Analysis of Laterally loaded long or Intermediate drilled shafts of small or large diameter in layered soil. Final report prepared for department of transportation, State of California (2004)
5. Basu, D., Salgado, R., Prezzi, M.: A continuum-based model for analysis of laterally loaded piles in layered soils. *Geotechnique* (2009)
6. Chin, J.T., Chow, Y.K., Poulos, H.G.: Numerical analysis of axially loaded vertical piles and pile groups. Comput. Geotech. **9**(4), 273–290 (1990)
7. Choo, Y.W., Kim, D.: Experimental development of the p-y relationship for large-diameter offshore monopiles in sands: centrifuge tests. J. Geotech. Geoenviron. Eng. **142**(1), 04015058 (2015)
8. Fleming, W.G.K.: A new method for single pile settlement prediction and analysis. Geotechnique **42**(3), 411–425 (1992)
9. Hajialilue-Bonab, M., Sojoudi, Y., Puppala, A.J.: Study of strain wedge parameters for laterally loaded piles. Int. J. Geomech. **13**(2), 143–152 (2011)
10. Hassan, A. M.: Winkler model for pile seismic analysis considering end constraints effects. HBRC J. (2017)
11. Higgins, W., Martindale, H., Chakraborty, T., Basu, D.: Assessment of the PY method for laterally loaded pile in sand. In: Indian Geotechnical Conference, pp. 833–836 (2010)
12. Khari, M., Kassim, K.A., Adnan, A.: Development of curves of laterally loaded piles in cohesionless soil. Sci World J. (2014)
13. Meyer, B.J., Reese, L.C.: Analysis of single piles under lateral loading (No. FHWA-TX-79–38+244–1 Intrm Rpt.). Center for Highway Research, University of Texas at Austin, TX (1979)
14. Rollins, K.M., Peterson, K.T., Weaver, T.J.: Lateral load behavior of full-scale pile group in clay. J. Geotech. Geoenviron. Eng. **124**(6), 468–478 (1998)
15. Borel, S., Bustamante, M., Gianeselli, L.: An appraisal of Chin method based on 50 instrumented pile tests. J. Ground Eng. 22–26 (2004)
16. Yang, M., Ge, B., Li, W., Zhu, B.: Dimension effect on P-y model used for design of laterally loaded piles. Procedia Eng. **143**, 598–606 (2016)
17. Zhang, C., Yu, J., Huang, M.: Winkler load-transfer analysis for laterally loaded piles. Can. Geotech. J. **53**(7), 1110–1124 (2016)

Quality Control Aspects for Casing Material and Coarse Filter for Earth Core Rockfill Dam

Uday Bhanu Chakraborty, N. P. Honkaradavar, Sandeep Dhanote, and S. Bajaj

Abstract Blasted prototype rockfill material from a multipurpose irrigation project which is under construction in India is considered for its quality control / assurance for this paper. The maximum particle size (d_{max}) of blasted rockfill material used in construction of the above project is 600 mm, and the maximum particle size of inclined and horizontal coarse filters is 20 mm and 80 mm, respectively. Following tests were conducted at site to check the quality and determine the field density, moisture content, grain size distribution and permeability as per relevant standards and field experiences:

 (i)   In-situ (Field) Density [1, 2]
 (ii)   Moisture Content [3]
 (iii)   Prototype Grain Size Distribution for Casing and Filter Materials [4]
 (iv)   Permeability [5]

All the above-mentioned tests were conducted at different stages/frequency of construction and determined material parameters. The results are presented, and necessary preventive action was also highlighted. From the testing, the test results were collected, i.e., field density, moisture content, field permeability, gradation, coefficient of uniformity (C_u), coefficient of curvature (C_c), finer percentage (>75 μ) and compared with design values. From the comparison, it is observed that the parameters determined from field tests almost match with design values. Highlighted all the observed deviations and provided the corrective measures based on the field conditions. Therefore, the quality control measures are very much essential to ensure the safety of the structure.

Keywords Rockfill · Quality control · Quality assurance · Field density · Gradation curve · Permeability

U. B. Chakraborty (✉) · N. P. Honkaradavar · S. Dhanote · S. Bajaj
Central Soil & Material Research Station, Hauz Khas, New Delhi 110016, India
e-mail: uday401133@rediffmail.com

1   Introduction

All over the world, generally rockfill materials are being applied in the construction of earth core rockfill dam (ECRD) and concrete faced rockfill dam (CFRD) as a casing/shell material because of their natural flexibility, ability to absorb large seismic energy and flexibility to various foundation circumstances. The use of modern construction equipments and available construction materials in the vicinity construct such dams cost-effective. The main purpose of the casing material is used to provide the stability to the structure.

This paper deals with the field testing, study of relative density [1, 2], gradation analysis of casing/shell and filter materials [4] and also study of the behavior of casing/shell material in aspect of permeability [5] for two main projects, viz. Polavaram project, Andhra Pradesh, and Kanhar dam project, Uttar Pradesh. The maximum particle size (d_{max}) of the prototype gradation casing/shell material as per approved construction is 600 mm. Overall performances of a rockfill dam depend upon the control exercised during construction, supervision and inspection stage. Proper quality control during construction is as important phenomenon as same as the design, and it helps to sustain the structure up to its design period. Quality does not mean to implement very rigid procedures to be laid down for during the construction stage. As every work has its own problems & limitations and therfore, procedures should match with the site conditions. Sequence of works for each zone is an essential activity to construct resilient structure. Figure 1 shows cross section view of Kanhar dam project.

Permeability, shear strength and gradation are the prime considerations in case of pervious fills. The general consideration for control of permeability should be that the permeability of the material increases toward the outer slopes of the dam embankment. The control of compaction is generally determined by relative density test which is a measure of the compactness of a pervious material with respect to the loosest and most compact states at which it can be placed.

MAXIMUM SECTION (50.485m) OF LEFT & RIGHT FLANK COMPOSITE DAM AT CHAINAGE Km. 1.68525 & Km. 2.003
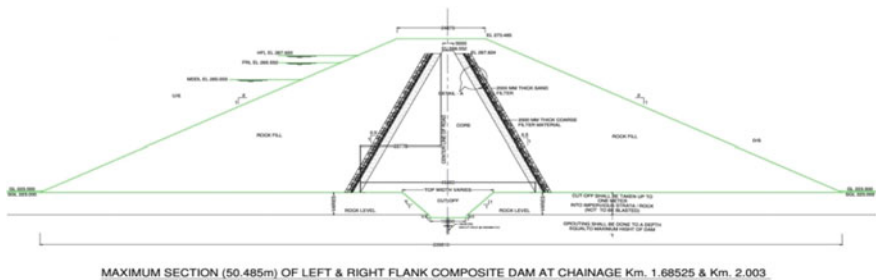
Fig. 1   Cross section of right section of Kanhar dam project

Table 1 Testing frequency of rockfill and filter material

Type of material	Test to be performed	Quantity	No. of test	Remarks
Casing/shell material	Gradation	1000 m^3	1 No	During the initial placement
		10,000 m^3 or each shift whichever is more frequent	1 No	After placement procedures have proved satisfactory and no significant changes in borrow area material
	Field density	1000 m^3	1 No	During the initial placement
		10,000 m^3 or each shift whichever is more frequent	1 No	After placement procedures have proved satisfactory and no significant changes in borrow area material
	Permeability	Monthly / 1,000,000	1 No	
Coarse filter	Gradation	1000 m^3	1 No	
	Field density	1000 m^3	1 No	

2 Testing Frequency

For pervious (rockfill & fillter) materials, the testing frequency is generally considerate as per IS 14690, and same has been shown in tabulated form in Table 1 [6]:

3 Construction Process for Earth Core Rockfill Dam

3.1 Placement and Spreading

Usually placement and spreading works started with gradation analysis and shape factor of each dumping yard/borrow area where rockfill material to be collected. Acceptable materials have to be transported from borrow area to working site by trucks or suitable conveying system. If the material are not fulfill the design requirement preciously not meet gradation criterion, grizzly screening (multi size boulder separators) to be installed and mix the materials as per their designed prototype gradation curve and transport by truck/conveyor system and spread by a bulldozer. During the dozing, the fines are moved onto the upper part of the layer, which creates a smoother working surface for the truck to place the next layer and the stratified

permeability. Oversize rocks are often pushed into a specified zone in the outer part of the dam, i.e., 'riprap' or the rock may break by using mechanical/pneumatic hammer. To meet the filter requirements, it is important to ensure that the contact between filters and rockfill material does not have an accumulation of large rocks [7].

3.2 Roller Type and Number of Passes

Compressibility of rockfill material is dependent on the various factors, viz. grading, degree of compaction (layer thickness, roller weight and number of passes), rock substance strength and the effect of wetting on the substance strength [8]. It is normal to specify smooth steel drum vibrating rollers to be used for compacting rockfill material. The roller is usually specified as having a static mass of between 10 and 15 tonnes. Roller trials are often specified to determine the number of passes. It is usual to require at least four passes of the roller. During site investigations, determine the degree of breakdown of rock under rollers may also be found which may influence the resulting density and particle size distribution, permeability and modulus of compressibility.

It was also studied that any additional compaction achieved after, say, 4 or 6 passes may not great influence the density, it only breaks the rock of the upper part of the layer. Therefore, it is common to limit the number of passes to 4 or 6, seldom more than 8 [7].

3.3 Addition of Water

Water is regularly added to the rockfill material to aid compaction and to weaken the rock-to-rock contact points in rock types which are weakened by wetting. The water should be added by spraying on to the dumped rockfill before spreading. Commonly, the amount of water is specified as a percentage of the volume of the rockfill. If the rock forming the fill is strong, produces few fines and is not greatly weakened by wetting, water may not be needed. Rolling trials can assist in assessing whether watering is needed and the amount of rolling required to achieve good compaction.

3.4 Durability Requirements

Rockfill is often required to be 'hard' and 'durable'. The means of measuring this are seldom specified, and in many dams, such a requirement will be unobtainable like where siltstone or sandstone is being used, which may breakdown on repeated exposure to wetting and drying. Breakdown only occurs on the surface of the rockfill and is not detrimental to the shear strength or compressibility of the rockfill as

a whole, provided the rockfill is well compacted and watered during compaction. Nevertheless, water should be used to control dust wherever necessary.

Hence, in general, there should be no requirements on durability for rockfill. The exception might be for some volcanic and altered granitic rocks which can deteriorate with. For riprap, or the outer layer of rockfill on the downstream slope, durability under wetting and drying is important and should be specified.

4 Inspection/Testing of Rockfill Material and Filters

Testing of rockfill material is very difficult to its large size. During the construction process, it requires determining the particle size distribution analysis, compacted field density and permeability. Particle size distribution (PSD) had a significant influence on the strength, permeability and compaction behavior of rockfill materials.

Rockfill material generally covers a range of particle sizes between 0.001 and 1000, and it is well known for containing wide-ranging grain composition. Therefore, the scaling distribution for grain composition is an essential index for studying the physical and mechanical properties. When the gradation of a rockfill material is changed, its permeability, deformation, strength and other properties are altered. During the compaction process of an earth core rockfill dam, the void reduction between grains is caused by natural settlement and artificial rolling.

4.1 Particle Size Distribution (PSD)

The PSD is likely to replicate the complexity and irregularity in structural properties of rockfill materials and can be used to study the physical behaviors between the whole and the parts of the materials. By using graphical representation (Fig. 2) and statistical analysis of prototype material, described a set of parameters like shape factors, coefficient of uniformity (C_u) and coefficient of curvature (C_c); and also find the maximum particle size and percentage fine (0.075 mm). Maximum particle size and percentage fine (0.075 mm) were obtained of the mentioned above projects are 600 mm and 0.49 % (i.e., <5 %), respectively.

4.2 Field Density

The degree of compaction of the rockfill materials is a key index for controlling the construction of earth core rockfill dams. The degree of compaction has an important consequence on the stability and seepage prevention of the dam. After rolling the materials to be dense and in the prototype gradation curve, it reflects that the void has been reducing steadily. Relative density is used as an indicator of compaction by

Prototype Gradation Analysis
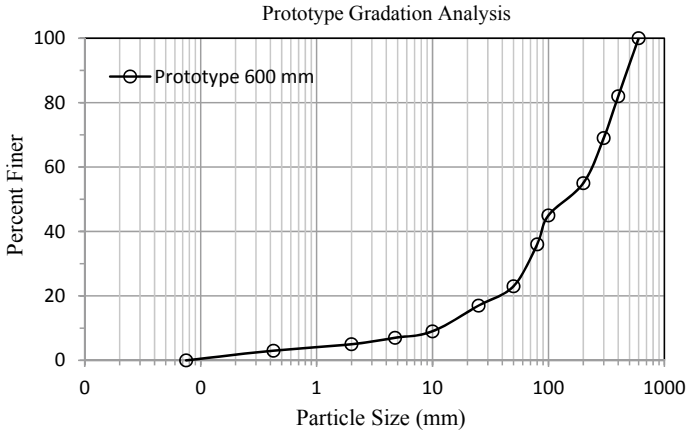
Fig. 2 Prototype grain size distribution curves

comparing the porosity during the loosest situation and the densest state. At site, the degree of compaction is measured by in-situ density.

Determining the in-situ density of casing material by the water replacement method as per IS 2720 part 33, a circular ring on the surface and a plastics film 0·1 mm thick, 2 to 4 m square (for small diameter rings); and 0.2 mm thick, 4 to 8 m square (for large diameter rings) are used to retain the water. The ring diameter shall be at least 3–4 times the size of the largest particle. The diameter usually ranges between 0.5 and 2.5 m in multiples of 0.5 m. The rings may be made of 4 to 8 rnrn mild steel sheet, and height of vertical flange will 10–20 cm. Pointer Gauge Assembly and Supports—Horizontal bar with supports resting on or outside the ring, fitted with an adjustable vertical pointer and lock nut and IS Sieves—100-mm, 80-mm, 40-mm, 25-mm, 20-rnm, 10-mm and 4.75-mm, 30 cm in diameter were used as required. Platform weighing machine of capacity up to 100 kg (digital type) also used for rockfill material measurement. Figure 3 shows the procedure to determine the field density using water replacement method and gradation analysis for rockfill material.

4.3 Field Permeability

Excavated a pit of 60 cm in diameter and height equal to the thickness of the compacted layer (around 80 cm) on the compacted surface of rockfill. Trim the vertical sides and fix the perforated circular cylinder as shown in Fig. 4. From the water tank, allowed the water into the pit. Let the water flow freely into the cylinder till the surrounding area gets fully saturated. Once the surrounding area of the cylinder got saturated, the inflow to the pit slowed down. Once it was confirmed that the inflow is equal to the out flow (constant flow = Q lit/s) of the cylinder, noted down the flow rate from the measuring water meter fitted to the inflow pipe. Constant head

Fig. 3 Determination of in-situ density of rockfill material using water replacement method

Fig. 4 Field permeability test to determine field permeability of rockfill material

permeability test was performed. Then, knowing the radius of pit (r cm), height of water head or pit (*H* cm)and rate of constant flow (*Q*), the permeability (*K*) has been calculated using the following equation:

$$K = \frac{Q}{5.5rH}$$
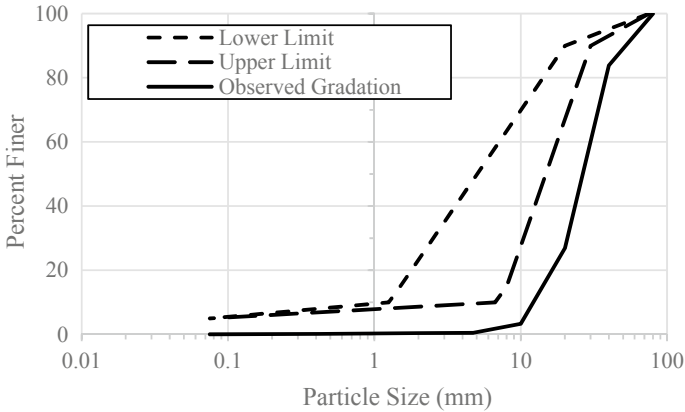
Fig. 5 Comparison of designed and observed gradation curves for Type-1 (bottom layer) horizontal filter

4.4 Filters

For carrying out in-situ density test for bottom layer of horizontal filter a cylinder of 30 cm in diameter and height equal to a layer thickness is used for determining in-situ density of bottom layer horizontal filter. Hollow cylinder was fixed on the filter and removed the filter material from inside using hand tool. The cylinder was kept on lowering as the material from inside removed till the layer thickness. The removed material was collected and weighed (W). In-situ density was calculated dividing the weight of material (W) by volume of cylinder (V). The excavated horizontal filter material from the cylinder was collected and sieved using following sieves: 80, 40, 20, 10, 4.75, 2.0, 0.425 and 0.075 mm.

Knowing the weight retained on each sieve, percentage weight retained on each sieve is calculated. Based on the percentage weight retained, cumulative percent finer is calculated and plotted the curve between sieve size v/s percent finer on a semi-log graph sheet (Fig. 5) for above of the one project. Compared the designed and observed gradation curves of bottom layer of horizontal filter. From the comparison, it is seen that the observed gradation curves deviate marginally and does not fit exactly into the designed gradation range (Fig. 4). This problem can be sorted out by stacking the stock pile of different sizes, mixing them properly and then placing in its zone so as to achieve the required gradation of Type-1 filter.

5 Conclusion

Ideal rockfill material is well graded, so it has a high density, strength and modulus after compaction and has a high permeability. This is not always practicable, if the

available rock tends to break down during the rolling. Therefore, rockfill material forms a gap-graded material with a high percentage of sand. There is tendency that the rockfill will segregate during on placement, with the coarser particles being more predominant in the lower half of the lift and the finer in the top half.

Gradations apply to the rockfill material below the upper surface of each layer which is usually finer because of breakdown under rolling action. The grading would be checked by a limited number of tests. Routine acceptance or rejection would be by inspection and only measured if it became necessary from a contractual viewpoint to confirm the percentage of finer particles was excessive. A guide to excessive finer fraction can be if the fill moves excessively as it is being rolled, or trucks bog on the fill. This also indicates the fill does not have a high permeability.

References

1. IS 2720 Part 33: Determination of dry density in place by the ring and water replacement method (1971)
2. ASTM D5030-04: Standard Test Method for Density of Soil and Rock in Place by the Water Replacement
3. IS 2720 Part 2: Determination of water content (second revision) (1973)
4. IS 2720 Part 4: Grain Size analysis (second revision) (1985)
5. IS 5529: Code of practice for in-situ permeability test: Part 1 Test in overburden (1985)
6. IS 14690: Quality control during construction of earth and rockfill dams—recommendations (1999)
7. Fell, R., Patrick MacGregor, P., et al.: Geotechnical Engineering of Dams, 2nd edn. CRC Press, London (2015)
8. IS 8826: Guidelines for design of large earth and rockfill dams (1985)

Study on Surface Soil Erosion of Bhogdoi River Basin Using GIS and Remote Sensing

Merina Englengpi and M. K. Dutta

Abstract The river Bhogdoi is a small but perennial river coming down from the foothills of Assam–Nagaland border into the plains of Assam and finally pours into the Brahmaputra. The river is surrounded by the hills of the Naga-Patkai range on the south and the floodplains of Brahmaputra on the North. Soil erosion is one of the most serious problems in recent times which affects both cultivable and forest lands. It creates serious problems in agriculture and water resources management. This paper emphasizes on determining the surface soil erosion around Bhogdoi River Basin. Since the study area experiences heavy rainfall, so it is obvious that rainfall plays an important role in study of surface soil erosion. Again, the change in land use/land cover plays an important role in surface soil erosion more specifically, the change in vegetation. This study evaluated the impact of combined effect of rainfall and LULC change and impact of change in vegetation on soil erosion. For this, Morgan, Morgan and Finney, MMF model was used. Various input parameters to the model were derived using RS and GIS using ArcGIS software, and finally soil erosion was estimated. In the combined effect, average soil erosion in 1975 has been found to be 5.18 kg/m^2 which has been increased to 5.32 kg/m^2 in 2008 followed by 5.53 kg/m^2 in 2018. In the study of impact of vegetation change, it has been found that average soil erosions in 1975, 2008 and 2018 were 3.39 kg/m^2, 3.43 kg/m^2 and 3.64 kg/m^2, respectively.

Keywords MMF model · Remote sensing and GIS · Soil erosion

1 Introduction

Soil erosion is one of the most serious problems in recent times which affects both cultivable and forest lands. It creates serious problems in agriculture and water

M. Englengpi (✉) · M. K. Dutta
Jorhat Engineering College, Jorhat, India
e-mail: merinadecember@gmail.com

M. K. Dutta
e-mail: mrinaldk@rediffmail.com

resources management by removing the top fertile soil and its subsequent deposition in reservoirs and lakes. Various human activities which include overgrazing, overcropping and deforestation can affect the level of nutrients and pollution in soil. Soil erosion by running water washes away the topsoil, thus making the land infertile. The use of Remote sensing and GIS technique can be used in soil erosion assessment studies. The input parameters required for soil erosion modeling can be generated by remote sensing. Geographical Information System helps in creation of a database for the catchment which is very much useful for carrying out spatial analysis thereby helping the decision-makers in framing appropriate measures for critically affected areas.

In order to demonstrate the estimation of surface soil erosion using RS and GIS techniques, Morgan–Morgan and Finney model has been applied in Bhogdoi River Basin which lies between the geographical territories of both Assam and Nagaland, India.

2 Study Area

2.1 Description of the Study Area

The study area lies within the geographical territories of both Assam and Nagaland. Geographically, the basin lies between 26° 17′ 17″ and 26° 49′ 22″ north lines of latitudes and 94° 1′ 30″ and 94° 29′ 2″ east lines of longitudes and covers an area of 1179.65 km^2 including both plains and hills within it. The Bhogdoi River has its source at Long Samtang of Mukokchung district of Nagaland (Naga Hills). In Nagaland, the river has a hilly course in the Tertiary Naga-Patkai ranges (Mukokchung district). In Assam, it flows through the southern Brahmaputra plains of Jorhat District. The Bhogdoi Basin enjoys a subtropical monsoon climate. The average annual rainfall in the area is around 215 cm (Fig. 1).

3 Methodology

3.1 Preparation of Spatial Database

The survey of India toposheets No. 83 F/10, F/14, J/1, J/2, J/3, J/4, J/5, J/6, J/7, J/9, J/10 (Scale 1:50,000) of 1975 were georeferenced, mosaic and used for preparation of base map using ArcGIS software. From the base map, the Bhogdoi River Basin was delineated along with river Bhogdoi and its tributaries (Fig. 2) by digitizing in GIS environment. Different attribute data like area, perimeter of the basin and length of the river were generated in GIS and saved in personal geodatabase.
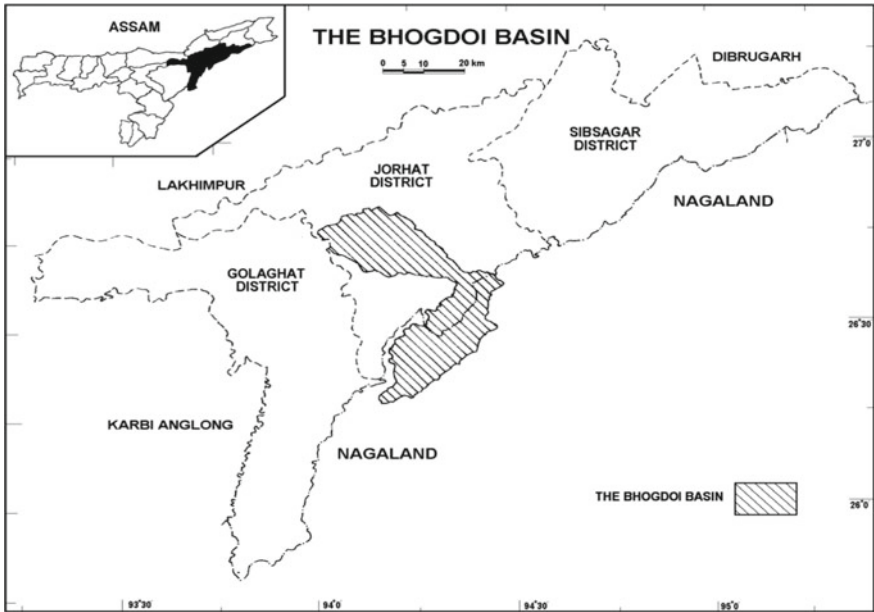
Fig. 1 Location map of the study area
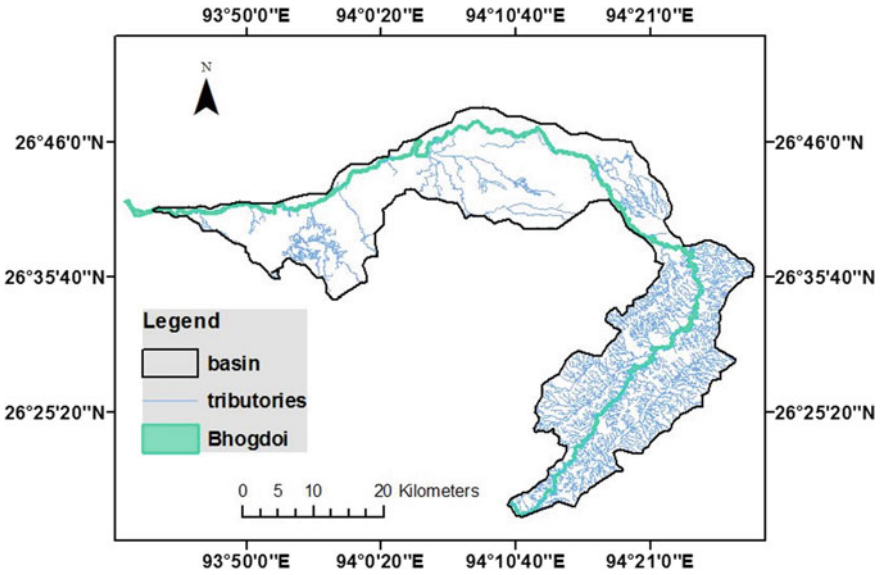
Fig. 2 Bhogdoi River Basin along with river Bhogdoi and its tributaries

3.2 Land Use/Land Cover Change Study

The base map of 1975 was used to prepare land use/land cover (LULC) map of 1975. IRS-P6 LISS-III satellite imagery acquired from National Remote Sensing Center (NRSC), Hyderabad, was georeferenced and registered with the base map using ground control points (GCPs) were used to map the land use/land cover status of Bhogdoi River Basin of the year 2008. Satellite imagery of Bhogdoi basin was downloaded from Google Earth Pro software and was used to map the land use/ land cover status of the year 2018. The land use/land cover map of 1975, 2008 and 2018 was prepared following on screen visual interpretation method by digitizing in ArcGIS 10.1. The attribute tables were created for the respective years to store the information such as area in square kilometer and type of the various land use/land cover categories. The different types of LULC digitized were settlement, cultivation, tea garden, water body, open scrub and forest, respectively.

3.3 Morgan–Morgan and Finney (MMF) Model

MMF model is a physically based empirical model and works by separating the process of soil erosion in the sediment phase and water phase. The water phase determines the runoff volume and the available energy of rainfall used to detach the soil particles. In the sediment phase of the model, the detachment of the soil particles is taken as a function of the soil erodibility, energy of rainfall and the interception of rainfall that is affected by vegetation. The MMF model makes comparison of the rate of predicted splash detachment with the transport capacity of the runoff or the overland flow, and the lower value of the two methods is taken as the rate of soil erosion, determining which one of these two (detachment or transport) is the factor of limitation [5].

Water Phase
In the water phase, rainfall energy was computed by

$$E = R \times (11.9 + 8.7 \times \log I) \tag{1}$$

where E is kinetic energy of rainfall (J/m^2), R is the annual rainfall (mm), and I is the intensity of erosive rain (mm/h). This is taken as 11 for temperate climate, 25 for tropical climate and 30 for strongly seasonal climate.

The overland flow was estimated by

$$Q = R \times \exp(-R_C/R_o) \tag{2}$$

where Q is the depth of overland flow (mm), R is the annual rain (mm), R_c is the soil moisture storage capacity under land cover (mm), and R_o is the mean rain per day (mm).

The soil moisture storage capacity was computed by

$$R_c = 1000 \times MS \times BD \times RD \times (E_t/E_o)^{0.5} \tag{3}$$

$$R_o = R/R_n \tag{4}$$

where MS is the moisture content of soil at field capacity, BD gives the bulk density of soil (mg/m^3), RD gives rooting depth of topsoil (m), E_t is the actual evaporation (mm/day), E_o gives the potential evaporation (mm/day), and R_n is the number of rainy days. RD is the soil depth from the surface to the A horizon base (up to an impermeable layer).

Sediment Phase

The detachment of soil by the rain drops was computed by

$$F = K \times (E \times e^{-aA})^b \times 10^{-3} \tag{5}$$

where F is the rate of soil detachment by raindrop impact (kg/m^2), K is the soil detachability index (g/J) defined as the weight of soil detached from the soil mass per unit of rainfall energy, E is the rainfall energy, and A is the percentage rainfall contributing to permanent interception and stream flow. The values of exponents are as follows: $a = 0.05$, $b = 1.0$

The distributed transport capacity map G was computed by

$$G = C \times Q^d \times \sin(S) \times 10^{-3} \tag{6}$$

where G is the transport capacity of overland flow (kg/m^2), C is the crop cover management factor, and S is the steepness of ground slope (°). The value of exponent $d = 2.0$.

3.4 Estimation of Soil Loss Using MMF Model

To determine the spatial distribution of average annual soil loss, the parameters of MMF models, viz. A, C, E_t/E_o and RD for land use/cover map were calculated using typical values of plant parameters [5] and are presented in Table 1, and soil parameters (K, MS and BD) are presented in Table 2. The land cover parameters and soil parameters were stored in attribute table associated with soil and land cover maps, respectively. From the LULC maps, the maps of percentage rainfall contributing to permanent interception and stream flow (A) map, ratio of actual to potential evapotranspiration (E_t/E_o) map and crop cover management factor (C) map were prepared. The soil map was prepared, and the soil type of entire region is mainly sandy loam/silty loam. From the soil map, the soil moisture content (MS) at field

Table 1 Values of plant parameters (For MMF model)

Land cover	A	E_t/E_o	C	RD
Settlement	20	0.10	0.1	0.00
Forest	30	0.9	0.08	0.1
Cultivation	25	0.58	0.3	0.05
Tea garden	25	0.8	0.5	0.1
Open scrub	35	0.8	0.05	0.05
Water body	0	1	0	0

Table 2 Soil parameter values (for MMF model)

Textural category of soil	MS	BD	K
Sand	0.08	1.5	0.3
Sandy loam	0.28	1.2	0.3
Loam	0.20	1.3	0.4
Silt loam	0.25	1.3	0.4
Clay loam	0.40	1.3	0.4
Silty clay loam	0.25	1.3	0.4
Clay	0.45	1.1	0.4

capacity map, bulk density (BD) of top layer map and soil detachability index (K) map were prepared in GIS environment. The overland flow (Q) map was generated using Eq. (2). R_c map was generated with integration of parameter maps (MS, BD, RD, E_t/E_o) using Eq. (3). The parameters R and R_n were calculated from the daily rainfall data. R_o was computed using annual rainfall (R) and number of rainy days (R_n). Finally, the rate of soil detachment by raindrop impact map (F) and transport capacity of overland flow map (G) were prepared using Eq. (5) and (6), respectively, and the minimum values from each of them were used for preparation of final soil loss map.

Finally, the combined effect of both rainfall and vegetation as well as the effect of vegetation alone was analyzed. In analyzing the effect of vegetation alone, the average rainfalls over last 49 years were taken, and the same value was applied for the three years (1975, 2008, and 2018).

The derivation of final soil loss map for the year 2018 is shown below (Figs. 3, 4 and 5):

In the same way, the soil loss maps for the year 1975 and 2008 were prepared to get the annual soil erosion in kg/m^2 (Figs. 6 and 7). The average soil erosion was then estimated for the three respective years. By this method, a combined effect of both rainfall and land use/land cover change was analyzed.

$$E = 47286.79 \text{ J/m}^2$$
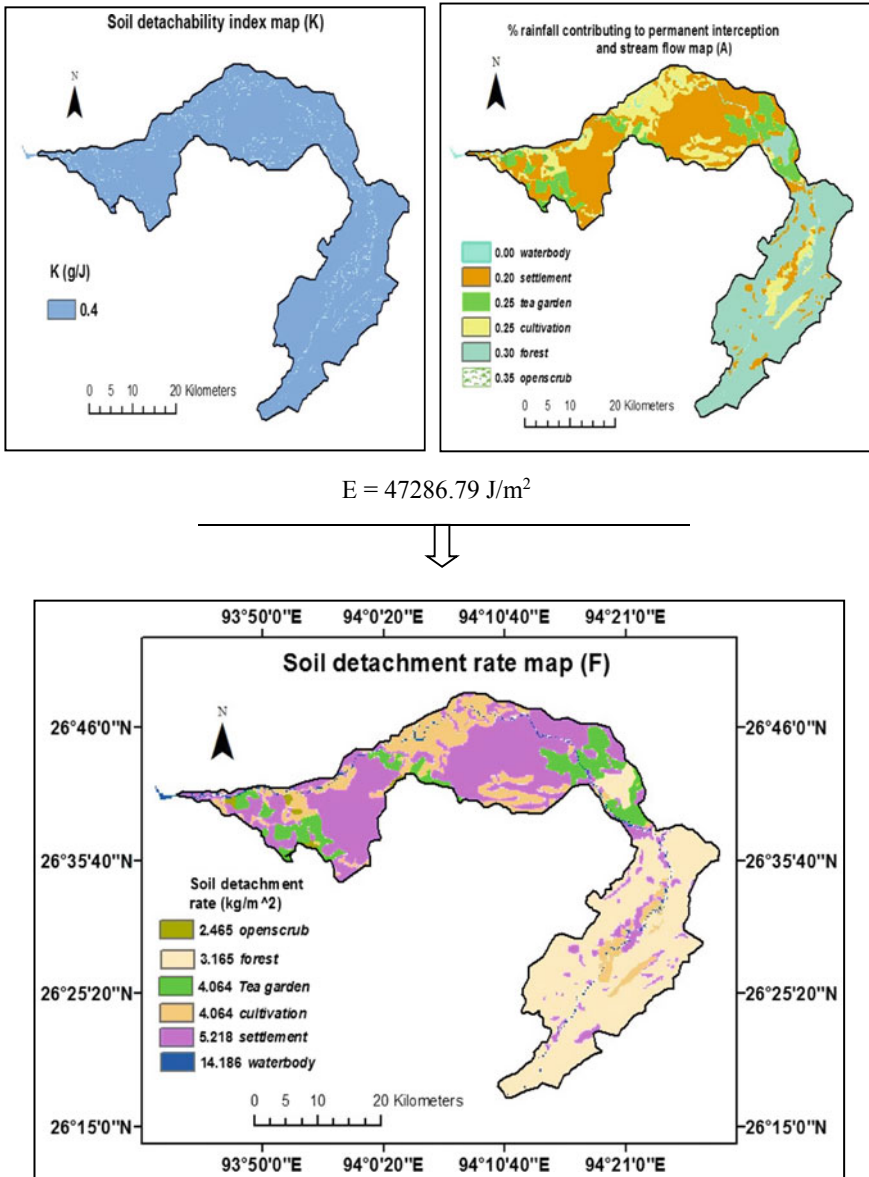
Fig. 3 Derivation of soil detachment map (*F*)
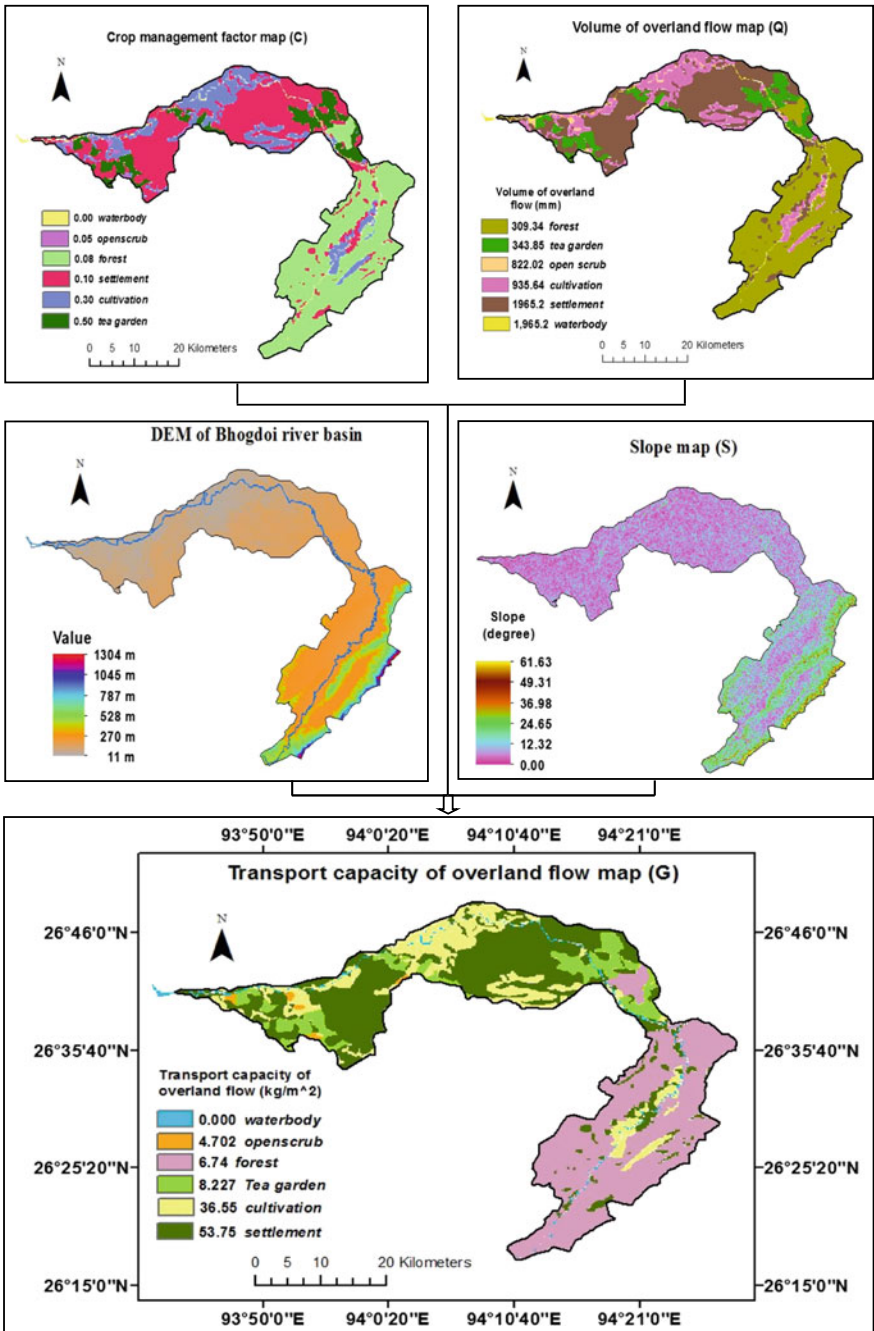
Fig. 4 Derivation of transport capacity of overland flow map (*G*)
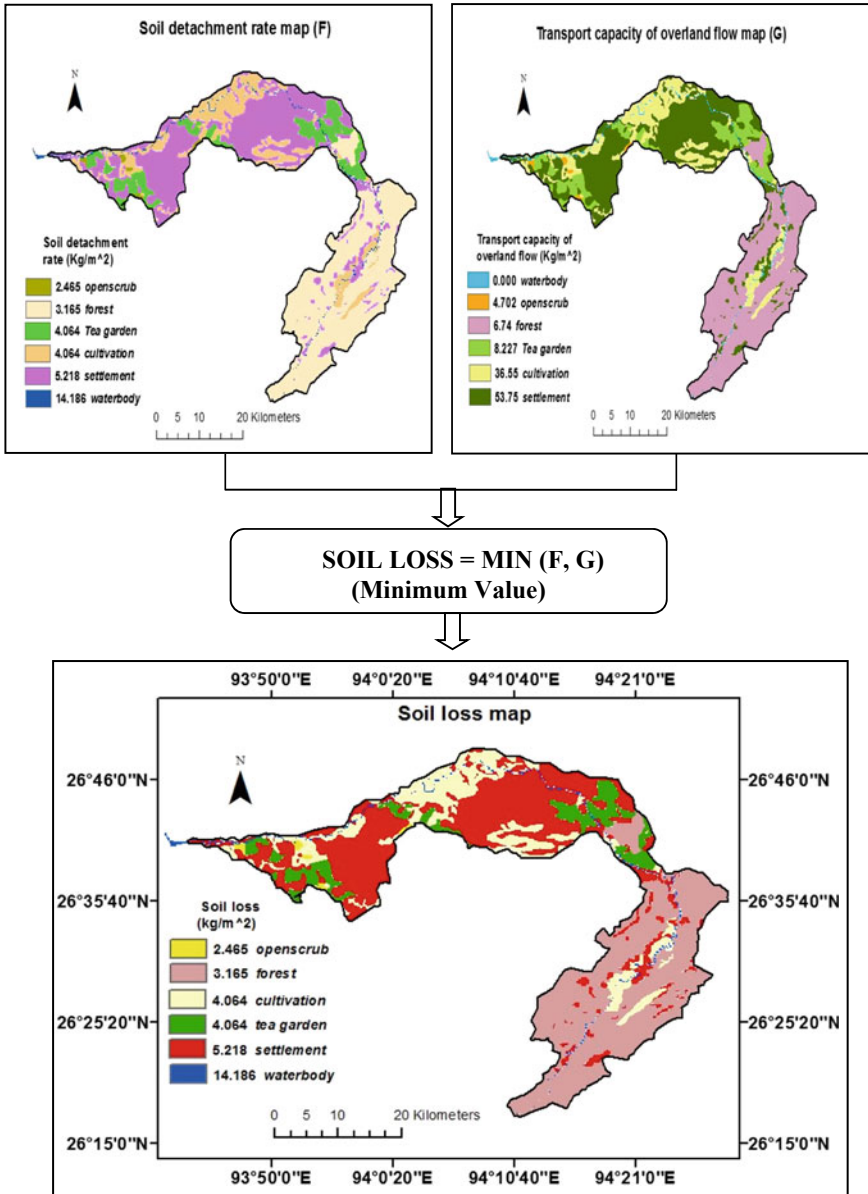
Fig. 5 Final soil loss map
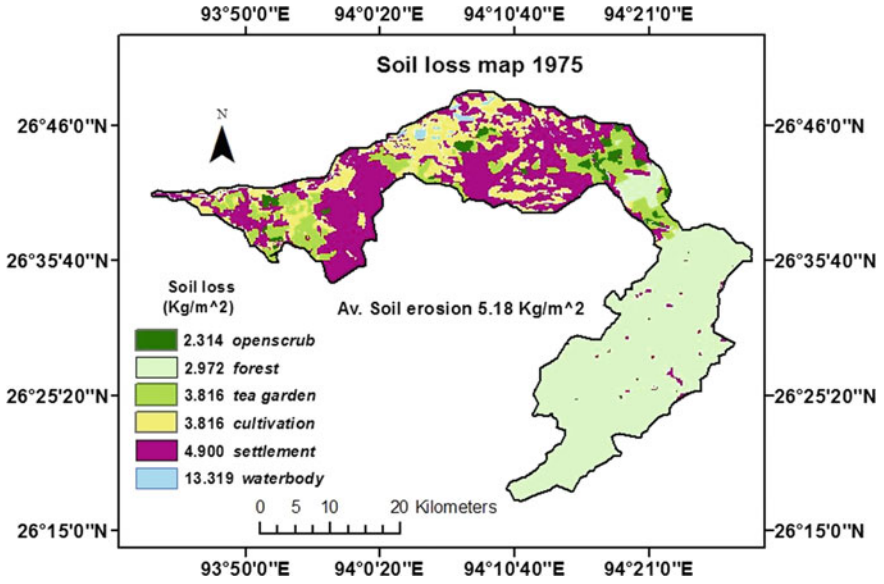
Fig. 6 Soil loss map of 1975
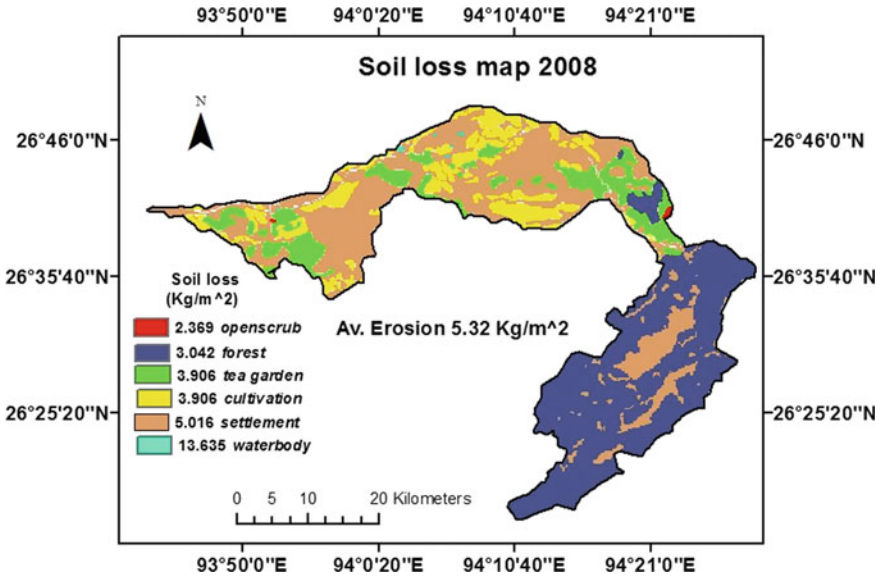
Fig. 7 Soil loss map of 2008

Table 3 Combined effects of rainfall and LULC change

Year	Annual rainfall (mm)	Area of the river basin in (km^2)	Total area covered by vegetation (km^2)	Soil erosion (kg/m^2)
1975	1845.2	1179.65	796.04	5.18
2008	1889	1179.65	698.60	5.32
2018	1965.2	1179.65	672.22	5.53

4 Results and Discussions

The change in land use/ land cover has great impact on soil erosion. In this study, a combined effect of rainfall and land use/ land cover has been analyzed for 1975, 2008 and 2018, respectively. Morgan, Morgan and Finney model has been used to estimate soil erosion. The rate of surface soil erosion depends mainly on the amount of rainfall for a particular period. More precipitation leads to the more amount of surface runoff which ultimately increased the soil erosion. The amount of soil erosion is also accentuated due to deforestation. From the study, it has also been observed that the amount of area covered by vegetation has decreased since 1975 which results in the more surface soil detachment resulting more erosion. The analysis of combined effects of rainfall and LULC change during the study period reveals that the rate of soil erosion was maximum in 2018 followed by 2008 and 1975, respectively. In 1975, the rate of soil erosion was about 5.18 kg/m^2 which were increased to 5.32 kg/m^2 in 2008 and 5.53 kg/m^2 in 2018 (Table 3). The increase in rate of soil erosion can be attributed due to decrease in vegetated cover and also increase in rainfall (Fig. 8).

5 Conclusion

The study of combined effect of annual rainfall over the study area and the LULC change reveals that the annual soil erosion was maximum in 2018 (5.53 kg/m^2) followed by soil erosion in 2008 (5.32 kg/m^2) and in 1975 (5.18 kg/m^2). Annual rainfall was maximum in 2018 (1965.2 mm) followed by annual rainfall in 2008 (1889 mm) and annual rainfall in 1975 (1845.2 mm). The result obtained from Morgan–Morgan and Finney model shows that surface soil erosion is minimum in forested areas and open scrub areas. Cultivated areas resulted in more soil loss than forested areas due to practicing of shifting agriculture, locally called 'jhum' cultivation that reduces the soil fertility, and no crops can be grown leaving the land as fallow land. Human built-up areas caused greater soil loss leaving the soil surfaced with little or no vegetation provides a prime opportunity for soil to be eroded by wind or water moving across the soil surface. Water body has resulted in maximum soil loss; it is because water is abundant and has a lot of power. It can detach soil particles and transport the detached particles downhill. These particles move from the field
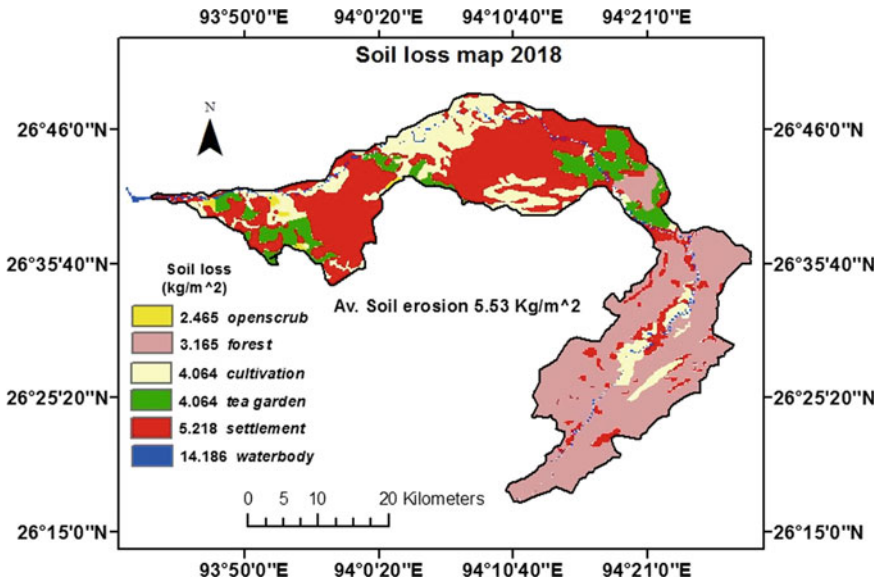
Fig. 8 Soil loss map of 2018

and end up in streams and waterways resulting in increase in siltation of the river bed.

References

1. Acharjee, S., Sarma, J.N.: A study of wetlands and their role in geological environment of the Bhogdoi river basin, Jorhat, Assam, using remote sensing and GIS. IJPSS **2**(10) (2012). ISSN: 2249–5894
2. Barman, S., Aggarwal, S., Dutta, M.K.: Soil erosion due to change in vegetated area in the Majuli Island of Assam. Int. J. Adv. Remote Sens. GIS Geogr. IJARSGG **1**(1), 8–19 (2013)
3. Bartsch, K.P., Miegroet, H., Boettinger, J., Dobrwolski, J.P.: Using empirical erosion model and GIS to determine erosion risk at Camp Williams. J. Soil Water Conserv. **57**, 29–37 (2002)
4. http://shodhganga.inflibnet.ac.in/bitstream/10603/5500/13/13
5. Morgan, R.P.C., Morgan, D.D.V., Finney, H.J.: A predictive model for the assessment of erosion risk. J. Agric. Eng. Res. **30**(245), 253 (1984)
6. Nath, M., Bora, A.: Depositional activities of the lower Bhogdoi river: Jorhat District, Assam. J. Indian Geomorphol. **1** (2012). ISSN 2320-0731, Indian Institute of Geomorphologists (IGI)
7. Pandey, A.: Soil erosion modelling using remote sensing and GIS. IJIRSET **5**(special issue 6) (2016). ISSN (Online): 2319-8753, ISSN (Print): 2347-6710
8. Shrestha, D.P.: Assessment of soil erosion in the Nepalese Himalaya: a case study in Likhu Khola Valley, Middle Mountain Region. Land Husb. **2**(1): 59–80 (1997)
9. Shrestha, D.P.: Lecture notes on soil degradation assessment and modelling. Department of Earth System Analysis, ITC, Enschede (2007)
10. Wilson, G.V., McGregor, K.C., Boykin, D.: Residue impacts on runoff and soil erosion for different corn plant populations. Soil Tillage Res. **99**, 300–307 (2008)
11. Wischmeier, W.H., Smith, D.D.: "Predicting rainfall erosion losses"—a guide to conservation planning. US Department of Agriculture, Agricultural handbook 537 (1978)

Effect of Freezing–Thawing Cycles on Suction Measurement of Unsaturated Soil

Jaimin Vaidya, Bhavita Dave, and Nitin H. Joshi

Abstract The basic relationship between the volumetric water content of soil and suction value is defined as soil–water characteristic curve or soil retention curve that plays an important role for determining properties of unsaturated soil and estimating its mechanical behavior. The present study is an attempt to evaluate the effect of freezing–thawing cycles on suction parameter of unsaturated soil. Suction is measured by filter paper method. Experiments have been conducted on 5 cycles of freezing–thawing of samples, and their soil–water characteristic curves have been developed with the change in its air entry value, and residual water content of soil for each cycle is presented in this paper.

Keywords Unsaturated soil · Soil water characteristic curve · Suction measurement

1 Introduction

1.1 Freezing–Thawing of Soil

Jammu and Kashmir is the coldest region in India. Indian meteorological department reports the temperature ranges from $-20\,°C$ in winter to $35\,°C$ in summer [1]. Freeze–thaw cycle causes frost action which leads to frost heave and thaw weakening. The former is due to formation of ice crystal, ice lenses, and later is due to melting of ice.

Silt is the most frost susceptible soil. Silt pores are large enough to transport an enough supply of moisture to the freezing front and small enough to promote suction and capillarity. Casagrande [2] observed that ice segregation did not appear in soils containing less than 1% of grains smaller than 0.02 mm. Efforts done to investigate the influence of freeze–thaw cycles on soil properties were reviewed

J. Vaidya (✉) · N. H. Joshi
The Maharaja Sayajirao University of Baroda, Vadodara, Gujarat, India
e-mail: jaiminvd4@gmail.com

B. Dave
S.V. National Institute of Technology, Surat, Gujarat, India

and summarized its influence in two parts: physical properties such as density and hydraulic permeability and mechanical properties such as ultimate strength, strain–stress behavior and resilient modulus. Loose soils tend to be densified, and dense soils become loose after freeze–thaw cycles, and both loose and dense soils may attain the same void ratio after a number of cycles. Having increased the large pores that are left after the thaw of ice crystals, permeability will increase.

Freezing can be of two types open and closed system. De Groot [3] defined an open system as exchange of matter, heat, work and energy with its surroundings. Jones (1987) defined open system freezing for soil as the condition where pore water in excess of that available in the voids of the soil is available to be moved to the surface of freezing to form segregated ice in frost susceptible soil. De Groot defined as closed system as exchange of heat, work and energy but no matter. Jones defined closed system of soil as no source of water available during the freezing process beyond the originally available in the voids of the soil or near the zone of freezing and the ice lenses may or may not form. In an open system, water is drawn up from a free surface through the soil as the freezing front moves downward. This movement of water due to freezing level creates ice lenses in the soil. In closed system, there is a redistribution of moisture to the freezing front occurs, and this movement causes an increase in water content and decrease in dry density near the freezing front.

1.2 Unsaturated Soil

According to Fredlund and Raharjdo [4], the unsaturated is generally neither in totally dry condition nor in saturated condition, but has degree of ranging from 0 to 100%. Theories developed for saturated and dry condition cannot be developed directly for unsaturated condition.

Terzaghi came up with a concept contractile skin which is nothing but a thin layer of air–water interface and suggested that the contractile skin might be in the order of $10-6$ mm in thickness. Lyklema [5] showed that the distribution of water molecules across the contractile skin takes the form of a hyperbolic tangent function. Properties of the contractile skin are different from that of ordinary water and have a water molecular structure similar to that of ice [6, 7].

1.3 Soil–Water Characteristic Curve

Soil–water characteristic curve (SWCC) or soil–water retention curve is a graphical presentation of suction pressure in soil with its varying volumetric water content as shown in Fig. 1 (Fredlund 1995, 2000). However, the term 'characteristic' shows that a distinctive relationship can characterize many of hydraulic and mechanical behavior of the unsaturated soil, despite of the high dependency of this relationship on the initial state such as sample's degree of saturation and void ratio, fabric, state
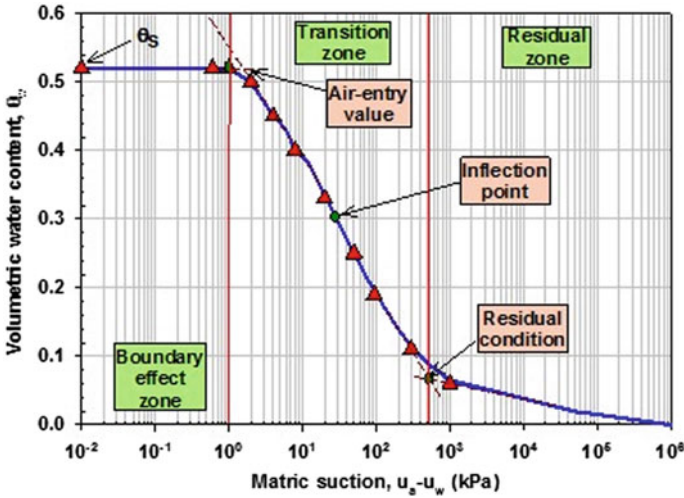
Fig. 1 Soil–water characteristic curve

of stress, hydraulic path and temperature. Air entry value is defined as the matric suction value that must be exceeded before air recedes into soil pores. The definitions of residual water content are based on developed statistically by various researchers, and each of them has different approach. It has no significant physical meaning and is only used for fitting parameters [8].

Brooks and Corey [9] defined residual water content as water content at which suction reaches infinity. This is the disadvantage of this method as it is not possible to extend SWCC to infinity. The soil suction up to 1,000,000 kPa is acceptable (Mitchell 1976). There is experiment evidence supporting this value provided by many researchers (Croney and Coleman 1961; Russam 1958; Vanapalli 1994; Fredlund 1964) [10]. van Genuchten in 1980 defined residual water content as the water content as soil suction of 1500 kPa. This is the limit of most soil suction testing device as models are used from agricultural and generally do not require to model beyond the wilting point. But in 1991, residual water content is defined as water content at which slope of SWCC and a coefficient of permeability go zero when soil suction becomes very large. But coefficient of permeability is a nonzero, finite number (Nitao and Bear 1996) so definition is an irony to the interpretation.

1.4 Empirical Models for SWCC

There are several empirical equations that have been proposed to describe SWCC such as Gardner (1959), Brooks and Corey (1964), van Genuchten [11], Fredlund and Xing [12], Gitirana and Fredlund [13], Fredlund and Pham (2006). Many SWCC equations take the form of a continuous function that is asymptotic at the extremities.

It is a zone between air entry value and residual suction where the curve has sufficient slope for calculation soil suction. van Genuchten [11] and Fredlund and Xing [12] empirical model is widely used.

1.4.1   Van Genuchten Fitting Method (VG Model)

The van Genuchten equation is the most common equation used SWCC equation. This equation has three parameters as follows:

$$w(\psi) = \frac{w_s}{\left[1 + (a\psi)^n\right]^m} \tag{1}$$

where 'a' is air entry fitting parameter, m and n are the parameters of fittings for inflection of curve and w_s is saturated water content. The above equation can be rearranged to solve suction in terms of water content.

$$\psi = \frac{1}{a}\left[\left(\frac{w_s}{w}\right)^{\frac{1}{m}} - 1\right]^{\frac{1}{n}} \tag{2}$$

The usage of this equation is limited to air entry value and the residual suction of a soil because of the asymptotic nature of equation.

1.4.2   Fredlund and Xing Fitting Method (FX Model)

They proposed the equation that has range beyond residual suction to completely dry conditions:

$$w(\psi) = C(\psi)\frac{w_s}{\left\{\ln\left[e + \left(\frac{\psi}{a}\right)^n\right]\right\}^m} \tag{3}$$

where $w(\psi)$ is water content at any soil suction; w_s is the saturated water content; a, n and m are the fitting soil parameters associated with the SWCC. The e is the base of natural logarithm. The correction factor $C(\psi)$ is written as follows:

$$C(\psi) = 1 - \frac{\ln\left(1 + \frac{\psi}{\psi_r}\right)}{\ln\left(1 + \frac{10^6}{\psi_r}\right)} \tag{4}$$

where ψ is any soil suction value and ψ_r is soil suction at residual conditions. Usually, correction factor is taken as 1. To calculate soil suction in terms of water content, the equation can be written as

$$\psi = a\left[e^{\left(\frac{w_s}{w}\right)^{\frac{1}{m}}} - e\right]^{1/n} \qquad (5)$$

1.5 Filter Paper Method for Suction Measurement

Filter paper technique is the only method from which both total and matric suction can be deduced. Using the filter paper method, the soil specimen and filter paper are brought to moisture equilibrium either in contact (matric suction) or not in direct contact (total suction) in a constant temperature environment Fig. 2. Direct contact between the filter paper and the soil allows water in the liquid phase and solutes to exchange freely. The water content of filter is measured after equilibrium is established. Then, by using the suitable filter paper calibration curve, the suction of the soil is estimated.

Different filter paper method calibrations are attributed by the different researchers. Whatman No. 42 filter paper was used to measure suction, and its calibration curve is given in Fig. 3.

2 Material and Its Properties

In this study, laboratory test was carried out on silty clayey sand as per IS code classification and unified soil classification system. The properties of soil are depicted in Table 1. Whatman Grade 42 filter paper was used having thickness of 200 μm and pore size of 2.5 μm.
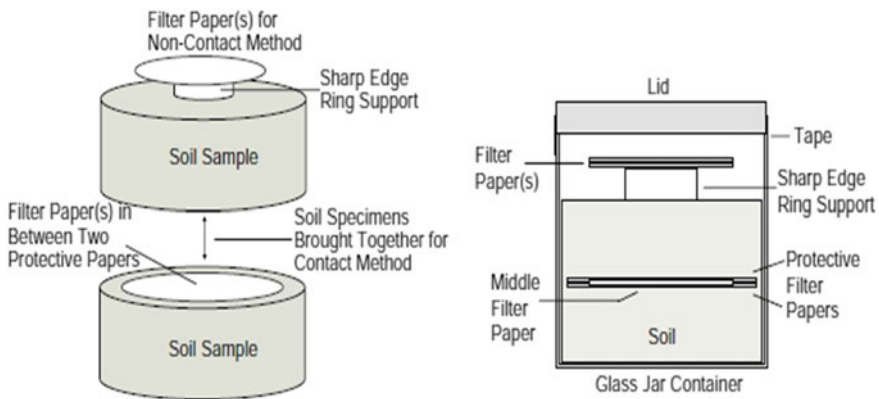
Fig. 2 Filter paper method to measure suction

$$\log_{10}S = 5.327 - 0.0779\,(wc_{fp})$$

$$\log_{10}S = 2.412 - 0.0135\,(wc_{fp})$$

$wc_{fp} = 45.26\%$
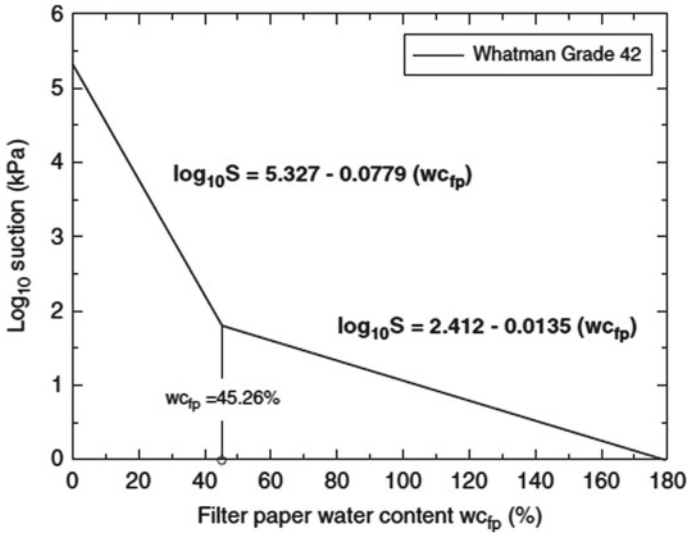
Fig. 3 Calibration curve for Whatman Grade 42 (ASTM D5298-10 [14])

Table 1 Properties of soil

Specific gravity	2.63
Liquid limit (%)	24.33
Plastic limit (%)	18.75
Plasticity index (%)	5.58
Maximum dry density (gm/cc)	1.86
Optimum moisture content	14

3 Testing Procedure

3.1 Specimen Preparation

To estimate suction, soil sample was prepared in consolidation ring and was removed and put in air tight container. Two cakes of soil sample were prepared at same degree of saturation as shown in Fig. 4. Water content at degree of saturation of 90, 80, 70, 60, 50, 40 and 30% was taken to prepare the sample by simple relation between water content, degree of saturation, mass of dry soil, void ratio and specific gravity. As shown in Fig. 2, three layers of filter paper were kept between the two cakes of the sample Fig. 4. Two layers of filter paper one above and one below the main filter paper were kept as a protecting layer.
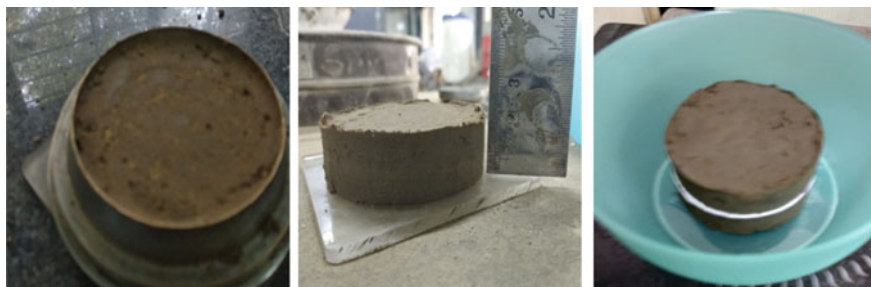
Fig. 4 Sample to measure suction

3.2 Freeze–Thaw Cycle

Samples were subjected to five cycles of freeze–thaw in closed system. Freezing was done below -23 °C for 24 h, and thawing was done for 23 h at normal temperature varying between 25 and 30 °C according to IS code 4332.4.1968. To obtain closed system for the sample, it was doubled wrapped with black polythene bag and kept in air tight container so that no moisture can come in or go out to or from the system. The samples were weighted before and after freeze–thaw cycles to see the difference in moisture before and after placing, and the change in weight for first two cycles was zero, and for rest cycles, it was ± 1 g for many samples. For few samples that have low moisture content (at $S_r = 60, 40, 30\%$) have no change in its weight which shows that there is no loss or gain of moisture.

3.3 Estimation of Soil–Water Characteristic Curve

ASTM D5298-10 code was used to follow guidelines for filter paper method of Whatman Grade 42 and its calibration curve Figs. 5, 6, 7, 8, 9 and 10 to estimate suction and empirical models of van Genuchten [11] and Fredlund and Xing [12] to estimate SWCC with the help of SOIL VISION software.

4 Results

The results by both empirical models are given in Table 2. The samples were subjected to five cycles of freeze–thaw because there was no much change in the parameters after third, fourth cycle. Figures 5, 6, 7, 8, 9 and 10 shows the SWCC found by VG model, and Figs. 11, 12, 13, 14, 15 and 16 shows SWCC found by FX model for zeroth to fifth cycle. Air entry value for 0 to 2 cycles for both model shows decrease in value, and then, from cycle 3, it was random but when compared between two fitting
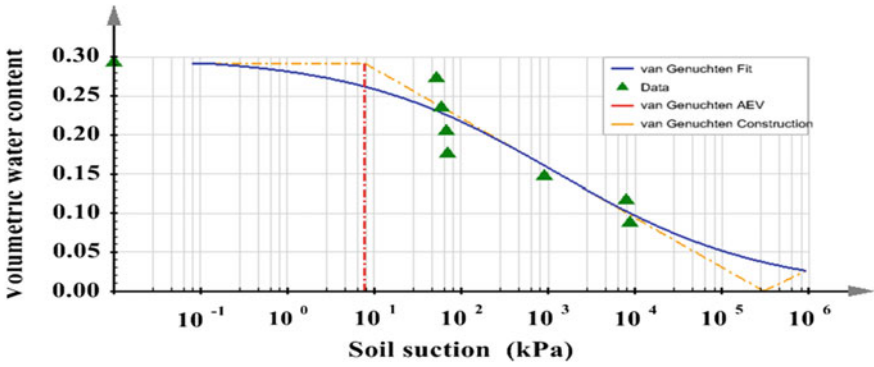
Fig. 5 van Genuchten fitting (zero cycle)
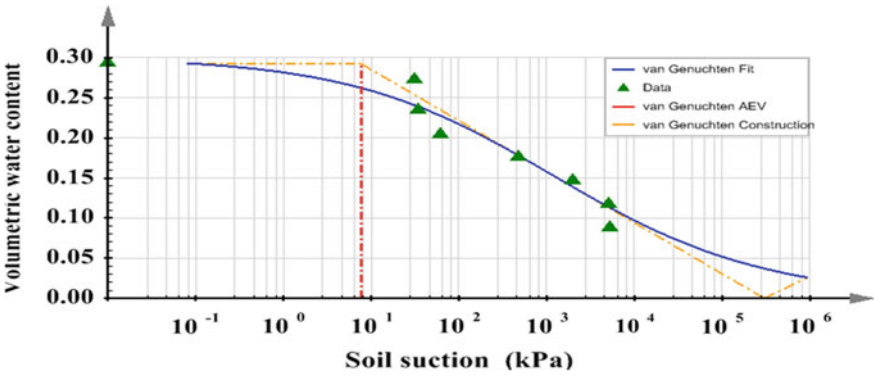
Fig. 6 van Genuchten fitting (first cycle)
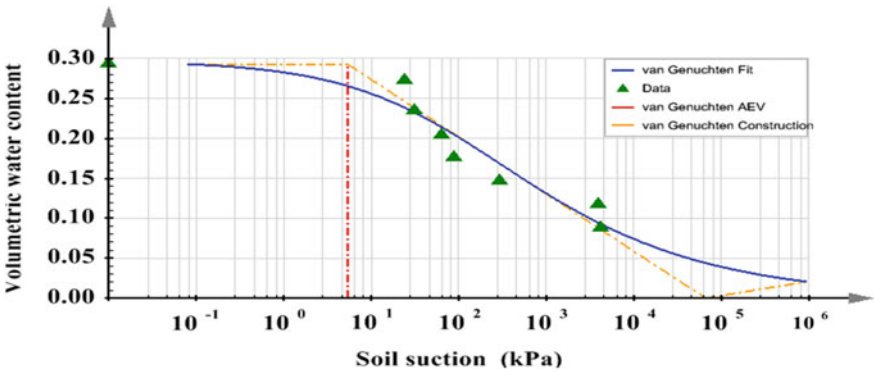
Fig. 7 van Genuchten fitting (second cycle)
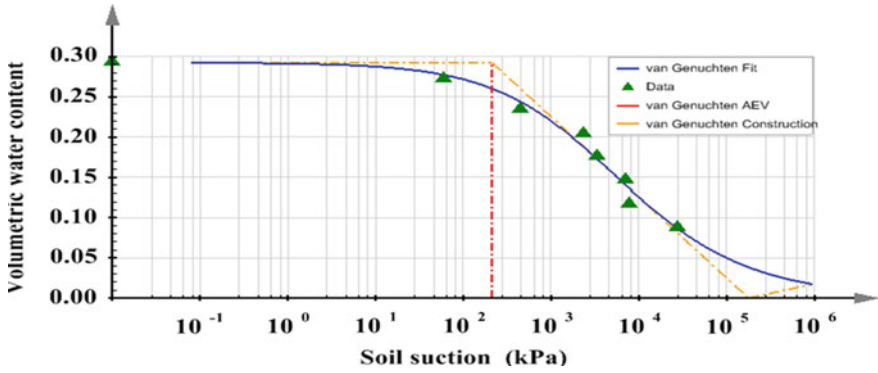
Fig. 8 van Genuchten fitting (third cycle)
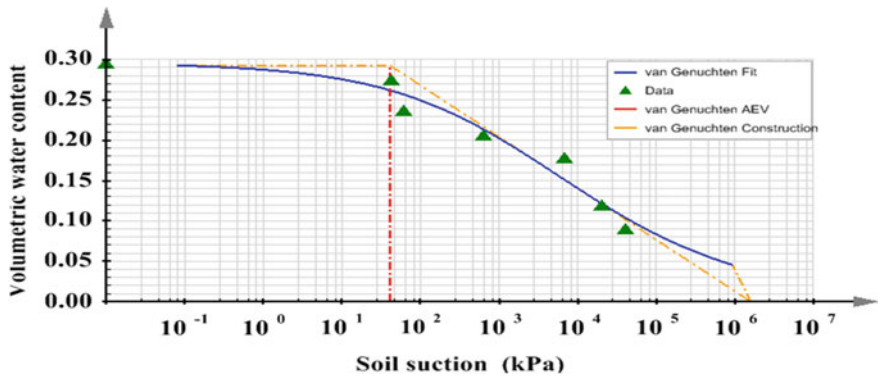

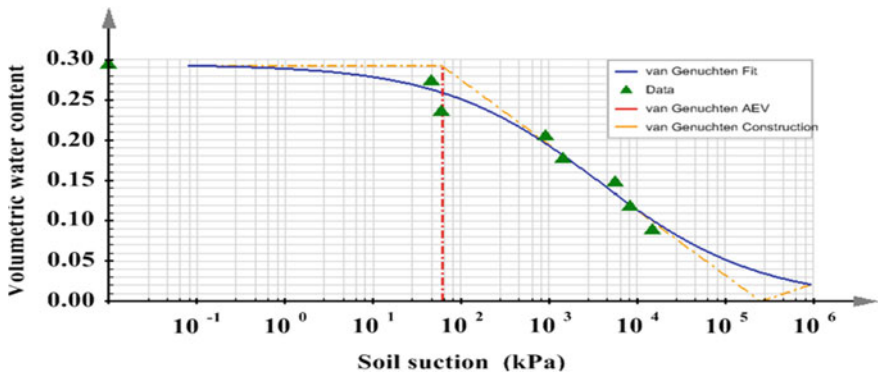**Fig. 9** van Genuvchten fitting (fourth cycle)

Fig. 10 van Genuchten fitting (fifth cycle)

Table 2 Fitting parameters with air entry value and residual water content for both models

VG model data

Cycles	0	1	2	3	4	5
α	0.006	0.001	0.001	0.0002	0.0003	0.0003
R^2	0.917	0.934	0.91	0.980	0.956	0.9688
Air entry (kpa)	48.02	7.68	5.45	226.83	41.4	60.63
Saturated W.C (%)	28.66	28.42	28.42	28.77	29.05	29.20
Residual W.C (%)	13	14	12	20	19	17.5
Residual pressure (Kpa)	1500	1500	1500	1500	1500	1500
n	3	0.38	0.517	0.612	0.418	0.489
m	6.84	0.902	0.562	0.957	0.754	0.9271

FX model data

A_f (kpa)	47.70	28.16	23.60	2500	2500	2500
R^2	0.915	0.965	0.982	0.9819	0.968	0.9705
Air entry (kpa)	40.08	21.79	20.67	217	223.24	67.48
Saturated W.C (%)	29.22	29.22	29.22	29.15	28.92	29.15
n	20	20	14.64	0.62	0.336	0.4622
m	0.111	0.084	0.126	1.62	1.59	2.12
Residual W.C (%)	18.33	19.75	17.21	5.35	11.66	3.83
Residual pressure (Kpa)	74.21	75.53	75.45	62,129	340,689	77,219
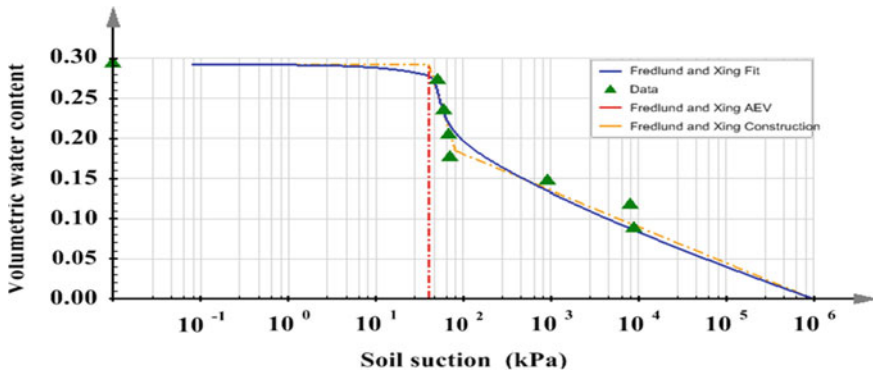
Fig. 11 Fredlund and Xing fitting (zero cycle)

models it was not much of difference except fourth cycle, while air entry parameter for VG model (α) was random and that for FX model (A_f) was decreasing up to cycle 2 and then remained same (2500 kPa). For all cycles for both models, saturated water content was same. For VG model, inflection parameters n and m have no significant change after second cycles of freeze–thaw, and that for FX model, there was sudden change between cycle 2 and 3. R^2 value close to 1 is most accurate fitted curve.
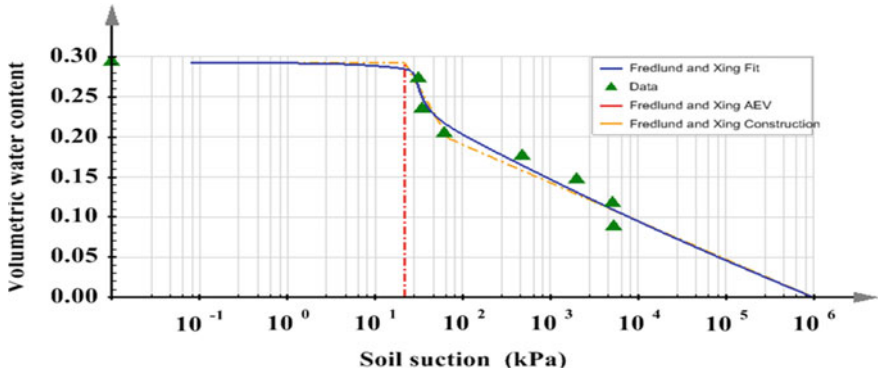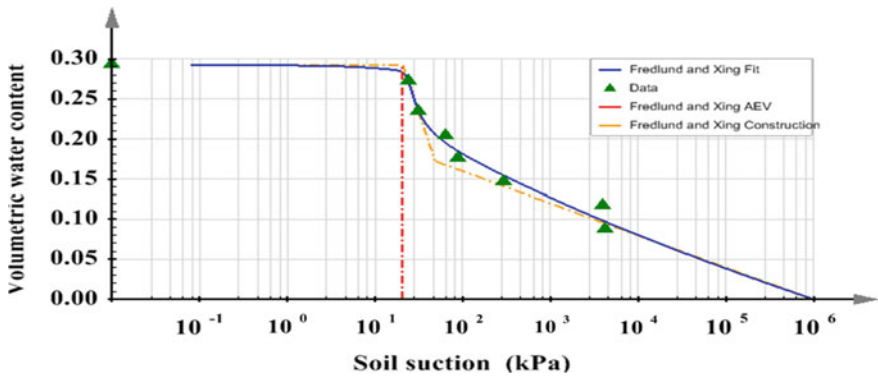
Fig. 12 Fredlund and Xing fitting (first cycle)
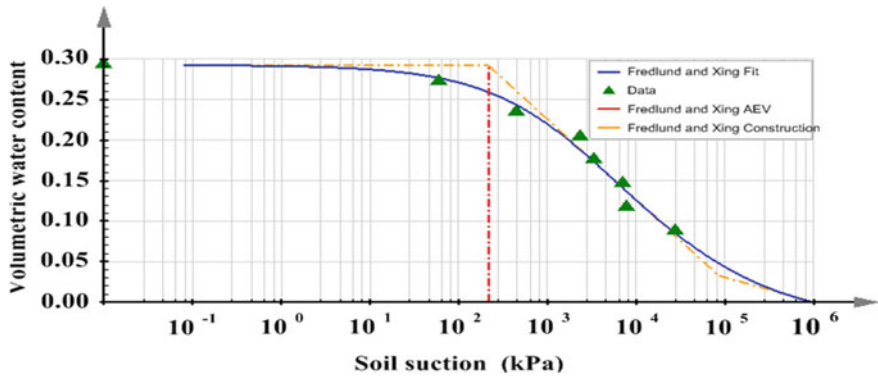

Fig. 13 Fredlund and Xing fitting (second cycle)

Fig. 14 Fredlund and Xing fitting (third cycle)
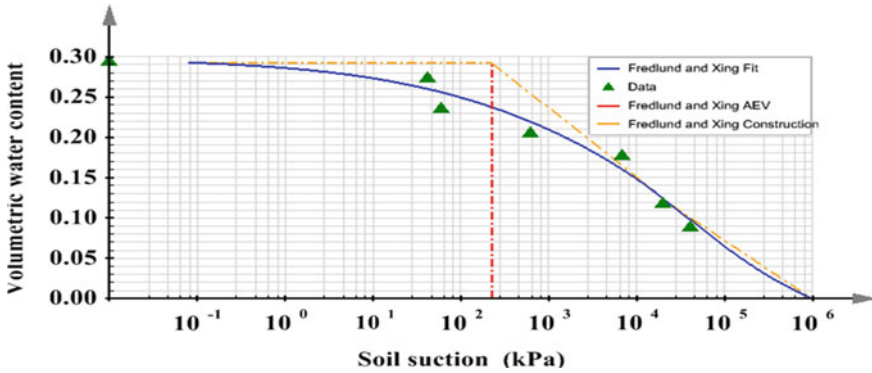
Fig. 15 Fredlund and Xing fitting (fourth cycle)
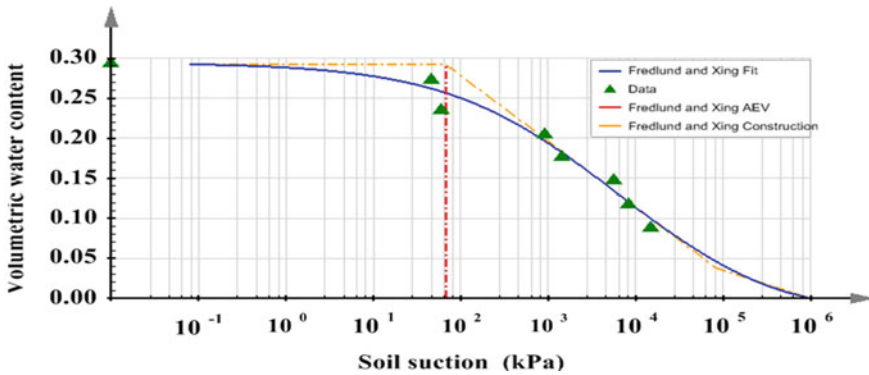

Fig. 16 Fredlund and Xing fitting (fifth cycle)

5   Conclusion

1. From van Genuchten SWCC graph, it can be seen that the construction line
    (orange dotted) goes below VG fit curve (blue curve) intersecting on X-axis and
    then joining the curve. This means that suction still exists though the soil has
    become dry which is practically incorrect. As per VG model, residual content is
    defined at 1500 KPa, but the results show that there is more suction value at low
    water content, which shows the limitation of VG model. But there is no such
    problem with FX model. Furthermore, as 1500 KPa is limitation for defining
    VG model to define residual content, it is best used when the suction value for
    soil is low, i.e., for coarse-grained soil like sand having bigger pores.
2. From no freeze–thaw (zeroth cycle) to its second cycle, there is decrease in air
    entry value and suction value because there may be increase in pore size during
    freezing. But from second to third to fourth cycle, there is sudden increase in
    air entry value and suction value for water content (at $S_r = 60$, 50, 40 and 30%)

except for that of VG model fourth cycle. It might be because of its limitation concluded above. This sudden increase may be due to decrease in pore size from adjacent increase in pore size, and equilibrium between filter paper and moisture in sample is due to suction taking place from path of decreased pore size.

3. In FX model, there is no change in air entry fitting parameter (A_f) after third cycle of freeze–thaw. But the change in air entry value is observed. This is due to sudden decrease of fitting parameter 'n' (slope parameter) from second to third cycle because of decrease in suction at higher water content (at $S_r = 90$, 80 and 70%) and increase in suction at lower water content (at $S_r = 60, 50, 40$ and 30%).

4. FX model shows very high residual suction pressure after third cycle which may be not possible. Therefore, other technique for measurement of suction is necessary to check the accuracy of filter paper method.

References

1. The weather for Srinagar, Jammu and Kashmir as per Indian Meteorological Department, Government of India. www.imd.gov.in
2. Casagrande, A.: Discussion of Frost heaving. Highway Research Board Proceedings **11**, 168–172 (1931)
3. Tolhoek, H.A., De Groot, S.R.: A discussion of the first law of thermodynamics for open systems
4. Fredlund, D.G., Rahardjo, H.: Soil Mechanics for Unsaturated Soils. Wiley, Hoboken (1993)
5. Lyklema, J.: Fundamental of interface and colloid science, vol. III, Academic, New York (2000)
6. Matsumoto, M., Kataoka, Y.: Study on liquid–vapour interface of water. I. Simulational results of thermodynamic properties and orientational structure. J. Chem. Phys. 885, 3233–3245 (1988)
7. Derjaguin, B.V., Churaev, N.V.: Structure of the boundary layers of liquids and its influence on the mass transfer in fine pores. In: Cadenhead, D.A., Danielli, J.F. (eds.) Progress in surface and membrane science, pp. 69–130. Academic, New York (1981)
8. Blight, G.E.: Unsaturated Soil Mechanics in Geotechnical Practice. CRC Press, Taylor and Francis Group, London (2013)
9. Brooks, R.H., Corey, A.T.: Hydraulic properties of porous media. Hydrology Paper No. 3, Colorado State Univ., Fort Collins, Colo. (1964)
10. Vanapalli, S.K., Sillers, W.S., Fredlund, M.D.: The Meaning and relevance of residual state to unsaturated soils. In: 51st Canadian Geotechnical Conference, Alberta (1998)
11. van Genuchten, M.T.: Closed formed equation for predicting the hydraulic conductivity of unsaturated soils. Soil Sci. Society Am. J. **44**, 892–898 (1980)
12. Fredlund, D.G., Xing, A.: Equation for the soil water characteristic curve. Can. Geotech. J. **31**, 533–546 (1994)
13. Ebrahimi-B, N., Gitirana, G.F.N., Jr., Fredlund, D.G., Fredlund, M.D., Samarasekera, L.: A lower limit for the water permeability coefficient. In: Proceedings of the 57th Canadian Geotechnical Conference (2004)
14. ASTM D5298-10 standard test method for measurement of soil potential (suction) using filter paper, annual book of ASTM standards, ASTM international, west Conshohocken,PA,USA.

Reviews on Mitigation Techniques of Offshore Jack Up Hazard by FEM Analysis

Arpit Parikh, S. J. Shukla, and S. R. Gandhi

Abstract It is very well observed that offshore sites mostly contain soft/loose soils may be of sand or clay or may be multiple layer of soil mixture under saturated condition. This particular soil undergoes large deformation on the installation of any offshore structure like jack up. It is also observed that jack up may tilt or sink under its own weight without any lateral load or hydrodynamic pressure or any natural hazard like liquefaction or hurricane. It may undergo punching shear failure due to the presence of soft soil. It may suffer failure due to jack up leg and foundation element connection failure. It gets affected by rotational stiffness, foundation fixity parameters. To overcome this situation, several techniques had been proposed by various researchers. Spudcan, anchors, mud mat, bucket foundation, suction caisson foundation, etc., are used to overcome such difficulties. These techniques of mitigation subsequently affect bearing capacity failure zones of soil. Sinking and tilting effects are due to overlapping of bearing capacity failure zones. Hence, by advancing changing in shape and spacing of jack up legs, sinking and tilting effects can be considerably reduced. In particular research paper, an attempt has been made to investigate the effects of various mitigation techniques by previous researchers. All field and laboratory studies along with soft computing with FEM-based software had been discussed. Considerable researchers had shown that provision of mud mat in jack up bottom increases stability of jack up structure. To visualize the various effects, FEM-based Plaxis 3D program had also been used.

Keywords Jack up foundation · PLAXIS 3D for jack up leg analysis · Bearing capacity failure

1 Introduction

Jack up foundation elements subjected to vertical axial loads, moments and lateral wave loads in the offshore regions create vital stability issues. The particular offshore

A. Parikh (✉) · S. J. Shukla · S. R. Gandhi
Sardar Vallabhbhai National Institute of Technology, Surat, India
e-mail: arpitparikh78@gmail.com

structures are mainly subjected to following kinds of failures. (A) Subjected to over-turning moment and leads to overturn. (B) Punch through failures, i.e., immediate bearing capacity failure or overlapping of failure zones. (C) Jack up foundation element sinking and tilting. How one can overcome these issues. The particular research paper reviews various techniques and methodologies for mitigating this kind of offshore geohazard. The research paper also highlights the recent trends and current practices, the old age techniques and their likely improvement with the time and lastly also discusses what the future holds in innovation in this area. Research paper highlights the improvement in resisting penetration of offshore jack up structure by suitable input parameters in FEM analysis.

2 Problem Statement Using Plaxis 3D

Here to get the clear idea of the problem faced by Oil & Gas Industries, author had modeled jack up foundation (jack up deck and four Number of jack up legs connected on periphery of deck plate) using conventional assumptions of finite element method which is embedded in offshore cohesive soil using FEM-based software Plaxis 3D (Fig. 1). Results of the same are represented in Fig. 2.
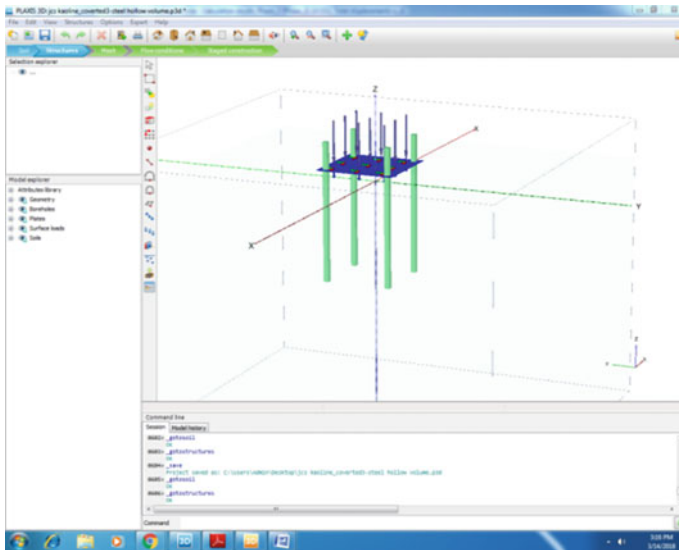
Fig. 1 Jack up and four number of legs embedded in Kaolin clay modeled in Plaxis 3D
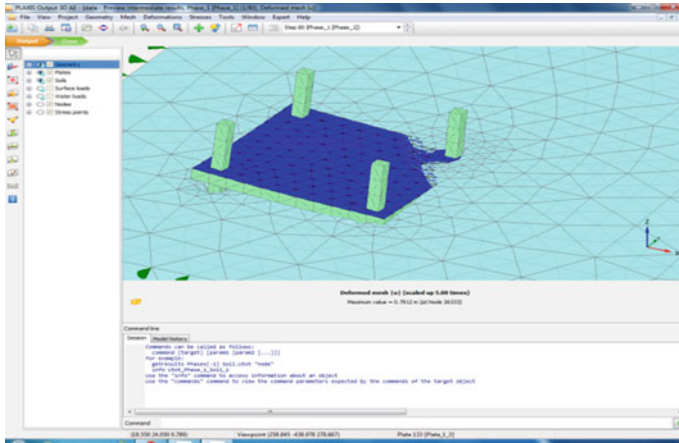
Fig. 2 Sinking and tilting behavior as observed in Plaxis 3D for jack up leg

3 Various Mitigation Practices

3.1 Mat-Supported Jack-Up Foundation

Scales [1] had worked in similar concepts. The findings of the scales have been reproduced here in terms of advantage of mat foundation to jack up.

A mat-supported rig with bottom bearings found to be very well suited for all types of environmental conditions. These types of rigs had performed very well under the event of hurricane also on extremely weak soils like Mississippi river delta area.

One more interesting advantage of jack up supported mat is it works as active damper in the entire system. Lowering of the mat at the particular site location allows the jack up deck to be jacked up out of the water very quickly. The lowered mat which is leveled to the seabed top acts as damper which gradually eliminates wave induced rig heave and therefore impacting or pounding on the bottom. This characteristic permits the jack up to move to more severe and harsh wave condition in comparison with other types of jack up.

3.2 Mat-Supported Jack-Up Foundation with Skirt

Stewart [2] has done extensive work in bearing capacity analysis and percentage increase in resisting overturning moment of jack up rig maleo producer which is supported by large cutout mats as shown in Figs. 3 and 4. Here, study has been carried out in soft clays on level seabed. Mud mat rigs will penetrate into the seabed until a depth where the soil bearing capacity is just sufficient to support the weight of the structureless its buoyancy weight. Particular mat penetrates in clay slowly.
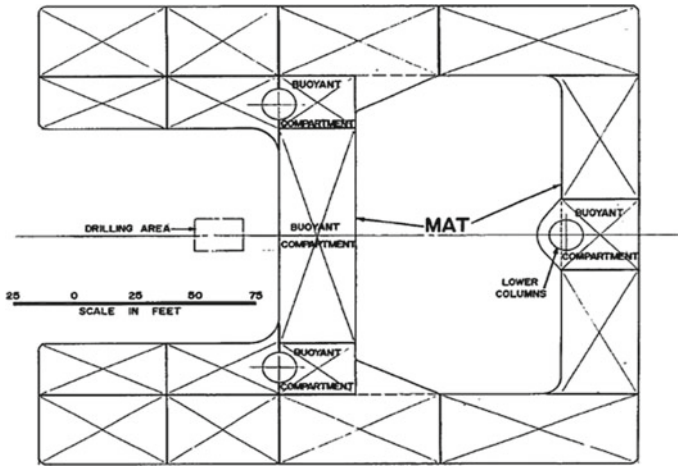
Fig. 3 Mat foundation for jack up in plan for Scales [1]
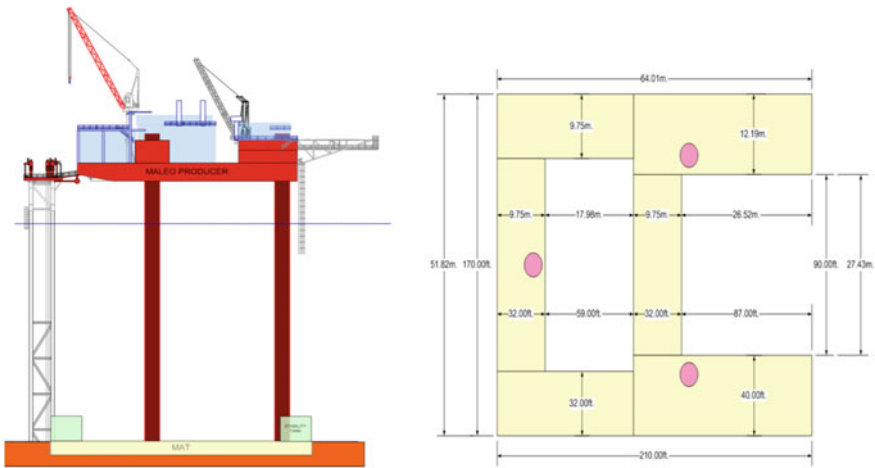

Fig. 4 Jack up rig with mat foundation with skirt

Jack up structure does not penetrate evenly. Jack up uneven penetration causes the structure to tilt back and forth and the bearing pressures to increase and decrease from one side of the mat to the other which are difficult to assess.

W. P. Stewart has made comparison of bearing capacity by taking initial bearing capacity of soil calculated by local soil investigation. Particular bearing capacity is considered as basic bearing pressure before placement and lowering the mat support to seabed. And then after lowering the mat-supported jack up at the site, the bearing pressure indicates rise of 50–66% compared to basic value. This is tabulated as

follows. Here, one can also visualize the effect of skirt—confinement of soil beneath skirt plate gives rise in bearing capacity by around 16% (Fig. 5; Table 1).

W. P. Stewart had also attempted calculation of mat overturning resistance. The mat-supported rig is mostly prone to overturn by mechanism of deep-seated slip circle failure or bearing capacity failure as local failure to be started at the edges of the mat.

Mat overturning resistance has been calculated by assuming strip foundation method for the mat cutouts. The strip foundation method proves to be better in comparison with the slip circle of method of soil. In this method, simple single force is acting vertically in the center of each cutout strips. The overturning resistance is taken as the sum of each force multiplied by its horizontal distance or lever arm, from assumed horizontal axis of rotation. The moment calculated from the axis of rotation may add or subtract to the overturning moment caused by environmental loading. This is generally combination of wind, wave and current forces and their
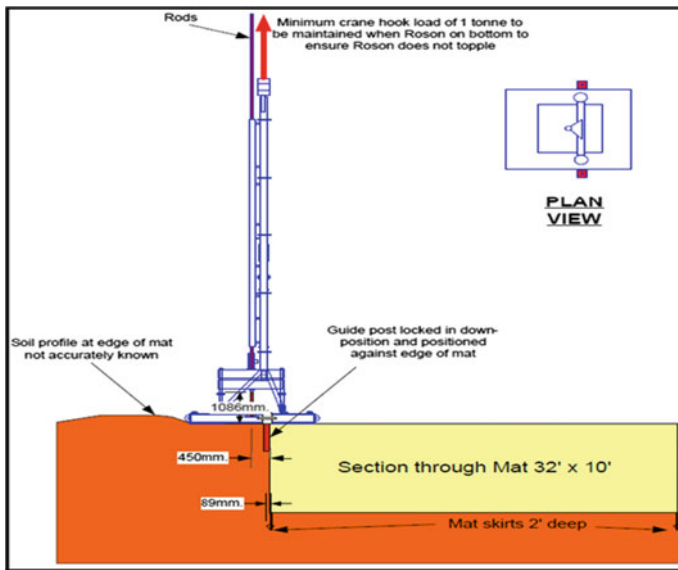

Fig. 5 Mat foundation in side elevation with clear view of skirts penetration (2′ Deep) in surrounding soil

Table 1 Comparison of bearing capacity results

Condition	q_{ult} kpa	q_{ult} Ratio
Avg. Max. bearing pressure at preload	29	Basic
Bearing pressure at mat bottom using avg. Cu	34	18%
As above with overburden pressure	43	50%
As above with O.B. + full skirt effect	48	66%

Table 2 Comparison of OTSF results

Condition	q_{ult} kpa	OTSF	OTSF Ratio
Avg. Max. bearing pressure at preload	29	1.70	Basic
Bearing pressure at mat bottom using avg. Cu	34	2.24	32%
As above with overburden Pressure	43	3.23	90%
As Above with O.B. + full skirt	48	3.72	119%

vertical distances above the assumed horizontal axis of rotation. Factor of safety against overturning or OTSF is defined as.

OTSF = (SRmoment-Wmoment)/OTmoment, where

SR moment = soil ultimate capacity resisting moment

W moment = (Weight –Buoyancy) moment

OT moment = overturning moment from environmental forces

Results are tabulated in Table 2 regarding benefit of providing mat foundation to jack up structure.

3.3 Spudcans to the Legs as Foundation Element

Eric J. Parker, Francesco Mirabelli & Lorenzo Paoletti [3] from Italy had studied the concept of predicting jack up leg penetration from the conventional mathematical expressions. They compared predicted and observed jack up spudcan leg penetrations in their research for 15 offshore sites. Although soft formulation for the same approach had not been mentioned in the research paper. They had attempted to give bearing capacity formulas for spudcan by making changes into conventional bearing capacity equations for various soil layers as well as in multiple soil layers (Fig. 6).

Some of the major conclusions of Eric and team can be mentioned here as follows.

Fig. 6 Spudcan geometry in vertical section
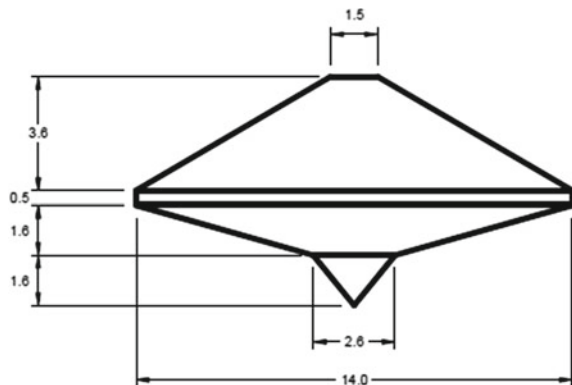
In general, jack-up leg penetration can be well predicted by simple bearing capacity equations. Practical spudcan penetration in sands usually stops when the maximum section comes to bear on the sand layer.

Leg penetrations can be large in normally consolidated clays. Penetration stops either at the base of Holocene Wedge or on silty/sandy interbeds. Predictions are most difficult in interbedded profiles, with the most critical cases being the presence of thin silty layers in soft layers. For purposes, the greatest risk of punch through is found in the Holocene wedge area.

Eric Parker and team have given various bearing capacity formula for different soil layer condition. This is not mentioned here. To visualize the advantage of the spudcan, one can use normal bearing capacity equation and modified bearing capacity equation given in the particular research paper.

3.4 Spudcans with Buoyancy Modules to the Legs as Foundation Element

An earlier solution by various researchers has been carried out to increase bearing capacity and increasing stability. Spudcan with buoyancy modules is suggested by Zhao Tianfenga and Sun Chengmeng [4] by considering problems associated with the retrieval operations of Jack up spudcan legs. Most of the cases in spudcan embedded legs are found that retrieving requires very heavy uplift pressure to remove spudcans which are embedded in intermediate layers of soil. Hence, to overcome these problems, spudcans with buoyancy modules have been suggested.

It is proposed to remove the soil resting on the upper surface of the spudcan and thus reduce the pull-out resistance during the extraction process after drilling. The new spudcan has three pontoons, each composed of three prismatic ballast cabins equipped with mud-filtering devices, jetting nozzles, jetting lines and gas injection lines. By injecting compressed air, the cabins can discharge ballast water through the mud-filtering devices on the pontoons, which act as drainage channels. Several mud fenders are positioned on the outside surfaces of the pontoon to protect the jetting nozzles, which are the outlets of the jetting lines inside the pontoon. Periodic jetting can be carried out to avoid soil consolidation near the leg. In comparison with existing spudcans, the buoyancy spudcans occupy the cavity space and reduce the amount of soil above the spudcan to gain a significant reduction in pull-out resistance. After the ballast water is discharged, buoyancy forces can also be acquired from empty pontoons to help leg extraction (Fig. 7).
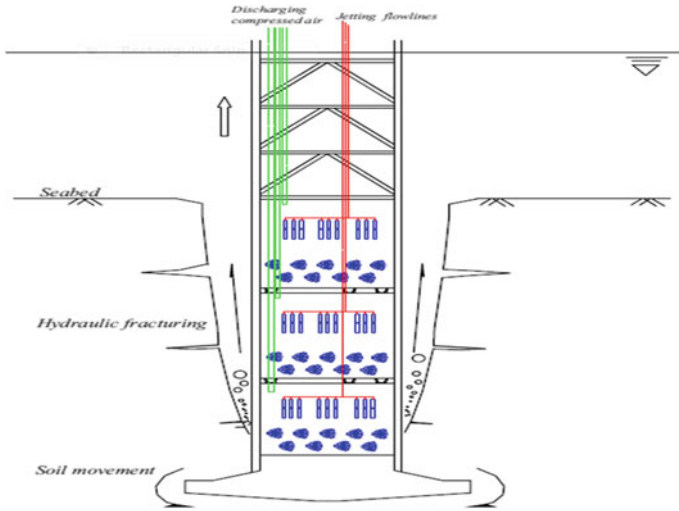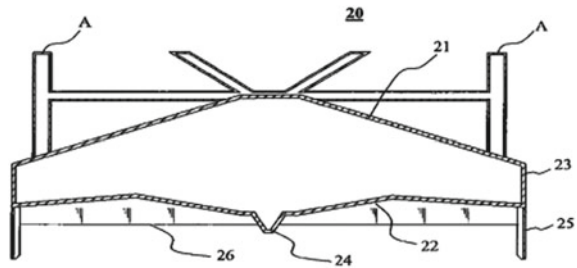
Fig. 7 Spudcan geometry in vertical section with buoyancy module

Fig. 8 Skirted spudcan geometry

3.5 Skirted Spudcans

Geir Swano and team had also worked on various aspects for improving performance of spudcan [5]. L. Kellezi, O. Koreta and S. S. Sundararajan [6] have performed research on various geometry of skirted spudcans and found that skirted spudcan is helpful in providing resistance to penetration and also helps in developing resistance against rotation for the combined VMH loading. It helps in resisting punching shear by providing confinement beneath the geometry inside seabed (Fig. 8).

4 Analytical Methodology

For the purpose of working out most practical and efficient foundation element, the following procedure is adopted. Author had studied the load penetration studies

Table 3 Offshore cohesive soil properties used in current FEM analysis

Soil properties	Value (kN/m^2)
Modulus of elasticity of soil, E	5000
Undrained shear strength of soil, Su	10

by taking jack up structure as intake and varying different foundation element with same pinned connection and rotational stiffness. Here, FEM analysis had been carried out using jack up weight including foundation element. Here, spudcan, skirt plate, mat foundation and oversize mat foundation have been checked with same jack up structure. All foundation elements are taken care of the same geometrical variance. Quantity of material consumption in different foundation element is maintained as constant to the extent possible to achieve economical option. Plaxis 3D FEM tool is used in analysis. Most of FEM elements are considered as planar 6 node plate elements for steel components and 10 node volume elements for soil volume (Table 3).

5 Analytical Results

See Figs. 9 and 10.

6 Plaxis 3D Result for Different Foundation Element Showing Penetration Under Static Condition of Loading in Offshore Cohesive Soil

7 Conclusion and Future Prospects

A. Figure 9 shows load penetration curves with different foundation element in axial compression, i.e., during installation. It indicates under normal condition jack up penetrates will be faster due to lesser initial shear strength of soil. Once it is associated with foundation element, it resists penetration subsequently depending on the geometry of foundation element and confinement provided beneath foundation element in seabed. The sequence of effectiveness of different foundation element is described in representative figure. Axial compression helps in estimation of preload capacity during installation. Once preload capacity is known, then punching shear should be easily avoided. Similarly, Fig. 10 shows jack up with different foundation element in uplift tension which helps in estimation of extraction forces. Figures 9 and 10 are important in developing monogram for specific jack up structure with different foundation element of equivalent dimensions. It helps in its lifecycle operations
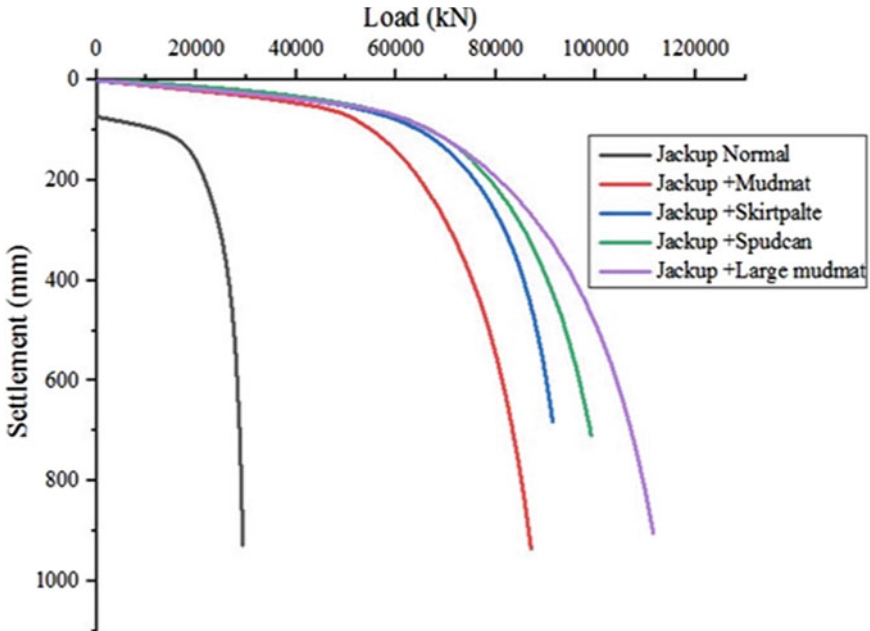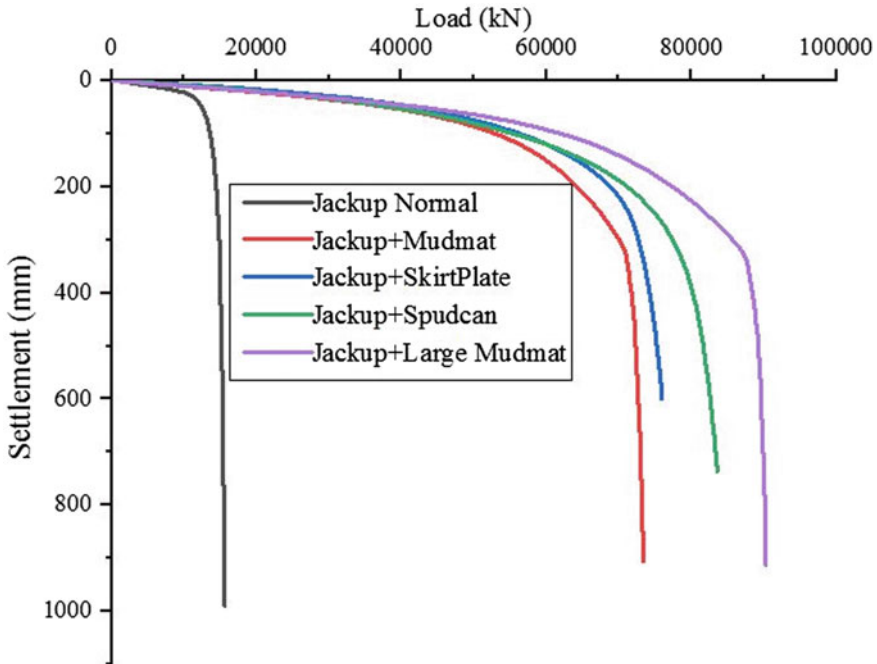
Load settlement curve for jackup with different foundation element
in installtion - axial compression for same airgap throughout

Fig. 9 Load settlement curves for jack up with foundation element in compression

to avoid offshore hazard by correct estimation of installation and extraction
forces (Figs. 11 and 12). Figures 13, 14, 15, 16 subsequently show penetration
records as derived from Plaxis 3D for specific nodes in axial compression for
different foundation elements as described in representative notations for the
figure. Figures 9 and 10 are most important for identical jack up structure in
use for its hazard-free life cycle operation and also in increasing its durability.

B. Here in particular, research papers submitted by various researchers about mat-
supported jack up, eventually researchers have found that mat acts as damper
to the system but no analytical work/ soft computing work has been done to
visualize the same effect. Dynamic analysis of mat-supported jack up legs
embedded in soil will fetch interesting results.

C. More geometrical variations of jack up leg foundation element shapes and
geometry can be studied which confines the soil during penetration or
installation of jack up will also help in mitigating offshore geohazard.

D. More variations in spacing of jack up legs in interaction with soil and
geometrical changes in shape of jack up leg also give fruitful results.

E. As jack up structures are bottom-based floating structure, the maintenance of
air gap, the clear height between the bottom of the deck plate of the jack up and
top of the seabed should also be not in transition zone of the waves to avoid

Load Settlement Curves for Jackup with different foundation element in Extraction - Uplift Tension in Offshore Cohesive Soil

Fig. 10 Load settlement curves for jack up with foundation element in tension

any geohazard. Placement of the hull is important aspect in avoiding hazard. Impacts of air gap during various operations of jack up structures should also be studied.

F. Generally, offshore installations alike jack up study should be carried out in station mode in shallow to deeper water where stability becomes a time-dependent phenomenon. A lapse of time in maintaining the jack up pressure on all legs (as applicable) may govern the conditions of stability studies.
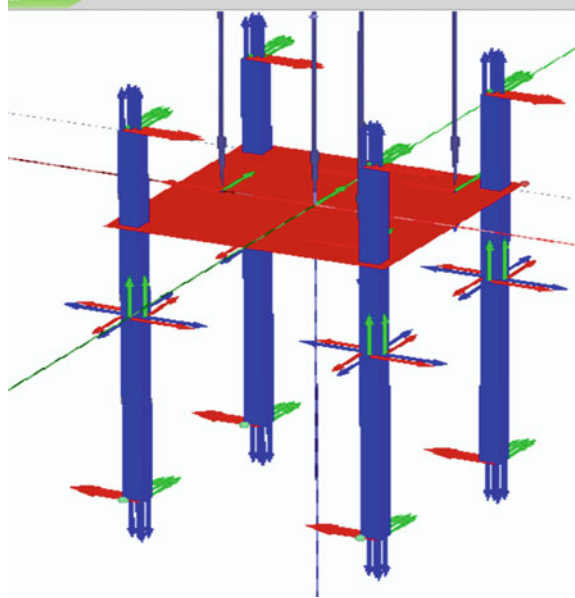
Fig. 11 Normal jackup in operation
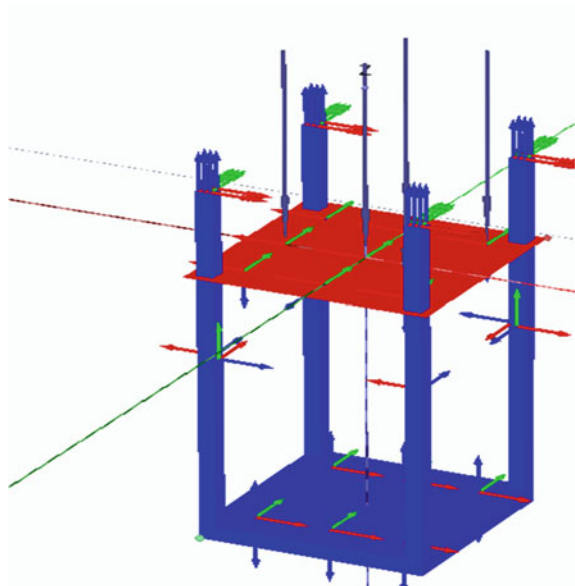

Fig. 12 Jackup with mat
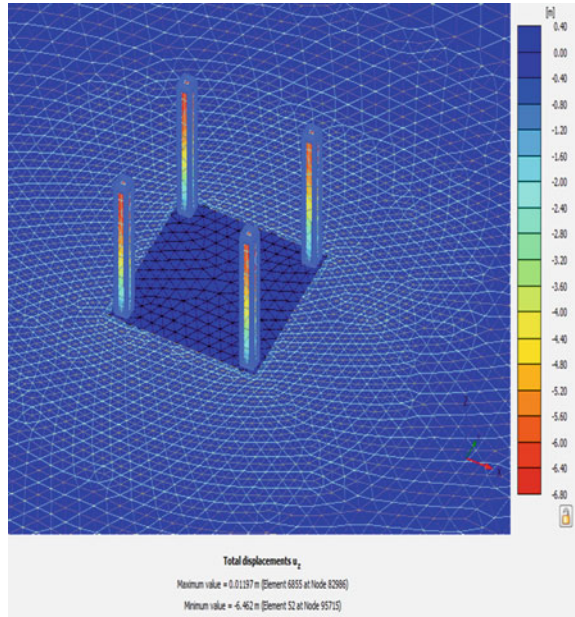
Fig. 13 Jackup penetration of 6.8 m

Fig. 14 Jackup skirt plate penetration of 6.7 m
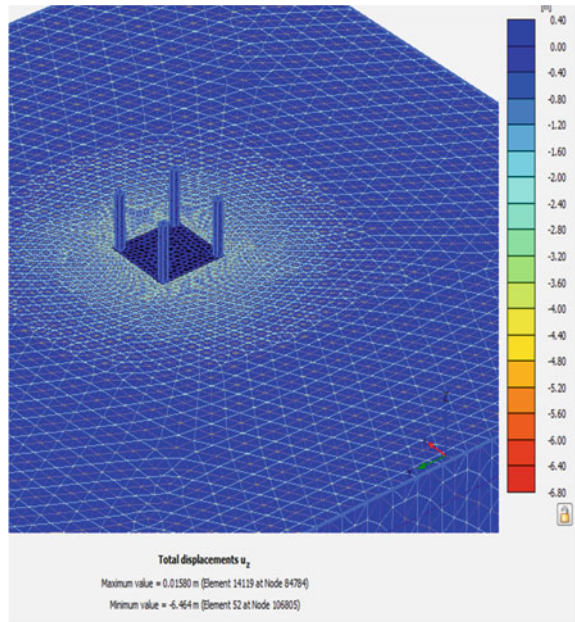
Fig. 15 Jackup spudcan penetration of 6.4 m

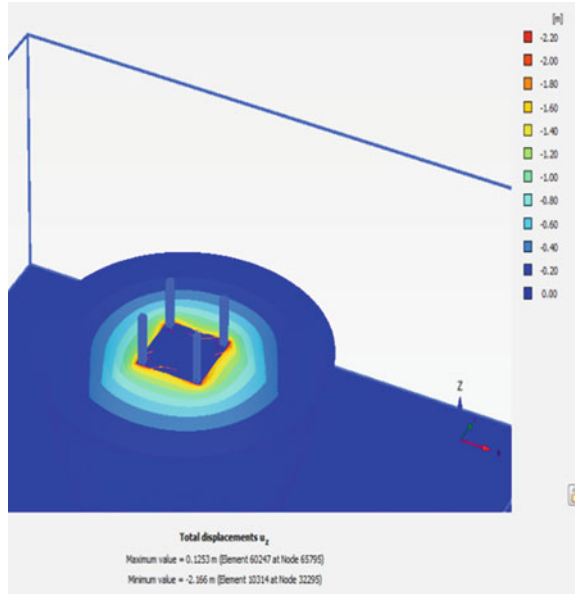**Fig. 16** Jackup mud mat penetration of 6.5 m
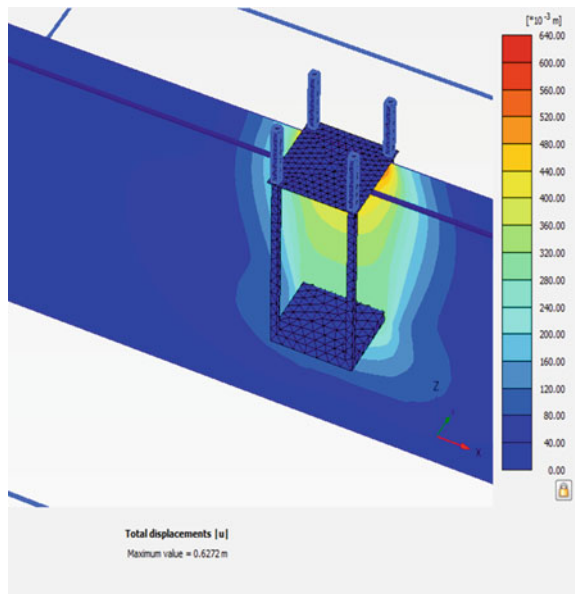
References

1. Scales, R.E.: A deep water mat-supported jack-up drilling unit with tubular telescoping columns and intermediate column frame. In: Offshore Technology Conference 1976, Jan 1. Offshore Technology Conference (OTC2504)
2. Stewart, W.P.: Mat-supported jack-up foundation on soft clay—overturning storm stability. The Jack-Up Platform—September 11th and 12th (2007)
3. Parker, E.J.: Mirabella, F., Paoletti, L.: Case histories paper: jack up rig spud can penetration: a 6000 ton load test, Italy (2008)
4. Zhao, T., Sun, C.: A new spud can with buoyancy modules for mobile jack-up rigs. Appl. Ocean Res. **47**, 154–162 (2014)
5. Svanø, G., Tjelta, T.I.: Skirted spud-cans—extending operational depth and improving performance. Marine Structures **9**(1), 129–148 (1996)
6. Kellezi, L. Koreta O. Sundararajan Geo S.S.: Skirted Spudcan- Soil interaction under combined loading- gap conditions after preloading, Copenhagen, Denmark (2017)

Response to Seismic Effect on Cable Stayed Bridges with Different Cable System Under Consideration of SSI

J. H. Gabra and Atul K. Desai

Abstract The prime aim of the study is to present response to seismic effect on cable stayed bridges with different cable system taking under consideration SSI. It is very much known that Soil Foundation Structure Interaction relies greatly on various factors such as soil and its properties, manner and type of structure and/or its foundation. The factors like the E.Q. induced motions/vibrations are also to be considered as important too. In this paper, the emphasis is on the simplified model and foundation on piles. For the modelling, author has used SAP2000 software. The study includes the response of the bridge modelled towards variation in the cable system under consideration of SSI. Quincy Bayview Bridge is taken as a reference, and six models are created with variation in cable system (ranging from original cable stayed bridge to suspension type, composite bridge and cable stayed suspension hybrid bridge). Soil modelling is done using the spring and dashpots (Kelvin element) for simulation of SSI effects. The results observed that effects of SSI have a substantial impact on selection of cable system for any cable stayed bridges

Keywords Cable stayed bridge · Modal time history analysis (MTHA) · Soil structure interaction (SSI) · SAP2000

1 Introduction

In the current socio-economic criteria, bridges are among the top in the list critical lifeline services. And as such, need of long span bridge has accumulated with boom of infrastructure. The want of unbelievable bridges of lengthy span is amassed after every passing day due to increase in population inhabiting across the globe, leading to increased importance for usage of material(s) with high to ultra-high strength blended with innovative structural system.

J. H. Gabra (✉)
Currently Research Scholar, SVNIT, Surat, Gujarat, India
e-mail: gabrason@gmail.com

A. K. Desai
Applied Mechanics Department, SVNIT, Surat, Gujarat, India

A few captivating and breathtaking bridges have been structured and worked over the most recent couple of decades than at some other similar time throughout the entire existence of development. The systems of cable supported bridges for the most part used to accomplish longer lengths can be easily categorized as cable stayed bridges (CSB's), suspension bridges (SB's), composite bridges (CB's), cable stayed suspension hybrid bridges (CSSHB's).

In normal to garner longer span bridges, CSB's and SB's are preferably selected/provided. CSSHB possesses superiority in preference SB's and/ or CSB's due to the fact it comprises advantages of each cable stayed nonetheless as suspension bridges.

Bridge, being long to super long structures for communication, its failures may/can lead to great and higher level of damage and loss to life and material comparable to that of catastrophic failures. This booms in the concept of prevention of such catastrophic accidents which may be possible by properly understanding the reasons that result(s) in failure of bridges.

Reasons for Failures of Bridges
The top and foremost reasons because of bridges become seriously compromised or collapse can be categorically listed as.

- Failures occurring during construction
- Failure occurring while bridge in service (in absence of any external action)
- Collapse in event of impact (may be due to collision)
- Failure caused due to onset of cyclone, tsunami, hurricane, flooding, ice or other floating objects; fire or explosion; *seismic activity*; falsework; incompetent design
- Combination of more than one of above

As a summary, causes commonly attributing to failures of bridge can be classified in a broader sense as: basic and plan inadequacies, erosion, development and supervision botches, unintentional over-burden and its effect, scour, & absence of upkeep or review.

Prevention is the best than cure concept leads to the methodology reflecting best way to avoid bridge failures. This attitude incorporates the concept of expecting them (failures) to happen and plan for them. It proves to be one of the ways to protect the public from injuries, loss of life, property damage and destruction. This enhances the interest in learning about ways to improve and update /upgrade bridge design and quality of construction and constructional practices adopted.

1.1 Soil–Structure Interaction (SSI)

Thus, seismic soil–structure interaction (SSI, hereafter) plays an important element in the understanding of seismic structure failure. The damage caused with foundation of bridges in earthquake(s) has emphasized the importance of understanding SSI

compared to free-field motions. Soil–structure interaction (SSI) thus is an important issue and must not be ignored in the seismic design of important structures including bridges. Thus, SSI, a complicated phenomenon [1], involving wave amplification—Seismic waves alter due to flexibility of soil, kinematic response—Soil displacement is causing structure to displace, Inertial Reactions—Stress movement continues and adds to displacement of structure.

This procedure (named SSI), in which the reaction of the soil impacts the movement of the structure and the movement of the structure impacts the reaction of the soil, presumes that both, soil and structure, are associated and not independent from one another.

SSI can be sub-categorized [2] as static SSI and kinematic or dynamic SSI. Also, soil–structure interaction [3, 4] can be broadly divided into two phenomena: Kinematic interaction and Inertial interaction.

Effects Soil–Structure Interaction (SSI)
SSI changes the dynamic qualities of the structural reaction essentially. These impacts were disregarded in the past; however, because of the failure of such huge numbers of enormous structure during seismic tremor occasion, the essentialness of SSI was figured it out. In this manner, SSI is given significance, and bunches of research work are proceeding to think about the impacts of SSI on different structures are condensed as

Alter the Natural Frequency of the Structure And Damping
Through the Soil Interaction effects
Travelling Wave effects.

2 Literature Survey

Examinations were completed in different investigations with respect to the impact of SSI on the tremor reaction of a few ordinarily structured extensions lately.

Spyrakos [5, 6] demonstrated that SSI enormously influences the seismic reaction of bridges driving towards progressively adaptable frameworks and expanded damping by using basic models which are linearly flexible.

Ciampoli and Pinto [7] explored on parametric examination on traditionally structured bridges established on shallow establishments thinking about inelastic reaction of the piers. Information of Eurocode good falsely produced accelerograms (far field excitations) was considered and reasoned that SSI impacts reliably diminished the pliability requests of the piers when contrasted with the system without SSI impacts.

Jeremic et al. [8] contemplated in detail the seismic reaction of the I-880 viaduct in Oakland, Calif. To conclude that "SSI can have both beneficial and detrimental effects on the response of the structure depending on the characteristics of the ground motion".

Zhang [9] conducted investigation on the effect of SSI on the response of 9/15 overcrossing in Los Angles and abstracted that ignoring SSI would lead to an underestimation of seismic forces.

Tongaonkar and Jangid [10] assessed the effects of SSI on three-span continuous deck bridges isolated with elastomeric bearings. They performed MTHA, assuming linear elastic behaviour for the isolation system and the piers of the bridge to conclude that consideration of SSI in the analysis will result in the enhancement of safety and reduction in design costs. They supplemented that under certain circumstances, isolation bearing displacements at abutment locations only might be underestimated if SSI is not accounted for in the analysis.

Mylonakis and Gazetas [11] took in thought a lot of real acceleration time histories recorded on delicate soil, utilizing an improved model for the bridge and its foundation, and presumed that the period protracting and expanded damping due to SSI impacts can detrimentally affect the forced seismic demands.

Examination Between Three Types of Cable Stayed Bridges Using Structural Optimization. In his work, a progressed and extensive numerical model was utilized to get the post-tensioning forces and the ideal structure of the three sorts of link/cable stayed bridge. The numerical technique dependent on limited component, B-spline bends and genuine coded hereditary calculation was embraced. The improvement represents every one of the factors that characterize the geometry and cross-segment of the bridge. Correlation between the three sorts, as far as post-tensioning forces and cost, was completed.

Siddharth Shah et al. [1] have given investigation in which spotlight is given on the impact of pylon's shape on the seismic reaction of cable stayed bridge. The examination uncovers that the pylon's shape has extraordinary impact in the seismic reaction of cable stayed bridge. Spread shape of the pylon is better for opposing seismic tremor longitudinal direction however feeble sidelong way, yet pyramid shape of the pylon is better as a result of its geometry in opposing quake power from any direction, and furthermore, SSI impacts are least for this situation. SSI impacts are transcendent for delicate soil conditions for all shapes of the pylon.

Zhang et al. [12] summarized that forces in the cables are significant in design of cable stayed bridges. By investigating a basic auxiliary system, the methodology utilizing the examination program MiDAS was delineated. The model was generated for the completed dead stage examination was outlined in detail, including the boundary and load combinations. The streamlining technique for unknown load factor was utilized to decide the forces in the cables to accomplish a perfect state. The perfect cable force is built up, and a development stage analysis is performed. The greatest cable forces were demonstrated to be in limits permissibility. The outcomes got uncovered that the technique exhibited for sure prompts ideal performance of the structure for the cable stayed bridge specifically and may be a valuable reference for the plan of other comparable bridges.

Wilson and Gravelle [13] studied modelling of a cable-stayed bridge for dynamic analysis and in their study, provide a detailed description of the development of one class of linear elastic finite element model for the dynamic analysis of a cable-stayed bridge. The bridge modelled in this study is the Quincy Bayview Bridge in Illinois..

2.1 Introduction to the Software

In the present study, the software used is SAP2000 v 20.2.1. It is a product of CSI, Berkeley, USA. It is used for analysing general structures ranging from bridges to stadiums, dams to industrial buildings, offshore to onshore structures, soil, etc. It has fully integrated programme that allows model creation, editing (modification), execution of the analysis, design optimization, review of results, etc., from within a single interface.

SAP2000 is a comprehensive and integrated design and finite element analysis tool. It offers features like.

- Multiple coordinate system; powerful graphical display
- Frame, cable and shell structural elements
- Wide range and variety of loading options including loading functions of time history, response spectrum, etc.
- Static and dynamic analysis; linear and nonlinear analysis; dynamic seismic analysis and pushover analysis; geometric nonlinearity including P-δ effect; nonlinear link and support analysis
- Frequency dependent link and support properties

3 Problem Studied

B.1 Quincy Bayview Bridge (Type I CB)
In the present study, a cable stayed bridge considered is similar to Quincy Bayview Bridge.

The Quincy Bayview Bridge, shown in Fig. 1, above was designed in 1983, and construction was completed in 1987. The bridge consists of two H-shaped concrete towers, double-plane fan type cables and a composite concrete-steel girder bridge
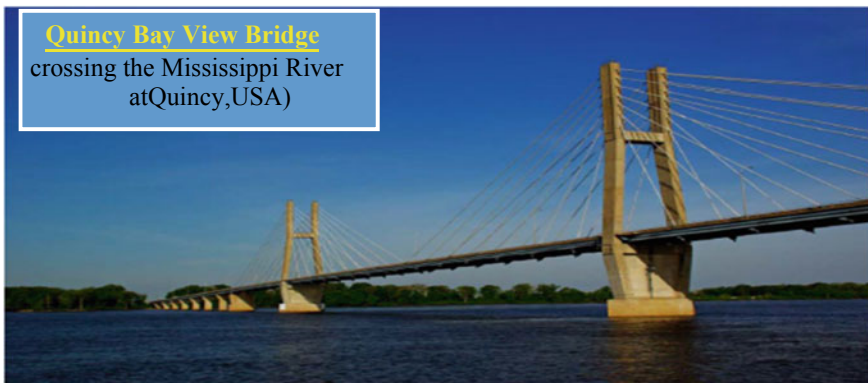

Quincy Bay View Bridge
crossing the Mississippi River atQuincy,USA)

Fig. 1   Quincy Bayview Bridge

deck. The main span is 900 ft (274 m), and there are two equal side spans of 440 ft(134 m) for a total length of 1780 ft (542 m). The tops of the towers are 232 ft (71 m) from the waterline. There are a total of 56 cables, 28 supporting the main span and 14 supporting each side span. The width of the deck from centre to centre of cables is 40 ft (12 m).

A typical cross section of the actual bridge deck is shown in Fig. 2. It is a simplified deck cross section between anchor points that was used to evaluate physical properties for the model. The road deck is a 9 in. precast post-tensioned concrete slab 46.5 ft wide with two non-structural precast parapets (traffic barriers). Five longitudinal steel stringers are spaced at equal transverse intervals of 7.25 ft. Floor beams transverse to the main girders at equally spaced intervals of 30 ft transfer stringer loads to two main girders at the outer edges of the deck. The cables are connected to the deck at the bottom flange of the main girders.

Each tower consists of two concrete legs, with dimensions of 14.5×7 ft (the larger dimension is in the longitudinal direction of the bridge), a lower strut (crossbeam) supporting the deck and an upper strut connecting the upper legs. There are three changes in the leg cross section over the height of the towers.

To avoid expansion joint, the bridge is modelled with roller joint supports at cantilever end (side spans), whereas the deck pylon support is roller and hinged support, respectively, along the longitudinal direction.

B.2 Quincy Bayview Bridge (Type II CSB)

This is a bridge with modified cable system, hence called composite bridge (Type II CSB) hereafter.

In this, the central span is converted to SB, whereas the side spans are cable stayed as shown in Fig. 3b hereafter. The material for hangers as well as suspension cable is same as that of stays. However, the diameter of suspension cable is taken as 0.4 m @ 9.613 kN/m, whereas hangers are of 0.1069 m diameter @ 0.263 kN/m, respectively. Sag to central span ratio is taken as 1/6. The hangers are placed/connected to deck at same respective location(s) where cable stays were connected to the deck in the originally designed CSB. The side spans are same as original CSB with 14 stay cables on each side as depicted in Figs. 2 and 3b, respectively.

B.3 Quincy Bayview Bridge (Type III CSB)

This is again a bridge with a modified cable system, hence called composite bridge (Type III CSB) hereafter. In this, the central span is converted to CB, whereas the side spans are cable stayed as shown in Fig. 3c.The material for hangers as well as suspension cable is same as that of stays. However, the diameter of suspension cable is taken as 0.4 m @ 9.614 kN/m, whereas hangers are of 0.1069 m diameter @ 0.631 kN/m, respectively. The hangers are placed/connected to deck at same respective location(s) where cable stays were connected to the deck in the originally designed CSB (side spans). There are a total of 28 cables in the central span with hangers spaced at 19 m c/c in the side span (suspension type).
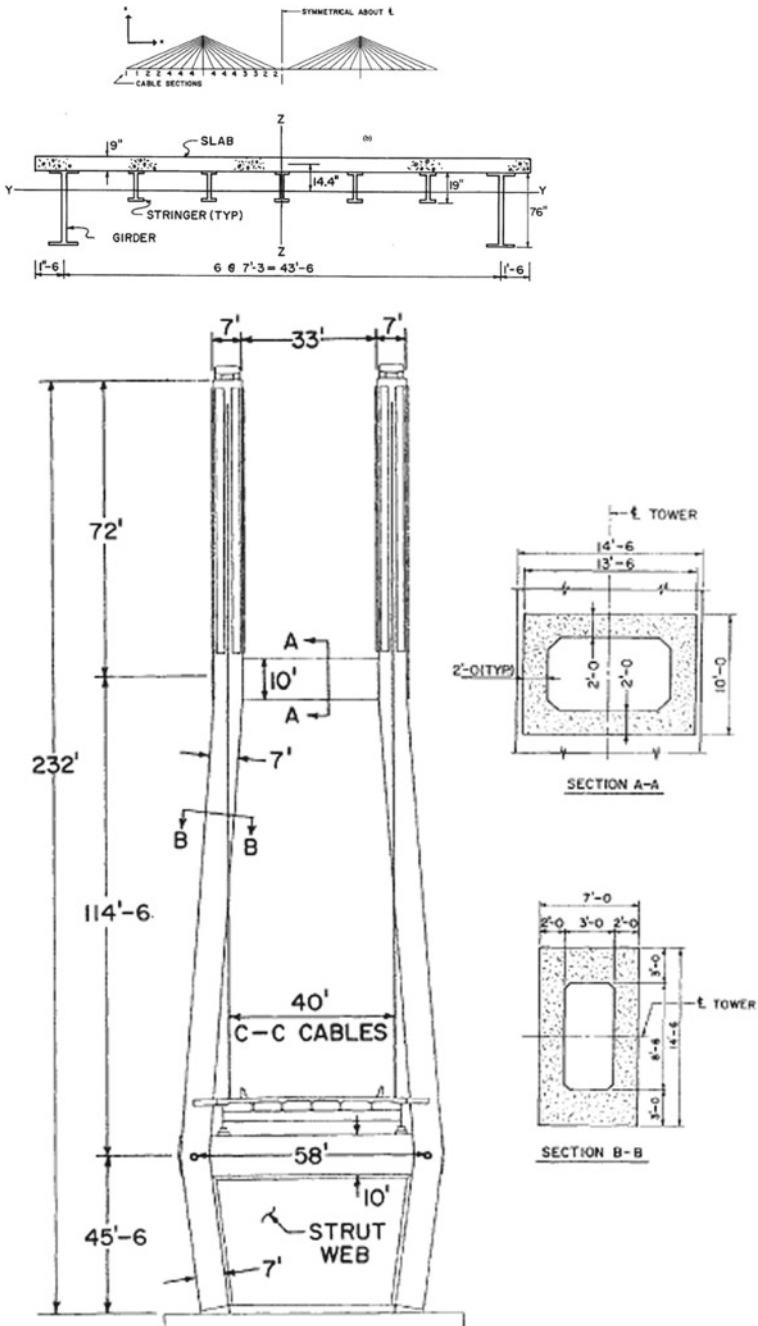
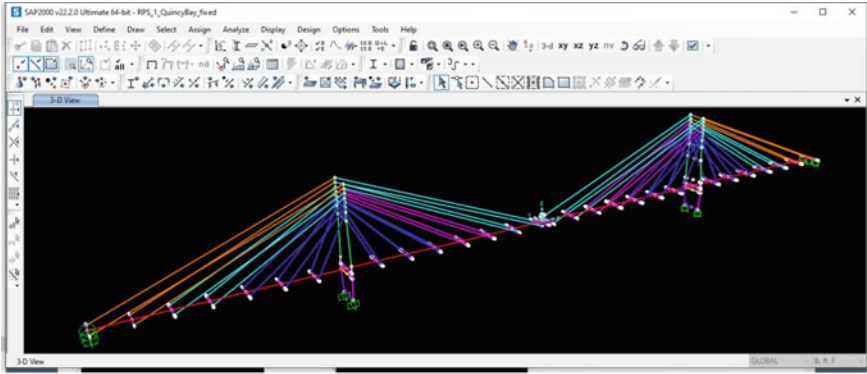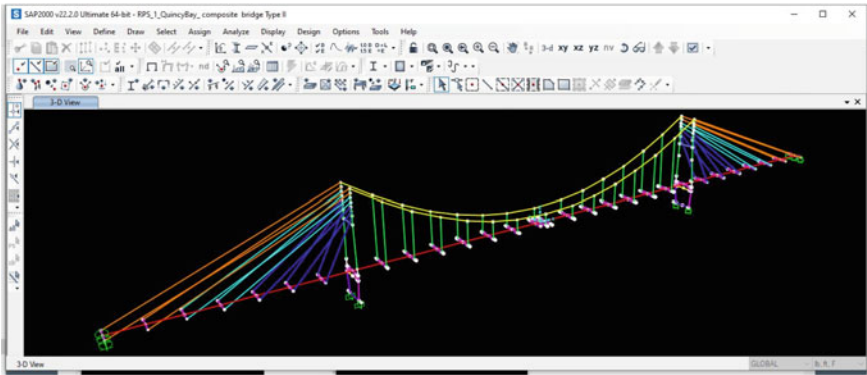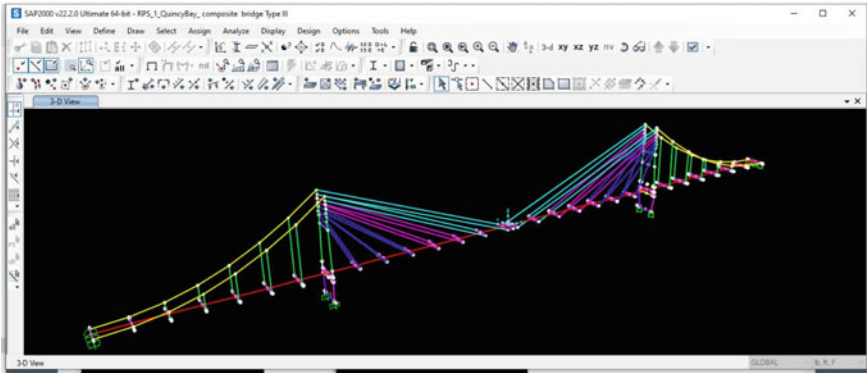**Fig. 2** Elevation, c/s and cable system of Quincy Bayview (Type I) [13]

a)CB Type I
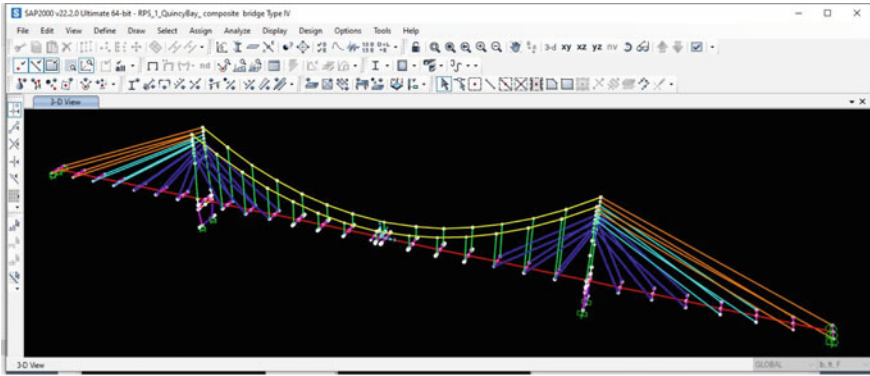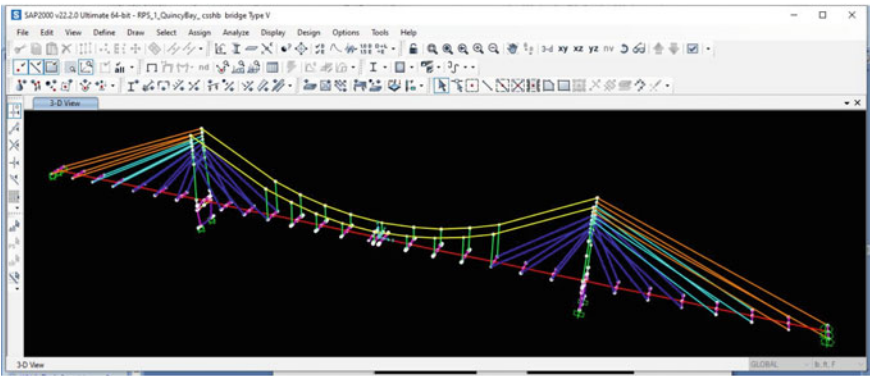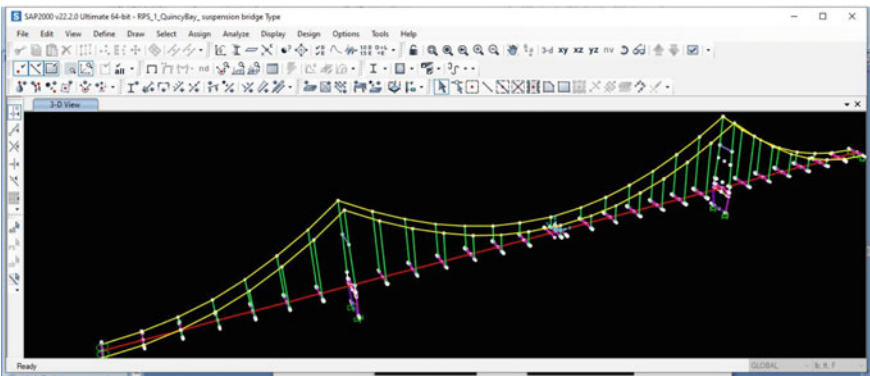

b) CSB Type II

c) CSB Type III

Fig. 3 Bridges with different cable systems

d) CSB Type IV

e) CSSHB Type V

f) SB Type VI

Fig. 3 (continued)

B.4 Quincy Bayview Bridge (Type IV CSB)

In this, the central span is converted to CB, whereas the side spans are cable stayed as shown in Fig. 3d hereafter. The material for hangers as well as suspension cable is same as that of stays. However, the diameter of suspension cable is taken as 0.4 m @ 9.614 kN/m, whereas hangers are of 0.1069 m diameter @ 0.631 kN/m, respectively. Sag to central span ratio is taken as 1/6. There are a total of 28 cables in the side spans and 12 in the central suspension portion with hangers spaced at 19 m c/c in the central span throughout. In the central span, the deck is further stiffened by providing three cable stays on each side, i.e. total 12 cable stays as shown in Fig. 3d.

B.5 Quincy Bayview Bridge (CSSHB type)

In this, the central span is converted to CB, whereas the side spans are cable stayed as shown in Fig. 3e hereafter. The material for hangers as well as suspension cable is same as that of stays. However, the diameter of suspension cable is taken as 0.4 m @ 9.614 kN/m, whereas hangers are of 0.1069 m diameter @ 0.631 kN/m, respectively. Sag to central span ratio is taken as 1/6. The hangers are provided at same points where there were stay cables in CB type, i.e. hangers are placed @ 19 m c/c.

B.6 Quincy Bayview Bridge (Suspension Bridge—SB type)

In this, the bridge is modelled by converting it to SB as shown in Fig. 3f hereafter. The material for hangers as well as suspension cable is same as that of stays. However, the diameter of suspension cable is taken as 0.4 m @ 9.614 kN/m, whereas hangers are of 0.1069 m diameter @ 0.631 kN/m, respectively. Sag to central span ratio is taken as 1/6. There hangers are placed at the same points where cable stays were attached to girder in case of original Quincy Bayview CB (i.e. with hangers spaced at 19 m c/c).

C1 Modelling of Bridge Structure

CSB like any other structure is divided into two main components namely super-structure and sub-structure. For finite element modelling of CSB, properties of material used and sections considered are entabulated in subsequent tables below. The finite element is developed using properties of material and section entabulated in Table 1 (Figs. 4 and 5).

C2 Modelling of Soil

The interaction between the pier footing and the soil is modelled using translational and rotational springs (Figs. 6 and 7) [1, 14].

The spring coefficients have been computed by the method suggested in Specification for Highway Bridges issued by Japan Road Association. In the suggested method, it should be mentioned that, when using Eqs. (1) and (2), the units of B_e and E must be centimetres and kgf/cm^2 (1 kgf/cm^2 = 98 kPa), respectively. The horizontal and rotational spring coefficients for each part of foundation are obtained by multiplying k by the area and the inertia moment of its surface perpendicular to the excitation direction, respectively. As for the bottom face of foundation, the soil reaction coefficient per unit area in horizontal direction is taken as 1/3 of *k*.

Table 1 Material used, cables and sections considered

Property	Steel	Concrete
Modulus of elasticity (E)	2.1×10^8 kN/m^2	2.985×10^7 kN/m^2
Unit weight	76.973 kN/m^3	24.993 kN/m^3
Poisson's ratio (μ)	0.3	0.25
Shear modulus (G)	8.077×10^7 kN/m^2	1.232×10^7 kN/m^2
Coeff. of thermal Expansion (α)	1.17×10^{-5}	0.55×10^{-5}

(a) Material used

Cable No.	Diameter (m)	Area (m^2)	Cable weight (kN/m)
1	0.1069	8.918×10^{-3}	0.686
2	0.0946	6.984×10^{-3}	0.537
3	0.0827	5.337×10^{-3}	0.411
4	0.0666	3.416×10^{-3}	0.263

(b) Cables used
(c) Sections considered

Component	Dimension	Material	Shape
Deck end beams	$h = 1.90$ m, bf $= 0.62$ m tf $= 0.08$ m, tw $= 0.04$ m	Steel	I- section
Deck Stringer beams	$h = 0.50$ m, bf $= 0.32$ m tf $= 0.02$ m, tw $= 0.01$ m	Steel	I-section
Stiffening wall	1.2 m thick	Concrete	Rectangular
Pylon bottom	(2.1336×4.4196)	Concrete	Solid rectangular
Pylon intermediate	(2.1336×4.4196)–0.9144 m dia hole	Concrete	Hollow rectangular
Pylon intermediate	(2.1336×4.4196)–(0.7897×0.9144) m	Concrete	Hollow rectangular box

$$k_0 = 1.2E/30 \tag{1}$$

$$k = k_0^{-0.75}\sqrt{B_e/30} \tag{2}$$

where

k_0 reference soil reaction coefficient,
E Young's modulus of elasticity for sil,
K the soil reaction coefficient per unit area,
B_e the width of foundation perpendicular to the considered direction.
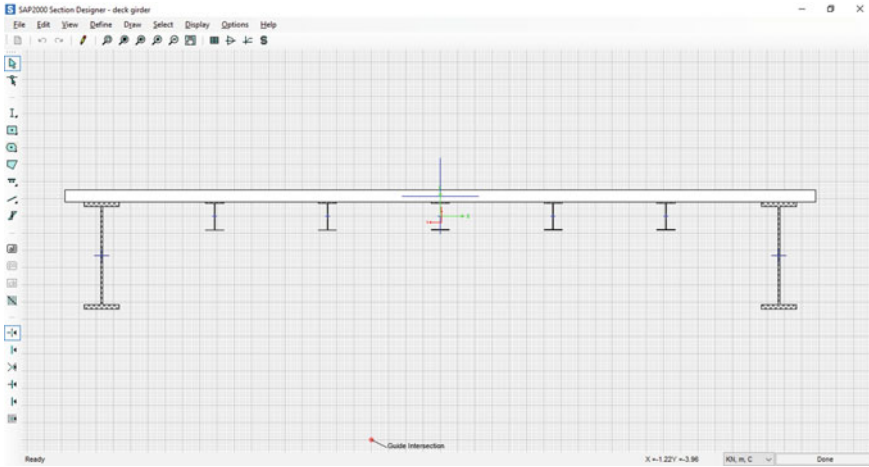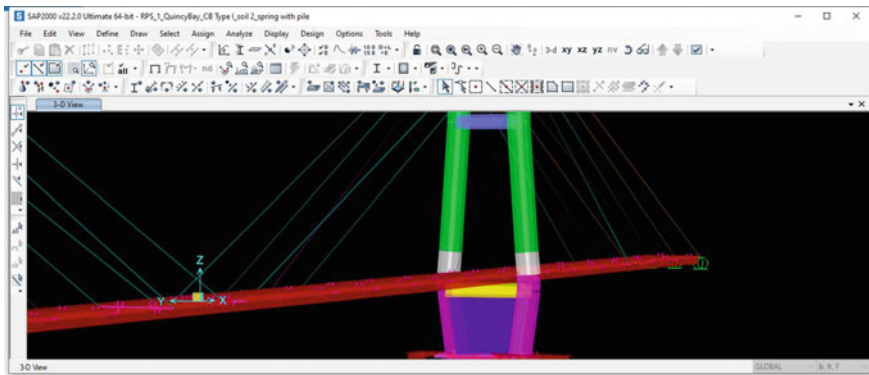
Fig. 4 C/s—deck girder

Fig. 5 3-D extruded view of pylon, Trans verse beams and stiffening walls

Three types of soils are in this study designated as soil type I, II, III in the Table 2.

C3 Details of acceleration Time History

- Name: Bhuj
- Magnitude: 7.7
- Duration: 133.53 s
- Peak Ground Acceln.: 1.0382 m/s^2
- Total No. of Acceln. records: 26,706.
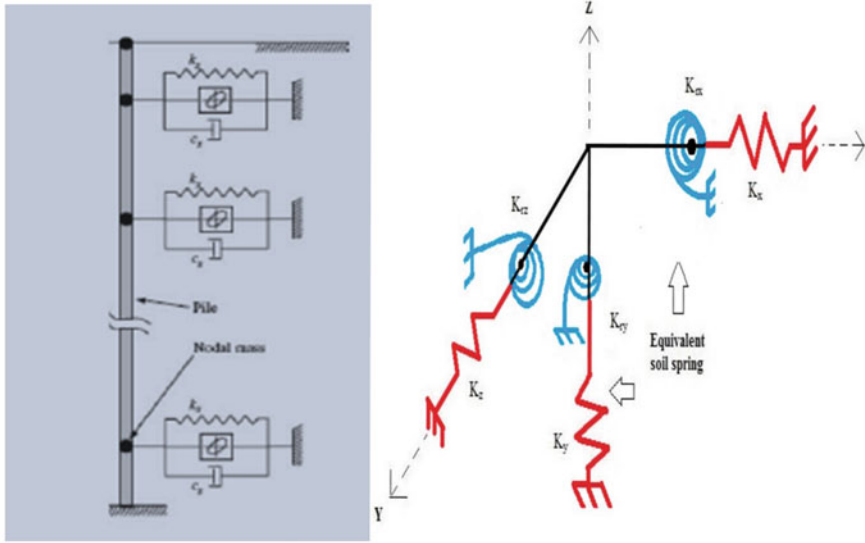
Fig. 6 Modelling of soil as spring and dashpot

Fig. 7 Soil 1 (hard clayey) modelled (Kelvin Element) applied at nodes of pile [14]. Adopted from Soneji and Jangid (2009)
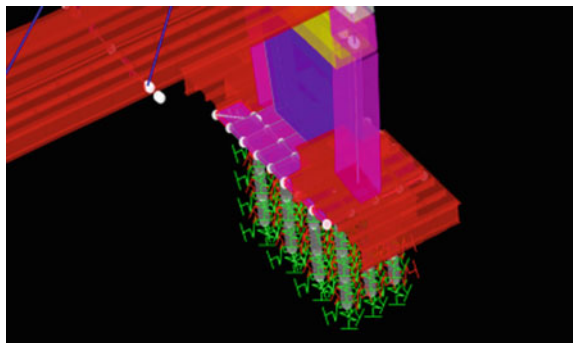
4 Analysis and Results

For evaluation of the seismic response, using Bhuj Earthquake near fault data, time history analysis (THA) was performed first on Quincy Bayview cable stayed bridge (CB_Type 1). This was followed subsequently on various bridges modelled as shown in Fig. 3. All the models are analysed subsequently to study the impact with and without SSI. For ascertaining SSI, three types of soils are considered as mentioned previously. The piles up to depth of 20 m are considered for all models (for SSI). Result(s) in Table 3 clearly reflect that bridge modelled (Quincy Bay) in the SAP2000 gives the results which are found similar with results presented in the literature (research paper referred)..

Table 2 Different properties including lateral and rocking stiffness coefficients [1]

S. No.	Soil properties	Soil I: Hard Clayey soil	Soil II::Soft Silty Soil	Soil III: Med Sandy soil
1	Unit Wt., Υ, kN/m^3	20	18	19
2	Shear strength, τ_s, kN/m^2	200	75	150
3	Poisson's ratio	0.3	0.4	0.35
4	Damping of soil, ξ	0.02	0.06	0.04
5	Shear Wave Velocity, V_s (m/s)	1050	83	309
6	Shear Modulus, G, kN/m^2	269×10^4	12,500	192,310
7	Young's Modulus, E, kN/m^2	700×10^4	35,000	500×10^3
8(a)	Soil stiffness, K_x (kN/m)	252×10^4	4.60×10^4	8.62×10^4
8(b)	Soil stiffness, K_y (kN/m)	1050×10^4	5.52×10^4	10.3×10^4
8(c)	Soil stiffness, K_z (kN/m)	1028×10^4	5.36×10^4	10.0×10^4
8d)	Soil stiffness, $K_{\theta x}$ (kN/m/rad)	8094×10^4	156×10^4	292×10^4
8e)	Soil stiffness, $K_{\theta y}$ (kN/m/rad)	309×10^4	21.6×10^4	40.4×10^4
8f)	Soil stiffness, $K_{\theta z}$ (kN/m/rad)	9808×10^4	532×10^6	729×10^6

Table 3 Time Period (first mode—CB Type I) different researchers

Modes	Paper results (Wilson and Gravelle)		Our results (SAP2000)		% Error	
	T (s)	f (Hz)	T (sec)	f (Hz)	T (sec)	f (Hz)
Mode-1 (lateral)	2.695	0.371	2.821	0.354	4.67	−4.58

The results of seismic time history analysis are entabulated in Table 3 for 24 cases (bridge and soil type). Table 4 demonstrates the change in time period with change in stiffness of soil underneath.

5 Conclusion

The results of seismic time history analysis are entabulated in Table 3 for 24 cases (bridge and soil type). Table 4 demonstrates the change in time period with change

Table 4 Modal time periods: bridges

1st Mode time PD, Sec., for different cases (soils)

[for 20 m depth of piles (foundation)]

Bridge type	W/O SSI	With SSI					
	(fixed base)	Soil I	% change	Soil II	% change	Soil III	% change
CB Type I	2.8214	2.3981	−15	2.4107	14.56	2.4002	−14.93
SB	3.9046	4.6735	19.69	4.6821	19.91	4.6774	19.79
CSB Type II	3.89	4.6495	19.53	4.6512	19.57	4.6498	19.53
CSB Type III	2.8291	2.4735	−12.57	2.5701	−9.16	2.4784	−12.4
CSB Type IV	3.028	3.6271	19.79	3.6328	19.97	3.6299	19.88
CSSHB Type	3.1958	3.8265	19.74	3.8312	19.88	3.8287	19.81

in stiffness of soil underneath. It depicts that the trend of change in time period (1st mode) follows almost the same trend with respect to bridge type for various cases. The increase in max in case of suspension bridge type (SB) and composite bridge type II (CSB) has a decreased time period in case of CSSHB type.Thus, SB and CSB type II have proved to be more flexible (has decreased stiffness) when compared to cable stayed bridge. Composite bridge type IV has more or less same stiffness, while CSSHB bears stiffness between CB and SB.

References

1. Shah, S.G., Solanki, C.H., Desai, J.A.: Effect of pylon shape on seismic response of CSB with SSI. IJSE **1**(3), 2010 (2010)
2. Kausel, E.: Early history of soil–structure interaction. Soil Dyn. Earthquake Eng. **30**(2010), 822–832 (2010)
3. Kramer, S.: Impact of soil-structure interaction on response of structures. EERI Technical Seminar Series
4. Stewart, J.P.: EERI; overview of soil-structure interaction principles
5. Spyrakos, C.C.: Assessment of SSI on the seismic response of short span bridges. Eng. Struct. **12**(1), 60–66 (1990)
6. Spyrakos, C.C.: Seismic behaviour of bridge piers including soil-structure interaction. Comput. Struct. **4**(2), 373–384 (1992).
7. Ciampoli, M., Pinto, P.E.: Effects Of Soil-Structure Interaction on inelastic seismic response of bridge piers. J. Structural Eng. ASCE **121**(5), 806–814 (1995)
8. Jeremic, B., et al.: Soil-foundation-structure interaction effects in seismic behavior of bridges. In: 13th World Conference on Earthquake Engineering Vancouver, B.C., Canada, 1–6 Aug 2004 Paper No. 294 (2004)
9. Makris, N.M., Zhang, J.: Seismic response analysis of a highway overcrossing equipped with elastomeric bearings and fluid dampers. J. Struct. Eng. **130**(6), 830–845 (2004)
10. Tongaonkar, N.P., Jangid, R.S.: Seismic response of isolated bridges with soil–structure interaction. Soil Dyn. Earthq. Eng. **23**, 287–302 (2003). https://doi.org/10.1016/S0267-7261(03)00020-4
11. Mylonakis, G., Gazetas, G.: Seismic soil-structure interaction: beneficial or detrimental? J. Earthquake Eng. **4**(3), 277–301 (2000). https://doi.org/10.1080/13632460009350372

12. Zhang, T., et al.: Dead load analysis of Cable-Stayed Bridge. In: 2011 International Conference on Intelligent Building and Management Proceedings of CSIT, vol .5. IACSIT Press, Singapore (2011)
13. Wilson, J., Gravelle, W.: Modelling of a cable-stayed bridge for dynamic analysis. Earthquake Eng. Structural Dyn. **20**,707–721 (1991)
14. Jaangid, R.S., Soneji, B.B.: Passive hybrid systems for earthquake protection of Cable Stayed Bridge. Eng. Structures **29**(1), 57–70 (2007)

Potential of Vibration Studies for Soil Characterization Around Proposed High-Speed Track Near Surat City

P. S. Rao, Atul K. Desai, and C. H. Solanki

Abstract High-speed corridors are necessary for national growth and hence are inevitable for the economic development of the country. The level of train-induced ground vibrations depends on various factors including the wave propagation at a site based on type of soil. Due increase in population, industrialization, and lack of space in the urban areas, numerous buildings are constructed near the vicinity of the railway tracks. Thus, dynamic analysis of such structures to evaluate its response to dynamic stresses induced due to train is finding increased application in civil engineering practice. In this study, the ground vibrations and its attenuation during the operation of the train at various frequencies is considered. The finite element modeling for the dynamic analysis is tackled here using conventional modeling capabilities normally available in most of the finite element programs. In this study, the computer program SAP2000 (CSI, 2000) is used for modeling. The passage of train over the track structure considered is idealized as a sinusoidal harmonic load. As vertical amplitude attenuates less and continues to exist for large distances compared to the horizontal amplitudes, vertical components are selected for the study. The vibration through the soil is found to follow the Bornitz equation, and thus, the attenuation coefficient for material damping is determined.

Keywords Bornitz equation · High-speed train · Attenuation

1 Decay of Motion in Soil Medium

Considering motion of train harmonic and sinusoidal in nature, if harmonic sine load is applied to a point load resting on an initially unloaded elastic medium, three types of waves will originate from the loading point. One is a surface wave whose horizontal and vertical amplitude decreases exponentially normal to the surface,

P. S. Rao (✉)
A. P. Shah Institute of Technology, Mumbai University, Thane, India
e-mail: poojasrao.brd@gmail.com

A. K. Desai · C. H. Solanki
Sardar Vallabhbhai Patel National Institute of Technology, Surat, India

while, in the far field, it decreases with distance along the surface at a rate inversely proportional to the square root of the surface distance. These waves are commonly known as Rayleigh (R) wave. The other two waves are termed as body waves, one of which propagates at the longitudinal wave speed of an elastic solid commonly known as primary (P) wave, and the other body wave travels at the shear wave speed of the medium and is known as shear (S) wave. Both body waves fall off in amplitude inversely proportional to the spherical distance from the source point when monitored in the interior of the elastic space. The Rayleigh waves propagate radially outward along a cylindrical wave front. The vertical ground displacement due to the Rayleigh wave arrival is much greater than that for P- and S-waves. Since P-waves are the fastest, they will arrive first followed by S-waves and then the Rayleigh waves. Out of these, Rayleigh waves carry a much larger portion of the total input energy about 67% compared to shear waves or primary waves which carry about 26% and 7%, respectively.

Maximum destruction caused to the nearby structures by vibratory energy is carried by Rayleigh (surface) waves traveling from the source of vibration. Generally, the decay or attenuation of vibrations with surface comprises of two factors namely geometric damping and material damping. A portion of this attenuation is caused by the distribution of constant amount of vibration energy on continuously increasing area of wave front. This type of damping is termed as radiation/geometric damping. The geometric damping depends on the type and location of the vibration source, and on the other hand, material damping is related with ground properties and vibration amplitude.

Mathematically, radiation or geometric damping is usually described by the following equation [1].

$$A_2 = A_1 \cdot \left[\frac{R_1}{R_2} \right]^n \tag{1}$$

where A_1 is the amplitude of vibration at distance R_1 from the source, A_2 is the amplitude of vibration at distance R_2 from the source, and n is the decay or attenuation coefficient due to geometrical damping. The value of attenuation coefficient, n, depends on the type of seismic wave, the location, and type of the source as given in Table 1.

Decay in the amplitude or vibration energy of the seismic waves is also associated with the material damping capacity of the geomaterials. Since soil is not perfectly elastic, the vibration energy is reduced due to friction and cohesion between the soil

Table 1 Attenuation geometric damping factor (n) with the source on the surface [2]

Source type	Induced wave	n
Point	Body wave	2.0
	Surface wave	0.5
Infinite line	Body wave	1
	Surface wave	0

particles. The decay or attenuation due to material damping is affected by the soil type and frequency of vibration [3]. The combined effect of radiation damping and material damping can be described by the following equation.

$$A_2 = A_1 \left[\frac{R_1}{R_2} \right]^n e^{-a[R_2 - R_1]} \tag{2}$$

where a is known as decay or attenuation coefficient due to material damping. Equation (2) is known as Bornitz equation and is used when amplitude of vibration is known at a small distance 'R' from the source. Damping of any vibrating system is a complicated parameter and comprises of two parts, namely material damping which is due to the hysteresis effect on the material and radiation damping due to dissipation of energy within the unbounded soil medium.

Material damping of soil ranges between 1 and 10% of the critical damping depending on material type, whereas radiation damping depends on several factors, and its value can be as high as 50% of the critical damping. Based on the results of measurement of man-made ground vibrations, researchers [4] have reported recommended values of attenuation coefficient 'a' for soil materials. Values of 'a' recommended by [4] for two values of vibration frequency (5 and 50 Hz) are given in Table 1. Subsequently [2] provided ranges of blow count values N_{SPT}, for each of the four classes of soils which are also included in Table 2.

Alternatively, considerably conservative results are obtained if it is assumed that the absorption coefficient linearly depends on frequency. Wave propagation due to train vibrations generates low strains where the soil can be assumed as a linear elastic medium. The nonlinear behavior of the soil is often neglected when the shear strain is $<10^{-5}$ [5]. Also, the value of shear wave velocity (V_S) of geomaterials decreases with increasing value of cyclic shear strain. However, for cyclic strain amplitudes less than 10^{-5}, the value of V_s remains practically constant. Surface waves include both Rayleigh and Love waves; however, for near-surface site characterization, the methods utilize only Rayleigh waves. The estimated value of the attenuation coefficient is obtained using the R-wave velocity (V_R), the frequency of the vibration, and the damping ratio (ζ) using the following equation.

Table 2 Values of frequency-dependent attenuation coefficient 'a' for four classes of soil material [3]

Class	Material damping coefficient a ($m - 1$)		Description of material
	5 Hz	50 Hz	
I	0.01–0.03	0.1–0.3	Weak or soft soils (NSPT < 5)
II	0.003–0.01	0.03–0.1	Competent soils (5 < NSPT < 50)
III	0.0003–0.003	0.003–0.03	Hard soils (15 < NSPT < 50)
IV	< 0.0003	< 0.003	Hard, competent rock (NSPT > 50)

$$a = \frac{2\pi f}{V_{R}} \tag{3}$$

From the above equation, the attenuation coefficient linearly increases with the operating or vibration frequency and is inversely proportional with the Rayleigh wave velocity. Alternatively, the independent-frequency attenuation coefficient [6] can be obtained from the following equation.

$$a_{o} = \frac{a}{V_{R}} = \frac{2\pi}{V_{R}} \ (\text{s/m}) \tag{4}$$

where a_{o} is the frequency-independent of attenuation coefficient in s/m.

2 Need for Current Study

National High-Speed Rail Corporation Limited, India (NHSRCL) for the first time is implementing the project of high-speed train corridor between Ahmedabad and Mumbai. This high-profile bullet train will be designed for an operating speed of 320 kmph to cover the distance of 526 km in just two hours fifty-eight minutes which currently is covered in seven to eight hours. Since this project is first of its kind in India, there has been no sufficient comprehensive literature available on the impact of train speed above 200 kmph on the vibration response of the track foundation soil in Indian terrain. Based on the research conducted in the past, FEM approach is adopted herein to study attenuation of motion of the surface waves resulting from geometrical and material-damping properties of the underlying soil layer near the proposed railway track in the Surat city. The properties of the soil based on laboratory assessment is presented in Table 3. The bedrock for the current study is presumed to be at the depth of 6 m from the ground level. A quarter car model was developed to simulate CRH3 type high-speed train so as to simulate dynamic effect of load

Table 3 Properties of soil near proposed high-speed track site

Description	Value	Unit
Density	15.57	kN/m^3
Water content	15	%
Liquid limit	34	%
Plasticity Index	13	---
Poisson's ratio	0.31	---
Modulus of elasticity	38.59	MPa
Shear modulus	15,871	kN/m^2
Shear wave velocity	100	m/s
IS classification	Soft to medium stiff inorganic sandy clays of low plasticity, CL	

moving on the ballastless track. The moving train is simulated by a sequence of moving wheel loads that may vibrate with certain frequency. The transmissibility of soil for vibrations induced by trains moving at different speeds was used to identify the cut-off frequency of the train. Two train speeds are considered in the study, one is smaller and the other is greater than the Rayleigh wave speed of the single-layered soil resting on a rock mass. The results of measurements were analyzed in the frequency domain, and the attenuation characteristics of foundation soil were studied in terms of frequency-independent attenuation coefficient, by applying Bornitz equation.

3 Critical Velocity of Single-Layered Soil Resting on Bedrock

Due to symmetry in the section along vertical plan, only half of the section is considered for analysis which has reduced analysis time considerably. To simulate the effect of bedrock, it is assumed that the bottom of the model is fixed, and to represent infinite extend in horizontal direction, transmitting boundaries are connected with the elements as shown in Fig. 1. These boundaries, which can fully absorb body waves propagating normal to the boundary, were initially proposed by Lysmer and Kuhlemeyer (1969). Accordingly, the damping coefficient for the horizontal and the vertical dampers are defined in the following by Eqs. 5 and 6.

$$C_h = -\rho V_p \ \& \ C_v - \rho V_S A \tag{5}$$

$$V_p = \sqrt{\frac{K}{\rho}} \ \& \ V_S = \sqrt{\frac{G}{\rho}} \tag{6}$$
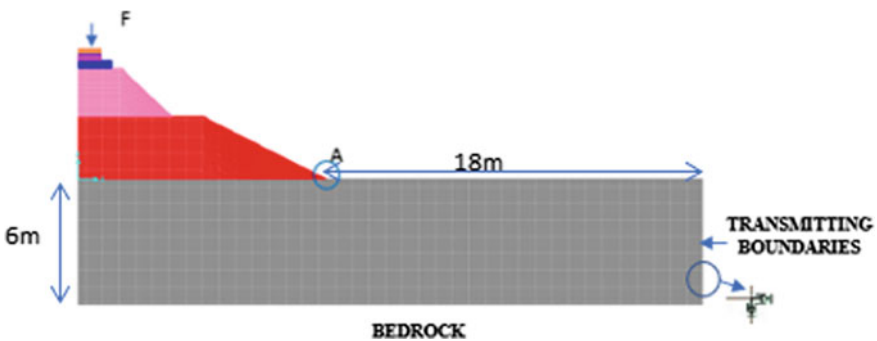

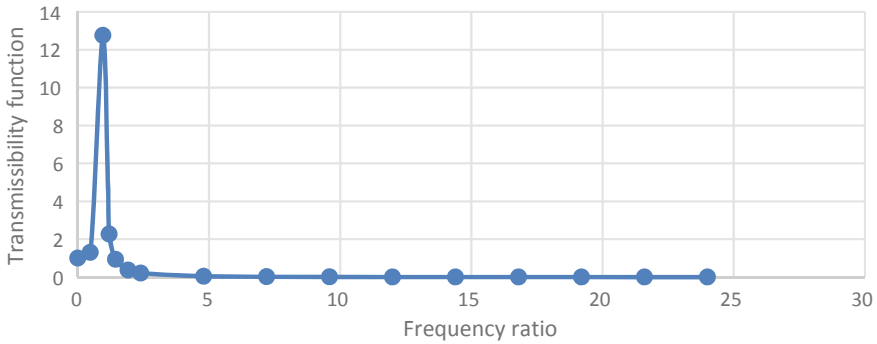**Fig. 1** FEM representation of the site

Fig. 2 Frequency response of the soil

In these equations, C_h and C_v are the horizontal and vertical coefficients of viscous dampers, V_p and V_s are the compressive and shear wave velocities in the soil, respectively, and A is effective nodal area for the node that is connected to the damper. Also, ρ, G, and K are mass density, shear modulus, and bulk modulus of soil.

In view of critical speed to be closely related to the wave velocity of the soil, the train running at a speed that is equal to the surface wave velocities of the supporting soil medium is called critical speed (V_{cr}) of the train. When train approaches speed equal to critical velocity, V_{cr} the deflection of track increases drastically. Correspondingly, the magnitude and impact of the vibrations become severe compared with the normal train induced vibration. Frequency response Fig. 2 revealed that maximum amplification occurs when the shear wave of the soil approaches 100 m/s. Thus, the critical velocity of the soil near the proposed site as computed based on dynamic analysis is 100 m/s.

4 Attenuation Characteristics of Soil Layer

Considering the configuration of CRH3-type high-speed train, it is simulated for a speed, moving at speed of 88 m/s (speed less than critical velocity of train) and 139 m/sec (speed greater than critical velocity of train), is done to comprehend attenuation characteristics of soil. From Table 4, it is observed that as the distance

Table 4 Value of 'n' and 'a' as worked out through curve-fitting method as measured value through simulation in SAP2000

Distance from the source	88 m/s		139 m/s	
	n	a	n	a
1 m	0.298	0.18	0.206	0.08
4 m	0.458	0.407	0.316	0.24

from the source increases, material damping property increases, but at a point, it is least affected by the frequency of vibration. For the accurate characterization of the soil, the readings must be taken as close to the source as possible. As per Table 1, it is deduced that the proposed site is characterized as Class I comprising of weak or soft soils with SPT $N < 5$. This goes well with the Indian Standard Classification as given in Table 3.

It is established from the present study that as velocity of propagation of waves through soil is vital information regarding the vibration problems of the adjacent buildings, the study helps to predict the vibration amplitude for multiple frequencies at varying distances.

5   Conclusion

The current study emphasizes on measurement of vertical displacement of particles induced by moving train and related geometrical and material damping properties of the surrounding soil. From the study, it can be concluded that for ground vibration developed from a periodic vibrating source (low frequency reciprocating type machinery), the attenuation follows Bornitz equation. Characterization of soil is done for the sites considered. The frequency-independent attenuation coefficient can be used for setting the vibration limits for buildings for varying distances depending on the soil type.

References

1. Athanasapoulos et al.: Soil dynamics and earthquake engineering. **19**, 277–288 (2000)
2. Woods, R.D.L: Dynamic effects of pile installations on adjacent structures. In: NCHRP 253, Transportation Research Board, National Academy Press, Washington DC (1997)
3. Drabkin, S., Lacy, H., Kim, D.S,: Estimating settlement of sand during construction vibration. J. Geotech. Eng. **122**(14), 920–928 (1996)
4. Woods, R.D., Jelede, L.P.: Energy attenuation relationships in construction vibrations. In: Vibration problems in Geotechnical Engineering—ASCE Convention in Detroit, Michigan (1985)
5. Lombaert, G.: Development and experimental validation of a numerical model for the free field vibrations induced by road traffic. PhD thesis, Katholieke Universiteit te Leuven (2001)
6. Wolf, J.P.: Dynamic soil-structure interaction. Prentice-Hall, Englewood Cliffs (1985)